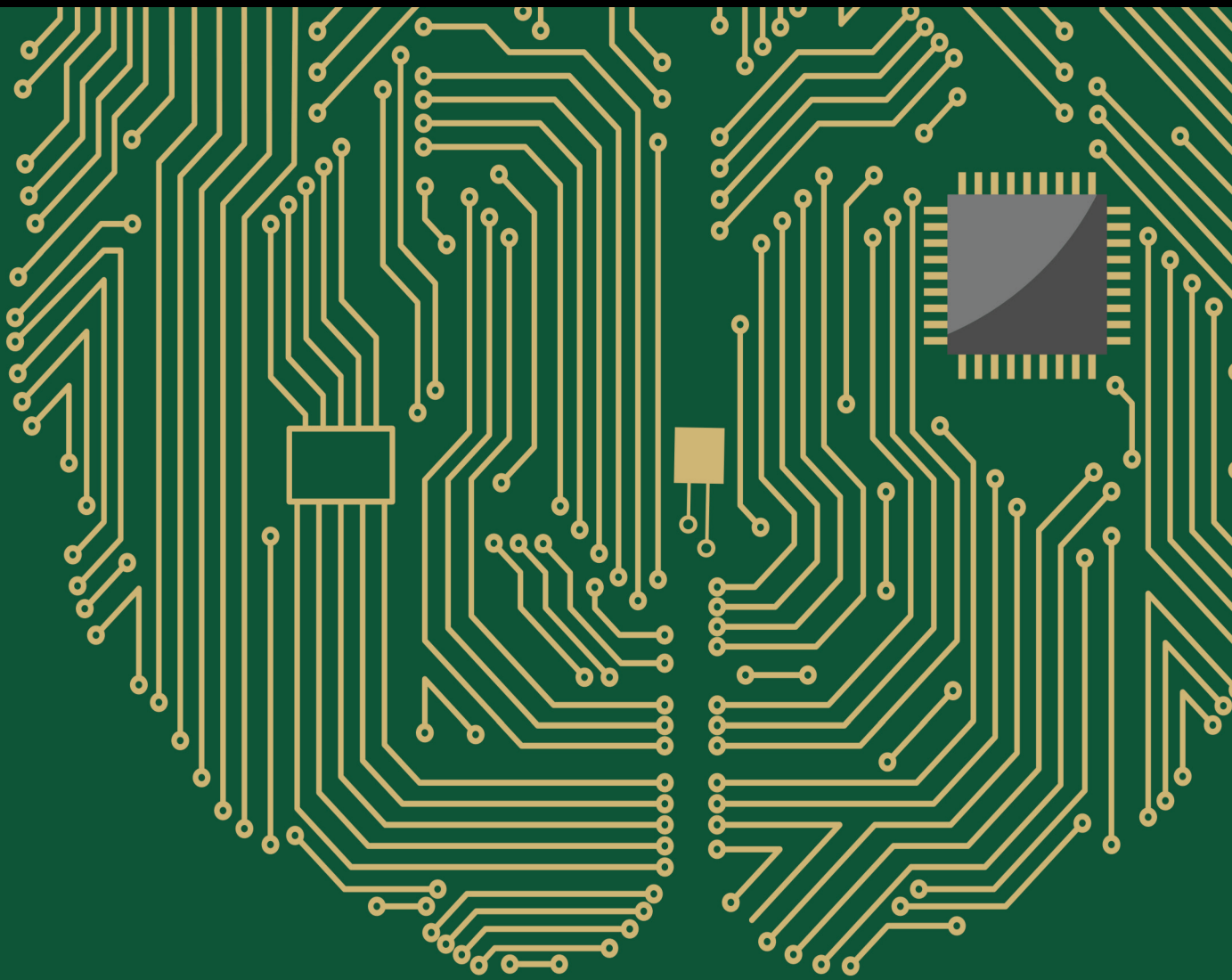


Advanced Computational Intelligence for Clinical Medical Information Processing

Lead Guest Editor: Dong Chen

Guest Editors: Changming Sun and Tuan D. Pham





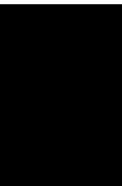
Advanced Computational Intelligence for Clinical Medical Information Processing

Computational Intelligence and Neuroscience

**Advanced Computational Intelligence
for Clinical Medical Information
Processing**

Lead Guest Editor: Dong Chen

Guest Editors: Changming Sun and Tuan D. Pham



Chief Editor

Andrzej Cichocki, Poland

Associate Editors

Arnaud Delorme, France
Cheng-Jian Lin , Taiwan
Saeid Sanei, United Kingdom

Academic Editors

Mohamed Abd Elaziz , Egypt
Tariq Ahanger , Saudi Arabia
Muhammad Ahmad, Pakistan
Ricardo Aler , Spain
Nouman Ali, Pakistan
Pietro Aricò , Italy
Lerina Aversano , Italy
Ümit Ağbulut , Turkey
Najib Ben Aoun , Saudi Arabia
Surbhi Bhatia , Saudi Arabia
Daniele Bibbo , Italy
Vince D. Calhoun , USA
Francesco Camastra, Italy
Zhicheng Cao, China
Hubert Cecotti , USA
Jyotir Moy Chatterjee , Nepal
Rupesh Chikara, USA
Marta Cimitile, Italy
Silvia Conforto , Italy
Paolo Crippa , Italy
Christian W. Dawson, United Kingdom
Carmen De Maio , Italy
Thomas DeMarse , USA
Maria Jose Del Jesus, Spain
Arnaud Delorme , France
Anastasios D. Doulamis, Greece
António Dourado , Portugal
Sheng Du , China
Said El Kafhali , Morocco
Mohammad Reza Feizi Derakhshi , Iran
Quanxi Feng, China
Zhong-kai Feng, China
Steven L. Fernandes, USA
Agostino Forestiero , Italy
Piotr Franaszczuk , USA
Thippa Reddy Gadekallu , India
Paolo Gastaldo , Italy
Samanwoy Ghosh-Dastidar, USA

Manuel Graña , Spain
Alberto Guillén , Spain
Gaurav Gupta, India
Rodolfo E. Haber , Spain
Usman Habib , Pakistan
Anandakumar Haldorai , India
José Alfredo Hernández-Pérez , Mexico
Luis Javier Herrera , Spain
Alexander Hošovský , Slovakia
Etienne Hugues, USA
Nadeem Iqbal , Pakistan
Sajad Jafari, Iran
Abdul Rehman Javed , Pakistan
Jing Jin , China
Li Jin, United Kingdom
Kanak Kalita, India
Ryotaro Kamimura , Japan
Pasi A. Karjalainen , Finland
Anitha Karthikeyan, Saint Vincent and the Grenadines
Elpida Keravnou , Cyprus
Asif Irshad Khan , Saudi Arabia
Muhammad Adnan Khan , Republic of Korea
Abbas Khosravi, Australia
Tai-hoon Kim, Republic of Korea
Li-Wei Ko , Taiwan
Raşit Köker , Turkey
Deepika Koundal , India
Sunil Kumar , India
Fabio La Foresta, Italy
Kuruva Lakshmanna , India
Maciej Lawrynczuk , Poland
Jianli Liu , China
Giosuè Lo Bosco , Italy
Andrea Loddo , Italy
Kezhi Mao, Singapore
Paolo Massobrio , Italy
Gerard McKee, Nigeria
Mohit Mittal , France
Paulo Moura Oliveira , Portugal
Debajyoti Mukhopadhyay , India
Xin Ning , China
Nasimul Noman , Australia
Fivos Panetsos , Spain

Evgeniya Pankratova , Russia
Rocío Pérez de Prado , Spain
Francesco Pistolesi , Italy
Alessandro Sebastian Podda , Italy
David M Powers, Australia
Radu-Emil Precup, Romania
Lorenzo Putzu, Italy
S P Raja, India
Dr.Anand Singh Rajawat , India
Simone Ranaldi , Italy
Upaka Rathnayake, Sri Lanka
Navid Razmjoo, Iran
Carlo Ricciardi, Italy
Jatinderkumar R. Saini , India
Sandhya Samarasinghe , New Zealand
Friedhelm Schwenker, Germany
Mijanur Rahaman Seikh, India
Tapan Senapati , China
Mohammed Shuaib , Malaysia
Kamran Siddique , USA
Gaurav Singal, India
Akansha Singh , India
Chiranjibi Sitaula , Australia
Neelakandan Subramani, India
Le Sun, China
Rawia Tahrir , Iraq
Binhua Tang , China
Carlos M. Travieso-González , Spain
Vinh Truong Hoang , Vietnam
Fath U Min Ullah , Republic of Korea
Pablo Varona , Spain
Roberto A. Vazquez , Mexico
Mario Versaci, Italy
Gennaro Vessio , Italy
Ivan Volosyak , Germany
Leyi Wei , China
Jianghui Wen, China
Lingwei Xu , China
Cornelio Yáñez-Márquez, Mexico
Zaher Mundher Yaseen, Iraq
Yugen Yi , China
Qiangqiang Yuan , China
Miaolei Zhou , China
Michal Zochowski, USA
Rodolfo Zunino, Italy

Contents

Retracted: Clinical Significance of EZH2 in Acute Myeloid Leukemia

Computational Intelligence and Neuroscience

Retraction (1 page), Article ID 9761597, Volume 2023 (2023)

Retracted: Comparison of the Effects of Open Surgery and Minimally Invasive Surgery on the Achilles Tendon Rupture Healing Based on Angiogenesis

Computational Intelligence and Neuroscience

Retraction (1 page), Article ID 9835651, Volume 2023 (2023)

Retracted: Effects of Fufang Banmao Capsule Associated with Sorafenib on Liver Function, Immune Status, Quality of Life Improvement, and Survival in Patients with Advanced Hepatocellular Carcinoma: A Retrospective Cohort Study

Computational Intelligence and Neuroscience

Retraction (1 page), Article ID 9817406, Volume 2023 (2023)

Retracted: Quality Evaluation of Ideological and Political Education in Universities Based on BP Neural Network

Computational Intelligence and Neuroscience

Retraction (1 page), Article ID 9840917, Volume 2023 (2023)

Retracted: Effect of Comprehensive Nursing on the Recovery of Gastrointestinal Function in Patients Undergoing Abdominal Operation

Computational Intelligence and Neuroscience

Retraction (1 page), Article ID 9840538, Volume 2023 (2023)

Retracted: Implementation of Evidence in Preventing Postoperative Sore Throat of Patients Undergoing General Anesthesia Intubation Using the i-PARIHS Framework

Computational Intelligence and Neuroscience

Retraction (1 page), Article ID 9834823, Volume 2023 (2023)

Retracted: Nonalcoholic Fatty Liver Hepatocyte-Derived lncRNA MALAT1 Aggravates Pancreatic Cell Inflammation via the Inhibition of Autophagy by Upregulating YAP

Computational Intelligence and Neuroscience

Retraction (1 page), Article ID 9831369, Volume 2023 (2023)

Retracted: Analysis of Factors Related to Adolescents' Physical Activity Behavior Based on Multichannel LSTM Model

Computational Intelligence and Neuroscience

Retraction (1 page), Article ID 9819806, Volume 2023 (2023)

Retracted: Effects of the Ultrasound-Guided Stellate Ganglion Block on Hemodynamics, Stress Response, and Gastrointestinal Function in Postoperative Patients with Colorectal Cancer

Computational Intelligence and Neuroscience

Retraction (1 page), Article ID 9814694, Volume 2023 (2023)

Retracted: Meta-Analysis of Knee Joint Function Recovery after Anterior Cruciate Ligament Reconstruction by Accelerated Rehabilitation Surgery

Computational Intelligence and Neuroscience

Retraction (1 page), Article ID 9893414, Volume 2023 (2023)

Retracted: Correlation between Sputum Bacterial Culture Positive Rate and Drug Sensitivity Test Results and Disease Severity in Inpatients and Its Clinical Significance: A Systematic Review and Meta-Analysis

Computational Intelligence and Neuroscience




Retraction (1 page), Article ID 9867361, Volume 2023 (2023)

Retracted: Correlation between Pain Scores and Disc Height Changes after Discectomy in Patients with Lumbar Disc Herniation: A Systematic Review and Meta-Analysis

Computational Intelligence and Neuroscience


Retraction (1 page), Article ID 9861787, Volume 2023 (2023)

A Soft Label Method for Medical Image Segmentation with Multirater Annotations

Jichang Zhang , Yuanjie Zheng , and Yunfeng Shi 




Research Article (11 pages), Article ID 1883597, Volume 2023 (2023)

Role of Intelligent Management Systems in Surgical Punctuality and Quality of Care

Gendi Li and Shenhui Huang 


Research Article (6 pages), Article ID 4921644, Volume 2022 (2022)

Posterior Injured Vertebra Column Resection and Spinal Shortening for Thoracolumbar Fracture Associated with Severe Spinal Cord Injury: A Retrospective Case-Control Observational Study

Zhiyue Shi , Yingsong Wang , Jingming Xie , Jin Zhou, Tingbiao Zhu, Tao Li, Zhi Zhao, Ying Zhang, Ni Bi, and Quan Li


Research Article (8 pages), Article ID 9000122, Volume 2022 (2022)

Effect and Safety of Painless and Conventional Endoscopic Management of Denture Impaction in the Esophagus

Li li Tian 


Research Article (6 pages), Article ID 9949875, Volume 2022 (2022)

Pan-Cancer Gene Analysis of m6A Modification and Immune Infiltration in Uterine Corpus Endometrial Carcinoma

Bing-fan Xie, Yan Xia, Dan-huan Lin, Bing Lian, Meng-li Zhang, Lu Liu, and Chun-Rong Qin 

Research Article (11 pages), Article ID 6530884, Volume 2022 (2022)


Research on Application of Meticulous Nursing Scheduling Management Based on Data-Driven Intelligent Optimization Technology

YanPing Zhai , Run Li, and ZhiLi Yan

Research Article (12 pages), Article ID 3293806, Volume 2022 (2022)


Contents

Effect of Early Rehabilitation Nursing on Motor Function and Living Ability of Patients with Traumatic Brain Injury Based on Orem's Self-Care Theory

Yuqin Yang and Lu Niu 

Research Article (9 pages), Article ID 7727085, Volume 2022 (2022)

Factors Influencing Adverse Pregnancy Outcomes in Gestational Diabetes Mellitus

Fang Zhao and Bo Xiao 


Research Article (8 pages), Article ID 5177428, Volume 2022 (2022)

[Retracted] Comparison of the Effects of Open Surgery and Minimally Invasive Surgery on the Achilles Tendon Rupture Healing Based on Angiogenesis

Fan Gong, Xiaoliang Li, Hanling Zhang, Jianke Wu, Guoxu Ma, Bowen Zhang, Jian Gao, Yi Ding, Yonglu Huang, Suoli Cheng, Xuebing Zhou, and Fei Zhao 


Research Article (8 pages), Article ID 1447129, Volume 2022 (2022)

[Retracted] Nonalcoholic Fatty Liver Hepatocyte-Derived lncRNA MALAT1 Aggravates Pancreatic Cell Inflammation via the Inhibition of Autophagy by Upregulating YAP

Di Liu, Weijie Yao, Kejun Liu, Genwang Wang, Bendong Chen, Zuozheng Wang, and Shaozhang Hou 


Research Article (9 pages), Article ID 2930960, Volume 2022 (2022)

Effect of Story Structure Instruction Based on Visual Analysis on Reading Comprehension Intervention for Dyslexic Students

Hanzhu Yang 


Research Article (8 pages), Article ID 9479709, Volume 2022 (2022)

Analgesic Effects, Birth Process, and Prognosis of Pregnant Women in Normal Labor by Epidural Analgesia Using Sufentanil in Combination with Ropivacaine: A Retrospective Cohort Study

Lijing Mao, Xiaoxiao Zhang, and Jing Zhu 


Research Article (9 pages), Article ID 1228006, Volume 2022 (2022)

Biological Mechanism on SIRT1/NLRP3/IL-18 Signaling Pathway of Acupuncture for Treatment of Ischemic Stroke with Center Poststroke Pain

Dan Zhou, Lanfang Zhang , Liwei Mao, Jingyu Cao, and Jiaqiang Gao


Research Article (10 pages), Article ID 8958742, Volume 2022 (2022)

[Retracted] Clinical Significance of EZH2 in Acute Myeloid Leukemia

Weiyun Jiao, Yuanyuan Liu, and Yangyi Bao 


Research Article (5 pages), Article ID 8741989, Volume 2022 (2022)

[Retracted] Effects of Fufang Banmao Capsule Associated with Sorafenib on Liver Function, Immune Status, Quality of Life Improvement, and Survival in Patients with Advanced Hepatocellular Carcinoma: A Retrospective Cohort Study

Xianghong Lai and Anmei Wang 


Research Article (8 pages), Article ID 6336107, Volume 2022 (2022)

[Retracted] Effect of Comprehensive Nursing on the Recovery of Gastrointestinal Function in Patients Undergoing Abdominal Operation

Lanlan Xiang, Wei Liu, and Yuanyuan Jin 


Research Article (10 pages), Article ID 1179321, Volume 2022 (2022)

Effect of Loratadine Tablets in Combination with Other Drugs on Nasal Physiological Function and T Lymphocyte Subsets in Patients with Allergic Rhinitis

Jie Zhang, Hongzheng Cheng, Yi Luo, Dan Kan, and Yinghuai Wang 

Research Article (8 pages), Article ID 3990427, Volume 2022 (2022)

Using Logistic Multivariate Analysis to Explore the Effects of Nursing and Psychological Factors on Motor and Cognitive Rehabilitation in Patients with Stroke: Based on a Retrospective Case-Control Study

Wenxin Lin, Liping Meng , Weimin Lou, Panpan Yang, and Min Huang


Research Article (8 pages), Article ID 1411670, Volume 2022 (2022)


Effect of Intelligent Operating Hole Towel in Cataract Patients

Suhui Xu, Meijuan Lan , Haiyan Cai, and Pei Zhang

Research Article (5 pages), Article ID 2638428, Volume 2022 (2022)


Clinical Image Feature Analysis and Diagnostic Efficacy Evaluation of Pulmonary Ultrasound in the Diagnosis of Congenital Pulmonary Airway Malformations in Children: Based on a Single Center, Retrospective Cohort Study

Dandan Liu, Gang Zhang , Jianyi Liao, Lan Jiang, Chun Cai, Xiao Li, Lei Lou, Bin Zhou, Huiyi Zeng,

Xiangang Yan, and Gang Yu 



Research Article (14 pages), Article ID 7490207, Volume 2022 (2022)

The Influence of Interpersonal Trust on Rural Residents' Willingness to Participate in Mutual Aid for the Aged: An Empirical Analysis Based on the Survey Data of Hubei and Henan Provinces

Beibei Liu and Yongyong Sun 


Research Article (11 pages), Article ID 2366425, Volume 2022 (2022)

Study on the Application Effect of the Case Teaching Method Based on Primary Teaching Principle in Clinical Teaching of Radiology

Tong Gong, Yuting Wang, Hong Pu, Longlin Yin , and Mi Zhou 


Research Article (8 pages), Article ID 3448182, Volume 2022 (2022)

A Transformer-Based Network for Change Detection in Remote Sensing Using Multiscale Difference-Enhancement

Gulinazi Ailimujiang, Yiliyaer Jiaermuhamaiti , Huxidan Jumahong, Huiling Wang, Shuangling Zhu, and Pazilaiti Nurmamaiti

Research Article (9 pages), Article ID 2189176, Volume 2022 (2022)




Research on the Audit Prediction Model of "Special Bonds + PPP" Project based on Machine Learning

Qianru Fang 

Research Article (11 pages), Article ID 4174473, Volume 2022 (2022)


Contents

Detecting Personal Medication Intake in Twitter via Domain Attention-Based RNN with Multi-Level Features

Shufeng Xiong , Vishwash Batra, Liangliang Liu, Lei Xi , and Changxia Sun 


Research Article (7 pages), Article ID 5467262, Volume 2022 (2022)

Research on the Development of Hospital Intelligent Finance Based on Artificial Intelligence

Mengxuan Ma 


Research Article (6 pages), Article ID 6549766, Volume 2022 (2022)

m6A-Related lncRNAs Predict Overall Survival of Patients and Regulate the Tumor Immune Microenvironment in Osteosarcoma

Yikang Bi, Depeng Meng, Ma Wan, Ning Xu, Yafeng Xu, Kaixuan Yuan, Pengcheng Liu, Hao Fang, Hai Hu, and Shenghui Lan 


Research Article (16 pages), Article ID 9315283, Volume 2022 (2022)

Effectiveness of Perioperative Comprehensive Evaluation of Hip Fracture in the Elderly

Tao Zhu, Jun Yu, Ye Ma, Yue Qin, Nan Li, and Haibo Yang 



Research Article (6 pages), Article ID 4124354, Volume 2022 (2022)

Effect of Restraint Stress on Pain Sensitivity, Spinal Trigeminal Nucleus Neurons, and Astrocytes in the Masseter Area of Rats

Feng Han 


Research Article (8 pages), Article ID 2345039, Volume 2022 (2022)

[Retracted] Correlation between Pain Scores and Disc Height Changes after Discectomy in Patients with Lumbar Disc Herniation: A Systematic Review and Meta-Analysis

Yuchen Zheng , Tao Lan, Xiaosheng Chen, Zhihao Hus, and Rui Zhang 


Research Article (9 pages), Article ID 2580004, Volume 2022 (2022)

A Retrospective Cohort Study of Neuroendoscopic Surgery versus Traditional Craniotomy on Surgical Success Rate, Postoperative Complications, and Prognosis in Patients with Acute Intracerebral Hemorrhage

Yong Li, Senyuan Yang, Xiaobin Zhou, Runlong Lai, and Dianhui Tan 


Research Article (9 pages), Article ID 2650795, Volume 2022 (2022)

Expression and Prognostic Role of CXCL1 Gene in Colorectal Adenocarcinoma

Chao Xia, Lifeng He, and Yi Sun 

Research Article (5 pages), Article ID 5504731, Volume 2022 (2022)

Clinical Efficacy and Safety of Different Dental Prosthetic Membranes in Guided Bone Regeneration during Dental Implants: A Meta-Analysis


Yan Guo, Linghan Su, Caidi Chen, Yan Liu, and Jianxue Li 

Research Article (9 pages), Article ID 3245014, Volume 2022 (2022)


Exploration and Practice of the Integrated Teaching Method of Mind Mapping in the Standardized Training of New Pharmacists

Li Yuan , Bei Chen, Zhaojun Wu, Gefei He, and Juanjuan Huang
Research Article (7 pages), Article ID 7985027, Volume 2022 (2022)



Safety and Efficacy of Single Condylar Knee Prosthesis When Treating Knee Single Compartment Osteoarthritis: A Prospective, Case-Randomized Controlled Study

Shaofeng Wang, Yang Wang, and Jiong Wang 
Research Article (8 pages), Article ID 3722619, Volume 2022 (2022)


The Efficacy and Safety of Mizoribine versus Mycophenolate Mofetil for the Treatment of Renal Transplantation: A Systematic Review and Meta-Analysis

Jie Chen, Hua Liu, Wenjun Yin, Zhengguang Xu, Zekai Chen, and Wingkeung Yiu 
Research Article (11 pages), Article ID 5717068, Volume 2022 (2022)

Research on the MEG of Depression Patients Based on Multivariate Transfer Entropy

Xinyu Zhang , Jicheng Xie, Changyu Fan, and Jun Wang 
Research Article (8 pages), Article ID 7516627, Volume 2022 (2022)


[Retracted] Quality Evaluation of Ideological and Political Education in Universities Based on BP Neural Network

Yunxia Ding , Wei Zeng, and Zhen Ning
Research Article (7 pages), Article ID 8336895, Volume 2022 (2022)


Effect of Compound Danshen Injection Combined with Magnesium Sulfate on Oxidative Stress, TNF- α , NO, and Therapeutic Efficacy in Severe Preeclampsia

Yanling Zhou , Juan Wang , Lei Wang , Jing Tang , and Chengwei Zhang 
Research Article (7 pages), Article ID 9789066, Volume 2022 (2022)

Role and Mechanism of Keap1/Nrf2 Signaling Pathway in the Regulation of Autophagy in Alleviating Pulmonary Fibrosis

Zhaoxing Dong, E. Gao Yin, Meijuan Yang, Xiaoyuan Zhao, Jing Li, and Wen Lei 
Research Article (9 pages), Article ID 3564871, Volume 2022 (2022)

[Retracted] Effects of the Ultrasound-Guided Stellate Ganglion Block on Hemodynamics, Stress Response, and Gastrointestinal Function in Postoperative Patients with Colorectal Cancer


An Xie, Xianjie Zhang, Feng Ju, Wen Li, Yukai Zhou, and Dan Wu 
Research Article (7 pages), Article ID 2056969, Volume 2022 (2022)

[Retracted] Correlation between Sputum Bacterial Culture Positive Rate and Drug Sensitivity Test Results and Disease Severity in Inpatients and Its Clinical Significance: A Systematic Review and Meta-Analysis

Wenjing Zhou and Jing Li 
Research Article (9 pages), Article ID 5102100, Volume 2022 (2022)

Contents

A Cross-Sectional Study on the Application of IS in Perioperative Pulmonary Function Training in Spine and Orthopedics

Ting Qiu, Yong Li, Jingjing Zhang, Xuanzhu Hou, Yuqi Wu, Yan Xu, Wenyue Chen, Jingjing Rui, Jin Yang, and Jing Qian 

Research Article (8 pages), Article ID 4546549, Volume 2022 (2022)

Optimisation of a Mouse Model of Cerebral Ischemia-Reperfusion to Address Issues of Survival and Model Reproducibility and Consistency

Zhenqian Liu, Mo Chen, Xu Duan, Yujia Zhai, Bin Ma, Zuowei Duan, Jiang Xu, and Haiyan Liu 


Research Article (10 pages), Article ID 7594969, Volume 2022 (2022)

[Retracted] Implementation of Evidence in Preventing Postoperative Sore Throat of Patients Undergoing General Anesthesia Intubation Using the i-PARIHS Framework

Qian Liu, Yiting Wang, Ruo Zhuang , Lei Bao, Liqun Zhu, and Yingfeng Zhou

Research Article (9 pages), Article ID 3151423, Volume 2022 (2022)

[Retracted] Analysis of Factors Related to Adolescents' Physical Activity Behavior Based on Multichannel LSTM Model

Guiling Chang and Jinfeng Liu 


Research Article (8 pages), Article ID 1022421, Volume 2022 (2022)

The Application of Image Processing Technology in Camera Picture

Yun Hong 


Research Article (11 pages), Article ID 9899610, Volume 2022 (2022)

Management and Analysis of Sports Health Level of the Elderly Based on Deep Learning

Liping Xiao , Limin Huang, Hongxia Chang, Li Ji, and Ji Li


Research Article (8 pages), Article ID 6044320, Volume 2022 (2022)

Research on Land Use Planning Based on Multisource Remote Sensing Data

Wei Jia, Tingting Pei, and Kai Lei 


Research Article (8 pages), Article ID 5851768, Volume 2022 (2022)

[Retracted] Meta-Analysis of Knee Joint Function Recovery after Anterior Cruciate Ligament Reconstruction by Accelerated Rehabilitation Surgery

Junxiang Xu , Minzhe Zheng, Zongxian Feng, Lingxiao Pan, and Zhaoxiang Peng



Research Article (8 pages), Article ID 5085143, Volume 2022 (2022)

Xingnao Kaiqiao Acupuncture Method Combined with Temporal Three-Needle in the Treatment of Acute Ischemic Stroke: A Randomized Controlled Trial

Zhongtao Song , Qingyuan Huang, Yuxia Guo, Xiaodong Song, Xuan Zhang, and Huajun Xiao


Research Article (7 pages), Article ID 8145374, Volume 2022 (2022)

Integration of Genetic and Immune Infiltration Insights into Data Mining of Multiple Sclerosis Pathogenesis

Xiaoyun Zhang , Ying Song, Xiao Chen, Xiaojia Zhuang, Zhiqiang Wei, and Li Yi 


Research Article (19 pages), Article ID 1661334, Volume 2022 (2022)

Design of Digital and Intelligent Financial Decision Support System Based on Artificial Intelligence

Tiejun Jia , Cheng Wang, Zhiqiang Tian, Bingyin Wang, and Feng Tian


Research Article (7 pages), Article ID 1962937, Volume 2022 (2022)

A Study on the Hedging Function of Gold in the Light of Economic Policy Uncertainty

Borui Xiao 


Research Article (16 pages), Article ID 1556475, Volume 2022 (2022)

Analysis of the Relationship between Transformational Leadership and Educational Management in Higher Education Based on Deep Learning

Haiying Meng 


Research Article (8 pages), Article ID 5287922, Volume 2022 (2022)

Metal Jewelry Craft Design Based on Computer Vision

Nan Li 

Research Article (11 pages), Article ID 3843421, Volume 2022 (2022)

Art Design Method of Industrial Products Based on Internet of Things Technology and Virtual VR

Yu Yu 


Research Article (10 pages), Article ID 9666827, Volume 2022 (2022)

Effects of Aerobic Exercise on the Serum Leptin Level and Heart Rate Variability in the Obese Girl Children

Cuihan Li , Shaojun Lyu, and Jianwei Zhang 


Research Article (6 pages), Article ID 2298994, Volume 2022 (2022)

Research on Mechanical and Carbonization Properties of Hybrid Fiber Iron Tailings Concrete Based on Deep Learning

Wenbo Zheng , Sheliang Wang, Yang Qu, Kangning Liu, and Liangwei Jia


Research Article (11 pages), Article ID 3475679, Volume 2022 (2022)

Novel High-Efficiency Nanocomposite Gate Design of Quantum-Dot Cellular Automata Based on Deep Learning

Yourun Zhu , Senlin Ren, and Xiaolong Li

Research Article (11 pages), Article ID 9596165, Volume 2022 (2022)


Monitoring and Analysis of Venture Capital and Corporate Fraud Based on Deep Learning

Ruijun Zhang and Lina Zheng 

Research Article (13 pages), Article ID 4589593, Volume 2022 (2022)

Contents

Design and Implementation of 3D Animation Data Processing Development Platform Based on Artificial Intelligence

Quansheng Gao 

Research Article (7 pages), Article ID 1518331, Volume 2022 (2022)

Fetal Meconium Peritonitis: A Clinical Study of Nine Cases

Fengping Fu , Xia Song , Fudan Huang , Hang Yuan , and Li Xiao 

Research Article (4 pages), Article ID 8658999, Volume 2022 (2022)

Retraction

Retracted: Clinical Significance of EZH2 in Acute Myeloid Leukemia

Computational Intelligence and Neuroscience

Received 26 September 2023; Accepted 26 September 2023; Published 27 September 2023

Copyright © 2023 Computational Intelligence and Neuroscience. This is an open access article distributed under the Creative Commons Attribution License, which permits unrestricted use, distribution, and reproduction in any medium, provided the original work is properly cited.

This article has been retracted by Hindawi following an investigation undertaken by the publisher [1]. This investigation has uncovered evidence of one or more of the following indicators of systematic manipulation of the publication process:

- (1) Discrepancies in scope
- (2) Discrepancies in the description of the research reported
- (3) Discrepancies between the availability of data and the research described
- (4) Inappropriate citations
- (5) Incoherent, meaningless and/or irrelevant content included in the article
- (6) Peer-review manipulation

The presence of these indicators undermines our confidence in the integrity of the article's content and we cannot, therefore, vouch for its reliability. Please note that this notice is intended solely to alert readers that the content of this article is unreliable. We have not investigated whether authors were aware of or involved in the systematic manipulation of the publication process.

Wiley and Hindawi regrets that the usual quality checks did not identify these issues before publication and have since put additional measures in place to safeguard research integrity.

We wish to credit our own Research Integrity and Research Publishing teams and anonymous and named external researchers and research integrity experts for contributing to this investigation.

The corresponding author, as the representative of all authors, has been given the opportunity to register their agreement or disagreement to this retraction. We have kept a record of any response received.

References

- [1] W. Jiao, Y. Liu, and Y. Bao, "Clinical Significance of EZH2 in Acute Myeloid Leukemia," *Computational Intelligence and Neuroscience*, vol. 2022, Article ID 8741989, 5 pages, 2022.

Retraction

Retracted: Comparison of the Effects of Open Surgery and Minimally Invasive Surgery on the Achilles Tendon Rupture Healing Based on Angiogenesis

Computational Intelligence and Neuroscience

Received 1 August 2023; Accepted 1 August 2023; Published 2 August 2023

Copyright © 2023 Computational Intelligence and Neuroscience. This is an open access article distributed under the Creative Commons Attribution License, which permits unrestricted use, distribution, and reproduction in any medium, provided the original work is properly cited.

This article has been retracted by Hindawi following an investigation undertaken by the publisher [1]. This investigation has uncovered evidence of one or more of the following indicators of systematic manipulation of the publication process:

- (1) Discrepancies in scope
- (2) Discrepancies in the description of the research reported
- (3) Discrepancies between the availability of data and the research described
- (4) Inappropriate citations
- (5) Incoherent, meaningless and/or irrelevant content included in the article
- (6) Peer-review manipulation

The presence of these indicators undermines our confidence in the integrity of the article's content and we cannot, therefore, vouch for its reliability. Please note that this notice is intended solely to alert readers that the content of this article is unreliable. We have not investigated whether authors were aware of or involved in the systematic manipulation of the publication process.

Wiley and Hindawi regrets that the usual quality checks did not identify these issues before publication and have since put additional measures in place to safeguard research integrity.

We wish to credit our own Research Integrity and Research Publishing teams and anonymous and named external researchers and research integrity experts for contributing to this investigation.

The corresponding author, as the representative of all authors, has been given the opportunity to register their agreement or disagreement to this retraction. We have kept a record of any response received.

References

- [1] F. Gong, X. Li, H. Zhang et al., "Comparison of the Effects of Open Surgery and Minimally Invasive Surgery on the Achilles Tendon Rupture Healing Based on Angiogenesis," *Computational Intelligence and Neuroscience*, vol. 2022, Article ID 1447129, 8 pages, 2022.

Retraction

Retracted: Effects of Fufang Banmao Capsule Associated with Sorafenib on Liver Function, Immune Status, Quality of Life Improvement, and Survival in Patients with Advanced Hepatocellular Carcinoma: A Retrospective Cohort Study

Computational Intelligence and Neuroscience

Received 1 August 2023; Accepted 1 August 2023; Published 2 August 2023

Copyright © 2023 Computational Intelligence and Neuroscience. This is an open access article distributed under the Creative Commons Attribution License, which permits unrestricted use, distribution, and reproduction in any medium, provided the original work is properly cited.

This article has been retracted by Hindawi following an investigation undertaken by the publisher [1]. This investigation has uncovered evidence of one or more of the following indicators of systematic manipulation of the publication process:

- (1) Discrepancies in scope
- (2) Discrepancies in the description of the research reported
- (3) Discrepancies between the availability of data and the research described
- (4) Inappropriate citations
- (5) Incoherent, meaningless and/or irrelevant content included in the article
- (6) Peer-review manipulation

The presence of these indicators undermines our confidence in the integrity of the article's content and we cannot, therefore, vouch for its reliability. Please note that this notice is intended solely to alert readers that the content of this article is unreliable. We have not investigated whether authors were aware of or involved in the systematic manipulation of the publication process.

Wiley and Hindawi regrets that the usual quality checks did not identify these issues before publication and have since put additional measures in place to safeguard research integrity.

We wish to credit our own Research Integrity and Research Publishing teams and anonymous and named external researchers and research integrity experts for contributing to this investigation.

The corresponding author, as the representative of all authors, has been given the opportunity to register their agreement or disagreement to this retraction. We have kept a record of any response received.

References

- [1] X. Lai and A. Wang, "Effects of Fufang Banmao Capsule Associated with Sorafenib on Liver Function, Immune Status, Quality of Life Improvement, and Survival in Patients with Advanced Hepatocellular Carcinoma: A Retrospective Cohort Study," *Computational Intelligence and Neuroscience*, vol. 2022, Article ID 6336107, 8 pages, 2022.

Retraction

Retracted: Quality Evaluation of Ideological and Political Education in Universities Based on BP Neural Network

Computational Intelligence and Neuroscience

Received 25 July 2023; Accepted 25 July 2023; Published 26 July 2023

Copyright © 2023 Computational Intelligence and Neuroscience. This is an open access article distributed under the Creative Commons Attribution License, which permits unrestricted use, distribution, and reproduction in any medium, provided the original work is properly cited.

This article has been retracted by Hindawi following an investigation undertaken by the publisher [1]. This investigation has uncovered evidence of one or more of the following indicators of systematic manipulation of the publication process:

- (1) Discrepancies in scope
- (2) Discrepancies in the description of the research reported
- (3) Discrepancies between the availability of data and the research described
- (4) Inappropriate citations
- (5) Incoherent, meaningless and/or irrelevant content included in the article
- (6) Peer-review manipulation

The presence of these indicators undermines our confidence in the integrity of the article's content and we cannot, therefore, vouch for its reliability. Please note that this notice is intended solely to alert readers that the content of this article is unreliable. We have not investigated whether authors were aware of or involved in the systematic manipulation of the publication process.

Wiley and Hindawi regrets that the usual quality checks did not identify these issues before publication and have since put additional measures in place to safeguard research integrity.

We wish to credit our own Research Integrity and Research Publishing teams and anonymous and named external researchers and research integrity experts for contributing to this investigation.

The corresponding author, as the representative of all authors, has been given the opportunity to register their agreement or disagreement to this retraction. We have kept a record of any response received.

References

- [1] Y. Ding, W. Zeng, and Z. Ning, "Quality Evaluation of Ideological and Political Education in Universities Based on BP Neural Network," *Computational Intelligence and Neuroscience*, vol. 2022, Article ID 8336895, 7 pages, 2022.

Retraction

Retracted: Effect of Comprehensive Nursing on the Recovery of Gastrointestinal Function in Patients Undergoing Abdominal Operation

Computational Intelligence and Neuroscience

Received 25 July 2023; Accepted 25 July 2023; Published 26 July 2023

Copyright © 2023 Computational Intelligence and Neuroscience. This is an open access article distributed under the Creative Commons Attribution License, which permits unrestricted use, distribution, and reproduction in any medium, provided the original work is properly cited.

This article has been retracted by Hindawi following an investigation undertaken by the publisher [1]. This investigation has uncovered evidence of one or more of the following indicators of systematic manipulation of the publication process:

- (1) Discrepancies in scope
- (2) Discrepancies in the description of the research reported
- (3) Discrepancies between the availability of data and the research described
- (4) Inappropriate citations
- (5) Incoherent, meaningless and/or irrelevant content included in the article
- (6) Peer-review manipulation

The presence of these indicators undermines our confidence in the integrity of the article's content and we cannot, therefore, vouch for its reliability. Please note that this notice is intended solely to alert readers that the content of this article is unreliable. We have not investigated whether authors were aware of or involved in the systematic manipulation of the publication process.

Wiley and Hindawi regrets that the usual quality checks did not identify these issues before publication and have since put additional measures in place to safeguard research integrity.

We wish to credit our own Research Integrity and Research Publishing teams and anonymous and named external researchers and research integrity experts for contributing to this investigation.

The corresponding author, as the representative of all authors, has been given the opportunity to register their agreement or disagreement to this retraction. We have kept a record of any response received.

References

- [1] L. Xiang, W. Liu, and Y. Jin, "Effect of Comprehensive Nursing on the Recovery of Gastrointestinal Function in Patients Undergoing Abdominal Operation," *Computational Intelligence and Neuroscience*, vol. 2022, Article ID 1179321, 10 pages, 2022.

Retraction

Retracted: Implementation of Evidence in Preventing Postoperative Sore Throat of Patients Undergoing General Anesthesia Intubation Using the i-PARIHS Framework

Computational Intelligence and Neuroscience

Received 25 July 2023; Accepted 25 July 2023; Published 26 July 2023

Copyright © 2023 Computational Intelligence and Neuroscience. This is an open access article distributed under the Creative Commons Attribution License, which permits unrestricted use, distribution, and reproduction in any medium, provided the original work is properly cited.

This article has been retracted by Hindawi following an investigation undertaken by the publisher [1]. This investigation has uncovered evidence of one or more of the following indicators of systematic manipulation of the publication process:

- (1) Discrepancies in scope
- (2) Discrepancies in the description of the research reported
- (3) Discrepancies between the availability of data and the research described
- (4) Inappropriate citations
- (5) Incoherent, meaningless and/or irrelevant content included in the article
- (6) Peer-review manipulation

The presence of these indicators undermines our confidence in the integrity of the article's content and we cannot, therefore, vouch for its reliability. Please note that this notice is intended solely to alert readers that the content of this article is unreliable. We have not investigated whether authors were aware of or involved in the systematic manipulation of the publication process.

In addition, our investigation has also shown that one or more of the following human-subject reporting requirements has not been met in this article: ethical approval by an Institutional Review Board (IRB) committee or equivalent, patient/participant consent to participate, and/or agreement to publish patient/participant details (where relevant).

Wiley and Hindawi regrets that the usual quality checks did not identify these issues before publication and have since put additional measures in place to safeguard research integrity.

We wish to credit our own Research Integrity and Research Publishing teams and anonymous and named external researchers and research integrity experts for contributing to this investigation.

The corresponding author, as the representative of all authors, has been given the opportunity to register their agreement or disagreement to this retraction. We have kept a record of any response received.

References

- [1] Q. Liu, Y. Wang, R. Zhuang, L. Bao, L. Zhu, and Y. Zhou, "Implementation of Evidence in Preventing Postoperative Sore Throat of Patients Undergoing General Anesthesia Intubation Using the i-PARIHS Framework," *Computational Intelligence and Neuroscience*, vol. 2022, Article ID 3151423, 9 pages, 2022.

Retraction

Retracted: Nonalcoholic Fatty Liver Hepatocyte-Derived lncRNA MALAT1 Aggravates Pancreatic Cell Inflammation via the Inhibition of Autophagy by Upregulating YAP

Computational Intelligence and Neuroscience

Received 25 July 2023; Accepted 25 July 2023; Published 26 July 2023

Copyright © 2023 Computational Intelligence and Neuroscience. This is an open access article distributed under the Creative Commons Attribution License, which permits unrestricted use, distribution, and reproduction in any medium, provided the original work is properly cited.

This article has been retracted by Hindawi following an investigation undertaken by the publisher [1]. This investigation has uncovered evidence of one or more of the following indicators of systematic manipulation of the publication process:

- (1) Discrepancies in scope
- (2) Discrepancies in the description of the research reported
- (3) Discrepancies between the availability of data and the research described
- (4) Inappropriate citations
- (5) Incoherent, meaningless and/or irrelevant content included in the article
- (6) Peer-review manipulation

The presence of these indicators undermines our confidence in the integrity of the article's content and we cannot, therefore, vouch for its reliability. Please note that this notice is intended solely to alert readers that the content of this article is unreliable. We have not investigated whether authors were aware of or involved in the systematic manipulation of the publication process.

Wiley and Hindawi regrets that the usual quality checks did not identify these issues before publication and have since put additional measures in place to safeguard research integrity.

We wish to credit our own Research Integrity and Research Publishing teams and anonymous and named external researchers and research integrity experts for contributing to this investigation.

The corresponding author, as the representative of all authors, has been given the opportunity to register their agreement or disagreement to this retraction. We have kept a record of any response received.

References

- [1] D. Liu, W. Yao, K. Liu et al., "Nonalcoholic Fatty Liver Hepatocyte-Derived lncRNA MALAT1 Aggravates Pancreatic Cell Inflammation via the Inhibition of Autophagy by Upregulating YAP," *Computational Intelligence and Neuroscience*, vol. 2022, Article ID 2930960, 9 pages, 2022.

Retraction

Retracted: Analysis of Factors Related to Adolescents' Physical Activity Behavior Based on Multichannel LSTM Model

Computational Intelligence and Neuroscience

Received 25 July 2023; Accepted 25 July 2023; Published 26 July 2023

Copyright © 2023 Computational Intelligence and Neuroscience. This is an open access article distributed under the Creative Commons Attribution License, which permits unrestricted use, distribution, and reproduction in any medium, provided the original work is properly cited.

This article has been retracted by Hindawi following an investigation undertaken by the publisher [1]. This investigation has uncovered evidence of one or more of the following indicators of systematic manipulation of the publication process:

- (1) Discrepancies in scope
- (2) Discrepancies in the description of the research reported
- (3) Discrepancies between the availability of data and the research described
- (4) Inappropriate citations
- (5) Incoherent, meaningless and/or irrelevant content included in the article
- (6) Peer-review manipulation

The presence of these indicators undermines our confidence in the integrity of the article's content and we cannot, therefore, vouch for its reliability. Please note that this notice is intended solely to alert readers that the content of this article is unreliable. We have not investigated whether authors were aware of or involved in the systematic manipulation of the publication process.

Wiley and Hindawi regrets that the usual quality checks did not identify these issues before publication and have since put additional measures in place to safeguard research integrity.

We wish to credit our own Research Integrity and Research Publishing teams and anonymous and named external researchers and research integrity experts for contributing to this investigation.

The corresponding author, as the representative of all authors, has been given the opportunity to register their agreement or disagreement to this retraction. We have kept a record of any response received.

References

- [1] G. Chang and J. Liu, "Analysis of Factors Related to Adolescents' Physical Activity Behavior Based on Multichannel LSTM Model," *Computational Intelligence and Neuroscience*, vol. 2022, Article ID 1022421, 8 pages, 2022.

Retraction

Retracted: Effects of the Ultrasound-Guided Stellate Ganglion Block on Hemodynamics, Stress Response, and Gastrointestinal Function in Postoperative Patients with Colorectal Cancer

Computational Intelligence and Neuroscience

Received 25 July 2023; Accepted 25 July 2023; Published 26 July 2023

Copyright © 2023 Computational Intelligence and Neuroscience. This is an open access article distributed under the Creative Commons Attribution License, which permits unrestricted use, distribution, and reproduction in any medium, provided the original work is properly cited.

This article has been retracted by Hindawi following an investigation undertaken by the publisher [1]. This investigation has uncovered evidence of one or more of the following indicators of systematic manipulation of the publication process:

- (1) Discrepancies in scope
- (2) Discrepancies in the description of the research reported
- (3) Discrepancies between the availability of data and the research described
- (4) Inappropriate citations
- (5) Incoherent, meaningless and/or irrelevant content included in the article
- (6) Peer-review manipulation

The presence of these indicators undermines our confidence in the integrity of the article's content and we cannot, therefore, vouch for its reliability. Please note that this notice is intended solely to alert readers that the content of this article is unreliable. We have not investigated whether authors were aware of or involved in the systematic manipulation of the publication process.

In addition, our investigation has also shown that one or more of the following human-subject reporting requirements has not been met in this article: ethical approval by an Institutional Review Board (IRB) committee or equivalent, patient/participant consent to participate, and/or agreement to publish patient/participant details (where relevant).

Wiley and Hindawi regrets that the usual quality checks did not identify these issues before publication and have since put additional measures in place to safeguard research integrity.

We wish to credit our own Research Integrity and Research Publishing teams and anonymous and named external researchers and research integrity experts for contributing to this investigation.

The corresponding author, as the representative of all authors, has been given the opportunity to register their agreement or disagreement to this retraction. We have kept a record of any response received.

References

- [1] A. Xie, X. Zhang, F. Ju, W. Li, Y. Zhou, and D. Wu, "Effects of the Ultrasound-Guided Stellate Ganglion Block on Hemodynamics, Stress Response, and Gastrointestinal Function in Postoperative Patients with Colorectal Cancer," *Computational Intelligence and Neuroscience*, vol. 2022, Article ID 2056969, 7 pages, 2022.

Retraction

Retracted: Meta-Analysis of Knee Joint Function Recovery after Anterior Cruciate Ligament Reconstruction by Accelerated Rehabilitation Surgery

Computational Intelligence and Neuroscience

Received 25 July 2023; Accepted 25 July 2023; Published 26 July 2023

Copyright © 2023 Computational Intelligence and Neuroscience. This is an open access article distributed under the Creative Commons Attribution License, which permits unrestricted use, distribution, and reproduction in any medium, provided the original work is properly cited.

This article has been retracted by Hindawi following an investigation undertaken by the publisher [1]. This investigation has uncovered evidence of one or more of the following indicators of systematic manipulation of the publication process:

- (1) Discrepancies in scope
- (2) Discrepancies in the description of the research reported
- (3) Discrepancies between the availability of data and the research described
- (4) Inappropriate citations
- (5) Incoherent, meaningless and/or irrelevant content included in the article
- (6) Peer-review manipulation

The presence of these indicators undermines our confidence in the integrity of the article's content and we cannot, therefore, vouch for its reliability. Please note that this notice is intended solely to alert readers that the content of this article is unreliable. We have not investigated whether authors were aware of or involved in the systematic manipulation of the publication process.

Wiley and Hindawi regrets that the usual quality checks did not identify these issues before publication and have since put additional measures in place to safeguard research integrity.

We wish to credit our own Research Integrity and Research Publishing teams and anonymous and named external researchers and research integrity experts for contributing to this investigation.

The corresponding author, as the representative of all authors, has been given the opportunity to register their agreement or disagreement to this retraction. We have kept a record of any response received.

References

- [1] J. Xu, M. Zheng, Z. Feng, L. Pan, and Z. Peng, "Meta-Analysis of Knee Joint Function Recovery after Anterior Cruciate Ligament Reconstruction by Accelerated Rehabilitation Surgery," *Computational Intelligence and Neuroscience*, vol. 2022, Article ID 5085143, 8 pages, 2022.

Retraction

Retracted: Correlation between Sputum Bacterial Culture Positive Rate and Drug Sensitivity Test Results and Disease Severity in Inpatients and Its Clinical Significance: A Systematic Review and Meta-Analysis

Computational Intelligence and Neuroscience

Received 25 July 2023; Accepted 25 July 2023; Published 26 July 2023

Copyright © 2023 Computational Intelligence and Neuroscience. This is an open access article distributed under the Creative Commons Attribution License, which permits unrestricted use, distribution, and reproduction in any medium, provided the original work is properly cited.

This article has been retracted by Hindawi following an investigation undertaken by the publisher [1]. This investigation has uncovered evidence of one or more of the following indicators of systematic manipulation of the publication process:

- (1) Discrepancies in scope
- (2) Discrepancies in the description of the research reported
- (3) Discrepancies between the availability of data and the research described
- (4) Inappropriate citations
- (5) Incoherent, meaningless and/or irrelevant content included in the article
- (6) Peer-review manipulation

The presence of these indicators undermines our confidence in the integrity of the article's content and we cannot, therefore, vouch for its reliability. Please note that this notice is intended solely to alert readers that the content of this article is unreliable. We have not investigated whether authors were aware of or involved in the systematic manipulation of the publication process.

In addition, our investigation has also shown that one or more of the following human-subject reporting requirements has not been met in this article: ethical approval by an Institutional Review Board (IRB) committee or equivalent, patient/participant consent to participate, and/or agreement to publish patient/participant details (where relevant).

Wiley and Hindawi regrets that the usual quality checks did not identify these issues before publication and have since put additional measures in place to safeguard research integrity.

We wish to credit our own Research Integrity and Research Publishing teams and anonymous and named external researchers and research integrity experts for contributing to this investigation.

The corresponding author, as the representative of all authors, has been given the opportunity to register their agreement or disagreement to this retraction. We have kept a record of any response received.

References

- [1] W. Zhou and J. Li, "Correlation between Sputum Bacterial Culture Positive Rate and Drug Sensitivity Test Results and Disease Severity in Inpatients and Its Clinical Significance: A Systematic Review and Meta-Analysis," *Computational Intelligence and Neuroscience*, vol. 2022, Article ID 5102100, 9 pages, 2022.

Retraction

Retracted: Correlation between Pain Scores and Disc Height Changes after Discectomy in Patients with Lumbar Disc Herniation: A Systematic Review and Meta-Analysis

Computational Intelligence and Neuroscience

Received 25 July 2023; Accepted 25 July 2023; Published 26 July 2023

Copyright © 2023 Computational Intelligence and Neuroscience. This is an open access article distributed under the Creative Commons Attribution License, which permits unrestricted use, distribution, and reproduction in any medium, provided the original work is properly cited.

This article has been retracted by Hindawi following an investigation undertaken by the publisher [1]. This investigation has uncovered evidence of one or more of the following indicators of systematic manipulation of the publication process:

- (1) Discrepancies in scope
- (2) Discrepancies in the description of the research reported
- (3) Discrepancies between the availability of data and the research described
- (4) Inappropriate citations
- (5) Incoherent, meaningless and/or irrelevant content included in the article
- (6) Peer-review manipulation

The presence of these indicators undermines our confidence in the integrity of the article's content and we cannot, therefore, vouch for its reliability. Please note that this notice is intended solely to alert readers that the content of this article is unreliable. We have not investigated whether authors were aware of or involved in the systematic manipulation of the publication process.

Wiley and Hindawi regrets that the usual quality checks did not identify these issues before publication and have since put additional measures in place to safeguard research integrity.

We wish to credit our own Research Integrity and Research Publishing teams and anonymous and named external researchers and research integrity experts for contributing to this investigation.

The corresponding author, as the representative of all authors, has been given the opportunity to register their agreement or disagreement to this retraction. We have kept a record of any response received.

References

- [1] Y. Zheng, T. Lan, X. Chen, Z. Hus, and R. Zhang, "Correlation between Pain Scores and Disc Height Changes after Discectomy in Patients with Lumbar Disc Herniation: A Systematic Review and Meta-Analysis," *Computational Intelligence and Neuroscience*, vol. 2022, Article ID 2580004, 9 pages, 2022.

Research Article

A Soft Label Method for Medical Image Segmentation with Multirater Annotations

Jichang Zhang , Yuanjie Zheng , and Yunfeng Shi 

School of Information Science & Engineering, Shandong Normal University, No. 1 Daxue Road, Changqing District, Jinan 250358, China

Correspondence should be addressed to Yuanjie Zheng; yjzheng@sdnu.edu.cn and Yunfeng Shi; yunfeng@sdnu.edu.cn

Received 22 June 2022; Revised 4 October 2022; Accepted 6 October 2022; Published 18 February 2023

Academic Editor: Changming Sun

Copyright © 2023 Jichang Zhang et al. This is an open access article distributed under the Creative Commons Attribution License, which permits unrestricted use, distribution, and reproduction in any medium, provided the original work is properly cited.

In medical image analysis, collecting multiple annotations from different clinical raters is a typical practice to mitigate possible diagnostic errors. For such multirater labels' learning problems, in addition to majority voting, it is a common practice to use soft labels in the form of full-probability distributions obtained by averaging raters as ground truth to train the model, which benefits from uncertainty contained in soft labels. However, the potential information contained in soft labels is rarely studied, which may be the key to improving the performance of medical image segmentation with multirater annotations. In this work, we aim to improve soft label methods by leveraging interpretable information from multiraters. Considering that mis-segmentation occurs in areas with weak supervision of annotations and high difficulty of images, we propose to reduce the reliance on local uncertain soft labels and increase the focus on image features. Therefore, we introduce local self-ensembling learning with consistency regularization, forcing the model to concentrate more on features rather than annotations, especially in regions with high uncertainty measured by the pixelwise interclass variance. Furthermore, we utilize a label smoothing technique to flatten each rater's annotation, alleviating overconfidence of structural edges in annotations. Without introducing additional parameters, our method improves the accuracy of the soft label baseline by 4.2% and 2.7% on a synthetic dataset and a fundus dataset, respectively. In addition, quantitative comparisons show that our method consistently outperforms existing multirater strategies as well as state-of-the-art methods. This work provides a simple yet effective solution for the widespread multirater label segmentation problems in clinical diagnosis.

1. Introduction

Recently, deep learning techniques have made impressive progress on image segmentation tasks and have become a popular choice in the computer vision community [1]. Typically, supervised learning in deep learning is based on the assumption that there is a ground truth (GT). However, the truth is a lie; that is, there is often a lack of human consensus on the category of an object [2–4]. Especially, in medical image segmentation, which is based on knowledge and experience, disagreements between raters are fairly common [5, 6]. Inter-rater variability, as frequently reported by relevant research in the clinical field, usually leads to difficulties in segmenting areas of high uncertainty [7, 8].

To mitigate this inter-rater variability, the most basic yet common approach is the majority voting approach, in which

opinions agreed by a majority of raters are taken as true. However, the majority voting approach essentially discards the rich information contained in the multirater labels through one-hot operation (e.g., the probability distribution [0.6, 0.3, and 0.1] is transformed into a hard label [1, 0, and 0]). To combat this issue, soft-label methods that average rater annotations have been intensively investigated [9, 10]. Furthermore, Islam and Glocker [11] introduced a label smoothing method that incorporates fuzzy information about edges into multirater soft labels, called spatially varied label smoothing (SVLS).

However, when we applied the soft labels method to the multirater optic cup (OC) and optic disc (OD) segmentation of the fundus image task, finding that the areas where segmentation errors occur coincides with the highly divergent areas to some extent, see Figure 1. As demonstrated

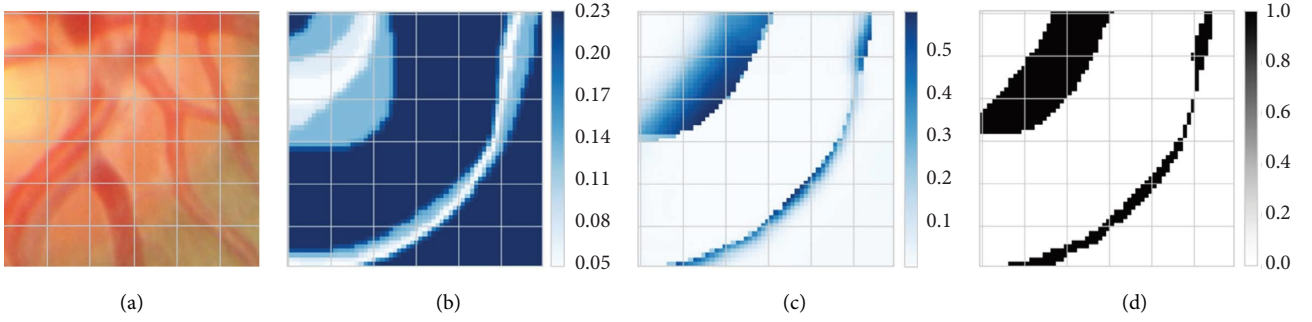


FIGURE 1: (a) Local visualization of an exemplary fundus image; (b) interclass variance map of annotations from six raters for OC and OD segmentation; (c) corresponding loss map of prediction; (d) corresponding error rates' map of prediction.

In Figure 2, the pixelwise loss and error rates of predictions are statistically positively correlated with the interclass variance which indicates the divergence between raters. We tentatively attempt to explain this phenomenon as follows:

- (i) An explanation is that the divergence area is highly uncertain, and the higher the uncertainty of the label, the lower the penalty imposed on the predicted distribution [12]. Highly uncertain annotations make it difficult to impose strong and precise constraints on the model, which is similar to weakly supervised learning that lacks accurate annotations [13]. The dependence on annotations in weakly supervised learning is weakened and replaced by a focus on features [14].
- (ii) Furthermore, we provide an intuitive interpretation that is more consistent with the multirater labels segmentation task: uncertainty reflects pixelwise image difficulty, where areas with high difficulty are more challenging for the model to accurately segment. Image difficulty, which is related to the visual characteristics of the images, such as image quality and occlusion of the area of the lesions, is one of the causal factors of inter-rater variability [15]. As demonstrated in Figure 1(a), the blood vessels occluding the edge region of the OD not only make ophthalmologists' judgment difficult but also hinder the accurate prediction of the deep neural network. In contrast to existing methods [16, 17] that treat difficulty as image level, we innovatively consider difficulty to be pixelwise for segmentation tasks.

In conclusion, the regions with high inter-rater variability have more difficult features but only weaker supervision, which could be a cause of mis-segmentation. In this work, we aim to improve the performance level of the soft label approach on multirater labels' segmentation task based on the previously mentioned explanations. A way to get the best of both sides is to increase the focus on image features while reducing the reliance on highly uncertain annotations. Consequently, we propose a supervised segmentation network that is constrained by consistency regularization. Specifically, consistency regularization exploits the augmentation invariance of images to optimize the feature space while avoiding relying simply on labels and compensating

for the disadvantage of unreliable local annotations. The uncertainty as the prior knowledge is formulated as the soft labels' interclass variance, which drives the proposed model's local difference training. In addition, the SVLS approach, which incorporates edge fuzziness into soft labels, is used to soften average expert labels.

Experiments are performed on a synthetic dataset with great disagreement as well as a real-world dataset. In these experiments, our method consistently outperforms existing multirater strategies and state-of-the-art (SOTA) methods. To verify the generalization of the proposed method, we additionally conduct generalization experiments on two other types of datasets.

In summary, the main contributions of this study are as follows:

- (1) To embed consistency/inconsistency of multirater into the model, the soft labels obtained by averaging softened annotations of raters are used as GT.
- (2) We provide thinking that disagreement among multiple raters, i.e., uncertainty, can be quantified from soft labels and used as prior knowledge to reflect the pixel-level difficulty of an image.
- (3) We propose to use consistency regularization to improve the model's attention to features and reduce dependence on GT, especially in regions of high uncertainty. Without introducing additional parameters, the accuracy of our method is improved over that of other methods on synthetic and real-world datasets.

2. Related Works

The problem of multirater labels' segmentation caused by inter-rater variability has started to pique the interest of researchers. There is a study showing that the observed labels depend on three causal factors: the true label, the expertise of the rater, and the image difficulty [16]. For the method of obtaining the true label, it is a common practice to use majority voting [18] and STAPLE [19] or other label fusion strategies to obtain the ground-truth labels [11, 20] so that they can be adapted to the general segmentation model. However, simple label fusion methods neither do take advantage of any image features nor do they carry the inter-

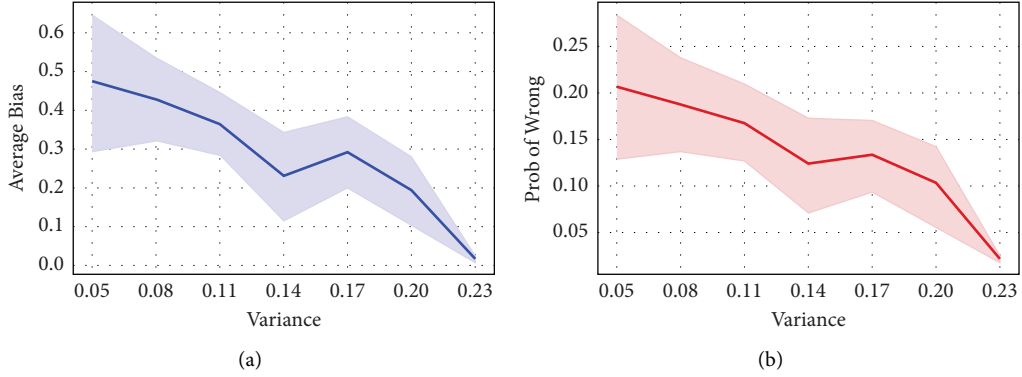


FIGURE 2: (a) Line graph of pixelwise interclass variances versus pixelwise loss; (b) line graph of pixelwise interclass variances versus pixelwise probability of misprediction. The abovementioned statistics are averaged on the validation set.

rater variability through to the model. Recently, several efforts have started to explore the expertise of the rater using label sampling strategies [21] or rater modeling strategies [22]. For instance, Zhang et al. [23] proposed to use confusion matrices to the model preference of annotators, obtaining segmentation prediction with the least noise by optimizing two coupled convolutional neural networks (CNNs). Yu et al. [15] proposed a multibranch model for the multirater glaucoma classification task, encouraging the specificity branch and the sensitivity branch to generate consistent/opposing predictions for consensus/disagreement samples. Ji et al. [24] proposed MRNet, which embeds the expertise of individual annotators into the model to generate calibrated predictions under different expertise levels for medical image segmentation.

However, there still lacks effective research on the image difficulty represented by image features in the multirater label segmentation task. Furthermore, we consider that multirater labels' segmentation is weakly supervised learning with inaccurate labels, which has not been explored before. Although our approach is uncertainty-driven, unlike works, such as Monte Carlo dropout [25] and ensembles [26, 27], that evaluate uncertainty and produce multiple segmentation hypotheses, our work aims to learn a deterministic single-output deep model.

3. Methodology

The main architecture of our model is illustrated in Figure 3, which is composed of three main parts: (a) segmentation network with consistency regularization for conveying more information about the input; (b) asymmetrical regularization part for generating uncertainty mask to realize local self-ensembling in supervised learning; (c) multirater labels fusion part for obtaining a soft label for each input as the supervised target containing uncertainty. In the test and application phase, just the trained network is required to predict the segmentation of the input image.

3.1. Problem Definition. In this article, we consider the problem of learning a segmentation model from labels annotated by multiple human raters. Given the images

$\{X^{W \times H \times L} = x_n\}_{n=1}^N$ and the corresponding one-hot labels $\{Y^{W \times H \times C} = y_n^{(r)}\}_{n=1, \dots, N}^{r=1, \dots, R}$ (W, H, L, C denote the width, height, channels, and classes), where N is the number of samples and R is the number of raters, each image is independently annotated by raters based on their personal experiences. The objective of the multirater label segmentation task is to learn the projection function $F(\cdot)$, mapping the input image x_n to the estimated prediction \hat{y}_n which is one-hot form encoded by the full probability distribution \hat{p}_n . In our article, \hat{p}_n is encouraged to be as similar as p_n , which is the soft label fused by Y_n .

3.2. Soft Labels. Recently, increasing studies have proposed training a model using soft labels for accounting for the high uncertainty in lesion or structure borders' delineation [11, 28–31]. Averaging multirater labels is an intuitive way to obtain soft labels in multirater annotation tasks as follows:

$$p_n = \frac{1}{R} \sum_{r=1}^R y_n^{(r)}. \quad (1)$$

Although the average strategy incorporates uncertainty from inter-rater variability into soft labels, it indulges the overconfidence of each rater. Therefore, we soften each hard label by SVLS and then average them to obtain p^n which contains spatial and inter-rater uncertainty as follows:

$$p_n^{(i,j)} = \frac{1}{R} \sum_{r=1}^R \frac{1}{\sum w} \sum_{a=1}^3 \sum_{b=1}^3 y_n^{r(i-a, j-b)} w^{(a,b)}, \quad (2)$$

where (i, j) is the position of pixel and w is a weight matrix which is obtained by $1/\sqrt{2\pi\sigma^2}e^{-|\vec{x}|^2/2\sigma^2}$ with $\sigma = 1$. SVLS determines the probability of the target pixel based on its neighboring pixels, achieved by a Gaussian-like weight matrix that is applied across the one-hot encoded rater labels $y^{(r)}$ to obtain a soft probability distribution.

The transmission of uncertainty information into the model is inseparable from the appropriate loss function. There is the performance of several common loss functions in Section 4.4, including soft cross-entropy loss, soft dice

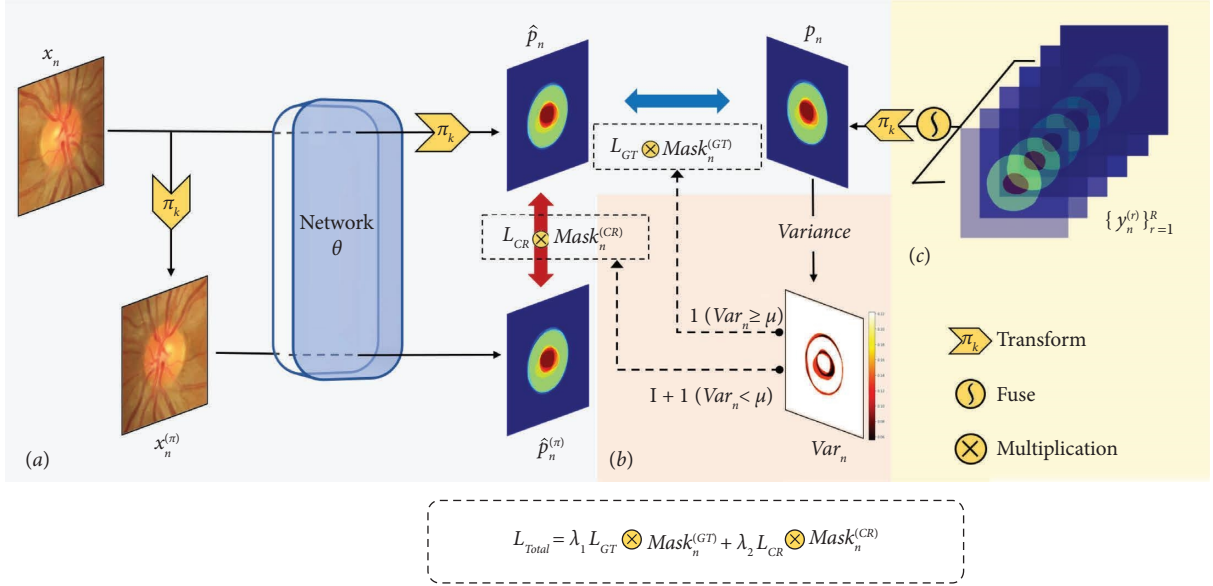


FIGURE 3: The architecture of our model consists of three parts: (a) segmentation network part; (b) asymmetrical regularization part; (c) multirater labels' fusion part.

loss, and soft focal loss. By comparison, the soft cross-entropy loss is selected as the optimization objective, encouraging the probability distribution of prediction \hat{p}_n to be identical to that of the soft label as follows:

$$\mathcal{L}_{GT} = - \sum_{n=1}^N p_n \log(\hat{p}_n). \quad (3)$$

3.3. Label Uncertainty Measure. It is equally crucial to model uncertainty at the pixel-level as to improve the model's performance, particularly in medical scenarios [25]. Unlike work that uses stochastic networks [32, 33] to model uncertainty, we improve multirater models using uncertainty as a source of prior knowledge. Specifically, we consider the pixelwise interclass variance $\{\text{Var}_n^{W \times H}\}_{n=1, \dots, N}$ that reflects the uncertainty caused by inter-rater variability and spatial variation. It is inversely proportional to entropy, meaning that the lower the variance, the greater the entropy and, hence, the greater the uncertainty. The appropriate uncertainty can enhance the generalization and calibration of the model. However, the high uncertainty would be detrimental to the model as noise. In the position of the $(i, j)^{th}$ pixel, the variance between classes $\text{Var}(p_n^{(i,j)})$ can be formulated by the following:

$$\text{Var}(p_n^{(i,j)}) = \frac{1}{C} \sum_{c=0}^{C-1} \left(p_n^{(i,j)}(c) - \frac{1}{C} \right)^2, \quad (4)$$

where $\sum_{c=0}^{C-1} p_n^{(i,j)}(c) = 1$. We propose to use uncertainty as a threshold to assign different optimization objectives to different areas of the image. Specifically, the labels of areas with high uncertainty are no longer decisive but are replaced with constraints on the feature space, which will be clarified in the next section. In areas with high rater agreement, soft labels and feature constraints work together to optimize the model. For convenience, we refer to this uncertainty-driven

local differential optimization as asymmetrical regularization. The threshold comes into play in the form of a mask of 0-1, acting directly on the loss function. Mask is differentiated into $\text{mask}_n^{(GT)}$ and $\text{mask}_n^{(CR)}$ based on the threshold, which correspond to areas of low and high uncertainty, respectively, as follows:

$$\begin{aligned} \text{mask}_n^{(GT)} &= \mathbb{1}(\text{Var}_n \geq \mu), \\ \text{mask}_n^{(CR)} &= \mathbf{I} + \mathbb{1}(\text{Var}_n < \mu), \end{aligned} \quad (5)$$

where $\mathbb{1}$ is the indicator function and \mathbf{I} is the identity matrix with the same shape as Var_n .

3.4. Consistency Regularization. To improve attention to features and optimize feature space, we propose using consistency regularization as an extra constraint on the model, which has been utilized in semisupervised learning [34] and unsupervised learning [35]. Consistency regularization is a type of self-ensemble learning because it only relies on the images themselves to learn. Inspired by Li et al. [34], we apply rotation consistency to this work. Specifically, there is a problem in the segmentation task using CNN: when the inputs of CNN are rotated, the corresponding network predictions would not be rotated in the same way [36] as follows:

$$\theta(\pi_k x_n) \neq \pi_k \theta(x_n), \quad (6)$$

where π_k is a rotation to the image (i.e., horizontal, vertical, or mixed flip) and θ is the parameters of the network. The feature space is automatically optimized when the model is encouraged to make the same judgments about elements before and after rotation. In this article, we use the soft cross-entropy loss function as the optimization target of rotation consistency regularization term:

$$\mathcal{L}_{CR} = - \sum_{n=1}^N \theta(\pi_k x_n) \log(\pi_k \theta(x_n)). \quad (7)$$

When formulas (3) and (7) are combined, the total loss function is as follows:

$$\mathcal{L}_{total} = -\lambda_1 \sum_{n=1}^N p_n \log(\hat{p}_n) - \lambda_2 \sum_{n=1}^N \theta(\pi_k x_n) \log(\pi_k \hat{p}_n), \quad (8)$$

where $\lambda_1 + \lambda_2 = 1$. By minimizing the loss function, the network is urged to focus more on the image content than on the regression of GT alone [37]. So far, image features can be fully expressed through self-ensembling. In regions of divergence where uncertainty is high, supervision of labels is entirely replaced by unsupervised self-ensembling. Without introducing extra parameters and structures, asymmetrical regularization is achieved by covering the soft label with an uncertainty-based mask (formulas (5) and (7)). Finally, updated formula (8) is shown as follows:

$$\mathcal{L}_{total} = -\lambda_1 \text{mask}_n^{(GT)} \sum_{n=1}^N p_n \log(\hat{p}_n) + -\lambda_2 \text{mask}_n^{(CR)} \sum_{n=1}^N \theta(\pi_k x_n) \log(\pi_k \hat{p}_n). \quad (9)$$

4. Experiments

In this section, we introduce the experimental dataset, implementation details, and evaluation metrics. In order to explore the best performance under different combinations of the loss and uncertainty threshold value, we conduct quantitative experiments with different setups on the MNIST and the RIGA validation set in Section 4.4. For comparison with other methods, the common label fusion approach and other SOTA approaches for multirater labels segmentation are used as the benchmark. The results are listed in Section 4.5, showing that our method can exploit the uncertainty of multirater annotations to improve segmentation performance. Additionally, ablation experiments are conducted to evaluate the efficacy of each component of our method.

4.1. Datasets

- (i) MNIST is a handwritten digits dataset with 60,000 training and 10,000 test examples. All images are 28×28 grayscale versions of the handwritten numbers 0–9. Zhang et al. [23] synthesized a dedicated dataset of multirater annotation tasks based on MNIST, which simulates raters with different biases to obtain multiple labels by using Morpho-MNIST software [38]. Specifically, the first rater provides good segmentation with approximate GT, the second rater tends to oversegment, the third rater tends to undersegmentation, the fourth rater is prone to the combination of small fractures and oversegmentation, and the fifth rater always annotates everything as the background. We train a model using all five raters' annotations and finally test the model performance on GT.
- (ii) RIGA is a publicly available dataset for joint OC and OD segmentation from the University of Michigan [39]. It includes a total of 750 color fundus images from three subsets: 460 images from MESSIDOR, 195 images from BinRushed, and 95 images from Magrabia. Each fundus image has six OC and OD

annotations carried out by six ophthalmologists. We select BinRushed and MESSIDOR as the training set, and Magrabia is selected as the test set, where all images are resized to 256×256 . In accordance with the experimental design of MRNet [24] and other methods [11, 23], the majority voting of six raters for each test image is used as the silver standard to evaluate the prediction.

- (iii) QUBIQ-Kidney and Prostate are subdatasets of Quantification of Uncertainties in Biomedical Image Quantification Challenge (QUBIQ) [40], which are specifically designed to evaluate inter-rater variability. The QUBIQ-Kidney images are 2D CT slices (20 cases for training and 4 cases for testing) in which the kidneys are manually annotated by three raters. The QUBIQ-Prostate images are 2D MRI slices (48 cases for training and 7 cases for testing) in which the prostate is manually annotated by six raters. To match the task objective of the QUBIQ challenge, GT and prediction are binarized at five probability levels (0.1, 0.3, 0.5, 0.7, and 0.9), and evaluation scores for all thresholds will be averaged.

4.2. Implementation Details. For a fair comparison, we employ the same network architecture as the baseline approach. Specifically, for the MNIST experiment, we use the U-Net architecture without pretraining as [23]. Moreover, for the RIGA experiment, the main framework utilizes the U-Net architecture with ResNet34 as the backbone. Parameters of the U-Net encoder are initialized with the pretrained model on ImageNet [41]. The abovementioned network is implemented with the PyTorch platform and trained/tested on a Tesla V100 GPU with 32 GB of memory. The proposed network is trained end-to-end using the Adam optimizer [42], and it takes about 4 hours to train our model with a mini-batch size of 4 for 60 epochs. The learning rate is set to 1×10^{-4} .

4.3. Evaluation Metrics. Various evaluation metrics, including the Dice similarity coefficient (DSC) and mean intersection over union (mIoU), were utilized to evaluate the performance of the proposed method for segmenting OC and OD relative to GT. These performance metrics are defined as follows:

$$\begin{aligned} \text{DSC}(\mathcal{D}) &= \frac{2 \times TP}{2 \times TP + FP + FN}, \\ \text{mIoU}(\mathcal{J}) &= \frac{TP}{FP + FN + TP}, \end{aligned} \quad (10)$$

where TP, FP, FN, and TN represent true positives, false positives, false negatives, and true negatives, respectively, in the evaluation confusion matrix. Note that a model with higher metric values can predict more precise segmentation masks. All experimental results are reported as the average of the ten experiments conducted on the test set.

4.4. Performance of Our Methods. Here, we provide a quantitative comparison among different loss functions including soft cross-entropy loss (CE), soft dice loss (DL), and soft focal loss [43] (FL). Table 1 displays the top five combinations of loss functions with the highest \mathcal{D} under the corresponding optimal hyperparameter settings, including the uncertainty threshold μ and the unsupervised loss weight λ_2 , where experiments are performed on the MNIST validation set. The proposed method exhibits the best performance when both the supervision loss and the consistency regularization loss are CE. In Figure 4, we further present the comparison of model accuracy at different μ and λ_2 settings under this loss function combination on the MNIST and RIGA validation set. Moreover, the average unsupervised proportion corresponding to different μ in the two datasets is performed in Figure 4. By comparison, the optimal (μ, λ_2) combinations on the MNIST and RIGA datasets are (0.5, 0.005) and (0.5, 0.002), respectively, with corresponding unsupervised proportions of 8% and 4%.

4.5. Comparisons with Other Methods. To demonstrate the advantage of the proposed method, we compare our method to the SOTA methods on the MNIST and RIGA datasets. We use the publicly released code with default parameters to retrain the SOTA methods with the same training/test set as ours for a fair comparison.

Table 2 quantitatively compares our framework to three hard label methods, five soft label methods, and other SOTA multirater labels' segmentation methods, including (a) Mode-UNet: UNet trained using a single label randomly selected; (b) MV-UNet: UNet trained using one-hot labels obtained by majority voting; (c) STAPLE-UNet: UNet trained using one-hot labels obtained by STAPLE [19]; (d) Average-UNet: UNet trained using soft labels obtained by average raters [31]; (e) GLS-UNet: UNet trained using soft labels smoothed by general label smoothing [44]; (f) Sharpen-UNet: UNet trained using soft labels smoothed by label sharpen [45] under temperature (T)=0.5 or 1.5; (g)

TABLE 1: The segmentation performance (mean \pm standard deviation) of different combinations of loss functions: supervised loss + consistency regularization loss.

Loss	μ	λ_2	Performance $\mathcal{D} \pm \text{std} (\%)$
CE and CE	0.005	0.5	94.09 \pm 0.51
CE and DL	0.005	0.5	93.55 \pm 0.78
DL and DL	0.005	0.1	92.39 \pm 1.09
DL and CE	0.005	0.1	91.15 \pm 1.16
FL and FL	0.005	0.5	89.91 \pm 0.59

Mixup-UNet: UNet trained using soft labels smoothed by Mixup; (h) SVLS-UNet: UNet trained using soft labels smoothed by SVLS [11]; (i) LNL [23]; (j) MRNet [24] on the MNIST and RIGA test sets.

As shown in Table 2, our proposed method consistently achieves superior performance compared with other methods. For value \mathcal{D} , our method outperforms the SOTA method by 1.13% on the synthetic MNIST dataset. Figure 5 shows the visualization results, wherein our method recovers the most realistic result from several annotations containing obvious human errors. Additionally, compared to the suboptimal MRNet method, the segmentation results predicted by the proposed method are smoother and more structured at the edge. For the real-world dataset RIGA, the performance improvement is especially prominent for the retinal OC segmentation, where the inter-rater variability is more significant, with a 2.29% increase in \mathcal{D} value over the current best method (listed in Table 2).

Figure 6(a) visualizes five examples of the silver standard and the corresponding segmentation results predicted by six different methods. As shown in Figure 6(b), the edge of OC occluded by blood vessels in the area with high inter-rater divergence (indicated by arrows) and, similarly, the high-incidence area of misprediction (red areas) by other methods. Compared to other methods, the proposed method shows lower prediction errors in the aforementioned area, demonstrating the robustness of our method to difficult features.

4.6. Ablation Studies. In this section, ablation studies are performed on the RIGA dataset over each component of the proposed method, including label smoothing (LS), consistency regularization (CR), and asymmetrical regularization (AR), as listed in Table 3. Meanwhile, the effect of different label smoothing techniques including GLS and Sharpen and SVLS on the performance of our method is also explored. The baseline model is the UNet trained using soft labels of average raters. All experiments are performed with the same network structure and training hyperparameters, Sections 4.2 and 4.4. \mathcal{D}_{ave} represents the average value of \mathcal{D}_{OC} and \mathcal{D}_{OD} .

As shown in Table 3, the segmentation performance of the model reaches SOTA when all components are activated. As we sequentially remove the proposed components from the U-Net Baseline, the model performance degrades gradually. In particular, the inclusion of CR improved the

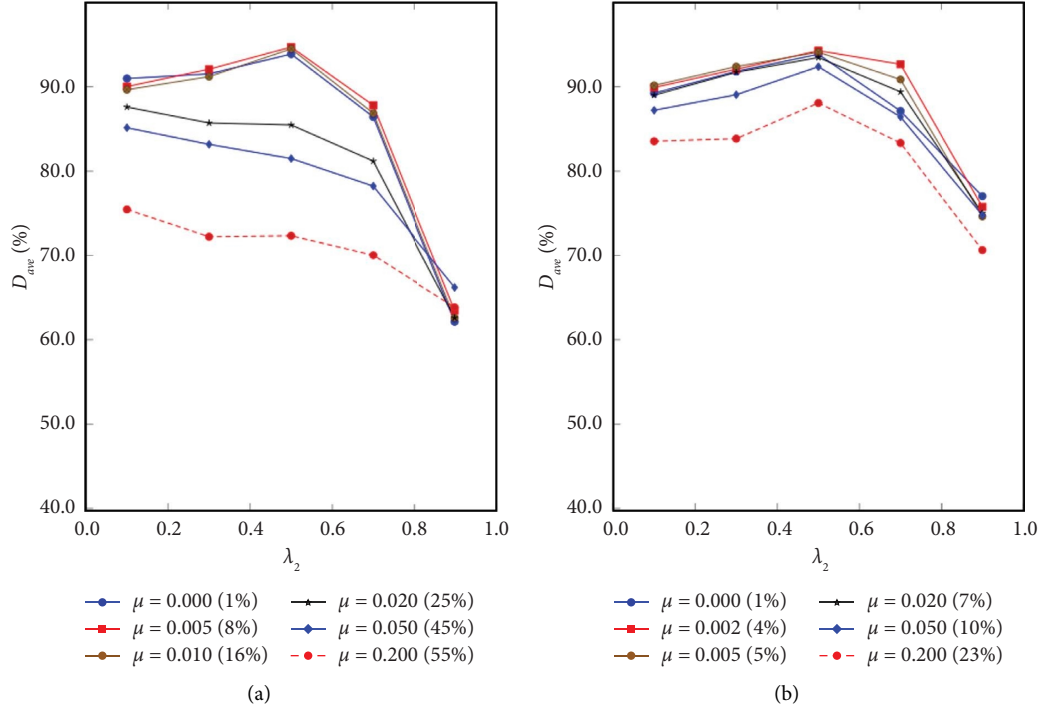
FIGURE 4: Segmentation accuracy under different μ and λ_2 on the (a) MNIST and (b) RIGA.

TABLE 2: Quantitative results with different strategies on the MNIST and RIGA test set.

Methods		MNIST		RIGA			
		\mathcal{D} (%)	\mathcal{F} (%)	\mathcal{D}_{OD} (%)	\mathcal{D}_{OC} (%)	\mathcal{F}_{OD} (%)	\mathcal{F}_{OC} (%)
Hard	Mode-UNet	62.89	57.30	96.90	82.41	94.62	75.09
	MV-UNet	89.14	80.59	97.03	84.92	94.35	73.47
	STAPLE-UNet	82.26	74.51	96.28	85.37	92.84	75.68
Soft	Average-UNet	90.54	82.85	97.04	85.40	94.52	76.58
	GLS-UNet	87.32	78.29	96.14	86.83	93.71	75.95
	Sharpen ^(T=0.5) -UNet	90.50	81.03	96.85	84.71	94.33	77.18
	Sharpen ^(T=1.5) -UNet	87.67	80.13	96.77	86.13	93.82	77.90
	Mixup-UNet	86.61	78.58	96.83	84.72	94.02	75.18
	SVLS-UNet	90.32	82.05	97.40	86.09	94.95	76.87
SOTA	LNL	84.52	76.33	97.67	87.56	95.46	78.76
	MRNet	93.63	88.09	97.60	86.54	95.78	78.19
	Ours	94.76	90.82	97.98	89.85	96.04	81.97

The best results are highlighted, and the second best results are italic.

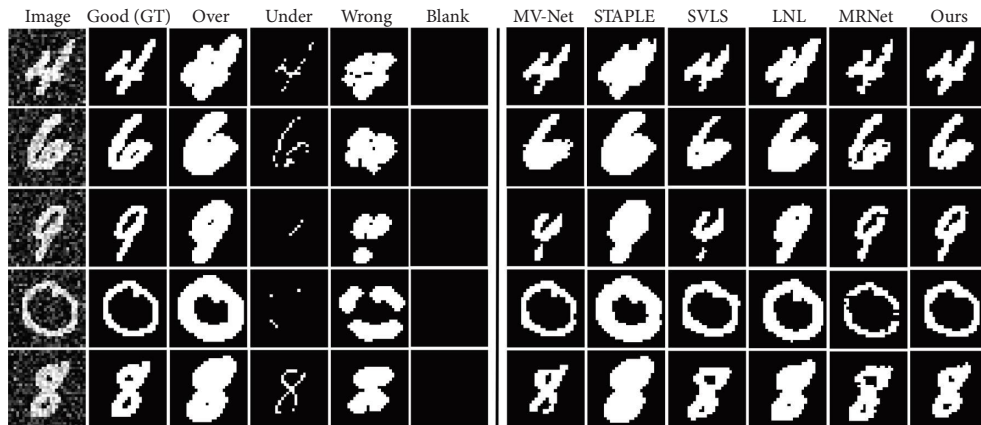


FIGURE 5: Visualization of five raters' annotations and predictions of six methods on the synthetic MNIST test set.

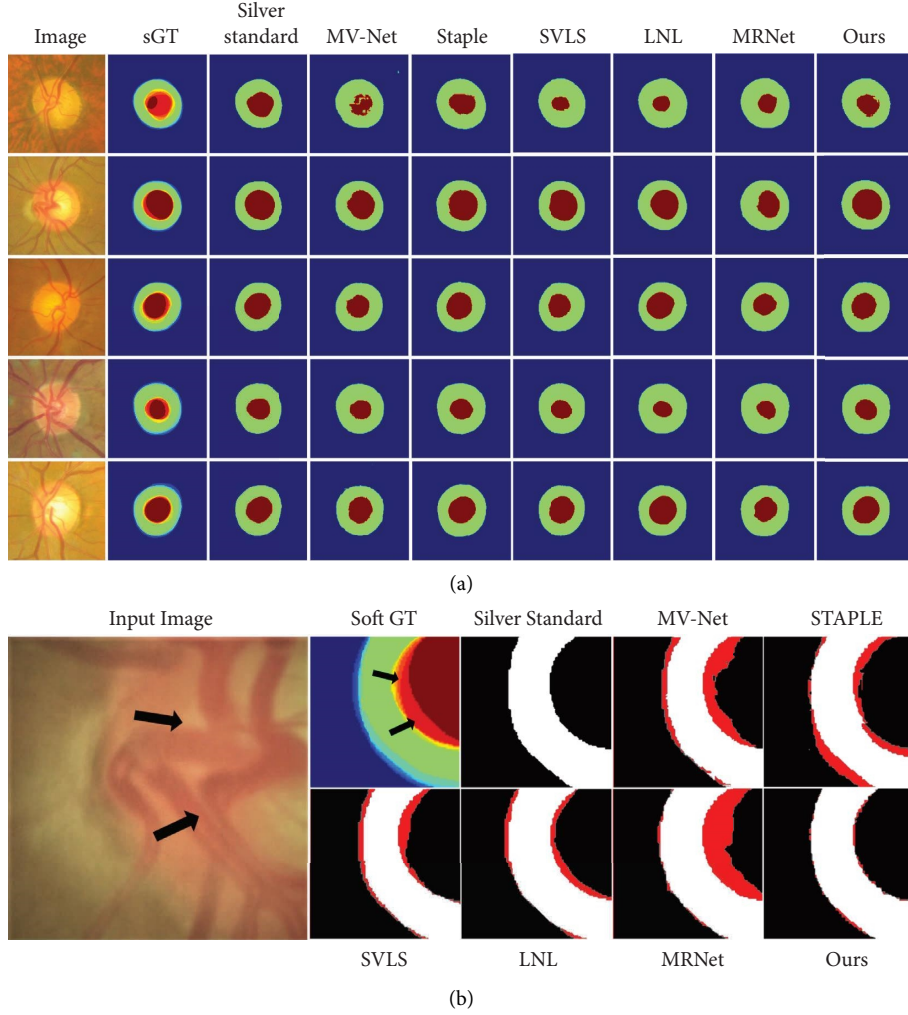


FIGURE 6: (a) Visualization of segmentation predictions on RIGA test set. (b) An example of a visualized partial map of predicted errors.

TABLE 3: Ablation experiment results on the RIGA dataset.

LS	Module		Performance $\mathcal{D}_{ave} \pm \text{std} (\%)$
	CR	AR	
SVLS	✓	✓	93.92 \pm 0.56
Sharpen ^(1.5)	✓	✓	93.55 \pm 0.73
GLS	✓	✓	93.49 \pm 0.63
SVLS	✓		93.36 \pm 0.71
Average	✓	✓	92.87 \pm 0.65
Average	✓		92.32 \pm 0.82
SVLS			91.74 \pm 0.78
Average			91.22 \pm 1.06

baseline by 1.10%. Then, the combination of CR and AR yielded an additional 0.55% improvement. This means that, in areas with higher rater inconsistency in annotations, the potential representation of image features is more reliable than in uncertain annotations. It is proved experimentally that features are also one of the important causes of observer variability rather than just the rater knowledge. In addition, adding SVLS alone improves \mathcal{D}_{ave} of baseline by 0.52% while utilizing it with CR and AR jointly improves \mathcal{D}_{ave} of the

proposed method without SVLS by 1.05%. It demonstrates that the positive effects of CR and AR are further strengthened under the threshold of uncertainty with SVLS.

4.7. Generalization Capability. To further verify the generalization capability of the proposed method, we additionally perform experiments on the kidney segmentation task of the QUBIQ multirater segmentation challenge. We use the same

TABLE 4: Quantitative results with different strategies on the QUBIQ-kidney and prostate test sets.

Methods	Kidney		Prostrate		#Parameters
	$\mathcal{D}^{(\text{soft})}$ (%)	$\mathcal{J}^{(\text{soft})}$ (%)	$\mathcal{D}^{(\text{soft})}$ (%)	$\mathcal{J}^{(\text{soft})}$ (%)	
MV-UNet	66.59	57.83	83.50	73.71	22.0M
STAPLE-UNet	65.01	56.31	83.36	73.69	22.0M
Average-UNet	69.33	58.21	85.82	77.02	22.0M
SVLS-UNet	70.04	58.65	86.11	77.38	22.0M
LNL	68.40	58.59	85.44	76.91	22.2M
MRNet	71.36	60.43	87.39	78.14	81.1M
Ours	70.25	59.08	87.67	78.55	22.0M

The best results are highlighted, and the second best results are italic.

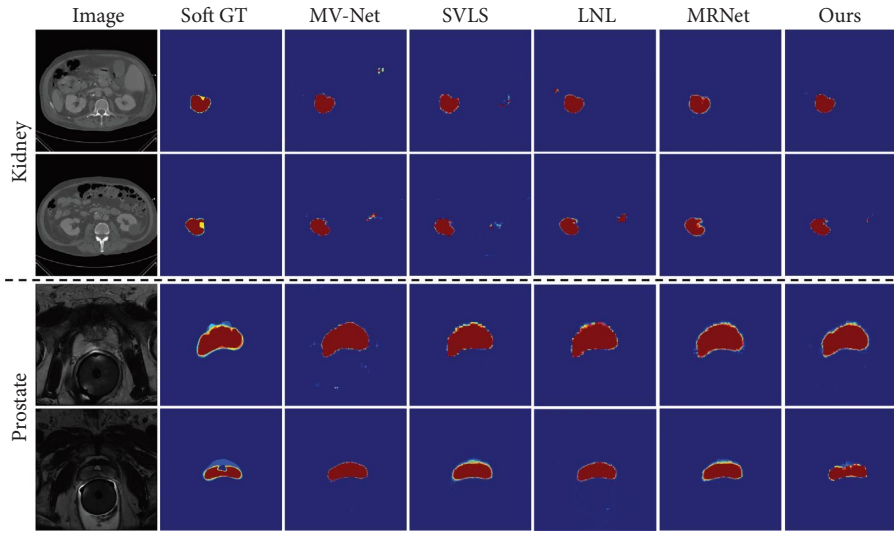


FIGURE 7: Visualization of segmentation predictions on the QUBIQ-kidney and prostate test sets.

multithreshold scores $\mathcal{D}^{(\text{soft})}$ and $\mathcal{J}^{(\text{soft})}$ as QUBIQ challenge, which can better evaluate the ability of the model to reflect potential inter-rater agreement/disagreement. Specifically, after the GT and prediction are binarized at multiple threshold levels (0.1, 0.3, 0.5, 0.7, and 0.9), the \mathcal{D} and \mathcal{J} metrics averaged across five thresholds are $\mathcal{D}^{(\text{soft})}$ and $\mathcal{J}^{(\text{soft})}$. As listed in Table 4, compared to the comparative methods, the proposed method achieves optimal performance on the QUBIQ-Prostate dataset and achieves sub-optimal performance on the QUBIQ-Kidney dataset. Furthermore, the advantage of a low number of parameters facilitates the application of our method to other multirater datasets. Several representative examples of the comparison methods for such two datasets are visualized in Figure 7.

5. Conclusion

In this article, we focus on the utilization of rich annotation information from multiple clinical raters, which are relatively less explored but widely presented in medical image segmentation. Based on the deep learning method using soft labels, we proposed a local self-ensembling learning model related to pixelwise variance with the intention of reducing the reliance upon uncertain local labels and optimizing the feature space. Our method achieves performance improvement over the soft labels' learning method without

requiring the introduction of extra parameters and structures. In addition, we incorporate structural uncertainty into soft labels via the label smoothing technique to further improve segmentation performance level. Empirical experiments demonstrated the overall superior performance of our method on a synthetic dataset and a real-world dataset. Our method provides a solution for automatically learning a reliable clinical-aided diagnosis system using multirater annotations.

Data Availability

The data used to support the findings of this study are available from the corresponding author upon request.

Conflicts of Interest

The authors declare that they have no conflicts of interest.

Acknowledgments

This work was supported by the National Natural Science Foundation of China (61773246 and 81871508), the Taishan Scholar Project of Shandong Province (TSHW201502038), and the Natural Science Foundation of Shandong Province (ZR2018ZB0419).

References

- [1] M. Mahmud, M. S. Kaiser, A. Hussain, and S. Vassanelli, "Applications of deep learning and reinforcement learning to biological data," *IEEE Transactions on Neural Networks and Learning Systems*, vol. 29, pp. 2063–2079, 2018.
- [2] G. Lakoff, *Women, Fire, and Dangerous Things: What Categories Reveal about the Mind*, University of Chicago Press, Chicago, IL, USA, 2008.
- [3] L. Aroyo and C. Welty, "Truth is a lie: crowd truth and the seven myths of human annotation," *AI Magazine*, vol. 36, no. 1, pp. 15–24, 2015.
- [4] K. Chen, L. Yao, D. Zhang, X. Wang, X. Chang, and F. Nie, "A semisupervised recurrent convolutional attention model for human activity recognition," *IEEE Transactions on Neural Networks and Learning Systems*, vol. 31, no. 5, pp. 1747–1756, 2020.
- [5] P. Brennan and A. Silman, "Statistical methods for assessing observer variability in clinical measures," *BMJ British Medical Journal*, vol. 304, no. 6840, pp. 1491–1494, 1992.
- [6] P. Bridge, A. Fielding, P. Rowntree, and A. Pullar, "Intra-observer variability: should we worry?" *Journal of Medical Imaging and Radiation Sciences*, vol. 47, no. 3, pp. 217–220, 2016.
- [7] L. Joskowicz, D. Cohen, N. Caplan, and J. Sosna, "Inter-observer variability of manual contour delineation of structures in CT," *European Radiology*, vol. 29, no. 3, pp. 1391–1399, 2019.
- [8] A. S. Becker, K. Chaitanya, K. Schawkat et al., "Variability of manual segmentation of the prostate in axial T2-weighted MRI: a multi-reader study," *European Journal of Radiology*, vol. 121, Article ID 108716, 2019.
- [9] J. C. Peterson, R. M. Battleday, T. L. Griffiths, and O. Russakovsky, "Human uncertainty makes classification more robust," in *Proceedings of the IEEE Conference on Computer Vision and Pattern Recognition*, pp. 9617–9626, Long Beach, CA, USA, August 2019.
- [10] T. Fornaciari, A. Uma, S. Paun, B. Plank, D. Hovy, and M. Poesio, "Beyond black & white: leveraging annotator disagreement via soft-label multi-task learning," in *Proceedings of the Conference of the North American Chapter of the Association for Computational Linguistics*, pp. 2591–2597, Mexico City, Mexico, June 2021.
- [11] M. Islam and B. Glocker, "Spatially varying label smoothing: capturing uncertainty from expert annotations," in *Proceedings of the Information Processing in Medical Imaging*, pp. 677–688, Springer, Berlin, Germany, June 2021.
- [12] D. Rolnick, A. Veit, S. Belongie, and N. Shavit, "Deep learning is robust to massive label noise," 2017, <https://arxiv.org/abs/1705.10694>.
- [13] Z.-H. Zhou, "A brief introduction to weakly supervised learning," *National Science Review*, vol. 5, no. 1, pp. 44–53, 2018.
- [14] M. Luo, X. Chang, L. Nie, Y. Yang, A. G. Hauptmann, and Q. Zheng, "An adaptive semisupervised feature analysis for video semantic recognition," *IEEE Transactions on Cybernetics*, vol. 48, no. 2, pp. 648–660, 2018.
- [15] S. Yu, H.-Y. Zhou, K. Ma et al., "Difficulty-aware glaucoma classification with multi-rater consensus modeling," in *Proceedings of the International Conference on Medical Image Computing and Computer-Assisted Intervention*, pp. 741–750, Springer, Berlin, Germany, October 2020.
- [16] J. Whitehill, T.-f. Wu, J. Bergsma, J. Movellan, and P. Ruolo, "Whose vote should count more: optimal integration of labels from labelers of unknown expertise," *Advances in Neural Information Processing Systems*, vol. 22, pp. 2035–2043, 2009.
- [17] R. Tudor Ionescu, B. Alexe, M. Leordeanu, M. Popescu, D. P. Papadopoulos, and V. Ferrari, "How hard can it be? Estimating the difficulty of visual search in an image," in *Proceedings of the IEEE Conference on Computer Vision and Pattern Recognition*, pp. 2157–2166, Las Vegas, NV, USA, June 2016.
- [18] J. E. Iglesias and M. R. Sabuncu, "Multi-atlas segmentation of biomedical images: a survey," *Medical Image Analysis*, vol. 24, no. 1, pp. 205–219, 2015.
- [19] S. K. Warfield, K. H. Zou, and W. M. Wells, "Simultaneous truth and performance level estimation (STAPLE): an algorithm for the validation of image segmentation," *IEEE Transactions on Medical Imaging*, vol. 23, no. 7, pp. 903–921, 2004.
- [20] Q. Liu, Q. Dou, L. Yu, and P. A. Heng, "MS-Net: multi-site network for improving prostate segmentation with heterogeneous MRI data," *IEEE Transactions on Medical Imaging*, vol. 39, no. 9, pp. 2713–2724, 2020.
- [21] M. H. Jensen, D. R. Jørgensen, R. Jalaboi, M. E. Hansen, and M. A. Olsen, "Improving uncertainty estimation in convolutional neural networks using inter-rater agreement," in *Proceedings of the International Conference on Medical Image Computing and Computer-Assisted Intervention*, pp. 540–548, Springer, Berlin, Germany, June 2019.
- [22] R. Tanno, A. Saeedi, S. Sankaranarayanan, D. C. Alexander, and N. Silberman, "Learning from noisy labels by regularized estimation of annotator confusion," in *Proceedings of the IEEE Conference on Computer Vision and Pattern Recognition*, pp. 11244–11253, Long Beach, CA, USA, June 2019.
- [23] L. Zhang, R. Tanno, M.-C. Xu et al., "Disentangling human error from ground truth in segmentation of medical images," *Advances in Neural Information Processing Systems*, vol. 33, pp. 15750–15762, 2020.
- [24] W. Ji, S. Yu, J. Wu et al., "Learning calibrated medical image segmentation via multi-rater agreement modeling," in *Proceedings of the IEEE Conference on Computer Vision and Pattern Recognition*, pp. 12341–12351, Nashville, TN, USA, June 2021.
- [25] A. Kendall and Y. Gal, "What uncertainties do we need in bayesian deep learning for computer vision?" *Advances in Neural Information Processing Systems*, vol. 30, 2017.
- [26] S. Lee, S. Purushwalkam Shiva Prakash, M. Cogswell, V. Ranjan, D. Crandall, and D. Batra, "Stochastic multiple choice learning for training diverse deep ensembles," *Advances in Neural Information Processing Systems*, vol. 29, 2016.
- [27] C. Rupprecht, I. Laina, R. DiPietro et al., "Learning in an uncertain world: representing ambiguity through multiple hypotheses," in *Proceedings of the IEEE International Conference on Computer Vision*, pp. 3591–3600, Venice, Italy, October 2017.
- [28] E. Kats, J. Goldberger, and H. Greenspan, "Soft labeling by distilling anatomical knowledge for improved MS lesion segmentation," in *Proceedings of the International Symposium on Biomedical Imaging*, pp. 1563–1566, IEEE, Venice, Italy, June 2019.
- [29] H. Li, D. Wei, S. Cao, K. Ma, L. Wang, and Y. Zheng, "Superpixel-guided label softening for medical image segmentation," in *Proceedings of the International Conference on Medical Image Computing and Computer-Assisted Intervention*, pp. 227–237, Springer, Berlin, Germany, October 2020.

- [30] C. Gros, A. Lemay, and J. Cohen-Adad, “SoftSeg: advantages of soft versus binary training for image segmentation,” *Medical Image Analysis*, vol. 71, Article ID 102038, 2021.
- [31] J. Lourenço-Silva and A. L. Oliveira, “Using soft labels to model uncertainty in medical image segmentation,” in *Proceedings of the International Conference on Medical Image Computing and Computer-Assisted Intervention*, pp. 585–596, Springer, Berlin, Germany, June 2022.
- [32] S. Hu, D. Worrall, S. Kneigt, B. Veeling, H. Huisman, and M. Welling, “Supervised uncertainty quantification for segmentation with multiple annotations,” in *Proceedings of the International Conference on Medical Image Computing and Computer-Assisted Intervention*, pp. 137–145, Springer, Berlin, Germany, June 2019.
- [33] M. Monteiro, L. Le Folgoc, D. Coelho de Castro et al., “Stochastic segmentation networks: modelling spatially correlated aleatoric uncertainty,” *Advances in Neural Information Processing Systems*, vol. 33, pp. 12756–12767, 2020.
- [34] X. Li, L. Yu, H. Chen, C.-W. Fu, L. Xing, and P.-A. Heng, “Transformation-consistent self-ensembling model for semi-supervised medical image segmentation,” *IEEE Transactions on Neural Networks and Learning Systems*, vol. 32, no. 2, pp. 523–534, 2021.
- [35] Q. Xie, Z. Dai, E. Hovy, T. Luong, and Q. Le, “Unsupervised data augmentation for consistency training,” *Advances in Neural Information Processing Systems*, vol. 33, pp. 6256–6268, 2020.
- [36] D. E. Worrall, S. J. Garbin, D. Turmukhambetov, and G. J. Brostow, “Harmonic networks: deep translation and rotation equivariance,” in *Proceedings of the IEEE Conference on Computer Vision and Pattern Recognition*, pp. 5028–5037, Honolulu, HI, USA, July 2017.
- [37] S. Wang, C. Li, R. Wang et al., “Annotation-efficient deep learning for automatic medical image segmentation,” *Nature Communications*, vol. 12, pp. 5915–6013, 2021.
- [38] D. C. Castro, J. Tan, B. Kainz, E. Konukoglu, and B. Glocker, “Morpho-MNIST: quantitative assessment and diagnostics for representation learning,” *Journal of Machine Learning Research*, vol. 20, pp. 1–29, 2019.
- [39] A. Almazroa, S. Alodhayb, E. Osman et al., “Agreement among ophthalmologists in marking the optic disc and optic cup in fundus images,” *International Ophthalmology*, vol. 37, no. 3, pp. 701–717, 2017.
- [40] B. Menze, Joskowicz, S. Bakas, A. Jakab, E. Konukoglu, and A. Becker, “Quantification of uncertainties in biomedical image quantification challenge at miccai,” 2020, <https://qubiq.grand-challenge.org/>.
- [41] A. Krizhevsky, I. Sutskever, and G. E. Hinton, “ImageNet classification with deep convolutional neural networks,” *Communications of the ACM*, vol. 60, no. 6, pp. 84–90, 2017.
- [42] I. Loshchilov and F. Hutter, “Decoupled weight decay regularization,” 2017, <https://arxiv.org/abs/1711.05101>.
- [43] T.-Y. Lin, P. Goyal, R. Girshick, K. He, and P. Dollár, “Focal loss for dense object detection,” in *Proceedings of the IEEE International Conference on Computer Vision*, pp. 2980–2988, Venice, Italy, June 2017.
- [44] R. Müller, S. Kornblith, and G. E. Hinton, “When does label smoothing help?” *Advances in Neural Information Processing Systems*, vol. 32, pp. 4694–4703, 2019.
- [45] D. Berthelot, N. Carlini, I. Goodfellow, N. Papernot, A. Oliver, and C. A. Raffel, “Mixmatch: a holistic approach to semi-supervised learning,” *Advances in Neural Information Processing Systems*, vol. 32, 2019.

Research Article

Role of Intelligent Management Systems in Surgical Punctuality and Quality of Care

Gendi Li and Shenhui Huang 

Operating Room of Huashan Hospital, Affiliated to Shanghai Fudan University Surgery, 200040 Shanghai, China

Correspondence should be addressed to Shenhui Huang; huibao@me.com

Received 21 July 2022; Revised 9 August 2022; Accepted 30 August 2022; Published 11 October 2022

Academic Editor: Dong Chen

Copyright © 2022 Gendi Li and Shenhui Huang. This is an open access article distributed under the Creative Commons Attribution License, which permits unrestricted use, distribution, and reproduction in any medium, provided the original work is properly cited.

Objective. The main objective is to illustrate the role of intelligent management systems in surgical punctuality and quality of care. **Methods.** 72 registered nurses were selected from our operating room, and 180 patients who needed surgery were randomly divided into the control group and the observation group for satisfaction survey and satisfaction analysis. **Results.** The correct rate of surgical clothing distribution and the qualified rate of clothing recovery were improved, and the punctuality rate of the operation was enhanced than before the implementation of the intelligent management system. The accurate positioning of surgical items and the accurate statistics of equipment use time were enhanced than before implementation. The error rate of surgical item preparation after implementation was lessened than before implementation. Both nursing satisfaction and patient satisfaction after implementation were increased than before implementation. **Conclusion.** The intelligent management system improves the punctuality of surgery and the quality of care in the operating room.

1. Introduction

Operation room is usually involved in multiple departments which offer important treatment and rescue for patients. The patients admitted to the operation room are generally with serious diseases and complex situations, which require the high-quality nurses. Nurses play an essential role in the operating room work, and the health and safety of patients are closely related to the effectiveness of nursing in the operating room. Traditional operating room management mostly adopted manual recording which not only increases the work burden but also prone to mistakes. In addition, the risk of adverse events easily occurred due to the complexity of operating room nursing work. Strengthening nursing quality in the management of the operating room and standardizing the behavior and operation of nursing staff contribute to reducing the incidence of adverse events and improving the satisfaction rate of patients.

With the development of medical technology and the improvement of surgical quality requirements, the hospital management staff turning attaches importance to the master

of operating room nursing technology to focus on the exploration of scientific management modes [1, 2]. Recently, the establishment of intelligent information in medical and health institutions throughout the country provides great convenience for medical staff. Moreover, the work efficiency of medical staff can be effectively improved based on the internet of intelligence and security [3]. As a new management mode, an intelligent management system has been employed to operating room work [4].

Intelligent operating room refers to the application of modern information technology in the operating room, and the use of high-tech software and hardware facilities can achieve modern operation process management [5]. The entry and exit of operating room medical staff can be obviously controlled by utilizing an information management system, which greatly reduces the wear of operating clothes and the operating cost of the hospital [6]. Moreover, the integration of all data in the operating room can significantly control the arrival time of medical staff in the operating room and improve the on-time opening rate [7]. Through the management of medical practices and transportation of

medical supplies, the patient's intraoperative and postoperative conditions can be followed up in time, which is convenient for medical staff to adjust the treatment plan according to the different states of patients [8]. Comprehensive operating room multisystem information can achieve information integration, effectively manage the flow of people, logistics, and highly improve the operation efficiency and perioperative quality control management.

In the present study, the improvement effect of an intelligent process management system on work quality in the digital process of the operating room was explored and analyzed the changes in related work quality of medical staff and patients' job satisfaction before and after implementation.

2. Methods

2.1. Participants. The study was approved by the ethics committee of Huashan Hospital, which is affiliated with Fudan University in Shanghai. From June 2019 to September 2021, 72 registered nurses aged 22 to 55 years old with an average age of (35.69 ± 8.456) were selected from the operating room of our hospital. 17122 surgeries were collected and adopted the traditional management mode and the intelligent management system in the operating room, respectively. 180 surgical patients ranging from 20 to 70 years old with average ages of (47.68 ± 12.76) years old and (44.97 ± 11.48) years old were randomly divided into prior implementation group (control group) and after implementation group (observation group) to investigate for satisfaction. The control group included 53 males and 37 females, and the observation group included 57 males and 33 females. There was no statistical divergence in baseline data between the two groups.

2.2. Inclusion and Exclusion Criteria. Inclusion criteria were as follows: I) all nurses have professional qualification certificate; II) the nursing age was more than 1 year and had working experience in a general hospital; III) the nurses are all women; IV) the patients requiring surgery; V) all participants signed informed consent.

Exclusion criteria were as follows: I) further education nurses; II) the nursing age was lower than 1 year; III) nurses without working experience in general hospital; IV) patients who do not require surgery; V) patients who do not sign informed consent.

2.3. Methods of Management Modes. The control group intervened with traditional management. The traditional management mode mainly includes manual registration of the identity of surgical staff, entering and leaving the operating room, receiving surgical clothing, and other medical behaviors. Drugs, equipment, and dressings in the operating room are kept in fixed locations by special personnel and checked regularly. Sterilization items in the operating room were marked with sterilization dates. The number of surgical instruments was counted and recorded by operators, and the

operating room nursing staff before and after the operation was to ensure the normal operation.

The observation group adopted the intelligent management system. (I) Surgical clothing management automation recorded operators' information to realize intelligent collection and recycling of clothes and shoes in the operating room. The management system tracked the washing and disinfection and used the status and inventory of surgical clothing and shoes in the operating room to remind logistics personnel to add or clean surgical clothing and shoes in time. At the same time, for efficient management level, the whole process of closed-loop management is required for surgical clothing and shoes. (II) Operation staff access control: intelligent identification of operating room medical staff strictly control the operating room irrelevant medical staff entry to effectively control the risk of infection in the operating room. (III) Operation staff behavior management: the combination of an intelligent management system and enterprise scheduling system accurately records the time point of medical staff entering and leaving the operating room to assure the on-time rate of operation. (IV) Operating room system management: according to the operating room management requirements, the historical data of the system reasonably are stored and maintained regularly to ensure the normal operation of all equipment. V) Operating room audit management: safety checked surgical instruments, medicines, blood transfusions, and consumables to form multi-dimensional knowledge database for data sharing.

2.4. Observation Indexes

- (I) The qualified recovery rate of surgical clothing was observed before and after the implementation of the intelligent management system. The quality rate of clothing recovery = cases of qualified cases of clothing returning after surgery / cases of medical staff $\times 100\%$.
- (II) Observed the on-time operation opening rate before and after the implementation of the intelligent system, with the operation starting at 8:30 as the standard.
- (III) Discrepancy before and after the implementation of the operating room nursing quality: five assessment team members with more than 10 years of nursing experience were selected, and the hospital operating room nursing quality questionnaires were used to evaluate the operating room nursing quality, including aseptic operation, surgical instruments for qualified, sterile items based nursing management, nursing documents, and operation 5 projects. The percentage system was adopted for each item, and the higher the score, the higher the quality of nursing in the operating room.
- (IV) Contrasted the satisfaction of medical staff before and after implementation. The satisfaction of medical staff was evaluated by the self-made satisfaction questionnaire of our hospital, which mainly included three aspects: changing clothes

flow schedule, operating room environment, and statistical reports. The total score of each aspect was 0 to 100, and the higher the score is, the higher the satisfaction will be.

- (V) The patient satisfaction questionnaire made by the hospital was adopted. The total score was 100 points, very satisfied: 90 points, satisfied: 75–90 points, general: 60–75 points, and unsatisfied: <60 points.

2.5. Statistical Analysis. SPSS 22.0 software (SPSS Inc., Chicago, USA) was utilized for statistical analysis of the obtained data. The measurement data were displayed as ($X \pm S$), and t -test was utilized for statistical analysis between the two groups. Counting data were displayed as rate (%), and divergence was performed by X^2 test (Chi-square test). $P < 0.05$ was considered as a statistically notable divergence.

3. Results

3.1. Divergence between Correct Rate of Distributing Surgical Clothing and Qualified Rate of Clothing Recovery before and after Implementation. The correct rate of distributing surgical clothing and the qualified rate of clothing recovery were both higher than before the implemented intelligent management system, with statistical significance ($P < 0.05$), as shown in Table 1.

3.2. A Class III Adverse Event Is One That Does Not Result in Any Impairment of the Patient's Body or Function despite the Occurrence of False Facts. The on-time rate of operation starting after the implementation of the intelligent management system was higher than before implementation, and the divergences were statistically notable ($P < 0.05$). The detection of potential safety hazards after the implementation of the intelligent management system was higher than before implementation, and incidences of Class III adverse events were lower after implementation compared to before implementation, but the divergence was not statistically notable ($P > 0.05$) as shown in Table 2.

3.3. Divergence of Surgical Items and Equipment of Medical Staff in Operating Room. The accurate positioning of surgical items and the accurate statistics of equipment use time after the implementation of intelligent management system were higher than before implementation, and the divergences were statistically notable ($P < 0.05$). The prepared surgical items incorrectly were lower after implementation compared to before implementation ($P < 0.05$), while the sterile items expire was lower after implementation compared to before implementation but the divergence was not statistically notable ($P > 0.05$) as shown in Table 3.

3.4. Divergence of Nursing Quality before and after Implementation. The qualified preparation of equipment, qualified preparation of aseptic materials qualified, emergency supplies intact, and qualified nursing technique

operation were higher than before implementation, and the divergences were statistically notable ($P < 0.05$) as shown in Table 4.

3.5. Discrepancy of Performance Appraisal Score of Operating Room Hospital. The work motivations of nurses were promoted after implementation compared to before implementation ($P < 0.05$). The job responsibility and the service attitudes were higher than before implementation; however, the divergences were without statistically notable ($P > 0.05$) as shown in Table 5.

3.6. Discrepancy of Satisfaction of Medical Staff before and after Implementation. The very satisfied number of nurses was more than before implementation, whereas the result did not reach statistical significance, and the divergences were statistically notable ($P > 0.05$). In addition, the satisfied number of nurses was more than before implementation, and the unsatisfied number of nurses was less than before implementation as shown in Table 6.

3.7. Discrepancy of Data between Control Group and Observation Group. 180 surgical patients were randomly divided into control group and observation group. The control group included 53 males and 37 females, and the observation group included 57 males and 33 females. There was no statistical divergence in baseline data between the two groups as shown in Table 7.

3.8. Comparison of Satisfaction of Patients before and after Implementation. The very satisfied number of patients was more than before implementation, while the result did not reach statistical significance, and the divergences were statistically notable ($P > 0.05$). In addition, the satisfied number of nurses was more than before implementation, and the unsatisfied number of nurses was less more than before implementation as shown in Table 8.

4. Discussion

In recent years, due to the continuous improvement of people's living standards and the continuous development of medical technology, patients have higher requirements for the quality of surgery, especially for the surgical staff and surgical environment [9]. It is widely known that the more personnel entering the operating room, the greater the impact on the operating room environment. Therefore, the entry and exit of personnel in the operating room must be strictly controlled. The traditional setting of full-time personnel to check and register the medical staff participates in the operation and issues the key to the locker of changing clothes and shoes. With the gradual development of the intelligent operating room system, the introduction of information technology into operating room management has become the trend of operating room construction [10–13]. The intelligent surgical management system not only effectively controls the entry and exit of operating room

TABLE 1: Divergence between the correct rate of distributing surgical clothing and qualified rate of clothing recovery before and after implementation (n, %).

Groups	Distribute surgical clothing correctly	Qualified rate of clothing recovery
Before implementation (n = 72)	66	58
After implementation (n = 72)	72	69
X ²	6.261	8.07
P	0.028	0.004

TABLE 2: A Class III adverse event is one that does not result in any impairment of the patient's body or function despite the occurrence of false facts (n, %).

Groups	The on-time opening rate of operation	Occurrence of potential safety hazards	Class III adverse events
Before implementation (n = 8561)	7734	7	5
After implementation (n = 8561)	8063	15	2
X ²	88.543	2.913	1.286
P	0.000	0.088	0.453

TABLE 3: Divergence of surgical items and equipment of medical staff in operating room (n, %).

Groups	Accurate positioning of surgical items	Sterile items expire	Prepare surgical items incorrectly	Accurate statistics of equipment use time
Before implementation (n = 8561)	7138	9	13	7389
After implementation (n = 8561)	8096	4	3	8350
X ²	546.348	1.925	6.256	726.444
P	0.000	0.267	0.021	0.000

TABLE 4: Divergence of nursing quality before and after implementation (n, %).

Groups	Equipment preparation qualified	Sterile articles qualified	Emergency supplies intact	Qualified nursing technique operation
Before implementation (n = 8561)	8079	8417	8348	8481
After implementation (n = 8561)	8365	8520	8496	8533
X ²	125.617	57.972	80.092	25.196
P	0.000	0.000	0.000	0.000

TABLE 5: Discrepancy of performance appraisal score of operating room hospital (n, %).

Groups	Work motivation	Job responsibility	Service attitudes
Before implementation (n = 72)	60	63	65
After implementation (n = 72)	69	70	68
X ²	6.028	4.823	0.886
P	0.026	0.055	0.532

TABLE 6: Discrepancy of satisfaction of medical staff before and after implementation (n, %).

Groups	Very satisfied	Satisfied	General	Unsatisfied
Before implementation (n = 72)	9	20	30	13
After implementation (n = 72)	13	37	20	2
X ²	0.352	4.947	3.064	9.005
P	0.647	0.03	1.115	0.003

TABLE 7: Discrepancy of data between control group and observation group ($\bar{X} \pm S$).

Groups	Age	Gender (male:female)
Before implementation ($n = 90$)	(47.68 \pm 12.76)	53:37
After implementation ($n = 90$)	(44.97 \pm 11.48)	57:33
P	0.136	0.541
χ^2	—	0.374

TABLE 8: Comparison of satisfaction of patients before and after implementation (n, %).

Groups	Very satisfied	Satisfied	General	Unsatisfied
Before implementation ($n = 90$)	21	29	26	14
After implementation ($n = 90$)	27	43	16	4
χ^2	1.023	4.537	3.106	6.173
P	0.4	0.048	0.112	0.023

personnel but also realizes the closed-loop tracking of surgical clothing [14]. The intelligent management system is of great help to the hospital to improve the regional management of operating room and standardize the behavior of medical staff [15].

The automatic and intelligent management of the distribution and recovery of operating clothes and shoes plays an important role in the management of the operating room [16]. Traditional operating room personnel receives surgical clothes and shoes through the manual record, while the surgical intelligent clothes sending machine is customized and developed based on the actual needs of the hospital. The dispensing machine is automatically associated with the operation schedule record of the hospital information system to realize the automatic dispensing of surgical clothes according to the size and effectively avoid the wrong dispensing of surgical clothes size [17]. The intelligent management system accelerated the turnover of surgical clothing via optimizing the changing process and simplified the counting process through the closed-loop tracking of washing, disinfection, receiving, and inventory of surgical clothing, which was more conducive to hospital logistics management [18]. What is more, the application of smart locker management also cultivated the habit of utilizing the wardrobe according to regulations and returning clothes in time, and the dressing recovery rate of medical staff was memorably boosted. The application of an intelligent management system not only lessened the workload of cleaning staff but also enhanced the satisfaction of medical staff to the changing process and operating room environment, bringing a better sense of experience to medical staff.

The on-time opening rate of operation is one of the indexes to evaluate the medical staff's behavior standard [19]. Before the application of the intelligent management system in the operating room, the operation is likely to be delayed due to the weak time concept of the operating room medical staff. In addition, there are often many and miscellaneous departments involved in the operation, and the operating room itinerant nurses often need to contact anesthesiologists and surgeons, which not only increases the working burden of the itinerant nurses but also increases the

hidden danger of operation safety [20]. After the application of the intelligent management system, the intelligent management system plays a good reminder role for the operating room medical staff through the planning of the operating room time and the operation information push function and effectively improves the on-time operation opening rate. Meanwhile, it improves the management level and service level of the hospital operating room and further effectively improves the medical behavior of medical staff and the quality of work [21]. The operation desk information can be sent to the nurse station in the ward, which is beneficial for nurses to prepare related work in advance. The operation desk information can also be pushed by the operation desk information, which ensures that the operation doctors can get the operation desk information in time, so as to arrange the time and work reasonably and avoid the operation delay due to other work.

There are many kinds of equipment and sterile items in the operating room. In order to improve the precision of equipment management and timely statistics on the use, recovery, and storage of sterile items, the intelligent management system can scan these equipment and sterile items to realize information sharing [22]. This study shows that the intelligent management system has the function of recording and identifying, which can effectively manage sterile items and surgical equipment, accurately count the use time of equipment and sterile dressing cycle, and effectively reduce the expiration and failure rate of sterile items. At the same time, the intelligent management system has a verification function, which greatly reduces the incidence of medical errors, ensures the smooth development of surgery, and directly ensures the safety of surgery.

Intelligent management system to adhere to the quality improvement as the basic concept can improve the medical staff's work initiative and stimulate the sense of responsibility. This study shows that after the application of intelligent management system, the performance evaluation score is significantly improved, and the distribution of performance evaluation can be reasonably completed in a short time, which is conducive to improving the satisfaction of medical staff. In addition, an intelligent operating room can fully integrate patient information, ensure accurate

operation, and reduce adverse events caused by improper operation of nursing staff, so as to ensure service quality and improve patient satisfaction.

5. Conclusion

Taken together, the efficiency of medical staff has been improved by intelligent management systems, which have changed the original manual management model. The intelligent management system can effectively improve the on-time operation opening rate, optimize the dressing process, improve the quality of nursing in the operating room, and reduce the occurrence of adverse events in the operating room, which is conducive to enhancing the satisfaction of medical staff and patients.

Data Availability

The datasets used and analyzed during the current study are available from the corresponding author upon reasonable request.

Ethical Approval

The authors are accountable for all aspects of the work in ensuring that questions related to the accuracy or integrity of any part of the work are appropriately investigated and resolved. The study was carried out in accordance with the ethical guidelines of the Declaration of Helsinki (as revised in 2013).

Conflicts of Interest

The authors declare that they have no conflicts of interest.

References

- [1] M. Fernandes, S. M. Vieira, F. Leite, C. Palos, S. Finkelstein, and J. M. C. Sousa, "Clinical decision support systems for triage in the emergency department using intelligent systems: a review," *Artificial Intelligence in Medicine*, vol. 102, Article ID 101762, 2020.
- [2] S. Chen, J. Huang, and Z. Gao, "Zhongguo yi liao qi xie za zhi," *Chinese Journal of Medical Instrumentation*, vol. 45, no. 1, pp. 42–45, 2021.
- [3] Q. U. Ain, S. Iqbal, S. A. Khan, A. W. Malik, I. Ahmad, and N. Javaid, "IoT operating system based fuzzy inference system for home energy management system in smart buildings," *Sensors*, vol. 18, no. 9, p. 2802, 2018.
- [4] H. G. Kenngott, M. Wagner, A. A. Preukschas, and B. P. Müller-Stich, "[Intelligent operating room suite: from passive medical devices to the self-thinking cognitive surgical assistant]," *Chirurg, Der*, vol. 87, no. 12, pp. 1033–1038, 2016.
- [5] V. Agnoletti, M. Buccioli, E. Padovani et al., "Operating room data management: improving efficiency and safety in a surgical block," *BMC Surgery*, vol. 13, no. 1, 2013.
- [6] B. P. Chang Md, J. C. Vacanti Md, Y. Michaud Rn Msn, H. Flanagan Md, and R. D. Urman Md Mba, "Emotional intelligence in the operating room: analysis from the Boston Marathon bombing," *Am J Disaster Med*, vol. 9, no. 2, pp. 77–85, 2014.
- [7] S. Franke, J. Meixensberger, and T. Neumuth, "Multi-perspective workflow modeling for online surgical situation models," *Journal of Biomedical Informatics*, vol. 54, pp. 158–166, 2015.
- [8] C. C. Lin, Y. P. Chen, C. C. Chiang, M. C. Chang, and O. K. S. Lee, "Real-time streaming of surgery performance and intraoperative imaging data in the hybrid operating room: development and usability study," *JMIR Med Inform*, vol. 8, no. 4, Article ID e18094, 2020.
- [9] M. Kunz and J. F. Rudan, "Patient-specific surgical guidance system for intelligent orthopaedics," *Advances in Experimental Medicine & Biology*, vol. 1093, pp. 225–243, 2018.
- [10] V. Bellini, M. Guzzon, B. Bigliardi, M. Mordonini, S. Filippelli, and E. Bignami, "Artificial intelligence: a new tool in operating room management. Role of machine learning models in operating room optimization," *Journal of Medical Systems*, vol. 44, no. 1, p. 20, 2019.
- [11] J. E. McGowan, J. D. Truweit, P. Cipriano et al., "Operating room efficiency and hospital capacity: factors affecting operating room use during maximum hospital census," *Journal of the American College of Surgeons*, vol. 204, no. 5, pp. 865–871, 2007.
- [12] A. Kjellin, L. Hedman, C. Escher, and L. Felländer-Tsai, "Hybrid simulation: bringing motivation to the art of teamwork training in the operating room," *Scandinavian Journal of Surgery*, vol. 103, no. 4, pp. 232–236, 2014.
- [13] W. Xiang and C. Li, "Surgery scheduling optimization considering real life constraints and comprehensive operation cost of operating room," *Technology and Health Care*, vol. 23, no. 5, pp. 605–617, 2015.
- [14] M. A. Cypko and M. Stoehr, "Digital patient models based on Bayesian networks for clinical treatment decision support," *Minimally Invasive Therapy & Allied Technologies*, vol. 28, no. 2, pp. 105–119, 2019.
- [15] M. Hensel, H. Wauer, A. Bloch, T. Volk, W. J. Kox, and C. Spies, "[Implementation of modern operating room management - experiences made at an university hospital]," *Anesthesiologie, Intensivmedizin, Notfallmedizin, Schmerztherapie: AINS*, vol. 40, no. 7, pp. 393–405, 2005.
- [16] A. Macario, "Implementing operating room management science: from the bench to the scheduling office," *European Journal of Anaesthesiology*, vol. 31, no. 7, pp. 355–360, 2014.
- [17] S. Riedl, "[Modern operating room management in the workflow of surgery. Spectrum of tasks and challenges of the future]," *Anaesthesist, Der*, vol. 52, no. 10, pp. 957–963, 2003.
- [18] T. Hüfner, M. Citak, J. Imrecke, C. Krettek, and T. Stübiger, "[Handling modern imaging procedures in a high-tech operating room]," *Unfallchirurg, Der*, vol. 115, no. 3, pp. 220–225, 2012.
- [19] J. Neumann, C. Angrick, C. Höhn et al., "Surgical workflow simulation for the design and assessment of operating room setups in orthopedic surgery," *BMC Medical Informatics and Decision Making*, vol. 20, no. 1, 2020.
- [20] M. Ma, P. Fallavollita, S. Habert, S. Weidert, and N. Navab, "Device- and system-independent personal touchless user interface for operating rooms: one personal UI to control all displays in an operating room," *International Journal of Computer Assisted Radiology and Surgery*, vol. 11, no. 6, pp. 853–861, 2016.
- [21] T. M. Coon, "Integrating robotic technology into the operating room," *American Journal of Orthopedics*, vol. 38, no. 2 Suppl, pp. 7–9, 2009.
- [22] S. Dharan and D. Pittet, "Environmental controls in operating theatres," *Journal of Hospital Infection*, vol. 51, no. 2, pp. 79–84, 2002.

Research Article

Posterior Injured Vertebra Column Resection and Spinal Shortening for Thoracolumbar Fracture Associated with Severe Spinal Cord Injury: A Retrospective Case-Control Observational Study

Zhiyue Shi , Yingsong Wang , Jingming Xie , Jin Zhou, Tingbiao Zhu, Tao Li, Zhi Zhao, Ying Zhang, Ni Bi, and Quan Li

Departments of Orthopaedic Surgery, 2nd Affiliated Hospital of Kunming Medical University, 374# Dianmian Road, Kunming 650101, Yunnan, China

Correspondence should be addressed to Jingming Xie; xiejingming@kmmu.edu.cn

Received 22 July 2022; Revised 26 August 2022; Accepted 3 September 2022; Published 6 October 2022

Academic Editor: Dong Chen

Copyright © 2022 Zhiyue Shi et al. This is an open access article distributed under the Creative Commons Attribution License, which permits unrestricted use, distribution, and reproduction in any medium, provided the original work is properly cited.

Background. Thoracolumbar spinal fracture associated with severe spinal cord injury (sSCI) is a kind of severe traumatic spine injury. Although various approaches are currently used to treat sSCI-related thoracolumbar fractures, the neurological function of patients has not been significantly improved by surgery. **Objective.** To evaluate the therapeutic effects of the new procedure of posterior injured vertebra column resection (PIVCR) and spinal shortening for the treatment of thoracolumbar fracture associated with sSCI. **Methods.** In this retrospective case-control observational study, we included 66 patients with thoracolumbar fractures associated with sSCI in our institution from January 2015 to December 2017. According to the different surgical approaches, the patients were allocated to group A ($n = 32$, received simple posterior decompression and fixation) and group B ($n = 34$, received PIVCR and spinal shortening). All patients' clinical and radiologic outcomes were collected to evaluate retrospectively. The clinical outcomes were gathered, including the intraoperative blood loss, operative time, visual analog scale (VAS) score, and American Spinal Injury Association (ASIA) impairment scale. The radiologic outcomes were collected involving the range of spinal shortening, canal encroachment, heights of the anterior edge of the vertebral body, and the Cobb angle. **Results.** There was no significant difference in the two groups regarding preoperative demographic data, VAS scores, segmental kyphosis Cobb, canal encroachment, and neurological status. The range of spinal shortening in group B was an average 1.57 ± 0.40 cm and $36.45 \pm 6.56\%$ of the height of the single spinal motion segment. Due to the characteristics of the surgical procedure, group B got complete decompression of the spinal cord and better postoperative canal decompression than group A. Thus, better clinical outcomes, including neurological improvement, loss of corrective Cobb angle, and VAS improvement, were shown in group B at the follow-up investigation than those in group A ($P < 0.05$). **Conclusion.** PIVCR and spinal shortening surgical procedure is a safe, reliable, and effective approach to treating thoracolumbar fracture associated with sSCI.

1. Introduction

According to incomplete estimates, the prevalence of SCI worldwide (spinal cord injury) is 223 to 755 people per million inhabitants, and the incidence of SCI per million inhabitants per year is about 10.4% to 195.4% [1, 2]. Severe spinal cord injury (sSCI) severely burdens society and families. A large portion of patients who suffer from traumatic spine injuries is mainly located in the thoracolumbar

junction, which could bring about the occurrence of neurological deficits with a rate of 22%-45% [3]. In order to alleviate the neural compression, correct segmental kyphosis, rebuild vertebral body height, construct and stabilize the spine, and enhance neurological recovery, therapeutic methods including surgery (anterior, posterior, and anterior combined with posterior approaches) and pharmacological therapy are adopted to treat thoracolumbar fracture associated with sSCI [4–8]. However, neurological improvement

is not always ideal by the treatments above, especially for those with complete neurological deficits. According to the research, the rate of neurological improvement for patients with traumatic sSCI in thoracic and thoracolumbar is only 22.4%, and merely 7.7% of patients with complete sSCI could get neurological improvement [9]. With the Frankel scale in thoracolumbar fracture, patients with incomplete sSCI could acquire postoperative neurological function improvement by an average of 1.3 grade [10, 11].

Surgical decompression early within 72 hours is found to significantly influence the potential for neurological improvement in patients with thoracolumbar spine injury [12]. Some studies have shown that high interspinous pressure in the injured spinal cord, spinal cord blood flow (SCBF) reduction, and interspinous circumstance disorder are critical factors that could affect the improvement of sSCI [13–16]. Effective methods urgently need to be adopted to improve the neurological deficit for thoracolumbar fractures. Posterior injured vertebra column resection (PIVCR) and spinal shortening could decompress the spinal cord circumferentially, reduce the tension of the spinal cord, improve spinal cord perfusion, and improve neurological deficit [17–25]. We applied PIVCR and spinal shortening to treat thoracolumbar fractures associated with sSCI and achieved significant neurological improvement. Therefore, it is necessary to study the clinical efficacy of PIVCR and spinal shortening in thoracolumbar fractures associated with sSCI.

To the best of our knowledge, this is the first retrospective study to report the utilization of PIVCR and spinal shortening for treating patients with thoracolumbar fractures associated with sSCI. This retrospective case-control observational study evaluated clinical effects by comparing the new approach (PIVCR and spinal shortening) and simple posterior decompression and fixation. The prime objective of this study is to determine whether the patients with thoracolumbar fracture associated with sSCI could get better clinical outcomes and neurological improvement with the surgery of PIVCR and spinal shortening than those with simple posterior decompression and fixation. The secondary objective of this study is to assess the safe range of spinal shortening in the thoracolumbar spine.

2. Methods

2.1. Ethical Approval. This study received ethical approval from the Ethics Committee at the 2nd affiliated Hospital of Kunming Medical University. Due to the retrospective characteristic, written informed consent was not applicable for this study.

2.2. Study Design and Patients. This retrospective case-control observational study was performed at the 2nd affiliated Hospital of Kunming Medical University. We included patients with thoracolumbar fractures associated with sSCI who received surgery in our institution from January 2015 to December 2017.

The inclusion criteria for eligible patients are as follows:

(1) without complete transection of the spinal cord in the

injury segment at preoperative magnetic resonance imaging (MRI); (2) severe neurological function impairment graded as A/B/C according to American Spinal Injury Association (ASIA) impairment scale; (3) single injured vertebral segment located at T10 to L1; and (4) TLICS scores ≥ 5 points. Patients with serious osteoporosis or without follow-up results were excluded from this study.

From January 2015 to December 2016, a total of 32 patients received simple posterior decompression and fixation and were assigned to group A as a control group. From January 2016 to December 2017, 34 patients received PIVCR and spinal shortening and were allocated to group B. All patients underwent surgery performed by the same medical team.

2.3. Surgical Procedures

2.3.1. Simple Posterior Decompression and Fixation in Group A. Under general anesthesia, a posterior midline incision was made. Pedicle screws were then implanted two or three levels by freehand technique. The fracture reduction was achieved by distraction from the screw and rod on both sides. Then, hemilaminectomy or laminectomy was performed on the side of the spinal cord with severe compression and the posterior aspect of the dural sac was decompressed. The dural sac was gently retracted and protected with a nerve retractor. The fragments of fracture in front of the dural sac were meticulously removed with a curette or pushed into vertebral body with a curette to receive further decompression. The spinal reconstruction was achieved by filling autogenous bone into the injured vertebra or filling a titanium mesh cage with autogenous bone into the injured vertebra segment. During operation, methylprednisolone (30 mg/kg) was used to protect the spinal cord before spinal canal decompression (Figure 1).

2.3.2. One-Stage Posterior Injured Vertebral Column Resection and Spine Shortening in Group B. Under general anesthesia, patients were placed in the prone position, and posterior midline incision was made. Pedicle screws including two or three levels upper and lower of the injured vertebral body were then implanted by freehand technique, respectively. The injured vertebral body did not need to be implanted. Through the costotransverse approach, the costotransverse joints and 2–3 cm of bilateral ribs in the thoracic segment were excised, respectively, and then the lateral wall of the vertebral body was exposed easily under meticulous subperiosteal dissection on each side. The spinous process, bilateral lamina, and complete facet joint of the injured level needed to be removed. Then, the dural sac and nerve roots were clearly exposed and the posterior aspect of the dural sac was decompressed. Dural sac and nerve root were then gently retracted and protected with a nerve retractor. The fragments of the fracture in front of the dural sac were meticulously pushed into the vertebral body with a curette to receive decompression and spinal cord safety. The pedicle on one side was removed. The vertebral body was removed with a curette or rongeur and upper and

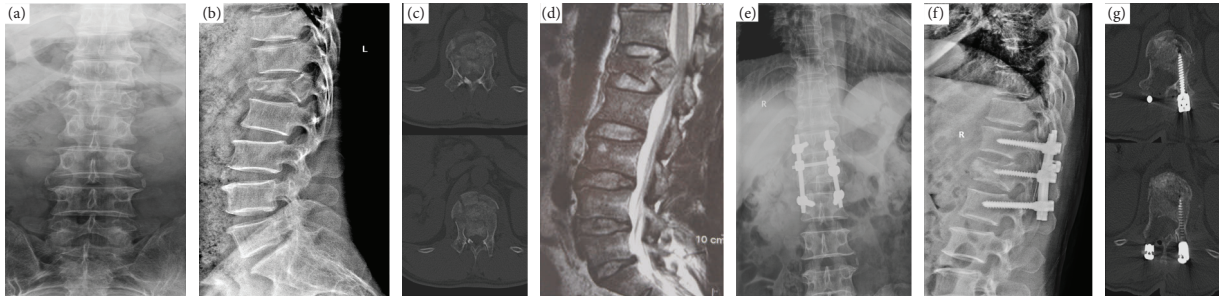


FIGURE 1: A 42-year-old male patient who was suffering from severe neurological deficit with a grade of ASIA B on admission. Preoperative X-ray (a, b) show L1 fracture with Cobb angle 22°, CT (c) with severe spinal canal encroachment, MRI (d) showed that the spinal cord was not transection in the injury segment. Undergoing simple posterior decompression fixation, patient achieved to correct segmental kyphosis deformity, restore vertebral body height (e, f), direct good decompress the neural elements (g) and neurological function improved to ASIA D.

lower intervertebral discs were removed. A temporary rod was placed when one side of the osteotomy was completed to keep the spinal stability. Subsequently, the same surgical process was performed on the opposite side. After the whole vertebral body as well as the upper and lower intervertebral discs were removed, the spinal cord was completely 360° decompressed. The spinal column was divided into two free segments into the cephalic and caudal sides, which were only connected by the spinal cord. The segmental kyphosis and spinal dislocation were easily got correction; meanwhile, safely controllable spine shortening was achieved (Figure 2). The principle of spine shortening was that the dural sacs should be not obvious shrinking and buckling. The spinal cord tension was reduced than preshortening through direct palpation on the dural sacs. Then, the permanent fixation rods were placed. If the dural sac was injured by accident, the repair was performed to reduce the risk of postoperative cerebrospinal fluid leakage. After accomplishing the process of spinal shortening, the height of the anterior and the resection space was measured. A titanium mesh filled with autograft bone was positioned in the midline of the inferior endplate of the cephalad vertebra and the superior endplate of the caudal vertebra from lateral side. The compression of the spine achieved the stability of the titanium mesh. Finally, a drain was placed, and the muscle, fascia, and skin were closed in sequence. During the operation, methylprednisolone (30 mg/kg) was used to protect neurological function 5 min before spinal canal decompression (Figure 3).

2.4. Clinical Outcomes and Radiologic Evaluation. The criteria were gathered to evaluate the clinical outcomes, including the intraoperative blood loss, operative time, VAS score, and ASIA impairment scale. The ASIA impairment scale assessed sensory and motor levels which were affected by the spinal cord injury and the VAS score assessed neurological outcomes and back pain.

Cobb angle, canal encroachment, heights of the posterior edge of the vertebral body, and range of spinal shortening were measured as the radiologic outcomes. Traumatic segment kyphosis was measured by Cobb angle between the upper and lower end plates of the adjacent vertebrae of the

fracture on the lateral radiograph. Radiologic assessment of spinal canal encroachment rate was calculated on computed tomography. As Lin et al. [11] demonstrated, the height of the posterior edge of the vertebral body was calculated as follows: the restore rate = [the height of the posterior edge of fractured vertebral body / (the height of the posterior edge of caudal vertebral body + the height of the posterior edge of the cephalad vertebral body) / 2] × 100%. Range and percentage of spinal shortening in a single spinal motion segment (total height of the posterior edge of vertebral body + cephalad disc + caudal disc) were calculated using the following equation on the postoperative lateral radiograph (Figure 4), range of spinal shortening: $X = (A + B) / 2 + C + D - E$, percentage of spinal shortening of single spinal motion segment: $Y = X / [(A + B) / 2 + C + D] \times 100\%$, in which A is the height of the posterior edge of the cephalad vertebral body, B is the height of the posterior edge of the caudal vertebral body, C is the height of the posterior edge of the cephalad disc, D is the height of the posterior edge of the caudal disc, and E is the height of the posterior edge of titanium mesh.

2.5. Statistical Analysis. Statistical analysis was performed by SPSS software (SPSS 17.0, IBM Corp, Armonk, NY). All quantitative data conformed to normal distribution by Kolmogorov-Smirnov test ($P > 0.05$). Therefore, the statistical description of the quantitative data was carried out by mean and standard deviation. The statistical description of the categorical data and ordinal data was carried out by number. For the further data analysis, methods including the t -test, the Pearson chi-square test, or Fisher exact test and Mann-Whitney U test were utilized, in which $P < 0.05$ represented the statistical significance.

3. Results

A total of 66 eligible patient cases were included in this retrospective case-control observational study, in which 32 patients received simple posterior decompression and fixation that were assigned to group A, and 34 patients received PIVCR and spinal shortening that was allocated to group

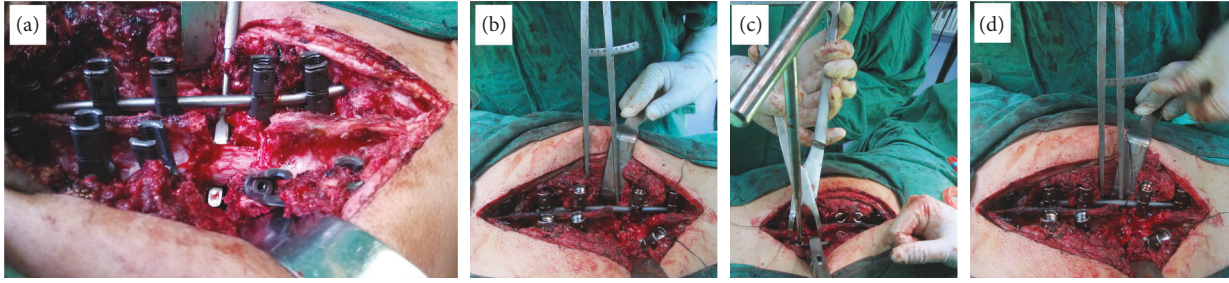


FIGURE 2: PIVCR and spinal shortening treated for T12 fracture associated with SCI. (a) shows posterior injured vertebral column resection; (b, c, d) show the spinal shortening procedure.

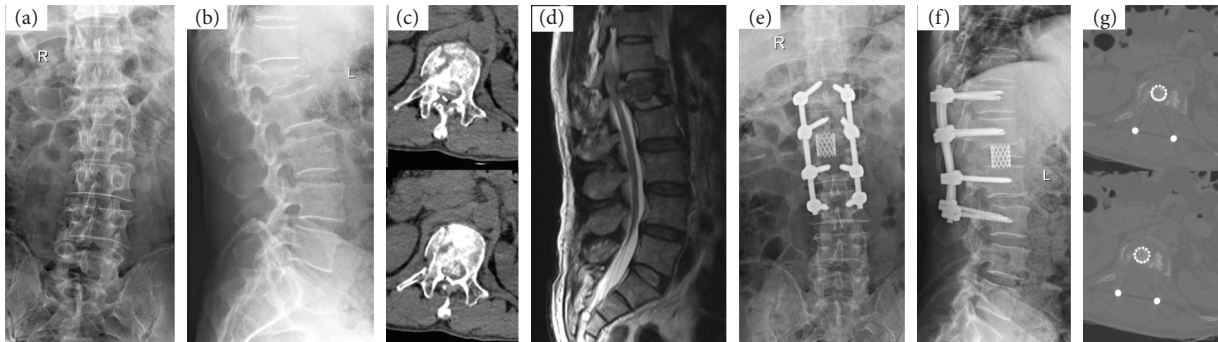


FIGURE 3: A 48-year-old male patient who was suffering from severe neurological deficit with a grade of ASIA A on admission. Preoperative X-ray (a, b) show L1 fracture with Cobb angle 19° , CT (c) with severe spinal canal encroachment, MRI (d) showed that the spinal cord was not transection in the injury segment. Undergoing PIVCR and spinal shortening, patient achieved to correct segmental kyphosis deformity, restore vertebral body height (e, f), direct good decompression the neural elements (g) and neurological function improved to ASIA E.

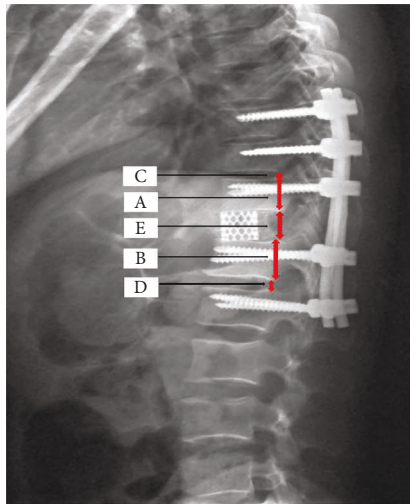


FIGURE 4: Range of spinal shortening and percentage of spinal shortening of single spinal motion segment (total height of posterior edge of vertebral body+cephalad disc+caudal disc) were calculated using the following equation on the postoperative lateral radiograph. Range of Spinal shortening: $X = (A + B)/2 + C + D - E$, percentage of spinal shortening of single spinal motion segments: $Y = X / [(A + B)/2 + C + D] \times 100\%$, where A is the height of posterior edge of cephalad vertebral body, B is the height of posterior edge of caudal vertebral body C is the height of posterior edge of the cephalad disc, D is the height of posterior edge of caudal disc, and E is the height of posterior edge of titanium mesh.

B. There was no significant difference in two groups regarding age, gender, injury segment, and the time from their initial injury to prior to surgery (Table 1).

Compared with those in group A, the blood loss and average operative time were significantly more and longer in group B. The height of the posterior edge of the vertebral body was improved from $91.40 \pm 1.04\%$ preoperative to $95.16 \pm 1.88\%$ postoperative, $94.32 \pm 1.61\%$ at final follow-up in group A, while $91.88 \pm 1.23\%$, 91.74 ± 7.03 , and $91.70 \pm 6.79\%$, respectively, in group B. The range of spinal shortening in group B was an average 1.57 ± 0.40 cm (range, 0.9 cm-2.28 cm) and $36.45 \pm 6.56\%$ of the height of the single spinal motion segment. Group B achieved better spinal shortening than group A ($P < 0.05$). The whole injured vertebral column and cephalad and the caudal intervertebral disc were removed in group B. Dural sacs were completely 360° decompressed, with significantly better decompression ($P < 0.05$) than group A (Table 2).

There was no neurological deterioration after surgery in any patient of the two groups. There was no significant difference in preoperative neurological impairment between the two groups ($P > 0.05$). At the final follow-up, the neurological improvement of patients in group B was 1.53 grades on average with the evaluation of ASIA impairment scale, which was significantly better than group A with 0.78 grades ($P < 0.05$). 89.47% of patients with incomplete deficit (ASIA B/C) in group B achieved more than 1 grade on the ASIA impairment scale, with mean recovery of around 1.79

TABLE 1: Characteristics of patients in simple posterior decompression and fixation group (group A, $n=32$) and PIVCR and spinal shortening group (group B, $n=34$).

Patients characteristic	Surgical approach		<i>P</i>
	Group A	Group B	
Median age (years)	37.28 ± 13.40	34.00 ± 11.43	0.288
Sex (M/F)	19/13	22/12	0.655
Duration from initial injury to prior to surgery	17.44 ± 4.23	18.26 ± 3.20	0.372
TLICS scores	7.41 ± 1.19	7.65 ± 1.04	0.384
The sites of injured vertebral segment			0.905
T10	2	3	
T11	4	5	
T12	13	11	
L1	13	15	

TABLE 2: Parameters of patients in simple posterior decompression and fixation group (group A, $n=32$) and PIVCR and spinal shortening group (group B, $n=34$).

Parameter	Group A	Group B	<i>P</i>
Operative time(min)	179.53 ± 30.12	264.26 ± 48.39	<0.001*
Blood loss (mL)	435.63 ± 222.61	564.41 ± 206.78	0.018*
Spinal canal encroachment rate			
Preop.	57.80 ± 9.90	59.50 ± 10.20	0.496
Postop.	14.30 ± 4.03	0	<0.001*
Heights of posterior edge of vertebral body (%)			
Preop.	91.40 ± 1.04	91.88 ± 1.23	0.614
Postop.	95.16 ± 1.88	91.74 ± 7.03	<0.001*
Final follow-up	94.32 ± 1.61	91.70 ± 6.79	<0.001*
Range of spinal shortening postop. (cm)	0.06 ± 0.03	1.57 ± 0.40	<0.001*
Percentage of spinal shortening of single spinal motion segment (%)	1.47 ± 0.57	36.45 ± 6.56	<0.001*

*indicated statistically significant. Preop indicates preoperative; postop, postoperative.

grades. Besides, 60% of patients with a complete deficit(ASIA A)in group B achieved more than 1 grade on the ASIA impairment scale, with a mean recovery of around 1.2 grades. 62.5% of patients with an incomplete deficit in group A achieved more than 1 grade on the ASIA impairment scale, with a mean recovery of around 1 grade. 31.25% of patients with complete deficit achieved more than 1 grade on the ASIA impairment scale, with mean recovery of around 0.56 grades (Table 3).

Local back pain was significantly relieved in all patients after the operation. At the final follow-up, the VAS scores in group A were lower than in group B ($P < 0.05$). There was no difference between the preoperative and postoperative segmental Cobb angle groups. However, the lost segmental Cobb angle in group A was more significant than in group B at the final follow-up ($P < 0.05$) (Table 4). For the complications, one patient in group A and one in group B encountered superficial tissue infection that healed following debridement. Three patients in group A and two patients in group B suffered from urinary tract infections. One patient in group B experienced pneumonia. All respiratory and urinary complications got cured within 2 weeks after the operation.

4. Discussion

Previous literature demonstrated that early surgical treatment, including anterior, posterior, or anterior combined with posterior approaches, and pharmacological therapy

TABLE 3: Neurological status of patients in simple posterior decompression and fixation group and PIVCR and spinal shortening group.

ASIA impairment scale on admission	Group A ($n=32$)					Group B ($n=34$)				
	A	B	C	D	E	A	B	C	D	E
A	11	2	2	1	0	6	5	1	1	2
B		5	2	1	0		2	2	3	3
C			1	2	5				1	8
Total	11	7	5	4	5	6	7	3	5	13

were performed to treat thoracolumbar with SCI and obtained advanced achievements [4–8]. However, neurological improvement is not always ideal after the surgery. The neurological recovery in patients with severe traumatic SCI is particularly limited, especially in those with complete deficits [9–11]. Thus, controversy on the surgical technique treatment is still existed in various thoracolumbar fractures associated with sSCI [4, 5, 11]. Moreover, doubt has also been raised regarding pharmacological therapy in some research, which does not recommend the administration of GM-1 ganglioside and methylprednisolone for the management of acute SCI [26].

The primary traumatic injury resulting from traumatic mechanical injury to the spinal cord could disrupt the dynamics of SCBF and local ischemia-reperfusion, which may result in a further inflammatory response and bring about additional severe neurological injury [8, 27]. The severity of

TABLE 4: Radiographic and clinic outcomes in simple posterior decompression and fixation group and PIVCR and spinal shortening group.

	Segmental kyphosis Cobb			VAS		
	Preop.	Postop.	At final follow-up	Preop.	Postop.	At final follow-up
Group A	24.84 ± 8.00	8.47 ± 2.82	11.19 ± 3.37	7.38 ± 1.24	3.34 ± 0.90	2.22 ± 1.34
Group B	26.85 ± 8.03	7.21 ± 3.38	8.26 ± 3.20	7.65 ± 1.07	3.06 ± 0.98	1.76 ± 1.02
P	0.313	0.105	0.001*	0.342	0.225	0.028*

*indicated statistically significant. Preop indicates preoperative; postop, postoperative; VAS, visual analog scale.

SCI is correlated with the degree of post-traumatic ischemia [28]. A large number of studies on SCI have shown that SCBF is significantly reduced after injury, which could lead to neurological deficits [16, 27, 29]. Werndle et al. and Gallagher et al. also confirm that the intraspinal pressure at the injury site is higher than subdural pressure below the injury or extradural pressure in traumatic SCI patients. Average intraspinal pressure from the patients with traumatic SCI is significantly higher than those without traumatic spinal cord injury, and the higher spinal cord perfusion pressure is correlated with increasing limb motor score [13, 14]. Therefore, surgery procedures including circumferential decompression, direct reduction of the tension in the spinal cord, and improvement of SCBF are all critical for neurological improvement in traumatic SCI patients.

In this study, 89.47% of patients with incomplete deficits underwent PIVCR and spinal shortening. At the final follow-up, patients achieved more than 1 grade on the ASIA scale with a mean recovery of around 1.79 grades. Besides, 60% of patients with complete deficit underwent PIVCR and spinal shortening, which achieved more than 1 grade on the ASIA scale with a mean recovery of around 1.2 grades at the final follow-up. However, 62.5% of patients with incomplete deficit underwent simple posterior decompression and fixation, achieving more than 1 grade on the ASIA impairment scale, with a mean recovery of around 1 grade. Only 31.25% of patients with complete deficit achieved more than 1 grade on the ASIA impairment scale, with a mean recovery of around 0.56 grades. The patients who underwent PIVCR and spinal shortening showed better clinical outcomes in neurological improvement than those who underwent simple posterior decompression and fixation surgery. Compared with the results reported by Harrop et al., Allain et al., and Lin et al., the recovery of neurological function was also significantly better in the group of PIVCR and spinal shortening [9–11]. PIVCR and spinal shortening may be important for neurological recovery in traumatic SCI. It could provide a new choice for the treatment of thoracolumbar fracture associated with sSCI.

Spine-shortening osteotomy has been a new procedure for the treatment of tethered cord syndrome with efficient reduction of neural tension and improvement of neurological deficit [21, 22]. PIVCR and spinal shortening could reduce the spinal cord tension, which could not only achieve the correction rate of spinal deformity safely and effectively but also reduce the risk of neurological deficit secondary to operative procedures and indeed improve neurological deficits [17–19]. Jarvis et al. also found that spinal shortening could provide the effect of spinal cord decompression, improvement in spinal cord perfusion, and improvement in

motor-evoked potentials (MEPs) when a reduction of MEP amplitude of greater than 50% occurred in severe spinal deformity correction [20]. The reperfusion of SCBF is of paramount importance in the improvement of spinal cord function after traumatic SCI. Proper range of spinal shortening brings about vasodilation of the arteries of the spinal cord, which could result in the concomitant reduction of resistance to blood flow and increase the diameter of the anterior spinal artery by 138% compared to base line. Moreover, SCBF could be increased by 111%–160% compared to the base line before shortening [19, 23, 25]. Based on the abovementioned studies, the spinal shortening could reduce the spinal tension and increase SCBF, which are critical for the neurological recovery in sSCI. Advantages including single posterior incision, circumferential decompression, correction in segmental kyphosis, direct reduction in the tension of the spinal cord, improvement of SCBF, intraspinal circumstances, and three-dimensional reconstruction could be brought about by PIVCR and spinal shortening. It could be hypothesized that the function of the remaining corticospinal tract may be waked up, and then it may create favorable conditions for the recovery of neurological function in patients with traumatic SCI in our study.

PIVCR is one of the corpectomy procedures to treat spinal deformity, which was first reported by Suk et al. in 2002 [30]. In the past decades, an increasing number of spinal deformity surgeons have used PIVCR to treat severe, rigid, and angular spinal deformity [31]. We first apply PIVCR procedure to treat thoracolumbar fracture associated with sSCI. The principle of PIVCR procedure in thoracolumbar fractures is appropriate spinal shortening. The total injured vertebrae with adjacent disks are resected completely to achieve 360° circumferential spinal cord decompression. Moreover, the space created by complete resection of vertebrae enables appropriate spinal shortening, reduction of spinal cord tension, and improvement of SCBF. The principle of spinal shortening was that the dural sacs should not be obvious shrinking and buckling. The main criterion to apply the PIVCR and spinal shortening procedure lies in no spinal cord complete transection at preoperative MRI, severe neurological deficit graded as ASIA A/B/C on the admission. PIVCR and spinal shortening are complex and risky techniques and can pose a challenge to surgeons. The risk of this procedure is that the surgical trauma is extensive and the intraoperative bleeding is massive compared to simple posterior decompression and fixation, while it could achieve circumferential decompression, better neurological recovery, less segmental Cobb loss, and fewer surgical complications. The non-neurological

complications of PVCR include the following: a. respiratory system-related complications: pneumonia, pleural effusion, pulmonary embolism, pleural injury, hemopneumothorax, and respiratory failure; b. wound infection; c. excessive bleeding and traumatic coagulopathy; d cardiovascular complications: cardiac arrest, heart failure, arrhythmia, hypotension, and myocardial infarction; and e. deep vein thrombosis [31]. In this study, the complications encountered were including superficial infection, urinary tract infections, and pneumonia.

Some previous studies investigated the safe shortening range by building shortening of spine animal models and clinical experience. Kawahara et al. have confirmed that spinal shortening within 1/3 of the vertebral segment is the safe range which does not result in dural sac deformity. The warning range of spinal shortening could be considered as between 1/3 and 2/3 of the vertebral segment with shrinking and buckling of the dural sac but no spinal cord deformity. The spinal shortening of more than 2/3 of the vertebral segment is a dangerous range that could result in compressing the spinal cord by buckled dura and spinal cord deformity [23]. Ji et al. demonstrate that shortening of 1/2 of a vertebral segment height is safe, while spinal shortening between 1/2 and 2/3 of a vertebral segment may lead to incomplete SCI in canines [25]. Lu et al. report that the tolerance of the spinal cord can be increased and spinal cord injury resulting from angulation can be avoided when the spinal cord is shortened by 1/4 to 2/4 [32]. According to the study by Modi et al., the maximum safe range of spinal shortening in the pig is much to 104.2% of one vertebral body height [24]. However, the conclusion drawn by Modi et al. is based on increasing the length in laminectomy before spinal shortening. A review including seven clinical articles confirms that spinal shortening of 20.5 mm (range, 14 mm–25 mm) is the safe and effective surgical approach for treating tethered cord syndrome in humans [22]. We firmly oppose shortening the whole resection gap in incomplete neurological deficit patients, which may lead to excessive shrinking and warping of the dural sac and neurological deficit. In our study, the spinal shortening range is 1.57 cm and 36.45% of the single spinal motion segment. The range of spinal shortening in our study is similar to the safe range of spinal shortening in the literature reported previously.

There are several limitations to the clinical outcomes of this study due to the characteristics of a retrospective study, especially the limited number of patients and the clinical outcomes which need to be increased for further study. Future clinical prospective studies with larger groups of patients should apply randomization, controlled, and blind approaches in multicenter. Moreover, further study will directly measure the changes in spinal cord tension and SCBF to illuminate its therapeutic mechanism on neurological recovery.

5. Conclusions

PIVCR and spinal shortening is a safe, reliable, and effective surgical method for the treatment of sSCI-related thoracolumbar fractures.

Abbreviations

PIVCR:	Posterior injured vertebra column resection
PVCR:	Posterior vertebra column resection
sSCI:	Severe spinal cord injury
SCBF:	Spinal cord blood flow
MRI:	Magnetic resonance imaging
ASIA:	American Spinal Injury Association
VAS:	Visual analog scale
MEP:	Motor-evoked potentials.

Data Availability

The datasets used and analyzed during the current study are available from the corresponding author upon reasonable request.

Conflicts of Interest

The authors declare that they have no conflicts of interest.

Acknowledgments

This study was supported by grants from the National Natural Science Foundation of China (No. 81560373, 81860403) and grants from the “Special and Joint Program” of Yunnan Provincial Science and Technology Department & Kunming Medical University (No. 2017FE467(-009)).

References

- [1] M. Wyndaele and J. J. Wyndaele, “Incidence, prevalence and epidemiology of spinal cord injury: what learns a worldwide literature survey?” *Spinal Cord*, vol. 44, no. 9, pp. 523–529, 2006 Sep.
- [2] S. B. Jazayeri, S. Beygi, F. Shokraneh, E. M. Hagen, and V. Rahimi-Movaghar, “Incidence of traumatic spinal cord injury worldwide: a systematic review,” *European Spine Journal*, vol. 24, no. 5, pp. 905–918, 2015 May.
- [3] F. Magerl, M. Aebi, S. D. Gertzbein, J. Harms, and S. Nazarian, “A comprehensive classification of thoracic and lumbar injuries,” *European Spine Journal*, vol. 3, no. 4, pp. 184–201, 1994.
- [4] T. Tan, J. Rutges, T. Marion et al., “Anterior versus posterior approach in traumatic thoracolumbar burst fractures deemed for surgical management: systematic review and meta-analysis,” *Journal of Clinical Neuroscience*, vol. 70, pp. 189–197, 2019 Dec.
- [5] P. Oprel, W. E. Tuinebreijer, and P. Patka, D. den Hartog, Combined anterior-posterior surgery versus posterior surgery for thoracolumbar burst fractures: a systematic review of the literature,” *The Open Orthopaedics Journal*, vol. 4, no. 1, pp. 93–100, 2010 Feb 17.
- [6] K. B. Wood and W. Li, D. S. Lebl and A. Ploumis, Management of thoracolumbar spine fractures,” *The Spine Journal*, vol. 14, no. 1, pp. 145–164, 2014 Jan.
- [7] Y. P. Charles and J. P. Steib, “Management of thoracolumbar spine fractures with neurologic disorder,” *Orthopaedics and Traumatology: Surgery & Research*, vol. 101, no. 1, pp. S31–S40, 2015 Feb.

- [8] D. C. Baptiste and M. G. Fehlings, "Update on the treatment of spinal cord injury," *Progress in Brain Research*, vol. 161, pp. 217–233, 2007.
- [9] J. S. Harrop, S. Naroji, M. G. Maltenfort et al., "Neurologic improvement after thoracic, thoracolumbar, and lumbar spinal cord (conus medullaris) injuries," *Spine*, vol. 36, no. 1, pp. 21–25, 2011.
- [10] J. Allain, "Anterior spine surgery in recent thoracolumbar fractures: an update," *Orthopaedics and Traumatology: Surgery & Research*, vol. 97, no. 5, pp. 541–554, 2011 Sep.
- [11] B. Lin, Z. W. Chen, Z. M. Guo, H. Liu, and Z. K. Yi, "Anterior approach versus posterior approach with Subtotal corpectomy, decompression, and reconstruction of spine in the treatment of thoracolumbar burst fractures," *Journal of Spinal Disorders & Techniques*, vol. 25, no. 6, pp. 1–317, 2011 Aug.
- [12] I. Qadir, K. D. Riew, S. R. Alam, R. Akram, M. Waqas, and A. Aziz, "Timing of surgery in thoracolumbar spine injury: impact on neurological outcome," *Global Spine Journal*, vol. 10, no. 7, pp. 826–831, 2020 Oct.
- [13] M. C. Werndle, S. Saadoun, I. Phang et al., "Monitoring of spinal cord perfusion pressure in acute spinal cord injury," *Critical Care Medicine*, vol. 42, no. 3, pp. 646–655, 2014 Mar.
- [14] M. J. Gallagher, F. R. A. Hogg, A. Zoumprouli, M. C. Papadopoulos, and S. Saadoun, "Spinal cord blood flow in patients with acute spinal cord injuries," *Journal of Neurotrauma*, vol. 36, no. 6, pp. 919–929, 2019 Mar 19.
- [15] C. H. Tator and M. G. Fehlings, "Review of the secondary injury theory of acute spinal cord trauma with emphasis on vascular mechanisms," *Journal of Neurosurgery*, vol. 75, no. 1, pp. 15–26, 1991 Jul.
- [16] A. Holtz, B. Nyström, and B. Gerdin, "Relation between spinal cord blood flow and functional recovery after blocking weight-induced spinal cord injury in rats," *Neurosurgery*, vol. 26, no. 6, pp. 952–957, 1990 Jun.
- [17] Y. Wang, J. Xie, Z. Zhao, Y. Zhang, T. Li, and Y. Si, "Changes in CSF flow after one-stage posterior vertebral column resection in scoliosis patients with syringomyelia and Chiari malformation Type I," *Journal of Neurosurgery: Spine*, vol. 18, no. 5, pp. 456–464, 2013 May.
- [18] J. M. Xie, Y. S. Wang, Z. Zhao et al., "Posterior vertebral column resection for correction of rigid spinal deformity curves greater than 100°," *Journal of Neurosurgery: Spine*, vol. 17, no. 6, pp. 540–551, 2012 Dec.
- [19] T. Li, Z. Zhao, Y. Wang et al., "A preliminary study of spinal cord blood flow during PVCR with spinal column shortening," *Medicine (Baltimore)*, vol. 99, no. 32, Article ID e21579, 2020 Aug 7.
- [20] J. G. Jarvis, S. Strantzas, M. Lipkus et al., "Responding to neuromonitoring changes in 3-column posterior spinal osteotomies for rigid pediatric spinal deformities," *Spine*, vol. 38, no. 8, pp. E493–E503, 2013.
- [21] A. W. Grande, P. C. Maher, C. J. Morgan et al., "Vertebral column subtraction osteotomy for recurrent tethered cord syndrome in adults: a cadaveric study," *Journal of Neurosurgery: Spine*, vol. 4, no. 6, pp. 478–484, 2006 Jun.
- [22] P. C. Hsieh, C. J. Stapleton, P. Moldavskiy et al., "Posterior vertebral column subtraction osteotomy for the treatment of tethered cord syndrome: review of the literature and clinical outcomes of all cases reported to date," *Neurosurgical Focus*, vol. 29, no. 1, p. E6, 2010 Jul.
- [23] N. Kawahara, K. Tomita, T. Kobayashi, M. E. Abdel-Wanis, H. Murakami, and T. Akamaru, "Influence of acute shortening on the spinal cord: an experimental study," *Spine*, vol. 30, no. 6, pp. 613–620, 2005 Mar 15.
- [24] H. N. Modi, S. W. Suh, J. Y. Hong, and J. H. Yang, "The effects of spinal cord injury induced by shortening on motor evoked potentials and spinal cord blood flow," *Journal of Bone and Joint Surgery*, vol. 93, no. 19, pp. 1781–1789, 2011.
- [25] L. Ji, X. Q. Dang, B. S. Lan et al., "Study on the safe range of shortening of the spinal cord in canine models," *Spinal Cord*, vol. 51, no. 2, pp. 134–138, 2013 Feb.
- [26] R. J. Hurlbert, M. N. Hadley, B. C. Walters et al., "Pharmacological therapy for acute spinal cord injury," *Neurosurgery*, vol. 72, no. supplement 2, pp. 93–105, 2013 Mar.
- [27] H. J. Senter and J. L. Venes, "Altered blood flow and secondary injury in experimental spinal cord trauma," *Journal of Neurosurgery*, vol. 49, no. 4, pp. 569–578, 1978 Oct.
- [28] M. G. Fehlings, C. H. Tator and R. Linden, "The relationships among the severity of spinal cord injury, motor and somatosensory evoked potentials and spinal cord blood flow," *Electroencephalography and Clinical Neurophysiology: Evoked Potentials Section*, vol. 74, no. 4, pp. 241–259, 1989.
- [29] N. E. Epstein, M. Alshareef, V. Krishna et al., "Effect of spinal cord compression on local vascular blood flow and perfusion capacity by," *Surgical Neurology International*, vol. 7, no. 26, pp. 682–685, 2016 Sep 22.
- [30] S. I. Suk, J. H. Kim, W. J. Kim, S. M. Lee, E. R. Chung, and K. H. Nah, "Posterior vertebral column resection for severe spinal deformities," *Spine*, vol. 27, no. 21, pp. 2374–2382, 2002.
- [31] J. M. Xie, Z. Q. Chen, J. X. Shen et al., "Expert consensus for PVCR in severe, rigid and angular spinal deformity treatment: the Kunming consensus," *Journal of Orthopaedic Surgery*, vol. 25, no. 2, Article ID 230949901771393, 2017 May-Aug.
- [32] Q. A. Lu, Y. S. Wang, J. M. Xie et al., "Effect of spinal shortening for protection of spinal cord function in canines with spinal cord angulation," *Medical Science Monitor*, vol. 25, pp. 9192–9199, 2019 Dec 2.

Research Article

Effect and Safety of Painless and Conventional Endoscopic Management of Denture Impaction in the Esophagus

Li li Tian 

Second Hospital of Shanxi Medical University, Digestive Endoscopy Center, Taiyuan 030001, Shanxi Province, China

Correspondence should be addressed to Li li Tian; tianlili202207@163.com

Received 5 July 2022; Revised 3 September 2022; Accepted 9 September 2022; Published 26 September 2022

Academic Editor: Dong Chen

Copyright © 2022 Li li Tian. This is an open access article distributed under the Creative Commons Attribution License, which permits unrestricted use, distribution, and reproduction in any medium, provided the original work is properly cited.

Objective. To improve the level of clinical diagnosis and treatment, reduce the incidence of complications, and provide the basis for clinicians to choose an appropriate treatment, this research explores the removal methods of the impacted denture in the esophagus by endoscopy. **Methods.** Based on the clinical information, treatment methods and complications of 72 patients with denture impaction in the esophagus admitted to our hospital from January 2016 to March 2021, which were divided into the group treated with painless endoscopy and the group treated with conventional endoscopy, retrospective analysis of the therapeutic effect and complications was conducted. **Results.** There was no statistically significant difference between the two groups in terms of denture removal rate ($P > 0.05$). There were statistically significant differences between the two groups in terms of operating time and incidence rates of complications during and after the procedure. The operating time of the group treated with painless endoscopy was significantly shorter than the group treated with conventional endoscopy ($P < 0.05$). The incidence rates of complications during and after the procedure of the group treated with painless endoscopy were significantly lower than the group treated with conventional endoscopy ($P < 0.05$). **Conclusions.** Compared with the conventional endoscopy, painless endoscopic management of denture impaction in the esophagus under general anesthesia with tracheal intubation improves the clinical efficacy and reduces the adverse reactions. Thus, it is worthy of clinical popularization and application.

1. Introduction

The upper digestive tract foreign body refers to the upper digestive tract that can not be digested and can not be discharged from the body. Once the upper gastrointestinal foreign body is diagnosed, the size, shape, type, quantity, and location of the foreign body should be known in time to formulate a treatment plan. At present, the common treatment methods for the gastrointestinal foreign body include natural discharge, endoscopic therapy, and surgery [1]. From the published literature, it can be seen that the patients with gastrointestinal foreign bodies in China are mainly treated with sharp foreign bodies such as date pit, bone, and denture. Due to the different types of upper gastrointestinal foreign body, the clinical symptoms and harmfulness are also different [2]. An upper gastrointestinal foreign body is a common digestive emergency in China, requiring emergency treatment. If not handled in time,

patients may suffer from complications such as fullness, clonic pain, pyloric obstruction, and even death [3, 4]. In China, 70%–75% of upper gastrointestinal foreign bodies are trapped in the esophagus, with the esophageal inlet being the most common [3, 5]. With the improvement in living standard, the utilization rate of the denture in elderly patients in China is high, and denture has become a common upper digestive tract foreign body. Because the sharp denture with metal clasps at both ends is easily immobilized in the alimentary canal wall and cannot be discharged from the body by itself, it is difficult to remove. If not removed in time, it may lead to massive bleeding, perforation, infection, and damage to adjacent organs, and even endanger life in serious cases. Therefore, it is particularly important for the timely treatment of esophageal immobilized dentures. Emergency gastroscopy for the treatment of the upper gastrointestinal foreign body is a method with high safety and success rate [5, 6], including ordinary gastroscopy and painless

gastroscopy. If the sharp object is incarcerated in the esophagus, the impaction of the food ball may cause high obstruction, which requires urgent endoscopic treatment. Compared with surgical operation, endoscopic foreign body removal has the advantages of less trauma, lower cost, and relatively simple operation, which has become the most important means for the treatment of the esophageal foreign body. However, in clinical practice, patients are often reluctant to cooperate in the removal of esophageal foreign bodies under local anesthesia because of fear. Moreover, if the surface local anesthesia is not sufficient, it may cause severe vomiting and struggle, head and neck twisting, and even sitting up, especially for patients with a short neck, mental tension, cervical diseases, and foreign bodies that are difficult to deal with. In these cases, when the gastroscope enters the closed esophageal entrance, it is difficult to see the relationship between the foreign body and the esophagus. If the operation is performed blindly, especially when the forceps are used to remove sharp foreign bodies, such as dentures and nails, because the foreign bodies are often pierced into the esophagus wall, the patient may experience muscle tension. If the doctor's operation is rough, forced clip out, complications will increase significantly. Mild cases of esophageal mucosal injury, bleeding, esophageal perforation and surrounding tissue infection, mediastinal abscess, and other complications, severe cases can injure the aorta, the formation of esophageal aortic fistula, the occurrence of massive bleeding and death. The general anesthesia operation does not involve the patient's cooperation problem. The nondepolarizing agent used can the maximum limit to remove esophageal muscle cramps or lower esophageal muscle tension, especially in the ring at the top of the esophagus pharyngeal constrictor flabby muscle, swallow, reduces the gastroscope to the operation field and friction resistance, promotes the insertion of a gastroscope, thereby reducing bleeding, guarantee the sharpness of the operation field, avoid the blindness of operation, reduce the occurrence of complications, is advantageous to the foreign body removed, And ultimately improve the success rate of surgery.

At present, there are few comparative studies on the safety and effectiveness of ordinary gastroscopy and painless gastroscopy in the treatment of esophageal denture incarceration. This study aims to analyze and compare the treatment success rate and intraoperative and postoperative complications of ordinary gastroscopy and painless gastroscopy in order to provide clinical guidance for the treatment of esophageal denture incarceration.

2. Data and Methods

2.1. The General Information. The clinical data of 78 patients diagnosed and treated with esophageal denture incarceration in the Second Hospital of Shanxi Medical University from January 2014 to May 2021 were retrospectively analyzed. There were 42 males and 36 females, with a male to female ratio of 1.17:1. The average age was (63.9 ± 7.96) years old from 51 to 82 years old, including 28 (35.9%) ≤ 60 years old, 34 (43.6%) from 61 to 70 years old, 15 (19.2%) from 71 to 80 years old, and 1 (1.3%) > 80 years old. 62 cases

(79.5%) and 16 cases (20.5%) were diagnosed within 24~48 hours after onset. 38 patients were treated by endotracheal intubation under general anesthesia, and 40 patients were treated by ordinary gastroscopy outside the class.

2.2. Methods. Preoperative preparation: after the patient was admitted to the emergency department of our hospital, detailed medical history was asked, and a chest X-ray examination was performed to determine the location of foreign bodies. For foreign bodies in the middle esophagus, a chest CT examination was required to observe the relationship between foreign bodies and the aorta and heart, and urgent blood routine examination, coagulation, and electrocardiogram examination were performed. Inform the patient's family and sign the consent form. Patients in the class were evaluated by professional anesthesiologists and treated under general anesthesia after endotracheal intubation, while patients outside the class were treated under ordinary gastroscopy.

Operating apparatus: Olympus Q260 endoscopic, Olympus Q290 endoscopic, Rubber cover, transparent cap, foreign body forceps, net basket, and trap.

Procedure: for the ordinary group, local anesthesia was performed in the oropharynx with lidocaine hydrochloride slurry; for the painless group, general anesthesia was performed in the state of tracheal intubation. The endoscope was slowly entered through the left piriform pit with a transparent cap, and the closed esophageal inlet mucosa was removed with the transparent cap to obtain a better operating field [7]. After careful observation, if a denture is found (see Figure 1), carefully explore the position and incarceration of a denture, remove incarceration with foreign body forceps (see Figure 2) and align the long axis of the denture with the axis of the esophagus, place one side of metal clapping into the transparent cap, and slowly remove the foreign body. If it is not easy to remove, the denture can be slowly put into the stomach cavity, or if the denture has entered the stomach cavity before treatment, the endoscope should be withdrawn first, and then the rubber sleeve should be put into the stomach cavity with the endoscope. With the aid of foreign body forceps, snare, or net baskets, the denture was loaded into the rubber sleeve (see Figure 3). The foreign body forceps clamped the denture and rubber sleeve, adjusted the direction of the denture to make the long axis of the denture consistent with the long axis of the esophagus, and slowly removed the denture. For the common group of patients, when the denture was taken to the esophagus entrance, the patient was instructed to swallow, the mandible was raised, and the denture was slowly removed. If the denture clings are deeply embedded in the esophageal wall or too large to pass through the esophageal inlet, and the removal fails, the patient will be transferred to surgical treatment.

2.3. Observation Indicators. The successful removal rate and operation time of foreign bodies were compared between the two groups, and the occurrence of intraoperative and postoperative complications were observed between the two groups.

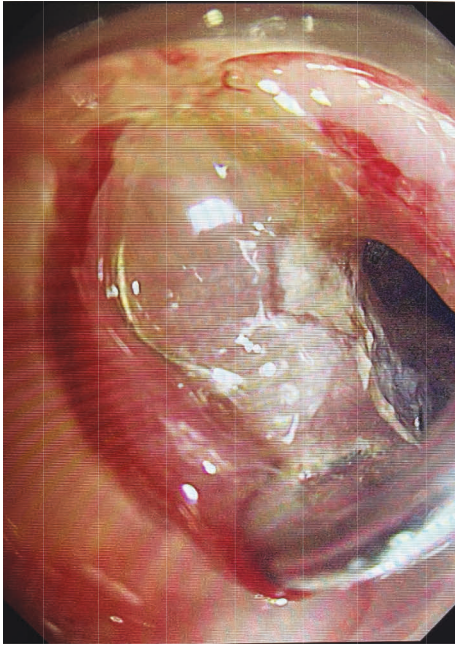


FIGURE 1: Esophageal incarceration denture.

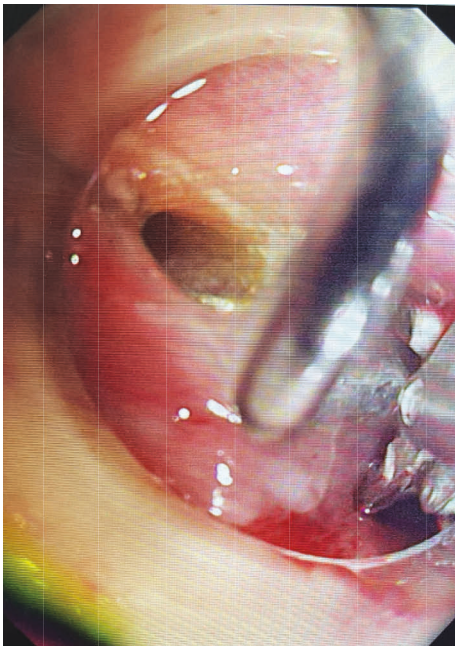


FIGURE 2: Foreign body forceps clamp denture.

2.4. Statistical Analysis. SPSS 23 statistical software was used for statistical analysis. All data were in accordance with normal distribution, the mean value of measurement data were expressed as mean \pm standard deviation ($\bar{x} \pm S$), the comparison between two groups was analyzed by two independent sample *T* test, the counting data were expressed as percentage (%), and the comparison between groups was conducted by χ^2 test. $P < 0.05$ was considered statistically significant.

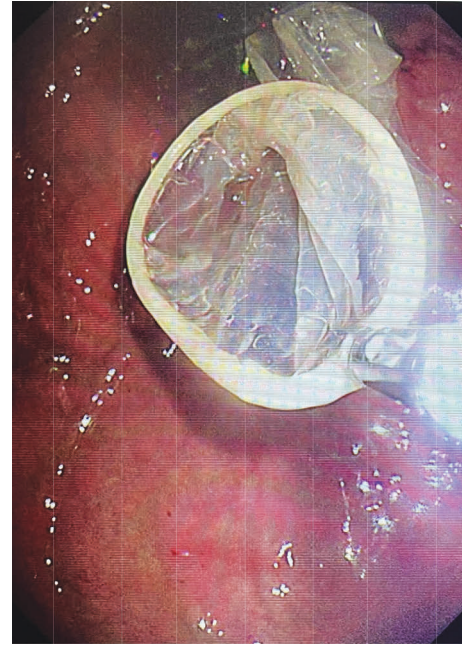


FIGURE 3: The denture in the stomach cavity is inside the rubber sheath.

3. Results

3.1. Comparison of Foreign Body Removal Success Rate and Removal Time between the Ordinary Group and the Painless Group. The success rate of foreign body removal in the painless group was 97.3%, lower than that in the normal group (87.5%), and the difference was not statistically significant ($P > 0.05$). The time of foreign body removal in the painless group was significantly shorter than that in the normal group, and the difference was statistically significant ($P < 0.05$), as shown in Table 1.

3.2. The Incidence of Intraoperative and Postoperative Complications in the Normal Group and the Painless Group. In terms of the incidence of total intraoperative and postoperative complications, the painless group was significantly better than the normal group, with statistically significant differences ($P < 0.05$), as shown in Table 2. No serious complications occurred in all patients, similar to previous studies [8]. No major bleeding was observed during the operation. For the small amount of bleeding, the hemostasis can be stopped by ice saline irrigation under endoscopy and endoscopic compression. For local mucous membrane injury, acid suppression, and protection of mucous membrane treatment. For the patients with esophageal perforation, endoscopic placement of the nasojejunal nutrition tube and nasal feeding diet improved significantly.

4. Discussion

The denture is a common cause of esophageal foreign body incarceration, which is mostly seen in the elderly [9]. However, due to the X-ray transparency of denture materials, it is often difficult to get a clear diagnosis in time,

TABLE 1: Comparison of extraction success rate and operation time between ordinary group and painless group.

Groups	Take out the successful (<i>n</i> , %)	Take out the failure (<i>n</i> , %)	Operating time (min, $\bar{x} \pm s$)
Normal group	35 (87.5%)	5 (12.5%)	17.55 \pm 1.77
Painless group	37 (97.3%)	1 (2.7%)	15.33 \pm 1.93
χ^2 (<i>t</i>)	1.464		5.290
<i>P</i>	0.226		0.000

TABLE 2: Comparison of intraoperative and postoperative complications between the normal group and the painless group (*n*, %).

Groups	Mucosal injury	Bleeding	Perforated	Infection	Aspiration	Total
Normal group	8 (20.0%)	2 (5.00%)	3 (7.50%)	1 (2.50%)	2 (5.0%)	16 (40.0%)
Painless group	3 (7.89%)	0 (0%)	1 (2.63%)	0 (0%)	1 (2.63%)	5 (13.15%)
χ^2	1.464	0.462	0.212	0	0	5.837
<i>P</i>	0.226	0.497	0.645	1.000	1.000	0.016

affecting treatment [10]. Therefore, esophageal denture incarceration is prone to a higher risk of complications, such as esophageal perforation, diverticulum, fistula formation, or intestinal obstruction, which may endanger life. How to treat esophageal denture incarceration in an effective way is of great significance to the life safety of patients.

At present, with the progress of various minimally invasive techniques under gastroscopy, gastroscopy has become the preferred treatment for the removal of upper gastrointestinal foreign bodies [11]. Endoscopic treatment of gastrointestinal foreign body has the advantages of small trauma, high success rate, low risk, and low cost [12, 13]. Studies have shown that emergency endoscopic extraction should be performed actively for dentures incarcerated in the esophagus [14–16]. Removal of an upper gastrointestinal foreign body by ordinary gastroscopy is simple and economical, but it is easy to cause adverse reactions such as nausea and vomiting in patients during the operation [17]. With the rapid development of medical technology, painless gastroscopy has become increasingly mature and widely used in clinical practice. However, there are still little research data on its application in removing incarcerated denture of the esophagus. Exploring the safe and effective extraction method of esophageal incarceration denture under endoscopy can better guide clinicians in choosing the appropriate treatment mode, improve the success rate of surgery and reduce clinical complications.

Observation and analysis of dentures incarcerated in the esophagus treated by emergency endoscopy in our department showed that most of them had sharp reverse multiple metal clasps, which were easily incarcerated in the three strictures of the esophagus, and the first stenosis (esophageal entrance) was more common [18, 19]. Usually, the esophagus entrance is closed and relatively narrow.

However, in the treatment of ordinary gastroscopy, the patient's treatment compliance is poor due to pharyngeal irritation, tension, and fear, and the operator needs to enter the scope several times. The patient's nausea and involuntary defensive actions make the operation more difficult [15, 20, 21]. Zhang et al. [22] study found that propofol intravenous anesthesia raised the success rate of the esophageal foreign body at the same time can shorten the treatment time, avoid taking too much for patients in the

process of foreign body reaction mucosal injury, at the same time can also be used for criminals, children and mental patients cannot cooperate with the special groups, such as expanded gastroscopy treatment indications. The painless method is general anesthesia under tracheal intubation, which can not only put the patient in an unconscious state but also relax the esophageal muscle of the patient. Muscle relaxation drugs cause the muscles at the entrance of the esophagus to be in a relaxed state, which relaxes the most easily incarcerated foreign bodies and reduces the operation difficulty of removing incarceration and removing foreign bodies [23]. In addition, under tracheal intubation and general anesthesia, the use of muscle relaxants can avoid secondary mucosal damage, and even perforation of the inverted metal clings at the entrance of the esophagus during the removal of partial removable dentures with occluded metal clings in the middle and lower segments of the esophagus and stomach, thus improving the success rate of removal and reducing the incidence of complications. From this retrospective study, we found that there was no statistically significant difference in the success rate of removing dentures between ordinary gastroscopy and painless endotracheal intubation under gastroscopy, suggesting that painless gastroscopy is an effective operation for removing occluded dentures. In terms of operation time and intraoperative complications, compared with the ordinary group, painless treatment with endotracheal intubation has obvious advantages, suggesting that painless gastroscopic removal of esophageal impingement denture is relatively safe and conducive to the smooth development of the treatment process. In addition, compared with ordinary gastroscopy, painless gastroscopy has fewer postoperative complications, suggesting that painless gastroscopy is relatively safe. Therefore, this study concluded that painless gastroscopy is a safe, effective, and ideal means for the treatment of esophageal incarceration dentures, with obvious overall advantages and worthy of widespread promotion and application in clinical practice.

Current problems that need to be improved: tools for foreign body removal: various applicable instruments that need to be developed because of the variety of foreign body types and shapes. ② Gastroscopy also has its own limitations: in cases where the foreign body is small, stays for a

long time, and the surrounding hematoma is formed, it is more difficult to clamp the foreign body because it does not show well. For patients with both ends of the foreign body inserted into the anterior and posterior walls of the esophagus, do not rush to clamp the foreign body after discovery. The operation should be cautious and careful, do not take it roughly and forcibly. Otherwise, it may cause perforation, and avoid surgery as much as possible. ③ When withdrawing the foreign body and gastroscope together, be sure to confirm whether the foreign body clamp grasps the foreign body firmly to avoid dropping the foreign body in the epiglottis when withdrawing or even aspirating to the trachea by mistake. If not handled properly, the consequences of accidental aspiration to the trachea are severe. ④ If other diseases or perforation risks are associated, timely hospitalization should be followed by treatment, and relevant departments should fully collaborate in preparing for resuscitation surgery.

5. Conclusion

In conclusion, compared with ordinary gastroscopy, painless gastroscopy is recommended for the clinical treatment of incarcerated dentures. Painless gastroscopy has high safety, high patient compliance and comfort, low incidence of adverse reactions, fewer postoperative complications, ideal prognosis, and simple operation. Of course, this study is a retrospective study, and some clinical data, such as the size of a denture and the number of a metal clasp, cannot be accurately counted, which may have a corresponding impact on the results. Therefore, more prospective, multi-center studies are needed to clarify further.

Data Availability

The datasets generated during and/or analyzed during the current study are available from the author on reasonable request.

Conflicts of Interest

The author declares that there are no conflicts of interest.

References

- [1] S. O. Ikenberry, T. L. Jue, M. A. Anderson et al., "Management of ingested foreign bodies and food impactions," *Gastrointestinal Endoscopy*, vol. 73, no. 6, pp. 1085–1091, 2011.
- [2] Institute of Public Health and Medical Health Management Chinese Enterprise Management Society, "Expert consensus on emergency management of esophageal foreign body in adult," *Chinese Journal of Critical Care Medicine*, vol. 13, no. 6, pp. 446–452, 2020.
- [3] D. Endoscopy Society of Chinese Medical Association, *Chinese journal of digestive endoscopy*, vol. 33, no. 1, pp. 19–27, 2016.
- [4] Q. Zhao, Y. Zhao, S. Li et al., "Impact of ambient temperature on clinical visits for cardio-respiratory diseases in rural villages in northwest China," *The Science of the Total Environment*, vol. 612, no. 5, pp. 379–385, 2018.
- [5] D. Xu, Q. L. Li, and P. H. Zhou, "The safety and feasibility of endoscopic treatment for upper gastrointestinal tract foreign bodies in elderly patients over 80 years old," *Chinese Journal of General Surgery*, vol. 22, no. 11, pp. 1078–1081, 2019.
- [6] J. H. Hu, J. H. Ma, and J. J. Li, "Emergency gastroscopic treatment of 152 cases of upper gastrointestinal foreign body and discussion," *Chinese Journal of Emergency Medicine*, vol. 26, no. 2, pp. 214–215, 2017.
- [7] S. Zhang, J. Wang, J. Wang, B. Zhong, M. Chen, and Y. Cui, "Transparent cap-assisted endoscopic management of foreign bodies in the upper esophagus: a randomized, controlled trial controlled trial," *Journal of Gastroenterology and Hepatology*, vol. 28, no. 8, pp. 1339–1342, 2013.
- [8] C. Sugawa, H. Ono, M. Taleb, and C. E. Lucas, "Endoscopic management of foreign bodies in the upper gastrointestinal tract: a review," *World Journal of Gastrointestinal Endoscopy*, vol. 16, no. 10, pp. 475–481, 2014.
- [9] A. A. Adeyemo and S. A. Ogunkeyede, "Denture impaction in the oesophagus: correlation of site and duration of impaction with sequelae," *Annals of Ibadan Postgraduate Medicine*, vol. 17, no. 1, pp. 65–70, 2019.
- [10] S. Samargandy, H. Marzouki, T. Al-Khatib, and M. Merdad, "Denture impaction causing an upper esophageal diverticulum," *Case Rep Gastrointest Med*, vol. 2019, Article ID 9621383, 2019.
- [11] D. Predescu, I. Predescu, C. Sarafoleanu, and S. Constantinoiu, "Oesophageal foreign bodies-from diagnostic challenge to therapeutic dilemma," *Chirurgia*, vol. 111, no. 2, pp. 102–114, 2016.
- [12] C. Lee, B. Kao, C. Wu et al., "Retrospective analysis of endoscopic management of foreign bodies in the upper gastrointestinal tract of adults," *I Chin Med Assoc*, vol. 82, no. 2, pp. 105–109, 2019.
- [13] W. C. Conway, C. Sugawa, H. Ono, and C. E. Lucas, "Upper GI foreign body: an adult urban emergency hospital experience," *Surg Endosc*, vol. 21, no. 3, pp. 455–460, 2007.
- [14] J. Z. Liu and P. H. Zhou, "Endoscopic treatment of upper gastrointestinal foreign body in 714 cases," *Chinese Journal of gastroendoscopy*, vol. 29, no. 1, pp. 46–47, 2012.
- [15] H. Xu, J. H. Lin, and Z. S. Li, "Endoscopic treatment of upper gastrointestinal foreign body in China," *Chinese Journal of gastroendoscopy*, vol. 33, no. 11, pp. 813–816, 2016.
- [16] J. Wu, L. Pang, and X. Y. Ma, "Clinical efficacy and safety analysis of painless gastroscopy and routine gastroscopy in the treatment of upper gastrointestinal foreign body," *Chinese Journal of Preventive Medicine*, vol. 16, no. 11, pp. 53–55, 2011.
- [17] Y. P. Zhai, "Comparison of conventional gastroscopy and painless gastroscopy in patients with upper gastrointestinal foreign body," *Chinese Journal of Medical Device Information*, vol. 27, no. 11, pp. 102–103, 2021.
- [18] M. H. Emara, E. M. Darwiesh, M. M. Refaey, and S. M. Galal, "Endoscopic removal of foreign bodies from the upper gastrointestinal tract: 5-year experience," *Clinical and Experimental Gastroenterology*, vol. 7, pp. 249–253, 2014.
- [19] S. H. Zhang, Y. Cui, X. R. Gong, G. Fang, C. Minhu, and Z. Bihui, "Endoscopic treatment of 561 cases of upper gastrointestinal foreign body in 10 years," *Chinese journal of digestive endoscopy*, vol. 25, no. 10, pp. 541–544, 2008.
- [20] M. Hua, X. F. Yan, and W. F. Zhang, "Analysis of risk factors for removal of gastrointestinal foreign body under gastroscopy," *Hebei medicine*, vol. 40, no. 11, pp. 1662–1666, 2018.
- [21] W. Y. Yu, X. P. Ding, and K. G. Zhang, "An exploratory scoring system for the successful removal of esophageal

- foreign bodies under gastroscopy,” *Journal of Anhui medical university*, vol. 54, no. 10, pp. 1656–1658, 2019.
- [22] J. Zhang, B. M. Wang, and H. L. Cao, “Application of intravenous anesthesia with propofol in the removal of esophageal foreign body,” *Tianjin medicine*, vol. 38, no. 9, pp. 804-805, 2010.
- [23] L. Y. Luo, “Effects of painless gastroscopy on stress response and adverse reactions of upper gastrointestinal foreign body,” *Forum on primary medicine*, vol. 24, no. 17, pp. 2424-2425, 2020.

Research Article

Pan-Cancer Gene Analysis of m6A Modification and Immune Infiltration in Uterine Corpus Endometrial Carcinoma

Bing-fan Xie, Yan Xia, Dan-huan Lin, Bing Lian, Meng-li Zhang, Lu Liu, and Chun-Rong Qin 

*The Reproductive Medical Center,
Shenzhen Maternity and Child Healthcare Hospital The First School of Clinical Medicine Southern Medical University,
Guangzhou 518000, Guangdong Province, China*

Correspondence should be addressed to Chun-Rong Qin; 2016150217@jou.edu.cn

Received 16 May 2022; Revised 21 June 2022; Accepted 11 July 2022; Published 26 September 2022

Academic Editor: Dong Chen

Copyright © 2022 Bing-fan Xie et al. This is an open access article distributed under the Creative Commons Attribution License, which permits unrestricted use, distribution, and reproduction in any medium, provided the original work is properly cited.

Objective. This investigation was to test the potential role of m6A-related long non-coding RNAs (lncRNAs) and immune infiltration as crucial factors in the diagnosis and treatment of uterine corpus endometrial cancer (UCEC). **Method.** The UCEC RNA-seq data were downloaded in the Cancer Genome Atlas (TCGA, <https://portal.gdc.cancer.gov/>). There were 587 samples totally, containing 543 UCEC cases and 35 healthy cases. The clinical information of UCEC cases included survival time, survival status, gender, age, stage, and TMN stage. Twenty-three m6A-related genes were found in published journals. The RNA-seq documents of UCEC were downloaded in the Cancer Genome Atlas (TCGA). The hub gene data of UCEC were downloaded from GEPIA2 database. The different packages of R language were applied to calculate and analyze in this research. **Results.** Among 587 cases in our study, we discovered 3039 lncRNAs in the TCGA-UCEC database. After the differential analysis, 23 m6A-associated genetics were screened and twenty-one m6A-associated differential genetics were found. In the end, we obtained 20 m6A-related lncRNAs. LNCTAM34A was considered as a predictive gene through univariate and multivariate Cox regression analysis. In addition to the above, patients with high LNCTAM34A expression had better outcomes than those with low LNCTAM34A expression. The high-risk cohort had greater scores of activated dendritic cells (aDCs), B cells, and T cell regulatory (Tregs) than low-risk cohort; in the meanwhile, high-risk cohort had lower scores of DCs and iDCs. Then, the high-risk cohort displayed greater scores in the immune functions of MHC class I, para-inflammation, and type I IFN response than those of low-risk cohort. Among 27 immune-inducible genes, the level of CD244, KIR3DL1, NRP1, PDCD1LG2, and TNFRSF8 was reduced in UCEC samples and the level of CD27, CD28, CD70, CD80, CD86, HAVCR2, ICOS, IDO1, LAIR1, PDCD1, TIGIT, TNFRSF18, -25, -9, -14, and VTCN1 was increased in UCEC samples. **Conclusion.** The key role of M6A-related lncRNAs in immune microenvironment in high-risk patients of UCEC. The patients with strong expression of LNCTAM34A have a good prognosis, and LNCTAM34A can be used as a prognostic gene for UCEC. m6A-related lncRNAs can be used as a potential treatment for UCEC. Our observations can be used as a hypothetical basis for future in vitro and animal experiments.

1. Introduction

Uterine corpus endometrial carcinoma (UCEC) is still the most frequently diagnosed disease of the female reproductive system in industrialized economies, accounting for over 83% in endometrial carcinoma (EC) [1, 2]. So, even though surgical intervention alone might help treat many UCEC patients, a massive number of female patients with

more aggressive histopathological type of the EC continue to have a worse prognosis. At present, there are two main problems in clinic, one of which is the problem of diagnosis, and the other is the difficulty of treatment. The difficulty of diagnosis reflects how to identify risk factors on the basis of biopsy. The difficulty of treatment lies in how to determine the type of adjuvant therapy by using the scope of adjuvant surgery and postoperative evaluation of risk biomarkers [3].

There is accumulating proof that genome destabilization, activation of oncogenes, abnormal methylated modifications, altered epigenetics, unusual expression of microRNAs, and changes in switching signaling processes are the key players and contribute to the malignant pathogenesis [4–7]. Methylation is an important epigenetic modification that is linked to oncogenesis [8]. In eukaryotes, N6-methyladenine (m6A) has been one of the most widely known methylation patterns [9]. According to recent findings, m6A modifications may behave as biologically relevant epigenetic indicators in biological mechanisms [10, 11].

m6A is one of the commonest RNAs modified in all eukaryotes, regulating RNA properties like the ability to splice and encode proteins through writers, erasers, and readers [12]. The m6A modification can be found in a variety of RNA and DNA molecules [13] and even alter the fate of carcinoma cells [14]. According to epi-transcriptomic research, m6A modifications in the transcribed various gene mutations like MYC are engaged in malignant growth and metastatic spread [15]. The abnormal interaction with both writers and erasers, which results from changes in their interpretation, has been connected to the pathological process of carcinoma [16]. However, the m6A genome of endometrial cancer remains unclear in terms of pan-cancer variations.

Despite increasing evidence that m6A factors influence the presence and progression of tumors, the involvement of the role of m6A modified lncRNAs in UCEC remains unknown [17]. A number of lncRNA studies have confirmed aberrant lncRNAs in UCEC specimens, and some of these lncRNAs networks may be important in the development of UCEC [18]. For example, LNC04080 has been observed to be significantly upregulated in EC tissue with involvement in EC carcinogenesis [18]. In addition, LNCTAM34A has been previously suggested to promote glioma proliferation and migration [19].

Based on the above, we undertook a pan-cancer genomic analysis of m6A regulatory factors and immune infiltration in this investigation to obtain a complete overview in EC, which would support in finding new prospects for carcinoma early diagnosis, therapies, and preventative measures.

2. Methods

2.1. Data Download. The UCEC RNA-seq data were downloaded in the Cancer Genome Atlas (TCGA, <https://portal.gdc.cancer.gov/>). There were 587 samples totally, containing 543 UCEC cases and 35 healthy cases. The clinical information of UCEC cases included survival time, survival status, gender, age, stage, and TMN stage. Twenty-three m6A-related genes were found in published journals [20–22].

2.2. Screening of Prognostic Genes. The package of org.Hs.eg.db was used by R language. 60488 gene IDs and 34446 symbols were obtained after conversion. The same profiles of gene symbol expression were merged by maximum value.

The package of normalizeBetweenArrays was used by limma. 24064 differential genes (adj. P. Val<0.5) were found between UCEC and normal cohorts. The lncRNAs were defined using lncRNA annotation file of the GENCODE website. 3039 lncRNAs were totally confirmed from TCGA-UCEC cohort. To assess the relationship between lncRNAs and 21 m6A-associated differential genomics, 20 lncRNAs were found by using the “rcorr” function in the Hmisc package with abs (cor-Filter) > 0.4 and $P < 0.05$. The differential genes of M6A were drawn by ggplot2 package of R language, and the box diagram of m6A-related lncRNA was drawn by ggpubr package of R language. The igraph package of R language is used to draw the lncRNA-related network of m6A.

2.3. Construction of lncRNA Risk Score Model. The construction of lncRNA risk score model was combined with the m6A correlation map of 20 lncRNA genes. The clinical data of patients including survival time and status were used for survival analysis by R language and univariate Cox regression. The prognostic genes were obtained from multivariate Cox regression analysis ($P < 0.05$). By the regression coefficients of the screened prognostic genes and their expression profiles, the risk scales were computed through the regression coefficients of screened prognostic genes and their expression profiles:

$$\text{Risk Score} = \sum \text{coef}(\text{lncRNAn}) \times \text{expr}(\text{lncRNAn}). \quad (1)$$

Note: coef(lncRNAn) represents the regression coefficient of lncRNAs and is obtained from multifactor Cox regression; expr (lncRNAn) represents the expression profile of lncRNAs.

Based on this formula, the risk score of each sample was derived [23]. All UCEC samples containing prognostic information were classified as high risk and low risk in accordance with the median risk score.

2.4. The Verification of UCEC Risk Score Model. The heat maps, sample risk status maps, and sample survival status maps were set up. The packages of pheatmap, ggplot2, survminer, and survivalROC were applied.

2.5. Investigation of Immune Infiltrating Cells and Functions. TCGA-UCEC expression profiling was conducted applying immunedeconv package of R language. The immunedeconv package enabled a variety of immune infiltration analysis methods, including quantiseq, timer, cibersort, cibersort_abs, mcp_counter, xcell, and epic. Xlsx was obtained from <https://onlinelibrary.wiley.com/doi/10.1002/jcp.29842>, containing 16 immune cells and 13 immune-related functions [24]. The ggpubr package of R language is used to draw ggboxmap function box diagrams and to distinguish between high risk and low risk. The gsva package of R language is used to calculate the ssGSEA score of the expression profile of the sample.

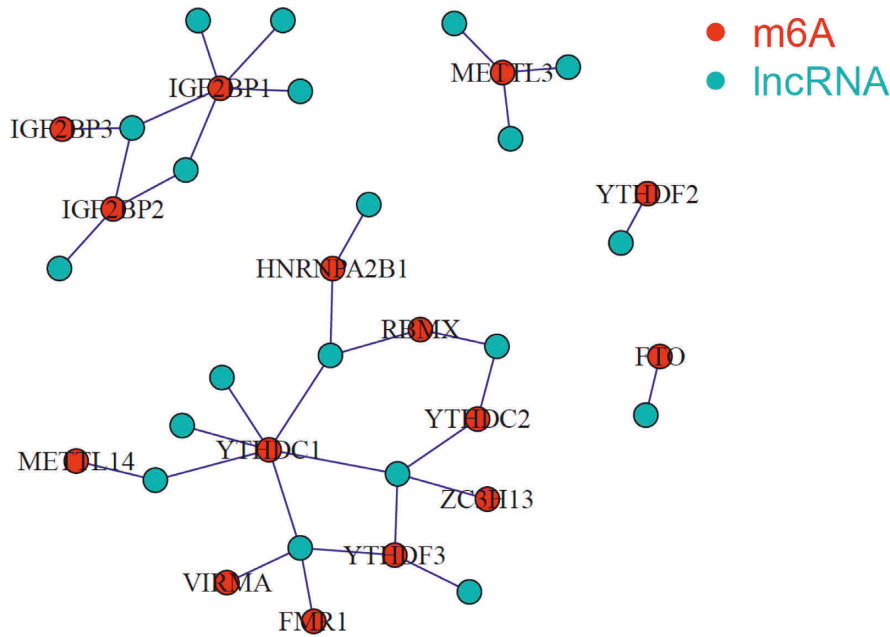


FIGURE 1: The co-expression networks indicated m6A-associated lncRNAs in UCEC. The red dots were m6A RNA methylated factors and the blue dots were m6A-associated lncRNAs.

2.6. Diagnostic Assessment of Hub Gene. The expression of LNCTAM34A gene in TCGA-UCEC was extracted and the expression differences of LNCTAM34A gene were plotted in box plots using the ggpubr package in R language. GEPIA2 database (<http://gepia2.cancer-pku.cn/>) was utilized to further confirm the difference in its expression in cancer and normal tissues. The specimens of UCEC were classified as high- and low-expression groups based on the median LNCTAM34A levels. The survival time and survival status of patients with UCEC were analyzed by the Kaplan–Meier curve.

3. Results

3.1. The Screening for m6A-Associated lncRNAs. In this study, a total of 587 samples were obtained from TCGA datasets, including 543 tumor samples and 35 normal samples. The medical characteristics of UCEC patients were analyzed by the above TCGA dataset. Based on the results of the differential analysis, 23 m6A-related genes were screened and 21 m6A-related differential genes were obtained. lncRNAs that were linked to the m6A methylation regulators ($\text{abs}(\text{cor-Filte}) > 0.4$ and $P < 0.05$) were defined as m6A-associated lncRNAs. The m6A-lncRNA correlation networks are displayed in Figure 1. Among 21 m6A-related differential genes, the upregulated genes were IGF2BP3, YTHDF1, YTHDF2, RBM15, HNRNPA2B1, IGF2BP1, METTL3, RBM15B, and YTHDC2 in UCEC. In addition, the down-regulated genes were YTHDC1, METTL14, FTO, ZC3H13, METTL16, RBMX, YTHDF3, VIRMA, WTAP, ALKBH5, FMR1, and IGF2BP2 in UCEC. The details are shown in Figure 2. Among the 15 m6A-lncRNAs in correlation network, the expressed levels were compared in the high-risk and low-risk groups (Figure 3). In the high-risk group, the

levels of FMR1, IGF2BP1, IGF2BP2, IGF2BP3, VIRMA, YTHDC1, YTHDF3, and ZC3H13 expressions were obviously higher than those in low-risk group (Figure 3). On the other hand, the levels of FTO, YTHDC2, and YTHDF2 in low-risk group were significantly reduced (Figure 3).

3.2. Construction of the UCEC Risk Model. Five lncRNA prognostic genes associated with disease risk were totally obtained by univariate Cox regression analysis, which were LINC02043, LINC00683, LNCTAM34A, FZD10-AS1, and MIR497HG (Figure 4(a), $P < 0.05$). Multivariate survival analysis using Cox's regression model was applied to support the significant predictive valuation of the five genomic mentioned at the first step. LNCTAM34A was considered as a prognostic gene (hazard ratio = 0.925).

3.3. The Verification of UCEC Risk Model. The Kaplan–Meier curves displayed that the cases in the high-risk cohort had a poor overall survival (OS) than those in the low-risk cohort (Figure 5(a)). The distributions of risk scores and survival status are shown in Figures 5(b) and 5(c), respectively. The ROC curves showed that high-risk cases were able to predict the OS in UCEC patient cohort. Moreover, the AUCs of OS at one, three, and five years were 0.679, 0.681, and 0.713 separately (Figure 5(d)). The AUCs of OS in the age, gender, tumor stage, and risk score were 0.510, 0.500, 0.533, and 0.576 (Figure 5(e)).

3.4. Immune Infiltration Analysis between the High and Low-Risk Groups. Differential expression immunologic response-related genotypes were evaluated between the low and high-risk groups to further investigate the possible

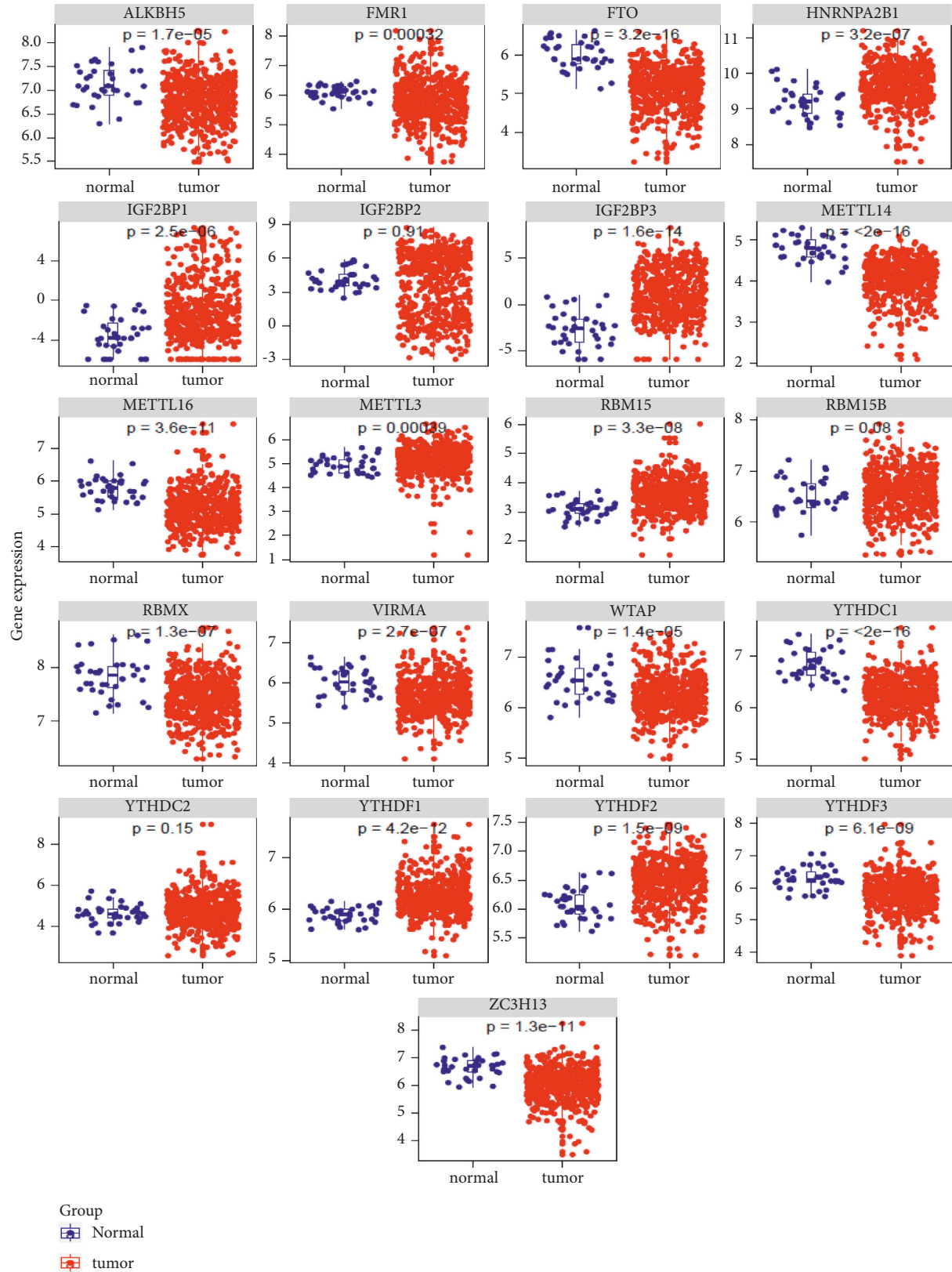


FIGURE 2: Among the 21 differential genes associated with m6A, there were 9 genes upregulated in UCEC (including IGF2BP3, YTHDF1, YTHDF2, RBM15, HNRNPA2B1, IGF2BP1, METTL3, RBM15B, and YTHDC2) and 12 genes downregulated (including YTHDC1, METTL14, FTO, ZC3H13, METTL16, RBMX, YTHDF3, VIRMA, WTAP, ALKBH5, FMR1, and IGF2BP2).

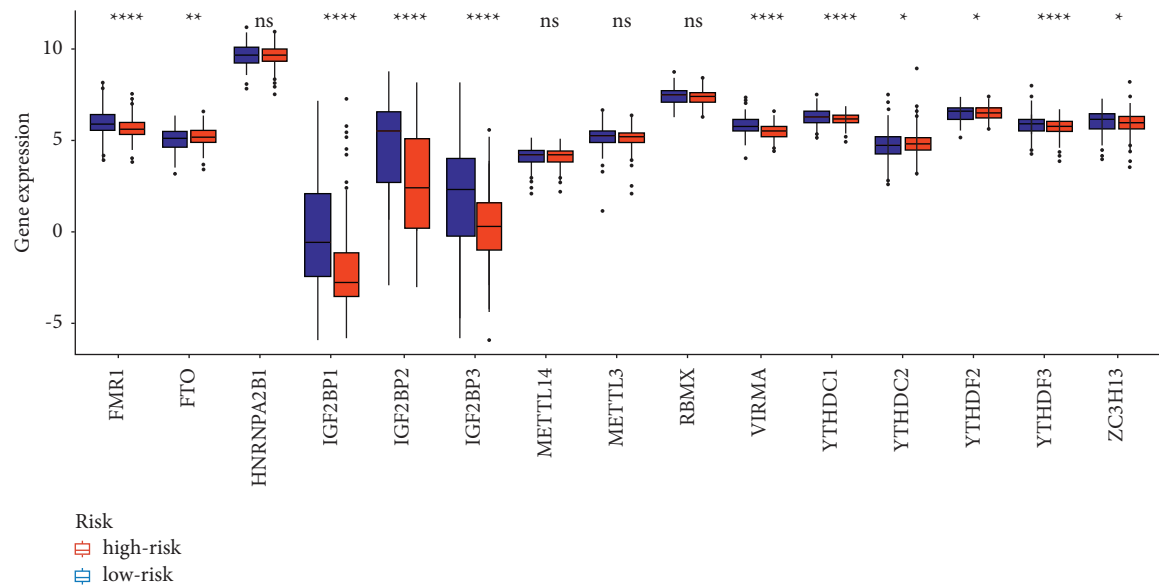


FIGURE 3: The expressed levels were compared in the high-risk and low-risk groups among the 15 m6A-lncRNAs in correlation network. * $P < 0.05$.

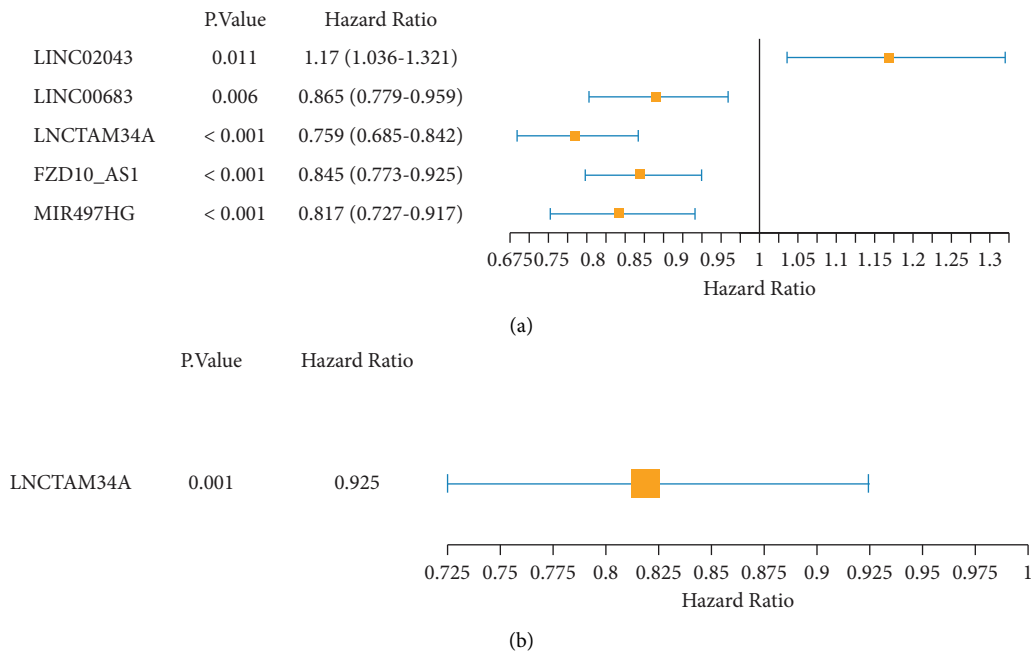


FIGURE 4: The univariate and multivariate Cox regression analysis was demonstrating five m6A-related lncRNAs.

underlying pathways of the predictive approach and its effectiveness in forecasting the effectivity of immunotherapeutic approaches. The results obtained from seven immuno-infiltration algorithms are displayed in Figure 6. The high and low-risk cohorts were classified via ssGSEA analysis. The infiltration of 16 subtypes of immune cells in high and low-risk cohorts is exhibited in Figure 7. According to Figure 7, high-risk cohort had greater scores of activated dendritic cells (DCs), B cells, and T cell regulatory (Tregs) than low-risk group; in the meanwhile, high-risk group had

lower scores of DCs and iDCs. Then, the high-risk group displayed greater scores in the immune functions of MHC class I, para-inflammation, and type I interferon (IFN) response than those of low-risk cohort (Figure 8). Among 27 immune-inducible genes, the levels of CD244, KIR3DLI, NRP1, PDCD1LG2, and TNFRSF8 were reduced in UCEC samples and the levels of CD27, CD28, CD70, CD80, CD86, HAVCR2, ICOS, IDO1, LAIR1, PDCD1, TIGIT, TNFRSF18, -25, -9, -14, and VTCN1 were increased in UCEC samples (Figure 9).

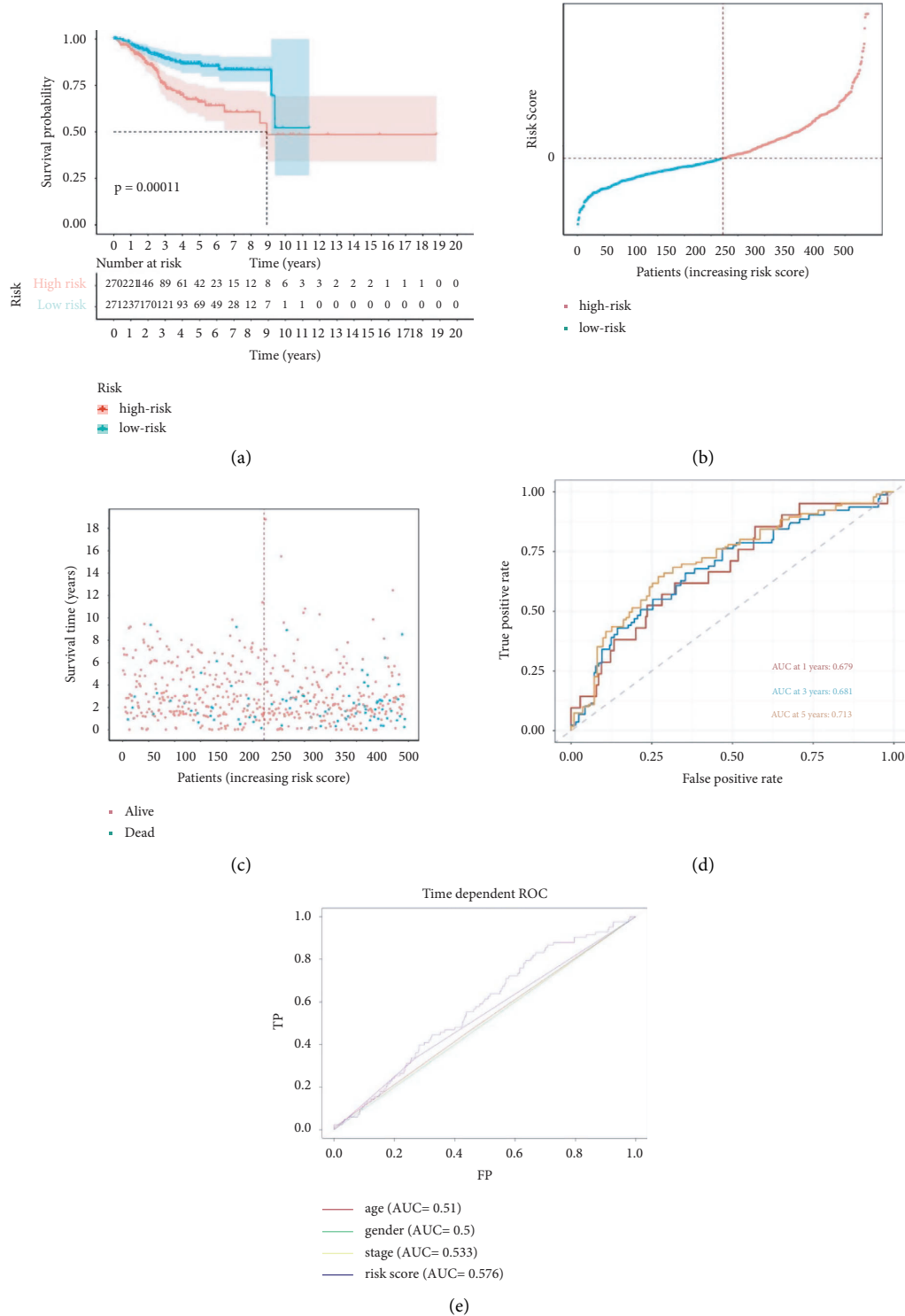


FIGURE 5: (a) The Kaplan–Meier curves. (b) Distributions of risk scores. (c) Survival status. (d) The AUCs at one, three, and five years to predict OS. (e) The AUCs of OS in the age, gender, tumor stage, and risk score.

3.5. Diagnostic Assessment of Hub Gene. According to the TCGA-UCEC data, we found that LNCTAM34A was expressed more strongly in normal specimens than that of UCEC samples ($P = 0.0036$, Figure 10(a)). Moreover, GEPIA2 database (<http://gepia2.cancer-pku.cn/>) was utilized to further confirm the difference in its expression in cancer and normal tissues.

Differential expression of m6A related to LNCTAM34A was remarkably stronger in UCEC patients than that in normal samples ($P < 0.05$, Figure 10(b)). The Kaplan–Meier curves suggested that the patients of the LNCTAM34A high-expression cohort had better OS than those in LNCTAM34A low-expression group ($P = 0.00012$, Figure 10(c)).



FIGURE 6: The heatmap displayed seven immuno-infiltration algorithms. The row of the heat map represents the different algorithms of immune cells; the column represents the sample. The rows were classified into seven types of immune infiltration and the columns were classified by high risk, low risk, and risk score.

4. Discussion

The emergence and advancement of UCEC is a multifactorial and complicated process [25]. The genetic information is translated into an extremely complicated RNA network for the most part. On the other hand, only 1% to 2% of transcripts are translated into proteins [26]. Therefore, RNA post-transcriptional regulation is particularly important because this post-transcriptional regulation can regulate the activity of tumor RNA transcription, thus changing the function and outcome of tumor cells [27]. lncRNAs are the transcription factors that are commonly regarded as transcribed far over 200 nucleotides which are not translated into proteins. Former research has linked the dysfunctional particular lncRNAs to the emergence and progression of malignancies. This research used pan-cancer genomic evaluation to profile m6A modification and expressed patterns of lncRNAs in order to gain a better insight into the underlying involvement of lncRNAs in human UCEC.

Among 587 cases in our study, we discovered 3039 lncRNAs in the TCGA-UCEC database. After the

differential analysis, 23 m6A-related genes were screened and 21 m6A-related differential genes were found. In the end, we obtained 20 m6A-related lncRNAs. LNCTAM34A was considered as a prognostic gene through univariate and multivariate Cox regression analysis. Moreover, the expression of LNCTAM34A was significantly stronger in normal cohort than that in UCEC cohort based on the TCGA-UCEC database. The patients of the LNCTAM34A high-expression cohort had better OS than those in LNCTAM34A low-expression group. LNCTAM34A was initially identified as an anti-sense RNA capable of modulating the cancerous inhibitor microRNA-34a in a variety of human malignancies [28]. Our results are consistent with data from previous studies, and in addition, our study is able to be interpreted through the pathways found [29]. Previous investigation found that LNCTAM34A-mediated upregulation of microRNA-34a levels was adequate to motivate the proper responses of cells to such stressful stimuli [29]. When exposed to multiple types of cellular strain, the collaboration of TP53 with other variables can initiate transcription at the microRNA-34a site, contributing to the formation of

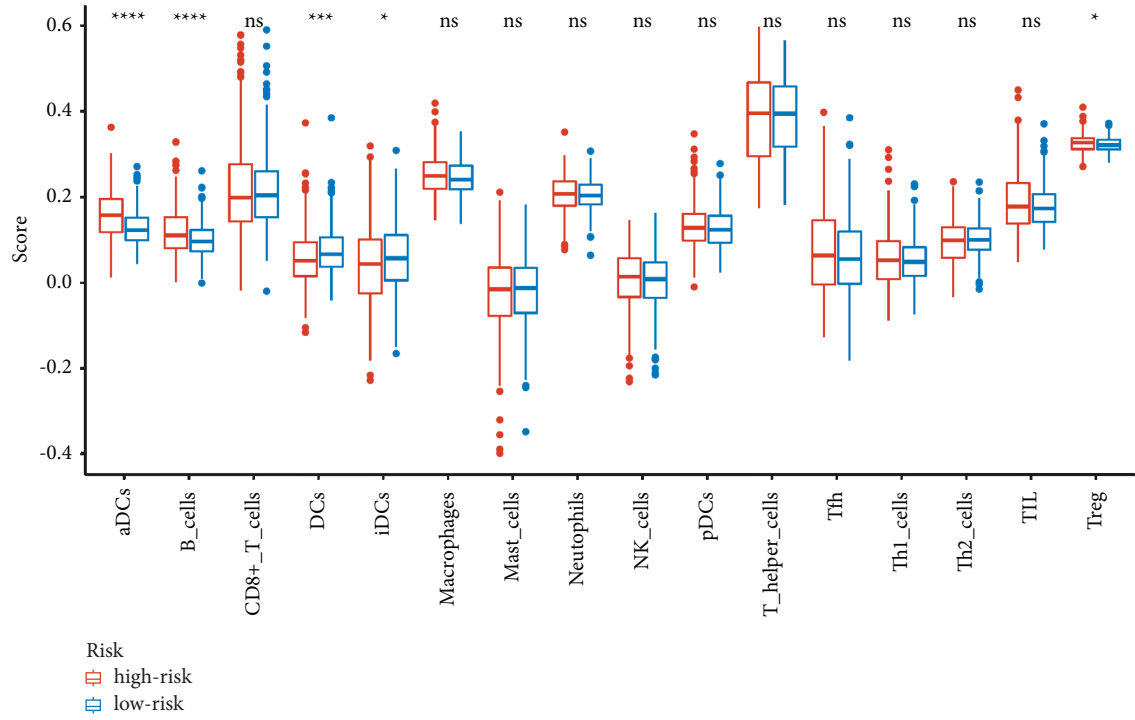


FIGURE 7: The comparison of immuno-infiltration scores was shown between high-risk and low-risk groups. * $P < 0.05$, *** $P < 0.001$, and **** $P < 0.0001$; ns indicated not statistically significant.

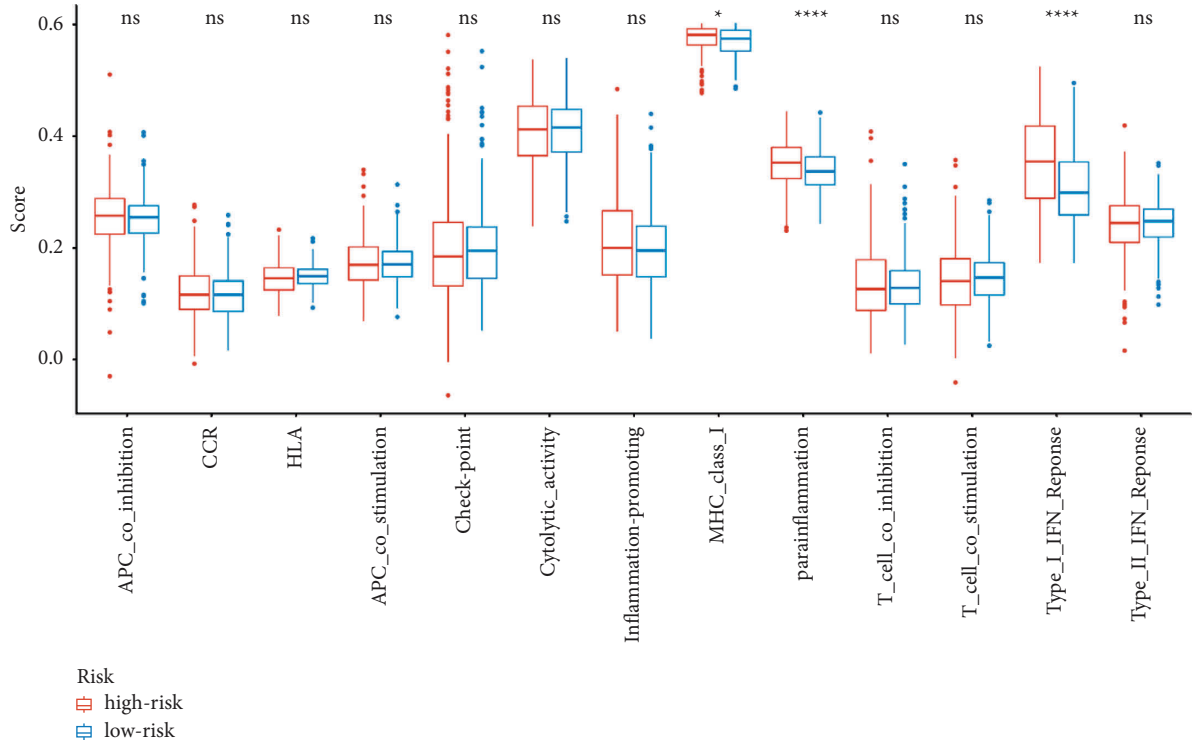


FIGURE 8: The comparison of immune functional scores was shown between high-risk and low-risk groups. * $P < 0.05$, *** $P < 0.001$, and **** $P < 0.0001$; ns indicated not statistically significant.

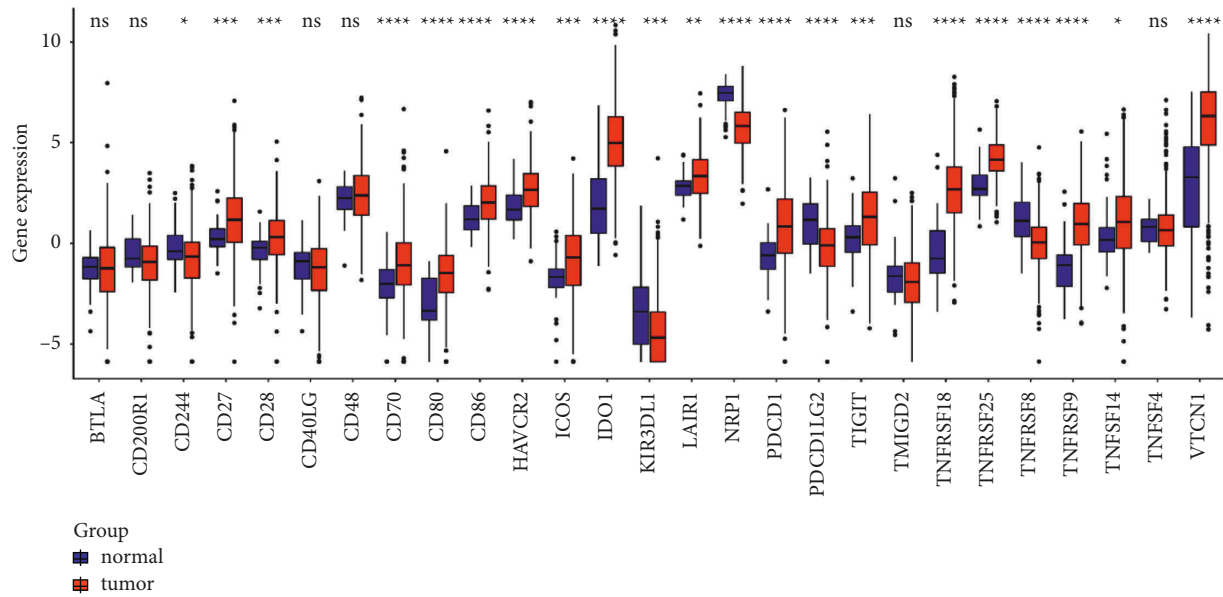


FIGURE 9: The levels of 27 immune-inducible genes were compared between normal and UCEC samples. * $P < 0.05$, ** $P < 0.01$, and so on; ns indicated not statistically significant.

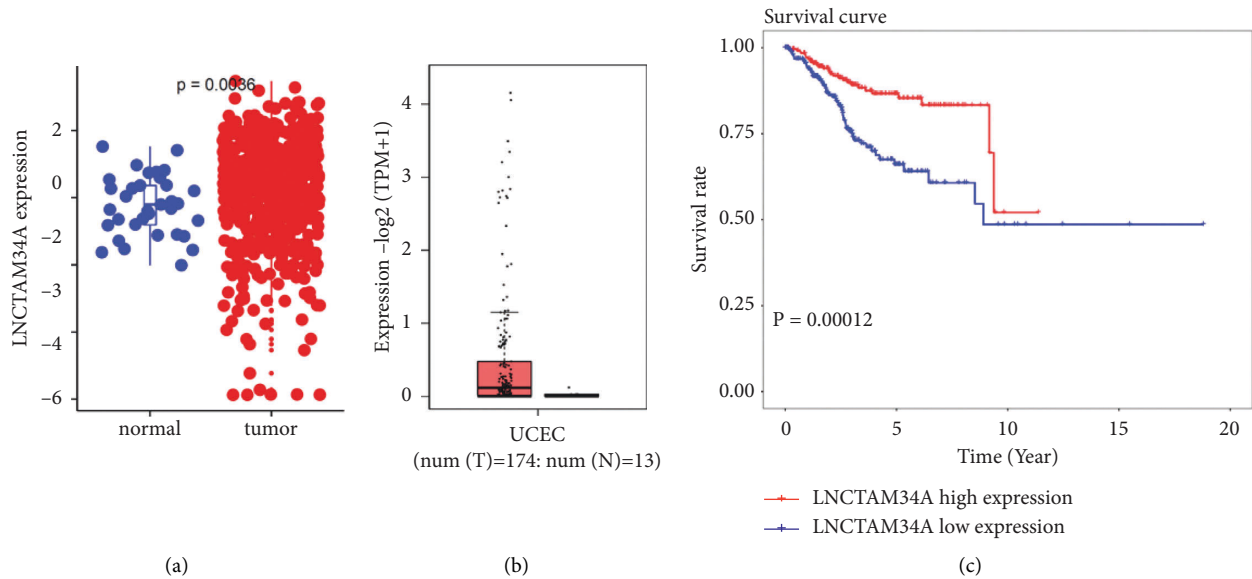


FIGURE 10: (a) The level of LNCTAM34A was expressed between normal and UCEC patients in TCGA database. (b) LNCTAM34A-related m6A genes were exhibited between normal and UCEC patients in GEPIA2 database. (c) The Kaplan–Meier curves were shown between LNCTAM34A high-expression and low-expression groups.

LNCTAM34A and miR34a [30, 31]. It has been reported that low-level expression of LNCTAM34A has been linked to a lower survival rate than that of high-level expression of LNCTAM34A in cancer patients [29]. In addition, worse outcomes of UCEC patients were discovered when occurrence of TP53 mutation, and low levels of microRNA and LNCTAM34A. Nevertheless, other studies have shown that LNCTAM34A is seen as a malignant promoter in glioma [19]. When LNCTAM34A was knocked out, glioma cell proliferation was inhibited, migration was diminished, and EMT rates were relatively low [19]. This contradictory conclusion may be due to the direct heterogeneity of the

different types of neoplasms [32]. Therefore, further exploration will need to be undertaken to explore the mechanisms of lncTAM34a regulation in UCEC.

The treatment of malignant tumours has been challenged by the properties of cancer relapse and metastasis [33]. Immunotherapy is one of the potential therapies for patients with UCEC, so m6A associated with regulating immune infiltration may have an effect on EC immune checkpoint inhibitors [34]. In our study, high-risk group had greater scores of activated dendritic cells (aDCs), B cells, and T cell regulatory (Tregs) than low-risk group; in the meanwhile, high-risk group had lower scores of DCs and iDCs. Then, the

high-risk group displayed greater scores in the immune functions of MHC class I, para-inflammation, and type I IFN response than those in the low-risk group. Among 27 immune-inducible genes, the levels of CD244, KIR3DL1, NRP1, PDCD1LG2, and TNFRSF8 were reduced in UCEC samples and the levels of CD27, CD28, CD70, CD80, CD86, HAVCR2, ICOS, IDO1, LAIR1, PDCD1, TIGIT, TNFRSF18, -25, -9, -14, and VTCN1 were increased in UCEC samples. Dendritic cells (DCs) have specific tumour antigens capable of inducing apoptosis in cancer cells, as well as nucleotide genes encoding pathogen-associated molecular patterns to trigger an immune response [35]. In the complex tumor microenvironment, B cells have diversity, and a variety of B cells regulate the occurrence and development of tumors. In the study of tumor invasion, B cells play an anti-tumor role by mediating T-cell immune function [36]. The findings indicated that immune-related genes exhibited positive correlation to the tumor infiltration of B cells and DCs in EC [37]. The histocompatibility complex (MHC) class I compound is a membrane-bound protein complex that is demonstrated on multinucleate human cells. MHC class I introduces intracellular signaling pieces to T-lymphocytes and initiates an excitation cascade when these cells recognize neoantigen. MHC class I loss by cancerous cells reduces tumor neoantigen demonstration to the immune response and thus reflects a potential mechanism of potential therapeutic tolerance even in malignancies that emerge to be excellent candidates for checkpoint suppression [38].

There are still a few drawbacks to in silico research. The expression patterns and diagnostic features used in this study were obtained from online databases with limited data, and the findings were not verified experimentally. We did, however, undertook multidimensional confirmation across several online databases, which provides strong backing for the relationships with both crucial biological markers recognized in our evaluation.

In conclusion, m6A-associated lncRNAs play a key role in the immune microenvironment of high-risk UCEC individuals. The patients with strong expression of LNCTAM34A have a good prognosis, and LNCTAM34A can be used as a prognostic gene for UCEC. m6A-related lncRNAs can be used as a potential treatment for UCEC. Our observations can be used as a hypothetical basis for future in vitro and animal experiments.

Data Availability

The datasets generated during analysed are not publicly available but are available from the corresponding author on reasonable request.

Conflicts of Interest

The authors declare that they have no conflicts of interest.

Authors' Contributions

All authors were responsible for conception and design, manuscript writing, and final approval of the manuscript.

Bing-Fan Xie provided administrative support. Yan Xia, Dan-Huan Lin, Bing Lianx, Meng-Li Zhang, Lu Liu, and Chun-Rong Qin provided research materials or patients and were responsible for data collection and compilation.

Acknowledgments

This study was supported by grants from the Funding Science Technology and Innovation Commission of Shenzhen Municipality (grant nos. JCYJ20180306172751035 and JCYJ20190809174605476) and Shenzhen Key Medical Discipline Construction (grant no. SZXK031).

References

- [1] J. Huvila, J. Pors, E. F. Thompson, and C. B. Gilks, "Endometrial carcinoma: molecular subtypes, precursors and the role of pathology in early diagnosis," *The Journal of Pathology*, vol. 253, no. 4, pp. 355–365, 2021 Apr.
- [2] H. Mahdy, M. J. Casey, and D. Crotzer, "Endometrial cancer," in *StatPearls [Internet]. Treasure Island (FL): StatPearls Publishing*, Tampa, Florida, United States, 2022 Jan.
- [3] Y. L. Wan, R. Beverley-Stevenson, D. Carlisle et al., "Working together to shape the endometrial cancer research agenda: the top ten unanswered research questions," *Gynecologic Oncology*, vol. 143, no. 2, pp. 287–293, 2016 Nov, PMID: 27593736.
- [4] N. Andor, C. C. Maley, and H. P. Ji, "Genomic instability in cancer: teetering on the limit of tolerance," *Cancer Research*, vol. 77, no. 9, pp. 2179–2185, 2017 May 1.
- [5] A. Nebbioso, F. P. Tambaro, C. Dell'Aversana, and L. Altucci, "Cancer epigenetics: moving forward," *PLoS Genetics*, vol. 14, no. 6, Article ID e1007362, 2018 Jun 7.
- [6] Z. Ali Syeda, S. S. S. Langden, C. Munkhzul, M. Lee, and S. J. Song, "Regulatory mechanism of MicroRNA expression in cancer," *International Journal of Molecular Sciences*, vol. 21, no. 5, p. 1723, 2020 Mar 3.
- [7] Y. P. Wang, J. T. Li, J. Qu, M. Yin, and Q. Y. Lei, "Metabolite sensing and signaling in cancer," *Journal of Biological Chemistry*, vol. 295, no. 33, pp. 11938–11946, 2020 Aug 14.
- [8] M. Klutstein, D. Nejman, R. Greenfield, and H. Cedar, "DNA methylation in cancer and aging," *Cancer Research*, vol. 76, no. 12, pp. 3446–3450, 2016 Jun 15.
- [9] Y. Zhang, X. Geng, Q. Li et al., "m6A modification in RNA: biogenesis, functions and roles in gliomas," *Journal of Experimental & Clinical Cancer Research*, vol. 39, no. 1, PMID: 32943100, p. 192, 2020 Sep 17.
- [10] J. Yang, J. Chen, X. Fei, X. Wang, and K. Wang, "N6-methyladenine RNA modification and cancer (Review)," *Oncology Letters*, vol. 20, no. 2, pp. 1504–1512, 2020 Aug, Epub 2020 Jun 16. PMID: 32724392; PMID: PMC7377110.
- [11] H. Heyn and M. Esteller, "An adenine code for DNA: a second life for N6-methyladenine," *Cell*, vol. 161, no. 4, pp. 710–713, 2015 May 7, Epub 2015 Apr 30. PMID: 25936836.
- [12] S. Zaccara, R. J. Ries, and S. R. Jaffrey, "Reading, writing and erasing mRNA methylation," *Nature Reviews Molecular Cell Biology*, vol. 20, no. 10, pp. 608–624, 2019 Oct, Epub 2019 Sep 13. PMID: 31520073.
- [13] S. Oerum, V. Meynier, M. Catala, and C. Tisné, "A comprehensive review of m6A/m6Am RNA methyltransferase structures," *Nucleic Acids Research*, vol. 49, no. 13, pp. 7239–7255, 2021 Jul 21.
- [14] H. Huang, H. Weng, and J. Chen, "m6A modification in coding and non-coding RNAs: roles and therapeutic

- implications in cancer,” *Cancer Cell*, vol. 37, no. 3, pp. 270–288, 2020 Mar 16.
- [15] D. Dixit, B. C. Prager, R. C. Gimple et al., “The RNA m6A reader YTHDF2 maintains oncogene expression and is a targetable dependency in glioblastoma stem cells,” *Cancer Discovery*, vol. 11, no. 2, pp. 480–499, 2021 Feb.
 - [16] Z. Chen, Y. Hu, L. Jin et al., “The emerging role of N6-methyladenosine RNA methylation as regulators in cancer therapy and drug resistance,” *Frontiers in Pharmacology*, vol. 13, Article ID 873030, 2022 Apr 6.
 - [17] Y. Chi, D. Wang, J. Wang, W. Yu, and J. Yang, “Long non-coding RNA in the pathogenesis of cancers,” *Cells*, vol. 8, no. 9, p. 1015, 2019 Sep 1.
 - [18] B. L. Li and X. P. Wan, “The role of lncRNAs in the development of endometrial carcinoma,” *Oncology Letters*, vol. 16, no. 3, pp. 3424–3429, 2018 Sep, Epub 2018 Jul 4. PMID: 30127944.
 - [19] Y. Chen, Y. Guo, S. Li et al., “Identification of N6-methyladenosine-related lncRNAs as a prognostic signature in glioma,” *Frontiers in Oncology*, vol. 12, Article ID 789283, 2022 Mar 3.
 - [20] J. Yu, W. Mao, S. Sun et al., “Identification of an m6a-related lncRNA signature for predicting the prognosis in patients with kidney renal clear cell carcinoma,” *Frontiers in Oncology*, vol. 11, Article ID 663263, 2021.
 - [21] H. Wang, Q. Meng, and B. Ma, “Characterization of the prognostic m6a-related lncRNA signature in gastric cancer,” *Frontiers in Oncology*, vol. 11, Article ID 630260, 2021.
 - [22] F. Xu, X. Huang, Y. Li, Y. Chen, and L. Lin, “m6A-related lncRNAs are potential biomarkers for predicting prognoses and immune responses in patients with LUAD,” *Molecular Therapy - Nucleic Acids*, vol. 24, pp. 780–791, 2021.
 - [23] J. Pan, Z. Huang, and Y. Xu, “m5C-Related lncRNAs predict overall survival of patients and regulate the tumor immune microenvironment in lung adenocarcinoma,” *Frontiers in Cell and Developmental Biology*, vol. 9, Article ID 671821, 2021 Jun 29.
 - [24] W. Jin, Y. Zhang, Z. Liu, Z. Che, M. Gao, and H. Peng, “Exploration of the molecular characteristics of the tumor-immune interaction and the development of an individualized immune prognostic signature for neuroblastoma,” *Journal of Cellular Physiology*, vol. 236, no. 1, pp. 294–308, 2021 Jan.
 - [25] J. Liu, R. Geng, S. Yang et al., “Development and clinical validation of novel 8-gene prognostic signature associated with the proportion of regulatory T cells by weighted gene Co-expression network analysis in uterine corpus endometrial carcinoma,” *Frontiers in Immunology*, vol. 12, Article ID 788431, 2021 Dec 14.
 - [26] M. Pertea, “The human transcriptome: an unfinished story,” *Genes*, vol. 3, no. 3, pp. 344–360, 2012.
 - [27] R. Shalgi, R. Brosh, M. Oren, Y. Pilpel, and V. Rotter, “Coupling transcriptional and post-transcriptional miRNA regulation in the control of cell fate,” *Aging (Albany NY)*, vol. 1, no. 9, pp. 762–770, 2009 Sep 8.
 - [28] J. T. Serviss, N. Andrews, J. Van den Eynden et al., “An antisense RNA capable of modulating the expression of the tumor suppressor microRNA-34a,” *Cell Death & Disease*, vol. 9, no. 7, p. 736, 2018 Jul 3.
 - [29] J. T. Serviss, N. Andrews, J. Van den Eynden et al., “An antisense RNA capable of modulating the expression of the tumor suppressor microRNA-34a,” *Cell Death & Disease*, vol. 9, no. 7, p. 736, 2018.
 - [30] N. Leveille, C. A. Melo, K. Rooijers et al., “Genome-wide profiling of p53-regulated enhancer RNAs uncovers a subset of enhancers controlled by a lncRNA,” *Nature Communications*, vol. 6, no. 1, p. 6520, 2015.
 - [31] A. Ashouri, V. I. Sayin, J. Van den Eynden, S. X. Singh, T. Papagiannakopoulos, and E. Larsson, “Pan-cancer transcriptomic analysis associates long noncoding RNAs with key mutational driver events,” *Nature Communications*, vol. 7, no. 1, Article ID 13197, 2016.
 - [32] I. Dagogo-Jack and A. T. Shaw, “Tumour heterogeneity and resistance to cancer therapies,” *Nature Reviews Clinical Oncology*, vol. 15, no. 2, pp. 81–94, 2018 Feb, PMID: 29115304.
 - [33] C. Bailey, J. R. M. Black, J. L. Reading et al., “Tracking cancer evolution through the disease course,” *Cancer Discovery*, vol. 11, no. 4, pp. 916–932, 2021 Apr.
 - [34] L. Wang, H. Hui, K. Agrawal et al., “m6 A RNA methyltransferases METTL3/14 regulate immune responses to anti-PD-1 therapy,” *The EMBO Journal*, vol. 39, no. 20, Epub 2020 Sep 23. PMID: 32964498, Article ID e104514, 2020 Oct 15.
 - [35] Z. K. Nazarkina and P. P. Laktionov, “[Preparation of dendritic cells for cancer immunotherapy],” *Biomeditsinskaya Khimiya*, vol. 61, no. 1, pp. 30–40, 2015 Jan-Feb, PMID: 25762597.
 - [36] V. Engelhard, J. R. Conejo-Garcia, R. Ahmed et al., “B cells and cancer,” *Cancer Cell*, vol. 39, no. 10, pp. 1293–1296, 2021 Oct 11, Epub 2021 Sep 30. PMID: 34597591.
 - [37] P. Chen, Y. Yang, Y. Zhang, S. Jiang, X. Li, and J. Wan, “Identification of prognostic immune-related genes in the tumor microenvironment of endometrial cancer,” *Aging (Albany NY)*, vol. 12, no. 4, pp. 3371–3387, 2020 Feb 19.
 - [38] L. A. Friedman, T. N. Bullock, E. A. Sloan, K. L. Ring, and A. M. Mills, “MHC class I loss in endometrial carcinoma: a potential resistance mechanism to immune checkpoint inhibition,” *Modern Pathology*, vol. 34, no. 3, pp. 627–636, 2021 Mar.

Research Article

Research on Application of Meticulous Nursing Scheduling Management Based on Data-Driven Intelligent Optimization Technology

YanPing Zhai¹ ,¹ Run Li,² and ZhiLi Yan²

¹Internal Medicine Teaching and Research Section, Shanxi Bethune Hospital, Shanxi, Taiyuan 030032, China

²School of Nursing, Shanxi University of Chinese Medicine, Shanxi, Taiyuan 030024, China

Correspondence should be addressed to YanPing Zhai; sxbqeyynk@sxtcm.edu.cn

Received 20 June 2022; Revised 25 July 2022; Accepted 3 August 2022; Published 12 September 2022

Academic Editor: Dong Chen

Copyright © 2022 YanPing Zhai et al. This is an open access article distributed under the Creative Commons Attribution License, which permits unrestricted use, distribution, and reproduction in any medium, provided the original work is properly cited.

The management of nursing scheduling in healthcare facilities have faced new challenges during the COVID-19 pandemic. With the rapid development of big data and artificial intelligence technology, data-driven intelligent medical services are what we need to study nowadays. This paper not only proposes reasonable solutions in areas such as refined nursing scheduling by using these scientific technologies to quickly realize the allocation of human resources in hospitals. It also accelerates the development of hospital informatization construction through computer technology, establishing a scientific and intelligent medical platform that meets the needs of users. Aiming at the problem of nursing scheduling in medical service data research, this paper proposes a complete plan by analyzing the development of the medical platform at this stage. Firstly, established an intelligent medical service platform, and studied the medical management from the perspective of data. Then, analyze the intelligent medical platform data by utilizing optimized algorithms, through reasonable analysis under various constraints, to get the basic nursing scheduling plan that meets the needs of medical institutions. Finally, considering the actual situation of emergency medical treatment, the decision classification model is introduced under the basic scheme to further screen out the optimal management scheme of modern medical treatment.

1. Introduction

The sudden outbreak of COVID-19 has had a severe impact on the lives of all mankind. Hospitals are the institutions most severely affected by the epidemic, mainly due to the centralized distribution of patients, which leads to the unbalanced allocation of medical resources and indirectly leads to a significant increase in the prevention and control costs and operating costs of medical institutions. COVID-19 has not only had a significant impact on the global healthcare industry, but also made more and more people value healthcare more. In the post-epidemic era, innovation and progress in the medical industry have become the focus of social attention, and patients' medical thinking and habits will change dramatically. Hospitals need to face the challenges and speed up the information construction process of

smart medical treatment [1]. In recent years, the problem of nurse scheduling has been concerned by many hospital administrators and related scholars [2]. A good scheduling is of great significance to the development of the unit. However, with the development of social information, manual scheduling has been obviously outdated, and nurses scheduling information is an inevitable development trend. Intelligent scheduling informatization based on big data is a multidisciplinary problem of nursing, management, operations and computer. Researchers need to have a more comprehensive understanding of this problem and solve it through performance-guided design, by improving market share and competitiveness, and then achieve sustainable development of hospitals.

At present, the world population is still increasing, and the development of medical care is in a difficult stage. At the

same time, the demand for medical personnel brought by the increase in the number of patients has not been well met, and there are also problems such as waste of health expenses, resulting in inadequate allocation of medical and health human resources [3]. What's more, hospital medical service efficiency is low. In the case of insufficient allocation of health human resources, there is still some idle personnel, wasting a large number of medical and health resources. Medical care in most countries is still in the low information stage of manual scheduling. Most hospital scheduling is done manually by the head nurse through experience. Such scheduling has many disadvantages. First of all, manual scheduling is inefficient and wastes a lot of time and resources. And with the development of modern hospitals, the number of nurses in the department and their needs are gradually increasing, and it will become more and more difficult to manually schedule shifts. Secondly, if multiple nurses put forward preference requirements, the head nurse is prone to be influenced by subjective factors in the schedule and cannot meet the requirements of each nurse with fairness and justice, which may cause dissatisfaction among nurses and also the conflicts between nurses and hospital management [4].

Therefore, the whole society should pay attention to how to effectively control hospital medical costs under the background of limited medical service resources. It is very important to improve the overall service quality of a hospital to ensure the service efficiency of medical and health personnel by rational allocation of nurses [5]. Considering that nurses serve patients in hospitals, the negative emotions of patients with diseases may also indirectly affect nurses' emotions, resulting in certain psychological pressure [6]. In addition to the influence brought by the special nature of nurses' work, there is a wrong concept of valuing medical care over nursing in the society, which is mainly influenced by factors including traditional culture. These adverse impacts on nurses' life and work, at the same time, affect patients' satisfaction with medical services, which may cause tension between nurses and patients [7, 8]. Then it will lead to greater uncertainty in the allocation of hospital human resources. When nursing work is heavy, additional temporary nurses need to be hired to meet the demand for medical and health services, which increases hospital costs to a certain extent. As shown in Figure 1, there are nurses doing nucleic acid tests for people during the COVID-19 pandemic.

On the one hand, although the overall strength of the global medical system has been greatly improved, the medical service system in most countries still faces great work pressure. Due to the imbalance between supply and demand of medical staff and patients, in order to better serve the people, it is necessary to optimize and reform the human resource management of hospitals [9]. Maximize the potential of hospital medical staff. Human resource management plays a very important role in both public and private hospitals. If the human resource management is inadequate and the professional strength of the staff cannot be fully brought into play, the waste of talents will be caused. On the other hand, In the long-term application of the traditional



FIGURE 1: Nurses' working pictures from Chongqing daily news report.

nursing scheduling mode, its shortcomings are gradually revealed. The traditional medical model is platform management, and nurses usually only perform their own duties [10]. Especially for young nurses, their lack of nursing experience and poor emergency response ability will increase the risk of adverse nursing events [11]. More importantly, nurses' psychological pressure will lead to lower work enthusiasm, thus forming a vicious circle. The rationality of the traditional scheduling method for nursing staff is not high. Sometimes, during the consultation period, the nurses will be busy and affect the observation of the patient's condition and health education, increasing the contradiction between the doctor and the patient.

The way to solve the above problems is to arrange nurses' working shifts reasonably, which can not only ensure the efficient completion of hospital nursing work, but also ensure that nurses can fulfill other social roles. As countries pay more and more attention to the medical and health field, hospitals should not only ensure the quality of service, but also try to meet the individual needs of medical staff from their perspective, by improving job satisfaction, and service efficiency to a certain extent [12]. Through the rational application of big data technology, artificial intelligence technology and the medical industry, the efficiency of human resource management has been effectively improved. For example, in the comprehensive evaluation of medical staff, it is no longer necessary for staff to collect all kinds of resources. Through the application of big data technology in the computer system, it can quickly call up the medical staff's attendance resources, daily work data, certificate data, diagnostic records, occupational assessment data, mental health data, etc [13]. A comprehensive and detailed personal career report is also available for human resource management. Meanwhile, the big data technology will also use the data comparison of job requirements to provide human resource managers with a reference job adjustment plan. Through daily work and post adjustment programs provided by big data technology, human resources can better carry out the allocation of medical human resources, ensuring the effective implementation of the work of various departments and departments, and promoting the overall operation quality and service effect of the hospital [14].

To sum up, COVID-19 certainly has had a significant impact on the medical industry. Medical service with Internet plus initiative will promote the trend of direct

connection between doctors and patients. Hospitals need to accelerate the construction of smart medical informatization, improve the ability of refined operation and management, and follow the trend to achieve sustainable development of hospitals. For industrial upgrading and industry development, the traditional medical industry has encountered many challenges and difficulties in labor management. For example, focus on the needs of different sub-scenarios in the medical industry, help the needs of refined labor management in the medical industry, and digitally empower enterprises to reduce costs and increase efficiency.

COVID-19 has accelerated the trend of direct access between doctors and patients. Hospitals should follow the trend, take precautions to build a smart hospital, by catching the express train named medical service with Internet plus initiative, to realize the sustainable development of the hospital. Accelerate the construction of the Internet hospital website, simulating the hospital entity, to increase the hospital brand weight in the virtual, and then improve the competitiveness with third-party platforms. Increase the information construction of hospitals, to meet the needs of patients' online medical consultation and inquiry to a greater extent, and improve the hospital's influence and market occupancy rate. Create online registration and hospital treatment channels to provide more convenient and fast medical services. Organization is fundamental. The hospital should set up a team, an operation department or a health service department, which is specially responsible for the operation and management of the Internet hospital, or entrust third-party platforms to manage and operate it. It is necessary to give full play to the commanding role of performance appraisal to guide and accelerate the advancement of medical service with Internet plus initiative. For those who provide services and attract hospital diagnosis and treatment through the hospital Websites, increase their performance incentives, fully revitalize their time, increase their treatment, and mobilize their enthusiasm, to achieve coordinated development with hospitals.

2. Related Studies

Hospital human resource management directly affects the overall service quality and effect of the hospital [15]. In order to provide patients with more efficient and safe medical services, it is necessary to carry out some reforms and innovations in hospital human resource management [16]. The intelligent scheduling system combines the business digital model to automatically calculate the demand of each position and generate the scheduling plan intelligently, convenient and efficient scheduling operation, preset a variety of scheduling rules. Different types of employees adopt different scheduling strategies to fully meet the multi-business needs of the medical industry. Enable the scheduling is real-time and transparent, that is, employees can view it at any time, effectively improving employee satisfaction and controlling labor costs. Nursing scheduling must conform to certain rules, if the arrangement of too few people, can not ensure the normal operation of the ward and

the patient's nursing needs. If there are too many people in the queue, the overflow of manpower will waste resources and increase the operating cost of the hospital. A good nursing scheduling system should be able to meet the needs of nurses' personal preference, nursing staff energy level, nurses' workload, shift balance, basic manpower requirements of each shift and other multi-dimensional requirements.

Western scholars have studied the scheduling problem of nurses earlier and put forward various methods in the essays. The nurses' scheduling model is mainly based on single objective model or changing multi-objective model into single objective problem model by weighting method. The research objectives mainly include reducing hospital salary costs, minimizing violation of hospital regulations, and maximizing the satisfaction of nurses' preferences. In addition, sometimes hospitals also consider how to reduce the number of nurses and reduce the overtime hours of nurses. Burke et al. [17] proposed heuristic sorting and variable neighborhood hybrid algorithm to solve nurse scheduling problems in reality by using weighted cost function as evaluation index. Sarkar et al. [18] proposed a heuristic framework with new features and a multi-parameter cost function based on variable waiting time. Finally, genetic algorithm toolbox was used to prove the feasibility of the framework and cost function. Mutingi and Mbohwa [19] proposed a simulation algorithm based on the concept of biological evolution to apply to nurse scheduling, which took into account user choice, user expectation and expert intuition and experience of decision makers.

The solution methods of nurse scheduling mainly include mathematical programming method and heuristic method. Most of the early studies adopted mathematical programming solution method. Musa and Saxena established mathematical programming model for several nurses and solved the problem using objective programming method [20]. Maenhout and Vanhoucke established a nurse scheduling model aiming at the penalty value of violation of nurses' assigned shifts, adopted the weighted sum method to transform the multi-objective problem into a single objective problem, and adopted the branch and bound method to solve the problem, and discussed the advantages and disadvantages of different branches and pruning methods in different scenarios [21].

However, the advantage of the accurate algorithm is that it can find the exact optimal solution of the problem, but the disadvantage is that for large-scale problems, the algorithm has high time complexity, and sometimes cannot be solved. The scale and high computational complexity of nurse scheduling problem determine that it is not suitable to be solved by an accurate algorithm. Legrain et al. [22] proposed a heuristic method based on local search, which is flexible, simple and easy to implement, and better than CPLEX solution. Topaloglu [23] proposed a multi-objective planning model of nurse scheduling with 10 hard constraints and 9 soft constraints. The sequential method and weighting method were used to transform the multi-objective function into a single penalty function for solving. Parr and Thompson [24] proposed to use neighborhood search to

solve the nurse scheduling problem using weighted cost function, and conducted a comparative experiment between sawing method and simulated annealing noise method, which proved that noise method could get a better scheduling scheme.

In recent years, more and more scholars use mixed mathematical methods to solve the problem of nurse scheduling. This is because the accurate algorithm consumes too much time to solve the multi-constraint and large-scale nurse scheduling problem and even cannot find the optimal solution. There are some defects in the heuristic algorithm, and there is no perfect scheme. Tassopoulos et al. proposed a two-stage variable domain search algorithm, which improved 48 instances in the benchmark problem of nurse competition and achieved better results [25]. Jaumard et al. promoted and extended the previous nurse scheduling model, proposed the 0–1 target nurse scheduling model based on the shortest path problem with resource constraints, and solved the model with column generation algorithm [26]. In recent years, there are also many studies on combinatorial algorithms, which can achieve better solution results. The optimization objectives proposed by Bard and Pumomo included minimizing mobile nurses and maximizing nurse satisfaction, establishing a multi-objective model, solving it by using column generation and integer programming, and completing an example verification in an American hospital [27]. Awadallah et al. proposed a hybrid algorithm using harmony search and mountain climbing algorithm, which can enhance the search ability of the algorithm and is suitable for solving a variety of nurse scheduling problems [28].

With the expanding influence of computer technology on all walks of life, there are more and more cross applications of science and technology and medical treatment. Abdennadher and Schlenkef supported semi-automatic generation of scheduling tables by imitating some thinking modes of human beings based on the idea of constraint programming [29, 30]. Cheng et al. [31] introduced and implemented a constraint-based nurse scheduling system by using a redundant modeling method. Hofe developed a nurse scheduling system based on hierarchical constraint satisfaction method on the basis of existing studies, and assays lists the practical application of this system [32]. In order to quickly get high-quality scheduling schedules, Muslija proposed an intelligent backtracking algorithm consisting of four steps and applied it into commercial software [33]. Also based on the variable neighborhood search algorithm, Burke et al. [34] proposed a hybrid heuristic sorting and variable neighborhood search algorithm (HVNS). Firstly, the algorithm uses heuristic method to generate the initial solution, and then optimizes the initial solution with variable neighborhood search algorithm. Finally, in order to jump out of the local optimal, the algorithm uses a heuristic restart mechanism to disturb the local optimal solution. Rahimian et al. [35] proposed a hybrid integer programming and variable neighborhood search algorithm. The algorithm first uses a greedy heuristic algorithm to generate the initial solution, and then optimizes

the solution using a variable neighborhood descent algorithm.

The study predicts the patient-related indicators, and then get the nurse allocation situation in a period of time in the future with the consideration of the total nursing time required by the patient, the effective nursing working time of nurses and the ratio of nurses to other medical staff, so as to formulate a reasonable method of nurse allocation according to the actual demand of the hospital. In the article [36], Valouxis and Housos adopted an approximate integer linear programming model to generate the initial solution of the nurse scheduling problem, and then adopted the local domain search method to optimize the initial solution. Nikola Todorovic proposed a colony optimization algorithm to solve the nurse scheduling problem in assay [37]. The algorithm simulates the foraging behavior of bees, including the process of scheduling and local search. Santos et al. proposed an integer programming method to solve the nurse scheduling problem in assay [38]. The algorithm starts to build the model of the problem and gives the integer programming formula of the problem. By referring to this formula, the algorithm gives a method to improve the performance of the IP solver.

Nursing scheduling is an important part of improving the efficiency of daily nursing management and rationally allocating hospital human resources [39]. The electronic nursing schedule can reduce the workload of the head nurse, facilitate the information exchange between different levels, and facilitate the nursing department to understand and manage the whole hospital manpower arrangement. In view of the low efficiency of paper scheduling and the diverse demands of different wards for scheduling, this paper designed a data-driven intelligent nursing scheduling management system, which fully considered the diversity of wards and the complexity of medical scheduling. This article aims to solve the hugely different needs of different wards for the setting of shifts and scheduling rules, and try to meet the diverse needs of each ward as much as possible.

3. Smart Medicine Based on Data

3.1. Data-Driven Medical Cloud Platform. The rapid development of Internet technology, promotes the continuous evolution of society towards informatization, networking and digitization. The focus of the Internet era has gradually shifted from the “Internet of Information,” with cloud computing, big data, and mobile Internet as the underlying technologies, to the “Internet of Value,” with block-chain, cryptography, and distributed consensus as the underlying technologies. A new round of technological revolution with block-chain as the underlying technology is coming. In recent years, block-chain technology and the field of smart medicine have been booming. Industry and academia have begun to try to combine these two, using block-chain’s features of de-centralization, high fault tolerance, immutability, traceability, anonymity and many others to solve the problems of data storage and privacy protection in the field of smart medicine. Then, realize storage and secure sharing

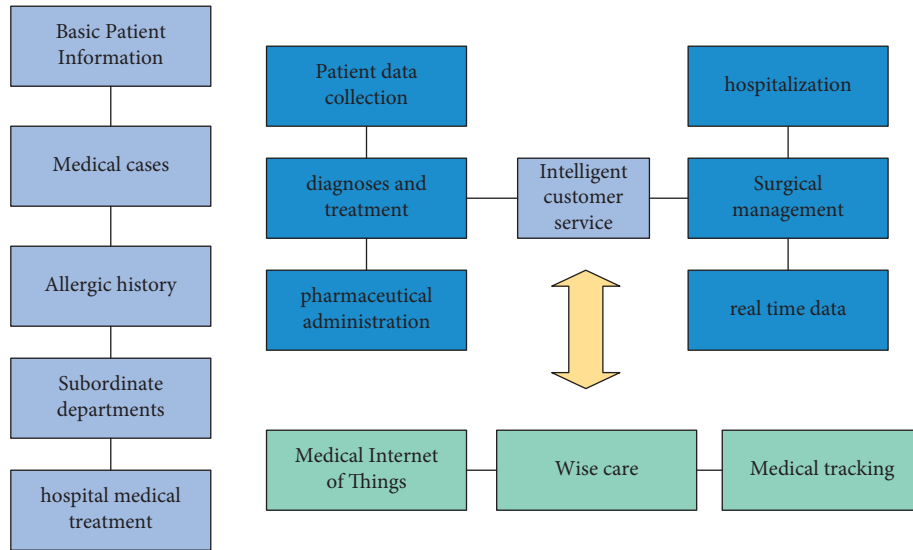


FIGURE 2: Data-driven framework of intelligent medical system.

of medical data among multiple entities. Medical image data continues to increase, and the amount of data stored, archived and invoked continues to rise; A large amount of data is stored and the interoperability is weak. Therefore, it is difficult to establish a unified shared resource management platform. The limitation of distance and talent makes primary medical care powerless. Doctor-patient information is sensitive, and information storage and sharing are difficult to be synchronized. This series of industry demand, all need to be supported by information technology, from a single system.

Medical information is about everyone's health information, and user data privacy is about ethics and regulation. For a long time, information and data in the medical industry have been in a closed environment. The information construction needs to get through the data between different platforms, and the data privacy, data security and other issues involved have been hindering the information construction of the medical industry. Due to the particularity of the medical industry, there are many personalized needs, and the needs of each department are different. Many hospital departments have the problem of independent division, and each department has a set of business, resulting in difficult data access and integration. With the development of medical equipment, more and more large-capacity archival data need to be preserved. These data grow very fast, and a large number of data need to be generated every day. At the same time, these data often need to be preserved for a long time. As the filing system of each hospital is not open, the medical data storage of the hospital is confronted with great challenges. Slow medical treatment has always been a pain point in the medical industry. How to solve this problem with the help of the digital process of the medical industry is the top priority in the digital transformation. With the emergence of big data analysis and AI technology, IT technology can help boost the diagnosis and treatment process, which can greatly save users' time to see a doctor.

However, the performance of traditional IT architecture is difficult to meet the needs of real-time analysis.

In the development of hospital human resource management, the sharing mechanism of hospital medical information can be built based on big data technology. Through the sharing and construction of medical information, the connection between various departments and departments can be effectively improved and the overall improvement of hospital service quality can be promoted. When the information of the hospital's human resources management is incorrect, it cannot promote the efficient development of related work. In order to solve this problem well, it is necessary to build a hospital's internal information management system, improve the circulation efficiency of hospital's internal information, and ensure that human resource management can play its corresponding work value. The framework of the smart medical platform based on the form of shared data is shown in Figure 2 in this paper. Data of multiple types and different departments are integrated and intelligent analysis is integrated to ensure the best results can be obtained through sharing.

3.2. Particle Swarm Optimization Algorithm Based on Medical Treatment. Particle swarm algorithm is also called particle swarm optimization algorithm (PSO). Simulate the behavior of birds randomly searching for food. In particle swarm optimization, the potential solution to every optimization problem is like a bird in the search space, called a particle. All particles have a fitness value determined by the optimized function, and each particle has a velocity that determines the direction and distance they "fly." The algorithm has the following advantages: simple and easy to operate, fast convergence speed, few setting parameters. And the general limitation condition is that when the number of steps or the corresponding accuracy is reached, the particle will stop moving. Particle swarm optimization algorithm, as a kind of

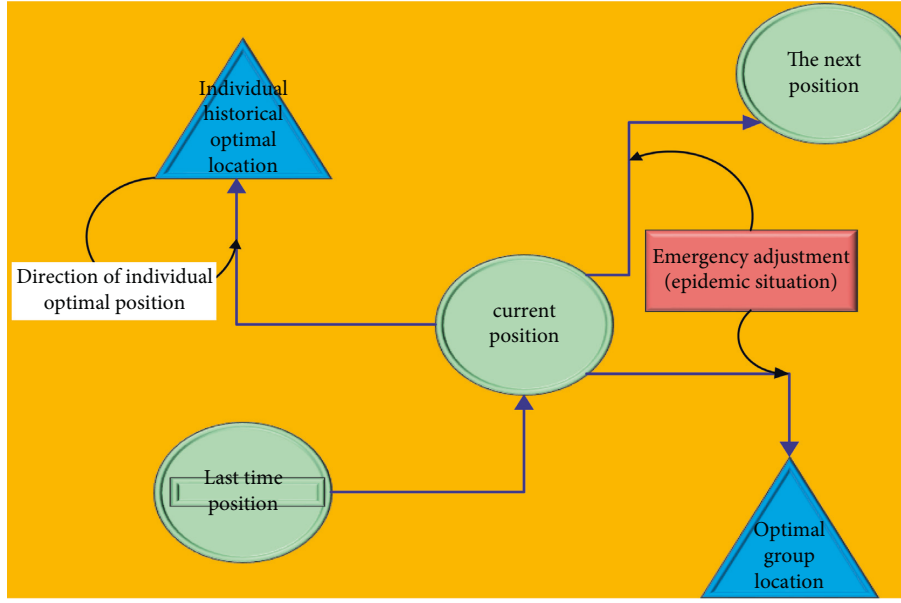


FIGURE 3: Update graph of nurse scheduling based on particle swarm optimization.

algorithm to find the optimal value, mainly relies on the iterative formula, which is updated as follows:

$$V_{id} = wV_{id} + C_1 \text{random}(0, 1)(P_{id} - X_{id}) + C_2 \text{random}(0, 1)(P_{gd} - X_{id}), \quad (1)$$

$$X_{id} = X_{id} + V_{id},$$

where w is the inertia factor and C is the acceleration constant. P_{id} represents the d -th dimension of the individual extremum of the i -th variable, and P_{gd} represents the d -th dimension of the global optimal solution.

Particle swarm optimization (PSO) initializes as a group of random particles (random solutions) and then iterates to find the optimal solution. In each iteration, the particle updates itself by tracking two extreme values: the first is the optimal solution found by the particle itself, which is called the individual extreme; The second is the optimal solution found so far for the whole population, which is called the global extremum. Or instead of using the entire population, you can use a fraction of it as a neighbor, called a local extremum. Combined with the actual hospital situation, it is necessary to consider the long-term effect of nurses on duty. When on duty, because the night shift work hours are long and reversed with the normal working hours, nurses generally do not want to work night shift, and the number of night nurses is small, so the night nurses are selected first, and the other nurses work day shift. First of all, according to the principle of voluntary, nurses who show willingness to work night shift will be given priority, and nurses who show reluctance to work night shift will be given priority under the same conditions. Secondly, according to the principle of fairness, nurses who worked less night shifts in a certain period of time (such as one year) should be considered first, and then nurses who did not work night shifts in the previous period should be considered, so as to avoid excessive fatigue caused by nurses working night shifts for too long.

The update process of particle swarm optimization algorithm based on nurse scheduling is shown in Figure 3. The neighborhood topology of PSO includes two kinds: one takes all the individuals in the population as the neighborhood of the particle; the other takes only some individuals in the population as the neighborhood of the particle. Neighborhood topology determines the optimal location of community history. Thus, PSO is divided into global PSO and local PSO. The global particle swarm algorithm includes the historical optimal value of the particle itself and the global optimal value of the particle population (the optimal value is determined by all particles).

As a swarm intelligence algorithm, particle swarm optimization has an obvious advantage that it can be encoded by real numbers instead of binary codes, and is easy to operate. Update mechanism of particle swarm optimization algorithm is only the global optimal solution to the information of other particles. And the algorithm does not need too much need to adjust the parameters. At the same time, the whole process with the current global optimal solution is updated iterations, also can quickly converge to global optimal location nearby, showing the fast convergence of the particle swarm optimization algorithm, the effectiveness and robustness, etc. At the same time, particle swarm optimization algorithm can achieve fast convergence to the final result, but it is easy to produce local optimal results. How to balance local optimization ability and global search ability is worth paying attention to, otherwise it is difficult to achieve good convergence effect.

Due to the impact of COVID-19, nurses have to pay more attention to epidemic prevention and control on the basis of their original duty, so the smart scheduling system should also take these factors into account. First, we divided the area into medium-high risk area or low-risk area, and then analyzed the data of medical duty on this basis. The first point is that the nurse clearly states the rest date and whether

the nurse can work on the first day. (If the nurse worked the night shift on the last day of the previous cycle, the nurse may not work on the first day of the new cycle). The third point is to determine the continuous work of the nurse at the end of the previous week. These data are used to calculate the continuous work of the nurse at the beginning of the new cycle. Fourth: determine the amount of work done by the nurse in the week when the new and old cycles are connected, and determine the workload of the nurse in the first week of the new cycle. The third and fourth items in the analysis information connect the old and new cycles, which is conducive to the hospital's fair and equitable management of nurses in the long term. According to the actual medical situation, the patient flow of the hospital was analyzed and predicted. We conducted preliminary detection according to the machine learning algorithm, which was convenient for the subsequent specific analysis of nurses on duty.

On the basis of intelligent forecasting, nurses were divided into day shift nurses and night nurse nurse in both groups. If the nurse scheduling for three shifts, chronic shift nurses can be divided into three groups. Thus when a nurse to work day shift, the night is no longer need to consider, so can reduce a lot of calculation, also meeting the requirements of the hard constraints directly, making the problem more simple. In addition, in the three-shift system, the working hours of each shift are generally similar, and the nurses' preference is not obvious. The classification should first consider the types of shifts that the nurses explicitly indicate to work or not to work, and then the nurses who are insufficient will be randomly assigned. In previous studies when nursing was a rapid shift, all nurses might work all shift types and there was no need to group nurses.

3.3. Medical Decision Classification Based on Big Data. Medical big data has a long history. There are written reports of clinical cases in ancient times. And with this, Islamic doctors in the Middle Ages further developed case records for teaching purposes. The forerunners of modern case records first appeared in Paris and Berlin in the early nineteenth century. Subsequently, clinical case records in the United States were developed in some teaching hospitals. In the twentieth century, clinical case data records were developed for direct use in patient care in hospital and outpatient Settings. There are many kinds of classification methods in data mining, such as decision tree method, FC nearest neighbor method, support vector machine, clustering algorithm, Logistic regression method, artificial neural network algorithm and so on. Among them, decision tree method is widely used in many problems because of its advantages of generating understandable rules, relatively small amount of calculation, processing continuous variables and classified variables, and clearly displaying which variables are more important.

Decision tree is a basic classification and regression method. The model of decision tree is a tree structure, which is usually composed of nodes and directed edges. There are two types of nodes: intermediate nodes and leaves. The intermediate node usually represents a certain feature or

attribute in the decision-making process, while the leaf node represents a classification or regression result. When leaf nodes represent classification results, such decision tree is also called classification tree. When leaf nodes represent regression results, a prediction real value is usually given. Such decision trees are also called regression trees. When using decision tree for classification or regression, a certain feature of the instance is tested starting from the root node. According to the test results, the instance is assigned to its corresponding child nodes, and then the process is repeated until the leaf node is reached. Finally, the instance is assigned to the corresponding category of the leaf node or the predicted value of regression.

XGBoost is an abbreviation for eXtreme Gradient Boosting, which has solved many real-world decision problems in recent years. XGBoost's excellent performance (both effectiveness and speed) made it the top solution in the screen data science competition for a long time, and it is still the model of choice for many big machine learning solutions. XGBoost is very excellent in parallel computing efficiency, missing value processing, control overfitting and prediction generalization ability. The base classifiers supported by XGBoost include decision trees and linear models. To prevent overfitting, XGBoost sets tree-based complexity as the regular term:

$$\Omega(f) = \gamma T + \frac{1}{2} \lambda \|w\|^2, \quad (2)$$

where, T is the number of leaf nodes of tree f , w is the vector formed by the output regression values of all leaf nodes. $\|w\|^2$ is the square of the $L2$ norm (modulus length) of this vector, and γ, λ is the hyperparameter. The objective function is as follows:

$$obj = \sum_{i=1}^N \left[g_i f_m(x_i) + \frac{1}{2} h_i f_m^2(x_i) \right] + \gamma T + \frac{1}{2} \lambda \sum_{j=1}^T w_j^2. \quad (3)$$

XGBoost also provides an approximate version of the above greed criterion, in short, using feature quantiles as segmentation candidates. In this way, the set of candidate points is reduced from traversal between the whole sample to traversal between several quantiles. Specifically, there are two strategies for selecting feature quantiles: global and local. Global is selected from the eigenvalues of all samples, and it only needs to be performed once before root node splitting. Local is selected from the eigenvalues of the samples contained in the nodes to be split, which should be carried out before each node is split. In general, since a global can only be partitioned once, it needs to be partitioned at a finer granularity.

Medical data is relatively special, so XGBoost optimization is a good fit for medical decision making. In order to speed up the selection of optimal segmentation points, XGBoost divides the eigenvalues into buckets according to the density distribution of eigenvalues, and uses the boundary value of the bucket as the candidate of the splitting points. Therefore, before training, the eigenvalues should be pre-sorted to find out the candidate cutting points, and then saved as a block structure, which is repeatedly used in

subsequent iterations, greatly reducing the amount of calculation. In the process of node splitting, the gain of each feature needs to be calculated, and the feature with the largest gain is finally selected to split.

Comprehensively consider the characteristics of nurses on duty, the gain calculation of each feature can be carried out by using multi-thread. That is, multi-thread parallel method is used to find the optimal segmentation point on different feature attributes, which can also play a role in preventing over-fitting. More importantly, the calculated splitting gain does not contain samples of missing values when searching for splitting points during training. In terms of logical implementation, in order to ensure completeness, samples missing the eigenvalue will be assigned to the left leaf node and the right leaf node respectively. After calculation of gain, the direction with large gain will be selected to classify samples containing the missing value. In the prediction stage, if there is no missing value in the training set but missing value in the test set, the default direction of the branch should be specified for the missing value (or the value that the specified value does not appear), and the missing value will be automatically divided into this branch during the prediction.

4. Experimental Results and Analysis

4.1. Experimental Setup. In the basic experiment phase, we chose the public data set INRC-2010, which consists of the test set provided by the 2010 contest, and mainly contains three types of questions: Sprint, Medium and Long. Each type of problem consists of three use cases: Early use cases, Late use cases, and Hidden instances. Sprint problems, Medium problems, and Long problems increase in size. The size of the problem for the early, Late, and Hidden instances of the same type increased. Through the above data to verify all the algorithms involved in this chapter, we compare and analyze the results of the algorithm in this paper with the best results of existing algorithms to verify the effectiveness of the algorithm in this paper. In order to verify the model more accurately, this paper will also simulate actual medical data for verification, the basic hardware requirements of the experiment are shown in Table 1.

Nurse scheduling is a NP-hard problem, which is small in scale but complicated. Python language is suitable for the implementation of nurse scheduling algorithm. In addition, Python is a good language for implementing this algorithm because of the excellent performance of machine learning algorithms. Python has the advantages of numpy, Matplotlib, SciKit-Learn, PANDAS, ipython and other tools in scientific computing. Pandas has the unrivaled advantage in handling medium data. It has become a major analysis tool in data analysis. Of course, Python also has powerful programming capabilities, which are different from R or MATLAB. Python has some very powerful data analysis capabilities, and it can also be used for crawler, game writing, and automatic operation and maintenance, which are widely used in these fields. These advantages make it possible for one technology to solve all business service problems, which fully demonstrates Python's ability to merge businesses. Using Python can greatly improve the efficiency of data analysis.

TABLE 1: Experimental environment configuration table.

Configuration	Parameters
Operating system	Windows10 (64)
CPU	Inter(R)Xeon(R)4116
Internal storage	128G
GPU	Tesla T4
Programming language	Python3.6
The text tool	BERT

4.2. Basic Time Analysis of the Model. Given the special nature of the healthcare industry, the value of time is Paramount. In order to verify the performance of the algorithm effectively, we analyze and compare the experimental results of the ANS algorithm and the algorithm in this paper from multiple perspectives. And then analyze and compare the advantages and disadvantages of the results obtained by the two algorithms and the length of the algorithm's running time (experiment S data Sprint, M said data Medium, BKS is known about the best results of the use case, Fb is algorithm each nurse scheduling problem cases to get the best solution, Fa is obtain the average solution algorithm to solve the use case, Ta is the average time for the algorithm to solve each use case).

Through traditional analysis and verification of examples in the dataset, the experimental results are obtained as shown in Figure 4. It can be clearly seen from Figure 4 that the variation rules of graph Fb, the best analysis result of the data obtained by the algorithm, and Graph Fa, the average result of the algorithm, are almost identical. The variations in the three plots are the same, which means that the optimal scheduling choices are the same. And in the analysis of individual data, the scheduling results are better than the fixed standard, which proves that the algorithm can greatly improve the efficiency of hospital nurses on duty. However, to our regret, not all of the results were better than the norm, and some experimental results did not meet the norm. not all of the results were better than the norm, and some experimental results did not meet the norm.

In order to exclude the error of the same type of data, we conducted the same experiment under data M, and the experimental results as shown in Figure 5 met the standard, but some data did not get the best value. That is, some data are not arranged in the best way, which may lead to the decline of hospital service evaluation in practical application.

In order to address the shortcomings of the traditional algorithm, our improved hybrid decision model was also verified under the data S and M. And Figure 6 shows the experimental results of the hybrid model under the data S. By comparing Figures 4 and 6, we can find that the number of optimal choices of the hybrid model is more than that of the traditional method, and it is easier for our algorithm to obtain the scheduling results of hospital demands based on the actual life.

In order to further verify the validity of the model, the experimental results of the mixed model under M data are shown in Figure 7. By comparing Figures 5 and 7, we can find that the number of optimal choices of the hybrid model

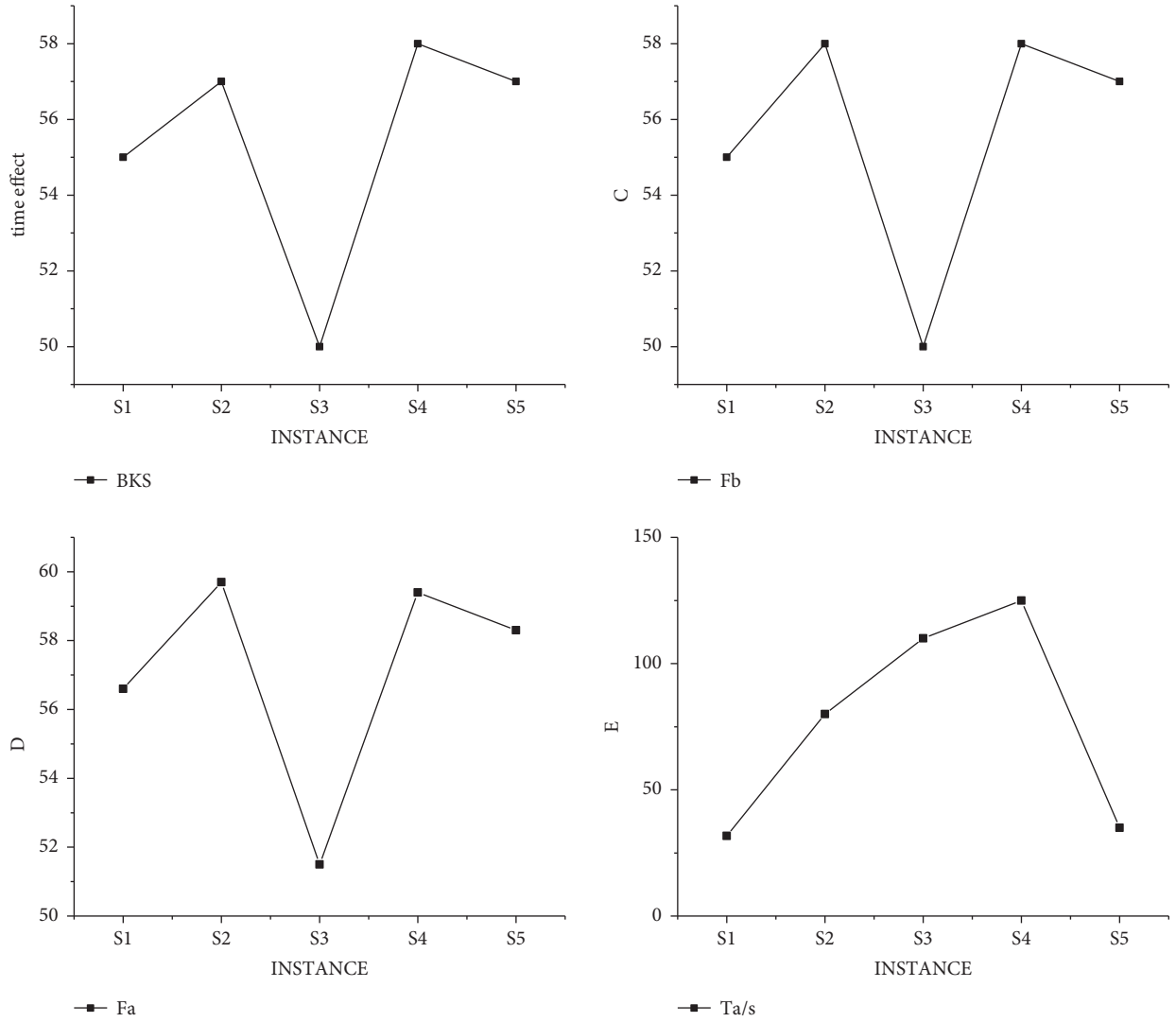


FIGURE 4: Experimental results of traditional algorithm in data S.

is still more than that of the traditional method. More importantly, the time of obtaining the standard value of the algorithm in this paper is significantly shorter than that of the traditional algorithm, indicating that the data processing efficiency of the algorithm is greatly improved.

The research on nurse scheduling problem belongs to the problem of selecting the optimal solution. This kind of algorithm research can further improve the processing efficiency through multi-threading (the time calculation of a scheduling problem is carried out under conventional splicing operation). The results of different threads of the mixed decision model under data S are shown in Figure 8. We obtained the experiment with small data through a large number of experiments, and the experimental result is that when solving each use case, all parameters of the two algorithms are the same, that is, the ending condition of the algorithm is the same. In this way, the best solution and the average solution are not calculated separately according to the different number of threads. But under the condition of

three threads, a unified value can better prove the objectivity of the experimental results. It can be seen from Figure 8 that the results of four threads are significantly better than those of two threads, but the progress is not linear due to data changes, which also conforms to the actual law. That is, there are individual emergencies in medical scheduling that we have to take into account.

By comparing the differences between Figures 5, 6 and 9, it is obvious that under the condition of conventional splicing, the running time of the improved hybrid algorithm is significantly reduced compared with that of the traditional algorithm. It shows that compared with random initialization methods, heuristic initialization methods generate high-quality solutions, which can reduce the number of iterations to a certain extent. And the experimental results show that the optimal solution of the hybrid algorithm is at least as good as that of the traditional algorithm, and the average solution is better than that of the conventional algorithm, and its time is shorter than that of the traditional algorithm.

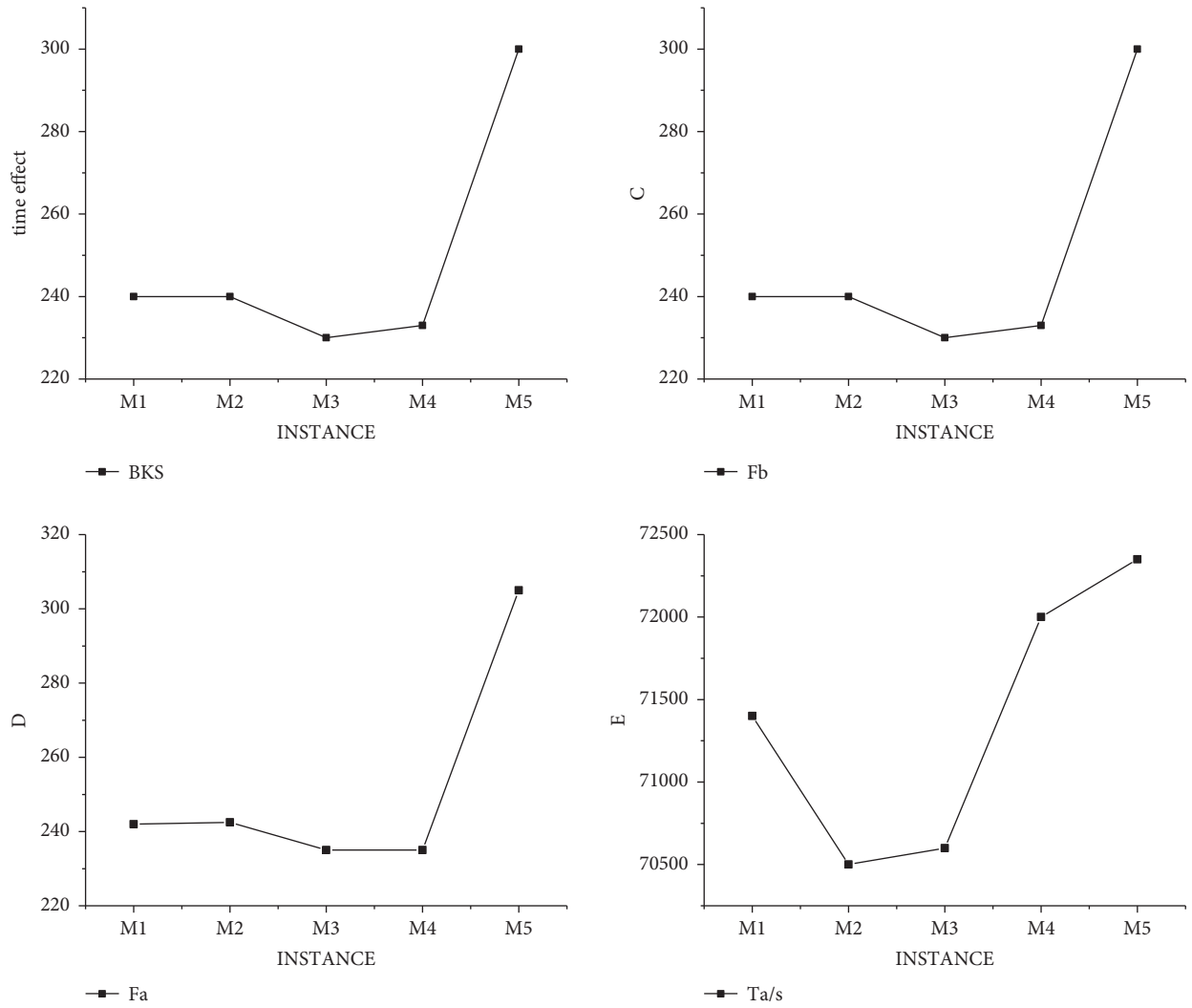


FIGURE 5: Experimental results of traditional algorithm in data M.

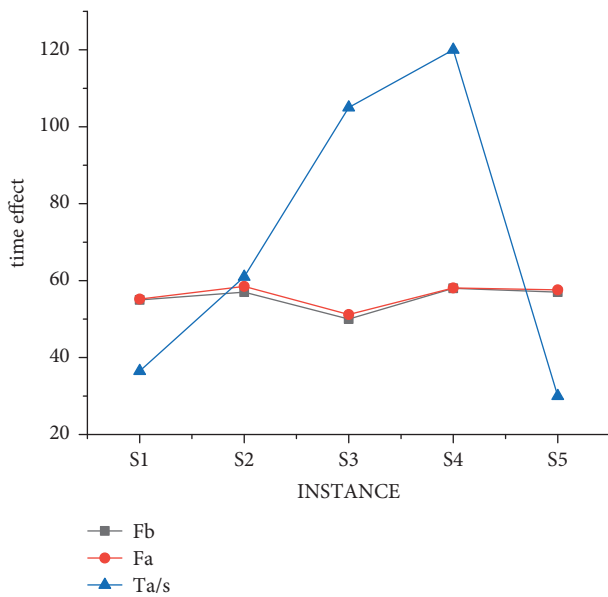


FIGURE 6: Results of mixed decision model under S data.

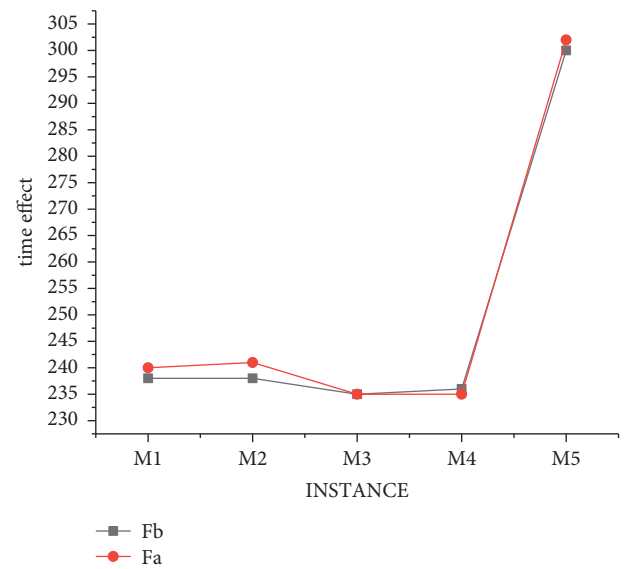


FIGURE 7: Results of mixed decision model under M data.

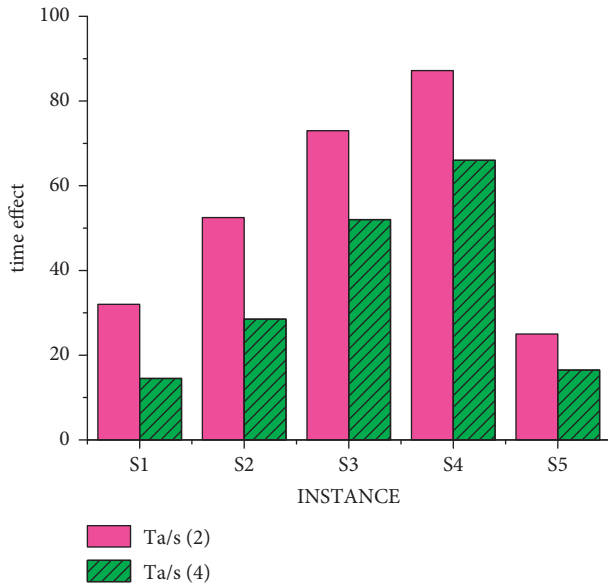


FIGURE 8: Time result of mixed decision model under S data.

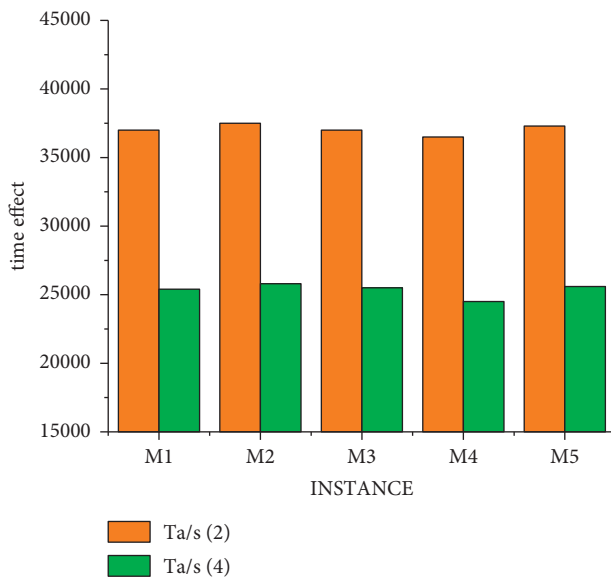


FIGURE 9: Time result of mixed decision model under M data.

In addition, by comprehensive comparison of experimental results under data S and M, the best solution obtained by the algorithm in this paper in use cases is the same as the known best solution, and the obtained solution is even better than the known best solution. And it can be seen that with the increase in the number of threads, the average time for solving use cases is getting shorter. This shows that the time performance of the improved algorithm is better than that of the traditional algorithm.

5. Conclusion

With the development of artificial intelligence, human beings have entered the era of intelligent data. How to give full

play to the maximum value of data is a common problem for all scientific researchers. Medical data application is one of the promising research fields. Hospital is a very special unit, involving a lot of professional departments and related departments. Under the impact of the global COVID-19 pandemic, the work of various departments and departments has become more difficult, so it is necessary to improve the rational allocation of existing resources in hospitals. Through the combination of optimization algorithm and decision algorithm, this paper proposes a scientific nursing scheduling scheme to ensure that professional medical staff can give full play to their strengths and provide medical services for patients. Only by closely combining computer technology with dependent services, can we realize the reform and innovation of hospital human resource management, ensuring the effective implementation of various human resource assignment work and enhancing the comprehensive strength of staff. In the future, more science and technology will be introduced into the medical industry. With the development of hardware technology, the talent gap of hospital departments will be filled, and the overall service potential of the hospital will be fully exerted.

Data Availability

The experimental data used to support the findings of this study are available from the corresponding author upon request.

Conflicts of Interest

The authors declare that they have no conflicts of interest to report regarding the present study.

References

- [1] S. Tian, W. Yang, J. M. L. Grange, P. Wang, W. Huang, and Z. Ye, "Smart healthcare: making medical care more intelligent," *Global Health Journal*, vol. 3, no. 3, pp. 62–65, 2019.
- [2] L. H. Aiken, Y. Xue, S. P. Clarke, and D. M. Sloane, "Supplemental nurse staffing in hospitals and quality of care," *The Journal of Nursing Administration: The Journal of Nursing Administration*, vol. 37, no. 7/8, pp. 335–342, 2007.
- [3] W. C. M. Yip, W. C. Hsiao, W. Chen, S. Hu, J. Ma, and A. Maynard, "Early appraisal of China's huge and complex health care reforms[J]. Health care policy in east asia: a world scientific reference," *Health Care System Reform and Policy Research in China*, vol. 1, pp. 51–83, 2020.
- [4] B. Maenhout and M. Vanhoucke, "An electromagnetic meta-heuristic for the nurse scheduling problem," *Journal of Heuristics*, vol. 13, no. 4, pp. 359–385, 2007.
- [5] L. Li and W. C. Benton, "Hospital capacity management decisions: e," *European Journal of Operational Research*, vol. 146, no. 3, pp. 596–614, 2003.
- [6] S. Fleischer, A. Berg, M. Zimmermann, K. Wuste, and J. Behrens, "Nurse-patient interaction and communication: a systematic literature review," *Journal of Public Health*, vol. 17, no. 5, pp. 339–353, 2009.

- [7] P. Copanitsanou, N. Fotos, and H. Brokalaki, "Effects of work environment on patient and nurse outcomes," *British Journal of Nursing*, vol. 26, no. 3, pp. 172–176, 2017.
- [8] S. De Simone, A. Planta, and G. Cicotto, "The role of job satisfaction, work engagement, self-efficacy and agentic capacities on nurses' turnover intention and patient satisfaction," *Applied Nursing Research*, vol. 39, pp. 130–140, 2018.
- [9] World Health Organization, *Imbalances in Rural Primary Care: A Scoping Literature Review with an Emphasis on the WHO European Region*, 2018.
- [10] D. Whitehead, "Health promoting hospitals: the role and function of nursing," *Journal of Clinical Nursing*, vol. 14, no. 1, pp. 20–27, 2005.
- [11] A. Purling and L. King, "A literature review: graduate nurses' preparedness for recognising and responding to the deteriorating patient," *Journal of Clinical Nursing*, vol. 21, no. 23-24, pp. 3451–3465, 2012.
- [12] S. M. Shortell, C. L. Bennett, and G. R. Byck, "Assessing the impact of continuous quality improvement on clinical practice: what it will take to accelerate progress," *The Milbank Quarterly*, vol. 76, no. 4, pp. 593–624, 1998.
- [13] D. A. Thompson, P. R. Yarnold, D. R. Williams, and S. L. Adams, "Effects of actual waiting time, perceived waiting time, information delivery, and expressive quality on patient satisfaction in the emergency department," *Annals of Emergency Medicine*, vol. 28, no. 6, pp. 657–665, 1996.
- [14] S. R. Jacoby and E. A. Scruth, "Negligence and the nurse: the value of the code of ethics for nurses[J]," *Clinical Nurse Specialist*, vol. 31, no. 4, pp. 183–185, 2017.
- [15] T. J. Vogus and L. E. McClelland, "When the customer is the patient: I," *Human Resource Management Review*, vol. 26, no. 1, pp. 37–49, 2016.
- [16] S. M. Lee, D. H. Lee, and C. Y. Kang, "The impact of high-performance work systems in the health-care industry: employee reactions, service quality, customer satisfaction, and customer loyalty," *Service Industries Journal*, vol. 32, no. 1, pp. 17–36, 2012.
- [17] E. K. Burke, J. Li, and R. Qu, "A hybrid model of integer programming and variable neighbourhood search for highly-constrained nurse rostering problems," *European Journal of Operational Research*, vol. 203, no. 2, pp. 484–493, 2010.
- [18] P. Sarkar, R. Chaki, and D. Sinha, "A heuristic framework for priority based nurse scheduling," *Advanced Computing and Systems for Security*, pp. 3–18, Springer, Singapore, 2017.
- [19] M. Mutingi and C. Mbohwa, "A Multi-Criteria Approach for Nurse Scheduling Fuzzy Simulated Metamorphosis Algorithm approach," in *Proceedings of the 2015 International Conference on Industrial Engineering and Operations Management (IEOM)*, pp. 1–7, IEEE, Dubai, UAE, March 2015.
- [20] A. A. Musa and U. Saxena, "Scheduling nurses using goal-programming techniques," *IIE Transactions*, vol. 16, no. 3, pp. 216–221, 1984.
- [21] B. Maenhout and M. Vanhoucke, "Branching strategies in a branch-and-price approach for a multiple objective nurse scheduling problem," *Journal of Scheduling*, vol. 13, no. 1, pp. 77–93, 2010.
- [22] A. Legrain, H. Bouarab, and N. Lahrichi, "The nurse scheduling problem in real-life," *Journal of Medical Systems*, vol. 39(1), pp. 1–11, 2015.
- [23] S. Topaloglu, "A shift scheduling model for employees with different seniority levels and an application in healthcare," *European Journal of Operational Research*, vol. 198, no. 3, pp. 943–957, 2009.
- [24] D. Parr and J. M. Thompson, "Solving the multi-objective nurse scheduling problem with a weighted cost function," *Annals of Operations Research*, vol. 155, no. 1, pp. 279–288, 2007.
- [25] I. X. Tassopoulos, I. P. Solos, and G. N. Beligiannis, "A two-phase adaptive variable neighborhood approach for nurse rostering," *Computers & Operations Research*, vol. 60, pp. 150–169, 2015.
- [26] B. Jaumard, F. Semet, and T. Vovor, "A generalized linear programming model for nurse scheduling," *European Journal of Operational Research*, vol. 107, no. 1, pp. 1–18, 1998.
- [27] J. F. Bard and H. W. Purnomo, "Preference scheduling for nurses using column generation," *European Journal of Operational Research*, vol. 164, no. 2, pp. 510–534, 2005.
- [28] M. A. Awadallah, M. A. Al-Betar, A. T. Khader, A. L. Bolaji, and M. Alkoffash, "Hybridization of harmony search with hill climbing for highly constrained nurse rostering problem," *Neural Computing & Applications*, vol. 28, no. 3, pp. 463–482, 2017.
- [29] S. Abdennadher and H. Schlenker, "INTERDIP—an Interactive Constraint Based Nurse scheduler," in *Proceedings of the First International Conference and Exhibition on the Practical Application of Constraint Technologies and Logic Programming*, PACLP, Berlin, Germany, April 1999.
- [30] S. Abdennadher and H. Schlenker, "Nurse Scheduling Using Constraint Logic programming," in *Proceedings of the AAAI/IAAI*, pp. 838–843, Berlin, Germany, July 1999.
- [31] B. M. W. Cheng, J. H. M. Lee, and J. C. K. Wu, "A nurse rostering system using constraint programming and redundant modeling," *IEEE Transactions on Information Technology in Biomedicine*, vol. 1, no. 1, pp. 44–54, 1997.
- [32] H. M. Hofe, "Conplan/siedaplan: Personnel Assignment as a Problem of Hierarchical Constraint satisfaction," in *Proceedings of the 3rd International Conference on Practical Applications of Constraint Technologies*, 1997.
- [33] N. Musliu, N. Gärtner, and W. Slany, "Efficient generation of rotating workforce schedules," *Discrete Applied Mathematics*, vol. 118, no. (1-2), pp. 85–98.
- [34] E. K. Burke, T. Curtois, G. Post, R. Qu, and B. Veltman, "A hybrid heuristic ordering and variable neighbourhood search for the nurse rostering problem," *European Journal of Operational Research*, vol. 188, no. 2, pp. 330–341, 2008.
- [35] E. Rahimian, K. Akartunali, and J. Levine, "A hybrid integer programming and variable neighbourhood search algorithm to solve nurse rostering problems," *European Journal of Operational Research*, vol. 258, no. 2, pp. 411–423, 2017.
- [36] C. Valouxis and E. Housos, "Hybrid optimization techniques for the workshift and rest assignment of nursing personnel," *Artificial Intelligence in Medicine*, vol. 20, no. 2, pp. 155–175, 2000.
- [37] M. J. Brusco and L. W. Jacobs, "A simulated annealing approach to the cyclic staff-scheduling problem," *Naval Research Logistics*, vol. 40, no. 1, pp. 69–84, 1993.
- [38] H. G. Santos, T. A. M. Toffolo, R. A. M. Gomes, and S. Ribas, "Integer programming techniques for the nurse rostering problem," *Annals of Operations Research*, vol. 239, no. 1, pp. 225–251, 2016.
- [39] N. Musliu, J. Gärtner, and W. Slany, "Efficient generation of rotating workforce schedules," *Discrete Applied Mathematics*, vol. 118, no. 1-2, pp. 85–98, 2002.

Research Article

Effect of Early Rehabilitation Nursing on Motor Function and Living Ability of Patients with Traumatic Brain Injury Based on Orem's Self-Care Theory

Yuqin Yang and Lu Niu 

The First People's Hospital of Lianyungang, The Affiliated Lianyungang Hospital of Xuzhou Medical University, The First Affiliated Hospital of Kangda College of Nanjing Medical University, Nanjing 222061, China

Correspondence should be addressed to Lu Niu; 760020220081@xzhmu.edu.cn

Received 6 June 2022; Revised 27 June 2022; Accepted 1 July 2022; Published 8 September 2022

Academic Editor: Dong Chen

Copyright © 2022 Yuqin Yang and Lu Niu. This is an open access article distributed under the Creative Commons Attribution License, which permits unrestricted use, distribution, and reproduction in any medium, provided the original work is properly cited.

Objective. To explore the effect of early rehabilitation nursing on motor function and living ability of patients with traumatic brain injury (TBI) based on Orem's self-care theory. **Methods.** A total of 60 patients with TBI treated in our hospital from February 2019 to June 2021 were enrolled. The patients were randomly divided into a control group and a research group. The control group adopted the early rehabilitation nursing model, while the research group adopted the early rehabilitation nursing model based on Orem's self-nursing theory. Nursing satisfaction, Fugl-Meyer score, NIH-SS score, Barthel index, quality of life score, and compliance were in the comparison of the two groups. **Results.** The nursing satisfaction of the research group was higher than that of the control group ($P < 0.05$). Compared with the control group, the Fugl-Meyer scores of the research group were higher at 1 month, 2 months, and 3 months after nursing ($P < 0.05$). After nursing, the NIH-SS score of the two groups decreased. In the comparison of the two groups, the NIH-SS score of the research group at 1 month, 2 months, and 3 months after nursing was lower ($P < 0.05$). After nursing, the Barthel index of the two groups increased. In the comparison of the two groups, the Barthel index of the research group was higher compared to the control group at 1 month, 2 months, and 3 months after nursing ($P < 0.05$). The scores of physiological function, psychological function, social function, and health self-cognition in the research group were lower ($P < 0.05$). The compliance rate of the research group was higher than that of the control group ($P < 0.05$). **Conclusion.** Patients with TBI receive early rehabilitation nursing based on Orem's self-care theory, which can effectively improve patient satisfaction and compliance and achieve the purpose of improving motor function and living ability. This nursing program is worth popularizing in the clinic.

1. Introduction

Brain injury, also known as traumatic brain injury (TBI) or head injury (HI), refers to brain injury caused by external violence in the head and neck, which can lead to disturbance of consciousness, memory loss, and neurological dysfunction [1]. TBI is a kind of injury with high morbidity, high mortality, and high disability rate. The prevalence rate of TBI in China is 783.3/100,000 population, second only to cerebrovascular disease and limb injury. However, the mortality and disability rate ranked first [2]. In the United States, the incidence of TBI is about 200/100,000 people; there are

500,000 new cases every year, and about 80,000 people die from TBI each year [3]. The fatality rate of mild, moderate, and severe TBI is 0.7%, 26% and 58%, respectively. The disability rate is 10%, 66%, and 100%, respectively [4]. The main causes of TBI include traffic accidents, industrial accidents, accidental falls, sports injuries, falls, dystocia, and surgical delivery. Wounds such as gunshot wounds and explosive wounds, as well as car accidents, fortifications, and building collapses, are the main causes of TBI in wartime [5]. TBI can occur in all age groups, and its distribution is polarized, that is, teenagers aged 15–24 (200/100,000 population) and people aged 65–75 (200/100,000 population).

The incidence of TBI in males was significantly higher compared to females, about 2:1, and the mortality rate was 3–4 times higher compared to females [6]. TBI occurs in youth and early adulthood, which are two critical periods in life. During this period, people not only need to learn knowledge but also need to master the skills for future life, but TBI limits their learning and ability development. Even have a significant impact on independent life [7]. TBI is the most common and crippling disease of the nervous system, which is the most disabling qualitative disease that can occur in patients with different degrees of motor and sensory dysfunction, with cognition and perception function, communication function, daily life self-care ability, behavior, psychological and social barriers; these dysfunction leads to higher morbidity. It seriously affects the quality of life of patients and brings a huge impact and heavy burden on patients, families, and society. In recent years, with the progress of medical technology, the overall mortality rate of brain trauma has dropped from 50% 30 years ago to about 30% now, but most of the surviving patients will be left with varying degrees of disability. In addition to physical and language dysfunction, cognitive impairment accounted for a large proportion [8].

Surgery is commonly employed in the treatment of TBI, but how to effectively providing nursing services for patients plays an important role in promoting postoperative rehabilitation and enhancing the quality of life of patients [9]. In order to explore the clinical nursing model suitable for TBI, further meet people's continuous pursuit of health, maximize the psychological and physiological satisfaction of patients with TBI, and reduce the burden on patients' families, nurses, and society. In recent years, major medical institutions have introduced self-care theory into nursing work [10]. Self-care theory is a nursing theory put forward by Dorothea Elizabeth Orem, Master of Nursing Education in the United States [11]. It was introduced into China in the middle and late 1980s, then gradually recognized by the nursing community, and applied to clinical practice guidance, education, and research. It includes self-care theory, self-care defect theory, and nursing system theory, which is composed of the nursing behavior provided by nurses and the behavior of patients. Nurses adopt three different nursing systems according to patients' self-care needs and ability, namely, complete compensation system, partial compensation system, and support-education system. It is widely employed in the nursing care of patients with TBI. In full compensation care, nurses take care of elderly TBI patients to meet all their needs. Nurses must make every effort for these patients to meet their therapeutic self-care needs. In partial compensatory nursing, both nurses and patients with TBI can play an important role in meeting the needs of therapeutic self-care. Nurses "help" patients complete self-care activities and make up for the deficiency of patients' self-care. According to the needs of patients, they can help and adjust their self-care ability, while patients try their best to complete what they can do independently, adjust their self-care ability, meet their self-care needs, and accept nurses' help. In the support-education system, patients with TBI need to learn how to self-care and the

patients are able to complete self-care activities but need temporary help. The help provided by nurses is psychological support, technical guidance, and the provision of a needed environment. In this system, the responsibility of a nurse is to "do it for him" and "do it for him" in the first two systems and transition to "educate and support him to do it." Early rehabilitation exercise refers to timely and correctly guiding patients to apply exercise therapy on the basis of a comprehensive evaluation of patients' postoperative physical function according to the principles of different people, gradual and orderly progress, perseverance, dynamic and static combination, and active participation [11]. The purpose of early rehabilitation exercise is to enhance muscle strength, increase the range of joint motion, and restore the function of lumbar vertebrae and lower extremities. The early rehabilitation nursing model based on Orem's self-care theory is to carry out early rehabilitation nursing for patients under Orem's self-care theory, in order to promote the recovery of motor function and living ability [12]. This study focuses on the effect of early rehabilitation nursing based on Orem's self-care theory on motor function and living ability of patients with TBI.

2. Patients and Methods

2.1. General Information. A total of 60 patients with TBI treated in our hospital from February 2019 to June 2021 were enrolled. The patients were randomly divided into a control group and a research group. The control group adopted the early rehabilitation nursing model, while the research group adopted the early rehabilitation nursing model based on Orem's self-nursing theory. In the control group, the age was 35–78 years old, with an average of (50.91 ± 3.53) years, including 15 males and 15 females, while in the research group, the age was 35–76 years old, with an average of (50.96 ± 3.65) years, including 16 males and 14 females. There was no statistical significance in the general data of the two groups. This study was permitted by the Medical Ethics Association of our hospital, and all patients noticed informed consent. This is a prospective study, and the baseline data of the two groups are balanced.

Inclusion criteria are as follows: (1) diagnostic criteria of TBI: clear history of TBI, confirmed by CT or MRI, and accorded with the diagnostic criteria of brain injury approved by the fourth National Academic Conference on Cerebrovascular Diseases; (2) age more than 14 years old and less than 60 years old and graduated primary school education level or above; (3) Glasgow coma scale (GCS) score ≤ 8 ; (4) Montreal Cognitive Assessment (MoCA) scale < 26 points; (5) no previous history of cognitive impairment and mental illness; and (6) informed consent.

Exclusion criteria are as follows: (1) age ≥ 60 years old or ≤ 14 years old and the educational level below primary school; (2) unstable vital signs; (3) MoCA > 26 points; (4) patients with severe language impairment, severe vision or hearing impairment, and bilateral upper limb dysfunction who could not be tested; (5) patients with the previous history of mental illness and pre-TBI with cognitive impairment or suspected cognitive impairment; (6) patients

with myocardial infarction or severe hepatic and renal dysfunction, severe infection, and severe diabetes; and (7) unconscious.

2.2. Treatment Methods. The control group received early rehabilitation nursing mode and carried out rehabilitation training with joint stability training as the core under the guidance of rehabilitation doctors and nurses in our hospital. First of all, nurses, family nurses, and patients were trained on the relevant knowledge of joint stability training of brain trauma, and rehabilitation doctors conducted rehabilitation training regularly with the participation of the three parties. The stability rehabilitation training program mainly includes antimuscle contracture training, flexion and extension muscle strength training, walking training, and joint impedance training. Meanwhile, rehabilitation doctors record the specific contents of stability training as videos and distribute them to patients for learning. Training is conducted twice a day for 60 minutes each time. The training process is carried out under the guidance of the rehabilitation therapist. It should be noted that attention should be paid to the safety risks in the rehabilitation process to ensure the quality and safety of rehabilitation training.

The research group accepted the early rehabilitation nursing model based on Orem's self-care theory: the Orem self-care model was employed throughout the whole nursing process of the intervention group. According to the patients' health needs, conditions, and existing nursing problems, the patients' self-care ability was comprehensively judged and dynamically evaluated, and different nursing systems and health education were given to guide the patients' self-care theory. Explain the significance and purpose of self-care and the responsibilities that patients and medical staff should bear in the process of rehabilitation training. And adjust flexibly according to the specific condition in the nursing process; the specific nursing process is as follows: (1) diagnosis and treatment: collect data by observing and talking with patients and their families and evaluate the patient's self-care needs, self-care ability, and self-care defects to determine why the patient needs care, and this analysis should be carried out continuously from the beginning to the end. In this step of the investigation, nurses should answer the following five questions: (1) what are the current therapeutic self-care needs of patients? (2) Are there any deficiencies in patients' self-care ability in order to meet these therapeutic self-care needs? (3) If there is a self-protection defect, what is the nature and why? (4) In order to achieve the purpose of treatment, should patients be helped to complete all their work or those self-care abilities that have been developed should be protected and encouraged? (5) What is the potential of patients' self-care ability in the future, such as increasing or deepening self-care knowledge, learning nursing techniques, and cultivating self-care desire? How to effectively and continuously integrate major self-care measures into daily life and self-care plans. (2) Planning and design: this step is the planning part of the procedure. According to the nursing diagnosis, the corresponding nursing plan is designed according to the three systems of

complete compensation, partial compensation, and auxiliary education in the nursing system theory. The specific plans are as follows: (1) complete compensation nursing: the patients are not fully awake after joint replacement surgery, the affected limbs use brace, traction and other bracing, drainage tubes, catheters, and so on, and the patients are unable to take care of themselves, their own hygiene, and daily life, and concomitantly, we should use complete compensation nursing system nursing with medical support to compensate for patients' lack of self-care. Nurses' behavior is to help them accept compensation and provide for all their self-care needs, including condition observation, cleaning respiratory tract, nutrition, keeping incision dry, keeping drainage tube unobstructed, observing local inflammation, recording body temperature changes, and basic life care such as washing, eating, defecation, cleaning perineum, skin care, medication, and so on. At the same time, it can meet the therapeutic self-care needs of patients, including helping patients turn over, massage the compressed site, measure vital signs, keep the indwelling catheter unobstructed, observe drainage, and so on. (2) Partial compensatory nursing: when the patient's vital signs are stable, conscious, and pain relieved, it generally refers to the second day after operation to before discharge. Nurses should continue to evaluate the patient's physical condition, postoperative rehabilitation exercise knowledge, skills, and self-care ability and provide partial compensatory nursing according to the difference in self-care ability. Let patients do what they can, change passivity into the initiative, mobilize patients' subjective initiative, and enhance patients' self-care ability and behavior ability, with emphasis on assistance, guidance, and education. During this period, the main goal of nursing is to teach patients specific skills of self-care and functional exercise. The functional exercise program and the training procedure for patients' self-care ability were formulated and photocopied and distributed to the patients themselves or their families, which were guided by the researchers. In the process of implementation, according to the specific conditions of each patient, adjust the exercise intensity and progress and help patients answer common questions in postoperative rehabilitation. (3) Support education and nursing: nurses use the support-education system to give psychological support to patients, provide counseling, carry out health education and nursing behavior guidance, and guide patients and their families to participate actively. Patients with brain trauma have different degrees of lack of knowledge in each rehabilitation stage. Nurses, as health promoters and educators, should provide relevant information and health education to patients and their families in the whole process of the disease. Make them master the methods of self-care, guide patients on how to prevent dislocation, let patients and their families actively participate in nursing activities, and achieve the goal of restoring independent living ability as soon as possible, including making the introduction of admission to the hospital; making the patients familiar with the ward environment and medical staff as soon as possible; reducing depression; talking with patients before operation; patiently introducing the basic knowledge of brain trauma, including

the basic principle and treatment effect; providing relevant information to patients; comforting and encouraging patients with successful examples of surgery; increasing treatment confidence; relaxing their spirit; eliminating worries and fears; and actively cooperating with medical care. After the operation, most patients may have fear and pain when using a venous pump and joint activity. Researchers should patiently explain to this kind of patients, eliminate their fear and anxiety, and encourage patients to build up confidence in overcoming the disease. (3) Implementation and evaluation: this step is the generation and management of the nursing relationship. Nurses implement the nursing system plan. Orem believes that nurses should: (1) assist patients (or family members) in self-care to achieve healthy results, (2) check completion against the requirements of the plan, (3) collect evidence that can show the effectiveness of nursing, and (4) compare with the results determined in the nursing system and evaluate the results with evidence.

2.3. Observation Index

2.3.1. Satisfaction. After consulting the literature and expert discussion, we designed patients' follow-up satisfaction, a total of 10 items, and recorded patients' satisfaction with follow-up management mode, health education, medical and nursing service, appointment registration process, and so on. It is assigned into four dimensions: very satisfied, satisfied, general, and dissatisfied. Satisfaction rate = very satisfaction rate + satisfaction rate + general rate.

2.3.2. Fugl-Meyer Motor Function Scale. Fugl-Meyer's motor function scale was used to evaluate the upper limb motor function and lower limb motor function before nursing and 1 month, 2 months, and 3 months after nursing. The upper limb motor function score was 66, and the lower limb motor function score was 34. The higher the score, the better the patient's motor function.

2.3.3. NIH-SS Scoring. The neurological function of the patients was evaluated with NIH-SS score before nursing and 1 month, 2 months, and 3 months after nursing, including 11 items such as level of consciousness, gaze, visual field, facial paralysis, upper limb movement, lower limb movement, ataxia, sensation, language, dysarthria, and neglect. The higher the score, the more obvious the neurological dysfunction.

2.3.4. Barthel Index. Before nursing and 1 month, 2 months, and 3 months after nursing, the Barthel index was employed to evaluate the ability of daily living before and after the intervention. The total score was 100. The higher the score, the stronger the ability to daily living.

2.4. Quality of Life Scale. The quality of life scale consists of four subscales, including physical, psychological, social, and health self-awareness, with a total of 29 items. Cronbach's α

coefficient of the scale is 0.79–0.91. The scale was scored by 1–5 grades. The lower the score, the higher the quality of life.

2.5. Compliance. Compliance is assigned into very compliance, compliance, noncompliance, and compliance rate = very compliance rate + compliance rate.

2.6. Statistical Analysis. The data were analyzed by SPSS 21.0 statistical software, and the measurement data were expressed by $(\bar{x} \pm s)$. *T*-test of independent samples was employed for comparison between groups; paired *t*-test was employed for comparison before and after treatment; and counting data were expressed by example *n* (%). χ^2 test was employed; $P < 0.05$ exhibited the difference was statistically significant.

3. Results

3.1. Comparison of Nursing Satisfaction. First of all, we compared the nursing satisfaction between the two groups: the research group was very satisfied in 24 cases, satisfactory in 5 cases and general in 1 case; the satisfaction rate was 100.00%; the control group was very satisfied in 14 cases, satisfactory in 10 cases, general in 1 case, and dissatisfied in 5 cases. The satisfaction rate was 83.33%. In the comparison of groups, the nursing satisfaction in the research group was higher, and the difference was statistically significant ($P < 0.05$). All the data results are indicated in Figure 1.

3.2. Fugl-Meyer Score Comparison. Secondly, we compared the Fugl-Meyer scores of the two groups. Before nursing, there exhibited no significant difference ($P > 0.05$). After nursing, the Fugl-Meyer score of both groups increased. Compared with the control group, the Fugl-Meyer scores of the research group were higher at 1 month, 2 months, and 3 months after nursing, and the difference was statistically significant ($P < 0.05$). All the data results are indicated in Table 1.

3.3. NIH-SS Score Comparison. Thirdly, we compared the NIH-SS scores of the two groups. Before nursing, there exhibited no significant difference ($P > 0.05$). After nursing, the NIH-SS scores of both groups decreased. Compared with the control group, the NIH-SS score of the research group was lower at 1 month, 2 months, and 3 months after nursing, and the difference was statistically significant ($P < 0.05$). All the data results are indicated in Table 2.

3.4. Barthel Index Comparison. Then, we compared the Barthel index. Before nursing, there exhibited no significant difference ($P > 0.05$). After nursing, the Barthel index of the two groups increased. The Barthel index of the research group was higher compared to the control group at 1 month, 2 months, and 3 months after nursing, and the difference exhibited statistically significant ($P < 0.05$). All the data results are indicated in Table 3.

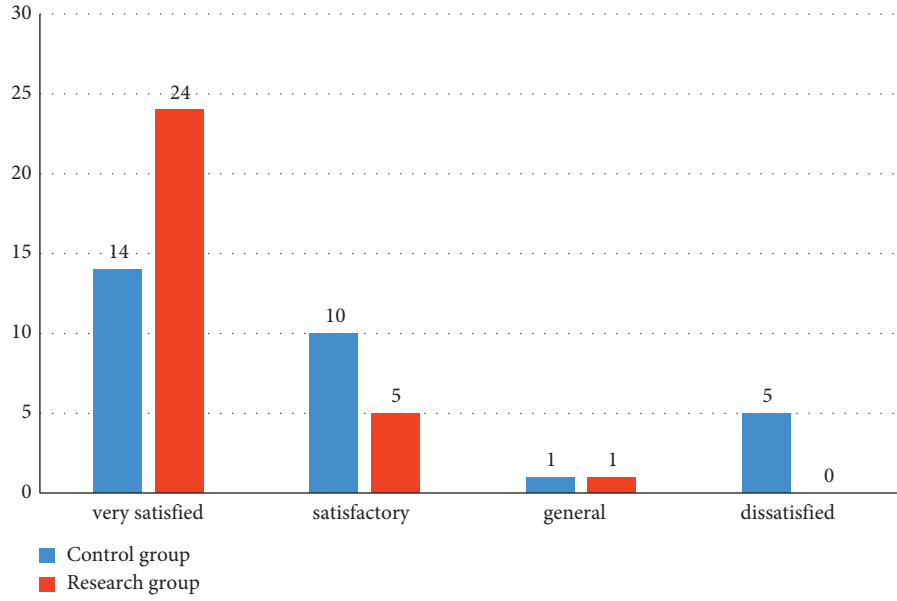


FIGURE 1: Comparison of nursing satisfaction between the two groups.

TABLE 1: Comparison of Fugl-Meyer score between the two groups [$\bar{x} \pm s$, points].

Grouping	N	Before nursing	1 month after nursing	2 months after nursing	3 months after nursing
Control group	30	31.96 \pm 4.53	44.06 \pm 3.12	54.91 \pm 2.41	62.59 \pm 3.46
Research group	30	31.82 \pm 3.56	57.93 \pm 2.56	65.18 \pm 4.23	74.81 \pm 3.13
t		0.133	18.823	11.554	14.345
P		> 0.05	< 0.01	< 0.01	< 0.01

TABLE 2: Comparison of NIH-SS scores between the two groups [$\bar{x} \pm s$, points].

Grouping	N	Before nursing	1 month after nursing	2 months after nursing	3 months after nursing
Control group	30	34.91 \pm 3.31	32.49 \pm 1.55	28.59 \pm 4.12	25.78 \pm 3.31
Research group	30	34.78 \pm 3.56	30.18 \pm 3.13	25.44 \pm 3.56	20.64 \pm 3.13
t		0.146	3.622	3.168	6.179
P		> 0.05	< 0.01	< 0.01	< 0.01

TABLE 3: Comparison of Barthel index between the two groups [$\bar{x} \pm s$, points].

Grouping	N	Before nursing	1 month after nursing	2 months after nursing	3 months after nursing
Control group	30	30.68 \pm 4.52	34.78 \pm 3.12	40.81 \pm 3.55	58.49 \pm 3.12
Research group	30	30.85 \pm 3.77	38.93 \pm 5.23	47.49 \pm 4.78	65.81 \pm 3.45
t		0.158	3.732	6.145	8.619
P		> 0.05	< 0.01	< 0.01	< 0.01

3.5. Comparison of Qualities of Life Scores. Next, we compared the scores of qualities of life between the two groups. Before nursing, there exhibited no significant difference ($P > 0.05$). After nursing, the scores of qualities of life of the two groups decreased. The scores of physiological function, psychological function, social function, and health self-cognition in the research group were lower than those in the control group, and the difference was statistically significant ($P < 0.05$). All the data results are indicated in Table 4.

3.6. Compliance Comparison. Finally, we compared the compliance of the two groups; the compliance rate of the

research group was higher; and the difference was statistically significant ($P < 0.05$). All the data results are indicated in Figure 2.

4. Discussion

TBI refers to the brain injury caused by external violence, which can lead to disturbance of consciousness, memory loss, and neurological dysfunction [13]. Studies have indicated that TBI has the characteristics of high morbidity, high mortality, and high disability rate [14]. Craniocerebral injury is the most common and crippling disease in nervous system diseases [15]. Patients may have varying degrees of

TABLE 4: Comparison of quality of life scores between the two groups[$\bar{x} \pm s$, Points].

Grouping	N	Physiological function		Psychological function		Social function		Healthy self-cognition	
		Before nursing	After nursing	Before nursing	After nursing	Before nursing	After nursing	Before nursing	After nursing
Control group	30	15.64 \pm 4.91	13.86 \pm 2.56 ^a	16.31 \pm 3.88	14.78 \pm 4.31 ^a	18.75 \pm 3.31	16.23 \pm 2.12 ^a	15.88 \pm 3.78	13.12 \pm 1.67 ^a
Research group	30	15.41 \pm 4.67	11.54 \pm 2.31 ^b	16.74 \pm 3.13	12.88 \pm 1.21 ^b	18.55 \pm 3.76	12.78 \pm 3.31 ^b	15.12 \pm 3.77	10.12 \pm 2.77 ^b
t		0.185	3.682	0.472	2.324	0.218	4.807	0.779	5.080
P		> 0.05	< 0.01	> 0.05	< 0.01	> 0.05	< 0.01	> 0.05	< 0.01

Note. The control group before and after nursing, ^a $P < 0.05$; the research group before and after nursing, ^b $P < 0.05$.

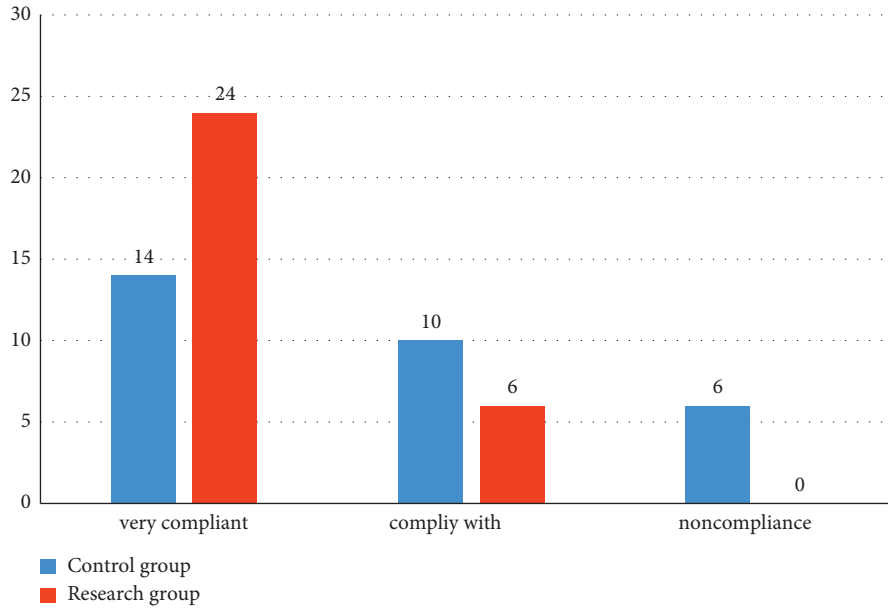


FIGURE 2: Comparison of compliance between the two groups.

motor and sensory dysfunction, accompanied by recognition, cognitive and perceptual functions, language communication functions, ability to take care of daily life, and behavioral, psychological, and social communication disorders; these dysfunctions lead to high disability rates and seriously affect the quality of life of patients [16]. It brings great influence and a heavy burden to the individual, family, and society of the patients. With the rapid development of transportation, the incidence of TBI is getting higher [17]. Today, with the rapid development of medical technology, great progress has been made in the treatment of TBI [18]. The overall mortality rate of TBI has decreased from 50% 30 years ago to about 30% at present, and the case fatality rate has dropped obviously [19]. However, as people often attach importance to life rescue while neglecting functional rehabilitation, the disability rate is greatly increased, and most of the surviving patients will leave behind varying degrees of disability. In addition to cognitive dysfunction, language dysfunction, and physical function accounted for a large part [20]. In the United States, some scholars published the meta-analysis report “early rehabilitation based on evidence: recommendations for Clinical practice” from 1999 to 2000. The results support the effectiveness of

existing early rehabilitation methods for patients with stroke and TBI [21]. The evidence demonstrates that perceptual rehabilitation training after stroke in the left and right hemispheres and rehabilitation training of attention, memory, and executive dysfunction after TBI contribute to functional improvement [22]. In 2005, American scholars systematically reviewed the literature on the efficacy of limb rehabilitation in patients with acquired brain injury published from 1998 to 2002 and put forward more specific and detailed practical standards, guidelines, and choices [23]. Other scholars’ studies performed meta-analysis, which also indicated that the therapeutic effect was affected by the type of cognitive impairment, course of the disease, type of TBI, and age and indicated sufficient evidence to confirm the effectiveness of attention training after TBI and visual-spatial training after unilateral neglect after stroke [24]. In China, as people pay more attention to limb functional rehabilitation, with the development of limb functional rehabilitation in Europe and the United States, and other developed countries, people gradually realize the impact of limb functional rehabilitation on rehabilitation. Limb functional rehabilitation has been paid more and more attention and become the focus [24].

After TBI, due to the mechanical damage of brain tissue caused by external forces, coupled with the secondary brain inflammatory response, it is more likely to bring about extensive nerve fiber damage, and the damage to brain tissue is more extensive [25]. Therefore, in terms of cerebrovascular disease, the brain is malleable, and the structure and function of the cerebral cortex can change as expected under the continuous action of external stimuli. After TBI, through the considerable intensity of learning and training, the dendrites and axons of neurons can establish new connections, or adjacent intact brain regions can replace the function of damaged brain regions, thus promoting behavioral changes [25]. Therefore, in the early stage of TBI, repeated rehabilitation training can promote the activation of latent pathways and dormant synapses, make the axons of related nerve cells sprout to form new synapses, and finally trigger synaptic regeneration, promoting brain function to carry out the functional repair, so as to reduce the degree of neurological disability. At present, the commonly used clinical cognitive rehabilitation methods include occupational therapy, computer-assisted cognitive training, virtual technology, and remote cognitive rehabilitation [26]. As the ability of TBI patients to process available information is weaker than that of normal people, effective psychological and behavioral patterns should be organically combined in the process of rehabilitation to broaden the information processing and information absorption capabilities of TBI patients, which is also very important to help TBI patients. Therefore, early rehabilitation nursing for patients with TBI is carried out by nurses. The cognitive rehabilitation intervention with the participation of patients' family members and therapists organically combines the mental and behavior patterns of patients. Through repeated training, patients can synthesize, and analyze information, so as to enhance their quality of life [27].

Orem's self-care theory was originally put forward by American nursing theorist Dorothea Orem [28]. Self-care is an individual's self-care behavior to meet the maintenance of their own life, health function, growth, development, and happiness, which is realized by meeting the existing self-care needs. In recent years, there have been more researches and applications on self-care behavior, which have developed rapidly, mainly focused on chronic diseases such as chronic obstructive pulmonary disease, asthma, heart failure, diabetes, hypertension, hemiplegia, and so on [28]. The results show that through self-nursing intervention, patients can master the relevant knowledge of TBI, correctly understand their self-worth, adapt to various changes caused by diseases, thus actively participate in the rehabilitation of TBI, and finally improve their quality of the patient. Orem's self-care theory emphasizes the individual's self-care ability, which is consistent with the holistic nursing concept of "patient-centered." Its purpose is to facilitate the individual's health status and the body's coping ability and function and has gradually become one of the main means of disease management [29]. The early rehabilitation nursing based on Orem's self-care theory was applied to the nursing of patients with TBI. According to the specific patients and different stages of the disease, the self-care ability was

dynamically evaluated, and different nursing systems were adopted. The self-care model suitable for different individuals and stages was worked out so that the nursing care of nursing patients at all levels was valued and compensated according to their self-care ability [30]. It can enable patients to correctly understand the disease and master the relevant self-care knowledge, so as to reduce the occurrence of complications, promote the limb function and survival ability of patients, enhance their self-confidence, and enable them to correctly deal with and accept the changes of internal and external environments, and show better social adaptability and enhance the quality of life. Patients with TBI participate in their own health decision-making and nursing from admission to discharge, encourage patients and their families to participate in nursing activities, mobilize patients' enthusiasm, explore their self-care potential, and give full play to their subjective initiative. It reflects the patient's own value and gives full play to the patient's self-care ability. At the same time, it shortens the nurse-patient relationship, enhances job satisfaction, enhances communication and understanding between nurses and patients, and promotes the harmonious development of the nurse-patient relationship [31, 32]. The same idea can be found in the study put forward by Zhiying Yang et al. [33], who have applied new methods in the study, and the conclusions drawn can also give some support to this study. There are some limitations in this study. First, the sample size of this study is not large, and it is a single-center study, so bias is inevitable. In future research, we will carry out multicenter, large-sample prospective studies, or more valuable conclusions can be drawn.

In conclusion, early rehabilitation nursing for TBI patients based on Orem's self-care theory can effectively improve patient satisfaction and compliance and achieve the purpose of enhancing motor function and living ability. The nursing scheme is worth popularizing in the clinic [34].

Data Availability

The data sets used and analyzed during the current study are available from the corresponding author upon reasonable request.

Conflicts of Interest

The authors declare that they have no conflicts of interest.

References

- [1] Y. Liu and D. Ma, "Effect of crisis management intervention combined with hyperbaric oxygen therapy on clinical efficacy, neurological function and prognosis of patients with emergency brain trauma," *Chinese Journal of nautical Medicine and Hyperbaric Medicine*, vol. 28, no. 5, pp. 583–588, 2021.
- [2] S. Zhao, P. Fang, and Y. Tao, "Effect of oral nursing intervention on pulmonary infection in patients with brain injury undergoing endotracheal intubation and general anesthesia during operation," *Nursing Research*, vol. 35, no. 16, pp. 2979–2982, 2021.

- [3] P. Chen, Y. Zheng, Z. he et al., "One case of planned catheter removal through periodic evaluation in patients with severe brain trauma," *Theory and practice of Rehabilitation in China*, vol. 27, no. 07, pp. 864–868, 2021.
- [4] G. Dagod, J. P. Roustau, and B. S. Bringuier-Branchereau, "Effect of a temporary lying position on cerebral hemodynamic and cerebral oxygenation parameters in patients with severe brain trauma," *Acta Neurochirurgica*, vol. 163, no. 9, pp. 2595–2602, 2021.
- [5] X. Qi, F. Gao, Y. Zhang, and L. Zhou, "Evaluation of the value and nursing quality of personalized nursing in patients with mild brain trauma," *Minerva Medica*, vol. 22, no. 55, pp. 188–194, 2021.
- [6] H. Yu Huang, C. S. Lee, and T. H. Chiu, "Clinical outcomes and prognostic factors for prolonged mechanical ventilation in patients with acute stroke and brain trauma," *Journal of the Formosan Medical Association*, vol. 121, no. 1, pp. 162–169, 2022.
- [7] F. Mario, G. Mario, P. Lara et al., "Mismatch between tissue partial oxygen pressure and near-infrared spectroscopy neuromonitoring of tissue respiration in acute brain trauma: the rationale for implementing a multimodal monitoring strategy[J]," *International Journal of Molecular Sciences*, vol. 22, no. 3, pp. 588–593, 2021.
- [8] H. Radabaugh, J. Bonnell, and O. Schwartz, "Use of machine learning to Re-assess patterns of multivariate functional recovery after fluid percussion injury: operation brain trauma therapy," *Journal of Neurotrauma*, vol. 38, no. 12, pp. 1670–1678, 2021.
- [9] H. Wang and A. Guo, "Study on the Sinicization of mini mental state examination scale and its reliability and validity in patients with TBI," *Nursing Research*, vol. 34, no. 24, pp. 4488–4490, 2020.
- [10] M. Koga, H. Toda, M. Kinoshita et al., "Investigation of the impact of preconditioning with lipopolysaccharide on inflammation-induced gene expression in the brain and depression-like behavior in male mice," *Progress in neuro-psychopharmacology & biological psychiatry*, vol. 103, no. 42, pp. 109978–44, 2020.
- [11] M. F. McCarty and A. Lerner, "Nutraceutical induction and mimicry of heme oxygenase activity as a strategy for controlling excitotoxicity in brain trauma and ischemic stroke: focus on oxidative stress," *Expert Review of Neurotherapeutics*, vol. 21, no. 2, pp. 157–168, 2020.
- [12] C. Pires Rita, O. Haldis, U. Eszter et al., "Xenon treatment after severe TBI improves locomotor outcome, reduces acute neuronal loss and enhances early beneficial neuro-inflammation: a randomized, blinded, controlled animal study," *Critical Care*, vol. 24, no. 1, pp. 19–24, 2020.
- [13] K. Faropoulos, D. Makris, and F. George, "The value of anti-epileptic therapy as a prophylactic factor for seizures in the management of moderate TBI[J]," *Future Sci. OA*, vol. 6, no. 10, pp. 197–200, 2020.
- [14] M. Forcione, A. M. Chiarelli, D. J. Davies et al., "Cerebral perfusion and blood–brain barrier assessment in brain trauma using contrast-enhanced near-infrared spectroscopy with indocyanine green: a review," *Journal of Cerebral Blood Flow and Metabolism*, vol. 40, no. 8, pp. 197–199, 2020.
- [15] A. Seyed Mostafa, S. Alireza, E. Mohammad Reza et al., "Efficacy of high-dose versus low-dose vitamin D supplementation on serum levels of inflammatory factors and mortality rate in severe TBI patients: study protocol for a randomized placebo-controlled trial," *Trials*, vol. 21, no. 1, pp. 1856–1859, 2020.
- [16] B. R. Narapareddy, L. Narapareddy, A. Lin et al., "Treatment of depression after TBI: a systematic review focused on pharmacological and neuromodulatory interventions[J]," *Psychosomatics*, vol. 61, no. 85, pp. 1898–1899, 2020.
- [17] S. Mitra, S. N. Khatri, M. Maulik, A. Bult-Ito, and M. Schulte, "Allosterism of nicotinic acetylcholine receptors: therapeutic potential for neuroinflammation underlying brain trauma and degenerative disorders," *International Journal of Molecular Sciences*, vol. 21, no. 14, pp. 1956–1959, 2020.
- [18] T. McMullan Jason, A. Ventura, and P. LeBlanc Dustin, "Emergency medical services TBI protocols do not reflect brain trauma foundation guidelines.[J]. Prehospital emergency care," *Official Journal of the National Association of EMS Physicians and the National Association of State EMS Directors*, vol. 25, no. 3, pp. 491–496, 2020.
- [19] H. Khormi Yahya, S. Ambikaipakan, O. C. Kelly, and D. Zygun, "Adherence to brain trauma foundation guidelines for intracranial pressure monitoring in severe TBI and the effect on outcome: a population-based study," *Surgical neurology international*, vol. 11, no. 44, pp. 488–493, 2020.
- [20] L. Giammattei, D. Starnoni, and R. Maduri, "Implementation of cisternostomy as adjuvant to decompressive craniectomy for the management of severe brain trauma," *Acta Neurochirurgica*, vol. 162, no. 3, pp. 469–479, 2020.
- [21] F. Chang, H. Z. Li, and S. Y. Zhang, "Working memory of patients with mild cognitive impairment due to brain trauma based on fNIRS," *Fa Yi Xue Za Zhi*, vol. 36, no. 1, pp. 52–60, 2020.
- [22] S. Sirena, M. Bridget, W. Evan, and S. Villapol, "Serum amyloid A is expressed in the brain after TBI in a sex-dependent manner," *Cellular and molecular neurobiology*, vol. 40, no. 7, pp. 73–78, 2020.
- [23] F. Pieter Francois, J. P. Andrew, B. Malcolm, S. Bernard, and K. Smith, "The utility of the brain trauma evidence to inform paramedic rapid sequence intubation in out-of-hospital stroke," *BMC Emergency Medicine*, vol. 20, no. 1, pp. 185–190, 2020.
- [24] D. Catherine, M. Dumont, P. Jean, A. Desautels, M. L. Fantini, and J. Montplaisir, "Sleep-wake disturbances in hospitalized patients with TBI: association with brain trauma but not with an abnormal melatonin circadian rhythm," *Sleep*, vol. 43, no. 1, pp. 174–178, 2020.
- [25] H. Watanabe, O. Nosova, and D. Sarkisyan, "Ipsilesional versus contralesional postural deficits induced by unilateral brain trauma: a side reversal by opioid mechanism," *Brain Communications*, vol. 2, no. 2, p. fcaa208, 2020.
- [26] A. Joris, S. C. Theresa, A. Beat et al., "TBI enhances the formation of heterotopic ossification around the hip: an animal model study," *Archives of orthopaedic and trauma surgery*, vol. 140, no. 8, pp. 185–190, 2020.
- [27] S.-Z. Qiu, G.-R. Zheng, B. Chen, J. J. Huang, G. Huang, and H. Hua, "Prognostic value of admission serum glucose-phosphate ratio in predicting the 6-month outcome of patients with severe TBI: a retrospective study," *Clinica Chimica Acta*, vol. 510, no. 566, pp. 1994–1996, 2020.
- [28] V. Evans, "Caring for traumatic brain injury patients: Australian nursing perspectives," *Critical Care Nursing Clinics of North America*, vol. 33, no. 1, pp. 21–36, 2021.
- [29] D. S. Mortimer and W. Berg, "Agitation in patients recovering from traumatic brain injury: nursing management," *Journal of Neuroscience Nursing*, vol. 49, no. 1, pp. 25–30, 2017.
- [30] X. Qi, "Application of brain state index and clinical pulmonary infection score in evaluating the prognosis of patients

- with brain injury coma complicated with pulmonary infection,” *Nursing research*, vol. 32, no. 4, pp. 658–661, 2018.
- [31] G. B. Goreth, “Pediatric mild traumatic brain injury and population health: an introduction for nursing care providers,” *Critical Care Nursing Clinics of North America*, vol. 29, no. 2, pp. 1578–165, 2017.
- [32] M. Bi, L. Meng, and L. Bai, “Effects of comprehensive nursing based on Orem’s self-care theory on symptom improvement and pregnancy outcome in patients with antiphospholipid syndrome: a retrospective cohort study,” *Computational and Mathematical Methods in Medicine*, vol. 19, p. 2022, Article ID 4133812, 2022 May.
- [33] Z. Yang, L. Shao, and Y. Teng, “Evaluation of the efficacy and adverse reactions of mirena combined with hysteroscopic surgery when treating AUB: based on a retrospective cohort study,” *Computational and Mathematical Methods in Medicine*, vol. 2022, 9 pages, Article ID 4082266, 2022.
- [34] C. S. Castañeda, S. O. Marysol, C. Luis, S. A. O. Suárez, and L. Rocha, “Propylparaben reduces the long-term consequences in Hippocampus induced by TBI in rats: its implications as therapeutic strategy to prevent neurodegenerative diseases,” *Journal of Alzheimer’s disease: JAD*, vol. 82, no. s1, pp. 184–186, 2020.

Research Article

Factors Influencing Adverse Pregnancy Outcomes in Gestational Diabetes Mellitus

Fang Zhao and Bo Xiao 

Obstetric, Hanyang Affiliated Hospital of Wuhan University of Science and Technology, Wuhan 430050, China

Correspondence should be addressed to Bo Xiao; api_81@sina.com

Received 24 May 2022; Revised 13 June 2022; Accepted 15 June 2022; Published 1 September 2022

Academic Editor: Dong Chen

Copyright © 2022 Fang Zhao and Bo Xiao. This is an open access article distributed under the Creative Commons Attribution License, which permits unrestricted use, distribution, and reproduction in any medium, provided the original work is properly cited.

Objective. Analysis of gestational diabetes risk factors and their impact on pregnancy outcomes. **Methods.** A retrospective analysis of pregnant women who delivered in the obstetrics ward of a tertiary hospital was performed, and the pregnant women were divided into a case group and a control group according to their compliance with the diagnostic criteria of GDM. The underlying pregnancy, delivery, and pregnancy outcomes of both groups were statistically analyzed. **Results.** The detection rate and incidence rate of gestational diabetes were 13.0%, and the incidence rate was 14.5% compared to pregnancy and childbirth complications between the two groups. No statistical differences in placental weight and cord length were found compared to the sex of the newborns by comparing the basic profile of the two groups of perinatal infants. There was no statistical difference between fetal growth restriction and neonatal abnormalities, while there was a statistical difference in neonatal outcomes between the two groups. **Conclusion.** Age, family history, and weight are the risk factors for GDM.

1. Introduction

Gestational diabetes mellitus (GDM) is the first occurrence or discovery of different degrees of glucose tolerance abnormalities during pregnancy with a total incidence ratio of 1% to 14% [1]. With the development of society, economy, and improvement of the living standards, global prevalence of GDM is increasing year by year especially in developing countries such as China where GDM has become one of the main chronic diseases endangering women's health. Poor blood sugar control during pregnancy not only affects the mother but also causes great harm to the newborn [2]. As a result, the study of GDM has become crucial and has received widespread attention from obstetricians [3]. With the Internet + health and medical services new service model continues to emerge [4]. Based on big data analysis, the use of mobile phones, QR codes, and the Internet to collect and manage basic information during pregnancy can effectively monitor GDM, thereby reducing GDM complications.

In 1979, the World Health Organization (WHO) regarded GDM as an independent type except for type 1 and type 2

diabetes [5]. With the improvement of economic conditions and the improvement of life comfort, the diversification of diets has led to an increase in the prevalence of GDM year by year. The clinical process of gestational diabetes is very complex. In the second and third trimesters of pregnancy, insulin-resistant substances such as estrogen and progesterone increase in the body of pregnant women, resulting in a decrease in the mother's sensitivity to insulin. To maintain the normal level of glucose metabolism in the body and increase the function of insulin secretion, the blood glucose level determines the influence of GDM on the outcome of pregnancy.

The latest domestic and foreign studies suggest that GDM is not only related to the adverse outcomes of premature maternal delivery, premature rupture of membranes, hypertension in pregnancy, hyperamniotic fluid, postpartum hemorrhage, and increased cesarean section rate. It also impacts adverse outcomes such as fetal distress, giant fetuses, and mild asphyxia. Therefore, increasing morbidity and mortality of pregnant women and perinatal infants is needed [6–10].

With the progress of medical diagnosis and treatment, paying attention to and strengthening the management of people at high risk of gestational diabetes can reduce the occurrence of adverse pregnancy and child outcomes. Pregnancy guidance and early screening for pregnant women with risk factors will prevent and reduce the occurrence of GDM. Intervene in people with mild dysglycemia by controlling divided meals, reducing excessive energy intake, increasing appropriate exercise, and promoting metabolism. For those with unsatisfactory blood sugar control, insulin therapy can be appropriately used. GDM pregnant women should regularly monitor blood glucose after childbirth, control glycogen intake, do more aerobic exercise, guide a healthy diet, and improve national health awareness [8, 11–14].

Although there are many kinds of research on GDM, the clinical process of GDM is complicated. It is necessary to conduct a statistically significant investigation on pregnant women with the same diagnostic criteria for gestational diabetes in the same period at the same medical institution, to understand the incidence of GDM and analyze and discuss various risk factors that impact the occurrence of GDM in pregnant women which provides a certain theoretical basis for the early prevention, diagnosis, and intervention of clinical GDM, in order to improve the pregnancy outcome.

Gestational diabetes mellitus (GDM) is any degree of impaired glucose tolerance that occurs or is first discovered during pregnancy [15]. In late pregnancy, due to the continuous increase of anti-insulin hormone secretion, insufficient insulin compensatory secretion or decreased insulin sensitivity results in abnormal glucose metabolism, resulting in impaired glucose tolerance during pregnancy (GIGT) or gestational diabetes. According to the World Health Organization (WHO) recommendation in 1998, gestational diabetes is divided into GIGT and GDM. GIGT is an early blood glucose steady-state change, which is just an intermediate state or transitional stage between normal blood glucose and gestational diabetes, rather than an independent type of gestational diabetes [16]. The clinical manifestations of GDM are polydipsia, polyphagia, polyuria, or recurrent vulvovaginal *Candida* infection symptoms or signs during pregnancy.

GDM blood glucose screening is the most effective method to reduce maternal and infant complications in pregnant women with gestational diabetes and to identify pregnant women at high risk of type 2 diabetes early. The blood glucose screening for pregnant women in our country started earlier in 1984 [17]. Previously, it was only available for pregnant patients with a history of adverse birth, macrosomia, polyhydramnios, diabetes, family history of obesity, and pregnancy with polyhydramnios. GDM was found in 0.05% of people with a positive oral glucose tolerance test (OGTT) for urine glucose [18]. With the improvement of people's living standards, changes in dietary structure, and advances in diagnostic methods, the prevalence of GDM blood sugar screening patients has gradually increased. The prevalence of GDM in our country was 1.75% in 1996, and the prevalence of GIGT was 8.39% [19]. The current epidemiology reports that

the prevalence of GDM in various countries ranges from 1% to 15%. Among them, the prevalence of GDM is 14% in the United States, 15% in Indians, and 7.3% in Vietnam [20]. The prevalence of GDM in Beijing, Shanghai, Guangzhou, and Hong Kong Special Administrative Region is 6.8%, 5.5%, 7.2%, and 8.1%, respectively [21] and is increasing yearly.

In the research on high-risk factors of GDM, age is closely related to the incidence of GDM, and the advanced age of pregnant women is a high-risk factor of GDM. Literature [22] believes pregnant women with BMI over 30 are more likely to develop GDM. Li et al. [23] found that the incidence of obese pregnant women and those with excessive weight gain during pregnancy giving birth to huge babies and the occurrence of GDM and pregnancy-induced hypertension is higher than that of normal body remodelling and low body remodelling, while prepregnancy body mass index and excessive weight gain are associated with newborns. Birth weight is related to pregnancy outcome. A family history of diabetes, malignant tumors in the parents, and prepregnancy BMI > 26 are risk factors for the occurrence of GDM. Obese women before and during the first trimester (within 18 weeks) are at risk of developing GDM. Literature [24] found that the incidence of non-White GDM is at high risk and believes that race is related to the incidence of GDM.

Clinical evidence shows that GDM can cause many adverse effects on pregnancy outcomes. GDM may cause fetal malformations, stillbirths, macrosomia, and long-term complications for the mother. Pregnancy-induced hypertension, hyperhydramnios, premature rupture of membranes, surgical delivery, and neonatal diseases in GDM pregnant women are higher than those of normal pregnant women and are closely related to blood sugar levels. Compared with age-appropriate GDM pregnant women, the adverse effects of older GDM pregnant women birth history, pregnancy-induced hypertension, maternal anemia, and low birth weight infants have a higher incidence. Literature [25] found in the study that 28.3% of patients with GDM are complicated with hypertension during pregnancy. In comparing delivery methods, there are also very significant differences in the rate of cesarean section and forceps use. In a few years postpartum, some women with GDM will develop diabetes (DM). Literature [26] reported that 10% of GDM develops into type 2 diabetes every year after childbirth, and 50% develops into type 2 diabetes within 5 years. BellH51 reports that there is 70% of pregnant women with GDM who develop type 2 diabetes.

In this article, a retrospective analysis of pregnant women, specifically those who gave birth in the obstetric ward of a tertiary hospital, was done. The pregnant women, who met the diagnostic criteria of GDM, were selected as the case group and control group for a controlled study.

2. Objectives and Methods

From June 1, 2013, to November 30, 2013, 1,038 pregnant women were hospitalized in the obstetric ward of a tertiary hospital for delivery. Five cases of unnatural conception, six cases of twins, 4 cases of prepregnancy hypertension, and 2 cases of kidney disease were excluded. There were 5 cases of

cardiovascular disease, 2 cases of liver disease, 2 cases of diabetes, 25 cases of hypothyroidism, 5 cases of nonhospital obstetrics during pregnancy, 6 cases of incomplete data, and 965 cases of pregnant women finally included in the study.

2.1. Research Objective

2.1.1. Choice of Case Group and Control Group. All 125 pregnant women who met the diagnostic criteria of GDM were selected as the case group [27], and all 840 pregnant women who gave birth at the same time without GDM and met the inclusion criteria were selected as the control group.

2.1.2. Inclusion and Exclusion Criteria. The inclusion criteria used in this article are as follows:

- (1) This pregnancy was a single pregnancy with natural conception.
- (2) There was no cardiovascular disease, hypertension, liver or kidney disease, diabetes, etc. before this pregnancy.
- (3) They have not taken drugs that interfere with lipid metabolism and glucose metabolism (such as phentolamine, cortisone, furosemide, etc.).
- (4) They were no previous endocrine and other related diseases (such as hyperthyroidism, hypothyroidism, Cushing's syndrome, etc.).
- (5) The pregnancy check-up is carried out in this hospital.
- (6) No other diseases affect pregnancy and fetal development.
- (7) It is not complicated by serious infectious diseases.

The exclusion criteria used in this article are as follows:

- (1) It is accompanied by malignant tumors.
- (2) There is serious dysfunction of important organs.
- (3) There are contraindications to the use of hypoglycemic drugs.
- (4) There are cognitive impairments, mental disorders, and poor treatment compliance.
- (5) Patients is suffering from polycystic ovary syndrome.
- (6) There is imminent delivery.
- (7) They have taken other hypoglycemic drugs on their own.
- (8) Islet cells have lacked insulin secretion function.
- (9) There are complications of gestational diabetes mellitus.

2.2. Research Methods. This study was designed with a retrospective analysis method to make statistics on the relevant conditions of pregnant women in both case and control groups to analyze the risk factors of GDM and pregnancy outcomes. The specific statistical indicators are as follows:

- (1) Basic information: maternal name, age (years old), height (m), blood pressure (mmHg), prepregnancy weight (kg), education level, previous medical history, family history of diabetes, and prepregnancy body mass index (BMI). $BMI = \text{weight}/\text{height}^2$ (kg/m^2).
- (2) History of pregnancy and childbirth: times of pregnancy, times of childbirth.
- (3) This pregnancy situation: Hepatitis B surface antigen carrying status, vaginal *Candida* test results, first birth weight (kg), OGTT weight (kg), weight within one week before delivery (kg), first fasting blood glucose (FPG), 75 g glucose tolerance test (OGTT), and pregnancy complications.
- (4) Circumstances during childbirth: delivery methods, complications during childbirth.
- (5) Newborn condition: placental weight (g), umbilical cord length (cm), newborn weight (g), gender, and newborn outcome.

2.3. Quality Control. The quality control principles are given as follows:

- (1) All medical records are reviewed and recorded by the researcher himself. The researcher has many years of obstetric work experience and a scientific and rigorous work attitude. He reviews and confirms the doubts reviewed in time. If any missing items are found, fill them up in time. After all the investigations are completed, professionals with rich obstetric experience will conduct a logical review of all the questionnaires and recheck and confirm the suspicious data to ensure the truthfulness and accuracy of the information.
- (2) Data processing and analysis quality control: Before data analysis, the data coding and input work were checked for errors, leaks, and logic checks. The repeated entry method is adopted, and the document verification procedure is established to reduce the human error of entering the data and ensure the reliability of the data.

2.4. Diagnostic Criteria. The diagnostic criteria used in this article are as follows:

- (1) Gestational diabetes: pregnant women undergo 75 g OGTT during 24–28 weeks of gestation, and their blood glucose levels are 5.1 mmol/L, 10.0 mmol/L, and 8.5 mmol/L, respectively, on an empty stomach and 1 and 2 hours after taking sugar. GDM is diagnosed if the blood glucose level meets or exceeds the above standards.
- (2) Premature delivery: delivery between 28 weeks and 37 weeks of pregnancy. The diagnostic criteria for polyhydramnios are B-ultrasound before childbirth indicating amniotic fluid dark area ≥ 8.0 cm, amniotic fluid index ≥ 25.0 cm, or total amniotic fluid

exceeding 2000 ml. Giant fetus: newborn birth weight ≥ 4000 g. Hypertension in pregnancy is a group of diseases that coexist with pregnancy and elevated blood pressure. At least 2 measurements of the same arm: systolic blood pressure ≥ 140 mmHg or diastolic blood pressure ≥ 90 mmHg. Neonatal asphyxia: Mild refers to 1 minute Apgar score < 8 points; ≤ 3 points is defined as severe asphyxia.

2.5. Statistical Analysis. Data analysis uses SPSS17.0 software and the measurement data conforms to a normal distribution as described by $\bar{x} \pm SD$ and t -test. The number of cases and percentages express the count data. χ^2 test is used. When $n \geq 40$ and all expected values $T \geq 5$, the hypothesis test uses Pearson χ^2 test; $n \geq 40$. When $1 \leq T \leq 5$, the hypothesis test uses the continuity-corrected χ^2 test; when $n < 40$ or $T < 1$, the Fisher exact probability method is used. Logistic regression analysis was used to study the related risk factors of gestational diabetes, and $P < 0.05$ indicated that the difference was statistically significant.

3. Results

3.1. GDM Detection Rate. One hundred twenty-five pregnant women were diagnosed with gestational diabetes and the incidence rate was 13.00%. Among these patients, there were 42 cases of abnormal fasting blood glucose at 75gOGTT, accounting for 33.6%; 50 cases of abnormal blood glucose one hour after taking sugar, accounting for 40%; 47 cases of abnormal blood glucose 2 hours after taking sugar, accounting for 37.6%.

Comparing the blood glucose levels of pregnant women between the two groups, the average fasting blood glucose level of 75gOGTT was (4.9 ± 0.8) mmol/L in the case group and (4.4 ± 0.4) mmol/L in the control group. The result was $P < 0.05$; that is, the difference was statistically significant; 1-hour blood glucose value of the case group was (9.3 ± 2.0) mmol/L, and the average of the control group was (7.0 ± 1.4) mmol/L, the result was $P < 0.05$, and the difference was statistically significant; the average of the 2-hour blood glucose value of the case group was (7.8 ± 1.6) mmol/L. The average of the control group is (6.1 ± 1.1) mmol/L, the result is $P < 0.05$, and the difference is statistically significant as shown in Table 1 and Figure 1. FBG is fasting blood glucose. OHG is one-hour blood sugar. THG is two hours of blood sugar.

3.2. Single Factor Analysis of GDM Risk Factors. This work considered the following risk factors: age, body mass index before pregnancy, weight and gain during pregnancy, and family history of diabetes.

Maternal age was divided into four groups: 209 cases in the 25-year-old group, 592 cases in the 25-29-year-old group, 137 cases in the 30-34-year-old group, and 27 cases in the ≥ 35 -year-old group, the number of patients in the case group was 25, 70, 22, and 8, and the number of controls was 184 cases, 522 cases, 115 cases, 19 cases, the result was

TABLE 1: Comparison of the blood glucose levels (Unit: mmol/L).

Item	Case group	Control group	t	P
FBG	4.9 ± 0.8	4.4 ± 0.4	7.7	0.001
OHG	9.3 ± 2.0	7.0 ± 1.4	11.9	0.001
THG	7.8 ± 1.6	6.1 ± 1.1	11.9	0.001

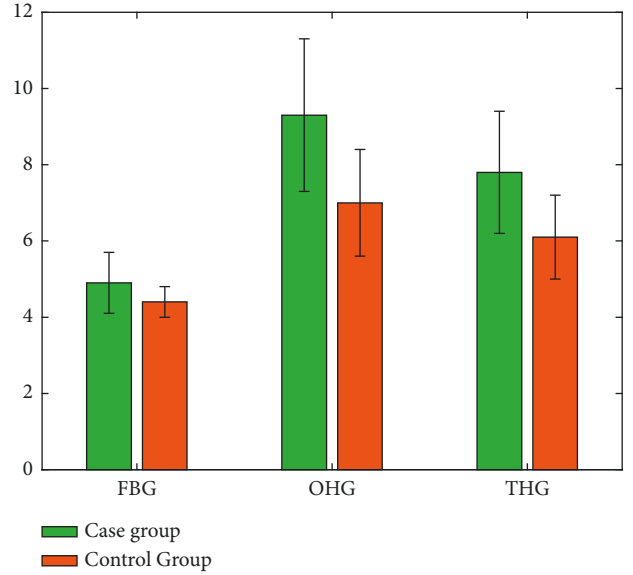


FIGURE 1: Comparison of the blood glucose levels.

$P < 0.05$, and the difference was statistically significant as shown in Table 2 and Figure 2.

The prepregnancy body mass index BMI was 15.0~40.0, with an average of 25.1 ± 4.2 in the case group and an average of 21.3 ± 3.4 in the control group. The pre-pregnancy BMI was divided into thin group (84 cases), normal group (559 cases), overweight group (240 cases), and fat group (82 cases), the numbers of cases in the case group were 0, 30, 57, and 38, and the numbers in the control group were 84, 529, 183, and 44, and the difference was statistically significant as shown in Table 3 and Figure 3.

At the first check-up, the weight was 39~103 kg, the average of the case group was 62.3 ± 10.1 kg, the average of the control group was 57.9 ± 9.1 kg, and the difference was statistically significant. The weight at OGTT was 40~107 kg, the average of the case group was 68.1 ± 10.2 kg, and the control group averaged 63.9 ± 8.8 kg, and the difference was statistically significant; within one week before delivery, the weight was 49~110 kg, the case group averaged 74.5 ± 10.6 kg, and the control group averaged 71.8 ± 9.2 kg. There is statistical significance. The average weight gain during pregnancy was 14.0 ± 5.6 kg in the case group and 12.3 ± 6.0 kg in the control group; the result was $P < 0.05$, and the difference was statistically significant, as shown in Table 4. WFC is weight at the first check-up. OGTT is weight at OGTT. WBD is weight within one week before delivery. WGP is weight gain during pregnancy.

There were 46 pregnant women with a family history of diabetes, 15 cases in the case group, 30 cases in the control group, 919 pregnant women who denied a family history of

TABLE 2: Comparison of the age of pregnant.

Age	Case group	Control group	χ^2	<i>P</i>
<25	25	184	8.68	0.03
25~29	70	522		
30~34	22	115		
≥35	8	19		

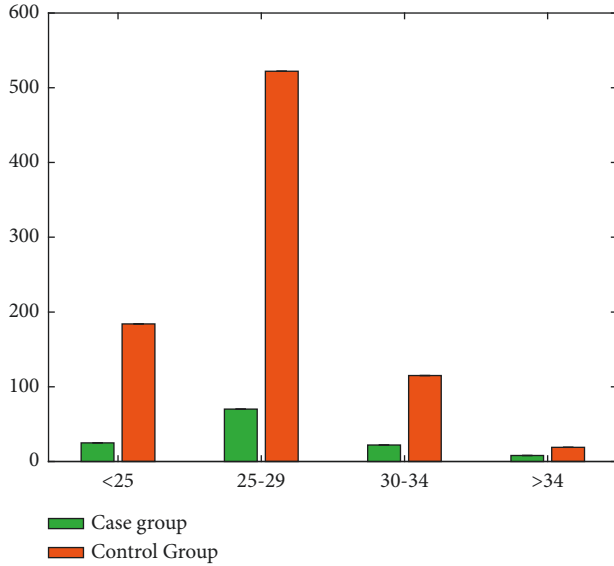


FIGURE 2: Distribution of the age.

TABLE 3: Comparison of prepregnancy body mass index.

BMI	Case group	Control group	χ^2	<i>P</i>
Thin	0	84	—	0.001
Normal	30	529		
Overweight	57	183		
Fat	38	44		

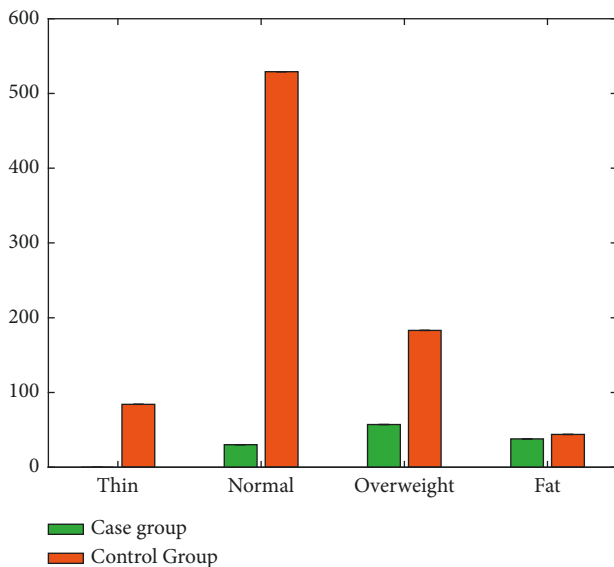


FIGURE 3: Distribution of the prepregnancy body mass.

TABLE 4: Comparison of pregnancy weight and weight gain.

Weight	Case group	Control group	<i>t</i>	<i>P</i>
WFC	62.3 ± 10.1	67.9 ± 9.0	5.0	0.001
OGTT	68.1 ± 10.2	63.9 ± 8.8	4.9	0.001
WBD	74.5 ± 10.6	71.8 ± 9.2	3.0	0.002
WGP	14.0 ± 5.6	12.3 ± 6.0	3.1	0.004

diabetes, 110 cases in the case group, and 810 cases in the control group. The difference was statistically significant as shown in Table 5.

3.3. Binary Logistic Regression Analysis of GDM Risk Factors.

The statistically significant factors in the univariate analysis were uniformly assigned and incorporated into the logistic regression model for analysis. The stepwise regression method was selected. The independent variable entry-level was 0.05, and the elimination level was 0.10 to screen the GDM influencing factors. Results: overweight or obesity, family history of diabetes, and maternal age entered the model, but the number of pregnancies, parity, weight, and gain during pregnancy and vaginal *Candida* were not entered into the model. Maternal overweight or obesity, family history of diabetes, and age are the main risk factors for GDM. The incidence of overweight or obesity is 8.56 times the normal body weight. The risk of GDM for pregnant women with a family history of diabetes is 3.2 times that of a family without diabetes. As the age of pregnancy increases, the risk of GDM increases by 1.1 times.

3.4. Comparison of Pregnancy Outcomes. In the two groups of maternal delivery methods, there were 565 cases (58.6%) of spontaneous deliveries and 400 cases (41.4%) of caesarean sections in the two groups, of which 60 cases of spontaneous delivery and 65 cases of caesarean section in the case group, and 505 cases of spontaneous delivery and 335 cases of caesarean section in the control group. The difference was statistically significant.

There were 140 preterm births, with an incidence rate of 14.5%, including 27 cases in the case group and 113 cases in the control group; 67 cases of premature rupture of membranes, with an incidence rate of 5.9%, including 23 cases in the case group and 44 cases in the control group; hypertension in pregnancy in 29 cases with an incidence rate of 3.0%, including 10 cases in the case group and 19 cases in the control group; 13 cases of polyhydramnios, an incidence rate of 1.4%, 10 cases in the case group and 3 cases in the control group; 36 cases of postpartum hemorrhage, the incidence rate 3.73%, 15 cases in the case group and 21 cases in the control group. The differences between the two groups were statistically significant in premature delivery, premature rupture of membranes, and hypertension in pregnancy, polyhydramnios, and postpartum hemorrhage.

The gender of newborns was 493 males, accounting for 51.1%, and 472 females, accounting for 48.9%; placental weight: the average weight of the case group was 578.2 ± 104.8 g, and the average weight of the control group was 575.5 ± 79.0 g, the result $P > 0.05$, and the difference

TABLE 5: Comparison of the family history of diabetes.

Family history	Case group	Control group	χ^2	P
Yes	15	30	16.6	0.001
No	110	810		

was not statistically significant; umbilical cord length: the average length of the case group is 56.1 ± 9.4 cm, the average length of the control group is 55.1 ± 9.3 cm, the result is $P > 0.05$, and the difference is not statistically significant.

There were 142 cases of fetal distress, with an incidence rate of 14.7%, including 29 cases in the case group and 113 cases in the control group; 2 cases of fetal growth restriction, with an incidence rate of 0.2%, including 1 case in the case group and 1 case in the control group; 64 cases of giant fetuses, with an incidence rate was 6.6%, with 14 cases in the case group and 50 cases in the control group; 4 cases of mild asphyxia, with an incidence rate of 7.7%, 3 cases in the case group and 1 case in the control group; 10 cases of neonatal deformity, with an incidence rate of 1.04%, including 2 cases in the case group and 8 cases in the control group. There was no statistically significant difference between the two groups in fetal growth restriction and neonatal abnormalities. Fetal distress, giant fetus, and mild asphyxia occurred in the two groups, and the difference was statistically significant.

4. Discussion

4.1. Incidence of GDM. Zhu et al. [28] reported an international survey of the incidence of GDM in mainland China in 2013, using the latest international general standard (IADPSG) diagnostic criteria [29]. The screening results of 17,186 pregnant women from different hospitals showed that the incidence of GDM is 17.5%. The incidence of GDM in this study is 13.0%, which is higher than the incidence of GDM reported in our country in the 8th edition of Obstetrics and Gynecology by 1% to 5% but is lower than the screening result of 17.5% in 2013. This may be related to living. The city, living conditions, and reported time differences are related. It has been reported that the global incidence of GDM has increased significantly in recent years [30], which may be related to improved diagnostic techniques, diversified diets, excessive emphasis on pregnancy, improved living conditions, and overnutrition. Increase the attention of pregnant women to GDM, reduce the occurrence of GDM and its adverse effects on pregnancy outcomes, and improve the health of mothers and children.

4.2. Risk Factors for GDM. During pregnancy, the mother's many hormones change, weakening the ability to regulate blood sugar and reducing insulin sensitivity, and it is prone to basic metabolic disorders. GDM is easy to develop in pregnant women with many risk factors, so it is necessary to understand the risk factors to achieve effective prevention. Common risk factors include maternal age, prepregnancy body mass index, overweight or obesity, family history of diabetes, etc. These factors are importantly related to the

occurrence of GDM and actively prevent them from reducing the harm caused by the disease.

The difference in age between the two groups of pregnant women was statistically significant. In the logistic regression analysis, the risk of GDM increased by 1.1 times with the increase in pregnancy age, indicating that older age is a risk factor for GDM in clinical practice. Correct guidance and age-appropriate pregnancy are important guarantees for the health of mothers and children.

In this study, the weight at the first check-up, the weight at the OGTT, and the weight within a week before delivery were statistically different between the two groups. The weight of pregnant women in the case group was significantly higher than in the control group. There was a statistically significant difference in the prepregnancy BMI between the two groups of pregnant women. The risk of overweight or obesity in the logistic regression analysis was 8.6 times that of normal weight. Explain that obesity or overweight is a risk factor for GDM. Therefore, a reasonable diet and strengthening exercise are vital in preventing and controlling the occurrence of GDM.

It was observed that there was a statistically significant difference in pregnant women with or without a family history of diabetes. Logistic regression analysis indicated that the risk of GDM for pregnant women with a family history of diabetes was 3.2 times that of family history without diabetes, indicating that a family history of diabetes is a risk factor for GDM. Pregnant and lying-in women with a family history of diabetes should pay more attention to healthy eating, regular obstetric check-ups, and early prevention.

The number of cases analyzed retrospectively is relatively small, and large samples, prospective, randomized controlled studies are needed to further clarify the relationship between umbilical artery blood flow parameters and poor pregnancy outcomes in gestational diabetes. In addition, the main subject of this study was a single-child GDM pregnant woman, and the results of the twin pregnancy study and the two-child pregnancy have not been studied. This study did not separately analyze the factors associated with specific adverse pregnancy outcomes in GDM pregnancies and will be further collected in future studies. Common adverse pregnancy outcomes were classified and the relevant influencing factors were analyzed to provide a reference for clinically accurate prevention.

5. Conclusion and Future Work

The incidence of gestational diabetes is 13.0%, which requires attention as it is a high ratio and needs to be controlled. Maternal age, family history of diabetes, and overweight or obesity are risk factors for GDM. Compared with non-GDM women, the pregnancy outcomes are, for example, premature delivery, premature rupture of membranes, hypertension during pregnancy, hyperamniotic fluid, postpartum hemorrhage, cesarean section, fetal distress, and occurrence of giant fetuses. Strengthen prepregnancy education, prepare well before pregnancy, enhance nutritional and dietary balance knowledge, monitor and

intervene GDM early throughout pregnancy, improve pregnancy outcomes, and improve maternal and infant health. Maternal age, family history of diabetes, and overweight or obesity are risk factors for the occurrence of GDM. Proactively promote a reasonable diet and appropriate exercise during pregnancy, paying particular attention to the proportion of energy intake and maintaining normal blood sugar in the body. It is very necessary during pregnancy to actively understand the effects of GDM. Further understand the risk factors and their impact on pregnancy outcome, strengthen the attention of pregnant women to GDM, actively control blood sugar, reduce the harm caused by high blood sugar to mothers and children, reduce the economic burden of society, and make a great contribution to the health of mothers and children.

In future, the proposed evaluation criteria could possibly be extended to describe how effective the proposed methods are in controlling these issues specifically from the perspective of the incidence of gestational diabetes.

Data Availability

The datasets used and analyzed during the current study are available from the corresponding author upon reasonable request.

Conflicts of Interest

The authors declare that they have no conflicts of interests.

Authors' Contributions

Zhao Fang put forward the idea of the paper and sorted out the data and papers by wavelet, and all authors participated in the preparation and review of the paper.

References

- [1] V. Ok, *Standards of Medical Care in Diabetes-2009 (American Diabetes Association): Executive Summary*, Diabetes Care, vol. 32, no. 1, Hayka, 2009.
- [2] Y. Yan, R. Zhang, and Y. Wei, "Change of serum lipocalin-2 level in pregnant women with gestational diabetes mellitus and its clinical significance," *Progress in Modern Biomedicine*, vol. 12, no. 24, pp. 4735–4737, 2012.
- [3] L. Bellamy, J. P. Casas, A. D. Hingorani, and D. Williams, *Lancet*, vol. 373, no. 9677, pp. 1773–1779, 2009.
- [4] Y. Wu, C. Wang, X. Liu et al., *Bioresource Technology*, vol. 211, no. 7, pp. 16–23, 2016.
- [5] F. G. Cunningham, N. F. Cant, and K. J. Leveno, *Williams Obstetrics*, p. 1363, McGraw-Hill Com. Inc, New York, 2002.
- [6] W. E. Consultation, "Appropriate body-mass index for Asian populations and its implications for policy and intervention strategies," *Lancet*, vol. 363, no. 9403, pp. 157–163, 2004.
- [7] T. D. Clausen, E. R. Mathiesen, T. Hansen et al., "Overweight and the metabolic syndrome in adult offspring of women with diet-treated gestational diabetes mellitus or type 1 diabetes," *Journal of Clinical Endocrinology & Metabolism*, vol. 94, no. 7, pp. 2464–2470, 2009.
- [8] N. F. Butte, "Carbohydrate and lipid metabolism in pregnancy: normal compared with gestational diabetes mellitus," *The American Journal of Clinical Nutrition*, vol. 71, no. 5, pp. 1256S–1261S, 2000.
- [9] A. Ferrara, "Increasing prevalence of gestational diabetes mellitus," *Diabetes Care*, vol. 30, no. 2, pp. 141–146, 2007.
- [10] C. G. Solomon, W. C. Willett, and V. J. Carey, "A prospective study of pregravid determinants of gestational diabetes mellitus," *JAMA*, vol. 278, no. 13, pp. 1078–1083, 1997.
- [11] J. Pei, "Big Data Mining in the Control of Epidemic," *Basic and Clinical Pharmacology and Toxicology*, pp. 428–430, 2020.
- [12] C. M. Boney, A. Verma, R. Tucker, and B. R. Vohr, "Metabolic syndrome in childhood: association with birth weight, maternal obesity, and gestational diabetes mellitus," *Pediatrics*, vol. 115, no. 3, pp. 290–296, 2005.
- [13] B. E. Metzger and D. R. Coustan, "Summary and recommendations of the fourth international workshop-conference on gestational diabetes mellitus. The organizing c," *Diabetes Care*, vol. 21, no. 2, pp. B161–B167, 1998.
- [14] D. A. Sacks, D. R. Hadden, M. Maresh et al., "Frequency of gestational diabetes mellitus at collaborating centers based on IADPSG consensus panel-recommended criteria: the hyperglycemia and adverse pregnancy outcome (HAPO) study," *Diabetes Care*, vol. 35, no. 3, pp. 526–528, 2012.
- [15] G. N. Brankston, B. F. Mitchell, E. A. Ryan, and N. B. Okun, "Resistance exercise decreases the need for insulin in overweight women with gestational diabetes mellitus," *American Journal of Obstetrics and Gynecology*, vol. 190, no. 1, pp. 188–193, 2004.
- [16] X. Jiang and W. Zeng, "Identification and classification of gestational diabetes," *Journal of Practical Obstetrics and Gynecology*, vol. 17, no. 5, pp. 257–258, 2001.
- [17] S. Reutrakul, N. Zaidi, K. Wroblewski et al., "Interactions between pregnancy, obstructive sleep apnea, and gestational diabetes mellitus," *Journal of Clinical Endocrinology & Metabolism*, vol. 98, no. 10, pp. 4195–4202, 2013.
- [18] H. S. Xu, D. J. Wang, R. C. Pace, and R. Jones, *The American Journal of Surgery*, vol. 163, no. 1, pp. 164–168, 1992.
- [19] C. Pan and Y. Liu, "Progresses in diabetology in China, 1996," *Zhonghua Yixue Zazhi*, vol. 76, no. 12, pp. 889–891, 1996.
- [20] X. Yang, B. Hsu-Hage, H. Zhang et al., "Gestational diabetes mellitus in women of single gravidity in Tianjin City, China," *Diabetes Care*, vol. 25, no. 5, pp. 847–851, 2002.
- [21] Y. p Lu, G. s Sun, X. y Weng, and L. Mao, "Evaluation of the glucose screening retest during pregnancy," *Zhonghua Fu Chan Ke Za Zhi*, vol. 38, no. 12, pp. 729–732, 2003.
- [22] C. C. Tebes, S. J. Tebes, K. Brown, and W. Spellacy, "Gestational diabetes and multiple gestations," *Obstetrics & Gynecology*, vol. 107, p. 65S, 2006.
- [23] J. Li and N. Feng, "The influence of pre-pregnancy body mass index and weight gain during pregnancy on the prognosis of mother and infant," *Maternal and Child Health Care of China*, no. 14, pp. 1901–1902, 2007.
- [24] Z. Qiang, J. Wang, and X. Qi, "A case-control study on risk factors of gestational diabetes mellitus," *Chinese Journal of Public Health*, vol. 22, no. 7, pp. 795–796, 2006.
- [25] A. Golbert and M. A. A. Campos, "Diabetes melito tipo 1 e gestação," *Arquivos Brasileiros de Endocrinologia e Metabologia*, vol. 52, no. 2, pp. 307–314, 2008.
- [26] P. Pharoah and Y. Adi, "Consequences of in-utero death in a twin pregnancy," *The Lancet*, vol. 355, no. 9215, pp. 1597–1602, 2000.
- [27] S. Pettis, *Gestational Diabetes Is Your Patient at Risk? Screening Most Pregnant Women between 24 and 28 Weeks of Gestation Is the Standard of Care. It Is Important for Clinicians*

to Identify and Treat Gestational Diabetes Early to Improve Perinatal Outcomes, 2005.

- [28] W Zhu, H Yang, Y Wei, and J.N.H.A. Yan, "Evaluation of the value of fasting plasma glucose in the first prenatal visit to diagnose gestational diabetes mellitus in China," *Diabetes Care*, vol. 36, no. 3, pp. 586–590, 2013.
- [29] International Association of Diabetes and Pregnancy Study Groups Consensus Panel, "International association of diabetes and pregnancy study groups recommendations on the diagnosis and classification of hyperglycemia in pregnancy," *Diabetes Care*, vol. 33, no. 3, pp. 676–682, 2010.
- [30] W. Li, S. Li, G. Feng, and Y Wang, "Species of npphp," *Zootaxa*, vol. 3838, no. 2, pp. 174–182, 2014.

Retraction

Retracted: Comparison of the Effects of Open Surgery and Minimally Invasive Surgery on the Achilles Tendon Rupture Healing Based on Angiogenesis

Computational Intelligence and Neuroscience

Received 1 August 2023; Accepted 1 August 2023; Published 2 August 2023

Copyright © 2023 Computational Intelligence and Neuroscience. This is an open access article distributed under the Creative Commons Attribution License, which permits unrestricted use, distribution, and reproduction in any medium, provided the original work is properly cited.

This article has been retracted by Hindawi following an investigation undertaken by the publisher [1]. This investigation has uncovered evidence of one or more of the following indicators of systematic manipulation of the publication process:

- (1) Discrepancies in scope
- (2) Discrepancies in the description of the research reported
- (3) Discrepancies between the availability of data and the research described
- (4) Inappropriate citations
- (5) Incoherent, meaningless and/or irrelevant content included in the article
- (6) Peer-review manipulation

The presence of these indicators undermines our confidence in the integrity of the article's content and we cannot, therefore, vouch for its reliability. Please note that this notice is intended solely to alert readers that the content of this article is unreliable. We have not investigated whether authors were aware of or involved in the systematic manipulation of the publication process.

Wiley and Hindawi regrets that the usual quality checks did not identify these issues before publication and have since put additional measures in place to safeguard research integrity.

We wish to credit our own Research Integrity and Research Publishing teams and anonymous and named external researchers and research integrity experts for contributing to this investigation.

The corresponding author, as the representative of all authors, has been given the opportunity to register their agreement or disagreement to this retraction. We have kept a record of any response received.

References

- [1] F. Gong, X. Li, H. Zhang et al., "Comparison of the Effects of Open Surgery and Minimally Invasive Surgery on the Achilles Tendon Rupture Healing Based on Angiogenesis," *Computational Intelligence and Neuroscience*, vol. 2022, Article ID 1447129, 8 pages, 2022.

Research Article

Comparison of the Effects of Open Surgery and Minimally Invasive Surgery on the Achilles Tendon Rupture Healing Based on Angiogenesis

Fan Gong, Xiaoliang Li, Hanling Zhang, Jianke Wu, Guoxu Ma, Bowen Zhang, Jian Gao, Yi Ding, Yonglu Huang, Suoli Cheng, Xuebing Zhou, and Fei Zhao 

Hand & Foot & Reconstruction Microsurgery,
People's Hospital of Ningxia Hui Autonomous Region (The First Affiliated Hospital of Northwest University for Nationalities),
Yinchuan 750002, Ningxia, China

Correspondence should be addressed to Fei Zhao; 18409489@masu.edu.cn

Received 30 May 2022; Revised 5 July 2022; Accepted 8 July 2022; Published 1 September 2022

Academic Editor: Dong Chen

Copyright © 2022 Fan Gong et al. This is an open access article distributed under the Creative Commons Attribution License, which permits unrestricted use, distribution, and reproduction in any medium, provided the original work is properly cited.

Objective. To compare the effect of three different surgical methods on rabbit Achilles tendon rupture. **Methods.** The Achilles tendon transection model was constructed by cutting off the inner half of the Achilles tendon. Rabbits were divided into 4 groups: model group, open surgery (OS) group, minimally invasive surgery (MS) group, and conservative treatment (CT) group. Biomechanical evaluation, H&E, and Picrosirius Red staining were applied to evaluate the histological changes and healing. RT-qPCR, Western blot, ELISA, and IHC staining were used to detect the expression of COLIII, IL-1 β , TNF- α , IL-6, CD31, VEGF, bFGF, and TGF- β 1. **Results.** Different surgery treatments significantly alleviated the histological changes in rabbits. The tension and elasticity of the Achilles tendon were significantly increased after surgery. In addition, surgery treatments notably alleviated the inflammatory responses *in vivo* via downregulation of IL-1 β , TNF- α , and IL-6 and promoted the tube formation in tissues through upregulating VEGF, bFGF, TGF- β 1, and CD31. Furthermore, MS exhibited best therapeutic efficiency on Achilles tendon rupture healing, compared with OS or CT. **Conclusions.** Our research revealed the superiority of MS in Achilles tendon rupture treatment at the molecular level compared with OS or CT.

1. Introduction

Achilles tendon rupture is a subtype of the prevalent tendon injuries [1, 2]. Most of the injuries happen in sports exercise, and the prevalence of injuries has been increasing among the sports participants [3, 4]. Nowadays, excessive strenuous exercise and repeated local inflammation can lead to the rupture of the Achilles tendon [5]. The clinical treatment outcome of Achilles tendon rupture is ideal due to the adopted surgical or nonsurgical treatments. However, the return to the sports before sufficient maturation of tendon can lead to repeat rupture, and this happens in 4.5%–12% and 2.8%–7.1% of cases after conservative treatment and surgeries, respectively [6].

Tendon healing includes overlapping and mutually dependent proliferative, inflammatory, and remodeling

stages. Inflammatory cells and erythrocytes enter the injury site during the initial inflammatory phase. Meanwhile, macrophages and monocytes often phagocytose the necrotic tissues in this phase. Then, the release of growth factors can promote the proliferation and angiogenesis of fibroblasts, and this phenomenon can lead to the migration of fibroblasts to the injury site. After that, the synthesis of type III collagen is initiated. The synthesis of type III collagen usually remains increased for about 42 days during the proliferative phase. Moreover, a bigger proportion of type I collagen is synthesized in the subsequent remodeling phase [7, 8].

At present, there are three major types of Achilles tendon rupture repair surgery: open surgery (OS), minimally invasive surgery (MS), and conservative treatment (CT). Each of these surgical methods has advantages and disadvantages.

For example, a previous study reported that the quality of healing after conservative treatment is poor, and the possibility of breaking again is also high [9]. Meanwhile, the side effect of CT is known to be limited, while the recovery period is too long [10]; the recovery period of MS is relatively short, and the side effect of MS is less obvious compared with OS [4, 11]. According to these studies, MS appears to be more conducive to the rupture and healing of the Achilles tendon, with less surgical injury and faster postoperative recovery. However, which surgical method is more efficient is not clear.

Thus, our study aimed to explore the efficiency of these three surgeries based on angiogenesis, as well as to investigate the underlying mechanism at molecular level. We hope our work would shed new light on finding the ideal treatments for rupture of the Achilles tendon.

2. Materials and Methods

2.1. Animal Model. The rabbit model of Achilles tendon rupture was constructed as recently described [12]. Thirty-two New Zealand white rabbits (SPF, half male half female, three-month-old, 3.5 ± 0.4 kg, Guangdong Medical Laboratory Animal Center, China) were raised in a pathogen-free environment, alternating light and dark for 12 h (8:00 am–8:00 pm). This experiment was carried out in accordance with the animal experiment guidelines, and the research plan was approved by the Animal Experiment Committee.

Rabbits were divided into four groups: model, MS, OS, and CT ($N = 8$, half male half female). All rabbits were modeled with Achilles tendon rupture. Model groups were not processed after modeling. The remaining groups were treated according to the group method.

Sodium pentobarbital (20 mg/kg body weight) was used to inject intravenously into the rabbits, and then we shaved the skin of right hind limb. The procedure of surgeries was used under the aseptic condition. The midline of the Achilles tendon was cut longitudinally with a gap. Subsequently, the paratenon was cut, and we then dissected the tendon of Achilles and plantaris from the surrounding tissues. After that, a scalpel was applied to cut off the middle of the Achilles tendon. The plantaris tendon was left intact as an internal splint. The severed tendon was not sutured. All models were performed on the right hind legs, and the left hind legs were used as an internal reference.

The rabbits in the CT group were treated with plaster to avoid movement. Rabbits in the OS group were treated with open sutures. After disinfection, the Achilles tendon was sutured directly by incising the skin, and then the skin was sutured layer by layer. In the MS group, minimally invasive suture was performed percutaneously. In brief, the ruptured Achilles tendon was sutured minimally through two proximal and two distal puncture routes. Suture line was Vicryl® (3.0, Polyglactin 910, Ethicon, USA). The recovery of the Achilles tendon in the early stage of healing (6 w) was analyzed.

2.2. Biomechanical Evaluation. Both ends of the left and right Achilles tendons of each rabbit were fixed on a test device (Lloyd, LS500, England). After fixing, a tensile test (10 mm/min) was performed. 1 kN electromechanical sensor (MTS Synergie, Eden Prairie, MN, USA) was applied to detect the stress-strain curve, and the elastic modulus (MPa) and failure stress (MPa) were calculated. The maximum force (N) required to break each sample was recorded as load until failure. For each rabbit, the percentage of the experimental side (right side, named treatment) to the health test (left side, named not treated, NT) was calculated.

2.3. H&E and Picrosirius Red Staining. The Achilles tendon tissue at the edge of the healing site was used for histological evaluation. The tissues were fixed (neutral formalin, 10%), sectioned, and deparaffinized. Hematoxylin was added and incubated at room temperature for 10 min, then 0.5% eosin solution was added and incubated at room temperature for 3 min. For the evaluation of collagen formation, Picrosirius Red solution was used to stain for 1 h. After washing and dehydrating, neutral gum was used to seal. The samples were observed under microscope (Olympus, Japan) at $\times 100$ magnification.

2.4. ELISA. IL-6 ELISA kit (PI335, Beyotime, China) and IL-1 β (ml02783) and TNF- α ELISA kit (ml001696, Mlbio, China) were used to detect. Achilles tendon tissues at the edge of the healing site were triturated and lysed, and the supernatant was collected by centrifugation (1,000 \times g, 4°C). Into each 96-well plate, 100 μ l of sample was added. Then, 100 μ l enzyme-labeled reagent was added and incubated at 37°C for 1 h. Subsequently, 50 μ l of chromogenic reagent A was added into each well and an equal volume of chromogenic reagent B was added. The mixture was shaken gently to mix the two stains evenly in the dark. After 15 min, 50 μ l stop solution was added to the reaction to halt color development. It was observed that the sample color changed from blue to yellow. Subsequently, the absorbance was detected. A blank well was used for zero adjustment and the detection wavelength used was 450 nm (680, Bio-Rad, USA). A standard curve was used to determine the concentrations of IL-6, IL-1 β , and TNF- α .

2.5. Reverse Transcription-Quantitative PCR (RT-qPCR). In the early stage of healing (6 weeks postoperatively), the Achilles tendon tissues at the edge of the healing site were collected, and TRIzol® reagent (Thermo Fisher Scientific) was applied to extract total RNA from tissues. Then, total RNA was reverse transcribed into complementary DNA (cDNA), followed by RT-qPCR examination using SYBR Green Master Mix on the ABI 7900 Real-Time PCR System. Real-time qPCRs were performed in triplicate under the following protocol: 94°C for 2 minutes, followed by 35 cycles (94°C for 30 s and 55°C for 45 s). The primer pairs were as follows: COL3A1 forward, 5'-TCACTGGTCTTTTGAG TTT-3' and reverse, 5'-GTGAGGAACAAGCCAGAGCT-3'; IL-6 forward, 5'-AAACTCTGCAAGATGCCACA -3'

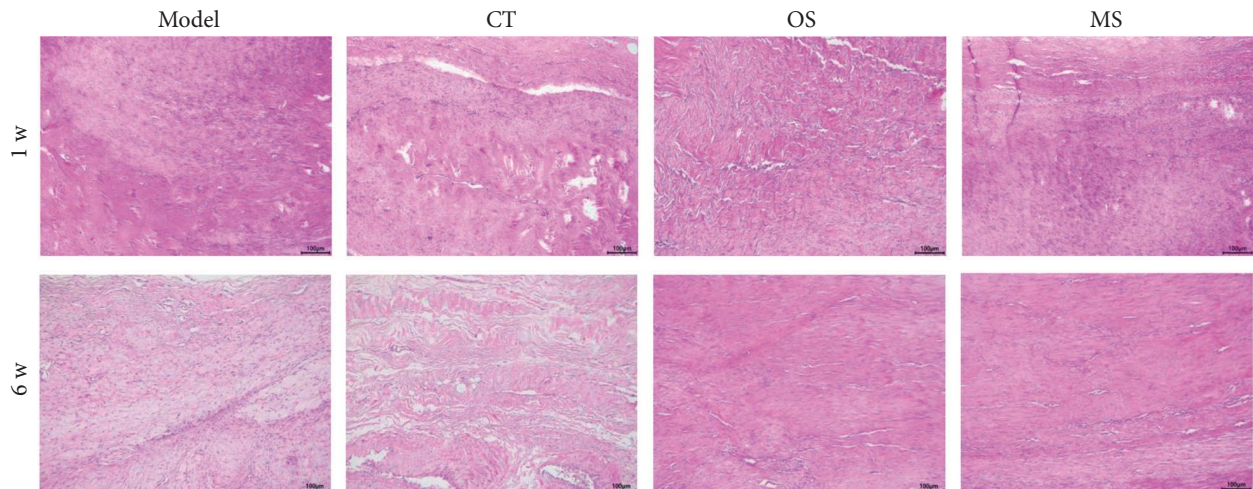


FIGURE 1: CT, OS, and MS alleviate the injury of the Achilles tendon rupture tissues. After 1 or 6 weeks of surgeries, the histological changes in Achilles tendon tissues of rabbits were observed by H&E staining.

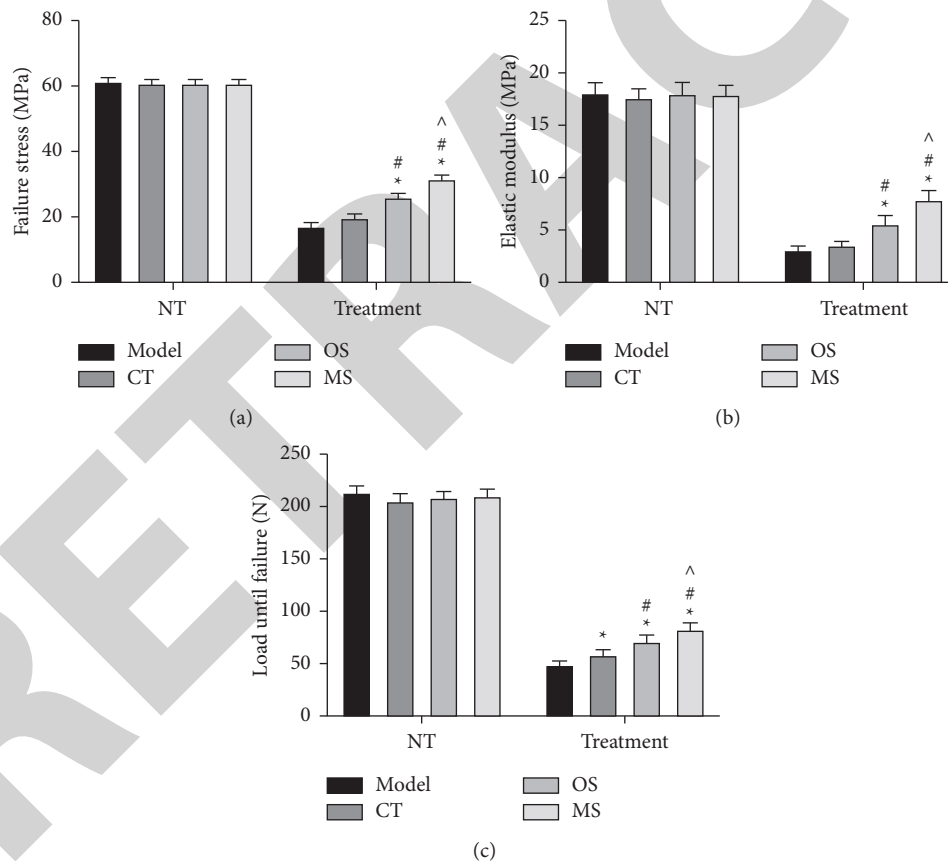


FIGURE 2: CT, OS, and MS promote the recovery biomechanical indicators of the Achilles tendon rupture tissues. (a) The effect of CT, OS, and MS on the elastic modulus of Achilles tendon. (b) The effect of CT, OS, and MS on the failure stress of Achilles tendon. (c) The effect of CT, OS, and MS on the failure stress of Achilles tendon. * $P < 0.05$, ** $P < 0.01$, and *** $P < 0.001$ compared to model. # $P < 0.05$, ## $P < 0.01$, and ### $P < 0.001$ compared to CT. ^ $P < 0.05$, ^# $P < 0.01$, and ^^ $P < 0.01$ compared to OS.

and reverse, 5'-GTCTGAGGCTCATTCTGCCC -3'; IL-1 β forward, 5'-GCAGGCACAGAACCAGTGGC-3' and reverse, 5'-GGAGTTCCTGCAGTCCAGCC -3'; TNF- α forward, 5'-ATGTTGTTCTCTATGGAGAA-3' and reverse, 5'-AATTTATTAATATTTAAATA -3'; VEGF forward, 5'-

CCTCAAATAAATGGCTAACT-3' and reverse, 5'-AATGTATAAATGGTTTTTAT-3'; bFGF forward, 5'-TCTTGGAAAGTGTAGGCTTA-3' and reverse, 5'-TATTTATATTGTATTTATAT-3'; β -actin forward, 5'-GTCCACCGCAAATGCTTCTA-3' and reverse, 5'-TGCTGTCACCTT

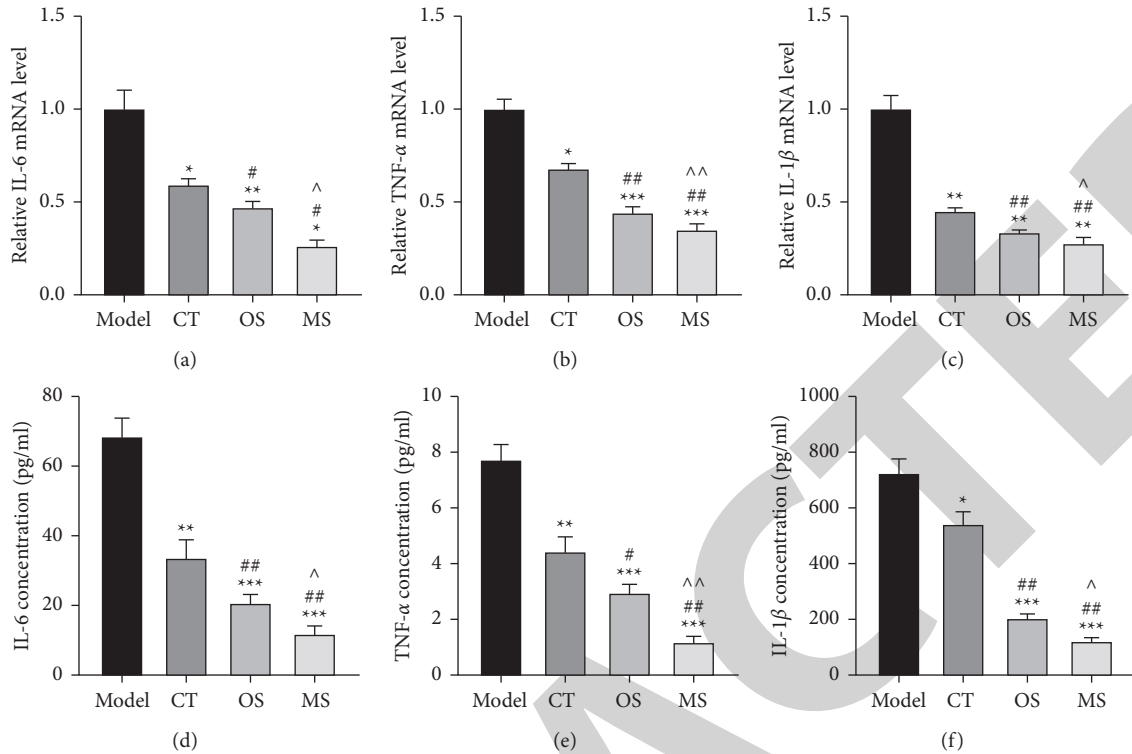


FIGURE 3: MS attenuates the inflammatory responses of the Achilles tendon rupture tissues in a rabbit model. The expressions of (a) IL-6, (b) TNF- α , and (c) IL-1 β in Achilles tendon tissues of rabbits were detected by RT-qPCR. The levels of (d) IL-6, (e) TNF- α , and (f) IL-1 β in Achilles tendon tissues of rabbits were detected by ELISA. * $P < 0.05$, ** $P < 0.01$, and *** $P < 0.001$ compared to model. # $P < 0.05$, ## $P < 0.01$, and ### $P < 0.001$ compared to CT. ^ $P < 0.05$, ^^ $P < 0.01$, and ^^ $P < 0.001$ compared to OS.

CACCGTTC-3'. The $2^{-\Delta\Delta Ct}$ method was used to quantify the data. β -Actin was applied for normalization.

2.6. Western Blotting. The Achilles tendon tissue at the edge of the healing site was lysed using RIPA lysis buffer (Beyotime). Equal amounts (20 μ g) of protein from each group were separated by SDS-PAGE electrophoresis. Separated proteins were transferred on to a PVDF membrane. Then, primary antibodies against COLI (ab239007, 1:1000, Cambridge, MA, USA), COLIII (ab239007, 1:1000), and GAPDH (ab179467, 1:1000) after blocking and HRP-conjugated secondary antibodies (Abcam; ab7356, 1:5000) were used to incubate with the membrane. All the antibodies were obtained from Abcam (MA, USA). ECL kit (Thermo Fisher Scientific) was applied to visualize the protein bands. β -Actin was used for normalization. The densitometry analysis was performed by IPP 6.0 (Image-Pro Plus 6.0).

2.7. Immunohistochemical (IHC) Staining. The Achilles tendon tissue at the edge of the healing site of rabbits was fixed, paraffin-embedded, and cut into sections (5 μ m thick). Paraffin sections were deparaffinized and rehydrated. Subsequently, the sections were heated, incubated for 25 min in 3% H₂O₂, washed, blocked, and incubated for 30 min. After that, primary antibodies (anti-CD31 and anti-VEGF) were applied to stain the samples overnight. Samples were treated with HRP-labeled secondary antibody. After 30 min of

incubation, diaminobenzidine (DAB) was applied for the development of color. All the antibodies originated from Abcam.

2.8. Statistical Analysis. Three independent experiments were performed in each group, and the mean \pm standard deviation (SD) was used to express all data. Difference between the two groups was analyzed using Student's t-test. Differences between the groups were performed using one-way analysis of variance (ANOVA) and Tukey's test (Graphpad Prism7). A significant difference was indicated by the result of $P < 0.05$.

3. Results

3.1. MS Alleviates the Injury and Promotes the Recovery Biomechanical Indicators of the Achilles Tendon Rupture Tissues. To compare the efficiency of three different surgeries for Achilles tendon rupture, H&E staining was performed. It was showed after 1 and 6 weeks of surgery, fibroblasts and angiogenesis in tissues of rabbits were significantly increased, while inflammatory infiltration (including inflammatory cells) was obviously alleviated. Meanwhile, the phenomenon after 6 weeks was more obvious, compared with 1 week. Furthermore, MS exhibited better anti-inflammatory and pro-angiogenesis effect to the ruptured Achilles tendon tissues, compared with OS and CT

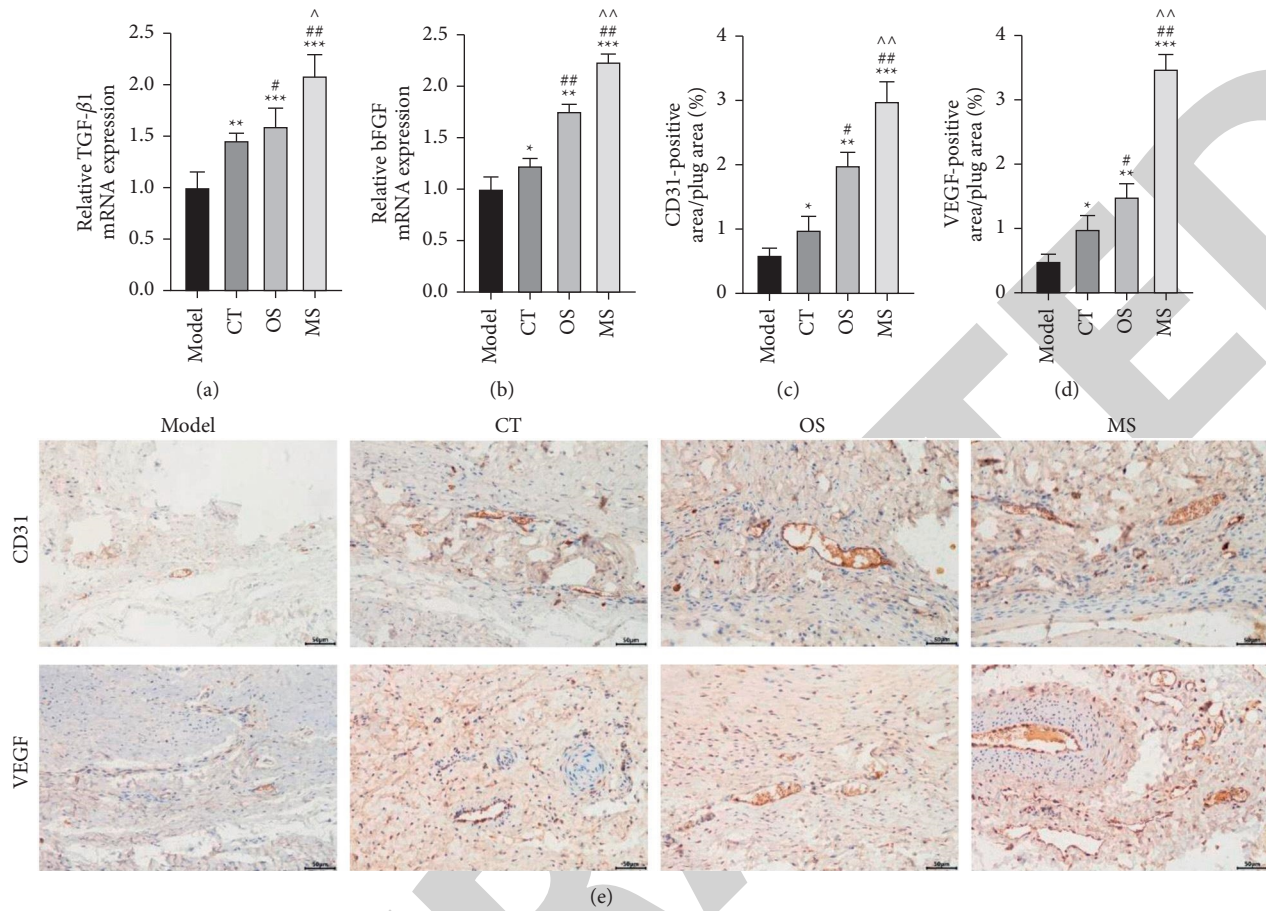


FIGURE 4: MS significantly promotes the angiogenesis of the Achilles tendon rupture tissues in a rabbit model. (a, b) The levels of bFGF and TGF-β1 mRNA in Achilles tendon tissues of rabbits were detected by RT-qPCR. (c, d, e) The protein levels of CD31 and VEGF in Achilles tendon tissues of rabbits were tested by IHC staining. * $P < 0.05$, $P^{**} < 0.01$, and $P^{***} < 0.01$ compared to model. # $P < 0.05$, ## $P < 0.01$, and ### $P < 0.001$ compared to CT. ^ $P < 0.05$, ^^ $P < 0.01$, and ^^^ $P < 0.01$ compared to OS.

treatment (Figure 1). Thus, the above results demonstrated that MS treatments could effectively alleviate the injury of the Achilles tendon rupture tissues in a rabbit model.

In addition, 6 weeks after modeling, the elastic modulus, failure stress, and load until failure indicators after OS and MS treatment all increased significantly (Figures 2(a)–2(c)). Moreover, the biomechanical indexes of the MS group were significantly higher than those of the OS group (Figures 2(a)–2(c)). This suggested that both OS and MS treatment could effectively restore the elasticity and strength of the Achilles tendon in the early stage, and the effect of MS was more significant.

3.2. MS Attenuates the Inflammatory Responses of the Achilles Tendon Rupture Tissues in a Rabbit Model. Next, we investigated the effect of different surgeries on inflammatory responses in Achilles tendon tissues. The data showed that the mRNA of IL-1β, TNF-α, and IL-6 in tissues of rabbits was significantly downregulated in the model group (Figures 3(a)–3(c)). All three surgical methods could effectively reduce the level of these inflammatory cytokines, and MS exerted the better anti-inflammatory effect compared with CT and OS. Similarly,

the data of ELISA demonstrated that three surgical methods significantly decreased the level of IL-1β, TNF-α, and IL-6 in tissues of rabbits, and MS exhibited the most anti-inflammatory effect (Figures 3(d)–3(f)). Taken together, all these data revealed that MS significantly attenuated the inflammatory responses in Achilles tendon rupture tissues of rabbits.

3.3. MS Significantly Promotes the Angiogenesis of the Achilles Tendon Rupture Tissues in a Rabbit Model.

In order to further analyze the molecular mechanisms affecting the healing of Achilles tendon rupture, this study firstly detected the levels of growth factors TGF-β1 and bFGF. The results showed that the levels of TGF-β1 and bFGF mRNA in tissues of rabbit model were greatly upregulated in three treatment groups compared with the model group (Figures 4(a) and 4(b)), while the CT group exhibited the lowest expression of TGF-β1 and bFGF mRNA compared with OS and CT groups. Moreover, the levels of TGF-β1 and bFGF mRNA in the MS group were significantly higher than those in the OS group (Figures 4(a) and 4(b)). These growth factors not only promoted the proliferation and differentiation of tissue cells but also participated in the induction of angiogenesis and promoted blood

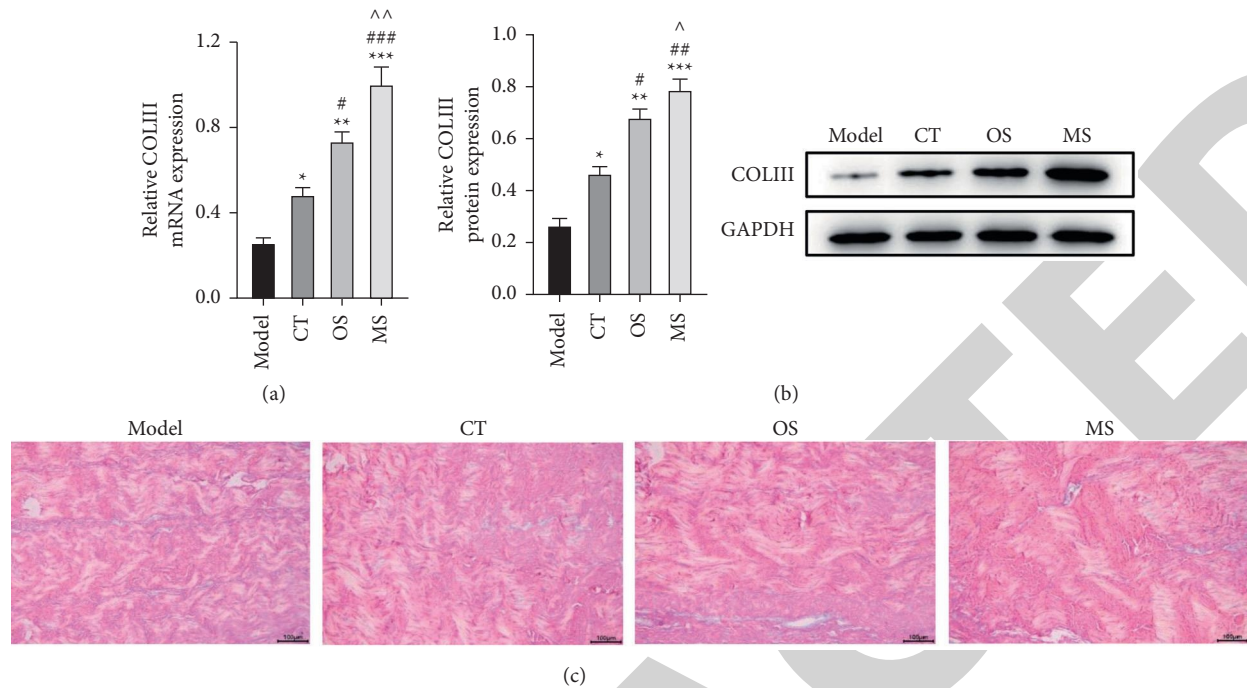


FIGURE 5: MS significantly promotes the healing of the Achilles tendon rupture tissues in a rabbit model. (a, b) The expressions of COLIII mRNA and protein in Achilles tendon tissue of rabbits were tested by RT-qPCR and Western blot. (c) The symptom of Achilles tendon rupture was observed by Picrosirius Red staining. * $P < 0.05$, ** $P < 0.01$, and *** $P < 0.001$ compared to model. # $P < 0.05$, ## $P < 0.01$, and ### $P < 0.001$ compared to CT. ^ $P < 0.05$, ^^ $P < 0.01$, and ^^ $P < 0.001$ compared to OS.

perfusion at the injured site. In this study, CD31 and VEGF were used to assess the growth of blood vessels. The results of IHC experiments showed that the CD31 and VEGF proteins in CT, OS, and MS groups all increased to varying degrees. The CD31 and VEGF levels of OS and MS group were significantly higher than those of the CT group. The MS group had the highest expression of CD31 and VEGF proteins (Figures 4(c)–4(e)). This suggested that compared to OS, MS was more helpful in retaining growth factors and promoting angiogenesis in the early stages of healing.

3.4. MS Significantly Promotes the Healing of the Achilles Tendon Rupture Tissues in a Rabbit Model. In the early stage of Achilles tendon repair, fibroblasts gradually migrated to the injury site and expressed COLIII. The up-regulation of the COLIII expression level within 6 weeks could reflect the early repair of Achilles tendon. The level of COLIII at 6 weeks could reflect the early repair of the Achilles tendon. The results indicated that three different treatments significantly upregulated the expressions of COLIII in Achilles tendon tissues at both mRNA and protein levels (Figures 5(a) and 5(b)). Furthermore, the effects of MS on COLIII mRNA and protein expressions were more significant, compared with CT and OS (Figures 5(a) and 5(b)). In addition, the results of Picrosirius Red staining showed that after treatment, the degree of fibrosis in the three groups was significantly increased. Among them, the fibers of the MS group were the most uniform and abundant (Figure 5(c)). This showed that at 6 weeks after surgery, MS was most conducive to the repair of Achilles tendon fibrosis.

4. Discussion

The main function of the Achilles tendon is flexion of the calf and foot extension. Once the Achilles tendon ruptures, it will seriously affect the patient's exercise ability and cause great inconvenience to the patient's daily life. There are two main treatments for closed Achilles tendon rupture: nonsurgical treatment (conservative treatment) and surgical treatment [13, 14]. The biggest complication of nonsurgical treatment is that the Achilles tendon is more likely to be broken again. At the same time, it requires a long time for plaster immobilization, which seriously affects the patient's quality of life [15, 16]. The surgical treatment is generally divided into two types: OS and minimally invasive surgery. OS has always been the "gold standard" for Achilles tendon rupture. However, scarring is easy to form after OS, and complications such as necrosis of the surrounding skin and exposure to Achilles tendon may occur [17–19]. The purpose of percutaneous surgery is to reduce the rate of re-fracture of the heel key and to minimize infection and soft tissue complications [20, 21]. MS also has some disadvantages. The broken form of the heel key is complicated and irregular, so percutaneous or minimally invasive surgery cannot be well exposed and repaired.

However, there are no systematic reports and studies in the literature that these two surgical methods are more effective. In addition, the underlying mechanism remains unclear. The results of a latest meta-analysis show that OS is more damaging to wounds, while MS seems to be more helpful in the early repair of Achilles tendon, and the long-term efficacy of the two is not significantly different [22]. In

order to evaluate the effects of OS and MS on the early healing of Achilles tendon rupture, rabbits were used for experimental analysis. The results show that 6 weeks after modeling, both OS and MS can promote the healing of the ruptured Achilles tendon, and MS more effectively restores the elasticity and bearing capacity of the Achilles tendon. In addition, the results also show that MS treatment can effectively inhibit the levels of inflammatory cytokines and promote the expression of growth factors TGF- β 1 and bFGF. Moreover, the results of this experiment also show that the repaired tissues of CT, MS, and OS groups all have the expression of VEGF and CD31 protein, while the levels of VEGF and CD31 in the MS group are the highest, suggesting that the blood vessels are the most abundant. Surgery can cause local ischemia and stress damage and promote the increase of inflammatory cytokines, which cause the loss of growth factors and inhibit angiogenesis [18]. This suggests that MS may accelerate Achilles tendon repair by promoting angiogenesis in the early stage of repair.

VEGF (approximately 45 kDa) is a homodimeric glycoprotein [23]. It plays a vital role in angiogenesis. In addition, it can bind VEGF receptor-1 and VEGF receptor-2, which are distributed in vascular endothelial cells [24]. Meanwhile, VEGF can induce angiogenesis in the development of embryo, which is crucial in wound healing in healthy adults [25]. In this research, we found that the surgery treatment could promote the angiogenesis, and it could upregulate the expression of VEGF. Previous studies indicated that VEGF upregulation could promote angiogenesis [26, 27]. VEGF and COLIII have a synergistic effect, and they work together to promote wound repair [28]. COLIII is a key protein for early Achilles tendon fibrosis, and it continues to increase within 6 weeks after healing [29–31]. The increase of COLIII indicates that the early healing degree is good and the speed is fast. The results of this study show that, corresponding to angiogenesis, the MS group also has the highest COLIII level. The function maintenance and repair of tendons are inseparable from the joint action of VEGF and COLIII [32]. In vitro study shows that VEGF can promote the expression of COLIII and promote fibrosis [33]. Based on this, the results of this study show that MS may promote the early repair of Achilles tendon rupture by promoting angiogenesis and the expression of COLIII, thereby accelerating healing. The expression of VEGF, COLIII, and other genes by different treatments may be related to the different effects of trauma, tissue repair, and subsequent inflammation. The mechanisms by which different treatments affect gene expression require in-depth studies.

MS has the advantages of both OS and CT. Compared with CT, MS can effectively repair the Achilles tendon and avoid the postoperative scarring and inflammation problems associated with OS.

5. Conclusion

In conclusion, MS, OS, and CT significantly promoted the repair of Achilles tendon injury. In addition, the anti-inflammatory and pro-angiogenesis effect of MS was much

better than other two treatments; the levels of COLIII (fibrotic markers) were more sensitive to MS, compared with CT and OS, suggesting that MS exhibited more significant therapeutic effects on Achilles tendon rupture, compared with CT and OS. Therefore, our study might shed new light on exploring the best methods for Achilles tendon rupture surgery. However, there is a big difference between animal research and human research. The mechanism by which MS promotes angiogenesis still needs to be studied in depth.

Data Availability

The datasets used and analyzed during the current study are available from the corresponding author upon reasonable request.

Conflicts of Interest

The authors declare that they have no conflicts of interest.

Acknowledgments

This study was supported by the Key Research and Development Project of Ningxia (grant nos. 2019BEG3036 and 2019BEG3044) and Ningxia Natural Science Foundation (grant nos. 2019AAC03172 and 2019AAC03170).

References

- [1] T. Notermans, P. Tanska, R. K. Korhonen, H. Khayyeri, and H. Isaksson, "A numerical framework for mechano-regulated tendon healing-Simulation of early regeneration of the Achilles tendon," *PLoS Computational Biology*, vol. 17, no. 2, Article ID e1008636, 2021.
- [2] S. H. Wirth, O. Andronic, F. Aregger, A. Jungwirth-Weinberger, T. Jentzsch, and A. Hecker, "Flexor hallucis longus hypertrophy secondary to Achilles tendon tendinopathy: an MRI-based case-control study," *European Journal of Orthopaedic Surgery and Traumatology*, vol. 31, no. 7, pp. 1387–1393, 2021.
- [3] B. D. Meeks, E. M. Kiskaddon, E. Erb, G. Gould, A. Froehle, and R. T. Laughlin, "Biomechanical comparison of tape versus suture in simulated achilles tendon midsubstance rupture," *The Journal of Foot and Ankle Surgery*, vol. 60, no. 4, pp. 697–701, 2021.
- [4] A. E. Roell, T. K. Timmers, D. J. C. van der Ven, and G. D. J. van Olden, "Rehabilitation after surgical repair of acute achilles tendon rupture: functional outcome with a follow-up of 6 months," *Journal of Foot and Ankle Surgery*, vol. 60, no. 3, pp. 482–488, 2020.
- [5] C. Chen and K. J. Hunt, "Open reconstructive strategies for chronic achilles tendon ruptures," *Foot and Ankle Clinics*, vol. 24, no. 3, pp. 425–437, 2019.
- [6] A. Grassi, S. Caravelli, M. Fuiano et al., "Epidemiology of achilles tendon rupture in Italian first division football (soccer) players and their performance after return to play," *Clinical Journal of Sport Medicine*, vol. 32, no. 1, pp. e90–e95, 2022.
- [7] I. Loturco, C. De la Fuente, C. Bishop et al., "Video-based biomechanical analysis of an unexpected Achilles tendon rupture in an Olympic sprinter," *Journal of Biomechanics*, vol. 117, Article ID 110246, 2021.

Retraction

Retracted: Nonalcoholic Fatty Liver Hepatocyte-Derived lncRNA MALAT1 Aggravates Pancreatic Cell Inflammation via the Inhibition of Autophagy by Upregulating YAP

Computational Intelligence and Neuroscience

Received 25 July 2023; Accepted 25 July 2023; Published 26 July 2023

Copyright © 2023 Computational Intelligence and Neuroscience. This is an open access article distributed under the Creative Commons Attribution License, which permits unrestricted use, distribution, and reproduction in any medium, provided the original work is properly cited.

This article has been retracted by Hindawi following an investigation undertaken by the publisher [1]. This investigation has uncovered evidence of one or more of the following indicators of systematic manipulation of the publication process:

- (1) Discrepancies in scope
- (2) Discrepancies in the description of the research reported
- (3) Discrepancies between the availability of data and the research described
- (4) Inappropriate citations
- (5) Incoherent, meaningless and/or irrelevant content included in the article
- (6) Peer-review manipulation

The presence of these indicators undermines our confidence in the integrity of the article's content and we cannot, therefore, vouch for its reliability. Please note that this notice is intended solely to alert readers that the content of this article is unreliable. We have not investigated whether authors were aware of or involved in the systematic manipulation of the publication process.

Wiley and Hindawi regrets that the usual quality checks did not identify these issues before publication and have since put additional measures in place to safeguard research integrity.

We wish to credit our own Research Integrity and Research Publishing teams and anonymous and named external researchers and research integrity experts for contributing to this investigation.

The corresponding author, as the representative of all authors, has been given the opportunity to register their agreement or disagreement to this retraction. We have kept a record of any response received.

References

- [1] D. Liu, W. Yao, K. Liu et al., "Nonalcoholic Fatty Liver Hepatocyte-Derived lncRNA MALAT1 Aggravates Pancreatic Cell Inflammation via the Inhibition of Autophagy by Upregulating YAP," *Computational Intelligence and Neuroscience*, vol. 2022, Article ID 2930960, 9 pages, 2022.

Research Article

Nonalcoholic Fatty Liver Hepatocyte-Derived lncRNA MALAT1 Aggravates Pancreatic Cell Inflammation via the Inhibition of Autophagy by Upregulating YAP

Di Liu,¹ Weijie Yao,¹ Kejun Liu,¹ Genwang Wang,¹ Bendong Chen,¹ Zuozheng Wang,¹ and Shaozhang Hou^{1,2} 

¹Department of Hepatobiliary Surgery, General Hospital of Ningxia Medical University, Yinchuan 750004, China

²School of Basic Medical Sciences, Ningxia Medical University, Yinchuan 750004, China

Correspondence should be addressed to Shaozhang Hou; 18409381@masu.edu.cn

Received 9 July 2022; Revised 5 August 2022; Accepted 8 August 2022; Published 31 August 2022

Academic Editor: Dong Chen

Copyright © 2022 Di Liu et al. This is an open access article distributed under the Creative Commons Attribution License, which permits unrestricted use, distribution, and reproduction in any medium, provided the original work is properly cited.

Background. Acute pancreatitis (AP) is one of the most common gastrointestinal disorders, which causes death with a high mortality rate of about 30%. The study aims to identify whether the nonalcoholic fatty liver disease (NAFLD)-derived lncRNA MALAT1 participates in the inflammation of pancreatic cell and its potential mechanism. **Methods.** The NAFLD cell model was constructed by treating HepG2 cells with FFA. The *in vitro* model of acute pancreatitis (AP) was established by the administration of caerulein on AR42J cells. MALAT1 and si-MALAT1 were transfected into pancreatic cells, and then exosomes were collected from the NAFLD cell model and then were cocultured with AR42J cells. Transmission electron microscopy was used to observe the morphology of exosomes. Oil Red O staining was applied to reveal the lipid deposition. The triglyceride, IL-6, and TNF- α levels were detected using ELISA. The MALAT1 level in exosomes was detected by qRT-PCR. The CD9, CD63, CD81, and CYP2E1, LC3II, and LC3I levels were detected by western blot. **Results.** MALAT1 was upregulated in NAFLD-derived exosomes and increased the levels of IL-6 and TNF- α in pancreatic cells. NAFLD-derived exosomes inhibited YAP phosphorylation, decreased the levels of IL-6 and TNF- α , and reduced the ratio of LC3II/LC3I protein in pancreatic cells. Silencing MALAT1 significantly returned the inhibitory effect of NAFLD on hippo-YAP pathway. YAP1 signal transduction inhibitor CA3 reversed the decrease of LC3II/LC3I expression and the increase of IL-6 and TNF- α levels induced by MALAT1 in the AP cell model. **Conclusions.** NAFLD-derived MALAT1 exacerbates pancreatic cell inflammation via inhibiting autophagy by upregulating YAP.

1. Introduction

Acute pancreatitis (AP) is able to cause death with high mortality rate of about 30%, which is one of the most common gastrointestinal disorders [1–3]. Pancreatic necrosis/apoptosis and systemic inflammation are the characteristics of AP [4]. Over the centuries, several studies have been conducted on the etiology and pathogenesis of AP [1]. Scholars have found that the main pathogenesis of AP is the undesired overactivation of trypsinogen in pancreatic cells [5]. However, the mechanisms regulating AP progression remain a matter of clarification.

Exosomes are vesicles secreted by cells that have a double plasma membrane structure, which carries specific cytokines of mother cells, including mRNA, miRNA, and lncRNA [6]. The role of exosomes in pancreatitis has been explored. For example, exosomal lnc-MMP2-2 increases vascular permeability and promotes lung cancer progression by promoting MMP2 expression [7]. Lnc-MKRN2-42:1 in exosomes from plasma samples is positively correlated with MDS-UPDRS III scores in patients with Parkinson's disease, and it may be involved in the development of Parkinson's disease [8]. Only one paper has reported the involvement of exosomal lncRNA in the progression of acute pancreatitis,

that is, rhodopsin suppresses acute pancreatitis by regulating the expression of cellular and exosomal lncRNA TUG1 [9]. The effect of lncRNA in NAFLD-derived exosomes on pancreatitis has not been explored previously.

Long noncoding RNA (lncRNA) is a special RNA molecule with a transcript length of more than 200 nucleotides and no protein-coding function [10]. The metastasis-associated lung adenocarcinoma transcript 1 (MALAT1), also is a long non-coding RNA [11]. One prior study found that lncRNA MALAT1 in exosomes from conditioned medium facilitates ischemic wound healing [12]. According to research, MALAT1 plays an important role in pancreatitis. Extracellular vesicle-shuttled MALAT1 promotes macrophage M1 polarization through miR-181a-5p/HMGB1 to induce acute pancreatitis [13]. MALAT1/miR-194/YAP1 has a regulatory effect on the progression of AP [14]. However, no data have been presented to verify the effect of NAFLD-derived lncRNA MALAT1 on the regulation of AP. It is reported that lncRNAs are involved in the progression of acute pancreatitis [15, 16], but the influence of NAFLD-derived MALAT1 in acute pancreatitis remains blurry.

In this study, the research aimed to uncover the influence of lncRNA MALAT1 in AP, and we hypothesized that NAFLD-derived MALAT1 could potentially affect the progression of AP and conduct a series of experiments to explore whether NAFLD-derived MALAT1 affects the progression of AP. The study is intended to provide a theoretical basis and potential targets for the treatment of clinical AP patient.

2. Materials and Methods

2.1. Isolation and Characterization of Exosomes. In this experiment, we borrowed the method of Thery *et al.* [17] to isolate exosomes. ExoQuick-TC (System Biosciences, Mountain View, CA) was used for the isolation of exosomes. We identified the isolated exosomes by transmission electron microscopy, western blot analysis, and nanoparticle tracking analysis.

2.2. Cell Culture. HepG2 and AR42J were obtained from the American Type Culture Collection (ATCC, Manassas, US). The cell lines HepG2 were cultured in Dulbecco's Modified Eagle Medium (DMEM) (Gibco, Paisley, UK, US) medium containing 10% fetal bovine serum (FBS, HyClone, UT, USA) for 24 h. AR42J were cultured in F-12K (Gibco) medium containing 20% FBS (HyClone) for 24 h. Then, the cells were incubated in an incubator at 37°C with 5% CO₂.

2.3. Cell Transfection. The sequences of si-NC and si-MALAT1 were obtained by GenePharma (Shanghai, China). HepG2 cells were transfected with si-NC and si-MALAT1 using Lipofectamine 2000 (Invitrogen, CA, USA) for 24 h. The transfected cells were used for further study.

2.4. Establishment of the NAFLD Cell Model and AP Cell Model. HepG2 treated with or without 1 mM free fatty acid (FFA, containing 2:1 v/v oleic acid and palmitic acid) for

24 h was used for subsequent experiments. In addition, AR42J cells cultured for 24 h were incubated with 20 nM caerulein (#C9026, Sigma-Aldrich, St Louis, MO, USA) for 48 h for the construction of AP cell model.

2.5. Oil Red O Staining. After fixing HepG2 cells in 10% formalin for 5 min, they were incubated with Oil Red O reagent for 30 min. The stained cells were then counterstained with hematoxylin for 1 min, and sections were dewaxed and rehydrated in xylene. Tissue sections were then incubated in Oil Red O reagent for 30 minutes and counterstained with hematoxylin for 1 min. Sections were finally imaged on a fluorescence microscope (IX-51, Olympus, Tokyo, Japan).

2.6. Quantitative Real-Time Reverse Transcription-Polymerase Chain Reaction (qRT-PCR). For the examination of the MALAT1 expressions, isolated from exosomes by TRIzol reagent (Ambion, Austin, TX). 1 µg of total RNA was reverse transcribed using the all-in-one miRNA qRT-PCR detection kit (GeneCopoeia Rockville, MD, USA). The qRT-PCR was performed on the CFX96 PCR detection system (Bio-Rad Laboratories, Hercules, CA, USA). The sequences used in qRT-PCR were presented as follows: MALAT1: 5'-GCT CTG TGG TGT GGG ATT GA-3' (F) and 5'-GTG GCA AAA TGG CGG ACT TT-3' (R); GAPDH: 5'-CCA GGT GGT CTC CTC TGA-3' (F) and 5'-GCT GTA GCC AAA TCG TTG T-3' (R). The 2^{-ΔΔCt} method was adopted to analyze relative fold change [18].

2.7. Western Blot. Cells were completely lysed in lysis buffer (Takara, Shiga, Japan) and extracted nuclear proteins and cytoplasmic proteins. The BCA protein assay kit (Pierce, Rockford, IL) was used to detect the corresponding protein densities. 50 µg of the sample was taken for SDS-PAGE electrophoresis and transferred to the PVDF membrane. Then, membranes were blocked with 5% skim milk. Membranes were then incubated with the corresponding primary antibodies, including anti-CD9 antibody (ab178860, 1:1000, Abcam, Cambridge, MA, USA), anti-CD63 antibody (ab188570, 1:5000, Abcam), anti-CD81 antibody (ab3778; 1:200, Abcam), anti-CYP2E1 antibody (ab52915, 1:10000, Abcam), anti-YAP-13 antibody (ab51072, 1:1000, Abcam), anti-phosphorylated-YAP antibody (ab185722, 1:1000, Abcam), anti-LC3II antibody (ab41037, 1:250, Abcam), anti-LC3I antibody (ab32360, 1:5000, Abcam), anti-LATS1 antibody (ab32452, 1:2000, Abcam), and anti-β-actin antibody (ab8226, 1:10000, Abcam) overnight at 4°C. β-actin was used as internal controls. Then, membranes were incubated with horseradish peroxidase-labeled secondary antibody (ab6721, 1:2000, Abcam) for 1 h at room temperature. Then, the specific protein bands were visualized using an enhanced chemiluminescent (ECL; Millipore, Shanghai, China).

2.8. Enzyme-Linked Immunosorbent Assay (ELISA). TNF-α ELISA and IL-6 ELISA kits (Thermo, MA, USA) were performed to measure TNF-α and IL-6 secretion and finally

the specific levels of TNF- α and IL-6 were determined by a standard curve.

2.9. Statistical Analysis. Data from at least three independent experiments were exhibited as mean \pm SD, analyzed by SPSS 17.0 statistical software. Paired Student's t-test was performed to compare the differences between the two groups. One-way ANOVA along with Bonferroni's posttest was used to analyze the differences between more than two groups. P value < 0.05 was considered statistically significant.

3. Results

3.1. MALAT1 Is Upregulated in NAFLD-Derived Exosomes. To assess whether the NAFLD cell model was successfully constructed, we examined the lipid deposition and triglyceride content in the hepatocytes and in the culture medium supernatant, respectively. The results indicated lipid deposition was remarkably increased in the FFA group (Figure 1(a)). The TG content was significantly elevated in the supernatant of HepG2 cell medium compared with the Control group (Figure 1(b), $p < 0.001$). Extracellular vesicles isolated from cell supernatant were characterized by the TEM. Vesicular morphology and a diameter between 50 and 150 nm were evident in TEM images (Figure 1(c)). Besides, we found that the isolated exosomes from the Control group and the FFA group expressed not only the exosomal markers CD9, CD63, and CD81 as expected but also hepatocyte marker proteins CYP2E1 (Figure 1(d)). We also examined the expression of MALAT1 in exosomes and found that the expression of MALAT1 was significantly increased after FFA induction, in contrast to in exosomes produced from HepG2 cells without FFA induction (Figure 1(e), $p < 0.001$). We cocultured the exosomes with pancreatic cells AR42J and measured the secretion levels of inflammatory factors in the pancreatic cell medium. The results showed the levels of IL-6 and TNF- α in the FFA group were obviously higher (Figure 1(e), $p < 0.001$). These results suggest that these hepatocytes are their primary source of the isolated exosomes wrapped in MALAT1. All illustrated that MALAT1 is upregulated in NAFLD-derived exosomes.

3.2. NAFLD-Derived Exosomes Exacerbate the Inflammatory Response and Inhibit YAP Phosphorylation and Autophagy in Pancreatic Cells. To investigate whether NAFLD-derived exosomes regulate the inflammatory response, YAP expression, and autophagy in pancreatic cells, we then cocultured exosomes with AR42J pancreatic cells. Figure 2(a) reveals inflammatory factors IL-6 and TNF- α level were increased in pancreatic cell cultures cocultured with exosomes relative to controls ($p < 0.001$). The level of YAP/p-YAP was obviously increased in the FFA group when compared with the Control group (Figure 2(b), $p < 0.001$). The levels of LC3II/LC3I in pancreatic cells were largely decreased after coculture of pancreatic cells and exosomes (Figure 2(c), $p < 0.001$). All of the above illustrates that

NAFLD-derived exosomes promote the inflammatory response and inhibit YAP phosphorylation and autophagy in pancreatic cells.

3.3. NAFLD-Derived Exosomes Inhibit Hippo-YAP Pathway, Suppress Autophagy, and Promote Inflammatory Responses in Pancreatic Cells via MALAT1. Based on the upregulation of MALAT1 in NAFLD-derived exosomes, the effects of NAFLD-derived exosomes on the inflammatory response and autophagy of pancreatic cells were investigated, as well as we speculated that MALAT1 may be involved in the regulatory process of exosomes in pancreatic cells. Figure 3(a) shows that the successful knockdown of MALAT1 in HepG2 cells ($p < 0.001$). Meanwhile, the MALAT1 level was significantly reduced in the exosomes extracted from FFA-induced HepG2 cells transfected with si-MALAT1 in relative to the FFA group (Figure 3(b), $p < 0.001$). Moreover, MALAT1 expression was elevated in pancreatic cells after cocultured with FFA-induced exosomes, and silencing MALAT1 reversed the increase in MALAT1 levels induced by FFA induction (Figure 3(c), $p < 0.001$). We further explored the effects of silencing MALAT1 on Hippo-YAP pathway, autophagy, and inflammation in pancreatic cells. Figures 3(d) and 3(e) show that LATS1 was much lower in the FFA group than that in the Control group ($p < 0.001$), while silencing MALAT1 effectively recovered this status ($p < 0.001$); the level of YAP/p-YAP showed an opposite trend ($p < 0.01$, $p < 0.001$). As shown in Figures 3(f) and 3(g), the levels of the LC3II/LC3I were reduced in the FFA group ($p < 0.001$), which was partly restored in the FFA + si-MALAT1 group ($p < 0.01$). Besides, FFA induction resulted in increased levels of IL-6 and TNF- α ($p < 0.001$), and silencing MALAT1 followed by FFA induction reversed the augment in IL-6 and TNF- α levels induced by FFA induction (Figure 3(h), $p < 0.01$). These suggested that NAFLD-derived exosomes inhibit the Hippo-YAP pathway, suppress autophagy, and promote inflammatory responses in pancreatic cells via upregulating MALAT1.

3.4. MALAT1 Exacerbates AP via Inhibiting Autophagy by Upregulating YAP. To further confirm the underlying molecular mechanism of MALAT1 in regulating AP, we then examined the effects of MALAT1 on YAP and autophagy in an *in vitro* model of AP. The results first showed the increased MALAT1 in pancreatic cells transfected with MALAT1 and the decreased MALAT1 in pancreatic cells transfected with si-MALAT1, indicating the successful overexpression and knockdown of MALAT1 in the *in vitro* model of AP (Figures 4(a) and 4(b), $p < 0.001$). Clearly, the *in vitro* model of AP with MALAT1 overexpression showed the increased expression of IL-6 and TNF- α levels ($p < 0.01$), while silencing MALAT1 decreased the IL-6 and TNF- α levels (Figure 4(c), $p < 0.05$). Besides, the level of LC3II/LC3I was reduced in the AP cell model with MALAT1 overexpression ($p < 0.001$), but such trend was significantly restored by the YAP inhibitor CA3 (Figures 4(d) and 4(e), $p < 0.01$). The inhibition of YAP CA3 inhibited the increase

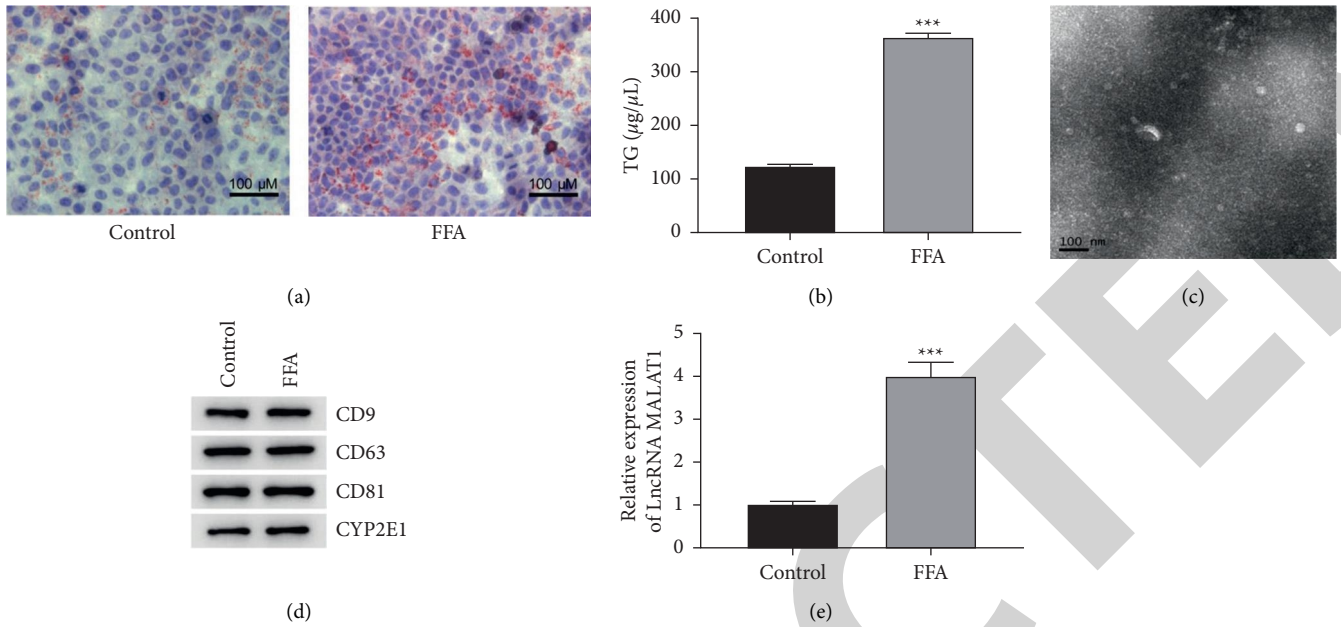


FIGURE 1: Increased expression of MALAT1 in NAFLD-derived exosomes exacerbates the inflammatory response in pancreatic cells. (a) Lipid deposition in NAFLD cell models was detected using Oil Red O staining. (b) TG in the supernatant of NAFLD cell model culture medium was detected by the ELISA assay. (c) Collected exosomes were observed by transmission electron microscopy. (d) CD9, CD63, and CD81 protein levels and liver marker CYP2E1 were investigated by western blot. (e) Expression of MALAT1 in exosomes was probed by qRT-PCR. *** $p < 0.001$ vs. Control group. TG: triglycerides.

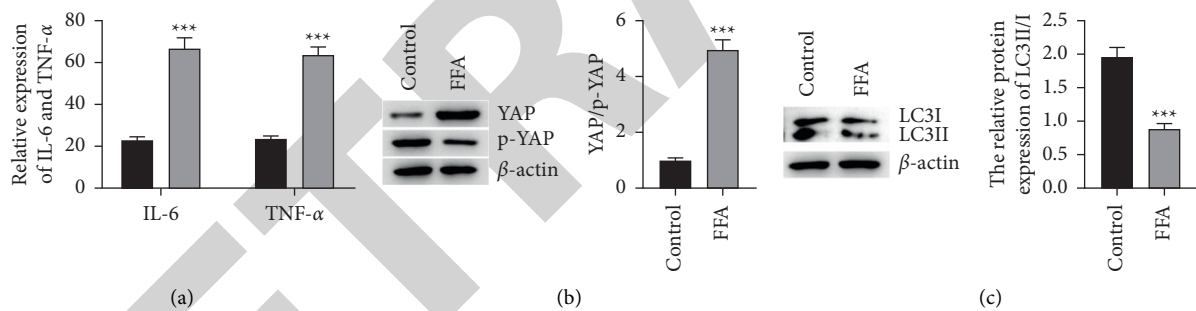


FIGURE 2: NAFLD-derived exosomes from nonalcoholic fatty liver activate YAP and inhibit autophagy in pancreatic cells. (a) The ELISA assay was used to detect levels of IL-6 and TNF- α . (b) The protein expression of YAP and phosphorylated YAP were detected by western blot. (c) The protein expression of LC3II and LC3I was detected by western blot. *** $p < 0.001$ vs. Control group.

of IL-6 and TNF- α level caused by MALAT1 (Figure 4(f), $p < 0.01$). The above indicated that MALAT1 exacerbates AP via inhibiting autophagy by promoting YAP.

4. Discussion

Exosomes perform cell-to-cell actions by delivering exosomal contents and regulating receptor cell [19–21]. Almost all types of cells can secrete exosomes, and exosomes are also widely present in body fluids [19, 22, 23]. The κ stem cell-derived exosomes prevent cardiac insufficiency via lncRNA MALAT1/NF- κ B/TNF [24]. Exosomal Hic-5 regulates osteosarcoma phenotype [25]. Human mesenchymal stem cells promote ischemic repairment and angiogenesis of diabetic foot through exosomal miRNA-21-5p [26]. In NAFLD, stressed/damaged hepatocytes release large amounts of EVs,

leading to the development of inflammation, fibrogenesis, and angiogenesis, which are key pathobiological processes in the progression of liver disease [27]. In this paper, we demonstrated that the FFA-induced NAFLD cell model secretes a large number of exosomes, when cocultured with AR42J pancreatic cancer cells, and inhibits YAP phosphorylation and autophagy in AR42J.

MALAT1 is the first lncRNA found to be involved in the occurrence and development of various cancers. MALAT1 can induce the metastasis and invasion of various cancer cells [28, 29]. Studies report that MALAT1 has pro-inflammatory effects, which was able to aggravate cardiac inflammation [30] and promote EC inflammation [31]. Furthermore, exosomal MALAT1 derived from HUVECs promoted inflammatory response in atherosclerotic mice [32]. Herein, we found that MALAT1 was upregulated in

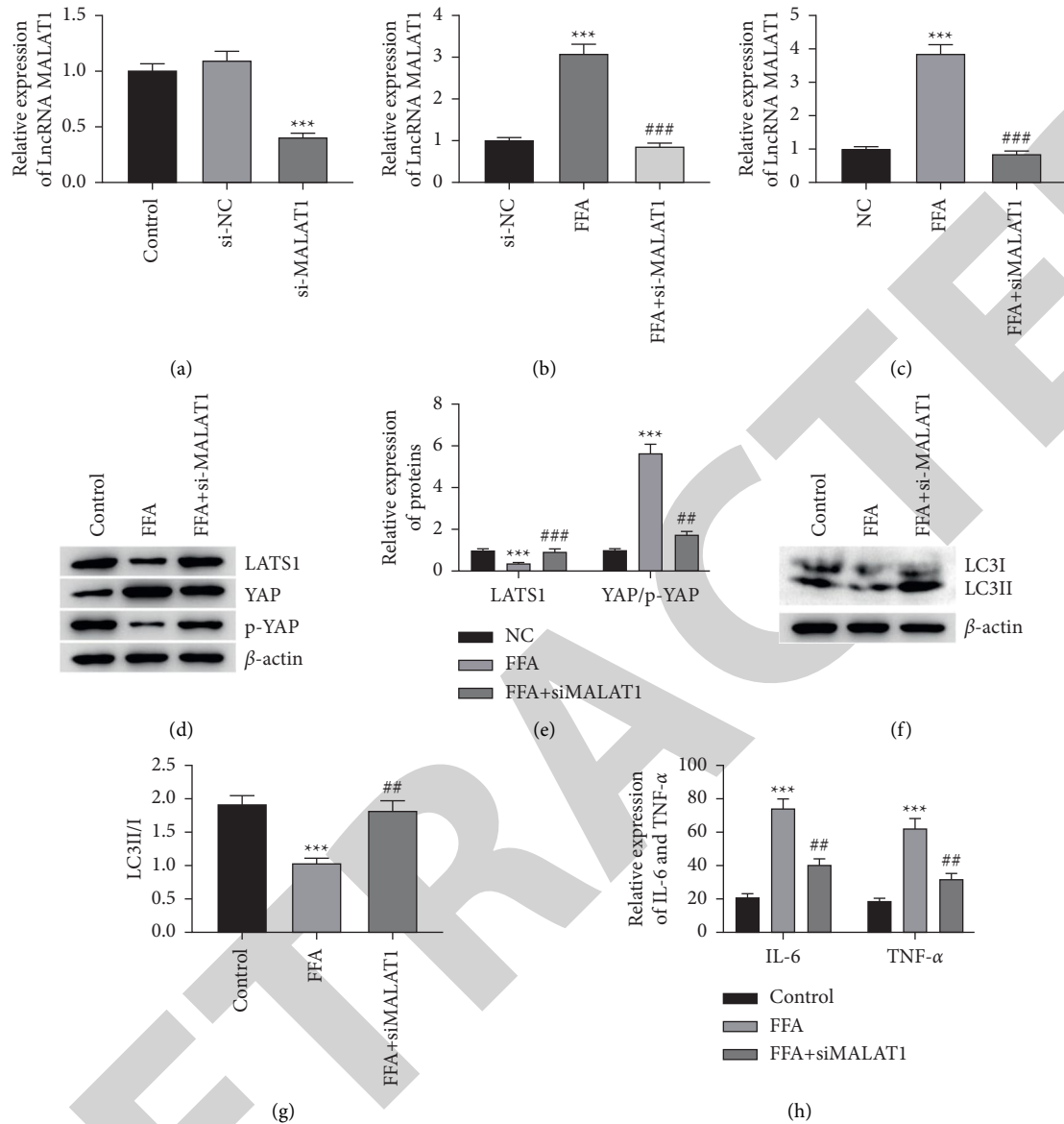


FIGURE 3: NAFLD-derived exosomes activate the Hippo-YAP pathway, suppress autophagy and inflammatory responses in pancreatic cells via MALAT1. (a) qRT-PCR was used to analyze MALAT1 levels in Human hepatocytes HepG2 following si-NC and si-MALAT1 transfection. (b) qRT-PCR was used to analyze MALAT1 levels in exosomes. (c) qRT-PCR analysis of MALAT1 expression in AR42J pancreatic cells after co-culture with NAFLD-derived exosomes. (d, e) Hippo-YAP pathway-associated protein LATS1, YAP and phosphorylated YAP were detected using western blot assay. (f, g) Autophagy-associated proteins LC3II and LC3I were measured by western blot assay. (h) ELISA assay was performed on the secretion levels of IL-6 and TNF- α . *** $p < 0.001$ vs. si-NC group/NC group/Control group; ## $p < 0.01$ and ### $p < 0.001$ vs. FFA group.

NAFLD-derived exosomes. Coculture of exosomes with AR42J pancreatic cells increased inflammatory factor levels in AR42J cell culture medium. Our subsequent study confirmed that NAFLD hepatocyte-derived exosomes promoted inflammatory responses in pancreatic cells through MALAT1. Our findings are consistent with those reported in previous studies that MALAT1 has pro-inflammatory effects.

The Hippo signaling pathway is a key regulator in the pathway, which consists of a series of conserved kinases that control organ size primarily by regulating cell proliferation and apoptosis [33], which have been researched in pancreas

development and pancreatic cancer [34, 35]. Moreover, the activation of Hippo signaling pathway participated in regulating ferroptosis in acute lung injury [36]. However, the function of Hippo signaling pathway in AP is still unclear. YAP (Yes-associated protein) is a major downstream effector of the Hippo pathway and mediates the effects of the Hippo pathway by regulating the gene expression [37, 38]. The Hippo-YAP axis has been reported to have a non-negligible role in regulating autophagy [39]. It is well known that Hippo plays an important role in the occurrence of inflammation. Naringin protects endothelial cells from apoptosis and inflammation by regulating the Hippo-YAP

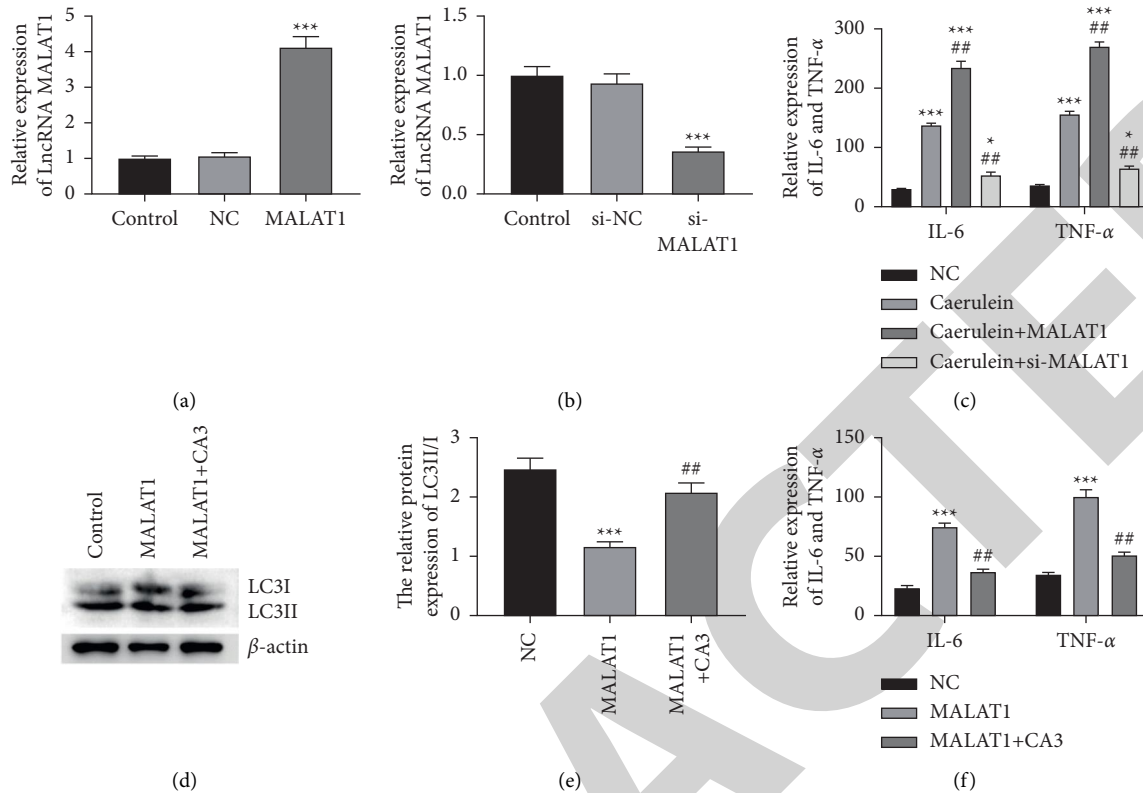


FIGURE 4: MALAT1 further inhibits autophagy by promoting YAP and eventually exacerbates AP. (a, b) The relative expression of MALAT1 in AR42J pancreatic cells transfected with MALAT1 and si-MALAT1 were examined using qRT-PCR assay. *** $p < 0.001$ vs. NC/si-NC group. (c) Levels of IL-6 and TNF- α was detected by ELISA assay in AR42J pancreatic cells treated with caerulein and/or transfected with MALAT1 and si-MALAT1. * $p < 0.05$ and *** $p < 0.001$ vs. NC group; ## $p < 0.01$ vs. Caerulein group. (d, e) The relative protein expression of LC3II and LC3I was measured by the western blot assay. (f) The levels of IL-6 and TNF- α were determined utilizing ELISA assay. *** $p < 0.01$ vs. NC group; ## $p < 0.01$ vs. MALAT1 group.

pathway [40]. Hippo/YAP pathway plays a critical role in effect of GDNF against A β -induced inflammation in microglial cells [41]. The inhibition of Hippo/YAP signaling pathway is required for magnesium isoglycyrrhizinate to ameliorate hepatic stellate cell inflammation and activation [42]. Our study shows that NAFLD hepatocyte-derived exosomes inhibit Hippo-YAP pathway and autophagy in pancreatic cells via MALAT1. The regulatory effect of MALAT1 on the Hippo-YAP pathway has been reported in the literature. Downregulation of MALAT1 inhibits the development of pancreatic cancer by activating the Hippo-YAP pathway [43]. MALAT1 interference decreased collagen accumulation and inflammation in high-glucose CFs and DCM mice [44]. Downregulation of MALAT1 suppressed the proliferation and adhesion of myeloma cells [45]. Furthermore, MALAT1 has been found to have regulatory effects on autophagy in a range of diseases. MALAT1 enhances the apoptosis of cardiomyocytes [46]. Long non-coding RNA MALAT1 affects the development of endometriosis [47] and promoted cell proliferation, yet inhibited apoptosis in colorectal cancer cells [48]. The results of this experiment are consistent with the theory and consistent with the existing literature reports.

We subsequently confirmed through rescue experiments that MALAT1 exacerbates AP by promoting YAP

and thereby inhibiting autophagy. The involvement of MALAT1 in the progression of pancreatitis has been documented. An important research study demonstrated that MALAT1/miR-181a-5p/HMGB1 induced AP [13]. Baicalin can affect the expression of miR-15a to prevent the occurrence of AP. Long noncoding RNA MALAT1, regulated by baicalin, targets miR-15a [49]. MALAT1 affects pancreatic cancer progress [50] and acts on AP via miR-194/YAP1 [14]. Treatment of MALAT1 overexpressing pancreatic cancer cells with CA3 in our research revealed that inhibition of YAP reversed the inhibition of autophagy and promotion of inflammatory response induced by MALAT1 overexpression. The role of Hippo pathway has been studied in the pancreas. Hippo signaling not only regulates pancreatic development by inactivating YAP [51], but also affects the differentiation and maintenance of the exocrine pancreas [52]. Proliferative and antiapoptotic action of exogenously introduced YAP in pancreatic cells [53]. YAP levels have a clear upward trend in alveolar and ductal cells of mice with pancreatitis and may be involved in regulating pancreatic tissue regeneration and stellate cell function [54]. Our study found that NAFLD-derived MALAT1 inhibits autophagy to further promote inflammatory responses by suppressing the Hippo-YAP pathway in pancreatic cells.

5. Conclusion

Taken together, our research is the first to clarify that exosomal lncRNA MALAT1 originating from NAFLD exacerbated pancreatic cell inflammation by regulating YAP inhibition of autophagy. This molecule may bring a major breakthrough in the clinical treatment of NAFLD. However, some potential mechanisms and Hippo signaling pathway regulation in AP are worthy further investigated.

Data Availability

The datasets used and analyzed during the current study are available from the corresponding author upon reasonable request.

Disclosure

Weijie Yao is the co-author.

Conflicts of Interest

The authors declare that they have no conflicts of interest.

Acknowledgments

This study was supported by the Key R&D Program of Ningxia Hui Autonomous Region, under 2021BEG03042 Special Fund for Innovation Platform of Ningxia Hui Autonomous Region Science and Technology Infrastructure Construction Plan (2020CXPT0007).

References

- [1] G. J. Wang, C. F. Gao, D. Wei, C. Wang, and S. Q. Ding, "Acute pancreatitis: etiology and common pathogenesis," *World Journal of Gastroenterology*, vol. 15, no. 12, pp. 1427–1430, 2009.
- [2] I. Gukovsky, A. S. Gukovskaya, T. A. Blinman, V. Zaninovic, and S. J. Pandol, "Early NF- κ B activation is associated with hormone-induced pancreatitis," *American Journal of Physiology - Gastrointestinal and Liver Physiology*, vol. 275, no. 6, pp. G1402–G1414, 1998.
- [3] C. E. Forsmark, S. Swaroop Vege, and C. M. Wilcox, "Acute pancreatitis," *New England Journal of Medicine*, vol. 375, no. 20, pp. 1972–1981, 2016.
- [4] Y. Liu, X. D. Chen, J. Yu et al., "Deletion of XIAP reduces the severity of acute pancreatitis via regulation of cell death and nuclear factor- κ B activity," *Cell Death & Disease*, vol. 8, no. 3, p. e2685, 2017.
- [5] D. Zhao, H. Ge, B. Ma et al., "The interaction between ANXA2 and lncRNA Fendrr promotes cell apoptosis in caerulein-induced acute pancreatitis," *Journal of Cellular Biochemistry*, vol. 120, no. 5, pp. 8160–8168, 2018.
- [6] Y. Wang, X. Fan, L. Xing, and F. Tian, "Wnt signaling: a promising target for osteoarthritis therapy," *Cell Communication and Signaling*, vol. 17, no. 1, p. 97, 2019.
- [7] D. m Wu, S. h Deng, T. Liu, R. Han, T. Zhang, and Y. Xu, "TGF- β -mediated exosomal lnc-MMP2-2 regulates migration and invasion of lung cancer cells to the vasculature by promoting MMP2 expression," *Cancer Medicine*, vol. 7, no. 10, pp. 5118–5129, 2018.
- [8] Q. Wang, C. Han, K. Wang et al., "Integrated analysis of exosomal lncRNA and mRNA expression profiles reveals the involvement of lnc-MKRN2-42:1 in the pathogenesis of Parkinson's disease," *CNS Neuroscience and Therapeutics*, vol. 26, no. 5, pp. 527–537, 2020.
- [9] X. Wen, B. He, X. Tang, B. Wang, and Z. Chen, "Emodin inhibits the progression of acute pancreatitis via regulation of lncRNA TUG1 and exosomal lncRNA TUG1," *Molecular Medicine Reports*, vol. 24, no. 5, p. 785, 2021.
- [10] X. F. Sheng, L. L. Hong, H. Li, F. Y. Huang, Q. Wen, and H. F. Zhuang, "Long non-coding RNA MALAT1 modulate cell migration, proliferation and apoptosis by sponging microRNA-146a to regulate CXCR4 expression in acute myeloid leukemia," *Hematology*, vol. 26, no. 1, pp. 43–52, 2021.
- [11] W. Tie and F. Ge, "MALAT1 Inhibits Proliferation of HPV16-Positive Cervical Cancer by Sponging miR-485-5p to Promote Expression of," *DNA and cell biology*, vol. 40, no. 11, pp. 1407–1417, 2021.
- [12] D. R. Cooper, C. Wang, R. Patel et al., "Human adipose-derived stem cell conditioned media and exosomes containing MALAT1 promote human dermal fibroblast migration and ischemic wound healing," *Advances in Wound Care*, vol. 7, no. 9, pp. 299–308, 2018.
- [13] J. Liu, Z. Niu, R. Zhang et al., "MALAT1 shuttled by extracellular vesicles promotes M1 polarization of macrophages to induce acute pancreatitis via miR-181a-5p/HMGB1 axis," *Journal of Cellular and Molecular Medicine*, vol. 25, no. 19, pp. 9241–9254, 2021.
- [14] L. Gu, J. Liu, D. Xu, and Y. Lu, "Reciprocal feedback loop of the MALAT1-MicroRNA-194-YAP1 pathway regulates progression of acute pancreatitis," *Medical Science Monitor*, vol. 25, pp. 6894–6904, 2019.
- [15] F. Hu, X. Tao, L. Zhao et al., "LncRNA-PVT1 aggravates severe acute pancreatitis by promoting autophagy via the miR-30a-5p/Beclin-1 axis," *American Journal of Tourism Research*, vol. 12, no. 9, pp. 5551–5562, 2020.
- [16] G. Song, J. Zhou, R. Song et al., "Long noncoding RNA H19 regulates the therapeutic efficacy of mesenchymal stem cells in rats with severe acute pancreatitis by sponging miR-138-5p and miR-141-3p," *Stem Cell Research & Therapy*, vol. 11, no. 1, pp. 420–434, 2020.
- [17] C. Théry, S. Amigorena, G. Raposo, and A. Clayton, "Isolation and characterization of exosomes from cell culture supernatants and biological fluids," *Current protocols in cell biology*, no. 1, p. Unit 3.22, 2006.
- [18] M. Adnan, G. Morton, and S. Hadi, "Analysis of rpoS and bolA gene expression under various stress-induced environments in planktonic and biofilm phase using 2- $\Delta\Delta$ CT method," *Molecular and Cellular Biochemistry*, vol. 357, no. 1–2, pp. 275–282, 2011.
- [19] J. Conde-Vancells, E. Rodriguez-Suarez, N. Embade et al., "Characterization and comprehensive proteome profiling of exosomes secreted by hepatocytes," *Journal of Proteome Research*, vol. 7, no. 12, pp. 5157–5166, 2008.
- [20] H. Valadi, K. Ekström, A. Bossios, M. Sjöstrand, J. J. Lee, and J. O. Lötvall, "Exosome-mediated transfer of mRNAs and microRNAs is a novel mechanism of genetic exchange between cells," *Nature Cell Biology*, vol. 9, no. 6, pp. 654–659, 2007.
- [21] A. Montecalvo, A. T. Larregina, W. J. Shufesky et al., "Mechanism of transfer of functional microRNAs between mouse dendritic cells via exosomes," *Blood*, vol. 119, no. 3, pp. 756–766, 2012.

- [22] L. Zitvogel, A. Regnault, A. Lozier et al., "Eradication of established murine tumors using a novel cell-free vaccine: dendritic cell-derived exosomes," *Nature Medicine*, vol. 4, no. 5, pp. 594–600, 1998.
- [23] S. Bala, J. Petrasek, S. Mundkur et al., "Circulating micro-RNAs in exosomes indicate hepatocyte injury and inflammation in alcoholic, drug-induced, and inflammatory liver diseases," *Hepatology*, vol. 56, no. 5, pp. 1946–1957, 2012.
- [24] B. Zhu, L. Zhang, C. Liang et al., " κ Stem cell-derived exosomes prevent aging-induced cardiac dysfunction through a novel exosome/lncRNA MALAT1/NF- κ B/TNF- signaling pathway," *Oxidative Medicine and Cellular Longevity*, vol. 2019, pp. 1–14, 2019.
- [25] L. Sha, D. Ma, and C. Chen, "Exosome-mediated Hic-5 regulates proliferation and apoptosis of osteosarcoma via Wnt/ β -catenin signal pathway," *Aging*, vol. 12, no. 23, pp. 23598–23608, 2020.
- [26] C. Huang, W. Luo, Q. Wang et al., "Human mesenchymal stem cells promote ischemic repairment and angiogenesis of diabetic foot through exosome miRNA-21-5p," *Stem Cell Research*, vol. 52, Article ID 102235, 2021.
- [27] A. Hernández, J. P. Arab, D. Reyes et al., "Extracellular vesicles in NAFLD/ALD: from pathobiology to therapy," *Cells*, vol. 9, no. 4, p. 817, 2020.
- [28] P. Ji, S. Diederichs, W. Wang et al., "MALAT-1, a novel noncoding RNA, and thymosin β 4 predict metastasis and survival in early-stage non-small cell lung cancer," *Oncogene*, vol. 22, no. 39, pp. 8031–8041, 2003.
- [29] S. Dhamija and S. Diederichs, "From junk to master regulators of invasion: lncRNA functions in migration, EMT and metastasis," *International Journal of Cancer*, vol. 139, no. 2, pp. 269–280, 2016.
- [30] H. Chen, X. Wang, X. Yan, X. Cheng, X. He, and W. Zheng, "RETRACTED: lncRNA MALAT1 regulates sepsis-induced cardiac inflammation and dysfunction via interaction with miR-125b and p38 MAPK/NF κ B," *International Immunopharmacology*, vol. 55, pp. 69–76, 2018.
- [31] P. Puthanveetil, S. Chen, B. Feng, A. Gautam, and S. Chakrabarti, "Long non-coding RNA MALAT1 regulates hyperglycaemia induced inflammatory process in the endothelial cells," *Journal of Cellular and Molecular Medicine*, vol. 19, no. 6, pp. 1418–1425, 2015.
- [32] H. Gao, X. Wang, C. Lin et al., "Exosomal MALAT1 derived from ox-LDL-treated endothelial cells induce neutrophil extracellular traps to aggravate atherosclerosis," *Biological Chemistry*, vol. 401, no. 3, pp. 367–376, 2020.
- [33] L. Xiao, X. Y. Shi, Z. L. Li et al., "Downregulation of LINC01508 contributes to cisplatin resistance in ovarian cancer via the regulation of the Hippo-YAP pathway," *Journal of gynecologic oncology*, vol. 32, no. 5, p. e77, 2021.
- [34] Y. Wu, P. Aegerter, M. Nipper, L. Ramjit, J. Liu, and P. Wang, "Hippo signaling pathway in pancreas development," *Frontiers in Cell and Developmental Biology*, vol. 9, Article ID 663906, 2021.
- [35] D. Ansari, H. Ohlsson, C. Althini et al., "The hippo signaling pathway in pancreatic cancer," *Anticancer Research*, vol. 39, no. 7, pp. 3317–3321, 2019.
- [36] W. Wang, L. Zhu, H. Li et al., "Alveolar macrophage-derived exosomal tRF-22-8BWS7K092 activates Hippo signaling pathway to induce ferroptosis in acute lung injury," *International Immunopharmacology*, vol. 107, Article ID 108690, 2022.
- [37] T. Moroishi, H. W. Park, B. Qin et al., "A YAP/TAZ-induced feedback mechanism regulates Hippo pathway homeostasis," *Genes & Development*, vol. 29, no. 12, pp. 1271–1284, 2015.
- [38] K. Tumaneng, K. Schlegelmilch, R. C. Russell et al., "YAP mediates crosstalk between the Hippo and PI(3)K-TOR pathways by suppressing PTEN via miR-29," *Nature Cell Biology*, vol. 14, no. 12, pp. 1322–1329, 2012.
- [39] D. Wang, J. He, B. Huang, S. Liu, H. Zhu, and T. Xu, "Emerging role of the Hippo pathway in autophagy," *Cell Death & Disease*, vol. 11, no. 10, p. 880, 2020.
- [40] H. Zhao, M. Liu, H. Liu, R. Suo, and C. Lu, "Naringin protects endothelial cells from apoptosis and inflammation by regulating the Hippo-YAP Pathway," *Bioscience Reports*, vol. 40, no. 3, Article ID BSR20193431, 2020.
- [41] J. Qing, X. Liu, Q. Wu et al., "Hippo/YAP pathway plays a critical role in effect of GDNF against $\alpha\beta$ -induced inflammation in microglial cells," *DNA and Cell Biology*, vol. 39, no. 6, pp. 1064–1071, 2020.
- [42] L. Li, J. Zhou, Q. Li, J. Xu, J. Qi, and H. Bian, "The inhibition of Hippo/Yap signaling pathway is required for magnesium isoglycyrrhizinate to ameliorate hepatic stellate cell inflammation and activation," *Biomedicine & Pharmacotherapy*, vol. 106, pp. 83–91, 2018.
- [43] Y. Zhou, T. Shan, W. Ding et al., "Study on mechanism about long noncoding RNA MALAT1 affecting pancreatic cancer by regulating Hippo-YAP signaling," *Journal of Cellular Physiology*, vol. 233, no. 8, pp. 5805–5814, 2018.
- [44] J. Liu, L. Xu, and X. Zhan, "lncRNA MALAT1 regulates diabetic cardiac fibroblasts through the Hippo-YAP signaling pathway," *Biochemistry and Cell Biology*, vol. 98, no. 5, pp. 537–547, 2020.
- [45] Y. Sun, T. Jiang, Y. Jia, J. Zou, X. Wang, and W. Gu, "lncRNA MALAT1/miR-181a-5p affects the proliferation and adhesion of myeloma cells via regulation of Hippo-YAP signaling pathway," *Cell Cycle*, vol. 18, no. 19, pp. 2509–2523, 2019.
- [46] H. Hu, J. Wu, X. Yu, J. Zhou, H. Yu, and L. Ma, "Long non-coding RNA MALAT1 enhances the apoptosis of cardiomyocytes through autophagy inhibition by regulating TSC2-mTOR signaling," *Biological Research*, vol. 52, no. 1, p. 58, 2019.
- [47] H. Liu, Z. Zhang, W. Xiong et al., "Long non-coding RNA MALAT1 mediates hypoxia-induced pro-survival autophagy of endometrial stromal cells in endometriosis," *Journal of Cellular and Molecular Medicine*, vol. 23, no. 1, pp. 439–452, 2019.
- [48] Y. Si, Z. Yang, Q. Ge et al., "Long non-coding RNA Malat1 activated autophagy, hence promoting cell proliferation and inhibiting apoptosis by sponging miR-101 in colorectal cancer," *Cellular and Molecular Biology Letters*, vol. 24, no. 1, p. 50, 2019.
- [49] J. Zhen, W. Chen, Y. Liu, and X. Zang, "Baicalin protects against acute pancreatitis involving JNK signaling pathway via regulating miR-15a," *The American Journal of Chinese Medicine*, vol. 49, no. 01, pp. 147–161, 2021.
- [50] J. e Lee, S. G. Cho, S. G. Ko, S. A. Ahmrad, A. Puga, and K. Kim, "Regulation of a long noncoding RNA MALAT1 by aryl hydrocarbon receptor in pancreatic cancer cells and tissues," *Biochemical and Biophysical Research Communications*, vol. 532, no. 4, pp. 563–569, 2020.
- [51] N. M. George, C. E. Day, B. P. Boerner, R. L. Johnson, and N. E. Sarvetnick, "Hippo signaling regulates pancreas de-

Research Article

Effect of Story Structure Instruction Based on Visual Analysis on Reading Comprehension Intervention for Dyslexic Students

Hanzhu Yang 

University of Leeds, Leeds LS29JT, UK

Correspondence should be addressed to Hanzhu Yang; hanzhuyang@yeah.net

Received 5 May 2022; Revised 3 June 2022; Accepted 7 June 2022; Published 29 August 2022

Academic Editor: Dong Chen

Copyright © 2022 Hanzhu Yang. This is an open access article distributed under the Creative Commons Attribution License, which permits unrestricted use, distribution, and reproduction in any medium, provided the original work is properly cited.

The application of artificial intelligence (AI) technology in the field of dyslexia is becoming increasingly abundant. However, the content of related literature shows that there is still a lack of systematic and comprehensive research in this field at home and abroad. By outlining the development of AI technology, the meaning, causes, and classification of learning disabilities, the most representative studies on the application of AI technology in dyslexia education, including four aspects of diagnosis, intervention, assessment, and services are analyzed. The study finds that AI technology can improve the conditions suffering from dyslexia and dysgraphia, and can serve the education of dyslexic children as a technical tool to overcome dyslexia. By summarizing the effect of story structure teaching based on visual analysis on reading comprehension intervention for students with dyslexia, it can provide useful references and references for related research.

1. Introduction

Dyslexia is a specific type of learning disability caused by a neurological problem that manifests as difficulty with spelling, decoding, and word recognition. In 2012, the International Dyslexia Association reported that 15–20% of school-age children across the United States have dyslexia, and up to 20% of children have partial dyslexia. For some students, dyslexia may even persist into adulthood. Dyslexia has serious implications for student learning, causing a variety of impairments such as spelling disorders, difficulty decoding words, and lack of fluency in reading aloud, and may also lead to problems in organizing learning strategies, language development, and motor development [1–7].

The existing research [8–10] shows that if children with reading problems are diagnosed and intervened with at an early age, up to 70% of students can be freed from the problem through special education or remedial education programs. This shows the importance of appropriate early intervention for dyslexia [11–14]. This study proposes a study of the effects of story structure instruction based on visual analysis on reading comprehension intervention for students with dyslexia in order to provide a basis for

promoting research and practice of dyslexia intervention methods in English language.

2. Definition of Relevant Concepts

2.1. Teaching Story Structure. Story structure is also known as story grammar, story composition, story mapping instruction, story mapping instruction, story schema, etc. This study defines story structure instruction as the presentation of important elements in a story by means of visual diagrams, including the main character, the situation, the main issue, what happens, and the ending of the story [15–18]. Readers improve their reading comprehension by mastering the elements in the story structure, establishing a story framework, and further analyzing the content of the text.

2.2. Dyslexia. According to the World Health Organization's definition, dyslexia (dyscalculia) is a state of reading or writing difficulty in which an individual is not different from other individuals in terms of general intellectual motivation, life circumstances, and educational conditions, and has no significant visual, hearing, or neurological impairments, but his or her reading or writing performance is significantly

below what it should be at the appropriate age [19–23]. Dyslexia is the most predominant type of learning disability, accounting for more than 70% of all children diagnosed with a learning disability. Studies have shown that up to 10–30% of children in English-speaking countries have dyslexia. The number of children learning Chinese, who have dyslexia is around 3–5%.

2.3. Reading Comprehension. This study defines reading comprehension as the process by which a reader extracts information from written materials, and uses reading strategies to turn the text into the complex cognitive process of integrating clues from the chapter with prior knowledge and experience in order to understand the meaning of the text, including surface contextual understanding vs. deep contextual understanding. Surface contextual understanding is the understanding of the clear message of the story, and for students, the answers to the questions can be found directly in the original text [24–26]. Deep contextual understanding is the understanding of the implicit message in the story that students are required to integrate the content of the story or to respond with their own experiences, such as the cause-and-effect relationship of the story, the main idea of the article, and the theme of the story, etc. [25].

3. Study Design

3.1. Study Object. In this study, one male and one female, a total of two dyslexic students in the fifth grade of an elementary school, were selected as experimental study subjects. The reference criteria were as follows: first, normal intelligence; second, the phenomenon of falling behind in reading achievement; and third, parental consent for the students to participate in the experimental instruction.

The researcher learned the following about the subjects by asking the classroom teachers and English teachers of the two subjects.

Subject A, male, 13 years old, had normal intelligence. In the usual teaching of reading comprehension, the student read aloud not by words, but randomly according to his own ideas; reading speed was slow; he could not use the clues in the article to infer the content of the article, and thus could not understand the general idea of the article, and his reading comprehension always showed a low level.

Subject B, female, 13 years old, had normal hearing and vision as well as neurology. The student knew a high amount of words, but had high spelling errors and often added or subtracted letters from words; was able to read word by word or with finger assistance, but had inaccurate comprehension of the text and had great difficulty expressing herself in writing. In daily learning, the student has poor generalization skills and often generalizes; has significant difficulty integrating contextual information.

3.2. Experimental Hypothesis. In this study, story structure instruction was used as the independent variable in the experiment, and the reading comprehension development level of dyslexic students was used as the dependent variable.

The research hypothesis was that story structure instruction could effectively promote the development of reading comprehension of dyslexic students.

3.3. Experimental Studies. The experiment was divided into three parts: a baseline period (A), an instructional intervention period (B), and a maintenance period (A'). The baseline period (A) lasted 2.5 weeks, consisted of two quizzes per week, for a total of five quizzes, and was designed to collect information about students' reading comprehension performance before the story structure instructional intervention. Students were asked to read the text themselves and were given a question-and-answer test without any prompting or feedback during the test period, in order to collect basic information about students' reading comprehension before the intervention. The demonstration phase (B) lasted for 6 weeks, with two experiments per week, for a total of 12 experiments. Table 1 shows the flow chart of the story structure instruction. In this phase, the researcher presented the "story train study sheet" after the students read the text aloud and guided them to add to the study sheet through a question and answer session. At the end of the instruction, students were given a reading comprehension quiz to collect changes in reading comprehension after the instructional intervention.

In the maintenance phase (A'), the test was administered two weeks after the end of the teaching period, for 2.5 weeks, twice a week. A total of 5 tests were administered to understand the effectiveness of the maintenance of the teaching experiment, no instruction was given during this period, and the same methods were used as in the baseline (A) phase.

3.4. Data Processing

3.4.1. Visual Analysis. This study used the A-B-A' experimental design in a single-subject experimental study, and visual analysis was the main method of data processing. The visual analysis mainly consisted of two parts, intrastage and interstage analysis. The following are the indicators used in this study.

(1) Intrastage Analysis

Estimated convergence: the convergence line within the phase, i.e., the slope of the data path. Up (/) is noted as progressive (+); down (\) is noted as regressive (–); and horizontal (–) is noted as smooth (=).

Convergence stability: the highest value of stage x the convergence stability criterion (20%) = acceptable stability range; the number of data points falling within the stability range of the convergence line \div total data points = convergence stability, above (including) 75%, which is stable; below 75%, which is unstable.

Average: the average of all information points within the phase.

Level range: the difference between the highest data point and the lowest data point within the phase.

TABLE 1: Teaching process of story structure.

Teaching program	Teaching procedure	Teaching time (min)
Lead the engine	Show the story title, predict the story content, and stimulate the students' interest in learning	5
Read the text	Focus on letting students understand the content of the story, reduce the reading burden of students with dyslexia, and lead students to read words and explain the meaning of new words. Students read the text aloud under the guidance of the teacher	5
Story structure teaching	Show the story train learning list, explain or review the five structural elements of the story. Use questions and answers to encourage students to find out the corresponding structure of the article, and fill in the answers in the story train learning list	15
Extended activities	Students should retell the story content or deduce the story content according to the content already filled in	5
Reading comprehension test	Show the reading comprehension test, the students read the article by themselves, and then collect the answers, and do not give them any hints or feedback	10

Level change: the difference between the last data point and the first data point within the phase.

Level stability: the highest value of the stage \times level stability standard (20%) = acceptable stability range; the number of data points falling within the stability range of the average level \div total data points = level stability, over (inclusive).

If it is 75%, it is stable; if it is less than 75%, it is unstable.

(2) Interstage Analysis

Convergence trend and effect change: refers to the convergence line path and change between phases.

Tendency to stable change: refers to the tendency to stable change between stages.

Level change: the difference between the last data point of the previous period and the first data point of the latter period.

Overlap percentage: the percentage of data points from the latter stage that falls within the range of data points from the former stage.

3.4.2. C Statistics. The C-statistic can compensate for the lack of visual analysis by examining whether the data changes within and between stages reach a significant level. It is calculated by the formula:

$$C = 1 - \frac{\sum_{t=1}^{N-1} (x_t - x_{t+1})^2}{2 \sum_{i=1}^N (x_i - \bar{x})^2},$$

$$Sc = \sqrt{\frac{N-2}{(N-1)(N+1)}}, \quad (1)$$

$$Z = \frac{C}{Sc},$$

In the formula, x represents the test score, \bar{x} represents the mean, and N represents the number of experiments.

The degree of stability of the data points can be determined from the Z-values obtained from the C-statistics. If the Z value reaches a significant level, then it means that the

data value of this stage has changed a lot; if the Z value does not reach the significant level, then it means that the data of this stage values vary a little.

4. Analysis of the Effect of Story Structure Teaching on the Overall Intervention of Reading Comprehension for Dyslexic Students

To explore the effect of story structure instruction on the overall intervention of reading comprehension for students with dyslexia, this study draws two a line graph of the change in overall reading comprehension scores for the six subjects was used to further ensure the reliability of the analysis by conducting visual analysis and C-statistical tests on the data. Reading comprehension included surface contextual understanding (out of 8) and deep contextual understanding (out of 8), with an overall reading comprehension score of 16 out of 16.

The overall reading comprehension scores of the two subjects in the three phases of baseline (A), instructional intervention (B), and maintenance (A') are shown in Figure 1. The tests were 1–5 baseline period, 6–17 teaching intervention period, and 18–22 maintenance period.

As shown in Figure 1, the reading comprehension scores of both subjects showed an increasing trend, and story structure instruction was positively correlated with reading comprehension scores. In the baseline period, both subjects' reading comprehension scores showed a low level, with little fluctuation in performance and stable reading comprehension performance. Subject A's performance was slightly higher than that of subject B, which might be related to subject A's better reading comprehension foundation. During the teaching intervention period, the reading comprehension scores of both subjects showed an increasing trend, with the highest score of 15 for subject A and the highest score of 16 for subject B, which was related to the seriousness of subject B's learning attitude. At the beginning of the instructional intervention, subject A's reading comprehension score was slightly higher than B's. As the instruction proceeded, subject B's reading comprehension

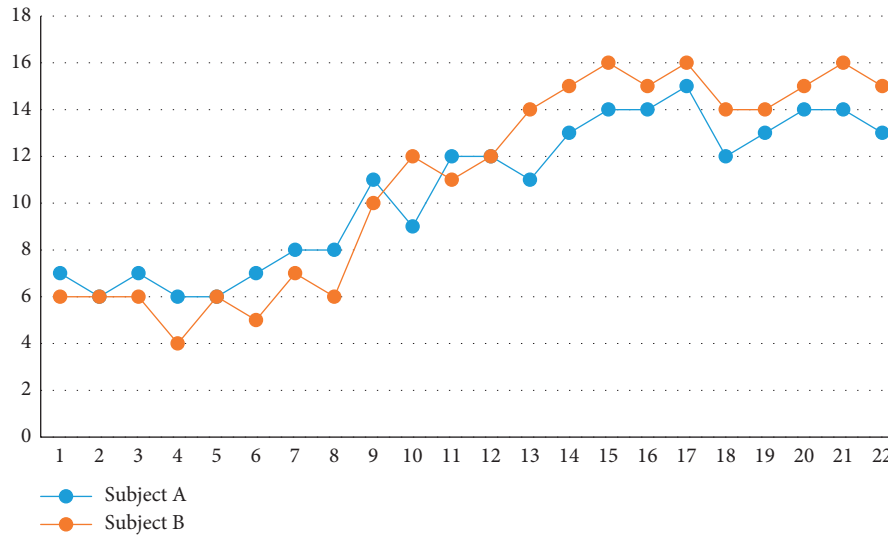


FIGURE 1: Line chart of reading comprehension for two subjects.

score exceeded A's, and the two subjects developed their reading comprehension at slightly different rates. During the maintenance period, both subjects' first reading comprehension scores decreased slightly and then immediately rose to a higher level and showed a stable trend. The decrease in subject B's first reading comprehension score during the maintenance period was smaller than that of A, indicating that story structure instruction was more effective in maintaining subject B's reading comprehension.

Thus, it is clear from the line graph that both subjects' reading comprehension scores improved as the instruction progressed, but there were interindividual differences in the speed and stability of development.

4.1. Analysis of the Effects of Story Structure Instruction on the Various Stages of Reading Comprehension Intervention for students with Reading Disabilities. Based on the scores of the two subjects' overall reading comprehension scores in the three phases of baseline (A), instructional intervention (B), and maintenance (A'), the information analysis table for each phase of overall reading comprehension scores was tallied and plotted, as shown in Table 2.

According to Table 2, subject A took the reading comprehension test five times during the baseline period, with convergent stability of 100% and a steady downward trend in reading comprehension scores. The mean value was 6.40, and the performance remained at a low level. Level range 6-7 (+1), level change 7-6 (-1), and level stability was 100%, with scores remaining stable. There was no significant difference in data variation within the phase ($C = -0.25$, $Z = -0.71$, $p > 0.05$), indicating that in this phase subject A's reading comprehension scores did not change significantly and was ready for instructional intervention. After entering the instructional intervention phase, subject A completed a total of 12 reading comprehension tests, with convergent stability of 83% and a steady upward trend in reading comprehension scores. The mean value was 11.08, which was an increase in performance compared to the baseline period.

Both the range and level change were 7-15 (+8), with level stability of 33% and a substantial increase in reading comprehension scores. The data change within the period reached a significant level of 0.01 ($C = 0.76$, $Z = 2.87$, $p < 0.01$), indicating that the reading comprehension scores of the A students in this period were significantly improved and the teaching effect was significant.

Subject A took a total of five reading comprehension tests during the maintenance period with convergent stability of 100% and a steady upward trend in reading comprehension scores. The mean value was 13.20, and the scores remained at a high level. The level range was 12-14 (+2), the level change was 12-13 (+1), and the level stability was 100%, with small changes in reading comprehension scores. There was no significant difference in data change within the period ($C = 0.46$, $Z = 1.31$, $p > 0.05$), indicating that the reading comprehension scores of subject A were stable and well maintained during this period. Subject B took a total of five reading comprehension tests during the baseline period and showed a decreasing trend in reading comprehension scores. The tendency stability was 60%, showing an unstable state, which may be related to the lower maximum value in this stage. Convergent stability is obtained by multiplying the highest value of the stage by the stability criterion to obtain an acceptable stability range, and the proportion of data points falling within the range is calculated to determine whether the convergence is stable or not. Lower convergent stability was derived due to the narrow range of acceptable stability resulting from the lower maximum value in the baseline period of subject B. However, the data did not show an improving trend and could enter the teaching intervention period. The mean value for this period was 5.60, keeping the scores low. The level range was 4-6 (+2), the level change was 6-6 (0), the level stability was 80%, and the scores remained stable. There was no significant difference in the data change within the phase ($C = -0.25$, $Z = -0.71$, $p > 0.05$), indicating that there was no significant change in the performance of subject B in this phase to intervene in teaching.

TABLE 2: Reading comprehension of the overall performance analysis table of each stage.

Stage order	Subject A			Subject B		
	Baseline A1	Intervention B1	Maintenance A1'	Baseline A2	Intervention B2	Maintenance A2'
Stage length	5	12	5	5	12	5
Estimated trend	—	—	—	—	—	—
	(−)	(+)	(+)	(−)	(+)	(+)
Trend stability	5/5	10/12	5/5	3/5	10/12	5/5
	100%	83%	100%	60%	83%	100%
Average value	Stabilize	Stabilize	Stabilize	Instability	Stabilize	Stabilize
	6.40	11.08	13.20	5.60	11.58	14.80
Level range	6-7	7-15	12-14	4-6	5-16	14-16
	(+1)	(+8)	(+2)	(+2)	(+11)	(+2)
Level change	7-6	7-15	12-13	6-6	5-16	14-15
	(−1)	(+8)	(+1)	(0)	(+11)	(+1)
Level stability	5/5	4/12	5/5	4/5	4/12	5/5
	100%	33%	100%	80%	33%	100%
C	Stabilize	Instability	Stabilize	Stabilize	Instability	Stabilize
Z	−0.71	2.87**	1.31	−0.71	3.39**	1.31

Note. * $p < 0.05$, Z test significance level 0.05; ** $p < 0.01$ and Z test significance level 0.01.

After entering the instructional intervention phase, subject B completed a total of 12 reading comprehension tests with convergent stability of 83% and a steady upward trend in reading comprehension scores. The mean value was 11.58, which was an increase in performance compared to the baseline period. Both the range and level change of the standards were 5–16 (+11), with level stability of 33% and a substantial increase in reading comprehension scores. The data change within the period reached a significant level of 0.01 ($C = 0.90$, $Z = 3.39$, $p < 0.01$), indicating that the reading comprehension scores of subject B improved significantly during this period and the teaching effect was significant. Subject B took a total of 5 reading comprehension tests during the maintenance period, with convergent stability of 100% and a stable upward trend in reading comprehension scores. The mean value was 14.80, and the performance remained at a high level. Level range 14–16 (+2), level change 14–15 (+1), level stability of 100%, and small changes in reading comprehension scores. There was no significant difference in the data change within the stage ($C = 0.46$, $Z = 1.31$, $p > 0.05$), indicating that the reading comprehension scores of subject B were stable and had a good maintenance effect in this stage.

4.2. Analysis of the Effect of Story Structure Teaching on the Interstage Intervention of Reading Comprehension for Dyslexic Students. Based on the scores of the two subjects' overall reading comprehension scores in the baseline (A), instructional intervention (B), and maintenance (A') periods, the interstage information analysis table for overall reading comprehension scores was tallied and plotted, as shown in Table 3.

As can be seen from Table 3, from the baseline period to the instructional intervention period, subject A's reading comprehension scores first decreased and then increased, and the tendency stability all showed stability. The change in level was 6-7 (+1), indicating that the reading

comprehension scores of subject A showed an immediate increase after the instructional intervention. The overlap percentage was 8%, and subject A scored at the baseline period level in only 1 out of 12 tests during the intervention period, indicating that the story structure instruction had a favorable effect on subject A's reading comprehension performance. The data change between phases was significantly different ($C = 0.87$, $Z = 3.80$, $p < 0.01$), indicating a significant improvement in subject A's reading comprehension performance between phases. From the instructional intervention period to the maintenance period, subject A's reading comprehension scores showed a steady upward trend. The change in level was 15-12 (−3), indicating a significant decrease in subject A's reading comprehension scores after withdrawal from instruction. The overlap percentage was 100%, indicating that all five reading comprehension scores of subject A in the maintenance period were within the range of changes in the intervention period and that the story structure instruction had a good maintenance effect. The data change between phases was significantly different ($C = 0.74$, $Z = 3.26$, $p < 0.01$), indicating a significant difference in subject A's reading comprehension scores between phases.

From the baseline period to the instructional intervention period, subject B's reading comprehension scores first decreased and then increased, and tended to change in stability from unstable to stable, with a level change of 6-5 (−1), indicating that after the intervention instruction, subject B's reading comprehension scores did not show an immediate increase. The overlap percentage was 16%, and subject B scored at the baseline period level on only 2 out of 12 tests during the intervention period, indicating that story structure instruction had a favorable effect on subject B's reading comprehension scores. The data change between phases was significantly different ($C = 0.93$, $Z = 4.06$, $p < 0.01$), indicating a significant improvement in subject B's reading comprehension performance between phases. From the instructional intervention period to the maintenance period, subject B's reading comprehension

TABLE 3: Reading comprehension overall achievement interstage analysis table.

Stage comparison	Subject A		Subject B	
	A1/B1	B1/A1'	A2/B2	B2/A2'
Towards the trend and the effect of the change	—	—	—	—
Trend to stability change	—+	++	—+	++
Level change	Stable to stable	Stable to stable	Instable to instable	Stable to stable
	6-7	15-12	6-5	16-14
	(+1)	(-3)	(-1)	(-2)
Percentage of overlap	1/12	5/5	2/12	5/5
	8%	100%	16%	100%
C	0.87	0.74	0.93	0.90
Z	3.80**	3.26**	4.06**	3.94**

Note. * $p < 0.05$, Z test significance level 0.05; ** $p < 0.01$ and Z test significance level 0.01.

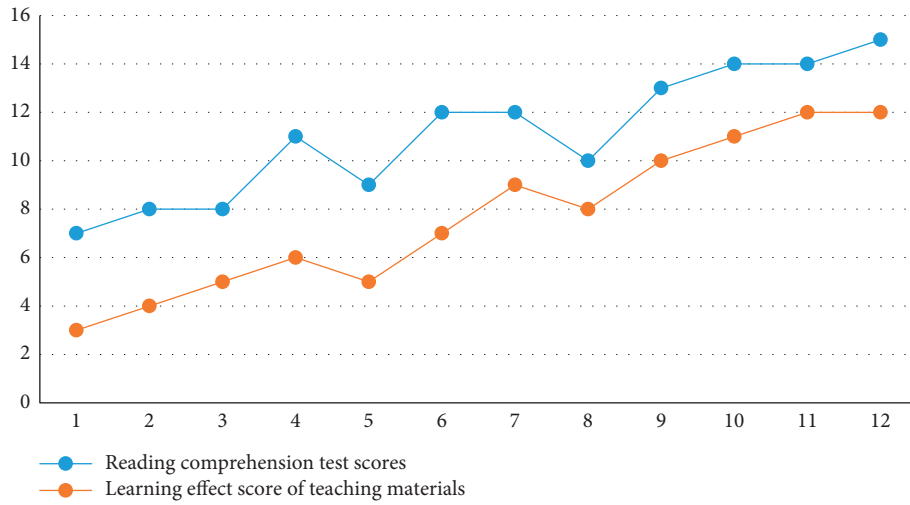


FIGURE 2: Subject A story structure line diagram of the change of learning effect and reading comprehension test results.

scores showed a steady upward trend. The change in level was 16-14 (-2), indicating a decrease in subject B's reading comprehension scores after withdrawal from instruction. The overlap percentage was 100%, indicating that all five reading comprehension scores of subject B in the maintenance period were within the range of changes in the intervention period and that the story structure instruction had a good maintenance effect. The data change between phases was significantly different ($C = 0.90$, $Z = 3.94$, $p < 0.01$), indicating a significant difference in subject B's reading comprehension scores between phases.

4.3. Comparison of Learning Effects of Story Structured Instructional Materials and Reading Comprehension Test Scores. To further illustrate the trends of the learning effects of story-structured instructional materials and reading comprehension test scores, the line graphs of the learning effects of instructional materials scores and reading comprehension test scores were plotted separately for two subjects during the instructional intervention period, as shown in Figures 2 and 3.

According to Figure 2, during the instructional intervention period, subject A's learning effectiveness scores for

instructional materials and reading comprehension test scores both showed an increasing trend, and the changes in both were basically the same. The reading comprehension test scores increased when the learning effectiveness scores of instructional materials increased and decreased when the learning effectiveness scores of instructional materials decreased. For example, in the second, fourth, sixth, ninth, and tenth experiments, subject A's learning effectiveness scores increased, and so did her reading comprehension test scores. In the 5th and 8th experiments, subject A's learning effectiveness scores decreased and his reading comprehension test scores also decreased.

According to Figure 3, during the instructional intervention period, subject B's learning effectiveness scores for instructional materials and reading comprehension test scores both showed an increasing trend, and the changes in both were basically the same. The reading comprehension test scores increased when the learning effectiveness scores of instructional materials increased and decreased when the learning effectiveness scores of instructional materials decreased. For example, in the second, fourth, fifth, seventh, eighth, and tenth experiments, subject B's learning effectiveness scores increased, and so did his reading

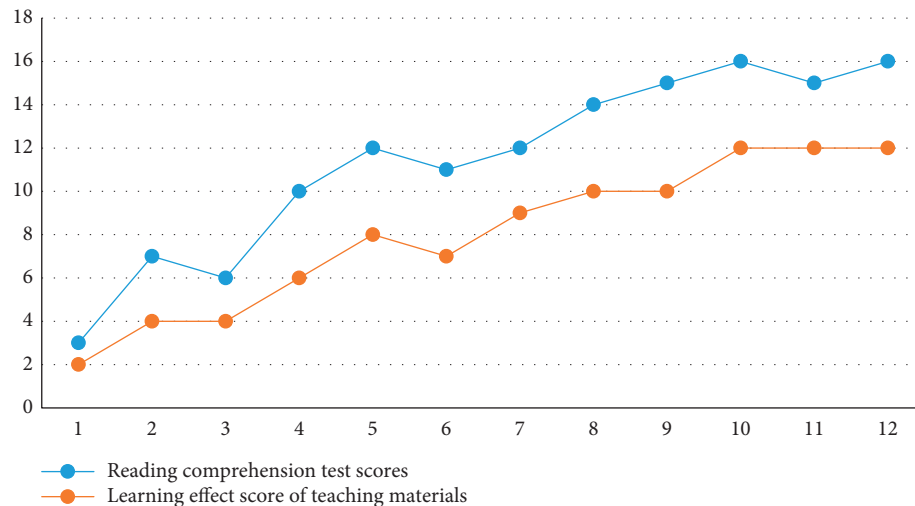


FIGURE 3: Subject B story structure line diagram of the change of learning effect and reading comprehension test results.

comprehension test scores. In the 6th experiment, subject B's learning effectiveness scores decreased and his reading comprehension test scores also decreased.

5. Conclusion

Combining the results of the line graph analysis of the two subjects, the learning effectiveness of the instructional materials of the two subjects during the instructional intervention period. The results scores showed high consistency with the reading comprehension test scores, both showing an increasing trend. Instructional material study learning effect scores increased, reading comprehension test scores increased accordingly, and learning effect scores for instructional materials decreased. Reading comprehension test scores also decreased. Thus, it can be shown that two subjects, who received story structure instruction after a change in the learning effect of story structure instruction, caused a change in reading comprehension test scores. The learning effect of story-structured instructional materials was consistent with reading comprehension test scores.

Data Availability

Data are available on request from the corresponding author.

Conflicts of Interest

The authors declare that they have no conflicts of interest in the publication of this work.

References

- [1] V. D. B. Paul and A. Helder, "Cognitive processes in discourse comprehension: passive processes, reader-initiated processes, and evolving mental representations," *Discourse Processes*, vol. 54, no. 5, 2017.
- [2] L. A. Staal, "The story face: an adaptation of story mapping that incorporates visualization and discovery learning to enhance reading and writing," *The Reading Teacher*, vol. 54, no. 1, 2000.
- [3] L. Li, B. Lei, and C. Mao, "Digital twin in smart manufacturing," *Journal of Industrial Information Integration*, vol. 26, no. 9, Article ID 100289, 2022.
- [4] L. Li, T. Qu, Y. Liu et al., "Sustainability assessment of intelligent manufacturing supported by digital twin," *IEEE Access*, vol. 8, pp. 174988–175008, 2020.
- [5] L. Li and C. Mao, "Big data supported PSS evaluation decision in service-oriented manufacturing," *IEEE Access*, vol. 8, no. 99, pp. 154663–154670, 2020.
- [6] L. Li, C. Mao, H. Sun, Y. Yuan, and B. Lei, "Digital twin driven green performance evaluation methodology of intelligent manufacturing: hybrid model based on fuzzy rough-sets AHP, multistage weight synthesis, and PROMETHEE II," *Complexity*, vol. 2020, no. 6, 24 pages, Article ID 3853925, 2020.
- [7] T. Boulineau, C. Fore, S. Hagan-Burke, and M. D. Burke, "Use of story-mapping to increase the story-grammar text comprehension of elementary students with learning disabilities," *Learning Disability Quarterly*, vol. 27, no. 2, pp. 105–121, 2004.
- [8] E. K. Washburn, R. M. Joshi, and E. Binks-Cantrell, "Are preservice teachers prepared to teach struggling readers?" *Annals of Dyslexia*, vol. 61, no. 1, pp. 21–43, 2011.
- [9] S. E. Shaywitz and B. A. Shaywitz, "The neurobiology of reading and dyslexia," *The ASHA Leader*, vol. 12, pp. 20–21, 2007.
- [10] H. W. Stevenson, J. W. Stigler, G. W. Lucker, Sy Lee, Cc Hsu, and S. Kitamura, "Reading disabilities: the case of Chinese, Japanese, and English," *Child Development*, vol. 53, no. 5, pp. 1164–1181, 1982.
- [11] H. Shu, C. McBride-Chang, S. Wu, and H. Liu, "Understanding Chinese developmental dyslexia: morphological awareness as a core cognitive construct," *Journal of Educational Psychology*, vol. 98, no. 1, pp. 122–133, 2006.
- [12] B. A. O'Brien, M. Wolf, L. T. Miller, M. W. Lovett, and R. Morris, "Orthographic processing efficiency in developmental dyslexia: an investigation of age and treatment factors at the sublexical level," *Annals of Dyslexia*, vol. 61, no. 1, pp. 111–135, 2011.
- [13] T. F. Denton and J. N. Meindl, "The effect of colored overlays on reading fluency in individuals with dyslexia," *Behavior Analysis in Practice*, vol. 9, no. 3, pp. 1–8, 2015.

- [14] X. Meng, O. Lin, F. Wang, Y. Jiang, and Y. Song, "Reading performance is enhanced by visual texture discrimination training in Chinese-speaking children with developmental dyslexia," *PLoS One*, vol. 9, no. 9, Article ID e108274, 2014.
- [15] E. Pedroli, P. Padula, A. Guala, M. T. Meardi, G. Riva, and G. Albani, "A psychometric tool for a virtual reality rehabilitation approach for dyslexia," *Computational and Mathematical Methods in Medicine*, vol. 2017, Article ID 7048676, 6 pages, 2017.
- [16] E. Q. Wang and A. M. Piper, "The invisible labor of access in academic writing practices: a case analysis with dyslexic adults," *Proceedings of the ACM on Human-Computer Interaction*, vol. 6, no. CSCW1, pp. 1–25, 2022.
- [17] W. Rasheed-Karim, "Intelligent tutoring systems, learning and cognitive styles of dyslexic students," *International Journal of Emerging Technologies in Learning*, vol. 16, no. 03, pp. 20–35, 2021.
- [18] P. Kadam, M. Thaker, G. Vyas, and A. Vegesna, "A learning ecosystem for dyslexic. EAI/Springer innovations in communication and computing," in *Proceedings of the International Conference on Mobile Computing and Sustainable Informatics - ICMCSI 2020*, pp. 29–39, Springer, Cham, December 2020.
- [19] J. P. Cardona, F. Alvarez, C. Velazquez, G. Dominguez, and J. Munoz, "Evaluation of remedial intervention with Mastery Learning approach for dyslexic children," in *Proceedings of the 2021 4th International Conference on Inclusive Technology and Education*, pp. 43–46, La Paz, Mexico, October 2021.
- [20] J. P. Cardona, F. Alvarez, C. Velazquez, G. Dominguez, and J. Munoz, "Font manipulation proposal to facilitate reading to dyslexic children," in *Proceedings of the 2021 4th International Conference on Inclusive Technology and Education*, La Paz, Mexico, October 2021.
- [21] F. Latifoglu, R. İleri, and E. Demirci, "Assessment of dyslexic children with EOG signals: determining retrieving words/re-reading and skipping lines using convolutional neural networks," *Chaos, Solitons & Fractals*, vol. 145, Article ID 110721, April 2021.
- [22] S. A. H. Minoofam, A. Bastanfard, M. R. Keyvanpour, and M. R. Keyvanpour, "RALF: an adaptive reinforcement learning framework for teaching dyslexic students," *Multi-media Tools and Applications*, vol. 81, no. 5, pp. 6389–6412, February 2022.
- [23] N. P. Guhan Seshadri, B. Geethanjali, and B. K. Singh, "Resting State EEG Signal Analysis in Indian Dyslexic Children," in *Proceedings of the 2020 1st International Conference on Power, Control and Computing Technologies, ICPC2T 2020*, pp. 300–304, Raipur, India, January 2020.
- [24] N. B. Mohamad, K. Y. Lee, W. Mansor, Z. Mahmoodin, C. W. N. F. Che Wan Fadzal, and S. Amirin, "Dyslexic frequency signatures in relaxation and letter writing," *Lecture Notes in Computer Science (Including Subseries Lecture Notes in Artificial Intelligence and Lecture Notes in Bioinformatics)*, vol. 12033119 pages, 2020.
- [25] N. P. Seshadri and B. K. Singh, "Hemispheric lateralization analysis in dyslexic and normal children using rest-EEG," in *Proceedings of the 2020 IEEE Recent Advances in Intelligent Computational Systems, RAICS*, pp. 37–41, Thiruvananthapuram, India, December 2020.
- [26] M. Sarah-May, E. Chew, and F. Carroll, "The review of dyslexic humanoid robotics for reinforcement learning," in *Proceedings of the Proceedings of the European Conference on E-Learning, ECEL*, P 654-657, England, October 2021.

Research Article

Analgesic Effects, Birth Process, and Prognosis of Pregnant Women in Normal Labor by Epidural Analgesia Using Sufentanil in Combination with Ropivacaine: A Retrospective Cohort Study

Lijing Mao,¹ Xiaoxiao Zhang,² and Jing Zhu ¹

¹Department of Obstetrics, Nantong Maternal and Child Health Hospital, Nantong 226000, China

²Anesthesiology Department, Nantong Maternal and Child Health Hospital, Nantong 226000, China

Correspondence should be addressed to Jing Zhu; 631406010315@mails.cqjtu.edu.cn

Received 30 June 2022; Revised 28 July 2022; Accepted 8 August 2022; Published 29 August 2022

Academic Editor: Dong Chen

Copyright © 2022 Lijing Mao et al. This is an open access article distributed under the Creative Commons Attribution License, which permits unrestricted use, distribution, and reproduction in any medium, provided the original work is properly cited.

Objective. The objective is to evaluate the analgesic, labor, and prognostic effects of patient-controlled epidural analgesia (PCEA) versus sufentanil in conjunction with ropivacaine in normal labor. **Methods.** Sixty pregnant women who had a normal delivery at our hospital between February 2019 and April 2021 were included. Pregnant women were arbitrarily assigned to a control group and a research group. Pregnant women in the control group received lidocaine analgesia and PCEA with sufentanil combined with ropivacaine in the research group. Satisfaction with care, fetal umbilical artery blood flow, VAS score, labor and bleeding, neonatal Apgar score and incidence of adverse events were analyzed. **Results.** First, we made a comparison of satisfactory performance of nursing care. The satisfaction rate of the research group was 100.00%, compared to 83.33% for the control group. Nursing satisfaction was higher in the research group, and the difference was statistically significant ($P < 0.05$). Following analgesia, PI, RI, and S/D values of umbilical artery blood flow were lower in the research group than those in the control group, but the difference was not statistically significant ($P > 0.05$). The VAS scores at 10 min, 20 min, and 30 min were found to be lower in the research group than in the control group after analgesia, and the difference was statistically significant ($P < 0.05$). Bleeding was significantly lower in the research group for all stages of labor, and the difference was statistically significant ($P < 0.05$). Apgar scores at 1 minute, 5 minutes, and 10 minutes postpartum were greater in the research group than in the control group, and the difference was statistically significant ($P < 0.05$). As a final note, the incidence of pruritus, hypotension, respiratory depression, nausea, and vomiting was found to be lower in the research group than in the control group, and the difference was statistically significant ($P < 0.05$). **Conclusion.** PCEA with sufentanil coupled with ropivacaine was used to perform labor analgesia. With significant reduction in maternal pain and assurance of labor, ropivacaine combined with sufentanil epidural labor analgesia did not reduce fetal umbilical artery blood flow without extended labor. It could not affect the labor process or the safety of the fetus, which is safe for the mother and fetus.

1. Introduction

In the process of delivery, pregnant women have severe pain due to uterine contraction and uterine dilatation, and many pregnant women choose cesarean section for fear of labor pain, which has an adverse impact on the physical and mental health of mothers and infants [1]. Pregnant women are often accompanied by bad emotions such as tension and fear in the process of delivery, and labor pain will aggravate

maternal tension and fear, which promote each other and form a vicious circle, and the final result is the lack of physical strength. A large amount of maternal consumption results in prolonged labor. Fetal distress may even occur, affecting maternal and infant safety. With the improvement of people's living standards, people put forward higher requirements for the comfort of medical activities. To this end, we strive to provide patients with "patient-centered" comfortable medical services by strengthening service measures

and optimizing the service environment [2]. With the development of anesthetic technology and the improvement of maternal requirements for labor analgesia, epidural labor analgesia is widely used in parturition, thus effectively relieving severe pain in the process of delivery [1, 2]. Epidural labor analgesia during the latent period did not prolong the duration of labor nor did it increase the rate of cesarean section. According to the 2016 version of the consensus of labor analgesia experts, labor analgesia begins with the need for pain relief, not the size of uterine dilatation [3]. For fear of prolonging the second stage of labor, some hospitals stop using analgesic pumps when the uterine mouth is full, but the latest research indicates that the whole process of labor analgesia does not change the delivery outcome, on the contrary, it can enhance the maternal satisfaction [4]. Labor analgesia can effectively reduce the fear of parturient, get sufficient rest in the whole process of labor, avoid unnecessary physical and oxygen consumption, and help to enhance the oxygenation function of the fetus, thus enabling the parturient to establish self-confidence. It has a positive effect on the physical and mental health of mothers and infants [5].

Normal physiological delivery is assigned into three stages of labor. The nature of labor pain in the first and second stages of labor is different, and the reason lies in the mechanism, source, and innervation of pain [6]. Ropivacaine hydrochloride injection is a long-acting amide local anesthetic with low cardiotoxicity and neurotoxicity. Low concentration ropivacaine has the advantage of separating sensorimotor block and rarely passes through the placenta [7]. When adopted in epidural space, the motor block effect of ropivacaine was weaker compared to other amide local anesthetics [8]. Sufentanil is a μ -opioid receptor agonist with good analgesic effect, which can cooperate with amide local anesthetics in epidural anesthesia to further reduce the dosage of local anesthetics, thus reducing the block of local anesthetics on the movement of lower limbs. The analgesic effect is faster and lasts longer, so as to achieve walking labor analgesia [9, 10]. Ropivacaine is a new type of long-acting amide local anesthetic, which blocks the conduction of excitement by inhibiting Na^+ channel. 0.1% ropivacaine had no blocking effect on the movement of human lower limbs. Ropivacaine is a left-handed stereoisomer. When local anesthetic poisoning occurs, the success rate of cardiopulmonary resuscitation is much higher compared to bupivacaine. In epidural anesthesia, the concentration of local anesthetic in cerebrospinal fluid is relatively low due to the blocking effect of arachnoid. In animal experiments, ropivacaine can cause a transient, reversible ascension to the medullary transmembrane channel [11]. Bupivacaine can enhance the permeability of fat-soluble membranes, and the effect of ropivacaine is relatively mild, so the toxicity of bupivacaine is stronger [12]. Animal model experiments show that the distribution of local anesthesia was different between intrathecal and epidural anesthesia, and the bioavailability of intrathecal ropivacaine decreased after epidural injection [13]. There exhibits no significant difference in sensory block between opium and Bubby. The motor block time and analgesic effect of the two drugs are similar.

Studies have indicated that the analgesic effect of Roopa is weaker compared to Bubby. In continuous epidural anesthesia, the recovery of sensory block was slower in patients using ropivacaine than in patients using bupivacaine [14]. Many studies have indicated that the longer the duration of analgesia, the higher the incidence of motor block with bupivacaine and ropivacaine [15]. Ropivacaine combined with opioids, such as fentanyl or sufentanil, can not only enhance the analgesic effect and prolong the analgesic time but also does not increase the incidence of motor block. Therefore, in the process of delivery, ropivacaine combined with sufentanil or fentanyl for maternal analgesia can promote the effect of maternal analgesia and strengthen maternal satisfaction rate [16]. This study focuses on the effects of PCEA combined with sufentanil and ropivacaine on maternal analgesia, labor process, and delivery outcome, in order to provide a theoretical basis for the clinical application of labor analgesia.

2. Patients and Methods

2.1. Normal Information. Sixty patients with natural delivery in our hospital from February 2019 to April 2021 were enrolled. The patients were randomly divided into control group and research group. The former received sufentanil for analgesia, whereas the latter received sufentanil combined with ropivacaine for PCEA. In the control group, the patients were aged from 20 to 34 years old, with an average of 27.23 ± 1.63 years old; In the research group, the age ranged from 20 to 35 years, with an average of 27.42 ± 1.58 years. There exhibited no statistical significance in the general data. This study was permitted by the Medical Ethics Association of our hospital, and all patients noticed informed consent.

Selection criteria: (1) According to the American College of Anesthesiologists (ASA) grade I~II. (2) All belong to full-term singleton parturient, head position. (3) The age was 20–35 years old and the weight was 60–85 kg. (4) There were no contraindications of intraspinal anesthesia and obstetrics. (5) Parturients voluntarily accept intrathecal labor analgesia.

Exclusion criteria: (1) Patients with abnormal coagulation function and easy bleeding. (2) Systemic infection increased intracranial pressure. (3) There are gestational diabetes, placenta previa, preeclampsia or eclampsia, heart disease, fetal intrauterine growth abnormalities, and other complications. (4) Have a history of mental illness, epilepsy, hysteria, and cannot cooperate normally. (5) Those who were evaluated by the obstetrician could not give birth through the vagina. (6) The parturients and their families refused to accept the pain relief of intraspinal delivery.

2.2. Treatment Methods. When regular uterine contractions appear, the following treatments were implemented: vital signs routine monitoring, upper extremity venous access opening, compound sodium chloride solution infusion, fetal heart rate monitoring, and uterine contraction intensity detection. When the cervix of the control group was enlarged to 3 cm, epidural puncture was performed in the L2-3 space and a 3.5 cm tube was placed on the cephalic side, no

blood or cerebrospinal fluid was withdrawn, and the test dose of 1.0% lidocaine was injected 3 ml, observe for 5 min to exclude intravascular catheter and subarachnoid administration. The research group was given sufentanil combined with ropivacaine for PCEA, and the loading dose of 10 ml (0.125% ropivacaine + 0.4 μ g/ml sufentanil) was injected uniformly through the epidural catheter. If the VAS score (visual analog score) of the parturient was still greater than 3 after the first dose of 15 min, the case was withdrawn from the study. After epidural analgesia took effect, PCEA pump (100 ml) was connected, PCEA regimen: background dose 10 ml/h, self-controlled dose 8 ml, locking time 15 min. Instruct the parturient when $VAS \geq 4$, press the drug by themselves, and stop the drug administration after the uterine mouth is fully opened.

2.3. Observation Indicator

2.3.1. Satisfaction. After consulting the literature and expert discussion, we designed patients' follow-up satisfaction, a total of 10 items, and recorded patients' satisfaction with follow-up management mode, health education, medical and nursing service, appointment registration process [17]. It is assigned into four dimensions: very satisfied, satisfied, general, and dissatisfied. Satisfaction rate = very satisfaction rate + satisfaction rate + general rate.

2.3.2. Fetal Umbilical Artery Blood Flow. The superior SONIXTABLET ultrasound instrument was used for examination. The probe frequency was set to 2.0~5.0 MHz, the sampling volume was 2 mm, and the angle between the pulsed Doppler sampling line and the blood vessel was less than 20°. The image of the umbilical artery was captured near the umbilical foramen on the side of the fetus. After finding the corresponding artery, when three consecutive regular waveforms appear on the ultrasound screen, the S and D values can be measured by freezing the image, and the resistance index RI [$RI = (S - D)/S$], Pulsatility index Pi [$PI = 2(S - D)/(S + D)$] and S/D value can be calculated automatically. All monitoring operations and data recording were performed by the same attending ultrasound doctor with rich clinical experience.

2.3.3. VAS Scoring. VAS for short draws a horizontal line from 0 to 10, with 0 for painless, and 10 for severe pain; The numbers in the middle represent different degrees of pain. Pregnant women write numbers and score according to their subjective pain feelings. 0–3 points indicate mild pain, 4–6 points indicate moderate pain, and 7–10 points indicate severe pain.

2.3.4. Parturient Stage of Labor. The following data were collected: the time of the first stage of labor, the time of the second stage of labor, and the amount of blood loss.

2.3.5. Apgar Scoring. The neonatal Apgar score was observed and recorded. According to the Apgar score, according to the five signs of skin color, heart rate,

respiration, muscle tone, and reflex after birth, normal newborns were normal with 2 points in each item, no respiratory depression, mild asphyxia under 7 points, and severe asphyxia below 4 points.

2.3.6. Incidence of Adverse Reactions. The adverse reactions such as pruritus, fever, hypotension, respiratory depression, nausea, and vomiting were observed and recorded.

2.4. Statistical Analysis. SPSS23.0 statistical software was adopted to process the data. The measurement data were presented as ($\bar{x} \pm s$). The group design *t*-test was adopted for the comparison and the analysis of variance was adopted for the comparison between multiple groups. Dunnett's *t*-test was adopted for comparison with the control group. The counting data were presented in the number of cases and the percentage, χ^2 test was adopted for comparison between groups, and bilateral test was employed for all statistical tests.

3. Results

3.1. Comparison of Nursing Satisfaction. First of all, we compared the nursing satisfaction. The research group was very satisfied in 23 cases, satisfactory in 6 cases and general in 1 case, with a satisfaction rate of 100.00%; In the control group, 8 cases were very satisfied, 8 cases were satisfied, 9 cases were general, and 5 cases were dissatisfied, the satisfaction rate was 83.33%; The nursing satisfaction of the research group was higher compared to the control group, and the difference was statistically significant ($P < 0.05$). All the data results are indicated in Figure 1.

3.2. Comparison of Fetal Umbilical Artery Blood Flow. Secondly, we compared the fetal umbilical artery blood flow. Before analgesia, there exhibited no significant difference ($P > 0.05$); After analgesia, the PI, RI, and S/D values of umbilical artery blood flow in the research group were lower than those in the control group, but the difference was not statistically significant ($P > 0.05$); All the data results are indicated in Table 1.

3.3. VAS Score Comparison. Secondly, we compared the VAS scores. Before analgesia, there exhibited no significant difference ($P > 0.05$); after analgesia, the VAS scores decreased. The VAS scores at 10 min, 20 min, and 30 min were lower compared to the control group, and the difference was statistically significant ($P < 0.05$). All data results are indicated in Table 2.

3.4. Comparison of the Stage of Labor and the Amount of Bleeding. Secondly, we compared the stage of labor and the amount of bleeding. The first stage of labor, the second stage of labor, the third stage of labor, and the amount of bleeding in the research group were lower compared to the control group, and the difference was statistically significant ($P < 0.05$). All the data results are indicated in Table 3.

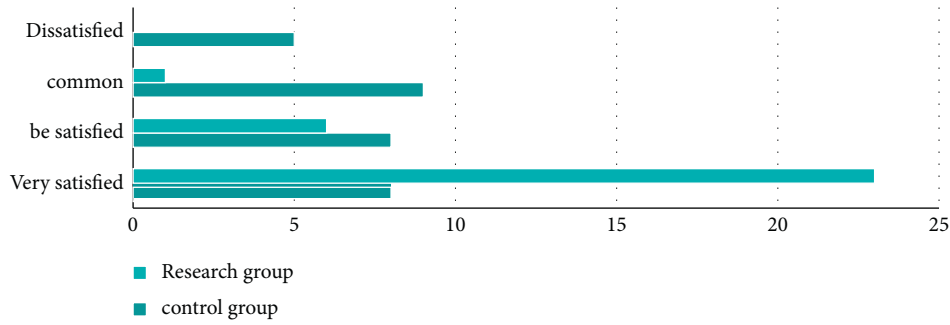


FIGURE 1: Comparison of the incidence of adverse reactions.

TABLE 1: Comparison of fetal umbilical artery blood flow between the two groups [$\bar{x} \pm s$].

Grouping	N	PI		RI		S/D	
		Before analgesia	After analgesia	Before analgesia	After analgesia	Before analgesia	After analgesia
Control group	30	0.80 ± 0.22	0.85 ± 0.16	0.55 ± 0.11	0.59 ± 0.12	2.34 ± 0.11	2.59 ± 0.16
Research group	30	0.81 ± 0.21	0.80 ± 0.21	0.56 ± 0.14	0.55 ± 0.21	2.35 ± 0.12	2.54 ± 0.33
<i>t</i> value		0.303	1.037	0.307	0.905	0.336	0.746
<i>P</i> value		>0.05	>0.05	>0.05	>0.05	>0.05	>0.05

TABLE 2: Comparison of VAS scores between the two groups [$\bar{x} \pm s$, points].

Grouping	N	Before analgesia	After analgesia 10 min	After analgesia 20 min	After analgesia 30 min
Control group	30	8.59 ± 1.21	6.69 ± 0.31	5.69 ± 1.22	3.55 ± 0.52
Research group	30	8.58 ± 1.22	5.31 ± 1.33	4.31 ± 1.21	2.21 ± 0.31
<i>t</i> value		0.031	5.534	4.398	12.123
<i>P</i> value		>0.05	<0.05	<0.05	<0.05

TABLE 3: Comparison of the stage of labor and blood loss between the two groups [$\bar{x} \pm s$].

Grouping	N	The first stage of labor (min)	The second stage of labor (min)	The third stage of labor (min)	Bleeding volume (ml)
Control group	30	445.81 ± 24.22	50.19 ± 3.66	24.91 ± 2.33	280.95 ± 25.44
Research group	30	430.19 ± 12.45	45.91 ± 4.32	20.91 ± 2.34	265.95 ± 20.52
<i>t</i> value		2.698	4.140	6.634	2.513
<i>P</i> value		<0.05	<0.05	<0.05	<0.05

TABLE 4: Comparison of Apgar score between two groups of newborns [$\bar{x} \pm s$, points].

Grouping	N	Birth 1 min Apgar scoring	Birth 5 min Apgar scoring	Birth 10 min Apgar scoring
Control group	30	9.01 ± 0.01	9.45 ± 0.12	9.82 ± 0.01
Research group	30	9.45 ± 0.44	10.00 ± 0.00	10.00 ± 0.00
<i>t</i> value		5.475	25.103	98.590
<i>P</i> value		<0.05	<0.05	<0.05

3.5. *Comparison of Neonatal Apgar Score.* Secondly, we compared the Apgar scores of newborns. The 1 min, 5 min, and 10 min Apgar scores of newborns in the research group were higher compared to the control group, and the difference was statistically significant ($P < 0.05$). All the data results are indicated in Table 4.

3.6. *Comparison of the Incidence of Adverse Reactions.* Finally, we compared the incidence of adverse reactions. The incidences of skin pruritus, hypotension, respiratory depression, nausea, and vomiting in the research group were

lower compared to the control group, and the difference was statistically significant ($P < 0.05$). All the data results are indicated in Figure 2.

4. Discussion

Pain in labor is a common physiological phenomenon, which accompanies the whole process of delivery [16]. According to the traditional view, when the uterine orifice is enlarged to 3 cm, the analgesic effect of labor in the spinal canal is the best. Early application of labor analgesia will reduce the intensity of uterine contraction, prolong the

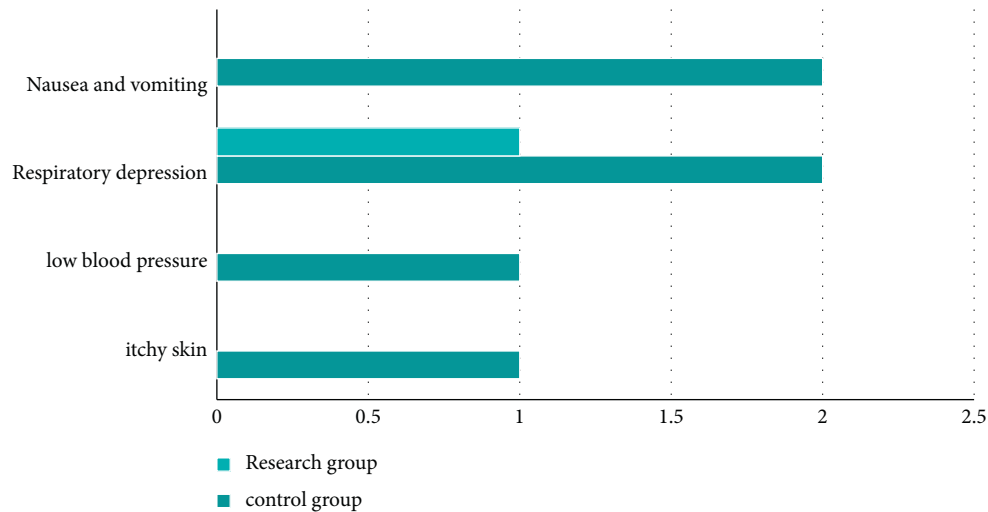


FIGURE 2: Comparison of the incidence of adverse reactions.

interval of uterine contraction, slow down the speed of uterine dilatation, and prolong the process of labor. However, in the process of clinical practice, it is found that many pregnant women have severe labor pain before entering the active stage. During the latent period of labor, fentanyl was injected into the epidural space of parturients, and the study indicated that there exhibited no difference in labor time and delivery outcome between labor analgesia and active labor analgesia [17]. Under the premise of ensuring medical safety, we pursue medical comfort and humanization. Make patients feel psychological and physical pleasure, no pain and no fear in the whole process of seeking medical treatment. As an important means of comfortable diagnosis and treatment in obstetrics, painless delivery is becoming more important. In China, in order to reduce labor pain, the main measure is to implement epidural painless delivery. According to authoritative data released by the World Health Organization (WHO) in 2010, the cesarean section rate in China is 46.2% (ranking first in the world), which is much higher than the upper limit of WHO cesarean section rate: 15% (of which 11.7% without surgical indication) [18]. The high rate of cesarean section has become not only a medical problem faced by the medical profession but also a serious “public health problem” faced by our country. Among the social factors of cesarean section, maternal inability to bear labor pain is the first cause [19]. In addition, some studies have indicated that labor analgesia can reduce the rate of cesarean section, so the promotion of labor analgesia has important social significance to change the current situation of high cesarean section rate in China [20]. This study focuses on the effects of PCEA combined with sufentanil and ropivacaine on maternal analgesia, labor process, and delivery outcome, in order to provide a theoretical basis for the clinical application of labor analgesia.

Traditional high concentration local anesthetic epidural labor analgesia can effectively relieve labor pain, but has a certain blocking effect on uterine contraction and lower limb motor function [21]. The first stage of labor: from regular uterine contractions to full opening of the uterine mouth.

The parturient women in the first stage of labor generally take 7–13 hours, while the parturients generally take 6–8 hours. The first stage of labor consists of the latent period and the active stage. In the first stage of labor, uterine contraction occurs, uterine muscle fibers elongate or even tear, and the decline of fetal head will lead to the dilation of the lower segment of uterus and cervix. The pain in the first stage of labor comes from uterine contraction and dilatation of the lower segment of the uterus and cervix, while the innervation of the uterine body and cervix comes from the visceral sensory nerves. The latent period of labor pain is usually dominated by T11-12, while the active phase is introduced through T10-11. The nature of labor pain in the first stage of labor is unclear and the location is uncertain, which belongs to the category of “visceral pain.” The intensity of labor pain in the first stage of labor is closely related to the intensity of uterine contraction, uterine pressure, and other factors, and the labor pain reaches the peak when the cervix is opened and 7–8 cm. The second stage of labor starts from the opening of the uterine orifice to the end of fetal delivery [22]. The pain in the second stage of labor comes from the expansion, pull and tear of the skin, muscle, fascia, and other tissues of the lower birth canal. The nerve conduction of labor pain in the second stage of labor comes from the lower birth canal, and the pain signal is transmitted along the pudendal nerve S234 and quickly uploaded to the nerve center. The nature of the second stage of labor pain is knife-like sharp pain, the pain site is relatively fixed, generally near the vagina, perineum, and rectum, belonging to the category of “body pain.” Due to the strong uterine contraction in the second stage of labor, some scholars believe that this stage is the coexistence of “visceral pain” and “physical pain.” The labor pain in the third stage of labor comes from cervical dilatation and uterine contraction during placental delivery [23]. Therefore, the ideal epidural labor analgesia requires that the block level be controlled at T10~L1 in the first stage of labor, and at S234 in the second and third stages of labor. In this way, we can achieve the goal of blocking only the sensory nerve without affecting the

motor nerve, so as to achieve the desire to eliminate labor pain without affecting uterine contraction. It should be noted that when the block level of epidural labor analgesia reaches T5, the intensity and frequency of uterine contraction decrease remarkably [24].

The ideal labor analgesia should have the following characteristics: convenient administration, quick effect, safe and reliable effect, can ensure the sobriety of the parturient and has little influence on the parturient, is not easy to pass through the placental barrier to affect the fetus, and only produces pain block, does not block the motor nerve, does not affect the maternal force and uterine contraction during delivery, and can be used to assist cesarean section at any time [25]. Medical experts and scholars have also been looking for methods of labor analgesia that meet these requirements. In 1847, Dr. Simpson used chloroform for labor analgesia. In 1920, a series of methods such as low epidural block and sacral block were used for labor analgesia. Epidural block was first used for labor analgesia by American physicians Graffagnin and Sevler in 1938. Epidural labor analgesia is very popular because of its definite analgesic effect, little influence on mother and infant, little influence on the course of labor, sober cooperation of parturient, and satisfying operation when the emergency needs to be converted to cesarean section during delivery. In 1979, Dr. Revil put forward epidural block as the most effective method of labor analgesia in Europe. Continuous epidural administration, patient-controlled analgesia (PCA) technology, and the use of new drugs make its application have a broader space, so that epidural labor analgesia has become the main means of obstetrical labor analgesia. The application of PCEA in labor analgesia was first reported in 1988 [26]. Epidural labor analgesia can not only effectively reduce maternal pain and meet the requirements of medical comfort but also can be combined with other disciplines. Some scholars use epidural labor analgesia combined with psychotherapy, the effect is obvious. The rate of cesarean section is greatly reduced [27].

Ropivacaine is a new type of amide with long-acting local anesthesia. It has a pure *S* (-) mirror structure, and its chemical structure is similar to that of bupivacaine and mepivacaine, except that the side chain of nitrogen hexane is replaced by propyl [28]. However, there is no consensus on whether PCEA administration mode should be combined with continuous background infusion. Scholars have found that continuous infusion of PCEA combined with background will lead to an increase in anesthetic dosage, but there is no further improvement in analgesic effect and maternal satisfaction, and even affect the process of labor [29]. However, more studies hold the opposite view, believing that PCEA combined with background infusion has a definite analgesic effect without increasing the anesthetic dosage [30, 31]. The differences in research methods, drug types, and drug doses are the possible reasons for the differences in the research results. Other scholars believe that the duration of epidural labor analgesia has a circadian rhythm, and the action time of the same dose of drugs in the daytime is longer than that at night [32]. It also suggests that we should consider the effect of circadian rhythm on

analgesia time, so as to make the research groups more comparable. The effect of circadian rhythm may be one of the possible factors contributing to the inconsistency of the above results. Recently, some scholars have put forward a new point of view on the background infusion mode. Through the latest computer integrated patient-controlled epidural analgesia (CI-PCEA) technology, the background infusion rate can be adjusted actively according to the individual needs of pregnant women [33]. If the puerperal presses PCEA1 to add drugs for the first hour, the background infusion speed is automatically adjusted from 0 to 5 mL/h; If the puerperal presses 2 times for 3 times, the background infusion speed is automatically adjusted to 10 mL/h or 15 mL/h; If the puerperal presses 0 times in the first hour, the background infusion rate will automatically decrease 5 mL/h. The researchers believe that compared with PCA without background infusion, CI-PCEA not only does not increase the dosage of anesthetics but also enhances maternal satisfaction with analgesia [34]. The authors changed the continuous infusion dose of 12 mL/h (0.0625% bupivacaine + 2 μ g/mL fentanyl) into a single epidural injection of 6 mL/30 min, which was named regular intermittent epidural administration (PIEB). Through regular intermittent epidural administration, if there is insufficient analgesia, the parturient can be treated with PCEA compressions, and if it cannot be relieved, a single epidural injection of 0.125% bupivacaine is required by the anesthesiologist to rescue [35]. The study found that compared with continuous background infusion of PCEA, there exhibited no significant difference between PIEB and its analgesic effect, but the number of maternal PCEA pressing was less, the dosage of anesthetics was remarkably reduced, and the satisfaction of maternal analgesia was promoted. In view of the different sources of pain in the first and second stages of labor, that is, labor pain in the latent period of the first stage of labor is usually controlled by T11-12, while in the active stage, it is transmitted through T10-11, and the pain signal of the second stage of labor is transmitted along the pudendal nerve S2hyd4 and quickly uploaded to the nerve center. Some scholars have explored the dual-tube epidural labor analgesia, puncturing the two-point T12-L1 and L4-5 space and inserting the epidural catheter respectively. Analgesics are given at the upper point in the first stage of labor, and drugs are given at the lower point in the second stage of labor. According to the different sources of pain in the process of labor, pain is given a "precise blow" [36]. The results indicate that this method can not only strengthen the satisfaction of parturient but also reduce the rate of lateral episiotomy and improve the long-term quality of life of parturients.

Although the side chain of nitrogen hexane was replaced by propyl, the potency of ropivacaine decreased. At present, PCEA is mostly adopted in intraspinal block labor analgesia with low concentration local anesthetics combined with analgesics. PCEA is more individualized, which can meet the analgesic needs of different parturients and reduce the dose [36, 37]. The ratio of anesthetic potency between ropivacaine and bupivacaine is about 5:8, but it also has some characteristics, such as inherent vasoconstrictor effect, lower

protein binding rate, higher clearance rate, and shorter elimination half-life. All these characteristics enable ropivacaine to avoid drug accumulation during multiple injections, thereby reducing the risk of systemic poisoning and greatly reducing cardiotoxicity and neurotoxicity [37]. In addition, the significant advantage of ropivacaine at low concentration is the separation of sensory and motor block, which makes it analgesic without affecting uterine contraction and movement, and is more suitable for obstetric anesthesia. Some scholars have confirmed that low concentration ropivacaine for epidural labor analgesia has no advantage compared with bupivacaine in analgesic effect and effect on mother and infant. Some scholars observed 40 parturients who underwent epidural labor analgesia. The two groups received continuous epidural infusion of 0.0625% ropivacaine + 2 $\mu\text{g/mL}$ fentanyl and 0.0625% bupivacaine + 2 $\mu\text{g/mL}$ fentanyl, respectively. The results indicated that there exhibited no significant difference in VAS score, sensorimotor block level, duration of labor, mode of delivery, and neonatal safety [38]. Neena et al. studied parturients with spontaneous delivery and normal fetal heart rate [39]. Patients received continuous epidural infusion of 0.0625% bupivacaine + 2 $\mu\text{g/mL}$ fentanyl and 0.1% ropivacaine + 2 $\mu\text{g/mL}$ fentanyl, respectively. 5 ml mixture was added per 5 min. If patients were ineffective within the same initial dose of 15 min, additional drugs were stopped after 90 minutes. The anesthetic effect was evaluated by analgesic effect, motor block, visual analogue scale, maternal hemodynamic parameters, and maternal satisfaction. The results indicated that there exhibited no significant difference. Even so, ropivacaine has become the first choice for epidural labor analgesia because of its sensorimotor separation and low cardiotoxicity.

Sufentanil is a central analgesic, which mainly activates μ receptor and has a powerful analgesic effect. Existing studies have found that sufentanil is more lipophilic than fentanyl, and its lipophilicity is about 2 times that of fentanyl and 1000 times that of morphine. Sufentanil can easily pass through nerve cell membrane and blood-brain barrier. Sufentanil has stronger analgesic effect and longer action time, so sufentanil has unique advantages in epidural labor analgesia. During intrathecal administration of sufentanil, it mainly acts on the opioid receptors on the surface of the spinal cord, and its analgesic effect is about 4/5 times higher compared to fentanyl [40]. The high placental transfer rate of sufentanil has raised concerns about the safety of sufentanil, but it has been reported that sufentanil is absorbed into the epidural space very little, so it has little effect on the fetus. Bullingham et al. conducted a randomized, double-blind, placebo-controlled trial involving 400 parturients [41]. All women received epidural anesthesia during the first stage of labor, using 0.08% ropivacaine + 0.4 $\mu\text{g/mL}$ sufentanil, and commonly used patient PCEA control mode. In the second stage of labor, parturients were arbitrarily assigned into two groups and received blind infusion of the same solution or placebo saline, respectively. The main observation index was the duration of the second stage of labor. The results indicated that there exhibited no difference in analgesia score, duration of labor, maternal and neonatal outcome between

the placebo group and the epidural group. The results indicated that sufentanil combined with low concentration ropivacaine could not prolong the second stage of labor and could be adopted for epidural labor analgesia. The original research papers published from 1995 to 2014 were searched in order to study which kind of local anesthesia combined with sufentanil was more suitable for epidural labor analgesia. The results of systematic review and meta-analysis indicated that sufentanil combined with bupivacaine, levobupivacaine, and ropivacaine could achieve satisfactory epidural labor analgesia, but the incidence of motor block of bupivacaine-sufentanil was higher. Although the analgesia duration of ropivacaine-sufentanil and levobupivacaine-sufentanil is longer, the rate of instrumental delivery is higher. This study still has some shortcomings. First, the quality of this study is limited due to the small sample size we included in the study. Secondly, this research is a single-center study and our findings are subject to some degree of bias. Therefore, our results may differ from those of large-scale multicenter studies from other academic institutes. This research is still clinically significant and further in-depth investigations will be carried out in the future.

In summary, Sufentanil PCEA combined with ropivacaine for labor analgesia can significantly reduce maternal pain and ensure delivery comfort. Epidural labor analgesia with ropivacaine combined with sufentanil does not reduce fetal umbilical artery blood flow, does not prolong the stage of labor, does not affect the process of delivery and fetal safety, and is safe for parturients and fetuses.

Data Availability

The data sets used and analyzed during the current study are available from the corresponding author upon reasonable request.

Conflicts of Interest

The authors declare that they have no conflicts of interest.

References

- [1] N. Gonzalez Meera, "Trehan gaurav, kamel ihab. Pain management during labor: Part 1—pathophysiology of labor pain and maternal evaluation for labor analgesia," *Topics in Pain Management*, vol. 37, no. 1, pp. 946–948, 2021.
- [2] X. Chen, M. Cai, X. Lei, and J Yu, "Obesity decreases the EC50 of epidural ropivacaine when combined with dexmedetomidine for labor analgesia," *Expert Review of Clinical Pharmacology*, vol. 14, no. 8, pp. 944–946, 2021.
- [3] D. Arnolds and B. Scavone, "Neuraxial labor analgesia failure rates in women with a body mass index $\geq 50 \text{ kg/m}^2$: a single-center retrospective study," *International Journal of Obstetric Anesthesia*, vol. 31, no. 45, pp. 941–945, 2021.
- [4] E. Wall Wieler and T. Bateman Brian, "Hanlon Dearman Ana, et al. Association of Epidural Labor Analgesia With Offspring Risk of Autism Spectrum Disorders," *JAMA Pediatrics*, vol. 31, no. 88, pp. 49–52, 2021.
- [5] P. Carlo, P. Jasmine, L. Dana, L. Saager, and T. T. Klumpner, "Difficulty in advancing flexible epidural catheters when establishing labor analgesia: an observational open-label

- randomized trial," *Anesthesia & Analgesia*, vol. 31, no. 66, pp. 931–935, 2021.
- [6] C. Mahesh, K. Lena, H. Samah, and S. S. Ahmed, "Knowledge and awareness of labor analgesia services available in our tertiary hospital among the pregnant women: a prospective study," *Bali Journal of Anesthesiology*, vol. 5, no. 2, pp. 931–934, 2021.
 - [7] A. Hassan, "Dexmedetomidine versus fentanyl as adjunct to ropivacaine-dexamethasone for labor analgesia: a randomized control study," *Research and Opinion in Anesthesia and Intensive Care*, vol. 8, no. 2, pp. 94–96, 2021.
 - [8] G. Li, H. Wang, X. Qi, X. Huang, and Y. Li, "Intrathecal dexmedetomidine improves epidural labor analgesia effects: a randomized controlled trial," *Journal of International Medical Research*, vol. 49, no. 4, pp. 535–536, 2021.
 - [9] H. Wang, B. Z. Yang, Q. Guo, and Z. Jing, "Effect of transcutaneous electrical acupoint stimulation combined with epidural labor analgesia on postpartum depression," *Zhen Ci Yan Jiu = Acupuncture Research*, vol. 46, no. 3, pp. 231–234, 2021.
 - [10] C. Delgado, L. Bollag, and W. Van Cleve, "Neuraxial labor analgesia utilization, incidence of postdural puncture headache, and epidural blood patch placement for privately insured parturients in the United States (2008–2015)," *Obstetric Anesthesia Digest*, vol. 41, no. 1, pp. 49–52, 2021.
 - [11] D. Chun-Mei, T. Ding, L. Shu, B. Lei, M. Xu, and L. Wang, "Neuraxial labor analgesia is associated with a reduced risk of postpartum depression: a multicenter prospective cohort study with propensity score matching," *Journal of Affective Disorders*, vol. 281, no. 64, pp. 40–43, 2021.
 - [12] R. Huang, Z. Jiang, Z. Zhao, and B. Wang, "The effect of programmed intermittent epidural bolus compared with continuous epidural infusion in labor analgesia with ropivacaine: a meta-analysis of randomized controlled trials," *Annals of Palliative Medicine*, vol. 10, no. 3, pp. 96–97, 2021.
 - [13] S. Hoffman, S. Abbey, W. Jane, and R. Kreiger, "Association of self-administered nitrous oxide for labor analgesia with maternal and neonatal process and outcome measures," *Journal of Obstetric, Gynecologic, and Neonatal Nursing*, vol. 52, no. 46, pp. 55–56, 2021.
 - [14] Y. Wu, F. Jung, A. Douglas, G. Konig, and R. C. Romeo, "Case report of remifentanyl labor analgesia for a pregnant patient with congenital methemoglobinemia type 1," *A&A Practice*, vol. 15, no. 1, pp. 95–96, 2021.
 - [15] Q. Liang, X. Wang, Y. Deng, L. Lu, T. Weng, and B. Fu, "Effect of an evidence-based activity management program on delivery outcomes in pregnant women after intraspinal labor analgesia," *American Journal of Tourism Research*, vol. 13, no. 4, pp. 3054–3063, 2021.
 - [16] Y. Katakura, Y. Nagamine, T. Goto, and H. Sumikura, "Association of chorioamnionitis with failed conversion of epidural labor analgesia to cesarean delivery anesthesia: a retrospective cohort study," *PloS one*, vol. 16, no. 5, pp. e0250596–52, 2021.
 - [17] B. Xiang, J. Yang, X. Lei, and J. Yu, "Adjuvant sufentanil decreased the EC50 of epidural ropivacaine for labor analgesia in healthy term pregnancy," *Drug Design, Development and Therapy*, vol. 15, no. 45, pp. 2143–2149, 2021.
 - [18] A. Cocoluto, G. Capogna, M. Camorcia, M. Hochman, and M. Velardo, "Analysis of epidural waveform to determine correct epidural catheter placement after CSE labor analgesia," *Local and Regional Anesthesia*, vol. 14, no. 64, pp. 103–108, 2021.
 - [19] J. Wang, L. Zhang, L. Zheng et al., "A randomized trial of the dural puncture epidural technique combined with programmed intermittent epidural boluses for labor analgesia," *Annals of Palliative Medicine*, vol. 10, no. 1, pp. 404–414, 2021.
 - [20] M. Mengie Workie, W. Birlik Chekol, and D. Yilkal Fentie, "Assessment of awareness, attitude and desire for labor analgesia and associated factors among pregnant women in Ethiopia: a cross-sectional study," *Pain and Therapy*, vol. 10, no. 45, pp. 591–595, 2020.
 - [21] R. Inoue, Y. Mazda, H. Tanaka et al., "Management of pregnancy and delivery in women with Kawasaki disease and residual coronary artery lesion with detailed analysis of labor analgesia: combined experience of 13 cases in two institutions," *JA Clinical Reports*, vol. 6, no. 1, pp. 67–958, 2020.
 - [22] L. Gabriel, J. Young, I. Hoesli, and T. Girard, "Generalizability of randomized trials of the programmed intermittent epidural bolus technique for maintenance of labor analgesia: a prospective single-centre cohort study," *Obstetric Anesthesia Digest*, vol. 40, no. 3, pp. 4956–4958, 2020.
 - [23] O. A. Ojo, J. E. Mehdiratta, B. H. Gamez, J. Hunting, and A. S. Habib, "Comparison of programmed intermittent epidural boluses with continuous epidural infusion for the maintenance of labor analgesia: a randomized, controlled, double-blind study," *Obstetric Anesthesia Digest*, vol. 40, no. 3, pp. 307–308, 2020.
 - [24] Z.-H. Liu, S. H. He, C. M. Deng, T. Ding, and M. J. Xu, "Neuraxial labor analgesia is associated with a reduced risk of maternal depression at 2 Years after childbirth: a multicenter, prospective, longitudinal study," *Obstetric Anesthesia Digest*, vol. 40, no. 3, pp. 596–597, 2020.
 - [25] G. Li, Y. Xiao, X. Qi et al., "Combination of sufentanil, dexmedetomidine and ropivacaine to improve epidural labor analgesia effect: a randomized controlled trial," *Experimental and Therapeutic Medicine*, vol. 20, no. 1, pp. 454–460, 2020.
 - [26] J. Murphy, J. Vaughn, K. Gelber, and A. Geller, "Readability, content, quality, and accuracy assessment of internet-based patient education materials relating to labor analgesia," *Obstetric Anesthesia Digest*, vol. 40, no. 2, pp. 391–394, 2020.
 - [27] Y. Song, W. Du, S. Zhou, Y. Zhou, Y. Yu, and Z. Xu, "Effect of dural puncture epidural technique combined with programmed intermittent epidural bolus on labor analgesia onset and maintenance: a randomized controlled trial," *Anesthesia and analgesia*, vol. 46, no. 75, pp. 13–14, 2020.
 - [28] E. Morell, F. M. Peralta, N. Higgins, and A. Suchar, "Effect of companion presence on maternal satisfaction during neuraxial catheter placement for labor analgesia: a randomized clinical trial," *Obstetric Anesthesia Digest*, vol. 40, no. 1, pp. 301–303, 2020.
 - [29] S.-Q. Zhou, J. Wang, Du Wei-Jia, Y. Song, and Z. Xu, "Optimum interval time of programmed intermittent epidural bolus of ropivacaine 0.08% with sufentanil 0.3 µg/mL for labor analgesia: a biased-coin up-and-down sequential allocation trial," *Chinese Medical Journal*, vol. 133, no. 5, pp. 484–486, 2020.
 - [30] O. A. Ojo, J. E. Mehdiratta, B. H. Gamez, J. Hunting, and A. S. Habib, "Comparison of programmed intermittent epidural boluses with continuous epidural infusion for the maintenance of labor analgesia: a randomized, controlled, double-blind study," *Anesthesia & Analgesia*, vol. 130, no. 2, pp. 426–435, 2020.
 - [31] J. Sun, Y. Xiao, L. Zou et al., "Epidural labor analgesia is associated with a decreased risk of the edinburgh postnatal depression scale in trial of labor after cesarean: a multicenter,

- prospective cohort study,” *BioMed Research International*, vol. 2020, no. 63, pp. 1–16, 2020.
- [32] S. Cai, J. Zheng, Q. Meng, J. Chai, R. Ma, and Y. Wang, “Investigation of the minimum local analgesic concentration of epidural sufentanil combined with ropivacaine for labor analgesia,” *Clinical Therapeutics*, vol. 42, no. 1, pp. 134–135, 2020.
 - [33] Y. Wang and M. Xu, “Comparison of ropivacaine combined with sufentanil for epidural anesthesia and spinal-epidural anesthesia in labor analgesia,” *BMC Anesthesiology*, vol. 20, no. 1, pp. 591–597, 2020.
 - [34] Y. Fan, W. Hou, S. Feng et al., “Programmed intermittent epidural bolus decreases the incidence of intra-partum fever for labor analgesia in primiparous women: a randomized controlled study,” *Archives of Gynecology and Obstetrics*, vol. 300, no. 6, pp. 1551–1557, 2019.
 - [35] C. W. Fidkowski, S. Shah, and M. R. Alsaden, “Programmed intermittent epidural bolus as compared to continuous epidural infusion for the maintenance of labor analgesia: a prospective randomized single-blinded controlled trial,” *Korean Journal of Anesthesiology*, vol. 72, no. 5, pp. 472–478, 2019.
 - [36] T. Zhang, Y. Yu, W. Zhang, and J. Zhu, “Comparison of dexmedetomidine and sufentanil as adjuvants to local anesthetic for epidural labor analgesia: a randomized controlled trial,” *Drug Design, Development and Therapy*, vol. 13, no. 412, pp. 1171–1175, 2019.
 - [37] G. Ahmet, “Epidural analgesia for labor pain: what has changed in the last 1 year? Literature review and clinical results our experience in labor analgesia,” *Journal of Clinical and Analytical Medicine*, vol. 31, no. 64, pp. 94–95, 2019.
 - [38] J. Xiao, W. Yi, and L. Wu, “Effects of electroacupuncture on reducing labor pain and complications in the labor analgesia process of combined spinal-epidural analgesia with PCEA,” *Archives of gynecology and obstetrics*, vol. 299, no. 1, pp. 491–495, 2019.
 - [39] N. Jain, P. Mathur, P. Soni, and P. Veena, “A comparative clinical study of intrathecal bupivacaine 2.5 mg with dexmedetomidine 5 μ g versus intrathecal bupivacaine 2.5 mg with fentanyl 25 μ g on the duration of labor analgesia using combined spinal epidural technique,” *Journal of Obstetric Anaesthesia and Critical Care*, vol. 9, no. 1, pp. 591–596, 2019.
 - [40] S. R. Miriam Ipe Shalini and S. Abraham, “A randomized controlled double blind study comparing the efficacy of epidural ropivacaine and bupivacaine with fentanyl for labor analgesia,” *Indian Journal of Clinical Anaesthesia*, vol. 5, no. 4, pp. 566–568, 2018.
 - [41] A. Bullingham, S. Liang, E. Edmonds, S. Mathur, and S. Sharma, “Continuous epidural infusion versus programmed intermittent epidural bolus for labor analgesia: a prospective, controlled, before-and-after cohort study of labor outcomes,” *Obstetric Anesthesia Digest*, vol. 38, no. 4, pp. 481–483, 2018.

Research Article

Biological Mechanism on SIRT1/NLRP3/IL-18 Signaling Pathway of Acupuncture for Treatment of Ischemic Stroke with Center Poststroke Pain

Dan Zhou,^{1,2} Lanfang Zhang³,, Liwei Mao,² Jingyu Cao,² and Jiaqiang Gao²

¹Clinical Medical College of Acupuncture and Rehabilitation, Guangzhou University of Chinese Medicine, Guangzhou, China

²Department of Rehabilitation, Guangzhou Tianhe District Chinese Medicine Hospital, Guangzhou, Guangdong 510665, China

³Physiotherapy Department, Guangdong Hospital of Traditional Chinese Medicine, Guangzhou 510120, Guangdong, China

Correspondence should be addressed to Lanfang Zhang; zlf408557063@163.com

Received 1 June 2022; Revised 28 June 2022; Accepted 12 July 2022; Published 26 August 2022

Academic Editor: Dong Chen

Copyright © 2022 Dan Zhou et al. This is an open access article distributed under the Creative Commons Attribution License, which permits unrestricted use, distribution, and reproduction in any medium, provided the original work is properly cited.

Objective. To evaluate the effect of acupuncture on an animal model of ischemic stroke with central poststroke pain (CPSP) through Sirtuin 1 (SIRT1)/NOD-like receptor thermal protein domain associated protein 3 (NLRP3)/interleukin-18 (IL-18) signaling pathway. **Methods.** Data mining was performed with R package “edgeR,” “limma,” “pathview,” etc., from NCBI Gene Expression Omnibus (GEO) database. Sprague Dawley (SD) rats were divided into 4 groups: sham operation group (Sham group, $n = 5$), poststroke central pain group (CPSP group, $n = 5$), poststroke central pain + acupuncture group (AP group, $n = 5$), central pain after stroke + acupuncture + SIRT1 inhibitor EX527 group (EX527 group, $n = 5$). Pain behavior testing was performed to determine the mechanical withdrawal threshold (MWT). Quantitative real-time PCR (qRT-PCR) was performed to verify the data mining results from the GEO database. **Results.** The KEGG key pathway map was created using the R package “pathview” package, demonstrating that the expression levels of NLRP3’s downstream inflammatory factors IL-18 were downregulated in both of siSIRT1 group compared to the control group and the NLRP3 reconstituted group compared to NLRP3 KO group. QRT-PCR results on animal models of CPSP ischemic stroke showed that the expression levels of SIRT1 were downregulated, the activation of the NLRP3 inflammasome was upregulated, and the expression levels of IL-18 were upregulated in the brain tissues of the surrounding area of the injury. As the pain threshold of CPSP rats was increased, the expression level of SIRT1 was upregulated, and the activation of NLRP3 inflammasome was downregulated. The expression level of IL-18 was downregulated after acupuncture treatment. **Conclusion.** Acupuncture may inhibit CPSP in an animal model of ischemic stroke by upregulating SIRT1 expression levels, inhibition of the activation of the inflammasome, and downregulating IL-18 expression levels.

1. Introduction

Stroke is an acute cerebrovascular disease characterized by high morbidity, complications, and high mortality. Central poststroke pain (CPSP), defined as pain associated with central nervous system damage, in general, is now preferred to describe the neuropathic pain after stroke [1]. CPSP is a neuropathic pain syndrome that can occur after a cerebrovascular accident. Most are caused by the sudden rupture of blood vessels in the brain or the blockage of local blood vessels in the body due to various factors and the inability of

blood to flow into the brain. This makes the patient’s language, hearing, and limb functions have certain obstacles, and the possibility of hemiplegia is high, which seriously affects the patient’s daily living ability and usually occurs 6 months after ischemic stroke [2]. This neuropathic pain syndrome is characterized by pain and sensory abnormalities in the body parts that correspond to the brain territory that has been injured by the cerebrovascular lesion [3]. CPSP is one of the most common neurological complications after stroke, which accounts for 1% to 14% of stroke patients [4], and seriously affects the prognosis and quality of life of

partitions. The most common presentations of CPSP are severe shoulder and hand pain. Shoulder and hand pain are common conditions among people who had a stroke, with its reported prevalence ranging from 12% to 49% [5, 6].

The pathogenesis of CPSP is not fully understood, and the treatment of CPSP is still based on drug therapy. Still, drug therapy can only partially relieve pain symptoms, and long-term use often leads to various adverse reactions. Acupuncture is a characteristic treatment of traditional Chinese medicine, which has the effect of channeling meridians and regulating qi and blood [7]. Acupuncture mainly stimulates the main acupuncture points on the affected limb, which plays a role in dredging the meridians, improving the joints, and reconciling qi and blood. At the same time, acupuncture and moxibustion are used together, focusing on regulating the yin and yang qi and blood of the liver, spleen, and kidney, dredging the meridians of the limbs, and achieving the purpose of both symptoms and root causes, which has been widely used in the rehabilitation treatment of common diseases in clinical departments [8].

Current clinical studies have confirmed that compared with drugs, acupuncture has a better therapeutic effect on CPSP and has a long-lasting effect and a low incidence of long-term adverse reactions [9]. However, the molecular mechanism of acupuncture for treating CPSP has not yet been elucidated, which has affected the further promotion of acupuncture. These patients suffer from allodynia and hyperalgesia after stroke, which is among the most troublesome sequelae of stroke [10]. Therefore, exploring the mechanism of action of acupuncture can lay a solid theoretical foundation for the prevention and treatment of CPSP by acupuncture, which is conducive to promoting the clinical application of acupuncture and has important clinical significance.

2. Method

2.1. Data Downloads from GEO. The RNA-seq data and annotation file were retrieved from NCBI Gene Expression Omnibus (GEO) (<http://www.ncbi.nlm.nih.gov/geo/>) with the *R* package “GEOquery.” RNA-Seq analysis of SIRT1 knockdown (KO) in the database of GSE171118 was performed based on the platforms of GPL23227 BGISEQ-500 (*Homo sapiens*) [11]. RNA-seq analysis of NOD-like receptor thermal protein domain associated protein 3 (NLRP3) KO and NLRP3 reconstituted in the database of GSE180707 was performed based on the platforms of GPL16791 Illumina HiSeq 2500 (*Homo sapiens*) [10].

2.2. Differentially Expressed Genes. The DEGs between the sirtuin 1 (SIRT1) group and control group of GSE180707 and between the NLRP3 KO group and NLRP3 reconstituted group of GSE171118 were screened and filtered out based on the *R* package “edgeR” [11] and “limma” [12, 13], requiring a fold-change (FC) > 1.0 or logFC < -1.0, and requiring the adjusted *P* values or false discovery ratio (FDR) < 0.05. The DEGs that differed - logFC > 1 or < -1 and

adjusted *P* values or FDR < 0.05 - between the siSIRT1 group and control group were also identified using a volcano plot with top DEGs marked by gene symbols.

2.3. Pathview Analysis of Key KEGG Pathway. A selected critical pathway of interest, the NLRP3 inflammasome signaling pathway (<https://www.kegg.jp/pathway/hsa04621+N00742>) for the DEGs between the siSIRT1 group and control group of GSE180707, and between NLRP3 KO group, and NLRP3 reconstituted group of GSE171118, was also performed for visualization by *R* package “pathview” on Kyoto Encyclopedia of Genes and Genomes graphs. The statistical cutoff was set to a *q* value ≤ 0.05 [14, 15].

2.4. Experimental Animals. Sixty male healthy SPF-grade SD rats, weighing 180 to 220 g, were purchased from Junke Biology, Nanjing China, license number: SYXK (Su) 2019-0064. The rats were kept in a suitable environment for 7 days, maintaining indoor humidity at 50–60%, the temperature at 20–25 °C, alternating day and night for 12 h/12h. They were allowed to eat and drink freely.

2.5. Experiment Grouping. According to the random number table, SD rats ($n = 20$) were divided into 4 groups: sham operation group (Sham group, $n = 5$), poststroke central pain group (CPSP group, $n = 5$), poststroke central pain + acupuncture group (AP group, $n = 5$), central pain after stroke + acupuncture + EX527 group (EX527 group, $n = 5$). EX527 (6-chloro-2,3,4,9-tetrahydro-1H-carbazole-1-carboxamide) was one of the inhibitors of the Sirtuin family [16]. We selected Neiguan, Renzhong, and Sanyinjiao points and gave acupuncture stimulation 30 min/time, once a day for 5 days. The EX527 group was intraperitoneally injected with EX-5275 mg/kg 30 minutes before the daily acupuncture treatment, and the rest of the operations were the same as those in the EA group. Rats in the Sham and CPSP groups were not treated with acupuncture [17].

2.6. Establishment of Rat CPSP Model. We established a rat CPSP model with the literature by Shih et al. [18]. The rats in the CPSP group, EA group, and EX527 group were fixed on the brain stereotaxic device after intraperitoneal injection of 10% chloral hydrate. The hair on the top of the rat's head was shaved, and the skin was disinfected with 75% alcohol and 2% iodine. The first skin was cut along the sagittal suture, the subcutaneous tissue was carefully separated, and the periosteum was separated to expose the sagittal suture and bregma. Using the bregma as the origin, refer to the positioning coordinates (right thalamic ventro-posterior lateral nucleus (VPL): 3.5 mm behind the bregma, 3.2 mm next to the midline, and 6.2 mm below the anterior bone). Under the stereotaxic guidance, the VPL was injected with type IV collagenase (dissolved 0.125U type IV collagenase in 1 μ l saline), then the wound was cleaned, and the scalp was sutured. Rats in the Sham group were injected with 1 μ l sterile saline.

2.7. Methods of Acupuncture Treatment. The rats were restrained and fixed on a self-made fixing device; insert the acupuncture needles into the Neiguan, Renzhong, and Sanyinjiao points of the rats in sequence. Neiguan acupoint was located on the inner side of the rat's forelimb, between the ulna fusiform suture about 3 mm away from the wrist joint, and there was one acupuncture point on the left and right sides. Renzhong acupoint was located about 1 mm in the middle of the rat's cleft lip and nose tip. Sanyinjiao was located about 1 cm above the tip of the medial malleolus of the rat's hind limbs, and there was an acupuncture point on the left and right sides. Each treatment was performed for 30 minutes.

2.8. Pain Behavior Testing with the Determination of Mechanical Withdrawal Threshold (MWT). The rats of each group were placed in a mesh cage with a metal mesh at the bottom at 1d before modeling and 1d, 3d, and 5d after modeling. After adapting to the environment for 30 minutes, we used an electronic mechanical pain meter to slowly and vertically puncture the center of the left hind foot of the rats. If the rats had the foot withdrawal reaction, it was positive, and the mechanical stimulation threshold was recorded. We repeated the operation at an interval of more than 10 minutes. The average value was taken as the mechanical withdrawal threshold of the rats until 3 positive reactions were recorded.

2.9. RNA Extraction and Quantitative Real-Time PCR. Quantitative real-time PCR (qRT-PCR) was performed to verify the results of data mining of the GEO database. After the pain behavior measurement was completed, the rats were anesthetized by intraperitoneal injection of 10% chloral hydrate. The skin was cut quickly and carefully to avoid pressing the brain tissue after the rat's neck was cut off with a decapitator. Then, we insert the curved forceps into the gap between the skull and the medulla oblongata, lift off the rat's skull, and remove the remaining skulls. After full exposure of the rat brain tissue, peeling is performed, then the brain tissue is removed, the filter paper absorbs the water and blood on the surface, and it is placed in a freezer at -80°C for storage. The manufacturer's instructions extracted total RNA from brain tissues using Trizol reagent (Takara, Kyoto, Japan). cDNA was synthesized using the PrimeScript reverse transcription-polymerase chain reaction kit (Takara, Kyoto, Japan). The qRT-PCR was performed in SYBR Green Master Mix (Roche). The 2- $\Delta\Delta C_t$ method was performed to analyze the data, and GAPDH was used as a loading control. The primer sequences are listed in Table 1.

3. Statistical Analysis

All values were expressed as mean \pm SEM. The statistical significance was determined by Student's *t*-test, performed by R package "ggpubr" and "ggplot2" with the function of `stat_compare_means`. $p < 0.05$ was taken as statistically significant.

4. Results

4.1. Identification of DEGs Related to SIRT1. The gene expression dataset of GSE171118, which contains 2 siSIRT1 samples and 2 normal control samples, was analyzed in the limma package with threshold parameters defined as fold change (FC) > 1 or < -1 and the adjusted *P* values < 0.05 . In total, 465 DEGs (173 high expression genes and 292 low expression genes) were identified between siSIRT1 samples and normal control samples, and there were 78 high expression genes and 170 low expression genes with the same threshold in the edgeR package (Table 2). Visualization was performed with volcano plot analysis to show the DEGs screened by limma (Figure 1) and edgeR (Figure 1(b)), respectively.

4.2. KEGG Pathway Analysis. From the path view KEGG pathway maps, it was observed that the expressions levels of NLRP3's downstream inflammatory factors interleukin-18 (IL-18) were downregulated in both of siSIRT1 group compared to the control group and NLRP3 reconstituted group compared to NLRP3 KO group, suggested that IL-18 expression levels were inhibited probably by SIRT1 expression activated and promoted. However, the expression levels of NLRP3 did not change significantly in the siSIRT1 group compared to the control group in the dataset of GSE171118.

4.3. Changes in Pain Behavior of Rats Measured by MWT. In the experiment on pain behavior, MWT values of the rats in the Sham group, CPSP group, AP group, and EX527 group were measured at 1d before modeling and at 1d, 3d, and 5d after modeling separately. We found that there was no statistical difference in MWT value of the rats in each group before the establishment of CPSP model, and there was no significant difference in MWT value of rats in the Sham group before and after modeling. Meantime, MWT value of the rats in the CPSP, EA, and EX527 groups was significantly decreased at d1-d3 compared with the Sham group; MWT value of the rats in the AP group was significantly increased compared with the CPSP group, while Figure 2 MWT value of the rats in the EX527 group was significantly decreased compared with the AP group (Figure 3).

4.4. mRNA Levels of NLRP3, SIRT1, and IL-18. The mRNA expression levels of NLRP3, SIRT1, and IL-18 on an animal model of ischemic stroke with CPSP were measured by qRT-PCR to validate the data mining findings from GEO. As illustrated in Figure 4(c), the expression levels of SIRT1 was downregulated and the activation of NLRP3 inflammasome was upregulated, the expression levels of IL-18 was upregulated in brain tissue around the injured area in animal model; as the pain threshold of CPSP rats was increased, the expression levels of SIRT1 were upregulated and the activation of NLRP3 inflammasome was downregulated, and the expression levels of IL-18 were downregulated after acupuncture treatment.

TABLE 1: Primer sequences used for the quantitative real-time polymerase chain reaction.

Gene	Forward primer (5'-3')	Reverse primer (5'-3')
SIRT1	GCTCGCCTTGCTGTGGACTTC	GTGACACAGAGATGGCTGGAAC TG
NLRP3	CCAGGAGTTCTTTGCGGCTA	GCCTTTTTTCGAAC TTGCCGT
IL-18	CAACCGCAGTAATACGGAGC	GATTCGTTGGCTGTTCCGGTC
GAPDH	ACAGCAACAGGTTGGTGGAC	TTTGAGGGTGCAGCGAACTT

TABLE 2: Results of differentially expressed mRNA of GSE171118.

Compare	Style	Identification tools	Log2FC_Cutoff	adjusted_Pvalue(FDR) _Cutoff	All differential expressed number	Upregulated number	Downregulated number	Total number after merging
siSIRT1 group versus normal control group	mRNA	limma	>1 or <-1	0.05	465	173	292	466
		edgeR	>1 or <-1	0.05	132	37	95	

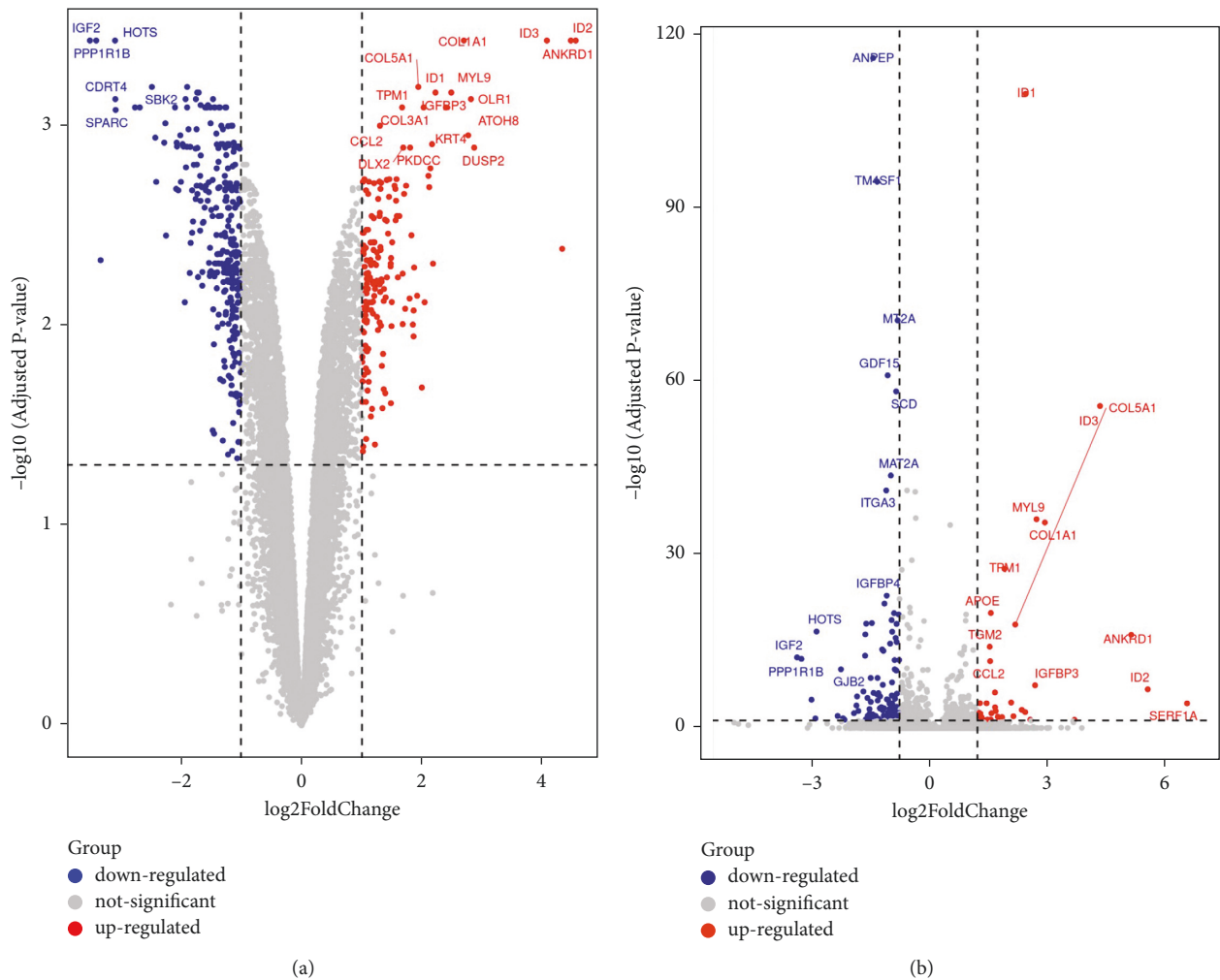
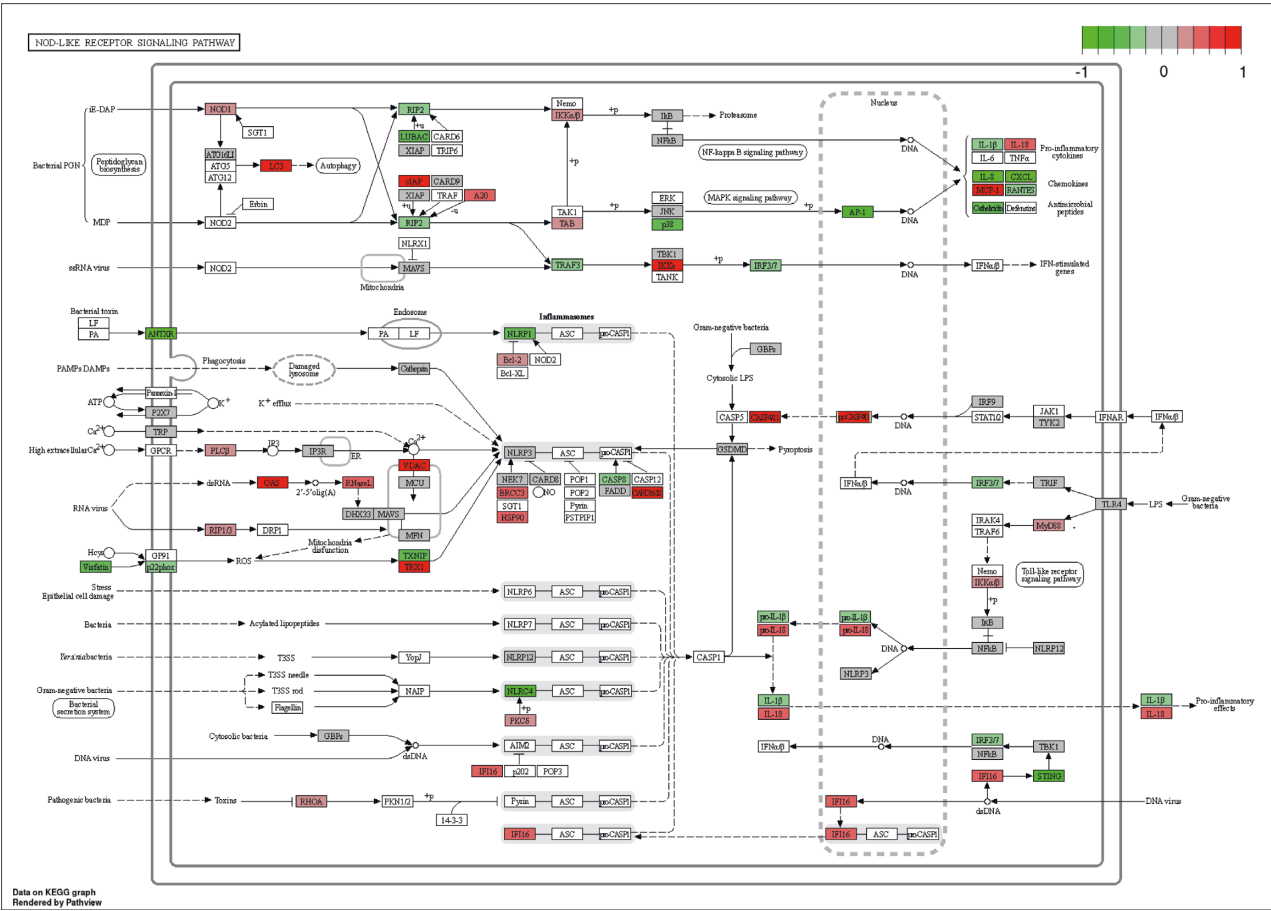


FIGURE 1: Volcano plot shows the DEGs between siSIRT1 and normal control samples. Fold change (FC) > 1 (in red) or < -1 (in blue) with adjusted P values or FDR < 0.05 are differentially increased or reduced in siSIRT1 samples relative to normal control samples. (a) Volcano plot performed by limma; (b) volcano plot performed by edgeR.



(a)
FIGURE 2: Continued.

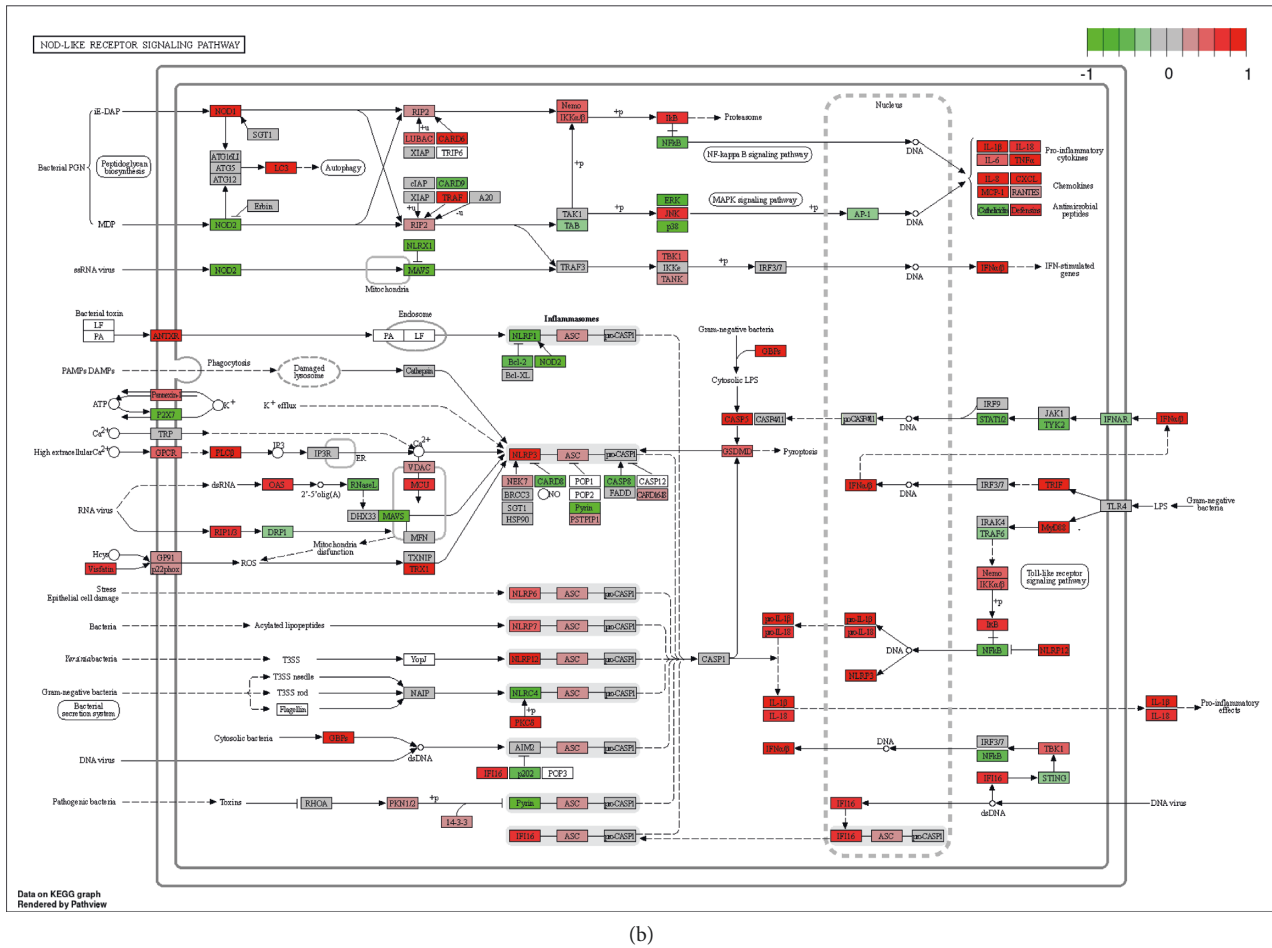


FIGURE 2: KEGG Pathway analysis of molecular signature of NLRP3 inflammasome signaling pathway, (a) Pathway analysis of siSIRT1 group compared to Control group; (b) Pathway analysis of NLRP3 reconstituted group compared to NLRP3 KO group; KEGG pathway analysis demonstrating upregulation or downregulation of multiple components of the complement pathway. Each box was one gene; the green boxes show the downregulated gene expression of mRNA while the red boxes show the upregulated gene expression.

5. Discussion

The neuropathic pain syndrome is caused by the corresponding ischemic or hemorrhagic lesions affecting the spinothalamic pathway [19]. The pathogenesis is not clear. It is usually characterized by sensory disturbances, persistent or intermittent pain, hyperalgesia, and hypersensitivity [20]. Studies have found that IL-17 can be detected in different central nervous system inflammatory states and is involved in neuropathic pain associated with multiple cirrhoses and autoimmune encephalomyelitis [21]. IL-17A can induce ATG5 and ATG7 to promote inflammation. It can also directly cause endothelial cells to release chemokines, thereby increasing leukocyte migration and the permeability of the blood-brain barrier, causing brain injury damage [22]. Based on current studies, we believe that CPSP was closely related to inflammation in the central nervous system. However, due to the complexity of inflammation signaling pathways, the mechanism has not yet been fully elucidated before.

SIRT1, as a NAD-dependent protein deacetylase, is involved in inflammatory responses, oxidative stress, and other processes. It also plays a cerebroprotective role in various inflammatory diseases of the nervous system by inhibiting the activation of the NLRP3 inflammasome and the immune upstream regulator IL-18 of NLRP3. SIRT1 can mediate gene silencing and life extension in yeast and fruit flies [23]. Homologs, including SIRT1-7, can catalyze protein deacetylation or adenosine diphosphate ribosylation. Its characteristic is that sirtuins need oxidized nicotinamide adenine dinucleotide (NAD⁺) undergo an enzymatic reaction to generate nicotinamide (NAM) as a negative feedback inhibitor [24]. Because of this NAD⁺ dependence, Sirtuins are classified as a group II group egg white deacetylase (Histon deacetylases, HDACs). SIRT1 is a kind of deacetylation that relies on NAD⁺ enzymes, a member of the SIRT family, which can regulate oxidative respiration, inflammation and various physical environments, and then participate in the regulation of various activities of the body.

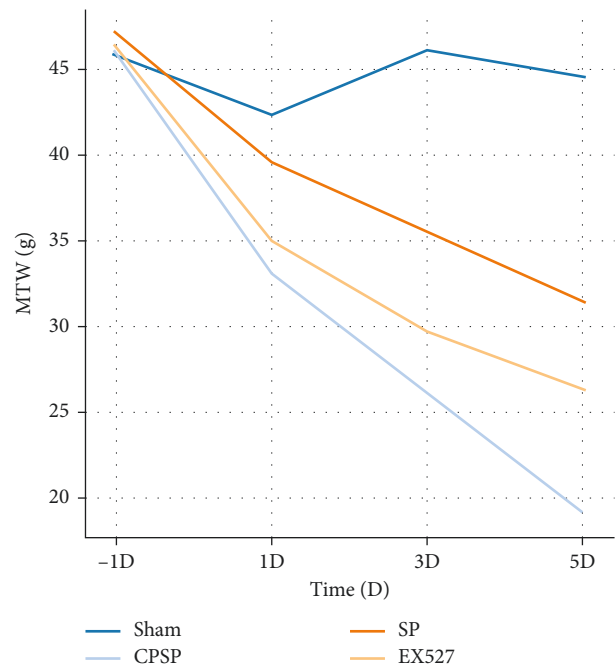


FIGURE 3: Changes in mechanical pain threshold in rats after establishing a central pain model after stroke. Compared with the Sham group, the MWT value of the left plantar in the CPSP group was decreased ($P < 0.05$); compared with the CPSP group, the MWT value in the AP group was increased ($P < 0.05$); compared with the AP group, MWT value in EX527 group was increased ($P < 0.05$).

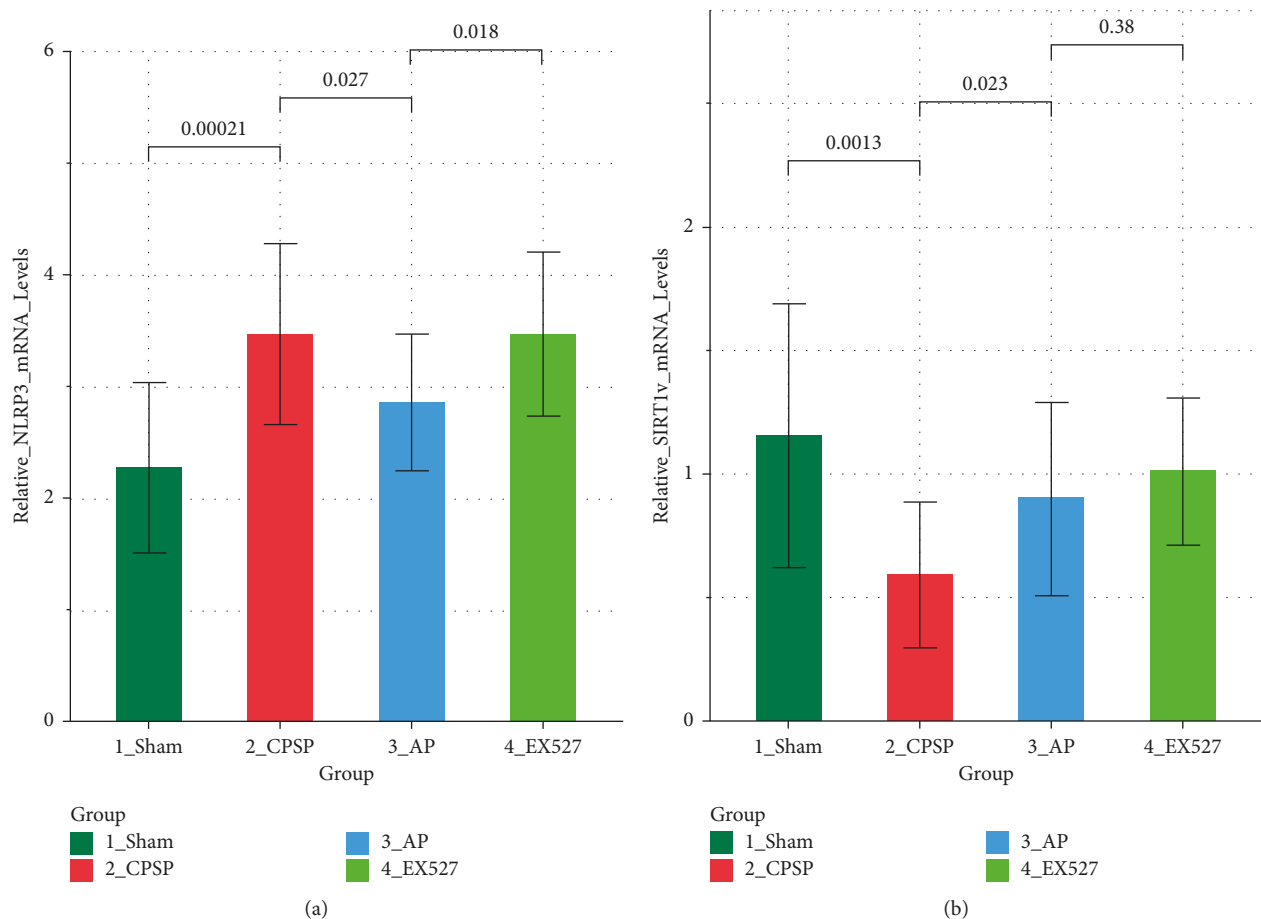


FIGURE 4: Continued.

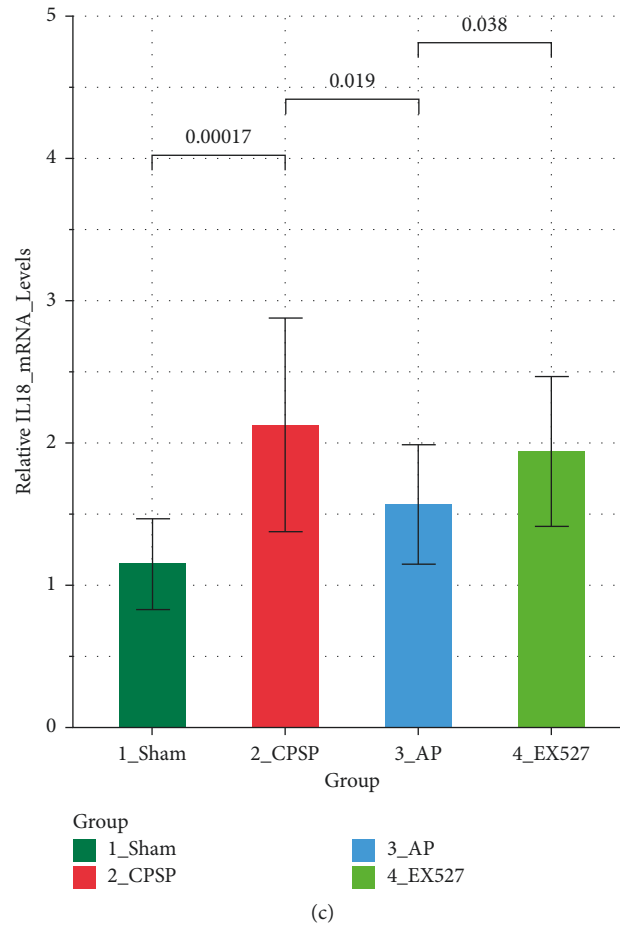


FIGURE 4: NLRP3, SIRT1 and IL-18 mRNA expression. (a) NLRP3, (b) SIRT1, and (c) IL-18 mRNA expression levels, which were normalized to GAPDH. $N=5$ in each group. Studies were repeated three times with highly similar results.

It is activated in a NAD⁺-dependent and non-NAD⁺-dependent manner. In addition, SIRT1 can target and regulate various transcription factors, such as NF- κ B, E2F1, p53, FOXOs, HIF-1, PGC-1 α , LXR, MyoD [25]. Under environmental stress, SIRT1 is transcribed to protein stimulation. Every step of life is dynamically regulated. At the post-transcriptional level, the HuR gene (also known as embryo-like lethal abnormal vision gene, ELAVL1) stabilizes SIRT1 by interacting with its 30-UTR mRNA SIRT1. Its activity is also regulated in many ways, such as its phosphorylation [26] and ubiquitination [27], or with AROS's [28] interaction with DBC1 [29]. The final expression and function of SIRT1 depend on the regulation of the redox festival. The research suggests that the use of bone marrow cell-specific SIRT1 knockout mouse models can be used in macrophage ablation. SIRT1 presents NF- κ B hyperacetylation, which leads to increased transcriptional activation of proinflammatory target genes [30]. The results of this study by establishing a model of CPSP in rats and performing interventional drug therapy in different groups are consistent with our speculations on reducing the pain threshold in CPSP rats. The expression level of SIRT1 in

brain tissue was downregulated, and NLRP3 and IL-18 expression levels were upregulated. Acupuncture could increase the pain threshold of CPSP rats, promote the expression levels of SIRT1, reduce the expression levels of NLRP3 and IL-18, and reduce the pain symptoms of rats. We found that the therapeutic effect of acupuncture could be reversed by a SIRT1 inhibitor, indicating that SIRT1 may play an important role in the process of acupuncture treatment of CPSP.

NLRP3 inflammasome is a polyprotein complex with NLRP3, ASC, and procaspase-1 as the core protein. When activated, it can rapidly induce the maturation and secretion of cytokines to trigger the body's inflammatory response [31]. It was found that the mouse lung tissue showed obvious pathological damage. At the same time, the expression levels of NLRP3 inflammasome and IL-18 in the lung tissue were upregulated by using intratracheal infusion of lipopolysaccharide to induce a mouse model of acute lung injury. The degree of lung injury in mice was significantly reduced after treatment with the NLRP3 inflammasome inhibitor MCC950. At the same time, the activation of NLRP3 inflammasomes in the lung tissues was reduced, and the

expression levels of IL-18 were downregulated, indicating that the activation of NLRP3 inflammasomes was inhibited, which play a protective role to reduce the subsequent secretion of IL-18, and reduce the levels of inflammation in the body [32].

In another animal experiment, the middle cerebral artery occlusion method was performed to establish a mouse cerebral ischemia-reperfusion model, and it was found that the expression of low-density lipoprotein receptor (LDLR) in the brain tissue of the model mouse was downregulated and induced the activation of NLRP3 inflammasome and the subsequent maturation, and the release of IL-18 eventually led to neuronal apoptosis. After treatment with the NLRP3 inflammasome inhibitor CY-09, the expression levels of IL-18 in the brain tissue were decreased, and the number of neuronal apoptosis was decreased, indicating that the NLRP3 inflammasome in the brain tissue can also regulate the maturation and secretion of IL-18 and other cytokines, and then participate in the body's inflammatory response. IL-18 are common proinflammatory cytokines that are closely related to a variety of neuropathic pain [33].

The present study observed that the pain threshold of CPSP rats increased after acupuncture treatment, the expression levels of SIRT1 in the brain tissue was upregulated, and the expression levels of NLRP3 and IL-18 were downregulated significantly. The pain threshold of rats was reduced, the expression levels of SIRT1 in the brain tissue were downregulated, and the expression levels of NLRP3 and IL-18 were upregulated.

There are also some shortcomings in this study. Although this study found that the improvement of stroke by acupuncture was related to the upregulation of SIRT1 expression levels in brain tissue and the significant downregulation of the expression levels of NLRP3 and IL-18, the specific in-depth mechanisms were not further studied. In addition, acupuncture effects may vary from acupuncture point to acupuncture point, and this study did not investigate. These will be the problems that need to be further solved in future research.

6. Conclusion

Acupuncture treatment of CPSP could inhibit the activation of the inflammatory body of NLRP3, and NLRP3's downstream inflammatory factors of IL-18 expression were inhibited.

Data Availability

The datasets used and analyzed during the current study are available from the corresponding author upon reasonable request.

Conflicts of Interest

The authors declare that they have no conflicts of interest.

References

- [1] M. U. Jahngir and A. I. Qureshi, "Dejerine roussy syndrome," in *StatPearls [Internet]* StatPearls Publishing, Treasure Island, FL, USA, 2021.
- [2] H. R. Choi, A. Aktas, and M. M. Bottros, "Pharmacotherapy to manage central post-stroke pain," *CNS Drugs*, vol. 35, no. 2, pp. 151–160, 2021.
- [3] H. Klit, N. B. Finnerup, and T. S. Jensen, "Central post-stroke pain: clinical characteristics, pathophysiology, and management," *The Lancet Neurology*, vol. 8, no. 9, pp. 857–868, 2009.
- [4] S. I. Hiraga, T. Itokazu, M. Hoshiko, H. Takaya, M. Nishibe, and T. Yamashita, "Microglial depletion under thalamic hemorrhage ameliorates mechanical allodynia and suppresses aberrant axonal sprouting," *JCI Insight*, vol. 5, no. 3, Article ID e131801, 2020.
- [5] H. Kocabas, F. Levendoglu, O. M. Ozerbil, and B. Yuruten, "Complex regional pain syndrome in stroke patients," *International Journal of Rehabilitation Research*, vol. 30, no. 1, pp. 33–38, 2007.
- [6] W. Petchkrua, D. J. Weiss, and R. R. Patel, "Reassessment of the incidence of complex regional pain syndrome type 1 following stroke," *Neurorehabilitation and Neural Repair*, vol. 14, no. 1, pp. 59–63, 2000.
- [7] Q. S. Huang, "Effect of acupuncture combined with speech rehabilitation in patients with motor aphasia after ischemic stroke," *Clinical Research*, vol. 30, no. 6, pp. 136–139, 2022.
- [8] L. L. Wei, "Application of acupuncture and rehabilitation training in the treatment of patients with hemiplegia after stroke," *Medicine and Health Research*, vol. 6, no. 12, pp. 86–88, 2022.
- [9] X. Zhang and Y. Zhu, "Clinical observation on electro-acupuncture treatment of thalamic pain after stroke," *Xinjiang Traditional Chinese Medicine*, vol. 30, no. 4, pp. 44–45, 2012.
- [10] B. Kumar, J. Kalita, G. Kumar, and U. K. Misra, "Central poststroke pain: a review of pathophysiology and treatment," *Anesthesia & Analgesia*, vol. 108, no. 5, pp. 1645–1657, 2009.
- [11] S. Leng, W. Huang, Y. Chen et al., "SIRT1 coordinates with the CRL4B complex to regulate pancreatic cancer stem cells to promote tumorigenesis," *Cell Death & Differentiation*, vol. 28, no. 12, pp. 3329–3343, 2021.
- [12] C. F. Budden, L. J. Gearing, R. Kaiser, L. Standke, P. J. Hertzog, and E. Latz, "Inflammasome-induced extracellular vesicles harbour distinct RNA signatures and alter bystander macrophage responses," *Journal of Extracellular Vesicles*, vol. 10, no. 10, Article ID e12127, 2021.
- [13] M. D. Robinson, D. J. McCarthy, and G. K. Smyth, "edgeR: a Bioconductor package for differential expression analysis of digital gene expression data," *Bioinformatics*, vol. 26, no. 1, pp. 139–140, 2010.
- [14] M. E. Ritchie, B. Phipson, D. Wu et al., "Limma powers differential expression analyses for RNA-sequencing and microarray studies," *Nucleic Acids Research*, vol. 43, no. 7, p. e47, 2015.
- [15] Á Nagy, A. Lánckzy, O. Menyhárt, and B. Györfy, "Validation of miRNA prognostic power in hepatocellular carcinoma using expression data of independent datasets," *Scientific Reports*, vol. 8, no. 1, p. 9227, 2018.
- [16] W. Luo and C. Brouwer, "Pathview: an R/Bioconductor package for pathway-based data integration and visualization," *Bioinformatics*, vol. 29, no. 14, pp. 1830–1831, 2013.
- [17] W. Luo, G. Pant, Y. K. Bhavnasi, S. G. Blanchard, and C. Brouwer, "Pathview Web: user friendly pathway

- visualization and data integration,” *Nucleic Acids Research*, vol. 45, no. W1, pp. W501–W508, 2017.
- [18] M. Gertz, F. Fischer, G. T. T. Nguyen et al., “Ex-527 inhibits Sirtuins by exploiting their unique NAD⁺-dependent deacetylation mechanism,” *Proceedings of the National Academy of Sciences*, vol. 110, no. 30, pp. E2772–E2781, 2013.
 - [19] C. Wang, Z. Chen, and G. Li, “Study on the standardized location method of acupoints in commonly used experimental animals,” *Tianjin Traditional Chinese Medicine*, vol. 33, no. 2, pp. 100–103, 2016.
 - [20] H. C. Shih, Y. H. Kuan, and B. C. Shyu, “Targeting brain-derived neurotrophic factor in the medial thalamus for the treatment of central poststroke pain in a rodent model,” *Pain*, vol. 158, no. 7, pp. 1302–1313, 2017.
 - [21] H. F. Lu, C. Y. Xu, L. Zhang et al., “A new central post-stroke pain rat model: autologous blood injected thalamic hemorrhage involved increased expression of P2X4 receptor,” *Neuroscience Letters*, vol. 687, pp. 124–130, 2018.
 - [22] R. A. Harrison and T. S. Field, “Post stroke pain: identification, assessment, and therapy,” *Cerebrovascular Diseases*, vol. 39, no. 3–4, pp. 190–201, 2015.
 - [23] L. Gao, P. P. Li, T. Y. Shao et al., “Neurotoxic role of interleukin-17 in neural stem cell differentiation after intracerebral hemorrhage,” *Neural regeneration research*, vol. 15, no. 7, pp. 1350–1359, 2020.
 - [24] H. Zhu, Z. Wang, J. Yu et al., “Role and mechanisms of cytokines in the secondary brain injury after intracerebral hemorrhage,” *Progress in Neurobiology*, vol. 178, Article ID 101610, 2019.
 - [25] N. Dali-Youcef, M. Lagouge, S. Froelich, C. Koehl, K. Schoonjans, and J. Auwerx, “Sirtuins: the ‘magnificent seven’, function, metabolism and longevity,” *Annals of Medicine*, vol. 39, no. 5, pp. 335–345, 2007.
 - [26] M. C. Haigis and L. P. Guarente, “Mammalian sirtuins—emerging roles in physiology, aging, and calorie restriction,” *Genes & Development*, vol. 20, no. 21, pp. 2913–2921, 2006 Nov 1.
 - [27] J. H. Lim, Y. M. Lee, Y. S. Chun, J. Chen, J. E. Kim, and J. W. Park, “Sirtuin 1 modulates cellular responses to hypoxia by deacetylating hypoxia-inducible factor 1 α ,” *Molecular Cell*, vol. 38, no. 6, pp. 864–878, 2010.
 - [28] T. Sasaki, B. Maier, K. D. Koclega et al., “Phosphorylation regulates SIRT1 function,” *PLoS One*, vol. 3, no. 12, p. e4020, 2008.
 - [29] Y. Yang, W. Fu, J. Chen et al., “SIRT1 sumoylation regulates its deacetylase activity and cellular response to genotoxic stress,” *Nature Cell Biology*, vol. 9, no. 11, pp. 1253–1262, 2007.
 - [30] E. J. Kim, J. H. Kho, M. R. Kang, and S. J. Um, “Active regulator of SIRT1 cooperates with SIRT1 and facilitates suppression of p53 activity,” *Molecular Cell*, vol. 28, no. 2, pp. 277–290, 2007.
 - [31] J. E. Kim, J. Chen, and Z. Lou, “DBC1 is a negative regulator of SIRT1,” *Nature*, vol. 451, no. 7178, pp. 583–586, 2008.
 - [32] F. Yeung, J. E. Hoberg, C. S. Ramsey et al., “Modulation of NF- κ B-dependent transcription and cell survival by the SIRT1 deacetylase,” *The EMBO Journal*, vol. 23, no. 12, pp. 2369–2380, 2004.
 - [33] L. Mao, A. Kitani, M. Similuk et al., “Loss-of-function CARD8 mutation causes NLRP3 inflammasome activation and Crohn’s disease,” *Journal of Clinical Investigation*, vol. 128, no. 5, pp. 1793–1806, 2018.

Retraction

Retracted: Clinical Significance of EZH2 in Acute Myeloid Leukemia

Computational Intelligence and Neuroscience

Received 26 September 2023; Accepted 26 September 2023; Published 27 September 2023

Copyright © 2023 Computational Intelligence and Neuroscience. This is an open access article distributed under the Creative Commons Attribution License, which permits unrestricted use, distribution, and reproduction in any medium, provided the original work is properly cited.

This article has been retracted by Hindawi following an investigation undertaken by the publisher [1]. This investigation has uncovered evidence of one or more of the following indicators of systematic manipulation of the publication process:

- (1) Discrepancies in scope
- (2) Discrepancies in the description of the research reported
- (3) Discrepancies between the availability of data and the research described
- (4) Inappropriate citations
- (5) Incoherent, meaningless and/or irrelevant content included in the article
- (6) Peer-review manipulation

The presence of these indicators undermines our confidence in the integrity of the article's content and we cannot, therefore, vouch for its reliability. Please note that this notice is intended solely to alert readers that the content of this article is unreliable. We have not investigated whether authors were aware of or involved in the systematic manipulation of the publication process.

Wiley and Hindawi regrets that the usual quality checks did not identify these issues before publication and have since put additional measures in place to safeguard research integrity.

We wish to credit our own Research Integrity and Research Publishing teams and anonymous and named external researchers and research integrity experts for contributing to this investigation.

The corresponding author, as the representative of all authors, has been given the opportunity to register their agreement or disagreement to this retraction. We have kept a record of any response received.

References

- [1] W. Jiao, Y. Liu, and Y. Bao, "Clinical Significance of EZH2 in Acute Myeloid Leukemia," *Computational Intelligence and Neuroscience*, vol. 2022, Article ID 8741989, 5 pages, 2022.

Research Article

Clinical Significance of EZH2 in Acute Myeloid Leukemia

Weiyun Jiao, Yuanyuan Liu, and Yangyi Bao 

Hematology Department, Hefei First People's Hospital, Hefei 23000, China

Correspondence should be addressed to Yangyi Bao; 2009030232@st.btbu.edu.cn

Received 23 June 2022; Revised 21 July 2022; Accepted 22 July 2022; Published 23 August 2022

Academic Editor: Dong Chen

Copyright © 2022 Weiyun Jiao et al. This is an open access article distributed under the Creative Commons Attribution License, which permits unrestricted use, distribution, and reproduction in any medium, provided the original work is properly cited.

In this paper, we have focused on the investigation of the expression level of the enhancer of zeste homolog 2 (EZH2) gene in bone marrow mononuclear cells of acute myeloid leukemia (AML) patients and analyze the relationship between EZH2 gene expression and EMI. The expression of EZH2mRNA in bone marrow mononuclear cells of 26 patients with incipient AML was detected by qRT-PCR, and the relationship between EZH2mRNA expression and clinical characteristics was analyzed. EZH2 mRNA expression was increased in 26 AML patients. EZH2 gene expression in male patients was significantly higher than that in female patients. The expression of EZH2 in the group with extramedullary infiltration (EMI) was significantly higher than that in the group without EMI. The patients were divided into different groups according to the chromosomal karyotype and prognosis. Statistical analysis showed that the expression level of the medium-risk group was significantly higher than that of the low-risk group, while there was no statistical difference in other groups ($P > 0.05$). The expression of EZH2 gene in AML patients was closely related to EMI, and the expression of EZH2 in AML cells was closely related to cell migration ability. EZH2 is expected to be one of the indicators of disease recurrence.

1. Introduction

Acute myeloid leukemia (AML) is a malignant tumor of hematopoietic stem and progenitor cells. The malignant proliferation of leukemia cells gradually replaces normal hematopoiesis in the body and invades extramedullary tissues and organs, resulting in anemia, bleeding, infection and organ enlargement, and ultimately death. In recent years, with the rapid economic development and increasingly serious environmental pollution, the annual incidence of leukemia is on the rise [1]. New epidemiological survey data show [2] that the mortality rate of leukemia in my country is as high as 4.28/10. It ranks eighth in malignant tumors.

AML is the most common type of adult leukemia. At present, with the emergence of new chemotherapy drugs and the continuous improvement and innovation of chemotherapy regimen, the remission rate of leukemia treatment has been significantly improved. 50–85% of AML patients can obtain complete response (CR) after standard regimen induction therapy [3]. The use of high-intensity consolidation chemotherapy and hematopoietic stem cell transplantation

has made the long-term survival rates to improve, but most patients will relapse after reaching CR and develop drug resistance to chemotherapy drugs or even progress to refractory leukemia and eventually death.

Considering that EZH2 plays an important role in malignant tumors and is closely related to tumor invasion and metastasis and poor prognosis, there are few studies on the overexpression of EZH2 in leukemia and its clinical significance. Therefore, in this study, the expression level of EZH2 gene in bone marrow mononuclear cells of AML patients was detected by qRT-PCR, and the relationship between its expression and clinical characteristics, treatment response, and prognosis were analyzed, providing a new indicator for the diagnosis, treatment, and prognosis evaluation of leukemia.

The enhancer of zeste homolog 2 (EZH2) plays the role of a proto-oncogene in malignant solid tumors, while hematological tumors have two states of gain and loss of function, which play a role in promoting or inhibiting cancer. EZH2 was found to be involved in the occurrence and development of AML. Momparler et al. [4] studied the function of EZH2 in AML in mice, and the results showed

that in the artificially constructed AF9 positive AML model mice, the trimethylation level of H3K27 was significantly reduced in the EZH2-deficient group. The expression of genes related to cell growth and differentiation, such as *Cdkn2a*, increased significantly, suggesting that EZH2 inhibits the differentiation of leukemia stem cells in AML, thereby promoting the occurrence of leukemia. DZNep, as an EZH2 inhibitor, has a significant inhibitory effect on cell clonogenesis in both human and mouse AML cell lines and has an antileukemia effect in leukemia mouse models, accompanied by upregulated expression of tumor suppressor genes *CDKN1A* and *FBX032* [5]. Domestic scholar Shenghao Wu found that EZH2 protein expression was significantly correlated with increased LDH, WBC, and shorter OS in bone marrow cells of AML patients. At the same time, EZH2 overexpression was accompanied by decreased miR-101 expression, suggesting that miRNA may have post-transcriptional regulation of EZH2 and promote the occurrence of leukemia [6].

In this paper, we have focused on the investigation of the expression level of the EZH2 gene in bone marrow mononuclear cells of AML patients and analyzed the relationship between EZH2 gene expression and EMI. The expression of EZH2mRNA in bone marrow mononuclear cells of 26 patients with incipient AML was detected by qRT-PCR, and the relationship between EZH2mRNA expression and clinical characteristics was analyzed. EZH2 mRNA expression was increased in 26 AML patients. EZH2 gene expression in male patients was significantly higher than that in female patients. The expression of EZH2 in the group with EMI was significantly higher than that in the group without EMI. The patients were divided into different groups according to the chromosomal karyotype and prognosis.

The remaining paper is organized as given in the following paragraph where a brief description of every section is provided.

In the subsequent section, a detailed discussion on the relationship between EZH2 gene expression and EMI is provided where it is clearly mentioned how data is collected. In Section 3, experimental results and observations are described in detail along with possible comparative evaluations which is followed by a brief discussion section. Finally, concluding remarks are provided at the end along with references.

2. Proposed Methodology

2.1. Participants. 26 patients with newly treated AML in our hospital from June 2018 to June 2021 were retrospectively analyzed. All patients were confirmed by bone marrow morphological cytology, immunohistochemical staining, or flow cytometry immunotyping. All specimens were collected with the informed consent of the subjects or their families and approved by the hospital ethics committee.

2.2. Isolation of Bone Marrow Mononuclear Cells. Routine bone marrow puncture was performed to extract 3–5 mL of the patient's bone marrow fluid, heparin was anticoagulated, and bone marrow mononuclear cells were isolated

by lymphocyte separation solution. After washing twice with PBS, 1 mL of Trizol was added, repeatedly beaten until no precipitation was found, and stored at -80°C for later use.

2.3. Total RNA Extraction. Total RNA was extracted according to Trizol instructions. After DEPC water was dissolved, the concentration and purity of RNA were determined by using a spectrophotometer. Only $2.0 > A_{260}/A_{280} > 1.8$ could be used for subsequent reverse transcription.

2.4. Reverse Transcriptional Reaction. Follow the instructions of TAKARA's Prime-Script reverse transcription kit. After fully mixing 1 μg total RNA, 1 μL Oligo(dT), and 18 μL dNTPmix, the mixture was placed at 65°C for 5 min and then cooled quickly on ice. After adding 45 μL Prime-Script buffer, 1 μL of the ribonuclease inhibitor, and finally, 1 μL of enzyme mix reverse transcriptase (200 U/ μL) were added until the final volume was 20 μL . After being treated at 42°C for 1 h and 70°C for 10 min, cDNA was cooled on ice, and the first strand obtained was immediately PCR or stored in an 80°C refrigerator for future use.

2.5. Real-Time PCR. The SYBR Green fluorescence quantitative PCR(RT-PCR) kit was used for detection. The upstream primer of EZH2 was 5'-GACCCTGACCTCTGTCTTACTF-3, and the downstream primer was 5'-GATgCTCCCAGGCAA AGATG-3. The upstream primer of internal reference GAPDH was 5''-TGAAGGTCGGAGTCAACGG-3, and the downstream primer was 5''-CTGGAA-GatGGTGATGGGATT-3. PCR amplification conditions were 95°C for 30 S, 95°C for 5 S, 60°C for 40 S, and 40 cycles. All reactions are set with 3 complex holes. The relative expression levels of target genes in the samples were expressed by the $2^{-\Delta\Delta\text{Ct}}$ method. The expression levels of the EZH2 gene were expressed as $2^{-\Delta\Delta\text{Ct}}$. The EZH2 mRNA of AML patients was multiplied by 10000, and 1 g of data was converted into a normal distribution and the Levene test for homogeneity of variance.

2.6. Statistical Analysis. SPSS23.0 statistical software was adopted to process the data. The measurement data were presented as $(\bar{x} \pm s)$. The group design *t*-test was adopted for comparison, and the analysis of variance was adopted for comparison between multiple groups. The Dunnett's test was adopted for comparison with the control group. The counting data were presented in the number of cases, the percentage, χ^2 test was adopted for comparison between the groups, and the bilateral test was employed for all statistical tests. Pearson correlation or Spearman rank correlation was used for correlation analysis. The Kaplan–Meier method was used for survival analysis. $P < 0.05$ was considered statistically significant.

3. Experimental Results

In this section, we are going to provide a detailed discussion on the effectiveness of the proposed scheme specifically with the supported experimental results which are collected

through the implementation of the proposed procedure in the underlined environment.

3.1. Basic Characteristics of AML Patients. The 26 patients with AML included 18 bone marrow tissue samples and 8 extramedullary tissue samples (see Table 1 for the main clinical characteristics and treatment scheme). Through analysis and comparison of the clinical data of the two groups, it was found that the age, proportion of primary immature cells in the bone marrow, proportion of peripheral immature cells, WBC, LDH, disease status, FAB (M2/M4/M5/other) typing, and chromosome karyotype distribution of the two groups were basically the same, and there was no significant difference ($P > 0.05$), but there were significant differences in gender, initial induction scheme, and consolidation enhancement scheme between the two groups ($P < 0.05$), which provided a reference basis for analyzing the relationship between EZH2 protein expression and clinical characteristics after combining the data of the two groups.

P value is the comparison between the BM group and the EMI group; BM % and PB % were the proportion of bone marrow and peripheral blood protonaive cells, respectively. M2 in FAB included L patients with M1, 4 patients with undefined AML and 3 patients with granulocytic sarcoma. In the induction scheme, only 1 cases of HA and 2 cases of MA were incorporated into the DA and IA groups, respectively. Consolidation and reinforcement program: A represents induction program + <4 courses of MD/HD-Ara-c, B represents induction program + 24 courses of MD/HD-Ara-C or Auto-HSCT, and C represents induction program + allo-HSCT. * represents $P < 0.05$ and ** represents $P < 0.01$.

3.2. EZH2 mRNA Expression Level in Bone Marrow Cells of AML Patients. T -test results of two samples showed that the EZH2 gene expression level in AML patients was significantly higher than that in normal controls ($P < 0.05$). The expression level of EZH2 mRNA in bone marrow mononuclear cells of 42 AML patients was detected by RT-PCR. The expression level of EZH2 mRNA in bone marrow cells of AML patients was 1.68 ± 0.73 (95%CI, 1.45–1.92). In the 10 normal controls, the rate was 0.87 ± 0.65 (95%CI, 0.40–1.34).

3.3. Expression and Clinical Characteristics of EZH2 mRNA in AML Patients. The expression of the EZH2 gene in the bone marrow of AML patients is closely related to the occurrence of EMI. In addition, the patients were divided into groups according to chromosome karyotype prognosis. The EZH2 gene expression level was 1.00 ± 0.05 in the low-risk group, 1.94 ± 0.60 in the medium-risk group, and 1.84 ± 0.64 in the high-risk group. The expression level of the EZH2 gene in bone marrow cells of AML patients was significantly correlated with males, proportion of juvenile cells in peripheral blood 30%, and $WBC > 35 \times 10^9/L$ ($P < 0.05$) but not with the FAB type, age, proportion of juvenile cells in the bone marrow, LDH level, and complex karyotype ($P > 0.05$). Statistical analysis showed that there was no significant

difference in the EZH2 expression level among the three groups ($P > 0.05$). However, the expression level of the EZH2 gene in the medium-risk group was significantly higher than that in the low-risk group ($P < 0.05$), suggesting that EZH2 may be one of the indicators for stratified diagnosis and prognosis assessment. According to whether patients were accompanied by EMI at the time of onset, patients were divided into the group accompanied by EMI and the group without EMI. The EZH2 gene expression level in the group accompanied by EMI was 2.04 ± 0.59 , while that in the group without EMI was 1.29 ± 0.72 . There was a significant difference Table 2 in the EZH2 gene expression level between the two groups ($P < 0.05$).

* indicates a significant difference between the low-risk group and the medium-risk group; BM % represents the proportion of bone marrow naive cells, PB % represents the proportion of peripheral blood naive cells, and EMI represents extramedullary infiltration (EMI). * represents $P < 0.05$ and * represents $P < 0.01$.

4. Discussion

EMI is one of the malignant biological features of AML. The impact of EMI on prognosis is still a controversial issue, but most studies show that EMI is closely related to a lower CR rate, higher risk of relapse, and poor prognosis. Just like the invasion and metastasis of malignant tumor cells, the EMI process of leukemia cells is also a complex process involving multiple factors and completed by multiple steps [7]. Most scholars believe that the alteration of the bone marrow microenvironment and degradation of the extracellular matrix are leukemia cells. The mechanism of extramedullary infiltration of leukemia cells may involve abnormal expression of adhesion factors on the surface of leukemia cells. The ability of leukemia cell adhesion or migration is enhanced, and then escape from the adhesion of the bone marrow stroma and escape into the bone marrow stroma and peripheral blood, and then operate chemotactic movement and adhere to the vascular endothelium under the action of chemokines. It then promotes the secretion of cellular matrix metalloproteinases to degrade the extracellular matrix and migrate to extramedullary tissues to form infiltrating lesions [8].

A literature study has shown that EZH2 is overexpressed in a variety of malignant tumors, especially solid tumors, and its expression is related to patients' clinical stage, tumor malignancy, tumor invasion and metastasis, chemotherapy resistance, and poor prognosis [9].

In vitro culture of primary bone marrow cells from patients with cellular lymphoma found that the expression of EZH2 protein in proliferating cells was significantly higher than that in quiescent cell lines. In addition, it has been demonstrated that overexpressed EZH2 promotes lymphoma formation by regulating the immunoglobulin IgH rearrangement [10].

At present, epigenetic modification has become an important mechanism to regulate gene expression. It is a modification mode independent of DNA sequence changes, mainly including DNA methylation, histone covalent

TABLE 1: Clinical characteristics and treatment of 26 patients with AML (median, range).

	<i>n</i>	BM (<i>n</i> = 18)	EMI (<i>n</i> = 8)	χ^2/Z	<i>P</i>
Sex (M/F)	26	12/6	5/3	5.378	0.019*
Age	26	34.2 (14.0–85)	32.8 (15–78.0)	−0.670	0.500
BM%	26	71.6 (24.8–93.6)	72.8 (23.7–92.4)	−0.500	0.615
PB%	26	45.8 (3.9–87.2)	46.7 (2.9–86.1)	−0.468	0.642
WBC $\times 10^9/L$	26	12.5 (0.7–102.9)	12.2 (0.6–99.7)	−0.995	0.354
LDH	26	356 (140.2–924.7)	367.2 (143.5–938.1)	−0.399	0.692
Status (incipient/recurrent)	26	13/5	4/2	−0.388	0.685
FAB (M2/M4/M5/other)	26	5/2/10/1	5/0/1/2	7.602	0.056
Normal/complex karyotype	22	17/2	2/1	0.008	0.945
Prognostic stratification (low/medium/high)	25	5/12/1	1/4/2	2.747	0.256
Induce (DA/IA)	26	1/17	7/1	8.50	0.003**
Consolidate (a/b/c)	20	10/1/4	4/2/0	8.299	0.015*

TABLE 2: Relationship between the bone marrow EZH2 mRNA expression level and clinical features in 38 AML patients.

Clinical features	<i>N</i>	EZH2 mRNA	95CI%	<i>F/t</i>	<i>P</i>
Sex				2.718	0.010*
Male	18	1.95 ± 0.65	1.65~2.22		
Female	8	1.39 ± 0.67	1.04~2.70		
Age				−0.496	0.627
	16	1.74 ± 0.72	1.42~2.01		
	10	1.63 ± 0.68	1.23~0.97		
FAB type				0.881	0.493
M1	2	1.55 ± 0.34	0.99~2.11		
M2	6	1.72 ± 0.51	1.39~2.01		
M3	4	1.92 ± 0.99	1.63~2.63		
M4	8	1.49 ± 0.66	1.15~1.84		
BM%				0.989	0.330
	10	1.55 ± 0.68	1.23~1.91		
	16	1.79 ± 0.72	1.65~2.22		
PB%				2.665	0.010*
	8	1.33 ± 0.65	1.04~1.75		
	18	1.95 ± 0.66	1.62~2.24		
WBC				2.081	0.044*
35	11	1.44 ± 0.75	1.05~0.84		
35	15	1.93 ± 0.69	1.59~2.05		
LDH				0.560	0.598
Normal	7	1.59 ± 0.98	0.58~2.63		
Increase	19	1.78 ± 0.69	1.47~2.06		
EMI				3.460	0.001**
No	7	1.28 ± 0.71	0.93~1.67		
Yes	8	2.05 ± 0.57	1.73~2.30		
Karyotype				1.625	0.326
Normal	20	1.97 ± 0.61	1.69~2.31		
Complex	6	1.54 ± 0.55	−5.39~7.65		
Prognostic stratification				2.77	0.082
Low risk	4	1.00 ± 0.04	0.51~1.46	−2.20	0.037*a
Medium crisis	16	1.95 ± 0.58	1.72~2.20		
High risk	6	1.84 ± 0.62	−0.56~3.65		

modification, and microRNA regulation. As a member of the PCG protein family, EZH2 is a catalytically active subunit of the PRC2 complex, which can induce trimethylation of histone H3K27 and then exert transcriptional inhibition on downstream target genes. Statistical analysis of the relationship between the expression of EZH2 and clinical features

showed that EZH2 mRNA and protein expression were correlated with the proportion of peripheral blood naive cells, WBC, and associated EMI. In addition, EZH2 mRNA was also closely correlated with gender and karyotype prognosis stratigraphy, and the expression level of EZH2 mRNA in the medium-risk group was significantly higher than that in the low-risk group. Wu et al. [5] showed that the EZH2 mRNA expression level in bone marrow cells was not related to gender, WBC, and LDH, while EZH2 protein in bone marrow tissues was associated with WBC $> 1.50 \times 10^9/L$ and increased LDH were significantly correlated, which was inconsistent with our results. In addition, this study believed that EZH2 mRNA and protein expression levels were inconsistent, which might be caused by the posttranscriptional regulation of EZH2 by Mir-101. Since our research group did not detect EZH2 mRNA and protein in the same specimen at the same time, and there are few studies in this area, it remains to be confirmed whether the mRNA and protein expression levels of EZH2 are consistent. Grubach et al. [11] and Tanaka al. [12] found that the expression level of the EZH2 gene in complex karyotype AML was significantly higher than that in normal AML patients. This study still has some shortcomings. Firstly, the quality of this study is limited due to the small sample size we included in the study. Secondly, this research is a single-center study, and our findings are subject to some degree of bias. Therefore, our results may differ from those of large-scale multicenter studies from other academic institutes. This research is still clinically significant, and further in-depth investigations will be carried out in the future.

5. Conclusion

The expression of the EZH2 gene in AML patients was closely related to EMI, and the expression of EZH2 in AML cells was closely related to cell migration ability. EZH2 is expected to be one of the indicators of disease recurrence. In this paper, we have focused on the investigation of the expression level of the EZH2 gene in bone marrow mononuclear cells of AML patients and analyzed the relationship between EZH2 gene expression and EMI. The expression of EZH2mRNA in bone marrow mononuclear cells of 26 patients with incipient AML was detected by qRT-PCR, and the relationship between EZH2mRNA expression and clinical characteristics was analyzed. EZH2 mRNA

Retraction

Retracted: Effects of Fufang Banmao Capsule Associated with Sorafenib on Liver Function, Immune Status, Quality of Life Improvement, and Survival in Patients with Advanced Hepatocellular Carcinoma: A Retrospective Cohort Study

Computational Intelligence and Neuroscience

Received 1 August 2023; Accepted 1 August 2023; Published 2 August 2023

Copyright © 2023 Computational Intelligence and Neuroscience. This is an open access article distributed under the Creative Commons Attribution License, which permits unrestricted use, distribution, and reproduction in any medium, provided the original work is properly cited.

This article has been retracted by Hindawi following an investigation undertaken by the publisher [1]. This investigation has uncovered evidence of one or more of the following indicators of systematic manipulation of the publication process:

- (1) Discrepancies in scope
- (2) Discrepancies in the description of the research reported
- (3) Discrepancies between the availability of data and the research described
- (4) Inappropriate citations
- (5) Incoherent, meaningless and/or irrelevant content included in the article
- (6) Peer-review manipulation

The presence of these indicators undermines our confidence in the integrity of the article's content and we cannot, therefore, vouch for its reliability. Please note that this notice is intended solely to alert readers that the content of this article is unreliable. We have not investigated whether authors were aware of or involved in the systematic manipulation of the publication process.

Wiley and Hindawi regrets that the usual quality checks did not identify these issues before publication and have since put additional measures in place to safeguard research integrity.

We wish to credit our own Research Integrity and Research Publishing teams and anonymous and named external researchers and research integrity experts for contributing to this investigation.

The corresponding author, as the representative of all authors, has been given the opportunity to register their agreement or disagreement to this retraction. We have kept a record of any response received.

References

- [1] X. Lai and A. Wang, "Effects of Fufang Banmao Capsule Associated with Sorafenib on Liver Function, Immune Status, Quality of Life Improvement, and Survival in Patients with Advanced Hepatocellular Carcinoma: A Retrospective Cohort Study," *Computational Intelligence and Neuroscience*, vol. 2022, Article ID 6336107, 8 pages, 2022.

Research Article

Effects of Fufang Banmao Capsule Associated with Sorafenib on Liver Function, Immune Status, Quality of Life Improvement, and Survival in Patients with Advanced Hepatocellular Carcinoma: A Retrospective Cohort Study

Xianghong Lai and Anmei Wang 

Department of Integrated Chinese and Western Medicine Oncology, Hangzhou Cancer Hospital, Hangzhou 310002, China

Correspondence should be addressed to Anmei Wang; 171841049@masu.edu.cn

Received 2 June 2022; Revised 1 July 2022; Accepted 8 July 2022; Published 23 August 2022

Academic Editor: Dong Chen

Copyright © 2022 Xianghong Lai and Anmei Wang. This is an open access article distributed under the Creative Commons Attribution License, which permits unrestricted use, distribution, and reproduction in any medium, provided the original work is properly cited.

Objective. A case-control study was carried out to explore the influences of Fufang Banmao capsule (FBC) associated with sorafenib on liver function, immune status, life quality, and survival in patients with advanced hepatocellular carcinoma (HCC). **Methods.** During January 2019 to October 2021, in our hospital, the clinical data of 144 patients with advanced HCC treated were collected and measured retrospectively. The patients were cured with transcatheter arterial chemoembolization (TACE) in the control group, and the patients were cured with FBC associated with sorafenib in the observation group. The clinical effect, liver function index, humoral immunity index (IgG, IgM, and IgA), cellular immunity index (CD3, CD4, CD4/CD8, and CD8), tumor marker alpha-fetoprotein (AFP), carcinoembryonic antigen (CEA), carbohydrate antigen 199 (CA199), and life quality were compared before and after treatment. **Results.** Regarding the therapeutic effects, the observation group had CR4, PR 48, SD 18, and PD2; the total remission rate was 97.22%. There were 2 individuals with CR, 32 with PR, 22 with SD, and 16 with PD in the observation group. 77.79% of the total remissions occurred. The total remission rate in the observation group was higher, and the difference was statistically significant ($P < 0.05$). A comparison of liver function index levels before and after treatment was done. As a result of treatment, the levels of AST, ALT, and TBIL lessened. In addition, the levels of AST, ALT, and TBIL in the observation group were lower as well, and the difference was statistically significant ($P < 0.05$). In the control group, the levels of serum IgG, IgM, and IgA were lower after treatment than before treatment, but in the observation group, the levels were higher. Additionally, the levels of IgG, IgM, and IgA were higher, and the difference was statistically significant ($P < 0.05$). With regard to the cellular immune indexes, compared to those before treatment, the CD3, CD4 and CD4/CD8 of the patients in the control group were lower, CD8 was higher, while CD3, CD4, and CD4/CD8 in the observation group were higher, CD8 was lower, and the difference was statistically significant ($P < 0.05$). AFP and CA199 levels lessened after treatment in the control group, indicating that the markers were reducing tumor growth, and the difference was statistically significant ($P < 0.05$). The value of CEA lessened, and the difference was statistically significant ($P < 0.05$). There was a marked decrease in AFP, CEA, and CA199 serum levels in the observation group compared to those before treatment, and the difference was statistically significant ($P < 0.05$). After treatment, the contents of AFP, CEA, and CA199 in the observation group were lower, and the difference was statistically significant ($P < 0.05$). In terms of the life quality after treatment, 36 patients (50.00%) had augmented KPS score and 38 patients (52.78%) had augmented ZPS score in the observation group, which was noticeably higher compared to the control group, and the difference was statistically significant ($P < 0.05$). The progression-free survival (PFS) of the observation group was 31.67 months (95% confidence interval was 0.09657~0.3019), and the PFS of the control group was 26.73 months (95% confidence interval was 3.313~10.36). The PFS time of the observation group was noticeably longer, and the difference was statistically significant ($P < 0.05$). **Conclusion.** FBC associated with sorafenib can noticeably strengthen the clinical effect of patients with advanced HCC, enhance the liver function and immune function of patients with advanced HCC, accelerate the speed of rehabilitation and ease clinical symptoms, reduce the level of tumor markers, strengthen the quality of life, and prolong the survival time of patients.

1. Introduction

Hepatocellular carcinoma (HCC) is the most common malignant tumor in the world with an upward trend year by year. The number of people in China is the highest in the world. Cytoreductive surgery is not only the first choice for the treatment, but also one of the most effective methods [1, 2]. In 2008, there were 700 thousand new cases of HCC in the world, and the incidence rate was 16 trillion. The Asia-Pacific region has a high incidence of liver cancer. More than 75% of the global HCC patients are concentrated in the Asia-Pacific region, and most patients are related to hepatitis B virus (HBV) infection [3, 4]. HCC patients in China account for more than 50% of the entire Asia-Pacific region [5]. The incidence of liver cancer is 26.68/100000 in China (39.42/100000 for men and 13.6/for women), which is second only to lung cancer and ranks second to lung cancer [6, 7]. In these areas with high incidence of liver cancer, it is urgent to find an effective treatment.

At present, cytoreductive surgery of tumor is still the primary choice and the most effective treatment for liver cancer. With surgical resection of liver lesions, the 5-year survival rate of patients has reached 60%–70% [8]. However, less than 20% of the patients can be surgically resected. HCC is usually discovered at a late stage for most patients, such as intrahepatic diffuse implantation, vascular invasion, or distant organ metastasis; the effect of surgical treatment in these patients is poor. In addition, HCC is not sensitive to chemotherapy and radiotherapy. Therefore, the treatment of advanced HCC still lacks effective treatment, which is still a major problem.

The pathogenesis of HCC is extremely complex and still not clear. However, some studies have found that the pathogenic factors affecting HCC are closely related to the geographical environment [9]. Hepatitis virus infection is strongly connected to the development and occurrence of HCC in the Asia-Pacific region. About 70% of HCC patients have HBV infection and about 20% of patients have hepatitis C virus (HCV) infection [9, 10].

HCC is a malignant tumor with rich blood supply [10]. In December 2005, Sorafenib (trade name Nexavar) was permitted by the Food and Drug Administration (FDA) of the US as a first-line drug of cancer and it was listed in China the next year. So far, Sorafenib is still the only first-line drug approved by many countries around the world for unresectable advanced HCC [11, 12]. Sorafenib is an oral pol- ykinase inhibitor that exerts its antitumor effect by suppressing tumor cell proliferation and angiogenesis. Intracellular signal transduction pathway Raf/MEK/ERK and extracellular VEGFR and PDGFR have been proved to be closely related to the occurrence of HCC. The latest study found that Sorafenib inhibits the expression of MMP-2 and Ki-67 by upregulating the expression of PS3 gene and inhibiting the expression of FoxM1 (ForkheadboxM1) gene, thus blocking the proliferation of HCC cells and invasion of surrounding organs [13, 14]. Sorafenib can interfere with the

above cellular signal transduction pathways, play a direct antitumor role in inhibiting the activities of c-Raf (Raf-1) and B-Raf, and play a dual antitumor role in antagonizing VEGFR-1,2,3 inhibiting the formation of tumor-related neovascularization.

Traditional Chinese medicine (TCM) preparation, especially TCM injection, is a great achievement in the field of medicine in China. However, its safety and efficacy have been widely concerned by the medical community since it was developed and listed on the market [15]. There has been more research suggesting that the application of TCM can noticeably reduce the incidence of radiation therapy and chemotherapy side effects and can enhance the cellular immunity and patients' life quality. Several TCM preparations have a synergistic effect on chemotherapy, which can not only prolong the duration of patients' survival, but also reduce the risk of metastasis and recurrence. Moreover, daily chemotherapy can increase the objective efficiency of chemotherapy. The TCM Fufang Banmao capsule (FBC), which is composed of Mylabris, ginseng, astragalus, *Acanthopanax senticosus*, mulberry, *Scutellaria barbata*, *Rhizoma Curcuma*, *Cornus officinalis*, *Ligustrum lucidum*, bear bile powder, and licorice, has the effect of breaking blood stasis and attacking white blood cells and phagocytic sores. Studies have indicated that in addition to inhibiting the growth of stem cells and apoptosis liver cancer cells, cantharidin also has a strong toxic effect, causing organ poisoning as well as necrosis [15, 16]. During January 2019 to October 2021, in our hospital, this study focuses on 144 patients with advanced HCC treated, which are reported as follows.

2. Patients and Methods

2.1. General Information. During January 2019 to October 2021, in our hospital, the clinical data of 144 patients with advanced HCC treated were collected and measured retrospectively. For the control group, the patients received TACE, while for the observation group, they received FBC plus sorafenib. There were 30 to 75 years of age in the control group and 31 to 76 years of age in the observation group. The control group average age was 52.18 ± 2.54 , while the observation group average age was 52.34 ± 8.61 . The general data were not statistically noticeable ($P > 0.05$). The Medical Ethics Association authorized this study, and all patients noticed informed consent forms.

Inclusion criteria include the following: (1) abdominal CT examination, a large amount of fluid in the abdominal cavity; (2) certain abilities for understanding, expressing themselves verbally, and writing are present in patients and their families; (3) take part in the study and sign the informed consent form voluntarily and follow the principle of randomization; and (4) patients without heart, liver, and kidney vital organ disorders.

Exclusion criteria include the following: (1) mental illness patients or family members, or those accepting treatment in connection with mental illness; (2) patients with

serious organ diseases; (3) exclusion of patients with KPS <70; (4) exclusion of patients with endocrine and metabolic diseases, such as severe diabetes, hyperthyroidism, and cardio-cerebrovascular diseases; and (5) exclusion of patients with a history of external injury and major operation within 1 month before treatment.

2.2. Treatment Methods. In the control group, patients were cured with liver TACE regimen. Seldinger puncture method, positive digital subtraction angiography (DSA), was performed after successful puncture; the location, quantity, and size of the tumor were accurately located; the guide wire catheter was inserted into the tumor feeding artery; and cisplatin and epirubicin were infused. The drug dose was used according to the individual condition of the patient. After operation, the guide wire was withdrawn, and the intervention point was pressed to stop bleeding. In the observation group, the patients were cured with FBC associated with Sorafenib and FBC orally (Guizhou Yibai Pharmaceutical Co., Ltd., Chinese medicine Z52020238), 3 tablets per time, twice a day. Oral administration during the intermission of chemotherapy: Each cycle was taken continuously for 21 days for 2 cycles as a course of treatment. Sorafenib (German Bayer Pharmaceuticals, imported Drug Registration no.: H20110599) 400 mg/times, twice a day. The subjects took the drug continuously and were originally scheduled to stop or reduce the dose when the patient developed a disease or could not tolerate side effects during treatment. After stopping or reducing the dose of sorafenib, the unified mode of administration was restored after the symptoms of the patients were enhanced. During chemotherapy, patients were given routine stomach protection, liver protection, immunity enhancement drugs, and early nutritional support treatment. The curative effects were evaluated at the end of one course of treatment.

2.3. Observation Index

2.3.1. Evaluation Standard of Curative Effect. The response assessment criteria in solid tumors (RECIST) were used as evaluation criteria, complete response (CR), partial response (PR), stable disease (SD), and progressive disease (PD) [17]. CR: No new lesions appeared after the lesions disappeared; PR: More than 30% less tumor diameter was measured in the trial phase compared with the baseline phase; SD: Between PR and PD; PD: A greater than 20% increase in maximum and minimum tumor diameters or the appearance of new lesions occurred as compared with the baseline phase. Objective response rate (ORR): $ORR = (CR + PR) / \text{total number} \times 100\%$. Disease control rate (DCR): $DCR = (CR + PR + SD) / \text{total population} \times 100\%$. A CT examination was performed on all patients before joining the group, and a final CT examination was conducted after the treatment had ended. The same researcher enhanced the baseline and tumor evaluation during the treatment period.

2.3.2. Liver Function Index Level. Before and after treatment, fasting venous blood of 3 mL was harvested, centrifuged 10 min, $3000 \text{ r} \cdot \text{min}^{-1}$, serum was separated, and serum

levels of glutamic oxaloacetic transaminase, glutamic pyruvic transaminase, and total bilirubin were examined by enzyme linked immunosorbent assay (ELISA) (Beckman Coulter Co., Ltd.).

2.3.3. Immune Function Index Level. The levels of serum CD3+, CD4+, CD8+, and NK before and after treatment were determined by Attune NxT acoustic focused flow cytometry and its supporting reagents, and CD4+/CD8+ was measured. The levels of IgM, IgG, and IgA in serum were measured by immune turbidimetry. The kits are all produced by Redd Company of the United States, and the testing operations are conducted in terms of the standards of the instructions, controlling intrabatch differences <10% and interbatch differences <15%.

2.3.4. Tumor Marker Level. The venous blood of 5 ml was taken before and after one course of treatment, and the blood vessels were collected in vacuum. At room temperature, 10 min was centrifuged with 4000 r/min, and the upper serum was taken for the determination of AFP, CEA, and CA199 in serum.

2.3.5. Quality of Life Score. The quality of life was evaluated by functional status score (Karnofsky, KPS) and physical status score (Zubrod-ECOG-WHO, ZPS).

2.3.6. Survival Follow-Up. Patients were followed up by outpatient clinic and telephone, and the progression-free survival (PFS) from the beginning of treatment to the time of tumor progression or death was calculated.

2.4. Statistical Analysis. In order to process data and create charts, SPSS 22.0 statistical software is used; measurement data are presented as mean \pm standard deviation ($\bar{x} \pm s$), and *t*-tests are used for comparison; counting data is presented by the number of patients and rate (%), and comparison is done by χ^2 test. Survival curves were measured by Kaplan–Meier methods, and multivariate analysis by logistic regression analysis; a statistical difference was observed, and $P < 0.05$ indicated that the difference between groups is statistically significant.

3. Results

3.1. Comparison of the Balance of Basic Data of Research Objects. Our first step was to compare the balance of basic data. The average age, body mass index, sex, age distribution, clinical stage, degree of differentiation, and metastasis site showed no noticeable difference, and the difference was statistically significant ($P < 0.05$). In Table 1, all data results are presented.

3.2. Comparison of Clinical Efficacy. We compared the therapeutic effects. In the observation group, there were CR4 ($n = 48$), PR ($n = 48$), SD ($n = 18$), and PD2 ($n = 18$). The total

TABLE 1: Comparison of general balance between groups (%).

Related factors	Observation group ($n = 72$)	Control group ($n = 72$)	t/χ^2	P
Average age (years)	52.34 ± 8.61	52.18 ± 2.54	0.151	> 0.05
Body mass index (kg/m^2)	24.78 ± 2.33	23.69 ± 2.56	2.672	> 0.05
Gender			1.039	> 0.05
Male	40 (55.56)	46 (63.89)		
Female	32 (44.44)	26 (36.11)		
Age distribution			0.516	> 0.05
30~44 years	18 (25.00)	16 (22.22)		
45~59 years	22 (30.56)	26 (36.11)		
60~75 years	32 (44.44)	30 (41.67)		
Clinical staging			0.113	> 0.05
III B period	40 (55.56)	42 (58.33)		
IV period	32 (44.44)	30 (41.67)		
Degree of differentiation			0.508	> 0.05
High differentiation	22 (30.56)	20 (27.78)		
Middle differentiation	40 (55.56)	44 (61.11)		
Low differentiation	10 (13.89)	8 (11.11)		
Transfer site			0.154	> 0.05
Lymph node	56 (77.78)	54 (75.00)		
Bone	16 (22.22)	18 (25.00)		

remission rate was 97.22%. In the control group, there were 2 individuals of CR, 32 of PR, 22 of SD, and 16 of PD. The total remission rate was 77.79%. The total remission rate of the observation group was higher, and the difference was statistically significant ($P < 0.05$). In Figure 1, all data results are presented.

3.3. Comparison of Liver Function Indexes. Before and after treatment, we compared the level of liver function index, with no noticeable difference before treatment, and the difference was statistically significant ($P < 0.05$). After treatment, the levels of AST, ALT, and TBIL lessened. Compared between the two groups, the levels of AST, ALT, and TBIL in the observation group were lower, and the difference was statistically significant ($P < 0.05$). In Table 2, all data results are presented.

3.4. Comparison of Humoral Immune Indexes before and after Treatment. Before and after treatment, we compared the level of humoral immunity, with no noticeable difference in the levels of IgG, IgM, and IgA before treatment, and the difference was statistically significant ($P < 0.05$). Compared to those before treatment, the serum levels of IgG, IgM, and IgA in the control group were lower, while in the observation group, they were higher, and in the observation group, they were higher compared to the control group, and the difference was statistically significant ($P < 0.05$). In Table 3, all data results are presented.

3.5. Comparison of Cellular Immune Indexes. We compared the cellular immune indexes. Before treatment, there was no noticeable difference in CD3, CD4, and CD4/CD8, and the difference was statistically significant ($P < 0.05$). After treatment, CD3, CD4, and CD4/CD8 in the control group lessened and CD8 augmented, while CD3, CD4, and CD4/

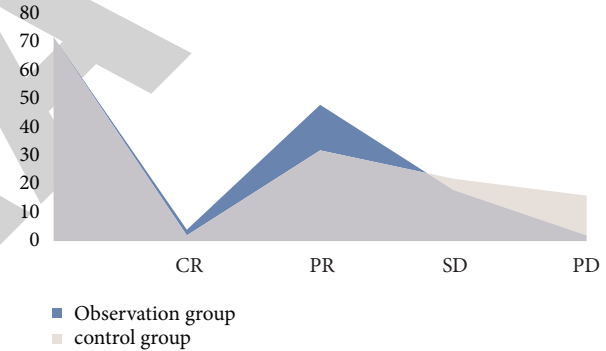


FIGURE 1: Comparison of clinical efficacy. The blue color refers to the observation group and the gray color refers to the control group.

CD8 in the observation group augmented, CD8 was lower than that before treatment, and CD3, CD4, and CD4/CD8 in the observation group were higher, while CD8 was lower, and the difference was statistically significant ($P < 0.05$). All results are indicated in Table 4.

3.6. Comparison of Tumor Markers. We compared the levels of tumor markers. There was no noticeable difference in serum AFP, CEA, and CA199 levels before treatment, and the difference was statistically significant ($P < 0.05$). After treatment, the contents of AFP and CA199 in the control group lessened compared with those before treatment, and the difference was statistically significant ($P < 0.05$). The value of CEA lessened, and the difference was statistically significant ($P < 0.05$). The serum levels of AFP, CEA, and CA199 in the observation group were noticeably lower than those before treatment, and the difference was statistically significant ($P < 0.05$). After treatment, the contents of AFP,

TABLE 2: Comparison of liver function indexes between groups ($\bar{x} \pm s$).

Grouping	N	AST (U/L)		ALT (U/L)		TBIL ($\mu\text{mol/L}$)	
		Before treatment	After treatment	Before treatment	After treatment	Before treatment	After treatment
Observation group	72	85.36 \pm 1.25	41.85 \pm 1.04 ^a	95.14 \pm 1.32	54.48 \pm 1.16 ^a	102.43 \pm 1.18	62.58 \pm 1.07 ^a
Control group	72	85.75 \pm 1.43	58.12 \pm 1.18 ^b	95.48 \pm 1.25	63.87 \pm 1.04 ^b	102.58 \pm 1.12	74.66 \pm 1.15 ^b
t-value		1.742	87.772	1.587	51.142	0.782	65.255
P-value		> 0.05	< 0.05	> 0.05	< 0.05	> 0.05	< 0.05

Note. Compared to observation group before treatment, ^a $P < 0.05$. Compared to control group before treatment, ^b $P < 0.05$.

TABLE 3: Comparison of humoral immune indexes between groups ($\bar{x} \pm s$, g/L).

Grouping	N	IgA		IgM		IgG	
		Before treatment	After treatment	Before treatment	After treatment	Before treatment	After treatment
Observation group	72	2.53 \pm 0.18	2.87 \pm 0.23 ^a	1.83 \pm 0.16	2.27 \pm 0.15 ^a	14.66 \pm 1.34	16.37 \pm 1.25 ^a
Control group	72	2.64 \pm 0.26	2.23 \pm 0.31 ^b	1.82 \pm 0.22	1.53 \pm 0.21 ^b	14.35 \pm 1.46	11.24 \pm 0.66 ^b
t-value		2.952	14.069	0.312	24.331	1.327	30.795
P-value		> 0.05	< 0.05	> 0.05	< 0.05	> 0.05	< 0.05

Note. Compared to observation group before treatment, ^a $P < 0.05$. Compared to control group before treatment, ^b $P < 0.05$.

TABLE 4: Comparison of cellular immune indexes between groups ($\bar{x} \pm s$).

Grouping	N	CD4		CD8		CD3		CD4/CD8	
		Before treatment	After treatment	Before treatment	After treatment	Before treatment	After treatment	Before treatment	After treatment
Observation group	72	36.31 \pm 3.38	40.85 \pm 4.14 ^a	28.45 \pm 2.23	24.45 \pm 2.67 ^a	59.64 \pm 4.35	65.58 \pm 6.25 ^a	1.23 \pm 0.13	1.48 \pm 0.12 ^a
Control group	72	36.37 \pm 3.76	31.45 \pm 3.05 ^b	28.23 \pm 3.22	30.35 \pm 2.83 ^b	59.48 \pm 4.17	56.23 \pm 5.24 ^b	1.21 \pm 0.15	1.11 \pm 0.15 ^b
t-value		0.101	15.511	0.477	12.867	0.199	9.728	0.855	16.344
P-value		> 0.05	< 0.05	> 0.05	< 0.05	> 0.05	< 0.05	> 0.05	< 0.05

Note. Compared to observation group before treatment, ^a $P < 0.05$. Compared to control group before treatment, ^b $P < 0.05$.

CEA, and CA199 in the observation group were lower, and the difference was statistically significant ($P < 0.05$). In Table 5, all data results are presented.

3.7. Comparison of Life Quality after Treatment. We compared the life quality after treatment. There was no noticeable difference in the number of patients with augmented KPS and ZPS scores before treatment, and the difference was statistically significant ($P < 0.05$). After treatment, KPS score augmented in 36 individuals (50.00%) and ZPS score augmented in 38 (52.78%) in the observation group, which was noticeably higher, and the difference was statistically significant ($P < 0.05$). In Table 6, all data results are presented.

3.8. The Survival Follow-Up Outcome. We compared the outcome of survival follow-up. The PFS of the observation group was 31.67 months (95% CI 0.09657~0.3019) and the control group PFS was 26.73 months (95% CI 3.313~10.36). The progression-free survival time of the observation group was noticeably longer, and the difference was statistically significant ($P < 0.05$). In Figure 2, all data results are presented.

4. Discussion

HCC is a kind of liver malignant tumor derived from epithelial tissue, which is highly malignant and invasive. HCC

is the most frequent type of primary liver cancer, accounting for 91.5%, and it ranks sixth among all types of cancers worldwide. HCC is the third in tumor-related deaths after lung and gastric cancers [18, 19]. However, how to treat liver cancer is difficult, and the prognosis is poor. The annual recurrence rate of surgical resection is high. Most patients are found at the late stage; thus, the treatment becomes more difficult, resulting in worse prognosis.

Sorafenib is an oral polykinase inhibitor to treat advanced unresectable liver cancer [20]. Sorafenib is so far the first and only systemically targeted drug approved by multiple national drug inspection authorities for advanced liver cancer [11]. Sorafenib inhibits hepatoma cell proliferation, metastasis, and tumor neovascularization mainly by inhibiting Raf-1 and a variety of tyrosine kinase receptors, including VEGFR-1/-2/-3, PDGFR- β , c-Kit, FLT-3, and RET. After the first oral administration of 400 mg bid sorafenib, the maximum plasma concentration (C_{\max}) was 2.3–3.0 $\mu\text{g/ml}$, and the peak time was generally 1.0–12.3 hours. After continuous administration of sorafenib, the steady-state plasma concentration was reached in about 7 days [11, 21]. Sorafenib has high bioavailability; however, a high-fat diet can reduce the bioavailability of sorafenib by about 29%. Therefore, it is recommended that patients take sorafenib on an empty stomach or 2 hours after meals to ensure maximum absorption. The binding rate of sorafenib to human plasma protein was high, and the in vitro

TABLE 5: Comparison of tumor markers between groups ($\bar{x} \pm s$).

Grouping	N	AFP (pg/ml)		CEA (ng/L)		CA199 (ng/L)	
		Before treatment	After treatment	Before treatment	After treatment	Before treatment	After treatment
Observation group	72	197.08 \pm 17.45	89.93 \pm 10.24 ^a	36.06 \pm 6.15	19.78 \pm 3.05 ^a	86.54 \pm 13.58	53.74 \pm 9.28 ^a
Control group	72	201.18 \pm 18.03	95.31 \pm 11.87 ^b	35.58 \pm 5.93	27.47 \pm 3.41 ^b	85.67 \pm 14.13	72.84 \pm 10.46 ^b
t-value		1.387	2.912	0.477	14.263	0.377	11.590
P-value		> 0.05	< 0.05	> 0.05	< 0.05	> 0.05	< 0.05

Note. Compared to observation group before treatment, ^a $P < 0.05$. Compared to control group before treatment, ^b $P < 0.05$.

TABLE 6: Comparison of quality of life between groups (n/%).

Grouping	N	KPS			ZPS		
		Raise	Stable	Drop	Raise	Stable	Drop
Observation group	72	22 (30.56)	36 (50.00)	14 (19.44)	23 (31.94)	35 (48.61)	14 (19.44)
Control group	72	36 (50.00)	23 (31.94)	13 (18.06)	38 (52.78)	25 (34.72)	9 (12.50)
t-value			6.281			6.442	
P-value			< 0.05			< 0.05	

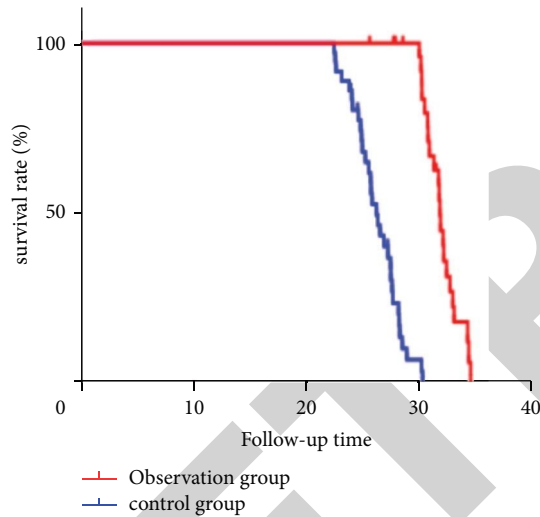


FIGURE 2: Comparison of survival follow-up outcomes. The red line refers to the observation group and the blue line refers to the control group.

experiment showed that the binding rate of sorafenib to human plasma protein was 99.5%. Sorafenib is cleared through liver metabolism and bile excretion [21]. Sorafenib is oxidized and metabolized by cytochrome P450 (CYP3A4) in the liver, and then 15% of the oxidative metabolites bind to glucuronide under the action of uridine diphosphate glucanoyl transferase 1A9. Studies have indicated that after oral administration of 100 mg sorafenib, 77% are excreted through feces and 19% through urine [22]. The elimination half-life of sorafenib is longer, up to 20–27 hours. The clinical efficacy of sorafenib when treating HCC has been confirmed by two phase III, randomized, double-blind, controlled, two large phase II clinical studies [22, 23]. Both SHARP and Oriental confirmed that sorafenib was effective and accurate when treating patients with advanced HCC,

and the adverse reactions were mild [23]. After that, Korean scholars reviewed and studied the efficacy of sorafenib when treating advanced HCC patients with extrahepatic metastasis. There exhibited a median survival time of 9.6 months and a median period when the disease progressed of 2.5 months. Some scholars conducted a similar retrospective study, showing that, after sorafenib treatment, the median survival time of advanced HCC patients was 9.9 months, and the median time of disease progression was 3.8 months [24]. People who benefit from sorafenib include those with multiple intrahepatic cancer foci, lymph node metastasis, vascular invasion, and extrahepatic distant organ metastasis [25]. Although the efficacy of sorafenib when treating late stage is noticeable, the emergence of drug resistance to sorafenib has become a major factor hindering the further prolongation of the overall survival time of patients. In addition, the side effects caused by sorafenib, HBV infection, liver background, and other factors caused the difference in the therapeutic effect of sorafenib. Taken together, all these studies have confirmed that sorafenib has a noticeable and positive effect on advanced HCC and can noticeably prolong the PFS time and total survival time of patients with advanced HCC. During the treatment process, the adverse reaction sorafenib is mild, tolerable without serious fatal reaction occurrence.

The common side effects of sorafenib are diarrhea, weight loss, skin reaction of hands and feet, hair loss, and hoarseness [25]. Most of them were mild adverse reactions of grade CTCAE1 or grade 2, which could be relieved after reduction or symptomatic treatment, and the fatal adverse reactions were very few. SHARP and Oriental studies did not report the fatal adverse reactions of sorafenib when treating advanced HCC [22, 23]. Zhang et al. found that basal concentrations of angiopoietin (Ang2) and vascular endothelial growth factor (VEGF) are independent predictors of survival and can evaluate the sensitivity of HCC patients to sorafenib [26]. However, this method is difficult to monitor and carry out in clinical work. Some studies have found that early hand and foot skin adverse reactions are an

independent prognostic factor of survival, and diarrhea can also be used as a predictor of survival [26]. Hand and foot skin reactions and diarrhea are also the most common adverse reactions when treated by sorafenib.

The TCM FBC, which is composed of Mylabris, ginseng, astragalus, *Acanthopanax senticosus*, Sangleng, *Scutellaria barbata*, Rhizoma Curcumae, *Cornus officinalis*, *Ligustrum lucidum*, bear bile powder, and licorice, has the effect of breaking blood stasis and attacking white blood cells and phagocytic sores. Its main ingredients include Mylabris, which belongs to the southern large Mylabris or yellow-black small Mylabris of turniaceae insects, can break blood stasis, attack toxin and phagocytic sores, and has the effect of anticancer, increasing white blood cells, and immune enhancement. Some previous studies have indicated that cantharidin can inhibit the growth of stem cells and accelerate the apoptosis of liver cancer cells, but it also has a strong toxic effect, causing organ poisoning and even necrosis [26, 27]. Astragalus membranaceus, which belongs to the dried root of Astragalus mongolicus or Radix Astragali, a perennial plant of Leguminosae, has the effects of replenishing qi and promoting yang, benefiting the body, promoting water and detumescence, detoxification, and muscle formation. Cancer cells are sensitive to chemotherapy due to astragalus saponins, its main component, which inhibits their growth [27]. The study also found that total astragalus saponins can inhibit the proliferation of mouse hepatoma H22 tumor cells, and its mechanism may be relevant to the enhancement of immune function [28]. Ginseng, the dried root of Panax ginseng, a perennial herb of Araliaceae, has the effects of tonifying vital energy, spleen and lung, and invigorating the mind. It has been found that ginsenosides can effectively reverse the multidrug resistance of HCC cells, and its mechanism may be related to the decrease of MDR1 and P-gp expression. There are also research findings; ginseng can successfully enhance the immunity of patients with liver cancer and reduce the incidence of adverse reactions [29]. *Acanthopanax senticosus*, Sangleng, *Scutellaria barbata*, zedoary, *Cornus officinalis*, *Ligustrum lucidum*, bear bile powder, licorice, and other drugs also have the effects of heat-clearing and detoxification, breaking blood stasis, tonifying and tonifying qi, and can enhance the clinical effect of chemotherapy in patients with liver cancer. From the aspect of TCM theory, FBC has comprehensive prescription and reasonable compatibility. It can promote the pathogenesis of qi stagnation, blood stasis, phlegm coagulation and dampness toxin by breaking blood stasis, attacking toxin and phagocytic sores, so that the functions of viscera, qi and blood and body fluid can be restored, and the balance between good and evil of the body can be restored. Modern medicine believes that FBC can promote the body's non-specific and specific immune function, strengthen the body's immune ability, noticeably increase the tumor inhibition rate, and resist leukopenia caused by chemotherapy.

In this study, FBC associated with sorafenib was effective when treating patients with advanced HCC. It was found that the total remission rate of the observation group was higher. The levels of AST, ALT, and TBIL in the observation group were lower. After treatment, the levels of IgG, IgM,

and IgA in the observation group were higher and the levels of CD3, CD4, and CD4/CD8 in the observation group were higher, while CD8 was lower. After treatment, the contents of AFP, CEA, and CA199 in the observation group were lower. KPS score augmented in 36 (50.00%) and ZPS score augmented in 38 (52.78%) in the observation group, which was noticeably higher after treatment. The progression-free survival time in the observation group was noticeably longer. Our results have shown that FBC associated with sorafenib can effectively inhibit the proliferation of tumor cells, enhance the immunity of patients, prolong their survival time, and improve their life qualities. There are some limitations in this study. First, the sample size of this study is not large, and it is a single-center study, so bias is inevitable. In future research, we will carry out multicenter, large-sample prospective studies, or more valuable conclusions can be drawn.

Conclusively, FBC associated with sorafenib has good clinical effect on patients with advanced HCC, which can noticeably enhance the quality of life of patients with liver cancer, inhibit the proliferation of tumor cells, enhance immune function and liver function, and promote the survival rate. However, for the longer-term effect, further clinical observation and follow-up are needed.

Data Availability

The datasets used and analyzed during the current study are available from the corresponding author upon reasonable request.

Conflicts of Interest

The authors declare that they have no conflicts of interest regarding the publication of this paper.

References

- [1] J. K. Heimbach, L. M. Kulik, R. S. Finn et al., "AASLD guidelines for the treatment of hepatocellular carcinoma," *Hepatology*, vol. 67, no. 1, pp. 358–380, 2018.
- [2] K. A. McGlynn, J. L. Petrick, and H. B. El-Serag, "Epidemiology of hepatocellular carcinoma," *Hepatology*, vol. 73, no. S1, pp. 4–13, 2021.
- [3] J. Hartke, M. Johnson, and M. Ghabril, "The diagnosis and treatment of hepatocellular carcinoma," *Seminars in Diagnostic Pathology*, vol. 34, no. 2, pp. 153–159, 2017.
- [4] L. Kulik and H. B. El-Serag, "Epidemiology and management of hepatocellular carcinoma," *Gastroenterology*, vol. 156, no. 2, pp. 477–491. e1, 2019.
- [5] A. J. Craig, J. Von Felden, T. Garcia-Lezana, S. Sarcognato, and A. Villanueva, "Tumour evolution in hepatocellular carcinoma," *Nature Reviews Gastroenterology & Hepatology*, vol. 17, no. 3, pp. 139–152, 2020.
- [6] European Association For The Study Of The Liver, "EASL clinical practice guidelines: management of HCC," *Journal of Hepatology*, vol. 69, no. 1, pp. 182–236, 2018.
- [7] R. K. Kelley and T. F. Greten, "Hepatocellular carcinoma — origins and outcomes," *New England Journal of Medicine*, vol. 385, no. 3, pp. 280–282, 2021.

Retraction

Retracted: Effect of Comprehensive Nursing on the Recovery of Gastrointestinal Function in Patients Undergoing Abdominal Operation

Computational Intelligence and Neuroscience

Received 25 July 2023; Accepted 25 July 2023; Published 26 July 2023

Copyright © 2023 Computational Intelligence and Neuroscience. This is an open access article distributed under the Creative Commons Attribution License, which permits unrestricted use, distribution, and reproduction in any medium, provided the original work is properly cited.

This article has been retracted by Hindawi following an investigation undertaken by the publisher [1]. This investigation has uncovered evidence of one or more of the following indicators of systematic manipulation of the publication process:

- (1) Discrepancies in scope
- (2) Discrepancies in the description of the research reported
- (3) Discrepancies between the availability of data and the research described
- (4) Inappropriate citations
- (5) Incoherent, meaningless and/or irrelevant content included in the article
- (6) Peer-review manipulation

The presence of these indicators undermines our confidence in the integrity of the article's content and we cannot, therefore, vouch for its reliability. Please note that this notice is intended solely to alert readers that the content of this article is unreliable. We have not investigated whether authors were aware of or involved in the systematic manipulation of the publication process.

Wiley and Hindawi regrets that the usual quality checks did not identify these issues before publication and have since put additional measures in place to safeguard research integrity.

We wish to credit our own Research Integrity and Research Publishing teams and anonymous and named external researchers and research integrity experts for contributing to this investigation.


The corresponding author, as the representative of all authors, has been given the opportunity to register their agreement or disagreement to this retraction. We have kept a record of any response received.

References

- [1] L. Xiang, W. Liu, and Y. Jin, "Effect of Comprehensive Nursing on the Recovery of Gastrointestinal Function in Patients Undergoing Abdominal Operation," *Computational Intelligence and Neuroscience*, vol. 2022, Article ID 1179321, 10 pages, 2022.

Research Article

Effect of Comprehensive Nursing on the Recovery of Gastrointestinal Function in Patients Undergoing Abdominal Operation

Lanlan Xiang,¹ Wei Liu,² and Yuanyuan Jin ²

¹Pediatric Surgery Department of Gastrointestinal Surgery, The First People's Hospital, Jingmen, Hubei Province, China

²Department of Gastroenterology, The First People's Hospital, Jingmen, Hubei Province, China

Correspondence should be addressed to Yuanyuan Jin; 18407244@masu.edu.cn

Received 8 June 2022; Revised 7 July 2022; Accepted 11 July 2022; Published 21 August 2022

Academic Editor: Dong Chen

Copyright © 2022 Lanlan Xiang et al. This is an open access article distributed under the Creative Commons Attribution License, which permits unrestricted use, distribution, and reproduction in any medium, provided the original work is properly cited.

Objective. The objective is to explore the effect of comprehensive nursing on the recovery of gastrointestinal function in patients undergoing an abdominal operation. **Methods.** Sixty patients undergoing abdominal surgery in our hospital from January 2019 to April 2021 were enrolled. The patients were arbitrarily assigned into control group and research group. The former group received routine nursing and the latter group received comprehensive nursing. Nursing satisfaction, gastrointestinal function, POMS-SF score, nutrition risk score, incidence of adverse reactions, and quality of life scores were compared. **Results.** The nursing satisfaction of the research group was higher than that of the control group, and the difference between the groups was statistically significant ($P < 0.05$). In terms of gastrointestinal function, the anal exhaust time eating time defecation time and bowel sound recovery time in the research group were significantly lower than those in the control group, and the difference between the groups was statistically significant ($P < 0.05$). In terms of POMS-SF score, the scores of tension-anxiety, depression-depression, fatigue-dullness, anger-hostility, and confusion-confusion in the research group were lower than those in the control group, while the energy-vitality score was higher than that in the control group, and the difference between the groups was statistically significant ($P < 0.05$). There was no significant difference in nutritional risk score among patients before nursing ($P > 0.05$); after nursing, the nutritional risk score decreased. Compared between the two groups, the nutritional risk score of the research group was lower when compared to the control group at 3 days, 5 days, and 7 days after nursing, and the difference between the groups was statistically significant ($P < 0.05$). In terms of the incidence of adverse reactions, the incidence of adverse reactions such as incision effusion, incision infection, incision dehiscence, and anastomotic leakage in the research group was lower when compared to the control group, and the difference between the groups was statistically significant ($P < 0.05$). Regarding quality of life scores, before nursing, there exhibited no significant difference of patients ($P > 0.05$); after nursing, the quality of life scores of patients decreased. Compared with the two groups, the physical function, psychological function, social function, and healthy self-cognition scores of the research group were all lower compared to the control group, and the difference between the groups was statistically significant ($P < 0.05$). **Conclusion.** Abdominal surgery patients received comprehensive care, which improved their mental health, reduced anxiety and depression levels, relieved fatigue and dullness, improved energy and vitality, and enhanced their overall mood. Meanwhile, it can also promote the recovery of gastrointestinal function in patients and reduce the incidence of adverse reactions.

1. Introduction

After the diagnosis of patients undergoing abdominal surgery, there are often a variety of bad emotions that affect the patient's eating, resulting in insufficient nutritional

intake and low spirits; the operation will cause harm to the body, which is bound to consume a lot of nutrition, thus affecting the recovery of gastrointestinal function [1]. Gastroparesis is one of the common complications of abdominal surgery, especially after radical gastrectomy and

pancreaticoduodenectomy [1]. Most of it occurs 1 to 2 days after the open diet or when the patient transitions from a liquid diet to a semi-fluid diet. The main symptoms are fullness or upper abdominal compression, no severe abdominal pain, vomiting a small amount to a large amount of gastric juice, containing bile; the symptoms can be significantly relieved after vomiting. Once it occurs after the operation, it often lasts for weeks, months, or even longer, so it is extremely difficult for clinical diagnosis and treatment. Due to different diagnostic criteria, the incidence of gastroparesis reported in some literature is 0.3% to 10% [2]. The incidence of gastroparesis after gastrectomy can be as high as 4.7% [3]. The etiology of gastroparesis after abdominal surgery is not yet clear, which may be related to the following factors: (1) whether there is gastric outflow tract obstruction before surgery: generally, patients with gastric outflow tract obstruction before surgery are more likely to develop postoperative gastric outflow tract obstruction than those without obstruction. more chance of gastroparesis; (2) whether there is an underlying disease that affects gastrointestinal motility: such as diabetes, hypothyroidism, scleroderma, etc.; (3) the way of reconstructing the digestive tract after gastrectomy: patients who underwent Billroth II anastomosis were more the incidence of gastroparesis is higher; and (4) the scope and degree of intraoperative lymph node dissection: the wider and more thorough the lymph node dissection, the more chance of gastroparesis. Basic studies have found that the possible mechanisms of gastroparesis are as follows [4, 5]. The main results are as follows: (1) surgical trauma itself activates the sympathetic nervous system and enhances the inhibitory activity of gastrointestinal sympathetic nerve in vivo. The activated sympathetic nerve fibers can not only inhibit the excited neurons of the gastrointestinal plexus but also inhibit gastric motility by directly binding the catecholamines released from the sympathetic nerve endings to the α and β receptors on the membrane of gastric smooth muscle cells, then inhibit the contraction of smooth muscle cells; (2) if the stomach is operated on, it will damage the vagus nerve or destroy the structural integrity of the stomach, resulting in an imbalance of gastric emptying; and (3) the secretion, metabolism, and regulation of gastrointestinal hormones are also affected to a certain extent [4].

With the progress of modern surgical theory, the concept of rapid rehabilitation surgery has gradually formed and changed the traditional model of gastrointestinal surgery since the beginning of this century, overturning many practices that are accustomed to, but have no evidence-based medicine [5]. Among them, the abandonment of nasogastric tube before and after the operation and the encouragement of early diet after operation attract people's attention. From past experience, surgeons generally take it for granted that nasogastric tubes are used in gastrointestinal surgery, in addition to maintaining gastric emptying during anesthesia and reducing the incidence of aspiration during operation. It can also promote the recovery of postoperative gastrointestinal function and reduce the occurrence of nausea, vomiting, abdominal distension, and pulmonary complications.

However, current clinical evidence shows that patients who do not routinely use nasogastric tubes recover intestinal function earlier and have a lower incidence of pneumonia [6–8]. The concept of rapid rehabilitation surgery also requires that patients be given a small amount of water and an open liquid diet on the day after operation, and gradually increase the amount and transition to a normal diet within a relatively short period of time after operation, and stop intravenous rehydration as soon as possible [9]. However, there is a contradiction between the renewal of modern surgical ideas and clinical reality. On the one hand, the number of elderly patients and severe patients after major surgery increased, the recovery of gastrointestinal function in these groups was slow, and the possibility of gastroparesis was remarkably higher compared to normal patients. Aspiration can cause reflux of gastric contents, which often leads to aspiration pneumonia and can be life-threatening [10]. On the other hand, rapid rehabilitation surgery requires early eating without a gastrointestinal decompression tube from the point of view of reducing perioperative trauma and stress, promoting early rehabilitation, shortening hospitalization days, and saving hospitalization costs. Therefore, how to identify the high-risk population of gastroparesis after abdominal surgery and take necessary measures to reduce the risk of reflux aspiration has deeper clinical significance than before. Comprehensive nursing intervention can be traced back to the middle of the 19th century; the United States took the lead in putting forward case management (CM), that is, managing patients as a whole. After a century of development, the term integrated management was formally formed in the middle of the 20th century, from which comprehensive nursing was developed and integrated with the thinking mode of the nursing procedure [11]. Comprehensive nursing is a new way of clinical nursing intervention, which is a perfect combination of nursing measures implemented by nurses in the process of holistic and comprehensive nursing for patients, in order to achieve an auxiliary method for the treatment of diseases [12]. Comprehensive nursing intervention needs to use multi-disciplinary knowledge to deal with the problems in clinical practice, through case assessment, planning, implementation, feedback, and adjustment, take appropriate nursing measures to meet the needs of patients. At present, the comprehensive nursing intervention has been widely adopted in various clinical fields. Some scholars have pointed out that comprehensive nursing measures such as cognitive intervention, progressive muscle relaxation training (PMR intervention), and group psychological intervention are adopted to observe the patients' mood, coping style, and quality of life before and within one month after receiving a comprehensive nursing intervention. The results indicated that comprehensive nursing intervention improved the mood of lung cancer patients undergoing chemotherapy, made patients adopt a positive coping style and enhanced their quality of life [13]. Based on this, the purpose of this study is to explore the effect of comprehensive nursing on the recovery of gastrointestinal function in patients undergoing abdominal surgery.

2. Patients and Methods

2.1. Normal Information. Sixty patients undergoing abdominal surgery in our hospital from January 2019 to April 2021 were enrolled. The patients were randomly divided into control group and research group. The former group received routine nursing and the latter group received comprehensive nursing. There were 18 males and 12 females in the control group and 17 males and 13 females in the research group with an average age of (45.31 ± 3.55) years (1974 years) and (45.75 ± 3.53) years (17 males and 13 females). There exhibited no statistical significance in the general data. This study was permitted by the Medical Ethics Association of our hospital, and all patients noticed informed consent. This study is a double-blind trial.

Selection criteria: meet (1) $18 \text{ years} \leq \text{age} \leq 80 \text{ years old}$, $\text{ASA I} \sim \text{II}$, $18 \text{ kg/m}^2 \leq \text{BMI} \leq 30 \text{ kg/m}^2$; (2) no previous cardiovascular and respiratory diseases; (3) no chest wall trauma or chest deformities; and (4) the expected duration of the operation is more than 3 hours.

Exclusion criteria: meet (1) $\text{ASA grade} \geq 3$; (2) severe hypertension and heart disease; (3) moderate or severe restrictive or obstructive pulmonary disease; and (4) anemia (hemoglobin is lower than 100 g/L).

2.2. Treatment Methods. The control group received routine nursing intervention in the department, issued disease guidance manuals to patients on the day of admission, evaluated admission, patiently carried out health education to patients, and explained to patients matters needing attention in disease-related self-management. Individual nursing guidance was given, and health education was the main way of education.

The research group received comprehensive care with the following specific measures:

- (1) A comprehensive nursing team was established, consisting of 2 senior medical oncology deputy chief physicians, 1 nutritionist, 1 psychological counseling and therapist, and 4 ward nursing responsible nurses (including head nurses and senior responsible nurses), a total of 8 people composition. Establish an intervention information file, uniformly register the enrolled patients, record the chemotherapy cycle and the date of each hospitalization and discharge, and collect survey data in a planned way; establish a WeChat group for patients in the intervention group, and push nutrition education information to patients irregularly after discharge. Comprehensive care team members review and answer patient nutritional and psychological questions every night.
- (2) Formulate comprehensive nursing intervention measures: use “comprehensive nursing”, “adjuvant chemotherapy”, “nutrition risk”, “comprehensive nursing”, “adjuvant chemotherapy”, and “nutritional risk” as search words to search China knowledge Network, Wanfang, PubMed, Medline, and other databases, read the relevant literature, refer to the

implementation methods of comprehensive nursing, and review and discuss the literature by the members of the group, and implement it after being reviewed by the experts in the hospital to ensure the scientific nature and feasibility of comprehensive nursing intervention measures. The final formulation of comprehensive nursing intervention measures includes: (1) nutritional assessment and education; (2) nutritional supplement intervention; and (3) psychological intervention.

- (3) Implementation of comprehensive nursing intervention measures:

Nutrition assessment and education: (1) after the patient was admitted to the hospital for the first time, the nurse in charge of the research group was responsible for receiving the patient, helping the patient understand the bed attending doctor, familiar with the ward environment, and creating a good bed environment. A good atmosphere for medical treatment lays a good foundation for further research. (2) Nutrition assessment: when admitted to the hospital for the first time, the responsible nurses used the dietary retrospective method to evaluate the nutritional status of patients and their families. The assessment included dietary rules, type and quantity of food intake, dietary nutritional requirements, and the presence or absence of partial eating, food fear, and food allergy, and asked patients about the main ways of intake of nutritional knowledge and assessed whether there were nutritional misunderstandings, etc. to fully understand the nutritional status of patients, so that dietitians can make personalized nutrition education plans for patients according to the results of the assessment; (3) Nutrition education: according to the individualized nutrition education plan, the responsible nurses adopted IIFAR information nursing method to carry out nutrition knowledge education to patients for 15–20 minutes each time [14]. IIFAR scheme: initial check: check the information the patient needs and choose the best time for the patient to receive the information. Information exchange conveys information and communicates to patients through a variety of forms. Through face-to-face conversation, we can distribute brochures to formulate nutritional meals according to dietary guidelines, watch nutrition promotion videos, organize patient education meetings, explain the contents of the bulletin board to patients, and carry out education according to their needs. WeChat can also promote nutrition science knowledge and other channels to ensure that patients receive information effectively. Final accuracy check: ensure the accuracy and validity of the information conveyed. Patients were asked about their learning experience at the end of each education and after re-admission, and patients were encouraged to briefly retell the learning content, deepen memory, and correct wrong cognition in time to prevent cognitive deviation, and reactions were adopted to evaluate whether patients mastered communication knowledge and whether their nutritional status had improved. Regular follow-up was conducted after discharge, and patients were asked about food intake, weight changes, and gastrointestinal discomfort reactions, and specific dietary guidance was given.

Nutritional supplement intervention: the daily food intake and times of patients in the intervention group were supervised and recorded by responsible nurses, and the eating situation and discomfort reaction of patients were observed. According to the results of the first PG-SGA assessment and the diet of the patients within one week after the first chemotherapy, the comprehensive nursing intervention group discussed the formulation of a specific nutritional intervention plan, which was constantly revised with the nutritional status of the patients. Patients in each chemotherapy cycle: according to the five-step model of nutritional intervention, oral nutritional supplement (ONS) is the first choice. Patients who cannot eat by mouth or those with severe gastrointestinal reactions can be supported by the placement of an enteral nutrition tube or peripheral intravenous nutrition, or the combination of parenteral and enteral nutrition. The prescription of parenteral nutrition and parenteral nutrition was jointly formulated by the research team, and the responsible nurses gave corresponding nursing measures, including parenteral nutrition nursing and enteral nutrition nursing.

Psychological intervention: (1) supportive psychotherapy: including mental health education and psychological emotion regulation. Responsible for nurses and head nurses to conduct psychological interviews with the families of newly admitted patients before chemotherapy, to understand the basic situation of patients, including family background, interests, understanding of the disease, and expectations of treatment, and to formulate a detailed treatment plan. According to the actual situation of patients to develop psychological counseling program for patients, specific methods remove unreasonable cognition and correctly understand the disease: medical staff uses their own professional knowledge to provide patients with professional guidance on the main treatment, adverse reactions, nursing, prognosis, and other aspects of the disease, so that patients have a more in-depth understanding of the occurrence and development of the disease, medical effects, and other aspects, so as to improve their cognitive level of disease treatment and their own situation. Help them understand the law of disease development and avoid negative psychological effects and negative emotions due to a lack of understanding of the disease; (2) guide the correct psychological cognition in the face of the disease: use accurate, distinct, kind, kind and positive language to communicate with the patients, guide the patients to face the disease correctly and reverse the traditional concept formed for a long time. Gradually eliminate the patients' fear of the disease itself and treatment, face the disease with an optimistic attitude, so as to achieve the goal of treating the disease and promoting physical and mental health; (3) instruct patients to carry out effective emotional regulation: teach patients to identify their own negative emotions, timely dredge, manage or establish the ability to seek help actively, carry out self-regulation and nursing in time, and effectively correct emotional problems. Enhance the ability of self-awareness and self-correction, and get rid of negative emotional problems such as pessimism and disappointment as soon as possible. Relaxation therapy:

relaxation therapy refers to training and learning, so that patients can consciously control their physical and mental activities, relax tension, achieve a state of peace of mind, physical and mental harmony, reduce the level of arousal, and adjust the function of the body from tension. From the second day of hospitalization, the psychological counseling therapist guided the patients to train according to the relaxation training procedure once a day in the afternoon. The specific methods are: (1) arrange a clean and quiet room with soft light, take a comfortable lying position and close your eyes slightly; (2) tell the patient to take a deep breath. Keep the rhythm natural and steady and focus on breathing; (3) according to certain instructions, patients are guided to tighten a certain muscle group first, and then relax, which can be carried out in the order from top to bottom, so as to relieve tension and anxiety; (4) after all parts of the body are relaxed, let this comfort be maintained for 3–5 minutes; (3) individualized psychological intervention: (1) in-depth communication: through in-depth communication between counseling therapists and patients and main caregivers, to understand the patient's personality and emotional characteristics, family-social situation, the process of seeking medical treatment and the cognition of disease and treatment. Fully understand the true thoughts of the patients and encourage them to express their doubts; (2) psychological counseling: give counseling, explanation, and comfort to patients with specific questions, fully combine "speech therapy" with "chemotherapy", and cooperate with necessary psychotherapy according to the situation, such as music therapy, suggestion therapy. Patients with a high matching degree and remarkable therapeutic effect can also be enrolled according to the situation to carry out collective psychological intervention with the patients in the intervention group, through common communication and learning, to explore good coping behavior, and to carry out psychological solutions and persuasion. To help patients eliminate tension and anxiety and improve their determination to overcome the disease; (3) family and social support: explain to the family members the important role of family support and help in the treatment and rehabilitation of patients, encourage them to actively cooperate with treatment and nursing, pay attention to the psychological changes of the main caregivers, and dredge patients with greater psychological stress. Provide positive emotional support for patients and reduce their psychological burden.

2.3. Observation Index

2.3.1. Satisfaction. After consulting the literature and experts' discussion, we designed patients' follow-up satisfaction, a total of 10 items, and recorded patients' satisfaction with follow-up management mode, health education, medical and nursing service, and appointment registration process [12]. It is assigned into four dimensions: very satisfied, satisfied, general, and dissatisfied. Satisfaction rate = very satisfaction rate + satisfaction rate + general rate.

2.4. Gastrointestinal Function

2.4.1. Profile of Mood States. Short Form (POMS-SF). The reliability of the Chinese simplified POMS questionnaire ranges from 0.62 to 0.82, with an average $r=0.71$, and the reliability is high. Chinese scholar Wang Jianping confirmed that the discrimination, reliability, and validity of POMS-SF in cancer patients met the requirements of psychometrics and were suitable for the detection of the emotional status of cancer patients in clinical practice [15]. POMS-SF consists of a subscale of six emotional situations: a positive scale: energy-vigor scale. The higher the score, the better the mood. The five subscales are negative scales: tension-anxiety (POMST), fatigue-retardation (POMSF), depression-depression-depression (POMSD), confusion-confusion (POMSC), and anger-hostility (AHPOM). The higher the score, the worse the mood. The total score (TMD) can be adopted as a separate indicator.

2.4.2. Nutrition Risk Screening Table. Nutrition risk screening table nutritional risk screening 2002, NRS-2002NRS2002, is based on a systematic review of 128RCT and is a nutrition assessment tool issued by the European Society for Parenteral Nutrition (EPSPEN) in 2003. Kondrup analyzed the reliability of NRS2002, its Kappa value is 0.67, and its content validity is expounded on the basis of literature research, so as to ensure a good content validity [16]. The scale consists of three parts: disease severity, nutritional damage, and age score, and is divided into the sum of the above three scores, that is, $0-7 \times \text{NRS2002}$ score <3 indicates no nutritional risk, and NRS2002 score ≥ 3 indicates nutritional risk.

2.4.3. Incidence of Adverse Reactions. The incidences of adverse reactions such as incision effusion, incision infection, incision dehiscence, and anastomotic leakage were calculated.

2.4.4. Quality of Life Scale. The quality of life scale consists of four subscales, including physical, psychological, social, and health self-awareness, with a total of 29 items [17]. The Cronbach's α coefficient of the scale is 0.79 to 0.91. The scale was scored by 1–5 grades. The lower the score, the higher the satisfaction.

2.5. Statistical Analysis. Using SPSS21.0 statistical software, before statistical analysis, the measurement data were examined by normal distribution and variance homogeneity analysis to meet the requirements of a normal distribution or approximate normal distribution, presented as $\bar{x} \pm s$, and repeated measurement data were analyzed by repeated measurement analysis of variance. T test was adopted to compare the two groups, n (%) was adopted as an example to represent the counting data, and χ^2 test was adopted. $P < 0.05$ indicated that the difference between the groups was statistically significant.

3. Results

3.1. Comparison of Nursing Satisfaction. In terms of nursing satisfaction, the research group was very satisfied in 24 cases, satisfactory in 5 cases, and general in 1 case, with a satisfaction rate of 100.00%; In the control group, 14 cases were very satisfied, 10 cases were satisfied, 1 case was general, and 5 cases were dissatisfied. The satisfaction rate was 83.33%; The nursing satisfaction of the research group was higher compared to the control group, and the difference between the groups was statistically significant ($P < 0.05$). All the data results are indicated in Figure 1.

3.2. Comparison of Gastrointestinal Function. In terms of gastrointestinal function, the anal exhaust time eating time defecation time and bowel sound recovery time in the research group were significantly lower than those in the control group, and the difference between the groups was statistically significant ($P < 0.05$). All the data results are indicated in Table 1.

3.3. POMS-SF Score Comparison. In terms of POMS-SF score, the scores of tension-anxiety, depression-depression, fatigue-dullness, anger-hostility, and confusion-confusion in the research group were lower than those in the control group, while the energy-vitality score was higher than that in the control group, and the difference between the groups was statistically significant ($P < 0.05$). All data results are indicated in Table 2.

3.4. Comparison of Nutritional Risk Scores. There was no significant difference in nutritional risk score before nursing ($P > 0.05$) but decreased after nursing. Compared with the two groups, the nutritional risk score of the research group was lower than that of the control group on the 3rd, 5th, and 7th day after nursing, and the difference between the groups was statistically significant ($P < 0.05$). All the data results are indicated in Table 3.

3.5. Comparison of the Incidence of Adverse Reactions. Regarding the incidence of adverse reactions, the incidence of adverse reactions such as incision effusion, incision infection, incision dehiscence, and anastomotic leakage in the research group was lower compared to the control group, and the difference between the groups was statistically significant ($P < 0.05$). All data results are indicated in Figure 2.

3.6. Quality of Life Score Comparison. There was no significant difference in the score of quality of life before nursing ($P > 0.05$) but decreased after nursing. The scores of physiological function, psychological function, social function, and health self-cognition in the research group were lower than those in the control group, and the difference between the groups was statistically significant ($P < 0.05$). All the data results are indicated in Table 4.

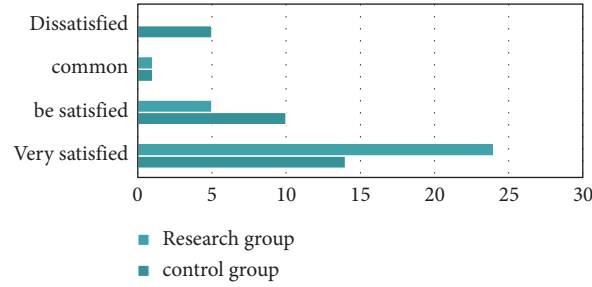


FIGURE 1: Comparison of nursing satisfaction between the two groups.

TABLE 1: Comparison of gastrointestinal function between the two groups [$\bar{x} \pm s, d$].

Grouping	N	Anal exhaust time	Feeding time	Defecation time	Bowel sound recovery time
Control group	30	2.05 ± 0.22	2.36 ± 0.34	2.89 ± 0.21	2.05 ± 0.36
Research group	30	1.73 ± 0.12	1.95 ± 0.12	2.16 ± 0.21	1.65 ± 0.31
t		6.994	6.228	13.463	4.611
P		< 0.05	< 0.05	< 0.05	< 0.05

TABLE 2: Comparison of POMS-SF scores between the two groups [$\bar{x} \pm s$, points].

Grouping	N	Tension-anxiety	Depression-depression	Fatigue-retardation	Anger-hostility	Confusion-chaos	Energy-vigor
Control group	30	9.98 ± 1.44	8.93 ± 1.21	6.78 ± 1.21	5.79 ± 0.53	5.65 ± 1.21	4.31 ± 1.22
Research group	30	7.35 ± 1.21	7.45 ± 1.21	4.43 ± 0.31	4.41 ± 0.63	4.13 ± 0.31	6.42 ± 0.95
t		7.658	4.737	10.304	9.180	6.665	7.474
P		< 0.05	< 0.05	< 0.05	< 0.05	< 0.05	< 0.05

TABLE 3: Comparison of nutritional risk scores between the two groups [$\bar{x} \pm s$, points].

Grouping	N	Before nursing	After nursing 3 d	After nursing 5 d	After nursing 7 d
Control group	30	4.96 ± 0.53	3.84 ± 0.31	3.05 ± 0.31	2.95 ± 0.31
Research group	30	4.98 ± 0.51	3.01 ± 0.31	2.64 ± 0.12	2.56 ± 0.11
t		0.148	10.369	6.755	6.493
P		> 0.05	< 0.05	< 0.05	< 0.05

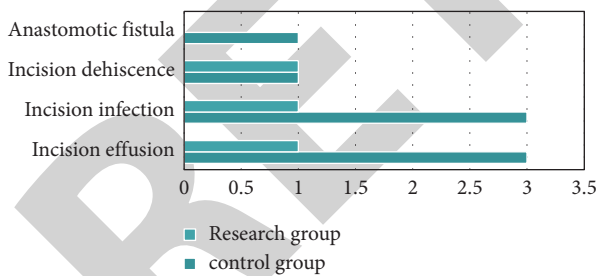


FIGURE 2: Comparison of the incidence of adverse reactions between the two groups.

4. Discussion

Delayed gastric emptying due to gastrointestinal motility disorders after abdominal surgery is collectively referred to as functional gastric emptying disorder or gastroparesis [17]. Therefore, during the comprehensive treatment of patients undergoing abdominal surgery, we must pay attention to the nutritional status of patients, such as not taking timely measures to improve the nutritional level of patients, and the decline of immunity of patients under malnutrition; it will

have a negative impact on the treatment effect and prognosis. Professor Shi Hanping proposed that nutrition education is the basic content of nutrition intervention and the first choice of nutrition therapy [18]. In the clinic, there are many nutritional misunderstandings in tumor patients, and the most common misunderstandings are taboos, thinking that supplementary nutrition will accelerate the growth of tumor cells. There are also more common misunderstandings, such as over-reliance on health products and superstitious vegetarian diet. The American Society for Parenteral and Enteral Nutrition (ASPEN) pointed out that reasonable nutritional intervention can effectively enhance the nutritional status of patients and remarkably promote their immunity [19]. Therefore, it is particularly important to eliminate bad cognition, spread scientific and healthy nutrition knowledge, provide reasonable and correct dietary nutrition advice for patients with nutritional needs, cooperate with effective nutritional intervention, and improve the nutritional status of patients. Comprehensive nursing intervention plays a positive role in delaying the loss of weight and nutritional index of patients undergoing abdominal surgery [19, 20]. Through reasonable and effective comprehensive nursing intervention for patients undergoing

TABLE 4: Comparison of quality of life scores between the two groups [$\bar{x} \pm s$, points].

Grouping	N	Physiological function		Psychological function		Social function		Healthy self-cognition	
		Before nursing	After nursing	Before nursing	After nursing	Before nursing	After nursing	Before nursing	After nursing
Control group	30	15.57 \pm 4.64	13.13 \pm 2.33a	16.67 \pm 3.53	14.34 \pm 4.31a	18.76 \pm 3.64	16.66 \pm 2.66a	15.75 \pm 3.53	13.55 \pm 1.77a
Research group	30	15.53 \pm 4.42	11.23 \pm 2.55 b	16.96 \pm 3.83	12.66 \pm 1.12 b	18.77 \pm 3.54	12.64 \pm 3.67 b	15.66 \pm 3.83	10.54 \pm 2.63 b
t		0.034	3.012	0.304	2.066	0.010	4.857	0.094	5.200
P		> 0.05	< 0.05	> 0.05	< 0.05	> 0.05	< 0.05	> 0.05	< 0.05

Note. comparison before and after nursing in the control group, ^a $P < 0.05$; Comparison before and after nursing in the research group, ^b $P < 0.05$.

abdominal surgery, we can reduce the negative impact of chemotherapy on the body, reduce the decline of patients' nutritional levels, and play a positive role in maintaining postoperative nutritional level. In the study of scholars, in the multi-disciplinary nursing intervention for patients undergoing abdominal surgery, it was found that there exhibited no statistically significant change in the nutritional index grade of the patients in the intervention group after 21 days of observation, and there exhibited a statistically significant difference after follow-up observation for 1 month, which is consistent with the results of this study. It indicates that nutritional intervention needs a process, and with the extension of time, it can indicate the advantage of its effect on the nutritional status of patients undergoing abdominal surgery. In this study, due to the short observation period, the more far-reaching and positive effect of comprehensive nursing intervention on the nutritional status of tumor patients need to be extended to the whole chemotherapy cycle in the future. Studies by some scholars have proved that nutritional support has a positive effect on improving the nutritional status of patients undergoing chemotherapy and the treatment of patients after abdominal surgery, which is similar to the results of this study [20]. Patients undergoing abdominal surgery often have some self-reported symptoms, such as nausea and vomiting, anorexia, and abdominal distension. Comprehensive nursing increased the part of patients' self-evaluation, fully considered the eating situation and the symptoms affecting eating, and effectively made up for the deficiency of relying solely on objective indicators to judge the nutritional status of patients. Studies of the 10th National gastric Cancer Congress and the third Sunshine Great Wall Cancer Congress also show that nutritional support during chemotherapy for patients undergoing abdominal surgery can improve nutritional status, enhance immunity and reduce adverse reactions caused by chemotherapy, similar to the results of this study [21]. From this, it can be inferred that the integration of management and maintenance evaluation and education into comprehensive nursing intervention measures can effectively enhance the nutritional status of patients undergoing abdominal surgery.

With the continuous progress of modern medicine, the mental health of patients has been paid more attention by the medical community [22]. WHO's new definition of health points out that patients should be treated as a whole, and the attention to diseases is not limited to the scope of

somatic diseases, but also to the mental health of patients. We can notice the importance of social and psychological factors to human physical and mental health [23]. After learning about the condition, patients with abdominal surgery will suffer a certain psychological impact, resulting in negative, evasive, and depressive emotions, and many patients are difficult to get rid of their own negative emotions, which seriously affect their quality of life and confidence in treatment [24]. Clinical observation shows that patients undergoing abdominal surgery have large mood fluctuations before and after operation, which leads to a concentrated outbreak of negative emotion in a short time. A large number of studies have shown that patients undergoing abdominal surgery have higher scores of anger, anxiety, depression, and fear than normal people [25–27]. With the extension of the rehabilitation cycle, the expression of bad emotion is more obvious. Previous studies have indicated that the causes of adverse psychological status in patients undergoing abdominal surgery are usually as follows: (1) stress reaction caused by confirmed disease; (2) worry about side effects after operation [28]; and (3) economic burden and self-perceived burden [29]. The cost of surgical treatment brings a huge financial burden to the patient's family. Repeated hospitalization and chemotherapy cause the loss of family role, which makes the patient produce negative emotions that drag down the family and become a family burden. As a result, negative emotions such as self-remorse, helplessness, depression, guilt, and anxiety appear. Therefore, when the patient's body and mind are extremely fragile, they need more care, support, and understanding from the family. Spiritual assistance and life care from family members play a positive role in building up confidence in overcoming the disease and improving treatment tolerance; (4) the uncertainty of the therapeutic effect and outcome of the disease [30]. At this stage, it is not enough to cure all cancers, the fear of death threats will also stimulate people's strong desire for survival and psychological expectations of the effectiveness of treatment, coupled with frequent and uncertain tumor metastasis. Anxiety and depression occur in patients with recurrent or worsening conditions; and (5) the influence of the hospital physical environment and social environment [31]. Compared with the psychological comfort brought by the family, the unfamiliar hospital environment is easy to make patients nervous, fear, and other discomfort, repeated hospitalization

makes patients have a conditioned reflex to the hospital environment, in addition, some medical staff cannot clearly feel the emotional changes of patients, impatience and kindness in the process of inquiring about the patient's condition or explaining matters needing attention may lead to negative psychological emotion. We can find that the causes of adverse psychological emotions in patients undergoing abdominal surgery are complex and need to be treated because of illness, and psychological intervention can get twice the result with half the effort if we give corresponding psychological intervention to the causes of the problems [32].

To help patients improve poor nutritional status, get rid of negative emotional disorders, and maintain a good physical and mental state to receive disease treatment is a necessary nursing measure for patients undergoing abdominal surgery. This study shows that comprehensive nursing intervention can effectively reduce the decline of patients' nutritional levels, alleviate the degree of anxiety and depression, and promote the improvement of patients' overall mood. It is suggested that the comprehensive nursing intervention program should be further promoted in clinical work to improve the malnutrition and psychological state of patients with malignant tumors undergoing adjuvant chemotherapy. With the continuous development of nutrition, the nutrition nurse treatment group (NST) appeared one after another and assumed the important responsibility of clinical nutrition knowledge dissemination and education. Due to the lack of understanding of the importance of NST, there are still few nutrition specialist nurses in our country. At present, the main clinical nutrition work is mainly undertaken by nutrition nurses [33]. However, in the actual work, the clinical nurses are closest to the patients and have more frequent contact. Training nutrition specialist nurses and setting up a comprehensive nursing team are more conducive to the implementation of the nutrition nursing plan. In the survey of patients undergoing abdominal surgery, it was found that 99.6% of patients had dietary misunderstandings, 93% of patients had not received formal nutrition education, and 70% of patients had doubts about how to eat scientifically [34]. The first two sources of nutrition knowledge for patients undergoing abdominal surgery are television (56.5%) and medical staff (54.4%), while the last two are magazines (25.5%) and dietitians (10.2%) [35, 36]. Medical staff and dietitians did not play their due role in nutritional treatment. Some data show that 76% of patients are not satisfied with clinical nutrition knowledge, 63% of patients want to receive nutrition knowledge education from nurses, and only 11% of nurses think that their nutrition knowledge reserve can meet the needs of patients [37, 38]. It can be noticed that clinical nurses are lack of professional nutrition knowledge. In the future talent echelon construction, we should pay attention to the training of specialist nurses and the establishment of a comprehensive nursing team. As people pay more attention to mental health, psychological intervention nursing, as a new nursing model, has been gradually integrated into clinical nursing work in recent years. A number of studies have indicated that it can play an important role in the treatment of diseases

with negative emotions such as anxiety and depression, and can effectively improve the quality of life of tumor patients [39–41]. In view of the fact that at present, psychological support and psychological intervention are mostly completed by nurses and lack of professional training and guidance, the professional study and training of psychological nursing should be strengthened in the future in order to ensure the safety of patients and enhance the effect of an intervention. The same idea can be found in the study put forward by other scholars [42, 43]. They have applied new methods in the study, and the conclusions drawn can also give some support to this study. There are some limitations to this study. First, the sample size of this study is not large and it is a single-center study, so bias is inevitable. In future research, we will carry out multi-center, large-sample prospective studies, or more valuable conclusions can be drawn.

In summary, patients undergoing abdominal surgery received comprehensive care, which enhanced their mental health, reduced the degree of anxiety and depression, relieved fatigue, dullness, energy, and vitality, and improved their overall mood. At the same time, it can also promote the recovery of gastrointestinal function and reduce the occurrence of adverse reactions.

Data Availability

The datasets used and analyzed during the current study are available from the corresponding author upon reasonable request.

Conflicts of Interest

The authors declare that they have no conflicts of interest.

References

- [1] S. Hajibandeh, S. Hajibandeh, S. Saeed, J. Bird, L. Kannappa, and I. Ratnayake, "Effect of hyaluronate-based bioresorbable membrane (Seprafilm) on outcomes of abdominal surgery: a meta-analysis and trial sequential analysis of randomised controlled trials," *Updates in surgery*, vol. 74, no. 3, pp. 865–881, 2021.
- [2] P. Dayalal, P. Kaushal, and C. Varsha, "A study to assess the effectiveness of structured teaching programme on knowledge regarding postoperative management among relatives of patients undergoing abdominal surgeries at enrolled hospitals of Mehsana City," *International Journal of Nursing Education and Research*, vol. 9, no. 2, pp. 314–315, 2021.
- [3] Y. Seok, E. E. Suh, S. Y. Yu, J. Park, H. Park, and E. Lee, "Effectiveness of integrated education to reduce postoperative nausea, vomiting, and dizziness after abdominal surgery under general anesthesia," *International Journal of Environmental Research and Public Health*, vol. 18, no. 11, pp. 6124–6435, 2021.
- [4] H. Merker, J. Sliker, S. Soppe, A. Keerl, and A. Nocito, "Performing total extraperitoneal inguinal hernia repair in patients with previous abdominal surgery is safe: an analysis of 1591 patients," *British Journal of Surgery*, vol. 108, no. 4, pp. 31–35, 2021.
- [5] O. Kouli and K. Omar, "V2 Evaluation of risk prediction models for postoperative pulmonary complications in adults undergoing major abdominal surgery: a systematic review and

- external validation study of the REspiratory Complications after abdomiNal surgery (RECON) cohort,” *BJS Open*, vol. 5, no. 1, pp. 4041–4045, 2021.
- [6] E. S. Bond, C. E. Soteropulos, Q. Yang, and S. O. Poore, “The impact of prior abdominal surgery on complications of abnormally based autologous breast reconstruction: a systematic review and meta-analysis,” *Journal of Reconstructive Microsurgery*, vol. 37, no. 7, pp. 566–579, 2021.
 - [7] L. N. Purcell, R. Reiss, V. J. Msosa, K. D. Westmoreland, and A. G. Charles, “Patient-reported quality of life after major abdominal operation in a resource-limited setting,” *Journal of the American College of Surgeons*, vol. 231, no. 4, pp. S127–S128, 2020.
 - [8] J. Sincavage, V. J. Msosa, L. N. Purcell, and A. G. Charles, “Postoperative complication and mortality after abdominal operation in a resource-poor setting,” *Journal of the American College of Surgeons*, vol. 231, no. 4, pp. S128–S426, 2020.
 - [9] Q. L. Hu, M. C. Grant, A. Hornor Melissa et al., “Technical evidence review for emergency major abdominal operation conducted for the agency for healthcare research and quality safety program for improving surgical care and recovery,” *Journal of the American College of Surgeons*, vol. 231, no. 6, pp. 994–996, 2020.
 - [10] K. Laks and S. Freeman, “Does a restrictive intravenous fluid strategy lead to improved outcomes in patients undergoing major abdominal surgery as compared with liberal intravenous fluids?” *Evidence-Based Practice*, vol. 24, no. 6, pp. 22–23, 2021.
 - [11] S. Singh, R. Jha, and M. Sharma, “The analgesic effect of bilateral ultrasound-guided erector spinae plane block in paediatric lower abdominal surgeries: a randomised, prospective trial,” *Indian Journal of Anaesthesia*, vol. 64, no. 9, pp. 762–496, 2020.
 - [12] K. Jakub, M. Kinga, S. Kinga, S. Urszula, and R. Kamil, “Mortality and morbidity prediction for older patients undergoing emergency abdominal surgery—comparison of the POSSUM, E-PASS score, and SASA score,” *Indian Journal of Surgery*, vol. 82, no. 4, pp. 551–558, 2020.
 - [13] “Complementary and alternative medicine - acupuncture therapy; Hubei Province hospital of traditional Chinese medicine details findings in acupuncture therapy (acupuncture therapy on postoperative nausea and vomiting in abdominal operation a bayesian Network meta analysis),” *Journal of Mathematics*, vol. 563, no. 75, pp. 31–34, 2020.
 - [14] A. A. Momin and E. M. Barksdale, “Zaem Lone, et al. Steinmetz. Exploring perioperative complications of anterior lumbar interbody fusion in patients with a history of prior abdominal surgery: a retrospective cohort study,” *The Spine Journal*, vol. 20, no. 7, pp. 301–304, 2020.
 - [15] R.-D. Wang, X. R. Sheng, W. X. Guan et al., “Flurbiprofen axetil for postoperative analgesia in upper abdominal surgery: a randomized, parallel controlled, double-blind, multicenter clinical study,” *Surgery Today*, vol. 50, no. 7, pp. 749–756, 2020.
 - [16] Ju Wang and J. Peng, “Prevention of internal hernia after abdominal operation,” *International Journal of Surgery*, vol. 47, no. 4, pp. 74–76, 2020.
 - [17] B. Teklewold, D. Pioth, and T. Dana, “Magnitude of abdominal wound dehiscence and associated factors of patients who underwent abdominal operation at st. Paul’s hospital millennium medical college, addis ababa, Ethiopia,” *Surgery Research and Practice*, vol. 2020, no. 75, pp. 491–495, 2020.
 - [18] J. Franko, S. Raman, N. Krishnan et al., “Randomized trial of perioperative probiotics among patients undergoing major abdominal operation,” *Journal of the American College of Surgeons*, vol. 229, no. 6, pp. 533–540e1, 2019.
 - [19] A. L. Lightner, N. P. McKenna, A. Alsughayer et al., “Biologics and 30-day postoperative complications after abdominal operations for crohn’s disease: are there differences in the safety profiles?” *Diseases of the Colon & Rectum*, vol. 62, no. 11, pp. 1352–1362, 2019.
 - [20] C. W. Snyder, P. D. Danielson, R. Gonzalez, and N. M. Chandler, “Effect of perioperative transfusion practices on serious complications after abdominal operation in pediatric patients with sickle cell disease,” *Journal of the American College of Surgeons*, vol. 229, no. 4, pp. e43–406, 2019.
 - [21] A. Schmitz, P. Haste, and M. Johnson, “03:27 PM Abstract No. 172 Transjugular intrahepatic portosystemic shunt (TIPS) creation to improve surgical candidacy prior to abdominal operation: a retrospective analysis,” *Journal of Vascular and Interventional Radiology*, vol. 30, no. 3, pp. S79–S142, 2019.
 - [22] Phenols and Department, “Of Anesthesiology Reports Findings in Phenols (Effects of sevoflurane inhalation anesthesia on cognitive and immune function in elderly patients after abdominal operation),” *Chemicals & Chemistry*, vol. 31, no. 75, pp. 485–486, 2019.
 - [23] L.-Q. Liang, Y.-Q. Jiao, and S.-L. Guo, “Effects of sevoflurane inhalation anesthesia on cognitive and immune function in elderly patients after abdominal operation,” *European Review for Medical and Pharmacological Sciences*, vol. 22, no. 24, pp. 8932–8938, 2018.
 - [24] P. Ssentongo, D. Brunke-Reese, A. E. Sentongo, E. M. Pauli, and D. I. Soybel, “Genetic variation in zinc transporter slc30a8/znt8 modifies risk of surgical stress induced hyperglycemia in patients undergoing major abdominal operation,” *Journal of the American College of Surgeons*, vol. 227, no. 4, pp. S101–S569, 2018.
 - [25] A. V. Fisher, S. A. Campbell-Flohr, B.-F. Maria et al., “Improving transitional care after complex abdominal operation: results of a telemedicine-based transitional care intervention,” *Journal of the American College of Surgeons*, vol. 227, no. 4, pp. 593–596, 2018.
 - [26] A. L. Lightner, N. P. McKenna, C. S. Tse et al., “Postoperative outcomes in ustekinumab-treated patients undergoing abdominal operations for crohn’s disease,” *Journal of Crohn’s and Colitis*, vol. 12, no. 4, pp. 402–407, 2018.
 - [27] A. L. Lightner, N. P. McKenna, C. S. Tse, L. E. Raffals, E. V. Loftus, and K. L. Mathis, “Postoperative outcomes in vedolizumab-treated Crohn’s disease patients undergoing major abdominal operations,” *Alimentary Pharmacology & Therapeutics*, vol. 47, no. 5, pp. 573–580, 2018.
 - [28] Y. Gao, X. Deng, H. Yuan et al., “Patient-controlled intravenous analgesia with combination of dexmedetomidine and sufentanil on patients after abdominal operation: a prospective, randomized, controlled, blinded, multicenter clinical study,” *The Clinical Journal of Pain*, vol. 34, no. 2, pp. 155–161, 2018.
 - [29] Z.-Y. Yao, Z. Jia, Y.-H. Xie et al., “Analgesic effect of dezocine in different doses on elderly patients undergoing abdominal operation under general anesthesia and its influence on stress response to postoperative tracheal extubation,” *European Review for Medical and Pharmacological Sciences*, vol. 21, no. 22, pp. 5223–5229, 2017.
 - [30] A. L. Lightner, L. E. Raffals, K. L. Mathis et al., “Postoperative outcomes in vedolizumab-treated patients undergoing abdominal operations for inflammatory bowel disease,” *Journal of Crohn’s and Colitis*, vol. 11, no. 2, pp. 185–190, 2017.

Research Article

Effect of Loratadine Tablets in Combination with Other Drugs on Nasal Physiological Function and T Lymphocyte Subsets in Patients with Allergic Rhinitis

Jie Zhang, Hongzheng Cheng, Yi Luo, Dan Kan, and Yinghuai Wang 

Putun Hospital Affiliated to Wuhan University of Science and Technology/Otorhinolaryngology, No. 1 Benxi Street, Qingshan District, Wuhan City 430081, Hubei Province, China

Correspondence should be addressed to Yinghuai Wang; 631406080302@mails.cqjtu.edu.cn

Received 15 June 2022; Revised 13 July 2022; Accepted 16 July 2022; Published 21 August 2022

Academic Editor: Dong Chen

Copyright © 2022 Jie Zhang et al. This is an open access article distributed under the Creative Commons Attribution License, which permits unrestricted use, distribution, and reproduction in any medium, provided the original work is properly cited.

Objective. To investigate the effects of loratadine tablets in combination with other drugs on nasal physiological function and T lymphocyte subsets in patients with allergic rhinitis (AR). **Methods.** A total of 120 AR patients treated in our hospital from February 2018 to February 2021 were randomly divided into control group and research group. The control group was given mometasone furoate nasal spray combined with loratadine tablets, while the research group was given budesonide combined with loratadine. The efficacy, duration of clinical symptom remission, immune function indicators, T lymphocyte subset, nasal physiological function, and incidence of adverse reactions were compared between the two groups. **Results.** The efficacy results of the two groups showed that the effective rate of the research group was 96.67%, while the effective rate of the control group was 83.33%. The effective rate in the research group was higher compared to the control group ($\chi^2: 5.925 P < 0.05$). The results of clinical symptom relief time showed that the clinical symptom relief time of nasal congestion, itching, runny nose, and sneezing in the research group was lower than that in the control group, and the difference was statistically significant ($P < 0.05$). The results of the comparison of immune function indicators showed that the IL-6, IL-8, and IgE of the research group were lower than those of the control group, while the Th1/Th2 of the research group were higher than those of the control group. There were no statistically significant differences in T lymphocyte subsets before nursing, but after treatment, the T lymphocyte subsets of the two groups decreased, and the level of CD3+, CD4+, CD8+, CD4+, and CD4+/CD8+ lymphocytes in the research group was lower than that of the control group, and the difference was statistically significant ($P < 0.05$). Before treatment, there exhibited no significant difference in nasal physiological function, but after treatment, the nasal physiological function of the two groups was enhanced, and the MTT, NR, and MCR of the research group were lower than those of the control group, and the difference was statistically significant ($P < 0.05$). Finally, the incidence of adverse reactions in the research group was lower compared to the control group, and the difference was statistically significant ($P < 0.05$). **Conclusion.** Budesonide and loratadine are effective in improving patient efficacy, T lymphocyte subsets, and nasal physiological function, and are safer.

1. Introduction

Allergic rhinitis (AR) is an IgE-mediated noninfectious disease of nasal mucosa characterized by the activation and infiltration of inflammatory cells [1]. The main inflammatory cells involved are mast cells and eosinophils. The main clinical symptoms of AR are nasal blockage, runny nose, nasal itching, and sneezing. Some patients are also accompanied by itching and tears, which are mainly seen in

patients with AR caused by pollen [2]. The main clinical symptoms are runny nose, nasal congestion, paroxysmal sneezing, nasal itching, sleep and breathing disorders, otitis media, sinusitis, and other complications [3]. When patients with AR are exposed to allergens such as dust mites, the immune response starts, and the immune response tends to develop in the direction of Th2 type immune response, which promotes Th2 cells to secrete allergy-related cytokines. These inflammatory factors further

promote B cells to secrete antigen-specific IgE (sIgE). When the allergen restimulates the immune process of the body, sIgE binds quickly to the allergen epitope and crosslink occurs, which makes mast cells degranulate and release allergic and inflammatory mediators, damage nasal mucosa and lead to AR [4].

Oxidative stress injury also plays an important role in the pathogenesis of AR [5]. Oxidative stress and related inflammatory pathways are mainly regulated by nuclear factor E2-related factor 2 (Nrf2)/heme oxygenase-1 (HO-1) pathway and NF- κ B signal pathway [6]. When Nrf2 binds to its corresponding inhibitory protein, ubiquitin degradation leads to a decrease in its activity. When the body is subjected to stress, reactive oxygen species can make nuclear factor E2-related factor 2 enter the nucleus, initiate HO-1 transcription and expression, inhibit NF- κ B signal pathway, and play an antioxidant role [7]. Regulatory T cells (Treg) are a class of T cells that express CD4, CD25, and transcription factor Foxp3. They dynamically regulate immune homeostasis by regulating Th1/Th2 balance. Some studies have indicated that the levels of IL-4 and effector T cells in patients with allergic diseases are significantly higher compared to patients without allergic diseases, while the levels of IL-10 and Treg are decreased [8]. Adoptive transfer of Treg cells can prevent or alleviate autoimmune diseases, resulting in immune tolerance to allergens [9]. Therefore, strengthening the level of Treg is an important strategy in the treatment of AR. Avoiding contact with allergens is still the main means of prevention and treatment of AR.

Loratadine tablets were often employed to treat children in the past [9]. Loratadine belongs to the second generation of antihistamine drugs, which play a good antiallergic effect mainly by inhibiting the binding of histamine to H1 receptor [10]. However, some studies have proved that the effect of loratadine alone in the treatment of AR has some limitations, and it is easy to relapse after drug withdrawal [11]. Based on this, it is necessary to explore other adjuvant treatments. A large number of studies have demonstrated that glucocorticoid has good anti-inflammatory and antiallergic effects, can significantly reduce a variety of inflammatory reactions, and alleviate nasal allergy [12]. Existing treatments or drugs can only relieve the symptoms of AR and need long-term medication, and adverse reactions caused by existing therapeutic drugs are constantly reported, such as liver and gastrointestinal diseases, lethargy, jaundice, nasal irritation, rashes, diarrhea, and so on. Meanwhile, the period of immunotherapy is long, the compliance of patients is poor, the treatment results vary greatly, and the treatment effect is not ideal. Therefore, it is necessary to actively explore an effective scheme for the treatment of patients. In the past, loratadine was often employed to treat children, although it has a certain effect but the overall effect needs to be enhanced [12]. Mometasone furoate nasal spray combined with loratadine, budesonide and loratadine can achieve good results in the treatment of AR, but there are few reports on the clinical efficacy of the two regimens in the treatment of AR. Therefore, in this study, the aim is to explore the efficacy of different drugs combined with loratadine tablets in the treatment of AR and the effects of T lymphocyte subsets and nasal physiological function.

2. Patients and Methods

2.1. General Information. One hundred and twenty patients with AR treated in our hospital from February 2018 to February 2021 were enrolled. The patients were randomly assigned into a control group and a research group. The control group was treated with mometasone furoate nasal spray combined with loratadine tablets, and the research group was treated with budesonide and loratadine. In the control group, the age was 18–74 years old, with an average of (45.66 ± 3.31) years, including 32 males and 28 females, while in the research group, the age was 18–76 years old, with an average of (45.33 ± 3.44) years, including 36 males and 24 females. There exhibited no statistical significance in the general data of the two groups. This study was permitted by the Medical Ethics Association of our hospital, and all patients signed informed consent.

Diagnostic criteria: according to the relevant diagnostic criteria mentioned in the clinical guidelines for allergic rhinitis issued by the American Society of Otorhinolaryngology and head and neck surgery in 2014 [13]: (1) there are two or more main symptoms such as nasal congestion, nasal itching, sneezing, and runny nose in clinic. The cumulative time of the symptoms may be more than 1 hour, and there can be both eye symptoms such as itching, conjunctival congestion, tears, and so on; (2) there are common watery secretions in the nasal cavity with edema and pallor of the nasal mucosa; and (3) the clinical manifestation of allergic rhinitis should be consistent with the results of skin prick test or serum specific IgE test.

Inclusion criteria: those who meet all of the following items can be included. (1) Patients, who meet the above diagnostic criteria; (2) 18 years old \leq age \leq 80 years old; (3) the total score of nasal symptoms (TNSS) ≥ 4 ; and (4) voluntarily participate in this study and sign the informed consent form for treatment.

Exclusion criteria: those, who meet any of the following items cannot be included. (1) Those who have taken H1-antihistamines, steroids, AH, decongestants directly acting on the eyes, nose and mouth, corticosteroids, antibiotics, and other drugs within 14 days before treatment; those who have received SLIT, SCIT immunotherapy, or hormone system therapy in the last year. Those, who received physiotherapy in traditional Chinese medicine and other traditional Chinese medicine fields such as acupuncture, moxibustion, cupping, inhalation of traditional Chinese medicine and other traditional Chinese medicine within 14 days before treatment; those who had taken proprietary medicine or decoction that had a significant effect on AR within 14 days before treatment, or those who could not be treated with acupuncture; (2) other types of rhinitis not caused by AR, such as runny nose, stuffy nose, sneezing, itching and ant sensation; (3) patients with respiratory infection within 14 days before enrollment, chronic paranasal sinusitis in previous history or chronic paranasal sinusitis demonstrated by X-ray examination of paranasal sinuses, nasal polyps, severe deviation of nasal septum, severe organic lesions in nasal cavity or undergoing surgery, patients with a history of respiratory diseases; (4) Asthma or

vasomotor rhinitis; (5) Serum aspartate aminotransferase (AST), alanine aminotransferase (ALT), creatinine and cystatin C (CysC) >1.5 times the upper limit of normal value; (6) there are serious primary diseases such as cardiovascular, liver, kidney, lung and blood, or serious diseases such as tumor and AIDS; (7) pregnant, lactating women, or persons with physical and mental disabilities; (8) by asking patients to identify those, who have used alcohol, hormone drugs and other medical history, or through the analysis of researchers, the probability of joining the group is low and the situation of joining the group is complicated; (9) patients, who have recently participated in other clinical drug studies; (10) there are people, who are allergic to the ingredients used in this study; and (11) those, who have joined the clinical trials of drugs in the past three months.

2.2. Treatment Methods. The control group was treated with loratadine (trade name: Kai Ruitan, Bayer Pharmaceutical Co., Ltd. (Shanghai), Chinese medicine: H10970410 10 mg/tablet, 6 tablets/box), one tablet at a time, once a day. Budesonide nasal spray (specification: 64 ug*120 sprays; nasal preparation; approval number: national drug standard J20180023; manufacturer: Sweden AstraZenecaAB) was treated twice a day at a dose of 64 ug.

The research group was treated with mometasone furoate nasal spray combined with loratadine tablets, and the treatment method of loratadine tablets was the same as that of the control group. In addition, patients were sprayed with mometasone furoate nasal spray per nostril (manufacturer: Schering-PloughLaboN.V. (Belgium), approval number: H20140100), once a day. Patients in both groups were treated continuously for 1 month.

2.3. Observation Index

2.3.1. Curative Effect Evaluation. The criteria for evaluating the curative effect are as follows: effective: after treatment, the symptoms such as sneezing, nasal itching, and runny nose disappeared, and the nasal secretion specific IgE test was negative; effective: after treatment, the symptoms such as sneezing, nasal itching, and runny nose were significantly relieved, and the nasal secretion specific IgE test was negative. Ineffective: after treatment, the symptoms such as sneezing, nasal itching, and runny nose were not significantly enhanced, and the specific IgE test of nasal secretions was negative and positive. Total effective rate = (number of effective cases + number of effective cases)/total number of cases \times 100%.

2.3.2. Clinical Symptom Relief Time. Statistics of the two groups of patients with a stuffy nose, nasal itching, runny nose, and sneeze clinical symptoms relief time.

2.3.3. Detection of Immune Function Index. In the early morning fasting state, after EDTA anticoagulation treatment, 3000 rpm, centrifugation 10 min, the upper serum was frozen at -80°C to be tested. The levels of IL-6, IL-8, IgE, and

Th1/Th2 in serum were examined by enzyme-linked immunosorbent assay (ELISA). All the kits are obtained from Redd Company of the United States and operate strictly in accordance with the standards of the instructions. The intrabatch differences are less than 10% and the interbatch differences are less than 15%.

2.3.4. T Lymphocyte Subsets Level. T lymphocyte subsets level: all patients employed EDTA-K2 anticoagulant tube to collect peripheral venous blood 2 mL under the condition of fasting in the morning, then stained with corresponding fluorescence-labeled monoclonal antibody, incubated 30 min at room temperature without light, employed FACSLysingsolution for hemolysis, and examined the levels of CD3+, CD4+, CD8+, and CD4+/CD8+ lymphocytes by flow cytometry.

2.3.5. Physiological Function of Nasal Cavity. Nasal physiological functions include nasal resistance (NR), nasal mucosal ciliary transit time (MTT), and nasal mucosal ciliary clearance rate (MCR). NR was examined by nasal resistance meter (manufacturer: GM, UK, model: NR6). The detection methods of MTT and MCR were saccharin clearance tests.

2.3.6. Incidence of Adverse Reactions. The incidence of adverse reactions in the two groups was calculated.

2.4. Statistical Analysis. SPSS23.0 statistical software was adopted to process the data. The measurement data were presented as ($\bar{x} \pm s$). The group design *t*-test was adopted for the comparison and the analysis of variance was adopted for the comparison between multiple groups. Dun-net-t test was adopted for comparison with the control group. The counting data were presented in the number of cases and the percentage, χ^2 test was adopted for comparison between groups, and a bilateral test was employed for all statistical tests.

3. Results

3.1. Comparison of Curative Effect. First of all, we compared the curative effects of the two groups: the research group was significantly effective in 36 cases, effective in 22 cases, ineffective in 2 cases, the effective rate was 96.67%; in the control group, 23 cases were significantly effective, 27 cases were effective, 10 cases were ineffective, and the effective rate was 83.33%. The effective rate in the research group was higher compared to the control group (χ^2 : 5.925 $P < 0.05$). All the data results are indicated in Figure 1.

3.2. Comparison of Clinical Symptom Relief Time. Secondly, we compared the clinical symptom relief time. The clinical symptom relief time of stuffy nose, itching, runny nose, and sneezing in the research group were lower compared to the control group, and the difference was statistically significant ($P < 0.05$). All the data results are indicated in Table 1.

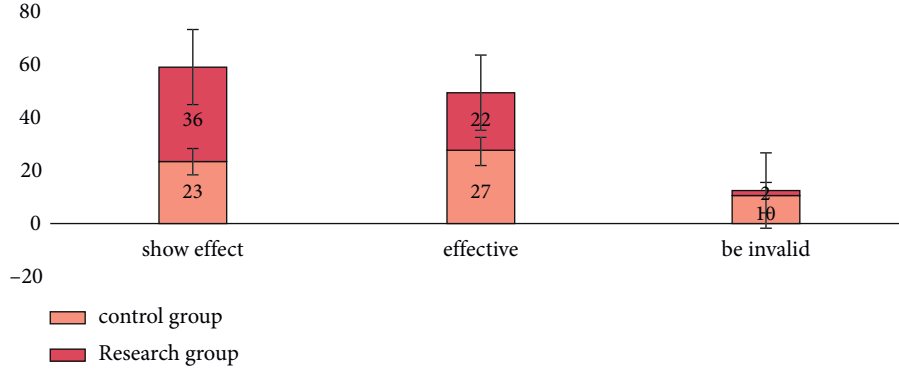


FIGURE 1: Comparison of curative effect between two groups of patients.

TABLE 1: Comparison of clinical symptom relief time between the two groups [$\bar{x} \pm s, d$].

Grouping	N	Nasal congestion	Nasal itching	Runny nose	Sneeze
Control group	60	5.94 ± 0.41	5.89 ± 0.67	6.98 ± 0.67	6.45 ± 0.41
Research group	60	4.19 ± 1.22	4.16 ± 0.34	4.33 ± 0.31	4.10 ± 0.35
t value		10.532	17.835	27.805	33.767
P value		<0.01	<0.01	<0.01	<0.01

3.3. Comparison of Immune Function Indexes. Thirdly, we compared the immune function indexes of the two groups. The IL-6, IL-8, and IgE of the research group were lower compared to the control group, while the Th1/Th2 of the research group was higher compared to the control group, and the difference was statistically significant ($P < 0.05$). All the data results are indicated in Table 2.

3.4. Comparison of T Lymphocyte Subsets. Then, we compared the T lymphocyte subsets of the two groups, there exhibited no significant difference before nursing, but after treatment, the T lymphocyte subsets of the two groups decreased, and the levels of CD3+, CD4+, CD8+ and CD4+/CD8+ lymphocytes in the research group were lower compared to the control group, and the difference was statistically significant ($P < 0.05$). All the data results are indicated in Table 3.

3.5. Comparison of Physiological Function of Nasal Cavity. Next, we compared the nasal physiological function of the two groups, there exhibited no significant difference before treatment, but after treatment, the nasal physiological function of the two groups was enhanced, and the MTT, NR, and MCR of the research group were lower compared to the control group, and the difference was statistically significant ($P < 0.05$). The results of all the data are indicated in Table 4.

3.6. Comparison of the Incidence of Adverse Reactions. Finally, we compared the incidence of adverse reactions, the incidence of adverse reactions in the research group was lower compared to the control group, the difference was statistically significant, and the difference was statistically significant ($P < 0.05$). All the data results are indicated in Figure 2.

4. Discussion

AR is an inflammatory disease of the upper respiratory tract mediated by a variety of immune cells and IgE [14]. AR has become a global medical and health problem; studies indicate that the global incidence of AR patients is 10%–40%. AR seriously affects the work and life of patients and brings heavy economic pressure to individuals and society [14]. AR is difficult to cure and has a wide range of diseases. Its prevalence rate is as high as 10% to 20% in the world, which has had a great impact on the daily life of patients [15]. The prevalence rate of AR in mainland China has reached 4% and 38%, and has indicated an upward trend in recent years. The pathogenesis of AR is complex, and is caused by two main factors: heredity and environment, which leads to nasal mucosal inflammation. Allergen is the initiating factor of an allergic reaction, and lymphocytes, immune factors, and inflammatory reactions are important reasons for the progression of AR [16]. Under normal circumstances, the cellular physiology of the body dynamically maintains a state of balance, but when the balance is destroyed by the intervention of various inflammatory mediators and cytokines, the immune system is rapidly activated, which can lead to mucosal vasodilation and plasma exudation, resulting in a prolonged course of the disease and nasal mucosal tissue remodeling [17]. Therefore, it is generally believed that overactivation of the immune system and to allergy induced by IgE are the main reasons for the progress of AR [17]. This study explored the efficacy of different drugs combined with loratadine tablets in the treatment of AR and the effects of T lymphocyte subsets and nasal physiological function.

In recent years, with the progress of society, especially in developed countries, air pollution is particularly serious. In the meantime, it has also become an important factor affecting AR. Qiong et al. pointed out that oak pollen exposure

TABLE 2: Comparison of immune function indexes between the two groups [$\bar{x} \pm s$].

Grouping	<i>N</i>	IL-6 (pg/ml)	IL-8 (ng/l)	IgE (IU/ml)	Th1/Th2
Control group	60	56.34 \pm 3.21	90.94 \pm 1.42	67.94 \pm 1.24	1.01 \pm 0.44
Research group	60	50.94 \pm 3.11	83.43 \pm 1.22	54.91 \pm 1.22	1.15 \pm 0.23
<i>t</i> value		9.358	31.073	58.021	2.184
<i>P</i> value		<0.01	<0.01	<0.01	<0.01

TABLE 3: Comparison of T lymphocyte subsets between the two groups [$\bar{x} \pm s$].

Grouping	<i>N</i>	CD3 + (%)	CD4 + (%)	CD8 + (%)	CD4 + /CD8 +
Control group	60	68.94 \pm 1.22	38.95 \pm 3.11	24.34 \pm 0.66	1.78 \pm 0.42
Research group	60	65.29 \pm 1.35	33.65 \pm 3.15	22.85 \pm 1.21	1.42 \pm 0.21
<i>t</i> value		15.538	15.538	8.373	5.938
<i>P</i> value		<0.01	<0.01	<0.01	<0.01

TABLE 4: Comparison of physiological function of nasal cavity between the two groups [$\bar{x} \pm s$].

Grouping	<i>N</i>	MTT (min)		NR (Pa/cm ³ ·s)		MCR (mm/min)	
		Before treatment	After treatment	Before treatment	After treatment	Before treatment	After treatment
Control group	60	21.53 \pm 3.31	17.39 \pm 3.34	0.29 \pm 0.06	0.19 \pm 0.03	7.78 \pm 1.23	5.39 \pm 0.16
Research group	60	21.95 \pm 3.34	13.81 \pm 2.14	0.28 \pm 0.01	0.14 \pm 0.05	7.72 \pm 1.26	4.12 \pm 0.31
<i>t</i> value		0.691	6.990	1.273	6.642	0.263	28.199
<i>P</i> value		>0.05	<0.01	>0.05	<0.01	>0.05	<0.01

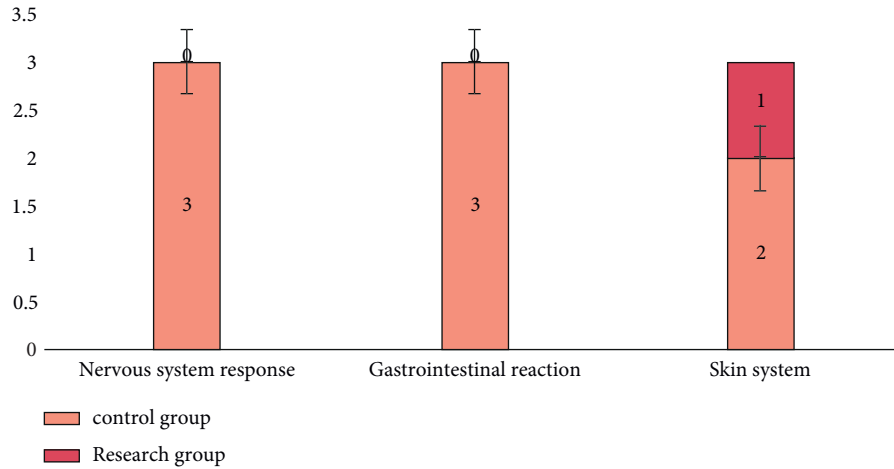


FIGURE 2: Comparison of the incidence of adverse reactions between two groups of patients.

to SO₂ and NO₂ will lead to the destruction of its own structure and a significant increase in the number of pollen grains, thus increasing the prevalence of allergic airway diseases in sensitized individuals [18]. Some scholars have pointed out that there is a significant correlation between PM_{2.5} and PM₁₀ and the prevalence of AR in adults. Total suspended particles, SO₂, and NO₂ in air pollutants are related to the increase in the prevalence of AR in children. Appropriate protective measures to the airway, such as wearing masks and reducing travel during pollen season, to reduce their exposure to air pollutants is an effective way to reduce the prevalence of AR. According to the severity of the patients, the corresponding standard drugs firstly should be taken, and the poor effect can be treated by further

operation. Secondly, selective neurotomy, plasma ablation of the turbinate, and so on can be considered. Pterygoid canal neurotomy is a common surgical method. At present, Western medicine often employs AH, GC and other drugs or adjuvant immunity, desensitization, and other treatments, but its safety and side effects are still open to question, and it has the characteristics of a long course of treatment and high price [19].

At present, it is recognized that the pathogenesis of AR is closely related to the immune inflammatory response mediated by IgE. Studies have indicated that the disorder of immune response caused by the imbalance of Th1/Th2 in the body can induce the synthesis of IgE, which is the main cause of the disease. Meanwhile, the transformation of IL-4

secreted by Th2 can accelerate the absorption and infiltration of EOS, and the increase of sensitivity to allergic factors aggravates the clinical symptoms. The IgE antibody on the surface of MC on the nasal mucosa can also bind to IgE during the occurrence of AR, promote the release of LTs and a large number of inflammatory factors, and then accelerate the occurrence and development of AR [20]. Recent studies have also found that the pathogenic factors of AR are also related to the release of SP, VIP, and NPY neuropeptides released by inflammatory cells in vivo, which accelerate the release of EOS and aggravate the symptoms [20]. Western medicine mainly treats AR by GC, LTs (leukotriene), AH (antihistamine), and other drugs. In recent years, through the practice and research of clinical workers, the efficacy of these conventional medicine has been widely demonstrated [21]. However, it also has many defects, such as AH generally has a central inhibitory effect, external nasal use of GC is easy to cause drug-induced rhinitis, nasal decongestant use for a long time will make turbinate atrophy, drug response will increase, anticholinergic drugs will decrease with the aggravation of symptoms, and so on [21].

The specific treatment of medicine can also be called desensitization therapy, mainly by improving the function of the body's immune system and weakening the overstimulation of external allergen reactions. It is an effective treatment for AR, which is divided into SLIT and SCIT [22]. The former is more easily accepted by patients, has more advantages in efficacy and safety, and is also suitable for children, while the latter can be used in combination with other drugs to achieve a better long-term effect. However, specific therapy also has some defects, such as too long treatment time, unstable curative effect, and long-term effective cooperation of patients. Chu et al. treated AR by blocking the nasal pterygoid canal, pharyngeal branch, and local ethmoid nerve [23]. However, most patients do not have a high degree of acceptance of surgical treatment, so they choose drug treatment.

Loratadine tablet is a tricyclic antihistamine with high efficiency and long-lasting effect, and it is a selective peripheral H1 receptor antagonist, which can relieve all kinds of symptoms caused by allergic reactions [24]. Antihistamines are available orally and intranasally. The first generation of antihistamine drugs such as chlorpheniramine and diphenhydramine is easy to cross the blood-brain barrier and bind to a large number of central H1 receptors, resulting in sedation, which is not recommended for clinical use [25]. In contrast, the second generation of antihistamines (cetirizine, levocetirizine, loratadine, desloratadine, and ebastine) can specifically bind to the peripheral H1 receptor and have a limited effect on permeating the blood-brain barrier, so it is safer. Glucocorticoid has a nonspecific anti-inflammatory effect. As a first-line drug in the clinical treatment of AR, glucocorticoid is mainly used in moderate and severe AR. It can effectively facilitate the nasal symptoms of children, but in the clinic, it is not easy for patients to master the correct spraying method and the use of anti-hormone drugs, and compliance is poor, which can easily lead to adverse reactions [26].

Mometasone furoate nasal spray is one of the most commonly employed topical corticosteroids in the clinic [27]. It belongs to the third generation of nasal corticosteroids, which can not only play a good local anti-inflammatory effect but also be administered by nasal spray. It can promote the drug to act directly on the nasal mucosa, thus can quickly and effectively alleviate the condition of children. In addition, studies have demonstrated that the combination of loratadine and loratadine is well tolerated, and mometasone furoate nasal spray has no significant effect on the plasma concentration of loratadine and its main metabolites [28]. Therefore, the use of mometasone furoate nasal spray combined with loratadine tablets in the treatment of children with AR can not only play a synergistic anti-inflammatory and antiallergic effect, so as to significantly facilitate the patient's condition and the level of inflammatory factors in the body. It can also facilitate the tolerance of patients to treatment. As a kind of glucocorticoid, budesonide is a locally effective anti-inflammatory drug. By inhibiting the release of inflammatory mediators, participate in the immune response of cytokines to achieve the purpose of treatment. Meanwhile, budesonide can protect against allergic reactions and prevent AR. The combination of the above two drugs can significantly facilitate the condition of patients with AR, enhance the effective rate of treatment, and promote the relief of clinical symptoms [29].

The changes in T lymphocytes play an important role in the occurrence and development of AR [30]. According to the cell surface differentiation antigen (CD), T lymphocytes are assigned into CD4+ and CD8+ subgroups and can be assigned into helper T cells (Th cells), and suppressor T cells (Ts cells) according to their functions. Therefore, the levels of T lymphocyte subsets and Th cell-related factors can reflect cellular immune status. In this study, budesonide and loratadine can significantly facilitate the changes of CD4+ and CD4+/CD8+ levels, and the levels of CD4+ and CD4+/CD8+ in the research group are significantly lower compared to the control group, indicating that budesonide and loratadine treatment can significantly facilitate the level of T lymphocyte subsets and avoid AR caused by over-activation of the immune system, which is consistent with the results reported by Germain et al. [30]. This is because budesonide and loratadine can reduce the excitability and sensitivity of parasympathetic nerves in sensitive areas of the nasal cavity, destroy nasal mucosa and weaken allergic reactions, so as to inhibit immune response and facilitate the level of T lymphocyte subsets [30]. Th cells can differentiate into Th1 and Th2, and the imbalance between these two cells will lead to the activation of immune-inflammatory factors and aggravate the local reaction in the nasal cavity, and lead to rhinitis. The production of IgE induced by the allergen is the main process leading to an allergic reaction, and IL-6 and IL-8 can stimulate the secretion of IgE by promoting the differentiation of acidic granulocytes. IL-6 and IL-8 can regulate the differentiation of Th cells and induce Th1/Th2 imbalance. Therefore, comparing the levels of IL-6 and IL-8 between the two groups can reflect the degree of immune response and inflammatory reaction. In this study, the two treatments could significantly affect the changes in IL-6 and IL-8 levels, and the levels of IL-6 and IL-8 in the research

group were significantly lower compared to the control group, indicating that budesonide and loratadine could significantly reduce the levels of serum IL-6 and IL-8 in patients with AR, which was consistent with the results reported by Philipp et al. [31]. This is because budesonide and loratadine treatment can promote hyperemia to dilate vasoconstriction, contribute to tissue edema absorption, alleviate inflammatory response, and facilitate local immune status. Our study still has some shortcomings. Firstly, the quality of this study is limited due to the small sample size we included in the study. Secondly, this research is a single-center study and our findings are subject to some degree of bias. Therefore, our results may differ from those of large-scale multicenter studies from other academic institutes. Our research is still clinically significant and further in-depth investigations will be carried out in the future.

In summary, compared with mometasone furoate nasal spray combined with loratadine tablets, budesonide and loratadine are more effective in the treatment of AR and can effectively improve the efficacy, T lymphocyte subsets and nasal physiological function of patients as well as with higher safety.

Data Availability

The datasets used and analyzed during the current study are available from the corresponding author upon reasonable request.

Conflicts of Interest

The authors declare that they have no conflicts of interest.

References

- [1] W. Weibin and Q. Yaqun, "Study on the efficacy of step-by-step antihistamine in the treatment of allergic rhinitis and its effect on the expression of inflammatory factors," *Journal of Shenyang Pharmaceutical University*, vol. 38, no. S1, pp. 80–82, 2021.
- [2] X. Gemin, G. Wenhai, and D. Min, "Study on the efficacy of Xiaoqinglong decoction and Xiaochaihu decoction in the treatment of allergic rhinitis of lung qi deficiency and cold type and the regulation of Treg cell-related factors," *Journal of practical Medicine*, vol. 37, no. 17, pp. 2287–2291, 2021.
- [3] H. Meixu, T. Susu, W. Daihua, X. Liu, and Q. Liu, "Dynamic Changes, Correlation of Basophils, and the Therapeutic Effect in Patients With Allergic Rhinitis During Allergen-specific Immunotherapy," *American journal of rhinology & allergy*, vol. 33, no. 42, pp. 883–885, 2021.
- [4] J. Y. Kim, D. Hwang, M. Jang, C. Rhee, and D. Han, "Clinical effectiveness of house dust mite immunotherapy in mono-versus poly-sensitized patients with allergic rhinitis: a systematic review and meta-analysis," *Rhinology journal*, vol. 0, no. 0, pp. 0–896, 2021.
- [5] H. Hongting, W. Guoyuan, and Z. Yi, "The long-term outcomes of posterior nasal neurectomy with or without pharyngeal neurectomy in patients with allergic rhinitis: a randomized controlled trial," *Brazilian journal of otorhinolaryngology*, vol. 45, no. 42, pp. 132–136, 2021.
- [6] P. Min, F. Zhengda, and X. Jianrong, "Analysis of systemic adverse reactions in patients with simple allergic rhinitis after subcutaneous immunotherapy with mite allergen injection," *Journal of adverse Drug reactions*, vol. 23, no. 4, pp. 190–195, 2021.
- [7] E. RodríguezPlata and G. L. HernándezSantana, "Real-life safety study of an accelerated cluster immunotherapy with a house-dust mite extract in patients with allergic rhinitis or rhinoconjunctivitis," *Allergo Journal International*, vol. 30, no. 7, pp. 189–192, 2021.
- [8] X. Manfang, Hu Ling, and Li Xiaonian, "Clinical study of mometasone furoate nasal spray combined with loratadine tablets in the treatment of children with allergic rhinitis," *Chinese Journal of Clinical Pharmacology*, vol. 36, no. 19, pp. 2989–2992, 2020.
- [9] D. Xiaochen and S. Maiqing, "Therapeutic effect of Shenling Baizhu Powder on allergic rhinitis and its effect on the content of substance P in nasal secretion," *When Zhenguo Medicine and Chinese Medicine*, vol. 31, no. 06, pp. 1406–1407, 2020.
- [10] W. W. Wei, Yu H. Wei, and Z. Bo, "Interleukin-17A up-regulates the microstromally myelopoietin production by nasal fibroblasts from patients with allergic rhinitis," *European archives of oto-rhino-laryngology: official journal of the European Federation of Oto-Rhino-Laryngological Societies (EUFOS): affiliated with the German Society for Oto-Rhino-Laryngology-Head and Neck Surgery*, vol. 278, no. 66, pp. 884–886, 2020.
- [11] Li Lei, R. Xiumin, and Xu ou, "Clinical observation of sublingual Dermatophagoides farinae drops in the treatment of allergic rhinitis," *Chinese otorhinolaryngology head and neck surgery*, vol. 27, no. 0=5, pp. 259–262, 2020.
- [12] Z.-Y. Liang, D. Yu-Qin, and T. Ze-Zhang, "A quantum dot-based lateral flow immunoassay for the rapid, quantitative, and sensitive detection of specific IgE for mite allergen sinsera from patients with allergic rhinitis," *Analytical and bio-analytical chemistry*, vol. 412, no. 8, pp. 713–716, 2020.
- [13] G. Lucia, S. Alexandru, and R. Daniela, "A comparison between mometasone furoate nasal spray and intranasal glycyrrhetic acid in patients with allergic rhinitis: a preliminary study in clinical practice," *Acta bio-medica: Atenei Parmensis*, vol. 91, no. 1-S, pp. 994–998, 2020.
- [14] H. Qiuju, W. Xin, L. Xia, J. Zheng, and H. Huang, "Effect of sublingual immunotherapy of Dermatophagoides farinae on the expression of specific IgG4 in patients with allergic rhinitis in Hainan," *Journal of Clinical Otorhinolaryngology, head and neck surgery*, vol. 34, no. 02, pp. 135–139, 2020.
- [15] Y. Quintai, L. Chunwei, and W. Weihao, "Infiltration pattern of gamma delta T cells and its association with local inflammatory response in the nasal mucosa of patients with allergic rhinitis," *International forum of allergy & rhinology*, vol. 9, no. 11, pp. 993–996, 2019.
- [16] N. Vijayan, P. Karthikeyan, N. C. Venkataramanujam, R. R. Kaipuzha, and D. T. Pulmoottil, "The association of absolute eosinophil count, serum immunoglobulin E and spirometry with co-morbid bronchial asthma in patients with allergic rhinitis," *Romanian Journal of Rhinology*, vol. 9, no. 35, pp. 151–154, 2019.
- [17] S. Dehnavi, F. Azad, R. Hoseini et al., "A significant decrease in the gene expression of interleukin-17 following the administration of synbiotic in patients with allergic rhinitis who underwent immunotherapy: A placebo-controlled clinical trial," *Journal of Research in Medical Sciences*, vol. 24, no. 1, pp. 51–1999, 2019.
- [18] W. Qiong, S. Qun, and C. Qiguo, "Characteristics of gene expression of peripheral blood fork head transcription factor p3 and cell antigen recognition receptor V γ subfamily in patients with allergic rhinitis complicated with nasal polyps before and after immunotherapy," *Journal of practical Medicine*, vol. 35, no. 14, pp. 2288–2292, 2019.

- [19] Ars Pharmaceuticals Inc, "ARSPharmaceuticalsAnnounces ResultsfromEPI-04ClinicalStudyofARS-1Intra-nasalEpinephrineSprayinAllergyPatientswith AllergicRhinitis," *MedicalLetterontheCDC&FDA*, vol. 35, no. 53, pp. 1899–1901, 2019.
- [20] C.-J. Zhou, F. Ma, and W.-J. Liao, "Restoration of immune suppress or function of regulatory Bcells collected from patients with allergic rhinitiswith Chinese medical formula YupingfengSan," *American journal of translational research*, vol. 11, no. 3, pp. 186–188, 2019.
- [21] G. Sánchez and C. Castro, "PrescriptionProfileandClinical OutcomesinPatientswithAllergicRhinitis TreatedwithOralAntihistaminesorNasalCorticosteroids," *International ArchivesofOtorhinolaryngology*, vol. 23, no. 3, pp. 314–317, 2019.
- [22] Immune System Diseases and Conditions-AllergicRhinitis, "Findings from University of Antioquiain the Area of Allergic Rhinitis Described(Differences in the NasalInflammatory Response to Cynodondactyl on From Ruraland Urban Areas in Patients With Allergic Rhinitis)," *Ecology Environment and Conservation*, vol. 44, no. 523, pp. 894–896, 2019.
- [23] J.-T. Chu, "Histamine H1 receptor genepolymorphism acts as abiologicalindicator of the prediction of the rapeutic efficacy in patients with allergic rhinitis in the Chinese H an population," *Journal of cellular biochemistry*, vol. 120, no. 1, pp. 183–184, 2019.
- [24] F. Gani, C. Lombardi, G. Bonizzoni et al., "The Characteristics of Severe Chronic Upper-Airway Disease(SCUAD) in Patients withAll ergic Rhinitis:A Real-Life Multi center Cross-Sectional Italian Study," *International archive sofallergyandimmunology*, vol. 178, no. 4, pp. 333–337, 2019.
- [25] A. T. W. Wardani, Wiratno, and D. Fatmawati, "Potential Immuno-modulatory activity of Probiotics containing Lactobacillus acidophilusand Lactobacillus caseitoin crease the ratio of IFN γ /IL-4 in patients with Allergic Rhinitis," *Bangladesh Journal of Medical Science*, vol. 18, no. 1, pp. 42–45, 2018.
- [26] Z. Yang, W. Zhen, and W. Dabin, "The levels and clinical significance of Th17, Treg, interleukin, adhesion factor and soluble E-selectin in peripheral blood of patients with allergic rhinitis complicated with asthma," *Chinese otorhinolaryngology head and neck surgery*, vol. 25, no. 08, pp. 453–454, 2018.
- [27] L. Chengyao, W. Xiangdong, and Z. Ming, "Effect of nasal glucocorticoid on the concentration of nitric oxide in nasal respiratory tract of patients with allergic rhinitis and non-allergic rhinitis," *Chinese otorhinolaryngology head and neck surgery*, vol. 25, no. 06, pp. 309–314, 2018.
- [28] Ç. S. Zeynep, Ç. Fatma, S. Şadan et al., "Smoking attitudes of the patients with allergic rhinitis:a comparison withasthma and chronicobstructive pulmonary disease. Are there-differences when only upper airwaysare involved?" *Tuberkuloz ve Toraks*, vol. 66, no. 1, pp. 192–195, 2018.
- [29] X. Xu, Q.-W. He, and W.-C. Xiao, "Effect of budesonideandcetirizine hydrochlorideon neuro trophic factor, airway function and chemokines CCL17 and CCL22 in patient-withallergicrhinitis," *Journal of Hainan Medical University*, vol. 23, no. 21, pp. 889–893, 2017.
- [30] N. Germain, S. Aballéa, and M. Romano, "Exploring The BurdenofIllnessandImpactofSQStandardisedGrassAllergyImmunotherapyTabletTreatment(AIT)onQualityofLife(QOL)in PatientswithAllergicRhinitis(AR)inGermanyandTheNetherlands," *ValueinHealth*, vol. 20, no. 9, pp. 89–93, 2017.
- [31] P. Badorrek, M. Müller, and W. Koch, "Specificityandreproducibilityofnasalbiomarkersinpatientswithallergicrhinitisafterallergenchallengechamberexposure," *AnnalsofAllergy, Asthma&Immunology*, vol. 118, no. 3, pp. 849–852, 2017.

Research Article

Using Logistic Multivariate Analysis to Explore the Effects of Nursing and Psychological Factors on Motor and Cognitive Rehabilitation in Patients with Stroke: Based on a Retrospective Case-Control Study

Wenxin Lin, Liping Meng , Weimin Lou, Panpan Yang, and Min Huang

Department of Rehabilitation Medicine, Zhejiang Hospital, Hangzhou 310000, China

Correspondence should be addressed to Liping Meng; 171849186@masu.edu.cn

Received 8 June 2022; Revised 6 July 2022; Accepted 8 July 2022; Published 19 August 2022

Academic Editor: Dong Chen

Copyright © 2022 Wenxin Lin et al. This is an open access article distributed under the Creative Commons Attribution License, which permits unrestricted use, distribution, and reproduction in any medium, provided the original work is properly cited.

Objective. Based on a retrospective case-control study, logistic multivariate analysis was employed to explore the effects of nursing and psychological factors on the rehabilitation of motor and cognitive function in patients with stroke. **Methods.** A total of 200 stroke patients treated from February 2019 to April 2020 were enrolled in our hospital. According to the results of exercise and cognitive rehabilitation, the patients with good rehabilitation were divided into the control group ($n = 140$) and the research group ($n = 60$). The effects of nursing and psychological factors on the rehabilitation of motor and cognitive function in patients with stroke were analyzed. **Results.** First of all, we compared the general data. There were significant differences in terms of age, years of education, occupational status, payment methods of medical expenses, family income and the course of the disease, and the difference was statistically significant ($P < 0.05$). There was no significant difference in general data ($P > 0.05$). Secondly, we compared the nursing effective rates. The nursing effective rates of the study group were 10 cases, 15 cases, 12 cases, and 23 cases, and the nursing effective rate was 61.67%. In the control group, 78 cases were markedly effective, 33 cases were effective, 25 cases were general and 14 cases were ineffective, and the nursing effective rate was 90.00%. The effective rate of nursing in the study group was higher than that in the control group, and the difference was statistically significant ($P < 0.05$). There was no significant difference in anxiety and depression scores before nursing ($P > 0.05$), but they decreased after nursing. In addition, the scores of anxiety and depression in the study group were higher than those in the control group, and the difference was statistically significant ($P < 0.05$). There was no significant difference in motor function and cognitive function between pre-nursing and post-nursing ($P > 0.05$); after nursing, the motor function increased and the score of cognitive function decreased. Furthermore, the motor function of the study group was lower compared to the control group, and the score of cognitive function of the study group was higher compared to the control group, and the difference was statistically significant ($P < 0.05$). The results of the Person correlation analysis showed that there was a significant correlation between nursing anxiety depression and the rehabilitation effect of motor cognitive function in stroke patients. The results of logistic regression analysis showed that age, family income, nursing efficiency, anxiety, and depression were the factors affecting the rehabilitation of motor and cognitive function in stroke patients. **Conclusion.** Age and family income may be the risk factors affecting the psychological mood of patients. Medical staff should pay attention to the negative emotion of patients and strengthen the nursing intervention of patients.

1. Introduction

Stroke, also known as cerebral apoplexy, is a sudden onset of symptoms lasting more than 24 hours or directly leading to death of local cerebrovascular blood circulation disorders [1]. Stroke, also known as stroke and cerebrovascular

accident, is a group of diseases caused by sudden obstruction or rupture of cerebral vessels and brain tissue damage, including ischemic and hemorrhagic stroke [2]. Stroke is a common neurological disorder, which has become the second leading cause of death endangering human life in Europe. With the rapid development of the medical level, the

survival rate of stroke patients has been remarkably promoted, but the subsequent high disability rate has become increasingly prominent. In accordance with the statistics of the World Health Organization, about 15 million patients worldwide suffer from stroke every year, about 5 million died after onset, and 5 million remain permanently disabled. In China, the annual incidence of stroke is about 250/100000, and the death rate is about 1.5 million. Its morbidity and mortality are among the highest in the world. In addition, 70%–80% of stroke survivors are unable to live independently because of disability [3]. The aging trend in China is becoming more and more serious. Due to the high-risk population of cerebrovascular disease in the elderly, the incidence of cerebrovascular disease remains high, which brings a huge burden to patients, patients' families, and society. For patients, the long-term illness will bring a variety of psychological problems, and these psychological problems will affect the physical recovery of patients.

Mental disorder is one of the most important secondary diseases of stroke [4]. The common psychological complications of stroke include depression, anxiety, mania, post-traumatic stress syndrome, emotional loss of control, apathy, and personality changes. The incidence of this kind of complication is high. In previous studies, the incidence of mental disorders caused by stroke varies greatly due to different psychological evaluation criteria, sampling locations, inclusion and exclusion criteria, and stroke course, ranging from 14.0% to 100% [5]. But overall, psychological problems are one of the important factors leading to a serious decline in the quality of life of patients with acute, convalescent, and chronic stroke. It has a significant impact on patients' functional recovery, disease development and complications, and even increases the risk of death [6]. The main manifestations of mental disorders caused by stroke are depression (PSD) and anxiety disorder (PSA). The fifth edition of the Diagnostic and Statistical Manual of Mental Disorders (DSM-5) defines depression as depression or lack of pleasure (loss of interest in things, unhappiness) lasting for more than two weeks and persistence of 4 or more of the following symptoms that affect normal daily life: sharp weight gain or sharp loss, insomnia or drowsiness, psychomotor agitation or deficiency, fatigue or lack of energy, sense of worthlessness or excessive guilt, lack of attention or loss of determination [7]. The incidence of depression is reported differently in related studies. The incidence of PSD is 25% to 65%. The risk of depression is the highest within 1 month after stroke, and some patients can recover on their own, but depressive symptoms persist in 1/3 of patients, especially in patients with severe depression, with an incidence of up to 30% in 1 year [7]. The meta-analysis indicated that the incidence of depression in patients with acute stroke was 28% (23% to 33%), 36% (29% to 43%) in recovery (2~6 months), and 31% (26% to 37%) in chronic phase (more than half a year) [8]. The incidence of PSD is high, but it has not been paid enough attention to. Doctors usually pay attention to the improvement of patients' symptoms in the process of disease diagnosis, treatment, and rehabilitation, ignoring patients' psychological problems, resulting in delayed identification and treatment of PSD. Patients with

depression can lead to a slow recovery of physical function, poor compliance for treatment and rehabilitation, increased medical consumption, reduced social activities, and reduced quality of life [9].

With the change of the concept of clinical nursing in China, the clinical nursing work with the core concept of "improving individual function and quality of life" pays more attention to the evaluation of physical and mental health of stroke patients, and has become an important link to enhance the rehabilitation effect of stroke patients [10]. The quality of life of stroke patients depends on the recovery of motor function and cognitive function. Rehabilitation training can effectively reduce the occurrence of stroke complications such as joint contracture, shoulder subluxation, shoulder-hand syndrome, and foot drop [11]. Stroke patients generally receive appropriate rehabilitation guidance and training during hospitalization or in professional rehabilitation institutions, and patients and caregivers can obtain certain rehabilitation knowledge, but due to the characteristics of stroke hemiplegia recovery, at least 45 minutes of moderate exercise rehabilitation training is carried out after discharge in order to ensure the rehabilitation effect during the rehabilitation period, it takes one day for patients who choose to rest at home. It is difficult to guarantee the quality of rehabilitation training. In addition, economic ability, traffic conditions, and other factors limit stroke patients to obtain timely professional rehabilitation guidance; patients are easy to miss the best opportunity for rehabilitation [10, 11]. Therefore, scholars have actively explored how to strengthen the functional recovery of stroke patients at home, although it has achieved certain results, it is still unable to meet the rehabilitation needs of patients. Based on this, this study focused on the effects of nursing and psychological factors on the rehabilitation of motor and cognitive function of stroke patients and carried out a logistic multivariate analysis to provide guidance for clinical stroke rehabilitation nursing.

2. Patients and Methods

2.1. General Information. A total of 200 stroke patients treated from February 2019 to April 2020 were enrolled in our hospital. According to the results of exercise and cognitive rehabilitation, the patients with good rehabilitation were divided into the control group ($n = 140$) and the research group ($n = 60$). With the permission of the Medical Ethics Association of our hospital, all patients signed the informed consent form.

Inclusion criteria were (1) in accordance with the diagnostic criteria revised by the 4th National Conference on Cerebrovascular Diseases in 1995 [12], the first stroke diagnosed by cranial CT and/or MRI examination; (2) 45–80 years old; (3) conscious (GCS >8), stable vital signs, no aphasia and the Montreal cognitive assessment (MoCA > 25); and (4) regular follow-up.

Exclusion criteria were (1) patients with a previous history of brain disease or injury; (2) patients with physical

dysfunction before investigation; (3) patients with a previous history of mental illness, dementia, cognitive impairment, and severe organic diseases; (4) patients with blindness, deafness and mute; and (5) those who refused to participate in the follow-up survey after explanation.

2.2. Treatment Methods

2.2.1. Nursing Methods. Rehabilitation nursing methods: rehabilitation training 30 minutes every time, twice a day, 5 days a week, regular training for 2 weeks, 10 minutes of active and passive training of shoulder joint, 10 minutes of active and passive training of elbow joint, and 10 minutes of wrist and hand function training. The convalesce should complete the traditional rehabilitation training on time and in accordance with the requirements of the experimental design and training.

2.2.2. Psychological Factor. Selfrating anxiety scale is a psychological scale compiled by William W. K. Zung to analyze the degree of anxiety and its changes in the course of treatment [13]. After decades of repeated use and verification, the scale has become one of the most commonly used psychological measurement tools for psychological counselors and psychiatrists. It is mainly used to evaluate the curative effect, but not for diagnosis. The higher the score, the more serious the symptoms. The total score of anxiety is normal if the total score is less than 50, mild for 50, moderate for 61, and severe for more than 70. The number of negative items indicates how many items the subjects did not respond to, and the number of positive items indicates how many items the subjects responded to. Total rough score: the scores of 20 items are added together, and the demarcation is assigned to 40 points.

Selfrating Depression scale (SDS) is a selfrating scale consisting of 20 items and assigned into 4 grades. The prototype is the Depression scale compiled by W. K. Zung (1965). The cut-off value of the SDS standard score was 53, of which 53–62 was mild depression, 63–72 was moderate depression, and more than 73 was severe depression.

2.3. Observation Index

2.3.1. General Information. Statistics of the two groups of patients' age, years of education, occupational status, medical expenses payment methods, family income, course of the disease, and gender.

2.3.2. Motor Function Score. Using the functional Independence rating scale (FIM), which is proposed by the American Association of Rehabilitation Medicine and the Society of Physical Medicine and Rehabilitation. It is a scale widely adopted in the world to evaluate the ability of patients' daily activities. Including selfcare ability, sphincter control, transfer, action ability, communication, and social cognition five dimensions, a total of 18 items, the total score of 180.126, the higher the score, the better the functional

independence of the patient. The FIM scale has good intragroup and intergroup reliability and good internal consistency.

2.3.3. Cognitive Function Score. The patients were evaluated with the MoCA scale and the total score of MoCA was 30 points and the evaluation time was about 5–10 minutes. The score was higher than 25 considered normal. Cognitive impairment is considered below the standard score, which needs to be examined.

2.4. Statistical Analysis. The data of this study were processed by SPSS26.0 statistical software, the counting data were expressed by $[n(\%)]$, the chi-square test was used, the measurement data were expressed by mean \pm standard deviation, t -test was used for comparison between groups, Pearson correlation analysis was used for normal distribution data, and Spearman correlation analysis was performed for skewness distribution data and grade data. Logistic regression was used to analyze the influencing factors. $P < 0.05$ indicated that the difference between groups is statistically significant.

3. Results

3.1. Comparison of General Data. First of all, compared with the general data there were significant differences in age years of education occupational status medical expenses payment mode family income and course of the disease, and the difference was statistically significant ($P < 0.05$). The gender difference was not significant and the data difference was not significant ($P > 0.05$). All the data results are indicated in Figure 1.

3.2. Comparison of Nursing Efficiency. Secondly, we compared the nursing effective rates. The nursing effective rates of the study group were 10 cases, 15 cases, 12 cases, and 23 cases, and the nursing effective rate was 61.67%. In the control group, 78 cases were markedly effective, 33 cases were effective, 25 cases were general and 14 cases were ineffective, and the nursing effective rate was 90.00%. The effective rate of nursing in the study group was higher than that in the control group, and the difference was statistically significant ($P < 0.05$). All the data results are indicated in Figure 2.

3.3. Comparison of Anxiety and Depression Scores. Thirdly, we compared the scores of anxiety and depression. Before nursing, there exhibited no significant difference ($P > 0.05$). The score for anxiety and depression in the study group was higher than that in the control group, and the difference was statistically significant ($P < 0.05$). All the data results are indicated in Table 1.

3.4. Comparison of Motor Function and Cognitive Function. Then, we compared the scores of motor function and cognitive function. Before nursing, there exhibited no significant difference ($P > 0.05$); After nursing, the motor

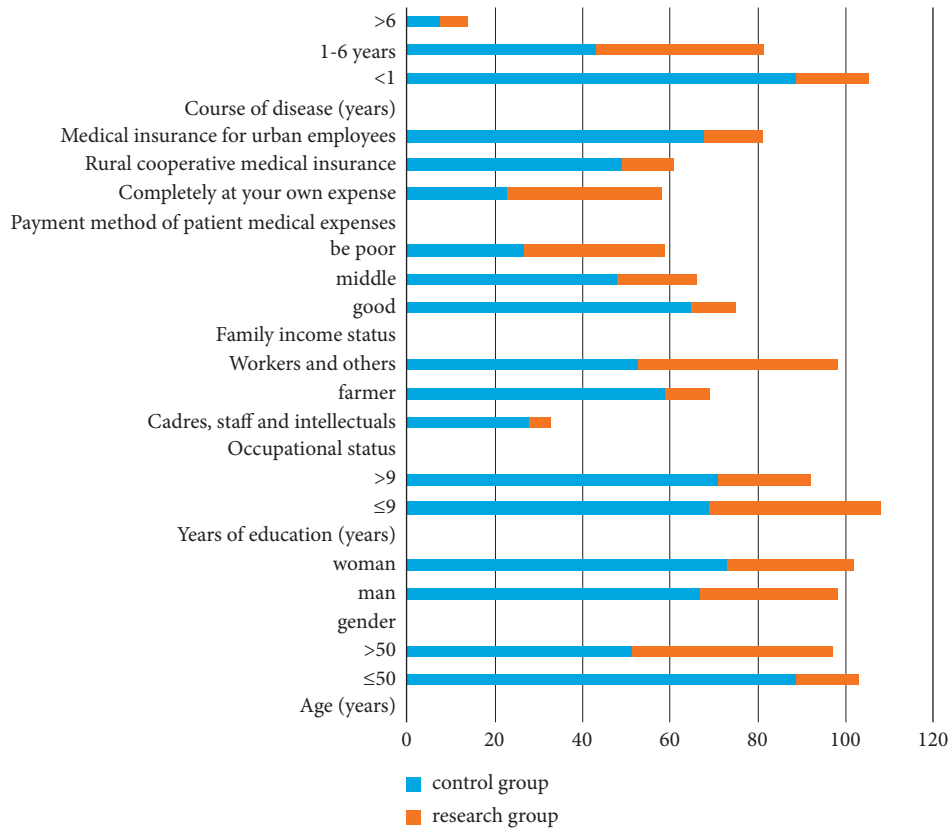


FIGURE 1: Comparison of general information of patients.

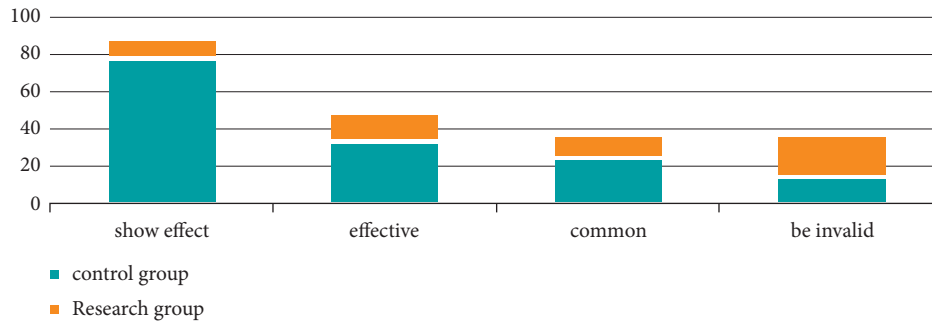


FIGURE 2: The effective rate of patient care in two groups.

TABLE 1: Comparison of anxiety and depression scores before and after nursing ($\bar{x} \pm s$, points).

Grouping	N	SAS		SDS	
		Before nursing	After nursing	Before nursing	After nursing
Control group	140	64.91 \pm 4.12	41.39 \pm 4.31	59.39 \pm 3.12	45.31 \pm 2.16
Research group	60	64.67 \pm 4.12	54.91 \pm 4.43	59.69 \pm 3.42	54.49 \pm 4.42
t value		0.377	20.160	0.605	19.725
P value		>0.05	<0.05	>0.05	<0.05

function increased and the cognitive function score decreased. The score of motor function in the study group was lower than that in the control group, while the score of cognitive function in the study group was higher than that in the control group, and the difference was statistically significant ($P < 0.05$). All the data results are indicated in Table 2.

3.5. *Correlation between Nursing and Psychological Factors and Rehabilitation Effect of Motor and Cognitive Function in Patients with Cerebral Apoplexy.* Next, we analyzed the correlation between nursing and psychological factors and the rehabilitation effect on motor and cognitive function of stroke patients. The results of the Person correlation analysis showed that nursing anxiety and depression were

TABLE 2: Comparison of motor function and cognitive function scores before and after nursing ($\bar{x} \pm s$, points).

Group	N	Motor function		Cognitive function	
		Before nursing	After nursing	Before nursing	After nursing
Control group	140	44.69 \pm 4.42	83.96 \pm 14.12	25.24 \pm 2.12	15.67 \pm 1.66
Research group	60	44.91 \pm 4.33	68.93 \pm 10.31	25.21 \pm 2.41	20.49 \pm 1.22
t value		0.324	7.434	0.087	20.256
P value		>0.05	<0.05	>0.05	<0.05

significantly correlated with the rehabilitation effect of motor cognitive function in patients with stroke, and the difference was statistically significant ($P < 0.05$). All the data results are indicated in Table 3.

3.6. Logistic Regression Analysis of the Influencing Factors of Motor and Cognitive Rehabilitation in Patients with Cerebral Apoplexy. Finally, we conducted a logistic regression analysis on the influencing factors of motor and cognitive rehabilitation in stroke patients. The results of the logistic regression analysis indicated that age, family income, nursing efficiency, anxiety, and depression were the factors affecting motor and cognitive rehabilitation in stroke patients, and the difference was statistically significant ($P < 0.05$). All the data results are indicated in Table 4.

4. Discussion

Stroke is an obvious chronic and refractory disease, which seriously endangers human health and life. It is generally divided into embolic cerebral infarction, cerebral hemorrhage, subarachnoid hemorrhage, and other unclassified strokes [17]. According to the statistics updated by the American Heart Association (AHA) in 2013, the prevalence rate of stroke in the United States (2.8%), the incidence rate (790000/year), and the mortality rate (120000 in 2009) are still high [18]. Clinical manifestations are often transient or permanent brain dysfunction symptoms and signs, with high incidence, high disability rate, high recurrence rate, and high mortality rate. In 2011, AHA and the American Stroke Association (ASA) updated the Stroke Primary Prevention guidelines, indicating that stroke is the main cause of dysfunction, and 15~30% of the survivors may be disabled [19]. In China, according to the guidelines for the Prevention and treatment of Cerebrovascular Diseases issued in 2007, it is estimated that there are about 2 million new stroke cases each year. About 75% of the survivors lost their ability to work and live to varying degrees, of which 40% were severely disabled [20]. In 2008, the third survey of the cause of death of residents in China indicated that cerebrovascular disease (mainly stroke) became the leading cause of death in the country. Therefore, the epidemiological situation of stroke in China is grim, and the responsibility for effective prevention and treatment of stroke is urgent and significant [21]. Rehabilitation training is the most effective way to enhance poststroke dysfunction in the treatment and rehabilitation of stroke. Meanwhile, it can strengthen the independence of life and the quality of life [22]. Stroke is a major event that

TABLE 3: Correlation between nursing and psychological factors and rehabilitation effect of motor and cognitive function in patients with cerebral apoplexy.

Factors	r	P
Nursing	0.881	<0.05
Anxiety	-0.685	<0.05
Depression	-0.866	<0.05

threatens human physical and mental health. Stroke patients often start their own psychological defense mode to deal with psychological stress after the onset of stroke. Improper use of psychological defense will adversely affect the treatment and prognosis of stroke. Stroke psychological disorder is a curable complication, the use of antidepressants can partially promote the psychological symptoms of patients, but in addition to drug treatment, the study of the influencing factors of mental disorders after stroke can provide an important intervention direction for the prevention and control of such complications [23]. Therefore, scholars have actively explored how to strengthen the functional recovery of stroke patients at home, although it has achieved certain results, it is still unable to meet the rehabilitation needs of patients. Based on this, this study focused on the effects of nursing and psychological factors on the rehabilitation of motor and cognitive function of stroke patients and carried out a logistic multivariate analysis to provide guidance for clinical stroke rehabilitation nursing.

Anxiety disorder is a common psychological and mental symptom of patients after illness [24]. Usually, proper anxiety will promote patients' sense of selfprotection and enhance their healthy behavior. A certain degree of anxiety after a stroke is a normal psychological reaction of human beings after their lives are threatened. However, the high level of anxiety symptoms of psychological measurement will affect the quality of life of patients, bring more medical consumption, increase the risk of poor prognosis and family burden, and even be life-threatening in serious cases [24, 25]. The incidence of poststroke anxiety (PSA) was 8%~29%, 20% in acute phase (13%~26%), 23% in convalescent stage (19%~27%), and 24% in chronic phase (19%~29%) [26]. The main manifestations of PSA are excessive or irrational fear or worry, patients are often worried, upset, fidgeting, excessive vigilance, and often accompanied by autonomic nervous hyperactivity, such as palpitations, tremors, dizziness, sweating, and gastrointestinal discomfort. Some patients have panic attacks because the anxiety symptoms of some patients are similar to those of stroke and are ignored and the incidence of anxiety is reported less, the attention to anxiety

TABLE 4: Logistic regression analysis of the influencing factors of motor and cognitive rehabilitation in patients with cerebral apoplexy.

Factors	<i>b</i>	S.E	Chi-square value	<i>P</i>	OR	95% CI for OR
Age	2.122	0.553	14.724	0.000	8.348	2.824–24.677
The number of years of education	1.221	1.432	0.727	0.394	3.391	0.205–56.133
Occupational condition	1.244	1.221	1.038	0.308	3.469	0.317–37.984
Payment method of medical expenses	2.561	1.874	1.868	0.172	12.949	0.329–509.811
Household income status	2.141	0.532	6.622	0.000	12.807	4.514–36.333
Nursing effective rate	2.550	0.532	22.975	0.000	12.807	4.514–36.333
Anxiety	−2.313	0.422	30.042	0.000	0.099	0.043–0.226
Depression	−2.144	0.451	22.599	0.000	0.117	0.048–0.284

symptoms is much lower compared to PSD. Studies indicate that 17% to 80% of PSA patients are also associated with PSD [26, 27]. So far, there are many studies on the influencing factors of PSA and depression. Scholars have investigated and verified the risk factors of psychological problems in stroke patients from different angles, but the results are still controversial [27]. The survey results of some scholars indicate that stroke patients generally have different types and degrees of psychological problems 2 weeks after illness (100%). This is related to the patient's education level, family background, stroke severity, and the degree of physical and speech disorders [28]. The investigation of other scholars indicated that the mood disorder after stroke was related to the type of stroke, the location of stroke focus, NIHSS score, and BI score at admission. However, some scholars believe that marital status, nerve injury, and daily activity ability have an influence on emotion [29]. There are also different research results on the effects of physical activity level and physical training on the psychology and spirit of stroke patients [30]. After the onset of stroke, the physique of stroke patients declined, and their cardiopulmonary endurance was about 50% of that of healthy people of the same age and sex, resulting in a serious lack of physical activity. The study on the psychological state of patients with stroke shows that rehabilitation exercise can improve the quality of life of patients, thus enhancing their psychological level [31]. However, there are also different research results. In a multicenter survey, we mainly observed the incidence, severity, and time process of anxiety and depression in stroke patients, and found that even if the patients' condition, characteristics, and exercise intensity were different. However, there exhibited no significant difference in the incidence and severity of anxiety and depression among patients in different rehabilitation centers, and patients with new psychological problems were found at each time. Some scholars have pointed out that some cognitive rehabilitation therapy can make patients' anxiety and depression states persist or even worsen, but the evidence intensity is not high and does not continue to demonstrate [31, 32].

Identifying patients' depressive symptoms and finding the risk of depression are very important for timely preventive measures, early and appropriate psychological intervention, and related treatment [32]. There are two explanations for the mechanism of poststroke depression PSD, one is physiological etiology, caused by brain lesions, and the other is psychogenic disorder, which is the patient's stress and emotional response to the disease. Therefore, the

assessment of depression in stroke patients is different from other diseases because of the characteristics of neurological diseases. Mental and psychological diseases such as energy decline, fatigue, irritability, sleep disorders, and lack of attention in depression may also be neurological symptoms caused by brain diseases [32, 33]. Patients may have both neurological and psychosocial symptoms, which makes psychological assessment more difficult. Then, the functional impairment of patients, such as aphasia, anosognosia, confusion, or dementia, will affect the reliability of doctor-patient communication and patient reporting in the evaluation process, which also becomes an obstacle in the diagnosis of depression. Nursing and psychological factors are common research contents in the influencing factors of cognitive and motor rehabilitation of stroke, but there are a lot of controversies. Previous studies have indicated that stroke patients with poor cognitive and motor rehabilitation have a higher incidence of depression [33]. Clinical epidemiological investigation shows that there are differences in rehabilitation effect, nursing effective rate, and psychological factors among stroke patients, indicating that there are some differences in rehabilitation effect among stroke patients with different psychological states and nursing effects. After the onset of stroke, age and family income are also one of the factors affecting the mental state of patients. In addition, stroke often occurs in the middle-aged and elderly. Middle-aged and elderly women in menopause or postmenopause are more likely to induce psychological disorders due to the decrease in estrogen levels [33, 34]. Some studies have indicated that stroke is a risk factor for depression during the course of 3 years, which may be related to the individual's psychological defense mechanism during psychological stress [34]. In addition, regarding patients ≤ 50 years old and with good family income status have better coping ability to deal with health problems [35]. Some scholars have also confirmed that the older the age is, the higher the risk of PSD is, especially within 2 months after onset, there is a significant correlation between age and depression [35, 36]. Although the incidence of stroke is younger, the physiological decline of the elderly makes the incidence of cerebrovascular diseases high in the elderly. The whole process of life development-transition theory holds that when an individual experiences transitional events in life, such as aging, sudden serious illness and other transitional events, personal role functions, goals, and life expectations will change due to the events. When the individual adjusts and adapts to the new

life situation, there will be stress, the mild ones will only have emotional ups and downs, and the serious ones will develop into depression. Therefore, the inconsistency of the results in the study may come from the differences in the age of the subjects [36]. Further research should divide the age group reasonably and consider the impact of a variety of transitional events such as age, and good family income. The same idea can be found in the study put forward by other studies [37, 38]. They have applied new methods in the study, and the conclusions drawn can also give some support to this study. There are some limitations to this study. First, the sample size of this study is not large and it is a single-center study, so bias is inevitable. In future research, we will carry out multicenter, large-sample prospective studies, or more valuable conclusions can be drawn.

In summary, nursing and psychological factors have a certain influence on the rehabilitation of motor and cognitive function of stroke patients. There is a significant correlation between nursing effect and anxiety and depression in the rehabilitation of motor and cognitive function of stroke patients. Age and family income may be risk factors affecting patients' psychological emotions, suggesting that medical staff should pay attention to patients' negative emotions and strengthen nursing intervention for patients in order to promote the rehabilitation effect of motor and cognitive function in stroke.

Data Availability

The datasets used and analyzed during the current study are available from the corresponding author upon reasonable request.

Conflicts of Interest

The authors declare that they have no conflicts of interest.

References

- [1] Y. Zhang, J. Xie, and L. Wang, "Effect of improved food intake training based on dietary preference on swallowing function in patients with stroke," *Chinese Journal of physical Medicine and Rehabilitation*, vol. 43, no. 12, pp. 1084–1086, 2021.
- [2] Y. Zhang, Y. Li, and Z. Huang, "Effect of continuous nursing of regional medical association on self-nursing ability and quality of life of stroke patients," *Journal of Nursing*, vol. 36, no. 22, pp. 87–90, 2021.
- [3] C. Huang, D. Liu, and J. Zhu, "Observation on the effect of intervention based on multidisciplinary collaborative diagnosis and treatment in patients with acute ischemic stroke," *Nursing Journal*, vol. 28, no. 21, pp. 62–66, 2021.
- [4] J. Zheng, H. Hu, and D. Li, "Observation and nursing care of patients with acute macrovascular occlusive ischemic stroke after thoracoscopic lobectomy," *PLA Journal of Nursing*, vol. 38, no. 10, pp. 77–79, 2021.
- [5] L. Ge, Y. Fang, and S. Rao, "A retrospective case-control study on late failure of arteriovenous fistula in hemodialysis patients and prediction of risk factors," *Computational and Mathematical Methods in Medicine*, vol. 2022, Article ID 8110289, 8 pages, 2022.
- [6] M. G. Maggio, D. Latella, G. Maresca et al., "Virtual reality and cognitive rehabilitation in people with stroke: An overview," *Journal of Neuroscience Nursing*, vol. 51, no. 2, pp. 101–105, 2019.
- [7] T. Loetscher, K. J. Potter, D. Wong, and R. das Nair, "Cognitive rehabilitation for attention deficits following stroke," *Cochrane Database System Review*, vol. 10, no. 11, Article ID CD002842, 2019.
- [8] F. S. Sarfo, U. Ulasavets, O. K. Opare-Sem, and B. Ovbiagele, "Tele-rehabilitation after stroke: an updated systematic review of the literature," *Journal of Stroke and Cerebrovascular Diseases*, vol. 27, no. 9, pp. 2306–2318, 2018.
- [9] T. Renton, A. Tibbles, and J. Topolovec-Vranic, "Neuro-feedback as a form of cognitive rehabilitation therapy following stroke: A systematic review," *PLoS One*, vol. 12, no. 5, Article ID e0177290, 2017.
- [10] Q. Wu, J. Zhou, and S. Wang, "Mediating effect of rehabilitation self-efficacy between PSD and post-stroke fatigue in elderly stroke convalescent patients," *Nursing Journal*, vol. 28, no. 17, pp. 64–69, 2021.
- [11] Ho Kim Sun, "Effects of dual transcranial direct current stimulation and modified constraint-induced movement therapy to improve upper-limb function after stroke: a double-blinded, pilot randomized controlled trial," *Journal of Stroke and Cerebrovascular Diseases*, vol. 30, no. 9, pp. 491–494, 2021.
- [12] X. Xue, "Application of hemiplegic limb rehabilitation training in nursing care of patients with cerebral infarction and its effect on quality of life-- comment on Clinical Nursing of Neurology," *Clinical Pharmacology and Therapeutics in China*, vol. 26, no. 08, pp. 836–837, 2021.
- [13] K. Kanika and G. Singh, "Commentary on: effect of a comprehensive E-rehabilitation Intervention alongside conventional stroke rehabilitation on disability and Health-Related quality of life: a Pre-Post comparison," *Journal of Rehabilitation Medicine*, vol. 3, no. 421, pp. 591–594, 2021.
- [14] T. Matsushita, S. Nishioka, and S. Taguchi, "Effect of improvement in sarcopenia on functional and discharge outcomes in stroke rehabilitation patients," *Nutrients*, vol. 13, no. 7, p. 2192, 2021.
- [15] M. Thornton, H. Jennifer, B. Krista, T. Dyks, H. Finestone, and M. MacKay-Lyons, "Development of a digital learning program for physiotherapists to enhance clinical implementation of aerobic exercise in stroke rehabilitation," *Archives of Physiotherapy*, vol. 11, no. 1, pp. 530–533, 2021.
- [16] M. Tay, "Hospital readmission in stroke survivors one year versus three years after discharge from inpatient rehabilitation: prevalence and associations in an asian cohort," *Journal of Rehabilitation Medicine*, vol. 53, no. 6, 2021.
- [17] A. Low Michelle, E. Power, and McG. Margaret, "Sexuality after stroke: exploring knowledge, attitudes, comfort and behaviours of rehabilitation professionals," *Annals of physical and rehabilitation medicine*, vol. 12, no. 42, pp. 56–59, 2021.
- [18] C. Raff, C. Mary, C. Chris, R. Lamont, S. Dean, and M. Tarrant, "Challenges of recruiting patients into group-based stroke rehabilitation research: reflections on clinician equipoise within the singing for people with aphasia (SPA) pilot trial," *Frontiers in Psychology*, vol. 12, no. 41, pp. 519–521, 2021.
- [19] R. Song, M. Park, T. Jang, J. Oh, and M. K. Sohn, "Effects of a tai chi-based stroke rehabilitation program on symptom clusters, physical and cognitive functions, and quality of life: a randomized feasibility study," *International Journal of*

- Environmental Research and Public Health*, vol. 18, no. 10, pp. 445–449, 2021.
- [20] R. S. Calabrò, G. Sorrentino, A. Cassio et al., “Robotic-assisted gait rehabilitation following stroke: a systematic review of current guidelines and practical clinical recommendations,” *European Journal of Physical and Rehabilitation Medicine*, vol. 57, no. 3, pp. 460–471, 2021.
 - [21] J. Lim, T. Lim, J. Lee, and H. SimChangYoonJung, “Patient-specific functional electrical stimulation strategy based on muscle synergy and walking posture analysis for gait rehabilitation of stroke patients,” *Journal of International Medical Research*, vol. 49, no. 5, 2021.
 - [22] H. Ahmad Ainuddin, M. H. Romli, T. A. Hamid, M. S F Salim, and L. Mackenzie, “An exploratory qualitative study with older Malaysian stroke survivors, caregivers, and healthcare practitioners about falls and rehabilitation for falls after stroke,” *Frontiers in Public Health*, vol. 9, no. 31, pp. 591–594, 2021.
 - [23] W. van MeijerenPont, J. Tamminga Sietske, H. Goossens Paulien et al., “Societal burden of stroke rehabilitation: costs and health outcomes after admission to stroke rehabilitation,” *Journal of Rehabilitation Medicine*, vol. 21, no. 45, pp. 42–45, 2021.
 - [24] N. Norouzi Gheidari, S. Archambault Philippe, K. Monte Silva et al., “Feasibility and preliminary efficacy of a combined virtual reality, robotics and electrical stimulation intervention in upper extremity stroke rehabilitation,” *Journal of Neuro-engineering and Rehabilitation*, vol. 18, no. 1, pp. 691–694, 2021.
 - [25] H. Bahia, P. Anita, C. Chiara et al., “Predictors of function, activity, and participation of stroke patients undergoing intensive rehabilitation: a multicenter prospective observational study protocol,” *Frontiers in Neurology*, vol. 12, no. 3, pp. 459–461, 2021.
 - [26] D. Lee and Y. Bae, “Short-term effect of kinesio taping of lower-leg proprioceptive neuromuscular facilitation pattern on gait parameter and dynamic balance in chronic stroke with foot drop,” *Healthcare*, vol. 9, no. 3, pp. 195–197, 2021.
 - [27] C. Breen Joan, “Abstract P209: community-based outpatient stroke rehabilitation program achieves excellent return to work outcomes: characteristics and rehabilitation outcomes of stroke survivors who return to work,” *Stroke*, vol. 52, no. 33, pp. 550–554, 2021.
 - [28] R. Annie, D. Ariane, and S. Morissette Gravel Anne, “Inclusion of relatives in stroke rehabilitation: perception of quality of services they received in the context of early supported discharged (ESD), in- and out-patient services,” *Topics in Stroke Rehabilitation*, vol. 28, no. 2, pp. 512–515, 2021.
 - [29] T. Hara, S. Aturan, A. McIntyre, and A. M. Burhan, “The effect of non-invasive brain stimulation (NIBS) on attention and memory function in stroke rehabilitation patients: a systematic review and meta-analysis,” *Diagnostics*, vol. 11, no. 2, pp. 531–536, 2021.
 - [30] I. Jeffares, N. A. Merriman, F. Doyle, and A. HorganHickey, “Inclusion of stroke patients in expanded cardiac rehabilitation services: a cross-national qualitative study with cardiac and stroke rehabilitation professionals,” *Disability & Rehabilitation*, vol. 44, no. 14, pp. 3610–3622, 2021.
 - [31] A. Kumar, Q. Fang, and P. Elena, “The influence of psychological and cognitive states on error-related negativity evoked during post-stroke rehabilitation movements[J],” *BioMedical Engineering Online*, vol. 20, no. 1, pp. 49–53, 2021.
 - [32] D. Edwards Jodi, E. Black Sandra, B. Shaun et al., “Canadian platform for trials in noninvasive brain stimulation (CanStim) consensus recommendations for repetitive transcranial magnetic stimulation in upper extremity motor stroke rehabilitation trials,” *Neurorehabilitation and Neural Repair*, vol. 35, no. 2, pp. 559–562, 2021.
 - [33] M. van Bloemendaal, S. A. Bus, F. Nollet, A. C. Geurts, and A. Beelen, “Feasibility and preliminary efficacy of gait training assisted by multichannel functional electrical stimulation in early stroke rehabilitation: a pilot randomized controlled trial,” *Neurorehabilitation and Neural Repair*, vol. 35, no. 2, pp. 566–569, 2021.
 - [34] H. Cai, T. Lin, L. Chen, and G. Weng Zhu ChenCai, “Evaluating the effect of immersive virtual reality technology on gait rehabilitation in stroke patients: a study protocol for a randomized controlled trial,” *Trials*, vol. 22, no. 1, p. 91, 2021.
 - [35] J. Wolf Timothy, “Doherty Meghan, Boone Anna, et al. Cognitive oriented strategy training augmented rehabilitation (COSTAR) for ischemic stroke: a pilot exploratory randomized controlled study,” *Disability and Rehabilitation*, vol. 43, no. 2, pp. 84–88, 2021.
 - [36] M. Kevdzija and G. Marquardt, “Stroke patients’ nonscheduled activity during inpatient rehabilitation and its relationship with the architectural layout: a multicenter shadowing study,” *Topics in Stroke Rehabilitation*, vol. 29, no. 1, pp. 9–15, 2021.
 - [37] A. Javeed, R. Sanam Shahla, S. Zhou, R. Riaz, S. U. Khan, and S. J. Kwon, “Heart risk failure prediction using a novel feature selection method for feature refinement and neural network for classification,” *Mobile Information Systems*, vol. 2020, Article ID 8843115, 11 pages, 2020.
 - [38] Z. Zhao and L. Feng, “Logistic regression analysis of risk factors and improvement of clinical treatment of traumatic arthritis after total hip arthroplasty (THA) in the treatment of acetabular fractures,” *Computational and Mathematical Methods in Medicine*, vol. 2022, Article ID 7891007, 10 pages, 2022.

Research Article

Effect of Intelligent Operating Hole Towel in Cataract Patients

Suhui Xu, Meijuan Lan , Haiyan Cai, and Pei Zhang

Second Affiliated Hospital Zhejiang University College of Medicine, Ophthalmology Department,
No. 88 Jiefang Road, Shangcheng District, Hangzhou, Zhejiang 310007, China

Correspondence should be addressed to Meijuan Lan; lanmj@zju.edu.cn

Received 21 June 2022; Revised 6 July 2022; Accepted 9 July 2022; Published 18 August 2022

Academic Editor: Dong Chen

Copyright © 2022 Suhui Xu et al. This is an open access article distributed under the Creative Commons Attribution License, which permits unrestricted use, distribution, and reproduction in any medium, provided the original work is properly cited.

Backgrounds. The eyeball and its ancillary tissues are important organs with the same shape and structure, and examining the surgical site is particularly important in ophthalmic surgery. A safe and easy-to-operate ophthalmic surgical hole towel is of great significance for improving the safety of ophthalmic surgery. **Objective.** To explore the effect of intelligent operating hole towel in cataract patients. **Methods.** From April 2020 to April 2021, 1220 cases of cataract patients who needed surgery in the second affiliated hospital Zhejiang University college of medicine, were recruited and randomly divided into the control group and the observation group. The control group adopted a disposable ophthalmic single-port operation cloth, and the intelligent surgical hole towel was used in the observation group. Incidences of surgical site errors, the amount of operation time, bacterial infections, and patient satisfaction were recorded. **Results.** The average operation time in the observation group had obviously reduced compared with the control group ($p < 0.05$). Moreover, patients' overall medical satisfaction in the observation group improved significantly compared with the control group ($p < 0.05$). **Conclusions.** The design and use of the new intelligent ophthalmic surgical hole towel can promote the efficiency of ophthalmic surgery, realize the intelligent verification of surgical eye, reduce the risk of surgical site errors and improve medical safety.

1. Introduction

Under the theme “Safe Surgery, Save Lives,” the 2007–2008 WHO Alliance for patient safety aims to improve surgical safety and save more lives worldwide. The Surgical Safety Checklist emphasizes that Surgical Safety checks include “before anesthesia (Sign in),” “before surgery (Time out),” and “before patients leave the operating room (Sign out).” WHO recommends the continuous optimization and development of surgical safety verification systems based on specific surgical procedures to ensure that the correct surgical site is marked on the patient's body and that the surgery is performed on the correct body part [1].

A cataract is an eye disease with clouding of the lens. With the aging of the global population, the incidence of cataracts is rising as the top treatable blinding eye disease worldwide. Since the rapid pace of eye surgery and the special anatomy of the eyeball, it is easy for the surgeon to confuse the eyes when covering the patients' eyes after the surgical field is disinfected, leading to the wrong covering of

the eyes and causing negative effects. In case of surgical field placement error, the surgical staff can timely find the error of surgical field placement during the “Time Out” safety check and suspend the operation. Although the surgical site error did not occur due to the timely intervention, ophthalmic surgery is mainly performed under local anesthesia. Patients are conscious that the error of eye tissue placement can easily cause a trust crisis of patients. Moreover, re-disinfecting towels and preparing all kinds of products increased the surgical staff's workload and affected the operation's efficiency [2]. In addition, the surgical towel is incorrect, and the surgical safety staff is not making proper checks leading to the surgical site error unidentified before “Time Out,” which may result in serious adverse events occurring. Therefore, “check the eyes when placing surgical towels” is significantly needed.

Before ophthalmology patients enter the operating room, medical staff confirm the patient's identity by using the patient's name and medical record number. The surgeon checks the medical record and image data to verify the

surgical safety of the surgical eyes [3]. In the procedure of surgical safety check, a new type of intelligent ophthalmic surgical hole napkin is added to assist in the surgical eye identification check. It can not only improve the visual perception of the surgical eye but also prevent the identification errors of the surgical site in the process of surgery [4, 5]. The new intelligent ophthalmic operating towel is based on the disposable ophthalmic operating towel and adds intelligent design in the key link of “operation cloth.” Currently, the surgical marker used in ophthalmology is an oily marker, which can only be used for cosmetic surgical markers [6, 7]. Special intelligent material is used in the new special intelligent surgical marker pen, which can react with the intelligent material of the surgical hole towel when completing the marking [8, 9]. The voice chip is embedded in the new smart surgical towel. When the surgical towel is unfolded, the voice prompts, “Please check the surgical eye.”

The disadvantage of the previous ophthalmic surgical towel is that it cannot be directly positioned on the front of the surgical site and usually requires another person to locate and operate correctly, which has the disadvantages of complex operation, easy contamination, and dispersion of surgical equipment preparation. Moving the towel hole caused a lot of inconvenience to the operation, extended the operation time, and increased the number of operation steps. It is necessary to design a towel to achieve the purpose of safety, convenience, and convenient operation. This study intends to promote the efficiency of ophthalmic surgery, realize the intelligent verification of surgical eye, reduce the risk of surgical site errors and improve medical safety through the design and use of the new intelligent ophthalmic surgical hole towel.

2. Methods

2.1. Participants. From April 2020 to April 2021, 1220 cases of cataract patients in the second affiliated hospital Zhejiang University were selected and randomly divided into two groups. There were 248 males and 362 females in the control group and 266 males and 344 females in the observation group. All patients in this study completed this study and no patients who dropped out halfway.

2.2. Inclusion and Exclusion Criteria. Inclusion criteria: (1) patients with cataracts need surgery; (2) no other serious diseases such as heart, liver, kidney, and other important organ dysfunction; (3) patients voluntarily participated and signed informed consent forms. Exclusion criteria: (1) patients with cataracts do not need surgery; (2) complicated with serious diseases such as heart, liver, kidney, and other important organ dysfunction; (3) poor treatment compliance; (4) incomplete clinical data or withdrawal; (5) not signing informed consent.

2.3. Methods

2.3.1. The Control Group. Disposable ophthalmic single-port operation hole towel was adopted in the control group.

Before the operation, the skin of the eye is disinfected and the patient's hair is covered with a headband. The disposable ophthalmic operation cloth includes the main body of the cloth and a single oval surgical eye hole. The back of the main body of the cloth is located on both sides of the surgical hole with glue, which is glued and fixed simultaneously. The surgical opening directly faces the patient's surgical eye, and the surgical towel is unfolded in turn according to the arrow pointing at the front of the towel.

2.3.2. The Observation Group. Intelligent surgical hole towels were used in the observation group. After the skin around the eyes is disinfected, the patient's hair is covered with a turban. Then, the procedure of towel laying for surgical holes follows the control group. When the operating hole towel was expanded to contact the operating eye with the intelligent operating mark, the voice suggested that the operating site was correctly exposed.

2.4. Observe Indicators. The data of surgical site errors, amount of the operation time, bacterial detection, and patient satisfaction were recorded.

2.5. Statistical Analysis. The SPSS 19.0 statistical software was employed to analyze data. The count data was expressed by the number of cases and percentage (%), and the χ^2 test performed the comparison between groups, *t*-test was used in independent samples. $p < 0.05$ indicates that the difference was statistically significant.

3. Results

3.1. Schematic Diagram of Surgical Towel and Marker Pen. As shown in Figure 1, the new intelligent ophthalmic surgical hole towel is displayed. Figure 1 A, B, C, and D represent voice prompt chips, and E refers to the smart surgery empty towel hole.

3.2. Basic Characteristics of the Patients. One thousand two hundred twenty cases of cataract patients who needed surgery were selected from April 2020 to April 2021 in the second affiliated hospital Zhejiang university hospital. The basic characteristics of the patients, including age, gender, and education level showed no statistical difference (Table 1).

3.3. The Incidents of Surgical Site Errors after Towel Placement and Surgical Site Errors. 5 cases of surgical site errors after towel placement were found in the control group, and no surgical site errors after towel placement were found in the observation group. Although compared between the two groups (the distinction does not prove a statistical significance, $p > 0.05$), it can be seen that the number of surgical site errors after towel placement found in the observation group was significantly lower than in the control group. Notably, there are no surgical site errors found in the observation group and the control group ($p > 0.05$) (Table 2).

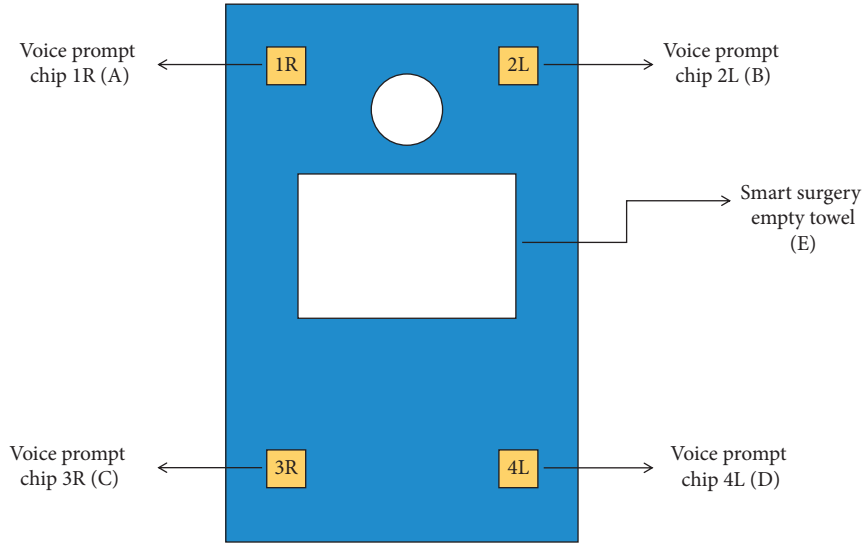


FIGURE 1: New intelligent ophthalmic surgical hole towel.

TABLE 1: Comparison of basic characteristics of the patients between the two groups.

Basic indexes	Observation group ($n = 610$)	Control group ($n = 610$)	χ^2	p
Age (year)				
65–70	115	126	1.835	0.402
60–65	358	365		
55–60	137	119		
Sex				
Male	266	248	1.089	0.324
Female	344	362		
Education level				
≤Primary school	371	394	1.873	0.392
Middle-high school	159	145		
>High school	80	71		

TABLE 2: The incidences of surgical site errors were compared between the two groups.

Groups	Observation group	Control group	χ^2	p
Surgical site errors after towel placement	0	5	5.021	0.062
Surgical site errors	0	0	0	1
n	610	610	—	—

3.4. Comparison of the Amount of Operation Time between the Two Groups. The average amount of operation time in the observation group is 20.93 ± 3.556 (min) and the average amount of operation time in the control group is 21.98 ± 4.127 (min). Results indicated the average amount of the operation time in the observation group had obviously contracted, $p < 0.05$, with a statistical difference (Table 3).

3.5. The Comparison of Bacterial Detection between the Two Groups. There was no statistically significant difference in bacterial detection between the two groups ($p > 0.05$). Results showed that only two bacterial infections occurred in

TABLE 3: Comparison of amount of the operation time between the two groups.

Groups	Amount of the operation time	t	p
Observation group	20.93 ± 3.556	4.749	$P < 0.001$
Control group	21.98 ± 4.127		

the control group and bacterial infections were detected in the observation group (Table 4).

3.6. Comparison of the Patients' Satisfaction between the Two Groups. The number of patient satisfaction in the observation group is 600 and the number of patient satisfaction in the control group is 585. Results suggested that patients' overall medical satisfaction in the observation group was improved by applying a new intelligent ophthalmic surgical hole towel combined with a surgical site marker pen (Table 5). The difference was a statistically significant comparison of the patient satisfaction between the two groups ($p < 0.05$).

TABLE 4: Comparison of bacterial detection between the two groups.

Groups	Bacterial detection			X^2	p
	N	Cases	Incidence (%)		
Observation group	610	0	0	3.007	0.249
Control group	610	2	0.328		

TABLE 5: Comparison of the patients satisfaction between the two groups.

Groups	Patients satisfaction			X^2	p
	N	Cases	Incidence (%)		
Observation group	610	600	98.361	6.618	0.015
Control group	610	585	95.902		

4. Discussion

Medical and health safety is a major issue affecting the health of hundreds of millions of people. With the improvement of people's economic level, more and more attention was focused on health. Meanwhile, higher requirements on the level and quality of medical and health services were put forward to the hospital. The eyes are the main organ for humans to collect information from the outside world. More than 80% of information is obtained from the eyes, so the average person attaches much more importance to their own eyes than other organs. Ophthalmology, as a special specialty, is characterized by the fact that most ophthalmic diseases need surgical treatment. Only a few can be treated with simple drugs or physical therapy. Therefore, the ophthalmic medical service is based on surgical treatment, supplemented by drugs and physical therapy. Surgery is needed to treat ocular plastic surgery, infection, trauma, tumor, cataract, and optometry. Surgical treatment not only involves equipment, instruments, and consumables but also involves the participation of medical and anesthesia professionals. And, due to the small surgery scale, the number of operations is far more than in other surgical specialties. In this way, the management of ophthalmic surgery is more strict and the quality of medical treatment is higher.

A cataract is the world's number one blinding eye disease. Cataracts are mainly because by lens metabolism disorder, lens protein denaturation, formation of turbidity, and blindness. With the rapid aging of the global population, the incidence of cataracts is increasing. According to incomplete statistics from the World Health Organization, there are about 500,000 new cataract blind people yearly [10, 11]. Currently, the number of cataract blindness in China is second only to India, ranking second in the world. With the development of health care, cataract surgery can restore nearly normal vision in most patients [12, 13]. Improving patients' visual ability and recovery is the key to improving patients' quality of life.

Surgical towels are the basic operation before the operation begins. Surgical pads not only keep the surgical area sterile but also prevent skin bacteria from entering the

incision, thereby reducing the risk of surgical site infection. The disadvantage of the original ophthalmic surgical towel is that it is not conducive to the safety verification of the surgical site. In the process of replacing the surgical towel, it will not only cause a lot of inconvenience to the surgical operation but also prolong the operation time, increase the number of operation steps, and significantly increase the possibility of contamination of the surgical area, which is easy to cause intraoperative infection [14]. In addition, ophthalmic surgery anesthesia is mainly performed under local anesthesia. Patients are conscious during the operation and are more prone to psychological stress reactions such as tension and anxiety under closed and dim operation orders for a long time. Therefore, it is necessary to improve. In this study, a kind of ophthalmic operation cloth is proposed. Although its structure is complex, it can realize intelligent operation site verification and is convenient for operation preparation and operation.

In 1957, the United States medical and health institutions on the health service patient satisfaction evaluation for the first time. Measuring patient satisfaction is the establishment and constitutes a prerequisite for hospital certification. Patient satisfaction has become a deterministic index of the quality and effect of the health service system. Patient satisfaction with surgery is considered an important factor affecting patients' overall medical satisfaction with the hospital. In the present study, the use of the new intelligent operating hole towel can promote the efficiency of ophthalmic surgery, realize the intelligent verification of surgical eye, reduce the risk of surgical site errors and improve medical safety. In addition, results showed that patients' overall medical satisfaction in the observation group was obviously improved compared with the control group. When high-quality medical services are advocated, high-quality medical technology can make patients feel safe and increase their trust in doctors.

There are also some shortcomings in this study. All the physicians were from the same surgical team in the second affiliated hospital Zhejiang university. Therefore, the results of this survey cannot fully represent the overall level and status of ophthalmic surgery in China. It is still necessary to expand the study's sample size and conduct followup statistics.

5. Conclusions

The intelligent operating hole towel gives the surgeon a more intuitive experience so that it can be attached to the patient's surgical site more quickly and accurately. The practicability of an intelligent operating hole towel can not only shorten the operation time to reduce the risk of surgical site infection but also strengthen the aseptic barrier to ensure the safety of patients, which is worthy of clinical promotion.

Data Availability

The datasets used and analyzed during the current study are available from the corresponding author upon reasonable request.

Ethical Approval

The authors are accountable for all aspects of the work in ensuring that questions related to the accuracy or integrity of any part of the work are appropriately investigated and resolved. The study was carried out in accordance with the ethical guidelines of the Declaration of Helsinki (as revised in 2013).

Conflicts of Interest

The authors declare that there are no conflicts of interest.

Acknowledgments



Project of the Department of Education y202147384.

References

- [1] N. Yu, L. Wu, J. Su, K. Huang, S. Zhao, and X. Chen, "One more paper towel, longer protection," *Journal of the American Academy of Dermatology*, vol. 82, no. 6, pp. e189–e190, 2020.
- [2] R. Jasper, S. Ahmed, and J. C. Blankenship, "Unintended delivery of surgical towel fibers into a vein graft during cardiac catheterization," *Cardiovascular Revascularization Medicine*, vol. 20, no. 11S, pp. 9–12, 2019.
- [3] S. Magalini, G. Pepe, S. Panunzi, C. Abatini, A. Di Giorgio, and M. Foco, "Observational study on preoperative surgical field disinfection: povidone-iodine and chlorhexidine-alcohol," *European Review for Medical and Pharmacological Sciences*, vol. 17, no. 24, pp. 3367–3375, 2013.
- [4] K. Nakajima, J. W. Milsom, D. A. Margolin, and E. J. Szilagyi, "Use of the surgical towel in colorectal hand-assisted laparoscopic surgery (HALS)," *Surgical Endoscopy*, vol. 18, no. 3, pp. 552–553, 2004.
- [5] B. Rumstadt, N. Roshanaei, and D. Schilling, "Gossypibom - das vergessene Bauchtuch [Gossypiboma - the retained surgical towel]," *Deutsche medizinische Wochenschrift*, vol. 133, no. 33, pp. 1673–1676, 2008.
- [6] S. Bathla, E. J. Nevins, P. L. Moori, and D. Vimalachandran, "Which pen? A comparative study of surgical site markers," *Journal of Perioperative Practice*, vol. 28, no. 1-2, pp. 21–26, 2018.
- [7] A. M. Driessche, "Surgical site markers: potential source of infection," *Orthopaedic Nursing*, vol. 31, no. 6, pp. 344–347, 2012.
- [8] B. Bell, J. O'Donovan, S. T. Wright, C. N. Gemelli, E. Knight, and R. Hirani, "Evaluation of a sterile surgical skin marker to indicate the optimal vein for venepuncture in the blood donation setting [published correction appears in *Vox Sang.* 2021 Sep 9]," *Vox Sanguinis*, vol. 115, no. 5, pp. 377–387, 2020.
- [9] W. H. Chan, S. Biswas, J. L. Ashworth, and I. C. Lloyd, "Congenital and infantile cataract: aetiology and management," *European Journal of Pediatrics*, vol. 171, no. 4, pp. 625–630, 2012.
- [10] A. García-Layana, G. Ciufo, E. Toledo et al., "The effect of a mediterranean diet on the incidence of cataract surgery," *Nutrients*, vol. 9, no. 5, p. 453, 2017.
- [11] A. S. Mursch-Edlmayr, L. J. Pomberger, P. Hermann, H. Wagner, S. Beka, and K. Waser, "Prospective comparison of apex-centered vs standard pupil-centered femtosecond laser-assisted capsulotomy in cataract surgery," *Journal of Cataract & Refractive Surgery*, vol. 47, no. 5, pp. 606–611, 2021.
- [12] G. Ye, B. Qu, Y. C. Tham et al., "A decision aid to facilitate informed choices among cataract patients: a randomized controlled trial," *Patient Education and Counseling*, vol. 104, no. 6, pp. 1295–1303, 2021.
- [13] E. D. Deeks, "Tropicamide/phenylephrine/lidocaine intracameral injection: a review in cataract surgery," *Clinical Drug Investigation*, vol. 39, no. 11, pp. 1133–1139, 2019.
- [14] P. Kongsap, "Central corneal thickness changes following manual small incision cataract surgery versus phacoemulsification for white cataract," *Rom J Ophthalmol*, vol. 63, no. 1, pp. 61–67, 2019.

Research Article

Clinical Image Feature Analysis and Diagnostic Efficacy Evaluation of Pulmonary Ultrasound in the Diagnosis of Congenital Pulmonary Airway Malformations in Children: Based on a Single Center, Retrospective Cohort Study

Dandan Liu,¹ Gang Zhang ,² Jianyi Liao,¹ Lan Jiang,¹ Chun Cai,² Xiao Li,² Lei Lou,² Bin Zhou,² Huiyi Zeng,² Xiangang Yan,² and Gang Yu ²

¹Department of Ultrasound Medicine, The Third Affiliated Hospital of Guangzhou Medical University, Guangzhou, China

²Department of Pediatric Surgery, The Third Affiliated Hospital of Guangzhou Medical University, Guangzhou, China

Correspondence should be addressed to Gang Zhang; utopia13cn@gzhmu.edu.cn and Gang Yu; 415371975@qq.com

Received 2 June 2022; Revised 29 June 2022; Accepted 5 July 2022; Published 18 August 2022

Academic Editor: Dong Chen

Copyright © 2022 Dandan Liu et al. This is an open access article distributed under the Creative Commons Attribution License, which permits unrestricted use, distribution, and reproduction in any medium, provided the original work is properly cited.

Objective. A single center, retrospective cohort study was conducted to analyze the clinical image features and diagnostic efficiency of pulmonary ultrasound in the diagnosis of congenital pulmonary airway malformations (CPAMs) in children. **Methods.** The starting and ending time of this study is from May 2019 to December 2021. This study included 200 children with CPAM diagnosed by prenatal ultrasound and postpartum CT imaging (aged from 1 hour to 3 years), including 103 males and 97 females. All of them were diagnosed by fetal ultrasound and were examined by chest X-ray (CXR), chest CT, and lung ultrasound (LUS). The clinical image characteristics and diagnostic efficiency of CXR, chest CT, and LUS in the diagnosis of CPAM in children were analyzed. **Results.** 200 lesions were limited to single lung, and the most common were right lower lobe, right lower lobe in 80 cases (40.0%), left lower lobe in 60 cases (30.0%), right upper lobe in 30 cases (15.0%), left upper lobe in 20 cases (10.0%), and right middle lobe in 10 cases (5.0%). Among the 200 cases of preoperative CT examination, 196 cases (98.00%) showed lesions and confirmed diagnosis, and 4 cases were missed. Chest X-ray showed multiple focal circular low-density shadow in the right lung, and the heart shadow and mediastinum moved slightly to the left. CXR showed multiple cystic transparent shadows in the left lower lung and slightly to the right of the mediastinum and heart. CXR showed multiple balloon cavities of different sizes in the right lung field, and the mediastinum and heart shadow shifted to the left. The direct signs of LUS (including single or multiple cystic lesions) were not significantly different from those of CXR, but the indirect signs were significantly higher than those of CXR. **Conclusion.** The most common CT findings of CPAM in children are cystic lesions, especially polycystic lesions, while LUS images of CPAM in children are various. LUS is a noninvasive and nonradiological examination method, which is easy to operate and repeat. LUS can be used for preliminary qualitative screening of CPAM in children, and the diagnostic value of indirect signs of LUS is better than that of CXR.

1. Introduction

Congenital pulmonary airway malformation (CPAM) is a congenital pulmonary dysplasia of unknown etiology. The essence of this disease is large airway obstruction and pulmonary parenchyma dysplasia. This malformation often occurs in the early stage of lung embryonic development [1]. In 1977, Tian et al. [2] divided the disease into types I, II, and

III according to the clinical and pathological features. In 2002, An et al. [3] changed the name of CCAM to CPAM and changed the original three-point method to a five-point method which was divided into 0–4 types according to the different parts of the airway where the malformations occurred. The latter two are widely used in clinic. CPAM is a hamartoma-like lesion characterized by a polycystic mass of lung tissue with abnormal bronchial proliferation. Its

incidence is 10410 000, which is slightly higher in men, often involving part of the lung lobe or the whole lobe. 80% of the lesions are located in a single lobe, and about 1% of the lesions occur in the bilateral lobes [3]. The clinical manifestations of the CPAM are generally dyspnea, fever, cough, and other nonspecific symptoms; some cases may also be asymptomatic. It has been reported in previous literature that the disease can be secondary to malignant tumors such as adenocarcinoma and squamous cell carcinoma. In addition, some cases are pathologically difficult to distinguish from low-grade pleural pulmonary blastoma (PPB) [4], so lobectomy is recommended no matter whether it is symptomatic or not. Because the clinical manifestations and laboratory results of CPAM are not specific, its diagnosis mainly depends on imaging examination, so it is necessary to study the imaging manifestations of CPAM.

With the development of prenatal ultrasound imaging technology, most CPAM can be diagnosed in the fetal period. It is reported in the literature that most of the children with CPAM have a good prognosis, and about 5% of them have respiratory symptoms after birth, which need to be diagnosed as soon as possible and surgical intervention should be carried out in time. Children who are asymptomatic after birth but those whose chest lumps are revealed by ultrasound often face a series of postpartum chest X-rays. When their CXR test is negative, they may also need to undergo chest enhanced CT for imaging diagnosis [5]. In addition, for children with twins or multiple births with CPAM, twins or even multiple births may need to be diagnosed by CXR or even chest enhanced CT. Lung ultrasound (LUS), as an important examination and therapeutic effect monitoring method for the diagnosis of lung diseases, has been successfully used to diagnose a variety of neonatal lung diseases, such as respiratory distress syndrome, wet lung, pulmonary hemorrhage, pneumonia, atelectasis, meconium aspiration syndrome, and pneumothorax. At present, although there are many reports about prenatal ultrasound diagnosis of CPAM, there is less literature about the ultrasonographic features of neonatal CPAM [6]. In this study, the clinical data of 200 children with CPAM were retrospectively analyzed, the ultrasonographic features of CPAM in neonatal period were summarized, the accuracy of CXR and LUS in the diagnosis of congenital pulmonary airway malformation was compared, and the clinical diagnostic value of neonatal LUS in CPAM was discussed. In this paper, the clinical image characteristics and diagnostic efficiency of LUS in the diagnosis of CPAM in children were analyzed retrospectively, in order to improve the understanding and diagnostic accuracy of the disease.

2. Patients and Methods

2.1. Patients Information. The starting and ending time of this study is from May 2019 to December 2021. This study included 200 children with CPAM diagnosed by prenatal ultrasound and postpartum CT imaging (aged from 1 hour to 3 years), including 103 males and 97 females. All the children were diagnosed by fetal ultrasound and were examined by CXR, chest CT, and LUS. This study was

approved by the Medical Ethics Association of our hospital, and all patients signed informed consent.

2.2. Investigation Methods. Chest CT examination: Siemens FROCE dual-source 194 layer ct, scanning range from the top of the chest entrance to the bottom of the lung, scanning parameters: plain scan tube voltage 120 kV, tube current 27 mAs. Dual-source scanning was used, including A ball tube voltage 70 kV, tube current 30–35 mAs tube voltage 150 kV, tube current 11–15 mAs, matrix 25 cm tube 25 cm, conventional slice thickness 3 mm and 0.6 mm thick lung window image, nonionic iodine contrast medium enhanced examination, nurse hand injection, and dose of 1.5 ml/kg.

LUS examination: using HITACHI ALOKA and PHILIPS ultrasonic diagnostic instrument, high frequency linear array probe, frequency 8–12 MHz. The LUS examination of the children was performed by two attending physicians who had received special lung ultrasound training. In the quiet state, the supine position, lateral position, and prone position were taken, and each lung was divided into three regions: anterior, lateral, and posterior regions, that is, 6 regions on both sides of the chest, which were bounded by the parasternal line, anterior axillary line, posterior axillary line, and spinal line on both sides of the chest, and each side of the lung was divided into three regions: the anterior area, the lateral area, and the posterior area, that is, six regions on both sides of the lungs. Each region of the lung needs to be scanned longitudinally (the probe is perpendicular to the ribs) and transversely (the probe walks along the intercostal space), and each region is scanned one by one from top to bottom, the order of which is, first, check the anterior area of the chest, the range between the parasternal line and the anterior axillary line; then check the lateral area of the chest, the range between the anterior axillary line and the posterior axillary line; finally, check the posterior area of the chest, the range between the posterior axillary line and the spinal line [7]. LUS observation index: direct signs included anechoic cystic lesions, high echo area, and low echo area, indirect signs included abnormal pleural line, A-line, B-line, pulmonary consolidation with bronchial inflation sign, pleural effusion, and mediastinal displacement.

CXR inspection: use GE1 instead of DR camera to shoot, and upload to Tianjian PACS system to read the film. The direct signs of X-ray findings included liquid cysts, gas-liquid cysts, air cysts, and multiple pulmonary cysts, while the indirect signs included emphysema, pulmonary consolidation, exudative lesions, and mediastinal displacement.

2.3. Image Analysis. The preoperative imaging data of all cases were collected retrospectively, including chest CT imaging diagnosis and images, CXR, and LUS imaging diagnosis and images. The imaging diagnosis was completed by two imaging doctors, one of whom had more than 10 years of work experience. The imaging data included the location of the lesion, the extent of involvement, the shape of the lesion and its surrounding manifestations, and whether there was systemic blood supply.

2.4. Statistical Analysis. SPSS 19.0 software was used for statistical analysis, the measurement data were expressed as $\bar{x} \pm s$, the counting data were expressed as constituent ratio (%), and the Fisher exact probability method was used for comparison between groups. *T*-test and χ^2 test were used to compare the two groups, and $P < 0.05$ indicates that there is significant difference between the two groups.

3. Results

3.1. Diagnosis Result. All the 200 lesions were confined to the single lung lobe, most commonly in the lower lobe of the right lung, 80 cases (40.0%) in the lower lobe of the right lung, 60 cases (30.0%) in the lower lobe of the left lung, 30 cases (15.0%) in the upper lobe of the right lung, 20 cases (10.0%) in the upper lobe of the left lung, and 10 cases (5.0%) in the middle lobe of the right lung.

3.2. Diagnostic Results and Images of Chest CT

3.2.1. Diagnostic Results of Chest CT. Among the 200 cases of preoperative CT, 196 cases (98.00%) showed the lesion and were clearly diagnosed, and 4 cases were missed.

3.2.2. Chest CT Image. According to the main imaging findings of the lesions were as follows: (1) single large cyst (6.00%) showed single diameter > 2 cm thin-walled cyst, with or without internal thin-walled separation. (2) The multiple large cysts (126 gamma 200~63.00%) showed several regular or irregular large cysts (diameter > 2 cm) with multiple small cysts or microcysts of different sizes, which were arranged adjacent to each other. Thin line-like separation could be seen in the larger cyst lumen, and the largest cyst was about 13.7 cm in diameter. The intercystic lung tissue showed emphysema in 16 cases and localized emphysema in 6 cases. (3) Multiple cysts (21.00%) showed tight arrangement of thin-walled cysts with similar size of ≤ 2 cm, and honeycomb-like microcysts were shown in 6 cases. 4 patchy high-density shadows (16 gamma 200) 8.33%: on CT plain scan, the lesions showed smooth or nonsmooth patchy high-density shadow, with or without surrounding small gaseous cysts, and showed inhomogeneous enhancement, irregular cyst-like enhancement in 3 cases, and multiple round cyst-like enhancement in 6 cases. Refer to Figures 1–3.

3.3. Diagnostic Results and Images of LUS

3.3.1. LUS Diagnosis Result. Of the 200 cases of preoperative LUS, 193 cases (96.50%) suggested the lesion and were clearly diagnosed, and 7 cases were missed.

3.3.2. CPAM LUS Images of Children before Operation. The main LUS findings of children with CPAM were as follows: Figure 4: right congenital cystic adenoid malformation of the lung, CT revealed multilocular cystic lesions in the middle and lower lobe of the right lung, cystic adenomatoid malformation (type II), irregular hypoechoic consolidation area in the middle and lower lobe of the right lung,

unsmooth and unclear pleural line, decrease or disappearance of A-line, dense B-line, or B-line fusion. Refer to Figures 4–9.

3.3.3. CPAM LUS Images of Children after Operation. The boundary is not clear and the internal echo is uneven. No abnormal echo was found after operation. Refer to Figures 10 and 11.

3.4. CXR Diagnostic Results and Images. Among the 200 cases of preoperative chest X-ray, only 102 cases (51.00%) showed lesions, but all of them were not clearly diagnosed, 98 cases were misdiagnosed, of which 23 cases were diagnosed as normal chest film, 20 cases were diagnosed as increased texture of both lungs or inflammation of both lungs, retrospective analysis of 55 cases of missed chest X-ray was done, and lesions could be found in all cases, showing flaky increased brightness shadow in 25 cases and irregular blurred shadow in 20 cases. Refer to Figures 12–15.

3.5. LUS and CXR Check Results. Compared with postnatal chest CT, there was no significant difference in direct signs (including single or multiple cystic lesions) between LUS and CXR, but the indirect signs of LUS were significantly higher than those of CXR, and the difference between groups was statistically significant ($P < 0.05$). All the data results are shown in Tables 1 and 2.

3.6. LUS and CXR Check Results. The design route of this study was shown in Figure 16.

4. Discussion

CPAM belongs to a kind of congenital chest malformation in children, which is not uncommon in childhood malformations [8]. Due to the popularity of prenatal diagnosis, most CPAM can be found prenatal, and it is estimated that the actual incidence is much higher. In 2002, it was divided into 4 types according to tissue origin: type 0, large solid interstitial tissue of bronchial origin, also known as acinar dysplasia, most of the dead fetus could not survive; type 1, bronchial/bronchiolar source, diameter ≥ 2 cm large sac; type 2, bronchiolar source, a large number of vesicles; type 3, bronchiolar trachea/alveolar source, solid tissue; type 4, peripheral source, most large single cyst. In the new classification, types 0 and 3 were not cystic structure, and types 1, 2, and 4 had no adenoma. A retrospective study showed that the prenatal diagnosis rate of CPAM was 85.7%, and the average diagnosis time was 21–24 weeks of pregnancy [9]. Prenatal ultrasound needs to determine the size, location, and morphological characteristics of the mass, such as large, small, solid, or mixed, as well as changes in size and source of blood supply. The prenatal ultrasound of CPAM can be divided into three types: type I (about 25% of cases) is single or polycystic of different sizes, with a maximum diameter of 10 cm; type II (about 25% of cases) is mixed with cyst and surrounding tissue, and ultrasound echo is enhanced; type

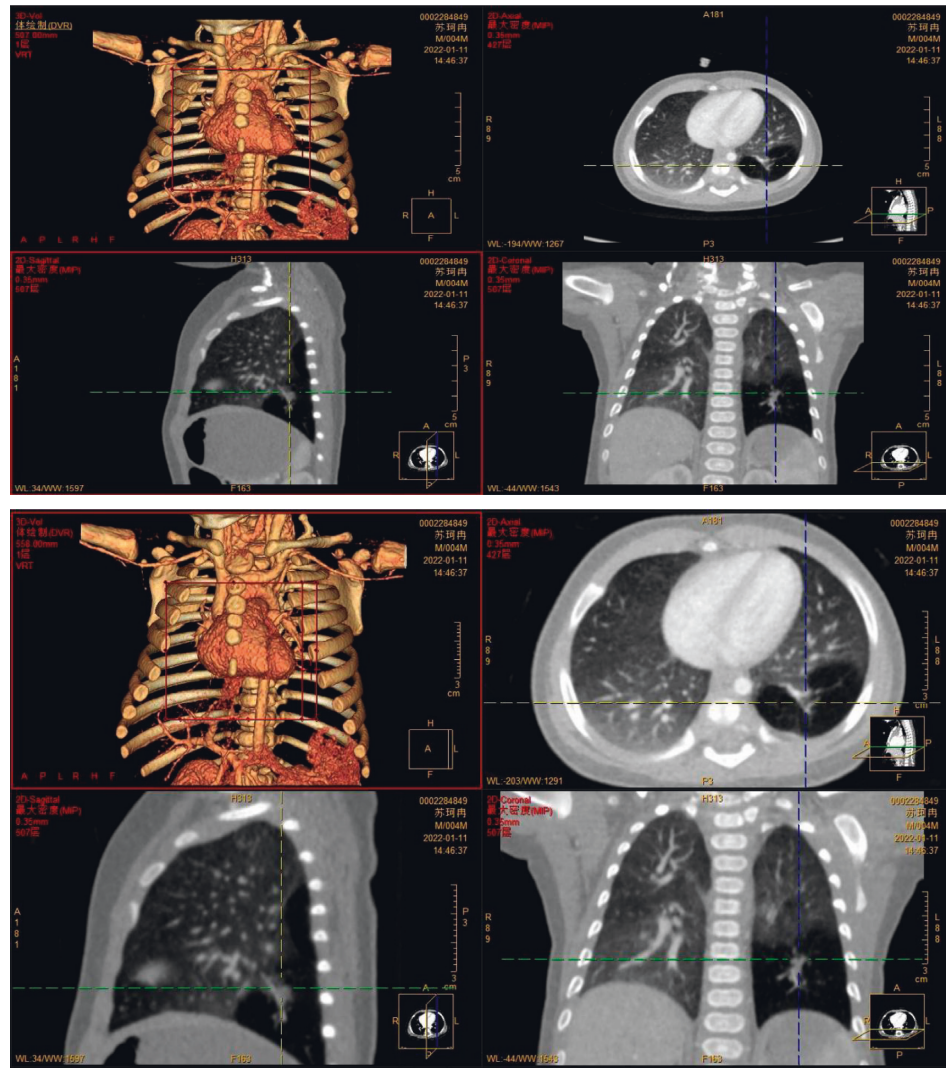


FIGURE 1: The brightness of the left lower lobe increased with a range of about 32.3 mm × 45.6 mm × 62.8 mm. The inner lung texture was sparse, with bronchovascular bundle running, no clear envelope at the edge, and no clear abnormal aortic blood supply. The remaining two lung fields were clear, lung texture was regular, and no abnormal tissue density shadow or space-occupying lesions were observed. Trachea and bronchus were unobstructed without stenosis or obstruction, and hilar shadow was not significant. No abnormal enhancement was found in both lungs on enhanced scan. The mediastinal structure was clear, no lesions were observed, and no enlarged lymph nodes were observed beside the trachea, under the carina, in front of the vessels, and behind the vena cava. There was no bilateral pleura thickening and no pleural effusion. Left lower lobe changes, considered congenital pulmonary airway malformation, cystadenoma malformation (type II).

III (about 50% of cases) contains microcystic masses ≤ 5 mm [3]. The sensitivity and specificity of prenatal ultrasound are 90% and 77%, respectively. Most congenital malformations can be found by prenatal MRI [8]. The sensitivity and specificity of MRI diagnosis of pulmonary malformations are more than 95%. However, the advantage of MRI and ultrasound in diagnosis and prognosis is not obvious. MRI only has certain significance in complex or mixed cases [10, 11]. Once prenatal CPAM is found, it should be monitored regularly and attention should be paid to possible complications, such as mediastinal swing, fetal edema, and polyhydramnios. Daddi et al. [12] used ultrasonic measurement of CPAM volume ratio (CCVR) as an index to predict risk; if $CVR > 1.6$, there is an 80% risk of fetal edema [13]. If $CVR > 0.84$, the probability of severe respiratory distress caused by polyhydramnios and ascites will increase

[14]. Other indicators include MRI lung volume, ultrasound ratio, and lung-to-head ratio, the main purpose of which is to monitor complications that may endanger fetal life [14].

Prenatal CPAM found that 70% of the children were found to be asymptomatic at birth, 30% of them had respiratory distress at birth, and 10% of them had severe respiratory distress requiring mechanical ventilation [15]. Fetal treatment includes glucocorticoid, minimally invasive, and fetal surgery [15]. For microencapsulated fetal edema, glucocorticoid therapy is more effective and less risky than open fetal surgery [15, 16]. The role of hormones is to reduce the production of fluid in the lungs and increase absorption, similar to the pathological changes in the later stage of the embryo. There were 3 cases of successful percutaneous sclerotherapy for type 2 and 3 CPAM. Catheterization in the thoracic cavity of the fetus with large sacs can be used for

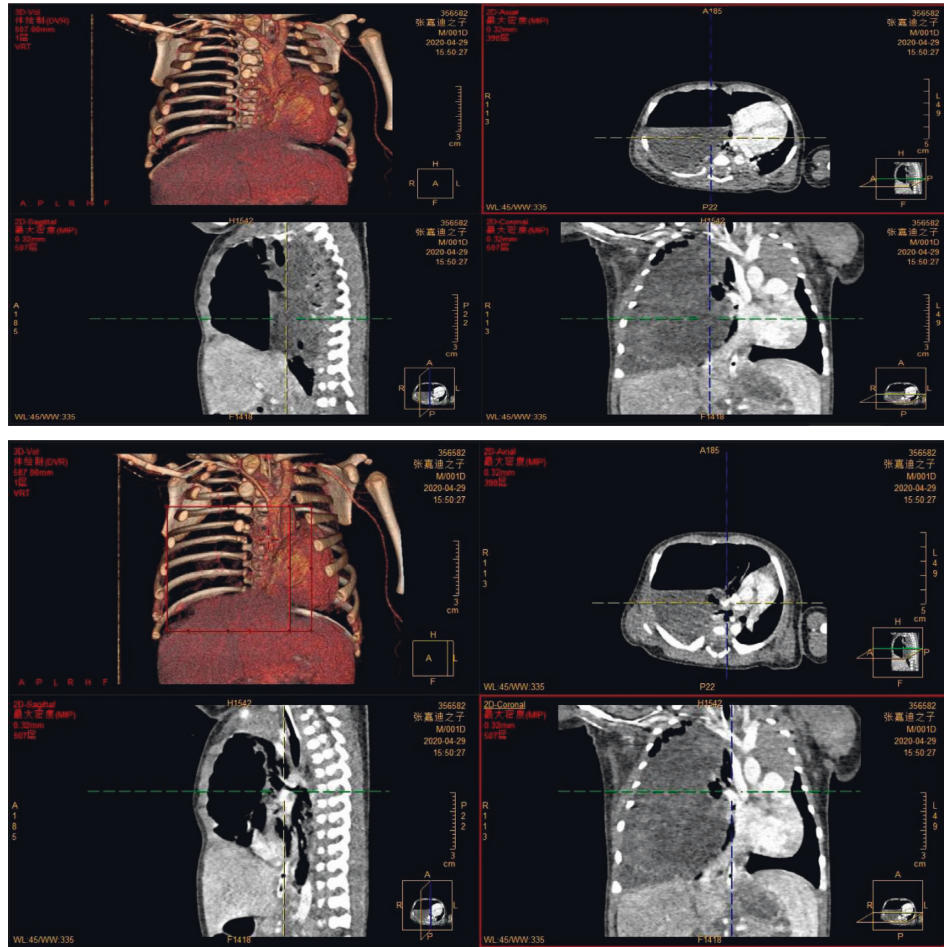


FIGURE 2: Multiple cystic transparent shadows can be seen in the right lung field with a range of $57 \times 68 \times 68$ mm and a clear boundary. The size of the inner capsule is different; the largest one is about $53 \times 48 \times 26$ mm. A large amount of liquid density shadows can be seen in the lung, and the liquid-gas plane can be seen. The mediastinum pushes to the left, pressing the left lung. Patchy and slightly high-density shadows were seen in the lower lobe of the left lung, with less clear boundaries. No thickening of the left pleura, no effusion of the left pleura. 1. Abnormal changes in the right lung, considered congenital cystadenoma malformation of lung (type I). Mediastinal displacement was obvious and left lung was compressed. Left lower lobe consolidation with a few exudative lesions.

both diagnosis and treatment of fetal edema. Due to the reaccumulation of fluid after catheterization, a better method is to use pleural amniotic shunt. In cases where lung development is completed in the third trimester and giant cysts lead to mediastinal swing, termination of pregnancy can be considered for immediate postpartum treatment. Induced labor is considered only for fetuses with no hope of treatment. Most of the cases without prenatal diagnosis were found with CPAM after the occurrence of pneumonia, and 1 case with prenatal diagnosis of CPAM had respiratory symptoms at 1 month after birth [9]. The positive rates of CPAM diagnosed by X-ray and CT were 50% and 100%, respectively. Large cysts can lead to displacement of the trachea and mediastinum. Abnormal blood vessels should be observed for enhanced CT. Differential diagnosis should include pulmonary sequestration, congenital lobar emphysema, and bronchogenic cyst. It is difficult to distinguish PPB from type 4 CPAM imaging, and finally pathological diagnosis is needed. The timing of CT examination for prenatal diagnosis of CPAM and asymptomatic children

after birth is still controversial. Some suggest that enhanced CT should be done before 6 months, and some should be completed before operation [17–20].

There is a consensus on surgical treatment for children with symptoms. There is no consensus on whether asymptomatic children need surgery. The reasons for supporting surgery are as follows: (1) infection during the observation period will increase the difficulty of operation and postoperative complications; (2) the nature of the tumor cannot be determined by imaging alone, especially the risk of pneumothorax, especially tension pneumothorax, between PPB and type 1 and 4 CPAM; (3) there is a risk of pneumothorax, especially tension pneumothorax; (4) some cases have the tendency of malignant transformation. It does not support the view of asymptomatic surgery: some cases have a tendency of degeneration, and surgery will increase the possible complications. It has been reported that 52 of the 90 cases received conservative treatment without obvious symptoms [21]. In detail, 20% of asymptomatic children develop symptoms, and a retrospective survey found that 45

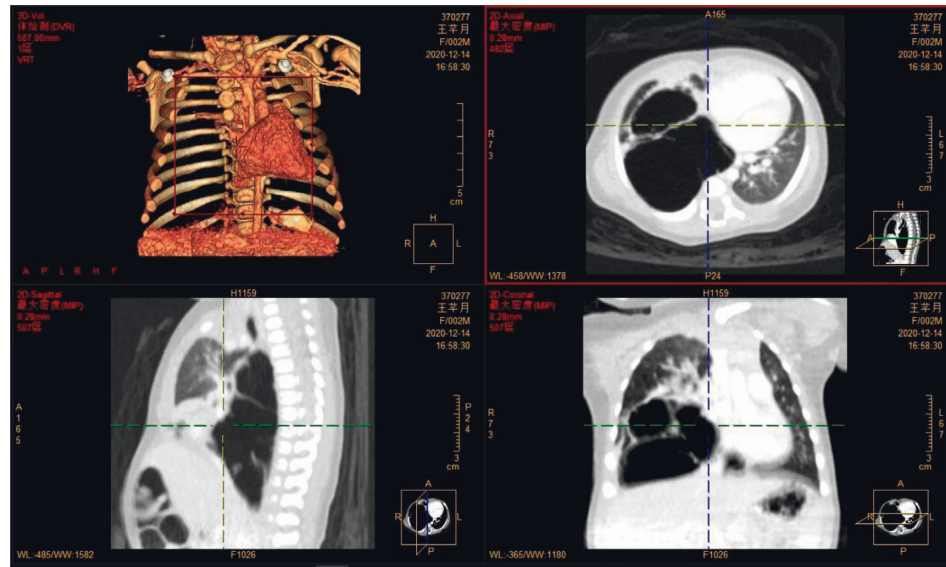


FIGURE 3: Multiple cystic lucid areas in the posterior segment of the upper lobe and lower lobe of the right lung, with a range of about $6.2\text{ cm} \times 6.8\text{ cm} \times 7.9\text{ cm}$, were displaced to the left by mediastinal compression. Multiple patchy and cordlike fuzzy shadows were seen in both lungs, partial consolidation was seen in the right lung, and air bronchial shadows were seen inside. Trachea and bronchus were unobstructed without stenosis or obstruction, and hilar shadow was not significant. The mediastinal structure was clear, no lesions were observed, and no enlarged lymph nodes were observed beside the trachea, under the carina, in front of the vessels, and behind the vena cava. There was no bilateral pleura thickening and no pleural effusion. Cystadenoma malformation (type I) was considered.

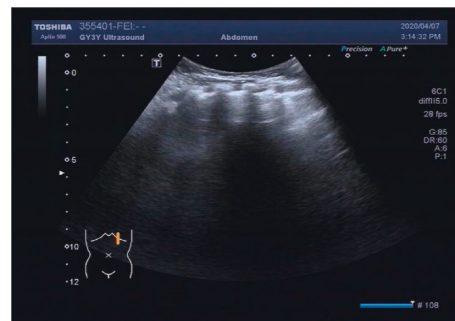


FIGURE 4: Left congenital cystadenoma. CT showed increased transmittance of the posterior segment of the upper lobe and the dorsal segment of the lower lobe of the left lung, with a range of about $38.5 \times 26.6 \times 42.9\text{ mm}$, with multiple round areas of different sizes, with a maximum diameter of about 7.7 mm , some of the walls slightly thicker, enhancement of the cyst wall, thickened pulmonary artery blood supply, and cystic adenomatoid malformation of the lung (type II). Ultrasound revealed irregular hypoechoic pulmonary consolidation areas, pleural lines were not smooth and unclear, A-lines decreased or disappeared, and dense B-lines or B-lines fused.

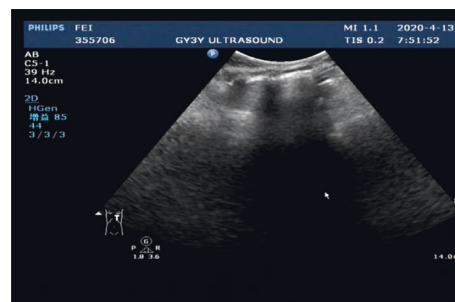


FIGURE 5: Right congenital cystic adenoid malformation of the lung, CT indicates abnormal changes of the right lung, considering congenital cystic adenomatoid malformation (type I); multiple cystic transparent shadow can be seen in the right lung field, the range is about $57 \times 68 \times 68\text{ mm}$, the boundary is clear, the size of the internal capsule is different, the largest is about $53 \times 48 \times 26\text{ mm}$, a large amount of fluid density shadow can be seen in it, the liquid-gas plane can be seen, and a little normal lung tissue can be seen near the middle lobe of the right lung. Ultrasound revealed a huge cystic echo in the right lung.

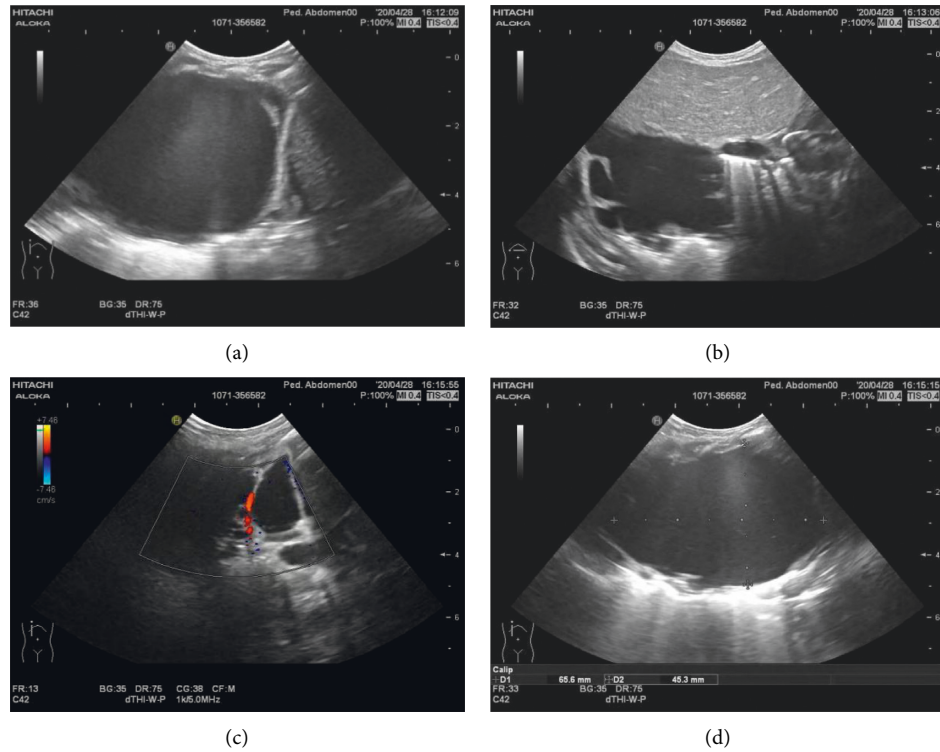


FIGURE 6: Ultrasound indicates irregular hyperechoic or mixed echo areas.

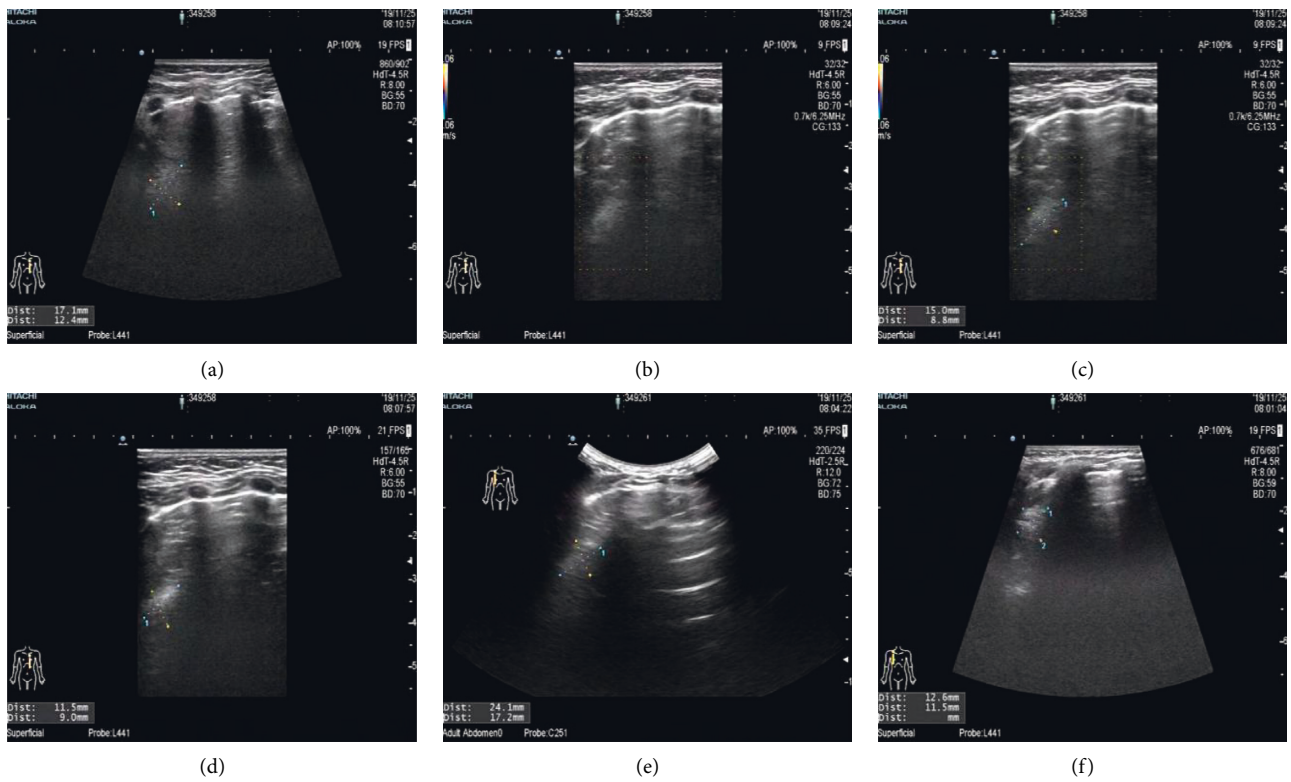


FIGURE 7: Ultrasound indicates irregular hyperechoic or mixed echo areas.

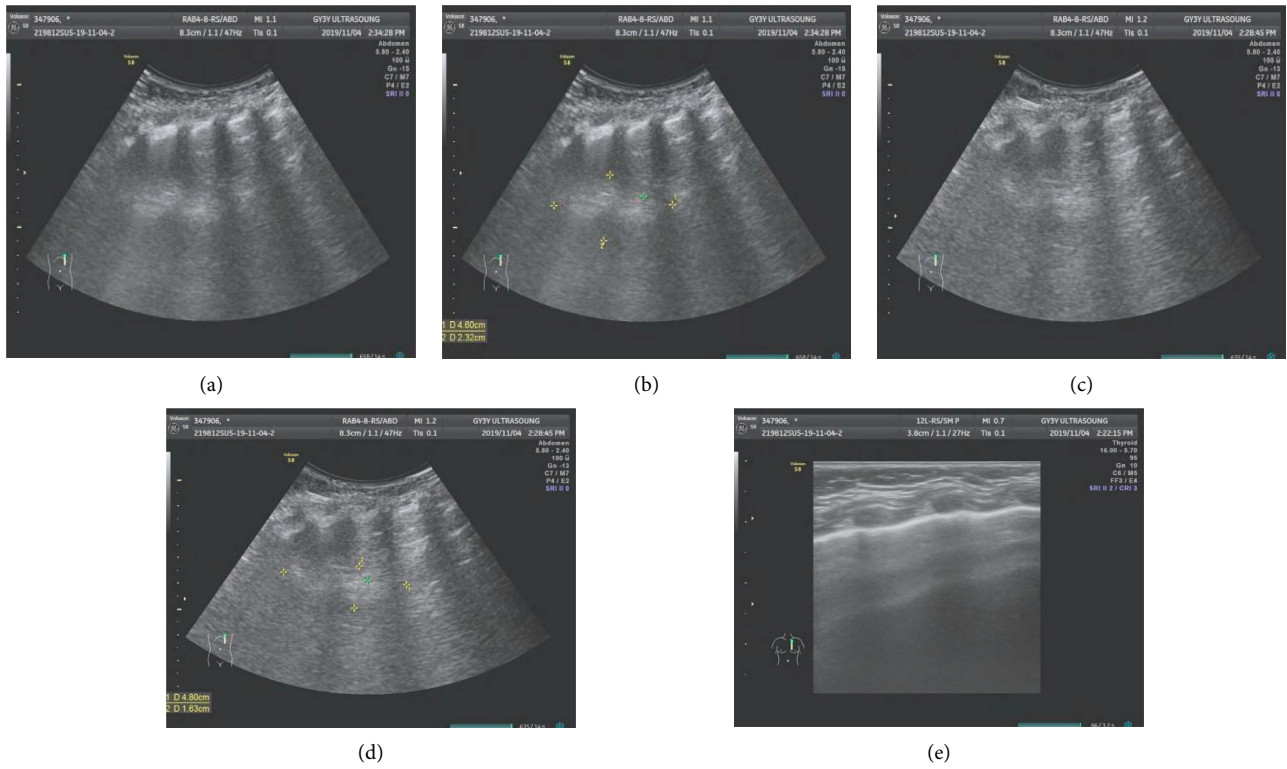
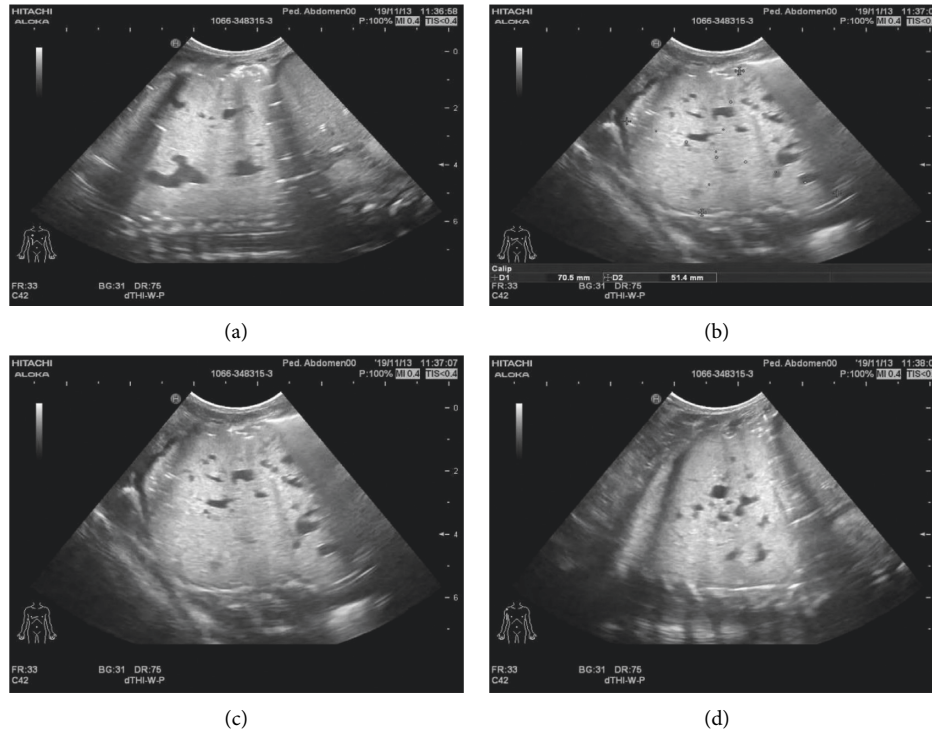


FIGURE 8: Ultrasound indicates irregular hyperechoic or mixed echo areas.

FIGURE 9: An irregular mixed echo mass can be seen in the right lung field, mainly solid, the size is about $71 \times 51 \times 47$ mm, the boundary is not clear, the irregular anechoic area can be seen inside, and the largest is about 20.9×10.4 mm. The left lung field was obviously squeezed and shifted to the left.

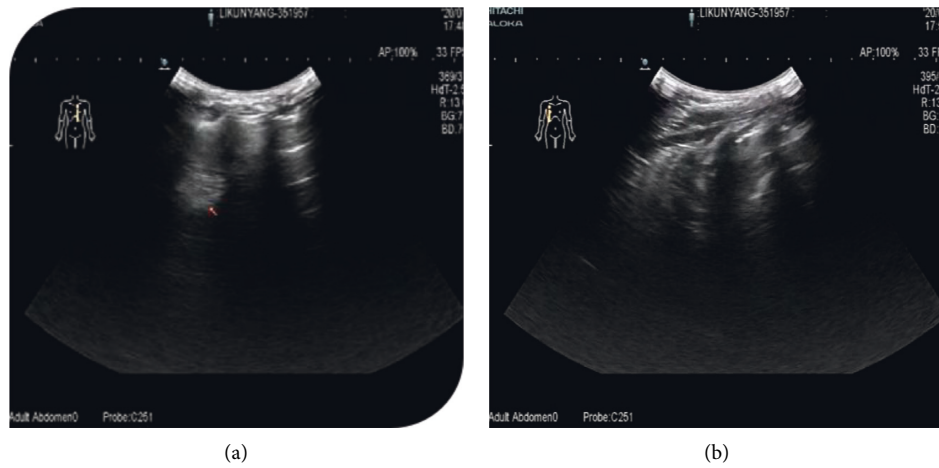


FIGURE 10: An irregular hyperechoic area can be seen in the upper part of the left lung field.

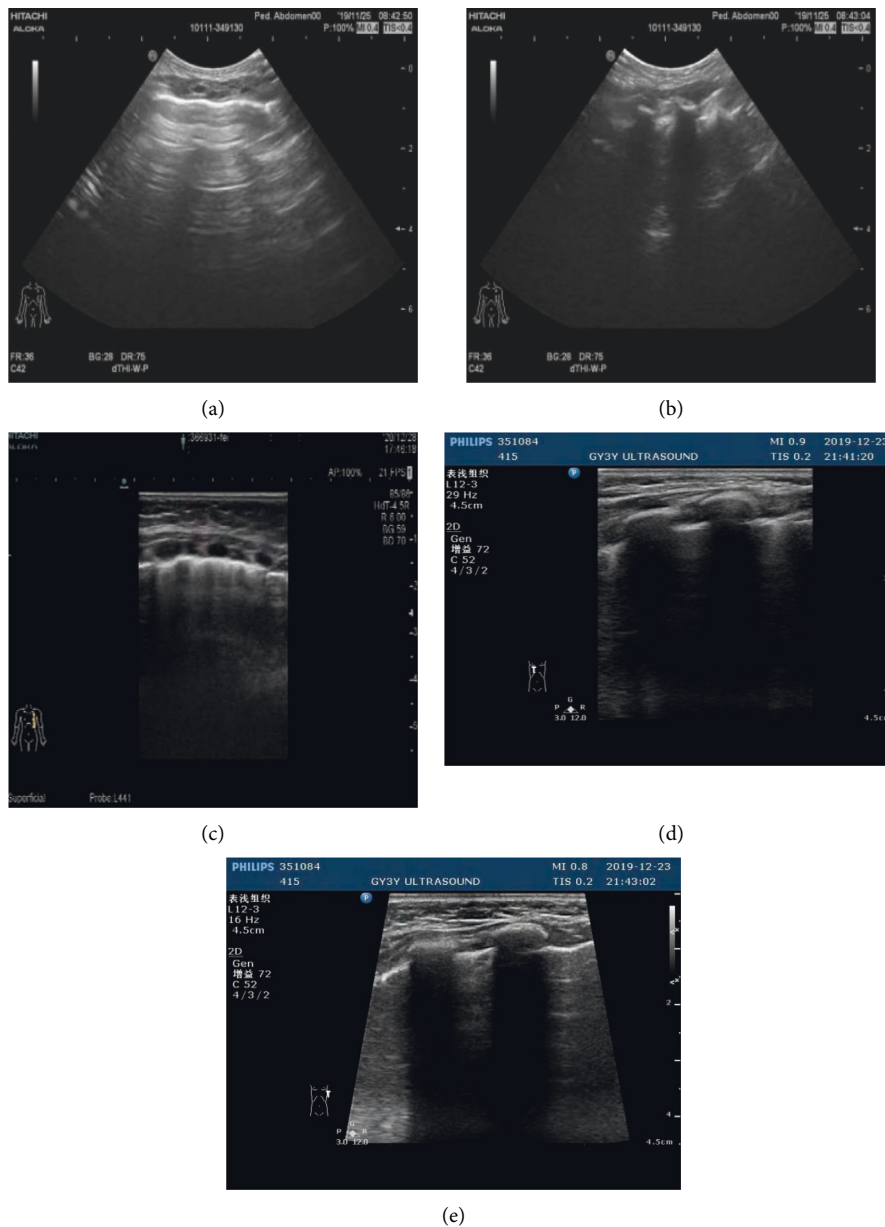


FIGURE 11: The pleural line of the bilateral lung field was smooth, the lung was slippery, the echo distribution of the lung field was uneven, part of the A-line disappeared, and there was no obvious abnormal mass echo and pleural effusion.

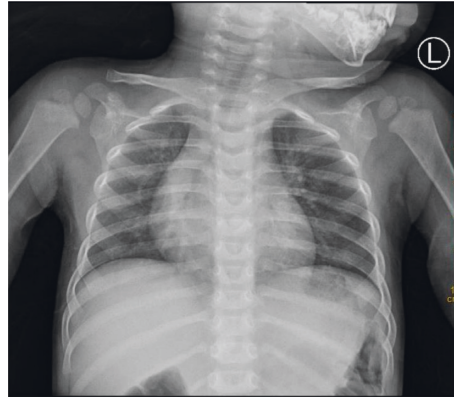


FIGURE 12: Both sides of the thorax are symmetrical, and the bones of the thorax are complete. The distribution of lung markings in both lungs is regular, with clear borders, and no signs of pulmonary congestion or congestion; both lung fields are clear, with no lung parenchyma or interstitial lesions; bilateral hilar size, shape, and location are not abnormal; no mediastinal widened.

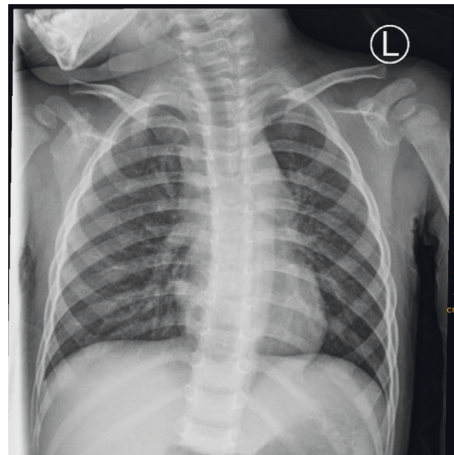


FIGURE 13: Both sides of the thorax are symmetrical, and the bones of the thorax are complete. The distribution of lung markings in both lungs is regular, with clear borders, and no signs of pulmonary congestion or congestion; both lung fields are clear, with no lung parenchyma or interstitial lesions; bilateral hilar size, shape, and location are not abnormal; no mediastinal widened.

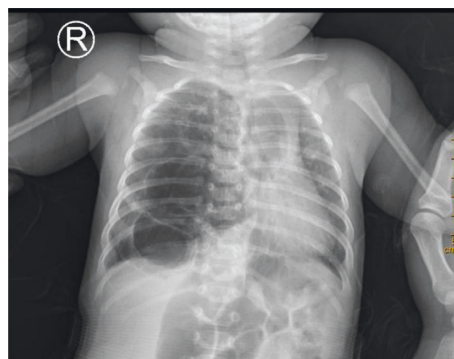


FIGURE 14: The right thorax was slightly full, and the right lung transparency was increased. Multiple cystic translucent areas were seen in the right middle and lower lung fields, with an area of about 46×67 mm, and the boundary was not clear. The lung markings of the left lung increased and thickened, and a few patchy blurred shadows were seen in both lungs, especially in the lower left lung, and the size, shape, and position of the left hilum were not abnormal; the trachea, mediastinum, and heart shadows shifted slightly to the left. The mediastinum was not widened. Consider cystadenoma malformation (type I).

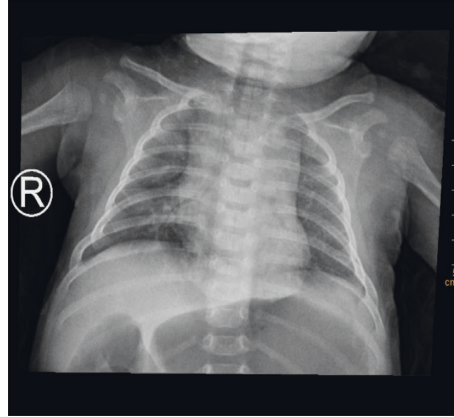


FIGURE 15: Both sides of the thorax are symmetrical, and the bones of the thorax are complete. In the right lower lung field, there was a local increase in transparency, and the lung texture was disordered, with a range of about 24×25 mm; the distribution of the lung texture in the other two lungs was regular, the edge was clear, and no signs of pulmonary congestion or congestion were found; the size, shape, and location of the bilateral hilum were unknown. See abnormal; no mediastinal enlargement.

TABLE 1: Comparison of direct and indirect signs between 1LUS and CXR [n/%].

Grouping	N	Direct sign	Indirect sign
LUS group	200	82 (41.00)	200 (100.00)
CXR group	200	80 (40.00)	86 (43.00)
χ^2		0.041	159.440
P		0.838	0.000

It is statistically significant that bold values are used to highlight differences.

TABLE 2: Comparison of indirect signs between pulmonary X-ray and pulmonary ultrasound [n/%].

Grouping	N	Pulmonary consolidation	Mediastinal displacement	Pleural effusion	Bronchial aeration	A-line	B-line	Pleural line	Exudative lesion
LUS group	200	132 (66.00)	120 (60.00)	6 (3.00)	80 (40.00)	186 (93.00)	200 (100.00)	182 (91.00)	—
CXR group	200	90 (45.00)	120 (60.00)	0 (0.00)	—	—	—	—	86 (43.00)
χ^2		17.856	0.000	0.616	—	—	—	—	—
P		0.000	1.000	0.947	—	—	—	—	—

It is statistically significant that bold values are used to highlight differences.

infants underwent surgery after symptoms, with an increase in intraoperative and postoperative complications compared with asymptomatic surgery [22]. The earlier the operation, the more beneficial to the development of the residual lung, which is also one of the reasons to support the early operation. At present, it is generally accepted whether to choose the operation and the best time should consider the following factors: (1) the space-occupying effect and symptoms of the cyst; (2) the requirements of the parents; (3) the evaluation of the anesthesiologist; (4) the experience of the surgeon. At present, the age of asymptomatic children undergoing surgery in China is from 6 months to 1 year. In the past, the standard operation was thoracotomy, but video-assisted thoracoscopy has become a widely accepted operation in recent years. In the United States, the proportion of video-assisted thoracoscopy is gradually increasing, and compared with thoracotomy, postoperative complications and hospital stay are similar [23]. Meta-analysis unveiled that the complications after thoracoscopic surgery were

reduced, and the hospitalization time was shortened, but the operation time was relatively prolonged [24]. Video-assisted thoracoscopic surgery requires one-lung ventilation to provide sufficient surgical space for the collapse of the lung on the affected side and low CO₂ pressure if necessary, with the cooperation of an experienced anesthesiologist. If thoracotomy is performed, it is best to use the muscle pull approach to avoid damage to the anterior patellar muscle, latissimus dorsi, and its nerves and to reduce postoperative pain and muscle atrophy. In the neonatal period, video-assisted thoracoscopic surgery is more difficult because of the small surgical space. But for newborns under 3 months old, video-assisted thoracoscopic surgery in experienced medical centers is also safe and effective, with a thoracotomy rate of between 3% and 12.2% [25]. The choice of lobectomy or partial lobectomy depends on whether to remove the lesion completely or to preserve healthy lung tissue as much as possible. Lobectomy is a standard operation, and partial lobectomy has been increasing in recent years because some

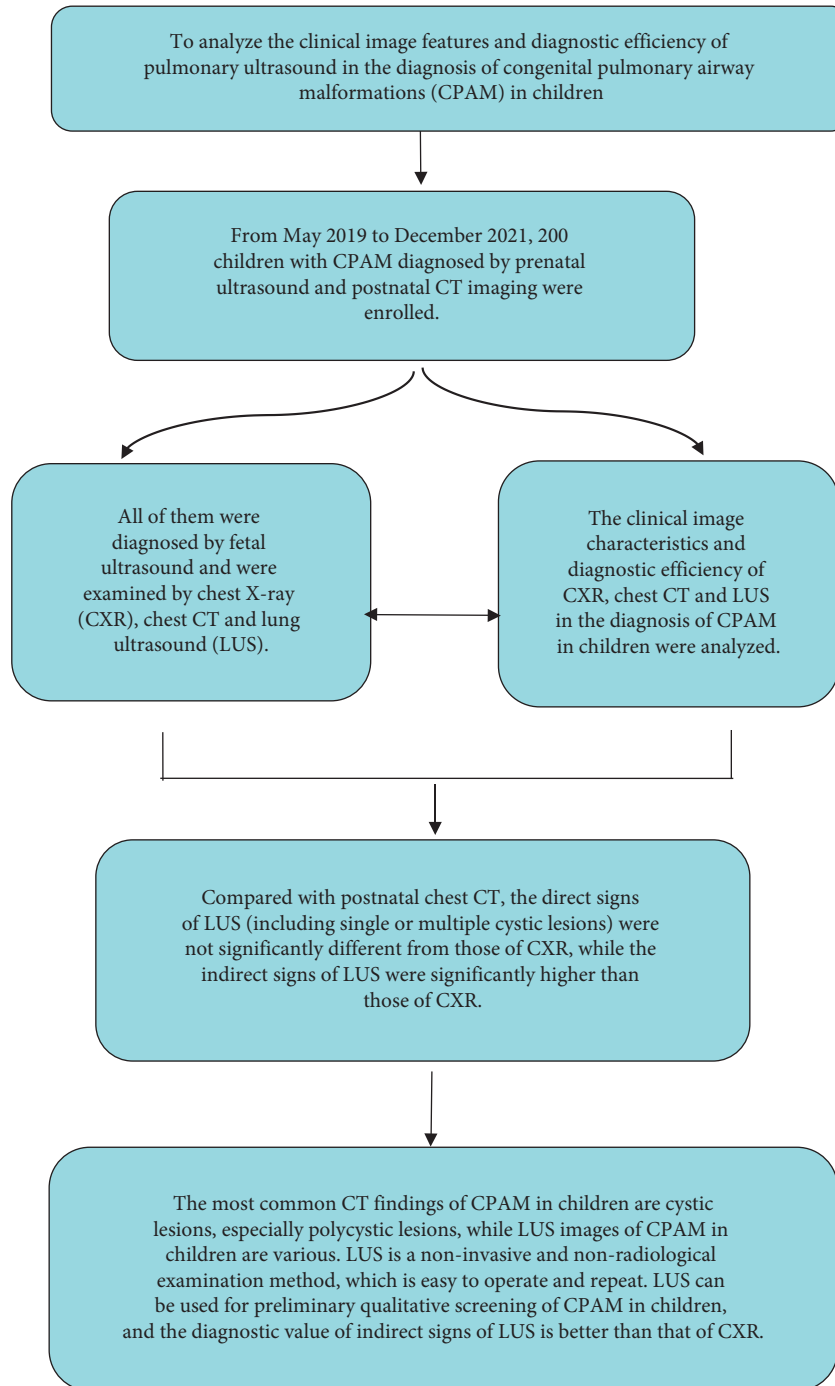


FIGURE 16: Research route.

lesions do not involve the whole lobe of the lung. Partial resection includes anatomical segmental resection, wedge resection, and nonanatomical segmental resection [25]. The benefit of lobectomy lies in the complete removal of the focus, no residue, avoiding the deterioration of the residual focus, and reducing postoperative air leakage. The operation space in the chest of children is small, and the more complex the local resection is, the more difficult it is. The recovery time after partial lobectomy is longer than that after lobectomy [26]. Video-assisted thoracoscopy cannot touch the

boundary of the mass by hand, and it is difficult to determine with the naked eye, and it is difficult to avoid residual lesions after partial resection. Unless multiple lesions involve several lobes, there is no definite basis for recommending partial resection, and local resection is only suitable for very limited lesions [25, 26]. CPAM is associated with two kinds of malignant tumors, one is PPB in infants or young children, and the other is bronchoalveolar carcinoma in adolescence or adults. Bronchoalveolar carcinoma and the characteristics of premolecular malignancy in type I CPAM mucin cells

occurred in many cases without complete resection of CPAM, which confirmed the relationship between bronchoalveolar carcinoma and type I CPAM. Pleuropneumoblastoma is a rare chest tumor, which is mostly diagnosed before 6 years of age. It can be divided into three types: type I, cystic type, type II, mixed type, and type III, solid. The clinical manifestations are lack of specificity, only repeated pulmonary infection, unexplained pneumothorax, and nonspecific X-ray findings. Neither imaging nor biological markers can clearly distinguish type I PPB from type 4 CPAM [27]. Some patients were even diagnosed as CPAM before delivery and confirmed as PPB after operation. PPB should be highly suspected in patients with family history, infantile spontaneous pneumothorax, renal cyst, intestinal polyp, thyroid hyperplasia, and gonadal tumor. 40% of PPB can find relevant clues, and the prognosis of patients with early diagnosis of cystic PPB is significantly better than that of patients with solid tumors. The incidences of CPAM and PPB are 120000 and 1250000, respectively; that is, 4% of CPAM may be pleural PPB.

Chest X-ray is an important imaging examination of pulmonary diseases in children, but for rare diseases such as CPAM, chest X-ray has low specificity and low sensitivity, which may lead to missed diagnosis and misdiagnosis [28]. It is reported that the sensitivity of chest X-ray in the diagnosis of CPAM is only 61% [28]. In the current study, only 51.67% of the lesions are indicated, and there is no clear diagnosis. However, no definite diagnosis was made in 29 cases, of which 8 cases were diagnosed as normal chest X-ray, 10 cases were diagnosed as increased texture of both lungs or inflammation of both lungs, retrospective analysis of 14 cases of missed chest X-ray was done, the lesions were found in 6 cases, and irregular blurred shadow was found in 6 cases. In this group of cases, CPAM chest film showed localized transmittance increased shadow, flaky blurred shadow, or focal multiple small gas and fluid shadow, which was easily confused with pneumonia, diaphragmatic hernia, pneumothorax, and other congenital pulmonary cystic lesions. In contrast, CT is the best method for the diagnosis of CPAM, and its sensitivity and specificity are much higher than those of ultrasound, chest X-ray, and other examination methods. In the study of Jeong et al. [29], the sensitivity and specificity for CT diagnosis of CPAM were 93.3% and 93.7%, respectively. In this study, the detection rate of CPAM lesions was 98.33%, which was much higher than that of chest X-ray (51.67%). However, the diagnosis rate of the first diagnosis is only 70.6%. The retrospective diagnosis test reflects that there is a certain correlation between the understanding of the disease and the diagnostic efficiency. It can be inferred that the low diagnosis rate of this group of cases is mainly related to the lack of understanding of the disease in the past. By strengthening the understanding of CPAM, the diagnostic accuracy of CPAM can be improved. In the diagnosis and treatment of CPAM, for children with high risk, asymptomatic after birth, disappearance of thoracic mass in the third trimester of pregnancy, and children with CPAM in twins or multiple births, the postnatal differential diagnosis of CPAM mainly relies on traditional CXR and CT. CXR is the first choice for the diagnosis of CPAM after birth. Its

manifestations include multiple focal low-density shadow, focal vesicular transparent shadow, focal hyperinflated or clouded mass in the lung, hyperventilation, mediastinal displacement, pneumothorax, and so on when the lesion is huge. However, postnatal examination based solely on CXR has great limitations, and the misdiagnosis rate is high. CT is the imaging standard for preoperative diagnosis of CPAM, but CT is radioactive and expensive, so it needs to be cooperated with children after the use of sedatives and often needs to be evaluated by chest CT. LUS has the advantages of simplicity, easy operation, strong repeatability, low cost, and less radiation. It is considered that LUS can accurately diagnose various lung diseases, and LUS is considered to be more accurate and sensitive than traditional CXR in the diagnosis of pneumothorax, pulmonary edema, pulmonary consolidation, and pleural effusion, avoiding repeated CT examination. Our study still has some shortcomings. Firstly, the quality of this study is limited due to the small sample size we included in the study. Secondly, this research is a single center study and our findings are subject to some degree of bias. Therefore, our results may differ from those of large-scale multicenter studies from other academic institutes. Our research is still clinically significant and further in-depth investigations will be carried out in the future.

In conclusion, the most common CT findings of CPAM in children are cystic lesions, especially polycystic lesions, while LUS images of CPAM in children are various. LUS is a noninvasive and nonradiological examination method, which is easy to operate and repeat. LUS can be used for preliminary qualitative screening of CPAM in children, and the diagnostic value of indirect signs of LUS is better than that of CXR (Figure 16).

Data Availability

The datasets used and analyzed during the current study are available from the corresponding author upon reasonable request.

Conflicts of Interest

The authors declare that they have no conflicts of interest.

Acknowledgments

This project is supported by the Science and Technology Projects in Guangzhou (202201020395) and Guangdong Provincial Science and Technology Plan Project (2014A020213021).

References

- [1] E. Y. Lee, S. O. Vargas, H. J. Park, D. Plut, K. A. Krone, and A. J. Winant, "Thoracic MDCT findings of a combined congenital lung lesion: bronchial atresia associated with congenital pulmonary airway malformation," *Pediatric Pulmonology*, vol. 56, no. 9, pp. 2903–2910, 2021.
- [2] J. Tian, H. Wu, C. Zhou, and A. Feinberg, "Imaging diagnosis of type I PPB and cystic congenital pulmonary airway

- malformation in children [J],” *Radiology practice*, vol. 36, no. 06, pp. 785–791, 2021.
- [3] P. An, X. Xiao, Y. Zhao, J. Zhou, J. X. Li, and Y. Xiong, “Prenatal ultrasound measurements of mild congenital pulmonary airway malformation and long-term prognosis: a retrospective cohort study,” *International journal of gynaecology and obstetrics: The Official Organ of the International Federation of Gynaecology and Obstetrics*, vol. 56, no. 53, pp. 953–958, 2021.
 - [4] R. Guo, Y. Zhai, H. Zhao, C. Rothenberg, and C. Stolar, “Experience of video-assisted thoracoscopy in the treatment of congenital pulmonary airway malformation in infants less than 3 months old [J],” *Chinese Journal of Pediatric surgery*, vol. 42, no. 04, pp. 304–309, 2021.
 - [5] S. Xiao and B. Jia, “Prenatal diagnosis and prognosis of congenital pulmonary airway malformation [J],” *Chinese Journal of Pediatric surgery*, vol. 42, no. 04, pp. 371–375, 2021.
 - [6] I. Goldsmith, G. Joseph, A. Umair, and S. Sharma, “An adult with episodic retrosternal chest pain: an unusual presentation of congenital pulmonary airway malformation – case report [J],” *Journal of Cardiothoracic Surgery*, vol. 16, no. 1, pp. 559–564, 2021.
 - [7] P. Chandrasekaran, S. Goergen, A. Robinson, A. Moghimi, and A. Malhotra, “Bilateral congenital pulmonary airway malformation in an extremely preterm infant,” *BMJ Case Reports*, vol. 14, no. 4, p. e242228, Article ID e242228, 2021.
 - [8] H. Sergei, K. Casper, M. Dhanya, P. Bagolan, and C. M. Burgos, “Development of a core outcome set for CPAM: study protocol of an international Delphi survey,” *BMJ open*, vol. 11, no. 4, pp. 494–496, 2021.
 - [9] D. H. Diona, V. H. Astrid, B. Glenn, and P. Pauwels, “An incidental finding of congenital pulmonary airway malformation type 3 during a forensic autopsy for a sudden infant death: a case report with a brief literature review[J],” *The American Journal of Forensic Medicine and Pathology*, vol. 744, no. 53, pp. 385–389, 2021.
 - [10] V. Gaia, T. Matthew, M. Corina, L. Parnell, and A. Hasan, “Bronchioloalveolar carcinoma arising in congenital pulmonary airway malformation in a neonate[J],” *Pediatric Pulmonology*, vol. 56, no. 5, pp. 912–917, 2021.
 - [11] J. Zheng, H. Tang, H. Xu, J. Li, X. Mao, and G. Liu, “Thoracoscopic versus open resection for symptomatic CPAM in neonates: a decade-long retrospective study[J],” *BMC Pulmonary Medicine*, vol. 21, no. 1, pp. 591–595, 2021.
 - [12] N. Daddi, V. Tassi, G. Rossi, and S. Mattioli, “P38.18 A rare case of pleomorphic carcinoma arising in adulthood type 1 congenital pulmonary airway malformation[J],” *Journal of Thoracic Oncology*, vol. 16, no. 3S, pp. 692–695, 2021.
 - [13] K. F. Lam Fiona, C. T. Lau, Y. M. On, and K. K. Y. Wong, “Comparison of thoracoscopy vs. thoracotomy on musculoskeletal outcomes of children with congenital pulmonary airway malformation (CPAM).[J],” *Journal of Pediatric Surgery*, vol. 56, no. 10, pp. 199–204, 2021.
 - [14] H. Khan, M. Kurup, S. Saikia et al., “Morbidity after thoracoscopic resection of CPAM (CPAM): single center experience over a decade[J],” *Pediatric Surgery International*, vol. 37, no. 5, pp. 459–464, 2021.
 - [15] A. E. Frick, H. Decaluwé, B. Weynand, M. Proesmans, and D. Van Raemdonck, “Invasive mucinous adenocarcinoma of the lung arising in a type 1 congenital pulmonary airway malformation in a 68-year-old patient: a case report[J],” *Acta Chirurgica Belgica*, vol. 121, no. 1, pp. 993–997, 2021.
 - [16] C. Ravindran, J. Kumar, and S. Sanjeev, “Bilateral congenital pulmonary airway malformation in an adult: report of a rare case[J],” *Journal of Advanced Lung Health*, vol. 1, no. 1, pp. 952–956, 2021.
 - [17] K. Bembem, D. Udayakumar, S. Mandal, N. Khurana, and V. Manchana, “Congenital pulmonary airway malformation with coexistent cytomegalovirus infection in an infant: an unusual presentation[J],” *Indian Journal of Pathology & Microbiology*, vol. 64, no. 1, pp. 591–597, 2021.
 - [18] R. Wagner, H. Li, L. Ayoub et al., “Epithelial cell-adhesion protein cadherin 26 is dysregulated in congenital diaphragmatic hernia and congenital pulmonary airway malformation,” *Pediatric Surgery International*, vol. 37, no. 1, pp. 49–57, 2020.
 - [19] K. Aziz, A. C. Jelin, A. M. Keiser, J. Schulkin, and E. B. Jelin, “Obstetrician patterns of steroid administration for the prenatal management of CPAM.[J],” *Journal of Neonatal-Perinatal Medicine*, vol. 14, no. 2, pp. 591–594, 2020.
 - [20] M. P. Bonasoni, G. Comitini, G. Tonni et al., “Prenatal diagnosis of fetal trisomy 5 mosaicism with congenital pulmonary airway malformation type 3: a case report,” *Fetal and Pediatric Pathology*, vol. 41, no. 3, pp. 516–522, 2020.
 - [21] P. Gloria, C. Sara, S. Giorgio et al., “Non-casual association between congenital pulmonary airway malformations/primary lung hypoplasia and congenital diaphragmatic hernia (CDH).[J],” *Frontiers in pediatrics*, vol. 8, no. 53, pp. 691–696, 2020.
 - [22] A. Hara, N. Hidaka, K. Nitahara, A. Sakai, S. Kido, and K. Kato, “Intrathoracic shunt displacement with massive pleural effusion after successful shunt placement in a hydropic fetus with multilocular macrocystic congenital pulmonary airway malformation,” *Journal of Clinical Ultrasound*, vol. 49, no. 2, pp. 149–153, 2020.
 - [23] J. Yu, Na Zhang, C. Chen, W. Zhong, B. Zhu, and D. Sun, “Diagnosis and treatment of congenital pulmonary airway malformation [J],” *Chinese Journal of Thoracic and Cardiovascular surgery*, vol. 34, no. 08, pp. 469–472, 2018.
 - [24] R. Giulio, “Pleuropulmonary blastoma type I and congenital pulmonary airway malformation type 4: distinct entities or sides of the same coin?[J],” *Virchows Archiv: An International Journal of Pathology*, vol. 477, no. 3, pp. 566–569, 2020.
 - [25] C. Zhou, J. Tian, H. Li, and M. Y. Lee, “Imaging diagnosis and misdiagnosis of congenital pulmonary airway malformation in children [J],” *Journal of Clinical Radiology*, vol. 38, no. 09, pp. 1738–1742, 2019.
 - [26] G. Zhou, L. Fan, Q. Yin, and M. D. Klein, “MRI findings of fetal pulmonary cystic lesions [J],” *Radiology practice*, vol. 34, no. 06, pp. 668–674, 2019.
 - [27] Y. Xu, H. Li, B. Jin, A. W. Flake, and D. Tibboel, “CT findings and diagnosis of congenital pulmonary airway malformation in children [J],” *Chinese Journal of Medical computer Imaging*, vol. 25, no. 02, pp. 165–169, 2019.
 - [28] Z. Shang, X. Duan, P. Zhang, W. Zhong, B. Zhu, and D. Sun, “Diagnosis and treatment of congenital pulmonary airway malformation [J],” *Chinese Journal of Thoracic and Cardiovascular surgery*, vol. 34, no. 10, pp. 606–608, 2018.
 - [29] Ba-Da Jeong, An Su-Ah, M. Y. Lee et al., “Comparison of the prognostic factors of fetuses with congenital pulmonary airway malformations according to type,” *Journal of Ultrasound in Medicine Official Journal of the American Institute of Ultrasound in Medicine*, vol. 39, no. 11, pp. 591–594, 2020.

Research Article

The Influence of Interpersonal Trust on Rural Residents' Willingness to Participate in Mutual Aid for the Aged: An Empirical Analysis Based on the Survey Data of Hubei and Henan Provinces

Beibei Liu and Yongyong Sun 

School of Public Administration, Central China Normal University, Wuhan 430000, China

Correspondence should be addressed to Yongyong Sun; yongyongs@ccnu.edu.cn

Received 8 June 2022; Revised 28 June 2022; Accepted 5 July 2022; Published 18 August 2022

Academic Editor: Dong Chen

Copyright © 2022 Beibei Liu and Yongyong Sun. This is an open access article distributed under the Creative Commons Attribution License, which permits unrestricted use, distribution, and reproduction in any medium, provided the original work is properly cited.

At present, there is a huge gap between supply and demand of old-age services in rural areas of China. Developing rural mutual old-age services is of great significance to remedy the gap. Based on the survey data of 1200 rural residents in Hubei and Henan provinces, this paper adopts binary logistic regression model to analyze the influence of special trust and general trust on rural residents' willingness to participate in mutual care for the aged. The results show that both special trust and general trust have an impact on rural residents' willingness to participate in mutual support for the elderly, but the effect of special trust on rural residents' willingness to participate in mutual support for the elderly is not significant. General trust has a significant promoting effect on rural residents' willingness to participate in mutual care for the aged. Chinese rural residents' trust in village cadres has a significant promoting effect on their willingness to participate in mutual assistance for the aged. The trust of ordinary friends significantly inhibited their willingness to participate. The educational level, living style, and economic status of Chinese rural residents have a positive impact on their willingness to participate in mutual care for the aged. Age, marital status, health status, and intergenerational relationship are inversely correlated with willingness to participate.

1. Introduction

According to the seventh national census data, the national population is 1,411.78 million, and the population aged 60 and above is 264.02 million, accounting for 18.70% (among them, the population aged 65 and above is 190.64 million, accounting for 13.50%). Compared with 2010, the proportion of the population aged 60 and above has increased by 5.44 percentage points [1]. The level of rural economic development is backward, the self-security ability of farmers is poor, and they do not have the economic ability and willingness to purchase professional pension services. The national security capacity is relatively inadequate. Although the coverage rate of rural old-age security (including residents' old-age insurance and minimum living security and "five guarantees") is relatively high on the whole, the level of

security is low and it cannot provide adequate old-age security. In addition, both public and private pension institutions in rural areas are lagging behind in development, and it is difficult to provide adequate pension services but also relatively common government failure and market failure phenomenon.

In this case, the development of rural mutual support for the elderly has become an important option to solve the problem. Compared with the development of other forms of old-age security, there are certain comparative advantages in promoting mutual support for the elderly among rural residents. It can not only better meet the rural elderly will not leave home but also fully explore and use the existing rural endowment resources, effectively alleviate the shortage of pension funds, services, talents, and other resources in rural areas, and reduce the pressure

of pension service. Since Qiantun Village, Feixiang County, Handan City, Hebei Province, established the rural mutual aid Happiness Home in 2008, Hebei, Gansu, Hubei, Guangxi, and other places have successively carried out the exploration of rural mutual aid old-age care innovation road. From the top-level design aspect, the Central government has incorporated mutual assistance for the elderly into national policies. From the Rural Revitalization Strategy Plan (2018–2020) in 2018 to the “No. 1 Document” of the Central Government, Resolutely Winning the Battle against Poverty in 2020, both emphasize the development of mutual assistance for the elderly in rural areas. From the point of view of the current practice model of mutual assistance for the aged in various places, it can be divided into two main types: one is centralized mutual assistance, where the elderly are gathered together, and the elderly provide each other with pension services and spiritual comfort, such as “rural mutual assistance happy home” and village community care center. The other is diaspora, in which elderly people live scattered at home and participate in mutual care services, such as the “Old Buddy Program” and the “Old Friends Circle”. Although different forms of mutual support for the elderly have achieved certain effects, but only a small scope of fire, unable to start a prairie fire, different mutual support for the elderly are facing an important problem, that is, rural residents have low willingness to participate in mutual support for the elderly. Studies show that only 47.9% of the rural elderly are willing to participate in mutual support for the aged [2], showing the characteristics of low quality, low level, and low willingness of the elderly to participate [3] [4] that rural mutual care for the elderly is not [5]. Some scholars have also found that family size, living style, intergenerational relationship, health status, economic status, and age and marital status in individual characteristic variables have a significant impact on the willingness of rural elderly to support each other for the aged [2, 6, 7]. So far, few scholars have studied the specific impact and effect of interpersonal trust on rural residents’ willingness to participate in mutual care for the aged. However, the mutual support for the aged in rural areas being explored in our country is essentially a voluntary social exchange, based on the voluntary cooperation of the elderly in rural areas, so who are the elderly willing to cooperate with the object? Who is not? Who influences older people’s willingness to cooperate? How to make use of these influencing factors to enhance the willingness to participate and promote the development of rural mutual care for the elderly? These are the questions to be answered in this paper.

2. Theoretical Basis and Research Hypothesis

2.1. Interpersonal Trust. Before analyzing the connotation of interpersonal trust, we need to understand the connotation of trust. Some scholars regard trust as an individual behavior [8]. However, more scholars believe that trust is a positive expectation of others’ behavior [9–12]. That is, an

individual’s positive expectation is that others will act in consideration of their own interests. Luhmann [12] divides trust into interpersonal trust and institutional trust. Interpersonal trust is based on the emotional connection established in interpersonal communication, while institutional trust is based on the regulation and restriction of norms, rules, and regulations in interpersonal communication [13]. Barber divides interpersonal trust into general trust and special trust: general trust is an individual’s expectation that those who maintain social interaction with him can act according to the role norms, usually the trust of others or strangers in the society; special trust refers to the expectation that the individual can fully shoulder the responsibility and trust of acquaintances, friends, and family members [9]. As a subset of trust, interpersonal trust is a kind of interpersonal relationship in essence. Relationship means that both sides of trust play a role. Therefore, from the perspective of trust objects, many researches divide interpersonal trust into special trust and general trust; special trust is based on acquaintance relationship and general trust facing general social members beyond acquaintance relationship [14, 15]. In short, face-to-face communities, mutual knowledge, and strong social control lead to special trust [16]. General trust is more likely to occur in large communities where strangers or nonacquaintances are the majority [17].

Domestic scholars believe that Chinese trust is significantly different from that of the West [18]. The interpersonal trust in Chinese society results from the inner “love is different” and “people are different”, which is consistent with the “differential pattern” proposed by Fei Xiaotong. In other words, different types of interpersonal trust are individual-centered and gradually weaken from inside to outside with the opening of the intimate distance [19]. Family members, relatives, and friends are the most trusted, followed by the rest of the people, the lowest degree of trust is frequent business contacts, classmates, and most people in society [20]. In this study, interpersonal trust is divided into special trust and universal trust according to the different trust objects of rural residents and the relationship between them. The trust of family members, relatives, and neighbors based on blood relationship and geographical relationship is special trust. The trust of village cadre and other friends is universal trust.

2.2. Rural Mutual Assistance for the Elderly. Domestic research on mutual assistance for the elderly is quite abundant. From the perspective of research content, existing research on mutual assistance for the elderly has discussed its connotation, historical evolution, development status, practice mode, participation intention, feasibility, development dilemma, path, and other aspects [5, 21–25]. From the perspective of research, existing studies have been analyzed from the perspective of institutional embeddedness, policy tools, historical anthropology, resocialization, and community governance [26–30]. Combing the existing research results, it can be seen that, on the one hand, the existing research has not paid enough attention to the participants of

mutual care for the aged. Rural residents are the participants of rural mutual care for the aged, and their willingness to mutual care for the aged is the premise and basis for the realization of mutual care for the aged. On the other hand, some scholars began to pay attention to the role of trust mechanism in mutual care for the aged, but they focused more on social capital, pointing out that social capital can influence the pension behavior of rural elderly through interaction effect, reciprocity effect, and mutual trust effect [31]. Abundant social capital can reduce all kinds of friction in the process of mutual aid and make mutual aid pension can still operate well [32]. Some scholars proposed to build trust mechanism, mutual norms, participation in the network to help the sustainable development of mutual care for the elderly. Trust is the core element of social capital, but few scholars have studied its specific influence and function on mutual pension.

2.3. Interpersonal Trust and Willingness to Participate in Mutual Care for the Aged. Rural mutual assistance for the aged is a kind of voluntary mutual assistance and cooperation. In voluntary cooperation, individual behaviors will inevitably affect others, and others' behaviors will also affect individual behaviors, and each individual will influence and interact with each other. These influences will be fed back to their actions of mutual assistance for the aged. Therefore, it is necessary to analyze the influencing factors of participation intention from the dynamic level. It has been proved by literature that trust is a necessary condition for the occurrence of farmers' cooperative behavior, and trust presents the form of differential pattern [34]. The "special trust" based on kinship and quasi-kinship is the action logic of Chinese farmers towards cooperation [35]. Trust is a key factor in promoting mutual pension participation. The cultivation of trust can promote people to reach tacit cooperation and form a good interaction between members of the organization [36]. As a core subset of trust, interpersonal trust affects individual behavior choices through interpersonal communication and interaction in rural residents' daily life and production, thus affecting their willingness to participate in mutual care for the aged.

2.4. Research Hypothesis. Based on the above analysis, it can be considered that the interpersonal trust of rural residents may be a key variable affecting the willingness of rural residents to participate in mutual care for the elderly, but the different types of trust it contains may have different effects. With the gradual transformation of Chinese society to modern society, the trust relationship in rural and local society gradually develops from "special trust" to "universal trust". Based on this, the following research hypotheses are proposed.

Research hypothesis 1: Rural residents' special trust has a positive impact on their willingness to participate in mutual support for the elderly. The more the rural residents trust their children, relatives, and neighbors, the more inclined they are to participate in mutual

support for the aged. On the contrary, they are not inclined to participate in mutual pension.

Research hypothesis 2: The general trust of rural residents has a positive impact on rural residents' willingness to participate in mutual care for the aged. According to previous studies, there is a "differential order pattern" in the trust structure of Chinese people, and the special trust is much higher than the general trust. Therefore, hypothesis 2 can be divided into: the higher the trust degree of rural residents to other friends and village cadres, the higher their willingness to participate in mutual pension; otherwise, they are less willing to participate in mutual pension.

Research hypothesis 3: Special trust has no significant impact on rural residents' willingness to participate in mutual care for the elderly, while general trust has a significant impact.

3. Data Source and Model Design

3.1. Data Sources. The research data are from self-tuning data of the research group in 2019. In July 2019, members of the research group took Zhijiang City of Hubei Province and Dengzhou City of Henan Province as the basic sampling framework, and adopted random sampling method to select a number of villages in each place to conduct a questionnaire survey. The purpose of the survey is to investigate the situation of rural residents' mutual support for the elderly, and the respondents are mostly middle-aged and elderly people in rural areas. The content of the questionnaire mainly includes three parts: personal basic information, social network, and the current situation of rural mutual support for the aged. The measure items in the questionnaire are all from the integration of existing literature, and some of the research measures are from western literature, and the method of back-translation is used to ensure the accuracy of the description of measure questions in the questionnaire. The questionnaire survey was completed by one-to-one structured questioning. 1500 questionnaires were distributed, 1200 were recovered, and 1056 valid questionnaires were obtained after eliminating invalid ones. A preliminary survey was conducted before the formal investigation to ensure the reliability and validity of the questionnaire.

3.2. Model Selection. In this paper, the willingness to support the elderly is a binary variable, that is, willing and unwilling. Therefore, this paper selects binary logistic regression model. The model is set as follows:

$$y_i = x'_i \beta + \varepsilon_i, \quad (1)$$

$$P(y = 1|x) = F(x, \beta), \quad (2)$$

$$P(y = 1|x) = F(\cdot, \beta) = \Lambda(x', \beta) = \frac{\exp(x', \beta)}{1 + \exp(x', \beta)}, \quad (3)$$

$$f(y_i|x_i, \beta) = [\Lambda(x'_i, \beta)]^{y_i} [1 - \Lambda(x'_i, \beta)]^{1-y_i}, \quad (4)$$

$$\ln f(y_i|x_i, \beta) = y_i \ln[\wedge(x'_i, \beta)] + (1 - y_i) \ln[1 - \wedge(x'_i, \beta)], \quad (5)$$

In the model, y_i is the dependent variable, X_i is the independent variable, β is the coefficient, and ε is the random disturbance term. Combined with this study, the final model is:

$$\begin{aligned} \log it P(\text{willingness}_i = 1 | \text{special trust}_i, \text{universal trust}_i, \text{controls}_i) \\ = \alpha_i \text{special trust}_i + \beta_i \text{universal trust}_i + \chi_i \text{controls}_i, \end{aligned} \quad (6)$$

where subscript i represents the i th rural resident to be interviewed. The explained variable is a 0–1 binary variable about the willingness of rural residents to participate in the mutual support for the elderly. If rural residents are willing to participate in the mutual support for the elderly, the value is 1; otherwise, it is 0. Special trust _{i} represents the special trust of i rural residents interviewed, and universal trust _{i} represents the general trust of the i th rural residents surveyed. Controls _{i} represents the control variable of the i th rural resident.

In this paper, IBM SPSS26.0 software is used to analyze variables at different levels. Model 1 only adds control variables for regression. Model 2 puts three variables of special trust on top of Model 1. Model 3 puts two variables of general trust based on Model 1. Model 4 puts all the variables for control variables, general trust, and special trust.

3.3. Variable Definition. According to the above theoretical analysis and research assumptions, variables are defined as follows.

The dependent variable is the willingness of rural residents to participate in mutual care for the aged, and the index used to measure it comes from the survey question “Are you willing to provide mutual care for the aged? The answer is designed with two choices, i.e., willing = 1 and unwilling = 0, which is a dichotomous-dependent variable.

The independent variables include special trust and universal trust. In the aspect of special trust, three variables are set up: trust to children, trust to relatives, and trust to neighbors. In the specific investigation process, considering the understanding and acceptance ability of rural residents, the above three variables were transformed into the following questions: “I think children: most of them are not trustworthy, most of them are not trustworthy, the trustworthy and untrustworthy are evenly divided, most of them are trustworthy, most of them are trustworthy” “I think relatives: “I think neighbors: Majority untrustworthy, Majority untrustworthy, Majority untrustworthy, Majority untrustworthy, majority trustworthy, majority trustworthy.” In terms of general trust, two variables are set: trust to village cadres and trust to other friends. These two variables were translated into the following question: “I think village cadres: the vast majority are not trusted, the majority are not trusted, the trustworthy and untrustworthy are evenly

divided, the majority are trusted, the vast majority are trusted.” “I think other friends: most untrustworthy, most untrustworthy, trustworthy and untrustworthy, most trustworthy, most trustworthy.” “Most untrustworthy, most untrustworthy, trustworthy and untrustworthy half, most trustworthy, most trustworthy” reflects the trust intensity and is assigned 1, 2, 3, 4, 5, respectively.

Control variables. According to the existing research conclusions, education level, family size, living style, intergenerational relationship, health status, economic status, age, and marital status among individual characteristic variables have a significant impact on the willingness of rural elderly to support each other for the aged [2, 6, 7]. In order to avoid research bias caused by omission of variables, other explanatory variables are controlled in this study, which are mainly divided into personal characteristics and family characteristics. One is personal characteristic variables, which mainly include gender, age, marital status, education level, and health status. Where, gender, assign “male” to 1 and “female” to 0; age is assigned according to different age groups; marital status was set as a categorical variable for four conditions in the questionnaire: unmarried, spousal, spousal (widowed), and spousal (divorced); education level, without any education is assigned 1, primary school is assigned 2, junior high school is assigned 3, senior high school is assigned 4, technical secondary school is assigned 5, and college or above is assigned 6; health status is the self-rated health status of the interviewees, and different health levels are assigned different values. The second is family characteristic variables, including intergenerational relationship, living style, and economic status. Where the intergenerational variables were set as frequency of visits by adult children, with a value of 1 per week, 2 for half a month, 3 for one month, 4 for several months (from February to May), 5 for half a year, and 6 for one year or more. Residence mode is set as a classification variable for different situations. Economic status is set as personal income and is a continuous variable (Table 1).

4. Data Analysis and Research Findings

4.1. Descriptive Statistics of the Current Situation of Rural Mutual Assistance for the Elderly. Among the rural residents surveyed, 49.6 percent were male and 50.3 percent were female. Most of them had education below primary school, accounting for 53.7%. The age was 50–69 years old, accounting for 55.5%. Most of them were married, accounting for 83.5%; The health status was mainly relatively healthy and very healthy, accounting for 59.3%. The main source of monthly income is labor income, accounting for 62.4%. The majority of residents lived with their spouses or their children, accounting for 70.4% (see Table 2).

Generally speaking, rural residents have a higher willingness to participate in mutual support for the elderly. To the question “Are you willing to provide mutual care for others?” When answering this question, 80.39% of respondents are willing to provide mutual care for the aged. Only 19.61% of the respondents answered that they are not willing to provide mutual care for the aged (see Figure 1).

TABLE 1: Variable description table.

The variable name		Variable assignment
The dependent variable		
Willingness	Are you willing to provide mutual care for others?	1 = yes 2 = no
The independent variables		
Special trust	1. Trust in children	1 = The vast majority are not credible
	2. Trust in your neighbor	2 = Most cannot be trusted
	3. Trust in relatives	3 = The trustworthy and the untrustworthy are half and half
General trust	1. Trust in village cadres	4 = Most trusted
	2. Trust in other friends	5 = Overwhelmingly credible
Control variables		
Gender		1 = male 0 = female
Age		1 = under 50 2 = 50–59 3 = 60–69 4 = 70–79 5 = 80–89 6 = More than 90
Degree of education		1 = unlettered 2 = primary school 3 = Junior high school 4 = senior high school 5 = secondary technical school 6 = above
Marital status		1 = unmarried 2 = have a spouse 3 = death of a spouse 4 = divorced
Health condition		1 = very health 2 = a healthier 3 = general 4 = less healthy 5 = It's not healthy
Personal annual income		1 = under 5000 CNY 2 = $5000 \leq x < 10000$ CNY 3 = $10000 \leq x < 20000$ CNY 4 = $20000 \leq x < 30000$ CNY 5 = $30000 \leq x < 40000$ CNY 6 = More than 40000 CNY
Living pattern		1 = live alone 2 = with spouse 3 = with children 4 = with spouse and children 5 = with relatives
Intergenerational relationship	Frequency of visits by adult children:	1 = every day 2 = half a month 3 = a month 4 = a few months 5 = half a year 6 = one year and above

TABLE 2: Basic information of the survey sample.

Project	Category	Percentage
Gender	Male	49.6
	Female	50.3
Degree of education	Unlettered	20.8
	Primary school	32.9
	Junior high school	27.5
	Senior high school	13
	Secondary technical school	2.5
	Above	3.3
Health condition	Very health	17.5
	a healthier	41.8
	General	24
	Less healthy	13.7
	It's not healthy	3
Marital status	Unmarried	2.3
	Have a spouse	83.5
	Death of a spouse	12.9
	Divorced	1.3
Age	Under 50	23.1
	50–59	29.5
	60–69.	26
	70–79.	17.4
	80–89.	3.6
	More than 90	0.5
Living pattern	Live alone	8.7
	With spouse	39.5
	With children spouse, children	18.3
	With relatives	30.9
		2.6

In terms of gender, there is a certain difference between male and female rural residents' willingness to participate in mutual care for the aged. The willingness of

Are you willing to provide mutual care for others?

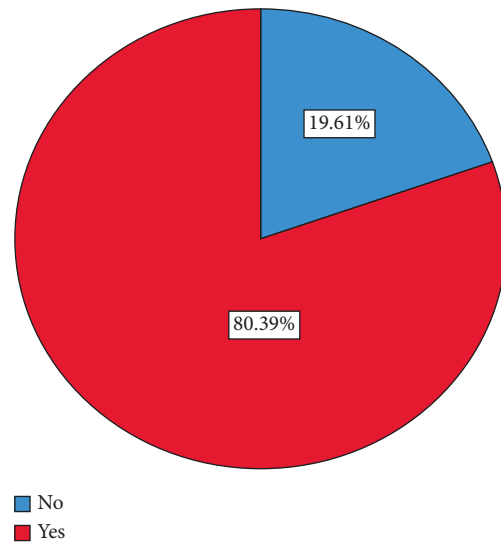


FIGURE 1: Willingness to participate in mutual pension.

female rural residents to participate in mutual care for the elderly was higher than that of male rural residents, and the willingness of female rural residents to participate in mutual care for the elderly reached 79.37%. In terms of age, rural residents of different age groups have different willingness to participate in mutual assistance for the elderly, showing the characteristics of younger people with higher willingness to participate and older people with lower willingness to participate. The willingness of rural residents under 70 years old to participate in mutual care for the elderly is higher, all above 80% level, and the willingness of rural residents under 50 years old to

participate in mutual care for the elderly is the highest. With the increase of age, the willingness to participate tends to decrease, and the willingness to participate of rural residents of all ages over 70 is around 60%. In terms of physical health, people with better physical health have higher willingness to participate, while those with poor physical health have lower willingness to participate. The rural residents of mutual endowment to participate are above the 80% level, health of rural residents' mutual endowment to participate reflected to participate in the transition between the good and bad health, very unhealthy and less healthy rural households mutual endowment to participate are around 65% level. In terms of marital status, there are differences among different marital status. Rural residents in the unmarried state are generally more willing to participate in mutual support for the elderly. In the married state, it is divided into different situations. Rural residents with spouse have a higher willingness to participate in mutual care for the aged, reaching 79.86%, while rural residents without spouse have a lower willingness to participate in mutual care for the aged, among which the widowed rural residents have the lowest willingness to participate in mutual care for the aged (see Table 3).

Most elderly people in rural China want to spend their old age at home, and their favorite way to provide for the aged is family care. 74.47% of respondents hope to choose family pension, 19.75% social institution pension (nursing home), 2.41% mutual support pension, and 3.37% other options (see Figure 2).

Since ancient times, there has been a concept of "raising children for old-age" in China. For most of the elderly in China, the main responsibility for supporting their children is their children. The findings of this study confirm this, 64.02 percent of the respondents said that children should be responsible for the elderly with children, followed by 8.05 percent who chose the elderly themselves, 21.86 percent who chose the government, their children, and the elderly, and 6.08 percent who chose the government (see Figure 3).

With the aggravation of China's aging population, the family's supporting function will gradually weaken. To solve the pension problem, we need to fundamentally change the traditional pension concept. However, according to the survey of this study, elderly people in rural China have a low awareness of the mutual assistance pension model. 66.9% of respondents have not heard of mutual support for the elderly, 26.6% of respondents have heard of it but do not know much about it, and only 6.4% of respondents have heard of it very well (see Figure 4).

In China's rural areas, with the aging of the population and the large-scale outflow of young and middle-aged labor force, the demand for elderly care services is increasing, and many elderly people have realized the necessity of mutual support for the elderly model. The survey of this study shows that 59.86 percent of respondents believe that it is necessary to develop mutual support for the elderly in the village, and people have recognized the necessity of mutual support for the elderly (see Figure 5).

4.2. Descriptive Statistics of Independent Variables and Control Variables. The core explanatory variables in this paper include special trust and universal trust element. Special trust mainly includes three variables: trust degree to children, trust degree to relatives, and trust degree to neighbors. General trust includes two variables: trust in village cadres and trust in other friends. Sex, age, education, marital status, and residence status were used as control variables. As shown in Table 3, in terms of the mean values of each variable, the mean values of the three variables in special trust are higher than those of the two variables in general trust. Among them, the mean value of trust in children is the largest, while that of other friends is the lowest. It shows that the current trust pattern of farmers based on family is obvious, and the interpersonal trust of farmers shows an obvious differential order pattern from close to sparse, from inside to outside. This is consistent with the traditional differential pattern theory and shows the family-oriented characteristics of traditional Chinese rural society summarized by previous researches. The difference is that the average trust degree of village cadres is higher than that of other friends. Since the reform and opening up, rural grassroots democracy construction has made certain achievements. Village cadres play a very important role in rural governance, and the average trust degree of farmers on village cadres is higher than that of other friends.

4.3. Multicollinearity Test. Before the regression analysis, considering that there may be internal correlations among variables such as rural residents' trust in children, relatives, neighbors, village cadres, and other friends, this paper makes a multicollinearity diagnosis for each variable. Generally, when $VIF > 3$, there is a certain degree of multicollinearity between the respective variables. When $VIF > 10$, there is a high degree of collinearity between the respective variables. By selecting trust in children as the dependent variable and the remaining variables as the independent variables, the estimated results of collinearity test are shown in Table 3. VIF is less than 10. Based on all the estimated results, the collinearity correlation degree between the respective variables is within a reasonable range (Table 4).

4.4. Binary Logistic Regression Results. In order to explain the effect of general trust and special trust on the willingness of rural residents to participate in mutual support for the aged, the regression results are shown in Table 5; three variables of special trust were added in model 2, two variables of general trust were added in model 3, and special trust and general trust were added in model 4. As the final model, the observed value of the Hosmer-Lemeshow statistic was 6.512, and the probability P was .590 and is higher than significant level α , so the null hypothesis should not be rejected. It is considered that there is no significant difference between the distribution derived from the actual value of the sample and that derived from the predicted value, and the goodness of fit of the model is better. From model 1 to model 4, Nagelkerke r^2 increased from 0.087 to 118, an increase of 35.632%. This shows that interpersonal trust plays an important role in

TABLE 3: Cross analysis of basic characteristic variables and willingness to participate in mutual pension.

Variable	Variable classification	Willingness to participate in mutual pension			
		Yes		No	
		Number	Percentage	Number	Percentage
Gender	Male	393	76.46	121	23.54
	Female	427	79.37	111	20.63
Age	≤50	206	85.12	36	14.88
	50–59	251	81.23	58	18.77
	60–69	219	80.22	54	19.78
	70–79	117	64.29	65	35.71
	80–89	22	57.89	16	42.11
	≥90	3	60.00	2	40.00
Marital status	Unmarried	19	79.17	5	20.83
	Have a spouse	694	79.86	175	20.14
	Death of a spouse	90	66.67	45	33.33
	Divorced	10	71.43	4	28.57
Health condition	Very healthy	155	84.70	28	15.30
	Healthier	360	82.19	78	17.81
	General	192	76.49	59	23.51
	Less healthy	90	62.50	54	37.50
	Not healthy	21	65.63	11	34.38

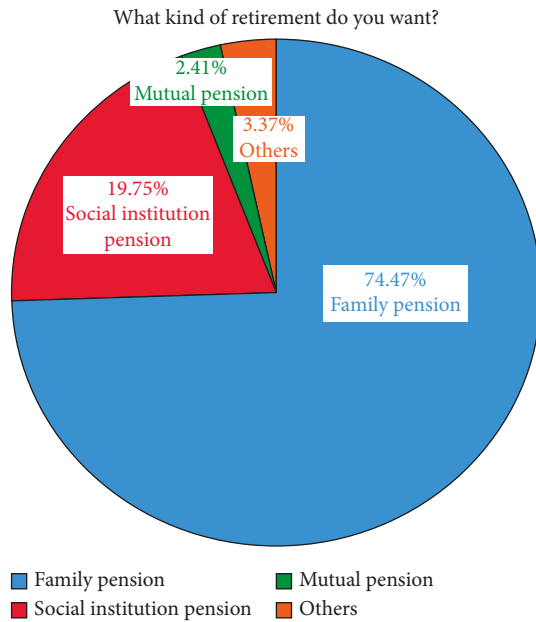


FIGURE 2: The choice of pension.

rural residents' willingness to participate in mutual support for the aged (Table 6).

- (1) From model 2 and model 3, the two regression results show that trust to children and trust to neighbors have a positive effect on the willingness of rural residents to participate in mutual support for the aged, that is to say, the higher the degree of trust to children and neighbors, the higher the willingness of mutual support and participation. The trust to relatives has a negative effect on the participation intention. The higher the trust degree to relatives, the lower the participation intention. The results support

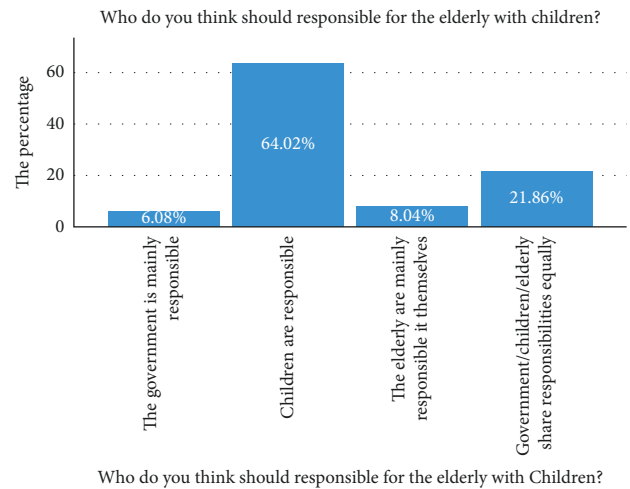


FIGURE 3: Elderly care responsibilities.

hypothesis 1 that the higher the trust level of rural residents towards their children and neighbors, the more likely they are to participate in mutual support for the aged, and vice versa, the less likely they are to participate in mutual support for the aged. However, the variable of trust in relatives has a negative effect on the willingness of rural residents to participate in mutual support for the aged. The possible explanation is that under the background of the current urbanization process in China, a large number of rural young and strong laborers have left their hometown and the outflow of rural labor forces blocks or limits the effectiveness of support. The old people in rural areas cannot rely on their children for their old-age support, while the relatives formed by blood relationship and

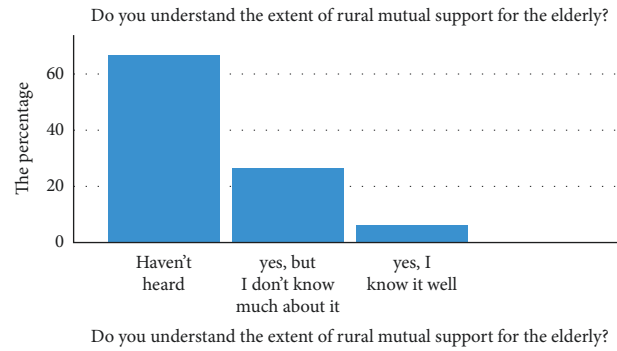


FIGURE 4: Understanding of mutual pension.

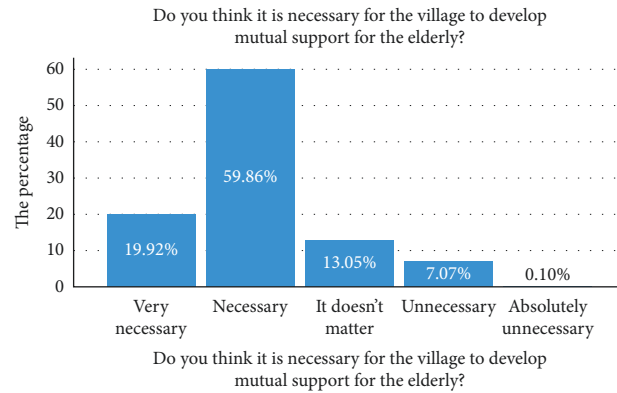


FIGURE 5: The necessity of developing the model of mutual support for the aged.

TABLE 4: Multicollinearity diagnosis.

	Nonstandardized coefficient		The standard coefficient		Sig.	Collinearity statistics	
	B	Standard error of	A trial version	t		Tolerance	VIF
(Constant)	2.765	0.119		23.143	0.000		
Trust in village cadres	0.077	0.028	0.094	2.741	0.006	0.643	1.556
Trust in neighbor	0.073	0.049	0.071	1.485	0.138	0.329	3.039
Trust in relatives	0.354	0.045	0.363	7.919	0.000	0.361	2.772
Trust in other friends	-0.023	0.030	-0.029	-0.761	0.447	0.528	1.895

A: dependent variable: trust degree of children

TABLE 5: Descriptive statistics of independent and control variables.

		Minimum	Maximum	Mean	Mean standard error
Special trust	Trust in children	1	5	4.67	0.023
	Trust in relatives	1	5	4.00	0.024
	Trust in your neighbor	1	5	3.91	0.023
General trust	Trust in village cadres	1	5	3.70	0.028
	Trust in other friends	1	5	3.53	0.029
Control variable	Gender	1	2	1.50	0.016
	Age	1	6	2.50	0.036
	Degree of education	1	6	2.54	0.038
	Marital status	1	4	2.13	0.013
	Health condition	1	9	2.43	0.032
	Personal annual income	1	6	2.52	0.044
	Living pattern	0	6	2.78	0.034
	Intergenerational relationship	1	6	4.07	0.074

TABLE 6: Regression results.

Change the amount	Model 1	Model 2	Model 3	Model 4
Trust in children		0.114 (0.163)		0.081 (0.165)
Trust in relatives		-0.518 (0.277)		-0.440 (0.246)
Trust in your neighbor		0.270 (0.231)		0.260 (0.262)
Trust in village cadres			0.273*** (0.133)	0.287*** (0.143)
Trust in other friends			-0.353*** (0.132)	-0.273*** (0.166)
Gender	0.219 (0.215)	0.209 (0.217)	0.199 (0.219)	0.196 (0.220)
Age	-0.091 (0.110)	-0.092 (0.111)	-0.123 (0.112)	-0.123 (0.1138)
Level of education	0.279** (0.124)	0.244** (0.126)	0.223** (0.125)	0.205** (0.127)
Marital status	-0.103 (0.247)	-0.157 (0.249)	-0.103 (0.249)	-0.146 (0.251)
Health condition	-0.242** (0.111)	-0.254** (0.113)	-0.232** (0.113)	-0.235** (0.114)
Personal annual income	0.090 (0.096)	0.078 (0.097)	0.084 (0.098)	0.076 (0.099)
Living pattern	0.108 (0.103)	0.116 (0.104)	0.102 (0.104)	0.103 (0.105)
Intergenerational relationship	-0.43 (0.053)	-0.053 (0.054)	-0.053 (0.054)	-0.060 (0.055)
Constant term	1.211 (1.012)	2.004 (1.371)	1.806 (1.175)	2.031 (1.379)
Chi-square	40.515 ($P = 0.001$)	46.241 ($P = 0.001$)	40.695 ($p \leq 0.001$)	52.813 ($P \leq 0.001$)
-2 logarithmic likelihood	628.249	622.065	612.697	609.128
Nagelkerke R^2	0.093	0.106	0.115	0.122

Note. Standard error in parentheses, standard regression coefficient outside parentheses; *, **, and *** were significant at the level of 0.05, 0.01, and 0.001, respectively.

geography can provide support to the old people nearby. When there is a need for old-age support, the old people can seek help from relatives; therefore, it is not a priority to participate in mutual support for the aged, so the trust of relatives has a negative effect on this variable.

- (2) The regression results of model 3 and model 4 show that in interpersonal trust, the two variables of universal trust have a significant effect on rural residents' willingness to participate in mutual support for the aged and have passed the significance test ($P < 0.001$). In the final model 4, the higher the trust of rural residents to the village cadres, the higher their willingness to participate in mutual support for the aged. Village cadres are grassroots organization managers such as village party secretaries and village committee directors who control the village's formal power resources. They are the village's elite; village elites play an important role in the modernization of Chinese villages. In the mutual support service for the aged, the higher the rural residents' trust to the village cadres,

the higher their willingness to participate, which is consistent with the scholars' theory of elite governance. Trust to other friends and mutual support participation intention showed the opposite effect, the lower the trust to other friends, the higher the mutual support participation intention. First, the trust of other friends has an important impact on the willingness of rural residents to provide for the elderly, we should pay full attention to this factor. Secoond, the Rural Society in China is an acquaintance society, in which the active subjects have enough understanding of each other due to long-term contact, and the degree of Information asymmetry interaction is low, as a result, rural residents are more willing to choose acquaintances as cooperative partners to reduce the risk of old-age care. Therefore, the more they distrust other friends, they are more willing to choose mutual assistance based on acquaintances, the more willing you are to participate.

- (3) The special trust variable had no significant effect on the willingness to participate ($P > 0.05$), but the

general trust variable had a significant effect on the willingness to participate ($P < 0.001$). Hypothesis 3 of this paper is demonstrated. Special trust has no significant effect on rural residents' willingness to participate in mutual care for the aged, while general trust has a significant effect. In today's rural society, the interpersonal trust pattern of rural residents is changing; before the traditional blood relationship as the core of relative closeness which is formed by the special trust relationship with the stability of the society is gradually changing, special trust occupying the leading status in the pattern of relationships is changing, the situation of interpersonal trust relationship gradually by the "special trust" the direction of "universal trust"; therefore, special trust has no significant effect on rural residents' willingness to participate in mutual care for the aged, while general trust has a significant effect.

- (4) Among the control factors, the controlling factors, gender, education level, living style, and economic status have a positive effect on the willingness to participate in mutual care for the elderly. In particular, educational level has a significant impact on willingness to participate. The higher the culture, the higher the willingness to participate. The four variables of age, marital status, health status, and intergenerational relationship have a reverse effect on rural residents' willingness to participate in mutual care for the aged. The younger the age, the higher the willingness to participate. Older people who live alone are more likely to participate in mutual care. Rural residents with poor health status had higher willingness to participate. The better the intergenerational relationship, the higher the frequency of home visits of adult children, the lower their willingness to participate. The possible explanation is that the elderly living alone and in poor health has greater demand for pension services, and their willingness to participate is higher.

5. Conclusion and Discussion

Based on the above analysis, the main conclusion of this paper can be summarized as follows. (1) Both special trust and general trust have an impact on rural residents' willingness to participate in mutual care for the aged, but the impact of special trust on rural residents' willingness to participate in mutual care for the aged is not significant. General trust has a significant promoting effect on rural residents' willingness to participate in mutual care for the aged. (2) Chinese rural residents' trust in village cadres has a significant promoting effect on their willingness to participate in mutual assistance for the elderly. The trust of ordinary friends significantly inhibited their willingness to participate. (3) Gender, education level, living style and economic status of Rural Chinese residents have a positive impact on their willingness to participate in mutual care for the elderly; In particular, the degree of education has a significant

promoting effect on the willingness to participate, the higher the degree of education of the elderly, the higher the willingness to participate in mutual support for the elderly. (4) There is an inverse correlation between age, marital status, health status, intergenerational relationship and rural residents' willingness to participate in mutual care for the aged. The older people who live alone have poor health, poor intergenerational relationship with their children, and higher willingness to participate in mutual support for the aged.

It should be pointed out that the willingness of rural residents to participate in mutual care for the aged will be affected by multidimensional factors. This study only analyzes from the perspective of interpersonal trust, and a more systematic investigation can be carried out by combining macrolevel factors with microlevel factors. In addition, the sample of this study is a representative sample of Chinese rural residents, and the research conclusion is only applicable to Chinese rural residents. In future studies, we still need to further expand the sample range and improve the external validity and robustness of research conclusions.

Data Availability

The datasets used and analyzed during the current study are available from the corresponding author upon reasonable request.

Conflicts of Interest

The authors declare that they have no conflicts of interest.

Acknowledgments

This study was supported by the project: A Study on the Construction of a New Rural Mutual Care Service Field Based on Social Networks (no. 18BSH164).

References

- [1] B. E. Sands, P. M. Irving, T. Hoops et al., "Ustekinumab versus adalimumab for induction and maintenance therapy in biologic-naïve patients with moderately to severely active Crohn's disease: a multicentre, randomised, double-blind, parallel-group, phase 3b trial," *Lancet (London, England)*, vol. 399, no. 10342, pp. 2200–2211, 2022.
- [2] G. Xu, "The construction of diversified rural old-age security System," *Changbai Journal*, no. 1, pp. 109–112, 2008.
- [3] H. Jin, *Exploration*, vol. 12, no. 6, pp. 155–161, 2014.
- [4] Z. Zhao, "The development dilemma and strategy of rural Mutual assistance pension model," *Journal of Hebei University (Philosophy and Social Science Edition)*, vol. 6, no. 1, pp. 72–75, 2015.
- [5] L. Zhang, T. Li, L. Huang et al., "Preparation and application of melamine cross-linked poly ammonium as shale inhibitor," *Chemistry Central Journal*, vol. 12, no. 1, pp. 44–49, 2018.
- [6] C. Yu, *Journal of Huazhong University of Science and Technology (Social Science Edition)*, vol. 7, no. 2, pp. 116–123, 2019.
- [7] J. Say Miranda and C. O'Driscoll, "Inter-rater variability in scoring of addenbrooke's Cognitive Examination-Third Edition (ACE-III) protocols," *Appl Neuropsychol Adult*, pp. 1–5, 2022.

- [8] B. Barber, "The logic and limits of trust," *Social Forces*, vol. 64, no. 1, pp. 51–58, 1983.
- [9] R. Hardin, "Conceptions and Explanations of trust," *Trust in Society Russell Sage Foundation*, 2001.
- [10] L.-T. Hosmer, "TRUST: the connecting link between organizational theory and philosophical ethics," *Academy of Management Review*, vol. 20, no. 2, pp. 379–403, 1995.
- [11] Y. Zheng, *Trust Theory*, China Radio and Television Press, 2006.
- [12] N. Luhmann, *Trust and Power*, John Wiley & Sons, New York, 1979.
- [13] R.-D. Putnam, *Bowling Alone: The Collapse of American Community*, ACM, New York: Simon & Schuster, 2000.
- [14] B.-A. Misztal, *Trust in Modern Societies: The Search for the Bases of Social Order*, Polity Press, Cambridge, UK, 1996.
- [15] R. Portes and P. Landolt, "Let's fight the next sovereign debt war now," *Economic Outlook*, vol. 20, no. 2, pp. 12–17, 1996.
- [16] D. Jan and N. Kenneth, "Predicting cross-national levels of social trust: Global pattern or Nordic Exceptionalism?" *European Sociological Review*, vol. 9, no. 4, pp. 769–771, 2005.
- [17] F. Wang, "A comparative study of trust between China, Japan and America," *Sociology Study*, no. 2, 1999.
- [18] Y. Yang, "'One of us': a case study of trust Construction process," *Journal of Sociology*, no. 2, 1999.
- [19] H. Yu, "Changing differential order: the change of farmers' interpersonal trust and its influencing factors: based on the five-wave questionnaire survey data of 40 villages in Jiangxi province from 2002 to 2015," *Journal of Central China Normal University (Humanities and Social Sciences Edition)*, vol. 9, no. 5, pp. 1–10, 2017.
- [20] Li. Dan and H. Bi, "A review of the development of mutual assistance for the elderly in China," *Scientific Research on Aging*, vol. 7, no. 1, pp. 44–53, 2020.
- [21] Q. Li and Y. Q. Liu, "Historical evolution, practice mode and development trend of rural mutual support for the elderly," *Journal of Northwest A&F University (Social Science Edition)*, vol. 10, no. 5, pp. 72–78, 2018.
- [22] J. Yang, "Mutual assistance pension model: characteristics, value and construction path," *Zhongzhou Journal*, vol. 8, no. 3, pp. 73–78, 2016.
- [23] L. C. Yang, "Practical dilemma and implementation path of rural empty nesters participating in mutual care for the elderly," *Journal of Agricultural Economics*, vol. 10, no. 8, pp. 81–83, 2019.
- [24] N. Liu, "Analysis on the types and operation mechanism of Mutual assistance social endowment in Rural China," *Population Research*, vol. 4, no. 2, pp. 100–112, 2019.
- [25] Y. Wang and Q. Wang, "The realistic dilemma and optimization path of Mutual aid pension in China," *China Economist*, vol. 12, no. 5, pp. 16–18, 2019.
- [26] H. Wang, "The logic of effective operation of multiple welfare from the perspective of policy tools: a case study of mutual-aid old-age care in S Village in northern Sichuan," *Journal of Public Administration*, vol. 8, no. 4, pp. 90–101, 2015.
- [27] J. Fang, *Ideological Front*, no. 4, pp. 78–82, 2015.
- [28] Y. Sun, G. Yang, and S. Liu, "Organization and management of voluntary mutual assistance for the elderly in China from the perspective of resocialization," *Reform and Strategy*, no. 2, pp. 120–122, 2017.
- [29] Y. Wan, "The cultivation of social capital in the model of mutual assistance for the aged from the perspective of community governance -- based on the experience of the American village Movement," *Journal of Northwest University*, no. 4, pp. 104–113, 2019.
- [30] N. Zhao, "Research on rural diversified pension model frPlease provide the full publication details for References [3, 6, 27, 30, 31].om the perspective of social capital," no. 2, pp. 30–35, 2018.
- [31] X. He, *Journal of Nanjing Agricultural University*, vol. 10, no. 5, pp. 1–8, 2020.
- [32] Li. Zhang and H. Bi, "Research on influencing factors of rural mutual assistance pension satisfaction based on AHP-Dematel Model," *Scientific Research on Aging*, vol. 5, no. 10, pp. 15–27, 2019.
- [33] S. Xu, *Research on Farmers' Cooperative Behavior and Trust: Based on the Perspective of Social Capital*, Shandong University, Shandong, 2006.
- [34] Q. Zhao and L. Yi, "Relationship networks and cooperative economy in Rural China: a social capital perspective," *Problems in Agricultural Economy*, vol. 13, no. 08, pp. 40–46, 2007.
- [35] H. Zhao, "Research on the development dilemma and countermeasures of mutual support for the elderly under the loss of social capital," *Learning and Exploration*, vol. 7, no. 9, p. 143, 2020.
- [36] H. A. O. Yaya and H. Bi, "Analysis on the willingness and influencing factors of the rural elderly to support each other in the community in Shandong Province," *Northwest Population*, vol. 6, no. 2, pp. 96–104, 2018.

Research Article

Study on the Application Effect of the Case Teaching Method Based on Primary Teaching Principle in Clinical Teaching of Radiology

Tong Gong, Yuting Wang, Hong Pu, Longlin Yin , and Mi Zhou 

Radiology, Sichuan Provincial People's Hospital, University of Electronic Science and Technology of China, Chengdu 610072, China

Correspondence should be addressed to Mi Zhou; 3170400009@caa.edu.cn

Received 6 June 2022; Revised 6 July 2022; Accepted 11 July 2022; Published 17 August 2022

Academic Editor: Dong Chen

Copyright © 2022 Tong Gong et al. This is an open access article distributed under the Creative Commons Attribution License, which permits unrestricted use, distribution, and reproduction in any medium, provided the original work is properly cited.

Objective. A case-control study explored the application of case-based teaching methods in the clinical teaching of radiology. **Materials and Methods.** 126 radiology interns of grade 2018 were selected by cluster sampling and randomly divided into the research group and the control group. The traditional teaching approach was used in the control group and the primary teaching principle was used in the research group. The teaching effects of the two groups were compared. **Results.** The interns' test scores, the research group's case summary multiple-choice questions, case-group multiple-choice questions, case analysis questions, theoretical total scores, and practical operation assessment scores were significantly higher than those of the control group, and the difference was statistically significant ($P < 0.05$). The total score of dimensions of the interns' critical thinking ability in the study group were significantly higher than those in the control group, and the difference was statistically significant ($P < 0.05$). The interns' perception of teachers, students' academic self-perception, students' perception of environment, students' social self-perception, and the total score of the DREEM scale in the study group were considerably greater than those in the control group, and the difference was statistically significant ($P < 0.05$). After teaching, the scores of systematic thinking ability and evidence-based thinking ability of the interns were significantly increased. The improvement in the study group was more significant than that in the control group, and the difference was statistically significant ($P < 0.05$). Following teaching, the scores of learning interest, self-management, plan implementation, and mutual cooperation of the interns in the two groups were significantly upregulated, and the difference was statistically significant ($P < 0.05$). Among them, the improvement of interns' abilities in the research group was significantly better than that in the control group, and the difference was statistically significant ($P < 0.05$). The scores of learning goal, learning process, learning effect, classroom environment construction, teaching strategy, and technology application in the research group were greater than those in the control group, and the difference was statistically significant ($P < 0.05$). The satisfaction rate of the study group was higher than that of the control group, and the difference was statistically significant ($P < 0.05$). **Conclusion.** The application of the case teaching method based on primary teaching principle in the radiology clinical teaching course is helpful to cultivate students' critical thinking ability and improve students' performance and classroom teaching effectiveness.

1. Introduction

The standardized training of radiology residents in China could be traced back to 1991. Through the standardized training in the department of radiology, the trainees can comprehensively grasp the imaging principle of common equipment in the department of radiology, the imaging

manifestations of common diseases, and the differential diagnosis of some rare diseases [1]. How to better improve the clinical practice ability and post competence of radiology residents is an urgent clinical practice problem for imaging medicine teachers [2]. At present, the training mode in the clinical practice teaching of radiology is mainly based on the traditional teaching mode, but the teaching method centered

on teachers, teaching materials, and topics can no longer meet the requirements of the hospital for medical students [3].

Typical case teaching method is a new teaching model in recent years. The typical case teaching method can not only encourage students to think independently and enhance their creative ability but also guide interns to combine theoretical knowledge with clinical practice. The classic case teaching method can guide students to actively think and summarize what they have learnt in time, making clinical practice teaching more vivid and concrete and achieve better teaching results [4, 5]. The primary teaching principle was first put forward by instructional design theorist Merrill in 2001. It is an important teaching principle summarized on the basis of studying various educational and teaching theories put forward by predecessors. It focuses on how to better facilitate learning and improve teaching effectiveness. The primary teaching principal advocates that under the purpose of “focusing on solving problems,” teaching should be carried out in a circle composed of activating old knowledge, demonstrating new knowledge, and applying new knowledge. It is a prescription teaching design principle to improve classroom teaching and attach importance to teaching effectiveness [6–8]. This principle completes the specific teaching tasks in a step-by-step situation of practical problems, which meets the requirements of learners’ psychological development, so it is suitable for the practical course of internal medicine nursing which is closely connected with the clinic. Some scholars have tried to apply the primary teaching principles to the classroom teaching of surgery and geriatric nursing, which has displayed a good teaching effect [9–13]. The results of this study has indicated that the primary teaching principle is helpful to improve the interns’ mastery of relevant knowledge and the ability to construct the knowledge system of radiology.

2. Materials and Methods

2.1. General Information. From October to December 2020, 126 interns in the Department of Radiology of grade 2018 were selected by the method of cluster sampling. All of them were enrolled in five-year clinical medicine major and randomly divided into two groups. There were 63 participants in the research group, including 52 boys and 11 girls. The age ranged from 20 to 23 (21.91 ± 0.93) years. The score of the first two academic years was (81.73 ± 0.22). There were 63 persons in the control group, including 50 boys and 13 girls. The age ranged from 19 to 23 (21.44 ± 1.36) years. The score of the first two academic years was (82.03 ± 0.45). There was no significant difference in age, sex, and performance between the two groups, so it was comparable.

Selective criteria are as follows: (1) all the participants had bachelor’s degree regardless of gender; (2) the participants had no cognitive, language, and intellectual impairment, and had basic reading and writing ability; (3) they all participated voluntarily.

Exclusion criteria are as follows: (1) non-radiology interns; (2) those who could not cooperate to complete all the teaching tasks; (3) those who dropped out halfway or did not match well.

2.2. Methods. The interns in the control group carried out the traditional teaching mode and the teacher responsibility system for clinical teaching, which was mainly taught by the teacher, and the teaching content is completed in accordance with the practice syllabus. Theoretical knowledge and clinical skills in radiology were taught. Teaching activities are regularly scheduled on a weekly basis and the teaching program was regularly checked and feedback is given in a timely manner. Regular surveys were conducted to determine the satisfaction of the trainees with the teaching situation and to identify any problems in teaching. Finally, based on feedback from various sources, the teachers changed their teaching methods.

The interns in the research group adopt the case teaching method based on the primary teaching principle based on the control group. The specific methods are as follows: (1) Preparation before teaching. Two weeks before the formal start of the course, the leader of the research group conducted a two-hour collective training for the interns. The training content was related to the primary teaching principles, including concepts, basic elements, implementation steps, and operation methods of the e-teaching platform. Prior to the start of the class, the average grades of 63 interns from the previous two academic years were stratified into three tiers: upper, middle, and lower. Two to three interns were placed in each stratum, and seven to eight interns were placed in groups to ensure homogeneity between groups. Because of the practice syllabus developed by the radiology department, the representative frequently-occurring diseases and common diseases were selected. The cases were compiled by experienced medical teachers and experienced teachers and the real cases can be adapted. Case explanation can be combined with multimedia courseware and other forms, including clinical data, questions to be discussed, and reference answers. (2) Teaching methods would focus on the problem or complete task. One week before class, the teacher issued a case and a learning task list (composed of complete tasks and sub-tasks) [14]. The complete task was a general task designed by teachers on the basis of textbook and learning situation analysis, which was divided into easy to difficult subtasks in accordance with the principle of the task sequence, which required interns to complete the task. Subtask: (1) review and consolidate the theoretical knowledge of related diseases; (2) integrate the theoretical knowledge of various diseases and systems; (3) formulate targeted diagnosis and treatment plans. Before class, the group leader was responsible for assigning 8 contents, consisting of the case introduction, nursing evaluation, disease diagnosis, treatment goal, diagnosis and treatment measures, effect evaluation, health education, and disease-related knowledge to the group members, and then discussing and making PPT and mind map of case analysis ideas [15]. During this period, nursing students could log on to the case database of the e-teaching platform to refer to the uploaded literature, website links, and other related materials [16]. When analyzing the case before class, the group judged the type of disease according to the clinical symptoms, reviewed the main points of the knowledge of the disease again, and learned new knowledge. After the preclass

discussion, each group of reporters made a centralized report and discussion to the teacher 2 days before class, and the teacher made suggestions for each group of reports and learned about the learning situation of nursing students in order to prepare for the lesson. (3) The content of new knowledge demonstrated by teachers should be consistent with the learning task list, combined with words, pictures, or videos to demonstrate the new knowledge in detail through analogy demonstration, picture imagination, intern debate competition, etc. [17]. After reviewing the old knowledge in class, 10 min was shown by 8 groups according to the mind map drawn by each group according to the diagnosis and treatment procedure in the form of slides to simulate the overall diagnosis and treatment process, which required that the disease diagnosis should be based on sufficient case basis. At the same time, when demonstrating new knowledge, we put forward relevant critical thinking problems and guide interns to use theoretical knowledge to solve problems step by step. (4) New knowledge was applied. As the interns gradually master knowledge, the teachers should gradually reduce guidance and finally provide interns with the opportunity to use new knowledge to solve variant problems [18]. The so-called variant problem was to change the problem situation around the teaching goal to make the interns follow suit [19]. (5) Convergence and integration. After first applying new knowledge to solve problems, interns needed further flexibility in selecting and applying new knowledge in real clinical cases in order to fully understand and integrate all aspects of knowledge [20]. The teachers needed to create opportunities for students to apply new knowledge flexibly. After classroom teaching, the students logged on to the e-teaching platform and learn similar cases of other causes in the case database. The cases came from real and complete clinical cases, which are closer to reality. The process of clinical diagnosis and treatment by learning the dynamic changes of the disease are practiced [21]. At the end of the self-study, the “discussion forum” of the e-learning platform course publishes the results of the case studies. The teacher guides students in speculation and communication.

2.3. Observation Index

2.3.1. Course Assessment Results. After the end of the practical teaching course, the two groups of interns took part in the closed-paper examination of the same test paper. The research group compiled the question bank. The test paper types were 10 case summary multiple-choice questions (20 points), 5 case group multiple-choice questions (20 points), 2 case analysis questions (60 points) with a total score of 100 points. In the case analysis questions, candidates were required to carry out nursing assessment according to the disease profile (15 points), put forward disease diagnosis results and measures (30 points), and carried out health education (15 points). The papers were marked by teachers and there was a unified reference standard.

2.3.2. Critical Thinking Ability. The Chinese version of critical thinking disposition critical thinking ability scale (CTDI CV) revised by Peng M.eici et al. [21] was used for

evaluation. The scale included 7 dimensions, consisting of truth seeking, open mind, analytical ability, systematic ability, curiosity, self-confidence, and cognitive maturity. There were 10 items in each dimension with 70 items. Using the Likert 6-level scoring method, the scores were from 1 to 6 points from strongly disagree to strongly agree with the 70 to 420 points. The Cronbach's α coefficient of the scale was 0.90. It was uniformly distributed by teachers through the questionnaire star platform before the beginning of the course and after the end of the course. The effective recovery rate of the two questionnaires was 100%.

2.3.3. Evaluation of Medical Education Environment. The DREEM scale was used for evaluation and five aspects were observed, including “students’ perception of learning,” “students’ perception of teachers,” “students’ academic self-perception,” “students’ perception of the environment,” and “students’ social self-perception” [22]. To judge the problems were existing in the medical education environment, all items from disagree to strongly agree were expressed on a scale of 0 to 4 with a full score of 200. According to the total score of the scale, the educational environment was divided into 4 grades. The educational environment had serious problems (0–50 points); the educational environment had many problems (51–100 points); the educational environment was good (101–150 points); and the educational environment was very good (151–200 points).

2.3.4. Clinical Thinking Ability Score. The clinical thinking ability rating scale compiled by Roberts et al. was used to evaluate the thinking ability of the two groups of radiology interns before and after teaching, with a total of 24 items [23]. Through the Likert 5 grade scoring method, the score was positively correlated with the clinical thinking level. The content validity of the questionnaire was 0.89 and the reliability coefficient of Cronbach' α was 0.91.

2.3.5. Autonomous Learning Ability. The autonomous learning scale was used to evaluate the self-learning ability of the two groups of interns before and after teaching [24]. The scale was divided into four dimensions, including learning interest, self-management, mutual cooperation, and plan implementation. The reliability and validity of the scale were 0.85 and 0.79, respectively.

2.3.6. Evaluation of Teaching Effectiveness. The effective teaching evaluation form of the new curriculum edited by Sun Wenbo was used to evaluate the effectiveness of classroom teaching [25]. It was attended by other teachers who were not substituted by the project group. The dimensions of nursing students include three items, such as learning goal (10 points), learning process (30 points), and learning effect (20 points), which mainly evaluated the achievement of learning goals, nursing students’ participation in activities and the level of intervention in problem solving. The teacher dimension included three items, consisting of classroom environment construction (10 points), teaching strategies (20

TABLE 1: The examination scores between the two groups of interns [$\bar{x} \pm s$, points].

Group	N	Multiple choice questions in case summary	Multiple choice questions of case group type	Case analysis questions	Total score of theory	Examination results of practical operation
R group	63	19.08 \pm 1.21	18.19 \pm 1.52	53.78 \pm 2.73	53.76 \pm 2.73	91.85 \pm 1.84
C group	63	16.21 \pm 1.65	17.24 \pm 2.08	49.21 \pm 3.55	49.25 \pm 3.48	82.61 \pm 2.11
t value		11.113	2.927	8.100	8.093	26.197
P value		<0.05	<0.05	<0.05	<0.05	<0.05

points), and technology application (10 points). The Cronbach's α coefficient of the scale was 0.89.

3.2.7. Teaching Satisfaction. Self-developed teaching satisfaction questionnaire had a total of 100 points. More than 90 points were regarded as very satisfied, less than 60 points were regarded as dissatisfied, and others were regarded as satisfactory. Satisfaction = (very satisfied + satisfied)/100%.

3.2.4. Statistical Analysis. The research data were entered by two people. The χ^2 test, t -test, and rank-sum test were carried out by SPSS25.0 statistical software. $P < 0.05$ indicated that the difference between the groups is statistically significant.

3. Results

3.1. The Examination Results between the Two Groups of Interns. First of all, we compared the test scores of the interns. The research group case summary multiple-choice questions, case group multiple-choice questions, case analysis questions, theoretical total scores, and practical operation assessment scores were significantly higher than those of the control group ($P < 0.05$, Table 1).

3.2. The Critical Thinking between the Two Groups of Interns. We compared the critical thinking of the two groups of interns. The total score of dimensions of the critical thinking ability of the interns in the study group were significantly higher than those in the control group ($P < 0.05$, Figure 1).

3.3. The Interns' DREEM Scale Scores between the Two Groups. We compared the scores of the two groups of interns on the DREEM scale. The total score of the DREEM scale were significantly higher than those in the control group, and the difference was statistically significant ($P < 0.05$). All results are shown in Table 2.

3.4. The Clinical Thinking Ability between the Two Groups of Interns. We compared the clinical thinking ability of the two groups of interns. Before teaching, there was no significant difference in the scores of systematic thinking ability and evidence-based thinking ability between the two groups ($P > 0.05$). After teaching, the scores of systematic thinking ability and evidence-based thinking ability of interns in the

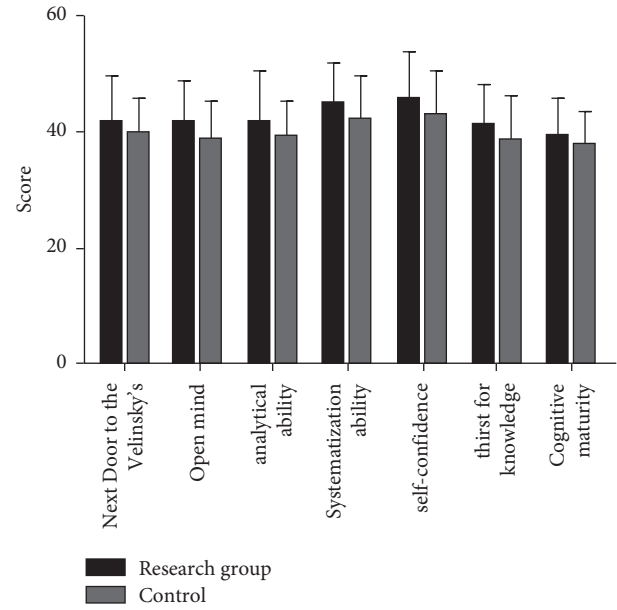


FIGURE 1: The critical thinking between the two groups of interns.

two groups increased significantly. Additionally, the improvement in the study group was more significant than that in the control group, and the difference was statistically significant ($P < 0.05$, Table 3).

3.5. The Scores of Learning Autonomy between the Two Groups of Interns. We compared the scores of learning autonomy between the two groups. Before teaching, there was no significant difference in all aspects of learning autonomy between the two groups ($P > 0.05$). After teaching, the scores of learning interest, self-management, plan implementation, and mutual cooperation of the two groups of interns were significantly higher than those before, and the difference was statistically significant ($P < 0.05$). Among them, the improvement of interns' abilities in all aspects in the study group was significantly better than that in the control group, and the difference was statistically significant ($P < 0.05$). The specific results are shown in Table 4.

3.6. The Classroom Teaching Effectiveness between the Two Groups. We compared the effectiveness of classroom teaching between the two groups. The research group scored

TABLE 2: The interns' DREEM scale scores between the two groups [$\bar{x} \pm s$].

Grouping	N	Students' perception of learning	Students' perception of teachers	Students' academic self-perception	Students' perception of the environment	Students' social self-perception	DREEM total score of the scale
Research group	63	33.22 \pm 2.83	29.08 \pm 2.41	23.07 \pm 1.66	32.68 \pm 3.62	19.89 \pm 1.73	139.62 \pm 6.44
Control group	63	31.58 \pm 2.51	23.36 \pm 2.01	16.37 \pm 1.94	29.24 \pm 3.01	15.44 \pm 1.56	108.52 \pm 5.92
t value		3.441	14.467	20.828	5.800	15.162	28.219
P value		<0.05	<0.05	<0.05	<0.05	<0.05	<0.05

TABLE 3: The clinical thinking ability of the two groups of interns ($\bar{x} \pm s$, points).

Grouping	N	Systematic thinking ability		Evidence-based thinking ability	
		Before teaching	After teaching	Before teaching	After teaching
Research group	63	30.36 \pm 2.83	40.15 \pm 1.48 ^b	18.56 \pm 3.87	26.38 \pm 0.79 ^b
Control group	63	29.83 \pm 2.52	33.52 \pm 1.84 ^a	18.47 \pm 3.31	20.49 \pm 0.98 ^a
t value		1.110	22.286	0.140	37.140
P value		>0.05	<0.05	>0.05	<0.05

Note. The comparison before and after teaching in the control group, a $P < 0.05$; The comparison of the research group before and after teaching, b $P < 0.05$.

TABLE 4: The learning autonomy scores between the two groups of interns before and after teaching ($\bar{x} \pm s$, points).

Grouping	N	Interest in learning		Self-management		Cooperate with each other		Plan implementation	
		Before teaching	After teaching	Before teaching	After teaching	Before teaching	After teaching	Before teaching	After teaching
Research group	63	18.33 \pm 4.13	24.78 \pm 3.37 ^b	28.87 \pm 4.36	35.84 \pm 3.21 ^b	13.19 \pm 2.14	17.38 \pm 3.63 ^b	18.26 \pm 2.51	23.81 \pm 4.26 ^b
Control group	63	19.12 \pm 4.32	20.24 \pm 3.76 ^a	28.21 \pm 4.51	31.27 \pm 3.22 ^a	13.26 \pm 3.72	15.27 \pm 3.81 ^a	18.73 \pm 2.84	20.26 \pm 5.45 ^a
t value		1.049	7.137	0.835	7.978	0.129	3.182	0.984	4.073
P value		>0.05	<0.05	>0.05	<0.05	>0.05	<0.05	>0.05	<0.05

Note. The comparison before and after teaching in the control group, a $P < 0.05$; the comparison of the research group before and after teaching, b $P < 0.05$.

significantly higher than the control group in the six items of learning objectives, learning process, learning effect, classroom environment creation, teaching strategies, and technology application ($P < 0.05$, Table 5).

3.7. The Teaching Satisfaction between Two Groups of Interns. We compared the teaching satisfaction of the two groups of interns. The study group was very satisfied in 34 cases, satisfied in 28 cases, and dissatisfied in 1 case, which the satisfaction rate was 98.41%. In the control group, 28 cases were very satisfied, 35 cases were satisfied, and 10 cases were dissatisfied. The excellent and good rate was 84.12%. The satisfaction rate of the study group was higher than that of the control group, and the difference was statistically significant ($P < 0.05$, Figure 2).

4. Discussion

As an important part of medical students' post-graduation education, resident clinical teaching is internationally recognized as a more scientific training method. The clinical teaching of residents is an important mean to train high-quality medical talents, which helps to improve the ability of

clinicians in an all-round way. It is also a strategic measure to promote the steady improvement of a medical level in our country. Radiology department is one of the important departments of the hospital, which integrates examination, diagnosis, and treatment. Many types of diseases need to be diagnosed by radiology examination. Therefore, it is very important to train high-quality radiology staff. This study attempted to apply the primary teaching principle to the case-oriented practice course, and to explore the application effect of case teaching based on the primary teaching principle in the clinical practice course of radiology. The students' knowledge recall is improved and their ability to make comprehensive assessments and decisions is significantly improved. Firstly, during the activation of the old knowledge stage, the group creates a mind map before class. Students pay attention to uncovering the relevance of the systematic knowledge related to the case and form a structured knowledge. The simplified text and images can organize a large amount of relevant case information [26]. Therefore, students will deepen their memory and improve their mastery of knowledge on the basis of understanding knowledge. Secondly, in the stage of activating old knowledge and demonstrating new knowledge in class, the teachers explain the clinical knowledge not mentioned or

TABLE 5: The classroom teaching effectiveness between the two groups ($\bar{x} \pm s$, points).

Grouping	N	Intern evaluation			Teacher evaluation		
		Learning goal	Learning process	Learning effect	Classroom environment construction	Teaching strategy	Application of technology
Research group	63	9.56 ± 0.23	28.11 ± 0.34	19.02 ± 0.56	9.38 ± 0.22	18.56 ± 0.72	9.12 ± 0.46
Control group	63	8.01 ± 0.14	20.07 ± 2.31	14.05 ± 1.21	7.26 ± 1.19	12.05 ± 2.33	7.05 ± 1.23
t value		46.691	27.331	29.587	13.905	21.188	12.511
P value		<0.05	<0.05	<0.05	<0.05	<0.05	<0.05

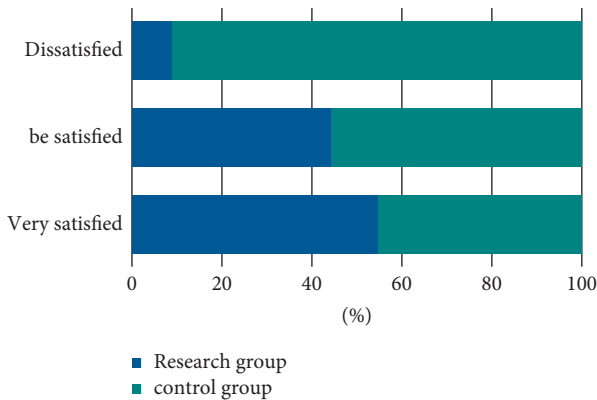


FIGURE 2: The comparison of teaching satisfaction between the two groups of interns.

less involved in textbooks. According to the case learning content reported by students, the new and old knowledge can be connected together to help students to further sort out and sum up case-related knowledge. In the stage of applying new knowledge, the students are able to apply new knowledge to practice for the first time and have a certain understanding of practical nursing procedures [27]. In the stage of integration, the students should learn similar cases based on the e-learning teaching platform. The construction of the students' knowledge system was made more systematic and structured through several practice sessions. The students' scores on case analysis questions requiring integrated understanding and decision-making have increased significantly. Finally, the interns in the research group realized more self-study and discussion of network resources based on the e-learning platform. The learning environment was easy, the degree of investment in learning was relatively high and the learning efficiency was high.

The intern DREEM scale was used to evaluate the students' comprehensive feelings of the medical education environment to find the weak links in the students' learning process. At the same time, it was possible to find the relevant contents of the hospital medical education environment that needed to be improved and provide strong evidence for improving the hospital clinical medical education environment. The scores of all dimensions of critical thinking ability of interns suggested that the primary teaching principle is helpful to the cultivation of critical thinking ability. The interns' perception of teachers, students' academic self-perception, students' perception of environment, students' social self-perception, and the total score of the DREEM scale were

significantly increased. This means that the teaching environment of our college is better and the implementation of mind mapping teaching in the practice of medical imaging can improve students' clinical thinking ability in an all-round way. Critical thinking is a judgment process of logical reasoning, analysis, and evaluation of specific problems in some specific situations by scientific methods [28, 29]. Critical thinking is an abstract thinking skill, which emphasizes that students should practice and use it repeatedly in the process of solving problems [30]. Teacher-oriented case teaching is a one-way knowledge transfer. Case discussions are short and students are prone to confusion of knowledge and learning fatigue. However, case studies based on primary teaching principles can give students more opportunities to exercise their thinking. In the part of focusing on problems, students analyze and study various resources independently around learning task sheets. In addition, the group discussion draws mind maps to present the thinking process of case analysis to effectively exercise their ability to promote the construction of logical thinking and effectively improve the ability to find the truth and analyze. In the link of demonstrating new knowledge, the teachers give encouragement to the content of students' case reports, so that students can observe and associate in analogy. The internal relationship is found what they have learned to enhance students' self-confidence in autonomous learning achievements and improve their open-mindedness. In the application of new knowledge and integration, the students understand and integrate the learning content from various perspectives through variant case drills, which is conducive to the cultivation of systematic thinking.

In addition, this study has indicated that the primary teaching principle can effectively improve the effectiveness of classroom teaching. The increased effectiveness of teaching may be due to the teacher's ability to stay close to the students' knowledge base when developing completed tasks. The sequence of questions is reasonably broken down to form a list of learning tasks and students' learning objectives are more clearly defined. Group cooperative learning before class is more willing to express their own views and stimulate learning motivation. The teachers explain new knowledge in class, combining with pictures, animation, and texts to give timely and comprehensive guidance to students. A relaxed, warm, and positive learning environment can be created to improve the satisfaction of classroom teaching. There are some limitations in this study. First, the sample size of this study is not large and it is a single-center study, so bias is inevitable. In future research, we will carry out multi-center, large-sample prospective studies, or more valuable conclusions can be drawn.

In conclusion, the application of the case teaching method based on primary teaching principle in the radiology clinical teaching course is helpful to cultivate students' critical thinking ability and improve students' performance and classroom teaching effectiveness.

Data Availability

The datasets used and analyzed during the current study are available from the corresponding author upon reasonable request.

Conflicts of Interest

The authors declare that they have no conflicts of interest.

References

- [1] Li ran, K. Yi, and K. Xiong, "Goal and significance of standardized training for radiology residents," *Journal of Qiqihar Medical College*, vol. 40, no. 4, pp. 494–496, 2019.
- [2] A. Prater, B. S. Rostad, E. L. Ebert, M. E. Mullins, and C. P. Ho, "Towards consensus: training in procedural skills for diagnostic radiology residents—current opinions of residents and faculty at a large academic center," *Current Problems in Diagnostic Radiology*, vol. 47, no. 6, pp. 387–392, 2018.
- [3] D. Castro, J. Yang, M. L. Greer et al., "Competency based medical education—towards the development of a standardized pediatric radiology testing module," *Academic Radiology*, vol. 27, no. 11, pp. 1622–1632, 2020.
- [4] M. Farashahi and M. Tajeddin, "Effectiveness of teaching methods in business education: a comparison study on the learning outcomes of lectures, case studies and simulations," *International Journal of Management in Education*, vol. 16, no. 1, pp. 131–142, 2018.
- [5] T. C. Guetterman and M. D. Fetters, "Two methodological approaches to the integration of mixed methods and case study designs: a systematic review," *American Behavioral Scientist*, vol. 62, no. 7, pp. 900–918, 2018.
- [6] Y. F. Zhang, L. Zhou, H. Q. Mao, F. H. Yang, Z. Chen, and L. Zhang, "Mitochondrial DNA leakage exacerbates odontoblast inflammation through gasdermin D-mediated pyroptosis," *Cell death discovery*, vol. 7, no. 1, pp. 381–384, 2021.
- [7] W. Zhao, L. He, W. Deng, J. Zhu, A. Su, and Y. Zhang, "The effectiveness of the combined problem-based learning (PBL) and case-based learning (CBL) teaching method in the clinical practical teaching of thyroid disease," *BMC Medical Education*, vol. 20, no. 1, 381, 2020.
- [8] Li Yang, Q. Ran, and L. Lin, "Mixed teaching design and application of basic nursing based on primary teaching principle," *Nursing practice and research*, vol. 19, no. 4, pp. 612–615, 2022.
- [9] M. Bi, Z. Zhao, J. Yang, and Y. Wang, "Comparison of case-based learning and traditional method in teaching post-graduate students of medical oncology," *Medical Teacher*, vol. 41, no. 10, pp. 1124–1128, 2019.
- [10] L. Sun, J. Wang, and R. Jin, "Study on the application of primary teaching principles in the practical course of internal medicine nursing," *Nursing Research*, vol. 34, no. 12, pp. 2189–2193, 2020.
- [11] Y. Su and F. Wang, "Study on the application of primary teaching principle in nursing teaching," *Scientific and technological information*, vol. 17, no. 12, pp. 119–120, 2019.
- [12] S. Safitri, F. Francisca, K. A. Handali, and T. D. Ariyanti, "Applying school effectiveness principle as school system: a case analysis in leading primary school in Indonesia," in *Proceedings of the Asia-Pacific Research in Social Sciences and Humanities*, pp. 696–705, Atlantis Press, Universitas Indonesia, May 2021.
- [13] D. Carrillo-Gallego, A. Maurandi-López, and P. Olivares-Carrillo, "From Pestalozzi's intuition principle to classrooms: the counting frame and innovations in the teaching of mathematics (Spain, nineteenth century)," *Paedagogica Historica*, vol. 2021, pp. 1–21, 2021.
- [14] Y. Sui and H. hope, "Exploration of flipped classroom teaching design based on the primary teaching principle," *Journal of Shanxi Normal University (Philosophy and Social Sciences edition)*, vol. 63, no. 2, pp. 93–99, 2018.
- [15] M. Y. G. Qi, "Application of mind mapping method based on case analysis in emergency nursing teaching of undergraduate nursing students," *Nursing management in China*, vol. 18, no. 12, pp. 1672–1677, 2018.
- [16] J. Ge, *Research on the Teaching Design of Primary School Mathematics circle Based on the Primary Teaching Principle*, Yangzhou University, Yangzhou, 2017.
- [17] Y. Zhao, *Research on Instructional Design of Information Technology in Senior High School Based on the Primary Teaching Principle*, Hunan normal University, Changsha, 2017.
- [18] M. Kaye, "Teaching complex content in OT education: using the multimedia principle of pretraining to foster meaningful learning," *American Journal of Occupational Therapy*, vol. 73, no. 4, Supplement_1, Article ID 7311520411, 2019.
- [19] E. B. Cahyanto, A. Nugraheni, I. S. Sukanto, M. Musfiroh, and N. B. Argaheni, "The effect of exercise mat Pilates on pain scale, anxiety, heart rate frequency in adolescent principle with primary dysmenorrhea in Surakarta," *Jurnal Ners dan Kebidanan Indonesia*, vol. 9, no. 1, pp. 29–38, 2021.
- [20] J. Zou, *Research on the Teaching Design and Application of Information Technology in Senior High School Based on the Primary Teaching Principle*, Nanjing normal University, Nanjing, 2016.
- [21] M. Peng, G. Wang, and J. Chen, "Study on the reliability and validity of critical thinking ability scale," *Chinese Journal of Nursing*, vol. 39, no. 9, pp. 7–10, 2004.
- [22] L. Zou, Wenli, and S. Zhang, "The application of organ system-based course teaching combined with case-based teaching in medical imaging teaching is discussed," *Chinese Journal of Lung Diseases (Electronic Edition)*, vol. 9, no. 06, pp. 697–699, 2016.
- [23] D. Roberts, "The clinical viva: an assessment of clinical thinking," *Nurse Education Today*, vol. 33, no. 4, pp. 402–406, 2013.
- [24] C. Yurdakul, "An investigation of the relationship between autonomous learning and lifelong learning," *International Journal of Educational research review*, vol. 2, no. 1, pp. 15–20, 2017.
- [25] W. Sun, *Research on Classroom Teaching Design of New Curriculum-- Exploration of "five Stars" Teaching Design*, p. 1, Zhejiang University Press, Hangzhou, 2005.
- [26] Y. Liu, L. Shen, and Y. Zhang, "The course design of traditional Chinese Medicine Pharmacy based on the primary teaching principle promotes the training of talents of

- traditional Chinese medicine,” *Journal of traditional Chinese Medicine Management*, vol. 27, no. 13, pp. 27–29, 2019.
- [27] S. P. P. Chin, E. Tsui, and C. S. Lee, “Enhancing learning effectiveness by adopting a knowledge-based usability guidelines,” *VINE Journal of Information and Knowledge Management Systems*, vol. 46, no. 1, pp. 123–152, 2016.
 - [28] C. K. Lo and K. F. Hew, “Using “first principles of instruction” to design SecondarySchool mathematics flipped classroom: the findings of two explor atoryStudies,” *Journal of Educational Technology & Society*, vol. 20, no. 1, pp. 222–236, 2017.
 - [29] X. Chen, Z. Yang, and X. Lan, “Micro-course teaching design under the guidance of primary teaching principles,” *Pharmaceutical education*, vol. 34, no. 1, pp. 41–44, 2018.
 - [30] L. Zhou and B. Lv, “Exploration on the teaching design of micro-course of physics experiment in senior high school under the primary teaching principle-- taking the parallel quadrilateral rule of force as an example,” *Physics in Hunan Middle School*, vol. 36, no. 6, pp. 25–27, 2021.

Research Article

A Transformer-Based Network for Change Detection in Remote Sensing Using Multiscale Difference-Enhancement

Gulinazi Ailimujiang,¹ Yiliyaer Jiaermuhamaiti ,¹ Huxidan Jumahong,¹ Huiling Wang,¹ Shuangling Zhu,² and Pazilaiti Nurmamaiti²

¹College of Network Security and Information Technology, YiLi Normal University, Yining 835000, China

²College of Electronics and Engineering, YiLi Normal University, Yining 835000, China

Correspondence should be addressed to Yiliyaer Jiaermuhamaiti; dg1533042@smail.nju.edu.cn

Received 7 May 2022; Revised 28 June 2022; Accepted 17 July 2022; Published 13 August 2022

Academic Editor: Dong Chen

Copyright © 2022 Gulinazi Ailimujiang et al. This is an open access article distributed under the Creative Commons Attribution License, which permits unrestricted use, distribution, and reproduction in any medium, provided the original work is properly cited.

Recently, transformer-based change detection methods have achieved remarkable performance by sophisticated architectures for extracting powerful feature representations. However, due to the existence of various noises in bitemporal images, there are problems such as loss of semantic objects and incompleteness that will occur in change detection. The existing transformer-based approaches do not fully address this issue. In this paper, we propose a transformer-based multiscale difference-enhancement U-shaped network and call it TUNetCD, for change detection in remote sensing. The encoder, which is composed of a multilayer Swin-Transformer block structure, can extract multilevel feature maps, further enhance these multilevel feature maps using a Swin-Transformer feature difference map processing module, and finally obtain the final change map using a lightweight decoder. We conducted comprehensive experiments on two publicly available benchmark datasets, LEVIR-CD and DSIFN-CD, to verify the effectiveness of the method, and our method outperformed other advanced transformer-based methods.

1. Introduction

The goal of remote sensing image change detection (CD) is to generate a binary change map (BCM) by comparing and analyzing two images taken at different times of day for the same area. Each pixel in the binary change map image consists of a 0 or a 1, corresponding to a change or no change in that pixel's position. The definition of change detection varies depending on the task. It is used for tasks such as urban area change detection [1, 2], environmental detection [3, 4], land use detection [5, 6], and disaster assessment [7]. Change detection methods that have been continuously updated in recent years are widely used in a variety of fields and are attracting the attention of more scholars.

Convolutional neural networks (CNNs) have gained wider applications in several fields of computer vision in recent years, such as image classification [5, 6], target detection [7], semantic segmentation [8], and face recognition [9]. CNN-based CD algorithms have also made significant

strides [8, 10–19]. Zhan et al. used a Siamese convolutional network in the CD task to extract two feature maps of diachronic images by two parallel weight-sharing convolutional branches and then compared the feature thresholds. Following that, many CD methods adopted this architecture [10]. Rahman F et al. proposed the Siamese network approach, which eliminates the threshold comparison with a decision network [11]. Following the success of fully convolutional networks (FCN) [8] and U-net [12] in image segmentation, its various variants now provide an effective method for change detection. Daudt et al. were the first to use FCN for CD tasks, proposing three FCN frameworks: FC-EF, FC-Siam-Conc, and FC-Siam-Diff [13]. However, because CNNs are more focused on local information, the extraction of global features is weak. Scholars have proposed a series of approaches to this problem. To extract multiscale features, Chen et al. proposed using ResNet as the encoder backbone and adding a pyramid self-attention structure [14].

Chen et al. then utilized the dual attention module to obtain long-range results [15]. Peng et al. proposed UNet++, which learns multiscale feature maps using dense skip connections and controls gradient convergence with residual blocks [16]. FCN was used by Zhang et al. to extract deep features, which were then fed into the proposed deep-supervised image fusion network (DSIFN) [17]. To improve encoder and decoder performance, Fang et al. proposed a densely connected U-type Siamese network [18].

The transformer proposed by Vaswani et al. was first used with great success on the neural machine translation (NMT) task of natural language processing (NLP) [19]. It was then widely used in various NLP fields. Dosovitskiy et al. proposed the vision transformer (ViT) as the first pure transformer algorithm, which was first used for computer vision (CV) tasks and proved to be effective in image classification tasks [20]. Meanwhile, due to transformer's superior semantic representation capability over CNN, many scholars applied the ViT method to various CV tasks and achieved comparable or better results than CNN. The Swin-Transformer shifted windowing scheme proposed by Liu et al. divides the window into multiple local windows and computes the self-attention hierarchy transformer within the local window [21]. This method effectively reduces the computational complexity of self-attention while also increasing accuracy. Xie et al. proposed combining the ViT encoder with a lightweight multilayer perceptron (MLP) decoder to form SegFormer, an efficient semantic segmentation framework that obtains multiscale features while avoiding complex decoders [22]. Bandara and Patel proposed unifying a hierarchically structured ViT encoder and an MLP decoder of the Siamese network framework to obtain multiscale long-range features [23]. The success of ViT and Swin-Transformer on various CV tasks, including CD, has aided in the development of further CD capabilities.

We designed a new network named transformer-based multiscale difference-enhancement U-shaped networks after being inspired by the previous work (TUNetCD).

Firstly, coregistered image pairs are concatenated as an input for the improved TUNetCD network, which can generate information using both global and fine-grained information. Second, numerous studies have demonstrated that shallow layers on the encoder side output fine-grained features, whereas deep layers output coarse-grained features. TUNetCD is being used to learn multiscale and semantic levels of visual feature representations to fine-tune the spatial details. To solve the CD task, we adopted a pure Swin-Transformer network with a U-shaped structure. Because TUNetCD's basic unit is a Swin-Transformer block, it can obtain both local fine-grained features.

The following are the main contributions of this paper:

- (1) To build the encoder and feature difference map processing module, we proposed TUNetCD, a

hierarchical U-shaped image change detection framework with LeWinTransformer as the main module.

- (2) To capture the local and global correlations of hierarchical multilevel features, we proposed a feature difference map processing module based on the LeWinTransformer block.
- (3) The superior experimental results on change detection datasets demonstrate the effectiveness and robustness of the proposed TUNetCD.

2. Related Work

In this section, the CNN framework for CD, the transformer mechanism, and the FCN method based on consistency regularization will be briefly illustrated.

2.1. CNN-Based CD Methods. In recent years, deep learning (DL) algorithms have attracted much attention. Deep learning models can learn multiple levels of representation and abstraction to help understand images and extract semantic information from them. In the field of remote sensing images processing, deep learning has also shown excellent performance [24] and is widely used in problems such as the remote sensing image change detection problem [25].

Most of the DL networks for CD tasks are based on convolutional neural networks. CNN-based CD methods usually enhance the semantic representation ability of network by changing the network structure, optimizing loss function, adding attention mechanism, and so on.

In terms of network structure, Zhan et al. [10] used a Siamese convolutional network in the CD task to extract two feature maps of diachronic images by two parallel weight-sharing convolutional branches and then compared the feature thresholds. Following that, many CD methods adopted this architecture. Daudt et al. [13] designed the first end-to-end training CD method and proposed three effective FCNN-based architectures. In [13], FC-EF concatenates the bitemporal images as the input of the network, while FC-Siam-conc and FC-Siam-diff leverage a Siamese structure, which can directly process bitemporal images. The most intuitive way to reduce the inherent locality of convolution operation is to increase the reception field. To extract multiscale features, Chen and Shi [14] proposed spatial-temporal attention neural network (STANet), using residual nets (ResNet) as the encoder backbone and adding a pyramid self-attention structure. Chen et al. [15] proposed dual attentive fully convolutional Siamese networks (DASNet) and then utilized the dual attention module to obtain long-range results. Compared with the shallow networks, STANet and DASNet have stronger feature extraction capability. Huang et al. [6] proposed dense connections (DenseNets) are built from dense blocks and pooling operations, where each dense block is an iterative

concatenation of previous feature maps. Among them, the UNet based on fully convolutional networks is the most popular and has become one of the standard CNN architectures for CD tasks with many extensions [24]. By adding a skip connection between encoder and decoder, UNet can better integrate deep semantic information and shallow spatial information, improving the accuracy of CD. Fang et al. [18] proposed the combination of Siamese network and UNet++ (SNUNet-CD) added dense connections between the features of different layers, so as to enhance the capability of the CD network.

In the remote sensing images, the changed pixels are far less than the unchanged pixels, so there exists a serious data imbalance in the CD task. Many scholars solved this problem by optimizing the loss function so that the changed and unchanged pixels participate in the loss calculation in the same proportion. Zhan et al. [10] proposed a weighted contrastive loss function, which increased the weight of the changed pixels in the loss calculation. STANet [14] and DASNet [15] further optimized the weighted contrastive loss function, and they proposed batch-balanced contrastive loss function and weighted double-margin contrastive loss function. In SNUNet proposed by Fang et al. [18], a hybrid loss function was used to optimize the network.

Since attention mechanism has achieved remarkable results in the CV task, many scholars have introduced attention mechanism into CD task. Chen et al. [15] introduced a dual attention module into the CD task to learn features that contain both channel information and spatial information. Fang et al. [18] proposed an ensemble channel attention module (CAM) to fuse the features of various levels, so as to generate stronger change features. In order to detect changes with different sizes, Chen and Shi [14] proposed a pyramid spatial-temporal attention module, which can extract features from different scales. Peng et al. [26] designed a dense attention method to extract richer and more effective features. Chen et al. [27] introduced the transformer into the field of CD for the first time and proposed bitemporal image transformer (BiT). First of all, BiT uses CNN to generate semantic features. Second, BiT leverages a transformer module to further process CNN features. Finally, BiT uses a prediction head module to generate the change maps.

Although the above methods have improved the ability of CD network to a certain extent, due to the inherent locality of convolution operation, the CNN-based methods cannot effectively extract long-term global features, thus limiting the ability of CD network. Unlike the previous methods, this article attempts to explore the potential of pure transformer network for the CD task.

2.2. Transformer-Based CD Methods. Dosovitskiy et al. [20] proposed the ViT as the first pure transformer algorithm. In image classification, ViT achieves comparable results with CNN-based algorithms. However, one drawback of ViT is that we need to pretrain ViT on a larger dataset, which makes the training of ViT inconvenient. The computational complexity of ViT is quadratic to the size of the input image,

so ViT is not suitable for the dense vision tasks. Liu et al. [21] proposed that Swin-Transformer used shifted windowing scheme to calculate self-attention in a local window, which not only reduced the computational complexity but also acquired the best results in several CV tasks. Motivated by ViT, BiT [27] firstly proposed a bitemporal image transformer network for effectively modeling spatial-temporal contexts, which innovatively proved the enhancing ability by combining a CNN and a transformer. A transformer-based Siamese network architecture (abbreviated by ChangeFormer) [23] is a hierarchical transformer in a Siamese network with a lightweight decoder, and it shows that good results can still be obtained without relying on the convolution operation. However, these mentioned transformer-based CD frameworks are merely capable of capturing global interdependencies of single-scale objects within each transformer layer, which tend to lose robustness in rich spatial scenes of remote sensing images. The local context information is essential for image change detection tasks since the neighborhood of a change pixel can be leveraged to restore its information, but previous works suggest that transformer shows a limitation in capturing local dependencies.

Inspired by the success of LeWin transformer in dense vision tasks, we introduce the LeWin transformer into the CD task and propose TUNetCD that is a pure LeWin transformer network with a multiscale difference-enhancement U-shaped structure. In our proposed method, we not only retain the original feature maps but also adopt the feature difference maps to model multiscale and multidepth change information, which will enhance the change intensity.

3. Methods

3.1. Framework Overview. As shown in Figure 1, the proposed NET consists of three major components: a hierarchical transformer encoder in a U-shape network to extract multiscale features, a feature difference map processing module, and a decoder. The LeWinTransformer block serves as the foundation for the first two components. Through the overlapped image patches, the encoder extracts hierarchical features. T , the feature difference map processing module, is used to improve the information of the changed areas. To predict the change map, the decoder aggregates the multi-level feature difference maps.

$\{X_1, X_2\} \in R^{H \times W \times 3}$ are the input bitemporal feature maps, where H , W , and C are height, width, and channel dimension of the feature map X_1, X_2 . We'll get the input feature map $X \in R^{H \times W \times 6}$ feature map after concatenating X_1 and X_2 . After entering it into the encoder X , we will first enter to the Overlap Patch Embedding module to convert X into image tokens and then use hierarchical LeWinTransformer to generate multilevel features $F_{enc}^i \in R^{(H/2^{i+1}) \times (W/2^{i+1}) \times C^i}$, where $i = \{1, 2, 3, 4\}$ and $C^{i+1} > C^i$, which will be further processed through the feature difference map processing module to generate multilevel features $F_{diff}^i \in R^{(H/4) \times (W/4) \times C_{emb}}$. The features are then passed to the decoder, which predicts the binary change map $F_{cm} \in R^{H \times W \times 2}$.

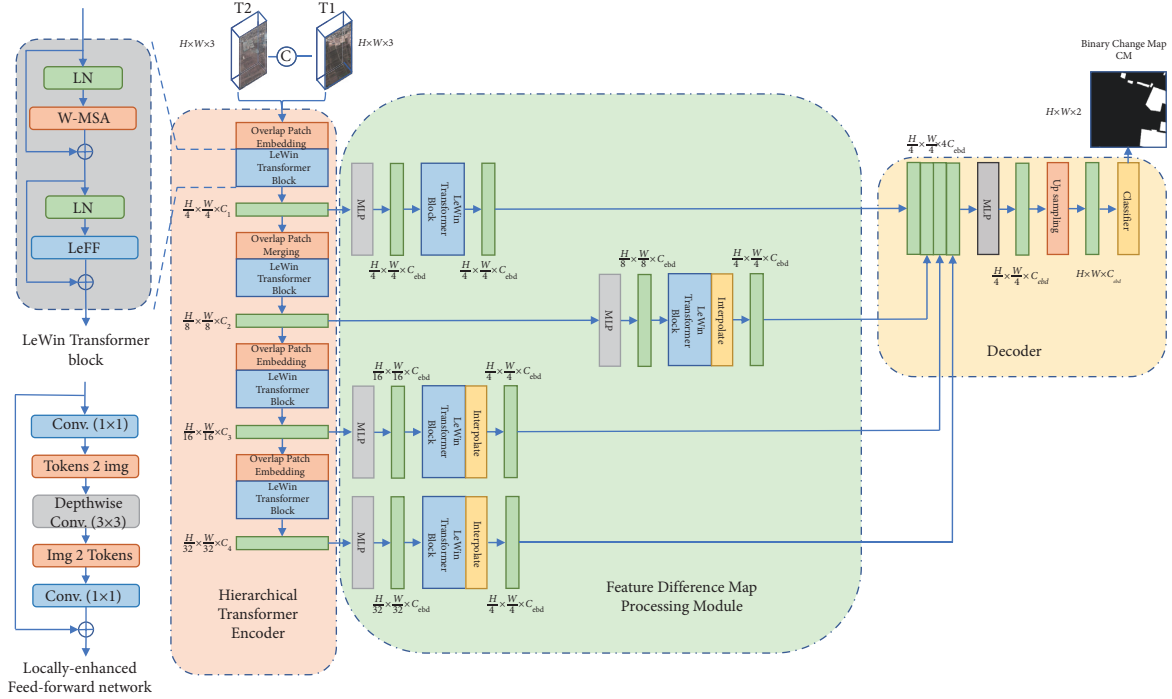


FIGURE 1: Overview of the TUNetCD.

3.2. Hierarchical Transformer Encoder

3.2.1. Overlapped Patch Merging. We used overlapping patch merging to tokenize the feature map and implemented downsampling to reduce computational consumption. In the Overlapped Patch Merging module, if given a hierarchical feature map $F^i \in R^{(H/2^{i+1}) \times (W/2^{i+1}) \times C^i}$ (i denotes the i_{th} stage), it unifies patch into feature map size as $F^{i+1} \in R^{(H/2^{i+1}) \times (W/2^{i+1}) \times C^{i+1}}$ and then iterates for any other features map in the hierarchy. As a result, we defined K as the patch size, S is the stride between two adjacent patches, and P is the padding size. We utilized a conv2D layer with $K = 7$, $S = 4$, and $P = 3$ for the initial merging, and $K = 3$, $S = 2$, and $P = 1$ for the rest.

3.2.2. LeWinTransformer Block. ViT is confronted with two major challenges: (1) when calculating global attention, self-attention must pay attention to all tokens, and the calculation cost increases quadratically with the number of tokens; (2) local context information is critical for all types of CV tasks, and the neighborhood of a change pixel must have significant differences. ViT has a limitation when it comes to capturing local dependencies.

Swin-Transformer is a module that replaces standard multihead self-attention based on (shifted) window multihead self-attention ((S) W-MSA). Other layers remained unchanged. We use the LeWinTransformer module, which is based on (S) W-MSA.

The locally enhanced window (LeWin) transformer block, as shown in the upper left of Figure 1, can obtain long-range dependencies by using the self-attention

mechanism in transformer or by adding the LeFF (locally enhanced feedforward network) module of the conversion operator to obtain local context information. Specifically, $(l-1)th$ assumes that, in the output feature F^{l-1} of the LeWinTransformer block, our LeWinTransformer block consists of two main parts: (1) nonoverlapping window multihead self-attention (W-MSA) and (2) locally enhanced feedforward network (LeFF). The calculation formulas of the block are as follows:

$$\begin{aligned} \hat{F}^l &= W - MSA(LN(F^{l-1})) + F^{l-1}, \\ F^l &= LeFF(LN(\hat{F}^l)) + \hat{F}^l, \end{aligned} \quad (1)$$

where \hat{F}^l and F^l are the outputs of the W-MSA module and LeFF module, respectively. LN represents the layer normalization.

The feature maps are partitioned into nonoverlapping windows, and each patch is calculated within each window.

(1) Window Multihead Self-Attention (W-MSA) Module. The W-MSA module divides the feature map into several nonoverlapping windows, and each window size is $N \times N$. The feature patches then calculated self-attention within each window. As shown in Figure 2, given the input feature map $F_{in} \in R^{H \times W \times C}$, where H , W , and C are height, width, and channel dimension of the feature map, F_{in} are partitioned into $N \times N$ nonoverlapping windows. Therefore, we define $F_{in}^i \in R^{N \times N \times C}$ as the feature of the i_{th} window, where $i \in \{1, 2, \dots, Z\}$ and $Z = (H \cdot W / N^2)$. F_{in}^i are flattened and transposed into $F^i \in R^{N^2 \times C}$. Subsequently, we perform self-attention on F^i in each window. Firstly, F^i is linearly

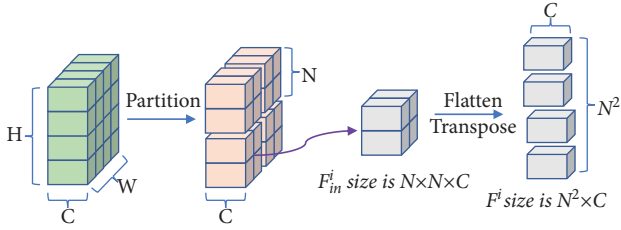


FIGURE 2: Feature map partition.

projected into query $Q^i \in \mathbb{R}^{N^2 \times C}$, key $K^i \in \mathbb{R}^{N^2 \times C}$, and value $V^i \in \mathbb{R}^{N^2 \times C}$ matrices.

$$\begin{aligned} Q^i &= F^i \cdot W^Q \\ K^i &= F^i \cdot W^K, \\ V^i &= F^i \cdot W^V, \end{aligned} \quad (2)$$

where W^Q , W^K , and W^V are learnable parameters and have the same dimensions of $\mathbb{R}^{C \times C}$, representing the weights of three linear projection layers, respectively. Second, we split Q^i , K^i , and V^i into h heads along the channel dimension, respectively. Then, they can be expressed as $Q^i = [Q_1^i, Q_2^i, \dots, Q_h^i]$, $K^i = [K_1^i, K_2^i, \dots, K_h^i]$, and $V^i = [V_1^i, V_2^i, \dots, V_h^i]$; the head dimension is $d_h = (C/h)$. The computation of k_{th} head self-attention in nonoverlapping windows can then be formulated as follows:

$$\text{Self-Attention}(Q_k^i, K_k^i, V_k^i) = \text{softmax}\left(\frac{Q_k^i \cdot K_k^i}{\sqrt{d_h}}\right) V_k^i, \quad (3)$$

where Q_k^i , K_k^i , and V_k^i represent the projection matrices of the query, key, and value for the k_{th} head, respectively. Third, the output tokens $F_{\text{out}}^i \in \mathbb{R}^{N^2 \times C}$ of the i_{th} window can be obtained by

$$F_{\text{out}}^i = \text{Concat}_{k=1}^h (\text{Self-Attention}(Q_k^i, K_k^i, V_k^i)) W^{\text{out}} + P, \quad (4)$$

where $\text{Concat}(\cdot)$ denotes the concatenating operation and $P \in \mathbb{R}^{N^2 \times C}$ is the relative position bias. They are taken from $\hat{P} \in \mathbb{R}^{(2N-1) \times (2N-1)}$ with learnable parameters, and $W^{\text{out}} \in \mathbb{R}^{C \times C}$ are learnable parameters. Then, we reshape F_{out}^i to obtain the output window feature map $F_o^i \in \mathbb{R}^{N \times N \times C}$. Finally, we merge all the patch representations $\{F_o^1, F_o^2, F_o^3, \dots, F_o^Z\}$ to obtain the output feature maps $F_{\text{out}} \in \mathbb{R}^{H \times W \times C}$.

(2) *Feedforward Network (FFN)*. As illustrated in Figure 3, Swin-Transformer's feedforward network (FFN) is composed of a 1×1 conv layer with a GELU activation, a depth-wise 3×3 conv layer with a GELU activation, and another 1×1 conv layer.

(3) *Locally Enhanced Feedforward Network (LeFF)*. The standard ViT's FFN has limited ability to leverage local context. To address this issue, we employed LeFFN to improve local context information. As shown in Figure 1, we first applied a linear projection layer to each token to

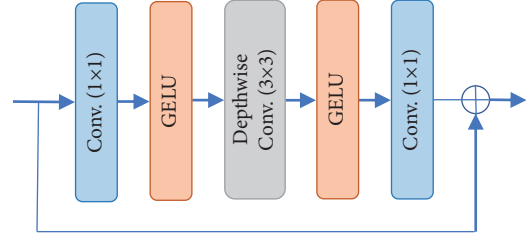


FIGURE 3: FFN.

increase the dimension of its features. The tokens were then reshaped into 2D feature maps, and local information was captured using a depth-wise convolution. The features were then flattened back to tokens, and the channels were shrunk via another linear layer to match the dimension of the input channels. After each linear/convolution layer, we used GELU as the activation function.

3.3. *Feature Difference Map Processing Module*. We obtained four multiscale feature maps from the encoder in the feature difference map processing module. The features with the smallest scale are considered high-level features because they contain rich semantic and attribute information. The sizes of the other three features gradually transition from high-level features to low-level features from small to large, and the features of which they primarily consist also change to texture and detailed information of ground objects. We can use feature difference map processing to take advantage of the interaction between high-level features and low-level features, guide the categories and attributes of low-level features with high-level features, and provide detailed information for high-level features. We used LeWinTransformer in the feature difference map processing module to strengthen and suppress information in each feature. In contrast to convolutions, the LeWinTransformer can capture long-range dependencies and attend to diverse information from a global perspective.

3.3.1. *MLP*. We first processed each multiscale feature through an MLP layer to unify the channel dimension to value C_{ebd} .

$$\hat{F}_{\text{out}}^i = \text{Linear}(C_i, C_{ebd})(F_{\text{out}}^i) \forall i, \quad (5)$$

where C_{ebd} denotes the embedding dimension.

3.3.2. *LeWinTransformer*

$$F_{l\text{-diff}}^i = \text{LeWinTransformer}(\hat{F}_{\text{out}}^i) \forall i. \quad (6)$$

3.3.3. *Upsampling*. We finally unsampled each multiscale feature to size of $(H/4) \times (W/4)$ as follows:

$$(F_{l\text{-diff}}^i) \forall i F_{\text{diff}}^i = \text{Upsample}\left(\left(\frac{H}{4}, \frac{W}{4}\right), \text{"bilinear"}\right)(F_{l\text{-diff}}^i) \forall i. \quad (7)$$

3.4. Decoder

3.4.1. Concatenation and Fusion. These feature maps with uniform channel dimension sizes are concatenated and then fused via an MLP layer as follows:

$$F_C = \text{Linear}(4C_{ebd}, C_{ebd}) \left(\text{Cat}(F_{\text{diff}}^1, F_{\text{diff}}^2, F_{\text{diff}}^3, F_{\text{diff}}^4) \right). \quad (8)$$

3.4.2. Upsampling and Classification. We upsampled the fused feature map F_c to the size of $H \times W$ by utilizing a transposed conv2d layer with stride of 4 and kernel size of 3. Finally, the upsampled feature map was processed through a MLP layer to predict the change mask $CM = \mathbb{R}^{H \times W \times 2}$. This process can be formulated as follows:

$$F = \text{ConvTranspose2D}(S = 4, K = 3)(F_C), \quad (9)$$

$$CM = \text{Linear}(C_{ebd}, 2)(F). \quad (10)$$

4. Experimental Setup

4.1. Datasets. For our experts, we used two publicly available CD datasets: LEVIR-CD [14] and DSIFN-CD [17]. The LEVIR-CD dataset is a building CD dataset with RS image pairs of resolution. We use 2048 patches as test datasets, 1024 patches as val datasets, and 7120 patches as train datasets, and we cropped nonoverlapping patches of size. The DSIFN dataset is a general CD dataset that includes changes to various landcover objects. We divided the original train dataset, val dataset, and test dataset into nonoverlapping patches of 14400, 1360, and 192 patches in the three sets of train dataset, val dataset, and test dataset, respectively.

4.2. Implementation Details. We implemented our model in Pytorch using NVIDIA 3070 GPU. We randomly initialized the network during training and applied data augmentation through random flip, random rescale (0.8–1.2), and random crop. We trained the models using the Cross-Entropy (CE) Loss and AdamW optimizer with weight decay equal to 0.01 and beat values equal to (0.9, 0.999). The learning rate is initially set to 0.0001 and linearly decays to 0 until trained for 200 epochs. We used a batch size of 2 to train the model.

4.3. Performance Metrics. To compare the performance of our model with SOTA methods, we reported F1 and Intersection over Union (IoU) scores with regard to the TUNetCD as the primary quantitative indices. Additionally, we reported precision and recall of the change category.

In order to quantitatively evaluate the performance of our proposed method, precision (P), recall (R), F1-score, and Intersection over Union (IoU) are utilized to compare the labels and our results, which are calculated as follows:

$$P = \frac{TP}{TP + FP}, \quad (11)$$

$$R = \frac{TP}{TP + FN}, \quad (12)$$

$$F1 = 2 \times \frac{P \times R}{P + R}, \quad (13)$$

$$\begin{aligned} IoU &= \frac{TP}{TP + FP + FN} \\ &= \frac{P \times R}{P + R - P \times R}, \end{aligned} \quad (14)$$

where true positive (TP) and true negative (TN) denote the number of changed and unchanged pixels detected correctly, respectively. False positive (FP) and false negative (FN) denote the number of changed and unchanged pixels detected incorrectly, respectively.

5. Results and Discussion

5.1. Comparative Experiments. In this section, we analyzed the results of our proposed TUNetCD method with the other four new methods on two CD datasets.

STANet [14] is a Siamese-based spatial-temporal attention network for CD.

SNUNet [17] is a multilevel feature concatenation method, in which a densely connected (NestedUNet) Siamese network is used for change detection.

The transformer-based method (BIT) [27] is used for the first time in the CD task, which obtains feature maps in a Siamese network with a ConvNet structure and then passes through a transformer encoder-decoder network to enhance the semantic tokens with the context-information semantic tokens, and finally the refined features are obtained to predict the change map.

ChangeFormer [23] is a transformer-based Siamese network architecture. It leverages the hierarchically structured transformer encoder and multilayer perception (MLP) decoder in a Siamese network architecture for change detection.

Table 1 presents the results of the aforementioned four methods on the test-sets of LEVIR-CD [14] and DSIFN-CD [17]. As can be seen from the table, the proposed TUNetCD network achieves better CD performance in four terms of precision, recall, F1, and IoU metrics. In particular, our TUNetCD improves previous baseline ChangeFormer in precision/recall/F1/IoU by 1.18/3.18/1.96/3.74 percentage (%) and 0.46/0.18/1.28/0.5 percentage (%), for LEVIR-CD and DSIFN-CD, respectively.

5.2. Ablation Study. It is well known that many factors can affect the model results, such as network structure and parameter initialization method. In this section, we mainly research the influences of feature difference map processing block on the TUNetCD model. For the factor, we conducted ablation experiments on the LEVIR-CD and DSIFN-CD datasets.

TABLE 1: The average quantitative results of different CD methods on two datasets.

Method		STANet	SNUNet	BIT	ChangeFormer	TUNetCD (ours)
LEVIR-CD	Precision (%)	83.81	89.18	89.24	92.05	93.23
	Recall (%)	91.00	87.17	89.37	88.80	91.98
	F1 (%)	87.26	88.16	89.31	90.40	92.36
	IoU (%)	77.40	78.83	80.68	82.48	86.22
DSIFN-CD	Precision (%)	67.71	60.60	68.36	88.48	88.94
	Recall (%)	61.68	72.89	70.18	84.94	85.12
	F1 (%)	64.56	66.18	69.26	86.67	87.95
	IoU (%)	47.66	49.45	52.97	76.48	76.98

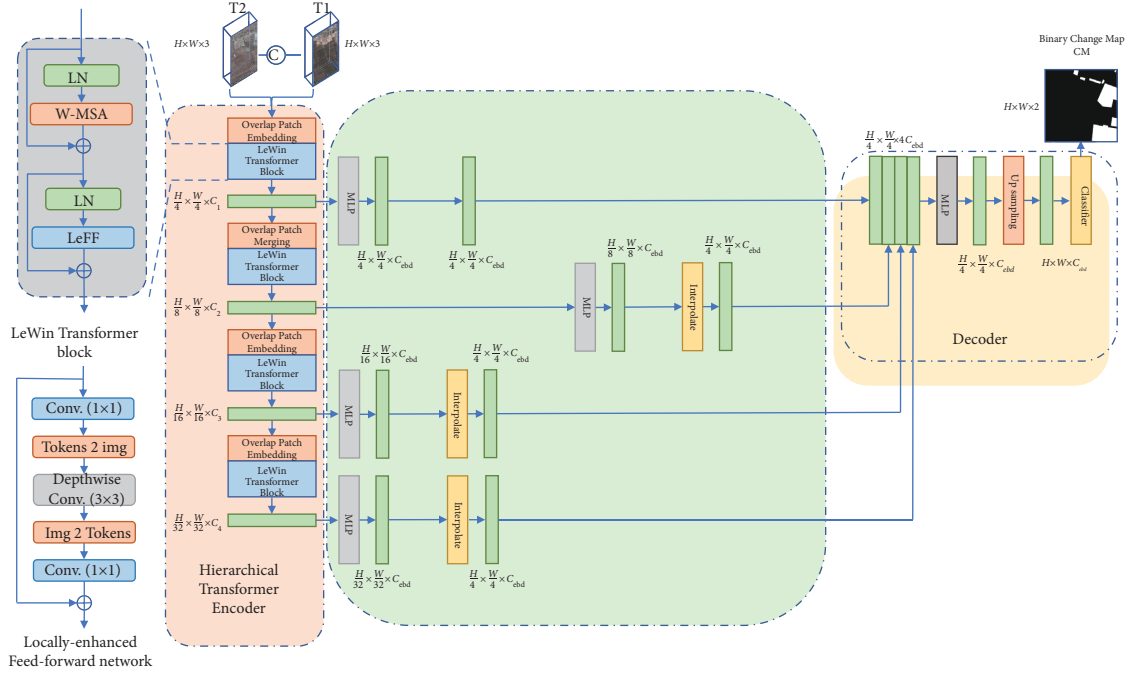


FIGURE 4: The structure of baseline.

TABLE 2: Ablation experiment of innovative modules.

Settings	Baseline	Baseline + LeWinTransformer block
LEVIR-CD	Precision (%)	91.65
	Recall (%)	87.50
	F1 (%)	89.53
	IoU (%)	81.04
DSIFN-CD	Precision (%)	87.31
	Recall (%)	82.78
	F1 (%)	84.98
	IoU (%)	73.88

Impact of feature difference map processing block: the feature difference map processing block contains a LeWinTransformer block. In experiments, we verify the validity of the block.

We gradually added LeWinTransformer block to the baseline. The detailed structure of the baseline is shown in Figure 4. Except for the LeWinTransformer block, everything looks similar to Figure 1 of this paper. We conducted an ablation experiment on two datasets. There are two

experiments: baseline, baseline + LeWinTransformer block. Table 2 shows the results of these two experiments. It can be seen that, without adding the LeWinTransformer block, the network performs poorly, with F1 of 89.53% and 84.98% on the two datasets LEVIR-CD and DSIFN-CD, respectively, which is a huge gap compared to other models that join the LeWinTransformer block.

The addition of the LeWinTransformer block to baseline is our proposed network. With the addition of the LeWinTransformer block module, the semantic information and location information in the feature maps are fully accessible at each level, facilitating the model in detecting the precise change regions. Due to the characteristics of P-R curves, in general, the detection rate tends to be low when the accuracy is high. Compared with the baseline and baseline + LeWinTransformer block, the P metric of the TUNetCD network achieves good results, although the R metric decreases slightly. F1 and IoU metrics achieve good performance, which proves that the LeWinTransformer block module proposed by TUNetCD can be used in combination with other modules to make further improvements in network performance.

6. Conclusion

The network consists of three parts to explore the potential of a pure transformer-based U-shaped structure: a hierarchical Swin-Transformer structure encoder, a feature difference map processing module, and a lightweight decoder. In the field of CD, this method provides good access to local context information than existing CD methods, other than focusing on global context information. We outperform recent attention-based (STANet and IFNet), Conv Net + transformer-based (BIT), and pure transformer structure (ChangeFormer) methods in terms of F1, IoU score, and overall acquisition. As a result, this study demonstrates that the LeWinTransformer block is well obtained in the hierarchical encoder and feature difference map processing module local context information, which effectively improves CD task performance.

In the future, we will conduct further research on unbalanced sample datasets, inaccurate supervision, and multiple types of changed areas to improve the performance of change detection, as well as improving the ability of the model in real-world scenarios.

Abbreviations

CD:	Change detection
BCM:	Binary change map
CNNs:	Convolutional neural network
FCN:	Fully convolutional networks
FC-EF:	Fully convolutional early fusion
FC-Siam-	Fully convolutional Siamese-concatenation
Conc:	
FC-Siam-	Fully convolutional Siamese-difference
Diff:	
DSIFN:	Deep-supervised image fusion network
NMT:	Neural machine translation
NLP:	Natural language processing
ViT:	Vision transformer
CV:	Computer vision
MLP:	Multilayer perceptron
DL:	Deep learning
STANet:	Spatial-temporal attention neural network
ResNet:	Residual nets
DASNet:	Dual attentive fully convolutional Siamese networks
FP:	False positive
FN:	False negative
TP:	True positive
TN:	True negative
P:	Precision
R:	Recall
IoU:	Intersection over Union.

Data Availability

The data are included within the article.

Conflicts of Interest

The authors declare that they have no conflicts of interest.

Acknowledgments

This study was funded by National Natural Science Foundation of China (62141206), Xinjiang Natural Science Foundation of China (2019D01C337), University Key Project (2020YSZD02), and Doctoral Research Startup Fund Project of Yili Normal University (2020YSBS005).

References

- [1] H. Jiang, X. Hu, K. Li, J. Zhang, J. Gong, and M. Zhang, "PGA-SiamNet: pyramid feature-based attention-Guided Siamese network for remote sensing Orthoimagery building change detection," *Remote Sensing*, vol. 12, no. 3, p. 484, 2020.
- [2] M. Tarawally, X. Wenbo, H. Weiming, T. D. Mushore, and M. B. Kursah, "Land use/land cover change evaluation using land change modeller: a comparative analysis between two main cities in Sierra Leone," *Remote Sensing Applications: Society and Environment*, vol. 16, Article ID 100262, 2019.
- [3] B. Wang, Z. Chen, L. Wu, X. Yang, and Y. Zhou, "SADA-net: a shape feature Optimization and multiscale context information-based Water Body extraction method for high-resolution remote sensing images," *Ieee Journal of Selected Topics in Applied Earth Observations and Remote Sensing*, vol. 15, pp. 1744–1759, 2022.
- [4] E. Weber and H. Kané, "Building Disaster Damage Assessment in Satellite Imagery with Multi-Temporal fusion," 2020, <https://arxiv.org/abs/2004.05525>.
- [5] T. He, Z. Zhang, H. Zhang, Z. Zhang, J. Xie, and M. Li, "Bag of tricks for image classification with convolutional neural networks," in *Proceedings of the IEEE/CVF Conference on Computer Vision and Pattern Recognition*, pp. 558–567, Long Beach, CA, USA, June 2019.
- [6] G. Huang, Z. Liu, L. Van Der Maaten, and K. Q. Weinberger, "Densely Connected Convolutional networks," in *Proceedings of the IEEE Conference on Computer Vision and Pattern Recognition*, pp. 4700–4708, Honolulu, HI, USA, July 2017.
- [7] T. Y. Lin, P. Dollár, R. Girshick, K. He, B. Hariharan, and S. Belongie, "Feature Pyramid Networks for Object detection," in *Proceedings of the IEEE Conference on Computer Vision and Pattern Recognition*, pp. 2117–2125, Honolulu, HI, USA, July 2017.
- [8] J. Long, E. Shelhamer, and T. Darrell, "Fully Convolutional Networks for Semantic segmentation," in *Proceedings of the IEEE Conference on Computer Vision and Pattern Recognition*, pp. 3431–3440, Athens, Greece, October 2018.
- [9] J. Deng, J. Guo, N. Xue, and S. Zafeiriou, "Arcface: Additive angular margin loss for deep face recognition," in *Proceedings of the IEEE/CVF Conference on Computer Vision and Pattern Recognition*, pp. 4690–4699, Long Beach, CA, USA, June 2019.
- [10] Y. Zhan, K. Fu, M. Yan, X. Sun, H. Wang, and X. Qiu, "Change detection based on deep Siamese convolutional network for Optical Aerial images," *IEEE Geoscience and Remote Sensing Letters*, vol. 14, no. 10, pp. 1845–1849, 2017.
- [11] F. Rahman, B. Vasu, J. Van Cor, J. Kerekes, and A. Savakis, "Siamese Network with Multi-Level Features for Patch-Based Change Detection in Satellite imagery," in *Proceedings of the 2018 IEEE Global Conference on Signal and Information Processing (GlobalSIP)*, pp. 958–962, IEEE, Anaheim, CA, USA, November 2018.
- [12] O. Ronneberger, P. Fischer, and T. Brox, "U-Net: Convolutional Networks for Biomedical Image segmentation," *International Conference on Medical Image Computing and*

- Computer-Assisted Intervention*, Springer Cham, New York, NY, USA, 2015.
- [13] R. C. Daudt, B. Le Saux, and A. Boulch, "Fully Convolutional Siamese Networks for Change detection," in *Proceedings of the 2018 25th IEEE International Conference on Image Processing (ICIP)*, pp. 4063–4067, IEEE, Athens, Greece, October 2018.
 - [14] H. Chen and Z. Shi, "A spatial-temporal attention-based method and a new dataset for remote sensing image change detection," *Remote Sensing*, vol. 12, no. 10, p. 1662, 2020.
 - [15] J. Chen, Z. Yuan, J. Peng et al., "DASNet: dual attentive fully convolutional Siamese networks for change detection in high-resolution Satellite images," *Ieee Journal of Selected Topics in Applied Earth Observations and Remote Sensing*, vol. 14, pp. 1194–1206, 2021.
 - [16] D. Peng, Y. Zhang, and H. Guan, "End-to-End change detection for high resolution Satellite images using improved UNet++," *Remote Sensing*, vol. 11, no. 11, p. 1382, 2019.
 - [17] C. Zhang, P. Yue, D. Tapete et al., "A deeply supervised image fusion network for change detection in high resolution bi-temporal remote sensing images," *ISPRS Journal of Photogrammetry and Remote Sensing*, vol. 166, pp. 183–200, 2020.
 - [18] S. Fang, K. Li, J. Shao, and Z. Li, "SNUNet-CD: a densely connected Siamese network for change detection of VHR images," *IEEE Geoscience and Remote Sensing Letters*, vol. 19, pp. 1–5, 2022.
 - [19] A. Vaswani, N. Shazeer, N. Parmar, P. Illia, and K. Łukasz, "Attention is all you need," *Advances in Neural Information Processing Systems*, vol. 30, 2017.
 - [20] A. Dosovitskiy, L. Beyer, A. Kolesnikov et al., "An Image Is worth 16x16 Words: Transformers for Image Recognition at scale," 2020, <https://arxiv.org/abs/2010.11929>.
 - [21] Z. Liu, Y. Lin, Y. Cao et al., "Swin transformer: hierarchical vision transformer using shifted windows," in *Proceedings of the IEEE/CVF International Conference on Computer Vision*, Article ID 10012, Montreal, QC, Canada, October 2021.
 - [22] E. Xie, W. Wang, Z. Yu, A. Anima, M. A. Jose, and L. Ping, "SegFormer: Simple and efficient design for semantic segmentation with transformers," *Advances in Neural Information Processing Systems*, vol. 34, 2021.
 - [23] W. G. C. Bandara and V. M. Patel, "A Transformer-Based Siamese Network for Change Detection," 2022, <https://arxiv.org/abs/2201.01293>.
 - [24] H. Jiang, M. Peng, Y. Zhong et al., "A Survey on deep learning-based change detection from high-resolution remote sensing images," *Remote Sensing*, vol. 14, no. 7, p. 1552, 2022.
 - [25] L. Khelifi and M. Mignotte, "Deep learning for change detection in remote sensing images: comprehensive Review and Meta-analysis," *IEEE Access*, vol. 8, Article ID 126385, 2020.
 - [26] X. Peng, R. Zhong, Z. Li, and Q. Li, "Optical remote sensing image change detection based on attention mechanism and image difference," *IEEE Transactions on Geoscience and Remote Sensing*, vol. 59, no. 9, pp. 7296–7307, 2021.
 - [27] H. Chen, Z. Qi, and Z. Shi, "Remote sensing image change detection with transformers," *IEEE Transactions on Geoscience and Remote Sensing*, vol. 60, pp. 1–14, 2022.

Research Article

Research on the Audit Prediction Model of “Special Bonds + PPP” Project based on Machine Learning

Qianru Fang 

Wenzhou Polytechnic, Wenzhou Higher Education Park, Wenzhou 325000, Zhejiang, China

Correspondence should be addressed to Qianru Fang; fqr@wzpt.edu.cn

Received 6 May 2022; Revised 30 May 2022; Accepted 3 June 2022; Published 11 August 2022

Academic Editor: Dong Chen

Copyright © 2022 Qianru Fang. This is an open access article distributed under the Creative Commons Attribution License, which permits unrestricted use, distribution, and reproduction in any medium, provided the original work is properly cited.

This paper aims at the whole-process tracking audit problem of “special bonds + PPP” mode (hereinafter referred to as “special bonds + PPP”) in public infrastructure construction projects and establishes an audit evaluation prediction model based on the theory and method of machine learning. Firstly, based on expert interviews and the actual working process of “special bonds + PPP,” the comprehensive evaluation index system of the whole process tracking audit is established. Secondly, innovate audit technology methods and apply machine learning theories and methods such as support vector machine, back propagation neural network, multinomial logistic regression, and random forest to the whole tracking audit of “special bonds + PPP.” Finally, the real case evaluation sample data are selected, and the four established models, that is, SVM, BP, Multinom, and RF, are trained and predicted. After comparative analysis, the RF model with the highest accuracy is selected as the evaluation prediction model.

1. Introduction

With the continuous enhancement of China’s comprehensive national strength, the demand for public infrastructure construction projects is surging. The PPP mode has become the main starting point of national infrastructure construction, but its financing difficulties are increasingly prominent. Such as local government special bonds have the advantages of the short issuance review period and low financing cost, and the “special bonds + PPP” mode of public infrastructure construction projects (hereinafter referred to as “special bonds + PPP”) financing mode emerges. It has become the main mode of government project investment and financing. At present, how to ensure the legality of the operation of “special bonds + PPP” and guarantee the project benefits is of great importance. A set of consistent whole-process tracking audit index system is needed, and an innovative evaluation method is needed to establish an audit prediction model to achieve effective supervision and audit prediction.

In domestic and foreign literature research and project practice, we divided scholars’ literature on PPP project tracking audit and special debt audit into the following three categories:

The first category is the research on key indicators of PPP project audit. Cheung [1] used the expert scoring method for multiparty evaluation and identifies effective risk, output benefits, project management ability, and technological innovation ability as key indicators of PPP project audit. Lu [2] drew lessons from the management mechanism of India and proposed that China should strengthen audit in key elements, work process, audit focus, risk assessment, and other aspects of PPP project. Jiang and Xu [3] proposed to start with the whole project cycle, focusing on the selection of optimal solutions, project progress, project investment, risk management and control, completion quality, project operation, and other key points to implement whole-process audit coverage, based on the comparison of the advantages and disadvantages of the VFM evaluation system both domestic and abroad. Li [4] suggested that a PPP project audit should focus on construction project quality, internal control, investment estimation, risk management, and other aspects. Wang and Zhang [5] believed that the key points of project audit are project screening, legal compliance of the implementation process, policy implementation,

and investment performance. Ye et al. [6] proposed that the partnership value, economy, efficiency, and effectiveness are the main contents of the audit of the PPP project. Based on the perspective of “dual identity” of government, Wang and Yan [7] believed that bonds risk, public interest, financial bearing capacity, and value for money evaluation report et al. are the key points of audit. Liu [8] studied the risk-oriented audit theory and put forward investment contract, policy implementation, social investment, construction management, and economic benefits as audit priorities. Liu [9] proposed the construction of an audit indicator system from the perspective of the project process, taking project stages of identification, preparation, procurement, implementation, and handover as dimensions.

The second category is the study of PPP project audit evaluation methods. Tang [10] summarized the current problems of PPP project audit efficiency and advocated using big data to carry out PPP project audit so as to avoid the shortage of sample reviews. Xiong [11] proposed that the application of cloud computing, big data, and other technology development means, as well as the application of audit tools, provide support for the full coverage of PPP project audit. Drawing on the PPP case of the British metro, Liang [12] proposed to use modern information technology execution and information transmission to build a trinity mechanism of entrustment to ensure full audit coverage. Liu et al. [13] established the VFM evaluation model and analyzed the PSC value of the comprehensive pipe gallery project and the LCC value in its PPP mode through actual cases. Xiang and Song [14] analyzed the interaction between risk factors of PPP projects and established a system dynamics model to strengthen the monitoring of financing risks. Zhao et al. [15] established a comprehensive performance rating model based on the matter-element extension evaluation method and evaluated PPP project performance index values as the matter-element to be evaluated. Liu et al. [16] used the BCC model and Malmquist index to evaluate the public governance performance of the PPP model in 31 provinces and cities from 2017 to 2019. Qin et al. [17] determined the index weight based on decision laboratory analysis (DEMATEL) and network analytic hierarchy process (ANP) and established the dynamic evaluation model of financing risk by using the extended approximate ideal solution (TOPSIS). Chang et al. [18] established the extension matter-element model of financing risk and used the correlation degree between the evaluation indexes and grades of the correlation degree function to evaluate the financing risk grade of the PPP project.

The third category is the key research of special bonds audit. Xiaoquan [19] believed that strengthening audit intensity in the whole life cycle of special bonds is conducive to reducing the risk of special bonds. Wen

et al. [20] proposed to strengthen audit of special bonds projects from three aspects: progress of bonds fund use, disclosure of bonds information, and investment and use of bonds funds, so as to prevent risks and improve benefits. Chai [21] believed that in the operation of government special bonds projects, the mode of bond issuance, the duration of bond issuance, and the mode of principal and interest repayment should be strengthened. Xu and Yang [22] analyzed the risk points of special bonds and summarized the rights and responsibilities of bonds issuing subjects, bonds size and structure, project selection, capital use efficiency, and sources of bonds repayment funds et al. as audit priorities. Cai [23] believed that the key point of special bonds supervision is whether the bidding, capital management, and construction management et al. of construction project and material procurement are standardized.

The above-given research focuses on the major links and key indicators of PPP projects and special debt audit, and PPP project evaluation methods. To a certain extent, they have ensured that the value for money, project progress control and risk control of single models such as PPP mode and special bonds mode meet the expected objectives. As an innovative mode with Chinese characteristics, special bonds and PPP combined mode is an innovative mode to solve the financing difficulties of the PPP mode. Currently, there are few studies that combine the application of artificial intelligence algorithms such as machine learning. In terms of audit evaluation and prediction, there is a lack of overall index systems and intelligent evaluation predicting tools for the audit supervision of “special bonds + PPP.”

Based on the research results of scholars, we propose to establish an appropriate audit evaluation and prediction model based on the theory and method of machine learning to carry out the whole-process tracking audit evaluation and prediction of “special bonds + PPP.” First of all, based on expert interviews and combined with the declaration and actual working process of “special bonds + PPP,” the key points of audit are identified, and the comprehensive evaluation index system of the whole process tracking audit is established, striving to cover all indicators. Secondly, innovate audit technology methods and apply machine learning theories and methods such as support vector machine, back propagation neural network, multinomial logistic regression, and random forest to the whole tracking audit of “special bonds + PPP.” Finally, design the experts evaluation questionnaire, select the real case, obtain original sample data, process the input, and output data in a quantitative way, and the four established models, that is, SVM, BP, Multinom, and RF, are trained and predicted. After comparative analysis, the RF model with the highest accuracy is selected as the evaluation prediction model. Meanwhile, this model is easy to operate and has a high level of versatility, which offers a theoretical and intelligent technical support for the “special bonds + PPP” audit activity coverage.

2. Construction of Whole-Process Tracking Audit Indicator System of “Special Bonds + PPP”

Based on the previous research and with expert interviews, this paper analyzes the audit focus of PPP project and special bonds, respectively, combines with the actual declaration and work process of “special bonds + PPP,” and based on the principle of full life cycle tracking audit coverage. The original evaluation indicators are extracted from the three dimensions of early project approval decision, midterm supervision and management, and later handover evaluation as the whole process tracking audit of “special bonds + PPP.” Then, select the national registered supervision engineers with practical work experience, senior engineers of the audit bureau, engineers of design institutes, college teachers, and scientific researchers with relevant knowledge as the survey objects. Through the “Sojump” app, the original audit evaluation index questionnaire is distributed to the respondents and analyzed, so as to build a whole process tracking audit evaluation index system including 3 primary indicators(as A), 23 secondary indicators (as B), and 68 tertiary indicators (as C), as shown in Table 1.

3. Data Source and Application

3.1. Sample Data Source and Pretreatment. This paper selects the real project of “special bonds + PPP,” which was selected by the ministry of finance, the project of the Zouping freight railway special line in Binzhou City, Shandong Province, as a case. Take the tertiary indicators C_1 – C_{68} and the overall evaluation of the project in Table 1 “special debt + PPP” whole process followup audit evaluation index system,” a total of 69 evaluation indicators, as the content of the questionnaire. Each evaluation index is set as excellent, good, medium, and poor in the four options. 50 questionnaires were sent to the registered supervision engineers of relevant engineering project management companies and 39 valid questionnaires were recovered. By analyzing the survey results of the overall evaluation item, 92.31% of the supervision engineers think the project is excellent or good, indicating that the project runs well. Therefore, the case data is used in the research of the next audit prediction model. Since the 69 index data collected in the questionnaire are descriptive data, they are analyzed and processed quantitatively according to the evaluation level from high to low. For C_1 – C_{68} indicators, 4 represents excellent, 3 represents good, 2 represents medium and 1 represents poor, the overall evaluation of the project is still expressed in four grades: excellent, good, medium, and poor. Sample data are excerpted in Table 2.

3.2. Application of Model Index Data. The valid sample data $X = \{X_1, \dots, X_n\}$, $Y = \{Y_1, \dots, Y_n\}$, $n = 1, \dots, 39$ of numbered 1–39 processed by the method described in “2 sample data sources and preprocessing” in this paper is adopted. C_1 – C_{68} index data in each sample $X_n = (x_1, \dots, x_i)$, $i = 1, 2, \dots, 68$ were taken as input data and overall evaluation

data Y_n , ($n = 1, 2, \dots, 39$) as output data. Using machine learning theories and methods such as support vector machine, back propagation neural network, multinomial logistic regression, and random forest, four models SVM, BP, Multinom, and RF are established, respectively.

The application process of valid sample data is as follows: (1) data are randomly classified. 50% of sample data are randomly selected from 39 data samples as the model training set (as TRS), and the other 50% of sample data as the model testing set (as TES). The testing set is independent of the training set and does not participate in training at all and is only used for the final evaluation of the model effect. (2) K -fold cross validation is adopted. In order to make better use of the limited sample data, increase the sample size and ensure the stability of generalization error, so as to obtain the ideal model, K -fold cross validation is needed. The training set is divided into K folds, of which $K - 1$ folds are used as $K - 1$ training sets(as TRS1~TRS $K-1$). By determining the fitting curve parameters, the classification model is established, and K different models are obtained, which are recorded as M , $M = \{M_1, \dots, M_K\}$. The k -th fold is used as the validation set (as VAS) to evaluate the effect of the model M and select the best hyper parameter to optimize the model. The above-given process was verified K times without a repeated sampling cycle to obtain the final required model. In this paper, according to the sample size, $K = 5$ is set to carry out a 5-fold cross-validation, training, and tuning of the model. (3) Final evaluation of model effectiveness. The four optimal models of SVM, BP, Multinom, and RF obtained after training are tested for their prediction accuracy through the testing set, and the prediction results are compared with the overall evaluation of the project of the samples in the testing set to select the most appropriate model.

4. Analysis of Modeling Ideas of Machine Learning-Related Models

4.1. Support Vector Machine Algorithm Model (as SVM). Support Vector Machine algorithm is a supervised learning and training classifier algorithm, whose goal is to accurately classify data by solving a geometrically spaced maximum hyperplane. The advantage of SVM is that it is based on the principle of structural risk minimization, which is suitable for the small sample situation existing in this paper and has good robustness. It helps us to grasp the key samples and delete redundant samples, thus overcoming the problems of “dimension disaster” and “overlearning” to a large extent.

The modeling idea is as follows:(1) given a training set $S = \{X_n, Y_n\}$, $X_n \in X \in R^i$, $n' = (1, 2, \dots, 20)$, n' is the number of training set samples, X as input space, each point $X_{n'}$ in the input space is composed of i attribute features as support vectors, and $Y_{n'} \in Y \in \{-1, 1\}$ is the target function to output data. In this paper, each X of the independent variable $X_{n'}$ in the audit prediction has 68 attribute features, that is, the C_1 – C_{68} index data in each sample is recorded as $X_{n'} = \{x_{n'1}, x_{n'2}, \dots, x_{n'68}\}$ as the input vector. The

TABLE 1: The whole-process tracking audit evaluation index system of “Special bonds + PPP.”

Primary indicators	Secondary indicators	Tertiary indicators
Preliminary project decision stage (A ₁)	Legitimacy of project identification process (B ₁)	Legitimacy of project initiation and screening procedures (C ₁) Completeness of procedures and documents (C ₂) Approval process compliance (C ₃)
	Rationality of investment estimation decision (B ₂)	Openness and transparency of the evaluation process (C ₄) Correctness of preparation basis (C ₅) Rationality of estimation accuracy (C ₆) Correctness of scheme preparation basis (C ₇)
	Feasibility of preliminary implementation plan (B ₃)	Accuracy of terms and duration of franchise contract (C ₈) Rationality of cooperation mode selection (C ₉) Legality of commercial contract (C ₁₀) Rationality of investment return mechanism (C ₁₁) Integrity report of value for money (C ₁₂) Pertinence of qualitative analysis content (C ₁₃) Accuracy of quantitative calculation (C ₁₄) Accuracy of annual discount rate determination (C ₁₅) Integrity of demonstration report (C ₁₆) Accuracy of calculation (C ₁₇)
	Accuracy of value for money reporting (B ₄)	Identification of financial expenditure responsibility (C ₁₈) Rationality of risk balance allocation (C ₁₉)
	Demonstration of financial affordability (B ₅)	Effectiveness of the combination of government resources and social capital (C ₂₀)
	Rationality of risk sharing (B ₆)	Whether excessively access to government support (C ₂₁) Completeness of procurement documents (C ₂₂) Transparency of information (C ₂₃)
	Compliance of procurement procedures (B ₇)	Standardization of response document review (C ₂₄) Compliance of contract signing (C ₂₅)
	Compliance of special bonds application (B ₈)	Completeness degree of application procedures (C ₂₆) Integrity of budgeting (C ₂₇) Accuracy of bonds accounting (C ₂₈)
	Solvency of special income (B ₉)	Self-balancing ability of project revenue (C ₂₉) Accuracy of solvency analysis (C ₃₀)

TABLE 1: Continued.

Primary indicators	Secondary indicators	Tertiary indicators
Mid-term supervision and management stage (A_2)	The performance of government supervision functions (B_{10})	Adequacy of supervision by relevant departments (C_{31}) Status of special bonds fund supervision (C_{32}) Familiarity degree of relevant personnel with special bonds policies and regulations (C_{33})
	Rationality of project financing (B_{11})	Rationality of financing structure (C_{34}) Economy of financing scheme (C_{35}) Accuracy of calculation results (C_{36})
	Rationality of special bonds use (B_{12})	Idle rate of special bonds funds (C_{37}) Connection between special funds and project schedule (C_{38}) Matching degree of project income period and bonds term (C_{39})
	Legality of construction procedures (B_{13})	Transparency of special fund information (C_{40}) Rationality of project planning decision (C_{41}) Completeness of relevant construction procedures (C_{42})
	Performance degree of the project company (B_{14})	Implementation of cooperation agreement (C_{43}) Management of quality safety and schedule (C_{44}) Reduction rate of engineering cost (C_{45})
	Mid-term performance assessment quality (B_{15})	Rationality of performance system (C_{46}) Rationality of the calculation of the incentive effect of the scheme (C_{47})
	Payment status of project completion (B_{16})	Rationality of settlement price (C_{48}) Rationality of completion settlement preparation (C_{49})
	Status of government feasibility gap subsidy (B_{17})	Rationality of preparation of completion final accounts (C_{50}) Rationality of stipulated pricing and subsidies (C_{51})
	Situation of finance and operation (B_{18})	Correctness of subsidy fund calculation (C_{52}) Authenticity and validity of account books and accounting statements (C_{53})
		Transparency of project operation (C_{54}) Rationality of user charges (C_{55})
Later handover evaluation stage (A_3)	Standardization of project handover (B_{19})	Compliance of transfer procedures (C_{56}) Integrity of handover content (C_{57})
	Economy of transfer subsidy amount (B_{20})	Realization rate of handover standard (C_{58}) Legality of asset appraisal procedures (C_{59}) Rationality of asset appraisal scheme (C_{60})
	Effectiveness of performance test (B_{21})	Standardization of performance test procedures (C_{61}) Rationality of performance test scheme (C_{62})
	Repayment degree of principal and interest of special bonds (B_{22})	Repayment rate of principal and interest (C_{63}) Coverage rate of special income repayment (C_{64}) Whether to provide efficient public goods or services (C_{65})
	Rationality of final performance evaluation (B_{23})	Public satisfaction (C_{66}) Environmental impact rate (C_{67}) Reduction rate of project investment (C_{68})

TABLE 2: Case evaluation sample data processing excerpt.

No	In															OE
	C ₁	C ₂	C ₃	C ₄	C ₅	C ₆	C ₇	C ₈	...	C ₆₄	C ₆₃	C ₆₆	C ₆₇	C ₆₈		
1	3	3	3	3	3	3	3	3	...	3	3	3	3	3	Good	
2	3	3	3	4	4	3	3	4	...	4	3	3	3	4	Excellent	
.	
.	
.	
9	3	3	3	3	2	2	2	2	...	2	3	2	2	2	Medium	
10	3	3	3	4	3	2	2	3		4	4	4	4	4	Excellent	
11	4	4	4	4	4	3	4	4		4	4	4	4	3	Excellent	
12	3	3	3	3	3	3	3	3		2	3	3	3	2	Good	
.	
.	
.	
38	4	4	4	4	4	4	4	4	...	4	4	4	4	4	Excellent	
39	4	3	4	4	4	4	4	3	...	3	3	4	4	3	Excellent	

Note: IN. represents index, No. represents simple number, OE represents overall evaluation of the project.

dependent variable Y_n is the overall evaluation of the project as the regression output value. (2) When the training set data is linear, on the basis of maximizing the hard interval, the relaxation variable $\xi \geq 1$ is introduced to maximize the soft interval, and the linear classifier model is learned and trained. (3) When the data of the training set is nonlinear, the inner product kernel function $K(x_i, x_j)$ is introduced, and the input vector X_n is mapped to a high-dimensional linear feature space, so that $Y_n = F(x_{n'1}, x_{n'2}, \dots, x_{n'68})$ trains the classifier in the high-dimensional feature space, and the decision function is obtained. (4) The relevant parameters of the separation hyperplane $w(x)$ with the largest geometric interval were determined and the SVM model was obtained. (5) The above steps, combined with the K -fold cross-validation method, were used to train the model with the training set and tune the model with the testing set to determine the optimal parameters and obtain the optimal SVM model.

4.2. Back Propagation Neural Network Algorithm Model (as BP). Back Propagation neural network is a multilayer feedforward neural network, which is the most widely used neural network model and a powerful data modeling tool. In essence, the algorithm takes the global sum of squares error of the network as the objective function and calculates the minimum value by using the gradient method. The advantage of BP lies in its ability to process the nonlinear transformed information with minimum input error. The ability of self-learning, self-adaptation, and generalization is good, and the fault tolerance rate is high [24].

The modeling idea is as follows (see Figure 1): (1) Back Propagation neural network structure is established. This paper adopts a single-layer feedforward neural network, which is composed of three neural network models: input layer X_n , $X_n = (x_1, \dots, x_{68})$, middle layer (1 hidden layer), and output layer Y_n . Neuron nodes of adjacent layers are fully connected by connection weight. (2) Back Propagation

neural network training is divided into signal forward propagation and error reverse feedback, and the training set is input into the network with a predetermined limiting value. After single hidden layer processing, when the global sum of squares error of the network meets the limiting value, that is, the output value is consistent with the output of the expected response, the training learning ends. If the global sum of squares error does not meet the limit value, that is, the output value is inconsistent with the expected response output, then the corrected error value is calculated and the connection weights and thresholds are modified layer by layer according to the back propagation network. (3) With the K -fold cross-validation method, the training set and verification set are trained and verified repeatedly until the global square sum error meets the limit value, so as to obtain the minimum error value and obtain the optimal BP model.

4.3. Multinomial Logistic Regression Algorithm Model (as Multinom). Multinomial Logistic Regression algorithm is a machine learning classification algorithm based on probabilistic nonlinear regression. The goal is to estimate the probability value through the logistic function, It is used to measure the relationship between dependent variables and multiple independent variables (characteristics). The advantage of multinomial is that through the convenient observation sample probability score, it can fundamentally solve the problem of how to do if the dependent variable is noncontinuous, the calculation cost is not high, and it is easy to understand and implement.

The modeling idea is as follows: (1) analyze the characteristics of valid samples $S = \{X_n, Y_n\}, n = 1, \dots, 39$ in this paper. The independent variable in each sample has 68 characteristic attributes, that is, C_1 – C_{68} index data in each sample, indicating that the number of events in this group is 68. The dependent variable Y is unique, that is, the overall evaluation of the project is one of the four grades of excellent, good, medium, and poor. Each grade is orderly,

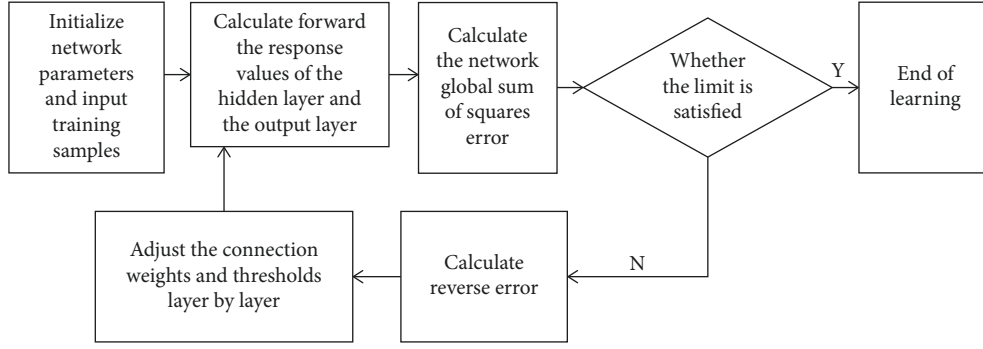


FIGURE 1: Modeling schematic diagram of back propagation neural network.

which belongs to the situation of multiclassification and order of response variables. Therefore, the ordered cumulative probability logistic regression model is established according to the characteristics of the samples. (2) Combining the K -fold cross-validation method with the maximum probability estimation method, the training set, and verification set are used to train and test continuously, and the optimal parameters are found to maximize the joint probability, and the optimal Multinom model is obtained.

4.4. Random Forest (RF) Algorithm Model. Random Forest is a supervised learning integration algorithm based on if-then-else rules. It generates many decision trees by randomly extracting variables and sample data and then summarizes the results of decision trees to become a random forest algorithm model. The advantage of RF is that it avoids the limitations of a single model. The accuracy of the integrated model is better than that of most single algorithms. The introduction of the randomness of feature subset and feature quantity makes RF not easy to fall into overfitting, fast training speed, and strong universality.

The modeling idea is as follows (see Figure 2): (1) data are randomly selected. Given the original training set $S_{n'} = \{X_{n'}, Y_{n'}\}$, $X_{n'} \in X \in R^i$, $n' = (1, 2, \dots, n')$, n' is the training set sample size, n' times are randomly selected with replacement, 1 sample is drawn each time, and the probability of the sample being selected is $1/n'$. This self-help sampling integration method is used to generate n' different train subsets, which are recorded as $TRS_1 \sim TRS_{n'}$. Samples in different train subsets can be repeated, and samples in the same train subset can also be repeated. Different train subsets are used to train a decision tree model one by one, which is recorded as $CART_1 \sim CART_{n'}$, and the models are irrelevant. The samples not selected form a validation set to test the generalization ability of $CART_1 \sim CART_{n'}$. In this paper, the sample size of the original training set $n' = 20$. (2) Characteristic variables are randomly selected. Each sample has F characteristic variables, randomly select f characteristic variables from F characteristic variables, Specify $f < F$, so that the optimal segmentation node can be found at each node to split the decision tree. The whole process does not prune.

Then, calculate the best splitting method according to the f characteristics, so as to improve the classification performance of $CART_1 \sim CART_{n'}$. In this paper, $F = 68$. (3) The model is integrated through voting. By using the regression analysis method, the prediction results of $CART_1 \sim CART_{n'}$ were obtained, and the optimal RF model is integrated by voting.

5. Comparative Analysis of Model Operation

5.1. Sample Application. Effective sample data numbered 1–39 as $S = \{X_n, Y_n\}$, $n = 1, \dots, 39$ processed in “2 Sample Data Sources and Preprocessing” in this paper were imported into “RStudio” software for model running. Check the training set and testing set established by the software according to the method of “3 Model Index Data Application” in this paper, and the software displays the randomly selected results of the machine. A total of 20 samples (3, 4, 6, 8, 9, 10, 15, 17, 20, 21, 23, 25, 26, 27, 28, 30, 31, 35, 36, 37, 38) were used to construct the original training set. The K -fold cross validation method is used to train and optimize the best SVM, BP, Multinom, and RF models, respectively. Another nineteen samples numbered 1, 2, 5, 7, 11, 12, 13, 14, 16, 18, 19, 22, 24, 29, 30, 32, 33, 34, and 39 were used to construct the testing set for the final effect evaluation of SVM, BP, Multinom, and RF models.

5.2. Model Fitting Results. Model fitting degree is an index to evaluate the consistency and precision of a theoretical model and actual data. The better the fitting degree is, the higher the consistency and precision will be. The performance of the observation model on the training set is as follows: (1) main parameters: in order to train various optimal machine learning models, it is necessary to continuously improve the main parameters of various model functions to tune the model. “Rstudio” software uses the maximum accuracy method to train the four optimal models of SVM, BP, Multinom, and RF, respectively. The running results show that the main parameters of the four models selected in this paper are as follows: SVM kernel function parameter $\sigma = 0.006142$, penalty factor $C = 5$; the number of samples selected for one training of BP is size = 5, and the attenuation

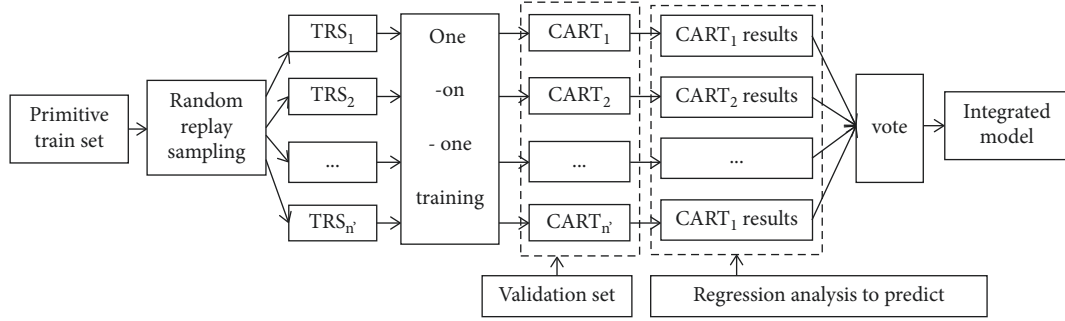


FIGURE 2: Schematic diagram of random forest modeling principle.

TABLE 3: Statistical table of model accuracy and Kappa.

Indicators	Model	Min	1st qu	Median	Mean	3rd qu	Max
Accuracy	SVM	0.5	0.7500000	1.0000000	0.8500000	1.00	1
	BP	0.5	0.7500000	1.0000000	0.8333333	1.00	1
	Multinom	0.5	0.6000000	0.6666667	0.7033333	0.75	1
	RF	0.5	0.6666667	0.8000000	0.7933333	1.00	1
Kappa	SVM	0.1111111	0.6	1.0000000	0.7422222	1.0	1
	BP	0.0000000	0.5	1.0000000	0.6666667	1.0	1
	Multinom	0.0000000	0.0	0.2727273	0.3545455	0.5	1
	RF	0.0000000	0.0	0.6428571	0.5285714	1.0	1

Note: Kappa means consistency.

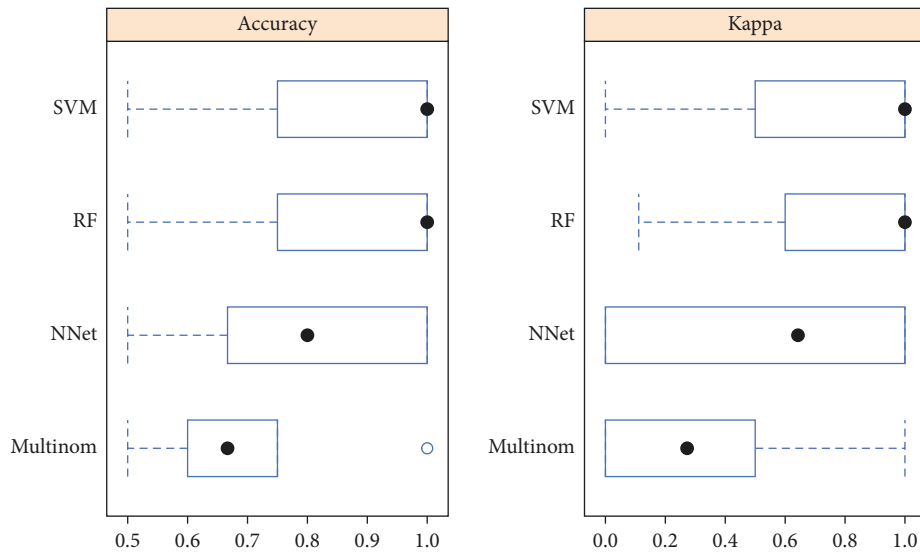


FIGURE 3: Comparison of accuracy and Kappa median.

TABLE 4: Statistical table model of sensitivity and specificity.

Indicators	Model	Class: excellent	Class: good	Class: medium
Sensitivity	SVM	0.6667	0.8333	1.00000
	BP	0.7500	0.5000	0.00000
	Multinom	0.5833	1.0000	0.00000
	RF	0.8333	1.0000	1.00000
Specificity	SVM	1.0000	0.7692	0.88889
	BP	0.7143	0.6923	0.94444
	Multinom	1.0000	0.5385	1.00000
	RF	1.0000	0.8462	1.00000

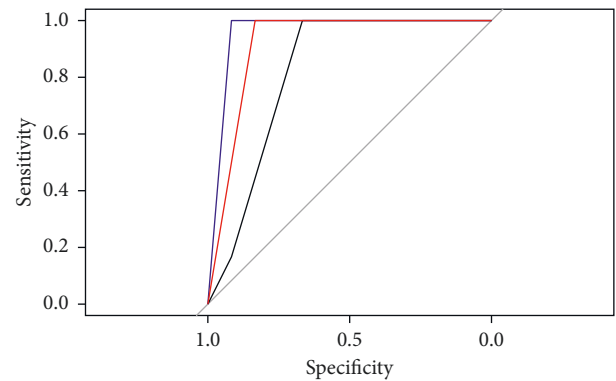


FIGURE 4: ROC curve of SVM model.

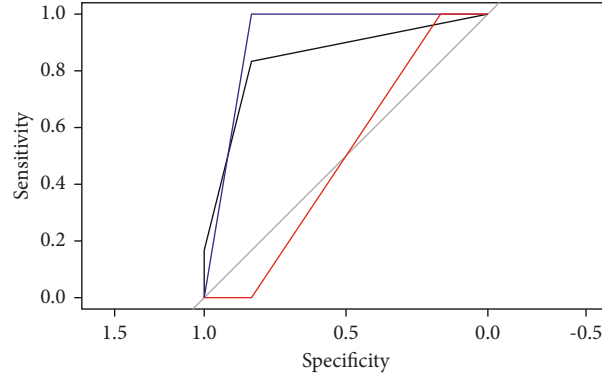


FIGURE 5: ROC curve of BP model.

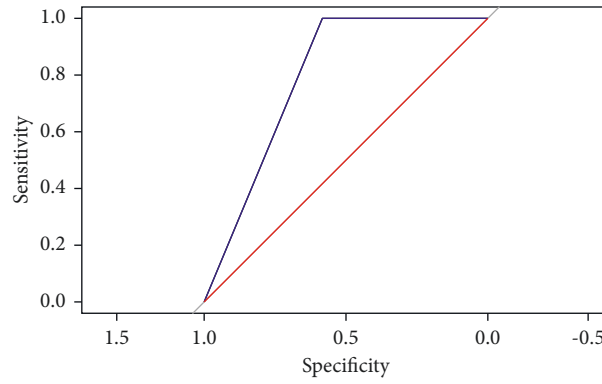


FIGURE 6: ROC curve of Multinom model.

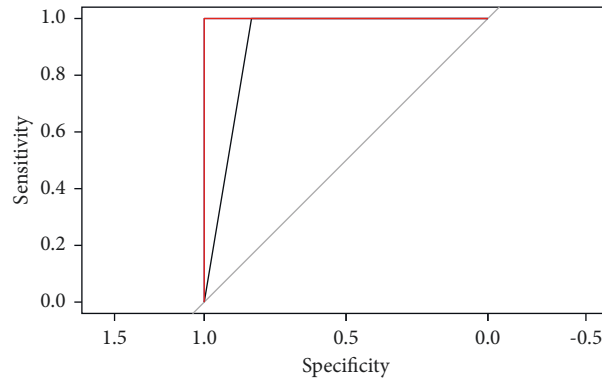


FIGURE 7: ROC curve of RF model.

factor of gradient descent method is $\text{decay} = 0.1$. Multinom determines regression coefficients on a X_n basis; RF is determined to randomly select $f = 35$ variables from 68 variables and use their optimal segmentation to split the nodes. (2) Comparison of fitting degree: By comparing the accuracy and consistency of the model with Minimum value (as Min), 25% Median (as 1st Qu), Median, Mean, 75% Median (as 3rd Qu.), and maximum (as Max) were compared and found (See Table 3 and Figure 3). RF and SVM fit better.

5.3. Prediction Results of the Model. The SVM, BP, Multinom, and RF models trained on the training set will be used to predict on the testing set. The performance of each model will be observed by the result output by RStudio software. (1) Sensitivity and specificity analysis. These two indexes are used to describe the performance of the classifier. The higher the sensitivity, the lower the leakage rate. The higher the specificity, the lower the misclassification rate. Comparing the sensitivity and specificity of the four models on class excellent, class good, and class medium (see Table 4), we can

TABLE 5: Comparison of models “RStudio” results and project OE raw data

PO	NO																		
	1	2	5	7	11	12	13	14	16	18	19	22	24	29	30	32	33	34	39
OE	G	E	E	E	G	E	E	M	E	G	E	E	G	E	G	E	E	G	E
SVM	G	E	E	G	G	E	E	M	E	G	G	E	G	E	G	E	M	M	G
BP	G	G	E	E	G	E	E	G	G	G	E	E	E	E	E	E	G	M	E
Multinom	G	G	E	E	G	E	G	G	E	G	G	E	G	E	G	E	G	G	G
RF	G	G	E	E	G	E	E	M	E	G	E	E	G	E	G	E	G	G	G

discover that the RF model has the highest value. (2) Roc curve analysis. The Roc curve is a curve representing subject operating characteristics. The point closest to the upper left corner of the coordinate is the critical value with higher sensitivity and specificity. The larger the area under the curve, the higher the accuracy. By comparing the Roc curves of the four models (see Figures 4–6), it was found that the area under the Roc curve of RF was the largest. (3) Comparison of predicted results. Compare the original project’s overall evaluation for each sample in the testing set with the predictions of the four models (see Table 5). The prediction accuracy of the SVM, BP, Multinom, and RF are 73.68%, 68.42%, 73.68%, and 84.21%, respectively, and the RF model has the highest accuracy. Based on the analysis of the model prediction results of the above three aspects, it is concluded that the prediction results of the RF model are the best.

6. Conclusion

This paper aims at the whole-process tracking audit problem of “special bonds + PPP” mode (hereinafter referred to as “special bonds + PPP”) in public infrastructure construction projects and establishes an audit evaluation prediction model. Based on theory and methods of machine learning, such as support vector machine, BP neural network, multinomial logistic regression, and random forest, we establish four models, that is, SVM, BP, Multinom, and RF to conduct a research with the following conclusions:

- (1) Based on the principle of tracking audit coverage in the whole life cycle, take the early project approval decision, medium-term supervision and management, and later handover evaluation as the three dimensions of the whole process tracking audit of “special debt + PPP,” and build an index system containing 68 evaluations, which can express the rationality, economy, efficiency, and sustainable development ability of the project in the whole process.
- (2) Innovate audit method, apply machine learning artificial intelligence algorithm to audit evaluation prediction, SVM, BP, Multinom, and RF audit evaluation prediction models are established.

Through RStudio software, the optimal parameters can be obtained quickly to tune the model and match with the evaluation criteria of the index system. The project survey data stored by the Ministry of Finance are true and effective. The operation of model training and prediction is simple and universal. The results showed that the RF model had a better fitting degree in training, and the sensitivity, specificity, and prediction accuracy of the trained model were the highest among the four models. RF model can greatly improve the efficiency of “special bonds + PPP” audit evaluation and prediction, which has a certain reference significance for carrying out full coverage of audit work.

This paper focuses on how to audit and predict “special debt + PPP” and establishes a matching overall evaluation index system and appropriate audit prediction model. In the future research, we will extend the RF audit prediction model to evaluation prediction in other fields, providing theoretical and intelligent technical support for full coverage of project audit activities of government departments.

Data Availability

The data used to support the study are included in the paper.

Conflicts of Interest

The author declares that there are no conflicts of interest.

Acknowledgments

This work was supported by the scientific research project of Education Department of Zhejiang Province--Research on the whole-process tracking audit system of “special bonds + PPP” mode for public infrastructure construction projects (Grant no. Y202044937).

References

- [1] E. Cheung, “Enhancing value for money in public private partnership projects,” *Journal of Financial Management of Property & Construction*, vol. 14, no. 1, pp. 7–20, 2013.

- [2] X. Lu, "Audit and reference of PPP infrastructure projects in India," *Audit Research*, vol. 31, no. 4, pp. 55–59, 2015.
- [3] H. Jiang and J. Xu, "International experience and enlightenment of PPP projects VFM quantitative evaluation," *Local Audit Research*, vol. 15, no. 06, pp. 105–112, 2018.
- [4] Z. Li, "Focus of PPP projects audit," *Chinese and Foreign Entrepreneurs*, vol. 33, no. 33, p. 56, 2016.
- [5] L. Wang and Y. Zhang, "Discussion on follow-up audit of PPP projects," *Audit Research*, vol. 32, no. 06, pp. 22–23, 2016.
- [6] X. Ye, D. Zhang, and S. Shi, "Research on the construction of PPP projects audit mechanism," *Construction Economy*, vol. 38, no. 08, pp. 49–54, 2017.
- [7] J. Wang and J. Yan, "Research on PPP government audit from the perspective of dual identity," *Audit Research*, vol. 34, no. 03, pp. 12–18, 2018.
- [8] Yu Liu, "Discussion on audit focus and mode based on key risk points of railway PPP projects," *China Internal Audit*, vol. 23, no. 11, pp. 22–27, 2019.
- [9] G. Liu, "Design of performance audit evaluation index system for environmental protection PPP projects—PSR framework model based on whole life cycle," *Financial Supervision*, vol. 21, no. 16, pp. 50–55, 2021.
- [10] L. Tang, "Difficulties and Countermeasures of PPP projects audit," *China Financialyst*, vol. 63, no. 03, pp. 54–55, 2018.
- [11] S. Xiong, "Idea and implementation path of full coverage of government audit PPP projects," *Financial supervision*, vol. 18, no. 10, pp. 65–70, 2018.
- [12] H. Liang, "Construction of PPP projects performance audit elements and Mechanism—Taking the UK subway PPP project performance audit as an example," *New Accounting*, vol. 9, no. 8, pp. 43–48, 2017.
- [13] H. Liu, J. Sun, and F. Li, "VFM evaluation of PPP mode applied to urban underground comprehensive pipe gallery," *Journal of Civil Engineering and Management*, vol. 33, no. 04, pp. 122–126, 2016.
- [14] P. Xiang and X. Song, "Risk evaluation of urban infrastructure financing under PPP mode," *Journal of Engineering Management*, vol. 30, no. 01, pp. 60–65, 2016.
- [15] Y. Zhao, J. Wang, Z. Chen, and R. Xie, "Research on PPP projects performance evaluation index system and comprehensive rating model," *Friends of Accounting*, vol. 36, no. 04, pp. 110–115, 2018.
- [16] J. Liu, J. Yuan, W. Lu, and L. Zhang, "Research on public governance performance of regional PPP model in the process of urbanization—a case study of 31 provinces and cities in China," *Journal of Engineering Management*, vol. 35, no. 35, pp. 1–6, 2021.
- [17] N. Qin, J. Wang, N. Zhang, Z. Wang, and W. Huang, "Dynamic evaluation of financing risk of urban rail transit PPP projects based on DEMATEL-TOPSIS," *Journal of Qingdao University of Technology*, vol. 42, no. 06, pp. 21–28, 2021.
- [18] S. Chang, K. Liu, and S. Liu, "Comprehensive evaluation of financing risk of comprehensive pipe gallery based on multi-level extension PPP model," *Journal of Civil Engineering and Management*, vol. 37, no. 05, pp. 115–121, 2020.
- [19] W. Xiaoquan, "Research on the impact of government audit on the risk of local government special bonds," *Audit Research*, vol. 36, no. 04, pp. 51–57, 2020.
- [20] L. Wen, W. Diao, B. Chen, and R. Jing, "Prevent risks, improve benefits, and strengthen the supervision of special bonds," *Financial Supervision*, vol. 20, no. 22, pp. 23–29, 2020.
- [21] Y. Chai, "Application and control of government special bonds financing," *China Market*, vol. 27, no. 33, pp. 28–29, 2020.
- [22] Bo Xu and W. Yang, "Analysis on risk points of local government special bonds," *Financial Science*, vol. 5, no. 06, pp. 77–85, 2020.
- [23] Li Cai, "Follow up audit path of local government special bonds policy from the perspective of internal audit," *China Internal Audit*, vol. 25, no. 06, pp. 42–44, 2021.
- [24] J. Chen, C. Li, and G. Ding, "Highway traffic safety evaluation based on BP neural network," *Journal of Tongji University*, vol. 36, no. 07, pp. 927–931, 2008.
- [25] J. Li, J. Bai, and B. Yu, "C-Mn yield forecasting model based on SVM," *IOP Conference Series: Earth and Environmental Science*, vol. 781, no. 2, 2021.
- [26] X. Yu and W. Lou, "Credit risk evaluation, early warning and empirical research of P2P online loan based on random forest," *Financial Theory and Practice*, no. 02, pp. 53–58, 2016.

Research Article

Detecting Personal Medication Intake in Twitter via Domain Attention-Based RNN with Multi-Level Features

Shufeng Xiong ¹, Vishwash Batra,² Liangliang Liu,¹ Lei Xi ¹ and Changxia Sun ¹

¹Henan Agricultural University, Zhengzhou 450002, China

²School of Computing and Mathematics, Keele University, Keele ST55AA, UK

Correspondence should be addressed to Changxia Sun; sunchangxia@henau.edu.cn

Received 11 June 2022; Revised 8 July 2022; Accepted 13 July 2022; Published 9 August 2022

Academic Editor: Dong Chen

Copyright © 2022 Shufeng Xiong et al. This is an open access article distributed under the Creative Commons Attribution License, which permits unrestricted use, distribution, and reproduction in any medium, provided the original work is properly cited.

Personal medication intake detection aims to automatically detect tweets that show clear evidence of personal medication consumption. It is a research topic that has attracted considerable attention to drug safety surveillance. This task is inevitably dependent on medical domain information, and the current main model for this task does not explicitly consider domain information. To tackle this problem, we propose a domain attention mechanism for recurrent neural networks, LSTMs, with a multi-level feature representation of Twitter data. Specifically, we utilize character-level CNN to capture morphological features at the word level. Subsequently, we feed them with word embeddings into a BiLSTM to get the hidden representation of a tweet. An attention mechanism is introduced over the hidden state of the BiLSTM to attend to special medical information. Finally, a classification is performed on the weighted hidden representation of tweets. Experiments over a publicly available benchmark dataset show that our model can exploit a domain attention mechanism to consider medical information to improve performance. For example, our approach achieves a precision score of 0.708, a recall score of 0.694, and a *F1* score of 0.697, which is significantly outperforming multiple strong and relevant baselines.

1. Introduction

Social media (Twitter, Facebook, etc.) encourages users to frequently express their thoughts, opinions, and other personal information of their lives. Existing studies have demonstrated that social media messages can provide knowledge for tracking public political opinion [1], detecting news events [2], and tracking the spread of infectious diseases [3]. Some research has also shown that social media can be used as a resource for mining public health information [4–6], especially in cases where the health data from official institutions is not readily available.

In this work, we focus on the task of medication intake detection, which is an individual level surveillance of drug safety [7] in the public health domain. The goal of the task is to automatically detect tweets that express clear evidence of personal medication consumption. For example, messages like indicate the author intakes medicine while indicates no intake.

There are two types of existing methods for this emerging task in the public health domain. The first involves applying traditional classification algorithms with hand-crafted features. For example, Kiritchenko et al. [8] exploited an SVM classifier with a variety of features for this task. Another one excludes the time-consuming effort of designing hand-crafted features by using deep neural networks and directly feeding word embedding as the input. Several methods based on CNNs (Convolutional Neural Networks) have achieved good performance [9–11].

Both of them have limitations. Traditional classification methods lack nonlinear mapping ability, although they can make full use of domain knowledge information (e.g., drug lexicon and domain word clusters) [8]. The neural-based methods based on pre-trained embeddings of words [12, 13] are domain-independent and are not very effective for a specific task [14, 15], for example, our medicine intake classification task. In addition, it is not always possible to train task-specific word embeddings due to limitations on

training resources. Despite some efforts to solve the problem of domain relevance at the feature level, for example, sentiment analysis on Nepali COVID-19 tweets [16], no relevant research work considering domain information has been found on our task.

To deal with the aforementioned limitations, we introduce a domain attention mechanism for recurrent neural networks with multi-level inputs to learn an informative representation of tweets. The attention mechanism enables the model the ability of learning domain-specific (medicine) matrix representation, which automatically weights the words in the text accordingly in the medication intake detection task. Meanwhile, the proposed model considers both word-level and character-level features as input features of the network. A prominent advantage of using character-level representation is that it is beneficial for many text analysis tasks [17–19], especially for informal text [20, 21], for example, tweets.

In particular, the proposed model generates word representations using a character-level CNN, which are fed to a highway network. We then concatenate them with pre-trained word embeddings, before feeding them to a BiLSTM network. Subsequently, as previously mentioned, the BiLSTM is introduced with an attention mechanism to distinctively attend on different words while learning the representation of the text. The attention-based BiLSTM also learns the representation of higher-level features in the whole text sequence of a tweet. Finally, softmax is applied to the final tweet representation for the classification task. We compared the experimental results obtained using our method with several strong and relevant baselines. We observe that our approach, with a micro-averaged F-score of 0.697 for Classes 1 and 2, achieves better performance on all other methods except ensemble approaches, which are more efficient than the standard approach. Altogether, this work introduces a novel attentional RNN framework with multi-level features that can effectively be applied to the personal medication intake detection task.

2. Related Work

Personal medication intake detection belongs to a short text classification task. Traditional representative methods for this task include statistical machine learning methods and deep learning methods. The vast majority of the first category is based on the vector space model, which is a typical method for tweet classification [22, 23]. Wang et al. [24] developed an SVM-based text classification algorithm. Chen et al. [25] and Jiang et al. [26] exploited the Naive Bayesian (NB) approach and KNN for this task, respectively. Wan et al. [27] implemented a new document classification method by integrating KNN and SVM, while Rogati et al. [28] investigated a large number of feature selection methods for text classification. However, these methods heavily depend on feature engineering, which cannot represent the grammatical and deep semantic information of words well.

Deep learning methods can automatically select features and therefore have become the mainstream methods for text

classification in recent years. The first step is to learn word representations using related methods [29–31]. Based on them, researchers initially adopted the CNN-based method to classify texts [32, 33]. Collobert et al. [33] extracted local features by using a convolutional layer. Kim [34] constructed a single-layer convolution network for sentence classification. Kalchbrenner et al. [35] proposed a CNN model with multi-layer dynamic k-Max pooling, taking random low-dimensional word vectors as input. Er et al. [36] developed an attention-based pooling component, which has the ability to obtain more semantic information. Yin et al. [37] developed a multi-channel variable-size CNN, which can support multiple pre-trained word embeddings and variable-size convolution kernel to obtain multi-granularity phrase features. Recently, the RNN-based model shows good performance. Lee et al. [38] exploited a convolutional recurrent neural network to process long text sequences. Lai et al. [39] proposed a bi-directional recurrent structure that can utilize the context information of words to classify text.

In addition, the participating systems of the SMM4H shared task are related to our method. These systems can be also divided into traditional statistic methods [8, 40] and neural network methods [10, 41]. Due to the characteristics of pursuing high-performance scores in evaluation tasks, most of them used ensemble technology. More details can be referred to the literature [9].

3. Background

3.1. Personal Medication Intake Detection. The primary objective of the personal medication intake detection task is the automatic classification of tweets mentioning medication intake, which is an emerging research topic in the public health domain based on social media. This is a three-class text classification task. Each medicine-mentioned tweet needs to be grouped into one of three categories: definite intake, non-intake, and possible intake. The details of these categories are as follows.

- (i) Define intake (Class 1)-The user expresses clear evidence of personal medication consumption, for example, “Benadryl and Tylenol are the only things saving me at night these last few nights.”
- (ii) Possible intake (Class 2)-It is suggested that one poster may have taken the medication, but there is no clear evidence, for example, “I would love to intravenously pump Motrin and caffeine into my body immediately.”
- (iii) Non-intake (Class 3)-There is no evidence showing that the user has consumed the medication, while it only mentions medication names, for example, “stay out of the heat, only drink water, and stay off your feet for a day or two. Tylenol is all you can take for pain.”

3.2. Character Convolutional Neural Network (CNN). Character Convolutional Neural Network (C-CNN) [17, 42] is fed characters instead of words, as in traditional CNN.

Given an input word w , which can be seen as a character sequence $C = \{c_1, c_2, \dots, c_n\}$, where n is the length of the word. The C-CNN applies the convolution operation on the character sequence to generate the feature map V_1 as follows:

$$V_1 = \text{Conv}(W, C) + b, \quad (1)$$

where Conv denotes the convolution kernel and W and b are learnable parameters. In practice, there are different convolution kernels for catching various features. A pooling layer, which is utilized to compress and obtain crucial features for the next layer, is usually applied after the convolution layer. The computing process can be written as

$$V_2 = \text{Pooling}(V_1). \quad (2)$$

There are two common pooling operations: max pooling and mean pooling. For example, max pooling chooses the maximum value in a pooling window as the output result of the pooling process. Several combinations of convolution and pooling layers could be used in practice for specific tasks.

3.3. Bi-Directional Long Short Term Memory (BiLSTM). The Long Short Term Memory (LSTM) network was introduced by Hochreiter et al. [43] and was refined and promoted by many works [44–46]. The LSTM solves the long-term dependency problem in the RNN model [47]. Given a sequence $X = \{x_1, x_2, \dots, x_n\}$ as input, the operations performed by the LSTM units are as follows:

$$\begin{aligned} s_t &= [h_{t-1}, x_t], \\ f_t &= W_f \cdot s_t + b_f, \\ i_t &= W_i \cdot s_t + b_i, \\ u_t &= W_u \cdot s_t + b_u, \\ C_t &= \delta(f_t) * C_{t-1} + \delta(i_t) * \tanh(u_t), \\ o_t &= W_o \cdot (s_t + b_o), \\ h_t &= \delta(o_t) * \tanh(C_t), \end{aligned} \quad (3)$$

where h_t is the output of the LSTM at time step t . W and b are the weights and bias, respectively, and δ is a sigmoid layer. In many NLP tasks, a bi-directional LSTM is used to obtain forward and backward information of words in a sequence. In BiLSTMs, it concatenates the outputs of the forward and backward hidden states as its output:

$$h_t = \left[\vec{h}_t, \overleftarrow{h}_t \right]. \quad (4)$$

4. Methods

Our proposed model combines the C-CNN and BiLSTM. It also introduces an attention mechanism in the BiLSTM for the personal medication intake detection task. The model consists of a character-level word embedding component, a word-level feature representation component (Character Language Model, CLM) that uses C-CNN, a sentence-level

feature representation component using BiLSTM, and a Domain Attention Component (DAC). An overview of our model is shown in Figure 1.

Since tweets are mostly informal, traditional word embeddings cannot represent it well. Therefore, we use a Character Language Model (CLM) to capture morphological features at the word level. Firstly, a character embedding e_c is created for each character in a word. Our model then converts the character embedding sequence into a vector using a CLM, which is a kind of C-CNN network. The structure of the CLM is as shown on the right in Figure 1.

Specifically, for every word w in a sentence, after passing it to convolutional and max pooling layers, our model utilizes a highway network[42, 48] to regulate the information flow:

$$\begin{aligned} \hat{C} &= g(W_h \cdot V_2 + b_h) \cdot t + V_2 \cdot (1 - t), \\ t &= H(W_t \cdot V_2 + b_t), \end{aligned} \quad (5)$$

where H is a nonlinear function, V_2 is calculated by equation (2), and t and $(1 - t)$ are called the transform gate and carry gate, respectively.

After obtaining \hat{C}_i , the representation of the i -th word at character-level, we concatenate it with its word embedding e_i to generate the final representation of the word:

$$\hat{e}_i = [\hat{C}_i, e_i]. \quad (6)$$

Subsequently, we feed a sentence $s = (\hat{e}_1, \hat{e}_2, \hat{e}_3, \dots, \hat{e}_n)$ into a BiLSTM network to get the hidden states $h = (h_1, h_2, h_3, \dots, h_n)$. In our experiments, we treat each tweet as one sentence and yet achieve good results since most of the tweets in our dataset are too short and mostly contain one or two sentences.

At this stage, the model performs a general processing on tweets. Therefore, for the medicine intake detection task, we introduce a DAC to attend to the specific domain information that is being used to detect a specific condition. The DAC aims to weigh the informative words for medicine intake highly. First, the result \hat{h}_k obtained by inputting h_k into a single-layer perceptron is used as the hidden representation of h . The weight value of a word is determined by the similarity of \hat{h}_k and a parameter D , here D can be seen as a domain context vector. After processing using a softmax function, a normalized attention weight matrix is obtained, which indicates the weight of each word in a sentence. Finally, the tweet representation u can be calculated as the weighted summation of the words in it. The output is computed as follows:

$$\begin{aligned} \hat{h}_k &= \tanh(W_a \cdot (h_k + b_a)), \\ a_k &= \frac{\exp(\hat{h}_k^\top \cdot D)}{\sum_k (\hat{h}_k^\top \cdot D)}, \\ u &= \sum_k a_k \cdot \hat{h}_k, \end{aligned} \quad (7)$$

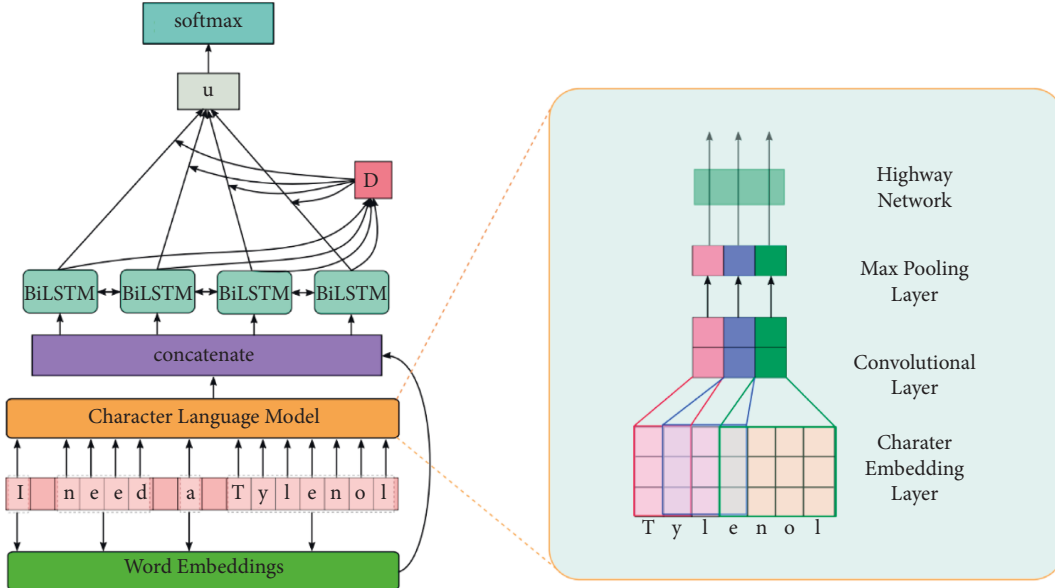


FIGURE 1: Framework of our model.

where W_a and b_a are the weight and bias, respectively. a_k stands for the attention value of the k -th word and measures the weight of each word in the sentence.

The vector representing the whole text sequence from a tweet or the tweet vector u is a higher-level representation and can be used directly as a feature for medicine intake detection:

$$p = \text{softmax}(W_s \cdot (u + b_s)). \quad (8)$$

The final optimization objective is to minimize the negative log likelihood of the correct labels:

$$L = - \sum_d \hat{p} \log p, \quad (9)$$

where \hat{p} represents the ground-truth label of the tweet.

5. Experiments

5.1. Dataset. Our experiments were conducted on a publicly available dataset from the 2nd SMM4H (Social Media Mining for Health) Shared Task on the AMMIA 2017 website. Using the Twitter download script and the tweet dataset description file provided by the organizers, we did not collect all the tweets since some of them are not available. Table 1 summarizes the statistics for the dataset. Classes 1, 2, and 3 stand for personal medication intake, possible medication intake, and no medication intake, respectively. Our training dataset is a combination of the originally provided training and validation datasets. We utilize 10-fold cross-validation when training our model.

5.2. Model Configuration and Training. We use pre-trained word embeddings to initialize the input of the neural network model. This is highly useful for NLP tasks [49, 50]. In our work, we use the embeddings trained by a word2vec

TABLE 1: Statistics of the dataset.

	Class 1	Class 2	Class 3	Total
Train	1648	2650	4246	8544
Test	1444	2267	2593	6304

model on Twitter data [51], which are of 400 dimensions. For character embeddings, we use a random initialization since there are no publicly available character embeddings in this case.

Within our experiments, we have two types of parameters, hyper-parameters and other settings. Specifically, the character embedding dimension is 15, the dimension of the hidden layer is 300, and the CLM has filters of width [1, 2, 3, 4] of size [15, 30, 45, 60] for a total of 180 filters. Additionally, the batch size, the learning rate, the dropout rate, and the $L2$ normalization factor are set to 100, $3e-4$, 0.3, and $5e-7$, respectively. In our training process, we used early stopping with a patience value of 40.

5.3. Baselines. We conducted comparative studies involving experiments with several baseline methods on the dataset, including neural network methods, traditional machine learning algorithms, and state-of-the-art methods for this task. In the first category, we choose the NB and SVM algorithms:

NB is a Naive Bayes classifier in which n -grams ($n = 1, 2, 3$) are used as features.

SVM is a Support Vector Machine classifier with n -grams ($n = 1, 2, 3$) features.

The neural network model is currently the dominant method for text processing. We chose the following representative methods:

BiLSTM uses a traditional bi-directional LSTM model for medicine intake detection, which represents a sentence with the hidden state of the last word of it.

CharCNN [18] is a classical model which performs text classification by using a character-level convolutional network.

AttRNN [52] concatenates the last hidden state, the first hidden states of an RNN with an attentive representation of a hidden state sequence as the features of a text sequence.

The third group is the top three systems from the SMM4H Shared Task:

InfyNLP [10] is the first system in the 2nd SMM4H Shared Task at AMIA 2017. It uses a stacked ensemble of shallow CNNs modeled as a classifier for this task.

UKNLP [41] is the second system in the Shared Task which utilizes a CNN network with a self-attention component.

NRC-Canada [8] exploited the SVM classifier with a variety of hand-crafted features, which is the third system on the SMM4H Shared Task.

5.4. Results and Discussion. Table 2 presents the performance of the different methods. We presented the micro-averaged Precision, Recall, and *F1* scores of Class 1 (personal medication intake) and Class 2 (possible medication intake). The best results are shown in bold text. The results with “#” are copied from their original papers. Following the setting in the SMM4H shared task, we report the micro-averaged scores over Class 1 and Class 2. It was observed that the proposed model performs the best over the *F1* score against strong baselines and top systems in the SMM4H shared task. Compared with other neural classification methods, the proposed domain attention component and CLM in our model improve the performance in the context of the task at hand. CharCNN and AttRNN methods perform less than our method, while BiLSTM performs poorly in this group because they are proposed for general text classification tasks, for example, topic classification. The former two methods perform better than BiLSTM because they introduce character-level information and attention components. NB and SVM, as they are represented in traditional machine methods, perform poorly because they cannot fully capture text semantic information compared to the NN model. At the performance of the top three systems is not as good as our method.

5.5. Ablation Test. In this subsection, we discuss the impact and contribution of the different components of our model. Specifically, we tested 3 settings. The first, we dismissed CLM only. In this case, the model did not capture character-level features. In the next setting, we remove the DAC only. Similarly, the model did not care about the domain information. Finally, we dismiss both CLM and DAC. In this case, the model degenerates to BiLSTM, which only just uses word-level features via BiLSTM encoding. Table 3 reports the results of this ablation study.

TABLE 2: Comparison results.

Model	Precision	Recall	<i>F1</i>
NB	0.675	0.631	0.650
SVM	0.679	0.664	0.668
BiLSTM	0.683	0.672	0.678
CharCNN	0.681	0.697	0.689
AttRNN	0.704	0.677	0.688
InfyNLP	0.725 [#]	0.664 [#]	0.693 [#]
UKNLP	0.701 [#]	0.677 [#]	0.689 [#]
NRC-Canada	0.704 [#]	0.635 [#]	0.668 [#]
Our model	0.708	0.694	0.697

TABLE 3: Comparison results with different settings.

Model	Precision	Recall	<i>F1</i>
w/o CLM and DAC	0.683	0.672	0.678
w/o CLM	0.701	0.683	0.693
w/o DAC	0.669	0.713	0.691
Full model	0.708	0.694	0.697

It is clear that both CLM and DAC are critical to the performance of our model. Removing one or both of them can cause performance degradation. In particular, we also observe that CLM seems to be less important than DAC, which means that the performance drops more as compared to removing CLM.

6. Conclusion and Future Works

Personal medication intake detection, aiming to automatically detect tweets that express clear evidence of personal medication consumption, is an essential research topic in the surveillance of drug safety. In this work, we proposed a domain attention component for recurrent neural networks, for example, LSTM, with multi-level feature representation of text from Twitter. Through experiments on the public benchmark dataset, we validated the performance of our model. Our model obtains the best performance of 0.697 *F1* score. Compared with multiple strong baselines, it showed a significant performance improvement.

Our method still has limitations on domain-specific knowledge representation due to the representation ability of the neural network model itself. Thus, it would be interesting to combine the knowledge base, for example, Knowledge Graph, with our model to obtain richer domain information for this task.

Data Availability

The data used to support the findings of this study have been deposited in the website <https://healthlanguageprocessing.org/sharedtask2/smm4h-sharedtask-2017/>

Conflicts of Interest

The authors declare that they have no conflicts of interest to report regarding the present study.

Acknowledgments

The author shall be thankful to Pingdingshan University for providing resources for this work. This work was supported in part by the MOE (Ministry of Education of China) Project of Humanities and Social Sciences (No. 19YJCZH198) and the Science and Technology Planning Project of Henan Province, China (No. 222102110423).

References

- [1] B. O'Connor, R. Balasubramanyan, B. R. Routledge, and N. A. Smith, "From tweets to polls: linking text sentiment to public opinion time series," in *Proceedings of the Fourth International AAAI Conference on Weblogs and Social Media*, Menlo Park, May 2010.
- [2] A.-M. Popescu and M. Pennacchiotti, "Detecting controversial events from twitter," in *Proceedings of the 19th ACM international conference on Information and knowledge management. ACM*, pp. 1873–1876, Ontario, Canada, October 2010.
- [3] A. Lamb, M. J. Paul, and M. Dredze, "Separating fact from fear: tracking flu infections on twitter," in *Proceedings of the 2013 Conference of the North American Chapter of the Association for Computational Linguistics: Human Language Technologies*, pp. 789–795, Stroudsburg, PA, USA, 2013.
- [4] L. Liu, W. Kunyan, Z. Xingting, D. Weng, L. Gao, and J. Lei, "The current status and a new approach for Chinese doctors to obtain medical knowledge using social media: a study of WeChat," *Wireless Communications and Mobile Computing*, vol. 2018, Article ID 2329876, , 2018.
- [5] L. Sinnenberg, A. M. Buttenheim, K. Padrez, C. Mancheno, L. Ungar, and R. M. Merchant, "Twitter as a tool for health research: a systematic review," *American Journal of Public Health*, vol. 107, no. 1, pp. 143–e8, 2017.
- [6] C. C. Freifeld, J. S. Brownstein, C. M. Menone et al., "Digital drug safety surveillance: monitoring pharmaceutical products in twitter," *Drug Safety*, vol. 37, no. 5, pp. 343–350, 2014.
- [7] A. Klein, A. Sarker, M. Rouhizadeh, K. O'Connor, and G. Gonzalez, "Detecting personal medication intake in twitter: an annotated corpus and baseline classification system," in *BioNLP 2017*, pp. 136–142, Association for Computational Linguistics, Stroudsburg, PA, USA, 2017.
- [8] S. Kiritchenko, S. M. Mohammad, J. Morin, and B. de Bruijn, "NRC-Canada at SMM4H shared task: classifying tweets mentioning adverse drug reactions and medication intake," in *Proceedings of the Social Media Mining for Health Applications Workshop at AMIA-2017*, Washington DC, DC, December 2017.
- [9] A. Sarker, M. Belousov, J. Friedrichs et al., "Data and systems for medication-related text classification and concept normalization from Twitter: insights from the Social Media Mining for Health (SMM4H)-2017 shared task," *Journal of the American Medical Informatics Association*, vol. 25, no. 10, pp. 1274–1283, 2018.
- [10] J. Friedrichs, D. Mahata, and S. Gupta, "InfyNLP at SMM4H task 2:stacked ensemble of shallow convolutional neural networks for identifying personal medication intake from twitter," in *Proceedings of the Second Workshop on Social Media Mining for Health Applications (SMM4H)*, Washington, DC, USA, 2017.
- [11] D. Mahata, J. Friedrichs, R. R. Shah, and J. Jiang, "Detecting personal intake of medicine from twitter," *IEEE Intelligent Systems*, vol. 33, no. 4, pp. 87–95, 2018.
- [12] H. Schwenk, "Continuous space language models," *Computer Speech & Language*, vol. 21, no. 3, pp. 492–518, 2007.
- [13] Y. Bengio, A. Courville, and P. Vincent, "Representation learning: a review and new perspectives," *IEEE Transactions on Pattern Analysis and Machine Intelligence*, vol. 35, no. 8, pp. 1798–1828, 2013.
- [14] P. Fu, Z. Lin, F. Yuan, W. Wang, and D. Meng, "Learning sentiment-specific word embedding via global sentiment representation," in *Proceedings of the Thirty-Second AAAI Conference on Artificial Intelligence (AAAI-18)*, pp. 4808–4815, Louisiana, LA, USA, February 2018.
- [15] H. Zamani and W. B. Croft, "Relevance-based word embedding," in *Proceedings of the 40th International ACM SIGIR Conference on Research and Development in Information Retrieval*, pp. 505–514, New York, NY, USA, August 2017.
- [16] Y. Ren, R. Wang, and D. Ji, "A topic-enhanced word embedding for Twitter sentiment classification," *Information Sciences*, vol. 369, pp. 188–198, nov 2016.
- [17] C. N. Dos Santos and B. Zadrozny, "Learning character-level representations for part-of-speech tagging," in *Proceedings of the 31st International Conference on International Conference on Machine Learning*, Beijing, China, June 2014.
- [18] X. Zhang, J. Zhao, and Y. LeCun, "Character-level convolutional net-works for text classification," in *Advances in Neural Information Processing Systems 28*, C. Cortes, N. D. Lawrence, D. D. Lee, M. Sugiyama, and R. Garnett, Eds., pp. 649–657, Curran Associates, Inc, New York, NY, USA, 2015.
- [19] R. Kavuluru, A. Rios, and T. Tran, "Extracting drug-drug interactions with word and character-level recurrent neural networks," in *Proceedings of the 2017 IEEE International Conference on Healthcare Informatics, ICHI*, Park City, Utah, USA, August 2017.
- [20] S. Vosoughi, P. Vijayaraghavan, and D. Roy, "Tweet2Vec: learning tweet embeddings using character-level CNN-LSTM encoder-decoder," in *Proceedings of the 39th International ACM SIGIR Conference on Research and Development in Information Retrieval*, pp. 1041–1044, Pisa, Italy, July 2016.
- [21] D. Liang, W. Xu, and Y. Zhao, "Combining word-level and character-level representations for relation classification of informal text," in *Proceedings of the 2nd Workshop on Representation Learning for NLP*, pp. 43–47, Vancouver, Canada, August 2017.
- [22] C. Sitaula, A. Basnet, A. Mainali, and T. B. Shahi, "Deep learning-based methods for sentiment analysis on Nepali COVID-19-related tweets," *Computational Intelligence and Neuroscience*, vol. 2021, Article ID 2158184, 2021.
- [23] T. B. Shahi, C. Sitaula, and N. Paudel, "A hybrid feature extraction method for Nepali COVID-19-related tweets classification," *Computational Intelligence and Neuroscience*, vol. 2022, pp. 1–11, Article ID 5681574, 2022.
- [24] Z. Q. Wang, X. Sun, D. X. Zhang, and X. Li, "An optimal SVM-based text classification algorithm," in *Proceedings of the 2006 International Conference on Machine Learning and Cybernetics*, pp. 1378–1381, Dalian, China, August 2006.
- [25] J. Chen, H. Huang, S. Tian, and Y. Qu, "Feature selection for text classification with Naïve Bayes," *Expert Systems with Applications*, vol. 36, pp. 5432–5435, 2009.
- [26] S. Jiang, G. Pang, M. Wu, and L. Kuang, "An improved K-nearest-neighbor algorithm for text categorization," *Expert Systems with Applications*, vol. 39, no. 1, pp. 1503–1509, 2012.
- [27] C. H. Wan, L. H. Lee, R. Rajkumar, and D. Isa, "A hybrid text classification approach with low dependency on parameter by integrating K-nearest neighbor and support vector machine,"

- Expert Systems with Applications*, vol. 39, no. 15, Article ID 11880, 2012.
- [28] M. Rogati and Y. Yang, "High-performing feature selection for text classification," in *Proceedings of the Eleventh International Conference on Information and Knowledge Management*, pp. 659–661, Virginia VA, USA, November 2002.
 - [29] Y. Bengio, R. Ducharme, P. Vincent, and C. Jauvin, "A neural probabilistic language model," *Journal of Machine Learning Research*, vol. 3, pp. 1137–1155, 2003.
 - [30] J. Pennington, R. Socher, and C. Manning, "Glove: global vectors for word representation," in *Proceedings of the EMNLP 2014*, pp. 1532–1543, Doha, October 2014.
 - [31] T. Mikolov, I. Sutskever, K. Chen, G. S. Corrado, and J. Dean, "Distributed representations of words and phrases and their compositionality," in *Proceedings of the NIPS*, pp. 3111–3119, Nevada, NV, USA, December 2013.
 - [32] C. Sitaula and T. B. Shahi, "Multi-channel CNN to classify Nepali covid-19 related tweets," 2021, <https://arxiv.org/>.
 - [33] R. Collobert, J. Weston, L. E. O. Bottou, M. Karlen, K. Kavukcuoglu, and P. Kuksa, "Natural language processing (almost) from scratch," *Journal of Machine Learning Research*, vol. 12, pp. 2493–2537, 2011.
 - [34] Y. Kim, "Convolutional neural networks for sentence classification," in *Proceedings of the 2014 Conference on Empirical Methods in Natural Language Processing (EMNLP)*, pp. 1746–1751, Doha, Qatar, October 2014.
 - [35] N. Kalchbrenner, E. Grefenstette, and P. Blunsom, "A convolutional neural network for modelling sentences," in *Proceedings of the ACL*, Maryland, MD, USA, June 2014.
 - [36] M. J. Er, Y. Zhang, N. Wang, and M. Pratama, "Attention pooling-based convolutional neural network for sentence modelling," *Information Sciences*, vol. 373, pp. 388–403, 2016.
 - [37] W. Yin and H. Schütze, "Multichannel variable-size convolution for sentence classification," in *Proceedings of the Nineteenth Conference on Computational Natural Language Learning*, pp. 204–214, Beijing, China, July 2015.
 - [38] J. Y. Lee and F. Dernoncourt, "Sequential short-text classification with recurrent and convolutional neural networks," in *Proceedings of the 2016 Conference of the North American Chapter of the Association for Computational Linguistics: Human Language Technologies*, pp. 515–520, San Diego, California, CA, USA, 2016.
 - [39] S. Lai, L. Xu, K. Liu, and J. Zhao, "Recurrent convolutional neuralnet works for text classification," in *Proceedings of the Twenty-ninth AAAI conference on artificial intelligence*, Texas, TX, USA, January 2015.
 - [40] B. G. Hb and S. Kp, "NLP_CEN_AMRITA @ SMM4H:health care text classification through class embeddings," in *Proceedings of the Social Media Mining for Health Applications Workshop at AMIA-2017*, Washington, DC, USA, 2017.
 - [41] S. Han, T. Tran, A. Rios, and R. Kavuluru, "Team UKNLP: detecting ADRs, classifying medication intake messages, and normalizing ADR mentions on twitter," in *Proceedings of the CEUR Workshop*, pp. 49–53, Switzerland, August 1996.
 - [42] Y. Kim, Y. Jernite, D. Sontag, and A. M. Rush, "Character-aware neural language models," in *Proceedings of the Thirtieth AAAI Conference on Artificial Intelligence*, Arizona, AZ, USA, March 2016.
 - [43] S. Hochreiter and J. Schmidhuber, "Long short-term memory," *Neural Computation*, vol. 9, no. 8, pp. 1735–1780, 1997.
 - [44] A. Graves, S. Fernández, and J. Schmidhuber, "Bidirectional LSTM net-works for improved phoneme classification and recognition," in *Proceedings of the ICANN 2005*, pp. 799–804, Warsaw, Poland, September 2005.
 - [45] F. A. Gers, J. Schmidhuber, and F. A. Cummins, "Learning to forget:continual prediction with LSTM," *Neural Computation*, vol. 12, no. 10, pp. 2451–2471, 2000.
 - [46] M. Sundermeyer, R. Schlüter, and H. Ney, "LSTM neural networks for language modeling," in *Proceedings of the INTERSPEECH 2012, 13th Annual Conference of the International Speech Communication Association*, pp. 194–197, Portland, Oregon, OR, USA, September 2012.
 - [47] B. A. Pearlmutter, "Learning state space trajectories in recurrent neural networks," *Neural Computation*, vol. 1, no. 2, pp. 263–269, 1989.
 - [48] R. K. Srivastava, K. Greff, and J. Schmidhuber, "Training very deep networks," in *Advances in Neural Information Processing Systems 28*, C. Cortes, N. D. Lawrence, D. D. Lee, M. Sugiyama, and R. Garnett, Eds., pp. 2377–2385, Curran Associates, Inc, New York, NY, USA, 2015.
 - [49] Y. Qi, D. Sachan, M. Felix, S. Padmanabhan, and G. Neubig, "When and why are pre-trained word embeddings useful for neural machine translation?" in *Proceedings of the 2018 Conference of the North American Chapter of the Association for Computational Linguistics: Human Language Technologies*, pp. 529–535, New Orleans, Louisiana, 2018.
 - [50] H. Xu, B. Liu, L. Shu, and P. S. Yu, "Double Embeddings and CNN-Based Sequence Labeling for Aspect Extraction," in *Proceedings of the ACL*, vol. 2, pp. 592–598, Melbourne, Australia, 2018.
 - [51] F. Godin, B. Vandersmissen, W. De Neve, and R. De Walle, "MultimediaLab @ ACL WNUT NER shared task: named entity recognition for twitter microposts using distributed word representations," in *Proceedings of the Workshop on Noisy User-generated Text*, pp. 146–153, Beijing, China, July 2015.
 - [52] C. Du and L. Huang, "Text classification research with attention-based recurrent neural networks," *International Journal of Computers, Communications & Control*, vol. 13, no. 1, pp. 50–61, 2018.

Research Article

Research on the Development of Hospital Intelligent Finance Based on Artificial Intelligence

Mengxuan Ma 

Hubei Cancer Hospital, Tongji Medical College, Huazhong University of Science and Technology, Wuhan, Hubei 430079, China

Correspondence should be addressed to Mengxuan Ma; mamengxuan752@qq.com

Received 28 April 2022; Revised 18 May 2022; Accepted 23 May 2022; Published 9 August 2022

Academic Editor: Dong Chen

Copyright © 2022 Mengxuan Ma. This is an open access article distributed under the Creative Commons Attribution License, which permits unrestricted use, distribution, and reproduction in any medium, provided the original work is properly cited.

Based on the development background of the interweaving and integration of computer technology and Internet technology, China's artificial intelligence industry is quietly rising. In the social life of the information age, the artificial intelligence industry represented by machine deep learning is playing a very important role. This study in combination with the background of the new health reform, in view of the reform of the medical industry, analyzes the connotation of financial wisdom based on the important role of the hospital financial development problems, puts forward the development direction of artificial intelligence hospital financial wisdom development measures, designed to meet the changing external environment demand, reduces human costs, and improves the overall efficiency of hospital financial fund management. Based on the evaluation results, this paper proposes the correct direction for the development of hospital intelligence finance by using the BP neural network model. After the analysis, it is found that the development of artificial intelligence is an important measure to promote the development of hospital intelligent finance. In other words, hospital intelligent financial management is the product of the continuous progress of artificial intelligence technology. At the present stage, the intelligent financial management problems of hospitals are mainly as follows: (1) lack of financial informatization, (2) lack of perfect financial risk early warning system, and (3) the phenomenon of "information island" in the financial system. After analyzing the above problems, the research believes that the development of hospital intelligent finance based on artificial intelligence needs to solve the above thorny problems, so as to improve the outcome of hospital intelligent finance development. The following work should be done: (1) strengthen the design of information sharing module, (2) intelligent control of the cost of hospitals, and (3) intelligent treatment of hospital accounting. Combining the development of artificial intelligence and hospital intelligent finance theory, combined with the actual trend of financial intelligence development under the background of artificial intelligence development in the new era, it provides scientific basis for the development of hospital intelligent finance.

1. Introduction

In a broad sense, financial management includes accounting, tax, audit, budget, and debt management, as well as investment, financing, and operation decisions [1–4]. China's financial management is divided into the following five development stages: (1) traditional stage, (2) computerization stage, (3) information stage, (4) intelligent stage, and (5) smart stage. "Smart finance" management is the product of the continuous progress of artificial intelligence technology, which provides a more novel path and a broader space for the transformation of the financial management field [5]. Its essential feature lies in the more scientific and humanized

management of value flow in economic activities, which is reflected in the organic combination of actual business development of hospitals, universities, and other entity organizations, which can liberate human resources and improve the ability to analyze and judge the judgment of financial status [6]. Starting from the development process of artificial intelligence and the superiority of intelligent finance, this paper discusses the innovative scheme of intelligent finance.

2. Problem Analysis

2.1. Insufficient Degree of Financial Informatization. At present, the degree of financial informatization in most

hospitals is not high, and the financial informatization is mainly reflected in accounting, but other financial work is still manually recorded, and the work efficiency is not high [7]. For example, many hospitals in the budgeting and budget implementation or through the financial personnel are using Excel forms for manual registration and summary [8]. As the general hospital involves multiple departments, with the continuous expansion of economic scale, there are more and more economic problems. In the process of manual registration and summary, it is easy to miss a recording, which will affect the budget preparation and implementation results [9]. For another example, in many hospitals in the financial reimbursement process, reimbursement application filling, form approval, reimbursement original attachments, and access to accounting vouchers and other links are manual. The degree of information is not high [10]. Traditional financial reimbursement process is generally divided into seven steps. The details are shown in Figure 1.

In the above mode, there may be multilevel approval according to the business needs, and the reimbursement agent needs to find different approval personnel for reimbursement approval [11]. Because the examination and approval personnel are mostly administrative leaders, the official duties are heavy, which may cause the phenomenon of the reimbursement agents running empty and reduce the reimbursement efficiency [12]. For the examination and approval personnel, the daily scattered and multiple examination and approval signatures take up a lot of time, and each examination and approval signature will also interrupt the working ideas of the examination and approval personnel, affecting the work efficiency. Financial personnel manually calculate the reimbursement amount and prepare accounting vouchers [13]. With the increasing volume of hospital business, there are more and more economic matters, and the efficiency of manual reimbursement is not high and easy to make mistakes [14]. If “mobile approval” and “online reimbursement” can be realized through information technology, the reimbursement operator can be reduced and the efficiency of financial reimbursement can be improved.

2.2. Lack of Perfect Financial Risk Early Warning System. Under the traditional financial mode of hospitals, post-management is the main management method of financial risks [15]. For financial management risks, there is a lack of prewarning and in-process control and a lack of dynamic financial risk management mechanism, which makes the financial risk management in hospital financial management have an obvious lag. In the financial management of hospitals, cash flow risk is the main financial risk faced [16]. For example, under the COVID-19 outbreak, some hospitals have closed all or some outpatients, resulting in a sharp decline in outpatients and chronic inpatients, the number of outpatient visits, and inpatients, and a sharp decline in medical income and cash flow. At the same time, the current cost of medical protective equipment, disinfection, and other equipment increased significantly, resulting in a significant

increase in cash flow expenditure [17]. The decrease of cash inflows and the increase of cash outflow make the hospital face huge financial problems, and the capital situation is severe [18]. Therefore, hospitals should strengthen the control of financial risks, especially cash flow, and establish a dynamic financial risk early warning system covering the whole process of economic business.

2.3. “Information Island” Problem. The financial system of most hospitals is completely connected with hospital information system, assets, and personnel management, and cannot realize information sharing. The problem of “information island” is very serious [19]. At the same time, because different suppliers provide different information systems, and the standards and specifications between each system are different, compatibility cannot be achieved, resulting in the effective integration of data resources between systems. For example, outpatient charges, hospitalization charges, and other income information. In the hospital information system, it is difficult to timely connect and share with the financial accounting system in real time. Therefore, the daily medical income and other accounting is still in the state of manual accounting [20]. The lack of connection between finance and purchase and supply system easily leads to the hospital material flow, capital flow, and information flow that cannot effectively form a virtuous cycle, which may cause the failure to match the accounts and the lack of data authenticity. At the same time, if the information is not effectively managed, it is difficult to carry out accurate financial accounting, and the operation and management problems cannot be found in time. It causes a lot of data collection or collation duplication, wastes a lot of resources, and seriously affects the efficiency of financial management.

3. The BP Neural Network Model

3.1. Algorithm of BP Neural Network Model under Hospital Intelligent Financial Model

3.1.1. Part 1: Basic Structure. Common neural networks can be divided into three parts: input layer, output layer, and several hidden layers. Figure 2 is a typical three-layer neural network structure and Figure 3 is the structure of each neuron model.

‘ X_n ’ represents the input value of the ‘ n ’ neuron, ‘ W_n ’ represents the connection weight value of the ‘ i ’ neuron, ‘ θ ’ is threshold values, ‘ Y_i ’ is the output value of the ‘ i ’ neuron. The resulting activation function is as follows:

$$y = f\left(\sum_{i=1}^n w_i x_i - \theta\right), \quad (1)$$

where the activation function refers to the introduction of nonlinear factors in the neurons, so that the neural network can be arbitrarily close to any nonlinear function. Sigmoid function, tanh function, and ReLU function are relatively extensive activation functions used in academic sessions. The threshold is a limited value. The difference result after

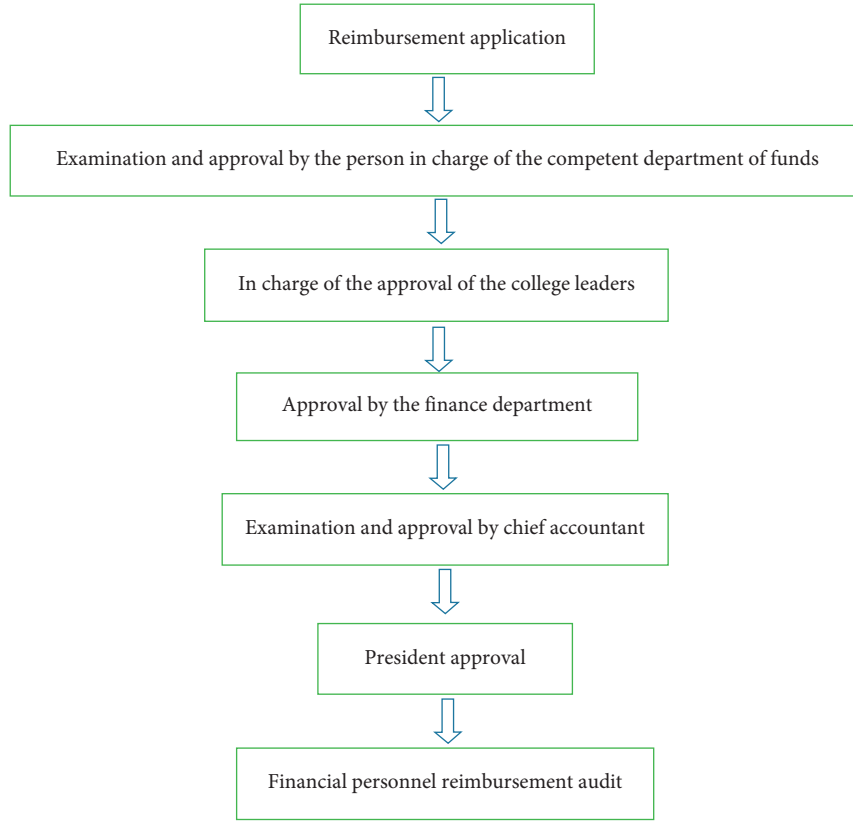


FIGURE 1: Traditional financial reimbursement process.

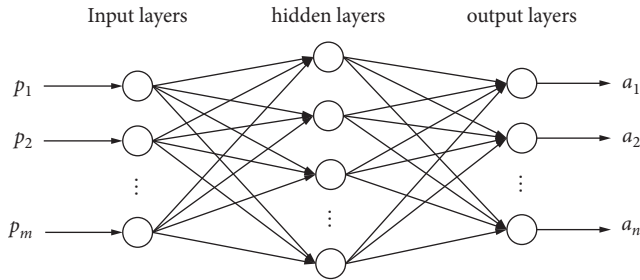


FIGURE 2: Basic structure.

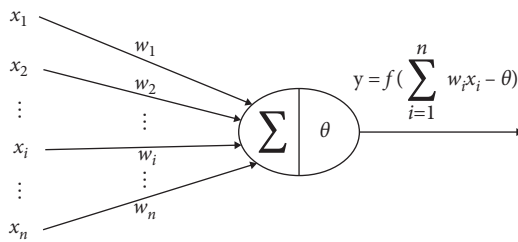


FIGURE 3: Structure of each neuron model.

the sum of ' $W_i X_i$ ' is finally expressed as inhibitory or activation events and gives the output result, which generally adopts the binary scientific counting method. If the difference is less than or equal to 0 and $Y=0$, state indicates inhibition. If the difference is greater than 0 and $Y=1$, state indicates activation.

3.1.2. Part 2: BP Training Method. To train a BP neural network, it is the adjustment and optimization of two parameters: weight and bias. The premise that the neural network can accurately reflect the training results is that the model is fully trained, and the optimal model parameters are obtained through the training: the connection weight ' W ' and ' θ '. The main training method of parameter learning is the BP algorithm, which is mainly based on the gradient descent algorithm, and it is also a common algorithm used to train the neural network model parameters in practical work. The main working principle of the gradient descent method is to solve the optimal solution of the parameters along the direction of the fastest local descent.

Two processes of the BP algorithm are forward and back propagation. The forward propagation is the signal, and the reverse propagation is the error. The error values are backpropagated without a given error range to correct the cell weights. Since the learning of parameters in the BP algorithm is based on the gradient descent algorithm, the core of gradient descent is the calculation of gradient. The training of neural networks is generally divided into four processes. The first process travels forward to calculate the error value between the output value and the actual value. The second process backpropagation calculates the contribution value of all neurons to the total error in each layer, mainly two classes of values of the output and hidden layers. A third process gradient was calculated to find the gradient of the total error against each model parameter for

parameter weights and threshold updates. The fourth process parameter is updated, updating the weights and thresholds.

3.1.3. Part 3: Select the Parameter. The number of nodes in the input layer is the number of input neurons. The number of points in the output layer is divided according to the analysis. If it is a classification problem, the corresponding number of nodes is the number of classification. If it is a regression problem, the corresponding number of nodes is equal to 1. The number of layers and the number of nodes in the hidden layer will make the model too pleasing to the training set and prone to overfitting, while the number of hidden layers and the number of hidden layer nodes are too small, underfitting will occur. There is no way to accurately determine the number of hidden nodes, and the specific number of hidden nodes can be formulated according to the empirical formula.

$$l < n, l < \sqrt{n+k} + i, l < 2\sqrt{n}. \quad (2)$$

In the abovementioned formula, ' l ' represents the number of nodes in the hidden layer, ' n ' represents the number of nodes in the input layer, ' k ' represents the number of nodes in the output layer, and ' i ' represents any constant between 0 and 9.

3.1.4. Part 4: Data Were Normalized. Data normalization is very important. The input layer will involve a variety of different indicators. These indicator dimensions and dimensional units are different, and different indicators will directly feedback the inaccuracy of the data results. The purpose of data standardization processing is to eliminate the influence of dimension, make the data index in the same order of magnitude, and each index is suitable for comprehensive comparative evaluation. The method used in this study is the normalization method, which changes the number into a decimal between 0 and 1. We get the following formula:

$$X_n(\text{new}) = \frac{X_n - X_{\min}}{X_{\max} - X_{\min}}. \quad (3)$$

In the abovementioned formula, ' X_n ' represents the original indicator, ' X_{\max} ' represents the maximum of ' X ' in all data, ' X_{\min} ' represents the minimum of ' X ' in all data, and ' $X_n(\text{new})$ ' is the new value obtained by normalization the original index ' X_n '.

3.2. BP Neural Network Model Data Processing. This study mainly uses MATLAB programming software to train and simulate the results of neural networks. The data mainly comes from the background financial data randomly selected from the intelligent finance development research of a hospital. The initial data sample has 3790 data sets, and the data classification is shown in Table 1.

In this study, the data were imported into MATLAB software for analysis. Based on the normalization method, all 3790 sets of data were the decimal between (0,1). After the

TABLE 1: Data classification.

Credit rating	A	B	C	D	E	F	Total
Sample size	41	1314	1864	428	129	14	3790

normalization analysis, 3000 sets of data were randomly selected as the training set, and the remaining 581 sets of data were used as the experimental set. On this basis, the accuracy of the model prediction is verified. The training step was 500, the expected error target was 0.001, and the learning step was 0.01.

In the above experiments, the number of hidden layer nodes was set to 7, 8, 9, 10, and 11, and the BP neural network model was trained by using the training set data. This paper mainly examines the training effect of different hidden nodes, from the following two aspects: first, to analyze the overall number of credit level identification errors. Second, to analyze the relative error of the deviation degree alone.

$$\text{error} = \text{Average} \left[\frac{\text{abs}(\text{Model output value} - \text{experimental value})}{\text{experimental value}} \right]. \quad (4)$$

For the regression prediction model, if the prediction can draw the predicted value and the real value in the same coordinate system. In the actual model, the judgment coefficient R^2 is usually used to evaluate the actual results of the regression model, which is to evaluate the degree to which the regression model explains the changes in the dependent variable y . The R^2 values range from 0–1, a percentage is usually used for the representation. If a regression model has an $R^2 = 0.7$, then this regression model is 70% interpretable of the predicted results. The academic circle agrees that R^2 is greater than 0.75, with a better model fit, and a high degree of interpretability. If R^2 is less than 0.5, it can be considered problematic in model fitting and not suitable in regression analysis.

The R^2 regression model was evaluated using the MATLAB model. The $R^2 = 0.99351$ calculated from the scoring data of the experimental set also reflects the good ability to estimate the financial risk in this paper and the high accuracy from the side. If this model is applied to the actual process of scoring financial indicators, it can help the hospital to accurately determine the score of each financial risk, so as to effectively help the hospital make a reasonable judgment of the estimated financial risk situation.

This chapter is mainly the simulation of the financial intelligence of the hospital neural network model, according to multiple secondary indicators. Through MATLAB software, using BP neural network model for model training and simulation and through the good simulation results of the model, it proved that the model can predict and evaluate the development of financial intelligence and can effectively help hospitals to predict financial risks, so as to reduce the possible fund management risk. In the future, the training effect can be improved by enriching and optimizing evaluation indicators, increasing training models, improving algorithms and other methods, and enhancing the interpretation ability of the neural network, so that the model can

more accurately predict financial management risks, reduce bad debts, and improve the financial intelligence level of the hospital.

4. Effective Measures of Intelligent Financial Mode of Hospitals under Artificial Intelligence

4.1. Strengthen the Information Sharing Module Design. Information sharing is mainly aimed at the efficient exchange of financial data in hospitals. In this mode, the network information platform can be used to integrate the financial data information of independent accounting units of each department, push the necessary financial data to the financial management personnel, and then define the content, and corresponding treatment plans are set up for classified control. Due to the different specific functions of hospital departments, data interaction and information transmission should be carried out according to the actual work and the principles of orderly, reasonable, and complete work so as to avoid repeated transmission and transmission of wrong information. In the specific preparation, the appropriate report template is selected in the system database according to the business development, and then the report data is retrieved according to the requirements of the template. The platform can screen, integrate, and summarize the data, and write the analysis and explanation of the report. Finally, realize the information exchange of independent financial subjects through the interactive platform. At the same time, the financial personnel can adjust the format of the financial report from the needs of themselves and the unit, carry out a comprehensive analysis and interpretation, focus on the surface abnormal data, and submit it to the management for review.

4.2. Intelligent Control of Hospital Costs. An important function of intelligent finance is accounting treatment, namely accounting function. The intelligent construction of the reimbursement module is to realize the automation and intelligent operation of a series of work such as voucher recording, storage, and bookkeeping in the interactive system. Due to the introduction of AI technology, the system can automatically identify the image content and use big data analysis processing. With the popularity of electronic invoice, intelligent financial system, invoice system depth interaction, and implement business credentials recorded in the core accounting system, the paper invoice content through AI identify key data such as billing, tax price, tax into digital language stored in the cloud. At the same time, intelligent finance can connect with the tax invoice query system to identify the authenticity of invoices and effectively control false businesses.

The financial personnel of the hospital shall submit the paperless examination and approval application in the OA office system after the system examination according to the established authority setting, and the process can be signed and approved in the OA system. After the OA review, the original voucher approval form and approval details will be

pushed to the financial accounting system. The financial personnel will review, and the document information will be encrypted by the smart financial system and will be displayed in the form of QR code on the documents, so as to realize the uniqueness and confidentiality of the data. Subsequently, the system automatically prints out the paper version of the accounting reimbursement documents, and the financial personnel will put the documents and the original vouchers into the accounting file cabinet in accordance with the provisions. The service mode of "smart finance" has the ability of memory feedback, which can analyze the daily entry writing rules of financial personnel and automatically make accounting entries for the identified economic business data, saving time and facilitating the follow-up review. At the same time, the data before and after the review can coexist, and it can be accurately and comprehensively be classified and archived according to the requirements of accounting standards. In the financial budget processing, "smart finance" service can handle the accounting vouchers according to the procedures. To analyze the financial operation data of the previous 3–5 years, a variety of budget models is combined to make a preliminary calculation of the capital flow of the future economic business. Then, the key indicators of the current market environment and policy situation changes is inputted into the system based on various factors to make a reasonable judgment on the cash inflow and outflow of the unit, capital demand, business prospects, and asset status. On this basis, the financial budget is drafted. After a review of the budget unit based on the opinions and suggestions of the budget subject, the next module is transferred for execution.

4.3. Intelligent Treatment of Hospital Accounting. Cost management accounting is one of the key links in the financial management, "financial" system has intelligent cost accounting and management module, and it confirms the current profit and loss accounting cost and cost responsibility center in time after the economic business occurs according to the cost accounting rules of the cost entity. If it cannot be confirmed, it can predict according to the past practice and conduct liquidation after the end of the accounting cycle. The cost management module mainly ensures that the accounting items can cover all links of the unit's economic business. In cost control, it divides and counts the costs of independent economic departments, and analyzes the actual economic benefits of independent financial units through cost analysis models, structural analysis, and trend prediction methods. The cost control intelligence module can prepare analysis reports for the management to use when adjusting the organizational management structure and business form.

5. Conclusion

The "smart" financial service model in the era of artificial intelligence has played a profound and revolutionary role in the reform of financial operation mechanism. It can strengthen the integration of modern intelligent technology

and management methods, strengthen the training of financial business talents, make them adapt to the financial management mechanism under the background of artificial intelligence, and deepen the “smart” service mode to better play the positive role of financial management.

Data Availability

Data are available upon request from the corresponding author.

Conflicts of Interest


The author declares no conflicts of interest.

References

- [1] L. G. Sui and J. Y. Chen, “Based on the Internet of things and cloud computing technologies to develop smart finance,” *Journal of Changchun Finance College*, vol. 11, no. 16, pp. 40–41, 2013.
- [2] L. Li, B. Lei, and C. Mao, “Digital twin in smart manufacturing,” *Journal of Industrial Information Integration*, vol. 26, no. 9, Article ID 100289, 2022.
- [3] Routledge, “Infrastructure planning and finance: a smart and Sustainable Guide for Local Practitioners,” *Reprints and Permissions*, vol. 14, no. 02, pp. 25–26, 2014.
- [4] L. Li, T. Qu, Y. Liu et al., “Sustainability assessment of intelligent manufacturing supported by digital twin,” *IEEE Access*, vol. 8, pp. 174988–175008, 2020.
- [5] N. . Hu, “Discussion of shanghai smart finance development,” *Journal of Shanghai Fisheries University*, vol. 3, no. 14, pp. 18–23, 2011.
- [6] M. Fan Ea -Ivanovici and M. C. Pan, “Crowdfunding as a smart finance and management tool: institutional determinants and well-being considerations,” *Evidence from Four Central and Eastern European Countries*, vol. 06, no. 14, pp. 33–36, 2022.
- [7] I. C. Focus, “IIASA. Carbon market and climate finance for climate-smart agriculture in developing countries,” *Climate Focus Inc*, vol. 12, no. 02, p. 152, 2011.
- [8] N. Hu and Y. Wang, “Analysis of building cloud-based smart finance platform of Shanghai,” in *Proceedings of the International Conference on Educational Technology and Management Science*, vol. 14, no. 06, p. 25, East Java Indonesia, October 2019.
- [9] L. E. Lang, “Financial points of entry. Sovereign wealth funds: hidden security threat or smart finance?” *Georgetown University*, vol. 08, no. 02, pp. 11–15, 2011.
- [10] T. Hayes, “Smart finance: claiming GST paid on water termination fees,” *Irrigation Australia the Official Journal of Irrigation Australia*, vol. 26, no. 1, pp. 1–5, 2011.
- [11] S. Huston, R. Rahimzad, and A. Parsa, *SmartSURFinance HustonReyhanehParsa 23April2014*, vol. 20, no. 3, pp. 56–59, 2015.
- [12] S. Huston, R. Rahimzad, and A. Parsa, “Smart’ finance for sustainable urban regeneration,” *Social Science Electronic Publishing*, vol. 6, no. 2, pp. 10–14, 2014.
- [13] D. Setyadi, H. E. Soegiarto, and I. N. Latif, “Sistem dan prosedur penjualan kredit sepeda motor pada Pt,” *Smart Multi Finance Kecamatan Melak Kabupaten Kutai Barat*, vol. 17, no. 21, p. 324, 2016.
- [14] A. Glossbrenner, “Smart guide to managing personal finance,” *John Wiley & Sons*, vol. 20, no. 08, pp. 201–205, New York, NY, USA, 2011.
- [15] S. L. Shofner, “The impacts of smart growth on municipal finance: perspectives of city planning directors,” *Across Texas*, vol. 24, no. 12, p. 241, 2000.
- [16] K. Jas Per and H. K. Sung, “CSO-state partnerships and social finance: smart social capital and shared incentives towards public-private partnership efficiency using social impact bonds,” *Social Science Electronic Publishing*, vol. 13, no. 2, pp. 102–103, 2012.
- [17] R. E. Lang, J. Lefurgy, and S. Hornburg, “From wall street to your street: new solutions for,” *Smart Growth Finance*, vol. 21, no. 5, p. 102, 2010.
- [18] J. Peng, “The study of the development and application situation of smart finance,” in *Proceedings of the 2020 5th International Conference on Humanities Science and Society Development (ICHSSD 2020)*, vol. 20, no. 14, pp. 18–20, 2020.
- [19] P. Guo, “Linq county build fiscal big data application platform and contribute to the construction of “smart finance”,” *Fiscal Science*, vol. 22, no. 14, pp. 56–58, 2019.
- [20] M. Witthaut, H. Deeken, and P. Sprenger, “Smart objects and smart finance for supply chain management,” *Logistics Journal nicht-referierte Veröffentlichungen*, vol. 44, no. 25, p. 132, 2017.

Research Article

m6A-Related lncRNAs Predict Overall Survival of Patients and Regulate the Tumor Immune Microenvironment in Osteosarcoma

Yikang Bi,^{1,2} Depeng Meng,³ Ma Wan,^{1,2} Ning Xu,^{1,2} Yafeng Xu,^{1,2} Kaixuan Yuan,^{1,2} Pengcheng Liu,^{1,2} Hao Fang,^{1,2} Hai Hu,^{1,2} and Shenghui Lan^{1,2} 

¹Department of Orthopaedics, The Eighth People's Hospital, Jiangsu University, Shanghai 200235, China

²Department of Orthopaedics, Xuhui Branch of The Sixth People's Hospital, Shanghai Jiao Tong University, Shanghai 200233, China

³Department of Orthopedics, Changzheng Hospital, Naval Military Medical University, Shanghai 200074, China

Correspondence should be addressed to Shenghui Lan; 17011010207@stu.suse.edu.cn

Received 1 June 2022; Revised 20 June 2022; Accepted 7 July 2022; Published 8 August 2022

Academic Editor: Dong Chen

Copyright © 2022 Yikang Bi et al. This is an open access article distributed under the Creative Commons Attribution License, which permits unrestricted use, distribution, and reproduction in any medium, provided the original work is properly cited.

Background. m6A-related lncRNAs have demonstrated great potential tumor diagnostic and therapeutic targets. The goal of this work was to find m6A-regulated lncRNAs in osteosarcoma patients. **Method.** The Cancer Genome Atlas (TCGA) database was used to retrieve RNA sequencing and medical information from osteosarcoma sufferers. The Pearson's correlation test was used to identify the m6A-related lncRNAs. A risk model was built using univariate and multivariable Cox regression analysis. Kaplan–Meier survival analysis and receiver functional requirements were used to assess the risk model's performance (ROC). By using the CIBERSORT method, the associations between the relative risks and different immune cell infiltration were investigated. Lastly, the bioactivities of high-risk and low-risk subgroups were investigated using Gene Set Enrichment Analysis (GSEA). **Result.** A total of 531 m6A-related lncRNAs were obtained from TCGA. Seven lncRNAs have demonstrated prognostic values. A total of 88 OS patients were separated into cluster 1, cluster 2, and cluster 3. The overall survival rate of OS patients in cluster 3 was more favorable than that of those in cluster 1 and cluster 2. The average Stromal score was much higher in cluster 1 than in cluster 2 and cluster 3 ($P < 0.05$). The expression levels of lncRNAs used in the construction of the risk prediction model in the high-risk group were generally lower than those in the low-risk group. Analysis of patient survival indicated that the survival of the low-risk group was higher than that of the high-risk group ($P < 0.0001$) and the area under the curve (AUC) of the ROC curve was 0.719. Using the CIBERSORT algorithm, the results revealed that Macrophages M0, Macrophages M2, and T cells CD4 memory resting accounted for a large proportion of immune cell infiltration. By GSEA analysis, our results implied that the high-risk group was mainly involved in unfolded protein response, DNA repair signaling, and epithelial-mesenchymal transition signaling pathway and glycolysis pathway; meanwhile, the low-risk group was mainly involved in estrogen response early and KRAS signaling pathway. **Conclusion.** Our investigation showed that m6A-related lncRNAs remained tightly connected to the immunological microenvironment of osteosarcoma tumors, potentially influencing carcinogenesis and development. The immune microenvironment and immune-related biochemical pathways can be changed by regulating the transcription of M6A modulators or lncRNAs. In addition, we looked for risk-related signaling of m6A-related lncRNAs in osteosarcomas and built and validated the risk prediction system. The findings of our current analysis will facilitate the assessment of outcomes and the development of immunotherapies for sufferers of osteosarcomas.

1. Introduction

Osteosarcoma (also known as osteogenic sarcoma or simply bone cancer) is the most frequent kind of bone cancer [1]. It is a type of invasive malignant neoplasm that develops from

primitive altered cells of mesenchymal origin (and hence is a sarcoma) and demonstrates osteoblastic differentiating and creates cancerous osteoid [1]. The most frequent histological kind of primary bone sarcoma is osteosarcoma [2]. It is particularly common among adolescents and young adults [3].

Despite the positive results of comprehensive surgical resection along with chemotherapy and radiotherapy, roughly 40–50 percent of patients develop lung dissemination [4]. Patients with lung metastatic tumors had a five-year life expectancy of only 28% [5]. Therefore, searching for new treatment targets and prognostic biomarkers is critical.

N6-methyladenosine (m6A) is the methylated adenosine that occurs at the N6 site and it is prevalently an epigenetic alteration in mRNA and noncoding RNAs (ncRNAs) [6]. The process of m6A is considered to be dynamic and reversible. Similar to other epigenetic regulatory mechanisms, the bioactivities of m6A are coordinated by “writer,” “reader,” and “eraser” [7]. The compound of m6A-writer acts as a methylase, allowing m6A to be installed. The m6A alteration is then identified by m6A-associated proteins, which are also called as readers. The erasers are demethylases that are in charge of eliminating the m6A alterations. Several investigations have shown that m6A alterations control carcinogenesis and progression [8]. The relevance of m6A variations in malignancy prediction is becoming clear.

Long noncoding RNA (lncRNA) is RNA with a transcriptome sequence of more than 200 nucleotides that are not transcribed into proteins [9]. lncRNA is involved in a number of physiological systems in cells, including cell growth and differentiation [10]. lncRNA influences gene transcriptions at three different sides: epigenetic regulation, transcription, and posttranscription. The abnormal pattern of lncRNA is linked to cancerous aggressiveness as well. Recent evidence has proved that lncRNA acts as tumorigenesis or repressors by participating in numerous signaling pathways [11]. For instance, SRY-box transcription factor 2 (SOX2) promotes development in colorectal cancer (CRC) by catalyzing methyl with methyltransferase-like protein 3 (METTL3) [12], whereas BCL2 interacting protein 3 (BNIP3) promotes cancer progression in breast cancer by catalyzing demethylation with FTO (fat mass and obesity-associated protein) [13]. Furthermore, lncRNAs have the potential to be used as prognosis markers in various types of tumors, such as prostate, breast, and liver cancers [14]. Recently, there has been a growing interest in the research framework between m6A and lncRNAs. Their regulating complex is implicated in tumor growth, migration, and metastasis in a variety of malignancies, giving new targets for cancer diagnostics and treatment. lncRNAs and m6A have been shown to have critical roles in controlling cancer bioactivity, but the mutual regulation mechanism between them is unknown. As a result, it is critical to investigate the possible biochemical reaction of these unregulated m6A-related lncRNAs in osteosarcoma. Therefore, determining the associations between the alterations of m6A-related lncRNAs and the courses of osteosarcoma may help to find biomarkers that can be considered predictive and prognostic markers.

2. Materials and Methods

2.1. The Process of Data Acquisition. The raw data and corresponding clinical information were downloaded from Genomic Data Commons of the TCGA

database (<https://xenabrowser.net/datapages/?cohort=GDC%20TARGET-OS&removeHub=https%3A%2F%2Fxcena.treehouse.gi.ucsc.edu%3A443>). These data contained three files of clinical data (TARGET-OS.clinical.tsv.gz), expression profiles (TARGET-OS.htseq_counts.tsv.gz), and survival information (TARGET-OS.survival.tsv). Clinical data of OS patients did not include normal controls; however, the data contained a variety of other clinical information (such as metastases, tumor grade, age, and gender). According to previous studies, these cases were grouped into two groups: metastases and nonmetastases, and the sample size was balanced between the two groups [15]. The available literature yielded a total of 20 m6A regulatory factors, including WTAP, METTL3, METTL14, METTL16, KIAA1429, ZC3H13, RBM15, HNRNPA2B1, IGF2BP1, IGF2BP2, IGF2BP3, YTHDC1, YTHDC2, FMR1, LRPPRC, YTHDF1, YTHDF2, YTHDF3, ALKBH5, and FTO.

2.2. Screening of Prognostic Genes. In accordance with the TCGA naming convention, all samples ending in 01A were OS samples, including 88 cases in total in our study. Gene IDs for TCGA-OS expression profiles were converted using the package (org.Hs.eg.db), obtaining a total of 34446 gene symbols. When there was a single symbol corresponding to multiple IDs, the expression profiles of identical gene symbols were merged by the maximum value. The GRCh38 annotation file was downloaded from the GENCODE website, which was used to differentiate the types of genes for TCGA-STAD expression profiles. The expression profiles of 20 m6A-related genes were extracted and box-line plots were plotted using the ggplot2 package. Correlation analysis was conducted on the expression profiles of all samples using the rcorr function of the Hmisc package. The correlation cor values and p values of the 10 m6A-related genes with lncRNA genes were obtained using Pearson analysis (p value < 0.05, cor Filter > 0.2) [16]. A total of 531 m6A-related lncRNAs were obtained.

2.3. Cox Regression Analysis. Clinical data packages for survival time and survival status were combined with 531 lncRNA gene expression profiles associated with m6A. One-way Cox regression analysis was performed using the R package survivor (p value < 0.05). Correlation analysis was carried out using the cor.test of the stats package (p value < 0.05).

2.4. Consistent Clustering Analysis. The expression profiles of seven lncRNA prognostic genes associated with disease risk were analyzed by consistent clustering using the R package consensus cluster plus, setting the number of clusters to 2.

2.5. Prognosis and the Immune Microenvironment in Coherent Clustering. The expression profiles of 9 prognostic genes were mapped using the pheatmap package, plus additional grouping tags (such as age and gender), and divided into Cluster 1, Cluster 2, and Cluster 3. Survival curve analysis

was performed with the `survfit` of the `surv.` package and plotted with the `ggsurvplot` function of the `survminer` package, grouped as Cluster1, Cluster2, and Cluster3. Using the CIBERSORT algorithm, immune infiltration of patient tissue is identified by 22 different types of immune cells. LM22 feature matrix file with CIBERSORT algorithm (1000 permutations) was applied to compare the immunocyte infiltration scores of Cluster1, Cluster2, and Cluster3.

Using the ESTIMATE package, immune scoring was calculated for TCGA-OS expression profiles, including ESTIMATE score, Immune score, Stromal score, and Tumor Purity. The box plots were drawn using the `ggplot2` package, grouped as Cluster1, Cluster2, and Cluster3. The significance of differences between groups was calculated by *T* test.

2.6. Constructing the Prognosis Diagnosis Model of TCGA-OS. Risk scores were calculated for the seven lncRNAs screened that were associated with OS risks. The calculation formula is as follows:

$$\text{Risk score} = \text{coef}(\text{lncRNA}_n) \times \text{expr}(\text{lncRNA}_n), \quad (1)$$

where $\text{coef}(\text{lncRNA}_n)$ represents the regression coefficient of lncRNA.

Based on this formula, the risk score of each group could be derived [17]. The median risk score was used to classify the OS samples containing survival information into a high-risk group and a low-risk group. The risk score distribution of the sample was plotted using the `ggplot2` package. The samples were divided into high-risk and low-risk groups. The survival curves were analyzed using the `survfit` function of the `survivor` package and plotted using the `ggsurvplot` function of the `survminer` package.

2.7. Immune Infiltration Analysis. The LM22 feature matrix file with the CIBERSORT algorithm (1000 permutations) was used to compare the immunocyte infiltration scores of the high-risk group and low-risk group. The risk core risk scores of Cluster1, Cluster2, and Cluster3 were compared, and differences between groups were calculated using a *t*-test. The box plot was obtained by using the `ggplot2` package.

2.8. Correlation of Immune Infiltration with lncRNA. The correlation between hub gene expression and immune infiltrating cells was calculated by the `cor.test` function of the `psych` package (spearman algorithm). Heatmaps were drawn with the `pheatmap` package to show the correlation heatmaps ($***P < 0.001$, $**P < 0.01$, and $*P < 0.05$). The colors from blue to red indicate a correlation *cor*-value from small to large.

2.9. Gene Set Enrichment Analysis (GSEA). GSEA analysis was performed using GSEA v4.2.2. Hallmarks (h.all.v7.5.1.symbols.gmt) were used to identify and illustrate specific signaling pathways.

3. Results

3.1. The m6A-Related Differential Genes and Identification of m6A-Related lncRNAs in OS. 88 samples of OS were derived from the TCGA database. The samples were divided into two subgroups: metastases (22 specimens) and nonmetastases (65 specimens). 3039 lncRNAs and 19135 mRNAs were obtained in total. 17,249 differential genes were found using the Limma package differential analysis (p value < 0.05). These differential genes were intersected with 20 m6A-related genes to obtain 10 m6A-related differential genes. These ten m6A-related differential genes included WTAP, METTL14, RBM15, IGF2BP1, IGF2BP2, IGF2BP3, YTHDC2, YTHDF2, YTHDF3, and FTO.

28 lncRNA prognostic genes associated with the risk of OS were found in total. Multifactor Cox regression analysis was continued for 28 lncRNAs obtained by single-factor regression using the R package SURVIVAL (p value < 0.05) [17]. A total of 7 lncRNA prognostic genes were screened for association with prognostic significance (Table 1). The expression profiles of 10 differential genes regulated by m6A and 7 lncRNA prognostic genes associated with risk factors were extracted separately. The correlation between m6A-related genes and lncRNAs is shown in Figure 1.

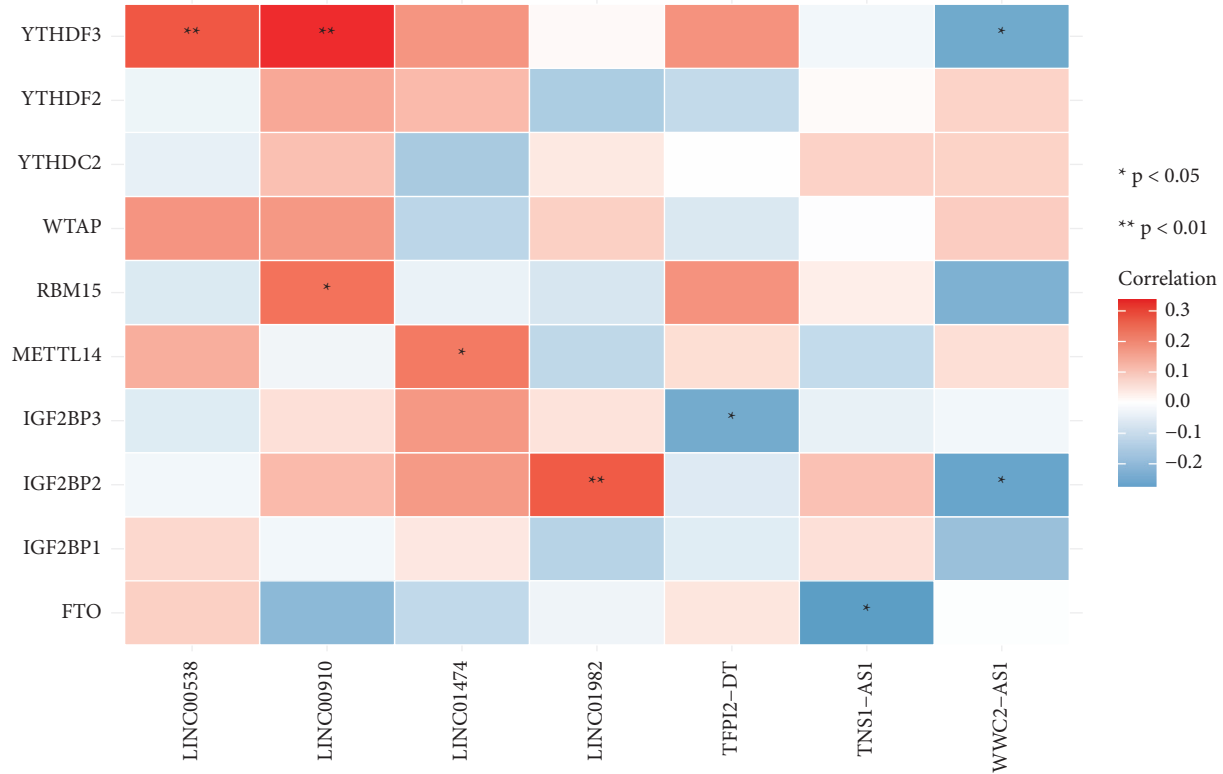
3.2. Consensus Clustering Categorized OS Patients according to m6A-Related Prognostic lncRNAs. Following the transcription of m6A-related predictive lncRNAs, consensus clustering was also used to divide OS patients into different clusters (Figure 2). Due to the similarities demonstrated by the expression profiles of m6A-related predictive lncRNAs, $k=3$ was discovered to be the best clustering consistency from $k=2$ to 9 (Figure 2(a)). A total of 88 OS patients were separated into cluster 1, cluster 2, and cluster 3. The overall survival rate of OS patients in cluster 3 was more favorable than that of those in cluster 1 and cluster 2 (Figure 2(b), $p=0.00081$).

3.3. Consensus Clustering Linked to Immune Infiltration. To explore the role of m6A-related prognostic lncRNAs in the osteosarcoma immune microenvironment, we then analyzed the difference in the immune score and immune cell infiltration level among cluster 1, cluster 2, and cluster 3. The average Stromal score was much higher in cluster 1 than those in cluster 2 and cluster 3 (Figure 3) ($P < 0.05$).

3.4. Risk Signaling of m6A-Related lncRNAs and Risk Prediction Model Showed Prognostic Value in Osteosarcoma. After calculating the risk scores of individual patients, the cases were divided into a high-risk group and a low-risk group based on the median risk score (Figure 4(a)). The heatmap showed changes in the risk score and expression levels of lncRNAs. The expression levels of lncRNAs used in the construction of the risk prediction model in the high-risk group were generally lower than those in the low-risk group (Figure 4(e)). Analysis of patient survival indicated that the survival of the low-risk group was higher than that of the

TABLE 1: Seven m6A-related lncRNAs with prognostic significance in osteosarcoma identified by Cox regression analysis.

lncRNA	Coefficient	HR (95% CI)	HR95%L	HR95%H	<i>p</i>
TNS1-AS1	-0.978	0.376 (0.191-0.74)	0.191	0.74	0.005
WWC2-AS1	1.095	2.989 (1.319-6.775)	1.319	6.775	0.009
TFPI2-DT	-1.124	0.325 (0.141-0.748)	0.141	0.748	0.008
LINC01474	-1.756	0.173 (0.049-0.609)	0.049	0.609	0.006
LINC00910	5.869	354.031 (3.782-33142.623)	3.782	33142.623	0.011
LINC01982	-0.972	0.378 (0.146-0.98)	0.146	0.98	0.045
LINC00538	1.201	3.324 (1.158-9.539)	1.158	9.539	0.026

FIGURE 1: The correlation between 10 m6A-related genes and 7 lncRNA prognostic genes. * $P < 0.05$; ** $P < 0.01$.

high-risk group ($P < 0.0001$, Figure 4(d)). The area under the curve (AUC) of the ROC curve was 0.719, indicating that the model showed medium accuracy in predicting the prognosis of osteosarcoma patients (Figure 4(e)). Our results showed that m6A-related lncRNAs had prognostic value and that the risk prediction model showed satisfactory performance in predicting the prognosis of patients with osteosarcoma (Figure 4).

3.5. Correlations between Immune Infiltration and m6A-Related lncRNAs in Osteosarcoma. The infiltration of 22 immune cell types in osteosarcoma samples was further analyzed using the CIBERSORT algorithm. The results revealed that Macrophages M0, Macrophages M2, and T cells CD4 memory resting accounted for a large proportion of immune cell infiltration (Figure 5). However, there were no significant differences in the proportion of most of the infiltrated immune cell types between the high- and low-risk

groups. The correlation coefficients between 22 types of immune cells are depicted in Table 2 and Figure 6.

3.6. The m6A-Related lncRNAs Subgroups Were Associated with Biological Characteristics of Osteosarcoma. Next, we analyzed differences in the biological responses of the subgroups generated using consensus clustering in order to further explore the relationships between m6A-related lncRNAs clustering subgroups and osteosarcoma biological characteristics. GSEA was used to explore the main KEGG signaling pathways in the two subgroups. Our results showed that the high-risk group was mainly involved in unfolded protein response, DNA repair signaling, and epithelial-mesenchymal transition signaling pathway and glycolysis pathway (Figures 7(a)–7(d)), which are related to the initiation of metastasis in cancer progression [18–20]. The low-risk group was mainly involved in estrogen response early and KRAS signaling pathway (Figures 7(e) and

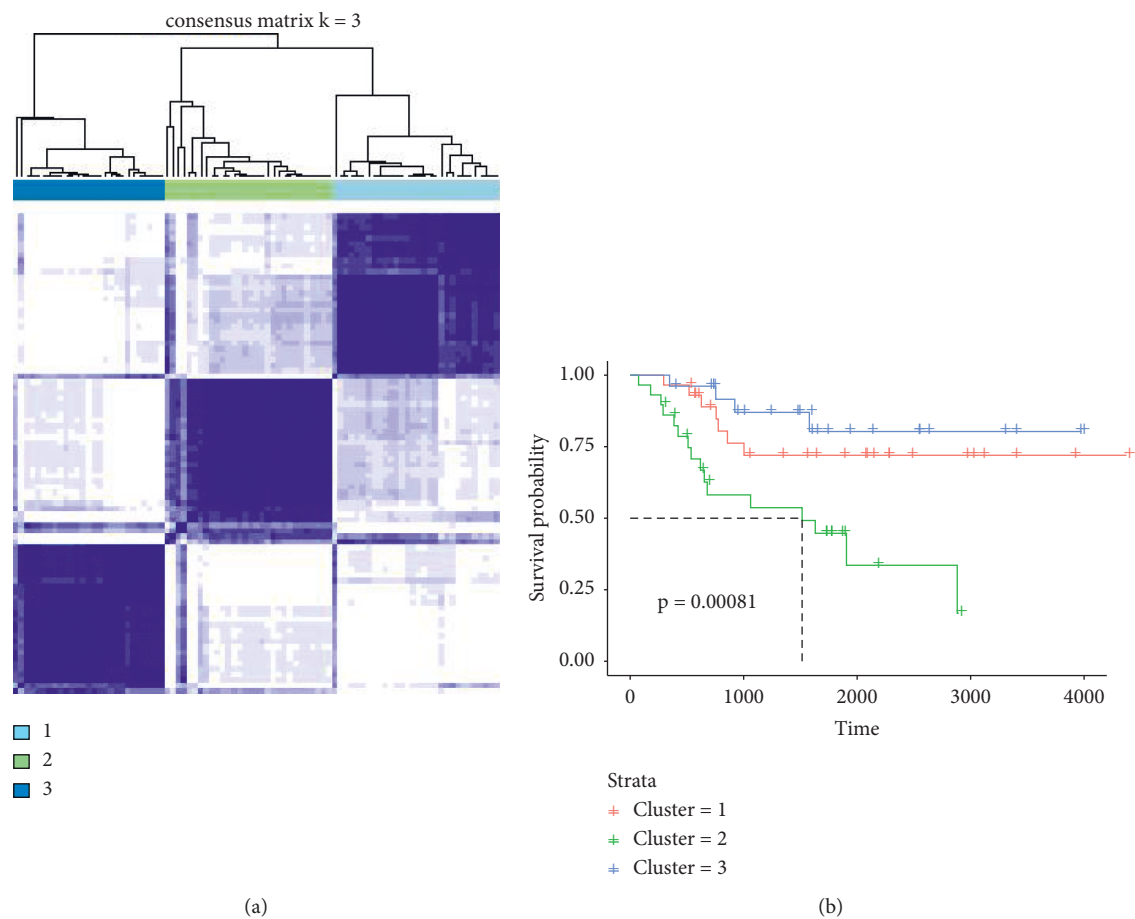


FIGURE 2: Continued.

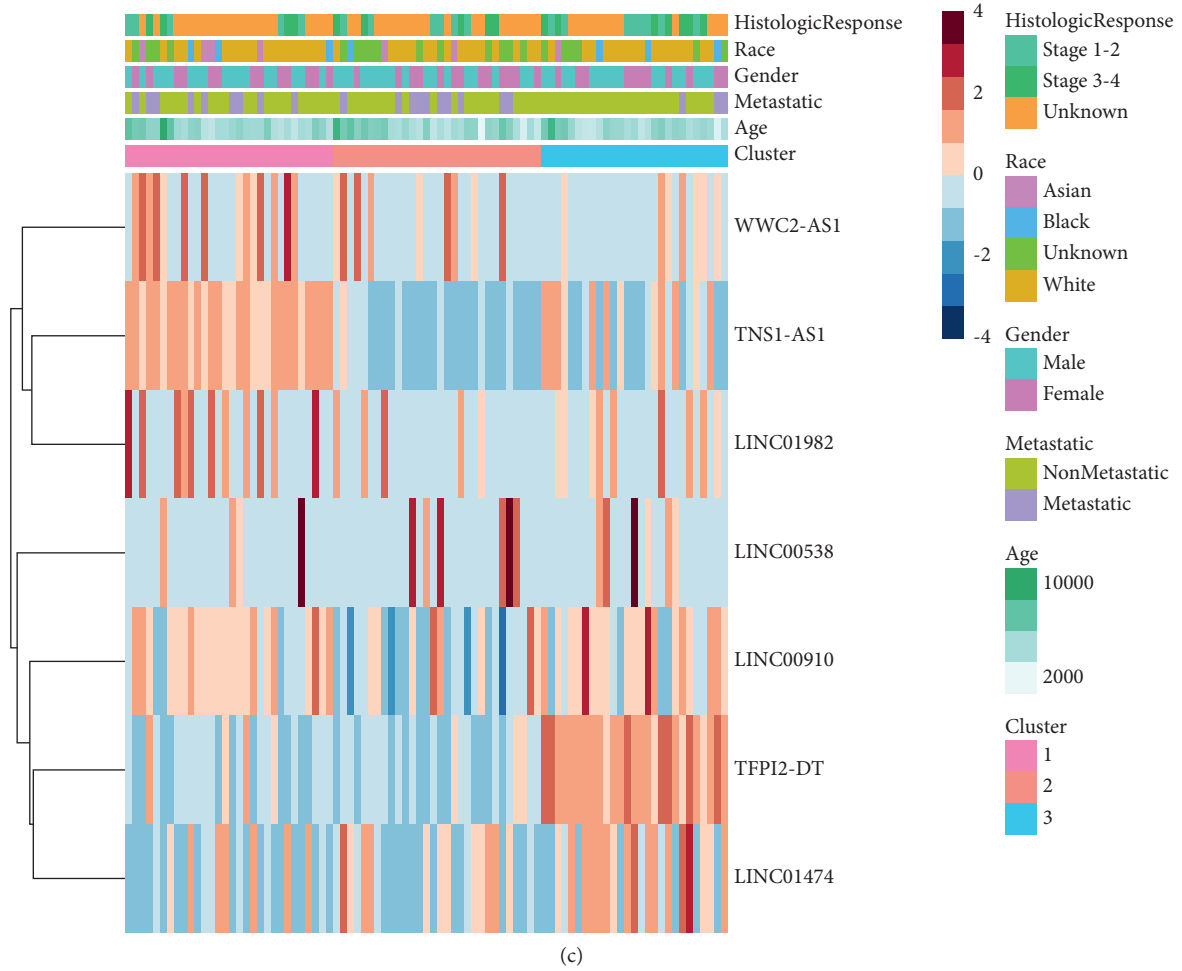


FIGURE 2: Consensus clustering of m6A-related prognostic lncRNAs. (a) TCGA osteosarcoma cohorts were grouped into three clusters according to the consensus clustering matrix ($k = 3$). (b) Overall survival analysis revealed a better overall survival of osteosarcoma patients in cluster 3 than those in cluster 1 and cluster 2. (c) The heatmap of the 3 clusters along with general information of patients.

7(f)), which are important for oncogene of osteosarcoma [21, 22]. These results indicated that there were differences in biological characteristics between high-risk and low-risk groups, which affected tumorigenesis and progression of osteosarcoma and survival of osteosarcoma patients.

4. Discussion

With the advancement of high-throughput sequencing methods and their widespread use in oncology, disclosing epigenomic irregularities during tumor onset and progression opens the door to the proof of identity of targeted therapies and predictive biomarkers in a range of tumors [23]. Current attention has been focused on the comprehensive detection of high sequencing results using publicly available databases, which has resulted in several major findings in the diagnosis and therapy of malignancies [17, 24]. Conversely, the involvement of m6A regulators in lncRNA deregulation in human cancer is unknown. Few research studies investigated the associations between m6A alterations and lncRNA-dependent osteosarcoma.

To elucidate the underlying biological mechanisms of the m6A-related lncRNA profile, we identified genes that were expressed differently between the metastases and non-metastases groups. A total of 7 lncRNA prognostic genes were screened for association with prognostic significance in osteosarcoma patients (including TNS1-AS1, WWC2-AS1, TFPI2-DT, LINC01474, LINC00910, LINC01982, and LINC00538). We did a clustering analysis based on the transcriptome of m6A-related predictive lncRNAs to further investigate the association between m6A-related lncRNAs and the clinical and pathological and biological aspects of AML. This analysis produced three subgroups, which were labeled as cluster 1, cluster 2, and cluster 3. The overall survival rate of OS patients in cluster 3 was more favorable than that of those in cluster 1 and cluster 2.

In addition, the samples were separated into two groups according to the average risk score: high-risk and low-risk groups after computing the risk scores of patient characteristics. GSEA suggested that the high-risk group was mostly engaged in unfolded protein response, DNA repair signaling, epithelial-mesenchymal transition signaling, and glycolysis signaling pathways. The low-risk group was

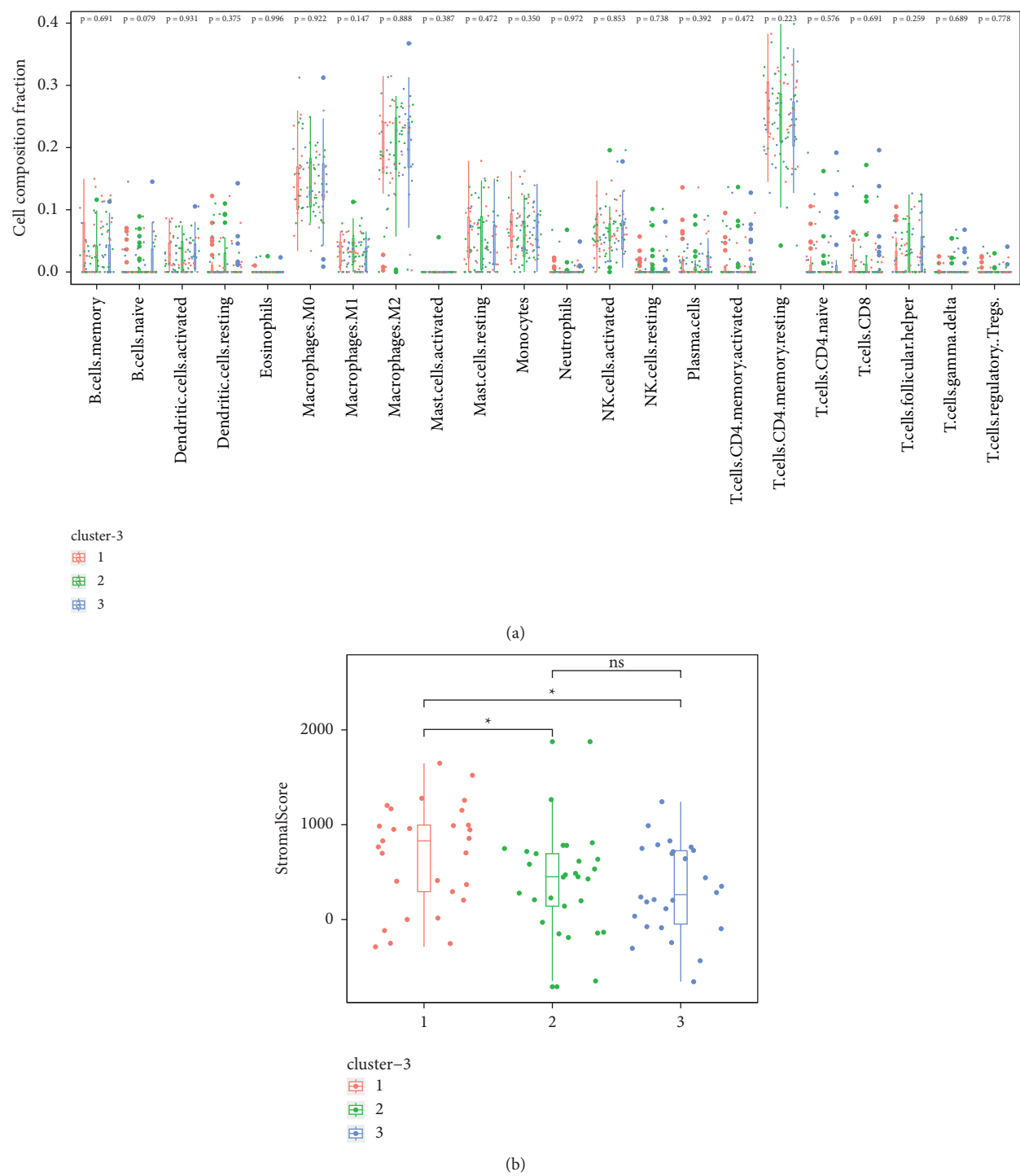


FIGURE 3: Continued.

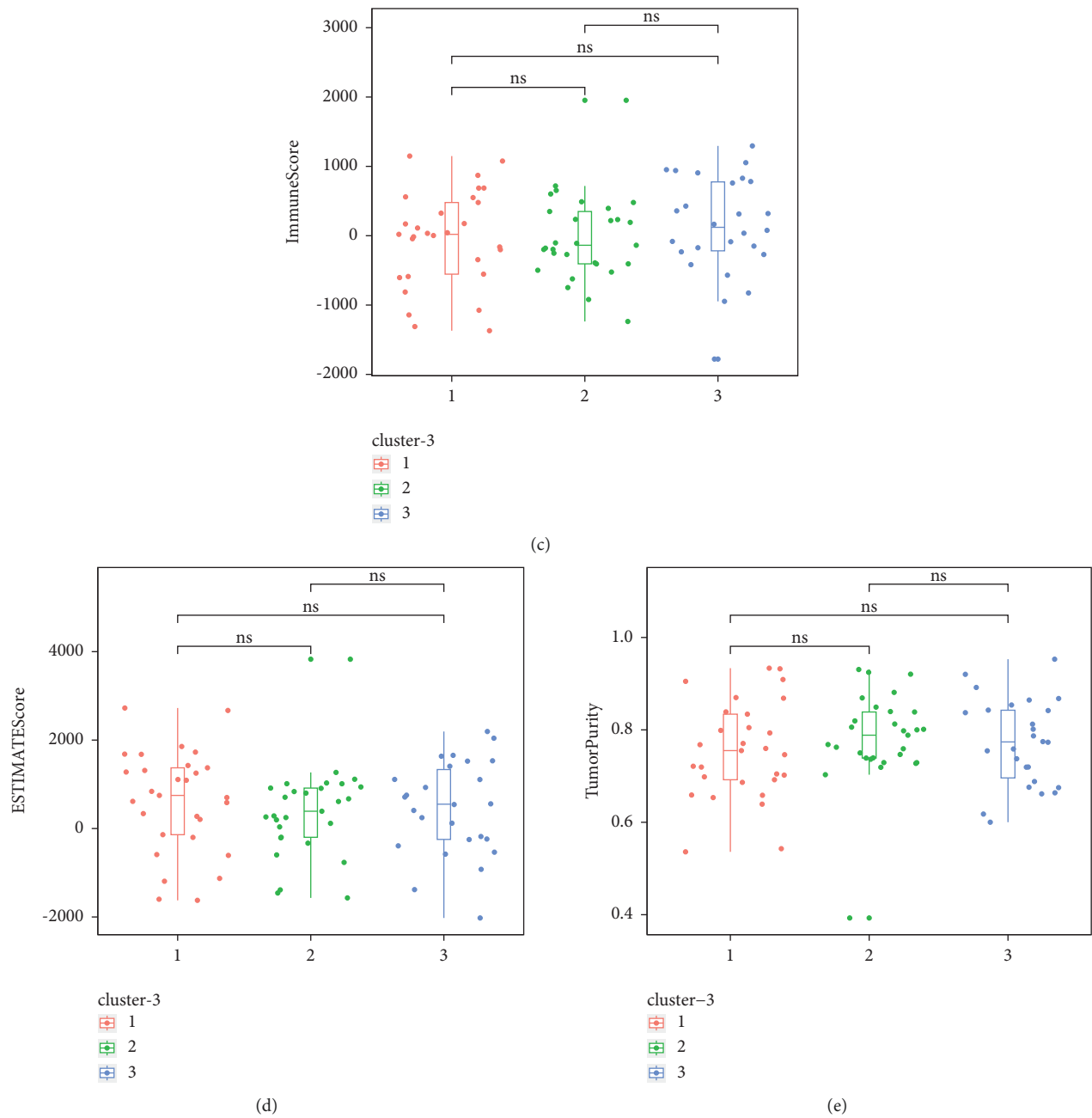
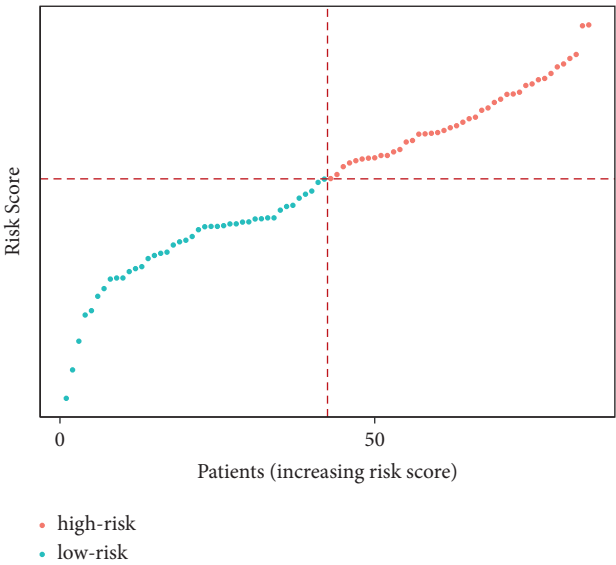
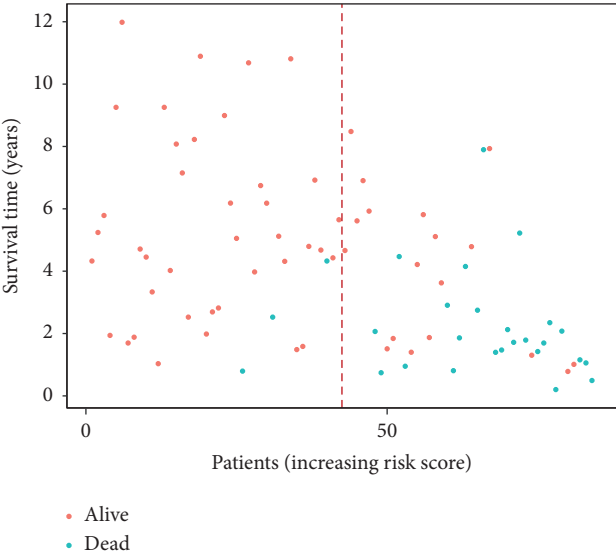


FIGURE 3: (a) The comparison of the immune score between the low-risk and high-risk groups ($p > 0.05$). (b–e) Comparison of immune score: (b) Stromal score, (c) Immune score, (d) ESTIMATE Score, and (e) Tumor Purity.



(a)



(b)

FIGURE 4: Continued.

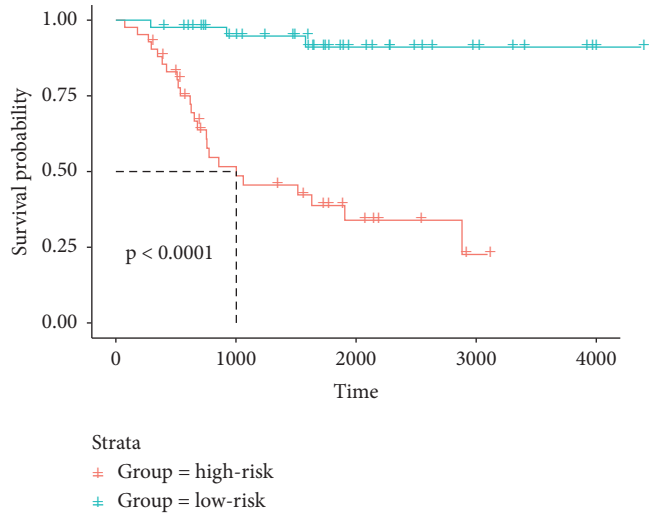
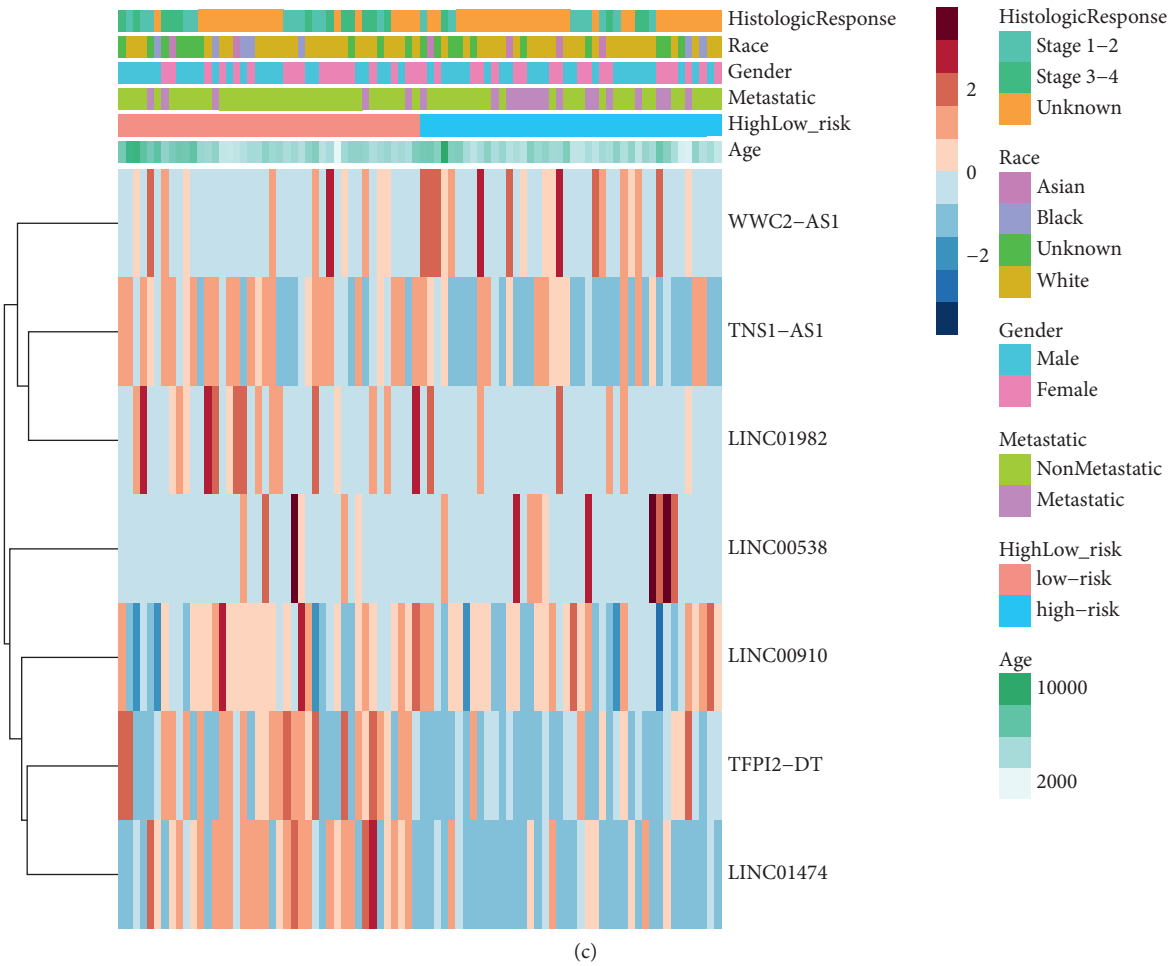


FIGURE 4: Continued.

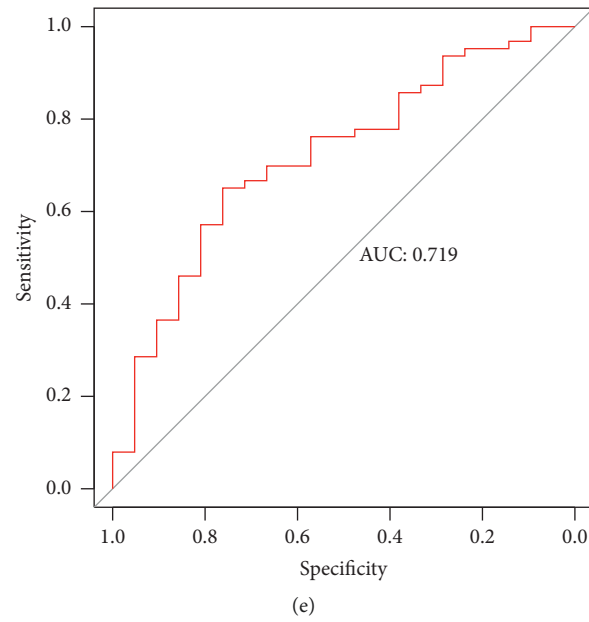


FIGURE 4: (a) The risk score distribution; (b) survival time scatter diagram; (c) clinical and pathological characteristics and varied lncRNA expression patterns in high- and low groups are depicted in a heatmap; (d) the risks model's Kaplan–Meier survival line; (e) ROC curve analysis.

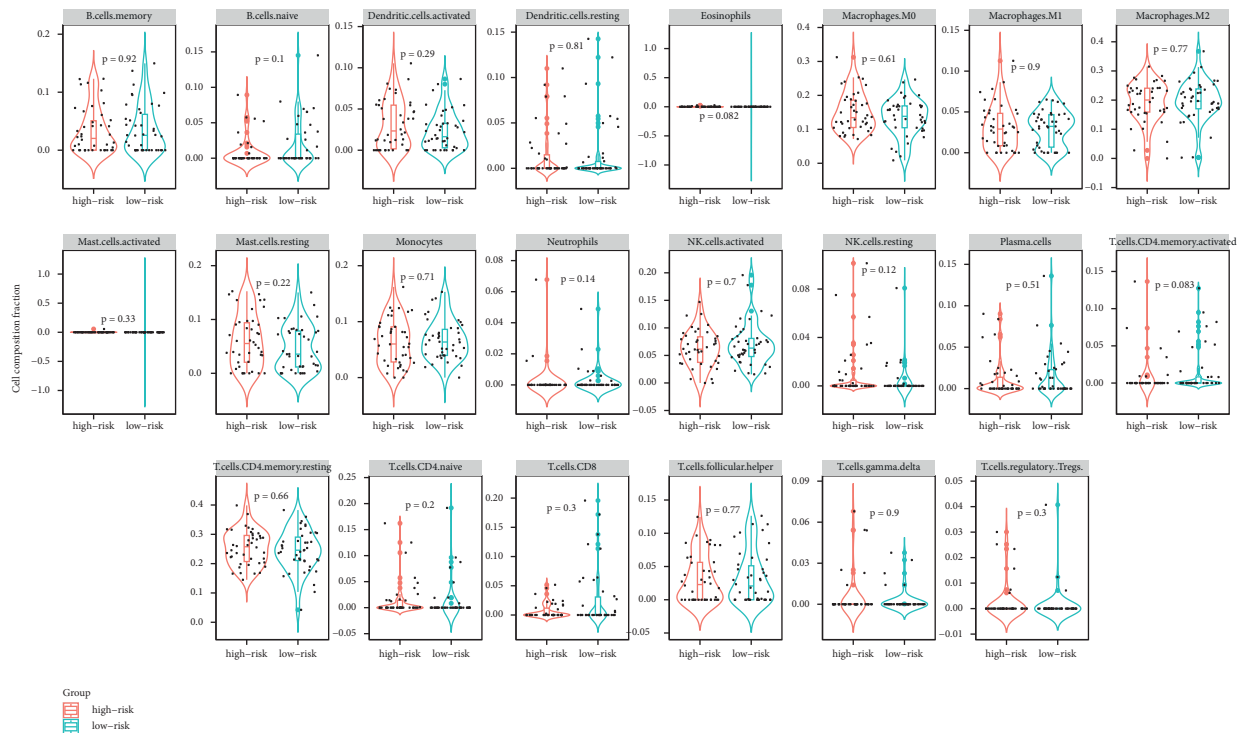


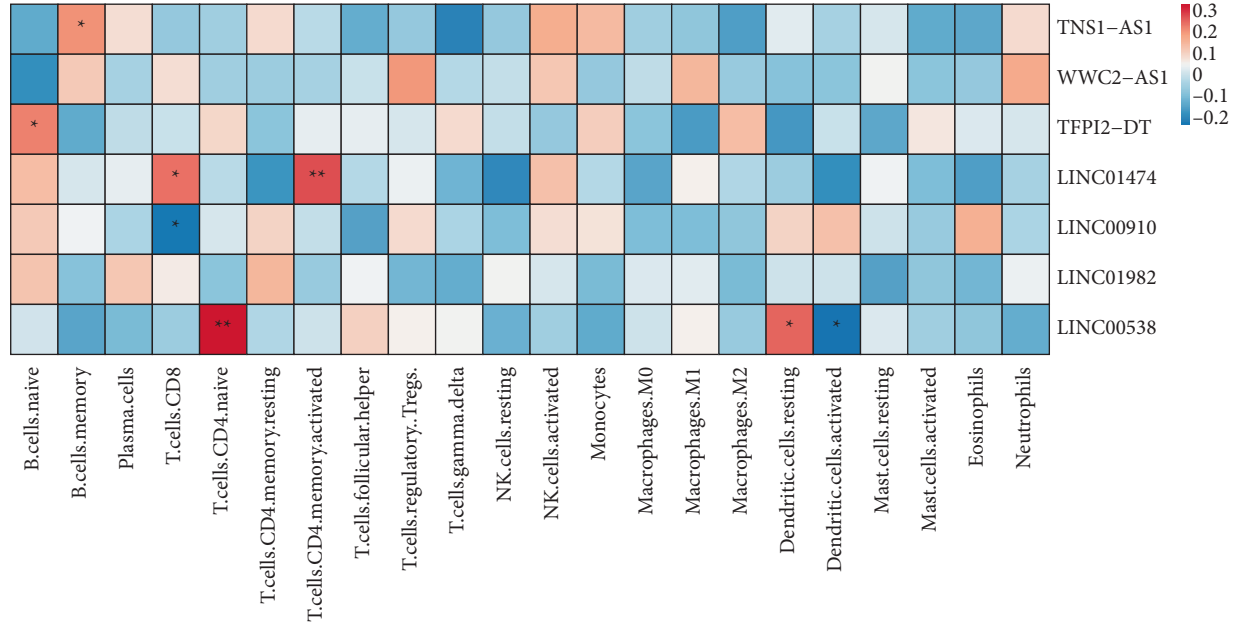
FIGURE 5: The violin plot of 22 tumor-infiltrating immune cell types in low- and high-risk groups. The infiltration of 22 immune cell types in osteosarcoma was analyzed by the CIBERSORT algorithm.

mainly involved in estrogen response early and KRAS signaling pathway. The low-risk group had a better overall survival rate than the high-risk group did. The ROC curve's

area under the curve (AUC) was 0.719, meaning that the model was somewhat capable of predicting the prognosis of osteosarcoma patients. According to a prior study, the active

TABLE 2: The correlations between immune infiltration and m6A-related lncRNAs.

lncRNA	Immune process	Positive (+)/negative (-) correlation	<i>r</i>	<i>P</i> value
TNS1-AS1	B cell memory	+	0.21	0.048
TFPI2-DT	B cells naive	+	0.23	0.034
LINC01474	T cells CD8	+	0.25	0.020
LINC01474	T cells CD4 memory activated	+		0.009
LINC00910	T cells CD8	-	-0.21	0.049
LINC00538	T cells CD4 naive	+	0.34	0.001
LINC00538	Dendritic cells resting	+	0.25	0.017
LINC00538	Dendritic cells activated	-	-0.23	0.035

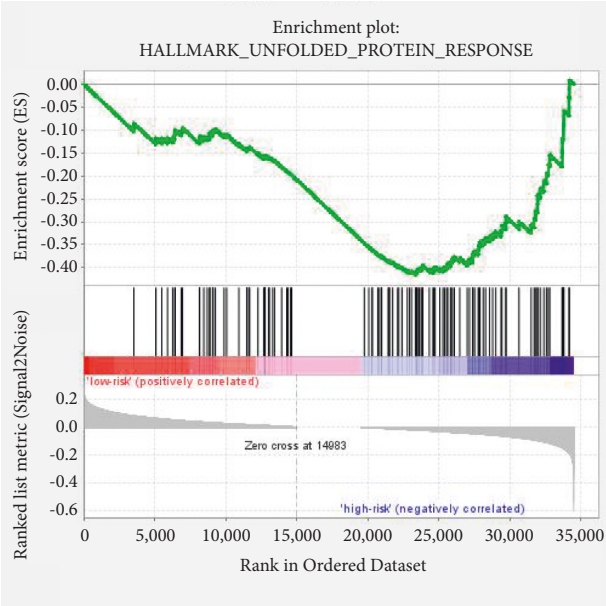
FIGURE 6: The correlations between immune infiltration and m6A-related lncRNAs. * $P < 0.05$; ** $P < 0.01$.

unfolded protein response was a key biochemical characteristic of osteosarcoma [25]. A large amount of evidence about the involvement of DNA damage response in osteosarcoma formation, survival, and treatments was assembled in a review paper [26].

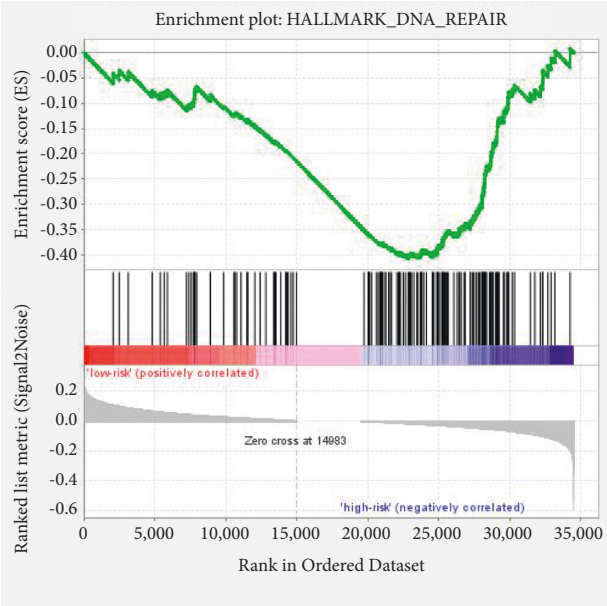
Diverse immune cells and released substances make up the immunological microenvironment [27]. Tumor cell invasion, immunological capabilities, and the activation of targeted therapies could all determine cancer patients' outcomes and forecast their responsiveness to immunotherapies [28, 29]. The immunological microenvironment and immune-related biochemical pathways could be altered by modulating the transcription of m6A regulatory or lncRNAs [30]. Our results revealed that Macrophages M0, Macrophages M2, and T cells CD4 memory resting accounted for a large proportion of immune cell infiltration. It is reported that M2 macrophages can encourage tumor progression [31, 32]. Especially, elevated infiltration of M2 macrophages has been linked to osteosarcoma metastases and poor patient outcomes, notwithstanding the adoption of intensive therapy regimens [33]. Moreover, exosomes from metastasis osteosarcoma cells have been shown to alter tumor-associated macrophage cellular signaling, boost the

M2 phenotype, and establish an immunosuppressive, tumor-promoting milieu via producing TGF β 2 [34]. However, there were no significant differences in the proportion of most of the infiltrated immune cell types between the high- and low-risk groups.

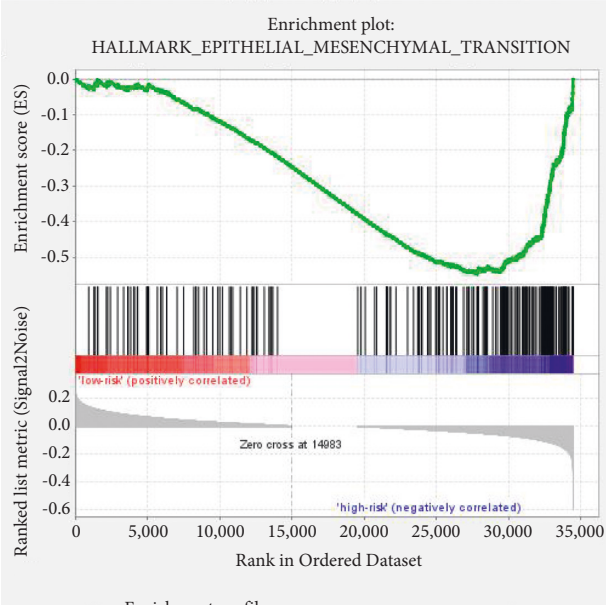
We investigated the association between m6A-related lncRNAs expression and the levels of immune infiltration in OS using CIBERSORT. TNS1-AS1 and TFPI2-DT were found positively correlated with B cell memory and B cells naive in our data, respectively. These results about immune infiltrate in osteosarcomas were consistent with previous studies [35, 36]. Additionally, the results uncovered that LINC01474 had a positive correlation with T cells CD8; however, LINC00910 was negatively related to T cells CD8. Other scholars believed that the significant infiltration of T cells CD8 activation in tumors may aid our signature's capacity to attain consistent predictive value [37]. There has been proof that programmed death-1 receptor (PD-1) plays a role in the evolution of osteosarcomas, and the proportion of PD-1 in blood CD8+ T cells is much higher in osteosarcomas patients [38, 39]. Moreover, LINC00538 was positively correlated with dendritic cells resting, in the meanwhile, negatively linked to dendritic cells activated in



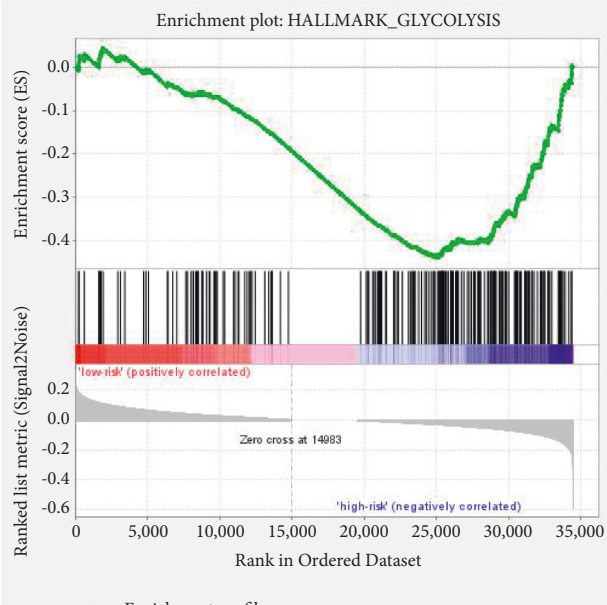
(a)



(b)



(c)



(d)

FIGURE 7: Continued.

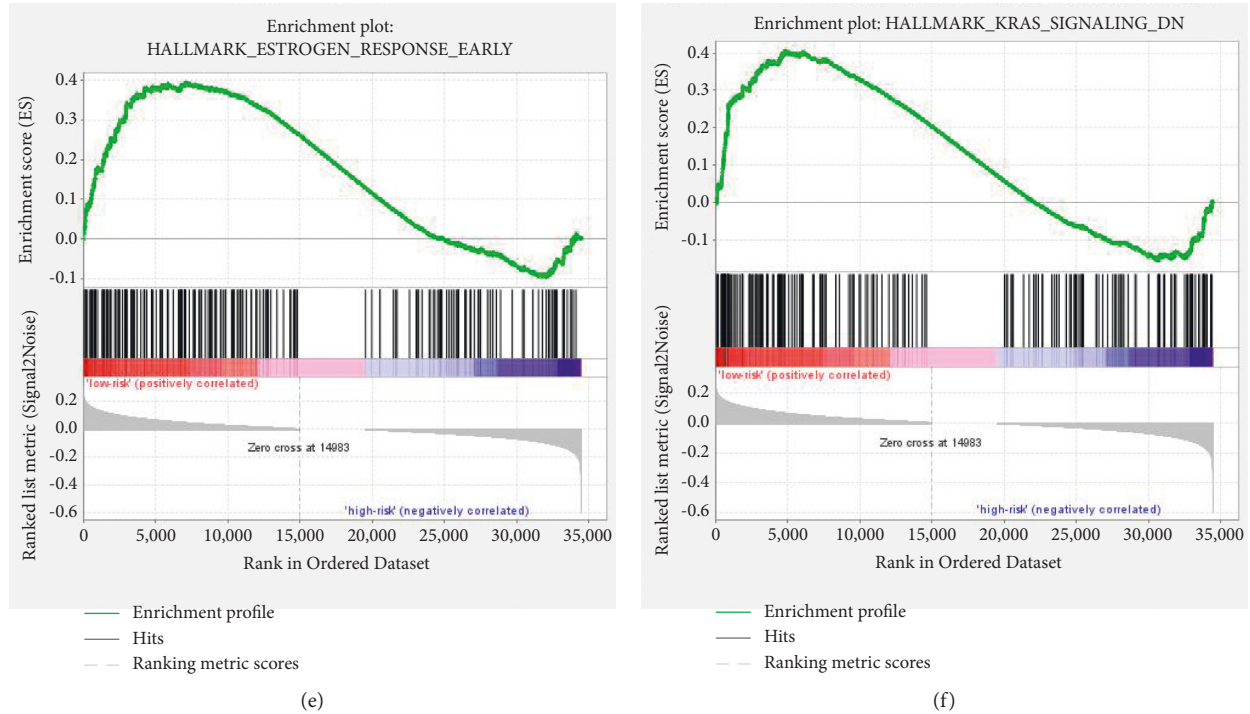


FIGURE 7: Abnormally activated signaling pathways in the two subgroups after Gene Set Enrichment Analysis. (a–d) Performed in the high-risk group, including unfolded protein response (ES = 0.42, $P = 0.02$, FDR = 0.110), DNA repair signaling pathway (ES = 0.41, $P = 0.0096$, FDR = 0.070), epithelial-mesenchymal transition signaling pathway (ES = 0.55, $P = 0.032$, FDR = 0.337), and glycolysis pathway (ES = 0.44, $P = 0.032$, FDR = 0.087). (e–f) Performed in the low-risk group, including estrogen response early (ES = 0.40, $P = 0.038$, FDR = 1.0) and KRAS signaling pathway (ES = 0.40, $P = 0.039$, FDR = 1.0).

our results. Previous studies demonstrated that the proportions of dendritic cells resting were positively correlated with the risk score of osteosarcomas [40] and LINC00538 was highly associated with worse outcomes of colon cancer patients [41].

There are some disadvantages to our study as well. First, for starters, the study's findings need to be verified by bigger external partners. Second, more specific methods of interaction between m6A and lncRNAs, as well as how this regulation pattern contributes to the reshaping of TME, should be investigated further. Third, it should be examined if m6A-related lncRNAs participate in other biological processes associated with cancer. Lastly, while the associations between the risk score and histopathological characteristics or TME had a significant difference, the medical variations should be confirmed again because the variance was not as apparent. To validate the prediction models built in our current investigation, additional research studies should incorporate specimens from other databases as well as an increasing number of clinical specimens. More research is needed to completely understand the signaling pathways of m6A-related lncRNAs in the carcinogenesis and development of osteosarcomas. This study has some limitations:

although the results of this study have some innovative and clinical significance, they have not been verified by more evidence, which makes this study incomplete, and a confirmatory study will be added in the future to make up for the shortcomings of this study.

In conclusion, our investigation showed that m6A-related lncRNAs remained tightly connected to the immunological microenvironment of osteosarcoma tumors, potentially influencing carcinogenesis and development. In addition, we looked for risk-related signaling of m6A-related lncRNAs in osteosarcomas and built and validated the risk prediction system. The findings of our current analysis will facilitate the assessment of the outcome and the development of immunotherapies for sufferers of osteosarcomas.

Data Availability

The datasets used and analyzed during the current study are available from the corresponding author upon reasonable request.

Conflicts of Interest

The authors declare that they have no conflicts of interest.

Authors' Contributions

Yikang Bi and Depeng Meng contributed equally to this work.

Acknowledgments

The authors gratefully acknowledge the support of the National Natural Science Foundation of China (no. 81601902), Research Fund of Shanghai Municipal Health Commission for Clinical Research in Medical Science (Grant no. 202040084), Medical Scientific Research Project of Xuhui District, Shanghai, China (Grant no. SHXH202009), and the Scientific Research Project of Shanghai Sixth People's Hospital Medical Group.

References

- [1] A. Luetke, P. A. Meyers, I. Lewis, and H. Juergens, "Osteosarcoma treatment - where do we stand? A state of the art review," *Cancer Treatment Reviews*, vol. 40, no. 4, pp. 523–532, 2014.
- [2] G. Ottaviani and N. Jaffe, "The epidemiology of osteosarcoma," *Cancer Treatment and Research*, vol. 152, pp. 3–13, Article ID 20213383, 2009.
- [3] S. Wang, L. Zhong, Y. Li et al., "Up-regulation of PCOLCE by TWIST1 promotes metastasis in Osteosarcoma," *Theranostics*, vol. 9, no. 15, pp. 4342–4353, 2019.
- [4] M. Hirahata, M. Osaki, Y. Kanda et al., "PAI -1, a target gene of miR-143, regulates invasion and metastasis by upregulating MMP -13 expression of human osteosarcoma," *Cancer Medicine*, vol. 5, no. 5, pp. 892–902, 2016.
- [5] X. Yu, L. Hu, S. Y. Li et al., "Long non-coding RNA Taurine upregulated gene 1 promotes osteosarcoma cell metastasis by mediating HIF-1 α via miR-143-5p," *Cell Death & Disease*, vol. 10, no. 4, p. 280, 2019.
- [6] L. He, H. Li, A. Wu, Y. Peng, G. Shu, and G. Yin, "Functions of N6-methyladenosine and its role in cancer," *Molecular Cancer*, vol. 18, no. 1, p. 176, Article ID 31801551, 2019.
- [7] K. D. Meyer and S. R. Jaffrey, "Rethinking m6A readers, writers, and erasers," *Annual Review of Cell and Developmental Biology*, vol. 33, no. 1, pp. 319–342, 2017.
- [8] T. Wang, S. Kong, M. Tao, and S. Ju, "The potential role of RNA N6-methyladenosine in Cancer progression," *Molecular Cancer*, vol. 19, no. 1, p. 88, Article ID 32398132, 2020.
- [9] Y. Chen, Z. Li, X. Chen, and S. Zhang, "Long non-coding RNAs: from disease code to drug role," *Acta Pharmaceutica Sinica B*, vol. 11, no. 2, pp. 340–354, 2021.
- [10] W. Wang, L. Min, X. Qiu et al., "Biological function of long non-coding RNA (LncRNA) xist," *Frontiers in Cell and Developmental Biology*, vol. 9, Article ID 645647, 2021.
- [11] M. Huarte, "The emerging role of lncRNAs in cancer," *Nature Medicine*, vol. 21, no. 11, pp. 1253–1261, 2015.
- [12] T. Li, P. S. Hu, Z. Zuo et al., "METTL3 facilitates tumor progression via an m6A-IGF2BP2-dependent mechanism in colorectal carcinoma," *Molecular Cancer*, vol. 18, no. 1, p. 112, Article ID 31230592, 2019 Jun 24.
- [13] Y. Niu, Z. Lin, A. Wan et al., "RNA N6-methyladenosine demethylase FTO promotes breast tumor progression through inhibiting BNIP3," *Molecular Cancer*, vol. 18, no. 1, p. 46, Article ID 30922314, 2019.
- [14] Y. Qian, L. Shi, and Z. Luo, "Long non-coding RNAs in cancer: implications for diagnosis, prognosis, and therapy," *Frontiers of Medicine*, vol. 7, Article ID 612393, 2020.
- [15] H. Tian, D. Guan, and J. Li, "Identifying osteosarcoma metastasis associated genes by weighted gene co-expression network analysis (WGCNA)," *Medicine*, vol. 97, no. 24, Article ID e10781, 2018.
- [16] H. Yuan, J. Liu, L. Zhao et al., "Prognostic risk model and tumor immune environment modulation of m5C-related LncRNAs in pancreatic ductal adenocarcinoma," *Frontiers in Immunology*, vol. 12, Article ID 800268, 2021.
- [17] J. Pan, Z. Huang, and Y. Xu, "m5C-Related lncRNAs predict overall survival of patients and regulate the tumor immune microenvironment in lung adenocarcinoma," *Frontiers in Cell and Developmental Biology*, vol. 9, Article ID 671821, 2021.
- [18] G. Wang, Y. Fan, P. Cao, and K. Tan, "Insight into the mitochondrial unfolded protein response and cancer: opportunities and challenges," *Cell & Bioscience*, vol. 12, no. 1, p. 18, 2022.
- [19] A. M. Lagunas, J. Wu, and D. L. Crowe, "Telomere DNA damage signaling regulates cancer stem cell evolution, epithelial mesenchymal transition, and metastasis," *Oncotarget*, vol. 8, no. 46, pp. 80139–80155, 2017.
- [20] D. M. Gonzalez and D. Medici, "Signaling mechanisms of the epithelial-mesenchymal transition," *Science Signaling*, vol. 7, no. 344, 2014.
- [21] N. A. Traphagen, S. R. Hosford, A. Jiang et al., "High estrogen receptor alpha activation confers resistance to estrogen deprivation and is required for therapeutic response to estrogen in breast cancer," *Oncogene*, vol. 40, no. 19, pp. 3408–3421, 2021.
- [22] H. J. Kim, H. N. Lee, M. S. Jeong, and S. B. Jang, "Oncogenic KRAS: signaling and drug resistance," *Cancers*, vol. 13, no. 22, p. 5599, 2021.
- [23] J. Zhao, D. C. Dean, F. J. Hornicek, X. Yu, and Z. Duan, "Emerging next-generation sequencing-based discoveries for targeted osteosarcoma therapy," *Cancer Letters*, vol. 474, pp. 158–167, 2020.
- [24] F. Zhong, F. Yao, Y. Cheng et al., "m6A-related lncRNAs predict prognosis and indicate immune microenvironment in acute myeloid leukemia," *Scientific Reports*, vol. 12, no. 1, p. 1759, 2022.
- [25] C. Shi, F. Zhao, T. Zhang et al., "A novel prognostic signature in osteosarcoma characterised from the perspective of unfolded protein response," *Clinical and Translational Medicine*, vol. 12, no. 3, p. e750, 2022.
- [26] F. Sadoughi, P. Maleki Dana, Z. Asemi, and B. Yousefi, "DNA damage response and repair in osteosarcoma: defects, regulation and therapeutic implications," *DNA Repair*, vol. 102, Article ID 103105, 2021.
- [27] E. Hayase and R. R. Jenq, "Role of the intestinal microbiome and microbial-derived metabolites in immune checkpoint blockade immunotherapy of cancer," *Genome Medicine*, vol. 13, no. 1, p. 107, 2021.
- [28] G. Price, A. Bouras, D. Hambardzumyan, and C. G. Hadjipanayis, "Current knowledge on the immune microenvironment and emerging immunotherapies in diffuse midline glioma," *EBioMedicine*, vol. 69, Article ID 103453, 2021.
- [29] K. Zhang, L. Ping, T. Du et al., "A ferroptosis-related lncRNAs signature predicts prognosis and immune microenvironment for breast cancer," *Frontiers in Molecular Biosciences*, vol. 8, no. 8, Article ID 678877, 2021.

- [30] F. Xu, X. Huang, Y. Li, Y. Chen, and L. Lin, "m6A-related lncRNAs are potential biomarkers for predicting prognoses and immune responses in patients with LUAD," *Molecular Therapy - Nucleic Acids*, vol. 24, pp. 780–791, 2021.
- [31] X. Fu, H. Shi, Y. Qi, W. Zhang, and P. Dong, "M2 polarized macrophages induced by CSE promote proliferation, migration, and invasion of alveolar basal epithelial cells," *International Immunopharmacology*, vol. 28, no. 1, pp. 666–674, 2015.
- [32] A. Schmieder, J. Michel, K. Schönhaar, S. Goerdts, and K. Schledzewski, "Differentiation and gene expression profile of tumor-associated macrophages," *Seminars in Cancer Biology*, vol. 22, no. 4, pp. 289–297, 2012.
- [33] F. Cersosimo, S. Lonardi, G. Bernardini et al., "Tumor-associated macrophages in osteosarcoma: from mechanisms to therapy," *International Journal of Molecular Sciences*, vol. 21, no. 15, p. 5207, 2020.
- [34] K. Wolf-Dennen, N. Gordon, and E. S. Kleinerman, "Exosomal communication by metastatic osteosarcoma cells modulates alveolar macrophages to an M2 tumor-promoting phenotype and inhibits tumoricidal functions," *OncoImmunology*, vol. 9, no. 1, Article ID 1747677, 2020.
- [35] H. Huang, M. Tan, L. Zheng et al., "Prognostic implications of the complement protein C1Q and its correlation with immune infiltrates in osteosarcoma," *OncoTargets and Therapy*, vol. 14, pp. 1737–1751, 2021.
- [36] J. Sun, H. Xu, M. Qi, C. Zhang, and J. Shi, "Identification of key genes in osteosarcoma by meta-analysis of gene expression microarray," *Molecular Medicine Reports*, vol. 20, no. 4, pp. 3075–3084, 2019.
- [37] J. Yang, A. Zhang, H. Luo, and C. Ma, "Construction and validation of a novel gene signature for predicting the prognosis of osteosarcoma," *Scientific Reports*, vol. 12, no. 1, p. 1279, 2022.
- [38] Z. Wang, B. Li, Y. Ren, and Z. Ye, "T-Cell-Based immunotherapy for osteosarcoma: challenges and opportunities," *Frontiers in Immunology*, vol. 7, p. 353, 2016.
- [39] B. Farhood, M. Najafi, and K. Mortezaee, "CD8 + cytotoxic T lymphocytes in cancer immunotherapy: a review," *Journal of Cellular Physiology*, vol. 234, no. 6, pp. 8509–8521, 2019.
- [40] C. Zhang, J. H. Zheng, Z. H. Lin et al., "Profiles of immune cell infiltration and immune-related genes in the tumor microenvironment of osteosarcoma," *Aging*, vol. 12, no. 4, pp. 3486–3501, 2020.
- [41] H. Tang, Y. Dou, Y. Meng, Q. Lu, L. Liang, and Y. Luo, "LINC00538 promotes the progression of colon cancer through inhibiting NKD2 expression," *JBON*, vol. 25, no. 6, pp. 2657–2664, 2020.

Research Article

Effectiveness of Perioperative Comprehensive Evaluation of Hip Fracture in the Elderly

Tao Zhu,¹ Jun Yu,¹ Ye Ma,¹ Yue Qin,¹ Nan Li,² and Haibo Yang¹ 

¹Department of Trauma Orthopedics, General Hospital of Ningxia Medical University, Ningxia, China

²Ningxia Medical University, Yinchuan 750004, China

Correspondence should be addressed to Haibo Yang; 184630509@smail.cczu.edu.cn

Received 26 May 2022; Revised 13 July 2022; Accepted 16 July 2022; Published 5 August 2022

Academic Editor: Dong Chen

Copyright © 2022 Tao Zhu et al. This is an open access article distributed under the Creative Commons Attribution License, which permits unrestricted use, distribution, and reproduction in any medium, provided the original work is properly cited.

Objective. The objective is to observe the effect of Comprehensive Geriatric Assessment (CGA) in the perioperative period of hip fracture. **Methods.** From October 2018 to October 2021, 155 patients over the age of 65 diagnosed with hip fracture and treated with surgery at the Department of Trauma Orthopaedics of General Hospital of Ningxia Medical University were randomly divided into two groups using a prospective research method. A total of 70 cases in the CGA group received a perioperative comprehensive assessment of the geriatric, and 85 cases in the control group received routine medical consultation. **Results.** Elderly patients with hip fractures have a high comorbidity index. Patients with abnormal daily activity before injury accounted for 55%, the abnormal rate of nutrition was 58.1%, the abnormal rate of cognition, anxiety, and depression was 81.8%, and 77.3% of the patients were in a weak state. There was no significant difference in age, gender, ASA grade, fracture type, and operation mode between the two groups, but there were significant differences in operation rate at 48 h ($\chi^2 = 22.153$; $P \leq 0.001$), preoperative waiting time ($Z = -6.387$; $P \leq 0.001$), total hospital stay ($Z = -11.756$; $P \leq 0.001$), and incidence of postoperative delirium ($\chi^2 = 23.897$; $P \leq 0.001$). **Conclusions.** The implementation of CGA shortened the preoperative waiting time and total hospital stay, increased the 48 h operation rate, and reduced the incidence of postoperative delirium.

1. Introduction

The number of elderly patients with osteoporotic fractures is increasing, and this type of elderly hip fracture seriously affects the quality of life and even the survival rate of patients. Early surgical treatment is advocated for elderly hip fractures. Some guidelines and consensus suggest that surgery should be performed within 48 hours, which can reduce the complications of long-term bed rest and postoperative mortality [1]. However, the difficulty in the treatment of such fractures is the comprehensive treatment and treatment in the perioperative period. Elderly hip fracture patients are often complicated with a variety of basic medical diseases. Some patients take a variety of drugs for a long time, which makes it difficult for orthopedic doctors to deal with them during the perioperative period and also becomes an important reason for delaying surgery [2]. At present, the treatment mode advocated is the

multidisciplinary cooperation mode between orthopedics doctors and internal medicine and anesthesiologists and even the co-management mode between geriatrics and orthopedics, so as to learn from each other's strengths and make up for their weaknesses in treatment, effectively reducing the preoperative waiting time and total hospital stay, so as to provide the treatment efficiency of hip fractures in the elderly [3]. Comprehensive geriatric assessment (CGA) is a multidisciplinary evaluation and treatment model that can make rapid adjustments to meet the operation conditions, reduce unnecessary preoperative examinations, improve the operation rate within 48 hours, reduce the total length of hospital stay, improve the daily activity score before discharge, and lower the incidence of postoperative delirium [4]. In this study, the elderly comprehensive evaluation method was used to evaluate the perioperative period of elderly hip fracture patients, and the patients with abnormal scores or high-risk patients were mainly

intervened in order to observe the effect of the application of the CGA method in the perioperative period of hip fracture.

2. Materials and Methods

2.1. Inclusion Criteria. Inclusion criteria include the following: (1) age greater than 65 years old; (2) the diagnosis was femoral neck fracture, intertrochanteric fracture of the femur, or fracture of the lesser trochanter; (3) clinical symptoms and imaging data were diagnosed as a hip fracture; and (4) family members and patients agreed to participate in this study.

2.2. Exclusion Criteria. The exclusion criteria include the following: (1) pathological fracture; (2) old fracture; (3) multiple fractures; and (4) patients with contraindications or failure to complete the operation. This study was reviewed and approved by the ethics committee of the General Hospital of Ningxia Medical University. All subjects were informed of the study and signed informed consent.

2.3. Case Source. From October 2018 to October 2021, 155 patients over 65 years of age were diagnosed with hip fracture and received surgical treatment in the orthopedic department of the General Hospital of Ningxia Medical University. The patients were divided into two groups according to the random number table method. A total of 70 cases in the CGA group received perioperative elderly comprehensive evaluation. There were 85 cases in the control group. After the two groups met the operation conditions, the operation was arranged as soon as possible and completed within 48 hours of hospitalization. There was no significant difference between the two groups in age, gender, ASA grade, fracture type and operation mode (Table 1).

2.4. Operation. After admission, routine examination is improved and surgical contraindications are improved; after CGA evaluation or medical consultation, surgery was performed. Closed reduction and cannulated screw fixation were used in patients with nondisplaced femoral neck fractures [5]. The displaced type was treated with half hip or total hip arthroplasty. Intramedullary or extramedullary fixation was used in patients with an intertrochanteric fracture [6]. The unstable type was treated with intramedullary fixation.

2.5. Contents of Comprehensive Evaluation and Intervention Measures for the Elderly. The geriatrician completes the geriatric comprehensive evaluation and records the evaluation form. Corresponding intervention measures should be taken for high-risk patients. The contents include the following. (1) Assessment of basic medical diseases: comprehensively understand the basic medical diseases of patients, quickly adjust the internal medical diseases to meet the operation conditions, reduce the waiting time and times of consultation, and reduce unnecessary preoperative

examination. (2) Mini-Nutritional Assessment (MNA-SF score): enteral nutrition support should be provided to patients with malnutrition (≤ 11), to promote rapid postoperative recovery. [7] (3) Physical activity assessment (Bathel ADL score): for patients at a high risk of postoperative falls (≤ 60), effective prevention or intervention shall be carried out by means of education, rehabilitation assistance, and application of fall prevention tools by orthopedic doctors and nurses. (4) Cognitive function was assessed by Mini-cog score and MMSE score, and anxiety and depression. Anesthesiologists and orthopaedics doctors should reduce the use of benzodiazepines and opioid analgesics during or after surgery for patients with high risk of delirium, poor postoperative cognitive function (Mini-cog: ≥ 1 , MMSE: ≤ 17), anxiety (SAS: ≤ 50), and depression (SAS: ≤ 52). Early psychological consultation and drug intervention (olanzapine and droperidol) were performed, while increasing the company of family members. Try to minimize intervention by transferring to the intensive care unit. V. Frail assessment (FRAIL score): for patients with frail status (≥ 3), strengthen nutritional status, strengthen rehabilitation exercise [8], strengthen nursing, and prevent falling again after the operation.

2.6. Diagnostic Criteria of Delirium. According to the diagnostic criteria of Diagnostic and Statistical Manual of mental disorder (Fourth revision) that delirium can be diagnosed if the following criteria are met: acute onset and fluctuating condition, inattention, disordered thinking, and the level of consciousness changes. Delirium can be diagnosed by having 1 and 2 and meeting 3 and 4. Postoperative delirium can be diagnosed from the day after the operation to the 7th day after the operation [9].

2.7. Postoperative Follow-Up. After the operation, the patients were followed-up by telephone or outpatient reexamination, took X-rays until the fracture healed, guided the hip functional exercise, and followed-up until the fracture healed.

2.8. Statistical Analysis. The Kolmogorov-Smirnov test is used to judge whether the measurement data conform to the normal distribution. The *t*-test is used for continuous measurement data and meeting normal distribution. The Mann-Whitney U rank sum test was used for comparison between measurement data groups that did not conform to normal distribution. Pearson is used for classified data χ^2 inspection. The data were statistically analyzed by SPSS20.0 analysis software. $P < 0.05$ was statistically significant.

3. Results

3.1. Comorbid State. There was no significant difference between the CGA group and the control group. However, the results showed that the patients had a high comorbidity index (Table 2).

TABLE 1: Comparison of general data between the study group and the control group.

Project	CGA group	Study group	χ^2/Z	P
Cases	70	85	—	—
Gender (female, %)	70.8	70.8	$\chi^2 = 0.227$	0.634 ^a
Age (years)	79.5	81.8	$Z = -0.658$	0.511 ^b
ASA (I, II/III, IV)	42/28 (60/40)	56/29 (65.9/34.1)	$\chi^2 = 0.233$	0.629 ^a
Femoral neck/intertrochanteric fracture (cases, %)	37/33 (52.9/47.1)	40/45 (47.1/52.9)	$\chi^2 = 0.233$	0.629 ^a
Operation mode				
Femoral neck fracture				
Cannulated screw (cases, %)	2 (5.4)	3 (7.5)		
Hemiarthroplasty (cases, %)	29 (78.4)	29 (72.5)	$\chi^2 = 2.542$	0.111 ^a
Total hip replacement (cases, %)	6 (16.2)	8 (20.0)		
Intertrochanteric fracture				
DHS (cases, %)	3 (9.0)	1 (2.2)	$\chi^2 = 2.542$	0.111
Intramedullary nail (cases, %)	30 (91.0)	44 (97.8)		

Note. a: χ^2 inspection; b: Mann-Whitney U test.

TABLE 2: Comparison of patients in study group and control group with diseases in internal medicine (cases, %).

Complicated with medical diseases	CGA group	Study group	χ^2	P value
Cardiovascular diseases	37 (52.9)	40 (47.1)	0.011	0.917
Respiratory diseases	11 (15.7)	15 (17.6)	0.471	0.492
Endocrine system diseases	21 (30.0)	19 (22.4)	0.341	0.559
Neurological and psychiatric diseases	30 (42.9)	28 (32.9)	0.376	0.540
Diseases of urinary system	8 (11.4)	6 (7.1)	0.459	0.498
Digestive system diseases	7 (10.0)	4 (4.7)	0.700	0.403
Combined with a medical disease	13 (18.6)	14 (16.5)	0.001	0.969
2 kinds	20 (25.0)	22 (25.9)	0.017	0.897
3 kinds	13 (28.6)	13 (15.3)	0.028	0.866
4 or more	7 (10.0)	6 (7.1)	0.162	0.687

TABLE 3: CGA evaluation of elderly hip fracture in study group and control group.

Assessment instrument	Cases	Median score (range)	Abnormal proportion (%)
ADL	75	65.0 (0 ~ 85)	55
MNA-SF	78	6.5 (3 ~ 20)	58.1
MMSE	55	13.5 (0 ~ 29)	81.8
SAS	53	45.0 (33 ~ 66)	18.9
SDS	53	48.5 (23 ~ 79)	68.2
FRAIL	53	3.0 (0 ~ 4)	77.3

3.2. CGA of Hip Fracture. Part of the evaluation content is due to the patient's dementia or inability to understand and cooperate to complete the evaluation scale. The patients had abnormal daily activity before the injury was 55%, the abnormal rate of nutrition was 58.1%, the abnormal rate of psychological assessment such as cognition, anxiety, and depression was 81.8%, and the patients in a weak state were 77.3% (Table 3).

3.3. 48 h Operation Rate, Preoperative Waiting, Length of Hospital Stay, Incidence of Postoperative Delirium, and ADL Score before Discharge. There were significant differences between the two groups in 48 h operation rate, preoperative waiting time, total hospital stay, and incidence of postoperative delirium (Table 4).

The implementation of geriatric comprehensive evaluation can improve the orthopaedic doctors' judgment of the

overall situation of patients, quantitatively evaluate the basic diseases, comorbid states, activity ability, nutrition, cognitive anxiety, depression, and weakness, and implement targeted preventive intervention and treatment measures, so as to finally improve the 48 h operation rate and shorten the preoperative waiting and total hospitalization time and can reduce the incidence of postoperative delirium. However, there was no significant difference in ADL scores between the two groups before discharge (Table 4).

4. Discussion

The incidence of hip fracture in the elderly is gradually increasing [10], with a long hospital stay, high medical cost, high incidence of complications, and high mortality, which brings a serious economic and human burden to the family and the country. According to the AAOS guidelines in the United States and the consensus of experts in the diagnosis and

TABLE 4: Comparison of 48 h operation rate, preoperative waiting, hospital stay, incidence of postoperative delirium, and ADL score between the CGA group and the general group.

Classification	CGA group	Study group	χ^2/Z	P value
48 h operation rate (cases, %)	23 (32.9)	10 (11.8)	$\chi^2 = 22.153$	$\leq 0.001^a$
Preoperative waiting (d)	5.9	8.7	$Z = -6.387$	$\leq 0.001^b$
Hospital stay (d)	20.8	23.6	$Z = -11.756$	$\leq 0.001^b$
Incidence of postoperative delirium (%)	15 (21.4)	27 (31.8)	$\chi^2 = 23.897$	$\leq 0.001^a$
ADL score (score)	50.5	51.7	$Z = -0.640$	0.522^b

Note. a: χ^2 inspection; b: Mann-Whitney U test.

treatment of elderly hip fractures in China [11, 12], the operation of fractures within 48 hours can reduce the incidence of complications and mortality. Because patients are often complicated with a variety of internal diseases, they need internal consultation and stabilization of internal diseases. Before the operation, they need a variety of examinations and reconsultations. In addition, oral anticoagulants are an important reason for the delay in operation [13, 14]. In order to reduce the waiting time before an operation, Grigoryan et al. [15] analyzed and summarized 18 studies and found that the cooperative treatment of elderly hip fractures by orthopedics and geriatric doctors can shorten the length of hospital stay and reduce in-hospital mortality and long-term mortality. Wu et al. [16] and others proposed that the joint management mode of orthopedics and geriatrics can shorten the preoperative waiting time and hospitalization time of patients and improve the treatment efficiency of hip fractures in the elderly. In addition, studies by Wu and others have shown that the application of the multidisciplinary cooperation model can shorten the preoperative stay in bed days, total hospital stay, postoperative out of bed activity time of elderly hip fracture patients, reduce hospitalization expenses and postoperative complications, and is more conducive to the recovery of hip function than the traditional model. In order to be more standardized and normalized, our research method was adjusted with reference to the 2018 China Guideline for the Diagnosis and Treatment of Senile Osteoporosis. During the research process, standardize the process according to the requirements of the guide at any time [17]. The above studies show that geriatrics or multidisciplinary cooperation can improve the treatment efficiency of hip fractures in the elderly and shorten the length of hospital stay and reduce the mortality rate [18]. Through routine preoperative CGA, this study can more comprehensively grasp the general situation of patients, reduce the number of consultations and waiting time, and reduce unnecessary preoperative examinations, so as to improve the 48 h operation rate and shorten the preoperative waiting time and total hospitalization time. Through the data, it can be found that the implementation of CGA can improve the 48 h operation rate to 28.6%, but the proportion is still not high. The reasons may be the lack of establishment of an emergency hospitalization or operation green channel [19], delayed evaluation, delayed operation on weekends, and other factors. The total length of stay was shortened to 20.8 days. However, compared with foreign or domestic large medical centers, it is still longer [20]. The length of stay is affected by many factors, including not only medical factors but also certain social factors [21].

Delirium is a common complication after hip fracture surgery in the elderly [22]. It can not only prolong the hospital stay and increase medical expenses but also induce dementia and seriously affect the rehabilitation of patients [23]. The pathogenesis of delirium is unclear, but preoperative targeted prevention and intervention is an effective prevention and treatment measure. CGA is a multidisciplinary evaluation and treatment model. Through the comprehensive evaluation of elderly patients, we comprehensively collect the physical, mental, and other information needs of elderly patients, including medical evaluation (disease diagnosis, elderly complications, and multiple drugs), physical ability evaluation (self-care ability, mobility, and balance ability), and psychopsychological evaluation, socioeconomic factors, and environmental evaluation. CGA is not only for the disease itself but also for the overall situation of elderly patients [24] and not only pays attention to physical conditions but also pays more attention to cognitive and psychological conditions [25, 26]. At present, the perioperative intervention effect of CGA on elderly hip fracture patients is not consistent, and there are very few studies on CGA in China [27]. For hip fracture patients over 65 years old, the implementation of CGA can reduce the mortality rate compared with the conventional group. Forni et al. [28] performed CGA on hip fracture patients over 70 years old with surgical treatment, which can reduce the mortality rate, shorten the length of hospital stay, and reduce the rate of functional loss. Hempenius et al. [28, 29] showed that the implementation of CGA for elderly hip fractures can reduce the incidence of postoperative delirium. The above results fully show that CGA can reduce the incidence of delirium after hip fracture in the elderly, reduce postoperative mortality, and reduce the loss of hip function. This study also found that CGA can evaluate the high-risk group of postoperative delirium before the operation, and effective treatment measures and targeted drugs can reduce the incidence of postoperative delirium.

5. Conclusions

CGA is an important adjuvant therapy tool in geriatrics. The results of this study show the advantages of CGA in the application of elderly hip fracture patients so that orthopedics doctors can more comprehensively grasp the overall situation of the elderly, evaluate and adjust to meet the operating conditions in the shortest time, reduce unnecessary consultation time, wait, and unnecessary preoperative examination, and improve the treatment efficiency of elderly hip fracture, which is worthy of clinical promotion.

Data Availability

The datasets used and analyzed during the current study are available from the corresponding author upon reasonable request.

Conflicts of Interest

The authors declare that they have no conflicts of interest.

References

- [1] J. F. Walker, Y. Yang, M. J. Moore et al., "Widespread paleopolyploidy, gene tree conflict, and recalcitrant relationships among the carnivorous Caryophyllales," *American Journal of Botany*, vol. 104, no. 6, pp. 858–867, 2017.
- [2] H. M. Pajulampi, H. K. Pihlajamäki, T. H. Luukkaala, J. J. Jousmaki, P. H. Jokipii, and M. S. Nuotio, "The effect of an in-hospital comprehensive geriatric assessment on short-term mortality during orthogeriatric hip fracture program-which patients benefit the most?" *Geriatr Orthop Surg Rehabil*, vol. 8, no. 4, pp. 183–191, 2017.
- [3] R. Biber, K. Singler, M. Curschmann-Hortner, S. Wicklein, C. Sieber, and H. J. Bail, "Implementation of a co-managed Geriatric Fracture Center reduces hospital stay and time-to-operation in elderly femoral neck fracture patients," *Archives of Orthopaedic and Traumatic Surgery*, vol. 133, no. 11, pp. 1527–1531, 2013.
- [4] Y. Zhou, Y. Rui, P. Lu et al., "[Research progress of multi-disciplinary team co-management models for geriatric hip fracture treatment]," *Zhongguo Xiu Fu Chong Jian Wai Ke Za Zhi*, vol. 34, no. 1, pp. 132–138, 2020.
- [5] Y. Rui, X. Qiu, J. Zou et al., "[Clinical application of multi-disciplinary team co-management in geriatric hip fractures]," *Zhongguo Xiu Fu Chong Jian Wai Ke Za Zhi*, vol. 33, no. 10, pp. 1276–1282, 2019.
- [6] Y. Zhou, Y. Ni, X. Li, H. Chen, and Y. Rui, "[Research progress in treatment of femoral neck fracture in the elderly]," *Zhongguo Xiu Fu Chong Jian Wai Ke Za Zhi*, vol. 33, no. 8, pp. 1033–1040, 2019.
- [7] C. Zeng, N. E. Lane, M. Englund et al., "In-hospital mortality after hip arthroplasty in China: analysis of a large national database," *The Bone & Joint Journal*, vol. 101-b, no. 10, pp. 1209–1217, 2019.
- [8] M. Baroni, R. Serra, V. Boccardi et al., "The orthogeriatric comanagement improves clinical outcomes of hip fracture in older adults," *Osteoporosis International*, vol. 30, no. 4, pp. 907–916, 2019.
- [9] G. Hecht, C. A. Slee, P. B. Goodell, S. L. Taylor, and P. R. Wolinsky, "Predictive modeling for geriatric hip fracture patients: early surgery and delirium have the largest influence on length of stay," *Journal of the American Academy of Orthopaedic Surgeons*, vol. 27, no. 6, pp. e293–e300, 2019.
- [10] Y. Jiang, Y. Luo, H. Lyu et al., "Trends in comorbidities and postoperative complications of geriatric hip fracture patients from 2000 to 2019: results from a hip fracture cohort in a tertiary hospital," *Orthopaedic Surgery*, vol. 13, no. 6, pp. 1890–1898, 2021.
- [11] J. Q. Kusen, B. Schafroth, B. Poblete et al., "The implementation of a Geriatric Fracture Centre for hip fractures to reduce mortality and morbidity: an observational study," *Archives of Orthopaedic and Traumatic Surgery*, vol. 139, pp. 1705–1712, 2019.
- [12] M. Gregersen, M. M. Mørch, K. Hougaard, and E. M. Damsgaard, "Geriatric intervention in elderly patients with hip fracture in an orthopedic ward," *J Inj Violence Res*, vol. 4, no. 2, pp. 51–57, 2012.
- [13] F. Xing, W. Chen, C. Long, F. Huang, G. Wang, and Z. Xiang, "Postoperative outcomes of tranexamic acid use in geriatric trauma patients treated with proximal femoral intramedullary nails: a systematic review and meta-analysis," *Orthopaedics and Traumatology: Surgery & Research*, vol. 106, no. 1, pp. 117–126, 2020.
- [14] A. V. Christiano, H. C. Elsevier, S. Sarker, G. Agriantonis, D. Joseph, and R. Hasija, "Improving outcomes after hip fracture at a safety net hospital with a standardised hip fracture protocol," *HIP International*, vol. 31, no. 5, pp. 696–699, 2021.
- [15] K. V. Grigoryan, H. Javedan, and J. L. Rudolph, "Orthogeriatric care models and outcomes in hip fracture patients: a systematic review and meta-analysis," *Journal of Orthopaedic Trauma*, vol. 28, no. 3, pp. e49–55, 2014.
- [16] X. Wu, M. Yang, and P. Zhang, "Geriatric orthopedic co-management reduces time-to-operation and hospital stay in geriatric hip fracture patients," *J Clin Orthop Re*, vol. 2, pp. 96–100, 2017.
- [17] M. Yuanzheng, W. Yipeng, and L. Qiang, "China guideline for the diagnosis and treatment of senile osteoporosis," *Chinese Journal of Practical Internal Medicine*, vol. 29, pp. 38–61, 2018.
- [18] C. Soong, P. Cram, K. Chezar et al., "Impact of an integrated hip fracture inpatient program on length of stay and costs," *Journal of Orthopaedic Trauma*, vol. 30, no. 12, pp. 647–652, 2016.
- [19] C. Wang, Y. Chang, Y. Zheng et al., "[Application of multi-disciplinary doctor-nurse collaboration team on the peri-operation management of geriatric hip fractures]," *Zhongguo Xiu Fu Chong Jian Wai Ke Za Zhi*, vol. 33, no. 10, pp. 1283–1286, 2019.
- [20] A. Van Heghe, G. Mordant, J. Dupont, M. Dejaeger, M. R. Laurent, and E. Gielen, "Effects of orthogeriatric care models on outcomes of hip fracture patients: a systematic review and meta-analysis," *Calcified Tissue International*, vol. 110, no. 2, pp. 162–184, 2021.
- [21] M. Loizzo, F. Gallo, and D. Caruso, "Reducing complications and overall healthcare costs of hip fracture management: a retrospective study on the application of a Diagnostic Therapeutic Pathway in the Cosenza General Hospital," *Ann Ig*, vol. 30, no. 3, pp. 191–199, 2018.
- [22] C. Bliemel, L. Oberkircher, D. A. Eschbach et al., "Impact of Parkinson's disease on the acute care treatment and medium-term functional outcome in geriatric hip fracture patients," *Archives of Orthopaedic and Traumatic Surgery*, vol. 135, no. 11, pp. 1519–1526, 2015.
- [23] L. Heyzer, R. Ramason, J. A. D. C. Molina, W. W. L. Chan, C. Y. Loong, and E. Kwek, "Integrated hip fracture care pathway (IHFCP): reducing complications and improving outcomes," *Singapore Medical Journal*, 2021.
- [24] C. Mittal, H. C. D. Lee, K. S. Goh et al., "ValuedCare program: a population health model for the delivery of evidence-based care across care continuum for hip fracture patients in Eastern Singapore," *Journal of Orthopaedic Surgery and Research*, vol. 13, no. 1, p. 129, 2018.
- [25] G. Lynch, R. Z. Shaban, and D. Massey, "Evaluating the orthogeriatric model of care at an Australian tertiary hospital," *International Journal of Orthopaedic and Trauma Nursing*, vol. 19, no. 4, pp. 184–193, 2015.

- [26] K. Milisen, M. D. Foreman, I. L. Abraham et al., “A nurse-led interdisciplinary intervention program for delirium in elderly hip-fracture patients,” *Journal of the American Geriatrics Society*, vol. 49, no. 5, pp. 523–532, 2001.
- [27] H. J. Roberts, J. Barry, K. Nguyen et al., “2021 John Charnley Award: a protocol-based strategy when using hemiarthroplasty or total hip arthroplasty for femoral neck fractures decreases mortality, length of stay, and complications,” *The Bone & Joint Journal*, vol. 103-b, no. 7 Supple B, pp. 3–8, 2021.
- [28] S. Forni, F. Pieralli, A. Sergi, C. Lorini, G. Bonaccorsi, and A. Vannucci, “Mortality after hip fracture in the elderly: the role of a multidisciplinary approach and time to surgery in a retrospective observational study on 23, 973 patients,” *Archives of Gerontology and Geriatrics*, vol. 66, pp. 13–17, 2016.
- [29] L. Hempenius, J. P. J. Slaets, D. van Asselt, G. H. de Bock, T. Wiggers, and B. L. van Leeuwen, “Outcomes of a geriatric liaison intervention to prevent the development of postoperative delirium in frail elderly cancer patients: report on a multicentre, randomized, controlled trial,” *PLoS One*, vol. 8, no. 6, Article ID e64834, 2013.

Research Article

Effect of Restraint Stress on Pain Sensitivity, Spinal Trigeminal Nucleus Neurons, and Astrocytes in the Masseter Area of Rats

Feng Han 

Department of Human Anatomy, Jilin Medical University, Jilin City 132013, Jilin Province, China

Correspondence should be addressed to Feng Han; han9598610@126.com

Received 24 May 2022; Revised 30 June 2022; Accepted 5 July 2022; Published 5 August 2022

Academic Editor: Dong Chen

Copyright © 2022 Feng Han. This is an open access article distributed under the Creative Commons Attribution License, which permits unrestricted use, distribution, and reproduction in any medium, provided the original work is properly cited.

To explore the changes of pain sensitivity (PS) in the masseter area (MA) in the rat model of psychological stress and the mechanism of action between spinal nucleus neurons and astrocytes in the trigeminal ganglion. The 40 Sprague-Dawley rats were randomly divided into control group (no treatment), group A (restraint stress (RS) 1 d), group B (RS 7 d), and group C (RS 14 d). The body weight growth rates (WGR) of rats in each group were compared and the difference of CORT and ACTH in serum was analyzed by ELISA. The open field test and the elevated “cross” maze test were adopted to detect the behavioral changes of rats. Finally, pain threshold of the MA in rats, the activation amount of brain tissue medulla oblongata parts astrocytes markers Glial fibrillary acidic protein (GFAP), and the protein expression of IL-1 β and IL-1RI were detected. The results showed the WGR at 7 d and 14 d was greatly lower than control group ($P < 0.01$). In addition, the activity level and serum CORT and ACTH levels AND mean pain threshold in the MA of groups B and C were greatly lower than control group ($P < 0.05$). The activation rate of GFRP in group C ($P < 0.01$) and the protein expression of IL-1 β and IL-1RI ($P < 0.05$) in rat trigeminal ganglion astrocytes of groups B and C was greatly higher than control group, indicating the increase of RS time, the release of IL-1 β and IL-1RI can activate neurons and astrocytes in spinal trigeminal nucleus (STN) nerve and increase the PS of the MA.

1. Introduction

With the development of society and the acceleration of the pace of life, the role of psychological stress in various diseases has become more and more prominent. Psychological stress has been reported to be a common risk factor for 75% to 90% of diseases [1].

Stress can stimulate a series of information transmission in the peripheral nervous system and the central nervous system. It is the process of the body dealing with external stimuli and challenges, resulting in a nonspecific adaptive mechanism, including environmental and psychological factors. Acute psychological stress can induce the body's natural immune system, enhance resistance to pathogenic microbial infection, and speed up wound healing. Chronic psychological stress will break the homeostasis of the internal environment, change the function of immune cells, lead to immune dysfunction, and induce a variety of physical and mental diseases, such as depression [2].

At present, there are many methods used to build stress animal models, mainly by directly exposing animals to the stress environment that cannot be avoided to make them produce corresponding stress response. When the body is stressed at the psychological level, it will activate the hypothalamic–pituitary–adrenal axis, thereby promoting the secretion of adrenocorticotropin by the pituitary gland and increasing the secretion of glucocorticoid in the body [3]. However, studies have shown that the occurrence and development of a large number of diseases are related to psychological stress, such as mental diseases like epilepsy, peptic ulcer, hypertension, rheumatoid diseases. [4]. Therefore, the establishment of stress animal models is of great significance for us to study the occurrence and development of related diseases. The methods of building animal models of psychological stress include the following: restraint method, forced swimming method, punitive drinking water method, etc. Among them, restraint method is a method that does not cause physical damage to animal

models [5]. The stress animal model after construction can be verified by open field test, elevated “cross” maze test, and sugar and water consumption tests.

Pain is a series of complex stress responses produced by the organism after the organism is stimulated by injury and often causes the individual to be depressed, slow in response, sympathetic excitement, and other reactions. Peripheral sensitization and central sensitization play an important role in the occurrence and development of pain [4]. According to statistics, the pain of the mouth and maxillofacial is one of the common and high-incidence parts of human pain diseases, among which the trigeminal nerve distributed in the maxillofacial tissue in the form of free nerve endings can feel the stimulation of injury. When the trigeminal nerve primary afferent nerve fiber transmits the pain to the sensory nucleus composed of the trigeminal nerve sensory main nucleus and spinal trigeminal nucleus (STN) in the brain stem, it conducts the pain conduction, and the STN neuron nerve plays a key role in the central sensitized process of the pain transmission system [6]. The nervous system is made up of neurons and glial cells, and astrocytes located in central nervous cells are also closely related to pain. A large number of studies have shown that GFAP, an astrocyte marker, is upregulated in the established masseter palpation model [7].

Currently, studies have shown that the body is stimulated by continuous low-intensity psychological stress, which will lead to the appearance of pain sensitivity (PS) in the mouth and maxillofacial region [8]. However, by constructing the rat model of psychological stress, the study on the effect of psychological stress on the PS of the masseter area (MA), STN neurons, and astrocytes in rats is less. Therefore, a rat psychological stress model was constructed with the restraint method, and the model was verified based on the open-field test, and the “cross” maze test was elevated, and then the influence of the increased stress time was tested on the pain threshold of the masseter area and the expression of glial fibrillary acidic protein (GFAP) in the brain tissue. The purpose of this study is to lay a foundation for the study of the mechanism of action of psychological stress on STN neurons and astrocytes during the nociceptive sensitivity of the MA in rats.

2. Materials and Methods

2.1. Establishment of Experimental Animal and RS Model. In this research, 40 SD male rats purchased from Shanghai Slack Laboratory Animal Co., LTD was selected as subjects. The average weight of all the rats was about 215 ± 10 g. The rats were kept in separate cages in the animal feeding laboratory, and the average temperature and relative humidity were kept at 23 ± 2 and $60 \pm 5\%$, respectively. All rats were fed standard feed, given natural light for 12 hours a day, and all rats were free to eat.

The freedom of movement of SD rats in the experimental group was restricted by using a cylindrical restraint device with a height of about 30 cm and a diameter of 10 cm made of elastic metal mesh, and the diameter of the restraint device was adjusted according to the growth condition of the experimental rats to ensure that the body of the rats was not

subjected to physical pressure. Forty SD rats were randomly divided into four groups: control group, test group A (RS 1 d), test group B (RS 7 d), and test group C (RS 14 d), with 10 rats in each group. The rats in the control group were kept in cages with no treatment every day, from 9:00 a.m. to 5:00 p.m.

2.2. Evaluation of Captive Stress Animal Models. Weight detection: rats in the four groups were weighed at 1, 7, and 14 days after RS stimulation and the WGR of the control group and the experimental group were calculated.

Detection of serum stress hormone content: on day 1, day 7, and day 14, rats were anesthetized by intraperitoneal injection of 1% pentobarbital sodium 50 mg/kg. A quantity of 1.5 ml of blood was taken from the heart and placed on ice for 30 min, then centrifuged at 3000 rpm for 15 min, and the supernatant was taken. Avidin-biocomplex-Enzyme-Linked Immunosorbent Assay (ABC-ELISA) was used to determine the content of CORT and ACTH in serum of rats. Monoclonal antibodies of rat CORT and ACTH were coated in a 96-well plate and were mixed with 100 μ L/well standard substance or serum to be tested, and then placed at 37°C for 2 h. After washing the reaction plate for five times, filter paper was used to print the dry reaction plate. The mixture was mixed with 100 μ L/hole and placed at 37°C for 1 h. After washing the reaction plate, 100 μ L/hole was added into the enzyme-labeled antibody and placed at 37°C for 30 min. After washing reaction plate, 100 μ L/hole working fluid was added to mix well, placed at 37°C to avoid light for 30 minutes. The final solution of 100 μ L/hole was mixed, and the absorbance value at 450 nm was detected in the microplate reader.

Open field test: rats were placed in a 100 \times 100 \times 80 cm open field test box in a low-light and sound-proof room on 1 d, 7 d, and 14 d after RS stimulation. After the rats were acclimated for 3 min, the total range (cm), the central range (cm), and the velocity (cm/s) of the rats were recorded within 15 min. After the experiment was completed, the chamber needed to be cleaned and 75% ethanol sprayed to treat the residual odor in the chamber.

Elevated “cross” maze test: rats were placed in the center of the “cross” structure made of opaque material about 70 cm above the ground at 1 d, 7 d, and 14 d after RS stimulation (upper and lower ends were open arms and left and right segments were closed arms. The wall length was 50 cm and the width was 10 cm), and the activity of the rats was recorded by camera within 5 min after the insertion. The final results were expressed as the percentage of retention time (%) and the percentage of retention times (%) in the open arm of each rat. After the experiment was completed, the chamber needed to be cleaned and 75% ethanol sprayed to treat the residual odor in the chamber.

2.3. Detection of PS of MA in Rats. The rats were placed in a quiet and closed space for 20 minutes prior to the restraint of stress stimulation, and for 1, 7, and 14 days after stimulation. Then, an electronic pain-measuring device was used to stimulate the MA about 1 cm below the middle line between

the eyes and ears of the rats. When the rats showed three or more times of avoidance, cowering, and vocalization, it indicated that the rats had pain response. At this time, the pressure value of the electronic pain-measuring device was recorded, and the mean value of five times of stimulation was taken as the pain threshold of the rat.

2.4. Glial Fibrillary Acidic Protein Detection in the Rat Trigeminal Ganglion. The rats were anesthetized with 1% pentobarbital sodium (50 mg/kg) intraperitoneally at 1 d, 7 d, and 14 d after RS stimulation. The rats were placed in a supine position. Perfusion needle was used to rise from the left ventricle of the rat to the aorta, and the prepared mixture of 4% paraformaldehyde, 0.2% saturated picric acid, and 0.1 mol/L PB was added. About 3 h later, the rat brain tissue was taken out for fixation and dehydration and placed in sucrose solution. After the brain tissue had sunk to the bottom, the medulla oblongata in the brain tissue was cut into sections 30 μ m thick and placed in 0.01 mol/L phosphate buffer (PBS). Sections were removed and washed with 0.01 mol/L PBS for 3 times \times 10 min. Donkey serum was added and incubated at room temperature for 30 min. The 1 : 5000 diluted monoclonal mouse Glial fibrillary acidic protein (GFAP) a fight and the 1 : 5000 diluted monoclonal rabbit anti-neun primary antibody were added, respectively, and incubated in warm shaker overnight. Washed with 0.01 mol/L PBS for 3 times \times 10 min, 1 : 500 diluted donkey anti-mouse IgG secondary antibody was added and incubated at room temperature for 3 h. After being washed with 0.01 mol/L PBS for 3 times \times 10 min, the staining results were observed under a laser confocal microscope after sealing, and Imag-Pro Plus image analysis software was used to process the results.

2.5. Analysis of Protein Expression of IL-1 β in Trigeminal Ganglion Astrocytes. The rat trident ganglion tissues obtained earlier were placed in the EP tube containing phenylmethylsulfonyl phosphating solution and placed in the icebox for enough tissue lysis. It was placed in a centrifuge and centrifuged at 12000 rpm for 3 min, then supernatant was taken. BCA kit (Shanghai Biyuntian Biotechnology Co., LTD., China) was used to determine protein concentration; the configured gel was fixed in the electrophoresis tank, and 6 μ L samples were added to each well to be tested; finally, PVDF membrane was used for transfer printing. After that, TBST solution was used for rinsing and sealing for 2 h. After rinse, 1 : 500 dilution of rabbit anti-IL-1 β I, 1 : 100 dilution rabbit anti-IL-1RI, and 1 : 5000 dilution rabbit anti- β -actin I were added, respectively, incubated at 4°C overnight. After rinsing, a 1 : 500 diluted donkey antirabbit secondary antibody was added and incubated at room temperature for 1 h. After rinsed, they were developed in a darkroom, and protein expression was detected by BeyoECL.

2.6. Statistics Process. SPSS19.0 software was used to conduct statistical processing of all data, and the data were misrepresented by mean \pm standard, and Duncan multiple

comparisons were used in ANOVA analysis for intergroup comparisons. When $P < 0.05$, the difference between the two groups was considered statistically significant.

3. Results

3.1. Effect of RS on Body Weight in Rats. In order to explore the influence of RS at different times on the weight of rats, the changes in the WGR of rats in the control group and the experimental group at 1, 7, and 14 days after RS stimulation were compared, and the results were shown in Figure 1. It showed that there was no statistically significant difference (SSD) in the WGR of rats when the stress stimulation was restrained for 1 d ($P > 0.05$). On the 7 d RS stimulation, the WGR of the control group was $64.1 \pm 6.2\%$, while that of the experimental group was $43.8 \pm 3.2\%$, and the WGR of the experimental group was greatly lower than that of the control group ($P < 0.01$). However, when the stress was restrained for 14 d, the WGR of the control group was $78.4 \pm 8.3\%$, while that of the experimental group was $64.6 \pm 5.7\%$, and the WGR of the experimental group was greatly higher than that of the control group ($P < 0.01$).

3.2. Effects of Bondage Stress on CORT and ACHT in the Serum of Rats. In order to explore the influence of RS at different times on serum-related indexes of rats, the differences in CORT and ACHT contents in the serum of the four groups of rats were detected and compared, and the results were shown in Figure 2. According to Figure 2, CORT content in blood of rats in the control group was 12.8 ± 2.6 ng/mL, rats in group A were 12.6 ± 4.4 ng/mL, rats in group B were 19.3 ± 4.7 ng/mL, and rats in group C were 25.1 ± 5.2 ng/mL. CORT content in serum of group B was greatly higher than that of control group ($P < 0.05$). The content of CORT in serum of group C was greatly higher than that of control group ($P < 0.01$).

According to Figure 3, the ACHT content in blood of rats in the control group was 28.1 ± 4.2 ng/mL, rats in group A were 31.2 ± 3.9 ng/mL, rats in group B were 48.3 ± 7.9 ng/mL, and rats in group C were 56.2 ± 8.7 ng/mL. The content of ACHT in serum of group B and group C was greatly higher than that of control group ($P < 0.01$).

3.3. Effects of Bondage Stress on Behavior in Rats. In order to compare the effects of bondage stress on the behavior of rats, open field test and elevated “cross” maze test were used to detect the behavioral changes of rats under different bondage stress. According to Table 1, in the open field test, there was no SSD between the total activity distance, central activity distance, and activity speed between the control group and group A ($P > 0.05$). The total active distance, central active distance, and active speed of rats in group B were greatly lower than those in control group ($P < 0.05$). The total active distance, central active distance, and active speed of group C were greatly lower than those of control group ($P < 0.01$). In the elevated “cross” maze test, there was no SSD between the control group and group A in the percentage of open-arm retention time and the percentage of open-arm retention

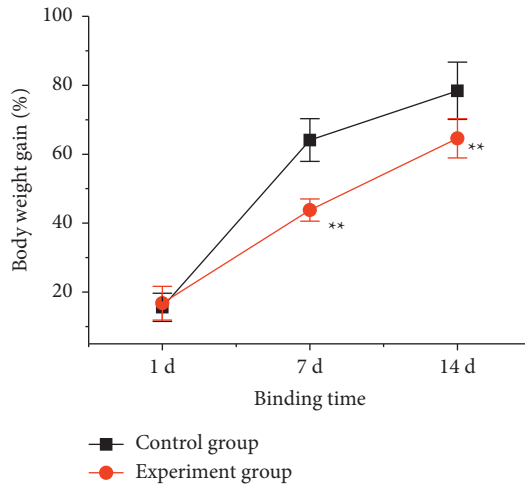


FIGURE 1: The WGR difference of rats after different time-RS stimulation. Note: ** meant there was an extremely SSD compared with the control group, $P < 0.01$.

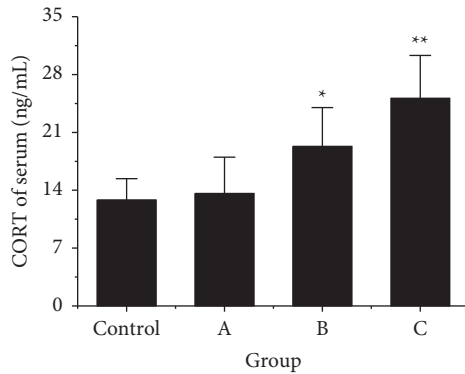


FIGURE 2: Comparison of CORT content in the serum of rats after RS. Note: * meant there was a SSD compared with the control group, $P < 0.05$; ** indicated that there was an extremely SSD compared with the control group, $P < 0.01$.

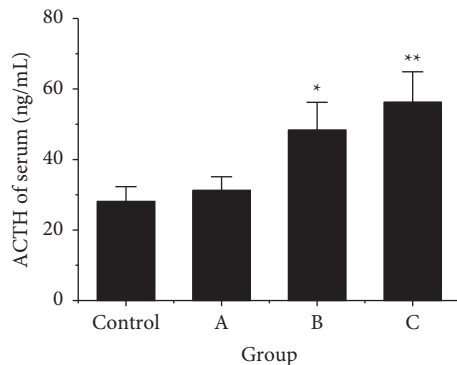


FIGURE 3: Comparison of ACTH content in the serum of rats after RS. Note: * meant there was a SSD after comparison with the control group, $P < 0.05$; ** indicated that there was an extremely SSD after comparison with the control group, $P < 0.01$.

times ($P > 0.05$). However, the percentage of open-arm retention time and the percentage of open-arm retention time in group B were greatly lower than those in the control group

($P < 0.05$). The percentage of open-arm retention time and open-arm retention times in group C was greatly lower than that in control group ($P < 0.01$).

3.4. Effect of RS on the PS of MA in Rats. In order to compare the effects of different RS on the PS of the MA in rats, an electronic pain-measuring device was used to detect the mean pain threshold of the MA in the control group and rats with RS stimulation on 1 d, 7 d, and 14 d, and the results were shown in Figure 4. According to Figure 4, the mean threshold of pain in the MA of rats in the control group was 98 ± 21 g, the mean threshold of pain in the MA of rats in group A was 97 ± 18 g, the mean threshold of pain in the MA of rats in group B was 79 ± 9 g, and the mean threshold of pain in the MA of rats in group C was 38 ± 10 g. After comparison, it showed that there was no SSD between the mean threshold of pain in group A and control group ($P > 0.05$), the mean threshold of pain in group B was greatly lower than that in control group ($P < 0.05$), and the mean threshold of pain in group C was greatly lower than that in control group ($P < 0.01$).

3.5. Immunofluorescence Staining of GFAP in STN Nerve in Rats after RS. In order to compare the effects of different time-RS on GFAP in STN in rats, immunofluorescence staining technology was used to detect the staining of GFAP in STN in brain tissues of rats. As shown in Figure 5, only a small number of GFAP positive neurons were found in the control group. The positive expression of GFAP in STN of rats in group A increased, while that in group B and group C increased greatly.

The activation rate of GFAP in STN nerve in rats was compared. As shown in Figure 6, the activation rate of GFAP in STN of rats in group C was greatly higher than that in the control group ($P < 0.01$); however, there was no SSD in the activation rate of GFAP in STN in the control group, group A, and group B ($P > 0.05$).

3.6. The Expression of IL-1 β Protein in Astrocytes Cells of Trigeminal Ganglion after RS. The protein expression changes differences of IL-1 β , IL-1R I, and reference genes β -actin in rat trigeminal ganglion astrocytes of each group were compared. From Figure 7, it can be found intuitively that the protein expression level of β -actin in star glial cells of trigeminal ganglia of rats in each group was nearly the same, while the protein expression of genes IL-1 β and IL-1RI was the lowest in the control group and highest in group C.

The protein expression differences of genes IL-1 β and IL-1RI in rat trigeminal ganglion astrocytes of each group were quantitatively analyzed. As shown in Figure 8, with the increase of the RS time, The protein expression of IL-1 β in star glia cells of trigeminal ganglia showed a gradually increasing trend in each group, and the expression of IL-1 β in group B was greatly higher than that in the control group ($P < 0.05$), and that in group C was greatly higher than that in the control group ($P < 0.01$). As shown in Figure 8(b), with the increase of the RS time, the expression of IL-1RI

TABLE 1: Comparison of behavioral changes in rats after RS (mean \pm standard).

Group	Total trip (cm)	Open field test		Elevated "cross" maze test	
		Central route (cm)	Activity speed (cm/s)	Percentage of open-arm retention time (%)	Percentage of open-arm retention (%)
Control group	4011 \pm 102	126 \pm 20	4.8 \pm 0.61	40 \pm 11	39 \pm 7
Group A	3824 \pm 110	113 \pm 18	4.7 \pm 0.43	36 \pm 10	33 \pm 10
Group B	2936 \pm 127*	76 \pm 19*	3.6 \pm 0.71*	24 \pm 7*	26 \pm 8*
Group C	2538 \pm 109**	61 \pm 12**	2.8 \pm 0.52**	21 \pm 9**	23 \pm 9**

Note: *meant there was a SSD after comparison with the control group, $P < 0.05$; **indicated that there was an extremely SSD after comparison with the control group, $P < 0.01$.

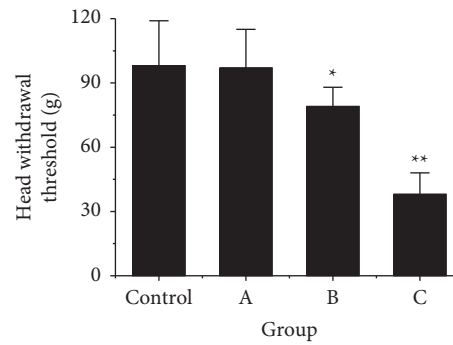


FIGURE 4: Comparison of the mean threshold of PS in the MA in rats after RS. Note: * meant there was a SSD after comparison with the control group, $P < 0.05$; **indicated that there was an extremely SSD after comparison with the control group, $P < 0.01$.

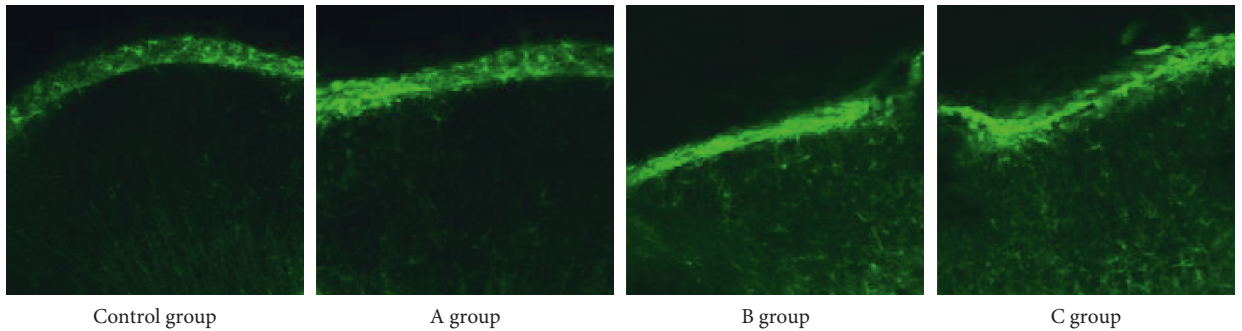


FIGURE 5: GFAP immunofluorescence staining in STN nerve in rats after RS.

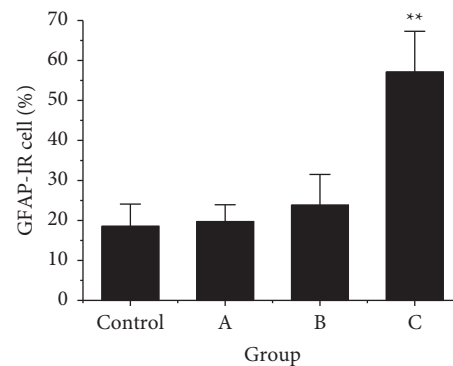


FIGURE 6: The activation rate of GFRP in STN of rats after RS. Note: **indicated a very SSD after comparison with the control group ($P < 0.01$).

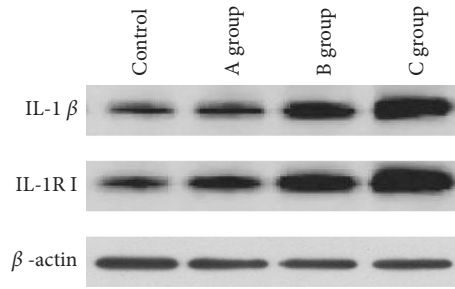


FIGURE 7: Western blot results of genes *IL-1β* and *IL-1RI* in rat trigeminal ganglion astrocytes.

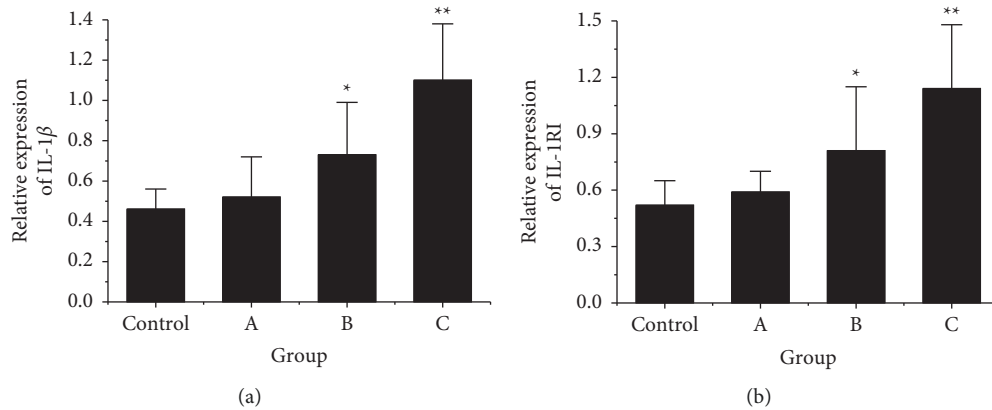


FIGURE 8: The quantitative results of *IL-1β* and *IL-1RI* proteins in rat trigeminal ganglion astrocytes. Note: (a) was the quantitative result of *IL-1β* protein expression; (b) was the quantitative result of *IL-1RI* protein expression; * indicated that there was SSD after comparison to the control group, $P < 0.05$; ** indicated that there were extremely SSDs after comparison to the control group, $P < 0.01$.

protein in star glial cells of trigeminal ganglia of rats in each group also showed a trend of gradual increase, and the expression of *il-1ri* protein in rats in group B was greatly higher than that in the control group ($P < 0.05$), and the expression of *IL-1RI* protein in rats in group C was greatly higher than that in the control group ($P < 0.01$). However, there was no SSD in *IL-1β* and *IL-1RI* protein expressions between the control group and group A ($P > 0.05$).

4. Discussion

In recent years, the methods used to construct animal models of psychological stress include electric foot stimulation, thermal stimulation, compulsive swimming treatment, restraint method, and so on, the stress model obtained by the restraint method can cause a typical nonspecific stress response in animals and does not cause direct trauma to the animal body [9, 10]. In this research, stress animal models were obtained by a restraint method. Results were found with the increase of bound time, and the model rats showed slow downward movement and WGR, and bondage stress model of rats serum levels of stress hormones. CORT and ACTH also increased with the increase of stress time reduce, indicating that the rat model with the constraints of this study to construct stress has been in a state of stress [11]. Studies have shown that psychological stress can affect the emotion-related hippocampus and other tissues in the brain

of rats, thereby causing behavioral changes in rats [12]. In this research, under the open-field test and the elevated “cross” maze test, it showed that with the increase of the stress time, the activity level of the rat model with RS decreased greatly, indicating that the rats had negative anxiety emotions, which was consistent with the results of Xin et al. [13].

The activity of atpase in the masseter of rats decreases gradually after they are subjected to psychological stress, which can increase the sensitivity of masseter myodynamia [14]. In this research, it showed that the mean pain threshold in the MA of rats decreased with the increase of stress time after stress stimulation was restricted, indicating that psychological stress would lead to the increase of PS in the MA of rats, which was consistent with Muzalev’s research results [15]. The reason for this phenomenon may be that when the rats are in a state of stress, they would increase the secretion of hormones such as epinephrine in their bodies, which would lead to local hypoxia and ischemia after increased muscle activity. The caudal subnucleus of the STN played an important role in the transmission of pain in the oral and maxillofacial regions. Okamoto et al. found that when the rats were subjected to compulsive swimming stress, the pain threshold of the mouth and maxillofacial region decreased, and the activation degree of neurons in the caudal subnucleus of the STN was significant increased [16]. When the astrocytes in the STN were activated, the specific markers of

GFAP expression would obviously rise [17]. This is consistent with the findings in this research that the proportion of GFAP positive neurons in the brain tissues of rats increased greatly with the increasing time of RS, indicating that astrocytes and neurons in the trigeminal nerve were greatly activated, which indicates that with the passage of stress time, the activation of astrocytes and neurons in the trigeminal nerve will become more and more obvious [18]. The relationship between astrocytes and neurons in trigeminal ganglion is an important part of nerve signal regulation. The activated glial cells release a series of inflammatory factors, such as interleukin-1 ($IL-1\beta$), which bind to the relevant receptors on the surface of the neuron, thereby enhancing the physiological activity of the neuron and finally aggravating the sensitivity of maxillofacial pain [19, 20]. It was found that with the increase of stress time, the protein expression of $IL-1\beta$ and $IL-1RI$ in rat trigeminal ganglion astrocytes increased greatly at 14 d of the stress, indicating that the release of $IL-1\beta$ and $IL-1RI$ can activate astrocytes, which in turn increases the sensitivity of the masseter pain in rats, which was consistent with the research results of Doyle et al. [21].

In this research, the RS method was used to construct rat models with different stress times. The stress rat model was verified by open-field test and elevated “cross” maze test. Subsequently, the changes in PS in the MA and the expression of astrocyte-specific marker GFAP in the brain tissues of the rat model were detected under different RS times. The results showed that the rat model of psychological stress was successfully constructed by restraint method, and the PS of the MA in the rat model increased with the increase of stress time. Finally, it was found that the STN neurons and astrocytes in rat brain may be activated due to the increase of the release of $IL-\beta$ and $IL-1RI$. However, only basic research was constructed, and the molecular regulatory mechanism that increases the sensitivity of masseter myalgia in rats after stress stimulation needs to be further studied. In conclusion, the results can lay a foundation for the subsequent research on the PS of MA caused by psychological stress.

Data Availability

The datasets used and analyzed during the current study are available from the author upon reasonable request.

Conflicts of Interest

The author declares that there are no conflicts of interest.

References

- [1] H. Miwa, T. Kondo, and T. Oshima, “Gastroesophageal reflux disease-related and functional heartburn: pathophysiology and treatment,” *Current Opinion in Gastroenterology*, vol. 32, no. 4, pp. 344–352, 2016.
- [2] J. F. Jin, X. Gao, and J. Y. Zhang, “Effects of psychological stress on phenotype and function of $CD11b^{+}Gr1^{+}$ myeloid cells,” *Journal of Harbin Medical University*, vol. 52, no. 3, pp. 199–205, 2018.
- [3] S. Assad, H. H. Khan, H. Ghazanfar et al., “Role of sex hormone levels and psychological stress in the pathogenesis of autoimmune diseases,” *Cureus*, vol. 9, no. 6, Article ID e1315, 2017.
- [4] M. A. Albert, E. M. Durazo, N. Slopen et al., “Cumulative psychological stress and cardiovascular disease risk in middle aged and older women: rationale, design and baseline characteristics,” *American Heart Journal*, vol. 192, pp. 1–12, 2017.
- [5] R. J. Field, J. A. C. Gallas, and D. Schuldburg, “Periodic and chaotic psychological stress variations as predicted by a social support buffered response model,” *Communications in Nonlinear Science and Numerical Simulation*, vol. 49, pp. 135–144, 2017.
- [6] M. J. M. Fischer, J. Schmidt, S. Koulchitsky, S. Klusmann, A. Vater, and K. Messlinger, “Effect of a calcitonin gene-related peptide-binding L-RNA aptamer on neuronal activity in the rat spinal trigeminal nucleus,” *The Journal of Headache and Pain*, vol. 19, no. 1, p. 3, 2018.
- [7] K. Nakamoto, F. Aizawa, M. Kinoshita, Y. Koyama, and S. Tokuyama, “Astrocyte activation in locus coeruleus is involved in neuropathic pain exacerbation mediated by maternal separation and social isolation stress,” *Frontiers in Pharmacology*, vol. 8, no. Suppl 1, p. 401, 2017.
- [8] Q. Li, M. Zhang, Y. J. Chen, Y. J. Wang, F. Huang, and J. Liu, “Oxidative damage and HSP70 expression in masseter muscle induced by psychological stress in rats,” *Physiology & Behavior*, vol. 104, no. 3, pp. 365–372, 2011.
- [9] A. Linson, T. Parr, and K. J. Friston, “Active inference, stressors, and psychological trauma: a neuroethological model of (mal) adaptive explore-exploit dynamics in ecological context,” *Behavioural Brain Research*, vol. 380, Article ID 112421, 2020.
- [10] S. Ueda, T. Yamaguchi, and A. Ehara, “Neonatal shaking brain injury changes psychological stress-induced neuronal activity in adult male rats,” *Neuroscience Letters*, vol. 718, Article ID 134744, 2020.
- [11] C. G. Titto, J. A. Negrão, T. D. S. Canaes et al., “Heat stress and ACTH administration on cortisol and insulin-like growth factor I (IGF-I) levels in lactating Holstein cows,” *Journal of Applied Animal Research*, vol. 45, no. 1, pp. 1–7, 2017.
- [12] J. E. Finnell, C. M. Lombard, A. R. Padi et al., “Physical versus psychological social stress in male rats reveals distinct cardiovascular, inflammatory and behavioral consequences,” *PLoS One*, vol. 12, no. 2, Article ID e0172868, 2017.
- [13] Y. Y. Xin, J. H. Wu, Z. X. Yao, Q. Guan, A. Aleman, and Y. Luo, “The relationship between personality and the response to acute psychological stress,” *Scientific Reports*, vol. 7, no. 1, Article ID 16906, 2017.
- [14] W. Lin, Y. Zhao, B. Cheng et al., “NMDAR and JNK activation in the spinal trigeminal nucleus caudalis contributes to masseter hyperalgesia induced by stress,” *Frontiers in Cellular Neuroscience*, vol. 13, p. 495, 2019.
- [15] K. Muzalev, C. M. Visscher, M. Koutris, and F. Lobbezoo, “Long-term variability of sleep bruxism and psychological stress in patients with jaw-muscle pain: report of two longitudinal clinical cases,” *Journal of Oral Rehabilitation*, vol. 45, no. 2, pp. 104–109, 2018.
- [16] I. Fukushi, S. Yokota, and Y. Okada, “The role of the hypothalamus in modulation of respiration,” *Respiratory Physiology & Neurobiology*, vol. 265, pp. 172–179, 2019.
- [17] please provide the complete details for reference [18].
- [18] K. Okamoto, A. Tashiro, Z. Chang, R. Thompson, and D. A. Bereiter, “Temporomandibular joint-evoked responses by spinomedullary neurons and masseter muscle are

- enhanced after repeated psychophysical stress,” *European Journal of Neuroscience*, vol. 36, no. 1, pp. 2025–2034, 2012.
- [19] M. E. Jones, C. L. Lebonville, J. E. Paniccia, M. E. Balentine, K. J. Reissner, and D. T. Lysle, “Hippocampal interleukin-1 mediates stress-enhanced fear learning: a potential role for astrocyte-derived interleukin-1 β ,” *Brain, Behavior, and Immunity*, vol. 67, pp. 355–363, 2018.
- [20] F. Liu, Y. Y. Zhang, N. Song et al., “GABAB receptor activation attenuates inflammatory orofacial pain by modulating interleukin-1 β in satellite glial cells: role of NF- κ B and MAPK signaling pathways,” *Brain Research Bulletin*, vol. 149, pp. 240–250, 2019.
- [21] S. Ayoub, A. Berbéri, and M. Fayyad-Kazan, “Cytokines, masticatory muscle inflammation, and pain: an update,” *Journal of Molecular Neuroscience*, vol. 70, no. 5, pp. 790–795, 2020.

Retraction

Retracted: Correlation between Pain Scores and Disc Height Changes after Discectomy in Patients with Lumbar Disc Herniation: A Systematic Review and Meta-Analysis

Computational Intelligence and Neuroscience

Received 25 July 2023; Accepted 25 July 2023; Published 26 July 2023

Copyright © 2023 Computational Intelligence and Neuroscience. This is an open access article distributed under the Creative Commons Attribution License, which permits unrestricted use, distribution, and reproduction in any medium, provided the original work is properly cited.

This article has been retracted by Hindawi following an investigation undertaken by the publisher [1]. This investigation has uncovered evidence of one or more of the following indicators of systematic manipulation of the publication process:

- (1) Discrepancies in scope
- (2) Discrepancies in the description of the research reported
- (3) Discrepancies between the availability of data and the research described
- (4) Inappropriate citations
- (5) Incoherent, meaningless and/or irrelevant content included in the article
- (6) Peer-review manipulation

The presence of these indicators undermines our confidence in the integrity of the article's content and we cannot, therefore, vouch for its reliability. Please note that this notice is intended solely to alert readers that the content of this article is unreliable. We have not investigated whether authors were aware of or involved in the systematic manipulation of the publication process.

Wiley and Hindawi regrets that the usual quality checks did not identify these issues before publication and have since put additional measures in place to safeguard research integrity.

We wish to credit our own Research Integrity and Research Publishing teams and anonymous and named external researchers and research integrity experts for contributing to this investigation.

The corresponding author, as the representative of all authors, has been given the opportunity to register their agreement or disagreement to this retraction. We have kept a record of any response received.

References

- [1] Y. Zheng, T. Lan, X. Chen, Z. Hus, and R. Zhang, "Correlation between Pain Scores and Disc Height Changes after Discectomy in Patients with Lumbar Disc Herniation: A Systematic Review and Meta-Analysis," *Computational Intelligence and Neuroscience*, vol. 2022, Article ID 2580004, 9 pages, 2022.

Research Article

Correlation between Pain Scores and Disc Height Changes after Discectomy in Patients with Lumbar Disc Herniation: A Systematic Review and Meta-Analysis

Yuchen Zheng , Tao Lan, Xiaosheng Chen, Zhihao Hus, and Rui Zhang 

Department of Spine Surgery, Shenzhen Second People's Hospital, The First Affiliated Hospital of Shenzhen University, Shenzhen 518035, China

Correspondence should be addressed to Yuchen Zheng; chinazuc@163.com and Rui Zhang; gukechinazuc@163.com

Received 16 May 2022; Revised 20 June 2022; Accepted 23 June 2022; Published 5 August 2022

Academic Editor: Dong Chen

Copyright © 2022 Yuchen Zheng et al. This is an open access article distributed under the Creative Commons Attribution License, which permits unrestricted use, distribution, and reproduction in any medium, provided the original work is properly cited.

Background. Surgery can reduce and improve lumbar disc herniation, but some patients still have pain after surgery, and the relationship between lumbar disc height and pain after surgery is still unclear. **Objective.** The main objective is to investigate the relationship between lumbar disc height and postoperative pain. **Methods.** We searched Pubmed, Web of Science, the Cochrane library, and Embase online for cohort studies or RCT studies on discectomy and assessed the quality of the included articles using the Newcastle-Ottawa Scale (NOS scale), with disc height (DH) and postoperative back pain as the main clinical outcome indicators, and the correlation coefficient between DH and back pain as the statistic to assess the pooled effect size. **Results.** 10 kinds of literature were included in this study for quantitative analysis. A total of 589 patients participated in the study. The follow-up time was between 1 and 2.3 years. Meta-analysis showed that after surgery, the relief of back pain was statistically significant ($MD = -2.57$, 95% CI $(-3.10, -2.04)$, $Z = -9.570$, $P < 0.0001$), the reduction of disc height was statistically significant ($MD = -0.82$, 95% CI $(-1.11, -0.52)$, $Z = -5.477$, $P < 0.0001$), the combined value of correlation coefficient Fisher's Z value was 0.33, 95% CI $(0.25, 0.42)$, with statistical significance ($P < 0.00001$), suggesting that the degree of back pain after surgery showed a moderate positive correlation with disc height in the short term. **Discussion.** After discectomy, the degree of pain is relieved, the disc height is reduced, and low back pain in the short term and disc height showed a moderate positive correlation, but the long-term correlation remains to be studied in depth.

1. Introduction

Lumbar disc herniation (LDH) is a common spinal disorder with low back and leg pain in the elderly. The cause is degeneration of the lumbar disc, which ruptures the annular fibers, exposes the nucleus pulposus, compresses nerve bundles, and causes persistent pain [1]. Lumbar disc herniation is clinically presented as a syndrome of lumbar and leg pain, and degenerative changes in intervertebral discs, trauma, pregnancy, and even heredity can cause its onset. For patients with mild symptoms, nonsurgical treatment (physical therapy, drug therapy, diet modification, lifestyle changes) is preferred, but for patients with severe symptoms, recurrent attacks, and ineffective treatment with nonsurgical methods, minimally invasive spinal techniques can be considered, and

especially, endoscopic spinal surgery is recommended [2]. Despite the excellent clinical outcome of surgery, it has been reported that 30% of patients still have low back pain (LBP) [3]. Factors such as unreasonable choice of surgical patients, unclear diagnosis, and outdated surgical instruments or techniques may be related to persistent postoperative low back pain, but the exact cause is unclear [4]. As the partially herniated nucleus pulposus tissue is removed in lumbar discectomy, the loss of intervertebral disc height (DH) or even lumbar instability may occur after the operation, or it may accelerate the degeneration process of surgery and cause the recurrence of low back pain or LDH [5]. Some studies [6] have shown that decreased DH after lumbar discectomy may be one of the causes of long-term low back and leg pain. However, some studies [7] suggested that the decrease in

intervertebral disc height in a short period of time contributed to the alleviation of pain, and in order to understand the correlation between DH and low back pain after lumbar discectomy, we performed this meta-analysis.

2. Materials and Methods

2.1. Database and Search Strategy. We searched Pubmed, Web of Science, the Cochrane library, and Embase online for the literature related to discectomy. We only included the literature published in the past 10 years from January 2011 to November 2021. The electronic search was performed with the keyword combination [discectomy] AND/OR [lumbar disc herniation] AND/OR [lumbar spine] AND/OR [percutaneous discectomy]. We set the screening criteria and screened the retrieved literature.

2.2. Literature Inclusion Criteria. (1) *Study Type*: all kinds of literature were observational studies or RCT literature, regardless of whether the research process uses blinding or not. For RCT literature, we only included one group related to discectomy in the random grouping into statistical analysis, and we did not limit the literature to prospective or retrospective cohort study; (2) *Study Subjects*: all patients were treated with disc herniation; (3) *Intervention Type*: all patients received discectomy for surgical intervention, and we did not limit the types of surgery to percutaneous endoscopic lumbar discectomy (PLED), microendoscopic discectomy (MED), or conventional lumbar discectomy (CLD) and did not limit the implantation of an annular closure device during surgery. (4) *Outcome Indicators*: we only included the literature reporting the intervertebral disc height (DH) and postoperative back pain. In order to eliminate the heterogeneity of indicator assessment, the way to assess the pain must be reported only by VAS (Visual Analogue Scale). The short term is defined as no more than 1 month after the operation, and the long term is defined as after 1 month after the operation. The VAS score data included in the literature contain or can be extrapolated mean and standard deviation.

2.3. Literature Exclusion Criteria. (1) We excluded all case-control studies, individual case studies, reviews, and meeting minutes. (2) We excluded patients whose study subjects are cervical discectomy. (3) We excluded studies that lack outcome indicators, or have no data. Lumbar disc herniation was excluded as a multisegment herniation, with a history of lumbar spine surgery, and diseases affect the evaluation of efficacy such as vertebral instability, spinal deformity, spinal stenosis, and severe osteoporosis. The types of excluded literature are reviews, animal experiments, conference papers, and repeated publications. (4) VAS scores designated as parts of the body (e.g., waist, legs) should be excluded. Studies with incomplete literature data and no access to authors in the associated literature should be excluded.

2.4. Literature Screening. The screened literature was imported into the software Note express for unified

management after retrieval and manual removal. The deduplication function of the software was used to exclude repeated literature. 2 researchers read the title and abstract for further screening. The screening results were cross-checked and discussed to determine the selected literature. If the original text could not be obtained from the Internet, the author of the original text was contacted by telephone or e-mail; if the original text could not be obtained, the literature was excluded.

2.5. Literature Quality Evaluation and Risk of Bias Assessment. The Newcastle-Ottawa Scale (NOS scale) [8] was used to analyze the quality of the included literature. The scale was used to evaluate the object selection, comparability, and outcome indicators of the literature. The maximum score was 9 points. The score of more than 5 points was considered good quality. The higher the score, the better the literature quality and the less bias.

2.6. Data Extraction and Analysis. 2 researchers independently extracted literature data: study type, location, patient age, height, weight, surgical method, surgical site, number of cohorts, follow-up time, and outcome indicators. After data extraction by 2 researchers, the results of each other were cross-checked, and the differences generated were discussed and finally determined.

2.7. Outcome Indicators. The main outcome indicators were the height of intervertebral disc height and the degree of back pain after operation (BP-VAS). There was no fixed standard for the calculation method of intervertebral disc height. We counted the DH calculation method included in the study and tried to analyze whether it would bring heterogeneity. The correlation coefficient between DH and BP-VAS in the literature was expressed by Pearson's correlation coefficient γ , and if not given directly in the literature, we will contact the original authors and calculate the correlation coefficient after obtaining the raw data. The significance of the values of the correlation coefficient γ is a very strong correlation, 0.8–1.0; strong correlation, 0.6–0.8; moderate intensity correlation, 0.4–0.6; weak correlation, 0.2–0.4; no correlation, 0–0.2.

2.8. Data Conversion. Before performing a meta-analysis of correlation coefficients, we need to convert the data (correlation coefficients γ), calculate Fisher's Z value and its SE value, and then import into meta-analysis software for inverse variance analysis [9]. The conversion formula is as follows:

$$\begin{aligned} \text{fisher's } Z &= 0.5 \times \ln \frac{1 + \gamma}{1 - \gamma}, \\ Vz &= \frac{1}{n - 3}, \\ Se &= \sqrt{Vz}. \end{aligned} \quad (1)$$

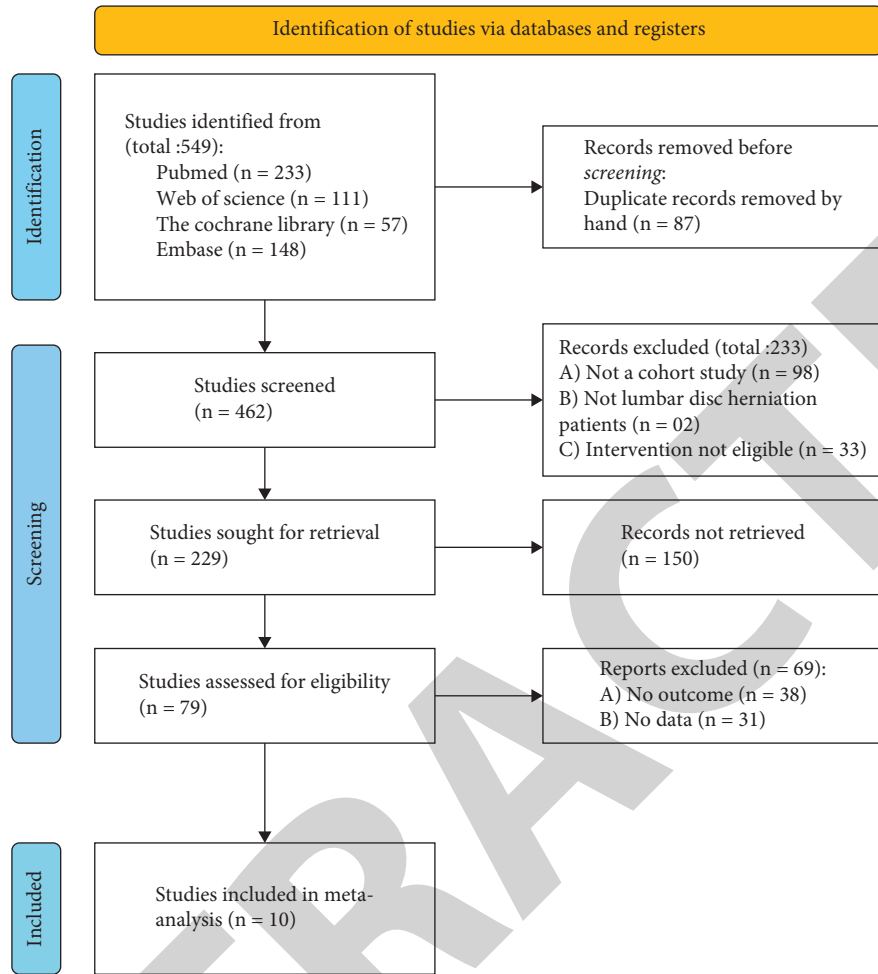


FIGURE 1: Literature selection flow chart.

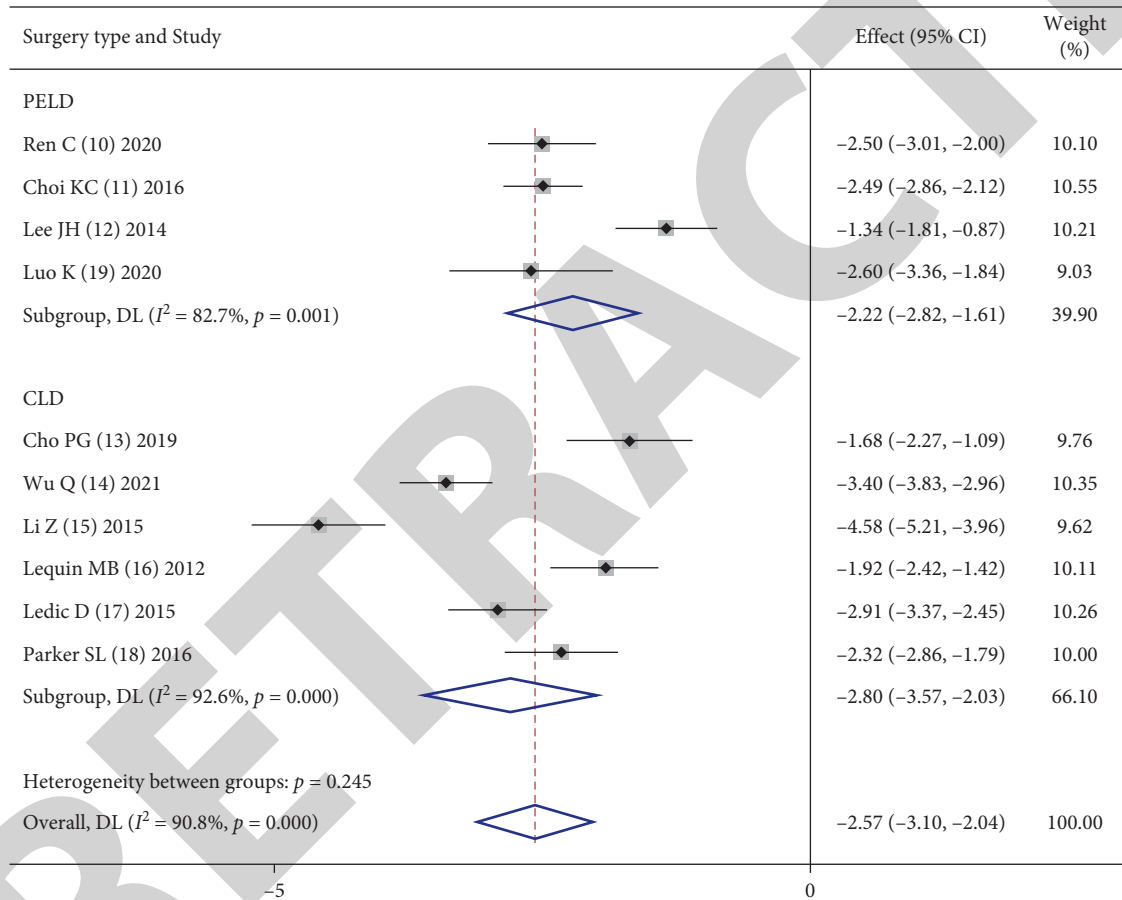
TABLE 1: Basic characteristics, intervention measures, intervention time and outcome indicators of the included literature.

Author and date of publication	Study design	Mean age (year)	Patients number	Surgery type	Surgery level	Follow-up time	DH method	Correlation coefficient γ	Outcomes
Ren C [10]	Prospective cohort study	45.6 \pm 12.2	54	PELD	L3-L4; L4-L5; L5-S1	1 years	Method 1	0.338	1/2/3/4/5
Choi KC [11]	Retrospective cohort study	38.3 \pm 10.3	100	PELD	L5-S1	2 years	Method 2	0.464	1/2/3/5
Lee JH [12]	Prospective cohort study	48.6 \pm 6.3	42	PELD	L3-L4; L4-L5; L5-S1	1 years	Method 1	0.255	1/2/3/4/5
Cho PG [13]	RCT	42.6 \pm 11.5	30	CLD	L3-L4; L4-L5; L5-S1	1 years	Method 1	0.521	1/2/3/4/5
Wu Q [14] 2021	Prospective cohort study	46.2 \pm 12	100	CLD	L3-L4; L4-L5; L5-S1	1.1 years	Method 1	0.335	1/2/3/4/5
Li Z [15]	Retrospective cohort study	38	72	CLD	L3-L4; L4-L5; L5-S1	2.3 years	Method 1	0.128	1/2/3/4/6
Lequin MB [16]	Prospective cohort study	42.3 \pm 11.4	45	CLD	L3-L4; L4-L5; L5-S1	1 years	Method 3	0.299	1/2/3/5
Ledic D [17]	Retrospective cohort study	38.3 \pm 9.5	75	CLD	L3-L4; L4-L5; L5-S1	2 years	Method 3	0.235	1/2/3/5
Parker SL [18]	Prospective cohort study	38 \pm 9	46	CLD	N/A	2 years	Method 2	0.233	1/2/3/6
Luo K [19]	Retrospective cohort study	45.6 \pm 10.9	25	PELD	L3-L4; L4-L5; L5-S1	1 years	Method 4	0.410	1/2/3/6

Outcomes: 1. back pain (VAS); 2. leg pain (VAS); 3. ODI score; 4. SF36 score; 5. disc height; 6. JOA score. DH method: Method 1 - the (anterior + posterior disc height)/2; Method 2 - the vertical distance between the posterior lower plate of the L5 vertebral body (VB) and the posterior upper plate of the sacrum; Method 3 - the distance between the anterior-inferior corner of the superior vertebra and the corresponding corner of the inferior vertebra. Method 4 - the (anterior disc height + central disc height + posterior disc height)/3. Abbreviations. PELD-percutaneous endoscopic lumbar discectomy. CLD-conventional lumbar discectomy. ODI - the Oswestry disability Index. JOA - Japanese orthopaedic association (JOA) score. N/A- not available.

TABLE 2: Quality assessment based on Newcastle-Ottawa scale (NOS).

Study	Case selection (/4)	Comparability (/2)	Outcome indicators (/3)	Total score (/9)
Ren C [10]	4	2	3	9
Choi KC [11]	4	2	2	8
Lee JH [12]	4	2	2	8
Cho PG [13]	4	2	3	9
Wu Q [14]	4	1	2	7
Li Z [15]	4	1	2	7
Lequin MB [16]	4	1	2	7
Ledic D [17]	4	2	2	8
Parker SL [18]	4	2	3	9
Luo K [19]	4	2	2	8



NOTE: Weights and between-subgroup heterogeneity test are from random-effects model

FIGURE 2: Changes in the degree of back pain before and after discectomy (grouped by surgical method).

2.9. Statistical Methods. (a) We used both STATA 16.0 (released by STATA Corp LLC) and Revman 5.3 (released by The Nordic Cochrane Centre, The Cochrane Collaboration, 2014) for analysis; (b) continuous variables were reported using mean difference (SMD) and 95% CI statistics, using STATA 16.0 software to analyze; (c) correlation coefficient analysis inputs Fisher's Z statistics and Se value after correlation coefficient γ conversion into Revman 5.3 software. The inverse variance was used for analysis, and the forest plot descriptive statistics were used for comparison. (d) The

I^2 analysis and Q test were used for literature heterogeneity. The $I^2 > 50\%$ or $P < 0.1$ indicated heterogeneity of the results. The random-effect model was used to obtain the SMD value, and otherwise, the fixed-effect model was used to obtain the SMD value; (e) if the heterogeneity analysis suggested heterogeneity between the kinds of literature, the subgroup analysis investigated the heterogeneity source. When the heterogeneity source could not be determined, the general description was adopted; (f) the funnel plot was used to represent the publication bias.

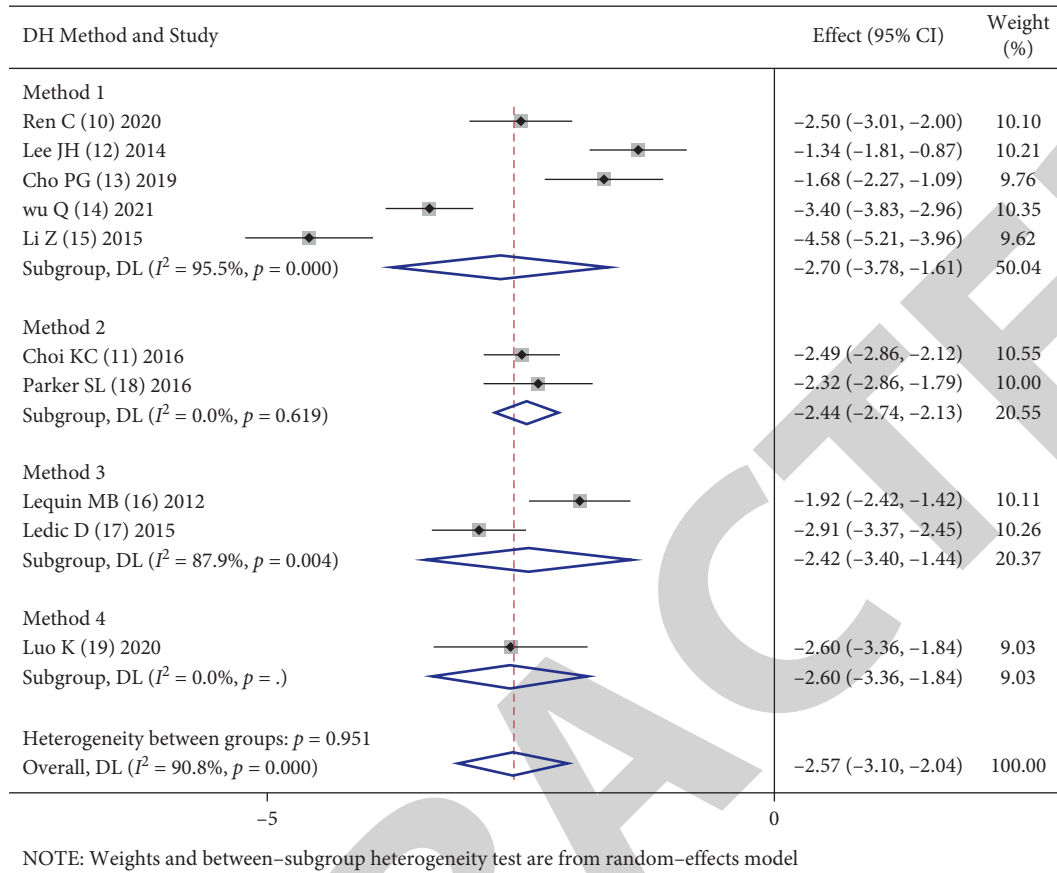


FIGURE 3: Changes in the degree of back pain before and after discectomy (grouped according to DH calculation method).

3. Results

3.1. Literature Screening Process and Results. Figure 1 shows the flow chart of literature selection, and finally, 10 kinds of literature were included in the quantitative analysis, with a total of 589 patients participating in the study.

3.2. Basic Characteristics of Literature. Ten kinds of literature were included in this study, including 4 retrospective cohort studies, 5 prospective cohort studies, and 1 RCT study. The minimum follow-up time was 1 year, and the maximum follow-up time was 2.3 years. The details are shown in Table 1.

3.3. Literature Quality and Bias Evaluation. In this study, all the included cases in the literature [10–19] were representative, with a less potential risk of bias. Some literature [14–16] did not describe the baseline data, and some literature did not describe the drop-out cases in detail [11,12,14–17,19]. However, the overall quality score of all literature was 7–9 points, with good quality, as shown in Table 2.

3.4. Meta-Analysis Results

3.4.1. Changes in the Degree of Pain (back) before and after Lumbar Discectomy. All literature [10–19] reported the back pain severity (BP-VAS). Meta-analysis was performed using

random-effect model. After the surgery, the back pain was significantly relieved, with statistical significance ($MD = -2.57$, 95% CI $(-3.10, -2.04)$, $Z = -9.570$, $P < 0.0001$).

Further subgroup analysis of the literature according to the surgical method or DH calculation method showed that there was still heterogeneity among the internal literature, but the degree of back pain relief was statistically significant among the literature ($P < 0.0001$), as shown in Figures 2 and 3.

3.4.2. Changes in Disc Height before and after Lumbar Discectomy (mm). All literature [10–19] reported the change in disc height before and after the operation. The random-effects model analysis was used to obtain that the disc height decreased after the operation. The decrease was statistically significant ($MD = -0.82$, 95% CI $(-1.11, -0.52)$, $Z = -5.477$, $P < 0.0001$).

Further subgroup analysis of the literature according to the surgical method or DH calculation method showed that there was still heterogeneity among the internal literature, and the decrease in disc height before and after the surgery was statistically significant ($P < 0.0001$), as shown in Figures 4 and 5.

3.4.3. Meta-Correlation Coefficient Analysis between the Degree of (back) Pain and Disc Height. There was no statistical heterogeneity in the reported correlation coefficient

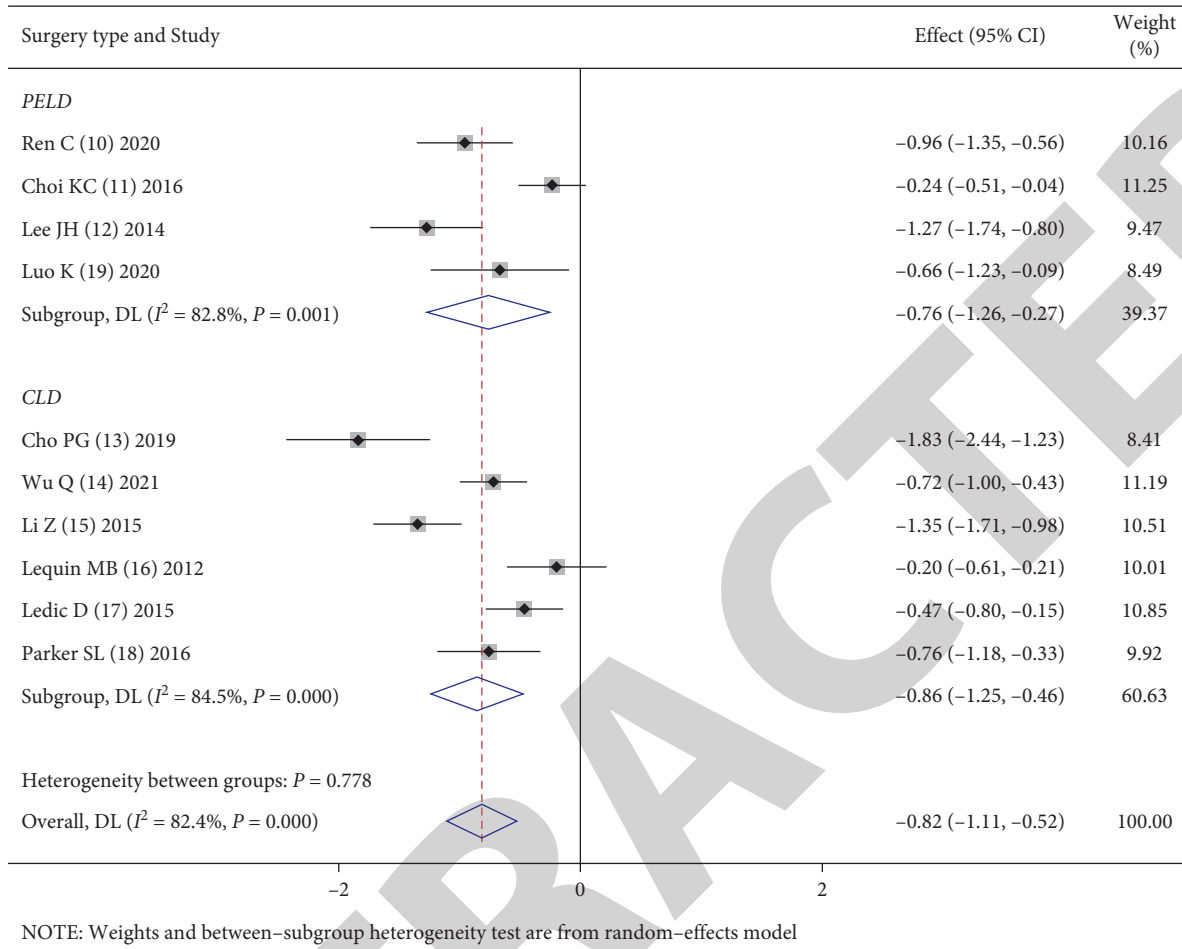


FIGURE 4: Changes of disc height before and after discectomy (grouped by surgical method).

between the 10 included literature ($I^2 = 0\%$, $P = 0.46$). Fixed-effect model was used, and meta-analysis showed that the combined value of the correlation coefficient Fisher's Z was 0.33, 95% CI (0.25, 0.42), with statistical significance ($P < 0.0001$), suggesting that there was a moderate positive correlation between the degree of back pain after surgery and disc height as shown in Figure 6.

3.4.4. Source of Heterogeneity and Sensitivity Analysis. In the analysis of the change indicator of disc height before and after the operation, there was statistical heterogeneity between the kinds of literature ($I^2 = 82.4\%$, $P = 0.01$). After the kinds of literature were divided into subgroups according to the operation method and DH calculation method, the internal heterogeneity was not eliminated. We speculated that the existence of heterogeneity may be related to multiple factors such as patient age level, disease type, operation method, and follow-up time.

In the correlation coefficient analysis, the random-effects model was used, and the results were similar to those of the fixed-effects model, showing that the results had good stability (good sensitivity).

3.4.5. Publication Bias Analysis. In the analysis of the correlation coefficient, the funnel plot shows that the two sides of the funnel are basically evenly distributed, suggesting that the publication bias is small, as shown in Figure 7.

4. Discussion

In this meta-analysis, we retrieved and identified 10 related articles with a total of 589 patients who underwent 2 types of surgery: PELD or CLD. All kinds of literature reported lower back pain (VAS) and disc height value. All patients had statistically significant pain relief and DH value reduction by comparing the data before and after the operation. We tried to analyze the kinds of literature. 221 patients underwent PELD surgery in 4 kinds of literature, 368 patients underwent CLD surgery in 6 literature. 5 kinds of literature used Method 1 DH calculation method, 2 kinds of literature used Method 2, 2 kinds of literature used Method 3, and 1 literature used Method 4. All blood pressure-VAS and DH statistical results show that pain relief can be achieved regardless of which discectomy is used, and disc height is reduced in any surgical method. The study by Orpen

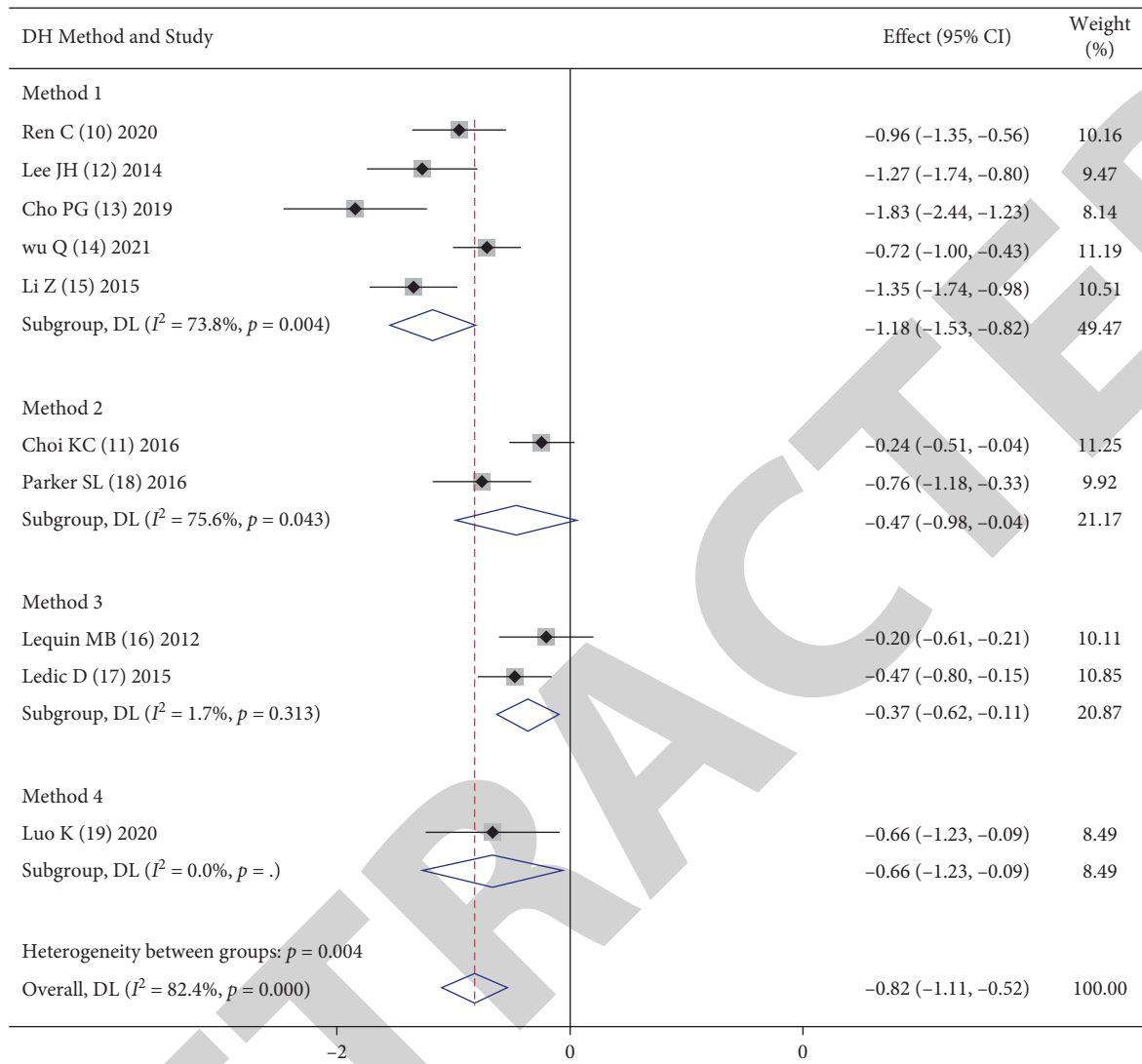


FIGURE 5: Changes in disc height before and after discectomy (grouped by DH calculation method).

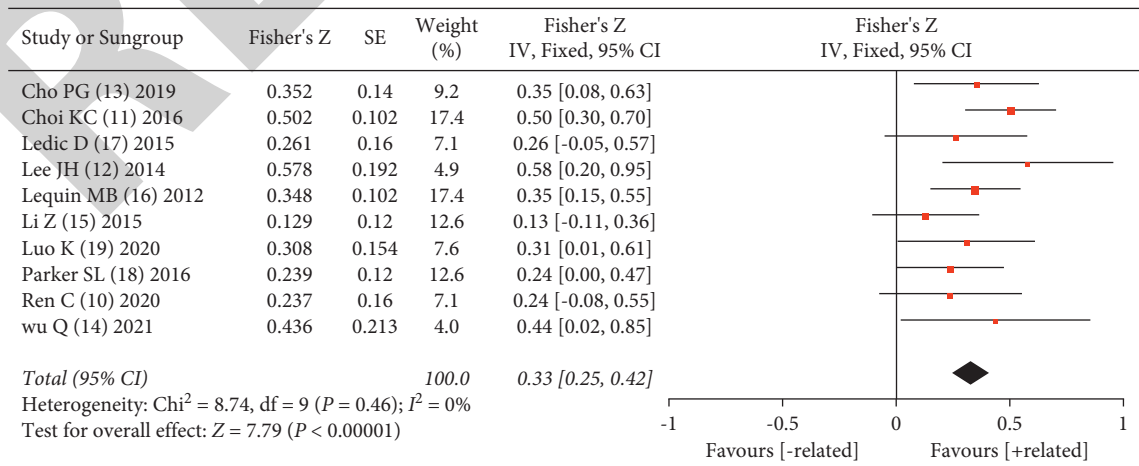


FIGURE 6: Correlation analysis between the degree of back pain after discectomy and disc height.

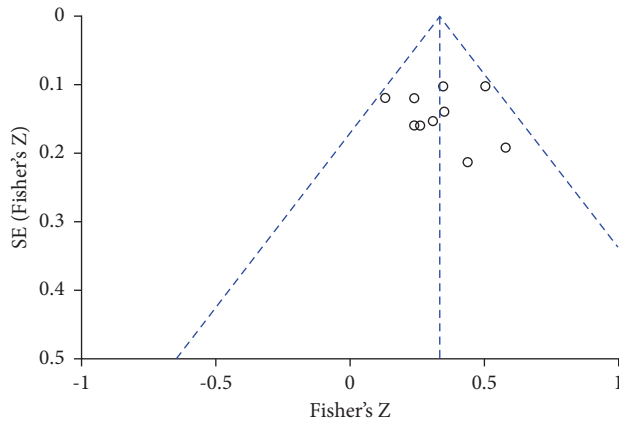


FIGURE 7: Funnel plot analysis.

et al. [20] concluded that the nucleus pulposus tissue is a gelatinous semiliquid substance with some fluidity. After a discectomy to remove a part of the nucleus pulposus tissue, the original integrity of the intervertebral disc has been damaged. The intervertebral disc capacity will gradually show degeneration and absorption phenomenon, so that the overall structure formed by the intervertebral disc and the upper and lower vertebral bodies are damaged. The height of the lesion space naturally decreases, which makes the intervertebral disc height decrease accordingly.

In this meta-analysis, we performed a summary of Fisher's Z transformation on the correlation coefficient γ between lower back pain (VAS) and disc height reported in each literature, and Revman's pooling was performed using the inverse variance method and presented in a forest plot, resulting in a fisher's Z pooling was 0.33, 95% CI (0.25,0.42), which was statistically significant ($P < 0.00001$), and the forest plot showed that there was a moderately strong correlation between lower back pain and disc height values. Studies [21] have shown that after discectomy, the destruction of vertebral annular integrity leads to significant changes in disc pressure and changes in disc height, which may be related to the amount of resection and the degree of disc bulging. A decrease in DH may lead to a decrease in the relative movement between the vertebrae, which can quickly reduce exercise-related pain [22]. However, with the decrease in the height of the intervertebral disc, the anterior and posterior longitudinal ligaments of the intervertebral disc become relaxed, and the range of motion of the lumbar spine increases, which may lead to adhesions and hyperplasia of the small joints, thus affecting the stability of the lumbar spine [23]. In the long term, decreased intradiscal pressure and increased facet loading after the loss of DH after discectomy have the potential to have adverse effects on the stability of the spine, increasing postoperative pain scores[24]. However, there are also some shortcomings in this study, as the maximum follow-up time of the studies we included was 2.3 years and no long-term follow-up was studied, so there are still some limitations to the correlation between lower back pain (VAS) and intervertebral disc height values.

10 RCTs were included in this study. The total score of the NOS methodology assessment was more than 7 points, with good quality. During subgroup analysis, heterogeneity was still shown in the 2 groups, which may be related to multiple factors such as patient age level, disease type, surgical method, and follow-up time. However, for the analysis of the correlation coefficient between the lower back pain (VAS) and disc height value, there was no heterogeneity among the literature, and the results were stable. The funnel plot showed that the distribution on both sides was symmetrical, suggesting that the publication bias was small. However, this study did not include long-term follow-up studies, and the study on this topic still needs to be further explored in terms of sample size.

5. Conclusion

This meta-analysis included 10 literature with a total of 589 patients. The results showed that the pain was relieved after discectomy, and the intervertebral disc height was reduced. There was a moderate positive correlation between low back pain and intervertebral disc height in a short period of time. However, the long-term correlation remains to be further studied.

Data Availability

No data were used to support this study.

Conflicts of Interest

The authors declare that they have no conflicts of interest.

References

- [1] L. Dang, Z. Chen, X. Liu et al., "Lumbar disk herniation in children and adolescents," *Neurosurgery*, vol. 77, no. 6, pp. 954–959, 2015.
- [2] F. Schils, B. Rilliet, and M. Payer, "Implantation of an empty carbon fiber cage crest or a tricortical iliac fiber cage autograft after cervical discectomy for single-level disc herniation: a prospective study [published correction appears in," *Journal of Neurosurgery: Spine*, vol. 18, no. 1, p. 107, 2013.
- [3] Frédéric, "Schils [corrected to schils, frédéric]; benedict, rilliet [corrected to rilliet, benedict]," *Journal of Neurosurgery: Spine*, vol. 4, no. 4, pp. 292–299, 2006.
- [4] S. L. Parker, S. K. Mendenhall, S. S. Godil, P. Siva subramanian, K. Cahill, and M. J. Ziewacz, "Incidence of low back pain after lumbar discectomy for herniated disc and its effect on patient-reported outcomes," *Clinical Orthopaedics and Related Research*, vol. 473, no. 6, pp. 1988–1999, 2015.
- [5] K. T. Kim, D. H. Lee, D. C. Cho, J. K. Sung, and Y. B. Kim, "Preoperative risk factors for recurrent lumbar disk herniation in L5-S1," *Journal of Spinal Disorders & Techniques*, vol. 28, no. 10, pp. E571–E577, 2015.
- [6] C. C. Apfel, O. S. Cakmakkaya, W. Martin, M. Richmond, S. George, and J. V. Pergolizzi, "Restoration of disk height through non-surgical spinal decompression is associated with decreased discogenic low back pain: a retrospective cohort study," *BMC Musculoskeletal Disorders*, vol. 11, no. 1, p. 155, 2010.

Research Article

A Retrospective Cohort Study of Neuroendoscopic Surgery versus Traditional Craniotomy on Surgical Success Rate, Postoperative Complications, and Prognosis in Patients with Acute Intracerebral Hemorrhage

Yong Li, Senyuan Yang, Xiaobin Zhou, Runlong Lai, and Dianhui Tan 

Department of Neurosurgery, First Affiliated Hospital of Shantou University Medical College, Shantou 515041, China

Correspondence should be addressed to Dianhui Tan; yli8@stu.edu.cn

Received 30 May 2022; Revised 30 June 2022; Accepted 9 July 2022; Published 5 August 2022

Academic Editor: Dong Chen

Copyright © 2022 Yong Li et al. This is an open access article distributed under the Creative Commons Attribution License, which permits unrestricted use, distribution, and reproduction in any medium, provided the original work is properly cited.

Objective. A case-control study was adopted to explore the effect of neuroendoscopy compared with traditional craniotomy on the success rate, postoperative complications, and prognosis of patients with intracerebral hemorrhage (ICH). **Methods.** The clinical data of 106 patients with ICH treated in our hospital from March 2019 to June 2021 were collected and analyzed retrospectively and divided into two groups according to different treatment methods. The patients who were cured by craniotomy were in the control group ($n = 53$), and those who received neuroendoscopic surgery were in the research group ($n = 53$). The clinical efficacy of patients was compared, and the cognition and daily living ability were evaluated by the Trier cognitive assessment scale, limb motor function score, and activity of daily living scale. The National Institutes of Health Stroke scale (NIHSS) and Glasgow coma scale (GCS) were used to compare the neurological function of the two groups before and after treatment, and the Glasgow outcome scale (GOS) and disability rating scale (DRS) were adopted to evaluate the functional prognosis. The simplified Fugl-Meyer motor function score was adopted to evaluate the patient's limb function, the Montreal cognitive assessment scale was adopted to evaluate the patient's cognitive function, the Barthel index score was adopted to evaluate the daily living ability of patients, and the treatment of patients was recorded. **Results.** In comparison with groups, the effective rate of treatment in the research group was higher, and the difference between groups was statistically significant ($P < 0.05$). Regarding the surgical indicators, the hospital stay, intraoperative blood loss, postoperative residual blood flow, and total hospital stay in the research group were remarkably lower, the hematoma clearance rate in the research group was remarkably higher, and the difference between groups was statistically significant ($P < 0.05$). After operation, the KPS scores indicated a gradual upward trend, and those of the research group were higher at 1 month, 2 months, and 3 months after operation. The Barthel index scores were compared. After treatment, the Barthel index scores increased. In comparison with the two groups, the Barthel index scores of the research group were higher at 1 month, 2 months, and 3 months after surgery, and the difference between groups was statistically significant ($P < 0.05$). The NIHSS, GCS, and DRS scores were compared. After treatment, the NIHSS, GCS, and DRS scores were decreased. In comparison with the two groups, the NIHSS, GCS, and DRS scores of the research group were remarkably lower, and the difference between groups was statistically significant ($P < 0.05$). With regard to the cognitive and physical function recovery after treatment, the MoCA score and Fugl-Meyer score of the research group were remarkably higher, and the difference between groups was statistically significant ($P < 0.05$). The quality of life scores were compared. After treatment, the quality of life scores decreased. In comparison with the two groups, the scores of physiological function, psychological function, social function, and healthy self-awareness of the research group were lower, and the difference between groups was statistically significant ($P < 0.05$). The incidence of postoperative complications in the research group was significantly lower than that in the control group, and the difference between groups was statistically significant ($P < 0.05$). **Conclusion.** Compared with conventional craniotomy, neuroendoscopic surgery can remarkably reduce the operation time and blood loss, enhance the hematoma clearance rate, and have a better prognosis, which is more conducive to the recovery of postoperative neurological function, life activities, and quality of life of patients.

1. Introduction

Intracerebral hemorrhage (ICH) refers to primary or non-traumatic rupture of cerebral blood vessels [1]. It is an acute cerebrovascular disease with acute onset, morbidity, disability, and mortality. It seriously harms people's physical and mental health and brings heavy economic burden to the family and society. There are 1.2–1.8 million new stroke patients in my country every year, with an annual prevalence rate of 2.50/100,000 and a mortality rate of 1.224/100,000, ranking second among all causes of death [2]. About 3/4 of the survivors have varying degrees of severity including incapacity to work, of which more than 40% are severely disabled. The morbidity and mortality of cerebrovascular diseases increased significantly in old age. With the trend of population aging, people over the age of 60 in China will account for more than 10% of the total population [3]. Cerebral hemorrhage directly damages the local brain tissue and destroys the nerve conduction pathway.

Hypertensive ICH accounts for 15% of all strokes, with rapid onset, rapid progression, and high mortality and disability rates [4]. According to the results of epidemiological surveys in my country, the annual incidence of hypertensive ICH is 50–80/10,000 people, and the age is mostly concentrated in 50–70 years old, of which 60–69-year-old patients account for 30.98% of the total, and the percentage of men is more than women [5]. ICH often occurs suddenly during emotional agitation or activity, accompanied by sudden symptoms of focal neurological impairment. After onset, it often reaches its peak within a few minutes to hours, often accompanied by elevated blood pressure, headache, vomiting, meningeal irritation sign, and disturbance of consciousness. According to some data, the mortality rate at 1 month after cerebral hemorrhage is extremely high, about 40%, and only 12%–39% of survivors do not have disabilities [6]. Another study shows that, in the survivors of cerebral hemorrhage, about 20% of patients have recurrent cerebral hemorrhage. The loss of direct medical expenses in my country caused by cerebral hemorrhage every year is nearly 20 billion, which brings pain to patients, seriously affects their life and work, and increases the economic burden of their families, bringing a heavy burden to the operation of national and social medical funds [7]. The onset of cerebral hemorrhage is sudden, the disease changes rapidly, and the consequences of delayed treatment are serious. Therefore, early diagnosis and treatment have become the focus of the treatment of cerebral hemorrhage. Starting the stroke channel as soon as possible and the cooperation between neurology and surgery can remarkably reduce the mortality and disability rate of patients.

Cerebral edema is the main complication of ICH, and its occurrence and development are the key factors leading to the deterioration of ICH [7, 8]. The main methods for clinical treatment of intracerebral hemorrhage are conservative medical treatment and surgical treatment, and there is no clear reason to prove the absolute advantage of these two methods. However, from the point of view of the treatment

effect and treatment process, the use of surgical methods is beneficial to clear the hematoma, enhance the ischemic problem, and reduce the injury of the involved hematoma to the patients, so it is more in line with the development of medicine. Melmed and other industry researchers have summarized clinical experiments and treatment data and found that neuroendoscopy can effectively remove the intracerebral hematoma, reduce the amount of bleeding during treatment, and enhance the treatment effect and prognosis [8]. The American Heart Association guidelines also point out that surgery has a positive effect on removing cerebral hematoma and the optimal treatment time is within 12 hours of onset. At present, the clinical treatment of cerebral hemorrhage mainly includes traditional cranial hematoma evacuation, burr hole hematoma drainage, microsurgical hematoma evacuation, and neuroendoscopic minimally invasive hematoma evacuation. Classical craniotomy with craniotomy for hematoma debridement has a large exposed area of brain tissue, which is prone to cause unnecessary damage, and the operation time is 5 times that of endoscopic surgery. Moreover, the hematoma clearance rate is low, and the patient needs to be injected with urokinase repeatedly to maintain his life after surgery, which easily increases the probability of intracranial infection. Microsurgery also requires stretching of the brain tissue, and excessive stretching increases the likelihood of cerebral ischemia and cerebral edema. In the context of medical development, neuroendoscopic minimally invasive surgery has become the main clinical surgical method for the treatment of cerebral hemorrhage due to its small trauma, less blood loss, and ability of completely removing brain edema. Clinical practice shows that the skin incision using neuroendoscopic surgery is only 3–4 cm and the blood loss is much lower than other surgical methods. This surgical method uses a transparent guide with a diameter of 1 cm to quickly establish a minimally invasive surgical channel, determine the location of the hematoma cavity, and determine the degree of hematoma removal, with good results [9]. In order to verify the therapeutic effect of neuroendoscopic surgery, the author retrospectively analyzed the effect of grouping treatment of hypertensive intracerebral hemorrhage patients who underwent surgery in our hospital.

2. Patients and Methods

2.1. Normal Information. The clinical data of 106 patients with ICH treated in our hospital from March 2019 to June 2021 were collected and analyzed retrospectively and divided into two groups according to different treatment methods. Patients cured by craniotomy were included in the control group ($n=53$), and patients who underwent neuroendoscopic surgery were included in the research group ($n=53$). In the control group, the age ranged from 64 to 85 years old, with an average of 66.12 ± 6.35 years old, including 20 males and 16 females. In the research group, the age ranged from 65 to 84 years, with an average of 67.08 ± 6.79 years, including 19 males and 17 females. The general data of

patients were not statistically significant. This study was permitted by the medical ethics committee of our hospital, and all patients noticed informed consent.

Selection criteria: (1) according to the Diagnostic Essentials of all kinds of Major Cerebrovascular Diseases in China 2019 formulated by Neurology Branch of Chinese Medical Association [10], the following accords with the diagnostic points of ICH: (2) acute onset, (3) admission within 48 hours after onset, (4) brain CT or MRI showing blood foci, (5) participating in relevant examination and treatment, and (6) complete clinical data.

Exclusion criteria: (1) complication with abnormal function of important organs, such as heart, liver, kidney, and lung, (2) mental illness, (3) the possibility of death in a short time, (4) patients with excessive hematoma, cerebral hemorrhage in other parts, or brain pain that need bone flap decompression, (5) complication with infectious diseases, and (6) incomplete clinical data.

2.2. Treatment Methods. Conventional craniotomy: for patients with supratentorial cerebral hemorrhage, the surgical incision avoids important intracranial vessels and functional areas, makes a horseshoe-shaped incision about 4 cm long, and grinds a bone window with a drill and a milling cutter. The intracerebral hematoma was removed as much as possible under the microscope, and the skull was routinely closed. For patients with preoperative brain herniation or patients with severe brain swelling after removal of the hematoma during surgery, decompressive craniectomy should be given. For patients with bleeding into the ventricle, unilateral or bilateral ventricle drainage should be performed. For patients with infratentorial ICH, the patient's side is prone. According to the location of the hematoma cavity, the posterior median or paramedian surgical incision is performed. After routine craniotomy, corticotomy is adopted to reach the hematoma cavity. The maximum amount of intracerebral hematoma is removed under the microscope. Ventricular drainage should be performed first in patients with hemorrhage or hydrocephalus.

Neuroendoscopic surgery: German Snake brand 0 degrees, 30-degree neuroendoscopy and a corresponding set of TV monitoring systems, good lighting system, and micro-devices corresponding to the operation are used. According to the CT level with the largest amount of hematoma, bypass the important arteriovenous vascular area or functional areas such as sensory and motor as the surgical route. After determining the surgical incision, make a straight incision about 3 cm in length, then drill the hole with a drill, and form a 2 cm × 2 cm bone window with a milling cutter. In this study, a 5 mL BD syringe was modified into a rigid transparent mirror sheath, and the sheath core was a catheter of appropriate size.

2.3. Observation Indicator

2.3.1. Efficacy Evaluation Criteria. The curative effect was evaluated by the scoring standard of neurological impairment of stroke established by the fourth National

Conference on Cerebrovascular Diseases in 1995. The National Institutes of Health Stroke scale [11] (NIHSS) was used to evaluate the degree of neurological impairment in patients with intracerebral hemorrhage. (1) Basic recovery: NIHSS score reduction $\geq 91\%$; (2) markedly effective: $46\% \leq$ IHSS score reduction $< 90\%$; (3) effective: $18\% \leq$ NIHSS score reduction $\leq 45\%$; (4) ineffective: NIHSS score reduction $< 17\%$. Note: efficacy calculation formula: (NIHSS score before treatment – NIHSS score after treatment)/NIHSS score before treatment $\times 100\%$. The total effective rate = (the number of Basic recovery cases + the number of markedly effective cases)/the total number of cases $\times 100\%$.

2.3.2. Collection of Surgical Indicators. The surgical indicators (operation time, intraoperative blood loss, hematoma clearance rate, total hospital stay, and postoperative residual blood volume) were observed. The hematoma volume before and after operation was measured and calculated by 3D-Slicer software, hematoma clearance rate = (preoperative hematoma volume – postoperative hematoma volume)/preoperative hematoma volume $\times 100\%$.

2.3.3. Barthel Index. The Barthel index [12] was adopted to evaluate the daily living ability of the patients before and after the intervention, with a total score of 100 points. The higher the score, the stronger the daily living ability.

2.3.4. Assessment of the Degree of Neurological Deficit. Before treatment and after 8 weeks of treatment, the neurological function of the two groups of patients was recorded, and the neurological deficit was scored by the National Institute of Health Stroke scale (NIHSS) [13], which included the level of consciousness, gaze, visual field, upper limb movement, lower limb movement, ataxia, facial paralysis, sensation, language, dysarthria, neglect, and distal motor function. The higher the score, the more serious the neurological damage of the patient.

2.3.5. Coma Level Assessment. Glasgow coma scale (GCS) [14] was used to evaluate the coma degree of patients, including eye opening, language, and exercise, with a full score of 15. The lower the score, the more severe the coma.

2.3.6. Functional Prognostic Assessment. The Glasgow outcome scale (GOS) [15] was adopted to assess the degree of disability of the patients, which was assigned into death (grade I), vegetative state (grade II: long-term coma, open eyes, and periodic eye opening-awake), severe disability (grade III: inability of taking care of themselves, conscious but with severe mental and physical disabilities), moderate disability (grade IV: ability of taking care of themselves in daily life and of engaging in some daily activities in specialized environments), and good recovery (grade V: return

to normal life, self-care, but there may be minor neurological or pathological defects).

2.3.7. Cognitive Function Assessment. Cognitive function recovery was assessed using the Montreal Cognitive Assessment (MoCA) [16], with 11 items, each with a score of 0 to 30, with higher scores indicating better cognitive function.

2.3.8. Motor Function Assessment. The recovery of motor function was assessed by the Fugl-Meyer score [17], with a score ranging from 0 to 100. The higher the score, the better the motor function.

2.3.9. Quality of Life Score. Quality of life scale includes four subscales, namely, physical, psychological, social, and health self-perception, a total of 29 items; the scale's Cronbach's alpha coefficient is 0.79–0.91. The scale uses a 1–5 scale; the lower the score, the higher the satisfaction.

2.4. Statistical Analysis. Statistical software SPSS22.0 was adopted to process data, count data were presented as n , %, and rank sum test was adopted for comparison of prognosis; measurement data was presented as $\bar{x} \pm s$, and t test was performed. $P < 0.05$ was considered statistically significant.

3. Results

3.1. Comparison of Treatment Effects. First of all, we compared the therapeutic effects, and the success rate was 100.00%. In the research group, 2 cases were cured, 23 cases were markedly effective, 27 cases were effective, 2 cases were ineffective, and the treatment effective rate was 96.23%. In the control group, 0 cases were cured, 10 cases were markedly effective, 34 cases were effective, 9 cases were ineffective, and the effective rate was 83.02%. In comparison with groups, the effective rate of the research group was higher, and the difference between groups was statistically significant ($P < 0.05$). All results are indicated in Figure 1.

3.2. Comparison of Surgery-Related Indicators of Patients. We compared the surgical indicators. The length of hospital stay, intraoperative blood loss, postoperative residual blood flow, and total hospitalization days in the research group were remarkably lower, the hematoma clearance rate in the research group was remarkably higher, and the difference between groups was statistically significant ($P < 0.05$). All results are indicated in Table 1.

3.3. Comparison of Postoperative KPS Score. We compared the postoperative KPS score. The research group was followed up to 3 months after operation, and 0 cases were lost. The control group was routinely followed up to 3 months after operation, and 0 cases lost follow-up. There was no significant difference before operation ($P > 0.05$); the KPS score increased gradually after operation, the KPS score at 1 month, 2 months, and 3 months after operation in the

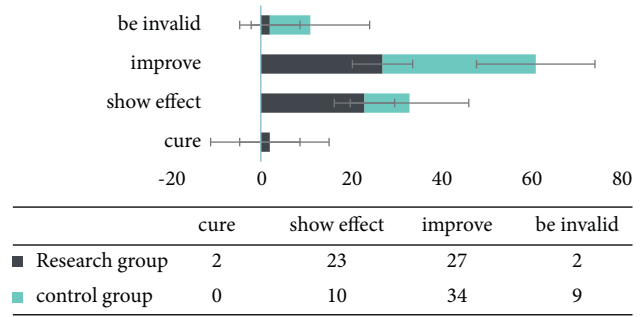


FIGURE 1: Comparison of the treatment effects of the two groups.

research group was higher than that in the control group, and the difference between groups was statistically significant ($P < 0.05$). All the results are indicated in Table 2.

3.4. Barthel Index Score Comparison. We compared the Barthel index scores. Before surgery, there was no significant difference ($P > 0.05$); after treatment, the Barthel index scores of patients increased. In comparison with the groups, the Barthel index scores of the research group were higher at 1 month, 2 months, and 3 months after the operation, and the difference between groups was statistically significant ($P < 0.05$). All results are indicated in Table 3.

3.5. Comparison of NIHSS, GCS, and DRS Scores. We compared the NIHSS, GCS, and DRS scores. Before treatment, there was no significant difference ($P > 0.05$); after treatment, the NIHSS, GCS, and DRS scores of patients were decreased. In comparison with the two groups, the NIHSS, GCS, and DRS scores of the research group were remarkably lower, and the difference between groups was statistically significant ($P < 0.05$). All results are indicated in Table 4.

3.6. Comparison of Cognitive and Physical Function Recovery of Patients after Treatment. We compared the recovery of cognitive and physical function after treatment. In comparison with the two groups, the MoCA score and Fugl-Meyer score of the research group were remarkably higher, and the difference between groups was statistically significant ($P < 0.05$). All results are indicated in Table 5.

3.7. Quality of Life Score Comparison. We compared the quality of life scores. Before treatment, there was no significant difference ($P > 0.05$); after treatment, the quality of life scores of patients decreased. In comparison with the two groups, the physical function, psychological function, social function, and healthy self-cognition scores of the research group were lower, and the difference between groups was statistically significant ($P < 0.05$). All results are indicated in Table 6.

3.8. Comparison of Postoperative Complications. We compared the postoperative complications. In the research group, 1 patient developed intracranial gas after operation, and the total incidence of postoperative complications was

TABLE 1: Comparison of surgery-related indicators between the two groups [$\bar{x} \pm s$].

Grouping	N	Operation time (min)	Intraoperative bleeding volume (ml)	Hematoma clearance rate (%)	Postoperative residual blood volume (ml)	Total hospitalization days (d)
Control group	53	1.24 ± 0.58^a	326.18 ± 96.83^a	76.82 ± 7.45^a	6.35 ± 1.17^a	16.65 ± 4.53^a
Research group	53	3.89 ± 1.25^b	42.24 ± 4.75^b	92.68 ± 8.87^b	4.16 ± 0.82^b	12.43 ± 3.12^b
t/χ^2		14.000	21.322	9.968	11.159	5.585
P		< 0.05	< 0.05	< 0.05	< 0.05	< 0.05

Note: the control group before and after treatment, ^a $P < 0.05$; the research group before and after treatment, ^b $P < 0.05$.

TABLE 2: Comparison of postoperative KPS scores between the two groups ($\bar{x} \pm s$, points).

Grouping	N	Before operation	One month after operation	2 months after operation	3 months after operation
Control group	53	70.31 ± 4.32	75.24 ± 4.76^a	77.46 ± 4.81^a	78.12 ± 4.85^a
Research group	53	71.45 ± 4.16	80.37 ± 5.41^b	83.48 ± 4.28^b	85.46 ± 5.96^b
t		1.384	5.183	6.807	6.954
P		> 0.05	< 0.05	< 0.05	< 0.05

Note: the control group before and after treatment, ^a $P < 0.05$; the research group before and after treatment, ^b $P < 0.05$.

TABLE 3: Comparison of Barthel index scores between the two groups [$\bar{x} \pm s$, points].

Grouping	N	Before operation	One month after operation	2 months after operation	3 months after operation
Control group	53	32.54 ± 3.34	47.33 ± 3.43^a	56.18 ± 5.41^a	78.31 ± 4.58^a
Research group	53	33.18 ± 3.75	59.45 ± 4.28^b	67.63 ± 3.95^b	86.43 ± 5.75^b
t		0.928	16.087	12.444	8.220
P		> 0.05	< 0.05	< 0.05	< 0.05

Note: the control group before and after treatment, ^a $P < 0.05$; the research group before and after treatment, ^b $P < 0.05$.

TABLE 4: Comparison of NIHSS, GCS, and DRS scores between two groups [$\bar{x} \pm s$, points].

Grouping	N	NIHSS scoring		GCS scoring		DRS scoring	
		Before treatment	After treatment	Before treatment	After treatment	Before treatment	After treatment
Control group	53	30.33 ± 3.16	22.33 ± 3.12^a	4.36 ± 1.23	8.44 ± 2.48^a	22.77 ± 3.83	16.18 ± 2.53^a
Research group	53	30.28 ± 3.53	14.36 ± 2.17^b	4.74 ± 1.46	13.38 ± 3.41^b	21.56 ± 3.43	12.45 ± 2.16^b
t		0.077	15.267	1.449	8.529	1.713	8.163
P		> 0.05	< 0.05	> 0.05	< 0.05	> 0.05	< 0.05

Note: comparison of control group before and after treatment, ^a $P < 0.05$; comparison of research group before and after treatment, ^b $P < 0.05$.

TABLE 5: Comparison of cognitive and physical function recovery between the two groups [$\bar{x} \pm s$, points].

Grouping	N	MoCA scoring	Fugl-Meyer scoring
Control group	53	20.17 ± 3.36^a	58.43 ± 8.77^a
Research group	53	25.28 ± 3.95^b	74.33 ± 10.26^b
t		7.174	8.576
P		< 0.05	< 0.05

Note: comparison of control group before and after treatment, ^a $P < 0.05$; comparison of research group before and after treatment, ^b $P < 0.05$.

1.89%. In the control group, there were 2 cases of recurrent hemorrhage, 3 cases of intracranial gas accumulation, 3 cases of intracranial infection, and 1 case of cerebral infarction. The total incidence of postoperative complications was 16.98%, the incidence of postoperative complications in the research group was remarkably lower, and the difference between groups was statistically significant ($P < 0.05$). All the results are indicated in Figure 2.

4. Discussion

The incidence of ICH has a gradually increasing trend. It poses a great threat to the health of people over 60 years old. ICH can cause acute mass effect, destroy surrounding brain tissue, and often lead to early death of the patient [18]. The space occupying effect of hematoma is an important cause of primary injury. According to epidemiological investigation and analysis, the incidence of cerebral hemorrhage accounts for 10% and 30% of stroke, and primary cerebral hemorrhage with hypertension accounts for 70% of spontaneous cerebral hemorrhage, of which 80% has a higher incidence; it also has high mortality (40% and 60%), high disability rate (50% and 85% survivors), and high recurrence rate [19]. Hypertensive ICH is mainly concentrated in the elderly (over 50 years old), but it shows a younger trend in recent years. The mortality and disability rate of hypertensive ICH are closely related to the location and volume of hemorrhage. With the same volume of hemorrhage, the survival rate of

TABLE 6: Comparison of quality of life scores between the two groups [$\bar{x} \pm s$, points].

Grouping	N	Physiological function		Psychological function		Social function		Healthy self-cognition	
		Before treatment	After treatment	Before treatment	After treatment	Before treatment	After treatment	Before treatment	After treatment
Control group	53	15.36 \pm 4.18	13.98 \pm 2.37 ^a	17.34 \pm 3.57	15.13 \pm 4.37 ^a	18.74 \pm 3.05	16.82 \pm 2.71 ^a	15.63 \pm 3.01	13.63 \pm 1.56 ^a
Research group	53	15.83 \pm 4.29	10.42 \pm 2.81 ^b	16.93 \pm 3.49	10.84 \pm 1.29 ^b	18.56 \pm 3.49	12.47 \pm 3.89 ^b	15.45 \pm 3.13	10.32 \pm 2.71 ^b
t		0.571	7.050	0.598	6.854	0.283	6.680	0.302	7.706
P		> 0.05	< 0.05	> 0.05	< 0.05	> 0.05	< 0.05	> 0.05	< 0.05

Note: comparison before and after nursing in the control group, ^a $P < 0.05$; comparison before and after nursing in the research group, ^b $P < 0.05$.

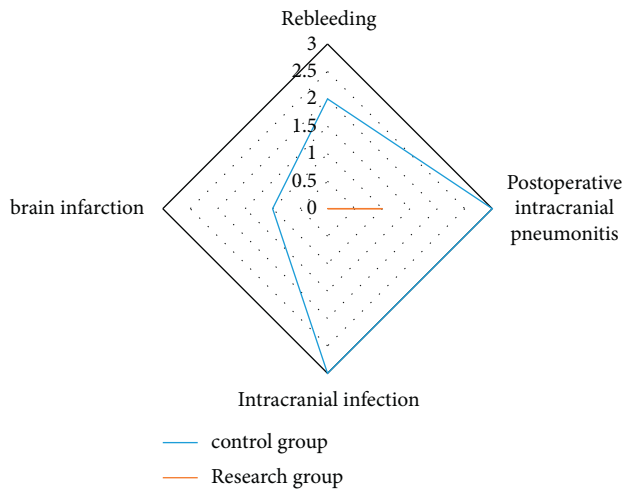


FIGURE 2: Comparison of postoperative complications between the two groups.

lobar hemorrhage is higher, and the mortality increases linearly with the increase of bleeding volume [20]. In 2000, Montes et al. reported that the 30-day mortality rate of patients with cerebral hemorrhage was about 35%–50%, half of them died within 2 days after onset, only 20% of the patients recovered after 6 months, and a few of them had the ability of living independently [21]. With the aggravation of the aging population and the irregularity of diet and life in our country, the incidence of cerebral hemorrhage is increasing year by year, which is a serious threat to people's health.

Medical treatment is the basic treatment of hypertensive intracerebral hemorrhage, and it is still the first choice for less bleeding, conscious consciousness, and mild neurological dysfunction. Diener et al. believe that the secondary damage after ICH is more serious than the injury caused by hemorrhage itself, so surgical removal of hematoma may be an effective method for the treatment of hypertensive ICH, but there is no statistical significance between STICHI phase response and medical conservative treatment based on the surgical study of ICH. The latest phase II study shows that surgical intervention for superficial hematoma has a better prognosis, indicating that reduction of scratching on brain tissue is effective [22]. It can enhance the effect of operation. Pasi et al. studies have indicated that the time window for stopping bleeding exceeds the previous understanding that

bleeding stops within 30 minutes [23]. The hematoma continues to expand due to continuous bleeding and rebleeding, and the mechanism is not clear. Peng et al. believed that the inflammatory cascade reaction led to physiological hemostatic dysfunction, resulting in the destruction of the blood-brain barrier and finally led to the expansion of hematoma [24]. It changed the traditional view that single reactive edema led to the deterioration of early nervous system symptoms and signs and indicated the necessity and importance of early surgical intervention. In addition to the space occupying effect, the toxic effect of hematoma also leads to brain damage. Qureshi and many other animal experiments have confirmed that the coagulation cascade reaction occurs and prothrombin is activated and transformed into thrombin, which leads to brain edema due to neurotoxicity [25]. Yang and Shao believe that the decomposition products of hematoma cause inflammatory reaction around hematoma, destroy the blood-brain barrier, produce inflammatory response, aggravate brain edema, lack local blood and oxygen supply, and induce brain cell apoptosis [26]. The decomposition of hematoma produces free radicals, attacks DNA, and causes oxidative damage to the brain.

At present, there are many schemes for the treatment of hypertensive intracerebral hemorrhage, and surgical treatment of intracerebral hemorrhage has unique advantages: clearing hematoma under direct vision, alleviating space occupying effect, reducing the pathophysiological effect of cytotoxic products after decomposition of blood clots on surrounding tissues, and reducing mortality and disability rate. From the point of view of pathophysiology, surgery may be a better choice for the treatment of cerebral hemorrhage. Early craniotomy for evacuation of hematoma has no obvious clinical significance because of severe trauma and conservative prognosis and internal medicine. With the development of technology, the mode of operation has gradually developed to minimally invasive, the concept of surgery has gradually undergone important changes, and the effect of surgery has gradually been widely recognized in clinical practice.

At present, the choice of surgical indications is different. Yang G thinks that the patients with worsening condition, late cerebral hernia, blood pressure, and respiration need drugs and machine maintenance is not ideal in medical and surgical treatment, so conservative treatment is recommended [26]. Gui et al. think that the amount of bleeding is

small, the mind is clear, no matter which kind of treatment is adopted, the outcome is very good, and conservative treatment is recommended [27]. There is a great controversy about the moderate amount of bleeding in 30 ml 60 ml and what kind of treatment. At present, the indications accepted by most doctors are as follows: (1) there is a certain degree of disturbance of consciousness or neurological symptoms, cerebral hernia has not yet formed, or early cerebral hernia should be actively treated; (2) the hemorrhage in the cerebellum is close to the brainstem. Unless the clinical symptoms are mild and the amount of bleeding is small, surgical treatment is the only effective treatment. When cerebellar hemorrhage exceeds 10 ml, there are surgical indications; (3) surgical treatment is not recommended for patients with brainstem hemorrhage, and surgical exploration can be given if vascular malformations and aneurysms are considered; (4) the curative effect of surgery is remarkable in theory, but it cannot be completely confirmed in clinic for the recovery of nerve function. The choice of operation needs to be considered, and whether to operate or not should be combined with the wishes of the family members.

The main purpose of surgery for patients with hypertensive ICH is to stop bleeding, remove hematoma, reduce intracranial pressure, and prevent and reduce a series of secondary pathological changes after hemorrhage. In addition, it can also improve the survival rate and quality of life of patients and promote the prognosis of patients. The disadvantages of craniotomy for evacuation of hematoma are large incision, large trauma, and long operation time, which is not conducive to the recovery of neurological function.

Since Auer first reported the endoscopic treatment of intracranial hemorrhage in 1985, neuroendoscopic technology has made great progress in the past 30 years and has been gradually adopted when treating intracranial tumors and hemorrhage. In this study, the advantages of neuroendoscopy were obtained by comparing the curative effect of neuroendoscopy and routine craniotomy group. In this study, by comparing the efficacy of the neuroendoscopy group and the routine craniotomy group, it was concluded that the neuroendoscopy group had the advantage of less trauma, and the diameter of the trauma caused by it was only 1.5 cm~2 cm. There were no repeated traction, compression, attraction, and other forms of damage to the important brain tissue around the hematoma, so as to reduce the postoperative reaction and enhance the prognosis of patients. Rennert et al. through the retrospective analysis of 23 cases of endoscopic treatment and 20 cases of microwindow craniotomy when treating cerebral parenchyma hemorrhage found that the prognosis of endoscopy group was remarkably better than craniotomy group [28]. Sun and other prospective studies compared the functional independence assessment (FIM) scale score, Barthel index score, and MP index at 6 months after operation [29]. It is concluded that neuroendoscopic surgery is more beneficial to the recovery of neurological function than craniotomy.

The results indicated that the effective rate of the research group was higher than the control group; the hospitalization time, intraoperative blood loss, postoperative residual blood flow, and total hospitalization days of the research group were remarkably lower than the control

group; the hematoma clearance rate of the research group was remarkably higher than the control group, and the KPS scores increased gradually. The KPS score and Barthel index of the research group were higher than the control group at 1 month, 2 months, and 3 months after operation. The scores of NIHSS, GCS, and DRS in the research group were remarkably lower than the control group, while the scores of MoCA and Fugl-Meyer in the research group were remarkably higher than the control group. The scores of physiological function, psychological function, social function, and health self-cognition in the research group were lower than the control group, and there were fewer post-operative complications. The reasons for this can be summarized as follows [29]. (1) Rapid decompression: the process of craniotomy in neuroendoscopic surgery is simplified, so most operations can be completed within 15 minutes for decompression. In completion within 2 h, of course, the proficiency of the operator is also an important factor affecting the operation time. In this study, the operation time of the neuroendoscopy group was remarkably better than the conventional craniotomy group. Some scholars' studies also show that the neuroendoscopy operation is relatively simple, the preparation time is shortened, and the operation time is relatively shortened [30]. (2) Less blood loss during surgery: most operations do not require blood transfusion; (3) there are good deep exposure, wider field of view, and high removal efficiency. The results of this study indicated that the hematoma clearance rate in the neuroendoscopy group ($93.5 \pm 4.7\%$) was remarkably better than that in the conventional craniotomy group ($90.5 \pm 5.2\%$), similarly to relevant domestic and foreign literature reports. (4) Complete hemostasis: hemostasis of direct vision under the endoscope can reduce the rebleeding rate; (5) the hospitalization cost of patients can also be reduced by reducing complications and hospitalization time.

Neuroendoscopic surgery still has certain limitations in some aspects: (1) the two-dimensional image of the endoscope and the "fish-eye" effect can easily lead to the illusion of the operator, so the operator is required to be more familiar with endoscopy; (2) the "two-dimensional" operation of the thalamus and brainstem is difficult. (3) Neuroendoscopy requires in-depth familiarity and understanding of the local anatomy; (4) internal and (5) special endoscopic surgical instruments are required. (6) The operation requires the cooperation of a professional team; (7) the number of cases is still small, and further research is needed. (8) The operating space and angle of the transparent endoscope sheath are arbitrarily limited. Nishihara et al. invented the transparent endoscopic sheath and achieved a satisfactory hematoma clearance rate [31]. In this study, the self-made transparent endoscope sheath is made from a medical syringe, which can provide a small but large endoscope working channel. A satisfactory hematoma clearance rate was achieved. However, it is found that the relative limitation of surgical space limits the application of other surgical instruments, such as bipolar electrocoagulation. Therefore, the working channel of the endoscope needs to be improved. There are some limitations in this study. First, the sample size of this study is not large and it is a single-center

study, so bias is inevitable. In future research, we will carry out multicenter, large-sample prospective studies, or more valuable conclusions can be drawn.

Neuroendoscopy technology is a pair of “wisdom eyes” brought to neurosurgeons by science and technology, and it is a prominent representative of the concept of “minimally invasive neurosurgery,” fast recovery, and low cost. As a new means of diagnosis and treatment, it enhances people’s understanding of some diseases and changes the concept of treatment of some diseases. With the continuous improvement of neuroendoscopy technology and the continuous development of surgical instruments, this surgical technique will become more and more mature and will be widely used in clinic.

Data Availability

The datasets used and analyzed during the current study are available from the corresponding author upon reasonable request.

Conflicts of Interest

The authors declare that they have no conflicts of interest.

Acknowledgments

This project was supported by Guangdong Provincial Medical Science and Technology Research Fund Project (A2018400) and Shantou Medical Healthcare Science and Technology Program, no. [2020]77.

References

- [1] I. C. Hostettler, D. J. Seiffge, and D. J. Werring, “Intracerebral hemorrhage: an update on diagnosis and treatment,” *Expert Review of Neurotherapeutics*, vol. 19, no. 7, pp. 679–694, 2019.
- [2] S. J. An, T. J. Kim, and B. W. Yoon, “Epidemiology, risk factors, and clinical features of intracerebral hemorrhage: an update,” *Journal of stroke*, vol. 19, no. 1, pp. 3–10, 2017.
- [3] A. L. de Oliveira Manoel, “Surgery for spontaneous ICH[J],” *Critical Care*, vol. 24, no. 1, pp. 1–19, 2020.
- [4] A. M. Thabet, M. Kottapally, and J. C. Hemphill, “Management of intracerebral hemorrhage,” *Critical Care Neurology Part I*, vol. 140, pp. 177–194, 2017.
- [5] J. Y. Kim and H. J. Bae, “Spontaneous intracerebral hemorrhage: management,” *Journal of stroke*, vol. 19, no. 1, pp. 28–39, 2017.
- [6] D. A. Wilkinson, A. S. Pandey, B. G. Thompson, K. Hua, and G. Xi, “Injury mechanisms in acute intracerebral hemorrhage,” *Neuropharmacology*, vol. 134, pp. 240–248, 2018.
- [7] C. Delcourt, S. Sato, S. Zhang et al., “Intracerebral hemorrhage location and outcome among INTERACT2 participants,” *Neurology*, vol. 88, no. 15, pp. 1408–1414, 2017.
- [8] K. R. Melmed, M. Cao, S. Dogra et al., “Risk factors for intracerebral hemorrhage in patients with COVID-19,” *Journal of Thrombosis and Thrombolysis*, vol. 51, no. 4, pp. 953–960, 2021.
- [9] C. Ma, M. E. Gurol, Z. Huang et al., “Low-density lipoprotein cholesterol and risk of intracerebral hemorrhage,” *Neurology*, vol. 93, no. 5, pp. e445–e457, 2019.
- [10] Y. J. Wang, Z. X. Li, H. Q. Gu et al., “Diagnostic points of major cerebrovascular diseases in China 2019 [J],” *Chinese Journal of Neurology*, vol. 09, pp. 710–715, 2019.
- [11] X. Wang, Li Shi, K. Han, P. P. Zhang, A. B. Cheng, and T. J. Liu, “Correlation analysis between blood glucose drift and National Institutes of Health Stroke scale score in 63 patients with acute anterior circulation ischemic stroke complicated with diabetes mellitus [J],” *Chinese Medicine and Clinic*, vol. 22, no. 03, pp. 216–218, 2022.
- [12] N. González, A. Bilbao, M. J. Bilbao, F. Ayala, O. Garcia-Gutierrez, and J. M. Hayas, “Psychometric characteristics of the Spanish version of the Barthel index,” *Aging Clinical and Experimental Research*, vol. 30, no. 5, pp. 489–497, 2018.
- [13] N. Kori, W. A. W. Zaidi, R. Remli et al., “A validation study of the bahasa Malaysia version of the national Institute of health stroke scale[J],” *Neurology Asia*, vol. 23, no. 3, pp. 14–15, 2018.
- [14] N. F. Cook, “The Glasgow coma scale,” *Critical Care Nursing Clinics of North America*, vol. 33, no. 1, pp. 89–99, 2021.
- [15] F. F. Mohamed, M. I. Ayman, and M. D. Amer, “Decompressive craniectomy in patients with malignant middle cerebral artery infarction: prognostic factors and timing dilemma[J],” *The Medical Journal of Cairo University*, vol. 89, no. June, pp. 701–707, 2021.
- [16] C. O’Driscoll and M. Shaikh, “Cross-cultural applicability of the montreal cognitive assessment (MoCA): a systematic review,” *Journal of Alzheimer’s Disease*, vol. 58, no. 3, pp. 789–801, 2017.
- [17] B. Singer and J. Garcia-Vega, “The fugl-meyer upper extremity scale,” *Journal of Physiotherapy*, vol. 63, no. 1, p. 53, 2017.
- [18] S. Hou, Y. Huang, G. Yang et al., “Epidemiological characteristics and clinical diagnosis and treatment of 557 cases of hypertensive ICH [J],” *Continuing medical education in China*, vol. 13, no. 32, pp. 154–158, 2021.
- [19] Li ao, S. Zhu, M. Chen, and B. Y. Luo, “Analysis of epidemiological and clinical characteristics of patients with hypertensive ICH [J],” *Chinese Journal of brain Diseases and Rehabilitation (Electronic Edition)*, vol. 8, no. 01, pp. 11–14, 2018.
- [20] G. Sun, X. Li, X. Chen, and Z. Xu, “Comparison of keyhole endoscopy and craniotomy for the treatment of patients with hypertensive cerebral hemorrhage[J],” *Medicine*, vol. 98, no. 2, pp. 180–182, 2019.
- [21] Y. Sun, B. Xu, and Q. Zhang, “Nerve growth factor in combination with oxiracetam in the treatment of hypertensive cerebral hemorrhage,” *Pakistan Journal of Medical Sciences*, vol. 34, no. 1, pp. 73–77, 2018.
- [22] H. C. Diener and G. J. Hankey, “Primary and secondary prevention of ischemic stroke and cerebral hemorrhage,” *Journal of the American College of Cardiology*, vol. 75, no. 15, pp. 1804–1818, 2020.
- [23] M. Pasi, A. Charidimou, G. Boulouis et al., “Mixed-location cerebral hemorrhage/microbleeds,” *Neurology*, vol. 90, no. 2, pp. e119–e126, 2018.
- [24] J. Peng, H. Wang, X. Rong, H. Xiang, p. Shen, and Y. Peng, “Cerebral hemorrhage and alcohol exposure: a review,” *Alcohol and Alcoholism*, vol. 55, no. 1, pp. 20–27, 2020.
- [25] A. I. Qureshi and M. H. Qureshi, “Acute hypertensive response in patients with intracerebral hemorrhage pathophysiology and treatment,” *Journal of Cerebral Blood Flow and Metabolism*, vol. 38, no. 9, pp. 1551–1563, 2018.
- [26] G. Yang and G. Shao, “Clinical effect of minimally invasive intracranial hematoma in treating hypertensive cerebral

- hemorrhage,” *Pakistan Journal of Medical Sciences*, vol. 32, no. 3, pp. 677–681, 2016.
- [27] C. Gui, Y. Gao, D. Hu, and X. Yang, “Neuroendoscopic minimally invasive surgery and small bone window craniotomy hematoma clearance in the treatment of hypertensive cerebral hemorrhage,” *Pakistan Journal of Medical Sciences*, vol. 35, no. 2, pp. 377–382, 2019.
- [28] R. C. Rennert, J. W. Signorelli, P. Abraham, and A. A. PannellKhalessi, *Expert Review of Neurotherapeutics*, vol. 15, no. 8, pp. 919–933, 2015.
- [29] G. Sun, T. Fu, Z. Liu, Z. Chen, and F. JinChi, “The rule of brain hematoma pressure gradient and its influence on hypertensive cerebral hemorrhage operation,” *Scientific Reports*, vol. 11, no. 1, p. 4599, 2021.
- [30] F. Song, B. Liao, and Yi Zhang, “Comparison of minimally invasive soft channel drainage and small bone window hematoma removal when treating hypertensive cerebral hemorrhage: a meta-analysis[J],” *Journal of Contemporary Medical Practice*, vol. 2, no. 12, pp. 17–20, 2021.
- [31] T. Nishihara, A. Teraoka, and A. Morita, “A transparent sheath for endo-scopic surgery and its application in surgical evacuation of spontaneousintracerebral hematomas Technical note,” *Journal of Neurosurgery*, vol. 6, p. 1055, 2000.

Research Article

Expression and Prognostic Role of CXCL1 Gene in Colorectal Adenocarcinoma

Chao Xia, Lifeng He, and Yi Sun 

Gastrointestinal Surgery Affiliated Xiaoshan Hospital, Hangzhou Normal University, Zhejiang, Hangzhou 311200, China

Correspondence should be addressed to Yi Sun; 2150011005@email.szu.edu.cn

Received 25 May 2022; Revised 28 June 2022; Accepted 1 July 2022; Published 2 August 2022

Academic Editor: Dong Chen

Copyright © 2022 Chao Xia et al. This is an open access article distributed under the Creative Commons Attribution License, which permits unrestricted use, distribution, and reproduction in any medium, provided the original work is properly cited.

In this manuscript, we have extensively examined expression and prognosis of CXCL1 gene in colorectal adenocarcinoma (COAD) using different cases of colorectal adenocarcinoma and tissues. To verify this, protein and mRNA expressions of cxcl1 were identified through RT-PCR and immunohistochemistry in 30 cases of colorectal adenocarcinoma and adjacent tissues, which were surgically resected from January to July 2021 in our hospital, and relationship between CXCL1 mRNA and clinicopathological features and protein expression was analyzed. CXCL1 mRNA in COAD carcinoma's expression was considerably higher than in the adjacent normal intestine. At the same time, CXCL1 diagnostic receiver operating characteristic (ROC) curve had preferably higher value of the diagnostic for area under curve (AUC) = 0.912, 95%, COAD ($P < 0.001$, CI = 0.825–0.969). We have observed that CXCL1 gene was closely linked with preoperative CEA level ($P = 0.007$) and gross tumor typing ($P = 0.039$). Finally, we have concluded that CXCL1 can be a possible biomarker for stress prognosis and diagnosis.

1. Introduction

Colorectal cancer (CRC) is a kind of cancer that affects the colon and rectum. CRC is one of the cancers with the highest rates of morbidity and death worldwide. According to data, approximately 1.8 million cases of the CRC and around 860,000 deaths are reported in the year 2018, which is approximately 10% of the overall cases of cancer and fatalities. CRC is considered as 3rd common malignancy and in terms of death ratio it is second [1]. CRC is one of China's top five malignancies in terms of morbidity and fatality [2]. In CRC patients, cancer metastasis is still the major cause of mortality. Patients have primary CRC and an 80–90 5-year overall rate of survival; however, patients with metastatic CRC have a 5-year rate of the survival of just 50 percent as low as 5–10 [3, 4]. CRC, like many other diseases, preferably cancers are assumed as a disease of type heterogeneous, in which tumor formation, progression, and metastasis are linked to genetic diversity, cellular environment, and external environmental effects [5].

CRC has a high incidence and fatality rate, and surgical resection is currently the most common therapeutic option

[6]. The earlier the CRC therapy begins, the better the outcome; early-stage cancer has a 5-fold survival rate compared to advanced disease [7]. Patients with tumor infiltration into the lamina propria (TNM stage TIS, N0, MO) had a 100 percent 5-year survival rate, but patients with invasive T1 (submucosal) or T2 (muscular) malignancy had a 90 percent 5-year survival rate. Those who were more aggressive but did not include lymph nodes (t3-4, N0, MO) had a 5-year survival rate of around 70%, whereas those who were regional lymph node positive had a 5-year survival rate of about 40% (any T, N1-3, MO). The 5-year survival rate for patients with distant metastases (any T, any N, M1) is around 5% [8]. Patients with successfully operated stage I cancer had a 5-year recurrence rate of 5%, 13% for stage II, and 33% for stage III, with recurrence rates varying from 9 to 22 percent for stage II to 17 to 44 percent for stage III, depending on the number of risk factors [9]. As a result, early detection and treatment of CRC are critical for the prognosis of patients.

CXC motif chemokine ligand 1 (CXCL1) is a tiny cytokine that belongs to the CXC chemokine family [10]. It was formerly identified as the Gro1 oncogene. Human melanoma cells release CXCL1, which has mitogenic characteristics and

is linked to melanoma aetiology [11, 12]. CXCL1 is a neutrophil chemoattractant that is produced by the cells of neutrophils, macrophages, and epithelial [13, 14]. CXCL1 is implicated in angiogenesis, inflammation, wound healing, and cancer, as well as blocking the oligodendrocyte precursor's migration in the spinal cord. CXCL1 gene is located on human chromosome 4 and is the gene of other CXC chemokines. Preliminary studies in mice have shown that CXCL1 can reduce the severity of multiple sclerosis and may provide neuroprotective function [15]. CXCL1 expression in colon cancer is much greater than in normal colon tissue, according to previous research. In metastatic CRC, high CXCL1 expression is a poor prognostic indicator; CXCL1 expression is linked to a poor prognosis in stage III CRC [16]. As a result, the role of CXCL1 in the diagnosis and prognosis of colonic adenocarcinoma was investigated in this study (COAD).

In this manuscript, we have extensively examined expression and prognosis of CXCL1 gene in colorectal adenocarcinoma (COAD) using different cases of colorectal adenocarcinoma and tissues. To verify this, protein and mRNA expressions of cxcl1 were identified through RT-PCR and immunohistochemistry in 30 cases of colorectal adenocarcinoma and adjacent tissues, which were surgically resected from January to July 2021 in our hospital, and relationship between CXCL1mRNA and clinicopathological features and protein expression was analyzed. CXCL 1 mRNA in COAD carcinoma's expression was considerably higher than in the adjacent normal intestine. At the same time, CXCL 1 diagnostic ROC curve had preferably higher value of the diagnostic for AUC=0.912, 95%, COAD ($P < 0.001$, CI = 0.825–0.969).

The rest of the paper is organized as follows.

In the subsequent section, the proposed evaluation mechanism is described in detail, where it is depicted clearly how various participants were selected and how the evaluation was carried out. In section 3, numerous results of the proposed scheme in terms of different evaluation metrics were presented along with possible justification and analysis. Finally, concluding remarks are given.

2. Methods

In this section, we are going to describe a detailed explanation of the proposed mechanism along with the participants.

2.1. Participants in the Evaluation Process. The surgically resected cancer tissue and normal adjacent colon tissue were collected from patients with colorectal adenocarcinoma in the department of colorectal and anal surgery in our hospital from January to July 2020. All patients did not receive radiotherapy or chemotherapy before operation. After operation, they were pathologically diagnosed as spinal cord injury and signed the informed consent.

2.2. Information Collection. Basic information and clinicopathological factors of patients were collected, including gender, age, preoperative carcinoembryonic antigen (CEA),

tumor/lymph node/metastasis (TNM) stage, tumor site, tumor gross type, tumor thrombosis, tumor size, number of tumors, positive lymph nodes, radical resection, tumor metastases, nerve invasion, and postoperative chemotherapy which were all factors to consider. The American Joint Commission on Cancer (AJCC) Lymph Node Metastasis Staging System (8th edition, 2017) [16] was used to identify and classify TNM staging. It is divided into left and right semicolon colons based on anatomical sites. The left semicolon colon includes the colon in the splenic flexure, descending colon, and sigmoid colon, while the right semicolon colon includes the colon in the cecum, ascending colon, hepatic flexure, and transverse colon [17]. Colectomy and regional lymph node dissection were the major surgical methods used.

2.3. Tissue Specimen Collection. After the tissue was surgically removed, the tumor about the size of soybeans and the normal colon tissue more than 3 cm adjacent to the tumor were cut out with ophthalmic scissors (note: the instruments for cancer tissue and normal colon tissue adjacent to the tumor were used separately), cut into pieces, and placed into a 1.5 ml EP tube. RNA protection solution (1 ml) was added to completely soak the tissue. Place the EP tube in a 4°C refrigerator test-tube rack overnight (allowing the RNA protection solution to mix well with the tissue). Transfer the EP tube to an -80°C refrigerator on the second day. The EP tube body is marked with the patient's name, hospitalization number, and operation date (collection date), and the EP tube cap is marked with the patient's hospitalization number. Each patient received 2 tubes of cancer and 2 tubes of adjacent normal colon tissue.

2.4. Extraction, Purification, and Identification of Tissue Total RNA. Total RNA was extracted from tissues in accordance with the instructions of Trizol. 2 μ L of RNA sample was taken, and the absorbance of RNA at 260 nm was measured by micro-UV spectrophotometer Q5000. The absorbance A260 and A280 of RNA at 260 nm and 280 nm was measured for quantitative RNA purity, and OD260/OD280 was recorded. The ratio of all samples was required to be $1.7 < \text{OD260/OD280} < 2.0$, lower than this value indicated that it contained protein impurities. Repurify it with chloroform. RNA integrity was determined by agarose gel electrophoresis.

2.5. Reverse Transcription. Total RNA was used as template to synthesize cDNA using invitrogen reverse transcription kit. Take a 0.2 ml DEPC-treated PCR tubes in which the reverse transcription reaction solution was prepared in an ice bath.

Reverse transcription reaction was performed according to the instructions of the reverse transcription kit. In the PCR tube, 1 μ of reverse transcription product, 0.25 μ L of upstream and downstream primers, PCR reaction mix 12.5 μ L, then ddH₂O supplement volume to 25 μ L. After mixing, the samples were immediately placed in PCR

TABLE 1: The upstream sequence of the primer for internal reference.

Name	Primer	Length
GAPDH	5'-CGGGAAATCGTGCGTGA-3'	116 bp
	5'-TCAGGCAGCTCGTAGCTCTT-3'	
CXCL1	5'-CAAACCGAAGtCATAGCCACA-3'	120 bp
	5'-CTCCTAAGCGATgCTCAAACA-3'	

apparatus for reaction according to the following procedures. After the reaction, the samples were stored at -20°C for later use. Reaction conditions are 95°C for 2 min, 95°C for 15 s, 62°C for 30 s, and a total of 35 cycles. All primers were synthesized by Shanghai Shengong Co., LTD. The upstream sequence of the for internal reference in Table 1. The detection of different genes in the same sample should be carried out in different PCR tubes. After amplification, the amplification curve and the melting curve were analyzed to obtain the cycle threshold (CT value). Finally, the differential multiple of CXCL1 expression in tumor tissues relative to normal tissues was calculated by $2^{-\Delta\Delta\text{CT}}$ method.

2.6. Statistical Analysis. The continuous data of the normal distribution were represented by Mean SD, and the continuous variables of the non-normal distribution were converted into dichotomy variables according to the median as the cut-off point. Chi-square test was used to analyze the correlation between clinical factors and CXCL1. And only normal distribution data can use *t*-test.

3. Results and Evaluation

In this section, a detailed analysis of various experimental results, specifically in terms of numerous evaluation metrics, is presented. For an easy follow-up, the proposed scheme is described with both discussion and experimental results.

3.1. Detection of CXCL1 Expression in COAD Patients and Adjacent Normal Colon Tissues. The study comprised thirty COAD patients, 20 men, and 10 women, with a median age of 58.75 years (range 34 to 80 years). RT-qPCR was used to identify real-time CXCL1 gene mRNA in 30 COAD patients (Figure 1). CXCL1 mRNA expression in COAD cancer tissues was considerably greater than in nearby normal intestinal tissues, according to a paired *T* test. Simultaneously, the CXCL1 diagnostic ROC curve revealed a greater diagnostic value for COAD ($P = 0.001$, $\text{AUC} = 0.912$, 95 percent $\text{CI} = 0.825\text{--}0.969$).

3.2. CXCL1 Expression in Cancer and Adjacent Normal Colon Tissues of COAD Patients. We grouped CXCL1 gene mRNA expression levels in cancer tissues of COAD patients into groups and calculated the relationship between CXCL1 gene mRNA expression and clinical factors of patients (Table 2). The results showed that CXCL1 gene was correlated with preoperative CEA level ($P = 0.007$) and gross tumor typing ($P = 0.039$).

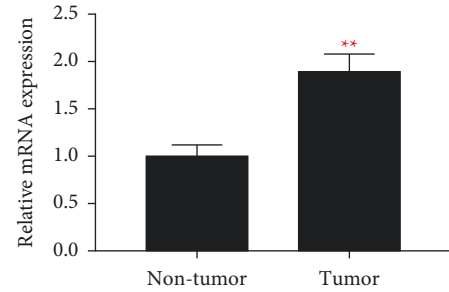


FIGURE 1: CXCL1 expression in cancer and adjacent normal colon tissues of COAD patients.

TABLE 2: CXCL1 expression in cancer and adjacent normal colon tissues of COAD patients.

Variable	Low	High	X ²	P
Gender				1.00
	Male	11	9	
	Female	5	5	
Age				1.00
	<65	11	9	
	>65	5	5	
CEA (ng/ml)				0.007
	1–5	11	13	
	>5	5	1	
TNM stage			2.576	0.517
	I	1	2	
	II	8	10	
	III	3	2	
	IV	2	1	
Location				1.00
	Right	3	3	
	Left	12	12	
Tumor type			6.782	0.038
	Invasive	1	2	
	Ulcerative	14	6	
	Mass	2	5	
Differentiation				0.682
	Well	13	14	
	Poor	2	1	
Tumor thrombus				0.702
	No	11	16	
	Yes	3	1	
Tumor size				1.00
	<5	3	2	
	>5	12	13	
Lymph node				0.148
	Negative	8	16	
	Positive	4	2	
Tumor transfer				0.622
	No	10	14	
	Yes	4	2	
Nerve infiltration				1.000
	No	13	13	
	Yes	2	2	

4. Discussion

Colon cancer is one of the common malignant tumors. 60% of patients have clinical and pathological evidence of liver

metastasis. Liver metastasis of colon cancer shows obvious organophilic, and the rates of simultaneous and isochronous liver metastasis are 43.7% and 56.3%, respectively [16]. This organophilic is a manifestation of directional migration of tumor cells. The “homing” theory holds that different organs have the special ability to capture or attract specific types of tumor cells by secreting chemokines. It has been confirmed that the directional metastasis process of some tumor cells shows similar characteristics to leukocyte chemotactic migration [17].

At present, surgical resection is still the main means of CRC treatment. The earlier the CRC is treated the better with survival rates about five times higher than for advanced cancer. So, early diagnosis and early treatment of colon cancer are particularly important for the prognosis of patients. At the time of initial diagnosis of CRC, only 15% of stage I patients were diagnosed, and most patients were already in the middle and late stage. Although colonoscopy is still the gold standard for detecting colon cancer, it is invasive, costly, and inconvenient, making it unsuitable for routine screening. Good tumor indicators have a high sensitivity and specificity for tumor diagnosis, and they help to detect malignancies early. Previous research on biological markers for colon cancer has had mixed findings. For colon cancer diagnosis and postoperative follow-up, serum carcinoembryonic antigen (CEA) is a useful tumor marker. Serum CEA level is positively correlated with tumor node metastasis (TNM) stage. The positive rates of serum CEA in TNM stage I, II, III, and IV patients were about 25%, 45%, 75%, and 85%, respectively. CEA has little significance for the early diagnosis of colon cancer. Therefore, to find more sensitive, more specific, and easier to operate biological markers is the current research focus.

In the study on the diagnostic value of CXCL1 in CRC, Wen et al. confirmed that the expression of CXCL1 in CRC was higher than that in normal colonic epithelium by real-time PCR and immunohistochemistry [18]. Sipos et al. found that on the basis of tissue microarray analysis, the matrix expression of MMP3 and CXCL1 can correctly distinguish high-grade dysplastic sessile adenoma stage and early CRC [19]. In the study of the role of CXCL1 on the occurrence and development of CRC, Ogata et al. [20] detected Groalpha immunohistochemistry in 62 primary CRC specimens and discussed the relationship between Groalpha expression and clinicopathological features; it was found that the expression of Groalpha was significantly correlated with tumor size, tumor stage, depth of invasion, lymph node metastasis, and survival rate. Wang et al. found that CXCL1 released by cancer cells induced microvascular endothelial cell migration and tubulation *in vitro*. In addition, prostaglandin E2 promotes tumor growth *in vivo* by inducing CXCL1 expression, resulting in increased tumor angiogenesis [21]. In the study of Hsu et al., transcriptome analysis of CXCL1 treated SW620 cells showed that CXCL1 could increase the expression of potential oncogenes in colon cancer. Analysis of public data showed that CXCL1 driven oncogenes and mir-105 had a negative impact on the prognosis of colon cancer [22]. Le Rolle et al. suggested that high CXCL1 expression is a biomarker of poor prognosis in

metastatic CRC [23]. Moreover, silencing CXCL1 inhibited the tumorigenic growth of KRAS mutant CRC cells. In the study of Cai et al., adiponectin partially promotes the aging of stromal cells in invasive colon cancer by producing CXCL1 and may be used as a therapeutic target for tumor patients [24].

Therefore, this study shows that CXCL1 may be a potential biomarker for the diagnosis and prognosis of load. This study verifies previous studies from the gene level. In terms of diagnostic value, the mRNA expression of CXCL1 in COAD cancer tissues is significantly higher than that in adjacent normal colon tissues, and ROC data show that CXCL1 does not significantly affect the prognosis of COAD. Because the number of patients included in this study is too small, there are certain limitations, and the research method is too single, and the reliability of the results needs to be further verified.

5. Conclusion

In this manuscript, we have extensively examined expression and prognosis of CXCL1 gene in colorectal adenocarcinoma (COAD) using different cases of colorectal adenocarcinoma and tissues. To verify this, protein and mRNA expressions of cxcl1 were identified through RT-PCR and immunohistochemistry in 30 cases of colorectal adenocarcinoma and adjacent tissues, which were surgically resected from January to July 2021 in our hospital, and relationship between CXCL1mRNA and clinicopathological features and protein expression was analyzed. CXCL 1 mRNA in COAD carcinoma's expression was considerably higher than in the adjacent normal intestine. At the same time, CXCL 1 diagnostic ROC curve had preferably higher value of the diagnostic for AUC = 0.912, 95%, COAD ($P < 0.001$, CI = 0.825–0.969). Experimental results have verified the exceptional performance of the proposed scheme in terms of various performance evaluation metrics.

In future, the proposed methodology has the capacity to be extended further by integrating it with existing state of the art approaches to form a hybrid and more useful approach.

Data Availability

The datasets used and analyzed during the current study are available from the corresponding author upon reasonable request.

Conflicts of Interest

The authors declare that they have no conflicts of interest.

Authors' Contributions

Chao Xia put forward the idea of the paper, and all authors participated in the preparation and review of the paper.

References

- [1] O. Stephen, M. Sain, U. J. Maduh, and D. U. Jeong, “An efficient deep learning approach to pneumonia classification

- in healthcare,” *Journal of healthcare engineering*, vol. 2019, pp. 1–7, Article ID 4180949, 2019.
- [2] R. Thapa, M. Lakhey, and P. K. Yadav, “Clinico-pathological study of colorectal carcinoma,” *Journal of the Nepal Medical Association*, vol. 52, no. 191, pp. 449–452, 1970.
 - [3] Y. Minamino, Y. Ohnishi, K. Kakudo, and M. Nozaki, “Isolation and propagation of neural crest stem cells from mouse embryonic stem cells via cranial neurospheres,” *Stem Cells and Development*, vol. 24, no. 2, pp. 172–181, 2015 Jan 15.
 - [4] A. Zhussupova, T. Takahashi, M. Miyao et al., “An E2F1-HOXB9 transcriptional circuit is associated with breast cancer progression,” *PLoS One*, vol. 9, no. 8, p. e105285, 2014.
 - [5] L. Sha, L. Dong, L. Lv, L. Bai, and X. Ji, “HOXB9 promotes epithelial-to-mesenchymal transition via transforming growth factor- β 1 pathway in hepatocellular carcinoma cells,” *Clinical and Experimental Medicine*, vol. 15, no. 1, pp. 55–64, 2015.
 - [6] A. Antonelli, S. M. Ferrari, D. Giuggioli, E. Ferrannini, C. Ferri, and P. Fallahi, “Chemokine (C-X-C motif) ligand (CXCL)10 in autoimmune diseases,” *Autoimmunity Reviews*, vol. 13, no. 3, pp. 272–280, 2014 Mar.
 - [7] K. Jin, J. Wang, H. Lan, and R. Zhang, “Laparoscopic surgery for colorectal cancer in China: an overview,” *International Journal of Clinical and Experimental Medicine*, vol. 7, no. 12, pp. 4635–4645, 2014 Dec 15.
 - [8] F. Rubin, R. Douard, and P. Wind, “The Functional Outcomes of Coloanal and Low Colorectal Anastomoses with reservoirs after low rectal cancer resections,” *The American Surgeon*, vol. 80, no. 12, pp. 1222–1229, 2014.
 - [9] C. Xu, E. C. Reichert, T. Nakano et al., “Deficiency of phospholipase A2 group 7 decreases intestinal polyposis and colon tumorigenesis in ApcMin/+ mice,” *Cancer Research*, vol. 73, no. 9, pp. 2806–2816, 2013.
 - [10] D. F. Smith, E. Galkina, K. Ley, and Y. Huo, “GRO family chemokines are specialized for monocyte arrest from flow,” *American Journal of Physiology Heart & Circulatory Physiology*, vol. 289, 2005.
 - [11] M. Subramaniam, S. A. Harris, M. J. Oursler, K. Rasmussen, B. L. Riggs, and T. C. Spelsberg, “Identification of a novel TGF- β -regulated gene encoding a putative zinc finger protein in human osteoblasts,” *Nucleic Acids Research*, vol. 23, no. 23, pp. 4907–4912, 1995.
 - [12] N. Iida and G. R. Grotendorst, “Cloning and sequencing of a new gro transcript from activated human monocytes: expression in leukocytes and wound tissue,” *Molecular and Cellular Biology*, vol. 10, no. 10, pp. 5596–5599, 1990.
 - [13] M. H. M. Vries, A. Wagenaar, S. E. L. Verbruggen, D. G. M. Molin, and M. J. Post, “CXCL1 promotes arteriogenesis through enhanced monocyte recruitment into the peri-collateral space,” *Angiogenesis*, vol. 18, no. 2, pp. 163–171, 2015.
 - [14] K. M. Omari, S. E. Lutz, L. Santambrogio, S. A. Lira, and C. S. Raine, “Neuroprotection and remyelination after autoimmune demyelination in mice that inducibly overexpress CXCL1,” *American Journal Of Pathology*, vol. 174, no. 1, pp. 164–176, 2009.
 - [15] M. Miyake, A. Lawton, S. Goodison et al., “Chemokine (C-X-C) ligand 1 (CXCL1) protein expression is increased in aggressive bladder cancers,” *BMC Cancer*, vol. 13, no. 1, pp. 1–7, 2013.
 - [16] F. Bray, J. Ferlay, I. Soerjomataram, R. L. Siegel, L. A. Torre, and A. Jemal, “Global cancer statistics 2018: GLOBOCAN estimates of incidence and mortality worldwide for 36 cancers in 185 countries,” *CA a cancer journal for clinicians*, vol. 68, pp. 394–424, 2018.
 - [17] F. Bray and I. Soerjomataram, “The changing global burden of cancer: transitions in human development and implications for cancer prevention and control,” *Cancer: disease control priorities*, vol. 3, pp. 23–44, 2015.
 - [18] Y. Wen, S. F. Giardina, D. Hamming et al., “GRO α is highly expressed in adenocarcinoma of the colon and down-regulates fibulin-1,” *Clinical Cancer Research*, vol. 12, no. 20, pp. 5951–5959, 2006.
 - [19] F. Sipos, T. M. Germann, B. Wichmann et al., “MMP3 and CXCL1 are potent stromal protein markers of dysplasia-carcinoma transition in sporadic colorectal cancer,” *European Journal of Cancer Prevention*, vol. 23, no. 5, pp. 336–343, 2014.
 - [20] H. Ogata, A. Sekikawa, H. Yamagishi et al., “GRO α promotes invasion of colorectal cancer cells,” *Oncology Reports*, vol. 24, no. 6, pp. 1479–1486, 2010.
 - [21] D. Wang, H. Wang, J. Brown et al., “CXCL1 induced by prostaglandin E2 promotes angiogenesis in colorectal cancer,” *Journal of Experimental Medicine*, vol. 203, no. 4, pp. 941–951, 2006.
 - [22] Y. L. Hsu, Y. J. Chen, W. A. Chang et al., “Interaction between tumor-associated dendritic cells and colon cancer cells contributes to tumor progression via CXCL1,” *International Journal of Molecular Sciences*, vol. 19, no. 8, p. 2427, 2018.
 - [23] A. F. le Rolle, T. K. Chiu, M. Fara et al., “The prognostic significance of CXCL1 hypersecretion by human colorectal cancer epithelia and myofibroblasts,” *Journal of Translational Medicine*, vol. 13, no. 1, p. 199, 2015.
 - [24] L. Cai, S. Xu, C. Piao, S. Qiu, H. Li, and J. Du, “Adiponectin induces CXCL1 secretion from cancer cells and promotes tumor angiogenesis by inducing stromal fibroblast senescence,” *Molecular Carcinogenesis*, vol. 55, no. 11, pp. 1796–1806, 2016.

Research Article

Clinical Efficacy and Safety of Different Dental Prosthetic Membranes in Guided Bone Regeneration during Dental Implants: A Meta-Analysis

Yan Guo,¹ Linghan Su,¹ Caidi Chen,² Yan Liu,³ and Jianxue Li¹ 

¹Department of Stomatology, The 940th Hospital of Joint Logistic Support Force of PLA, Lanzhou 730050, China

²Endocrinology Department, The 940th Hospital of Joint Logistic Support Force of PLA, Lanzhou 730050, China

³The 940th Hospital of Joint Logistics Support Force of PLA, Lanzhou 730050, China

Correspondence should be addressed to Jianxue Li; lijianxue6@163.com

Received 24 May 2022; Revised 23 June 2022; Accepted 4 July 2022; Published 31 July 2022

Academic Editor: Dong Chen

Copyright © 2022 Yan Guo et al. This is an open access article distributed under the Creative Commons Attribution License, which permits unrestricted use, distribution, and reproduction in any medium, provided the original work is properly cited.

Objective. To evaluate clinical efficacy and safety of absorbable and non-absorbable dental restorative membranes in guided bone regeneration (GBR). Articles concerning absorbable and non-absorbable prosthetic membrane-related studies of GBR were screened from multiple databases. In the end, 526 postoperative patients who met eligibility criteria were screened for the study from eight trials. The results showed that the repair success rate of the experimental group (absorbable dental restorative membrane) was higher than that of the control group (non-absorbable dental restorative membrane) (RR = 1.18, 95% CI [1.11, 1.26]), and the total physical therapy effect was $P < 0.0001$, $I^2 = 0\%$, and the height of bone graft in the experimental group was higher than that in the control group (MD = 0.67, 95% CI [0.11, 1.23]). The thickness of bone graft in the experimental group was higher than that in the control group (MD = 0.43, 95% CI [0.30, 0.56], $P < 0.00001$, $I^2 = 61\%$), and the adverse events in the experimental group were less than those in the control group (RR = 0.31, 95% CI [0.18, 0.51], $P < 0.00001$, $I^2 = 13\%$). Absorbable prosthetic membrane is superior to non-absorbable prosthetic membrane in clinical efficacy and safety.

1. Introduction

Guided Bone Regeneration (GBR) originated from the field of periodontology in guided tissue regeneration technology. It is a biofilm made of biomaterials, which erect a biological barrier between bone defects and gingival soft tissue [1–3]. GBR prevents epithelial cells and fibroblasts in soft tissue and soft tissue from growing into the bone defect area. This process ensures that the osteogenesis process is completed on the premise of no interference of fibroblasts. Finally, GBR can realize complete bone repair of the defect area, which needs oral repair membrane [4].

Oral repair membrane is a biocompatible material. The repair membrane is placed between oral soft tissue and bone defect by surgery to establish a biological barrier to create a relatively closed bone regeneration environment [5, 6]. Oral repair film can be divided into absorbable film and non-

absorbable film according to whether the material can be degraded. In the past, patients used titanium membrane (non-absorbable membrane) as a protective barrier membrane because titanium membrane could not be fully absorbed. This process limited the supply of blood plasma and then hindered the blood supply in the bone graft area, which had a significant impact on the recovery of patients to a certain extent [7–9]. However, it has good plasticity and can bend, trim the contour, adapt to various bone defect forms, better stabilize the wound, and guide bone regeneration [10].

Although the absorbable membrane risks rapid degradation, it makes the new bone tissue adhere to the biofilm. Absorbable membrane promotes the early tissue integration and the production of transmembrane blood vessels, avoids the inward growth of connective tissue, increases the stability of gingival tissue, and reduces gingival atrophy [11]. Also, it can reduce patient

complications without the need for second-stage surgical removal of the membrane.

Although there are several research studies about comparison between absorbable and non-absorbable dental restorative membrane in guided bone regeneration, there is little comprehensive analysis for the topic. Therefore, we conducted this research to overall analyze the difference in absorbable and non-absorbable dental restorative membrane in guided bone regeneration.

In this paper, we have evaluated clinical efficacy and safety of absorbable and non-absorbable dental restorative membranes in guided bone regeneration (GBR). For this purpose, both absorbable and non-absorbable prosthetic films for GBR were selected from multiple databases (PubMed, Web of Science, Cochrane Library, and China National Knowledge Infrastructure), whereas Review Manager 5.2 was used for meta-analysis, sensitivity analysis, and bias analysis. After the screening process, 526 postoperative patients were extracted from 8 trials which are those patients who finally met the qualification criteria to conduct this meta-analysis.

2. Proposed Method or Strategy

To ensure the scientificity, we followed PRISMA statement and the methods of Cao et al. [12].

2.1. Literature Search Strategy. We have searched the randomized controlled trials published by PubMed, ScienceNet, Cochrane Library, and China National knowledge Infrastructure from January 1, 2000, to September 1, 2021, using the following search terms:

- (1) Absorbable dental repair membrane.
- (2) Bone regeneration.
- (3) Clinical effect. The search strategy involves medical subject headings (mesh) and text words combined by the Boolean operator "AND."

We will conduct a comprehensive search in multiple databases without restrictions on language or publication status. In order to maximize the specificity and sensitivity of the search, the author should also refer to the list of retrieved references to find other relevant studies not found through the search strategy.

A comprehensive review of potentially relevant articles was conducted to ensure that they met all inclusion criteria, as follows:

- (1) Studies comparing patients receiving absorbable and non-absorbable dental repair membranes.
- (2) Studies comparing patients receiving absorbable and non-absorbable dental repair membranes.
- (3) GBR patients.
- (4) Between absorbable and non-absorbable dental restorative membranes, indexes for evaluating curative effect or other relevant indexes are included.
- (5) The full text is available for reference.

Studies were excluded according to the following pre-determined exclusion criteria:

- (1) Studies on other subjects.
- (2) Comparison of other interventions.
- (3) Lack of research on available data.
- (4) Comments, abstracts, and reproduction of publications.

2.2. Data Extraction and Quality Assessment. Two pairs of reviewers independently screened the titles, abstracts, and full-text articles of potentially qualified studies and resolved their differences through discussion. The following data parameters were extracted: name of main author, study country, patient population in the study, number of participants in each group, patient age, patient gender, characteristics of drug intervention during follow-up in each group, and outcome measurement in each group. The Cochrane bias risk tool in Review Manager 5.2 was used to evaluate the effectiveness of qualified randomized controlled trials. Egger's test and funnel plot program were used to assess the risk of bias in the study.

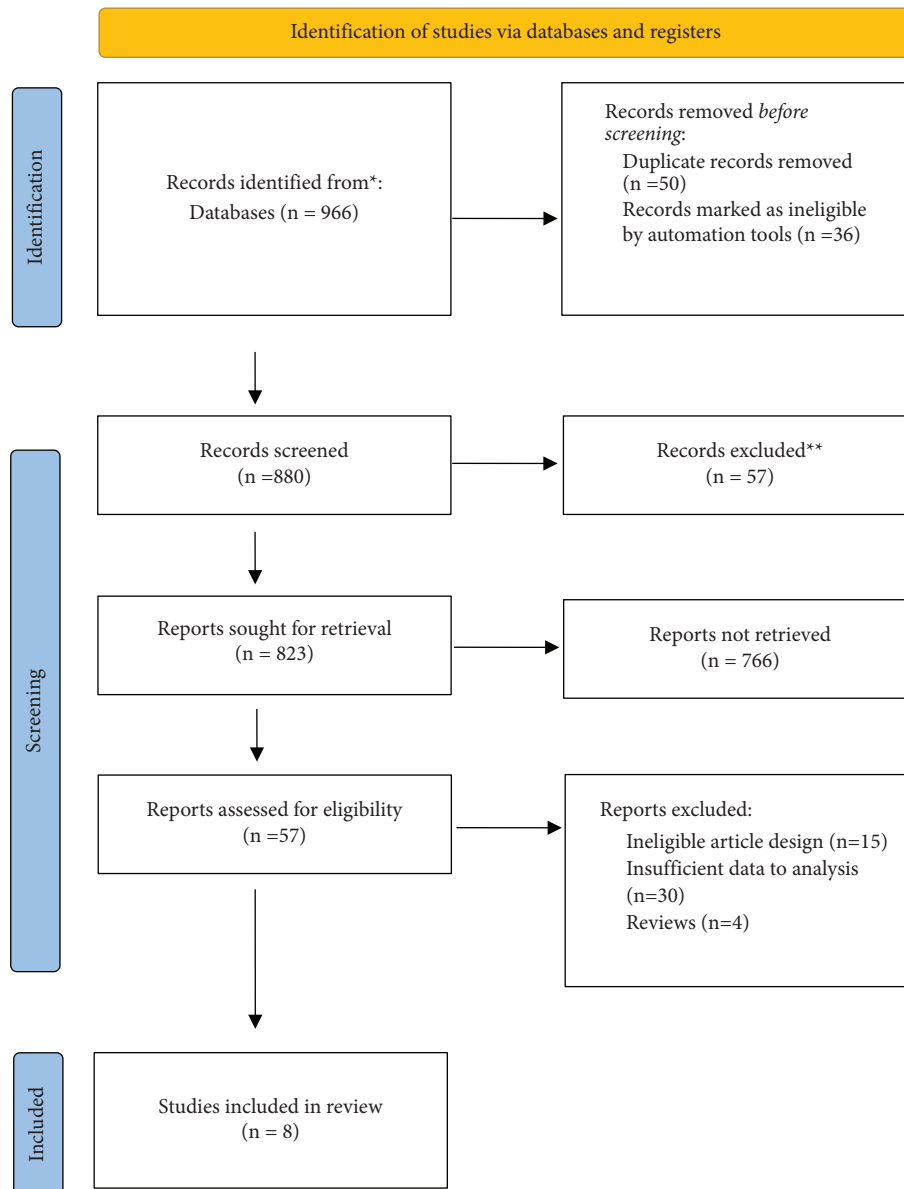
2.3. Statistical Analysis. Review Manager (version 5.2, Cochrane Collaboration, 2011) is used to evaluate the impact of the results in the selected report. In order to measure the consistency of effect size (or and MD), DerSimonian and Laird random effect models were used for paired meta-analysis, and the combined estimates and 95% CI between two groups were calculated. 0% to 40% of heterogeneity is considered "may not be important," 30% to 60% is considered "moderate heterogeneity," 50% to 90% is considered "substantial heterogeneity," and 75% to 100% is considered "considerable heterogeneity."

If $P < 0.05$ or $I^2 > 50\%$, the random effect model was used for analysis; if $P \geq 0.05$ and $I^2 \leq 50\%$, the fixed effect model was used for analysis. When heterogeneity exists, the random effect model is used, while the fixed effect model is applied. Publication bias was examined by visual examination of the funnel plot and using Egger's test. Sensitivity analysis was performed by deleting one study at a time to observe the impact of individual results on the overall analysis.

3. Results

3.1. Search Process. The initial search yielded 966 articles from four databases, including PubMed, Embase, Web of Science, and CNKI. After the first screening, 880 records were retained. By screening titles and abstracts, additional 823 records were excluded because they were review articles, letters, case reports, comments, or editorials. Then, 57 articles were remained. Eight articles were further excluded for various reasons, including different research designs or insufficient available data.

Finally, 8 studies [13–20] met the inclusion criteria and were included in this meta-analysis, with a total of 526 patients. The process followed PRISMA guidelines, including the reasons for excluding the study, as shown in Figure 1.



*Consider, if feasible to do so, reporting the number of records identified from each database or register searched (rather than the total number across all databases/registers).

**If automation tools were used, indicate how many records were excluded by a human and how many were excluded by automation tools.

FIGURE 1: PRISMA flowchart detailing the search strategy for study inclusion.

3.2. Characteristics of Included Studies. Table 1 lists the main characteristics of the eight tests. These studies included 526 patients (263 patients in the experimental group and 263 patients in the control group). All 8 articles were published from 2016 to 2020. The sample size is between 26 and 100.

3.3. Results of Quality Assessment. The Cochrane bias risk assessment tool was used to assess the risk of inclusion in the study. Of these 8 articles, only 1 study found a high risk of selection bias, performance bias, detection bias, abrasion bias, reporting bias, and other bias (Figures 2 and 3).

Given the deviation summary, only 1 clue has different deviation. Visual examination of the funnel chart of studies reporting efficiency showed some asymmetry, and the Egger test showed little evidence of publication bias.

3.4. Results of Heterogeneity Test

3.4.1. Heterogeneity Analysis of Successful Repair between Experiment and Control Groups. Meta-analysis of successful repair. The overall results showed that the repair success rate of the experimental group was higher than that of the control

TABLE 1: Characteristics of eligible studies.

Study	Year	Country	Groups	Sex (male/female)	Age (years)	<i>n</i>	Years of onset
Basler	2018	Switzerland	Resorbable membrane	11/12	56.6 ± 17.4	12	January 2015 to January 2018
			Non-resorbable membrane			11	
Cui	2019	China	Resorbable membrane	44/36	47.4 ± 4.25	40	February 2016 to February 2018
			Non-resorbable membrane			40	
Huang	2016	China	Resorbable membrane	63/37	50.8 ± 1.9	50	August 2013 to February 2015
			Non-resorbable membrane			50	
Naenni	2016	Switzerland	Resorbable membrane	13/14	51.85 ± 29.7	13	March 2010 and January 2013
			Non-resorbable membrane			14	
Wang	2018	China	Resorbable membrane	39/37	40.25 ± 18.75	38	July 2017 to July 2018
			Non-resorbable membrane			38	
Wang	2020	China	Resorbable membrane	49/45	42.4 ± 5.55	47	December 2017 to December 2018
			Non-resorbable membrane			47	
Yang	2016	China	Resorbable membrane	41/25	45.07 ± 6.5	33	January 2014 to January 2015
			Non-resorbable membrane			33	
Zhuang	2016	China	Resorbable membrane	36/24±	36.4 ± 9.09	30	January 2013 to May 2015
			Non-resorbable membrane			30	

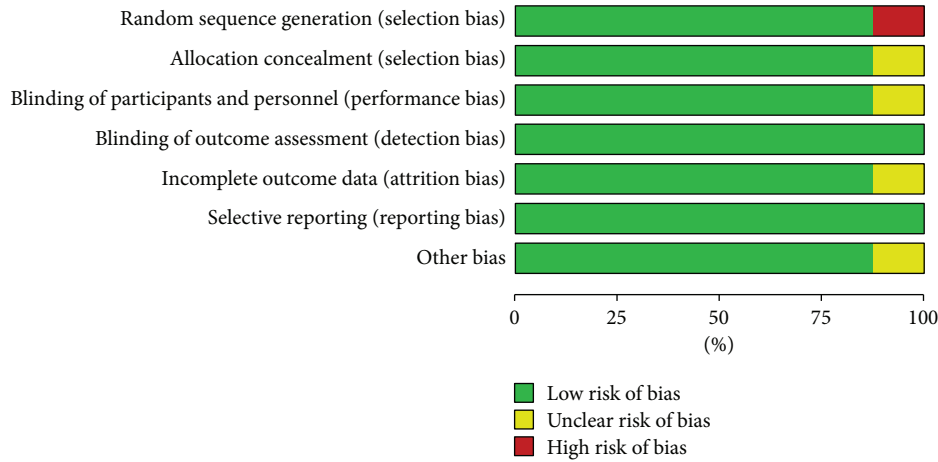


FIGURE 2: Graph of the risk of bias: green = low risk; yellow with question mark = unclear; and red = high risk.

group (RR = 1.18, 95% confidence interval [1.11, 1.26], and the total effect was $P < 0.0001$, $I^2 = 0\%$ fixed effect model) (Figure 4).

3.4.2. Heterogeneity Analysis of Height of Bone Graft between Experiment and Control Groups. Similarly, the first mic-turition (min) between the experimental group and the control group was meta-analyzed. The overall results showed that the height of bone transplantation in the experimental group was higher than that in the control group (MD = 0.67, 95% confidence interval [0.11, 1.23], overall $P = 0.02$, $I^2 = 99\%$, using random effect model) (Figure 5).

3.4.3. Heterogeneity Analysis of Bone Graft Thickness between Experiment and Control Groups. For residual urine, it was reported in 7 studies. The overall results showed that the thickness of bone graft in the experimental group was higher than that in the control group (MD = 0.43, 95% confidence interval [0.30, 0.56], $P < 0.00001$, $I^2 = 61\%$, using random effect model) (Figure 6).

3.4.4. Heterogeneity Analysis of Adverse Events between Experiment and Control Groups. To better assess the safety of different therapies, we collected data on adverse events. The overall results showed that the adverse events in the experimental group were less than those in the control group (RR = 0.31, 95% confidence interval [0.18, 0.51], $P < 0.00001$, $I^2 = 13\%$, using the fixed effect model) (Figure 7).

3.5. Results of Sensitivity Analysis and Publication Bias. To assess the sensitivity of the articles, we deleted a study to observe the effect of individual outcomes on the overall efficacy of urinary retention. In Figure 4, the result shows $I^2 = 0\%$ high heterogeneity. When Wang's article [18] was deleted, the results change the most, indicating the robustness of the included study (Figure 8).

We used funnel plots to assess the efficiency of urinary retention. Visual results showed symmetrical shape. The P value of Egger test was 0.218, indicating that there was no publication bias in this study (Figure 9).

	Random sequence generation (selection bias)	Allocation concealment (selection bias)	Blinding of participants and personnel (performance bias)	Blinding of outcome assessment (detection bias)	Incomplete outcome data (attrition bias)	Selective reporting (reporting bias)	Other bias
Basler 2018	+	+	+	+	+	+	?
Cui 2019	+	+	+	+	+	+	+
Huang 2016	-	+	+	+	+	+	+
Naenni 2016	+	+	?	+	+	+	+
Wang 2018	+	+	+	+	?	+	+
Wang 2020	+	+	+	+	+	+	+
Yang 2016	+	+	+	+	+	+	+
Zhuang 2016	+	?	+	+	+	+	+

FIGURE 3: Risk of bias for each study, using three colors: green = low risk; yellow with question mark = unclear; and red = high risk.

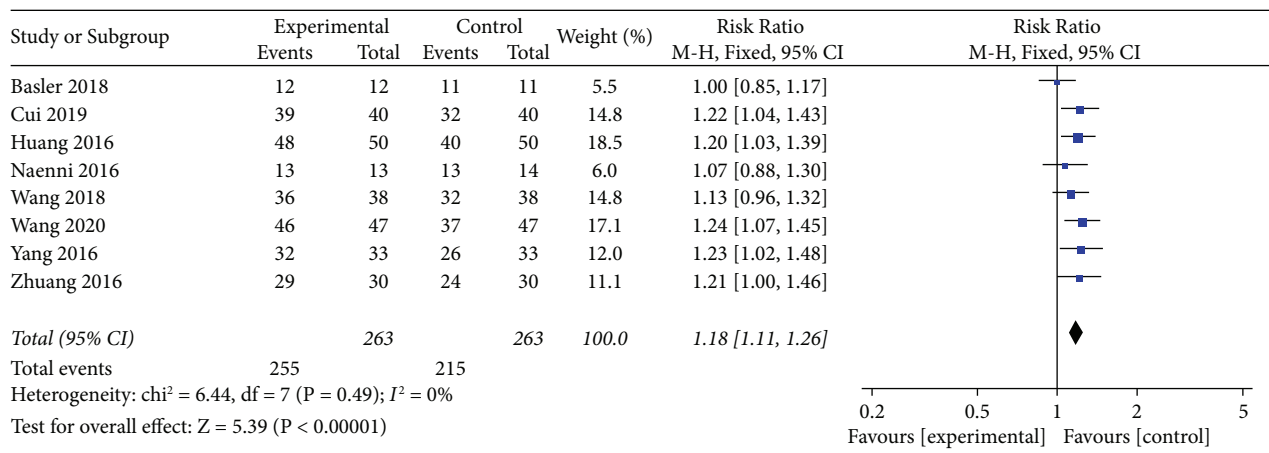


FIGURE 4: Forest plots for the effects for successful repair in experiment versus control groups.

4. Discussion

From our results, we can find that absorbable dental restorative membrane had higher successful repair than non-absorbable dental restorative membrane in guided bone regeneration. In addition, height of bone graft and bone graft

thickness were both higher in absorbable dental restorative membrane than non-absorbable dental restorative membrane. In the comparison of safety, absorbable dental restorative membrane was worse than non-absorbable dental restorative membrane. These results showed that absorbable dental restorative membrane was better than non-

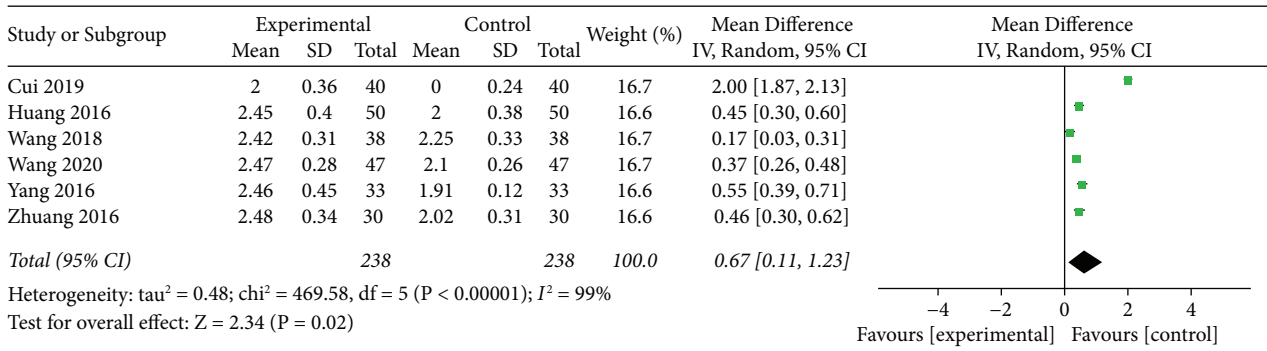


FIGURE 5: Forest plots for the height of bone graft in experiment versus control groups.

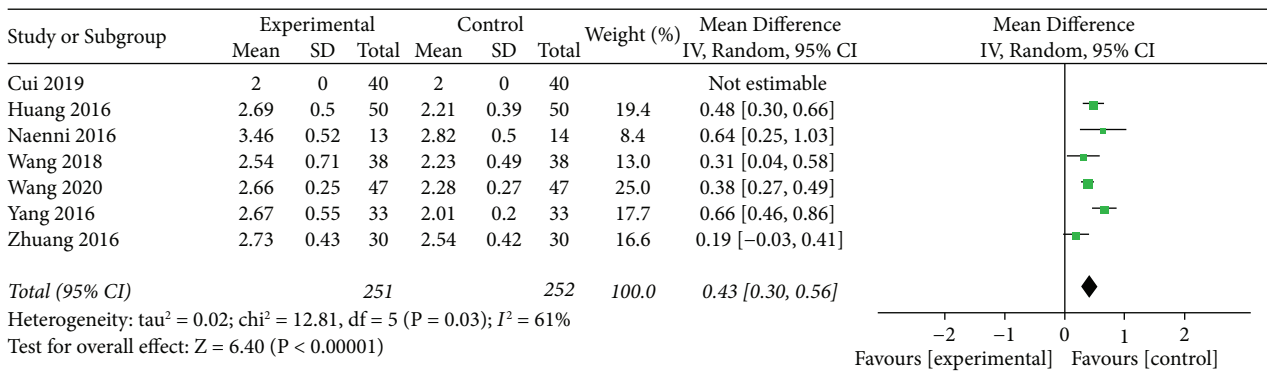


FIGURE 6: Forest plots for bone graft thickness in experiment versus control groups.

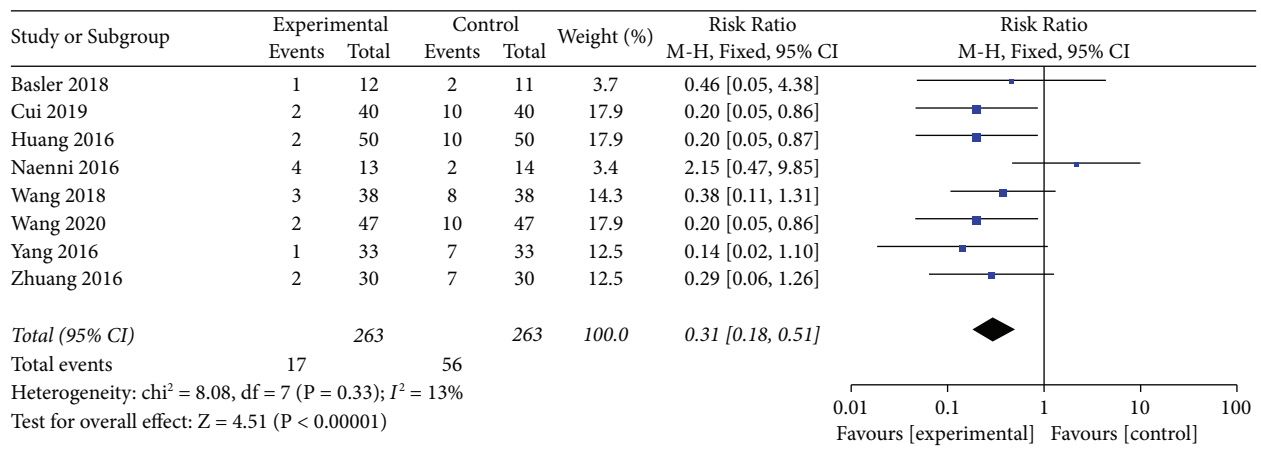


FIGURE 7: Forest plots for adverse events in experiment versus control groups.

absorbable dental restorative membrane in clinical effects and safety. These were consistent with Zhang's study [21] that bone regeneration guided by absorbable biofilm in patients with GBR improves the success rate of dental implantation and has high safety.

With the development of dental implants, implant denture has become one of the conventional treatment

methods for repairing dentition defects or deletions, and the methods are constantly simplified [22, 23]. The safety and reliability are gradually improved. Guided bone regeneration (GBR) is often widely used to treat periodontal diseases and repair maxillary sinus defects and bone defects. Oral repair membrane has the characteristics of high efficiency, short time consumption, thick osteogenesis, and high

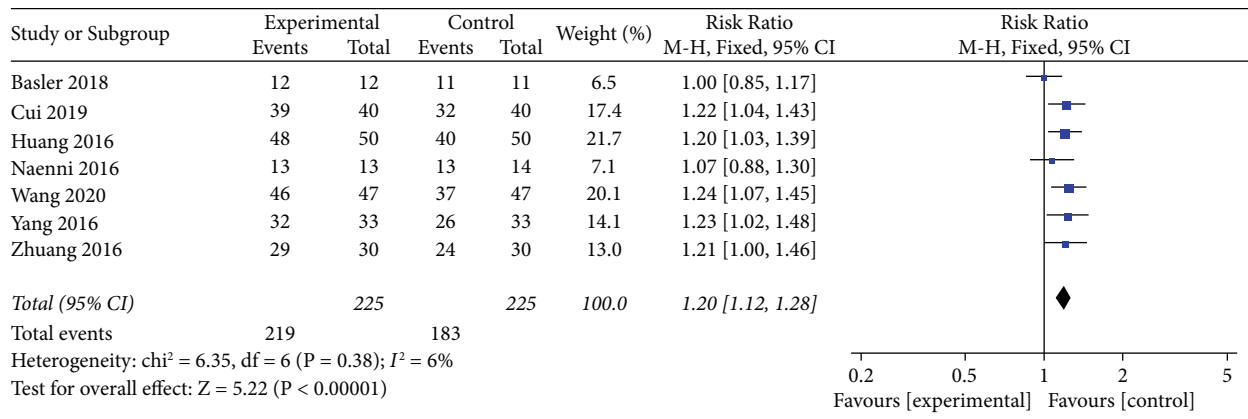


FIGURE 8: Sensitivity analysis of effects for successful repair between experiment and control groups.

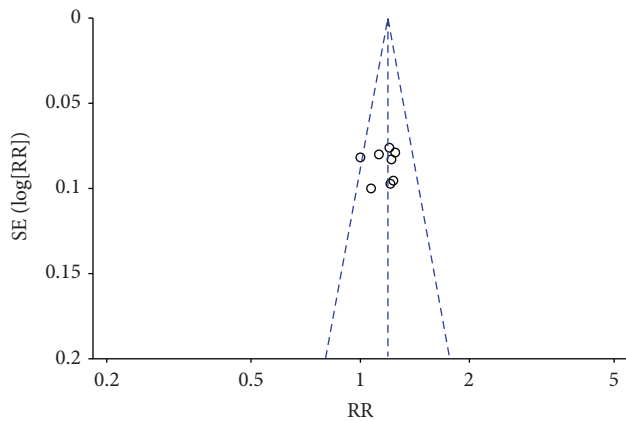


FIGURE 9: Funnel plot of publication bias.

osteogenesis [24]. The primary function of the oral repair membrane is to prevent epithelial cells and connective tissue cells from entering the regeneration area and create and maintain a space for the unrestrained growth of pluripotent stem cells and osteoblasts [25]. It is widely used in stomatology, such as periodontal mucosa, oral implant, and alveolar surgery.

Non-absorbable membrane (titanium membrane) was a commonly used oral repair material in the past. It has the characteristics of stable space, good resistance strength, and hard texture [26]. It plays a specific role in promoting the growth of bone grafts. However, it also has some adverse effects, such as preventing the excellent absorption of blood by bone graft, prolonging patients' recovery time, and requiring secondary surgery [27]. The incidence of postoperative complications is high, and the osteogenic effect is poor.

The absorbable membrane has collagen composition similar to periodontal connective tissue, including weak immunogenicity and cytotoxicity [28]. The absorbable membrane can promote the chemotaxis of periodontal ligament (PDL) cells and gingival fibroblasts. In addition, it can encourage hemostasis, is easy to operate, and degrades physiologically. Calcification and ossification can occur when approaching bone [29].

5. Conclusion

In this paper, we have evaluated clinical efficacy and safety of absorbable and non-absorbable dental restorative membranes in guided bone regeneration (GBR). For this purpose, both absorbable and non-absorbable prosthetic films for GBR were selected from multiple databases (PubMed, Web of Science, Cochrane Library, and China National Knowledge Infrastructure), whereas Review Manager 5.2 was used for meta-analysis, sensitivity analysis, and bias analysis. After the screening process, 526 postoperative patients were extracted from 8 trials which are those patients who finally met the qualification criteria. The present study showed that absorbable dental restorative membrane was better than non-absorbable dental membrane both in clinical effects and safety. However, our findings should be carefully considered with caution due to small sample size. Studies in various areas with large study population are essential to further confirm our findings in the future. There are some limitations in this study. Firstly, more indicators should be included, and this could be conducted in the future. Secondly, more research studies from various areas could be analyzed in the next research.

In future, we are keen to extend the proposed study to other domains and diseases preferably in smart healthcare sector.

Data Availability

The datasets used and analyzed during the current study are available from the corresponding author upon reasonable request.

Disclosure

Yan Guo and Linghan Su are co-first authors.

Conflicts of Interest

The authors declare that they have no conflicts of interest.

Authors' Contributions

Yan Guo and Linghan Su contributed equally to this study. The conception of the paper was completed by Caidi Chen and Yan Liu. The data processing was completed by Caidi Chen, Yan Liu, and Jianxue Li. All authors participated in the review of the paper.

Acknowledgments

This study was supported by the general project of Natural Science Foundation of Gansu Province (20JR10RA006).

References

- [1] D. Monteiro and B. S. Kim, "Utilizing anorganic bovine bone (bio-oss) with absorbable and nonabsorbable membranes placed over the lateral window: histomorphometric and clinical," *International Journal of Periodontics Restorative Dent*, vol. 25, 2005.
- [2] G. Khoury, P. Lahoud, and R. Younes, *Use of Grafting Materials in Sinus Floor Elevation: Biologic Basis and Current Updates*, Springer International Publishing, Berlin, Germany, 2015.
- [3] B. J. Anguelov, "Trabeculectomy with absorbable and non-absorbable sutures of the scleral flap in primary open angle glaucoma," *国际眼科杂志*, vol. 3, p. 1, 2003.
- [4] X. Yong, *The Clinical Effect Of Oral Biofilm In Guiding Of Bone Regeneration During Dental Implant*, Northeast Asia Publishing, Berlin, Germany, 2015.
- [5] X. F. Jiao and D. O. Stomatology, "Study on the clinical effect of oral prosthetic membrane material guided bone regeneration in dental implantation," *China Medical Cosmetology*, 2017.
- [6] I. Rocchietta, P. Schupbach, C. Ghezzi, and M. Maschera, "Soft tissue integration of a porcine collagen membrane: an experimental study in pigs," *The International Journal of Periodontics and Restorative Dentistry*, vol. 32, no. 1, pp. e34–e40, 2012.
- [7] S. S. Wallace, S. J. Froum, S. C. Cho et al., "Sinus augmentation utilizing anorganic bovine bone (Bio-Oss) with absorbable and nonabsorbable membranes placed over the lateral window: histomorphometric and clinical analyses," *The International Journal of Periodontics and Restorative Dentistry*, vol. 25, no. 6, pp. 551–559, 2005.
- [8] D. Pfoerringer, N. Harrasser, H. Muehlhofer et al., "Osteoinduction and -conduction through absorbable bone substitute materials based on calcium sulfate: in vivo biological behavior in a rabbit model," *Journal of Materials Science*, vol. 29, pp. 11–17, 2018.
- [9] M. Lopez, S. Olate, A. L. Lanata-Flores et al., "New bone formation in a bone defect associated to dental implant using absorbable or non-absorbable membrane in a dog model," *International Journal of Clinical and Experimental Pathology*, vol. 6, no. 11, pp. 2292–2299, 2013.
- [10] E. A. Sallum, A. W. Sallum, F. H. Nociti, R. A. Marcantonio, and S. D. Toledo, "New attachment achieved by guided tissue regeneration using a bioresorbable polylactic acid membrane in dogs," *The International Journal of Periodontics and Restorative Dentistry*, vol. 18, no. 5, pp. 502–510, 1998.
- [11] A. Joop, B. Rahlf, N. C. Gellrich, A. Kampmann, C. V. See, and M. Stoetzer, "Examination of local periosteal microcirculation after application of absorbable and non-absorbable membranes," *Journal of Oral Implantology*, vol. 43, no. 6, pp. 462–467, 2017.
- [12] M. Cao, X. Wu, and J. Xu, "A systematic review and meta-analysis of neostigmine for urinary retention after surgeries," *Translational Andrology and Urology*, vol. 11, no. 2, pp. 190–201, 2022.
- [13] C. Zy, "Effects of two different oral repair membrane materials on implant guided bone regeneration," *Grassroots Medical Forum*, vol. 23, pp. 1371–1372, 2019.
- [14] H. Hb, "Clinical study on the effect of dental restorative membrane in guided bone regeneration during dental implantation," *Shenzhen Journal of integrated traditional Chinese and Western Medicine*, vol. 26, pp. 127–128, 2016.
- [15] L. Zhou, "Evaluation of the effect of dental restorative membrane material in guiding osteogenesis during dental implantation," *Heilongjiang Medicine Journal*, vol. 29, pp. 781–783, 2016.
- [16] W. Hj, "Application of Haiao oral repair membrane in guided bone regeneration during dental implantation and analysis of its adverse reactions," *Modern diagnosis and treatment*, vol. 31, pp. 1764–1765, 2020.
- [17] Y. Qy, "Comparative study on guided bone regeneration of different oral restorative membrane materials in dental implantation," *Chin J Mod Drug Appl*, vol. 10, pp. 94–95, 2016.
- [18] C. P. Qx, "Clinical effect of different oral restorative membrane materials on guided bone regeneration during dental implantation," *Medical Information*, vol. 31, pp. 59–60, 2018.
- [19] T. Basler, N. Naenni, D. Schneider, C. H. F. Hammerle, R. E. Jung, and D. S. Thoma, "Randomized controlled clinical study assessing two membranes for guided bone regeneration of peri-implant bone defects: 3-year results," *Clinical Oral Implants Research*, vol. 29, no. 5, pp. 499–507, 2018.
- [20] N. Naenni, D. Schneider, R. E. Jung, J. Husler, C. H. F. Hammerle, and D. S. Thoma, "Randomized clinical study assessing two membranes for guided bone regeneration of peri-implant bone defects: clinical and histological outcomes at 6 months," *Clinical Oral Implants Research*, vol. 28, no. 10, pp. 1309–1317, 2017.
- [21] J. Zhang, "Application and effect of absorbable repair membrane in guided bone regeneration of dental implant," *Chinese Community Doctors*, vol. 17, no. 8, pp. 120–128, 2018.
- [22] E. Battistella, E. Varoni, A. Cochis, B. Palazzo, and L. Rimondini, "Degradable polymers may improve dental practice," *Journal of Applied Biomaterials and Biomechanics*, vol. 9, no. 3, pp. 223–231, 2011.
- [23] U. Sakallioğlu, U. Yavuz, M. Lütfioglu, I. Keskiner, and G. Açıkgöz, "Clinical outcomes of guided tissue regeneration with Atrisorb membrane in the treatment of intrabony defects: a 3-year follow-up study," *The International Journal of Periodontics and Restorative Dentistry*, vol. 27, no. 1, pp. 79–88, 2007.
- [24] P. A. Rodriguez, A. L. Lenarduzzi, M. Amer, and L. Sierra, "Bone-regeneration after Apical Surgery Using Reabsorbable Membrane and Powder Bone," in *Proceedings of the Meeting of the Continental European Division of the International Association of Dental Research (CED-IADR) with the Scandinavian Division (NOF) 2011*, Barcelona, Spain, September 2011.
- [25] T. Cao, K. Ohno, T. Shirota, and K. Michi, "Bone defect healing by nonabsorbable membrane for guided tissue regeneration," *Dental Medicine Research*, vol. 18, pp. 214–218, 2012.
- [26] S. Medel, M. Alarab, H. Kufaishi, H. Drutz, and O. Shynlova, "Attachment of primary vaginal fibroblasts to absorbable and

- nonabsorbable implant materials coated with platelet-rich plasma,” *Female Pelvic Medicine & Reconstructive Surgery*, vol. 21, no. 4, pp. 190–197, 2015.
- [27] B. Shao, Y. Lu, and J. Sui, “Application of dental restorative materials in bone regeneration in dental implantation,” *World Latest Medicine Information*, vol. 101, 2016.
- [28] F. H. Nociti, M. Â N. Machado, C. M. Stefani, E. A. Sallum, and A. W. Sallum, “Absorbable versus nonabsorbable membranes and bone grafts in the treatment of ligature-induced peri-implantitis defects in dogs,” *Clinical Oral Implants Research*, vol. 12, no. 2, pp. 115–120, 2001.
- [29] S. J. Froum, S. H. Froum, and P. S. Rosen, “A regenerative approach to the successful treatment of peri-implantitis: a consecutive series of 170 implants in 100 patients with 2- to 10-year follow-up,” *The International Journal of Periodontics and Restorative Dentistry*, vol. 35, no. 6, pp. 857–863, 2015.

Research Article

Exploration and Practice of the Integrated Teaching Method of Mind Mapping in the Standardized Training of New Pharmacists

Li Yuan , Bei Chen, Zhaojun Wu, Gefei He, and Juanjuan Huang

Department of Pharmacy, The First Hospital of Changsha, Changsha 410005, China

Correspondence should be addressed to Li Yuan; 31808220314@stu.suse.edu.cn

Received 1 June 2022; Revised 24 June 2022; Accepted 29 June 2022; Published 31 July 2022

Academic Editor: Dong Chen

Copyright © 2022 Li Yuan et al. This is an open access article distributed under the Creative Commons Attribution License, which permits unrestricted use, distribution, and reproduction in any medium, provided the original work is properly cited.

Objective. The objective is to analyze the application effect of mind map in the standardized training of new pharmacists, providing reference information for the standardized training and teaching methods of new pharmacists. **Methods.** 24 new pharmacists in pharmacy were selected as experimental samples. The mind map integration teaching method was applied in the standardized training, which involved two parts of pharmaceutical professional knowledge theory and practical skills. The relevant theoretical knowledge of the new pharmacists was evaluated by the examination paper. Their clinical practice ability was evaluated by the expert group on-the-spot assessment score, and the final scores were calculated by two parts. Paired *t*-test was used to analyze the training effect of theoretical knowledge and clinical practice ability of participants before and after training. **Results.** All pharmacists have passed the examination. The average score of theory test was (85.8 ± 5.2) , the average score of skill examination was (83.1 ± 6.0) , and the total score was (84.1 ± 5.0) . Before and after training, the total scores of 9 core competencies of pharmacists before and after training have significant difference $(18.87 \pm 4.06$ and 21.40 ± 2.68 , $P < 0.01$). **Conclusion.** The standardized training for new pharmacists through the mind map integration teaching method can effectively improve their core competence and post competence. This training method is worth using for reference and promotion.

1. Introduction

The Development Plan of Medicine and Health points out that the number of hospital pharmacists in China should reach 850,000 by 2020. The standardized training of pharmacists should be strengthened, and the on-the-job training system and professional qualification system of pharmacists should be improved. Pharmacists should be equipped with the relevant policies in hospitals and pharmacies [1]. According to the statistics of China Health Statistical Yearbook 2021, 497,000 pharmacists in medical institutions in China have obtained technical titles by the end of 2020, which is still far from the target of 850,000 pharmacists [2]. In the future, there will be a large number of new pharmacists to enter the hospital. New pharmacists in hospitals refer to pharmacists who have recently graduated or who have obtained the qualification of junior pharmacists within two years. Most of them are fresh graduates lacking practical experience in working in hospitals. It is necessary to change the role of students to pharmaceutical professionals and

technicians as soon as possible, to meet the requirements of different positions. It is a new problem for hospital and pharmacy department to strengthen the standardized training of new pharmacists to make them competent pharmacists and to ensure the safety of patients' medication. Standardized training of pharmacists is an important link in the growth of pharmaceutical talents in hospitals, but there has been a lack of standardized system and objective standards for the training of newly recruited pharmacists in our country [3]. At present, a set of effective standardized training course system for new pharmacists has not been formed in China. The notice from the Ministry of Health's Department of Science and Education concerns the implementation in 1999 of standardized training for hospital pharmacists, but the outline did not specify the specific model of standardized training of hospital pharmacists in our country [4]. However, the training model, training objectives, training level, and degree of standardization have not yet reached a unified consensus. Mind mapping integrated teaching method is a new training method, which has

been popularized and applied in multi-disciplinary and multi-post staff training. Its training effect has been affirmed by many instructors and participants. In this study, our center combines the mind map integrated teaching method with the standardized training of new pharmacists, taking the new pharmacists in the department of pharmacy as the research object to conduct a systematic theoretical and practical training for a period of 6 months. The training effect is evaluated by the way of examination and assessment, and the experiences and lessons are analyzed and summarized. It can be used as a reference for the further development and system improvement of standardized training for new pharmacists in the later stage.

2. Methods

2.1. Training Object. In this study, 24 new pharmacists from our center were selected as the research object.

2.1.1. Inclusion Criteria

- (1) Pharmacists who joined the department of pharmacy or obtained the qualified title of junior pharmacist within 2 years before December 2020 were included in the study;
- (2) New pharmacists volunteered to participate in this study.

2.1.2. Exclusion Criteria

- (1) Pharmacists who do not want to cooperate in the research process.

There were six men and 18 women, aged from 21 to 30 years, with an average age of (25.08 ± 2.48) , seven have bachelor's degrees and 17 have master's degrees.

2.2. Training Mode. Based on the demand-oriented training mode of pharmacists for different positions and paying attention to practical operation, the basic process is shown in Figure 1.

2.2.1. Training Demand Survey. The research group consulted the relevant literature, compiling a questionnaire and investigating the students' learning needs for pharmacists with different professional titles before training[5–9]. A total of 1152 pharmaceutical professionals from 99 medical institutions or community health service centers in 13 prefecture-level cities and 1 autonomous prefecture in Hunan Province were selected. 1141 valid questionnaires were collected. The survey shows that the training needs of pharmacists in different positions are different. Pharmacists in outpatient and emergency pharmacies have a strong demand for training in prescription review and rational use of antibiotics, which are closely related to their work. Inpatient pharmacies and static dispensing center pharmacists have a strong demand for training in rational use of antibiotics, rational use of auxiliary drugs, and prescription

review due to the use of drugs by patients in all clinical departments of the hospital. Clinical pharmacists need to participate in a series of work, such as pharmaceutical rounds, pharmaceutical consultation, and pharmaceutical consultation. In addition to the basic requirements for pharmaceutical professional knowledge, we also pay more attention to clinical medical knowledge, evidence-based medicine, key case analysis, and case discussion. At the same time, we also observe the demand for medicine and pharmaceutical humanities of pharmacists, which may be related to the change of the demand of the patients for pharmacists. Pharmacists reflect the original intention of changing the pharmaceutical care model. The service is "patient-centered," and the treatment of patients reflects more humanistic care.

2.2.2. Construct the Detailed Rules for Training Implementation. According to the notice of the Department of Science and Education of the Ministry of Health on the implementation of the standardized training syllabus for Hospital Pharmacists and the Annex "standardized training outline for Hospital Pharmacists" (1999), organize experts to formulate the implementation rules for the training of new pharmacists in our hospital (referred to as "training rules"), including training objectives, implementation objects, curriculum outline, training cycle, training teachers, examination methods, examination standards, and other specific implementation measures.

The training content includes two modules: Professional knowledge and professional skills. The professional knowledge part is the theoretical knowledge training, and the professional skills part is the practical exercise. The specific training courses are shown in Table 1. The purpose of the training is to make hospital pharmacists master the basic knowledge, basic theories, and basic skills necessary for hospital pharmacy. The training of hospital pharmacists should be able to skillfully master the basic knowledge of pharmacy, pharmaceutical-related professional knowledge, laws and regulations, and other comprehensive knowledge. Problem-based teaching method (PBL) or case-based teaching method (CBL) can be adopted in teaching methods. Mind map can be integrated into teaching methods to stimulate the initiative and enthusiasm of new pharmacists.

2.2.3. Implement Training. According to the training implementation rules made in the previous period, the teaching teachers were selected and the training was unified. The training is divided into two stages: the first stage carries on the theoretical centralized training in the online and offline integration mode of the first Hospital in Changsha. The second stage is divided into groups and into different positions of the pharmacy department.

2.2.4. Evaluation and Assessment of Training Effect. Before the implementation of the training, the new pharmacists who participated in the training conducted a theoretical examination. At the end of the training course, they

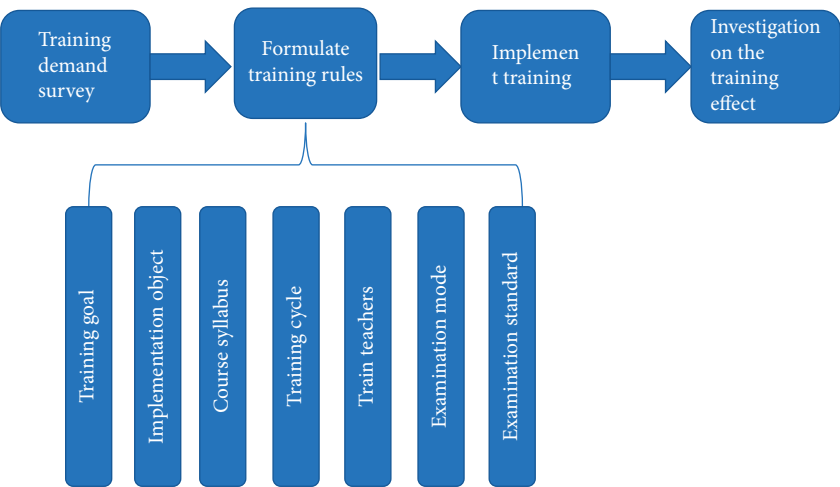


FIGURE 1: An integrated training model based on the needs of different positions of pharmacists and focusing on practical operation.

TABLE 1: Outline of training courses for new pharmacists.

Module classification	Professional knowledge (required)	Professional skills (required)	Professionalism (elective)
	Basic knowledge of pharmacy Professional knowledge related to pharmacy Laws and regulations, rules and regulations Drug policy	Capacity of drug supply and allocation Pharmaceutical care ability Drug management ability Interpersonal communication skills Scientific research ability Emergency handling capacity	Cultural building Moral accomplishment Adaptability
School hours	30	56	12
Teaching method	Online and offline integration, centralized training	Group practice (outpatient pharmacy, inpatient pharmacy, pharmacy, and clinical pharmacy)	Online and offline integration, centralized training
Teaching team	Pharmaceutical expert, clinical pharmacist	Senior dispensing pharmacist and clinical pharmacist	Director of pharmacy

will take part in the theoretical knowledge test and professional skill operation examination. The members of the examination group shall be pharmacists with professional titles in pharmacy and more than 5 years working experience in outpatient and emergency department or hospital adjustment. The examination team formulates the theoretical test paper and the examination standard of skill operation.

- (1) The total score consists of theoretical and skill scores, of which theory accounts for 40% and skills account for 60%. The main contents of the theoretical examination are the syllabus, the teaching contents of the teachers, and the related knowledge issued by the state, with a total score of 100. Skills assessment uses 4 items of on-site prescription/doctor's order review, drug dispensing, medication account, and simulated patient medication consultation to complete the practice assessment. Each item of the score is 25 points, and the total score is 100 points.
- (2) Two months after the end of the pharmacist core competence evaluation training, referring to the relevant literature, a self-designed evaluation table

was used to evaluate the changes of pharmacist core competence before and after training [10–14]. The scale is evaluated from 9 aspects, including emergency treatment, therapeutic drug testing, adverse reaction report, prescription review, drug storage and maintenance, special drug management, medication guidance and consultation, drug dispensing, and competence in prescription. Basically competent and incompetent are scored, and their weights are 4, 3, 2, and 1, respectively, with a total score of 39 points. Calculating each score and total score, the higher the score, the stronger the pharmaceutical care ability. At the same time, the competency rate is counted and the post competency of the students is evaluated. The calculation formula is as follows: competency rate = competent number + basic competent number/total number.

2.3. Statistical Methods. Using SPSS23.0 software, *t*-test was conducted for the score of theory examination, skill operation, and core competence of pharmacists before and after

training conforming to normal distribution. $P < 0.05$ or $P < 0.01$ was set as a significant difference, and there was statistical significance.

3. Results

3.1. Exam Results. All pharmacists have passed the examination, with a pass rate of 100%. The average score of theory test was (85.8 ± 5.2) , the average score of skill examination was (83.1 ± 6.0) , and the total score was (84.1 ± 5.0) . It shows that the trained pharmacists have mastered the basic knowledge and skills of pharmaceutical care. Taking the prescription audit and practical training courses in professional skills upgrading training, new pharmacists draw their own mind maps after training to help memorize knowledge points and operation points as shown in Figure 2.

3.2. Comparison of Core Competence Scores of Pharmacists before and after Pharmacist Training. Two months after the training, the score of the pharmacist's core competence is shown in Table 2. After training, the scores of pharmacists' core competence were significantly improved. The total scores of 9 pharmacists' core competence before and after training had significant difference before and after the training (18.87 ± 4.06 vs. 21.40 ± 2.68 , $P < 0.01$), indicating that the core competence of pharmacists was significantly improved after training.

The change of post competency of new pharmacists before and after training is shown in Figure 3. The post competency rate of pharmacists was significantly improved after training. Among them, the competencies of emergency management, therapeutic drug monitoring, adverse reaction reports, prescription reviews, drug storage and maintenance, special drug management, drug guidance and consultation, and drug dispensing and prescription/order review increased by 20.84%, 25.00%, 29.17%, 33.33%, 25.00%, 20.83%, 33.34%, 25.00%, and 37.50%, respectively. The prescription/doctor's order review, medication guidance, and consultation and prescription review with low competency rate before training are greatly improved, indicating that the training is highly targeted and meets the job needs of pharmacists.

4. Discussion

4.1. The Training Mode Dominated by Practical Operation Is Beneficial to Improve the Training Effect. Most of the new pharmacists in the hospital are fresh graduates, lack of practical experience, their knowledge is relatively narrow, and their service skills are relatively weak. They need to change their roles from students to pharmaceutical professionals in order to meet the requirements of different positions. In recent years, after active exploration and practice of standardized training model for hospital pharmacists in many regions and hospitals, Beijing area has initially established a standardized training system for hospital pharmacists in Beijing area. Some hospitals in Shaanxi and Henan have also explored the standardized training model for hospital pharmacists [5, 15–18].

Strengthening the standardized training of new pharmacists, especially in terms of practical skills, is not only an effective way to improve their skills but also an important link to ensure patients' drug safety and improve hospital medical quality and safety. The traditional training mode based on medical and pharmaceutical professional knowledge has played an important role in the early continuing education and standardized training system for pharmacists [19–21]. However, with the increasing requirements of pharmaceutical care and the deepening of rational drug use, pharmacists should not only have solid professional knowledge but also have all-round service skills. A systematic training plan formulated in our center can be targeted to improve the abovementioned skills of new pharmacists and set corresponding assessment standards. Through practical operation, pharmacists can understand their job responsibilities, work contents, system, and standard operating procedures from all aspects, which can not only meet the requirements of pharmacist post competence but also improve the comprehensive quality of pharmacists. The results of this study show that all the trainees passed the examination and the passing rate was 100%. The average score of the theory test was (85.8 ± 5.2) , the average score of the skill examination was (83.1 ± 6.0) , and the total score was (84.1 ± 5.0) . The result shows that the new pharmacists have a high enthusiasm to participate in the training, and they have good participation in the training mode dominated by practical operations. Under this training mode, they can fully stimulate their interest in learning and make them better master the basic knowledge and skills of pharmaceutical care.

The implementation of the practice-led training model for new pharmacists is that the pharmacist team of our hospital fully understands the training programs and needs in different positions and professional titles after detailed investigation in the early stage. The pharmacist training system and model with our characteristics is formed through the careful formulation of the teaching syllabus and training courses by pharmaceutical experts. Through the analysis of the research results, a preliminary understanding of the knowledge reserve of new pharmacists combined with the knowledge and skill requirements of various positions of pharmacists in our hospital. The training courses are reconstructed, the course contents and teaching methods are carefully designed, and the training model of centralized theoretical training and grouping skills practice is implemented. This training model takes pharmacists as the center, following the concept of "teaching according to needs" and paying attention to practical training, and can solve the problems of pertinence and effectiveness of training.

4.2. Integrate Various Teaching Methods to Improve the Core Competence of Pharmacists. The results of this study show that after 2 months of theoretical training and skill operation practice, the total scores of the 9 core competencies of new pharmacists are (18.87 ± 4.06) and (21.40 ± 2.68) . There was significant difference before and after training ($P < 0.01$), and the post competency rate of pharmacists was significantly improved after training. The competency rates of 9

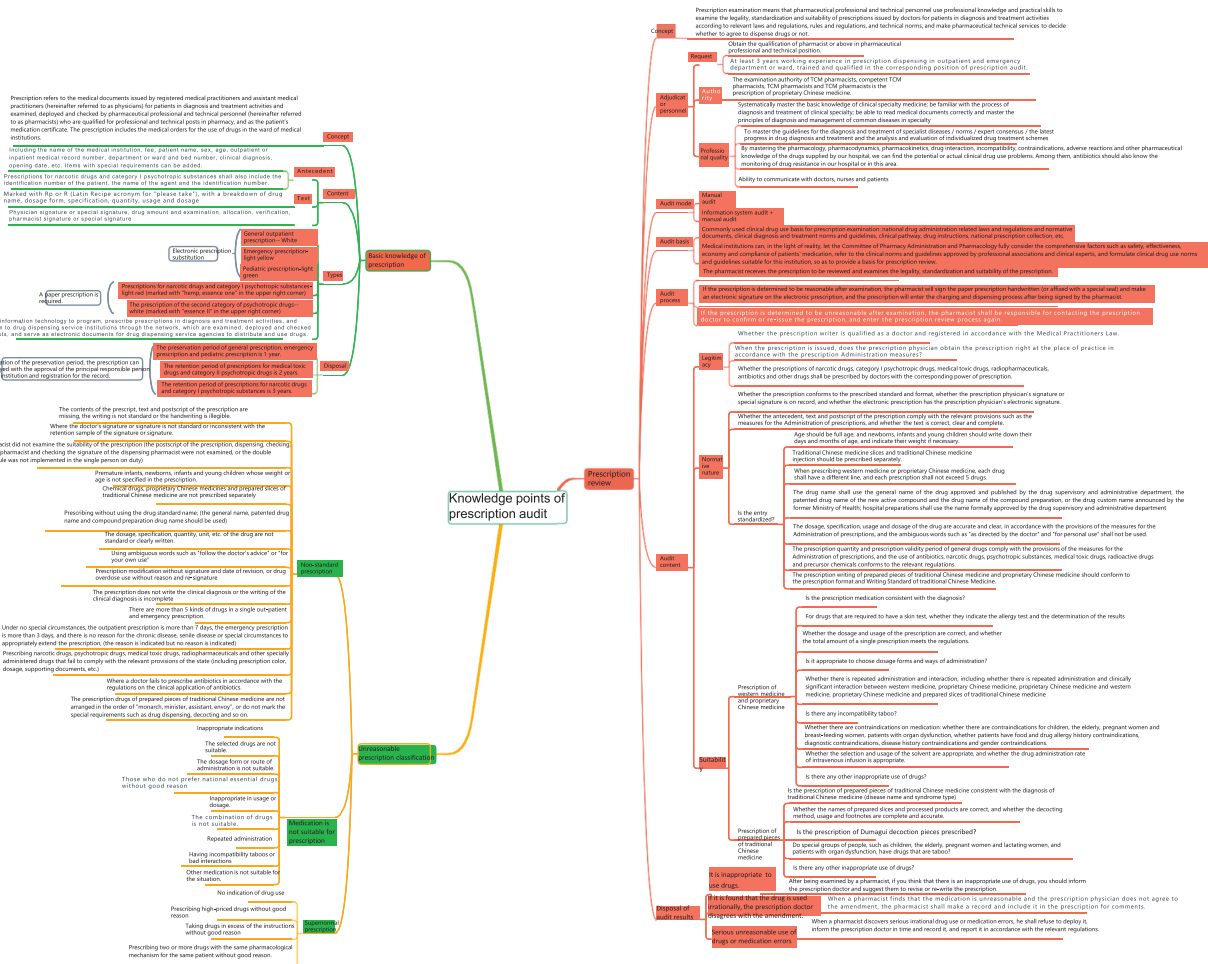


FIGURE 2: Mind map of prescription review and practical training points.

TABLE 2: Comparison of core competence scores of pharmacists before and after training.

[illegible]

indicators such as prescription review, drug dispensing, medication guidance, and adverse reaction reports were greatly improved, especially the prescription/doctor's order review, medication guidance, consultation, and prescription review with low qualification rate before training, indicating that the training is highly targeted and meets the job needs of pharmacists.

In the past, the training was mainly based on pharmaceutical theoretical knowledge training, but our training outline was implemented in two stages. In the first stage, centralized theoretical training was carried out in the hospital learning platform in online and offline integration mode. In

the second stage, groups were divided into different positions in the pharmacy department for practical training. Theory training had 30 class hours and skills practice had 56 class hours. The total score is composed of theory and skills accounting for 40% and 60%, respectively, which is enough to highlight the new training mode of new pharmacists dominated by skill practice. At the same time, we integrate a variety of effective teaching methods, which could help new pharmacists memorize theoretical knowledge, systematically sort out the knowledge system, and achieve integration [22–24]. Encountering new problems in skills practice, stimulating divergent thinking, and combining practice and theory to

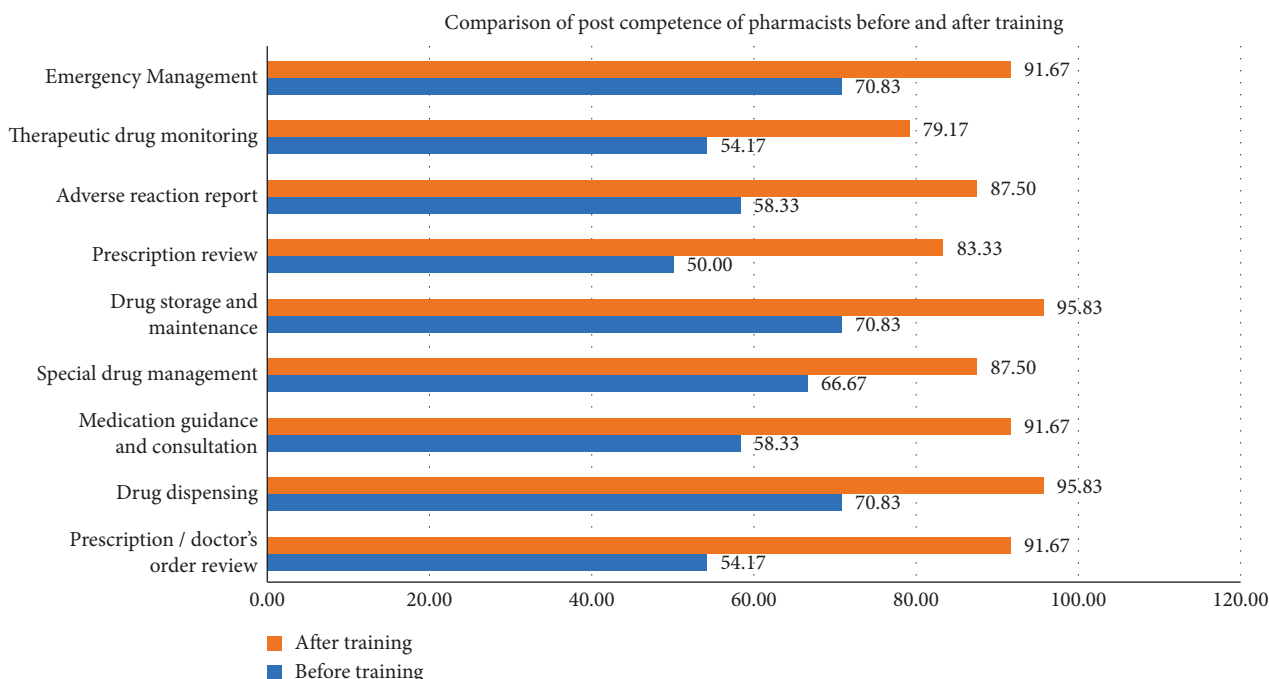


FIGURE 3: Comparison of post competency rate of new pharmacists before and after training.

form a new mind map deepen the understanding and analysis of theoretical knowledge and gradually adapt to the complex and changeable process of dealing with clinical problems.

At present, our research is mainly limited to Hunan Province with a small number of participants. We will expand our research to the whole China in the follow-up study in order to reduce the limitations of the research.

In conclusion, the implementation of the demand-oriented training model for new pharmacists can grasp the weak links of pharmacists' theories and skills for targeted training, which not only strengthens the skills of rational use of drugs but also enables new pharmacists to have a new understanding of the profession of pharmacists. First of all, the research group has an in-depth understanding of the weak links in the theories and skills of new pharmacists and then formulates well-targeted training rules. At the same time, the integration of various teaching methods is used to improve the core competence of pharmacists, which plays a positive role in improving the level of rational drug use and the construction of pharmaceutical talents.

Data Availability

The datasets used and analyzed during the current study are available from the corresponding author upon reasonable request.

Conflicts of Interest

The authors declare that they have no conflicts of interest.

Acknowledgments

This study was supported by Changsha Municipal Natural Science Foundation (kq2014007).

References

- [1] W. Renfa, "Circular of the Ministry of Health on the Issuance of the Medium-And Long-Term Talent Development Plan for Medicine and Health," 2011, http://www.gov.cn/zwgg/2011-04/28/content_1854246.html.
- [2] China Health Statistics, "China Health Statistics Yearbook," 2021, <https://www.yearbookchina.com/navibooklist-n3022013080-1.html>.
- [3] Y. Xie, C. Wu, and S. Jia, "The practice of mind mapping combined with CPBL teaching method in clinical pharmacist teaching [J]," *Continuing medical education in China*, vol. 11, no. 25, pp. 57–60, 2019.
- [4] X. Shi, J. Zhang, and X. Liu, "Construction of standardized training system for outpatient pharmacists," *Shanghai medicine*, vol. 39, no. 5, pp. 61–63, 2018.
- [5] Z. Chen, Y. Chen, and J. Shen, "Exploration and practice on the construction of standardized pre-post training system for hospital pharmacists," *Chinese Journal of Hospital Pharmacy*, vol. 41, no. 22, pp. 2273–2277, 2021.
- [6] Z. Gu, Y. Huang, and X. Xi, "The enlightenment of New Zealand prescription pharmacist training system to China," *Chinese Journal of Hospital Pharmacy*, vol. 42, no. 3, pp. 223–228, 2022.
- [7] W. Zhao, Yi Yang, and K. Tian, "The enlightenment of American drug treatment management model to the capacity building of pharmaceutical care in primary health care institutions in China," *Chinese Journal of New drugs*, vol. 28, no. 11, pp. 1292–1296, 2019.
- [8] ran Zhou, Y. Fang, and F. Xiaojun, "Evaluation of the effect of modified mini clinical drill evaluation teaching method in standardized training of clinical pharmacists," *Chinese pharmaceutical industry*, vol. 30, no. 18, pp. 13–16, 2021.
- [9] H. Chang, X. Lin, and J. Lin, "The enlightenment of American resident pharmacist training model to the establishment of standardized training system for hospital pharmacists in

- China,” *Chinese Pharmaceutical Affairs*, vol. 35, no. 7, pp. 835–840, 2021.
- [10] T. Ma, R. Fang, and J. Wu, “Preliminary construction of standardized training system for pharmaceutical personnel in junior hospitals,” *Journal of traditional Chinese Medicine Management*, vol. 26, no. 7, pp. 25–26, 2018.
 - [11] Li Yue, W. Wang, and Y. Luo, “Investigation and study on the core factors of post competence of pharmacists in pharmacy [J],” *Higher medical education in China*, vol. 17, no. 9, pp. 11–12, 2018.
 - [12] J. Cai, “Application of mind mapping teaching method in occupational exposure protection training of newly recruited nurses,” *Medical frontier*, vol. 9, no. 30, p. 221, 2019.
 - [13] Z. Wang, T. Zhang, and Y. Li, “Application of CBL teaching method in standardized training of pharmacists in medical institutions,” *Continuing medical education in China*, vol. 13, no. 7, pp. 35–39, 2021.
 - [14] H. Tian, B. Wang, and H. Yao, “Design of competency-based pharmaceutical care system for pediatric dispensing pharmacists,” *Practical drugs and clinical practice*, vol. 22, no. 10, pp. 1116–1120, 2019.
 - [15] S. Ren, J. Bian, D. Wu, J. Zhen, and W. Zhang, “Discussion on the optimization of standardized training mode for resident pharmacists in Beijing,” *Chinese pharmacy*, vol. 31, no. 6, pp. 755–758, 2020.
 - [16] Y. Chu, Z. Yin, and L. Yan, “Investigation on the current situation of core competence of new pharmacists and its enlightenment to standardized training of hospital pharmacists,” *Chinese Journal of Hospital Pharmacy*, vol. 39, no. 19, pp. 1985–1988, 2019.
 - [17] R. Cao, Li Qi, and X. Meng, “Application of layered training model in hospital pharmacist training,” *Medical information*, vol. 32, no. 3, pp. 28–30, 2019.
 - [18] Y. Chu, Z. Yin, and L. Yan, “Construction of standardized training course system for new pharmacists and test of its reliability and validity,” *Modern Applied Pharmacy in China*, vol. 37, no. 16, pp. 2011–2015, 2020.
 - [19] Y. Zou, B. Wu, and Y. Shi, “Construction of hierarchical training plan for pharmacists in inpatient pharmacy,” *Chinese Journal of Hospital Pharmacy*, vol. 41, no. 20, pp. 2138–2141, 2021.
 - [20] Y. Huang, H. Liu, and M. Leng, “Study on the current situation and problems of Pharmaceutical Care in Primary Medical institutions in China (2): analysis of the current situation of pharmacist team construction,” *Chinese Journal of Hospital Pharmacy*, vol. 39, no. 1, pp. 1–6, 2019.
 - [21] X. Xi, D. Yao, and Y. Huang, “Study on the current situation and problems of clinical pharmaceutical care in tertiary hospitals in China (2): analysis of the current situation of clinical pharmacist team construction,” *Chinese pharmacy*, vol. 53, no. 6, pp. 472–476, 2018.
 - [22] H. P. Tian, C. R. Sun, L. Wang, and X. T. Lu, “Establishment and practice of standardized mode of pre-job training for pharmacists in the dispensary of the emergency department,” *Pharmaceutical Care and Research*, vol. 18, no. 6, pp. 460–464, 2018.
 - [23] A. Lim, G. Arora, B. McInerney, M. Vienet, K. Stewart, and K. Galbraith, “Evaluation of a new educational workplace-based program for provisionally registered pharmacists in Australia,” *Currents in Pharmacy Teaching and Learning*, vol. 12, no. 12, pp. 1410–1416, 2020.
 - [24] S. A. Gernant, “Optimizing the role of pharmacy technicians in patient care settings: Nationally recognized, standardized training for technicians in pharmacist-delivered cognitive services,” *Journal of the American Pharmacists Association*, vol. 58, no. 1, pp. 9–11, 2018.

Research Article

Safety and Efficacy of Single Condylar Knee Prosthesis When Treating Knee Single Compartment Osteoarthritis: A Prospective, Case-Randomized Controlled Study

Shaofeng Wang,¹ Yang Wang,² and Jiong Wang³ 

¹Department of Orthopedics, Jinshan Tinglin Hospital, Shanghai 201505, China

²Department of Orthopedics, Seventh Medical Center of PLA General Hospital, Beijing 100700, China

³Department of Orthopedics, Caidian District People's Hospital, Wuhan 430100, Hubei Province, China

Correspondence should be addressed to Jiong Wang; 2016150208@jou.edu.cn

Received 23 May 2022; Revised 10 June 2022; Accepted 28 June 2022; Published 30 July 2022

Academic Editor: Dong Chen

Copyright © 2022 Shaofeng Wang et al. This is an open access article distributed under the Creative Commons Attribution License, which permits unrestricted use, distribution, and reproduction in any medium, provided the original work is properly cited.

Objective. The aim of this study is to explore the safety and efficacy of single condylar knee prosthesis when treating knee single compartment osteoarthritis by measuring the decrease of hemoglobin, total postoperative blood loss, maximum reduction of HCT, and knee joint activity. **Methods.** A total of 80 patients with knee joint single compartment osteoarthritis treated in our hospital from January 2020 to December 2021 were studied. They were randomly assigned to a study group ($n = 40$) and a control group ($n = 40$). The study group was treated with total knee prosthesis, while the control group was treated with simple knee prosthesis. The decrease rate of hemoglobin, the amount of bleeding, and the maximum decrease of hematocrit were compared after treatment. The range of motion of knee joint was evaluated by the Fugl-Meyer motor function scale (FM-B) and Berg balance scale (BBS). **Results.** The decrease of hemoglobin in the study group at 24 hours, 36 hours, and 48 hours after treatment was remarkably lower ($P < 0.05$). The total blood loss and the maximum reduction of hematocrit (HCT) in the study group were lower ($P < 0.05$). The range of motion (ROM) of the knee joint in the study group at 6 and 12 months after treatment was remarkably higher than that before treatment and remarkably higher compared to the control group ($P < 0.05$). The FM-B scale and BBS scale of the studied cohort at 6 and 12 months after treatment were remarkably higher than those before treatment and were remarkably higher compared to the control's ($P < 0.05$). **Conclusion.** The unicondylar knee prosthesis is safer and more effective in the treatment of noncompartmental osteoarthritis of the knee, facilitating less trauma and perioperative blood loss and enhancing the patient's motion and balance.

1. Introduction

Knee joint single compartment osteoarthritis (single-compartment osteoarthritis of the knee joint) is an obvious bone and joint disease [1]. The disease shows chronic progression and the pathology is dominated by noninflammatory changes, such as articular cartilage degeneration and secondary hyper osteogeny. The disease mostly occurs in the middle-aged and elderly accompanied with the increasing age of prevalence rate, and the incidence rate in female is higher than that in male [2, 3]. The main clinical symptoms are joint pain, stiffness, swelling, and limitation of

movement, which bring great pain and inconvenience to the patients' life and work.

Anatomically, the knee joint can be assigned into three compartments, including medial compartment, lateral compartment, and patellofemoral compartment. Knee arthritis can affect any of these compartments and damage to any compartment can lead to loss of knee joint function [4]. Clinically, the early pathological changes in patients with 1/3 were limited to one compartment, in which the medial compartment was more common, and the lateral inter-compartment and patellofemoral compartment were rarely involved [5, 6]. The early stage of knee osteoarthritis is

mainly a mild dull pain in the part of the knee, which is often aggravated after activity and proper rest may be relieved. However, as the disease progresses, the symptoms will become more and more serious [7–9].

At present, orthopedic clinic has a variety of step-by-step treatment for knee osteoarthritis at different stages of development [10]. The surgical methods for the treatment of single compartment osteoarthritis include total knee arthroplasty and single condylar replacement. Total knee arthroplasty as a clinical near-perfect treatment for advanced knee osteoarthritis, its long-term postoperative survival rate and excellent and good rate have basically been recognized by most scholars [11, 12]. However, because the human knee joint is unique in its own structure and lower limb force line, there are not a few knees osteoarthritis manifested by unilateral compartment in clinic, mainly the medial knee compartment as the mainstream. It accounts for about half of all patients with knee osteoarthritis. However, at present, for some patients with medial compartment, whether it is suitable for direct total knee arthroplasty, there are still objections at home and abroad [13–15]. For this reason, as early as the late 1960s, some scholars had proposed a surgical treatment for single compartment osteoarthritis of the knee joint, which was called single condylar replacement [16]. Single condylar knee prosthesis replacement preserves the relatively healthy knee compartment of the patient through the compartment replacement of the knee joint lesion of the patient. After more than half a century of development, a surgical technique has been gradually improved and perfected. Compared with total knee arthroplasty, it has the advantages of small incision, nonvalgus patella, preservation of quadriceps femoris, no interference with suprapatellar bursa and extension device, less trauma, and early weight bearing after operation. This operation retains as much normal bone and soft tissue as possible, causing less surgical trauma to patients, and the time of the operation is relatively shorter. It has even become the last surgical treatment for some patients with knee osteoarthritis. Therefore, a prospective, case-randomized controlled study was conducted to study the safety and efficacy of unicompartment knee prosthesis when treating knee single compartment osteoarthritis.

2. Patients and Methods

2.1. General Information. Eighty patients (80 knees) with knee joint single compartment osteoarthritis who were cured from January 2020 to December 2021 were enrolled in our hospital as the subjects of the study. The 80 patients were arbitrarily assigned into studied and controlled groups. There were 40 cases (40 knees) in the study group and 40 cases (40 knees) in the control group. 20 males and 20 females were in the research cohort, who aged from 48 to 64 years old (mean age 55.36 ± 4.22). There were 21 cases of right knee and 19 cases of left knee. 21 males and 19 females were in the controlled cohort, who aged from 48 to 65 years old (mean 53.42 ± 4.17). The lesions were located in the right knee in 21 cases and the left knee in 19 cases. There exhibited no significant difference in sex, age, and course of disease.

The inclusion criteria of this study are as follows:

- (1) The anterior and posterior cruciate ligaments and the medial and lateral collateral ligaments were normal.
- (2) The symptoms of pain or tenderness in the medial compartment of the knee joint are obvious, but there were no obvious symptoms in other compartments.
- (3) Weight-bearing standing knee X-ray showed that the medial compartment had osteoarthritis manifestations of grade III–IV by Kellgren–Lawrence (K–L) classification, and other compartments were normal or had no imaging manifestations of grade III or above.
- (4) There was no varus and valgus deformity of knee joint or varus $\leq 15^\circ$. The deformity could be corrected by manipulation.
- (5) Flexion deformity $< 15^\circ$, ROM $\geq 90^\circ$.

The exclusion criteria of this study are as follows:

- (1) Patients with abnormal blood coagulation found by laboratory examination.
- (2) The patient had recently or is currently using some kind of an anticoagulant.
- (3) Patients with ischemic heart disease or chronic cardiac insufficiency, atrial fibrillation, and stent implantation.
- (4) Patients with previous history of thrombosis and cerebral infarction.
- (5) Patients with active infection.
- (6) Patients with severe cardiac and pulmonary insufficiency; patients with liver insufficiency (pay special attention to patients with low albumin), patients with renal insufficiency.
- (7) Patients with hemoglobin < 90 g/L or with other hematological disorders.
- (8) Unable to complete the research for various reasons.

2.2. Treatment Methods

2.2.1. Technical Route. The technology roadmap is as indicated in Figure 1.

2.2.2. Treatment Scheme. After a clear diagnosis was made, the patient and his or her family agreed to or requested artificial joint replacement treatment. The patients needed to complete the necessary perioperative tests to exclude inappropriate factors. The patients then underwent elective surgery.

The operation plan of the control group: total knee joint surface prosthesis replacement: after anesthesia was effective, a supine position was taken, catheterization was normal, routine disinfection area, sterile sheet, and a protective film was routinely applied in the operation area. The thighs were preset with an inflatable tourniquet. A straight anterior incision of the knee was taken, about 10–12 cm, bended the knee and valgus the patella. During the operation, it was common to see the injury of the cartilage surface of femur, tibia, and patella, the formation of peripheral osteophyte,

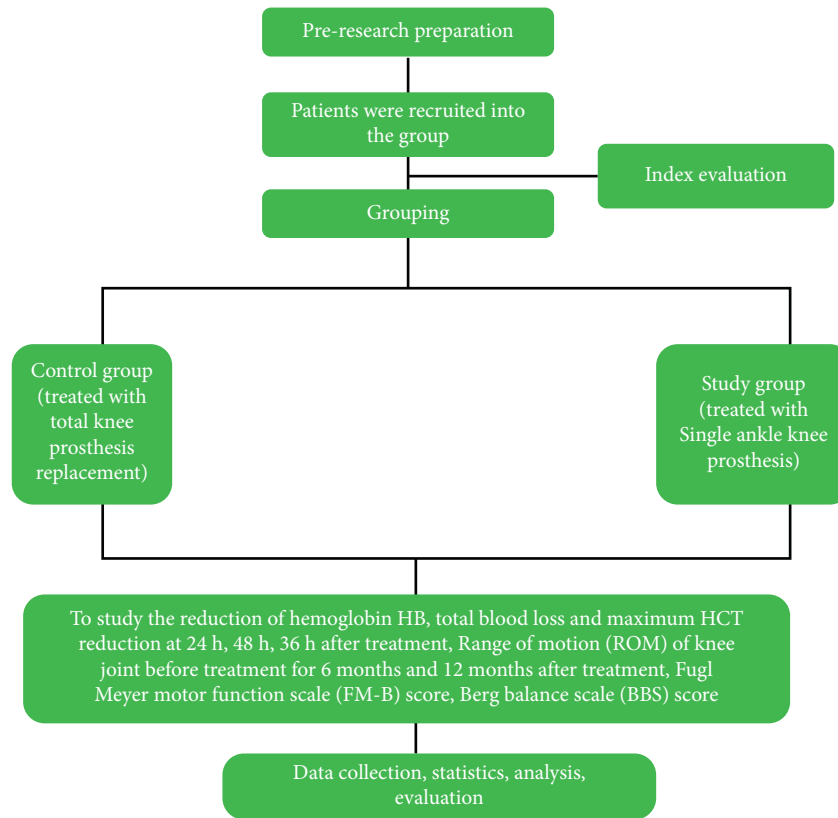


FIGURE 1: Technology roadmap.

synovial hyperemia, hyperplasia and hypertrophy, removal of hyperplastic synovium, residual meniscus and anterior and posterior cruciate ligament, and removal of osteophyte and loose body. According to the biological force line of the lower limb, the tibial plateau, anterior and posterior condyle of femur, distal end, oblique plane, and groove were cut to repair the articular surface of patella. After patella shaping, the corresponding test model, flexion, and extension joint, joint stability, ROM, force line, and patellar trajectory were all satisfactory. Then, the joint prosthesis was gradually implanted into the knee joint with bone cement. Burn gauze pressure bandaging, no drainage tube after the operation, total knee joint surface prosthesis replacement side prosthesis-enrolled Zimmer NexGen knee joint prosthesis, the operation was performed by the same group of surgeons.

Operation plan of the research group: After the effect of anesthesia, the patients were taken in a supine position, normal indwelling catheterization, routine disinfection area, aseptic sheet, upper limb driving belt and tourniquet, and a protective film was routinely applied in the operation area. A 10 cm incision was made longitudinally on the medial line of the patella of the affected knee. The skin, subcutaneous tissue, and fascia were cut layer by layer and the joint capsule was cut in the medial side of the patella. The osteophyte at the edge of the femoral condyle and tibial plateau were removed, and the soft tissue appropriately was released. If necessary, it was checked whether there were lesions on the cartilage surface of the patella, the articular surface of the lateral compartment

cartilage and whether the cruciate ligament was normal. Finally, the surgical indications were confirmed. The external positioning rod of tibial bone marrow was installed to locate the osteotomy. The positioning rod in the femoral bone marrow was inserted to determine the location of osteotomy and then osteotomy. The tibial plateau prosthesis was installed, and the knee joint was flexed and extended to test the stability of the knee joint and the tension of the surrounding soft tissue. The femoral prosthesis was installed to test the model, fully flexion, and extend the knee joint to ensure that the movement of the patella would not be hindered during flexion and extension. The bone surface was rinsed, the bone cement was mixed, the tibia prosthesis and femur prosthesis were placed in turn, the excess bone cement was scraped off, the bone cement was pressed to harden completely, and the knee joint was kept to the neutral position during the period. Bite forceps to repair the osteophyte around the patella. The placement of high polyethylene gasket, full flexion, and extension of the knee joint can carry out a sufficient range of activities. Patellar movement trajectory was normal without hindrance. The drainage tube was retained, the drainage device was connected, and the incision was sutured layer by layer. OxfordPhase3 knee prosthesis made by Biomet Company was enrolled for unicondylar knee prosthesis replacement and all the operations were performed by the same group of surgeons.

The blood routine, ion routine, ESR and C-reactive protein, and the positive and lateral position of knee joint

X-ray were examined after operation. The drainage tube was removed when the drainage volume was less than 100 ml within 48 hours. The antibiotics were used to prevent infection if necessary. Subcutaneous injection of enoxaparin sodium (4000iu, once a day) was given on the first day after operation and rivaban (10 mg, once a day) was taken orally from the second day to 5 weeks after operation.

Active quadriceps contraction exercises, ankle flexion and extension exercises, and straight leg raising exercises were carried out on the first day after operation. Knee flexion and extension exercises and walker-assisted weight-bearing walking were carried out on the second day after operation and gradually increased the range of flexion and extension of the knee joint and full weight-bearing walking according to the situation. On the first day after operation, 5 kg weights (rice bags or salt bags) were placed on the knee joint after operation and straightening exercises were carried out until the knee joint could straighten itself. The dressing was changed regularly and the healing of the incision was observed. The patients with good incision healing, no fever, no infection, knee joint reached 0° extension position 90° flexion position can be discharged, patients were advised to continue functional exercise, anticoagulant therapy, and timely reexamination.

2.3. Observation Index

- (1) The decrease of hemoglobin at 24 hours, 36 hours, and 48 hours after treatment.
- (2) The total postoperative blood loss and the maximum reduction of hematocrit (HCT).
- (3) The ROM of knee joint was studied before treatment, 6 months after treatment, and 12 months after treatment.
- (4) The scores of Fugl-Meyer motor function scale (FM-B) were studied before treatment, 6 months after treatment, and 12 months after treatment. In the FM-B scale, there were seven items: unsupported sitting position, healthy side spreading reaction, affected side spreading reaction, standing under support, standing without support, standing on healthy side, and standing on affected side [17]. The score of 0–2 for each item was scored according to three levels and a score of 0 to 14 indicated that the balance function was impaired. The lower the score, the more serious the balance dysfunction.
- (5) The scores of the Berg balance scale (BBS) were studied before treatment, 6 months after treatment, and 12 months after treatment. The score of BBS scale ranged from 0 to 56 and the higher the score, the stronger the balance ability [18]. From 0 to 20, the balance function was poor, the patient needs to ride in a wheelchair; 21–40 indicated a certain balance ability, the patient can walk with assistance; 41–56 indicated the balance function was better, the patient can walk independently. A score of less than 40 indicated the risk of falling.

2.4. Statistical Analysis. The research data were statistically analyzed by SPSS24.0 software, and the data of normal distribution were expressed by mean \pm standard deviation and accepted independent sample *t* test. The counting data were tested by chi-square test and the grade data were tested by the Fisher exact method.

3. Results

3.1. The Decrease of Hemoglobin at 24 Hours, 36 hours, and 48 hours after Treatment. As indicated in Table 1, the decrease of hemoglobin in the study group at 24 hours, 36 hours, and 48 hours after treatment was lower compared to that of the control group ($P < 0.05$, Table 1).

3.2. The Total Blood Loss and Maximum Reduction of HCT after Operation. As indicated in Table 2, the total postoperative blood loss and the maximum reduction of HCT in the study group were remarkably lower ($P < 0.05$).

3.3. The ROM of Knee Joint Was Studied before Treatment, 6 months after Treatment, and 12 months after Treatment. As indicated in Table 3, ROM of the knee joint at 6 and 12 months after treatment in the study group was remarkably higher than that before treatment and remarkably higher compared to that of the control group ($P < 0.05$).

3.4. The Score of FM-B Scale before Treatment, 6 months after Treatment, and 12 months after Treatment. The FM-B scale scores of the study group after 6 months and 12 months of treatment were remarkably increased compared with those before treatment and were remarkably higher compared to those of the control group ($P < 0.05$, Table 4).

3.5. The Score of BBS Scale before Treatment, 6 months after Treatment, and 12 months after Treatment. After 6 months of treatment, the BBS scale scores of the study group after 12 months of treatment were remarkably increased compared with those before treatment and higher compared to the control group ($P < 0.05$, Table 5).

4. Discussion

Knee single compartment osteoarthritis is a chronic degenerative joint lesion [19]. At present, the number of patients with knee osteoarthritis in single compartment is increasing year by year and the incidence rate is high. According to statistics, the prevalence rate of people over 60 years old is 49%. The prevalence rate of people over 75 years old is as high as 80% [20]. Currently, the incidence of knee single compartment osteoarthritis is increasing year by year, which may become the fourth largest factor leading to disability by 2020 [21].

For patients with knee osteoarthritis, there are not many clinical methods that can be taken, mainly to reduce the weight-bearing and activity of the joint to delay the progress of the disease [22]. Early use of nonresidual drugs to control

TABLE 1: The decrease of hemoglobin at 24 h, 36 h, and 48 h after treatment.

Grouping	After treatment 24 h (g/L)	After treatment 36 h (g/L)	After treatment 48 h (g/L)
Control group ($n = 40$)	13.54 ± 2.19	24.82 ± 3.11	36.99 ± 4.08
Study group ($n = 40$)	8.35 ± 1.12	15.69 ± 2.23	19.24 ± 3.02
χ^2 value	13.344	15.088	22.116
P value	<0.05	<0.05	<0.05

TABLE 2: The total blood loss and the maximum reduction of HCT after operation.

Grouping	Total postoperative blood loss (ml)	Maximum HCT reduction (%)
Control group ($n = 40$)	381.54 ± 105.19	0.05 ± 0.02
Study group ($n = 40$)	191.38 ± 75.12	0.03 ± 0.01
t value	9.304	5.567
P value	<0.05	<0.05

TABLE 3: The ROM of knee joint before treatment, 6 months after treatment, and 12 months after treatment.

ROM of the knee joint	Before treatment	Treatment for 6 months	Treatment for 12 months
Control group ($n = 40$)	105.82 ± 12.11	$109.12 \pm 9.39^*$	$113.19 \pm 8.25^*$
Study group ($n = 40$)	$105.69 \pm 12.03^*$	$118.14 \pm 11.44^*$	$126.23 \pm 8.35^*$
t value	0.048	3.855	7.026
P value	0.962	<0.05	<0.05

*represents that the 6-month and 12-month treatment in this group were compared with those before treatment, $P < 0.05$.

TABLE 4: The scores of FM-B before treatment, 6 months after treatment, and 12 months after treatment.

FM-B scale score (points)	Before treatment	Treatment for 6 months	Treatment for 12 months
Control group ($n = 40$)	7.52 ± 1.12	$9.24 \pm 0.22^*$	$11.29 \pm 0.64^*$
Study group ($n = 40$)	7.49 ± 1.09	$11.08 \pm 0.13^*$	$13.71 \pm 0.15^*$
t value	0.121	45.539	23.284
P value	0.904	<0.05	<0.05

*represents that the 6-month and 12-month treatment in this group were compared with those before treatment, $P < 0.05$.

TABLE 5: The scores of BBS before treatment, 6 months after treatment, and 12 months after treatment.

BBS scale score (points)	Before treatment	Treatment for 6 months	Treatment for 12 months
Control group ($n = 40$)	30.23 ± 2.37	$42.09 \pm 2.47^*$	$46.59 \pm 2.32^*$
Study group ($n = 40$)	30.18 ± 2.42	$49.25 \pm 1.01^*$	$53.36 \pm 1.14^*$
t value	0.093	16.969	16.564
P value	0.926	<0.05	<0.05

or alleviate the symptoms of patients, oral drugs involved in cartilage metabolism to prevent the progression of the disease. In clinical practice, it is considered that total knee prosthesis replacement and single condylar knee prosthesis replacement are effective methods for the treatment of single compartment osteoarthritis. The clinical application of total knee prosthesis replacement is long. The prosthesis design and operation technology are perfect, it can effectively relieve pain, restore function, and the survival rate of prosthesis is high. However, the pain-sensitive areas of some patients' knee joint are located on the medial side and the imaging findings are only unilateral compartment lesions of the knee joint. Therefore, with the continuous progress of artificial joint materials, design and surgical techniques, condylar knee prosthesis replacement has been applied to a certain extent when treating patients with knee osteoarthritis. Single ankle replacement for knee joint single compartment osteoarthritis

has been favored by the majority of knee surgeons because of its obvious advantages and characteristics, such as less surgical trauma, short operation time and hospital stay, low hospitalization cost, satisfactory short-term effect, and so on. Riddle et al. reported that the number of American condylar knee prosthesis replacement increased by an average of 32.5% per year from 1998 to 2005 [23]. More and more researchers have believed that condylar knee arthroplasty can relieve pain and improve the quality of life of patients with osteoarthritis in single compartment, especially in medial compartment [24–32]. Therefore, a prospective, case-randomized controlled study was conducted to study the safety and efficacy of unicompartmental knee prosthesis when treating knee single compartment osteoarthritis.

The results showed that the decrease of hemoglobin HB in the study group at 24 hours, 36 hours, and 48 hours after treatment was lower compared to that of the control group.

The total blood loss and the maximum reduction of HCT in the study group were lower. The ROM of the knee joint in the study group at 6 and 12 months after treatment was remarkably higher than that before treatment and remarkably higher compared to the control group. The scores of FM-B scale and BBS scale in the study group at 6 and 12 months after treatment were remarkably higher than those before treatment and were remarkably higher compared to the control group. This study has shown that single condylar knee prosthesis is more safe and more effective when treating knee single compartment osteoarthritis. Additionally, it is more beneficial to reduce trauma, reduce perioperative blood loss, and improve the exercise and balance ability of patients.

Compared with total knee prosthesis replacement, single condylar knee prosthesis replacement has unique advantages: The main results are that the conventional choice of single condylar knee replacement is to use the lower limb fixator to suspend the lower limbs of the replacement side to facilitate the gap measurement. The release and balance of soft tissues is not emphasized, so there is no need to release the collateral ligament. The whole joint is more stable, the movement function is better, it is more conducive to the recovery of motor function and improve the balance ability of the limb. Second, the proprioceptive sensation of the joint can be close to normal to the maximum extent. Then, only a small amount of osteotomy is performed in the lesion compartment and sufficient bone mass is retained for possible secondary revision surgery. The effect of revision is similar to that of the primary total knee prosthesis replacement [33]. Lastly, functional exercises should be carried out earlier because of small incision, less bleeding, and less postoperative complications. 30 patients (32 knees) were followed up for an average of 53 months, of which 21 patients had polyethylene wear and only 2 patients needed revision surgery, and the thickness of polyethylene exceeded that of 10 mm [34]. Berger et al. followed up 51 patients (62 knees) with single condylar replacement with bone cement type of knee joint [35]. Taking revision or imaging prosthesis loosening as the standard, the 10-year survival rate was 98% and the 13-year survival rate was 95.7%. Swienckowski et al. reported 41 patients (46 knees) with single condylar replacement of knee joint, whose 11-year survival rate was 92% [36]. Hopper GP et al. have indicated that patients undergoing unicompartmental knee prosthesis replacement have a higher quality of life than patients with total knee prosthesis replacement, specifically in 96.7% of patients who can participate in sports activities, while only 63.3% of patients with total knee prosthesis replacement [37]. In 1988, Mac Kinnon et al. reported that the 57-month survival rate of knee unicompartmental replacement was about 95% [38]. In 1998, Murray et al. reported that the 10-year survival rate after knee joint unicompartmental replacement was about 98% [39]. In 2004, Naudie et al. reported that the 5-year and 10-year survival rates after unicompartmental knee replacement were 94% and 90%, respectively [40]. Romanowski et al. performed 13 cases of single condylar replacement with small incision, and the survival rate of 8-year follow-up was 93% [41]. Argenson et al. basically agree with these views through research and

they believe that computer-aided systems will also increase the accuracy of surgery in the future [42]. Therefore, it can be considered that unicompartmental knee prosthesis replacement has the advantages of high efficacy and safety when treating knee single compartment osteoarthritis. There are some limitations in this study. First, the sample size of this study is not large and it is a single-center study, so bias is inevitable. In future research, we will carry out multicenter, large-sample prospective studies, or more valuable conclusions can be drawn.

To sum up, the unicompartmental knee prosthesis is safer and more effective in the treatment of noncompartmental osteoarthritis of the knee, facilitating less trauma and perioperative blood loss and enhancing the patient's motion and balance.

Data Availability

The datasets used and analyzed during the current study are available from the corresponding author upon reasonable request.

Conflicts of Interest

The authors declare that they have no conflicts of interest.

References

- [1] G. Fan and G. Tang, "Comparative analysis of single condylar and total knee arthroplasty when treating single compartment osteoarthritis of knee joint," *Medical frontier*, vol. 11, no. 16, pp. 38-39, 2021.
- [2] F. Jian, J. Ban, and J. Gao, "Clinical effect of single condylar replacement when treating knee joint unicompartment osteoarthritis," *Zhejiang Trauma surgery*, vol. 26, no. 3, pp. 535-536, 2021.
- [3] J. C. Stoddart, O. Dandridge, A. Garner, and C. J. van Arkel, "The compartmental distribution of knee osteoarthritis-a systematic review and meta-analysis," *Osteoarthritis Cartilage*, vol. 29, no. 4, pp. 445-455, 2021.
- [4] H. Ansari, J. Pandit, and T. Takahashi, "Kinematically aligned total knee arthroplasty or mechanically aligned total knee arthroplasty," *Journal of Knee Surgery*, vol. 31, no. 10, pp. 999-1006, 2018 Nov.
- [5] Y. Hou, W. Xun, and S. Song, "Clinical effect of single condylar replacement and high tibial osteotomy with Tomofix internal fixation when treating single compartment knee osteoarthritis," *Chinese Journal of Experimental surgery*, vol. 37, no. 3, pp. 568-570, 2020.
- [6] J. M. Jennings, L. T. Kleeman-Forsthuber, and M. P. Bolognesi, "Medial unicompartmental arthroplasty of the knee," *Journal of the American Academy of Orthopaedic Surgeons*, vol. 27, no. 5, pp. 166-176, 2019 Mar 1.
- [7] Li. Cheng, J. Zhang, and Li. Qiang, "Comparison of total knee arthroplasty and single condylar arthroplasty when treating knee single compartment osteoarthritis," *Chinese Journal of Anatomy and Clinic*, vol. 22, no. 2, pp. 121-126, 2017.
- [8] S. Oussedik, M. P. Abdel, J. Victor, M. W. Pagnano, and F. S. Haddad, "Alignment in total knee arthroplasty," *The Bone & Joint Journal*, vol. 102-B, no. 3, pp. 276-279, 2020 Mar.
- [9] G. Xi, H. H. Wang, and H. Li, "Short-term outcomes of Oxford unicompartmental knee arthroplasty with coronal

- subluxation of the knee: a retrospective case-control study," *Journal of Orthopaedics and Traumatology*, vol. 23, no. 1, pp. 1–9, 2022.
- [10] Bo. Huang, "Clinical observation of single compartment knee arthroplasty when treating medial single compartment osteoarthritis of knee joint in the elderly [J]," *Chinese practical medicine*, vol. 16, no. 13, pp. 137–139, 2021.
 - [11] K. Kizaki, A. Shanmugaraj, F. Yamashita et al., "Total knee arthroplasty using patient-specific instrumentation for osteoarthritis of the knee: a meta-analysis," *BMC Musculoskeletal Disorders*, vol. 20, no. 1, p. 561, 2019 Nov 23.
 - [12] M. Deng, Y. Hu, Z. Zhang, H. Zhang, Y. Qu, and G. Shao, "Unicondylar knee replacement versus total knee replacement for the treatment of medial knee osteoarthritis: a systematic review and meta-analysis," *Archives of Orthopaedic and Trauma Surgery*, vol. 141, no. 8, pp. 1361–1372, 2021 Aug.
 - [13] E. Castiello and S. Affatato, "Progression of osteoarthritis and reoperation in unicompartmental knee arthroplasty: a comparison of national joint registries," *The International Journal of Artificial Organs*, vol. 43, no. 3, pp. 203–207, 2020 Mar.
 - [14] S. Toyoda, T. Kaneko, T. Igarashi, K. Takada, and S. Yoshizawa, "Higher patellofemoral compressive force does not affect anterior knee pain in anatomical bi-cruciate retaining total knee arthroplasty: in vivo prospective analysis of guided motion prosthesis," *Clinical Biomechanics*, vol. 88, p. 105444, 2021 Aug.
 - [15] S. Witjes, A. Hoorntje, K. L. M. Koenraadt, G. M. M. J. Kerkhoffs, and R. C. I. van Geenen, "Higher function scores and satisfaction in patients with anteromedial osteoarthritis compared with other wear patterns of the knee: 2 Years after both total and unicondylar knee arthroplasties," *Journal of Knee Surgery*, vol. 33, no. 07, pp. 629–635, 2020 Jul.
 - [16] F. Huang, D. Wu, J. Chang et al., "A comparison of mobile- and fixed-bearing unicompartmental knee arthroplasties in the treatment of medial knee osteoarthritis: a systematic review and meta-analysis of 1,861 patients," *Journal of Knee Surgery*, vol. 34, no. 04, pp. 434–443, 2021 Mar.
 - [17] C. J. Lesley, K. Gert, and J. B. J. Bussmann, "Are the hierarchical properties of the Fugl-Meyer assessment scale the same in acute stroke and chronic stroke?" *Physical therapy*, vol. 94, no. 7, pp. 977–986, 2018.
 - [18] G. Beckers, D. Mazy, P. Tollet, and O. Van Nieuwenhove, "Knee mega-prosthesis in the management of complex knee fracture of the elderly: a case series and review of the literature," *Acta Orthopaedica Belgica*, vol. 87, no. 2, pp. 347–351, 2021 Jun.
 - [19] N. Walter, J. Weber, M. Kerschbaum et al., "Revision arthroplasty after unicompartmental knee arthroplasty," *Journal of Orthopaedic Surgery and Research*, vol. 16, no. 1, p. 666, 2021 Nov 12.
 - [20] S. Romagnoli, J. A. Vitale, and M. Marullo, "Outcomes of lateral unicompartmental knee arthroplasty in post-traumatic osteoarthritis, a retrospective comparative study," *International Orthopaedics*, vol. 44, no. 11, pp. 2321–2328, 2020 Nov.
 - [21] T. Y. Voravitvet, C. Chen, C. Y. Lin, and M. H. Cheng, "Lymphedema microsurgery reduces the rate of implant removal for patients who have pre-existing lymphedema and total knee arthroplasty for knee osteoarthritis," *Journal of Surgical Oncology*, vol. 121, no. 1, pp. 57–66, 2020 Jan.
 - [22] J. Beckmann, M. K. Meier, C. Benignus, A. Hecker, and E. Thienpont, "Contemporary knee arthroplasty: one fits all or time for diversity?" *Archives of Orthopaedic and Trauma Surgery*, vol. 141, no. 12, pp. 2185–2194, 2021 Dec.
 - [23] W. Shi, Y. Jiang, X. Zhao, H. Zhang, Y. Wang, and T. Li, "The influence of posterior tibial slope on the mid-term clinical effect of medial-pivot knee prosthesis," *Journal of Orthopaedic Surgery and Research*, vol. 16, no. 1, p. 563, 2021 Sep 15.
 - [24] F. Bernard de Villeneuve, C. Jacquet, S. Puech, S. Parratte, M. Ollivier, and J. N. Argenson, "Minimum five years follow-up of total knee arthroplasty using morphometric implants in patients with osteoarthritis," *The Journal of Arthroplasty*, vol. 36, no. 7, pp. 2502–2509, 2021 Jul.
 - [25] R. S. Aujla and C. N. Esler, "Total knee arthroplasty for osteoarthritis in patients less than fifty-five years of age: a systematic review," *The Journal of Arthroplasty*, vol. 32, no. 8, pp. 2598–2603, 2017 Aug.
 - [26] W. J. Wang, M. H. Sun, J. Palmer et al., "Patterns of compartment involvement in end-stage knee osteoarthritis in a Chinese orthopedic center: implications for implant choice," *Orthopaedic Surgery*, vol. 10, no. 3, pp. 227–234, 2018 Aug.
 - [27] X. Sun, X. Gao, X. Sun, and Z. Su, "Comparison of clinical and radiographic results between total knee arthroplasties using medial pivot and posterior-stabilized prosthesis," *Medicine (Baltimore)*, vol. 100, no. 4, p. e23809, 2021 Jan 29.
 - [28] P. B. White, S. Turcan, J. R. Satalich, A. S. Ranawat, and C. S. Ranawat, "Clinical outcomes of a modern total knee arthroplasty prosthesis compared to its predecessor at 5-year follow-up: matched pair analysis," *The Journal of Arthroplasty*, vol. 35, no. 11, pp. 3150–3155, 2020 Nov.
 - [29] R. Redelbach, A. Mahnke, and J. O. Anders, "Digital measurement of individual motor and proprioceptive skills in patients with osteoarthritis of the knee prior to total knee replacement," *Zeitschrift für Orthopädie und Unfallchirurgie*, vol. 159, no. 05, pp. 513–520, 2021 Oct.
 - [30] W. Shi, Y. Jiang, C. Wang, H. Zhang, Y. Wang, and T. Li, "Comparative study on mid- and long-term clinical effects of medial pivot prosthesis and posterior-stabilized prosthesis after total knee arthroplasty," *Journal of Orthopaedic Surgery and Research*, vol. 15, no. 1, p. 421, 2020 Sep 17.
 - [31] J. B. Seeger, J. P. Schickschneit, C. Schuld et al., "Instrumented gait analysis in patients with medial osteoarthritis of the knee after mobile-bearing unicompartmental knee arthroplasty," *The Knee*, vol. 25, no. 3, pp. 392–397, 2018 Jun.
 - [32] A. Nakajima, M. Yamada, M. Sonobe et al., "Three-year clinical and radiological results of a cruciate-retaining type of the knee prosthesis with anatomical geometry developed in Japan," *BMC Musculoskeletal Disorders*, vol. 22, no. 1, p. 241, 2021 Mar 3.
 - [33] J. Soong, Y. Ou Yang, Z. M. Ling, S. L. Chia, N. N. Lo, and S. J. Yeo, "Cruciate retaining and posterior stabilized total knee arthroplasty in severe varus osteoarthritis knee: a match-pair comparative study in an Asian population," *Journal of Orthopaedic Surgery*, vol. 29, no. 3, Article ID 230949902110552, 2021 Sep-Dec.
 - [34] Y. Tu, T. Ma, T. Wen, T. Yang, L. Xue, and H. Xue, "Does unicompartmental knee replacement offer improved clinical advantages over total knee replacement in the treatment of isolated lateral osteoarthritis? A matched cohort analysis from an independent center," *The Journal of Arthroplasty*, vol. 35, no. 8, pp. 2016–2021, 2020 Aug.
 - [35] Y. H. Kim, J. W. Park, and Y. S. Jang, "Long-term (up to 27 Years) prospective, randomized study of mobile-bearing and fixed-bearing total knee arthroplasties in patients <60 Years of age with osteoarthritis," *The Journal of Arthroplasty*, vol. 36, no. 4, pp. 1330–1335, 2021 Apr.
 - [36] G. Yang, X. Jiao, Q. Li et al., "Hybrid Oxford uni-compartmental knee arthroplasty has lower residual cement

- extrusion than cemented arthroplasty in treating end-stage unicompartmental knee osteoarthritis,” *BMC Musculoskeletal Disorders*, vol. 22, no. 1, p. 833, 2021.
- [37] S. Toyoda, T. Kaneko, Y. Mochizuki et al., “Minimally invasive surgery total knee arthroplasty is less popular, but the prosthesis designed specifically for MIS provides good survival and PROMs with a minimum follow-up of 10 years,” *Journal of Orthopaedic Surgery and Research*, vol. 16, no. 1, p. 95, 2021 Jan 29.
 - [38] N. G. Patel, R. J. Napier, J. R. A. Phillips, and A. D. Toms, “The first knee prosthesis to go through beyond compliance: a new standard for the safe introduction of orthopaedic implants,” *The Surgeon*, vol. 18, no. 6, pp. e27–e32, 2020.
 - [39] D. A. Crawford, K. R. Berend, and E. Thienpont, “Unicompartmental knee arthroplasty,” *Orthopedic Clinics of North America*, vol. 51, no. 2, pp. 147–159, 2020 Apr.
 - [40] J. Itou, U. Kuwashima, M. Itoh, and K. Okazaki, “Anterior prominence of the femoral condyle varies among prosthesis designs and surgical techniques in total knee arthroplasty,” *BMC Musculoskeletal Disorders*, vol. 22, no. 1, p. 784, 2021 Sep 12.
 - [41] R. D’Ambrosi, A. Nuara, I. Mariani, F. Di Feo, N. Ursino, and M. Hirschmann, “Titanium niobium nitride mobile-bearing unicompartmental knee arthroplasty results in good to excellent clinical and radiographic outcomes in metal allergy patients with medial knee osteoarthritis,” *The Journal of Arthroplasty*, vol. 36, no. 1, pp. 140–147, 2021 Jan.
 - [42] M. G. J. Gademán, L. N. Van Steenberghe, S. C. Cannegieter, R. G. H. H. Nelissen, and P. J. Marang-Van De Mheen, “Population-based 10-year cumulative revision risks after hip and knee arthroplasty for osteoarthritis to inform patients in clinical practice: a competing risk analysis from the Dutch Arthroplasty Register,” *Acta Orthopaedica*, vol. 92, no. 3, pp. 280–284, 2021 Jun.

Research Article

The Efficacy and Safety of Mizoribine versus Mycophenolate Mofetil for the Treatment of Renal Transplantation: A Systematic Review and Meta-Analysis

Jie Chen,¹ Hua Liu,² Wenjun Yin,¹ Zhengguang Xu,¹ Zekai Chen,¹ and Wingkeung Yiu ¹

¹Urinary Surgery, The First Affiliated Hospital of Jinan University, Guangzhou, China

²Urinary Surgery, Southern Hospital of Southern Medical University, Guangzhou, China

Correspondence should be addressed to Wingkeung Yiu; 18404112@masu.edu.cn

Received 5 May 2022; Revised 22 June 2022; Accepted 25 June 2022; Published 22 July 2022

Academic Editor: Dong Chen

Copyright © 2022 Jie Chen et al. This is an open access article distributed under the Creative Commons Attribution License, which permits unrestricted use, distribution, and reproduction in any medium, provided the original work is properly cited.

Background. Mizoribine (MZR) is widely used in Asia due to its high safety and low cost, and comparative studies of its safety and efficacy with the first-line drug mycophenolate mofetil (MMF) have been carried out. This paper aimed to compare the efficacy and safety of MZR and MMF in immunosuppressive therapy of renal transplantation by meta-analysis. **Methods.** We searched randomized controlled trials (RCTs) comparing MZR versus MMF for renal transplantation in PubMed, Excerpta Medica Database (EMBASE), Cochrane Library, Web of Science, WanFang Database, China National Knowledge Infrastructure (CNKI), and Chinese Biomedical Database (CBM). Articles were assessed for their risk of bias using the Cochrane Collaboration. Forest plots and funnel plots were also performed on the included articles. **Results.** A total of twelve studies with 1103 patients were selected in the analysis. No significant difference were observed between the MZR group and the MMF group for the rate of acute rejection (RR = 1.50, 95% CI 1.11 to 2.01, $P = 0.008$), patient survival (RR = 1.01, 95% CI 0.99 to 1.03, $P = 0.56$), graft survival (RR = 1.02, 95% CI 1.00 to 1.04, $P = 0.12$), leucopenia (RR = 0.69, 95% CI 0.44 to 1.10, $P = 0.12$), and liver damage (RR = 0.72, 95% CI 0.46 to 1.13, $P = 0.15$). The MZR group was associated with a lower risk of gastrointestinal disorder (RR = 0.28, 95% CI 0.13 to 0.62, $P = 0.002$) and cytomegalovirus infection (RR = 0.59, 95% CI 0.42 to 0.84, $P = 0.003$) but had a higher risk of hyperuricemia (RR 1.79, 95% CI 1.17 to 2.75, $P = 0.007$). No significant publication bias was observed among included studies. **Discussion.** MZR is similar to MMF in efficacy, and in terms of safety, MZR has a lower risk of gastrointestinal disorder and cytomegalovirus infection but a higher risk of hyperuricemia.

1. Introduction

Renal transplantation has been widely carried out all over the world, which would be the most mature solid organ transplantation technology at present [1]. With the renewal and application of new immunosuppressive drugs, the maturity of matching technology and renal transplantation technology, the incidence of short-term rejection after transplantation has been significantly reduced, and the incidence of adverse prognostic events caused by rejection has been reduced [2, 3]. When the shortage of organs cannot be overcome at present, how to ensure the longest functional survival of available organs is one of the hot issues discussed in clinical work.

The triple immunosuppressive regimen of calcineurin inhibitors (CNIs) combined with antiproliferative drugs and hormones has been widely used to prevent and treat rejection after renal transplantation [4, 5]. The application of CNI is the basis for the success of renal transplantation, but CNIs can cause many adverse reactions, which limit their long-term application in the clinical practice of organ transplantation. The combined use of antiproliferative drugs can reduce the dosage of CNIs, then reduce its renal injury, and will not increase the incidence of rejection [6]. Antiproliferative immunosuppressants mainly include mizoribine (MZR), azathioprine (AZA), and mycophenolate mofetil (MMF). AZA is rarely used in recipients after renal transplantation because of its severe hepatotoxicity and bone

marrow suppression toxicity [7]. MMF is currently recommended as the first-line drug of antiproliferative drugs, but the application of MMF after renal transplantation is easy to cause gastrointestinal reactions such as diarrhea, abdominal pain, leucopenia, infection, and liver function damage. As a new immunosuppressant, MZR has been used in clinics. Its immunosuppressive mechanism is similar to MMF. It inhibits the *de novo* synthesis of guanosine monophosphate by competitively inhibiting hypoxanthine monophosphate nucleoside dehydrogenase and guanosine monophosphate synthase so as to inhibit the synthesis of RNA and DNA, further inhibit the proliferation and activation of *T* and *B* lymphocytes, and inhibit both cellular immunity and humoral immunity [8, 9].

In recent years, there have been some studies on the efficacy and safety of MZR compared with MMF in recipients after renal transplantation [10–12]. Some studies have shown that the effectiveness of high-dose MZR in antirejection treatment after renal transplantation is equivalent to MMF, which is even better than MMF in pulmonary infection, leucopenia, and gastrointestinal disorder. However, some literatures have reported that MZR has fewer adverse reactions as its immunosuppressive effect is weaker than MMF [13, 14]. In our paper, meta-analysis was used to analysis the literature of randomized controlled trials (RCTs) comparing MZR and MMF so as to evaluate the efficacy and safety of MZR and MMF in renal transplant recipients in order to provide evidence-based basis for clinical rational selection of immunosuppressants.

2. Methods

2.1. Literature Search Strategy. We performed a systematic search for relevant literature from the following databases up to April 2022 in PubMed, Excerpta Medica Database (EMBASE), Web of Science, Cochrane Library, WanFang Database, Chinese BioMedical Database (CBM), and China National Knowledge Infrastructure (CNKI). Search terms were constructed by using Boolean operator “AND” or “OR” of the following keywords: (1) mizoribine; (2) mycophenolate mofetil; (3) renal transplantation; and (4) kidney transplantation. No language restrictions were applied on searches. We attempted to identify additional studies by reviewing the reference lists to identify any studies that our search strategy may have missed.

2.2. Study Selection. We considered studies to be eligible for inclusion if they met the following criteria:

- (1) Population: patients after renal transplantation
- (2) Study design: randomized controlled trials (RCTs)
- (3) Intervention and control: researches comparing patients receive MZR and MMF
- (4) Outcomes: efficacy outcomes, such as acute rejection and patient survival; safety outcomes, such as leucopenia, cytomegalovirus infection, and hyperuricemia

- (5) Language: the publication was available in either English or Chinese

2.3. Data Extraction and Quality Assessment. Two authors (JChen and HLiu) collected data independently, and any different opinions between the two authors were resolved by discussions with the third author for a consensus decision. The data extracted from each article included basic information (study design, author’s name and country, publication year, duration, and time of follow-up), and patient’s demographic details (sample size, age, sex, and drug dosage). We used the Cochrane Risk of Bias Tool for methodological quality as all the included studies were RCTs.

2.4. Statistical Analysis. Meta-analysis was performed using Review Manager (version 5.4, Nordic Cochrane Centre) and STATA (version 14.0, STATA Corporation). We expressed dichotomous outcome data as risk ratios (RRs) with 95% confidence intervals (CIs) and continuous outcome data as mean differences (MDs) with 95% CIs. Heterogeneity of the data was assessed using I^2 values. If I^2 was $<50\%$, we used a fixed-effect model to pool the data; otherwise, we used a random-effect model for meta-analysis. The funnel plot and Egger’s test was conducted to assess the potential publication bias.

3. Results

3.1. Search Process. A total of 1038 potentially eligible studies were identified. Of the identified articles, 125 were duplicates and removed, 789 articles were excluded after reading the titles and abstracts. After the full-texts screening, 12 RCTs, including 1103 patients, met the inclusion criteria and were then included in this meta-analysis [15–26]. The details of our literature search and selection process are shown in Figure 1.

3.2. Characteristics of the Included Studies. The baseline characteristics of the selected studies are presented in Table 1. In total, 1103 patients were included. All 12 articles were published from 2003 to 2020, six came from China, five came from Japan, and one came from Korea. Four articles were published in Chinese and the others were in English. The time of follow-up ranged from 6 to 50 months.

3.3. Results of Quality Assessment. Overall, all the trials were deemed to be at unclear risk of allocation concealment (selection bias) and blinding of participants and personnel (performance bias), five studies were deemed to be at unclear risk of random sequence generation (selection bias), and all studies did not have high risk of bias (Figure 2(a)). A summary of all kind of bias in each study is shown in Figure 2(b).

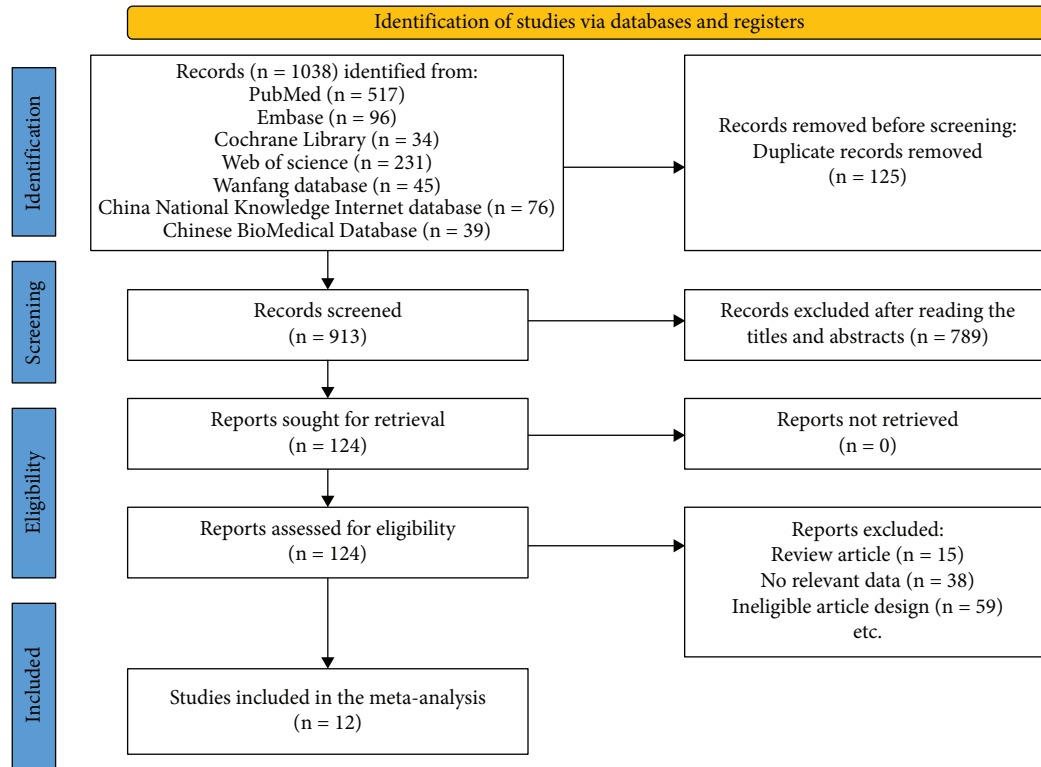


FIGURE 1: Flowchart of the literature search and study selection.

3.4. Meta-Analysis of Efficacy Outcomes

3.4.1. Acute Rejection. Ten studies comprising 983 patients provided information regarding acute rejection. The MZR group demonstrated significantly lower rate of acute rejection (RR = 1.50, 95% CI 1.11 to 2.01, $P = 0.008$, $I^2 = 0\%$, fixed-effect model) compared with the MMF group (Figure 3).

3.4.2. Patient Survival. Patient survival was reported in nine studies involving 743 patients. Pooled results failed to show statistically significant differences for patient survival between the MZR and MFF group (RR = 1.01, 95% CI 0.99 to 1.03, $P = 0.56$, $I^2 = 0\%$, fixed-effect model) (Figure 4).

3.4.3. Graft Survival. In the evaluation of difference of graft survival between the MZR group and MMF group, ten articles involved 804 patients were included. Similarly, no statistical significance of graft survival incidence was found between the two groups (RR = 1.02, 95% CI 1.00 to 1.04, $P = 0.12$, $I^2 = 0\%$, fixed-effect model) (Figure 5).

3.5. Meta-Analysis of Safety Outcomes

3.5.1. Leukopenia. A total of 762 patients enrolled in nine studies were compared on the frequency of leukopenia. There was no significant difference in the incidence of leukopenia for those patients who received MZR compared with MMF (RR = 0.69, 95% CI 0.44 to 1.10, $P = 0.12$, $I^2 = 36\%$, fixed-effect model) (Figure 6).

3.5.2. Liver Damage. Two studies contributed to analysis of liver damage. No significant difference in incidence of liver damage was detected in patients who were treated with MZR compared with MMF (RR = 0.72, 95% CI 0.46 to 1.13, $P = 0.15$, $I^2 = 0\%$, fixed-effect model) (Figure 7).

3.5.3. Gastrointestinal Disorder. Ten trials evaluated gastrointestinal disorder between the MZR group and MMF group. Significant heterogeneity was found ($P = 0.01$, $I^2 = 56\%$). Consequently, the random-effect model was applied. The MZR group was markedly beneficial in improving gastrointestinal disorder compared with the MMF group (RR = 0.28, 95% CI 0.13 to 0.62, $P = 0.002$) (Figure 8).

3.5.4. Cytomegalovirus Infection. With regard to cytomegalovirus infection, seven trails involving 532 patients were selected. The pooled analysis showed that the MZF group had a significantly lower rate of cytomegalovirus infection than the MMF group (RR = 0.59, 95% CI 0.42 to 0.84, $P = 0.003$, $I^2 = 38\%$, fixed-effect model) (Figure 9).

3.5.5. Hyperuricemia. All the included studies had data available for analysis of hyperuricemia. The MZR group showed a significantly higher incidence of hyperuricemia compared with the MMF group (RR 1.79, 95% CI 1.17 to 2.75, $P = 0.007$, random-effect model). There is significant heterogeneity between the included studies ($P = 0.002$, $I^2 = 63\%$) (Figure 10).

TABLE 1: Trial design and baseline characteristics of the 12 trials included in the meta-analysis.

Study	Country	Language	Study design	No. of patients		Gender (M/F)		Age		Dosages		Follow-up	Duration
				MZR	MMF	MZR	MMF	MZR	MMF	MZR	MMF		
Ming 2003	China	Chinese	RCT	20	20	-	-	-	-	100 mg/d	1.5 g/d	6 months	2001
Yan 2008	China	Chinese	RCT	100	100	-	-	-	-	50-100 mg/d	1 ~ 1.5 g/d	12 months	2002
Han 2010	China	Chinese	RCT	35	35	23/12	23/12	41.6 ± 10.5	42.1 ± 10.6	150-200 mg/d	1 ~ 1.5 g/d	12 months	September 2004 to November 2005
Chen 2012	China	Chinese	RCT	33	28	21/12	18/10	40.2 ± 11.5	38.6 ± 9.9	150-200 mg/d	1 ~ 1.5 g/d	6 months	January 2010 to October 2010
Ju 2013	Korea	English	RCT	110	109	70/40	64/45	44.6 ± 10.9	44.2 ± 11.1	100-300 mg/d	1 ~ 2 g/d	6 months	July 2008 to January 2011
Takahara 2013	Japan	English	RCT	16	19	9/7	15/4	36.1 ± 7.2	39.7 ± 11.3	350-600 mg/d	1 ~ 2 g/d	12 months	July 2005 to June 2007
Yoshimura 2013	Japan	English	RCT	40	38	23/17	20/18	41 ± 13	35 ± 14	6 mg/kg/d	25 mg/kg/d	24 months	October 2004 to July 2007
Yoshimura 2014	Japan	English	RCT	12	12	7/5	5/7	50 ± 10	50 ± 13	6 mg/kg/d	1 g/d	36 months	October 2007 to April 2010
Ishida 2016	Japan	English	RCT	41	42	26/15	27/15	41.7 ± 14.4	42.3 ± 12.5	700 mg/d	2 g/d	12 months	October 2008 to December 2013
Ushigome 2016	Japan	English	RCT	90	81	56/34	50/31	42.5 ± 13.5	39.2 ± 13.1	6 mg/kg/d	30 mg/kg/d	24 months	February 2006 to June 2008
Shi 2019	China	English	RCT	22	20	20/2	16/4	30.4 ± 7.7	29.4 ± 8.4	3 mg/kg/d	1.5 g/d	36 months	January 2012 to August 2014
Huang 2020	China	English	RCT	40	40	21/19	18/22	27.5 (3-57)	28.5 (6-54)	3 mg/kg/d	15 mg/kg/d	50.7 months	March 2014 to March 2017

MZR, mizoribine; MMF, mycophenolate mofetil.

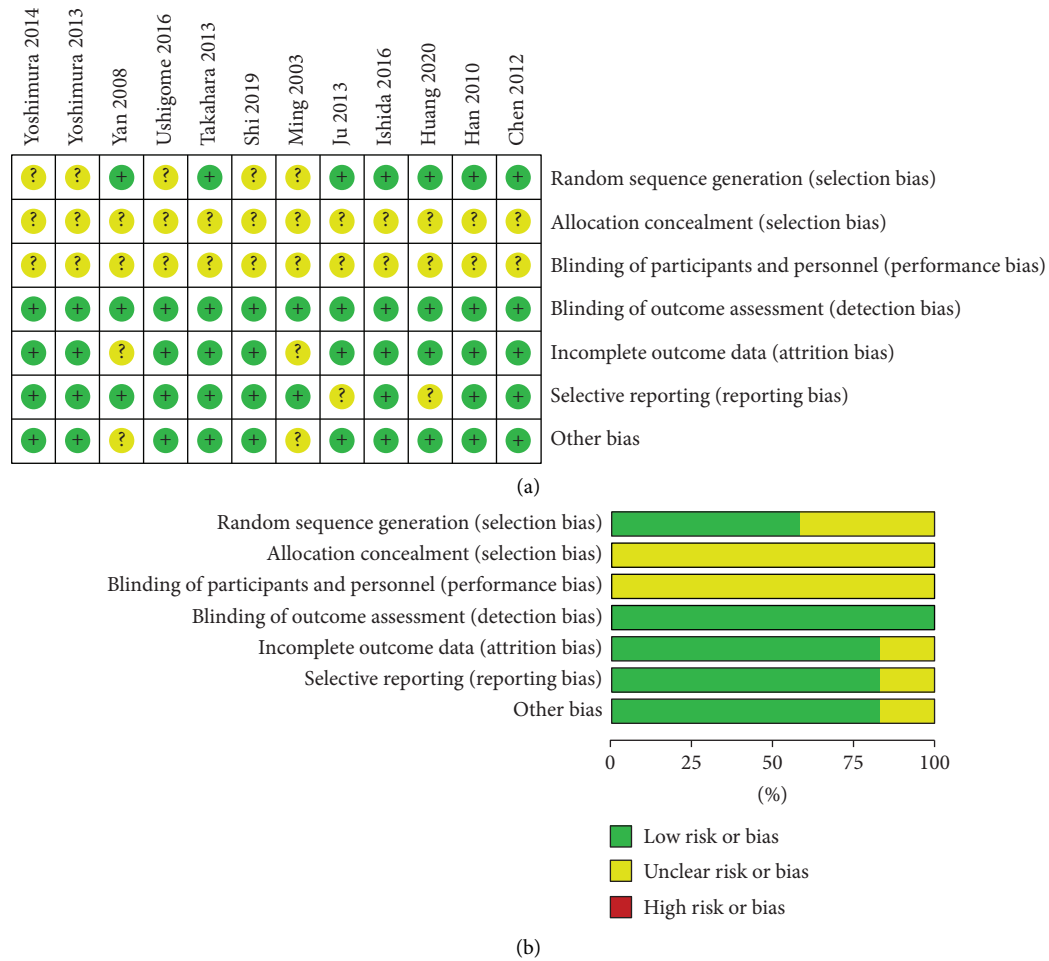


FIGURE 2: Quality assessment of included studies. (a) Risk of bias summary of each included study; (b) Overall risk of bias of included studies.

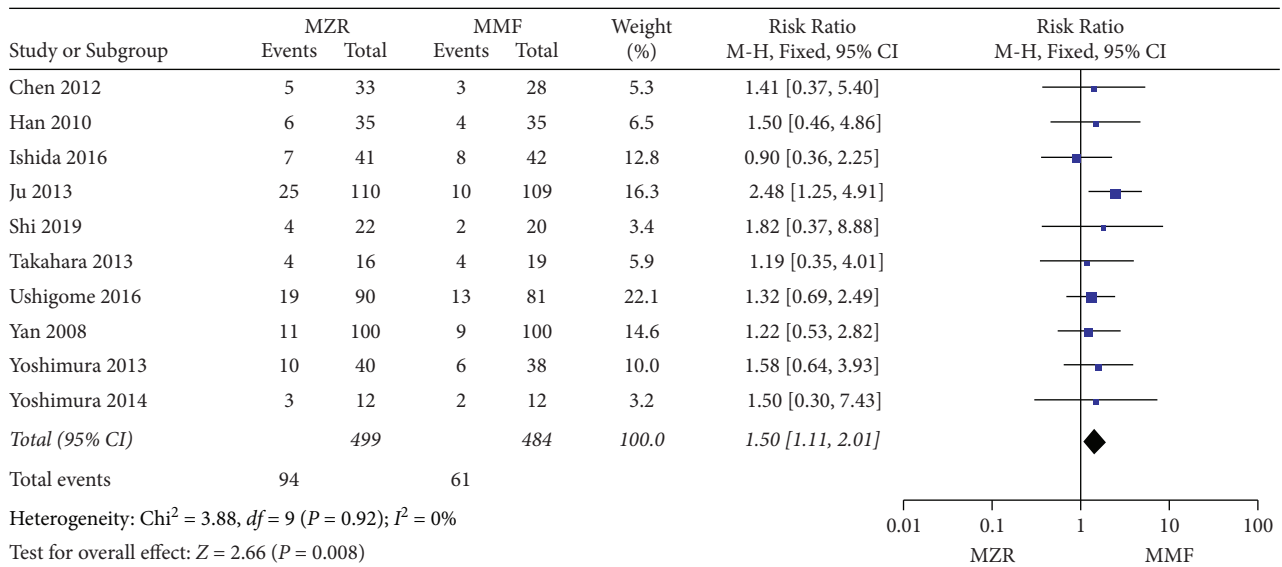


FIGURE 3: Forest plot: MZR versus MMF for acute rejection. MZR, mizoribine; MMF, mycophenolate mofetil; CI, confidence interval; df, degrees of freedom.

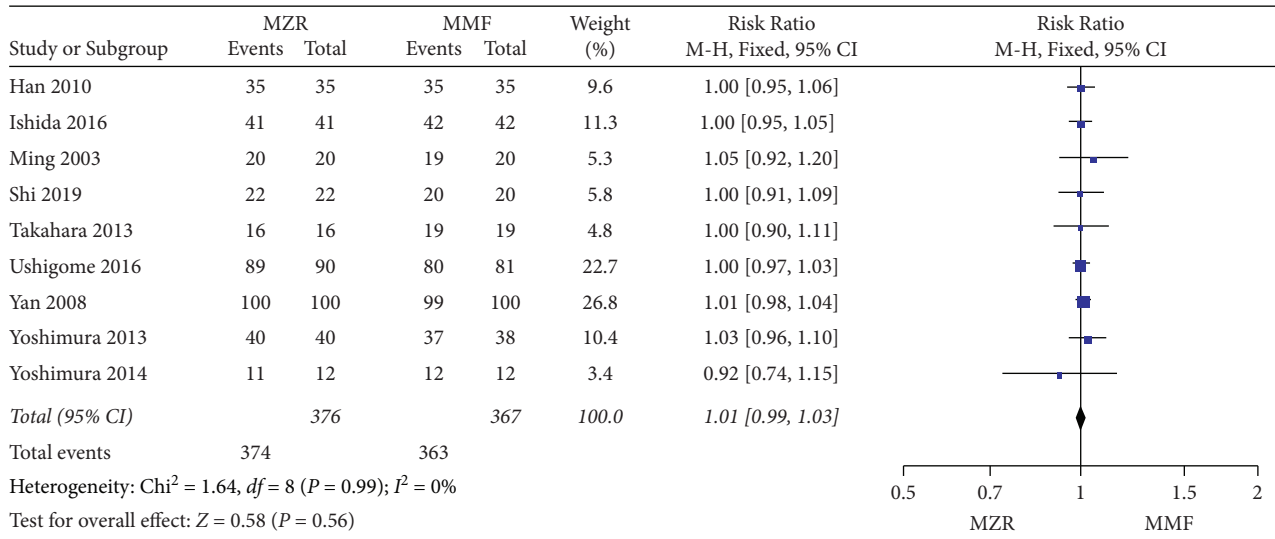


FIGURE 4: Forest plot: MZR versus MMF for patient survival. MZR, mizoribine; MMF, mycophenolate mofetil; CI, confidence interval; df, degrees of freedom.

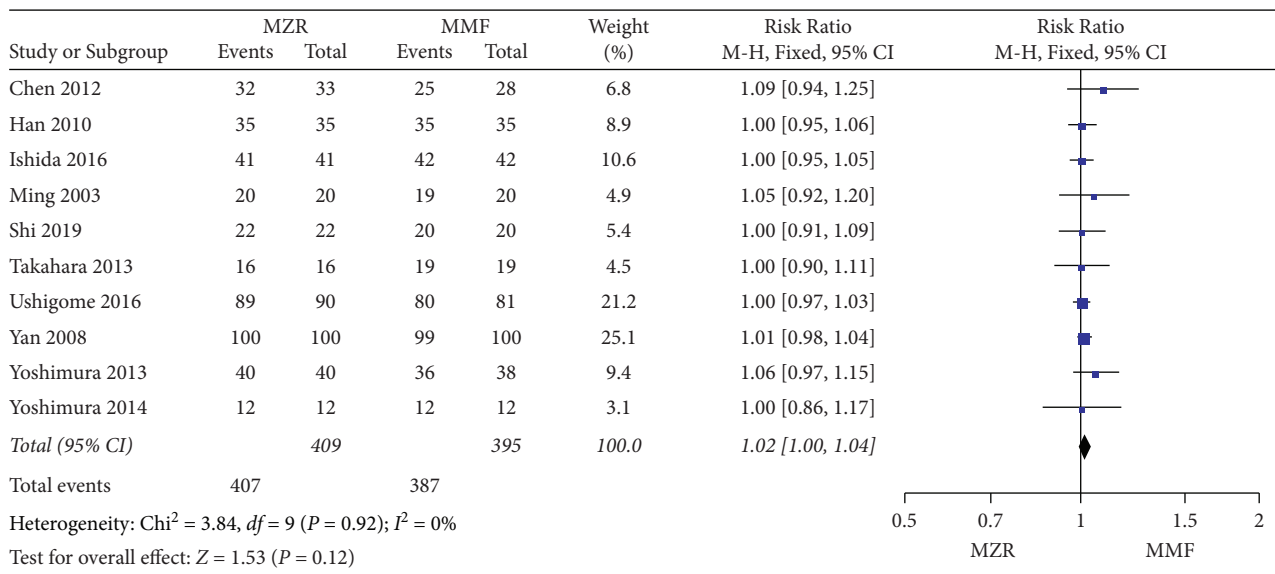


FIGURE 5: Forest plot: MZR versus MMF for graft survival. MZR, mizoribine; MMF, mycophenolate mofetil; CI, confidence interval; df, degrees of freedom.

3.6. Publication Bias. The publication bias test was conducted when the included studies were at least ≥ 10 by using the funnel plot and Egger's test, so we performed the tests on the outcomes of acute rejection, graft survival, gastrointestinal disorder, and hyperuricemia. The funnel plots for acute rejection and graft survival were visually symmetrical, and Egger's test also showed no significant publishing bias (acute rejection, $P = 0.764$; graft survival, $P = 0.618$). Even though the shape of funnel plots for gastrointestinal disorder and hyperuricemia showed some evidence of asymmetry, the P value of Egger's test was nonsignificant (gastrointestinal disorder, $P = 0.185$; hyperuricemia, $P = 0.327$) (Figure 11).

4. Discussion

At present, renal transplantation mainly relies on the classic triple immunosuppressive therapy of calcineurin phosphatase inhibitor, MMF, and hormone to control acute rejection. However, AZA has significant hepatotoxicity and hematotoxicity, MMF is often accompanied by opportunistic virus infection that is difficult to control, and it is expensive [27, 28]. Therefore, the transplantation urgently needs new drugs with a good curative effect, good safety, and moderate price so as to provide more choices for clinicians.

As an antimetabolic immunosuppressant, MZR has mild adverse reactions. According to early studies, its

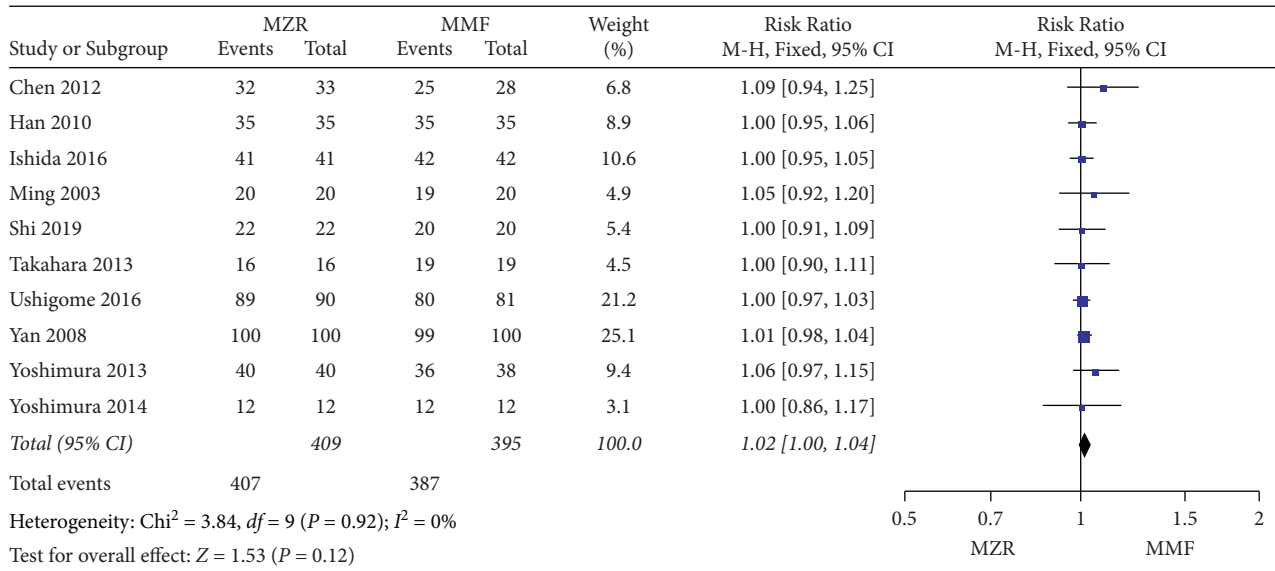


FIGURE 6: Forest plot: MZR versus MMF for leukopenia. MZR, mizoribine; MMF, mycophenolate mofetil; CI, confidence interval; df, degrees of freedom.

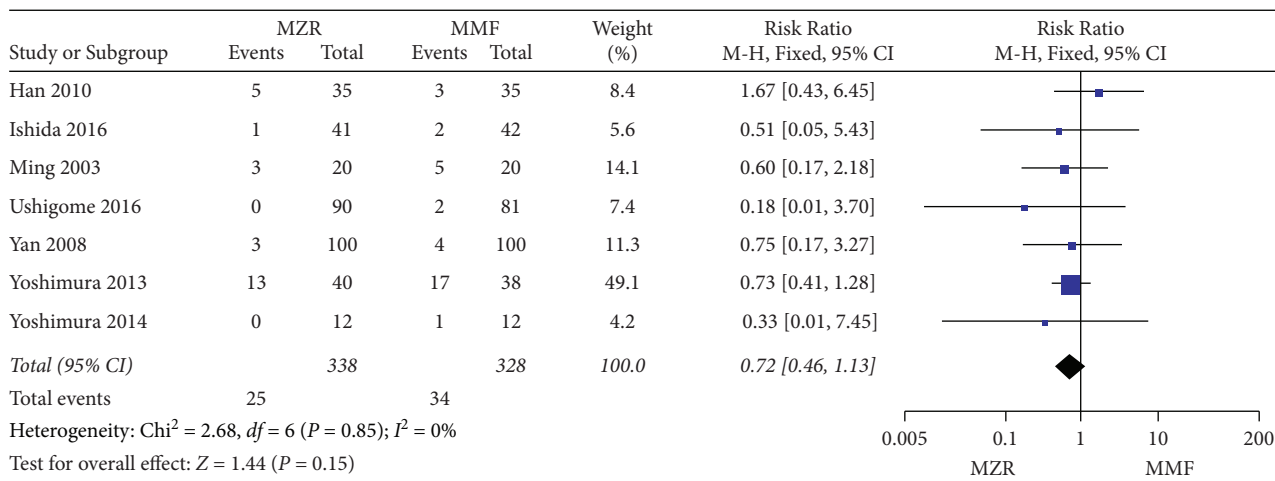


FIGURE 7: Forest plot: MZR versus MMF for liver damage. MZR, mizoribine; MMF, mycophenolate mofetil; CI, confidence interval; df, degrees of freedom.

antirejection effect is also weaker than MMF, so it is not widely used in countries other than Japan. International reports on the application of MZR in the field of renal transplantation also come from Japan [29, 30]. It was developed as an antifungal drug in the early stage and later found to have an anticell proliferation effect. In the twenty-first century, it is usually used as an alternative drug for MMF after renal transplantation in Asia, especially in China, Japan, South Korea, and other countries [16, 19, 23]. The main reasons for choosing MZR to replace MMF are as follows:

- (1) MZR has an active structure similar to the antiviral drug ribavirin, so it has a certain inhibitory effect on a variety of viruses, while Japanese scholars believe that MZR may also have a certain inhibitory effect on

BK virus (BKV) in the diagnosis and treatment of patients with BKV urine after renal transplantation

- (2) Early Brennan and other scholars have verified that MMF immunosuppressive regimen is one of the risk factors of BKV reactivation
- (3) The immunosuppressive effect of low-dose (1-3 mg/kg/d) MZR after renal transplantation is weaker than that of MMF, while high-dose (5-6 mg/kg/d) MZR is considered to provide the same immunosuppressive intensity as MMF

Therefore, in theory, when MMF is converted to MZR, it can not only rely on its anti-BKV activity but also increase the self-specific immune effect against BKV due to the decrease of immunosuppression so as to comprehensively inhibit the replication of BKV [31-33].

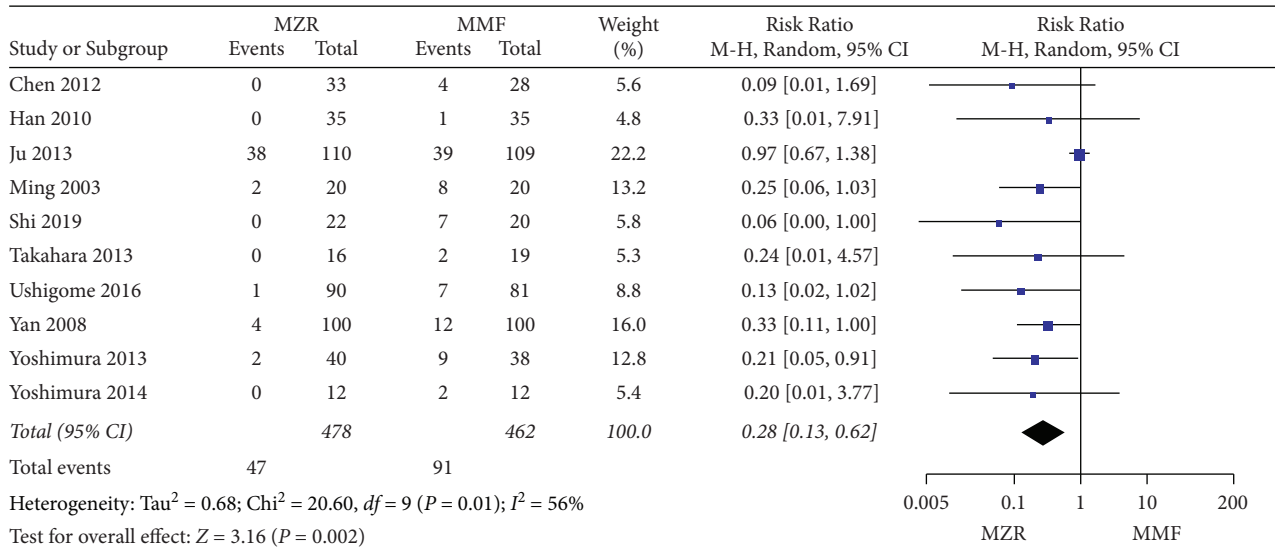


FIGURE 8: Forest plot: MZR versus MMF for gastrointestinal disorder. MZR, mizoribine; MMF, mycophenolate mofetil; CI, confidence interval; df, degrees of freedom.

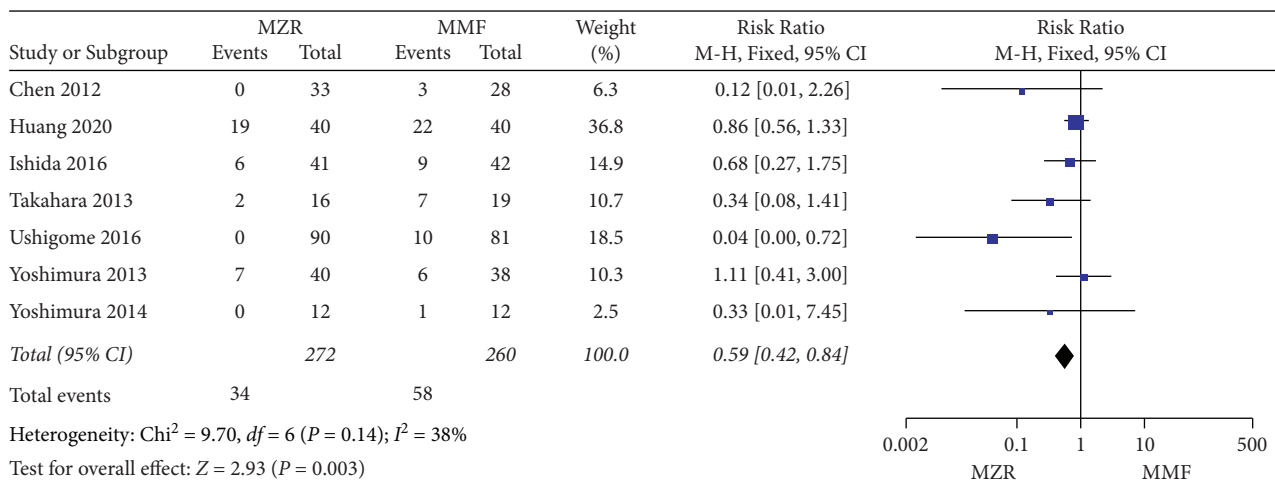


FIGURE 9: Forest plot: MZR versus MMF for cytomegalovirus infection. MZR, mizoribine; MMF, mycophenolate mofetil; CI, confidence interval; df, degrees of freedom.

In our paper, the meta-analysis was used to evaluate the efficacy and safety of MZR and MMF in renal transplant recipients. The results showed that there was no significant difference in the incidence of acute rejection, patient survival, and graft survival rate between MZR and MMF groups, which were consistent with the results of Xing et al.[34]. In terms of safety, there was no significant difference in the incidence of leucopenia and liver damage between the MZR group and MMF group, but the incidence of gastrointestinal disorder and cytomegalovirus infection in the MZR group was lower than that in the MMF group, while the incidence of hyperuricemia was higher than that in the MMF group. Except that the difference in the incidence of cytomegalovirus infection was inconsistent with the research results of Li et al. [35], other safety results were consistent, and it may be related to the fact that Li's study

only included four literatures for cytomegalovirus infection, while we included seven, and the result was more reliable.

The good tolerance of MZR in the gastrointestinal tract has obvious advantages. It can be used as an alternative treatment for diarrhea in renal transplant recipients so as to improve the compliance of renal transplant recipients. Infection is one of the main complications after renal transplantation, and it is also an important factor affecting the survival rate of recipients and transplanted kidneys, especially cytomegalovirus infection [36]. Mild cases are asymptomatic viremia, and severe cases are often life-threatening. MZR has been proved to inhibit cytomegalovirus in vitro in a dose-response relationship [37]. Its antiviral mechanism may be similar to its chemical structure and broad-spectrum antiviral drug ribavirin. MZR can reduce the incidence of infection without increasing the risk of

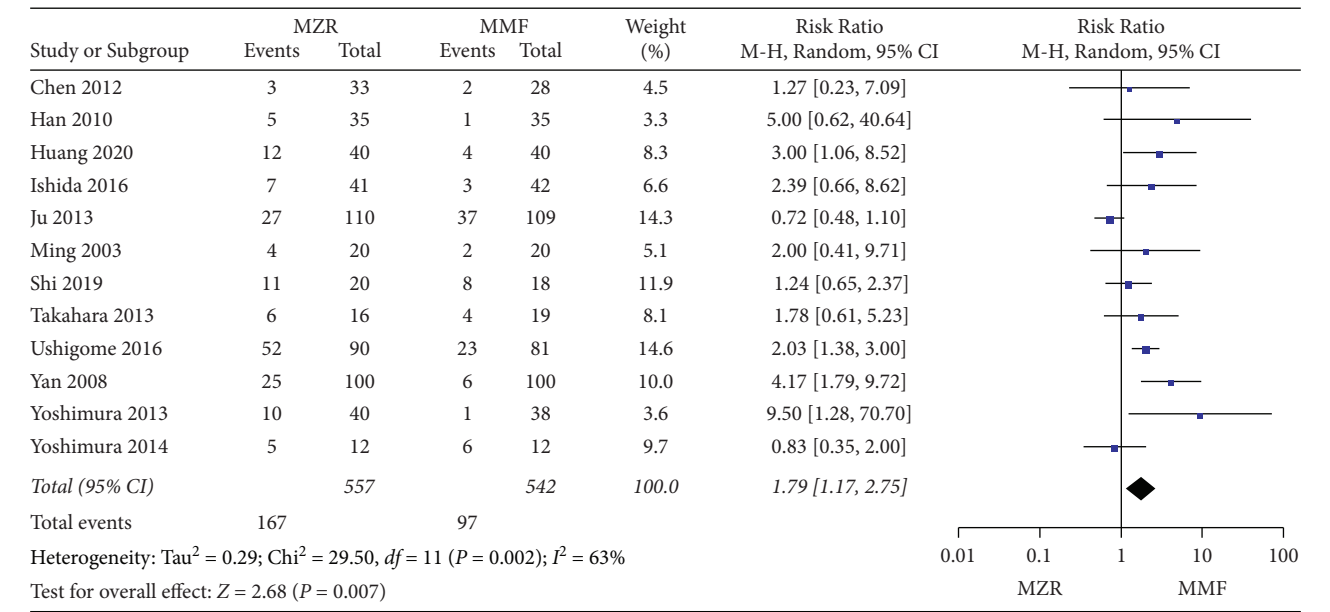


FIGURE 10: Forest plot: MZR versus MMF for hyperuricemia. MZR, mizoribine; MMF, mycophenolate mofetil; CI, confidence interval; df, degrees of freedom.

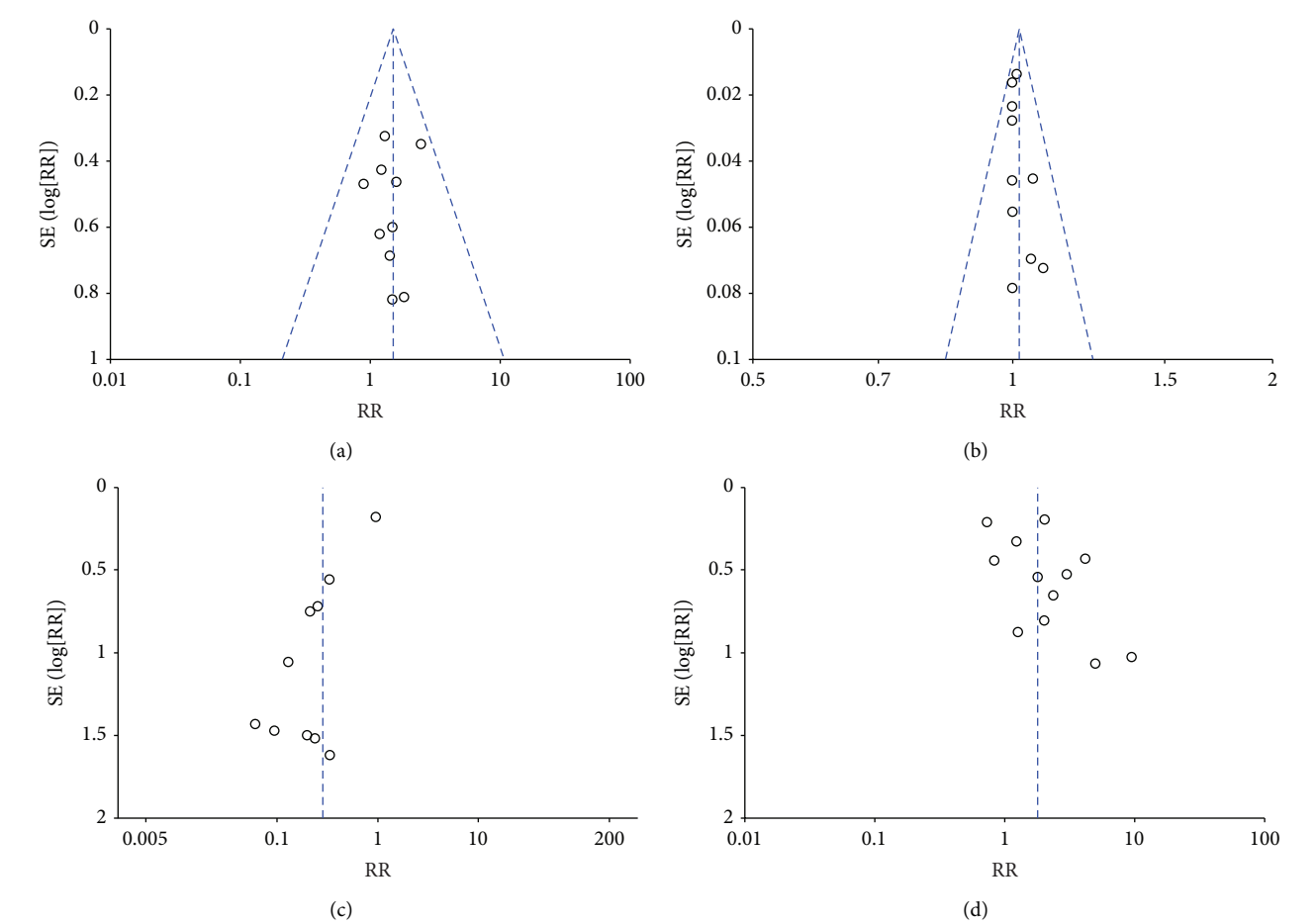


FIGURE 11: Funnel plot for publication bias in this meta-analysis (a) Acute rejection; (b) Graft survival; (c) Gastrointestinal disorder; (d) Hyperuricemia.

rejection. It can effectively help renal transplant recipients through the high-risk infection period especially for high-risk infection recipients such as perioperative lung infection, retransplantation, and the use of polyclonal antibodies.

Hyperuricemia is a common adverse reaction of MZR. It mainly leads to the increase of guanine and xanthine nucleoside by inhibiting the activity of hypoxanthine nucleoside phosphate dehydrogenase so as to increase xanthine and uric acid, which is positively correlated with the drug dose. Therefore, the blood uric acid level of the recipient should be monitored during the administration of MZR [38]. If necessary, the dose of MZR can be reduced or uric acid lowering drugs such as allopurinol and benzbromarone can be added to maintain the normal blood uric acid level.

There were still some limitations in this study: (1) Although 12 literatures were included, the sample size was only 1103, which was still small; (2) the follow-up time ranged from 6 to 50 months due to the small number of literatures, and it was impossible to make subgroup analysis of short-term and long-term effects; (3) the research population was limited to China, Japan, and South Korea, and there was a lack of research on other regions; and (4) the dosage of each study and the type of transplanted renal were different, which may affect the accuracy of the final conclusion.

5. Conclusions

In conclusion, there is no significant difference in the efficacy of rejection between MZR and MMF in the prognosis of renal transplantation. In terms of safety, there is also no significant difference between the two groups in the incidence of leucopenia and liver damage; compared with the MMF group, the incidence of gastrointestinal disorder and cytomegalovirus infection in the MZR group was lower, but the incidence of hyperuricemia was higher. Limited to the design and quality of the included study, more large samples, more regions, and longer follow-up RCTs are needed to verify the conclusion.

Data Availability

The datasets used and analyzed during the current study are available from the corresponding author upon reasonable request.

Conflicts of Interest

All authors have completed the ICMJE uniform disclosure form. The authors have no conflicts of interest to declare.

Authors' Contributions

Jie Chen and Hua Liu contributed equally to this work.

References

- [1] P. J. Morris, R. J. Johnson, S. V. Fuggle, M. A. Belger, and J. D. Briggs, "Analysis of factors that affect outcome of primary cadaveric renal transplantation in the UK," *Lancet* (North American Edition), vol. 354, no. 9185, pp. 1147–1152, 2019.
- [2] R. Boissier, V. Hevia, H. M. Bruins, K. Budde, A. Figueiredo, and J. Olsburgh, "The risk of tumour recurrence in patients undergoing renal transplantation for end-stage renal disease after previous treatment for a urological cancer: a systematic Review - ScienceDirect," *European Urology*, vol. 73, no. 1, pp. 94–108, 2018.
- [3] J. D. Schold, B. Kaplan, R. J. Howard, A. I. Reed, D. P. Foley, and H. U. Meier-Kriesche, "Are we frozen in time? Analysis of the utilization and efficacy of pulsatile perfusion in renal transplantation," *American Journal of Transplantation*, vol. 5, no. 7, pp. 1681–1688, 2005.
- [4] Y. Qin, F. Zhang, B. Shen et al., "Efficacy and safety of enteric-coated mycophenolate sodium in patients with de novo and maintenance renal transplantation," *International Journal of Clinical Practice*, vol. 68, pp. 17–22, 2014.
- [5] D. Y. H. Yap and T. M. Chan, "Treatment of lupus nephritis: practical issues in Asian countries," *International Journal of Rheumatic Diseases*, vol. 18, no. 2, pp. 138–145, 2015.
- [6] A. Sonoda, K. Wada, K. Mizukami et al., "Deep ulcers in the ileum associated with mycophenolate mofetil," *Internal Medicine*, vol. 56, no. 21, pp. 2883–2886, 2017.
- [7] F. Ljuca, S. Imamović, D. Mesić et al., "Micophenolat Mofetil versus Azathioprine: effects on renal graft function in early posttransplant period," *Bosnian Journal of Basic Medical Sciences*, vol. 9, no. 2, pp. 156–160, 2009.
- [8] S. Cao, G. O. Aboge, M. A. Terkawi et al., "Mycophenolic acid, mycophenolate mofetil, mizoribine, ribavirin, and 7-nitro-indole inhibit propagation of babesia parasites by targeting inosine 5'-Monophosphate dehydrogenase," *The Journal of Parasitology*, vol. 100, no. 4, pp. 522–526, 2014.
- [9] J. Sobiak, M. G. Yda, M. Malec, and M. Chrzanowska, "Pharmacokinetics of mycophenolate mofetil metabolites in older patients on the seventh day after renal transplantation article in press," *Transplantation Proceedings*, vol. 53, pp. 358–365, 2021.
- [10] K. Akioka, K. Masuda, S. Harada et al., "Acute renal failure caused by hyperuremic acidemia in ABO-incompatible kidney transplant maintained with cyclosporine and high-dose mizoribine: a case report," *Transplantation Proceedings*, vol. 45, no. 7, pp. 2815–2818, 2013.
- [11] Y. Shi, H. Liu, X. G. Chen, and Z. Y. Shen, "Comparison of mizoribine and mycophenolate mofetil with a tacrolimus-based immunosuppressive regimen in living-donor kidney transplantation recipients: a retrospective study in China," *Transplantation Proceedings*, vol. 49, no. 1, pp. 26–31, 2017.
- [12] A. Boyd, A. Brown, J. Patel et al., "Basiliximab with delayed tacrolimus improves short-term renal outcomes post-liver transplantation—a real-world experience," *Transplantation Proceedings*, vol. 53, no. 5, pp. 1541–1547, 2021.
- [13] K. Sugimoto, N. Sakata, S. Fujita et al., "Cure of relapsing nephrosis by an allogeneic marrow graft for chronic myelogenous leukemia," *Pediatric Nephrology*, vol. 28, no. 6, pp. 975–978, 2013.
- [14] S. Ashimine, Y. Watarai, T. Yamamoto et al., "Neither pre-transplant rituximab nor splenectomy affects de novo HLA antibody production after renal transplantation," *Kidney International*, vol. 85, no. 2, pp. 425–430, 2014.
- [15] A. Ming, M. Lin, M. Zhao, L. Yue, M. Li, and L. Fan, "Application of mizoribine in cadaveric renal transplantation," *Journal of Clinical Urology*, vol. 18, no. 01, pp. 6–7, 2003.

- [16] Q. Yan, H. Chen, Y. Jiang, S. Xie, Z. Shen, and W. Kui, "Application of mizoribine in clinical kidney transplantation," *Chin J Organ Transplant*, vol. 29, no. 1, pp. 14-15, 2008.
- [17] S. Han, B. Shen, Y. Fan, and Y. Zhu, "Comparison of two triple immunosuppressive regimens of mizoribine and mycophenolate mofetil in renal transplant patients," *Chin J New Drugs*, vol. 19, no. 7, pp. 595-598, 2010.
- [18] L. Chen, L. Liu, Y. Qian, M. Cai, X. Zhang, and B. Shi, "Efficacy and safety of mizoribine in early postoperative renal transplantations," *Chin J Organ Transplant*, vol. 33, no. 1, pp. 18-21, 2012.
- [19] M. K. Ju, K. H. Huh, K. T. Park et al., "Mizoribine versus mycophenolate mofetil in combination therapy with tacrolimus for de novo kidney transplantation: evaluation of efficacy and safety," *Transplantation Proceedings*, vol. 45, no. 4, pp. 1481-1486, 2013.
- [20] S. Takahara, K. Takahashi, T. Akiyama et al., "Randomized comparative trial of mizoribine versus mycophenolate mofetil in combination with tacrolimus for living donor renal transplantation," *Clinical and Experimental Nephrology*, vol. 17, no. 6, pp. 899-904, 2013.
- [21] N. Yoshimura, H. Ushigome, K. Akioka et al., "The beneficial effect of high-dose mizoribine combined with cyclosporine, basiliximab, and corticosteroids on CMV infection in renal transplant recipients," *Clinical and Experimental Nephrology*, vol. 17, no. 1, pp. 127-133, 2013.
- [22] N. Yoshimura, H. Ushigome, S. Nobori et al., "Usefulness and safety of high-dose mizoribine on ABO-incompatible living related kidney transplantation using anti-cd20 and anti-cd25 antibodies without splenectomy: 3-year results," *Transplantation Proceedings*, vol. 46, no. 2, pp. 391-394, 2014.
- [23] H. Ushigome, K. Uchida, K. Nishimura et al., "Efficacy and safety of high-dose mizoribine combined with cyclosporine, basiliximab, and corticosteroids in renal transplantation: a Japanese multicenter study," *Transplantation Proceedings*, vol. 48, no. 3, pp. 794-798, 2016.
- [24] H. Ishida, S. Takahara, N. Amada et al., "A prospective randomized, comparative trial of high-dose mizoribine versus mycophenolate mofetil in combination with tacrolimus and basiliximab for living donor renal transplant: a multicenter trial," *Experimental and Clinical Transplantation :Official Journal of the Middle East Society for Organ Transplantation*, vol. 14, no. 5, pp. 518-525, 2016.
- [25] Y. Shi, H. Liue, X. G. Chen, and Z. Y. Shen, "Efficacy and safety of mizoribine combined with tacrolimus in living donor kidney transplant recipients: 3-year results by a Chinese single center study," *Transplantation Proceedings*, vol. 51, no. 5, pp. 1337-1342, 2019.
- [26] Y. Huang, M. Han, D. Yang et al., "Comparative study of mizoribine and mycophenolate mofetil combined with a calcineurin inhibitor-based immunosuppressive regimen in patients with alternative donor hematopoietic cell transplantation," *Biology of Blood and Marrow Transplantation*, vol. 26, no. 9, pp. 1663-1669, 2020.
- [27] H. R. Whalen, J. A. Glen, V. Harkins et al., "High inpatient tacrolimus variability is associated with worse outcomes in renal transplantation using a low-dose tacrolimus immunosuppressive regime," *Transplantation*, vol. 101, no. 2, pp. 430-436, 2017.
- [28] J. Bamoulid, A. Roodenburg, O. Staack et al., "Clinical outcome of patients with de novo C1q-binding donor-specific HLA antibodies after renal transplantation," *Transplantation*, vol. 101, no. 9, pp. 2165-2174, 2017.
- [29] K. Koshino, H. Ushigome, T. Nakao et al., "Usefulness of follow-up biopsies at one year after ABO-incompatible kidney transplantation," *Transplantation Proceedings*, vol. 46, no. 2, pp. 385-387, 2014.
- [30] N. Ichimaru, K. Yamanaka, T. Kato et al., "Risk factors and incidence for lipid abnormalities in kidney transplant patients," *Transplantation Proceedings*, vol. 47, no. 3, pp. 672-674, 2015.
- [31] L. Ye, F. Xiao, J. Xie et al., "Synergistic renoprotective effects of sesame oil and erythropoietin on ischemic kidney injury after renal transplantation," *AMB Express*, vol. 10, no. 1, p. 4, 2020.
- [32] J. Sobiak and M. Resztak, "A systematic Review of multiple linear regression-based limited sampling strategies for mycophenolic acid area under the concentration-time curve estimation," *European Journal of Drug Metabolism and Pharmacokinetics*, vol. 46, no. 6, pp. 721-742, 2021.
- [33] X. Ding, X. Zhu, Y. Zhang et al., "Influence of serum uric acid levels in response to the conversion from mycophenolate mofetil to mizoribine in kidney transplant recipients," *Transplantation Proceedings*, vol. 45, no. 1, pp. 190-193, 2013.
- [34] S. Xing, J. Yang, X. Zhang, and P. Zhou, "Comparative efficacy and safety of mizoribine with mycophenolate mofetil for Asian renal transplantation—a meta-analysis," *Clinical Biochemistry*, vol. 47, no. 7-8, pp. 663-669, 2014.
- [35] N. Li, S. Tang, Z. F. Zhu, L. Jing-Li, X. Zhang, and D. Pharmacy, "Efficacy and safety of mizoribine and mycophenolate mofetil after renal transplantation: a Meta-analysis," *Chinese Journal of Hospital Pharmacy*, vol. 38, no. 10, pp. 1102-1109, 2018.
- [36] K. Sallam, G. D. Bhumireddy, V. D. Evuri et al., "Sirolimus adverse event profile in a non-clinical trial cohort of heart transplantation patients," *Annals of Transplantation*, vol. 26, p. e923536, 2021.
- [37] Y. Qian, B. Shi, J. Ao, and H. Yang, "Clinical application of mizoribine in minimizing virus infection risk in renal graft recipients," *Chin J Organ Transplant*, vol. 27, no. 12, pp. 723-724, 2006.
- [38] J. Ao, X. Xiao, H. Zhang, and H. Yang, "The conversion of mizoribine to treat myelosuppression after renal transplantation," *Journal of Clinical Urology*, vol. 19, no. 7, pp. 435-436, 2004.

Research Article

Research on the MEG of Depression Patients Based on Multivariate Transfer Entropy

Xinyu Zhang ^{1,2}, Jicheng Xie,^{1,2} Changyu Fan,^{1,2} and Jun Wang ^{1,2}

¹School of Geographic and Biologic Information, Nanjing University of Posts and Telecommunications, Nanjing, China

²Smart Health Big Data Analysis and Location Services Engineering Research Center of Jiangsu Province, Nanjing University of Posts and Telecommunications, Nanjing, China

Correspondence should be addressed to Jun Wang; wangj@njupt.edu.cn

Received 24 April 2022; Revised 27 May 2022; Accepted 3 June 2022; Published 20 July 2022

Academic Editor: Dong Chen

Copyright © 2022 Xinyu Zhang et al. This is an open access article distributed under the Creative Commons Attribution License, which permits unrestricted use, distribution, and reproduction in any medium, provided the original work is properly cited.

The pathogenesis of depression is complex, and the current means of medical diagnosis is single. Patients with severe depression may even have great physical pain and suicidal tendencies. Magnetoencephalography (MEG) has the characteristics of ultrahigh spatiotemporal resolution and safety. It is a good medical means for the diagnosis of depression. In this paper, multivariate transfer entropy algorithm is used to study MEG of depression. In this paper, the subjects are divided into the same brain region and the multichannel combination between different brain regions, and the multivariate transfer entropy of patients with depression and healthy controls under different EEG signal frequency bands is calculated. Finally, the significant difference between the two groups of experimental samples is verified by the results of independent sample *t*-test. The experimental results show that for the same combination of brain channels, the multivariate transfer entropy in the depression group is generally lower than that in the healthy control group, and the difference is the best in γ frequency band and the largest in the frontal region.

1. Background Introduction

Depression is an affective disorder. Its main clinical manifestations are long-term depression, loss of interest in many things, insomnia, and even self-mutilation [1–4]. According to the data released by the World Health Organization, there are about 340 million patients with depression in the world, with a prevalence rate of 35%. There are 1 million suicidal deaths caused by mental illness every year. Depression has become the second largest disease burden after ischemic heart disease. In the suicide population, 40% of people die because of depression without timely and systematic treatment [5–7]. Therefore, how to distinguish whether patients suffer from depression is particularly important.

The development of information technology [8–11] has brought new opportunities and challenges to the diagnosis and treatment of depression [12–14]. MEG is a real-time monitoring technology used to record the brain magnetic field signal generated by neuronal activity and monitor the brain electrophysiological activity through the waveform,

amplitude, and frequency of the signal [15–19]. MEG has a time resolution of millisecond, which can record neuron signals in real time without measuring brain metabolism; high spatial resolution of MEG can locate brain lesions accurately. MEG is a safe and repeatable detection method. MEG signals can penetrate the scalp without damage and invasion.

The brain can be regarded as a complex nonlinear system. As an index of nonlinear system, entropy is used to measure the complexity of nonlinear system [20, 21]. At present, the methods of sample entropy and approximate entropy have been applied to the analysis of brain magnetic and electricity data [22, 23]. On this basis, the multivariate transfer entropy used in this paper covers the dynamic characteristics and directionality, and is suitable for the complexity study of nonlinear systems. Partial information decomposition algorithm is a new algorithm for complex multivariate systems. Its main principle is to decompose the interaction of multivariate variables into four non negative and non-overlapping parts, and can separate collaborative

and redundant structures. In view of the imperfect research on MEG in China, especially the research on the connectivity between patients with depression and normal brain regions stimulated by emotional pictures is relatively few. Therefore, the multivariate transfer entropy algorithm used in this paper to study the complexity and correlation of multiple channels of MEG can provide some preliminary understanding and help for the future clinical diagnosis of depression and the study of brain functional area connectivity.

2. The Source of Experimental Data

The MEG data of the experimental study comes from 13 groups of MEG data collected by the MEG center of the Brain Hospital Affiliated to Nanjing Medical University, including 8 groups of healthy subjects and 5 groups of patients with depression. The depression samples are patients with depression in the inpatient department of the hospital, including 3 male patients and 2 female patients. Their ages range from 18 to 35, with an average of 25. The healthy samples are from interns in the hospital of Nanjing Medical University and medical post-graduates. Their ages range from 20 to 28, with an average age of 23. All subjects have normal sensory stimulation, have no history of infectious diseases, exclude other mental diseases, do not contraindicated brain magnetic resonance examination, do not take psychiatric inhibitors recently, and sign an informed agreement with the ethics committee of Nanjing Medical University after informing the experiment and related matters.

The original data collected by MEG is .meg4 file, uses SPM8 software to adjust the corresponding time delay, converts the data in the -200 ms– 600 ms time interval into MATLAB for calculation and processing, and finally corrects the baseline of the processed data and reduces the frequency. The processed data structure is the data dimension.

3. Introduction of Multivariate Transfer Entropy Algorithm and Frequency Division

3.1. Multivariate Transfer Entropy Algorithm

3.1.1. Symbolization of Original Sequence. Symbolic dynamics is a complex and abstract mathematical theory to study symbolic dynamical systems. In symbolic dynamics system, the state of the system can be expressed as an infinite sequence of finite abstract symbols. In the middle and late 1960s, due to the increasingly active research on chaos, it began to become a powerful tool for analyzing various complex sequences. In the mid-1990s, people began to analyze symbolic time series. Symbolic time series is a new way to analyze information. It includes symbolic dynamics theory, chaotic time series analysis, and information theory, which makes the signal analysis simple, fast, and effective.

Symbolization mainly adopts the means of “coarse graining” to transform the original time series into the specified symbol series according to certain mapping rules. The symbolic time series can remove a large amount of redundant information on the basis of retaining the characteristics of nonlinear dynamics. Then, the key information

is obtained by studying the dynamic characteristics of the symbol sequence.

The symbolic algorithm used in this experiment is the static scale symbolic method in symbolic dynamics. For the study of static symbolization, Wessel and other people proposed the time series four symbol static scale symbol method in the study of heart rate in patients with chronic heart failure.

The mapping rules are as follows:

$$s_i(x_i) = \begin{cases} 0: u_1 < xi \leq (1+a)u_1 \text{ or } (1+a)u_2 \leq xi < u_2, \\ 1: (1+a)u_1 < xi < \infty \text{ or } -\infty < xi < (1+a)u_2, \\ 2: (1-a)u_1 \leq xi < u_1 \text{ or } u_2 < xi \leq (1-a)u_2, \\ 3: (1-a)u_2 < xi < (1-a)u_1. \end{cases} \quad (1)$$

$1 \leq i \leq N$ represents the symbol position corresponding to the symbolic original time series, u_1, u_2 is the average of the sampled signals greater than or equal to zero and less than zero in the original sequence. a is a special constant with a normal value range of $[0.03, 0.07]$, because it will lose details if it is too large, and it will aggravate the influence of noise if it is too small, so it cannot better capture the dynamic information in the signal. In order that the processed signal will not lose the dynamic characteristics of the time series, it is usually taken as $a = 0.05$.

3.1.2. Multivariate Transfer Entropy. At present, nonlinear dynamics method [24, 25] has been widely used in brain science research. For the study of EEG signals, the nonlinear dynamic methods mainly include correlation dimension, Lyapunov exponent, Kolmogorov entropy, approximate entropy, and sample entropy. However, there are few studies on nonlinear dynamic methods of MEG signals at home and abroad. At present, the relevant nonlinear dynamic methods used in MEG research mainly include Lempel Ziv, correlation dimension, and entropy statistics.

Human brain is a complex nonlinear system, and its left and right hemispheres are asymmetric. The transfer entropy can obtain the dynamic characteristics of the nonlinear system and its direction. Therefore, the study of asymmetric entropy transfer algorithm can just meet the characteristics of brain. The traditional transfer entropy algorithm is only aimed at the research of binary connectivity, that is, the connectivity between two variables. For the MEG signals of depression, the signals of MEG channels in the same functional area and between different functional areas may affect each other.

Therefore, the experiment in this paper takes multivariate transfer entropy as the measurement value, which can study the coupling between multiple variables. Compared with the traditional transfer entropy algorithm, the analysis of the experimental results is more accurate. Because the calculation process is sensitive to noise and requires high parameters, the multivariate transfer entropy is generally calculated after symbolic processing of the corresponding original time series, the specific algorithm processing procedures is shown in Figure 1.

The definition of multivariate transfer entropy can be given by multivariable transfer entropy and the symbolization of the original sequence, that is, the X sequence is mapped into a symbolic sequence according to the symbolization rules, $S = \{s_1, s_2, \dots, s_i, \dots, s_n\}$. Sequence Y is mapped to a sequence of symbols, $J = \{j_1, j_2, \dots, j_i, \dots, j_n\}$, $j_i \in A$ ($A = 0, 1, 2, 3$). Sequence Z is mapped to the corresponding symbolic order, $K = \{k_1, k_2, \dots, k_i, \dots, k_n\}$, $k_i \in A$ ($A = 0, 1, 2, 3$); multivariate transfer entropy is defined as $I_{S \rightarrow J}^{TE} \approx I_{S \rightarrow J}^{DT E} = \sum p(s_{n-\tau}, j_n, s_{n-\tau-1}, j_{n-\tau+1}, j_{n-\tau}, j_{n-\tau-1}, k_{n-\tau}, k_{n-\tau-1}) \cdot \log(p(s_{n-\tau}, j_n, s_{n-\tau-1}, j_{n-\tau+1}, j_{n-\tau}, j_{n-\tau-1}, k_{n-\tau}, k_{n-\tau-1}) / p(j_n, s_{n-\tau-1}, j_{n-\tau+1}, j_{n-\tau}, j_{n-\tau-1}, k_{n-\tau}, k_{n-\tau-1})) \cdot p(s_{n-\tau-1}, j_{n-\tau+1}, j_{n-\tau}, j_{n-\tau-1}, k_{n-\tau}, k_{n-\tau-1}) / p(s_{n-\tau}, s_{n-\tau-1}, j_{n-\tau+1}, j_{n-\tau}, j_{n-\tau-1}, k_{n-\tau}, k_{n-\tau-1})$.

3.2. The Filtering of EEG Band. The filter is mainly used to process signals, filter out the signals we do not need, and leave the required signal information. Generally, filters are divided into low-pass filter, band-pass filter, band stop filter, and high pass filter according to frequency characteristics. According to the difference of impulse response, the digital filter is divided into finite impulse response (FIR) filter and infinite impulse response (IIR) filter. FIR filter is an all zero structure, so the system is very stable and has the characteristics of linear phase. All signals in the effective frequency range will not have phase error. An FIR filter with band pass of 14–30 Hz is designed on the MATLAB platform, which can filter the EEG signal to obtain segment a in the EEG signal. The frequency response of the filter is as follows:

Figure 2 is the frequency response function of the band-pass filter. The allowable frequency is 1430 Hz, which is cut off in other frequencies. Figure 3 is the time domain waveform of the unprocessed EEG signal, and Figure 4 is the time domain diagram of EEG signal filtered on the band. It can be seen that the fluctuation of the signal is chaotic. After the original signal is transformed from the time domain to the frequency domain, 1430 Hz is extracted, and then transformed to frequency domain to obtain β EEG signal. It can be seen that the waveform of β signal is obviously different from the original data. After that, the EEG time domain diagram under B (<4 Hz, delta), (4~7 Hz, theta), (8~13 Hz, alpha), and C (>30 Hz, gamma) can be obtained by using a similar method.

4. Frequency Division Results and Analysis of Symmetrical and Asymmetric Brain Regions

4.1. Verifying the Difference with Relative Error. In order to study the differences between patients with depression and healthy subjects in different brain regions, this characteristic parameter is defined to characterize the relative difference of

the mean value of multivariate transfer entropy between the two groups of experimental samples.

$$\sigma = \frac{\text{MsteEn}_p - \text{MsteEn}_h}{\text{MsteEn}_h}. \quad (2)$$

MsteEn_p represents the mean value of multivariate transfer entropy of patients with depression corresponding to brain channel combination (including symmetric channel combination and asymmetric channel combination). MsteEn_h represents the mean value of multivariate transfer entropy of the corresponding brain region channel combination (including symmetric channel combination and asymmetric channel combination) of healthy control group. σ represents the change range of multivariate transfer entropy of brain channel magnetoencephalogram signal in depression group relative to the healthy control group. The greater the absolute value of σ , the more obvious the difference between them; $\sigma < 0$ represents that the multivariate transfer entropy of patients with depression is smaller than that of normal subjects; $\sigma > 0$ represents that the multivariate transfer entropy of patients with depression is greater than that of normal subjects.

4.1.1. Symmetrical Brain Area Analysis. After calculating the differences of each symmetrical brain region under different frequency bands and the differences of different brain regions under each frequency band with MATLAB [26–28], we can draw a difference comparison columnar statistical chart. It is inconvenient to show all pictures due to space limitation. Take the differences of each symmetrical brain region under frequency band A and the differences of each frequency band in the central region as an example, as shown in Figures 5 and 6.

Figure 5 is the difference comparison statistical diagram of each symmetrical brain region by filtering the EEG signal to the θ band. It can be seen from the figure that under this band, the relative difference of frontal region is the largest, and the effect is the best to distinguish patients with depression from healthy subjects; Figure 6 is the difference comparison statistical chart of filtering EEG signals to each frequency band after selecting the central region as the study brain region. It can be seen from the figure that for this brain region, filtering the EEG signal in the δ band has the best effect on distinguishing patients with depression from healthy subjects; therefore, when using the multivariate transfer entropy algorithm to distinguish patients with depression from healthy subjects, if most of the EEG signals collected are in the θ band, the frontal region is the best; if the collected EEG signal mainly comes from the central region, the best discrimination effect is when the EEG signal is filtered in δ band.

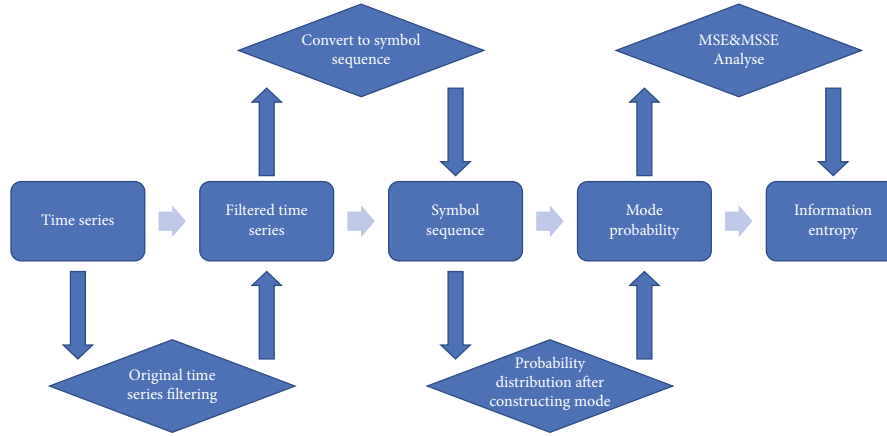


FIGURE 1: Algorithm flowchart.

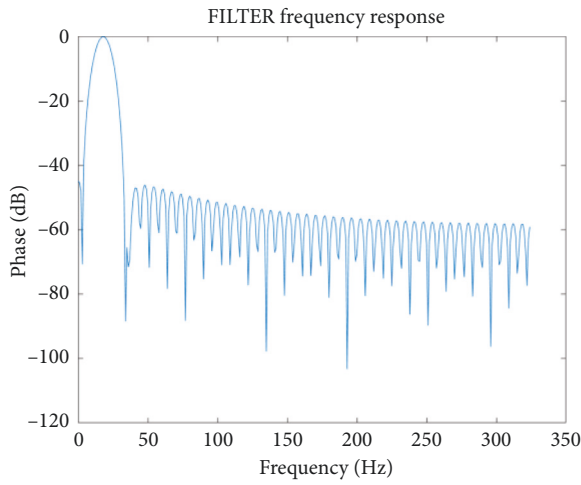


FIGURE 2: Filter frequency response.

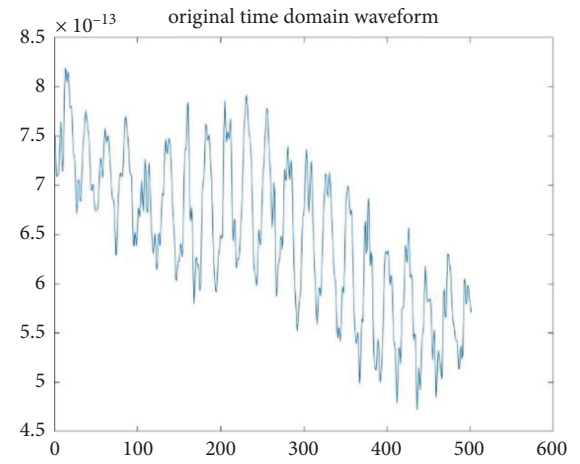


FIGURE 3: Time domain diagram of original EEG signal.

4.1.2. Asymmetric Brain Area Analysis. After calculating the differences of asymmetric brain regions in different frequency bands and the differences of asymmetric brain regions in different frequency bands with MATLAB, we can draw a difference comparison columnar statistical chart. It is inconvenient to show all pictures due to space limitation, taking the multivariate transfer entropy difference between the combination of asymmetric channels from temporal region to central region under δ band and asymmetric channels from left temporal region to left central region under different frequency bands as an example, as shown in Figures 7 and 8.

Figure 7 represents the multivariate transfer entropy difference comparison of the asymmetric channels from the left temporal region to the left central region under different frequency bands. The connection strength difference between the brain region channel combination depression patient group and the healthy control group under each frequency band is obvious, and the discrimination relationship is $\theta > \delta > \alpha > \beta > \gamma$; the multivariable sign transfer entropy difference between depression and healthy people under frequency band θ is greater than that under other frequency bands. Figure 8 represents the relative difference

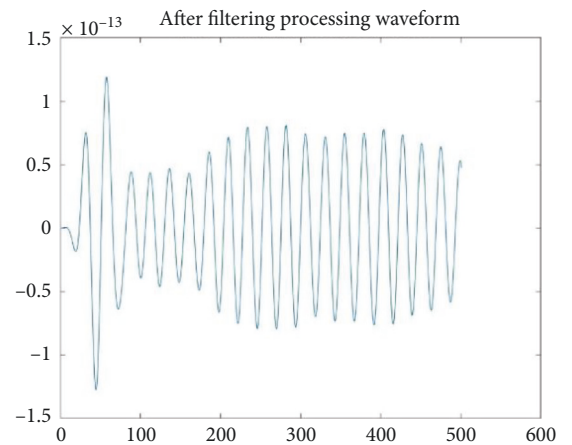


FIGURE 4: Time domain diagram of filtered b-band EEG signal.

under the asymmetric channel combination from temporal region to central region in the δ band. The connection strength of each brain region channel combination, depression patient group, and healthy control group is significantly different, and the differentiation relationship is left temporal region to right center > left temporal region to left

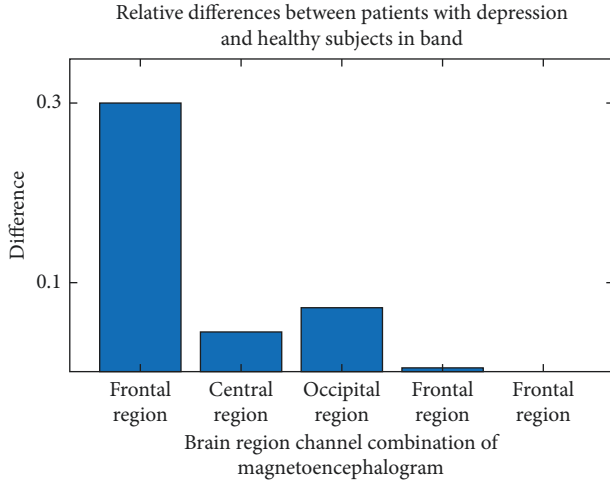


FIGURE 5: Differences of symmetrical brain regions in θ frequency band.

center > right temporal region to left center > right temporal region to left center > right temporal region to right center. The multivariate transfer entropy of depression and healthy people under the combination of left temporal region to right central channel is more different than that under other channel combinations.

4.2. Improved Multivariate Transfer Entropy Analysis for Brain Magnetic Channel Signals in the Same Brain Region.

The study of the four brain regions is divided into left brain region \rightarrow right brain region and left brain region \rightarrow right brain region connectivity analysis. In multivariate analysis, a single variable is controlled as a known condition. When analyzing the central channel of the corresponding brain region of the left and right hemispheric connectivity of the same brain region and the symmetrical and asymmetric channels of the left and right brain regions, when analyzing a single channel, the other two channels remain unchanged as a known condition, and the multivariate transfer entropy of different channel combinations is calculated. Then, do independent sample t -test analysis on differentiated individual subjects to verify whether the normal control group and patients with depression can be significantly distinguished in the corresponding brain regions. Secondly, with the differentiation between the four functional areas, patients with depression and healthy control group are compared. Finally, based on the calculation results of multivariate transfer entropy of the same sample under different stimuli, combined with the existing physiological basis, the changes of brain connectivity in patients with depression and healthy controls under different stimuli are analyzed.

The frontal area is an important part of the brain. The frontal area mentioned in this experiment roughly corresponds to the prefrontal part of the brain and has advanced cognitive functions such as thinking ability. According to the brain asymmetry and the analysis of the same brain area, three frontal channels (left middle and right) are selected to calculate the corresponding multivariate transfer entropy.

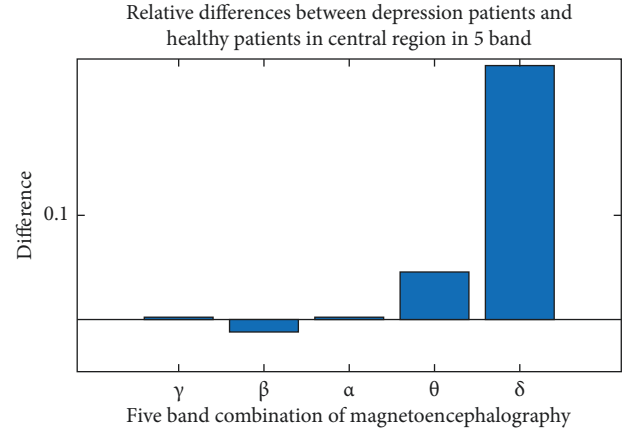


FIGURE 6: Differences of various frequency bands in the central region.

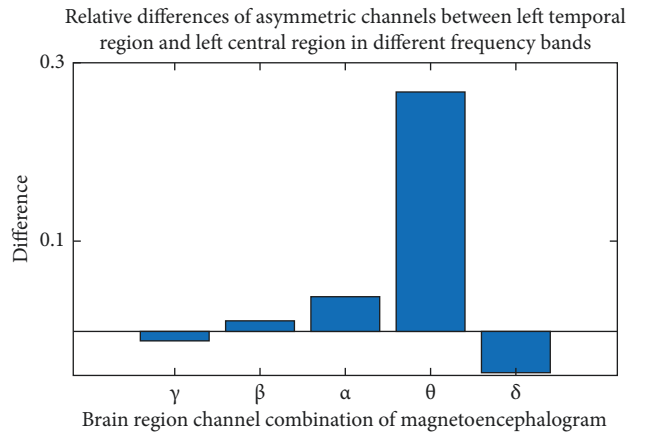


FIGURE 7: Relative difference between left frontal area and left central area under each frequency band.

Because there are too many different combinations of the three channels, the study of simple symmetric channels is too one-sided. In order to make the above experimental conclusions more rigorous, we not only study the symmetric channels but also analyze each channel combination in the left and right frontal regions. For the frontal channel combination, the multivariate transfer entropy in the healthy control group is significantly higher than that in the depression group, but it does not rule out the existence of individual channel combinations. In order to better study the statistical significance of the sample data and study the significance of distinguishing between depression patients and healthy controls in the frontal channel, an independent sample t -test is performed on each channel combination data with SPSS software to verify the significance of multivariate transfer entropy algorithm in distinguishing depression patients and healthy controls. Because there are too many t -test results, only two groups of t -test results are selected here as an example. The P value of t -test results of independent samples in left and right symmetrical frontal area under γ band is $0.004 < 0.05$, that is, there is a significant difference between depression group and healthy control group, as shown in Figures 9 and 10.

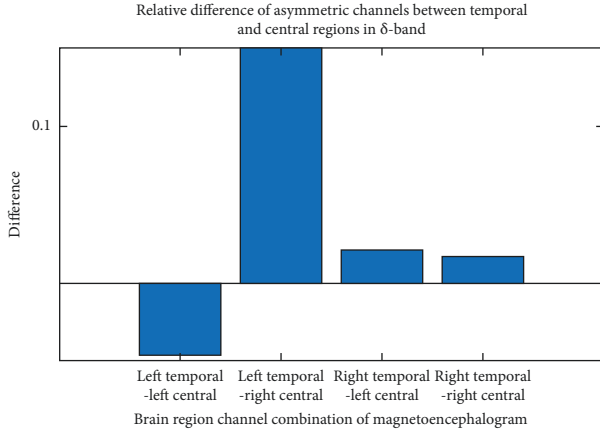


FIGURE 8: Relative difference between temporal region and central region in δ band.

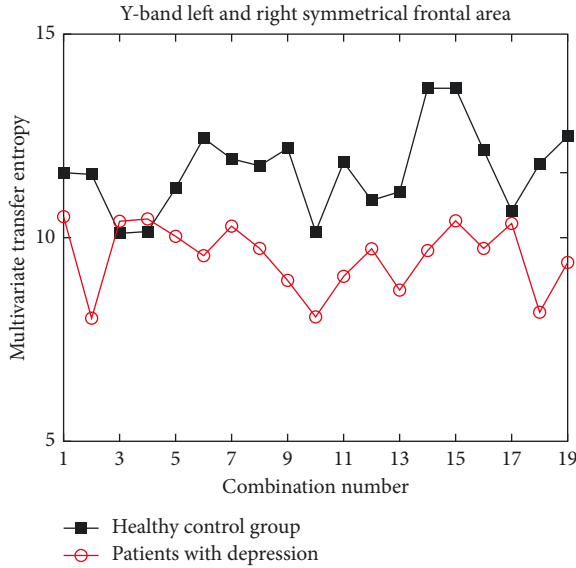


FIGURE 9: Multivariate transfer entropy of left and right symmetrical frontal region in band γ .

Figure 9 shows the comparison of multivariate transfer entropy in the left and right symmetrical frontal regions of patients with depression and healthy controls under band γ . The horizontal axis coordinate is the combination of symmetrical and asymmetric channels in the corresponding brain region, and the vertical axis coordinate is the improved multivariate transfer entropy. The black line represents the healthy control group and the red line represents the depression group. It can be seen from the figure that the multivariate transfer entropy of the healthy control group is generally higher than that of the patients with depression, and the difference is significant. Therefore, taking the γ band subfrontal channel as the research object can provide reference significance for the clinical diagnosis of distinguishing healthy people from patients with depression.

4.3. Counter Example Analysis of Multivariate Transfer Entropy of Brain Magnetic Channels in Different Brain

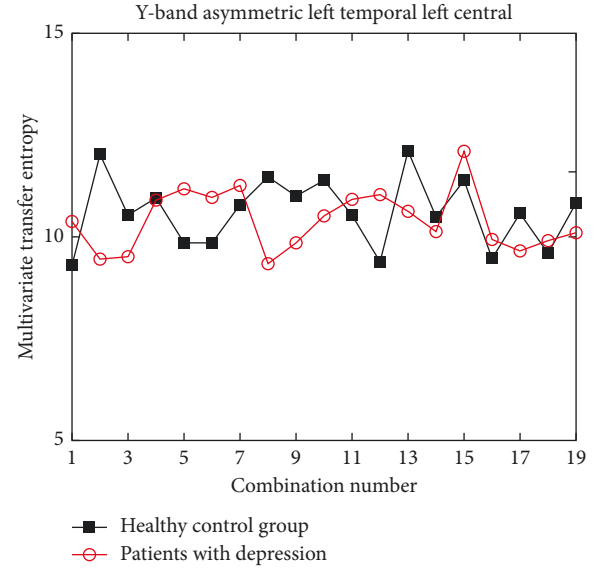


FIGURE 10: Multivariate transfer entropy of left temporal and left central region under γ band.

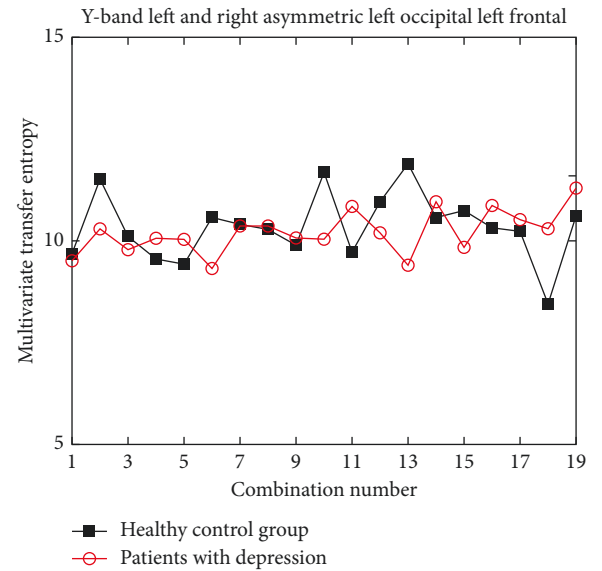


FIGURE 11: Multivariate transfer entropy of left occipital and left frontal region under γ band.

Functional Areas. Under different wave bands, for the channel combinations that meet the difference in different brain functional areas, the improved multivariate transfer entropy in the healthy control group is significantly higher than that in the depression group, but it does not rule out the existence of individual channel combinations. Due to space limitations, it is not convenient to show all the example diagrams in this paper. Here, only two indistinguishable counter examples are shown, as shown in Figures 10 and 11.

The experimental results show that under the γ band, the discrimination between the left temporal region \rightarrow the left central region, the left frontal region \rightarrow the left occipital region is small, and the two are close and almost indistinguishable. Therefore, when selecting asymmetric brain

regions as the research object under γ band, we need to carefully consider the specific brain regions selected, such as between the left temporal region and the left central region, which is difficult to provide reference significance for clinically distinguishing healthy people from patients with depression.

5. Summary

The results show that the multivariate transfer entropy method and frequency division brain region research proposed in this paper can well distinguish the symmetrical channel combination of various symptomatic brain regions of normal people and patients with depression. The synergistic value of multiple TE: the symmetrical meridians of frontal lobe in healthy people are significantly higher than those in patients with depression, especially when the target object is the frontal lobe of γ band, the difference is the most significant, which indicates that the brain activities of healthy people have better connectivity than those in patients with depression. We hope that the experimental methods provided in this paper will help to further study the difference between patients with depression and healthy people, which can provide some help for clinical diagnosis and treatment of depression.

Data Availability

The data used to support the findings of this study are available from the corresponding author upon request.

Conflicts of Interest

The authors declare that there are no conflicts of interest.

Acknowledgments

Project was supported by Students' Innovation and Entrepreneurship Training Program (Grant No. SZDG2021034).

References

- [1] E. Rejaibi, A. Komaty, F. Meriaudeau, S. Agrebi, and A. Othmani, "MFCC-based Recurrent Neural Network for automatic clinical depression recognition and assessment from speech," *Biomedical Signal Processing and Control*, vol. 71, p. 14, 2022.
- [2] S. Hashempour, R. Boostani, M. Mohammadi, and S. Sanei, "Continuous scoring of depression from EEG signals via a hybrid of convolutional neural networks," *IEEE Transactions on Neural Systems and Rehabilitation Engineering*, vol. 30, pp. 176–183, 2022.
- [3] Y. Zheng, Y. Xia, W. Ye, and C. Zheng, "The effect of skin-to-skin contact on postoperative depression and physical recovery of parturients after cesarean section in obstetrics and gynecology department," *Computational and Mathematical Methods in Medicine*, vol. 2022, Article ID 9927805, 8 pages, 2022.
- [4] J. Xu, K. He, K. Zhang et al., "Low-dose copper exposure exacerbates depression-like behavior in ApoE4 transgenic mice," *Oxidative Medicine and Cellular Longevity*, vol. 2021, Article ID 6634181, 30 pages, 2021.
- [5] L. Xu, J. Hou, and J. Gao, "A novel smart depression recognition method using human-computer interaction system," *Wireless Communications and Mobile Computing*, vol. 2021, Article ID 5565967, 8 pages, 2021.
- [6] J. Yang, G. Zhou, Z. Ou, N. Jia, and D. Wang, "The effect and mechanism of exercise training on rats with poststroke depression based on the intestinal flora," *Computational and Mathematical Methods in Medicine*, vol. 2021, Article ID 3567447, 12 pages, 2021.
- [7] M. Dai, Q. Wei, Y. Zhang, C. Fang, P. Qu, and L. Cao, "Predictive value of red blood cell distribution width in poststroke depression," *Computational and Mathematical Methods in Medicine*, vol. 2021, Article ID 8361504, 6 pages, 2021.
- [8] L. Li, B. Lei, and C. Mao, "Digital twin in smart manufacturing," *Journal of Industrial Information Integration*, vol. 26, no. 9, Article ID 100289, 2022.
- [9] L. Li, T. Qu, Y. Liu et al., "Sustainability assessment of intelligent manufacturing supported by digital twin," *IEEE Access*, vol. 8, pp. 174988–175008, 2020.
- [10] L. Li and C. Mao, "Big data supported PSS evaluation decision in service-oriented manufacturing," *IEEE Access*, vol. 8, pp. 154663–154670, 2020.
- [11] L. Li, C. Mao, H. Sun, Y. Yuan, and B. Lei, "Digital twin driven green performance evaluation methodology of intelligent manufacturing: hybrid model based on fuzzy rough-sets AHP, multistage weight synthesis, and PROMETHEE II," *Complexity*, vol. 2020, no. 6, 24 pages, Article ID 3853925, 2020.
- [12] Z. Ma, "Mental health education of freshmen in higher vocational colleges under information technology," in *Proceedings of the 2021 4th International Conference on Information Systems and Computer Aided Education, ICISCAE*, pp. 701–705, IEEE, New York, NY, USA, September 2021.
- [13] D. Lamela, J. Cabral, S. Coelho, and I. Jongenelen, "Personal stigma, determinants of intention to use technology, and acceptance of internet-based psychological interventions for depression," *International Journal of Medical Informatics*, vol. 136, Article ID 104076, 2020.
- [14] F. Li, "Opportunities and challenges of educational psychology under the influence of information technology," in *Proceedings of the 2020 5th International Conference on Mechanical, Control and Computer Engineering ICMCE*, pp. 1802–1805, IEEE, Harbin, China, December 2020.
- [15] J. Liu, S. Sun, Y. Liu et al., "A novel MEGNet for classification of high-frequency oscillations in magnetoencephalography of epileptic patients," *Complexity*, vol. 2020, Article ID 9237808, 9 pages, 2020.
- [16] Weber, J. Douglas, G. Sudre et al., "A Real-Time Software Interface for Magnetoencephalography," *Computational Intelligence and Neuroscience*, vol. 2011, p. 17, Article ID 327953, 2011.
- [17] M. Altamura, T. E. Goldberg, B. Elvevg et al., "Prefrontal cortex modulation during anticipation of working memory demands as revealed by magnetoencephalography," *International Journal of Biomedical Imaging*, vol. 2010, Article ID 840416, 10 pages, 2010.
- [18] Z. Yuan, W. Yan, J. Wang, J. Li, and F. Hou, "Analysis of depression magnetoencephalography based on modified permutation entropy," in *Proceedings of the 2018 11th International Congress on Image and Signal Processing, Bio-Medical Engineering and Informatics, CISP-BMEI*, pp. 1–5, IEEE, Beijing, China, October 2018.

- [19] J. Hu, W. Yan, J. Wang, J. Li, and F. Hou, "Analysis of bi-variate time series of magnetoencephalography for depression based on granger kernel method. 3rd international conference on biological information and biomedical engineering," in *Proceedings of the 3rd International Conference on Biological Information and Biomedical Engineering*, pp. 213–218, VDE, Hangzhou, China, July 2019.
- [20] T. Lei and R. Li, Y. Man and H. Fu, Dynamics analysis and fractional-order approximate entropy of nonlinear inventory management systems," *Mathematical Problems in Engineering*, vol. 2021, Article ID 5516703, 8 pages, 2021.
- [21] A. M. Adam, E. N. Gyamfi, K. A. Kyei, S. Moyo, and R. S. Gill, "A New EEMD-Effective Transfer Entropy-Based Methodology for Exchange Rate Market Information Transmission in Southern Africa Development Community," *Complexity in Financial Markets*, vol. 2021, Article ID 3096620, 8 pages, 2021.
- [22] K. S. Manic, R. Biju, W. Patel et al., "Extraction and evaluation of corpus callosum from 2D brain mri slice: a study with cuckoo search algorithm," *Computational and Mathematical Methods in Medicine*, vol. 2021, Article ID 5524637, 2 pages, 2021.
- [23] X. Fu, Y. Wang, and A. Belkacem, A. Nasreddine, Q. Zhang, C. Xie, Y. Cao, H. Cheng, and S. Chen, "Integrating optimized multiscale entropy model with machine learning for the localization of epileptogenic hemisphere in temporal lobe epilepsy using resting-state fMRI," *Journal of Healthcare Engineering*, vol. 2021, Article ID 1834123, 10 pages, 2021.
- [24] A. Naseem, M. A. Rehman, and J. Younis, "Some Real-Life Applications of a Newly Designed Algorithm for Nonlinear Equations and its Dynamics via Computer Tools," *Complexity, Dynamics, Control, and Applications of Nonlinear Systems with Multistability*, vol. 2021, Article ID 9234932, 9 pages, 2021.
- [25] S.-C. Chang, "Study on nonlinear dynamics and chaos suppression of active magnetic bearing systems based on synchronization," *Mathematical Problems in Engineering*, vol. 2021, Article ID 5549775, 10 pages, 2021.
- [26] W. Guo, Y. Zhao, R. Li, H. Ding, and J. Zhang, "Active Disturbance Rejection Control of Valve-Controlled Cylinder Servo Systems Based on MATLAB-AMESim Cosimulation. Complexity," *Learning and Adaptation for Optimization and Control of Complex Renewable Energy Systems*, vol. 2020, Article ID 9163675, 10 pages, 2020.
- [27] F. Jiang, M. Li, J. Wen, Z. Tan, and W. Zhou, "Optimization analysis of engine intake system based on coupling matlab-simulink with GT-power," *Mathematical Problems in Engineering*, vol. 2021, Article ID 6673612, 17 pages, 2021.
- [28] Y. Zhang, Y. Zhang, J. Chen, W. Yan, Z. Chen, and J. Wang, "Magnetoencephalogram analysis of depression based on multivariable sign transfer entropy," *Journal of Physics: Conference Series*, vol. 1592, 2020.

Retraction

Retracted: Quality Evaluation of Ideological and Political Education in Universities Based on BP Neural Network

Computational Intelligence and Neuroscience

Received 25 July 2023; Accepted 25 July 2023; Published 26 July 2023

Copyright © 2023 Computational Intelligence and Neuroscience. This is an open access article distributed under the Creative Commons Attribution License, which permits unrestricted use, distribution, and reproduction in any medium, provided the original work is properly cited.

This article has been retracted by Hindawi following an investigation undertaken by the publisher [1]. This investigation has uncovered evidence of one or more of the following indicators of systematic manipulation of the publication process:

- (1) Discrepancies in scope
- (2) Discrepancies in the description of the research reported
- (3) Discrepancies between the availability of data and the research described
- (4) Inappropriate citations
- (5) Incoherent, meaningless and/or irrelevant content included in the article
- (6) Peer-review manipulation

The presence of these indicators undermines our confidence in the integrity of the article's content and we cannot, therefore, vouch for its reliability. Please note that this notice is intended solely to alert readers that the content of this article is unreliable. We have not investigated whether authors were aware of or involved in the systematic manipulation of the publication process.

Wiley and Hindawi regrets that the usual quality checks did not identify these issues before publication and have since put additional measures in place to safeguard research integrity.

We wish to credit our own Research Integrity and Research Publishing teams and anonymous and named external researchers and research integrity experts for contributing to this investigation.

The corresponding author, as the representative of all authors, has been given the opportunity to register their agreement or disagreement to this retraction. We have kept a record of any response received.

References

- [1] Y. Ding, W. Zeng, and Z. Ning, "Quality Evaluation of Ideological and Political Education in Universities Based on BP Neural Network," *Computational Intelligence and Neuroscience*, vol. 2022, Article ID 8336895, 7 pages, 2022.

Research Article

Quality Evaluation of Ideological and Political Education in Universities Based on BP Neural Network

Yunxia Ding , Wei Zeng, and Zhen Ning

Jiangxi University of Technology, Nanchang 330098, China

Correspondence should be addressed to Yunxia Ding; dingyunxia@jxut.edu.cn

Received 14 April 2022; Revised 12 May 2022; Accepted 25 May 2022; Published 18 July 2022

Academic Editor: Dong Chen

Copyright © 2022 Yunxia Ding et al. This is an open access article distributed under the Creative Commons Attribution License, which permits unrestricted use, distribution, and reproduction in any medium, provided the original work is properly cited.

At present, there are some problems in the research of curriculum ideological and political quality evaluation, such as insufficient theme attention, insufficient theoretical research, incomplete data collection, and so on. This study aims to use the BP neural network in the ideological and political quality evaluation system so that the system can more comprehensively and accurately reflect the actual situation of students and point out the direction for the development of students' ideological and political education. The construction of this system can provide a very considerable and accurate way for the quality evaluation of ideological and political education of college students and especially solves the problems of human subjective, factor errors, and the setting of evaluation index weights in the evaluation system.

1. Introduction

Since the reform and opening up, the reform of ideological and political theory classroom teaching in universities nationwide has been continuously going on, although great achievements have been made. However, the reform of classroom teaching of ideological and political theory course has been concentrated on teaching content and curriculum, while the reform of classroom teaching index system evaluation of ideological and political theory course seems to be rather lagging behind [1–3]. The so-called teaching quality evaluation is to assess the standard, efficiency, and quality of teaching activities according to the teaching objectives, and to estimate and judge the value of teaching. The talent training effect is the primary standard for the evaluation of curriculum ideological and political construction. It is necessary to establish and improve the multidimensional evaluation system and supervision and inspection mechanism of curriculum ideological and political construction effect, and implement it in all kinds of evaluation work and deepen the reform of education and teaching in colleges and universities.

Although many teachers engaged in teaching ideological and political theory courses also attach great importance to the research and summary of teaching experience and methods, the research results of the classroom teaching

evaluation index system with weight are rare. Based on the above analysis, how to improve the teaching level and quality of ideological and political theory courses in universities, the study of classroom teaching evaluation index and its system is fundamental to improve the level and quality. Therefore, the construction of a curriculum ideological and political quality evaluation system is of great significance. It is the guarantee measure to promote the full implementation of curriculum ideological and political education, the measurement standard to test the quality of curriculum ideological and political teaching, and the feedback mechanism to improve the effectiveness of curriculum ideological and political education.

This study is the first attempt to use the BP neural network modeling to evaluate the effectiveness of online ideological and political education in universities. The research results show that the BP neural network can effectively improve the precision of college ideological and political classroom teaching quality evaluation and provide a new method and way for college ideological and political classroom teaching quality evaluation.

2. Features of BP Neural Network Model

The artificial neural network model does not require any a priori formula and has the advantages of self-learning, self-

organization, self-adaptation, good fault tolerance, and strong nonlinear mapping ability, which is especially suitable for the processing of pattern recognition, data mining, and classification problems with complex variables and relationships.

The BP neural network is the most widely used artificial neural network algorithm, and the characteristics of the BP neural network model are as follows: each layer neuron is only connected with the neighboring layer neuron; there is no connection between neurons in each layer; and there is no feedback connection between neurons in each layer. The learning process is characterized by two parts: forward propagation of data and backward propagation of error, and the most suitable network model for the sample is built by continuously reducing the error. The BP neural network has infinite approximation of nonlinear mapping capability, powerful parallel processing capability, self-learning, self-organization and self-adaptability, data inclusion capability, and effective complex variable processing capability, which is especially suitable for multivariate function simulation, pattern recognition, judgment, classification, data processing, and other problems.

The BP neural network model is currently widely used in various disciplines. Wang [4] proposed a general public budget revenue forecasting analysis model based on gray forecasting and BP neural network and applied it in the case of Wuxi city. Ma [5] evaluated the effectiveness evaluation of online ideological and political education in colleges and universities based on the BP neural network. Wu et al. [6] studied the error compensation for airborne laser ranging based on the BP neural network. Lee et al. [7] integrated a cloud-based BP system with CPOE to improve self-management of the hypertensive patients and carried out a randomized controlled trial. These existing studies provide a reference for the work of this study.

3. The Problems of the Traditional Evaluation System of Ideological and Political Education in Universities

3.1. Single Evaluation Subject. Nowadays, the evaluation system of teachers' teaching quality is commonly carried out in all universities in China, such as students' evaluation of teachers, peer evaluation, administrative leaders' evaluation, experts' evaluation, and teachers' self-evaluation. The subjects of evaluation are students, peer teachers, administrators, and teachers' self-evaluation, which are usually evaluated by some combination of these four evaluation subjects, each of which has its own advantages and disadvantages. No matter which evaluation method is used, it is a one-sided evaluation with limitations, while teachers' teaching activity is a comprehensive activity with complexity and creativity.

3.2. Incomplete Evaluation Indicators. The teaching quality evaluation index is what evaluation index is the angle or dimension of measuring things. At present, most higher educational institutions in China have established a teaching quality evaluation index system, and the evaluation content

versions of each university are similar, including teaching methods, teaching attitudes, teaching effects, and other aspects. The content of the evaluation is relatively simple, as if classroom theoretical teaching is all the evaluation of teaching quality. Some important contents, such as practical training teaching, engineering practice ability, students' comprehensive quality, and whether the specification and quality of cultivated talents meet the needs of the society, are excluded from the evaluation scope, forming a narrow object of teaching evaluation and a flat object coverage, which cannot comprehensively reflect the teaching quality.

3.3. Distortion of Evaluation Results. In recent years, the participation of college students as the main body in teachers' teaching evaluation has become a common way of teaching evaluation in China's universities. As the direct objects of classroom teaching, students have the most detailed understanding and deepest feelings about teachers' teaching attitude, teaching level, teaching effect, and teachers' moral standards, so they have the most right to evaluate. However, it is a long-standing controversial issue whether students, as the main subjects of teaching quality monitoring and evaluation, are objective and credible in their evaluation results. Those who resist and oppose are mainly from teachers, and there are many good teachers. There are two main reasons for this: one is that good teachers with strong dedication, strict requirements for students, and never "accommodating" students in examination results are not "well-rewarded," and the other is that they are worried that it will mislead teachers to lower their requirements for students and cater to and accommodate students, which will have a negative impact on teaching quality. The practice of teaching quality monitoring and evaluation proves that these two tendencies do exist, and to a certain extent, they also distort the results of teaching quality monitoring and evaluation.

4. Construction of the Evaluation System of Ideological and Political Education Quality in Universities Based on BP Neural Network

4.1. Teachers' Teaching Quality Evaluation Index System. The evaluation index system refers to an organic whole with an internal structure composed of multiple indexes representing the characteristics of all aspects of the evaluation object and their interrelations. There must be a certain logical relationship between each index. They should not only reflect the main characteristics and states of each subsystem from different aspects, but also reflect the internal relationship between each subsystem. Each subsystem is composed of a group of indicators, which are independent and connected with each other to form an organic unity. The construction of the index system is hierarchical, from top to bottom, from macro to micro, forming an inseparable evaluation system.

Teaching quality evaluation must first determine a scientific teaching quality evaluation index system. In this study, based on the in-depth interviews with some teachers

TABLE 1: Teaching quality evaluation index system of college teachers.

Primary indicators	Secondary indicators	Tertiary indicators
Teacher teaching quality	I ₁ Instructional prerequisites	I ₁₁ Teachers' commitment and responsibility to teaching
		I ₁₂ Teachers' ability to teach and learn
		I ₁₃ Teachers' subject knowledge
		I ₁₄ Teachers' research achievements and research ability
	I ₂ Teaching process	I ₂₁ The scientific nature of teaching content and the effective information it contains
		I ₂₂ Reasonableness of teachers' teaching methods
		I ₂₃ The development of students' interest in learning
		I ₂₄ Whether the teacher has a suitable professional personality and teaching characteristics
	I ₃ Teaching effect	I ₂₅ Adaptability of teaching contents to students' needs
		I ₂₆ Teachers' compliance with school teaching regulations and discipline
		I ₃₁ The ideological, political, and moral qualities of students
		I ₃₂ Students' acquisition of basic professional knowledge and general knowledge
		I ₃₃ The improvement of students' practical and self-efficacy

and students of a university and the summary of teaching quality evaluation research theories and practices in higher educational institutions at home and abroad, a comprehensive evaluation index system of teachers' teaching quality in various aspects such as teachers' teaching prerequisite factors, teaching process, and teaching effect is constructed (Table 1).

4.2. Teaching Quality Evaluation Model and Application

4.2.1. Evaluation Model Construction. From the evaluation index system of teaching quality of university teachers, it can be seen that the factors affecting their teaching quality mainly include four categories of teaching prerequisites, such as teachers' commitment and responsibility to teaching, teachers' education and teaching ability, teachers' subject knowledge quality, and teachers' scientific research achievements and scientific research ability. The factors involved in the teaching process are six categories: the scientificity of the teaching contents and the amount of effective information contained in them, the reasonableness of the teaching methods, the cultivation of students' interest in learning, the appropriateness of the teachers' professional personality and teaching characteristics, the adaptability of the teaching contents to the students' needs, and the teachers' compliance with the school's teaching regulations and discipline. The improvement of students' political thought and moral quality, the acquisition of students' basic professional knowledge and general knowledge, and the improvement of students' practice and self-development ability are represented as $I_{11}, I_{12}, I_{13}, I_{14}, I_{21}, I_{22}, I_{23}, I_{24}, I_{25}, I_{26}, I_{31}, I_{32}, I_{33}$. If the teaching quality evaluation process of university teachers is modeled as a BP neural network system, the system is studied by taking teaching quality as the output of the system and all the influencing factors affecting teaching quality as the input of the system (multiple inputs).

The BP network is a hierarchical feedforward neural network consisting of an input layer, intermediate layer, and output layer. The intermediate layer can be extended into multiple layers; the neurons are connected between adjacent layers and within the same layer according to a certain

structure; and the learning training is conducted in the way the teacher shows and teaches to determine the threshold value of each neuron and the weight value between each neuron, so that the neural network has a certain "function" or "intelligence." However, the BP neural network itself has some defects and shortcomings, mainly including slow convergence speed, easy to input local minimal, difficult to determine the appropriate number of hidden layers and hidden nodes, and poor prediction effect on data with large numerical quantity relationship [6–9]. To address the shortcomings of "slow convergence speed" and "poor prediction for data with large numerical relationships," the standard BP algorithm (i.e., absolute error backpropagation algorithm) is improved by applying the relative error of the data as the error signal. This study applies the relative error of data as the error signal to improve the standard BP algorithm (i.e., absolute error backpropagation algorithm) in order to improve the accuracy of the BP neural network. For establishing the neural network model with the function of "university teaching quality evaluation," this study adopts the "three-layer" BP network, the number of neurons in the first input layer (13 evaluation indexes affecting its teaching quality) is 13, the number of neurons in the second intermediate layer is 28, and the number of structural neurons in the third layer is 28. The number of neurons of the third output layer (teaching quality) is 1. The BP network [10–14] is trained by using the teaching quality evaluation data to find out the correlation between the teaching quality and the evaluation indexes of university teachers. Then, they further rely on the trained BP network to calculate the teaching quality of teachers under different influencing factors (each evaluation index).

The specific learning training algorithm is implemented as follows:

- (1) N sets of training samples from the teaching quality evaluation data are selected as the BP network input and output samples for training, and the remaining data are used as the test samples. For the k th sample, we set the BP network input pattern vector $U^k = (u_1^k, u_2^k, \dots, u_s^k)$ (s is the number of neurons in the network input layer 13) corresponding to the desired

output vector $X^k = (x_1^k, x_2^k, \dots, x_q^k)$ (q is the number of neurons in the network output layer 1), the output layer unit input vector $M^k = (m_1^k, m_2^k, \dots, m_q^k)$, the output layer unit output vector $N^k = (n_1^k, n_2^k, \dots, n_p^k)$, the intermediate layer unit input vector $G^k = (g_1^k, g_2^k, \dots, g_p^k)$, the intermediate layer unit output vector $H^k = (h_1^k, h_2^k, \dots, h_p^k)$ (p is the number of intermediate layer neurons 28), input layer to intermediate layer connection weight is v_{jt} ($j = 1, 2, \dots, p$; $t = 1, 2, \dots, q$), intermediate layer unit threshold is θ_j ($j = 1, 2, \dots, p$), output layer unit threshold is γ_t ($t = 1, 2, \dots, q$), η is the learning rate, and network response function $f(x) = 1/(1 + e^{-x})$.

- (2) We assign the initial values of weights and thresholds $w_{ij}(n)$, $v_{jt}(n)$, $\gamma_t(n)$, and $\theta_j(n)$ to random values in the interval $[-1, 1]$, and set $n = 0$ and $k = 0$.
- (3) We set $k = k + 1$, assign the values of $I_{11}, I_{12}, I_{13}, I_{14}, I_{21}, I_{22}, I_{23}, I_{24}, I_{25}, I_{26}, I_{31}, I_{32}, I_{33}$ of the k th set of sample data in the N sets of training samples to the elements $U_1^k, U_2^k, U_3^k, U_4^k, U_5^k, U_6^k, U_7^k, U_8^k, U_9^k, U_{10}^k, U_{11}^k, U_{12}^k, U_{13}^k$ in the input pattern vector U^k , and assign the values of teacher teaching quality I to the elements X_1^k in the output vector X^k .
- (4) According to equations (1) and (2), the actual outputs of the intermediate layer and the output layer are calculated as h_j^k and n_t^k .

The output layer is as follows:

$$\begin{cases} \text{input: } m_t^k = \sum_{j=1}^p v_{jt} h_j^k - \gamma_t, & (t = 1, 2, \dots, q; k = 1, 2, \dots, N), \\ \text{output: } n_t^k = f(m_t^k), \end{cases} \quad (1)$$

$$\begin{cases} \text{input: } g_j^k = \sum_{i=1}^s w_{ij} u_i^k - \theta_j & (j = 1, 2, \dots, p; k = 1, 2, \dots, N), \\ \text{output: } h_j^k = f(g_j^k). \end{cases} \quad (2)$$

- (5) The steepest gradient descent method is used to learn multilayer error correction for the network. The standard BP algorithm usually uses absolute error as the error transfer signal in the process of calculating values, which often makes the error large. This is due to the fact that absolute error tends to invariably magnify the overall error value of the system without considering the relationship with the actual value, which results in less accurate and slower final prediction results. The use of relative error as the transmission signal of the BP neural network error can well avoid the impact of such shortcomings. That is, the absolute error in the standard BP algorithm $(x_t^k - n_t^k)$ is replaced by the relative error $(x_t^k - n_t^k)$, and the generalized error sum of each unit in the

output and intermediate layers is calculated by using equations (3) and (4).

$$d_t^k = \frac{(x_t^k - n_t^k) n_t^k (1 - n_t^k)}{(x_t^k)^2}, \quad (t = 1, 2, \dots, N), \quad (3)$$

$$e_j^k = \left[\sum_{t=1}^q d_t^k \cdot v_{jt} \right] h_j^k (1 - h_j^k), \quad (j = 1, 2, \dots, p). \quad (4)$$

- (6) If $k = N$, then we go to equation (7); otherwise, we go to equation (4) to continue the execution.
- (7) We correct the connection weights v_{jt} and thresholds γ_t with the generalized error of each unit in the output layer d_t^k and the output of each unit in the intermediate layer h_j^k , as shown in equations (5) and (6); we correct the connection weights h_j^k and thresholds θ_j with the generalized error of each unit in the intermediate layer e_j^k and the input of each unit in the input layer, $U^k = (u_1^k, u_2^k, \dots, u_s^k)$, as shown in equations (7) and (8); and we set $k = 0$.

$$v_{jt}(n+1) = v_{jt}(n) + \eta \sum_{k=1}^N d_t^k h_j^k, \quad (5)$$

$$\gamma_t(n+1) = \gamma_t(n) + \eta \sum_{k=1}^N d_t^k, \quad (6)$$

$$\theta_j(n+1) = \theta_j(n) + \eta \sum_{k=1}^N e_j^k, \quad (7)$$

$$w_{ij}(n+1) = w_{ij}(n) + \eta \sum_{k=1}^N e_j^k u_i^k. \quad (8)$$

- (8) It is recalculated with the new weights and thresholds $h_j^k n_t^k$ ($k = 1, 2, \dots, N$). According to the accuracy requirement, if for each k ($k = 1, 2, 3, \dots, N$) and each t ($t = 1, 2, 3, \dots, q$) are satisfied: $\|x_t^k - n_t^k\| < \varepsilon$ (ε is a given precision and set $\varepsilon = 10^{-6}$) then learning stops. Otherwise, we set $k = 0$, go to equation (4), and remodify the weights and thresholds until the error accuracy requirement is satisfied.
- (9) Using the trained BP network [15–18], the values of $I_{11}, I_{12}, I_{13}, I_{14}, I_{21}, I_{22}, I_{23}, I_{24}, I_{25}, I_{26}, I_{31}, I_{32}, I_{33}$ in the input test samples are assigned to the elements $U_1^k, U_2^k, U_3^k, U_4^k, U_5^k, U_6^k, U_7^k, U_8^k, U_9^k, U_{10}^k, U_{11}^k, U_{12}^k, U_{13}^k$ in the input pattern vector U^k , and the values of the elements n_1^k in the output vector, i.e., $N^k = (n_1^k, n_2^k, \dots, n_q^k)$, the value of teacher teaching quality I , are predicted by simulation.

4.2.2. System Implementation and Application. In this study, a total of 30 students in different classes taught by teachers of two main courses in a university are used as the survey samples, and the surveyed students rate the teachers' performance on each subevaluation index and the overall

TABLE 2: Results of teaching quality.

Number	Overall teaching quality score	Relative error (%)	Number	Overall teaching quality score	Relative error (%)
1	90	0	16	95.22	5.8
2	65.53	9.22	17	74.91	-0.12
3	77.17	2.89	18	47.4	5.33
4	81.36	8.48	19	81.91	9.21
5	98.26	9.18	20	64.17	6.95
6	64.84	8.07	21	60.79	1.32
7	81.55	8.73	22	65.08	8.47
8	60.57	0.95	23	81.12	8.16
9	80.14	6.85	24	92.67	2.97
10	74.44	-0.75	25	60.75	1.25
11	60.25	0.42		63.96	6.6
12	48.66	8.13		77.94	3.96
13	60.62	1.03	Inspection sample	82.15	9.53
14	60.85	1.42		60.85	1.42
15	60.95	1.58		61.22	2.03

situation of teachers' teaching quality, respectively. The scores for the overall situation of each index are 1 (poor), 2 (general), 3 (good), and 4 (excellent), corresponding to scores of 45, 60, 75, and 90, respectively.

Using the established evaluation model [17, 18] of university teachers' teaching quality, the first 25 sets of survey data were fitted to the designed evaluation model to solve the unknown parameters in the evaluation model, and the last 5 sets of survey data were used as the test sample data. The evaluation model with the determined parameters was used to calculate the data of the 25 groups of samples that participated in the modeling and the data of the 5 groups of samples that did not participate in the modeling. Combined with the evaluation model, the data were processed with the simulation software system for evaluating the teaching quality of college teachers developed by Microsoft Visual Studio based on the Windows 8 x64 platform, and the results shown in Table 2 are obtained. From the table, it can be seen that the results obtained by the teacher teaching evaluation model based on the optimized neural network are very good, and the relative error is less than 10%.

5. Suggestions for Optimizing the Effectiveness of Ideological and Political Teaching in Universities

5.1. Establish a High-Quality and High-Skilled Ideological and Political Science Teachers' Team. Cultivating teachers' comprehensive quality and establishing a high-quality and high-skilled civic and political science teachers' team are the main prerequisites for strengthening and improving the effectiveness of ideological and political teaching in universities under the new situation. Combined with the actual situation, ideological and political teachers first need to cultivate theoretical literacy, constantly enrich themselves on the basis of establishing the awareness of lifelong learning, learning advanced knowledge, paying attention to social hotspots, while keeping good contact with students, understanding students' confusion and needs, and helping them solve problems in time; second, they need to cultivate

moral cultivation, use the method of linking theory to practice to teach students, and be a good role model for them. This method of using practical actions to educate students is more effective than purely theoretical teaching, and it is easy to gain students' recognition; finally, it is necessary to cultivate the educational ability, to play a variety of roles in teaching, such as organizer, guide, coordinator, and manager, to respect the main position of students, to create an equal and harmonious teaching environment, to strengthen practical teaching while focusing on theoretical teaching, and to further improve the relevance and effectiveness of teaching, and effectiveness.

5.2. Pay Attention to the Cultivation of Students' Sense of Identity in Ideology and Politics. Understanding students' needs and cultivating students' sense of identity in ideology and politics are important basis for strengthening and improving the effectiveness of ideological and political teaching in universities under the new situation. Students are the main body of classroom teaching, and today, with the continuous development of new curriculum reform, it has become the consensus of college education to play the main role of students and respect students' interests and demands. Compared with other courses, the ideological and political course has certain advantages in the propagation and learning of party policies. Teachers need to use this advantage to highlight the role and charm of the ideological and political course and inspire students to pay attention to the ideological and political learning. In addition, teaching ideology and politics is a practical subject, and when teaching in practice, it is necessary to combine students' interests and personality characteristics to design activities, and to cultivate students' healthy personalities while enjoying their body and mind. Therefore, civic teachers need to stimulate students' participation in practical teaching through multiple channels, give students more free time and space in the specific practice process, and guide them to use what they have learned to solve real-life problems, so that they can further realize the importance and necessity of ideological and political teaching and thus develop a sense of identity.

5.3. Reflect the Rationality and Scientificity of Teaching Objectives. The setting of teaching objectives is crucial for any lesson; ideological and political teaching in universities is no exception; and teaching objectives are the main basis for judging the degree of effectiveness of its teaching. Ideological and political teaching emphasizes the combination of theoretical and practical teaching, among which the setting and selection of practical teaching objectives have a direct impact on teaching content, teaching evaluation, and teaching form, and should be paid great attention. The general goal is the general goal of theoretical teaching, which is to improve students' understanding of the connotation and spirit of Marxism, their ability to apply Marxist concepts and methods, to establish correct learning concepts, to clarify their duties and obligations, and to take the initiative to learn and move forward in the direction of excellent socialist builders through participation in practical activities. It should be noted that the specific goal system should cover various aspects, such as knowledge, skills, and emotions.

5.4. Play the Role of Modern Media to Improve the Effect of Teaching Mode. In today's increasingly popular network, multimedia computers and other media gradually come into the life of college students, changing their learning style and thinking mode; multimedia computers and other media are new media in the background of the new situation; and there are certain differences with traditional media. The teachers of higher education need to compare the new media with the traditional media on the basis of understanding the characteristics of the new media, give the traditional media new connotation, and establish an interactive teaching method that meets the requirements of the new situation, so as to achieve the purpose of enriching the content of ideological and political teaching and improving the relevance and effectiveness of ideological and political teaching. Second, they need to respect students' main position, design teaching around students, and change students' passive acceptance into active learning; finally, they need to build an equal and harmonious teaching environment, and promote the realization of equality and dialogue among subjects.

5.5. Optimize and Improve the Teaching Environment. Optimizing and improving the teaching environment are an inevitable trend to strengthen and improve the effectiveness of ideological and political teaching in universities under the new situation. Therefore, ideological and political teachers should optimize and improve the teaching environment from multiple perspectives, eliminate negative factors as much as possible, and provide students with a harmonious, equal, and relaxed learning atmosphere. Marx has stressed that the environment is the main factor affecting human character, and it is reasonable to make the environment compatible with human nature. A harmonious environment has positive significance to the excavation and transformation of external factors of ideological and political teaching, plays a positive role in the development of the integration of direct and indirect teaching, and has an important influence on the enhancement of teaching

integration, so civic and political science teachers should build learning contexts, cognitive contexts, and humanistic sensitization through multiple channels. Therefore, civic teachers should build learning contexts, cognitive contexts, and humanistic contexts through multiple channels to improve the effectiveness of ideological and political teaching while reflecting its charm.

6. Conclusions

In this study, the process of evaluating the teaching quality of college teachers as a system is studied from the perspective of input, output, information, and control of the system, and computer technology and mathematical methods are simultaneously applied as tools in the study of this problem of teaching quality in universities. Based on the survey questionnaire on the teaching quality of college teachers and the collection and analysis of survey data, the principle and method of the evaluation model of teaching quality of college teachers are elaborated based on the optimized BP neural network theory, and the software system of evaluation of teaching quality of college teachers is developed from the perspective of computer database development and program design. The software imported the survey data (including the comprehensive evaluation score of teaching quality and the evaluation score of its influencing factors) for the calculation of the teaching quality score, and compared and analyzed the calculated values of the test samples with the survey data values, and the degree of their conformity was quite good.

The results of the teacher teaching evaluation model based on an optimized neural network are very good, and the relative error is less than 10%, which indicated that it was practical to use the optimized BP neural network theory method for the analysis and calculation of teaching quality evaluation of college teachers.

Data Availability

The data used to support the findings of this study are available from the corresponding author upon request.

Conflicts of Interest

The authors declare that they have no conflicts of interest.

Acknowledgments

This work was supported by the General Project of Higher Education Reform Research in Jiangxi Province (JXJG-20-24-5) and the Jiangxi Province University Humanities and Social Sciences Research Youth Program (JC20218).

References

- [1] Y. Li and F. Pioneer, "Research on the evaluation of teaching quality of college Civics classroom based on DA-BP algorithm," *Microcomputer Applications*, vol. 35, no. 9, pp. 128–131, 2019.
- [2] Q. Cui and Z. Sun, "The use of big data in promoting the quality improvement of ideological and political education in

Research Article

Effect of Compound Danshen Injection Combined with Magnesium Sulfate on Oxidative Stress, TNF- α , NO, and Therapeutic Efficacy in Severe Preeclampsia

Yanling Zhou ¹, Juan Wang ², Lei Wang ³, Jing Tang ⁴, and Chengwei Zhang ⁵

¹Department of Obstetrics, Yantaishan Hospital, Yantai 264000, China

²Department of Clinical Laboratory, Zhangqiu District People's Hospital, Jinan 250200, China

³ICU, The Affiliated Qingdao Central Hospital of Qingdao University, The Second Affiliated Hospital of Medical College of Qingdao University, Qingdao 266042, China

⁴Department of Gynaecology, Zhangqiu District Maternity and Child Care Hospital, Jinan 250200, China

⁵Medical Laboratory and Diagnostic Center, Jinan Central Hospital, Jinan 250013, China

Correspondence should be addressed to Chengwei Zhang; zhangchengwei@jnzxhospital.cn

Received 11 April 2022; Revised 1 June 2022; Accepted 24 June 2022; Published 18 July 2022

Academic Editor: Akansha Singh

Copyright © 2022 Yanling Zhou et al. This is an open access article distributed under the Creative Commons Attribution License, which permits unrestricted use, distribution, and reproduction in any medium, provided the original work is properly cited.

Aims. This study is designed to explore the effect of compound Danshen injection combined with magnesium sulfate on TNF- α , NO, oxidative stress, and therapeutic efficacy in severe preeclampsia (S-PE). **Methods.** Sixty S-PE patients were placed into the control group and the therapy group, randomly. The control group was under the treatment of magnesium sulfate, and the therapy group was under the treatment of compound Danshen injection with magnesium sulfate. After treatment, the therapeutic efficacy of the two groups was comparatively analyzed. **Results.** 7 days after treatment, DBP, SBP, and 24 h urinary protein were sharply lower than those before treatment. The 24 h urinary protein was notably lower in the therapy group. After treatment, the expression level of TNF- α in both groups was notably higher than before treatment, while NO level was higher than that before treatment. Furthermore, D-D level in two groups was dramatically decreased compared to that before treatment. Moreover, Fib, PT, and APTT in two groups showed statistically significant differences after 7 days. The contents of ALT, AST, BUN, and Scr in therapy group were notably lower than those in control group. **Conclusion.** Our results indicated that compound Danshen injection could improve renal function, blood hypercoagulability, and oxidative stress level and had a better therapeutic effect on S-PE.

1. Introduction

Preeclampsia (PE) is a unique disease of women during pregnancy. The main clinical manifestations are hypertension, edema, proteinuria, and other symptoms after 20 weeks of pregnancy [1–4], causing systemic multi-system dysfunction and even irreversible damage in pregnant women [5–7] and seriously threatening maternal and infant health. The incidence of PE is about 5% [8, 9]. Therefore, timely and effective treatment is of significant meaning to the prognosis of PE patients. At present, the pathogenesis of PE is not completely clear [10], among which the theory of placental shallow implantation and the theory of vascular endothelial

injury are the main theories. As the core factor of inflammatory response, excessive TNF- α can directly damage vascular endothelial cells and cause placental shallow implantation, placental ischemia, and hypoxia [11–14]. NO acts as an endogenous vasodilator released by endothelial cells. When its synthesis, release, and activity are inhibited and destroyed, it will further lead to abnormal vasoconstriction and dysfunction, which will worsen local or systemic ischemia and hypoxia and worsen the condition of patients with severe PE (S-PE) [15]. Compound Danshen injection has the effects of promoting blood circulation, preventing platelet aggregation, removing free radicals, protecting vascular endothelial cells, and improving cell resistance to

hypoxia [16, 17]. Studies [18, 19] have shown that compound Danshen injection has certain therapeutic efficacy in treating S-PE. However, it has not been reported whether compound Danshen injection can affect the changes of clinical parameters such as blood pressure by reducing $\text{TNF-}\alpha$ and increasing NO level.

Magnesium sulfate is the drug of choice for relieving spasm of S-PE, which can relax skeletal muscle and effectively control the patient's central nervous system. Although the therapeutic effect of magnesium sulfate has been recognized by clinical trials, excessive blood concentration of the drug may cause dizziness, nausea and vomiting, abdominal pain and diarrhea, and other suspected mild poisoning [20, 21], which threatens the safety of patients to a large extent. Therefore, magnesium sulfate often needs to be used in conjunction with other drugs to reduce the degree of adverse reactions and improve the efficacy. In this study, compound Danshen injection was used to treat S-PE patients, in order to observe the clinical efficacy and the effect on $\text{TNF-}\alpha$ and NO.

2. Materials and Methods

2.1. Research Objects. 60 patients with S-PE who underwent regular prenatal examination and were hospitalized in the department of obstetrics of our hospital were selected. Patients were placed into therapy group and control group. 30 patients in control group were treated with magnesium sulfate. 30 patients in therapy group were under the treatment of compound Danshen injection on the basis of control group. All pregnant women signed the informed consent form.

2.2. Diagnostic Criteria for S-PE

- (i) Systolic blood pressure (SBP) ≥ 160 mmHg and/or diastolic blood pressure (DBP) ≥ 110 mmHg
- (ii) Proteinuria (++) and above
- (iii) Serum creatinine (Scr) ≥ 1.2 mg/dL (1 mg/dL = 88.402 $\mu\text{mol/L}$)
- (iv) Platelet (Plt) $< 100 \times 10^9/\text{L}$

S-PE can be diagnosed with any of these laboratory results.

2.3. Inclusion and Exclusion Criteria. Inclusion criteria were as follows:

- (i) Met the diagnostic criteria of moderate to S-PE in Obstetrics and Gynecology
- (ii) No previous history of PE
- (iii) The gestational age of onset < 34 weeks, and the gestational age of delivery was 28–33 weeks
- (iv) No other treatment was received before admission
- (v) Normal basic coagulation function before pregnancy
- (vi) Full participation in treatment and related examinations and complete clinical data

- (vii) Signed informed consent and approved by the medical ethics committee of our hospital

Exclusion criteria were as follows:

- (i) Complicated with severe cardiac, hepatic, and renal insufficiency
- (ii) With diabetes, hypertension, and other chronic diseases [22]
- (iii) With malignant neoplastic diseases
- (iv) Related treatment contraindications
- (v) Communication disorders
- (vi) Poor compliance

2.4. The Treatment. Patients in both groups were on bed rest, their fetal heart rates were closely monitored, and they were given oxygen inhalation. Routine examinations such as electrocardiogram, metabolic indicators, renal function indicators, coagulation indicators, and electrolytes were performed. The control group was under the conventional treatment and magnesium sulfate. 5 g magnesium sulfate was dissolved in 20 mL 5% glucose solution and dropped within 30 minutes. Then, 15 g magnesium sulfate was dissolved in 500 mL 5% glucose solution and dropped for 2 hours. The total amount of magnesium sulfate used for 24 hours should not exceed 30 g. One course of treatment is one week.

The therapy group was treated with compound Danshen injection in addition to the basic treatment of the control group. Compound Danshen injection (16 ml) was injected into 250 ml 5% glucose solution, once a day.

2.5. Evaluation Criteria for Clinical Effect

- (1) Cured: the patient's clinical symptoms disappear, blood pressure $< 140/90$ mmHg, and no symptoms of proteinuria or edema
- (2) Effective: the patient's clinical symptoms improved and blood pressure was 140/90 mmHg to 150/100 mmHg, with slight proteinuria and slight edema
- (3) Ineffective: the patient's symptoms did not improve, and the condition was gradually transformed from mild PE to S-PE

Total effective rate = ((cured + effective)/total number of cases) $\times 100\%$.

2.6. Detection of $\text{TNF-}\alpha$. Enzyme-linked immunosorbent assay (ELISA) was used for $\text{TNF-}\alpha$ detection. The experiment was carried out in the laboratory of our hospital, and all operation procedures were strictly carried out according to the product instructions.

2.7. Detection of NO. The nitric acid reductase method was used to detect NO in serum. This experiment was completed in the laboratory of our hospital, and each experiment was conducted in strict accordance with the instructions.

2.8. Detection of Endothelial Protein C Receptor (EPCR) and Thrombomodulin (TM). The levels of EPCR and TM were examined by ELISA before and after treatment.

2.9. Detection of Lipid Peroxide (LPO). The catalase (CAT) level was determined by ammonium molybdate colorimetry, and the LPO level was determined by thiobarbituric acid colorimetry before and after treatment.

2.10. Coagulation Function. Before and after 7 days of treatment, 1.5 ml of fasting venous blood was taken from both groups and added with sodium citrate for anticoagulation. The serum was extracted by centrifugation at 3000 r/min at 4°C for 10 min. The levels of fibrinogen (Fib), prothrombin time (PT), D-dimer (D-D), and activated partial thrombin time (APTT) were determined by coagulation analyzer.

2.11. Liver and Kidney Function. The contents of liver and kidney function indexes in peripheral blood, including blood urea nitrogen (BUN), aspartate aminotransferase (AST), blood creatinine (Scr), and alanine aminotransferase (ALT), were detected by automatic blood biochemical analyzer.

2.12. Statistical Analysis. The measurement data were presented as $(\bar{x} + s)$ and analyzed by *t*-test. The numeration data were presented as N (%), and analyzed by χ^2 test. SPSS 22.0 software was used for data analysis. The *t*-test was applied to data analysis between groups. When $p < 0.05$, the difference was considered statistically significant.

3. Results

3.1. Comparison of Clinical Parameters between the Two Groups before Treatment. The age of patients in the therapy group was 24–38 years old, the average age was 28.6 ± 4.9 years old, the gestational age was 28–33 weeks, and the average gestational age was 29.90 ± 2.40 weeks. There were 22 cases of cesarean section and 8 cases of vaginal delivery. Patients in the control group were 25–39 years old, with an average age of 29.1 ± 4.8 years old. The gestational age of pregnant women was 28–33 weeks, with an average gestational age of 29.70 ± 2.80 weeks. There were 23 cases of cesarean section and 7 cases of vaginal delivery. Before treatment, there was no obvious difference in parameters between the two groups ($p > 0.05$).

3.2. Comparison of TNF- α and NO between the Two Groups. There was no significant difference in TNF- α level between the two groups before treatment. TNF- α level in two groups was evidently reduced after treatment, and the decrease was more obvious in therapy group. The level of TNF- α in the two groups was notably different after 7 days ($p < 0.05$, Figure 1(a)).

There was no obvious difference in NO level between the two groups prior treatment. The level of NO in the control group increased sharply after treatment. Also, the level of

NO in the therapy group increased more obviously after treatment than before treatment. The difference of NO level between the two groups after treatment was statistically significant ($p < 0.05$, Figure 1(b)).

3.3. Comparison of EPCR and TM Levels between the Two Groups. There was no obvious difference in EPCR and TM levels between the two groups before treatment ($p > 0.05$). After treatment, the levels of EPCR and TM in two groups were lower than before treatment ($p < 0.05$). The levels of EPCR and TM in the therapy group were lower than those in the control group ($p < 0.05$, Table 1).

3.4. Comparison of CAT and LPO Levels between the Two Groups. Before treatment, there was no statistical significance in CAT and LPO levels between the two groups ($p > 0.05$). After one week of treatment, CAT level in both groups was higher ($p < 0.05$), LPO level was lower than that before treatment, and the range of change in the therapy group was greater than that in the control group ($p < 0.05$, Table 2).

3.5. Comparison of Coagulation Function Indexes before and after Treatment. Before treatment, there were no evident differences in serum coagulation indexes Fib, D-D, PT, and APTT between two groups ($p > 0.05$). The levels of Fib and D-D in two groups after treatment were lower, while PT and APTT levels were higher than those before treatment ($p < 0.05$). The levels of Fib and D-D in the therapy group were lower, while the levels of PT and APTT were higher than those in the control group ($p < 0.05$, Table 3).

3.6. Comparison of Liver and Kidney Function Indexes. Before receiving treatment, there was no difference in the levels of ALT, AST, BUN, and Scr between two groups ($p > 0.05$). After 7 days of treatment, the levels of ALT, AST, BUN, and Scr in two groups were lower than those before treatment ($p < 0.05$). The levels of ALT, AST, BUN, and Scr in the therapy group were lower than those in the control group ($p < 0.05$, Table 4).

3.7. Comparison of Clinical Effective Rate between the Two Groups. Before treatment, there were no differences in SBP, DBP, and 24 h urine protein between two groups ($p > 0.05$). Compared with before treatment, blood pressure levels in the two groups declined after treatment, and the decrease was more obvious in the treatment group. After treatment, there were notable differences in blood pressure levels between the two groups ($p < 0.05$, Figure 2). After 7 days of treatment, the 24 h urinary protein in the therapy group was dramatically lower than that in the control group ($p < 0.05$, Figure 3). The total effective rate in the therapy group was 93.0%, and the total effective rate in the control group was 76.7%. The overall effective rate of the therapy group was maintained at a high level ($p < 0.05$, Figure 4).

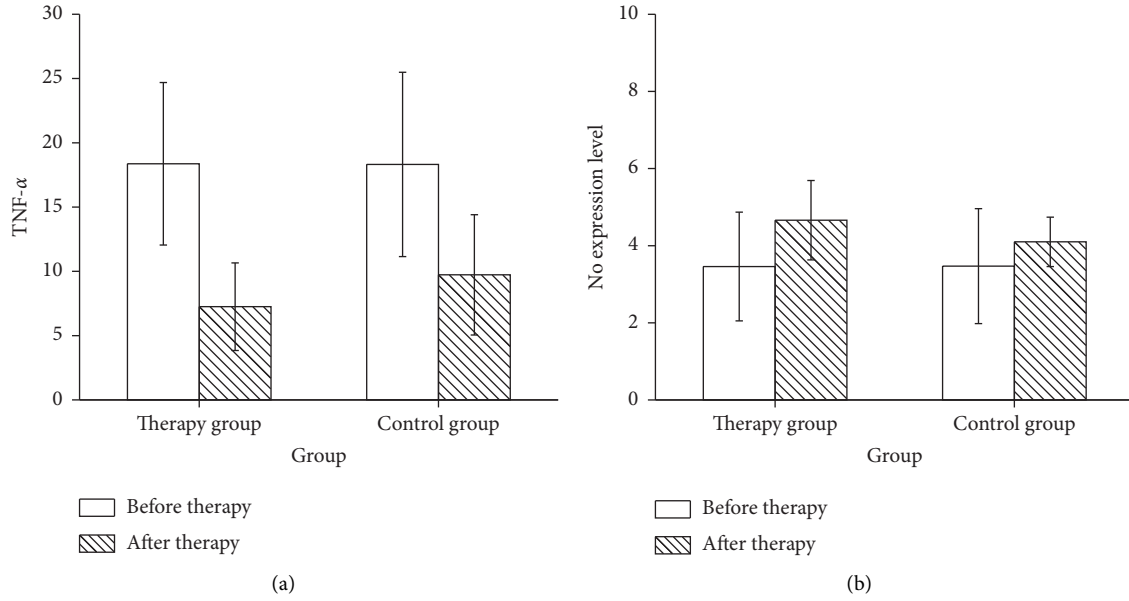


FIGURE 1: Comparison of TNF- α and NO levels between two groups. (a) Comparison of TNF- α before and after treatment. (b) Comparison of NO before and after treatment.

TABLE 1: Comparison of EPCR and TM levels before and after treatment ($\bar{x} + s$).

Parameters	Control group		Therapy group	
	Before treatment	After treatment	Before treatment	After treatment
EPCR ($\mu\text{g/L}$)	217.03 \pm 9.41	165.31 \pm 13.43	217.96 \pm 9.53	142.21 \pm 12.41
TM ($\mu\text{g/L}$)	89.21 \pm 8.25	60.97 \pm 8.14	89.51 \pm 6.67	49.02 \pm 8.45

TABLE 2: Comparison of CAT and LPO levels before and after treatment ($\bar{x} + s$).

Parameters	Control group		Therapy group	
	Before treatment	After treatment	Before treatment	After treatment
CAT (U/mL)	4.92 \pm 0.88	7.34 \pm 1.34	4.99 \pm 0.94	8.36 \pm 1.45
LPO (nmol/L)	14.75 \pm 2.31	11.34 \pm 2.12	14.88 \pm 2.44	9.98 \pm 1.98

TABLE 3: Comparison of serum coagulation function indexes before and after treatment ($\bar{x} + s$).

Parameters	Control group		Therapy group	
	Before treatment	After treatment	Before treatment	After treatment
Fib (g/L)	3.93 \pm 0.42	3.19 \pm 0.33	3.96 \pm 0.45	2.89 \pm 0.29
D-D (mg/L)	2.64 \pm 0.33	2.12 \pm 0.27	2.63 \pm 0.36	1.66 \pm 0.24
PT (s)	10.18 \pm 1.54	11.91 \pm 1.74	10.19 \pm 1.57	13.31 \pm 1.81
APTT (s)	31.10 \pm 3.54	33.02 \pm 3.71	31.19 \pm 3.47	35.01 \pm 3.87

TABLE 4: Comparison of liver and kidney function indexes before and after treatment ($\bar{x} + s$).

Parameters	Control group		Therapy group	
	Before treatment	After treatment	Before treatment	After treatment
ALT (U/L)	34.71 \pm 3.51	26.61 \pm 3.09	34.77 \pm 3.68	21.78 \pm 2.83
AST (U/L)	45.85 \pm 5.62	31.79 \pm 4.23	45.73 \pm 5.41	25.47 \pm 2.98
BUN (mmol/L)	6.20 \pm 0.64	4.02 \pm 0.47	6.18 \pm 0.58	3.30 \pm 0.41
Scr ($\mu\text{mol/L}$)	323.73 \pm 43.77	280.74 \pm 34.27	321.99 \pm 43.59	22.38 \pm 31.87

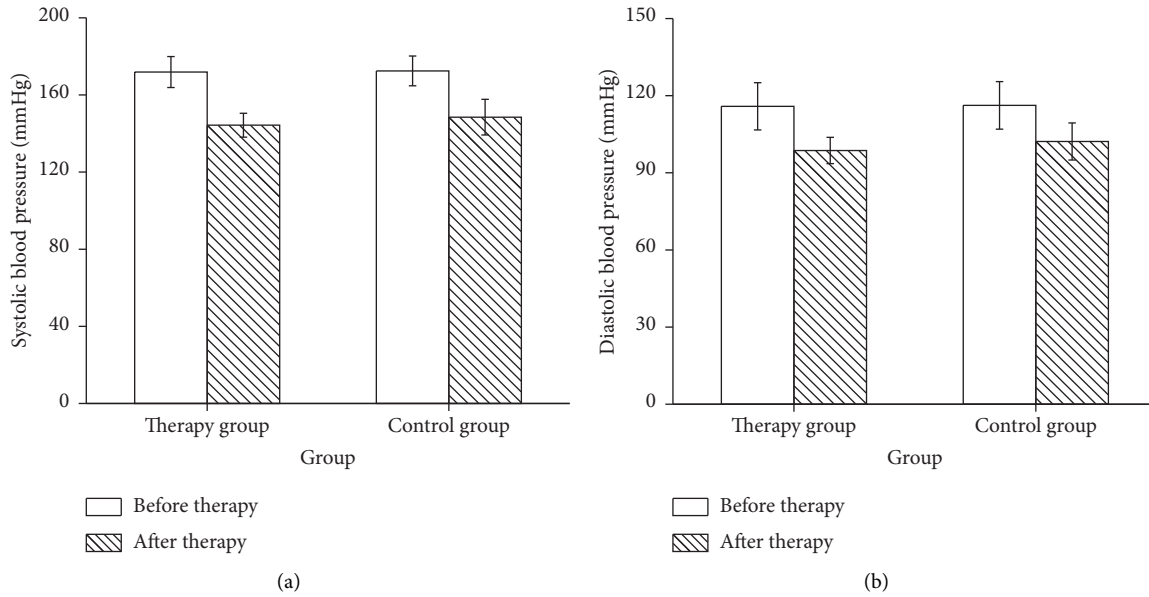


FIGURE 2: Comparison of blood pressure levels between two groups before and after treatment. (a) SBP. (b) DBP.

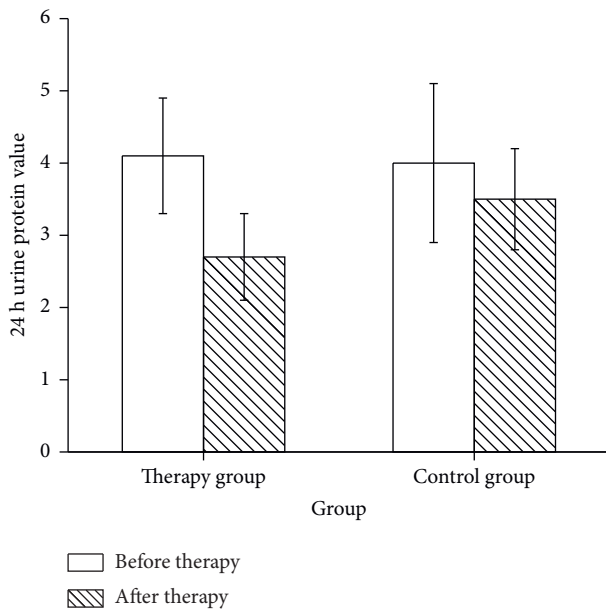


FIGURE 3: Comparison of 24 h urine protein between two groups before and after treatment.

4. Discussion

S-PE is mainly manifested by continuous elevated blood pressure and renal impairment and may also be accompanied by persistent headache, visual impairment, epigastric pain, and other clinical symptoms, which bring discomfort to pregnant women and directly threaten the safety of the lives of mothers and infants [7, 23]. Conventional treatments such as hypotension, spasmolysis, and sedation have been proved to be effective for mild PE, but the outcome optimization effect of the above methods on S-PE is limited. Compound Danshen injection has been used for the

treatment of acute myocardial infarction and angina pectoris, and its effective component tanshinone can protect the myocardium, remove oxygen free radicals, and improve blood flow. Pregnant women with S-PE have some pathological manifestations similar to myocardial infarction, such as systemic arteriolar spasm, placental atherosclerosis, and decreased blood perfusion. Therefore, compound Danshen injection was added into the treatment plan of pregnant women with S-PE as an auxiliary drug.

The study showed that $\text{TNF-}\alpha$ in both groups was decreased after treatment, and the decrease was more obvious in the therapy group. The lower the $\text{TNF-}\alpha$ level, the higher the probability of S-PE disease improvement, suggesting that compound Danshen injection combined may play a certain effect on PE patients by reducing the $\text{TNF-}\alpha$ level. The level of NO in both groups increased after treatment, and the increase was especially significant in the therapy group. The higher the NO level is, the stronger the S-PE could be controlled, suggesting that magnesium sulfate combined with compound Danshen injection may play a therapeutic role in S-PE by increasing the level of NO. Therefore, it can be inferred that compound Danshen injection is related to reducing $\text{TNF-}\alpha$ and increasing NO level.

The blood pressure of S-PE patients was decreased significantly after treated with magnesium sulfate combined with compound Danshen injection [24]. In our study, SBP, DBP, D-D, Fib, and 24 h urinary protein in two groups were significantly decreased after treatment. Moreover, PT and APTT were increased in both groups. In patients with S-PE, vasospasm and contraction of liver vessels lead to hypoxic-ischemic injury of liver tissues [25]. The contents of ALT, AST, and other liver function landmark enzymes increased significantly, which can quantitatively reflect the degree of liver function injury and clinical treatment effect. With the increase of urinary protein, the patients' renal function injury was aggravated, followed by glomerular dilatation and

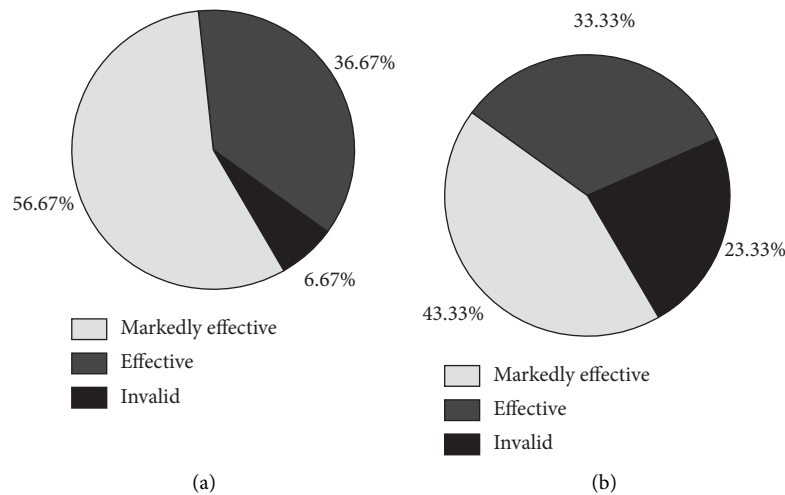


FIGURE 4: Comparison of clinical effective rate between the two groups. (a) Effective rate of therapy group. (b) Effective rate of control group.

renal tubule spasm and gradually decreased renal blood flow and glomerular filtration excess, leading to the increase of BUN and Scr [26]. Our results showed that the levels of ALT, AST, BUN, and Scr in two groups were decreased after treatment, suggesting that the two treatments have the effect of optimizing liver and kidney function. The levels of ALT, AST, BUN, and Scr in the therapy group were lower, indicating that compound Danshen injection-assisted therapy can further improve the liver and kidney functions of patients with S-PE, and its efficacy is more outstanding. Consistent with the previous results [27, 28], our therapeutic effect was better, which was possibly due to the insufficient sample size. In conclusion, compound Danshen injection adjuvant therapy can optimize the clinical manifestations of S-PE and reduce systemic hypercoagulability.

Data Availability

The data used to support the findings of this study are available on reasonable request from the corresponding author.

Conflicts of Interest

The authors declare that they have no conflicts of interest.

References

- [1] American College of Obstetricians and Gynecologists, "Hypertension in pregnancy," *ACOG Technical Bulletin*, vol. 219, pp. 1–8, 1996.
- [2] M. A. Brown, W. M. Hague, J. Higgins et al., "The detection, investigation and management of hypertension in pregnancy: full consensus statement," *The Australian and New Zealand Journal of Obstetrics and Gynaecology*, vol. 40, no. 2, pp. 139–155, 2000.
- [3] M. A. Brown, M. D. Lindheimer, M. deSwiet, A. VanAssche, and J. Moutquin, "The classification and diagnosis of the hypertensive disorders of pregnancy: statement from the international society for the study of hypertension in pregnancy (ISSHP)," *Hypertension in Pregnancy*, vol. 20, no. 1, pp. IX–14, 2001.
- [4] O. V. Golovchenko, M. Y. Abramova, V. S. Orlova, I. V. Batlutskaya, and I. N. Sorokina, "Clinical and genetic characteristics of preeclampsia," *Archives of Razi Institute*, vol. 77, no. 1, pp. 275–281, 2022.
- [5] F. K. Baghbahadorani and S. Miraj, "The impact of Silymarin on improvement of platelet abnormalities in patients with severe preeclampsia," *Electronic Physician*, vol. 8, no. 5, pp. 2436–2442, 2016.
- [6] A. M. Maged, A. M. Hashem, S. H. GadAllah, M. E. Mahy, W. A. I. Mostafa, and A. Kotb, "The effect of loading dose of magnesium sulfate on uterine, umbilical, and fetal middle cerebral arteries Doppler in women with severe preeclampsia: a case control study and fetal middle cerebral arteries Doppler in women with severe preeclampsia: a case control study," *Hypertension in Pregnancy*, vol. 35, no. 1, pp. 91–99, 2016.
- [7] J. Textoris, D. Ivorra, A. Ben Amara et al., "Evaluation of current and new biomarkers in severe preeclampsia: a microarray approach reveals the VSIG4 gene as a potential blood biomarker," *PLoS One*, vol. 8, no. 12, p. e82638, 2013.
- [8] American Journal of Obstetrics and Gynecology, "A. Report Of the national high blood pressure education program working group on high blood pressure in pregnancy," *American Journal of Obstetrics and Gynecology*, vol. 183, no. 1, pp. 1–22, 2000.
- [9] S. Meher and L. Duley, "Prevention of Pre-eclampsia Cochrane Review authors. Interventions for preventing pre-eclampsia and its consequences: generic protocol," *Cochrane Database of Systematic Reviews*, vol. Issue 2, 2005.
- [10] D. Mihu, C. Razvan, A. Malutan, and C. Mihaela, "Evaluation of maternal systemic inflammatory response in preeclampsia," *Taiwanese Journal of Obstetrics & Gynecology*, vol. 54, no. 2, pp. 160–166, 2015.
- [11] F. M. Fong, M. K. Sahemey, G. Hamed, R. Eytayo, and D. Yates, V. Kuan, S. Thangaratinam, and R. T. Walton, "Maternal genotype and severe preeclampsia: a HuGE review," *American Journal of Epidemiology*, vol. 180, no. 4, pp. 335–345, 2014.
- [12] O. A. Reyes and G. M. Gonzalez, "Carbetocin versus oxytocin for prevention of postpartum hemorrhage in patients with severe preeclampsia: a double-blind randomized controlled

- trial,” *Journal of Obstetrics and Gynaecology Canada*, vol. 33, no. 11, pp. 1099–1104, 2011.
- [13] Y. S. Serin, B. Özçelik, M. Bapbuð, H. K yl yc , D. Okur, and R. Erez, “Predictive value of tumor necrosis factor alpha (TNF- ) in preeclampsia,” *European Journal of Obstetrics & Gynecology and Reproductive Biology*, vol. 100, no. 2, pp. 143–145, 2002.
 - [14] M. A. Guven, A. Coskun, I. E. Ertas, M. Aral, B. Zencirci, and H. Oksuz, “Association of maternal serum CRP, IL-6, TNF- , homocysteine, folic acid and vitamin B12 levels with the severity of preeclampsia and fetal birth weight,” *Hypertension in Pregnancy*, vol. 28, no. 2, pp. 190–200, 2009.
 - [15] V. L. Roger, A. S. Go, D. M. Lloyd-Jones et al., “Heart disease and stroke statistics-2012 update,” *Circulation*, vol. 125, no. 1, pp. e2–e220, 2012.
 - [16] K. Yang, G. Dong, Y. Tian, and J. Li, “Effects of compound Danshen injection combined with magnesium sulfate on serum MPO and hs-CRP in patients with severe preeclampsia,” *Experimental and Therapeutic Medicine*, vol. 16, no. 1, pp. 167–170, 2018.
 - [17] X. Zhao, H. Wang, Y. Gao, and Y. Wang, “Effects of compound danshen injection combined with magnesium sulfate on pregnancy-induced hypertension syndrome under the guidance of empirical mode decomposition algorithm-based ultrasound image,” *Journal of Healthcare Engineering*, vol. 2021, p. 9026223, 2021.
 - [18] Z. Zhai, Y. Li, Y. Yang et al., “ENOS G894T gene polymorphisms and hyperhomocysteinemia in the predisposition to venous thromboembolism,” *Chest*, vol. 140, no. 4, pp. 23–26, 2011.
 - [19] Y. S. Kanwar, J. Wada, L. Sun et al., “Diabetic nephropathy: mechanisms of renal disease progression,” *Experimental Biology and Medicine*, vol. 233, no. 1, pp. 4–11, 2008.
 - [20] L. Duley, A. M. G lmezoglu, and D. J. Henderson-Smart, “Magnesium sulphate and other anticonvulsants for women with pre-eclampsia,” *Cochrane Database of Systematic Reviews*, vol. 2, p. CD000025, 2003.
 - [21] P. Talungchit, T. Liabsuetrakul, and G. Lindmark, “Development and assessment of indicators for quality of care in severe preeclampsia/eclampsia and postpartum hemorrhage,” *Journal for Healthcare Quality*, vol. 35, no. 3, pp. 22–34, 2013.
 - [22] D. Gupta, A. Choudhury, U. Gupta, P. Singh, and M. Prasad, “Computational approach to clinical diagnosis of diabetes disease: a comparative study,” *Multimedia Tools and Applications*, vol. 80, no. 20, pp. 30091–30116, 2021.
 - [23] M. A. Aracil, R.-B. Rodr guez, C. M. Bernal et al., “Maternal perinatal characteristics in patients with severe preeclampsia: a case-control nested cohort study,” *International Journal of Environmental Research and Public Health*, vol. 18, no. 22, p. 11783, 2021.
 - [24] D. He, S. Wu, H. Zhao, Z. Zheng, and W. Zhang, “High normal blood pressure in early pregnancy also contribute to early onset preeclampsia and severe preeclampsia,” *Clinical and Experimental Hypertension*, vol. 40, no. 6, pp. 539–546, 2018.
 - [25] C. Barr, P. Pudwell, and N. Smith, “Postpartum microvascular functional alterations following severe preeclampsia,” *American Journal of Physiology - Heart and Circulatory Physiology*, vol. 320, no. 4, pp. H1393–H1402, 2021.
 - [26] T. Tzur, R. Rimon, and J. Herzlich, M. J. Kupferminc, “Progression from isolated gestational proteinuria to preeclampsia with severe features,” *Acta Obstetrica et Gynecologica Scandinavica*, vol. 100, no. 9, pp. 1620–1626, 2021.
 - [27] S. S. Juan-Reyes and H. Gomez-Olivan, “Oxidative stress in pregnancy complicated by preeclampsia,” *Archives of Biochemistry and Biophysics*, vol. 681, p. 108255, 2020.
 - [28] L. Youssef, J. Miranda, M. Blasco et al., “Complement and coagulation cascades activation is the main pathophysiological pathway in early-onset severe preeclampsia revealed by maternal proteomics,” *Scientific Reports*, vol. 11, no. 1, p. 3048, 2021.

Research Article

Role and Mechanism of Keap1/Nrf2 Signaling Pathway in the Regulation of Autophagy in Alleviating Pulmonary Fibrosis

Zhaoxing Dong,¹ E. Gao Yin,² Meijuan Yang,² Xiaoyuan Zhao,² Jing Li,² and Wen Lei ²

¹Department of Respiratory Medicine, Hua Mei Hospital, University of Chinese Academy of Sciences, Ningbo Institute of Life and Health Industry, University of Chinese Academy of Sciences, Ningbo, 315010, China

²The First Ward, Department of Pulmonary and Critical Care Medicine, The Second Affiliated Hospital of Kunming Medical University, Kunming, 650101, China

Correspondence should be addressed to Wen Lei; b20160503231@stu.ccsu.edu.cn

Received 24 May 2022; Revised 6 June 2022; Accepted 8 June 2022; Published 18 July 2022

Academic Editor: Dong Chen

Copyright © 2022 Zhaoxing Dong et al. This is an open access article distributed under the Creative Commons Attribution License, which permits unrestricted use, distribution, and reproduction in any medium, provided the original work is properly cited.

A variety of internal and external lung diseases may eventually lead to pulmonary fibrosis, and insufficient autophagy is closely related to pulmonary fibrosis. This research is aimed to explore the mechanism of autophagy to alleviate pulmonary fibrosis. Then, a mouse model of pulmonary fibrosis induced by boromycin and histopathological lesions of the lungs of mice were observed by HE staining, which Masson staining assessed the degree of fibrosis in the lung tissue by detecting the expression of hydroxyproline in the tissue. RT-qPCR and western blotting were used to detect the levels of autophagy and Keap1/Nrf2 signaling pathway-related proteins. It was proved that autophagy-related proteins MAP1LC3(LC3) and Beclin 1 were decreased in mice with pulmonary fibrosis, while the expression of p62 was increased. Mice with pulmonary fibrosis worsened after injection of a 3-MA autophagy inhibitor, while injection of autophagy activation of rapamycin agent promoted Nrf2 nuclear mobilization. In a word, autophagy relieves pulmonary fibrosis through the activation of the Keap1/Nrf2 signaling pathway.

1. Introduction

Pulmonary fibrosis is an inflammatory disease characterized by the proliferation of fibroblasts and the accumulation of extracellular matrix accompanied by inflammatory damage [1]. Most patients with pulmonary fibrosis have an unknown etiology (idiopathic). Idiopathic pulmonary fibrosis (IPF) with pulmonary fibrosis as the main manifestation is the most common disease, which can lead to progressive loss of lung function [2]. Pulmonary fibrosis seriously affects human respiratory function. After normal lung tissue is replaced by fibrotic tissue, respiratory function will be significantly reduced [1]. The morbidity and mortality of pulmonary fibrosis are increasing year by year and the average survival time after diagnosis is only 2.8 years. These claims have shown a poor prognosis clinically [3, 4].

Therefore, it is of great significance to explore the mechanism of pulmonary fibrosis.

Autophagy is a process of engulfing one's own cytoplasmic proteins or organelles and coating them into vesicles and fusing with lysosomes to form autophagic lysosomes and degrading the contents it encapsulates. It is a conservative decomposition of cells' metabolic needs that can also achieve the renewal of organelles [5]. In the literature, various mechanisms have found that autophagy plays an important role in the regulation of lung diseases, especially in diseases of pulmonary fibrosis [6]. The proliferation of fibroblasts is a major feature of pulmonary fibrosis and autophagy can maintain the normal life and progression of lung fibroblasts. Additionally, transforming growth factor-1 (TGF- β 1) can induce fibroblasts to myofibroblasts differentiation, which leads to pulmonary fibrosis, mainly through

the inhibition of autophagy, indicating that the intervention of autophagy can be an effective measure to prevent pulmonary fibrosis [7]. The direct impact of autophagy on pulmonary fibrosis has also been proved, for example, bleomycin-induced pulmonary fibrosis can be improved by inhibiting apoptosis of pulmonary epithelial cells through autophagy. Likewise, the destruction of inhibition of cellular protease after autophagy blocking can induce the occurrence of interstitial lung disease [8, 9]. Therefore, exploring the mechanism of autophagy regulating the progression of pulmonary fiber can provide a new treatment idea for alleviating pulmonary fibrosis.

Keap1-Nrf2 is one of the important mechanisms of cell defense against oxidative stress damage. After the Keap1-Nrf2 signaling pathway is activated, the nuclear transcription factor Nrf2 enters the nucleus and activates the transcription of a variety of antioxidant genes, thereby reducing cell damage caused by ROS [10–12]. Studies have found that the Keap1-Nrf2 signaling pathway has an important effect on autophagy, and the expression of autophagy gene will also decrease after Nrf2 is knocked out [13]. In addition to it, induction of autophagy can be regulated by the systemic level feedback of Nrf2 based on oxidative stress response [14]. Meanwhile, studies have shown that Keap1-Nrf2 is associated with pulmonary fibrosis, and the protective effect of p65 in pulmonary fibrosis can be reversed by Nrf2 knockout [15]. The activation of the Keap1-Nrf2 feedback loop can promote the antioxidant response of autophagy to improve the harmful effects of excessive oxidative stress. In this paper, we have explored the mechanism of autophagy in pulmonary fibrosis and to clarify the mechanism of the interaction between Keap1/Nrf2 signaling pathway and autophagy in pulmonary fibrosis. For this purpose, various experimental studies, specifically on mouse dataset, were performed to verify the expected outcome and claims of the proposed model.

2. Materials and Methods

In this section, a detailed description of the experimental studies, their possible setup, and approval from the concerned authority (if needed and applicable) is provided. Additionally, status of the animal, mouse in this case, and the effects of the proposed solution of their status are described in detail.

2.1. Animals. Animal experiments were approved by the Animal Experiment Ethics Review Committee of Kunming Medical University (Lot Number: kmmu2021756). Forty-eight male, which were 8-week-old C57BL/6 mice, weighing about 18–22 g and SPF grade. These mice were fed for seven days to adapt to the environment and then randomly divided into 4 groups such that every group has 12 mice.

Grouping: (i) Sham operation group (Sham), (ii) bleomycin (BLM) group, (iii) BLM + autophagy inhibitor (3-MA) group, and (iv) BLM + autophagy activator rapamycin (RAPA) group. Initially, twelve (12) hours before the experiments, mice were forced to fast (as no food was

provided) and gave them only water. All experimental mice were anesthetized with 2% sodium pentobarbital and administered by intraperitoneal injection of 0.056 mg/kg. After the mice did not respond, they were placed on a fixed plate and the limbs and head of the mice were fixed. Skin and sterilize sharp scissors are used to cut a small vertical 0.5 cm wound up in the center of the neck. The cortex and muscle layer were peeled off to expose the trachea and used a 1 ml syringe to push the BLM (2.5 mg/kg) along the lower edge of the cartilage ring and injected into the airway (0.9% sodium chloride injection in the Sham group), and then turned the test bench. The BLM (0.9% sodium chloride injection in the Sham group) was let to reach the small airways in the lungs, arrange, and suture the wound. To prevent wound infection, mice were given amikacin lotion on the wound 3 days after the operation. On the basis of the successful construction of pulmonary fibrosis mice, subsequent BLM mice were injected with autophagy inhibitor (3-MA) and autophagy activator (rapamycin) for intervention to complete various tests in subsequent experiments.

2.2. Culture of Pulmonary Fibrosis Cells (PFC). Lung tissue was extracted from a 10-week-old male mice in the aseptic state, cut into 0.5–1 mm³ tissue blocks, sterilized with PBS, and rinsed twice to remove blood and floating connective tissue. The tissue mass was transferred into a 50 mL centrifuge tube and 0.25% trypsin 5 mL was added. The tissue mass was digested at 37°C for 5–10 min and shake the tube gently by hand during digestion. Gently blown and discarded the upper suspension, added trypsin 5 mL to the tissue mass for further digestion for 5–10 min, centrifuged, collected the supernatant and added it to Dulbecco's Modified Eagle's Medium (DMEM) containing 20% BSA to stop digestion, and blown and collected the supernatant. These steps were repeated three times. The collected supernatant was centrifuged at 1000 r/min for 10 min. The supernatant was discarded and added with 10% fetal bovine serum (FBS) DMEM medium was blown away and inoculated in the culture flask, placed in the incubator (5% CO₂, 37°C) for 2 h, discarded the supernatant, replaced with fresh medium, and continued the culture.

2.3. RT-qPCR. After collecting mouse lung tissue or lung fibrocytes, the total RNA was extracted using TRIzol reagent (Invitrogen; Thermo Fisher Scientific Inc.) according to the manufacturer's instruction. Then, cDNA was synthesized using reverse transcription kit (Bio-Rad Laboratories Inc.). Finally, cDNA was used as a template to detect RT-qPCR reaction with PCR kit (Takara Bio Inc.). The results were obtained, and the method of $2^{-\Delta\Delta C_t}$ was used to analyze the relative expression level.

2.4. Western Blotting. Initially, (i) extracted the protein of cells and tissues, (ii) used the BCA kit to determine the protein concentration, (iii) prepared a polyacrylamide gel of the corresponding concentration according to the molecular weight of the protein, and (iv) adjusted the sample amount

according to the protein concentration. After the electrophoresis was completed, the protein was transferred to the PVDF membrane, which was pretreated with formaldehyde (transferred conditions were 4°C, 90 mA, and 1.5 h). Blocked with 5% skimmed milk powder for 1 h, and then added the (i) diluted primary antibody, (ii) transglutaminase 3 (LC3) antibody (1:1000 dilution), (iii) Beclin1 antibody (1:500 dilution), (iv) p62 antibody (1:2000 dilution), (v) Keap1 antibody (1:2000 dilution), and (vi) Nrf2 antibody (1:1000 dilution) at 4°C overnight. Added HRP-labeled secondary antibody and incubated at room temperature for 1 h. ECL color development, gel imaging system imaging analysis, semiquantitative determination of expression level, and ImageJ analysis of band gray value were performed.

2.5. Hematoxylin and Eosin (H&E) Staining. The slices were routinely dewaxed, which was (i) washed with water for 10 s, (ii) washed with hematoxylin dye solution for 10 min, (iii) rinsed with running water for 1 min, (iv) washed with 1% hydrochloric acid alcohol for 10 s, (v) rinsed in running water for 1 min, (vi) washed with warm water returned to blue for 1 min, (vii) put in eosin dye solution for 30 s, and (viii) washed in water for 10 s. Gradient alcohol dehydration, transparent xylene, mounting with neutral gum, and observed the cell morphology under a fluorescence microscope and took pictures and recorded.

2.6. Masson Staining. After the lung tissue was embedded and fixed in paraffin, the tissue section was stained according to the instructions of the Masson staining kit, and then the staining of the section was observed under a microscope.

2.7. Determination of Hydroxyproline (HYP). After grinding the lung tissue into a homogenate shape, detected the content of HYP in the homogenate according to the instructions of the hydroxyproline detection kit.

2.8. Statistical Analysis. GraphPad Prism 8 software was used to draw relevant statistics and SPSS19.0 was used for statistical analysis. Data differences between groups were analyzed by *t*-test (Student's test) and one-way ANOVA where $P < 0.05$ indicated a significant difference and $P < 0.01$ indicated a very significant difference, respectively.

3. Experimental Results and Observations

In this section, various observations and the experimental study are reported and described in detail how effective the proposed approach is. Each experiment was performed using sophisticated procedure such as safety of both animals and scientists. The experimental results and observations of various groups are compared against each other, which were carried out under similar environmental conditions.

3.1. Expression of Autophagy-Associated Proteins and Keap1/Nrf2 Pathway-Associated Proteins in BLM-Induced PF.

BLM-induced lung fibrosis mouse lung tissue was taken as a sample to detect autophagy and Keap1/Nrf2 pathway-related protein expression. Comparison with mice in the Sham group, RT-qPCR, and Western Blot tests, showed a significant decrease in the expression of autophagy-related proteins LC3 and Beclin 1 in BLM mice (Figures 1(a), 1(b), and 1(d), $P < 0.05$) and a significant increase of p62 (Figures 1(c) and 1(d), $P < 0.05$). At the same time, RT-qPCR and Western Blot detection of proteins related to the Keap1/Nrf2 signaling pathway showed that the expression of Keap1 was significantly increased in BLM mice (Figures 1(e) and 1(g), $P < 0.05$), while the expression of Nrf2 was significantly decreased than that of the Sham group (Figures 1(f), 1(g), $P < 0.05$).

3.2. Autophagy Attenuates the Pathological Damage and Collagen Accumulation of Pulmonary Fibrosis. HE staining and Masson staining were performed on mouse lung tissue to observe pathological changes. The results of HE staining showed that the lung tissue structure of the BLM-perfused mice was severely damaged and the alveoli were significantly reduced and deformed (Figure 2(a)). The results of Masson staining showed that the lung tissue of the mice perfused with BLM was disordered and there was a large amount of collagen deposition (Figure 2(b)). However, treatment with autophagy activator RAPA partially restored BLM-induced alveolar structural damage and inhibited BLM-induced collagen deposition (Figures 2(a) and 2(b)). The autophagy inhibitor 3-MA has the opposite effect (Figures 2(a) and 2(b)). In addition, by detecting the content of HYP in the lung tissue, it was found that compared with the Sham group ($0.52 \pm 0.02 \mu\text{g}/\text{mg}$), the content of HYP in the lung tissue of the BLM perfusion ($1.81 \pm 0.03 \mu\text{g}/\text{mg}$) group was significantly increased (Figure 2(c)). Similarly, autophagy inhibitor 3-MA further increased the content of HYP while autophagy activator RAPA reduced it (Figure 2(c)).

3.3. The Expression of Autophagy-Related Proteins and Keap1/Nrf2 Pathway-Related Proteins in Lung Fibroblasts Cell. Comparison with PFC group, RT-qPCR, and Western Blot tests showed a significant decrease in the expression of autophagy-related proteins LC3 and Beclin 1 in the PFC+BLM group (Figures 3(a), 3(b), and 3(d), $P < 0.05$) and a significant increase of p62 (Figures 3(c), and 3(d), $P < 0.05$). This result is consistent with the detection results in the BLM-induced mouse model of PF. The expression of proteins related to the Keap1/Nrf2 signaling pathway was also detected by RT-qPCR. The results showed that the expression of Keap1 was significantly increased in PFC + BLM group (Figures 3(e), 3(g), $P < 0.05$), while the expression of Nrf2 was significantly decreased, compared with the PFC group (Figure 3(f), 3(g), $P < 0.05$).

3.4. Effects of Autophagy on Proliferation and Apoptosis of PFC Cells. CCK-8 test results showed that compared with the PFC group, the proliferation activity of cells in the PFC + BLM group was significantly increased (Figure 4(a)).

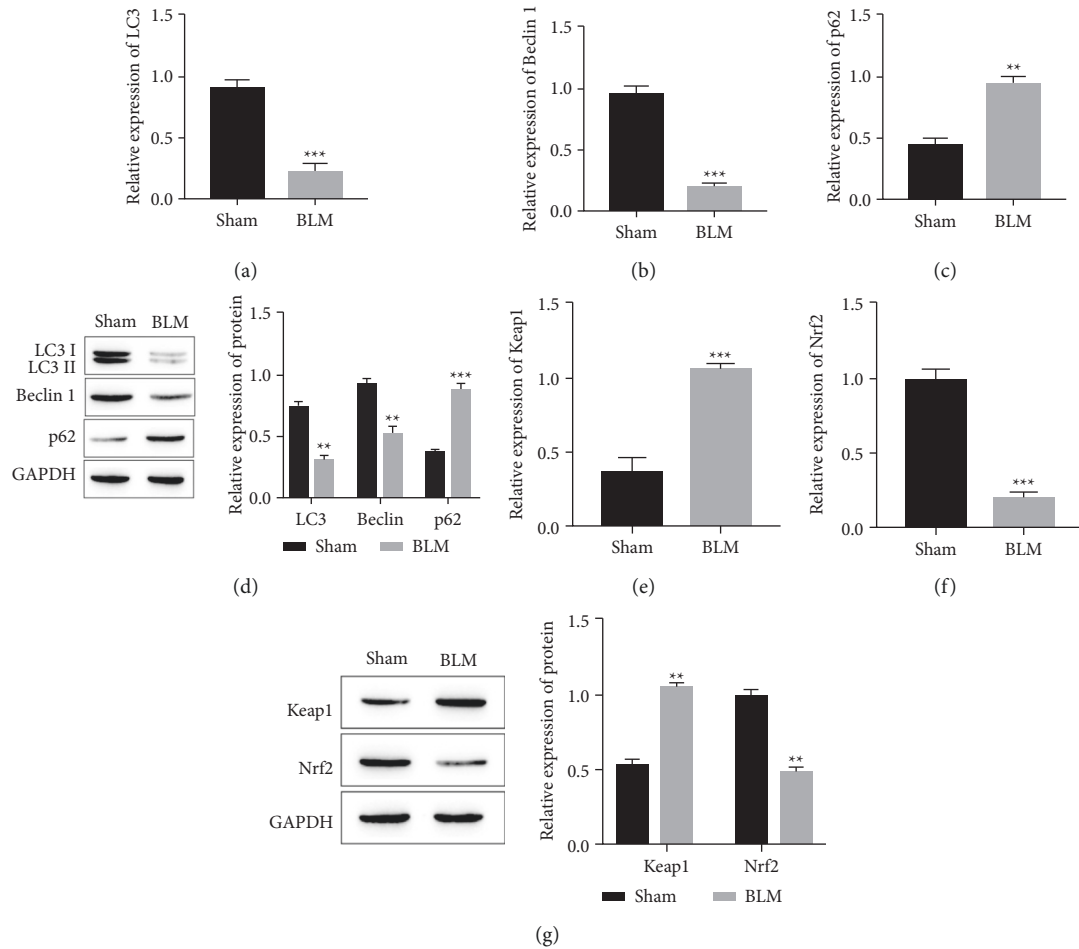


FIGURE 1: The expression levels of autophagy and KEAP1/Nrf2 signaling pathway-related proteins in pulmonary fibrosis mouse models. (a) The expression level of LC3 was detected by RT-qPCR. *** $P < 0.001$ vs. Sham group. (b) The expression level of Beclin 1 was detected by RT-qPCR. *** $P < 0.001$ vs. Sham group. (c) The expression level of p62 was detected by RT-qPCR. ** $P < 0.01$ vs. Sham group. (d) The expression levels of autophagy-related proteins of LC3, Beclin 1, and p62 by Western blotting assay. ** $P < 0.01$, *** $P < 0.001$ vs. Sham group. (e) The expression level of KEAP1 was detected by RT-qPCR. *** $P < 0.001$ vs. Sham group. (f) The expression level of Nrf2 was detected by RT-qPCR. *** $P < 0.001$ vs. Sham group. The expression levels of KEAP1/Nrf2 signaling pathway-related proteins of KEAP1 and Nrf2 by Western blotting assay. ** $P < 0.01$ vs. Sham group.

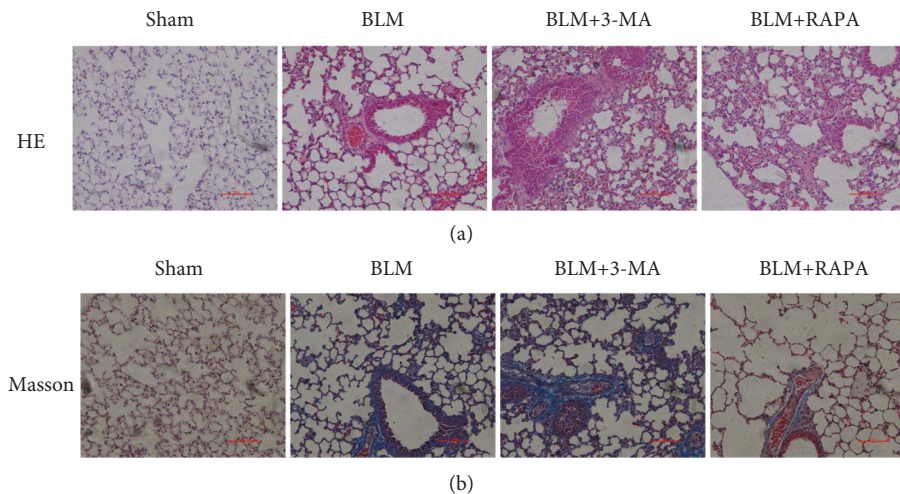


FIGURE 2: Continued.

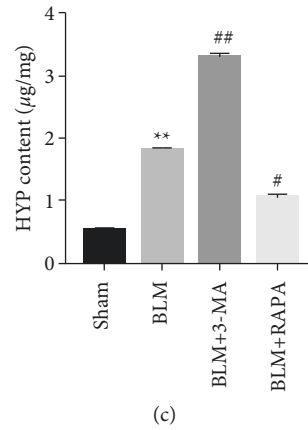


FIGURE 2: The effect of autophagy on BLM-induced PF. (a) HE staining to detect histopathological changes. (b) Masson staining to detect collagen accumulation. (c) The kit detects the content of HYP in lung tissue. ** $P < 0.01$ vs. Sham group. # $P < 0.05$, ## $P < 0.01$ vs. BLM group.

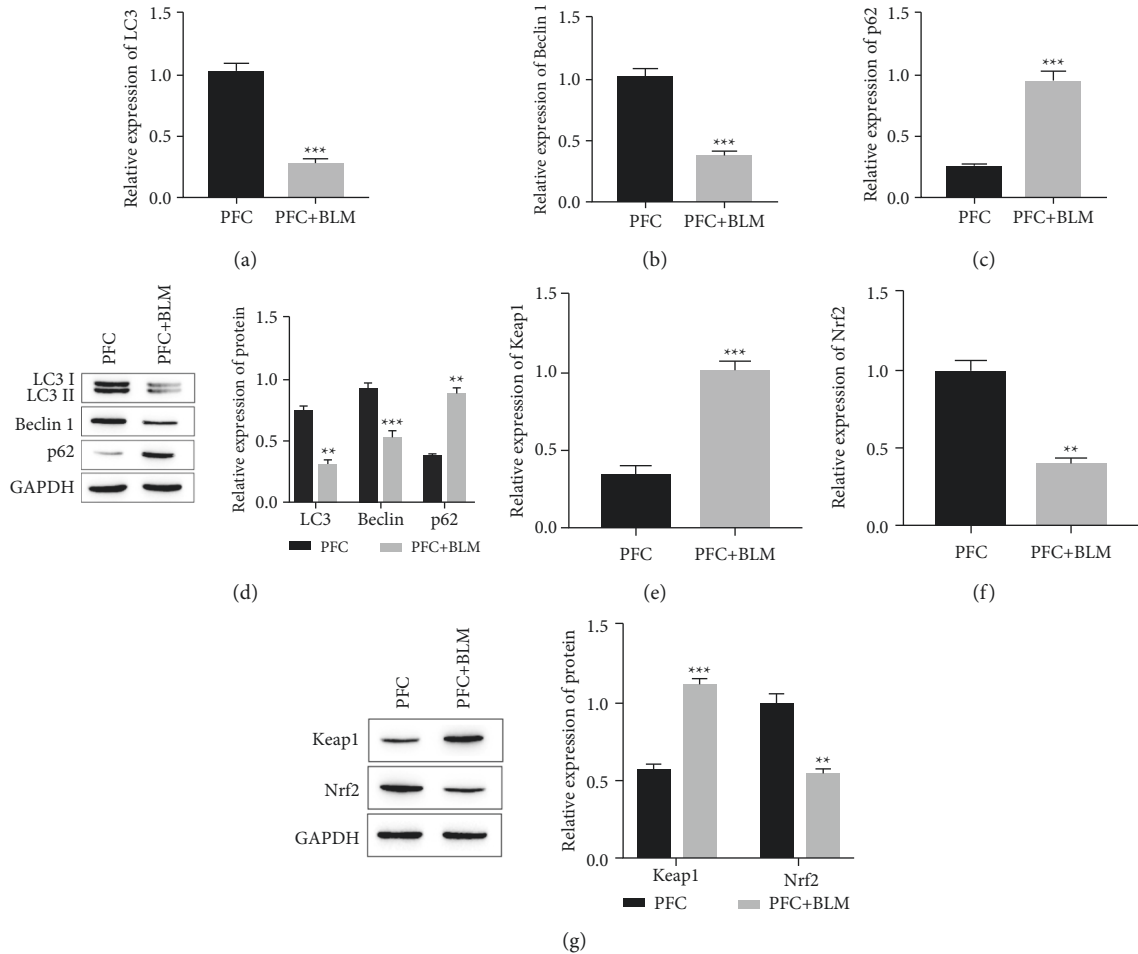


FIGURE 3: The expression levels of autophagy and KEAP1/Nrf2 signaling pathway-related proteins in PFC cells. (a) The expression level of LC3 was detected by RT-qPCR. *** $P < 0.001$ vs. PFC + BLM group. (b) The expression level of Beclin 1 was detected by RT-qPCR. *** $P < 0.001$ vs. PFC + BLM group. (c) The expression level of p62 was detected by RT-qPCR. ** $P < 0.01$ vs. PFC + BLM group. (d) The expression levels of autophagy related proteins of LC3, Beclin 1, and p62 by Western blotting assay. ** $P < 0.01$, *** $P < 0.001$ vs. PFC + BLM group. (e) The expression level of KEAP1 was detected by RT-qPCR. *** $P < 0.001$ vs. PFC + BLM group. (f) The expression level of Nrf2 was detected by RT-qPCR. ** $P < 0.01$ vs. PFC + BLM. The expression levels of KEAP1/Nrf2 signaling pathway-related proteins of KEAP1 and Nrf2 by Western blotting assay. ** $P < 0.01$ vs. PFC + BLM group.

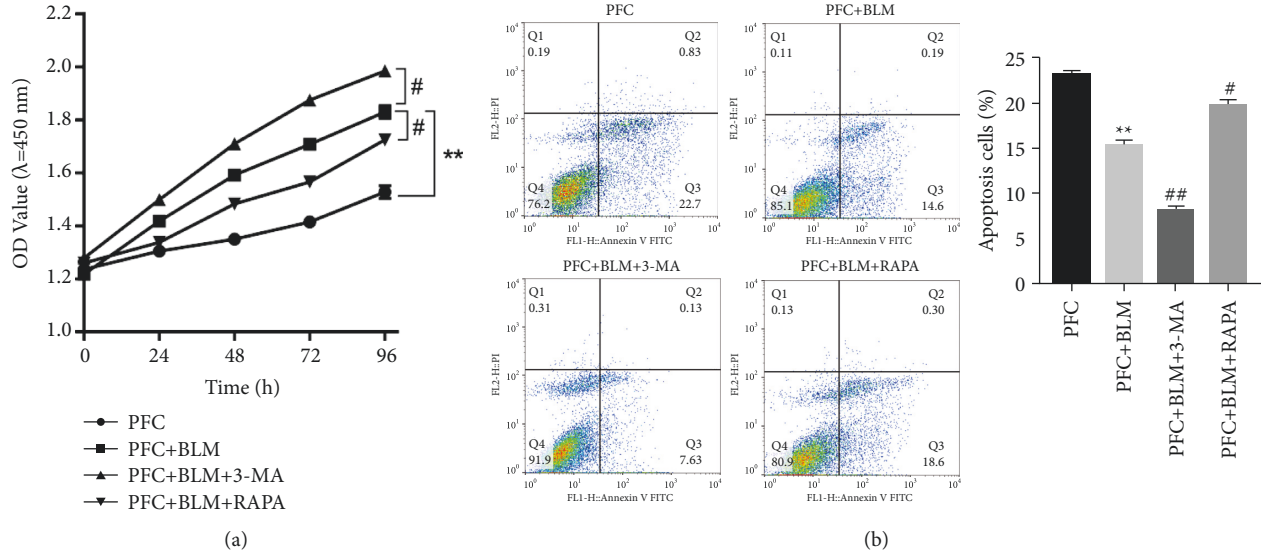


FIGURE 4: Effects of autophagy on proliferation and apoptosis of PFC cells. (a) The cell proliferation of PFC cells were examined by CCK-8 assay. $**P < 0.01$ vs. PFC group. $\#P < 0.05$ vs. PFC + BLM group. (b) The cell apoptosis of PFC cells were examined by CCK-8 assay. $**P < 0.01$ vs. PFC group. $\#P < 0.05$, $\#\#P < 0.01$ vs. PFC + BLM group.

However, when the autophagy activator was applied, the proliferation activity of PFC cells was attenuated, while the autophagy inhibitor had the opposite effect, which could further promote the proliferation activity of cells (Figure 4(a)). The results of flow cytometry detection of apoptosis showed that compared with the PFC group, the apoptosis in the PFC + BLM group was significantly declined, and the autophagy activator could enhance the occurrence of apoptosis in the PFC, while the autophagy inhibitor could further reduce the occurrence of apoptosis in the PFC cells (Figure 4(b)).

3.5. Autophagy Affects Cell Proliferation and Apoptosis through Keap1/Nrf2 Signaling Pathway. RT-qPCR and Western Blot results showed that compared with the PFC group, the expression of Keap1 was significantly higher in the PFC + BLM group, and the expression of Nrf2 was significantly decreased in the PFC + BLM group, but the application of autophagy activator of RAPA could significantly reduce the expression of Keap1 and increase the expression of Nrf2 in the PFC + BLM group, while the autophagy inhibitor of 3-MA could further promote the expression of Keap1 and reduce the expression of Nrf2 (Figures 5(a)–5(c)). CCK-8 test results showed that compared with the PFC group, the proliferation activity of cells in the PFC + BLM group was significantly increased, but the proliferation activity of cells was significantly decreased after the overexpression of Nrf2, and the opposite result was obtained after the knockdown of Nrf2 (Figure 5(d)). The results of flow cytometry detection of cell apoptosis showed that compared with the PFC group, the apoptosis of the PFC + BLM group was significantly decreased. When the autophagy activator was added, the occurrence of cell apoptosis could be promoted, while when the autophagy inhibitor was added, the occurrence of cell apoptosis could be further weakened (Figure 5(e)).

4. Performance Evaluation: General Discussion

Pulmonary fibrosis leads to progressive fibrosis and loss of lung function, making it a progressive and fatal lung disease. The occurrence of pulmonary fibrosis will have obvious tissue pathological features such as fibroblast proliferation, cell inflammation of the deposited interstitium of the outer matrix, or collapse of alveolar cells [16]. At present, research on the treatment of pulmonary fibrosis is vigorously carried out, but the road to successful treatment is still very long, and the proposal of new treatment strategies is also very necessary [17]. Autophagy is proposed as an effective intervention for the prevention and improvement of pulmonary fibrosis. The proposed research work shows that autophagy can alleviate the occurrence of pulmonary fibrosis by activating the Keap1/Nrf2 signaling pathway, and autophagy activators can probably effectively slow down lung injury from BLM-induced pulmonary fibrosis mice, as well as increase the apoptosis of lung fibrotic cells and inhibit the proliferation of lung fibrotic cells, while autophagy inhibitors produce the opposite result.

BLM is used as an antibiotic in the treatment of cancer, but it can produce dangerous side effects, namely, bleomycin pulmonary toxicity, which can lead to loss of lung function [18]. Studies have shown that 2–46% of patients treated with this drug will be accompanied by the side effect of pulmonary toxicity [19–21], and the mortality rate of BLT is 1–2% [22, 23]. Patients who receive bleomycin during surgery and require oxygen support are also prone to pulmonary toxicity in a state of hypoxia, which may be caused by the induction of superoxide anion [24]. At the same time, in the state of hyperoxia, oxygen-free radicals can inactivate antioxidant enzymes and cause the death of oxygen-sensitive cells, leading to the death of alveolar cells [25]. The pulmonary toxicity of bleomycin can cause the destruction of lung structure and cause pulmonary fibrosis, specifically by

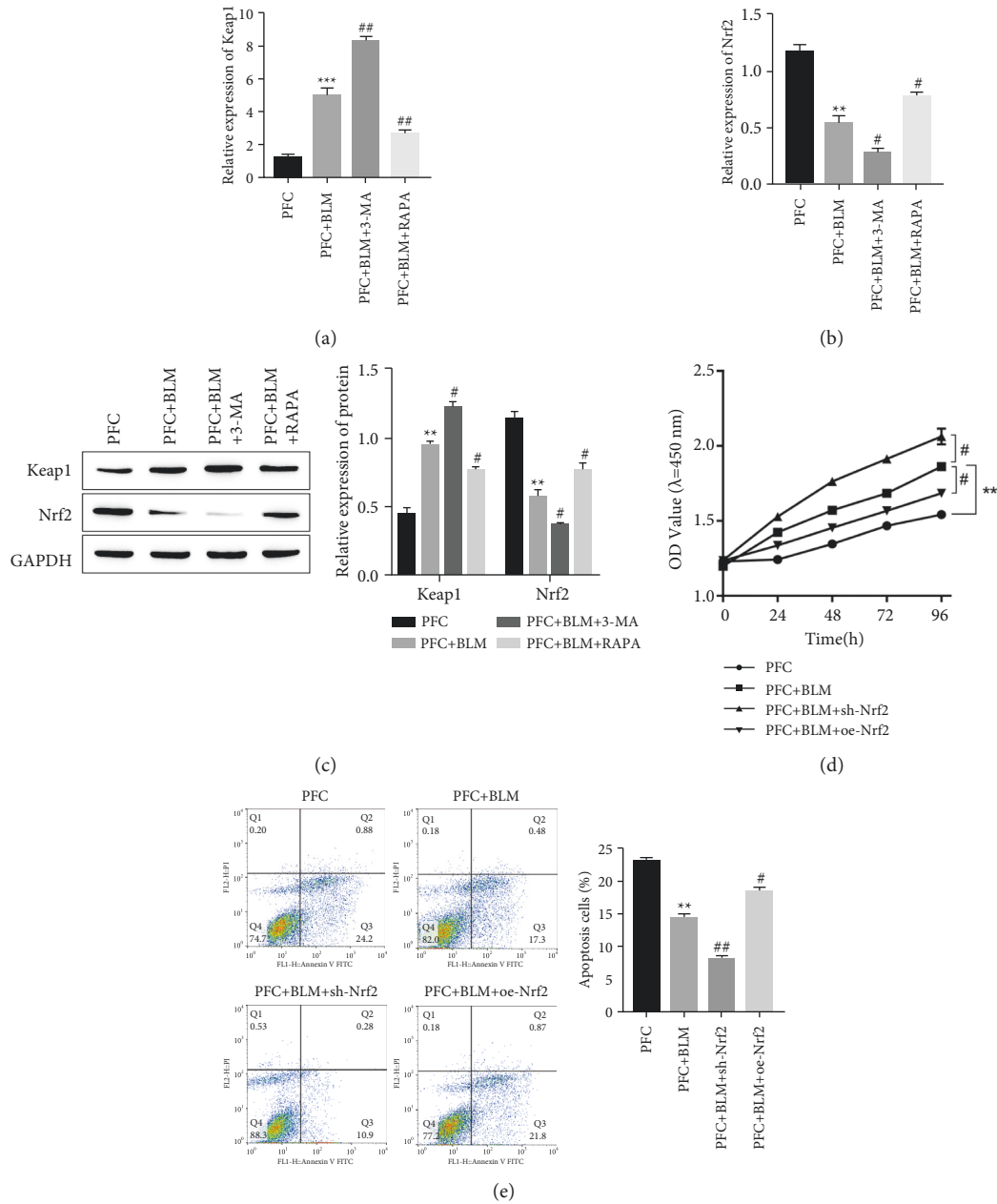


FIGURE 5: Autophagy affects cell proliferation and apoptosis through KEAP1/Nrf2 signaling pathway. (a) The expression levels of KEAP1 by RT-qPCR. *** $P < 0.001$ vs. PFC group. ## $P < 0.01$ vs. PFC + BLM group. (b) The expression levels of Nrf2 by RT-qPCR. ** $P < 0.01$ vs. PFC group. # $P < 0.05$ vs. PFC + BLM group. (c) The expression levels of KEAP1 and Nrf2 by Western blotting assay. ** $P < 0.01$ vs. PFC group. # $P < 0.05$ vs. PFC + BLM group. (d) The cell proliferation of PFC cells were examined by CCK-8 assay. ** $P < 0.01$ vs. PFC group. # $P < 0.05$ vs. PFC + BLM group. (e) The cell apoptosis of PFC cells were examined by CCK-8 assay. ** $P < 0.01$ vs. PFC group. # $P < 0.05$, ## $P < 0.01$ vs. PFC + BLM group.

affecting the transcription of fibroblasts and the increase of collagen production or the increase of hydroxyproline level [26]. In this study, in mice with bleomycin-induced pulmonary fibrosis, we found that the alveolar structure of the mice was damaged, the alveolar septum was widened, a large amount of collagen deposition appeared, and the content of hydroxyproline increased.

Autophagy is a self-protection mechanism of cells in a bad environment or external stimuli such as starvation, hypoxia, and DNA damage [27]. When autophagy occurs,

some proteins play a key role, and Beclin1 and LC3 are two typical autophagy markers [28]. Among them, p62 also plays an important role in autophagy, p62 is an important indicator of the dynamic process of autophagy, and p62 can bind to the autophagy substrate LC3. By detecting the expression of LC3II and p62 in the lung tissue of IPF patients, it was found that the down-regulation of LC3II expression and the up-regulation of p62 expression proved that there is insufficient autophagy in the lung tissue of IPF patients [29]. In addition, it was also found that compared

with normal lung, the expression of Beclin1 in IPF lung fibroblasts was down-regulated and LC3II was inhibited [30, 31]. Similarly, in this study, we found that in BLM-induced pulmonary fibrosis mice, the expressions of LC3 and Beclin1 were significantly decreased, while the expression of p62 was significantly increased, which was consistent with the results of previous studies and also showed the important role of autophagy in the progression of pulmonary fibrosis.

As an inducible transcription factor, Nrf2 can play an adaptive protective role in the state of cellular oxidation and protein toxic stress, thereby maintaining the continuation of redox signals [32]. In addition, the regulatory role of Nrf2 in the inflammatory response has also been reported [33]. Similarly, Nrf2 also plays an important role in pulmonary fibrosis, and it can participate in the fine-tuning of autophagy in response to oxidative stress levels [14]. The role of Nrf2 as a “master regulator” in the antioxidant response has been proven to play a key role in bleomycin-induced pulmonary fibrosis, and it has also become a biomarker and potential therapeutic target [34]. The role of Keap1/Nrf2 signaling pathway has received extensive attention. Studies have found that the activation of Keap1/Nrf2 signaling pathway can regulate autophagy and apoptosis regulated by ROS [35, 36], and the feedback loop of Keap1/Nrf2 can be maintained by p62 [37]. In this study, we have found that the expression of Keap1 and Nrf2 are abnormal in mouse models of pulmonary fibrosis and pulmonary fibrosis cells, that is, Keap1 is highly expressed and Nrf2 is low, indicating that the Keap1/Nrf2 signaling pathway is affected by lung fibrosis. In this study, it was observed that autophagy activators can reverse the abnormal expression of Keap1 and Nrf2 and activate the Keap1/Nrf2 pathway. Autophagy inhibitors have achieved the opposite result in the experimental setup.

5. Conclusions

In this paper, we have explored the mechanism of autophagy to alleviate pulmonary fibrosis. Formation of pulmonary fibrosis mouse model was induced by Boromycin and observed lung histopathological lesions in mice by HE staining, which shows the degree of fibrosis in tissue by Masson staining and detecting hydroxyproline expression in lung tissue. RT-qPCR and western blotting detected autophagy and Keap1/Nrf2 signaling pathway-related proteins. Furthermore, we have found that expression of LC3, Beclin 1, and Nrf2 are decreased in PF mouse model and cells. The expression of p62 and Keap1 are increased. Autophagy can reduce BLM-induced alveolar structural damage and inhibit the occurrence of collagen deposition. Autophagy alleviating pulmonary fibrosis through activation of Keap1/Nrf2 signaling pathway. This study provides a new treatment strategy for PF.

In future, we are eager to explore and investigate the expected performance of the proposed solution and perform experiments on human beings, preferably volunteers, instead of mice.

Data Availability

The authors confirm that the data supporting the findings of this study are available within the article.

Conflicts of Interest

The authors declare that they have no conflicts of interest.

Authors' Contributions

Zhaoxing Dong and E gao Yin are co-first authors, and they have the same contribution. (I) Conception and design: Zhaoxing Dong. (II) Administrative support: E gao Yin. (III) Provision of study materials or patients: Zhaoxing Dong. (IV) Collection and assembly of data: all authors. (V) Data analysis and interpretation: E gao Yin. (VI) Manuscript writing: all authors. (VII) Final approval of manuscript: all authors.

Acknowledgments

This paper was supported by National Natural Science Foundation of China (81860018) and Kunming Medical Joint Special Fund (2017FE468(-210), 2019FE001(-166)).

References

- [1] X. Lv, K. Li, and Z. Hu, “Autophagy and pulmonary fibrosis,” *Advances in Experimental Medicine & Biology*, vol. 1207, pp. 569–579, 2020.
- [2] R. Ganesh, R. Bram, Z. Yuan et al., “An official ATS/ERS/JRS/ALAT clinical practice guideline: treatment of idiopathic pulmonary fibrosis. An update of the 2011 clinical practice guideline,” *American Journal of Respiratory and Critical Care Medicine*, vol. 192, 2015.
- [3] J. Lawrence and R. Nho, “The role of the mammalian target of rapamycin (mTOR) in pulmonary fibrosis,” *International Journal of Molecular Sciences*, vol. 19, no. 3, 2018.
- [4] B. Ley, H. R. Collard, and T. E. King, “Clinical course and prediction of survival in idiopathic pulmonary fibrosis,” *American Journal of Respiratory and Critical Care Medicine*, vol. 183, no. 4, pp. 431–440, 2011.
- [5] L. Krustev, T. Tashev, A. Pokrovskij et al., “Effects of reduced diet and physical stress on liver lysosomes. Morphological and biochemical studies,” *Nahrung*, vol. 22, no. 3, pp. 309–313, 1978.
- [6] K. Mizumura, S. Cloonan, M. E. Choi et al., “Autophagy: friend or foe in lung disease?” *Annals of the American Thoracic Society*, vol. 13, pp. S40–S47, 2016.
- [7] M. L. Sosulski, R. Gongora, S. Danchuk, C. Dong, F. Luo, and C. G. Sanchez, “Deregulation of selective autophagy during aging and pulmonary fibrosis: the role of TGF β 1,” *Aging Cell*, vol. 14, no. 5, pp. 774–783, 2015.
- [8] K. Wang, T. Zhang, Y. Lei et al., “Identification of ANXA2 (annexin A2) as a specific bleomycin target to induce pulmonary fibrosis by impeding TFEB-mediated autophagic flux,” *Autophagy*, vol. 14, no. 2, pp. 269–282, 2018.
- [9] A. Hawkins, S. H. Guttentag, R. Deterding et al., “A non-BRICHOS SFTPC mutant (SP-CI73T) linked to interstitial lung disease promotes a late block in macroautophagy disrupting cellular proteostasis and mitophagy,” *American*

- Journal of Physiology - Lung Cellular and Molecular Physiology*, vol. 308, no. 1, pp. L33–L47, 2015.
- [10] V. R. Muthusamy, S. Kannan, K. Sadhaasivam et al., “Acute exercise stress activates Nrf2/ARE signaling and promotes antioxidant mechanisms in the myocardium,” *Free Radical Biology and Medicine*, vol. 52, no. 2, pp. 366–376, 2012.
 - [11] D. L. Palliyaguru, D. V. Chartoumpekis, N. Wakabayashi et al., “Withaferin A induces Nrf2-dependent protection against liver injury: role of Keap1-independent mechanisms,” *Free Radical Biology and Medicine*, vol. 101, pp. 116–128, 2016.
 - [12] E. Kubo, B. Chhunchha, P. Singh, H. Sasaki, and D. P. Singh, “Sulforaphane reactivates cellular antioxidant defense by inducing Nrf2/ARE/Prdx6 activity during aging and oxidative stress,” *Scientific Reports*, vol. 7, no. 1, Article ID 14130, 2017.
 - [13] Z. Tang, B. Hu, F. Zang, J. Wang, X. Zhang, and H. Chen, “Nrf2 drives oxidative stress-induced autophagy in nucleus pulposus cells via a Keap1/Nrf2/p62 feedback loop to protect intervertebral disc from degeneration,” *Cell Death & Disease*, vol. 10, no. 7, 2019.
 - [14] O. Kapuy, D. Papp, T. Vellai, G. Banhegyi, and T. Korcsmaros, “Systems-level feedbacks of NRF2 controlling autophagy upon oxidative stress response,” *Antioxidants*, vol. 7, no. 3, 2018.
 - [15] J. Yao, J. Zhang, W. Tai et al., “High-dose paraquat induces human bronchial 16 HBE cell death and aggravates acute lung intoxication in mice by regulating keap1/p65/nrf2 signal pathway,” *Inflammation*, vol. 42, no. 2, pp. 471–484, 2019.
 - [16] E. S. White, M. H. Lazar, and V. J. Thannickal, “Pathogenetic mechanisms in usual interstitial pneumonia/idiopathic pulmonary fibrosis,” *The Journal of Pathology*, vol. 201, no. 3, pp. 343–354, 2003.
 - [17] K. M. Antoniou, G. A. Margaritopoulos, and N. M. Siafakas, “Pharmacological treatment of idiopathic pulmonary fibrosis: from the past to the future,” *European Respiratory Review*, vol. 22, no. 129, pp. 281–291, 2013.
 - [18] E. C. Gabazza, O. Taguchi, and Y. Adachi, “Bleomycin-induced lung fibrosis: the authors should have used another method to induce pulmonary lesions resembling human idiopathic pulmonary fibrosis,” *American Journal of Respiratory and Critical Care Medicine*, vol. 165, no. 6, pp. 845–846, 2002.
 - [19] B. D. Cheson, “Pharmacology of cancer chemotherapy: miscellaneous chemotherapeutic agents,” in *Cancer Principles and Practice of Oncology*, V. T. De Vita Jr, S. Hellmann, and A. S. Rosenberg, Eds., pp. 452–459, Lippincott Williams&Wilkins, Pennsylvania, USA, 2001.
 - [20] J. Hay, S. Shahzeidi, and G. Laurent, “Mechanisms of bleomycin-induced lung damage,” *Archives of Toxicology*, vol. 65, no. 2, pp. 81–94, 1991.
 - [21] K. Jules-Elysee and D. A. White, “Bleomycin-induced pulmonary toxicity,” *Clinics in Chest Medicine*, vol. 11, pp. 1–20, 1990.
 - [22] P. W. C. Van Barneveld, T. H. W. Van Der Mark, D. T. H. Sleijfer, N. H. Mulder, H. S. Koops, and R. Peset, “Predictive factors for bleomycin-induced pneumonitis,” *American Review of Respiratory Disease*, vol. 130, pp. 1078–1081, 1984.
 - [23] U. B. Chaudhary and J. R. Haldas, “Long-term complications of chemotherapy for germ cell tumours,” *Drugs*, vol. 63, no. 15, pp. 1565–1577, 2003.
 - [24] T. S. Ingrassia, J. H. Ryu, V. F. Trastek, and E. C. Rosenow, “Oxygen exacerbated bleomycin pulmonary toxicity,” *Mayo Clinic Proceedings*, vol. 66, no. 2, pp. 173–178, 1991.
 - [25] R. M. Jackson, “Pulmonary oxygen toxicity,” *Chest*, vol. 88, no. 6, pp. 900–905, 1985.
 - [26] E. Azambuja, J. F. Fleck, R. G. Batista, and S. Menna Barreto, “Bleomycin lung toxicity: who are the patients with increased risk?” *Pulmonary Pharmacology & Therapeutics*, vol. 18, no. 5, pp. 363–366, 2005.
 - [27] B. Levine and G. Kroemer, “Autophagy in the pathogenesis of disease,” *Cell*, vol. 132, no. 1, pp. 27–42, 2008.
 - [28] I. Tanida, T. Ueno, and E. Kominami, “LC3 and autophagy,” *Methods in Molecular Biology*, vol. 445, pp. 77–88, 2008.
 - [29] A. S. Patel, L. Lin, A. Geyer et al., “Autophagy in idiopathic pulmonary fibrosis,” *PLoS One*, vol. 7, no. 7, Article ID e41394, 2012.
 - [30] R. S. Nho and P. Hergert, “IPF fibroblasts are desensitized to type I collagen matrix-induced cell death by suppressing low autophagy via aberrant Akt/mTOR kinases,” *PLoS One*, vol. 9, no. 4, Article ID e94616, 2014.
 - [31] A. Ricci, E. Cherubini, D. Scozzi et al., “Decreased expression of autophagic beclin 1 protein in idiopathic pulmonary fibrosis fibroblasts,” *Journal of Cellular Physiology*, vol. 228, no. 7, pp. 1516–1524, 2013.
 - [32] G. Shanmugam, A. K. Challa, S. H. Litovsky et al., “Enhanced Keap1-Nrf2 signaling protects the myocardium from isoproterenol-induced pathological remodeling in mice,” *Redox Biology*, vol. 27, Article ID 101212, 2019.
 - [33] S. Qin, R. H. du, S. S. Yin, X. Liu, G. Xu, and W. Cao, “Nrf2 is essential for the anti-inflammatory effect of carbon monoxide in LPS-induced inflammation,” *Inflammation Research*, vol. 64, no. 7, pp. 537–548, 2015.
 - [34] K. Mukaigasa, L. T. P. Nguyen, L. Li, H. Nakajima, M. Yamamoto, and M. Kobayashi, “Genetic evidence of an evolutionarily conserved role for Nrf2 in the protection against oxidative stress,” *Molecular and Cellular Biology*, vol. 32, no. 21, pp. 4455–4461, 2012.
 - [35] G. Filomeni, D. De Zio, and F. Cecconi, “Oxidative stress and autophagy: the clash between damage and metabolic needs,” *Cell Death & Differentiation*, vol. 22, no. 3, pp. 377–388, 2015.
 - [36] A. K. Verma, A. Yadav, J. Dewangan et al., “Isoniazid prevents Nrf2 translocation by inhibiting ERK1 phosphorylation and induces oxidative stress and apoptosis,” *Redox Biology*, vol. 6, pp. 80–92, 2015.
 - [37] K. Hayashi, K. Dan, F. Goto et al., “The autophagy pathway maintained signaling crosstalk with the Keap1-Nrf2 system through p62 in auditory cells under oxidative stress,” *Cellular Signalling*, vol. 27, no. 2, pp. 382–393, 2015.

Retraction

Retracted: Effects of the Ultrasound-Guided Stellate Ganglion Block on Hemodynamics, Stress Response, and Gastrointestinal Function in Postoperative Patients with Colorectal Cancer

Computational Intelligence and Neuroscience

Received 25 July 2023; Accepted 25 July 2023; Published 26 July 2023

Copyright © 2023 Computational Intelligence and Neuroscience. This is an open access article distributed under the Creative Commons Attribution License, which permits unrestricted use, distribution, and reproduction in any medium, provided the original work is properly cited.

This article has been retracted by Hindawi following an investigation undertaken by the publisher [1]. This investigation has uncovered evidence of one or more of the following indicators of systematic manipulation of the publication process:

- (1) Discrepancies in scope
- (2) Discrepancies in the description of the research reported
- (3) Discrepancies between the availability of data and the research described
- (4) Inappropriate citations
- (5) Incoherent, meaningless and/or irrelevant content included in the article
- (6) Peer-review manipulation

The presence of these indicators undermines our confidence in the integrity of the article's content and we cannot, therefore, vouch for its reliability. Please note that this notice is intended solely to alert readers that the content of this article is unreliable. We have not investigated whether authors were aware of or involved in the systematic manipulation of the publication process.

In addition, our investigation has also shown that one or more of the following human-subject reporting requirements has not been met in this article: ethical approval by an Institutional Review Board (IRB) committee or equivalent, patient/participant consent to participate, and/or agreement to publish patient/participant details (where relevant).

Wiley and Hindawi regrets that the usual quality checks did not identify these issues before publication and have since put additional measures in place to safeguard research integrity.

We wish to credit our own Research Integrity and Research Publishing teams and anonymous and named external researchers and research integrity experts for contributing to this investigation.

The corresponding author, as the representative of all authors, has been given the opportunity to register their agreement or disagreement to this retraction. We have kept a record of any response received.

References

- [1] A. Xie, X. Zhang, F. Ju, W. Li, Y. Zhou, and D. Wu, "Effects of the Ultrasound-Guided Stellate Ganglion Block on Hemodynamics, Stress Response, and Gastrointestinal Function in Postoperative Patients with Colorectal Cancer," *Computational Intelligence and Neuroscience*, vol. 2022, Article ID 2056969, 7 pages, 2022.

Research Article

Effects of the Ultrasound-Guided Stellate Ganglion Block on Hemodynamics, Stress Response, and Gastrointestinal Function in Postoperative Patients with Colorectal Cancer

An Xie,¹ Xianjie Zhang,¹ Feng Ju,¹ Wen Li,¹ Yukai Zhou,¹ and Dan Wu² 

¹Department of Anesthesiology, People's Hospital of Deyang City, Deyang, Sichuan 618000, China

²People's Hospital of Deyang City, No. 173 Taishan Road, Deyang, Sichuan Province, China

Correspondence should be addressed to Dan Wu; 18407026@masu.edu.cn

Received 26 May 2022; Revised 20 June 2022; Accepted 23 June 2022; Published 14 July 2022

Academic Editor: Dong Chen

Copyright © 2022 An Xie et al. This is an open access article distributed under the Creative Commons Attribution License, which permits unrestricted use, distribution, and reproduction in any medium, provided the original work is properly cited.

Objective. The aim of the study was to study the effects of the ultrasound-guided stellate ganglion block on hemodynamics, stressful response, and postoperative gastrointestinal functions in patients with colorectal cancer. **Methods.** A total of 100 patients with colorectal cancer hospitalized from January 2021 to December 2021 were selected. After anesthesia induction, the right stellate ganglion block was performed under ultrasound guidance in the research group and the general anesthesia was performed in the control group. The heart rate (HR), mean arterial pressure (MAP), epinephrine, cortisol, self-rating anxiety scale (SAS), Ramsay sedation score (RSS), postoperative bowel sound recovery time, anal exhaust time, and the incidence of gastrointestinal adverse reactions 24 hours after operation were studied pre- and post-24-hour anesthesia induction. **Results.** Following 24-hour operation, the HR and MAP values were largely reduced ($p < 0.05$). Following 24-hour operation, epinephrine and cortisol became obviously higher ($p < 0.05$). After 24-hour operation, the levels of epinephrine and cortisol in the research group were greatly lower. The score of the SAS in the study cohort was less than that of the controls ($p < 0.05$). The RSS of the research group was obviously increased ($p < 0.05$). The recovery time of intestinal sound and the anal exhaust time of the study cohort became remarkably shorter ($p < 0.05$). The incidence of gastrointestinal adverse reactions 24 hours after operation of the study cohort was much less common ($p < 0.05$). **Conclusion.** The ultrasound-guided stellate ganglion block can reduce the fluctuation of blood circulation during radical resection of colorectal cancer, reduce postoperative gastrointestinal dysfunction and stress reaction, relieve patients' anxiety, and contribute to the recovery of gastrointestinal function.

1. Introduction

Colorectal cancer is a malignant disease with a high incidence. Most of the patients had no obvious symptoms in the early stage, and most of the patients are found in the middle and the late stage. Common clinical manifestations are usually changes in defecation habits, such as abdominal pain and diarrhea [1]. Among the global cancer diseases, the incidence of colorectal cancer is the third and the mortality rate is the second [2]. In 2015, there were 387600 new colorectal cancer patients in China, accounting for 9.87% of all new cancer patients. A total of 187100 patients died of colorectal cancer, accounting for 8.01% of all cancer patients [3]. From the global perspective, the incidence of colorectal cancer in the United States has been

declining in the past decade, while the incidence and mortality of colorectal cancer in China have increased year by year [4–6]. Apparently, colorectal cancer has become a major public health problem that threatens health of residents around the world.

So far, the most important and effective treatment for colorectal cancer is surgical treatment [7, 8]. In addition, the disturbance is caused by operation in varying degrees [9, 10]. Long-term postoperative inhibitions probably cause an increase in the incidence of postoperative intestinal obstruction [11]. The severe cases can increase the risk of reoperation with systemic inflammatory response syndrome or multiple organ dysfunction syndromes [14, 15].

Previous studies have shown that the stellate ganglion block (SGB) can inhibit surgical stress and inflammation and

adjust the level of gastrointestinal hormones in rats undergoing gastrointestinal surgery [16], so that the digestive function of rats undergoing gastrointestinal surgery can quickly return to normal [17, 18]. The stellate ganglion is a ganglion formed by the combination of the inferior cervical ganglion, and the first thoracic ganglion and receives the T1~T2 nerve at the same time. Its branches can innervate the blood vessels, sweat glands, pilus muscle, bone, joints, and so on. The medial side of the stellate ganglion is the esophagus, trachea, recurrent laryngeal nerve, and long cervical muscle. The lateral side is the anterior scalenus muscle. The front is the carotid sheath, vertebral artery, and vertebral vein, and the rear is the cervical transverse process. It reversibly blocks the stellate ganglion and its adjacent sympathetic ganglia to block the preganglionic and postganglionic nerve fibers in the innervation area of these ganglia so that the disorder of autonomic nerve function can be relatively balanced. However, there are few studies on the stellate ganglion block and early recovery of gastrointestinal function in clinical work.

2. Materials and Methods

2.1. General Information. A total of 100 patients with colorectal cancer hospitalized from January 2021 to December 2021 were selected. A total of 100 patients with colorectal cancer were randomly divided into the study cohort and the control cohort, including 50 cases, respectively. In the research group, there were 25 males and 25 females, aged from 48 to 69 years old, with an average age of (58.36 ± 4.22) years. The body mass index was $18.5 \sim 24.0 \text{ kg/m}^2$, with an average BMI of $(21.48 \pm 2.33) \text{ kg/m}^2$. In the control group, there were 24 males and 26 females, aged from 47 to 69 years, with an average age of (58.42 ± 4.17) years. The body mass index was $18.6 \sim 24.0 \text{ kg/m}^2$, with an average BMI of $(21.51 \pm 2.29) \text{ kg/m}^2$.

Inclusion criteria were as follows: (1) patients who underwent colorectal cancer surgery within a limited period of time; (2) patients aged between 45 and 65 years old; (3) ASA grade I~II; (4) cardiopulmonary function was basically normal, no obvious heart, liver, kidney, endocrine diseases, preoperative laboratory, and related imaging examination results were not significantly abnormal.

Exclusion criteria were as follows: (1) patients with a history of upper respiratory tract infection within 2 weeks; (2) those with an obvious abnormality of heart, liver, and renal function; (3) those with a history of drug and alcohol abuse; (4) those with a history of allergy to narcotic drugs; (5) long-term use of anticoagulant drugs; (6) those with skin injury or infection at the puncture point of the neck; (7) those with an abnormal immune system; (8) those who refused to participate in this study; (9) the clinical data were incomplete.

2.2. Methods

2.2.1. Technical Route. As shown in Figure 1.

2.2.2. Treatment Regimen. The patients visited the day before the operation and were asked about their relevant medical history. The patient and his family were informed

about the anesthesia-related procedures and possible complications.

The control group received routine general anesthesia. After entering the room, the peripheral venous pathway was established. The electrocardiogram, heart rate, blood oxygen saturation, noninvasive arterial blood pressure, and EEG bispectral index were monitored by using the Drager Infinity C500 anesthesia monitor. All patients were given general anesthesia by endotracheal intubation. Anesthesia induction consisted of midazolam 0.03 mg/kg , fentanyl $3 \sim 5 \mu\text{g}\cdot\text{kg}^{-1}$, propofol $1.5 \sim 2.0 \text{ mg}\cdot\text{kg}^{-1}$, and cis atracurium $0.2 \text{ mg}\cdot\text{kg}^{-1}$. The patient's BIS was in the range of 45 to 55, the muscle was completely relaxed, and endotracheal intubation was performed using a visual laryngoscope. After successful intubation, mechanical ventilation was performed, and the tidal volume was $6 \sim 8 \text{ ml}\cdot\text{kg}^{-1}$. The partial pressure of end-expiratory carbon dioxide was maintained at $35 \sim 45 \text{ mmHg}$, and the respiratory rate was adjusted according to the partial pressure of end-expiratory carbon dioxide. Continuous intravenous infusion of propofol and remifentanyl was used for sedation and analgesia during anesthesia maintenance. The maintenance dose was adjusted according to the BIS value, which should be maintained in the range of 50~60. For the fluctuation of hemodynamics during operation, under the condition of ensuring the appropriate depth of anesthesia, the blood pressure was maintained in the range of $\pm 20\%$ of the basic value. Above or below this range, urapidil or ephedrine can be administered to regulate blood pressure. When the blood pressure was reduced, fluid replacement treatment can be carried out according to the specific conditions. The heart rate would be maintained at 50~100 beats/min. If it was higher or lower than this range, after excluding the causes of blood loss, arrhythmia, and improper depth of anesthesia, intravenous injection of esmolol or atropine can adjust the heart rate.

In the research group, the right stellate ganglion block was performed under ultrasound guidance after anesthesia induction. After induction of general anesthesia, the planetary ganglion was blocked at the level of the seventh cervical vertebra on the right under the guidance of ultrasound. The medical staff arranges the patient to lie down, turns the patient's head to the left, disinfects the puncture point, and spreads a surgical towel. After determining the structures of the thyroid, carotid artery, vertebral artery, inferior thyroid artery, trachea, and esophagus, the puncture needle was inserted from the lateral transverse plane of the probe, and the carotid sheath was pushed to the outside as far as possible. To avoid vascular damage, when the tip of the needle entered the deep side of the prevertebral fascia on the surface of the cervical longus muscle, 0.2% ropivacaine hydrochloride 4 ml is slowly injected after pumping no blood, gas, or cerebrospinal fluid.

Tropisetron was administered intravenously 30 minutes preoperation ending. The intravenous analgesia pump was routinely used in all patients after operation. The formula was fentanyl $10 \mu\text{g}\cdot\text{kg}^{-1}$ + tropisetron 4 mg + dexmedetomidine $0.1 \mu\text{g}\cdot\text{kg}^{-1}\cdot\text{h}^{-1}$ diluted to 100 ml to relieve postoperative pain. After the patient entered the anesthesia recovery room, a suitable position for the patient was arranged. In addition to

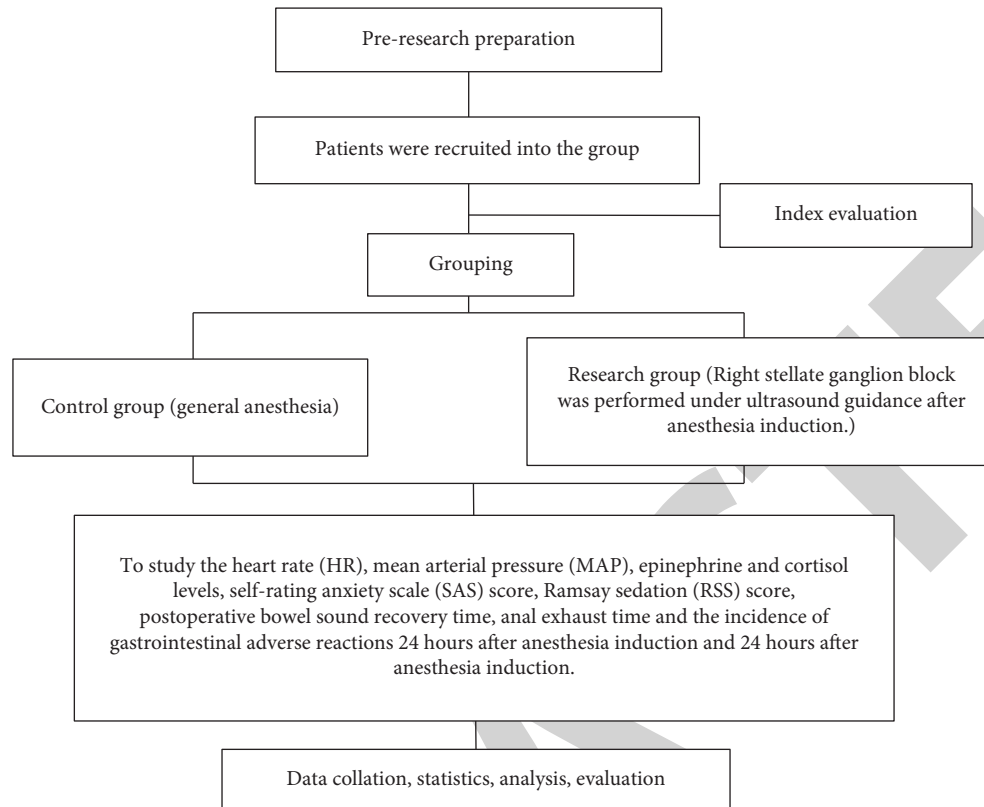


FIGURE 1: Technology roadmap.

psychological support measures by using words such as comfort and encouragement, nurses needed to make use of nonverbal skills, such as guiding patients to communicate with patients by blinking, nodding, and shaking their heads. Mental health education was given after the patients were fully conscious. According to the patient's own tolerance, the nurse carried out massage nursing to the patient according to the standard of gentle operation.

2.2.3. Observation Indicators

- (1) To study the heart rate (HR) and mean arterial pressure (MAP) before anesthesia induction and 24 hours after operation.
- (2) To study the levels of epinephrine and cortisol before and 24 hours after anesthesia induction, peripheral blood 5 ml was collected and centrifuged at 3000 for 5 minutes. The supernatant (plasma) was stored in a refrigerator at -80°C . The levels of adrenaline and cortisol were detected by using the ELISA kit. All ELISA kits are purchased from the CUSABIO company.
- (3) To study the scores of the self-rating anxiety scale (SAS) and the Ramsay sedation score (RSS) during anesthesia recovery, the score of the SAS was divided into 4 grades, including 20 items [19], of which, 15 items were described by negative words, calculated according to 1–4 scores. 5 items were described by positive words, calculated according to 4–1 scores.

The anxiety score of each item was added to get a rough score. On this basis, the integer part of the number multiplied by 1.25 was the final anxiety score. According to the standard of the Chinese norm, if the score was ≥ 50 , it was considered that the patient has anxiety disorder. The Ramsay sedation score scale was proposed by Ramsay in 1974 [20] and the Cronbach's α coefficient was 0.94. The score range of the scale was 1–6.

- (4) To study the recovery time of intestinal sound and the time of anal exhaust after operation.
- (5) To study the incidence of gastrointestinal adverse reactions 24 hours after operation.

2.3. Statistical Analysis. The statistical analyses of the results were carried out by SPSS 24.0. Statistical figures were plotted by Graphpad Prism 8.0. Data conforming to a normality distribution were represented as the mean \pm standard deviation ($\pm s$). The paired samples *t*-test was employed for intragroup comparisons, and the independent sample *t*-test was used for inter-group comparisons. $p < 0.05$ was considered statistically significant.

3. Results

3.1. The HR and MAP Values Were Studied before and 24 Hours after Anesthesia Induction. Twenty-four hours after operation, the HR and MAP values in both groups were

TABLE 1: Comparison of the HR before and 24 hours after anesthesia induction.

Group	Before induction of anesthesia (times/min)	24 hours after operation (times/min)
Control group ($n = 50$)	78.54 ± 7.19	$73.82 \pm 6.11^*$
Research group ($n = 50$)	78.35 ± 7.12	$71.69 \pm 6.23^*$
t value	0.133	1.726
p value	0.894	0.087

Note: the symbol*represents the comparison of 24 hours before and 24 hours after anesthesia induction in this group, $p < 0.05$

significantly lower than those before anesthesia induction ($p < 0.05$). See Tables 1 and 2.

3.2. The Levels of Epinephrine and Cortisol before and 24 Hours after Anesthesia Induction. Following 24-hour operation, the levels of epinephrine and cortisol in both groups were significantly higher than those before anesthesia induction ($p < 0.05$). Twenty-four hours after operation, the levels of epinephrine and cortisol in the research group were considerably lower than those in the control group ($p < 0.05$) (see Tables 3 and 4).

3.3. The Score of the SAS Scale and the RSS Scale during the Recovery Period of Anesthesia. The score of the SAS in the study cohort was considerably less than that in the control group ($p < 0.05$). The RSS score of the research group was greatly higher ($p < 0.05$) (see Table 5).

3.4. The Recovery Time of Intestinal Sound and the Time of Anal Exhaust after Operation. The recovery time of intestinal sound and the anal exhaust time in the study cohort became statistically shorter ($p < 0.05$) (see Table 6).

3.5. The Incidence of Gastrointestinal Adverse Reactions 24 Hours after Operation. The incidence of gastrointestinal adverse reactions 24 hours after operation in the research group was remarkably lower than that in the control group ($p < 0.05$) (see Table 7).

4. Discussion

Colorectal cancer is a malignant tumor of the digestive system, which is caused by genetic, environmental, and other factors. The global mortality rate of colorectal cancer is about 50%, with the fourth fatality rate [23]. The incidence of the disease is increasing in many countries because of their bad habits [24]. Nowadays, people's material life has improved significantly. These factors have led to the fastest increase in the incidence of colorectal cancer in China [25]. The main treatment for patients with early colorectal cancer is surgery, while patients with advanced colorectal cancer are treated with surgery on the basis of preoperative radiotherapy and chemotherapy [26]. However, operation and anesthesia can cause stress and inflammatory reactions and prolong the time needed for gastrointestinal recovery after operation [27, 28].

The sympathetic nervous system is widely distributed in the palace of primary and secondary lymphoid organs. The adrenergic receptors are also widely distributed in immune cells such as macrophages and neutrophils. When

sympathetic excitation occurs, sympathetic postganglionic fibers release catecholamines to activate adrenergic receptors of immune cells in lymphoid organs [29, 30]. In addition, sympathetic excitation can inhibit parasympathetic excitability. Surgical stimulation increased sympathetic excitability, aggravated perioperative inflammatory reaction, and delayed the recovery time of postoperative gastrointestinal function [31]. Therefore, choosing appropriate anesthesia, maintaining appropriate intraoperative management measures, and taking appropriate intervention measures to prevent excessive excitation of the sympathetic nervous system are very important for patients to quickly recover gastrointestinal function for anesthesiologists.

The stellate ganglion is a kind of a sympathetic ganglion. Its fibers can widely dominate the skin of the heart, brain, throat, shoulder and neck, trachea and bronchus, lung, and chest wall [32]. The stellate ganglion block refers to the injection of local anesthetic into the stellate ganglion and the loose connective tissue around it to inhibit the excitement of nerve cells by blocking the flow of sodium ions into the cell membrane. Reducing impulse transmission can achieve the purpose of reversibly blocking the stellate ganglion and its branches [33]. In recent years, ultrasound technology has become more and more mature and it has been widely used in all kinds of nerve block anesthesia. With the application of ultrasonic imaging technology in the process of the stellate ganglion block, we can observe the nerves, the blood vessels, the pleura, and other important tissues in real time and locate them accurately. We can also observe the specific location of the puncture needle and the distribution of anesthetics. By properly adjusting the puncture needle to make the drug spread evenly, we avoid an incomplete block and improve the success rate of puncture. Under the guidance of this visualization technique, we can use the minimum amount of anesthetic to achieve the best anesthetic effect and reduce the incidence of complications of the stellate ganglion block. Ultrasound has no radiation and will not cause damage to the human body during operation, which makes it more popular in clinics. Based on the advantages of ultrasound, the effects of the ultrasound-guided stellate ganglion block on hemodynamics and stressful response in patients with colorectal cancer were studied.

The results have proved that the ultrasound-guided stellate ganglion block can reduce the fluctuation of blood circulation, reduce the concentration of epinephrine and cortisol in peripheral blood, and reduce gastrointestinal dysfunction and stress reaction after operation. The anxiety can be relieved during the perianesthetic period so that the patients pass the anesthetic recovery period safely. This was mainly because all patients in this study underwent the

TABLE 2: Comparison of the map value before and 24 hours after anesthesia induction.

Group	Before induction of anesthesia (mm Hg)	24 hours after operation (mm Hg)
Control group ($n = 50$)	95.19 ± 9.08	$92.54 \pm 9.19^*$
Research group ($n = 50$)	95.24 ± 9.02	$91.38 \pm 9.12^*$
t value	0.028	0.634
p value	0.978	0.528

Note: the symbol*represents the comparison of 24 hours before and 24 hours after anesthesia induction in this group ($p < 0.05$).

TABLE 3: Comparison of the epinephrine levels before and 24 hours after anesthesia induction.

Group	Before induction of anesthesia (pg/ml)	24 hours after operation (pg/ml)
Control group ($n = 50$)	151.82 ± 32.11	$219.05 \pm 52.02^*$
Research group ($n = 50$)	151.69 ± 32.03	$175.03 \pm 41.01^*$
t value	0.020	4.699
p value	0.984	<0.01

Note: the symbol*represents the comparison of 24 hours before and 24 hours after anesthesia induction in this group, $p < 0.05$.

TABLE 4: Comparison of cortisol levels before and 24 hours after anesthesia induction.

Group	Before induction of anesthesia (ng/ml)	24 hours after operation (ng/ml)
Control group ($n = 50$)	82.12 ± 18.39	$174.19 \pm 39.25^*$
Research group ($n = 50$)	82.14 ± 18.44	$129.23 \pm 30.35^*$
t value	0.005	6.408
p value	0.996	<0.01

Note: the symbol*represents the comparison of 24 hours before and 24 hours after anesthesia induction in this group, $p < 0.05$.

TABLE 5: Comparison of the score of the SAS scale and the RSS scale during the recovery period of anesthesia.

Group	SAS scale (score)	RSS scale (score)
Control group ($n = 50$)	53.52 ± 4.12	3.24 ± 0.05
Research group ($n = 50$)	47.49 ± 1.09	5.18 ± 0.13
t value	10.005	98.489
p value	<0.01	<0.01

TABLE 6: Comparison of the recovery time of the bowel sound and the anal exhaust time after operation.

Group	Postoperative bowel sound recovery time (h)	Anal exhaust time (h)
Control group ($n = 50$)	57.23 ± 3.37	80.29 ± 2.64
Research group ($n = 50$)	38.18 ± 2.42	58.71 ± 1.15
t value	32.467	52.991
p value	<0.01	<0.01

TABLE 7: Comparison of the incidence of gastrointestinal adverse reactions 24 hours after operation.

Group	Nausea (case/%)	Vomiting (case/%)	Abdominal distension (case/%)	Incidence of gastrointestinal adverse reactions (case/%)
Control group ($n = 50$)	2/4.00	3/6.00	5/10.00	10/20.00
Research group ($n = 50$)	1/2.00	0/0.00	1/2.00	3/4.00
t value				4.640
p value				0.031

ultrasound-guided stellate ganglion block by the same anesthesiologist. Some studies pointed out that the left stellate ganglion block can increase left ventricular diastolic pressure and myocardial oxygen consumption, weaken myocardial

contractility, reduce the left ventricular ejection fraction, and increase the cardiac QT interval, while the right stellate ganglion block can effectively reduce sympathetic nerve activity, reduce cardiac oxygen consumption, and has little

effect on circulatory fluctuation [34, 35]. In addition, the stellate ganglion block can regulate autonomic nerve function, inhibit hyper sympathetic nerve, dilate the diameter of central and peripheral blood vessels, weaken stress response in vivo, and maintain normal blood perfusion in tissues and organs of the whole body [36]. The stellate ganglion block can also prolong the atrial effective refractory period and increase cardiac electrophysiological stability [37], which indicates maintaining the stability of the circulatory system in patients. Moreover, the stellate ganglion block can inhibit abnormally active sympathetic activity, reduce the levels of catecholamine and cortisol, weaken the body's stress response, and promote the recovery of human immune function to further inhibit inflammation [38]. At the same time, it can improve the blood circulation of the hypothalamus [39] and make the patients pass through the recovery period safely. It has been found that the stellate ganglion block can inhibit oxidative stress and early inflammatory response in patients with hemorrhagic shock, inhibit hypothalamic sympathetic nerve excitation, improve local tissue ischemia and hypoxia, and shorten the intestinal peristalsis time and anal exhaust time [40]. There are some limitations in this study. First, the sample size of this study is not large and it is a single-center study, so bias is inevitable. In future research, we will carry out multicenter, large-sample prospective studies, or more valuable conclusions can be drawn.

In conclusion, the ultrasound-guided stellate ganglion block can reduce the fluctuation of blood circulation during radical resection of colorectal cancer, the concentration of epinephrine and cortisol in peripheral blood, and gastrointestinal dysfunction and stress reaction after operation. The anxiety can be relieved during the perianesthetic period to promote the recovery of gastrointestinal function after operation.

Data Availability

The datasets used and analyzed during the current study are available from the corresponding author upon reasonable request.

Conflicts of Interest

The authors declare that they have no conflicts of interest.

References

- [1] W. Q. Chen, H. Li, and K. X. Sun, "[Report of cancer incidence and mortality in China, 2014]," *Zhonghua Zhongliu Zazhi*, vol. 40, pp. 5–13, 2018.
- [2] N. Wang, S. Liu, and L. Yang, "Interpretation of global cancer statistical report 2018," *Electronic Journal of Comprehensive Oncology Therapy*, vol. 5, no. 1, pp. 87–97, 2019.
- [3] R. Zheng, K. Sun, and S. Zhang, "Analysis of the prevalence of malignant tumors in China in 2015," *Chinese Journal of Oncology*, vol. 41, no. 1, pp. 19–28, 2019.
- [4] X. Wang, "Prevention and treatment of colorectal cancer from epidemiology," *Health report*, vol. 2, no. 10, p. 6, 2021.
- [5] Department of Planning Development and Informatization, "Department of Planning Development and Informatization Healthy China Action (2019-2030)," 2019, <http://www.nhc.gov.cn/guihuaxxs/s3585u/201907/e9275fb95d5b4295be8308415d4cd1b2.shtml>. 2019-07-15.
- [6] The Bureau of Disease Control and Prevention, "Circular of the CDC of the National Health Commission on Launching the National Cancer Prevention and Control Week 2020," 2020, <http://www.nhc.gov.cn/jkj/s5878/202003/8f30acddc9f84132a414233e8937d431.shtml.%202020-03-23>.
- [7] C. Aquina, S. Mohile, M. Tejani et al., "The impact of age on complications, survival, and cause of death following colon cancer surgery," *British Journal of Cancer*, vol. 116, no. 3, pp. 389–397, 2017.
- [8] A. Page, A. Ejaz, G. Spolverato et al., "Enhanced recovery after surgery protocols for open hepatectomy-physiology, immunomodulation, and implementation," *Journal of Gastrointestinal Surgery*, vol. 19, no. 2, pp. 387–399, 2015.
- [9] K. Rtibi, S. Selmi, D. Grami, H. Sebai, M. Amri, and L. Marzouki, "Irinotecan chemotherapy-induced intestinal oxidative stress: underlying causes of disturbed mucosal water and electrolyte transport," *Pathophysiology*, vol. 24, no. 4, pp. 275–279, 2017.
- [10] A. Montalbán Arques, M. Chaparro, J. Gisbert, and D. Bernardo, "The innate immune system in the gastrointestinal tract: role of intraepithelial lymphocytes and lamina propria innate lymphoid cells in intestinal inflammation," *Inflammatory Bowel Diseases*, vol. 24, no. 8, pp. 1649–1659, 2018.
- [11] Z. Moghadamyeghaneh, G. Hwang, M. Hanna et al., "Risk factors for prolonged ileus following colon surgery," *Surgical Endoscopy*, vol. 30, no. 2, pp. 603–609, 2016.
- [12] G. Theodoropoulos, I. Papanikolaou, T. Karantanos, and G. Zografos, "Post-Colectomy assessment of gastrointestinal function: a prospective study on colorectal cancer patients," *Techniques in Coloproctology*, vol. 17, no. 5, pp. 525–536, 2013.
- [13] G. Theodoropoulos, N. Memos, K. Peitsidou, T. Karantanos, B. G. Spyropoulos, and G. Zografos, "Synbiotics and gastrointestinal function-related quality of life after elective colorectal cancer resection," *Annals of Gastroenterology*, vol. 29, no. 1, pp. 56–62, 2016.
- [14] E. Schneider, O. Hyder, B. Brooke et al., "Patient readmission and mortality after colorectal surgery for colon cancer: impact of length of stay relative to other clinical factors," *Journal of the American College of Surgeons*, vol. 214, no. 4, pp. 390–398, 2012.
- [15] Y. Chen, "Chinese expert consensus and path Management Guide for accelerated Rehabilitation surgery (2018)," *Chinese Journal of Anesthesiology*, vol. 38, no. 01, pp. 8–13, 2018.
- [16] H. Li, D. Xia, and W. Huiping, "Effect of preoperative stellate ganglion block on gastrointestinal function after abdominal operation in rats," *Journal of Clinical Anesthesiology*, vol. 33, no. 01, pp. 66–70, 2017.
- [17] W. W. Zung, "A rating instrument for anxiety disorders," *Psychosomatics*, vol. 12, no. 6, pp. 371–379, 1971.
- [18] W. Zhou and Z. Wang, "Research progress of analgesia and sedation nursing for patients with mechanical ventilation in ICU," *Chinese Journal of first Aid of Integrated traditional Chinese and Western Medicine*, vol. 24, no. 5, pp. 556–560, 2017.
- [19] C. M. Ding, J. He, and W. Y. Liao, "Regulation of WNT/ β -catenin signaling by carbamoyl-phosphate synthetase 2, aspartate transcarbamylase, and dihydroorotase (CAD) in colorectal cancer cell," *International Journal of Clinical and Experimental Medicine*, vol. 10, no. 12, Article ID 16243, 2017.

Retraction

Retracted: Correlation between Sputum Bacterial Culture Positive Rate and Drug Sensitivity Test Results and Disease Severity in Inpatients and Its Clinical Significance: A Systematic Review and Meta-Analysis

Computational Intelligence and Neuroscience

Received 25 July 2023; Accepted 25 July 2023; Published 26 July 2023

Copyright © 2023 Computational Intelligence and Neuroscience. This is an open access article distributed under the Creative Commons Attribution License, which permits unrestricted use, distribution, and reproduction in any medium, provided the original work is properly cited.

This article has been retracted by Hindawi following an investigation undertaken by the publisher [1]. This investigation has uncovered evidence of one or more of the following indicators of systematic manipulation of the publication process:

- (1) Discrepancies in scope
- (2) Discrepancies in the description of the research reported
- (3) Discrepancies between the availability of data and the research described
- (4) Inappropriate citations
- (5) Incoherent, meaningless and/or irrelevant content included in the article
- (6) Peer-review manipulation

The presence of these indicators undermines our confidence in the integrity of the article's content and we cannot, therefore, vouch for its reliability. Please note that this notice is intended solely to alert readers that the content of this article is unreliable. We have not investigated whether authors were aware of or involved in the systematic manipulation of the publication process.

In addition, our investigation has also shown that one or more of the following human-subject reporting requirements has not been met in this article: ethical approval by an Institutional Review Board (IRB) committee or equivalent, patient/participant consent to participate, and/or agreement to publish patient/participant details (where relevant).

Wiley and Hindawi regrets that the usual quality checks did not identify these issues before publication and have since put additional measures in place to safeguard research integrity.

We wish to credit our own Research Integrity and Research Publishing teams and anonymous and named external researchers and research integrity experts for contributing to this investigation.


The corresponding author, as the representative of all authors, has been given the opportunity to register their agreement or disagreement to this retraction. We have kept a record of any response received.

References

- [1] W. Zhou and J. Li, "Correlation between Sputum Bacterial Culture Positive Rate and Drug Sensitivity Test Results and Disease Severity in Inpatients and Its Clinical Significance: A Systematic Review and Meta-Analysis," *Computational Intelligence and Neuroscience*, vol. 2022, Article ID 5102100, 9 pages, 2022.

Research Article

Correlation between Sputum Bacterial Culture Positive Rate and Drug Sensitivity Test Results and Disease Severity in Inpatients and Its Clinical Significance: A Systematic Review and Meta-Analysis

Wenjing Zhou and Jing Li 

Department of Laboratory Lianyungang TCM Hospital Affiliated to Nanjing University of Chinese Medicine, Lianyungang, Jiangsu 222004, China

Correspondence should be addressed to Jing Li; fsyy01270@njucm.edu.cn

Received 16 May 2022; Revised 6 June 2022; Accepted 8 June 2022; Published 14 July 2022

Academic Editor: Dong Chen

Copyright © 2022 Wenjing Zhou and Jing Li. This is an open access article distributed under the Creative Commons Attribution License, which permits unrestricted use, distribution, and reproduction in any medium, provided the original work is properly cited.

Objective. To systematically evaluate the correlation between the positive rate of sputum bacterial culture and the results of drug sensitivity test and the severity of the disease and its clinical significance, so as to provide evidence-based medicine for clinical application. **Methods.** PubMed, Embase, ScienceDirect, Cochrane Library, China Knowledge Network Database (CNKI), China VIP Database, Wanfang Database, and China Biomedical Literature Database (CBM) online database were used. The retrieval time limit was from the establishment of the database to the present. Data for all included studies were extracted by two independent researchers, and the risk of bias for the quality of each included study was assessed by the Cochrane Handbook 5.1.0 criteria. RevMan5.4 statistical software was used to analyze the collected data by meta. **Results.** In the end, 6 RCT articles were included. Overall, 613 samples were included in 6 RCT studies. The correlation between the positive rate of sputum bacterial culture in inpatients and the severity of the disease was meta-analyzed. The heterogeneity test results showed that $\chi^2 = 177.20$, $df = 3$, $P < 0.00001$, and $I^2 = 98\%$, indicating that there was obvious heterogeneity among the included research data. It was considered that there was a correlation between the positive rate of sputum bacterial culture and the severity of the disease. The correlation between the results of the drug sensitivity test of inpatients and the severity of the disease was evaluated. The results of the heterogeneity test showed that $\chi^2 = 0.00$, $df = 1$, $P = 1 > 0.05$, and $I^2 = 0\%$, indicating that there was no heterogeneity among the included research data. In addition, the combined effect of WMD was analyzed by the fixed effect model. The combined effect dose WMD test was $Z = 6.58$ ($P < 0.00001$). It was considered that there was a correlation between the results of the drug sensitivity test and the severity of the disease. **Conclusion.** There is a correlation between positive sputum culture and drug sensitivity test results and the severity of the disease in hospitalized patients. In clinical practice, for hospitalized patients, the positive sputum bacterial culture rate and drug sensitivity test results can be used to guide the appropriate use of antibiotics. Due to the low input from the literature, more studies with higher methodological quality and longer follow-up are needed for further validation.

1. Introduction

Pulmonary infection is a common respiratory disease. Influenza and pneumonia were combined as the eighth leading cause of death in the United States in 2011, according to the Centers for Disease Control and Prevention [1]. There are many kinds of pathogens that cause pulmonary infection,

including bacteria, fungi, viruses, atypical pathogens, and parasites. Due to the widespread use of a variety of antimicrobials, the pathogen spectrum of pulmonary infection is diversified. According to relevant reports [2], the mortality rate of hospitalized pneumonia patients is 11.7%. The mortality rate of pneumonia patients in the pencil ICU is as high as 45% [3]. Without timely anti-infective treatment, it is

easy to develop into cause systemic inflammatory response syndrome and then involve other organs, even lead to death of patients [4]. If antibiotics are abused, it will lead to an increase in the number of drug-resistant strains; if only empirical use of antibiotics, it is difficult to control infection, so it is necessary to select appropriate antibiotics according to the results of drug sensitivity. The selection methods of antibiotics for pulmonary infection include empirical selection and etiological diagnosis. Empirical drug selection is based on clinical data, previous pathogenic diagnosis, and experience in anti-infective treatment. Selection of anti-infective drugs that may be sensitive to anti-infective therapy was done. Etiological diagnostic drug selection refers to the method of selecting sensitive antibiotics for anti-infective treatment according to the results of the microbial culture and drug sensitivity test. When selecting drugs, the drug sensitivity test shows that they are sensitive to many kinds of antibiotics at the same time and then choose antibiotics with high sensitivity, narrow antibacterial spectrum, and low toxicity [5]. At present, some infection indexes such as C-reactive protein and procalcitonin are often used to diagnose pulmonary infection, but these indexes are lack of specificity. Bacteriological examination as a pathogen type of infectious disease is easy to be disturbed by many factors, so it is difficult to provide gold standard for disease diagnosis and treatment and its clinical application significance is low [6].

When bacterial infection occurs in human lungs or bronchi, the amount of sputum increases significantly. Sputum bacterial culture is performed by collecting the patient's sputum as a sample and growing the sample in a culture medium to observe the growth of bacteria. The identification of bacteria that have grown can identify the pathogenic bacteria in sputum, such as pneumococci, *Moraxella catarrhalis*, and *Klebsiella pneumoniae* [7]. It is helpful to the diagnosis and treatment of lower respiratory tract infectious diseases. In addition, the TB sputum culture cycle is long, usually taking half a month to a month, and it takes 2 months to get results for a complete dosing [8]. The pathogenic information of lung and bronchial lesions can be obtained through sputum culture, and then targeted intervention and treatment. The pharynx, larynx, and tonsils belong to the upper respiratory tract, and their diseases can also be obtained by expecting sputum culture to obtain pathogenic information. Based on the results of sputum culture, sensitive antibiotics can be selected. The drug sensitivity test is the abbreviation of the drug sensitivity test. The method is to take samples containing pathogenic bacteria from the infection site of the patient and inoculate them on a certain culture medium. At the same time, stick the paper with antibiotics on the surface of the culture medium and then observe the culture results. It is suitable to understand the sensitivity of pathogenic microorganisms to various antibiotics, so as to guide the rational selection of antibiotics in clinic. If a pathogen needs a small dose of antibiotics to inhibit and kill it, we say that the pathogen is sensitive to the antibiotic [9]. If a pathogenic bacterium needs a large dose of antibiotics to inhibit and kill it, we call it insensitive or resistant to this kind of antibiotics. If the

pathogenic bacteria are sensitive to antibiotics, the larger the bacteriostatic circle is, and if the pathogenic bacteria are not sensitive to antibiotics, the smaller the bacteriostatic zone is. The size of the bacteriostatic zone is proportional to whether it is sensitive or not. The drug sensitivity test can guide the rational use of drugs [10]. Based on this, this study systematically evaluated the correlation between the positive rate of sputum bacterial culture and the results of the drug sensitivity test and the severity of the disease, as well as the clinical guiding significance, so as to provide evidence-based medicine for clinical use.

2. Research Contents and Methods

2.1. Sources and Retrieval Methods of Documents. The computer searched The Cochrane Library, Embase, PubMed, Web of Science, SinoMed, China Knowledge Network, Wanfang data knowledge Service platform, and VIP. The Chinese search words were "hospitalized patients, positive rate of sputum bacterial culture, results of drug sensitivity test, severity of disease, correlation, and clinical guiding significance." The search time limit was to build each database to 2022–4.

2.2. Inclusion and Exclusion Criteria of Literature

2.2.1. Literature Inclusion Criteria. (1) Research type: the randomized controlled trials (RCTs) were included on the correlation between sputum bacterial culture positive rate and drug sensitivity test results and disease severity in all inpatients in China. The language was limited to Chinese. (2) Participants: patients with positive rate of sputum bacterial culture were tested for drug sensitivity.

2.2.2. Document Exclusion Criteria. (1) It was not a randomized controlled study. (2) The data report was incomplete and the data cannot be used. (3) Repeated the research content and the latest research. (4) The full text cannot be obtained.

2.3. Quality Evaluation and Data Extraction

(1) Data for all included studies were extracted by two independent researchers, and the risk of bias for the quality of each included study was assessed by the Cochrane Handbook 5.1.0 criteria. The differences were resolved through discussion or asked the third researcher to negotiate and decide. The extracted data included the first author, year of publication, group, number of cases, age, prognosis index, and so on. The modified Jadad scale was used to evaluate the quality of the study, including the generation of random sequence (appropriate 2, unclear 1, and inappropriate 0), allocation concealment (appropriate 2, unclear 1, and inappropriate 0), blind (implementation 2, unclear 1, and unimplemented 0), and withdrawal and loss of follow-up (description

1 and undescribed 0). 0–3 was classified as low-quality research and 4–7 as high-quality research.

- (2) Data extraction: the extracted data were transformed as follows and then the data were analyzed by meta with RevMan5.0 software. The conversion formula is as follows [11]:

$$\begin{aligned} \text{Fisher's } Z: Z &= 0.5 * \ln\left(\frac{(1+r)}{(1-r)}\right), \\ Vz &= \frac{1}{(n-3)}, \\ Sez &= Vz \Delta 0.5, \\ r &= \frac{(e^{\Delta 2z} - 1)}{(e^{\Delta 2z} + 1)}. \end{aligned} \quad (1)$$

2.4. Outcome Indicators. All the studies included were sputum bacterial culture positive rate and drug sensitivity test results to evaluate the severity of inpatients. The correlation between sputum bacterial culture positive rate and drug sensitivity test results to evaluate the severity of inpatients was expressed by Pearson correlation coefficient r value, so the Pearson correlation coefficient r value was used as the comprehensive outcome index. A negative value of r indicated a positive correlation between the positive rate of sputum bacterial culture and the results of the drug sensitivity test to evaluate the severity of hospitalized patients.

2.5. Statistical Processing. RevMan5 software was used for meta-analysis. Continuous variables were represented by standardized mean difference (SMD) and its 95%CI. If there was no statistical heterogeneity among the studies ($P > 0.100$, $I^2 < 50\%$), the fixed effect model was used for analysis. Otherwise, the random effect model was used for analysis. If there was statistical heterogeneity, the sources of heterogeneity and subgroup were analyzed the factors that may lead to heterogeneity among the studies. If there is statistical heterogeneity but without clinical heterogeneity or statistically significant difference between the two groups, the random effect model was used for analysis. The sensitivity analysis was carried out by remerging the calculation after excluding the literature one by one. When the heterogeneity between the two groups was too large or unable to find the data source, descriptive analysis was used. Publication bias was analyzed by Egger's test. $P < 0.05$ means the difference is statistically significant.

3. Results and Analysis

3.1. The Literature Retrieval and the Basic Situation of Literature Inclusion. 2133 articles were obtained by computer database search, and 432 articles were obtained after eliminating repeated studies. 56 articles were obtained from preliminary reading of titles and abstracts, irrelevant studies, reviews, case reports, and no control literature were

excluded. 17 articles were initially included, and full text was carefully read. 11 articles with incomplete data and no main outcome indicators were excluded. Finally, 6 RCTs were included [12–17]. In total, 613 samples were analyzed by meta. The basic features included in the literature are shown in Table 1.

3.2. Evaluation of the Quality of the Methodology Included in the Literature. Six RCT literature studies were included to report the baseline of patients, and the included six studies all gave detailed intervention measures and follow-up time. RCT did not describe in detail the number and reasons of blindness and loss of follow-up or withdrawal. Risk bias is shown in Figure 1 and 2.

3.3. Results of Meta-Analysis

3.3.1. Meta-Analysis of Fisher's Z Intermediate Conversion Value. Due to the large number of data, this paper only showed positive results.

3.3.2. Correlation between the Positive Rate of Sputum Bacterial Culture and the Severity of the Disease. A total of 613 samples were included in 6 RCT studies. The correlation between the positive rate of sputum bacterial culture and the severity of the disease was analyzed by meta. The heterogeneity test results showed that $\text{Chi}^2 = 177.20$, $\text{df} = 3$, $P < 0.00001$, and $I^2 = 98\%$, indicating that there was obvious heterogeneity among the included research data. It was considered that there was a correlation between the positive rate of sputum bacterial culture and the severity of the disease. The results are shown in Figure 3.

3.3.3. Correlation between the Results of Drug Sensitivity Test and the Severity of the Disease. Six RCT studies were included with 613 samples. The correlation between the results of the drug sensitivity test and the severity of the disease in inpatients were assessed. The heterogeneity test results showed that $\text{Chi}^2 = 0.00$, $\text{df} = 1$, $P = 1 > 0.05$, and $I^2 = 0\%$, indicating that there was no heterogeneity among the included research data, and the combined effect WMD was analyzed by the fixed effect model. The combined effect dose WMD test was $Z = 6.58$ ($P < 0.00001$). It was considered that there was a correlation between the results of the drug sensitivity test and the severity of the disease. The results are shown in Figure 4.

4. Discussion

Nosocomial infections include infections that occur during hospitalization and acquired in the hospital but after discharge [18]. Nosocomial infections mainly include pneumonia, urinary tract infection, and hematogenous infection [19], which mostly occur in patients with mechanical ventilation, urinary catheterization, intravenous catheterization, and long-term use of antibiotics [20]. The common pathogens are *Klebsiella pneumoniae*, *Acinetobacter baumannii*,

TABLE 1: Basic characteristics of the literature.

Include the literature	Year of publication	N	Age	Average age	Disease type	Correlation coefficient between the positive rate of sputum bacterial culture and the severity of disease	Correlation coefficient between the results of drug sensitivity test and the severity of the disease	Conclusion
Fan Xin	2019	53	24–77	53.47 ± 6.38	Pneumonia	$r = -0.495$	-	Most of the patients with acute exacerbation of bronchiectasis were positive for sputum culture, suggesting that there was a certain correlation between the severity of the disease and the positive results of sputum culture.
Tian Yu	2015	60	33–68	50.4 ± 7.2	Chronic obstructive pulmonary disease	$r = -0.673$	-	Sputum culture was positive, indicating that the patient had bacterial infection, and AECOPD was related to the severity of bacterial infection.
Zhao Mingli	2013	100	68–89	78.38 ± 5.87	Chronic obstructive pulmonary disease	$r = -0.839$	-	Pulmonary fungal infection, especially <i>Aspergillus</i> infection, may be one of the causes of persistent wheezing in patients with chronic obstructive pulmonary disease.
Zhang Yaodong	2012	96	25–56	36.93 ± 4.53	Pneumonia	-	$r = 0.732$	The drug resistance rate of most bacteria is positively correlated with the frequency of antibiotics. According to the disease severity of inpatients, the monitoring of bacterial drug resistance and the management of clinical application of antibiotics should be strengthened.
Zhong Jiao	2011	104	33–84	56.39 ± 4.34	Pneumonia	-	$r = 0.811$	The drug resistance of bacteria is related to the severity of the disease in inpatients, suggesting that the clinical use of antibiotics should be standardized to reduce the production of drug-resistant bacteria.
Peng Min	2008	200	6–34	15.39 ± 2.44	Acute attack of bronchial asthma	$r = 0.133$	-	The main inducing factors of asthma attack were upper respiratory tract infection, followed by dust mites, house dust, and pollen. Lower respiratory tract infection is relatively rare, and the positive rate of sputum culture is low, which is not the main inducing factor of asthma attack.

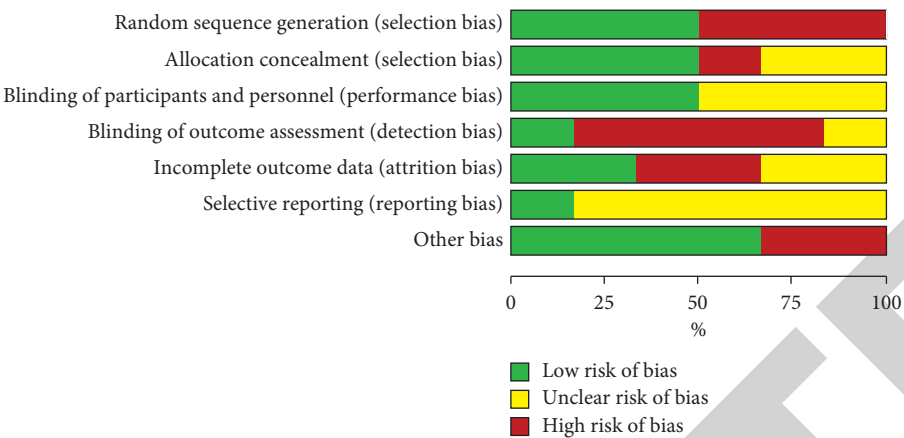


FIGURE 1: Risk of bias assessment of included studies.

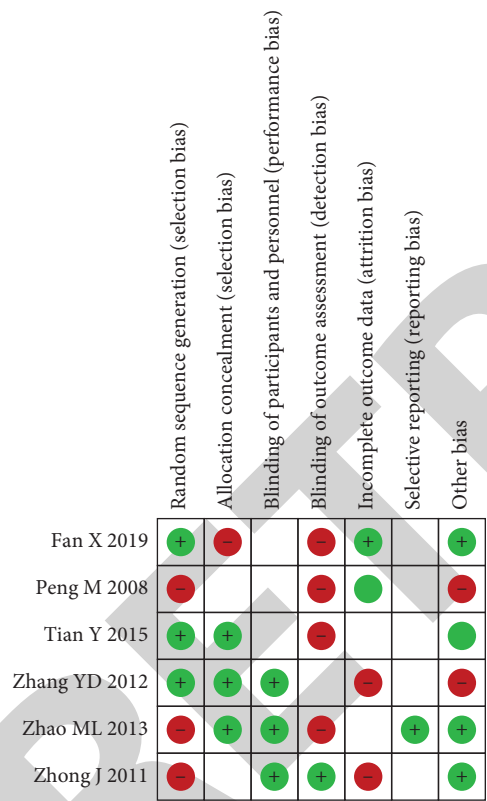


FIGURE 2: Summary chart of risk bias of included studies.

Escherichia coli, *Pseudomonas aeruginosa*, and *Staphylococcus aureus* [21]. Hospital-acquired infection is one of the main causes of death of critically ill patients [22]. The main cause of hospital-acquired infection is that the pathogenic bacteria develop drug resistance due to long-term or large-scale antibiotic treatment during hospitalization. Therefore, clinicians need to be familiar with and master the characteristics of hospital-acquired infection in actual work. This helps reduce the incidence of infection in patients. The current study showed that the main pathogens of hospital-acquired infection were Gram-negative bacteria dominated by *Acinetobacter baumannii*, *Pseudomonas aeruginosa*,

Klebsiella pneumoniae, and *Escherichia coli*, Gram-positive bacteria dominated by *Staphylococcus aureus*, and fungi dominated by *Candida* [23]. The drug resistance of pathogens of hospital-acquired infection is suitable for the delayed use of antibiotics, which can not only increase the mortality of patients but also increase the drug resistance of bacteria in hospital [24]. Charles-Edouard Luyt et al. mentioned that 30% of the antibiotics used by hospitalized patients are unnecessary for patients and are not the most preferred antibiotics for the pathogen [25]. The long-term use of these antibiotics may lead to the emergence of bacterial resistance. To a certain extent, the distribution of bacteria is different from that in the general ward and the types of drug resistance of pathogens are wider than those in the general ward. Ramesh Venkataraman et al. analyzed the isolated strains of each flora collected, and in terms of the proportion of multiple drug-resistant bacteria [26]. The proportion of immobile bacteria, *Klebsiella*, *Escherichia coli*, *Pseudomonas*, and staphylococci was 87.5%, 75.5%, 61.9%, 58.9%, and 2.4%, respectively. Among Gram-negative bacteria, extended-spectrum β -lactamase-producing strains accounted for 34%, including *Klebsiella* (41.1%), *Escherichia coli* (26.4%), and *Pseudomonas* (23.5%). Carbapenem antibiotics are used as the first-line treatment of extended-spectrum β -lactamase-producing *Klebsiella pneumoniae* with the rapid increase of carbapenem-resistant strains, and the choice of antibiotic therapy is very limited [27]. Wirlaine Glaucel Maciel et al. have believed that the production of metallo- β -lactamases is one of the important reasons for the resistance of *Pseudomonas aeruginosa* to β -lactam antibiotics including carbapenem antibiotics [28]. In their study, drug sensitivity tests showed that polymyxin B and colistin could be used as treatment options. The study of Voichița Lăzureanu et al. showed that the resistance rate of *Acinetobacter baumannii* to carbapenem antibiotics increased gradually [29]. Colistin was the only drug that maintained low resistance to *Acinetobacter baumannii* among the antibiotics used in this study. Ainihayati Noordin et al.'s research showed that 34% of methicillin-resistant *Staphylococcus aureus* (MRSA) was resistant to ciprofloxacin, ERY, and gentamicin, but sensitive to vancomycin and teicoplanin [30]. These reports suggest the prevalence of

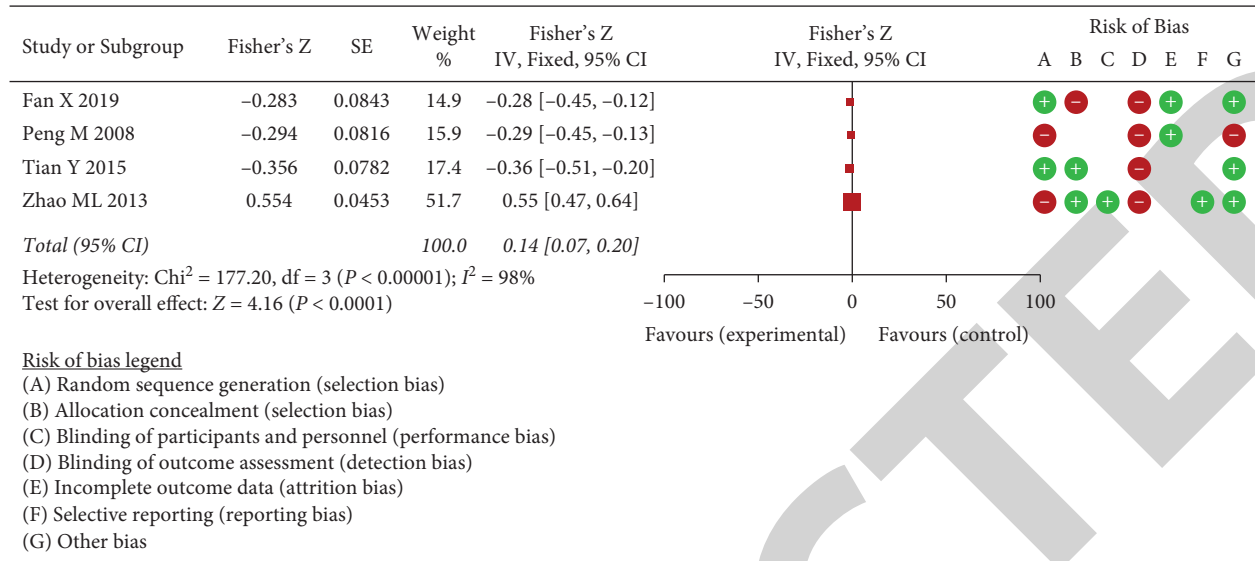


FIGURE 3: Forest plot of the positive rate of sputum bacterial culture and the severity of the disease.

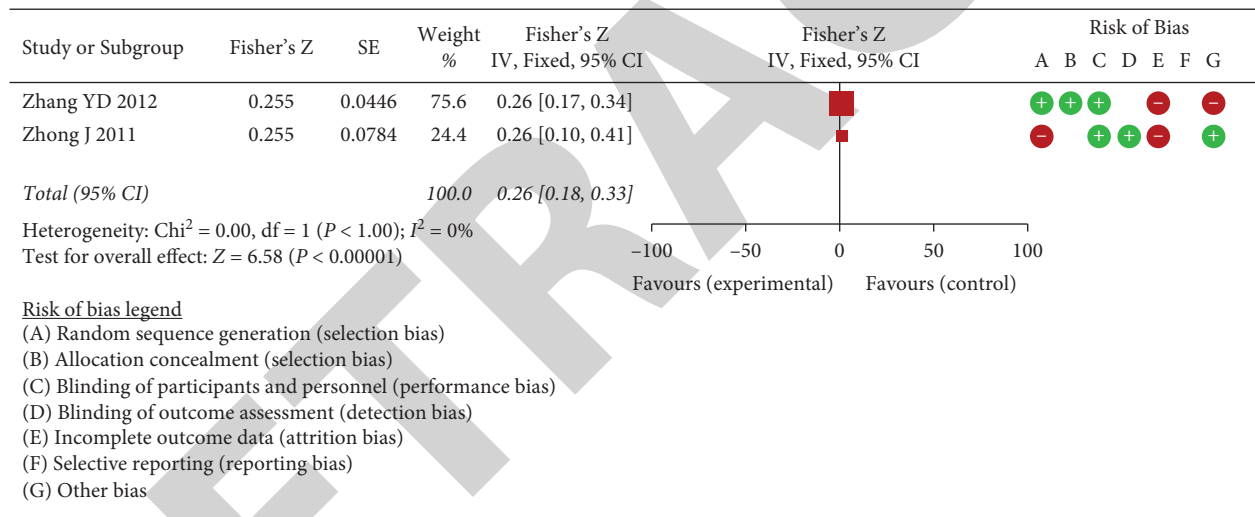


FIGURE 4: Forest plot of drug sensitivity test and the severity of the disease.

multi-drug-resistant bacteria, only a few advanced antibiotics maintain a low resistance rate, and some antibiotics cannot be used in some cases because of their side effects, resulting in more limited use of antibiotics.

Pulmonary infection can be life-threatening, especially for patients with low immune function and potential pulmonary dysfunction, such as cystic fibrosis and chronic obstructive pulmonary disease. According to the World Health Organization, lung infection was the leading cause of death in 2012. Eradicating lower respiratory tract infection is an arduous task [31]. Long-term use of antibiotics can easily lead to bacterial drug resistance. In view of bacterial drug resistance, if we do not selectively select sensitive antibiotics for pathogens, it will not only increase the economic burden but also delay the disease. Therefore, the etiological diagnosis of pulmonary infection is particularly important. The quality of sputum samples has a great influence on the diagnosis of

sputum culture. Specimens from the lower respiratory tract may be contaminated by upper respiratory secretions during collection, and some poorly collected specimens may be composed entirely of upper respiratory secretions [32–35]. Either way, it can lead to the wrong conclusion that an organism that settles in the upper airway is causing pneumonia. Therefore, the standard practice of the diagnostic laboratory is to use indicators to evaluate the quality of sputum samples, which indicate that sputum samples are obtained from the lower respiratory tract. This includes evaluating the number of squamous epithelial cells (Secs) and polymorphonuclear cells (Pmns) in Gram staining smears [36]. Infection is a common complication of inpatients, and it may lead to prolonged hospitalization and high medical costs and even lead to death, so the prevention of infection is particularly important. Preventive measures mainly include the following: (1) strict central venous

catheterization nursing. After 15 days of catheterization, the incidence of hematogenous infection increased sharply [37]. Therefore, regular removal and replacement of tubes should be taken into consideration. (2) Limit the application of acid inhibitors. Acid inhibitors can increase the incidence of delayed septicemia with the extension of time. The incidence will gradually increase, especially Gram-negative bacilli and fungal septicemia [38]. (3) Oral care and withdrawal as soon as possible. Sean van Diepen et al. have believed that raising the head of the bed, oral care with chlorhexidine and withdrawing the machine as soon as possible can reduce ventilator-associated pneumonia [36]. (4) Clean environment and hand hygiene. Patti et al. believed that a clean environment can reduce the spread of pathogens [39]. The hands of health care workers in the intensive care unit can also pollute the indoor environment after being contaminated, including the head of the patient's bed and sphygmomanometer cuff, which can also increase the risk of infection. (5) Limit the use of antibiotics. The study has shown that contact isolation, hand hygiene, and antibiotic control can be used as basic preventive measures for methicillin-resistant *Staphylococcus aureus* and multi-drug-resistant *Acinetobacter baumannii* infection [40–42]. Some scholars feel that communication and continuing education can reduce central venous catheter-related blood flow infection [43]. Typically, hospitalized patients are critically ill, in poor baseline condition, and the pathogens are mostly multi-drug-resistant bacteria. The choice of antibiotics available is very limited, and treatment is difficult, factors that can lead to a poor prognosis or even death.

Finally, we included 6 RCT articles. A total of 613 samples were analyzed by meta. The correlation between the positive rate of sputum bacterial culture and the severity of the disease was analyzed by meta. The results of the heterogeneity test showed that $\text{Chi}^2 = 177.20$, $\text{df} = 3$, $P < 0.00001$, and $I^2 = 98\%$, indicating that there was obvious heterogeneity among the included research data. In addition, it was considered that there was a correlation between the positive rate of sputum bacterial culture and the severity of the disease. Through the inclusion of 6 RCT studies, the correlation between the results of the drug sensitivity test of inpatients and the severity of the disease was analyzed by meta. The results of the heterogeneity test showed that $\text{Chi}^2 = 0.00$, $\text{df} = 1$, $P = 1 > 0.05$, and $I^2 = 0\%$, indicating that there was no heterogeneity among the included research data, and the combined effect of WMD was analyzed by the fixed effect model. The combined effect dose WMD test was $Z = 6.58$ ($P < 0.00001$). It can be considered that there was a correlation between the results of the drug sensitivity test and the severity of the disease. Due to the status of inpatients and the application of invasive measures, there is a high incidence of infection. This prolongs hospital stays and even aggravates the condition, leading to death [44–46]. Generally, culture drug sensitivity tests for pathogenic bacteria take a long time and require empirical treatment by the physician. The resistant and heterogeneous nature of the infecting bacteria, as well as the underlying illness of the patient, make it impossible for the patient to use some antibiotics, which makes it very difficult for doctors to use

empirical drugs. Therefore, the sputum culture test is used to determine whether patients are infected with bacteria. Combined with the results of the drug sensitivity test, medication for patients can achieve rational use of drugs and achieve the purpose of treating diseases [47].

In conclusion, there is a certain correlation between the sputum bacterial culture positive rate and drug sensitivity test results of inpatients and the severity of the disease. Based on the results of sputum culture, sensitive antibiotics can be selected for hospitalized patients. Due to less literature input, more studies and follow-up with higher methodological quality are needed for further verification.

Data Availability

No data were used to support this study.

Conflicts of Interest

The authors declare that they have no conflicts of interest.

References

- [1] T. I. G. A. B. U. Tigabu and A. L. E. M. Getaneh, "Staphylococcus aureus, ESKAPE bacteria challenging current health care and community settings: a literature review," *Clinical Laboratory*, vol. 67, no. 7, 2021.
- [2] B. A. T. O. O. L. Sadia, D. A. L. I. A. Almaghaslah, and A. L. Q. A. H. T. A. N. I. Ali, "Aetiology and antimicrobial susceptibility pattern of bacterial isolates in community acquired pneumonia patients at Asir region, Saudi Arabia," *International Journal of Clinical Practice*, vol. 75, no. 2, Article ID e13667, 2021.
- [3] A. N. A. R. Homann, L. A. U. R. A. Niebling, S. T. E. F. E. N. Zehnle et al., "A microfluidic cartridge for fast and accurate diagnosis of *Mycobacterium tuberculosis* infections on standard laboratory equipment," *Lab on a Chip*, vol. 21, no. 8, pp. 1540–1548, 2021.
- [4] Y. U. L. I. A. Yulia, J. O. S. E. P. H. I. N. E. Mariza, Soedarsono, and F. Herawati, "Bacterial profile and antibiotic use in pneumonia patients at dr. Soetomo general hospital," *Current Respiratory Medicine Reviews*, vol. 16, no. 1, pp. 21–27, 2020.
- [5] A. Jitmuang, T. Naksanguan, and R. Sirijatuphat, "Implementation of the World health organization's global antimicrobial resistance surveillance system (GLASS) for the surveillance of sputum specimens collected from patients at siriraj hospital," *Journal of the Medical Association of Thailand =: Chotmaihet thangphaet*, vol. 103, no. 3, pp. 198–209, 2020.
- [6] P. A. T. R. I. C. K. Stafler, G. A. L. Zaks Hoffer, O. D. E. D. Scheuerman et al., "Diagnostic value of sputum cultures in children under 2 years of age with chronic suppurative lung diseases," *Pediatric Pulmonology*, vol. 55, no. 12, pp. 3421–3428, 2020.
- [7] P. Kolia-Diafouka, S. Carrère-Kremer, M. Lounnas et al., "Detection of *Mycobacterium tuberculosis* in paucibacillary sputum: performances of the Xpert MTB/RIF ultra compared to the Xpert MTB/RIF, and IS6110 PCR," *Diagnostic Microbiology and Infectious Disease*, vol. 94, no. 4, pp. 365–370, 2019.
- [8] J. A. M. E. S. Como, M. A. T. T. H. E. W. A. Moffa, N. I. T. I. N. Bhanot et al., "Potential false-positive urine *Legionella* enzyme immunoassay test results," *European*

- Journal of Clinical Microbiology & Infectious Diseases*, vol. 38, no. 7, pp. 1377–1382, 2019.
- [9] R. E. N. A. N. M. A. R. I. C. H. I. Mauch, C. L. Rossi, L. U. C. I. O. Nolasco da Silva et al., “Secretory IgA-mediated immune response in saliva and early detection of *Pseudomonas aeruginosa* in the lower airways of pediatric cystic fibrosis patients,” *Medical Microbiology and Immunology*, vol. 208, no. 2, pp. 205–213, 2019.
 - [10] N. Collins, D. Amin, and K. Kentosova, “Children’s sputum-induced positive bacteria culture is superior to cough swab positive bacteria culture, and its role in evaluating the success of eradication treatment of *Pseudomonas aeruginosa*,” *Pediatric Pulmonology*, vol. 54, no. Suppl.2, p. S276, 2019.
 - [11] F. A. K. H. R. I. Fakhri, M. A. R. W. A. L. I. Marwali, B. U. D. I. W. A. R. D. H. A. N. A. Budiwardhana, P. S. Roebiono, A. U. Rahajoe, and M. Caesario, “Diagnosing infection after infant open heart surgery: role of procalcitonin,” *Asian Cardiovascular & Thoracic Annals*, vol. 27, no. 8, pp. 641–645, 2019.
 - [12] J. I. A. N. Du, W. E. I. Shu, Y. U. H. O. N. G. Liu et al., “Development and validation of external quality assessment panels for mycobacterial culture testing to diagnose tuberculosis in China,” *European Journal of Clinical Microbiology & Infectious Diseases*, vol. 38, no. 10, pp. 1961–1968, 2019.
 - [13] Yu Tian, “Study on the relationship between acute exacerbation of chronic obstructive pulmonary disease and bacterial infection [J],” *Chinese and foreign medical research*, vol. 13, no. 27, pp. 8–10, 2015.
 - [14] M. Zhao, H. Chen, and Y. Wang, “Study on the relationship between positive sputum fungal culture and persistent wheezing in patients with chronic obstructive pulmonary disease,” *Chinese Journal of Hospital infection*, vol. 23, no. 19, pp. 4647–4649, 2013.
 - [15] Y. Zhang, H. Wang, and J. Hu, “Analysis of the correlation between bacterial drug resistance and the use of antibiotics,” *Chinese pharmacist*, vol. 15, no. 11, pp. 1632–1633, 2012.
 - [16] J. Zhong, Z. Yan, and W. Zhao, “Investigation of bacterial drug resistance in our hospital and analysis of its correlation with the use of antibiotics,” *Chinese Journal of Antibiotics*, vol. 36, no. 02, pp. 160–163, 2011.
 - [17] M. Peng, P. Liu, and C. Li, “Analysis of the relationship between acute attack of bronchial asthma and allergen sputum culture,” *Journal of Liaoning University of traditional Chinese Medicine*, vol. 1997, no. 06, pp. 168–170, 2008.
 - [18] F. O. U. A. D. Hala, M. Mona, A. Halim, and F. Hebatallah, “Influence of Handprint Culture Training on Compliance of Healthcare Workers with Hand Hygiene,” *Interdisciplinary perspectives on infectious diseases*, vol. 2018, Article ID 3727521, 2018.
 - [19] E. L. L. I. O. T. L. Naidus, M. A. R. Y. T. Lasalvia, E. D. W. A. R. D. R. Marcantonio, and S. J. Herzig, “The diagnostic yield of noninvasive microbiologic sputum sampling in a cohort of patients with clinically diagnosed hospital-acquired pneumonia,” *Journal of Hospital Medicine*, vol. 13, no. 1, pp. 34–37, 2018.
 - [20] C. Chatla, N. Mishra, M. Jojula, R. Adepu, and M. Puttala, “A systematic review of utility of urine lipoarabinomannan in detecting tuberculosis among HIV-positive tuberculosis suspects,” *Lung India*, vol. 38, no. 1, pp. 64–73, 2021.
 - [21] G. I. N. A. Hong, H. E. A. T. H. E. R. B. Miller, S. A. R. A. H. Allgood, R. Lee, N. Lechtzin, and S. X. Zhang, “Use of selective fungal culture media increases rates of detection of fungi in the respiratory tract of cystic fibrosis patients,” *Journal of Clinical Microbiology*, vol. 55, no. 4, pp. 1122–1130, 2017.
 - [22] G. V. Mukamolova, O. Turapov, J. Malkin, G. Woltmann, and M. R. Barer, “Resuscitation-promoting factors reveal an occult population of tubercle bacilli in sputum,” *American Journal of Respiratory and Critical Care Medicine*, vol. 181, no. 2, pp. 174–180, 2010.
 - [23] R. I. S. S. E. R. Risser, B. A. R. O. N. E. Barone, C. L. A. R. K. Clark, and D. L. Simpkins, “Noncomparative, open label, multicenter trial of cefixime for treatment of bacterial pharyngitis, cystitis and pneumonia in pediatric patients,” *The Pediatric Infectious Disease Journal*, vol. 6, no. 10, pp. 1002–1006, 1987.
 - [24] G. B. Rogers, M. P. Carroll, N. M. M. Zain et al., “Complexity, temporal stability, and clinical correlates of airway bacterial community composition in primary ciliary dyskinesia,” *Journal of Clinical Microbiology*, vol. 51, no. 12, pp. 4029–4035, 2013.
 - [25] N. Soler, C. Agusti, J. Angrill, J. Puig De la Bellacasa, and A. Torres, “Bronchoscopic validation of the significance of sputum purulence in severe exacerbations of chronic obstructive pulmonary disease,” *Thorax*, vol. 62, no. 1, pp. 29–35, 2007.
 - [26] S. Z. Nasr, “Inducing sputum in patients with cystic fibrosis could be helpful, but is time-consuming and expensive,” *The Journal of Pediatrics*, vol. 158, no. 5, p. 862, 2011.
 - [27] D. Bottai, G. Batoni, S. Esin et al., “Expression of SA5K, a secretion antigen of *Mycobacterium tuberculosis*, inside human macrophages and in sputum from tuberculosis patients,” *FEMS Microbiology Letters*, vol. 226, no. 2, pp. 229–235, 2003.
 - [28] S. U. T. A. N. T. A. N. G. J. A. I. Methawee, F. A. S. K. S. R. I. Kiaticchai, and C. H. A. I. C. U. M. P. A. R. Kimyaluk, “Evaluation of an immunochromatographic test kit for detecting MYCOBACTERIUM tuberculosis complex in sputum samples and on solid and in liquid cultures,” *Southeast Asian Journal of Tropical Medicine & Public Health*, vol. 45, no. 2, pp. 357–364, 2014.
 - [29] R. U. S. C. O. N. I. Rusconi, R. A. N. C. I. L. I. O. Rancilio, A. S. S. A. E. L. Assael et al., “Counterimmunoelectrophoresis and latex particle agglutination in the etiologic diagnosis of presumed bacterial pneumonia in pediatric patients,” *The Pediatric Infectious Disease Journal*, vol. 7, no. 11, pp. 781–788, 1988.
 - [30] M. Palaci, R. Dietze, D. J. Hadad et al., “Cavitary disease and quantitative sputum bacillary load in cases of pulmonary tuberculosis,” *Journal of Clinical Microbiology*, vol. 45, no. 12, pp. 4064–4066, 2007.
 - [31] M. Zaki, D. Raafat, and A. A. Metaal, “Relevance of serology for *Mycoplasma pneumoniae* diagnosis compared with PCR and culture in acute exacerbation of bronchial asthma,” *American Journal of Clinical Pathology*, vol. 131, no. 1, pp. 74–80, 2009.
 - [32] F. Karpati and J. Jonasson, “Polymerase chain reaction for the detection of *Pseudomonas aeruginosa*, *Stenotrophomonas maltophilia* and *Burkholderia cepacia* in sputum of patients with cystic fibrosis,” *Molecular and Cellular Probes*, vol. 10, no. 6, pp. 397–403, 1996.
 - [33] N. G. O. C. A. Dang, M. A. R. T. A. Mourao, and S. J. O. U. K. J. E. Kuijper, “Direct detection of *Mycobacterium tuberculosis* in sputum using combined solid phase extraction-gas chromatography-mass spectrometry,” *Journal of Chromatography, B: Analytical Technologies in the Biomedical and Life Sciences*, vol. 986–987, pp. 115–122, 2015.

Research Article

A Cross-Sectional Study on the Application of IS in Perioperative Pulmonary Function Training in Spine and Orthopedics

Ting Qiu, Yong Li, Jingjing Zhang, Xuanzhu Hou, Yuqi Wu, Yan Xu, Wenyue Chen, Jingjing Rui, Jin Yang, and Jing Qian 

Infection Control Administration Department, The Affiliated Hospital of Nanjing University Medical School, Nanjing 210008, China

Correspondence should be addressed to Jing Qian; 2111807010@e.gzh.edu.cn

Received 25 May 2022; Revised 7 June 2022; Accepted 13 June 2022; Published 6 July 2022

Academic Editor: Carlo Ricciardi

Copyright © 2022 Ting Qiu et al. This is an open access article distributed under the Creative Commons Attribution License, which permits unrestricted use, distribution, and reproduction in any medium, provided the original work is properly cited.

Background. The incentive spirometer (IS) is a mechanical device that promotes lung expansion and can be used to prevent and treat postoperative pulmonary complications. In this study, the preventive effect of pulmonary function training with IS on the improvement of pulmonary function and pulmonary complications was observed. **Methods.** From May 2019 to April 2021, 69 scoliosis patients with impaired moderate and severe lung function were divided into the traditional pulmonary training group ($n = 32$) and IS-enhanced pulmonary training group ($n = 35$). The patient underwent lung function testing after admission and one week after the start of training and chest CT on the third day after surgery. **Results.** The average age was 13.47 and 15.66, respectively ($p = 0.223$). The Cobb angles were 83.84 and 83.97 ($p = 0.756$), respectively, and no statistical difference between the parameters of lung function was detected. After 1 week of respiratory function training, significant improvement in lung function testing parameters including VC%, FVC%, FEV1%, FEV1/FVC, FEV1/VC, and MVV% was found in both groups. Analysis of covariance showed more significant improvement in IS-enhanced group compared to the conventional training group ($p < 0.05$). The incidence of postoperative pulmonary atelectasis was lower in IS-enhanced group than in traditional groups (2.9% vs. 21.9%, $p = 0.043$) with no difference in the overall incidence of pulmonary complications ($p = 0.164$) and shorter preoperative and total hospitalization in the IS-enhanced group. **Conclusion.** Compared to traditional pulmonary function training, IS-enhanced training can significantly accelerate the improvement of pulmonary function testing parameters, shorten the preoperative pulmonary function training time, reduce the incidence of postoperative pulmonary tension complications, and accelerate postoperative rehabilitation.

1. Introduction

Surgery is the main treatment for scoliosis. As one of the most important physiological dysfunction caused by scoliosis, impaired lung function is an important factor affecting the safety of surgical indications and the perioperative period. Studies have shown that impaired lung function can induce respiratory failure and even death [1]. It is extremely important to improve lung function and its compensatory ability by preoperative pulmonary function training for reducing postoperative lung complications and improving the safety of surgery. Traditional methods of preoperative respiratory rehabilitation training have been shown to have a significant effect on improving the patient's respiratory

function, including lip compression, balloon blowing, breathing exercises, etc. The disadvantage is that the training process lacks clear quality control indicators and is difficult to self-assessment. This depends heavily on the patient's understanding and compliance, thus significantly reducing the efficiency of training.

Unlike traditional lung function training methods, the incentive spirometer (IS) is a mechanical device to assist lung dilation, which helps patients keep their lungs in good condition by increasing the total lung capacity (TLC) and lung compliance, improving oxygen supply, and maintaining the smoothness of the small airways. IS provides clear feedback during breathing training, which enables patients to set and achieve lung function training goals.

Studies have shown that IS can effectively improve a patient's breathing function during the perioperative period of chest and abdomen surgery, which improves surgical tolerance and reduces the occurrence of postoperative lung complications. IS is also widely used in the scoliosis orthopedic perioperative period, but its actual role in the improvement of perioperative lung function is lack of a clear evaluation.

The purpose of this study is to evaluate the role of IS in the training of pulmonary function during scoliosis orthopedic perioperative surgery and its effect on postoperative complications.

2. Information and Methods

2.1. Subjects. Patients undergoing scoliosis orthopedic surgery at the Spinal Surgery Center of Drum Tower Hospital, affiliated with Nanjing University Medical College, from May 2019 to May 2021, whether patients who had normal communicational skills and cognition, and had no correlative surgical treatment history, were enrolled.

2.1.1. Inclusion Criteria. Inclusion criteria include the following: (1) malformations affecting congenital or recurrent scoliosis of the chest; (2) Cobb angle: 50–100°; (3) age: 12–18 years; with the completion of lung function examination and respiratory function training program, gender is unlimited; and (4) the lung function report shows moderate and severe pulmonary dysfunction.

2.1.2. Exclusion Criteria. Exclusion criteria include the following: (1) patients with simple lumbar scoliosis and an upper lateral terminal cone below the L1 segment; (2) patients who combine other diseases and are unable to cooperate with examination and training; (3) patients with severe heart, liver, and kidney dysfunction; (4) blood gas analysis at the time of admission showed severe respiratory failure; and (5) patients combined with other underlying lung diseases.

2.1.3. Remove Criteria. Remove criteria include the following: (1) patients who voluntarily withdraw from this study or who are unable to operate for other reasons; (2) lung function is determined by the diagnostic criteria for ventilation dysfunction, such as guidelines from the American Thoracic Society and the European Respiratory Society [1, 2]; and (3) the expected value of FVC <80% was diagnosed as restrictive ventilation dysfunction, while FEV1/FVC <92% was diagnosed with obstructive ventilation disorder [2].

2.2. Research Methods. 75 patients who met the above-mentioned criteria after preliminary examination were collected after admission. Excluding 6 patients who did not agree to participate in the study and those who could not operate, a total of 69 patients (guardians) signed informed consent. Patients were randomly divided into traditional pulmonary training group and IS-enhanced pulmonary

training group. The former is trained in traditional pulmonary training during perioperative period, while the latter is given training in traditional pulmonary and increased IS-enhanced pulmonary training. The lung function of the patient was measured at the time of admission to the hospital and after the completion of the training program lasting 1 week. It is confirmed that those who meet the surgical standards will undergo surgery after multidisciplinary consultation in the anesthetic department and other relevant disciplines. Those who do not meet the criteria continue to train in the above manner until the day before the operation. After surgery, it was determined whether to transit through the ICU as per the patient's cardiopulmonary function. The preoperative breathing training was continued after entering the ward. Chest CT flat sweep was used to assess the occurrence of lung complications 3 days after the surgery. Observation indicators are as follows: ① lung function at the time of admission and after one week of training; ② number of days of preoperative respiratory training; ③ postoperative respiratory complications; ④ time spent in the hospital after surgery; and ⑤ hospitalization costs and overall satisfaction. The research program was approved by the Ethics Committee of Drum Tower Hospital, affiliated with Nanjing University Medical College. Traditional pulmonary training is as follows: ① lip breathing: the patient aspirates with his nose and bulged the upper abdomen; holds the breath for 1–2 s after the lips slowly exhale through the mouth, while exhaling side count to 7 and exhale (inhale and exhale at 1:2); ② abdominal movement breathing: the patient places his hand on the abdomen and helps to contract the abdominal muscles when inhaling; takes a deep, slow breath, at which point the chest can be seen clearly lifted and the abdomen sinks; then, relaxes the abdomen and gently exhales breath; ③ muscle breathing: the nurse places his hands under the rib arch of the patient's abdomen and instructs the patient to inhale with his nose; the abdomen puffs outwards and then resists the nurse's hands when inhaling; holds the breath for 1–2 s to open the alveoli; uses mouth to slowly exhale gas when exhaling, and practices several times before the patient can practice on his own; ④ blow balloons: the patient takes a seat or a stand position and does the balloon movement; takes a deep breath, then holds the balloon, and blows all the gas from your lungs into the balloon until he cannot blow it out. The above method is professionally directed by the nurse to the patient. This is practiced 20 min per action, 3 times a day, and lung function tests are conducted again after 1 week. IS training is done with the Raventon Respiratory Trainer (Leventon S.A.U., SPIRO-BALL, L25913000 4000 ml). The patient sits on a chair and holds a lung capacity meter, moving the yellow indicator on the right side of the instrument up and down to the target milliliter (the initial training target is set at 70% of lung capacity based on lung function test results). Inhale deeply and evenly with mouth to keep the float in a raised state, and keep the small yellow ball in the smiley position for as long as possible and then exhale normally. Repeat 10 to 12 times per hour and 3 times a day for 1 hour, and repeat the lung function test after 1 week. The preoperative training regimen is continued on days 1 to 5 after surgery.

2.3. Lung Function Tests. Lung function testing is performed by fixed personnel using the German Jaeger lung function tester for patients after admission and one week after the completion of the exercise program. Observation indicators included vital capacity as a percentage of projected value (VC%), forced vital capacity as a percentage of predicted value (FVC%), percentage of forced expiratory volume in one second (FEV1%), forced expiratory volume in one second/forced vital capacity (FEV1/FVC, %), forced expiratory volume in one second/vital capacity (FEV1/VC, %), and maximal voluntary ventilation as a percentage of the estimated value (MVV%). Estimates are calculated based on the patient's age, weight, and finger spacing. The degree of lung impairment is based on current guidelines of the American Thoracic Society + European Respiratory Society and is diagnosed as restrictive ventilation dysfunction at an estimated FVC value < 80% [1, 2]. FEV1/FVC < 92% is the diagnostic criteria for obstructive ventilation disorders.

2.4. Postoperative Respiratory Complications. On the third day after surgery, a routine chest CT scan was performed to observe whether there was atelectasis, lung infection, and pleural effusion.

2.5. Days Living in the Hospital before and after Surgery Were Recorded. Pain scores on days 1, 2, and 5 after surgery were recorded using a numeric rating scale (NRS) of pain.

2.6. Statistical Analysis. SPSS 23 statistical software is used for data processing and statistical analysis. Categorical variable data are expressed as counts or percentages, and continuous variables are expressed as means and standard deviations. Covariance analysis was used to compare lung function before and after one week of training. The inter-group outcome indexes between groups included lung complications and lung function, and *t*-test and chi-square test were used for comparison. All statistical tests were bilateral probability tests, and $p < 0.05$ was considered a statistically significant difference.

3. Results

A total of 75 patients who underwent scoliosis orthosis at the Spine Surgery Center of the Drum Tower Hospital affiliated to Nanjing University School of Medicine were admitted to the hospital and met the inclusion and exclusion criteria after preliminary examination from May 2019 to May 2021. In this study, a total of 6 patients were excluded based on the exclusion criteria. A total of 69 patients (guardians) signed informed consent forms by excluding 6 patients who did not agree to participate in this study and other reasons that they could not undergo surgery. It was randomly divided into the traditional pulmonary training group ($n = 34$) and IS-enhanced pulmonary training group ($n = 35$). Among them, 2 people voluntarily withdrew from the traditional pulmonary training group during the research process and 32 people finally completed the traditional training of the study. There

were no significant differences in age (13.46 ± 6.36 vs. 15.66 ± 8.28 , $p = 0.233$) and gender composition (male/female: 15/17 vs. 17/18, $p = 0.89$). The Cobb angle was 83.34 ± 7.93 in the traditional pulmonary training group and 83.97 ± 8.48 in the IS-enhanced pulmonary training group; there was no significant difference between the groups ($p = 0.756$). The basic lung function indicators of the two groups of patients are shown in Table 1. There was no significant difference in the degree and type of respiratory impairment ($p = 0.621$), and all presented with predominantly restrictive ventilation dysfunction.

There were no significant differences in the indicators of lung function upon admission between the two groups ($p > 0.05$). After one week of breathing training, both the traditional pulmonary training group and IS-enhanced pulmonary training group improved significantly ($p > 0.01$). Covariance analysis showed significant improvements in all other indicators except FEV1/VC ($p = 0.031$), indicating that the addition of stimulated spirometry training improved lung function more significantly than traditional training after 1 week of training. The improvement of other indicators varied significantly, indicating that added incentive spirometry training more significantly improved lung function after 1 week of training than conventional training (as shown in Table 2).

The incidence of postoperative pulmonary complications in both groups is shown in Table 3. No significant difference in the number of overall pulmonary complications between the two groups ($p = 0.164$) was found. However, the incidence of atelectasis in the traditional pulmonary training group (7/32, 21.9%) was much higher than that in the IS-enhanced pulmonary training group (1/35, 2.9%) ($p = 0.043$).

Comparison of hospital stay and postoperative pain scores between the two groups is shown in Table 4. The number of days living in the hospital before the traditional pulmonary training and IS-enhanced pulmonary training groups was 15.72 ± 9.65 and 11.34 ± 4.65 , respectively. The difference was significant ($p = 0.024$). The number of days living in the hospital after surgery was 15.13 ± 7.07 and 12.40 ± 2.50 , with significant differences ($p = 0.046$). The total length of days living in the hospital also varied significantly ($p = 0.014$). There was no significant difference in pain scores on day 1 after surgery between the traditional pulmonary training and IS-enhanced pulmonary training groups ($p = 0.085$), while there was a statistical difference on day 2 postoperatively ($p < 0.001$), the difference was not significant on day 5 after surgery. In summary, there were significant differences between the two groups ($p = 0.006$).

4. Discussion

4.1. Impaired Respiratory Function Is an Important Complication of Scoliosis and Seriously Affects the Preoperative Safety of the Spinal Orthopedic Surgery. Scoliosis is the third largest "killer" affecting the health of children and adolescents with an incidence between 0.47% and 5.2% [3]. The incidence of scoliosis is about 1% in China. Scoliosis not only affects the appearance of the child but also causes pulmonary

TABLE 1: Basic information for both groups of patients.

Project	Traditional pulmonary training group ($n = 32$)	IS-enhanced pulmonary training group ($n = 35$)	p value
Age (year, $\bar{x} \pm s$)	13.47 ± 6.36	15.66 ± 8.28	0.233
BMI (kg/m^2 , $\bar{x} \pm s$)			
Gender (male/female)	15/17	17/18	0.890
Cobb angle ($\bar{x} \pm s$)	83.34 ± 7.93	83.97 ± 8.48	0.756
Pulmonary dysfunction (moderate/severe)	23/9	27/8	0.621
VC actual/predicted value (%)	48.69 ± 7.64	49.03 ± 7.19	.850
FVC actual/predicted value (%)	49.22 ± 8.08	49.55 ± 8.58	0.870
FEV1 actual/predicted value (%)	44.73 ± 8.13	44.68 ± 8.18	0.980
FEV1/FVC (%)	91.17 ± 9.21	90.22 ± 6.69	0.630
FEV1/VC (%)	91.99 ± 8.85	91.79 ± 6.07	0.912
MVV actual/predicted value (%)	52.01 ± 9.09	51.10 ± 9.89	0.696

VC: vital capacity; FC: forced vital capacity; FEV1: forced expiratory volume in one second; MVV: maximal voluntary ventilation.

TABLE 2: Analysis of covariance of lung function in two groups after completion of one-week training (analysis of covariance).

Covariant	Traditional pulmonary training group	IS-enhanced pulmonary training group	p value
VC actual value/predicted value (%)	48.69 ± 7.64	49.03 ± 7.19	0.85 (0.311)
First entered the hospital	60.46 ± 9.69	64.12 ± 7.68	0.09 (1.374)
After 1 week of training	11.77 ± 3.39	15.09 ± 3.39	
Difference p value	0.0001	0.0001	0.006(8.116)
FVC actual value/predicted value (%)	49.22 ± 8.08	49.55 ± 8.58	0.87 (0.005)
First entered the hospital	60.77 ± 9.62	65.96 ± 9.01	0.026(0.533)
After 1 week of training	11.55 ± 3.36	16.41 ± 2.91	
Difference p value	0.0001	0.0001	0.0001(40.081)
FEV1 actual value/predicted value (%)	44.73 ± 8.13	44.68 ± 8.18	0.98(0.848)
First entered the hospital	57.99 ± 7.92	63.98 ± 8.37	0.004(0.092)
After 1 week of training	13.27 ± 2.09	19.31 ± 2.85	
Difference p value	0.0001	0.0001	0.0001(97.02)
FEV1/FVC (%)	91.17 ± 9.21	90.22 ± 6.69	0.63(2.371)
First entered the hospital	94.72 ± 9.38	98.06 ± 7.20	0.105(1.46)
After 1 week of training	3.55 ± 7.16	7.84 ± 5.07	
Difference p value	0.009	0.0001	0.006(7.983)
FEV1/VC (%)	91.99 ± 8.85	91.79 ± 6.07	0.912(3.746)
First entered the hospital	95.65 ± 9.27	99.02 ± 6.53	0.088(3.336)
After 1 week of training	3.66 ± 7.49	7.23 ± 6.64	
Difference p value	0.009	0.0001	0.031(4.841)
MVV actual value/predicted value (%)	52.01 ± 9.09	51.10 ± 9.89	0.696(0.308)
First entered the hospital	59.12 ± 8.91	65.24 ± 12.59	0.026(3.331)
After 1 week of training	7.12 ± 3.44	14.14 ± 5.01	
Difference p value	0.0001	0.0001	0.0001(44.759)

hypertension and impaired lung function [4–6]. In children with scoliosis, the elastic resistance of the lungs increases, the compliance decreases, the lung volume decreases, and the lung ventilation volume decreases due to the gradual change of bone structure and muscle structure [7]. Studies have shown that changes in lung function have a clear correlation with the degree of scoliosis. Patients with mild scoliosis deformity and Cobb angle below 60° have good compensatory lung function. Patients with moderate deformities and a Cobb angle of 60° – 90° will have a significant decrease in VC, MVV, and FEV1, below 80% of the normal estimate. Patients with severe malformations and Cobb angles above 90° have VC, MVV, and FEV1 falling below 50% of normal estimates, with a minimum of only about 30%. The effect of scoliosis on respiratory function is also related to its etiology. Congenital scoliosis (CS) is particularly affecting respiratory

function and can develop severe respiratory dysfunction. The effect on respiratory function is mainly manifested as a restrictive ventilation dysfunction regardless of the cause of scoliosis. The preoperative lung function test results of the enrolled patients in this study also met this feature.

Surgical orthopedics is the main means of treating scoliosis. However, lung injury, as one of the most common physiological dysfunctions caused by scoliosis, has become an important factor affecting surgical indications and perioperative safety. On the one hand, the presence of preoperative lung dysfunction can affect the safety of surgery; on the other hand, spinal orthopedics, in addition to its effects on the diaphragm and thoracic cage (anesthesia, wound pain, surgical stimulation, medications, and metabolic changes) has other causes of pulmonary complications. These combined factors can reduce lung volume and flow

TABLE 3: Postoperative pulmonary complications in two groups (chi-square test).

	Whole group ($n = 67$)	Traditional pulmonary training group ($n = 32$)	IS-enhanced pulmonary training group ($n = 35$)	p value
Pulmonary complications				
Yes	14 (20.9%)	9 (28.1%)	5 (14.3%)	0.164
No	53 (79.1%)	23 (71.9%)	30 (85.7%)	
Pneumonia yes	6 (9%)	4 (12.5%)	2 (5.7%)	0.587
No	61 (91%)	28 (87.5%)	33 (94.3%)	
Pleural effusion Yes	9 (13.4%)	5 (15.6%)	4 (11.4%)	0.885
No	58 (86.6%)	27 (84.4%)	31 (88.6%)	
Atelectasis Yes	18 (26.9%)	7 (21.9%)	1 (2.9%)	0.043
No	59 (88.1%)	25 (78.1%)	34 (97.1%)	

TABLE 4: Length of hospitalization, hospitalization cost, and pain score before and after surgery of the two groups of patients (t -test and chi-square test).

Whole group $n = 67$	Traditional pulmonary training group $n = 32$	IS-enhanced pulmonary training group $n = 35$	F value	p value
Length of preoperative hospital stay	15.72 ± 9.65	11.34 ± 4.65	12.96	0.024
Length of postoperative hospital stay	12.13 ± 7.07	9.37 ± 2.53	24.24	0.044
Total length in hospital	27.78 ± 14.65	20.66 ± 5.93	17.81	0.014
Postoperative pain score			8.107	.006
Day 1	2.09 ± 0.86	1.77 ± 0.65	3.060	0.085
Day 2	1.41 ± 0.71	0.77 ± 0.65	14.65	0.000
Day 5	0.28 ± 0.46	0.11 ± 0.32	3.026	0.087
Cost	21.12 ± 4.87	19.68 ± 2.69	7.49	0.148

rate by 10% to 30%. In addition, VC and MVV are also reduced accordingly, and there is even a risk of developing postoperative pulmonary insufficiency or respiratory failure. The maximum preoperative ventilation volume has been reduced by 40% or less, and postoperative complications and the occurrence of ARDS may be greatly increased [8].

4.2. Lung Function Training Is an Important Part of the Perioperative Period of Spinal Orthopedic Surgery. Improving the compensatory capacity of lung function has always been the most important work in the perioperative period of scoliosis patients. Studies have shown that good respiratory exercises increase respiratory muscle strength by 35% to 55% and endurance by 19% to 55% [9]. Traditional preoperative respiratory rehabilitation training methods mainly include lip reduction breathing, balloon blowing, breathing exercises, etc. The resistance generated by the slow exhalation of the lip shrinking causes the isobaric pressure (2–5 cm H₂O) point of the airway to move towards the distal end of the airway, which prevents the small airway from collapsing and narrowing during exhalation. This facilitated the discharge of alveolar air. The prolongation of the exhalation time is also conducive to the full discharge of gas in the lungs and prevents the airway from collapsing. Balloon blowing training can lengthen the exhalation time, slow down the airflow, and increase the internal pressure of the trachea to avoid premature collapse of the bronchi and small bronchi, thereby effectively eliminating residual gas in the lungs, improving the imbalance of ventilation/blood flow,

reducing the dilution of functional residual gas to inhale the fresh air, increasing alveolar PCO₂, and thus improving gas exchange and ventilation function. Respiratory exercises can increase the volume of lung ventilation, enhance the function of the respiratory muscles, reduce the residual air volume in the alveoli after forceful exhalation, and reduce the degree of alveolar expansion. Exercise can also improve breathing type, improve respiratory efficiency, increase muscle strength in the patient's limbs, and improve skeletal muscle dysfunction caused by chronic respiratory diseases.

4.3. IS-Enhanced Pulmonary Training and Its Role in Perioperative Lung Function Training. The lack of clear quality control indicators and the difficulty of self-assessment in the traditional respiratory function exercise process have a relationship with the patient's understanding and compliance, thus significantly reducing the efficiency of training. The Incentive Spirometer (IS) mimics sighing and yawning movements to help patients take an active approach to rhythmic deep breathing, increase tidal volume by promoting diaphragm respiration and alveolar opening, basal ventilation, penetrating pulmonary pressure, and in turn improve respiratory muscle status, promote airway secretion discharge, and assist to maximize lung expansion to prevent and reverse lung atelectasis [10–17]. An excitatory spirometer, also known as a sustained maximum inhalator, encourages patients to maximize inhalation and maintain >3 s by monitoring the flow or volume of breath. The excitatory spirometer is equipped with a display device that

helps the healthcare provider guide the patient to the desired training effect, while the patient can also visually monitor the performance of their workout through the display [18].

Many studies have shown that IS can prevent the development of postoperative complications. Renault et al. [19] randomly divided 36 patients after coronary artery bypass surgery into deep breathing training group ($n=18$) and IS group ($n=18$). Although there were no significant differences in FVC and FEV between the two groups, the pulmonary complications in the IS group were significantly less than those in the deep breathing group. Alaparathi et al. [20] divided 260 patients undergoing laparoscopic abdominal surgery into four groups: diaphragmatic respiratory training group, volume IS group, flow IS group, and control group. FVC and FEV1 improved in all patients the day after surgery, while improvements were more prominent in the IS group. Rollin et al. [17] analyzed 84 patients and found that 5 of them had pneumonia in the routine care group, while none in the IS group had pneumonia. Koo and Hwang [21] divided 63 patients with epigastric surgery into control groups ($n=31$) and IS groups ($n=32$). Pulmonary complications occurred in 5 cases (16.1%) in the control group, compared with none in the IS group ($p=0.018$).

However, Thomas and McIntosh [22] evaluated and compared the preventive effects of IS, IPPB, and deep breathing training in preventing pulmonary complications during epigastric surgery. The OR value for the development of pulmonary complications was 0.44 compared with patients without physical therapy, and the value was 0.43 for deep breathing training compared with patients without physical therapy. IS has included 46 studies in its role in preventing postoperative pulmonary complications, 35 without conclusions due to methodological defects, while 10 of 11 studies did not support the effect of IS. In the only study to support the outcome, IS, deep breathing training, and IPPB were equally effective in preventing lung complications after abdominal surgery. This evidence does not support that the use of IS after cardiac or abdominal surgery reduces the incidence of postoperative pulmonary complications. The findings suggest that IS deep breathing training after epigastric surgery is beneficial for preventing postoperative pulmonary complications, but there is no supportive evidence for differences between different treatments. The review by Carvalho et al. [23] included 30 studies (14 abdominal surgery, 13 cardiac surgery, and 3 thoracic surgery; total sample size is 3370). 5 studies (3 abdominal surgery, 1 cardiac surgery, and 1 thoracic surgery) compared the effects before and after IS interventions. No significant differences were found. The authors did not support the use of IS after surgery because no significant differences were found in the results. A Cochrane review [24] focused on coronary artery bypass surgery, including 7 studies of 592 patients; results were found to be superior to physiotherapy, positive pressure ventilation, active cycle breathing, or preoperative education. Patients with IS have poorer lung function and arterial support and no improvement in muscle strength compared with positive pressure ventilation. There is no evidence that IS reduces

pulmonary complications or improves lung function after coronary artery bypass surgery. Another Cochrane review of epigastric surgery yielded similar results [25].

The subjects involved in the above studies are patients with basically normal preoperative lung function, and the subjects of this study are those whose lung function due to scoliosis has been moderately and severely impaired. The use of IS in the perioperative phase of scoliosis orthopedics has also been reported in the past, but most studies have included it as part of routine respiratory function training and have not independently quantified it. The results of this study show that the combination of stimulated lung capacity training based on traditional respiratory training can effectively improve the improvement of lung function indicators per unit time. After one week of training, the excitation spirometry training group had more significant improvements in the VC measured value/predicted value (%), FVC measured value/predicted value (%), FEV1/FVC (%), FEV1/VC (%), FEV1/VC (%), and MVV measured/predicted value (%) compared with the traditional training group. In particular, the MVV improvement was more significant, suggesting that the addition of stimulated lung capacity training can more effectively improve the ventilation effect of the small airways.

Effective lung function training is also beneficial for patients' postoperative recovery. It can be seen that the improvement of respiratory function with the addition of IS training is more significant from this study, the preoperative respiratory function exercise time is significantly shortened, the postoperative pain score is significantly reduced, and the recovery time is shorter. In this study, the incidence of atelectasis alone in the postoperative complications of the IS-enhanced pulmonary training group was significantly improved, and the overall incidence of lung complications did not have a significant statistical change from that of the traditional pulmonary training group. Possible reasons are as follows: (1) the sample size of this study is still relatively small; (2) although the traditional training group did not improve lung function as much as the motivated lung capacity group within one week, its preoperative breathing training time was longer, and both groups of patients underwent surgery after the lung function training reached a certain standard. Therefore, the preoperative lung function training method had a limited impact on the occurrence of overall postoperative complications.

4.4. Attention for Is Training. The biggest advantage of IS is that it provides clear feedback during training, which can motivate patients to work hard to achieve the goals of each training session. Therefore, it is necessary to set a reasonable daily lung capacity training goal during use. The initial goal can be set according to lung function at the time of admission and then gradually increased according to the patient's condition. In addition, the completion of the goal still depends on patient compliance while an excitation spirometer provides visual feedback. Therefore, individualized training programs should be evaluated and implemented

according to the specific situation of each patient, and the completion of the goals should be recorded every day and adjusted on time.

The clinical effect of IS is still controversial due to the lack of clinical evidence and the lack of clear standards for the use procedures and norms of IS, but the treatment and prevention effect of IS for pulmonary complications during the perioperative period is still generally agreed [26, 27]. The use of IS has four parameters: number of training sessions per day, target inhalation, number of breaths completed per session, and length of breath held after inhale, each of which varies greatly as described in the setup literature [28]. The motivational spirometer is not recommended alone and should be used in conjunction with other respiratory training measures according to the 2011 edition of the American Guidelines for Clinical Practice in Respiratory Care, including deep breathing, encouraging coughing, and early activity [29]. Reasonable anesthesia options are also important for preventing postoperative complications. Therefore, the guidance and implementation of traditional methods of respiratory function training should also not be relaxed when using motivated lung capacity training. In addition, IS includes two types: flow type and volume type, of which the volume type should be preferred in clinical use, especially for pediatric patients. The IS parameters used in this study are set by combining the characteristics of scoliosis patients and the previous experience of our center, and good results have been achieved in actual use.

4.5. Deficiencies of This Study. To more effectively observe the effects of IS in the perioperative period, the inclusion criteria for this study were set to patients with moderate and severe respiratory function at the time of admission and no severe respiratory failure, which greatly limited the sample size of the study and may have an impact on the outcome. Most patients with scoliosis orthopedic surgery have mild respiratory dysfunction, and a larger sample is needed for further study.

5. Conclusion

In this study, the preventive effect of pulmonary function training with IS on the improvement of pulmonary function and pulmonary complications was observed. IS is more conducive to the quantification of perioperative lung function training indicators and the standardization of processes, which is conducive to improving the efficiency of lung function training [30].

Data Availability

The datasets used and analyzed during the current study are available from the corresponding author upon reasonable request.

Conflicts of Interest

The authors declare that they have no conflicts of interest.

Authors' Contributions

The conception of the paper was completed by Ting Qiu, and the data processing was completed by Yong Li. All authors participated in the review of the paper.

References

- [1] M. R. Miller, R. Crapo, J. Hankinson et al., "General considerations for lung function testing," *European Respiratory Journal*, vol. 26, no. 1, pp. 153–161, 2005.
- [2] L. Zhu and L. Dong, "Diagnosis of lung function Chinese," *Journal of Tuberculosis and Respiratory Diseases*, vol. 35, no. 3, pp. 235–237, 2012.
- [3] M. R. Konieczny, H. Senyurt, and R. Krauspe, "Epidemiology of adolescent idiopathic scoliosis," *Journal of Children's Orthopaedics*, vol. 7, no. 1, pp. 3–9, 2013.
- [4] M. Y. Dong, K. L. Zai, and J. C. Chen, "Determinant of pulmonary limitation in adolescents with idiopathic thoracic scoliosis," *Chinese Journal of Orthopedics*, vol. 18, no. 3, pp. 134–136, 1998.
- [5] R. De la Garza Ramos, C. R. Goodwin, and N. Abu-Bonsrah, "Patient and operative factors associated with complications following adolescent idiopathic scoliosis surgery: an analysis of 36,335 patients from the Nationwide Inpatient Sample," *Journal of Neurosurgery: Pediatrics*, vol. 25, no. 6, pp. 730–736, 2016.
- [6] X. Y. Li, Z. Li, F. Feng et al., "Correlation between severity of adolescent idiopathic scoliosis and pulmonary artery systolic pressure: a study of 338 patients," *European Spine Journal*, vol. 25, no. 10, pp. 3180–3185, 2016.
- [7] H. L. Xia and W. Y. Chen, "Physical therapy is observed before lateral spinal process in children," *The Orthopedic Journal of China*, vol. 5, no. 6, p. 566, 1998.
- [8] M. D. Ravishankar Vedantam, G. Lawrence, M. D. Lenke, J. Haas, and D. A. Linville, "A prospective evaluation of pulmonary function in patients with adolescent idiopathic scoliosis relative to the surgical approach used for spinal arthrodesis," *Spine*, vol. 25, no. 1, pp. 82–90, 2000.
- [9] B. Bain and I. Jacobs, "Respiratory muscle fatigue during simulated air combat maneuvering," *Aviation Space & Environmental Medicine*, vol. 68, no. 1, p. 118, 1997.
- [10] R. H. Bartlett, M. L. Brennan, A. B. Gazzaniga, and E. L. Hanson, "Studies on the pathogenesis and prevention of postoperative pulmonary complications," *Surgery Gynecology & Obstetrics*, vol. 137, pp. 925–933, 1973.
- [11] S. Dohi and M. I. Gold, "Comparison of two methods of postoperative respiratory Care," *Chest*, vol. 73, pp. 592–595, 1978.
- [12] J. A. Renault, R. Costa-Val, and M. B. Rossetti, "Respiratory physiotherapy in the pulmonary dysfunction after cardiac surgery," *Revista Brasileira de Cirurgia Cardiovascular*, vol. 23, pp. 562–569, 2008.
- [13] R. L. Wilkins, *Lung expansion therapy Egan's Fundamentals of Respiratory Care*, R. L. Wilkins, J. K. Stoller, and R. M. Kacmarek, Eds., Mosby Elsevier, St. Louis, 2009.
- [14] M. Westwood, K. Griffin, K. Roberts, M. Williams, K. Yoong, and T. Digger, "Incentive Spirometer decreases respiratory complications following major abdominal Surgery," *The Surgeon*, vol. 5, pp. 339–342, 2007.
- [15] P. Agostini, B. Naidu, H. Cieslik et al., "Effectiveness of incentive Spirometer in patients following thoracotomy and lung resection including those at high risk for developing

- pulmonary complications," *Thorax*, vol. 68, pp. 580–585, 2013.
- [16] P. Pasquina, M. R. Tramer, J. M. Granier, and B. Walder, "Respiratory physiotherapy to prevent pulmonary complications after abdominal surgery: a systematic review," *Chest*, vol. 130, pp. 1887–1899, 2006.
 - [17] K. E. Rollins, S. Aggarwal, A. Fletcher et al., "Impact of early incentive spirometer in an enhanced recovery program after laparoscopic donor nephrectomy," *Transplantation Proceedings*, vol. 45, pp. 1351–1353, 2013.
 - [18] I. Spirometry, *Critical Care Therapy and Respiratory Care Section* National Institutes of Health, Bethesda, MD , USA, 2013.
 - [19] J. A. Renault, R. Costa-Val, M. B. Rosseti, and N. M. Hourri, "Comparison between deep breathing exercises and incentive spirometer after CABG surgery," *Revista Brasileira de Cirurgia Cardiovascular*, vol. 24, pp. 165–172, 2009.
 - [20] G. K. Alaparathi, A. J. Augustine, R. Anand, and A. Mahale, "Comparison of diaphragmatic breathing exercise, volume and flow incentive spirometer, on diaphragm excursion and pulmonary function in patients undergoing laparoscopic surgery: a randomized controlled trial," *Minim Invasive Surg*, vol. 2016, Article ID 1967532, 2016.
 - [21] M. Koo and S. Hwang, "Comparison of effects of exhalation and inhalation breathing exercises on pulmonary function and complications in elderly patients with upper-abdominal surgery," *J Korean Acad Nurs*, vol. 46, pp. 514–522, 2016.
 - [22] J. A. Thomas and J. M. McIntosh, "Are incentive spirometry, intermittent positive pressure breathing, and deep breathing exercises effective in the prevention of postoperative pulmonary complications after upper abdominal surgery? A systematic overview and meta-analysis," *Physical Therapy*, vol. 74, no. 1, pp. 3–10, 1994.
 - [23] C. R. Carvalho, D. M. Paisani, and A. C. Lunardi, "Incentive spirometry in major surgeries: a systematic review," *Revista Brasileira de Fisioterapia*, vol. 15, no. 5, pp. 343–350, 2011.
 - [24] E. R. Freitas, B. G. Soares, J. R. Cardoso, and A. N. Atallah, "Incentive spirometry for preventing pulmonary complications after coronary artery bypass graft," *Cochrane Database of Systematic Reviews*, vol. 9, p. CD004466, 2012.
 - [25] P. do Nascimento Junior, N. S. Modolo, S. Andrade, M. M. Guimaraes, L. G. Braz, and R. El Dib, "Incentive spirometry for prevention of postoperative pulmonary complications in upper abdominal surgery," *Cochrane Database of Systematic Reviews*, no. 2, p. 006058, 2014.
 - [26] A. E. M. Eltorai, G. L. Baird, A. S. Eltorai et al., "Perspectives on incentive spirometry utility and patient protocols," *Respiratory Care*, vol. 63, no. 5, pp. 519–531, 2018.
 - [27] A. E. M. Eltorai, A. L. Szabo, V. Antoci et al., "Clinical effectiveness of incentive spirometry for the prevention of postoperative pulmonary complications," *Respiratory Care*, vol. 63, no. 3, pp. 347–352, 2018.
 - [28] SK. Sum, YC. Peng, SY. Yin, and P F Huang, "Using an incentive spirometer reduces pulmonary complications in patients with traumatic rib fractures: a randomized controlled trial," *Trials*, vol. 20, p. 797, 2019.
 - [29] R. D. Restrepo, R. Wettstein, L. Wittnebel, and M. Tracy, "Incentive spirometry: 2011," *Respiratory Care*, vol. 56, no. 10, pp. 1600–1604, 2011.
 - [30] T. J. Overend, C. M. Anderson, S. D. Lucy, C. Bhatia, B. I. Jonsson, and C. Timmermans, "The effect of incentive spirometry on postoperative pulmonary complications: a systematic review," *Chest*, vol. 120, no. 3, pp. 971–978, 2001.

Research Article

Optimisation of a Mouse Model of Cerebral Ischemia-Reperfusion to Address Issues of Survival and Model Reproducibility and Consistency

Zhenqian Liu, Mo Chen, Xu Duan, Yujia Zhai, Bin Ma, Zuowei Duan, Jiang Xu, and Haiyan Liu 

Department of Neurology, The Second Affiliated Hospital of Xuzhou Medical University, Xuzhou 221000, China

Correspondence should be addressed to Haiyan Liu; 14519155@xzyz.edu.cn

Received 24 May 2022; Revised 9 June 2022; Accepted 13 June 2022; Published 6 July 2022

Academic Editor: Dong Chen

Copyright © 2022 Zhenqian Liu et al. This is an open access article distributed under the Creative Commons Attribution License, which permits unrestricted use, distribution, and reproduction in any medium, provided the original work is properly cited.

Middle cerebral artery occlusion (MCAO) induced brain ischemia-reperfusion model in Mice is essential for understanding the pathology of stroke and investigating potential treatments, in which a variety of methods may be employed to block the middle cerebral artery (MCA), the most common being through the insertion of a monofilament; however, in vivo ischemia-reperfusion models are associated, particularly in mice, with high variability in lesion volume and high mortality. We aimed to optimise a mouse model of cerebral ischemia-reperfusion, addressing issues of mouse survival, model reproducibility, and consistency. The model was optimised in two ways: first, insert the monofilament directly through the internal carotid artery rather than through the external or common carotid artery, and second, by extending the length of the silicone coating on the monofilament, the length of the silicone coating enables embolization of the beginning of the middle cerebral artery, as well as the anterior cerebral artery and part of the posterior communicating artery. *Results:* We assessed various parameters, including blood flow changes in the middle cerebral artery, stability of the infarct area, correlation between infarct volume percentages and neurological deficit scores, mortality, weight changes, and wellbeing. We found that optimisation of the surgical procedure may improve mouse wellbeing and reduce mortality, through reduced weight loss and decrease the variability. In conclusion, we suggest that the optimisation of the model is superior for the study of both short and long-term outcomes of ischemic stroke. These results have considerable implications on stroke model selection for researchers.

1. Introduction

Stroke is one of the leading causes of adult mortality and disability [1]. Ischemic strokes in humans arise most commonly from blockage of the middle cerebral artery (MCA) and its branches [2]. Stroke animal models play an essential role in the investigation of mechanisms and drug development [3]. Over the last four decades, a variety of animal stroke models, including the intraluminal MCA occlusion (MCAO) model [4, 5], photothrombosis model [6], craniotomy model [7], atherothrombotic model [8, 9], and embolic stroke model [10], have been developed. Intraluminal MCAO in mice is the most frequently used model of stroke as it allows the restoration of blood flow after

the induction of focal ischemia thus mimicking human ischemic stroke, exhibiting a penumbra, being highly reproducible and having no craniotomy [11, 12]. Many efforts have been made to improve this model [4, 13–15], but the survival rate, success rate, and stability of the model remained unsatisfying and diverse among different individual studies [16]. Which may be due to the variation of lateral circulation and excessive vascular damage and the difficulty of the operation procedure [17, 18].

To allow for permit reperfusion the vessel through which the monofilament is inserted, which is either the common carotid artery (CCA) [19] or the external carotid artery (ECA) [20], remains permanently ligated. Permanent ligation of the CCA prevents restoration of blood flow through

the internal carotid artery this structure has a high anatomical variability and hemodynamic abnormality [21]. The alternative is to insert the monofilament via the ECA, also known as the classical procedure [22], ECA transection in rats can induce ischemic lesions of the mastication and swallowing muscles [23, 24], if vascular supply to the ECA is compromised this has been shown, in rats, affecting drinking behaviours and increasing body weight loss post-MCAO, to have a detrimental effect on the animal's wellbeing [25]. New research suggests that post-MCAO mortality in mice is not primarily caused by ischemic brain damage, but secondarily by inadequate food and/or water intake [26].

The posterior communicating artery (PCoA) and the proximal segment of the anterior cerebral artery (ACA) collateral blood flow during occlusion may cause inconsistent infarction: variable residual flow within the MCA territory, which has been well characterized, [27, 28]. Thus, we investigated an optimised surgical approach in mice avoiding ECA, pterygo palatine artery (PPA) ligation, survival rate, and wellbeing can be improved in mice, extending the length of silicone coating on monofilament reduces the collateral blood supply from ACA and PCoA to MCA, variability within this model will be reduced.

2. Materials and Methods

2.1. Animals. The experimental procedures were approved by the Laboratory Animal Ethics Committee of Xuzhou Medical University (No. 201702w012). All procedures were carried out in accordance with the National Institutes of Health Guide for the Care and Use of Laboratory Animals (NIH Publications No. 8023, revised 2011).

A total of 120 Kunming (KM) male mice (Xuzhou Medical University Laboratory Animal Centre, China) at 10 weeks, weighing 20–23 g were used in our study. The mice were randomly divided into one of the following experimental groups: sham-operated group, internal carotid artery access group (ICA1 group) (Figure 1(a)), internal carotid artery access group + long silicone coated monofilament (ICA2 group) (Figure 1(b)), external carotid artery access group (ECA1 group) (Figure 1(c)), external carotid artery access group + long silicone coated monofilament (ECA2 group) (Figure 1(d)).

The animals were housed in a controlled environment with an ambient temperature of 25°C and relative humidity of 65%, under a 12 h light/dark cycle, and were allowed free access to water and food. Observations were conducted once per day before surgery and every 6 hours after surgery to monitor the health of the animals.

2.2. Surgery

2.2.1. Anesthetic. Animals were anaesthetized with an intraperitoneal injection of ketamine and diazepam. A heating pad was employed to maintain the core temperature of $37 \pm 0.5^\circ\text{C}$, measured with a rectal temperature probe. Before starting surgery, the depth of anesthesia was assessed by toe pinch. If no response was elicited, the surgery would be started.

2.2.2. Measurement of Cerebral Blood Flow (CBF). CBF in the MCA was monitored by using a laser Doppler flowmeter (LDF; PeriFlux system 5000; Perimed, Stockholm, Sweden), territory an incision (1 cm) was made on the skin overlying the calvarium, and the skin was pulled laterally to affix a microtip. The microtip was placed perpendicular to the surface of the right parietal skull (1 mm posterior and 5 mm lateral to the bregma). [29] only mice with 75% flow reduction after monofilament insertion were included in this study. We recorded MCA blood flow primarily preoperatively, at 0 minutes and 80 minutes after insertion of the monofilament.

2.2.3. MCAO. The ICA1 and ICA2 groups were operated with a monofilament inserted from the ICA, the ECA1 and ECA2 groups were operated with a monofilament inserted from the ECA (Figure 1). The difference between groups 1 and 2 is the different lengths of the silicone coating on the monofilament, 2 mm for 1 and 4 mm for 2. The ICA2 performs an optimised procedure.

The mouse was placed on the operating table in a supine position under a stereo dissecting microscope, disinfection of fur with 75% ethanol.

(1) The Classic MCAO Model. (i) Vessel separation. after dissection of the carotid triangle, the common carotid artery (CCA), ECA, ICA, and occipital artery (OA) were identified. Cut into 20 mm segments with 6-0 sutures. place a permanent suture around the ECA, as far distally as possible, and another temporary suture on the ECA distal to the bifurcation (ii) Monofilament insertion. A temporary knot is tied in the proximal end of the CCA with a suture to prevent blood leakage, the ICA is clamped closed with a micro-arterial clip, and a small hole is cut between the permanent and temporary suture on the ECA. A 12 mm long 6-0 silicone coating monofilament (monofilament size 6-0, coating diameter 0.2 ± 0.01 mm, coating length 2 mm or 4 mm) is introduced into the ECA. The ECA distal to the permanent suture is completely severed, the free segment of the ECA is pulled outward and upward so that it runs parallel to the course of the ICA, and the monofilament is slowly fed downstream into the ICA. When the monofilament enters at a depth of 9–10 mm while resistance is felt, the suture on the ECA is tied tightly to secure the nylon monofilament and open the temporarily blocked CCA. (iii) Ligation suture. Remove the monofilament after 80 min and close the surgical incision layer by layer. (iv) Surgical care. All mice received subcutaneous buprenorphine (0.05 mg/kg; Temgesic, Schering-Plough Europe, Belgium) for pain relief at 1 h before surgery. The animals were maintained at $37 \pm 0.5^\circ\text{C}$ during and after surgery until they were fully recovered from anesthesia, when they were returned to their solitary cages in a heated (25–26°C) environment with free access to food and water.

(2) Optimised MCAO Model. (i) Vessel separation. After dissection of the carotid triangle, CCA, ECA, ICA, OA, and PPA were identified (Figure 2(a)). (ii) Monofilament

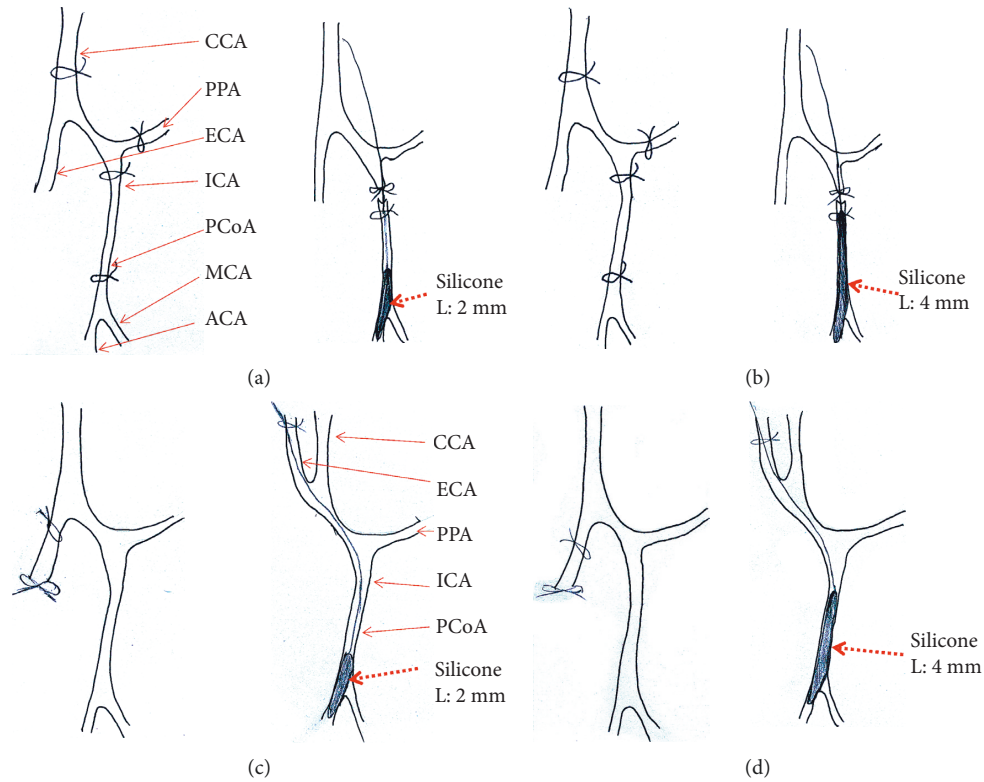


FIGURE 1: Schematic diagrams of the 4 MCAO procedures with large vessels and operating location: (a) ICA1 procedure, (b) ICA2 procedure, (c) ECA1 procedure, and (d) ECA2 procedure. Abbreviations: CCA, Common carotid artery; ECA, External carotid artery; ICA, Internal carotid artery; OA, Occipital artery; PPA, Pterygopalatine artery; PCoA, Posterior communicating artery.

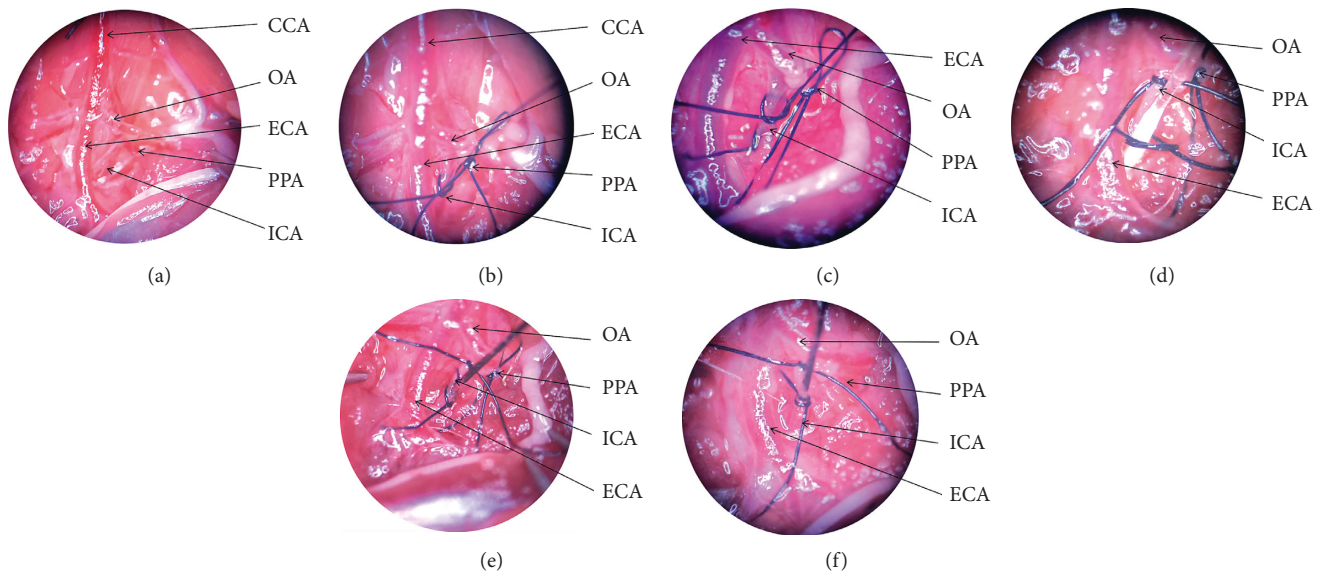


FIGURE 2: The surgical procedures of Optimised MCAO model. Notes: (1) Expose vital vessels by carefully separating the carotid triangle. (2) The thick OA emanating from the beginning of the ECA often forms a crossover with the ICA, eliminating the interference of the OA and accurately locating the PPA and ICA.

insertion. Temporary knots were tied in CCA, PPA with sutures place a permanent suture around the ICA, as far distally as possible, and another temporary suture on the ICA distal to the bifurcation (Figures 2(b) and 2(c)), a small hole is cut between the permanent and temporary suture on

the ICA. A 12 mm long 6-0 silicone coating monofilament (monofilament size 6-0, coating diameter 0.2 ± 0.01 mm, coating length 2 mm or 4 mm) is introduced into the ICA (Figure 2(d)), and the monofilament is slowly fed downstream into the ICA. When the monofilament enters at a

depth of 9–10 mm while resistance is felt, the suture on the ICA is tied tightly to secure the nylon monofilament (Figure 2(e)). The ICA distal to the permanent suture is completely severed and open the temporarily blocked CCA, PPA (Figure 2(f)), (iii) Ligature suture. Remove the monofilament and suture ICA permanent after 80 min, close the surgical incision layer by layer. (iv) Surgical care, Same as (A).

2.3. Neurological Severity Score (NSS). NSS scores were performed on each group of mice at 24 h, 72 h, and 1 w postoperatively, respectively.

The tests include the evaluation of motor (raising the mouse by the tail, placing the mouse on the floor), sensory (placing test and proprioceptive test), reflex (reflex absence and abnormal movements), and balance (beam balance tests) deficits on a scale of 0 to 18 (0: normal score; 18: maximal deficit score) [30].

2.4. Measurement of Infarct Volume Percentage. 24 h postoperative, mice were euthanized and brains collected for measurement of infarct size using 2,3,5-triphenyl tetrazolium chloride (TTC; Sigma, St. Louis, MO, USA) histology and digital image analysis, as previously described [31]. Their brains were subsequently removed and frozen at -80°C for 2 min, then cut into slices with a thickness of 2 mm from the cephalic to the caudal portion. Brain sections were incubated in 2% 2,3,5-TTC at 37°C for 15 min before imaging. The infarct volume percentage was corrected using standard methods (whole contralateral hemispheric volume-ipsilateral nonischemic hemispheric volume) and it was expressed as a percentage of the whole brain volume. Brain infarct volume percentages were measured and calculated using Image-Pro Plus 6.0 software.

2.5. Model Success Rate. The success rate of the model was calculated using an NSS score of 4 or more and the appearance of white infarct lesions on TTC staining as criteria for evaluating the success of the model, respectively, 24 h after surgery.

TTC solution is a clear, redox indicator that turns red only when applied to live cells. Brain tissue in the infarcted area appears white and any form of blood on the surface of the brain is considered a brain haemorrhage. We use the presence of white infarcted lesions as a criterion for successful modelling, and any locally dark red brain tissue is considered a model failure, as is the presence of brain haemorrhage.

2.6. Survival Rate. Calculated as the percentage of animals alive in each group 24 h, 72 h, 1 w postoperative.

2.7. Wellbeing Assessment. 24 h, 72 h, and 1 w postoperatively, a general neurological scale (Clark general) was used to evaluate the wellbeing of mice [32]. The Clark general test addresses the hair, ears, eyes, posture, spontaneous activity,

and epileptic behaviour of the animals. For each of the six general deficits measured, the scores in the six areas are summed to provide a total general score ranging from 0 to 28.

2.8. Weight Change. Mice were weighed before, 24 hours, 72 hours, and 1 w after the operation and compared to their preoperative body weight. Rate of weight change = (preoperative weight at each time point – postoperative weight)/preoperative weight.

2.9. Statistical Analysis. Parametric data are presented as the means \pm SEM, and nonparametric data are presented as the medians \pm interquartile ranges. Statistical analysis was performed using SPSS software (SPSS Inc., Chicago, IL, USA). Parametric data were analysed via one-way ANOVA, *t*-test and nonparametric data via Kruskal-Wallis ANOVA on ranks, followed by Dunn's posthoc testing. Correlations were analysed using Spearman's correlation. Model Success Rate and survival rate between the groups were compared using the Fisher exact test. The level of statistical significance was defined as $P < 0.05$.

3. Results

3.1. Cerebral Blood Flow Reduction (CBF). All groups of mice except the sham-operated group showed a significant drop in blood flow during surgery, and we analysed the drop in blood flow after monofilament insertion compared to the preoperative baseline blood flow ($P < 0.01$), the percentage decrease in blood flow immediately after middle cerebral artery embolization in each group was as follows: Sham: 0%, ICA1: $(86.91 \pm 3.47)\%$, ICA2: $(86.48 \pm 4.09)\%$, ECA1: $(87.96 \pm 3.39)\%$, ECA2: $(86.79 \pm 42.5)\%$, no statistically significant difference between the 4 groups ($P > 0.05$) (Figure 3(a)). It was suggested that the insertion of the monofilament had an embolic effect on the main trunk of the middle cerebral artery in all four groups of mice. During ambulatory blood flow monitoring for 80 min, the percentage decrease in MCA blood flow in each group of mice was as follows: Sham: 0%, ICA1: $(47.41 \pm 8.28)\%$, ICA2: $(81.17 \pm 4.72)\%$, ECA1: $(46.07 \pm 3.15)\%$, ECA2: $(81 \pm 3.98)\%$, Inter-group comparisons suggest a statistical difference only between groups 1 and 2 ($P < 0.05$) (Figure 3(b)), Extending the monofilament's Silicone-coated length may result in a sustained disruption of MCA blood flow.

3.2. Model Success Rate. The success of the model was judged by the presence of distinct white infarct lesions on TTC staining. 24 h postoperative, the model success rates for each group were: Sham: 0, ICA1: 33.3%, ICA2: 93.3%, ECA1: 26.7%, ECA2: 53.3%. ICA2 group, which used the optimised procedure, had a significantly higher model success rate than the ICA1, ECA1, and ECA2 groups (Figure 4). In the ICA2 group, the infarct foci were distributed in the neocortex, striatum, thalamus, and hippocampus, with a better consistency of infarct areas.

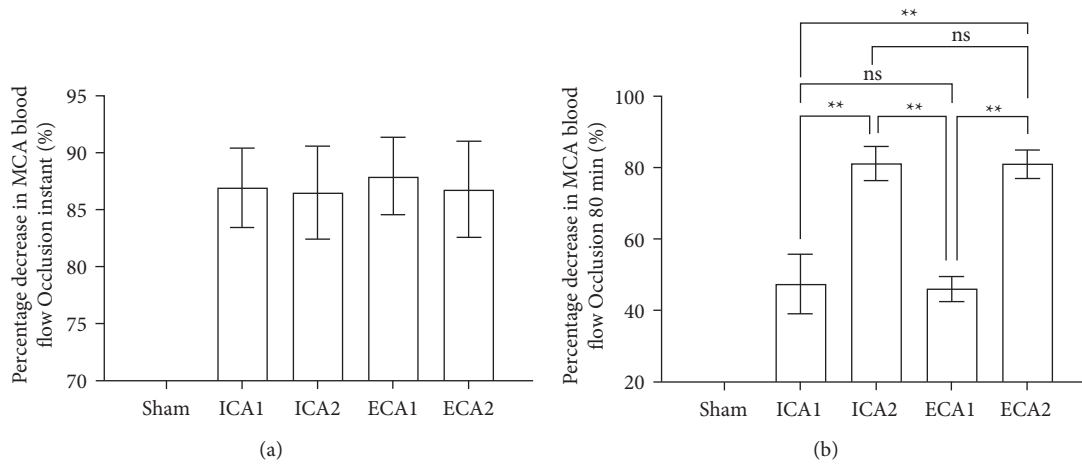


FIGURE 3: Percentage decrease in MCA blood flow. (a) No significant difference in the percentage decrease in MCA flow between the groups ICA1, ICA2, ECA1, and ECA2 after monofilament insertion, $P > 0.05$, $n = 15$. (b) 80 minutes after insertion of the monofilament, the percentage decrease in MCA flow was significantly greater in ICA1 and ECA1 than in ICA2 and ECA2. $*P < 0.05$, $n = 15$, while there was no significant difference between groups 1 and 2 $P > 0.05$, $n = 15$. Values are expressed as mean \pm SD.

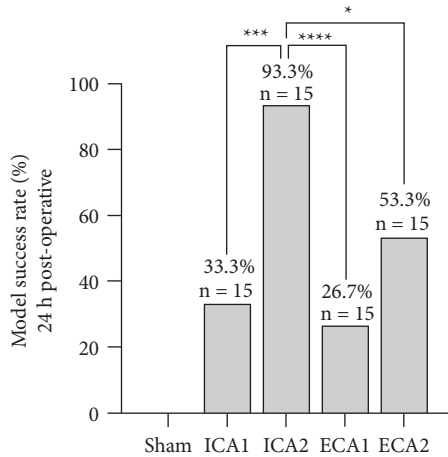


FIGURE 4: Model success rate for each group, 24 h postoperatively. The success rate of the model in the ICA2 group was higher than in the ICA1, ECA1, and ECA2 groups, and the difference was statistically significant. $*P < 0.05$, $***P < 0.001$, $****P < 0.0001$, $n = 15$.

3.3. Correlation between Cerebral Infarct Volume Percentage and Neurological Severity Score (NSS). At 24 h postoperatively, the correlation between NSS and the percentage of infarct volume was analysed. Only the ICA2 group had a strong correlation between NSS and the percentage of cerebral infarct volume, with an optimised surgical approach, the NSS allows for a more accurate assessment of the extent of brain damage (Figure 5).

3.4. Postoperative Weight Change. The body weights of the mice were measured before, 72 h, 24 h, and 1 w after surgery. At 24 h postoperatively, during intergroup comparison, there was a difference in weight change between the groups, but there is little difference between the groups (Figure 6(a)). At 72 h postoperatively, in intergroup comparison, the change in body weight in the ECA1 and ECA2 groups were

significantly greater than that in the ICA2 groups (Figure 6(a)). The difference in weight change between the ICA1 group and ECA1 group and ECA2 group as follows: $(9.4 \pm 0.4)\%$, $(7.5 \pm 0.4)\%$, $****P < 0.0001$, $n = 15$ (Figures 6(b) and 6(c)). At 1w postoperatively, the intra-group comparison suggested that the weight of the ICA2 group recovered to 24 h postoperatively. There was no significant difference in the rate of weight change in the ICA2 group at 24 h and 1 w postoperatively (Figure 6(a)), it was suggested that the body weight of mice in ICA2 groups gradually recovered at 1 week postoperatively. The difference between ICA2 and ECA1 and ECA2 further increased, respectively: $(17.4 \pm 1.0)\%$, $(18.8 \pm 1.1)\%$, $****P < 0.0001$, $n = 15$ (Figures 6(b) and 6(c)). The mice in the ECA1 and ECA2 groups did not recover their feeding ability and gradually lost weight at 1 week postoperatively. With the classical operation, the mice showed increasing weight changes after the operation without recovery, and with the optimised operation, the mice showed decreasing weight changes after the operation with gradual weight recovery.

3.5. Survival Rates at Different Time Points Postoperatively. The survival rate of the mice was counted at 24 h, 72 h, and 1 w postoperatively. 24 hours postoperatively, with no significant difference in survival between the four groups, but the Survival rates of the ICA1 and ICA2 groups were higher than those of the ECA1 and ECA2 groups at the two postoperative time points (72 h, 1 w). It is worth pointing out that at 24 h and 1 w postoperatively, there was no significant difference in survival rates between the ICA1 and ICA2 groups using the ICA access and between the ECA1 and ECA2 groups using the ECA access (Figure 7). It is suggested that ICA access could reduce the mortality of the mice postoperative.

3.6. Wellbeing Assessment. Clark general scores were performed at 24 h, 72 h, and 1 w postoperatively. The ICA2

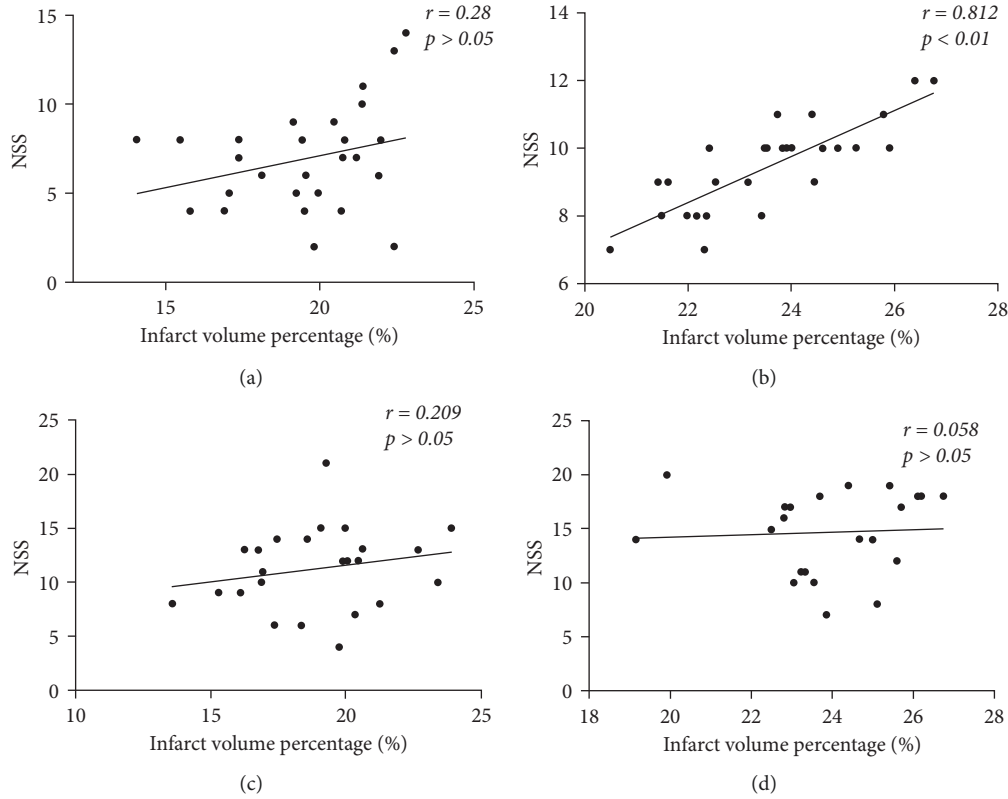


FIGURE 5: Correlation analysis between NSS and percentage of cerebral infarct volume at 24 h postoperatively. (a) There was no correlation between NSS and the percentage of cerebral infarct volume in the ICA1 group $r = 0.28$, $P > 0.05$, $n = 15$. (b) In the ICA2 group, NSS was significantly correlated with the percentage of cerebral infarct volume $r = 0.812$, $P < 0.01$, $n = 15$. (c) In the ECA1 group, there was no correlation between NSS and percentage of cerebral infarct volume $r = 0.209$, $P > 0.05$, $n = 15$. (d) In the ECA2 group, there was no correlation between NSS and percentage of cerebral infarct volume $r = 0.0588$, $P > 0.05$, $n = 15$.

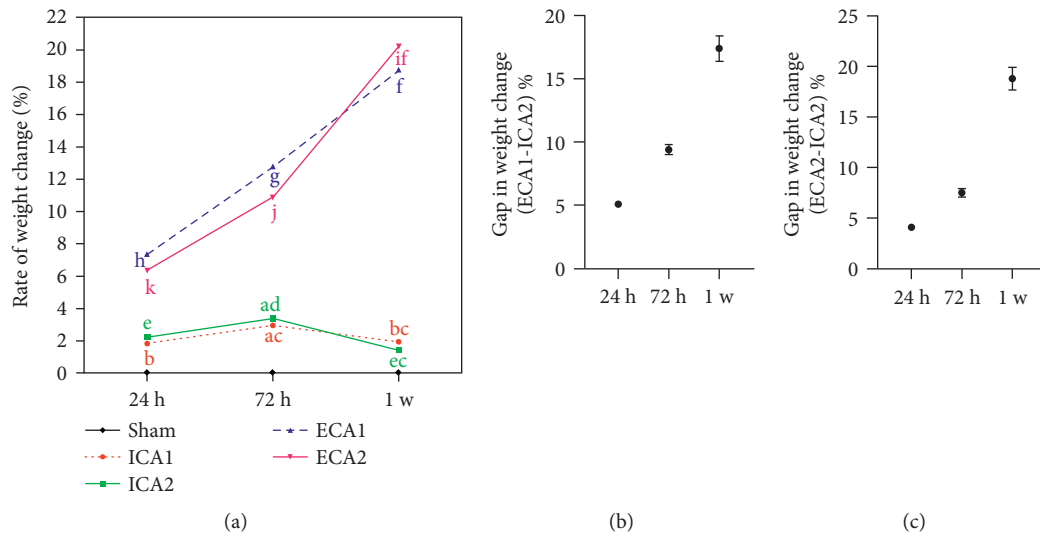


FIGURE 6: Comparison of rates of weight change, 24 h, 72 h, 1 w postoperatively. (a) Intergroup comparison: at 2 postoperative time points (72 h, 1 w), there was a statistically significant difference in weight change in the ICA2 group compared to ECA1 and ECA2 groups respectively **** $P < 0.0001$, **** $P < 0.0001$, **** $P < 0.0001$, **** $P < 0.0001$, $n = 15$. Intragroup comparison: no significant difference in the rate of weight change in the ICA2 group at the 2 postoperative time points (24 h, 1 w) $P > 0.05$, $P > 0.05$, $n = 15$. (b) The difference in weight change between the ECA1 group and the ICA2 group at different time points. (c) The difference in weight change between the ECA2 group and the ICA1 group at different time points. Notes: The letters a, b, c, d, e, f, g, h, i, j, k mark the differences between intergroup and intragroup, the letters are different between the two points suggesting that there is a difference and that the difference is statistically significant, the letters are repeated between the two points suggesting that there is no difference.

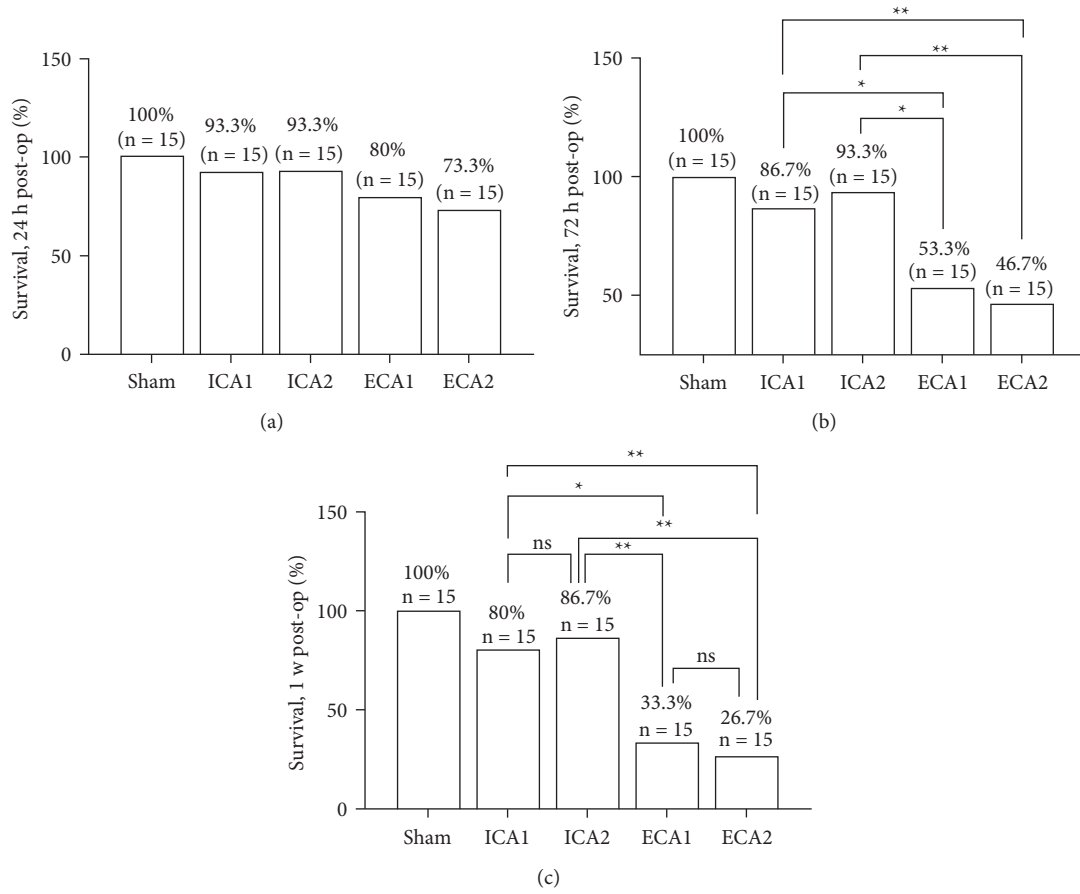


FIGURE 7: Survival rates between groups at different time points postoperatively. (a) No statistically significant difference in survival rate between groups at 24 h postoperatively $P > 0.05$, $n = 15$. (b) At 72 h postoperatively, the survival rate in the ECA1 group was significantly lower than that in the ICA1 and ICA2 groups, $*P < 0.05$, $n = 15$, the survival rate in the ECA2 group was significantly lower than that in the ICA1 and ICA2 groups $**P < 0.01$, $n = 15$ (c) At 1 week postoperatively, there was no difference in survival rates between the ECA1 and ECA2 groups, and similarly between the ICA1 and ICA2 groups, $P > 0.05$, $n = 15$. survival rates in the ICA2 group were significantly higher than those in the ECA1 and ECA2 groups $**P < 0.01$, $n = 15$.

group showed a statistically significant difference in the Clark score compared to the ECA1 and ECA2 groups, at three postoperative time points (24 h, 72 h, 1 w) (Figure 8(a)). At 24 h, 72 h, and 1 w postoperatively, the difference between the ICA2 group and the ECA1 and ECA2 groups in Clark general score were 3.8 ± 1.0 and 4.4 ± 1.1 , 6.4 ± 1.6 and 5.0 ± 1.3 , 10 ± 0.7 and 11.3 ± 0.8 respectively (Figures 8(b) and 8(c)). Subsequently, the gap in Clark general scores increased the longer the postoperative period, whereas there was no gap in the ICA2 group for intergroup comparisons at different times, 1 w after surgery, ICA2 group scores gradually recovered and mice showed an improvement in wellbeing, it is suggested that ICA access can improve well-being in mice by reducing vascular damage.

4. Discussion

High mortality and high heterogeneity have been major obstacles in mouse MCAO models [33], resulting in an inability to assess long-term functional outcomes and waste of animals and medicine [34].

Our study focuses on the optimisation of a mouse model of cerebral ischemia-reperfusion. On the one hand, by avoiding damage to the ECA, PPA, and other vessels [24], the survival rate and the wellbeing of the mice are improved by ICA access. Thus, optimising surgical approaches greatly minimizes mortality bias and allows the study of long-term morphological and functional sequelae of stroke in mice. On the other hand, The present study indicated that the consistency and reproducibility of the infarct area of the model was improved by extending the length of the silicone coating, which improved the correlation between behavioural scores and actual brain damage. This method will reduce the number of animals required and provide scientific, economic, and ethical benefits.

The current procedure of ECA access is well established and a simplified method of ligating the CCA has also been proposed. However, ligation of the CCA on one side has a non-negligible effect on haemodynamics, and there is no blood supply to the ECA, PPA, and other vessels on the operated side. Impaired PPA leads to dysphagia and ophthalmoplegia, impaired masticatory muscle function, and feeding difficulties after ECA damage (the results of the

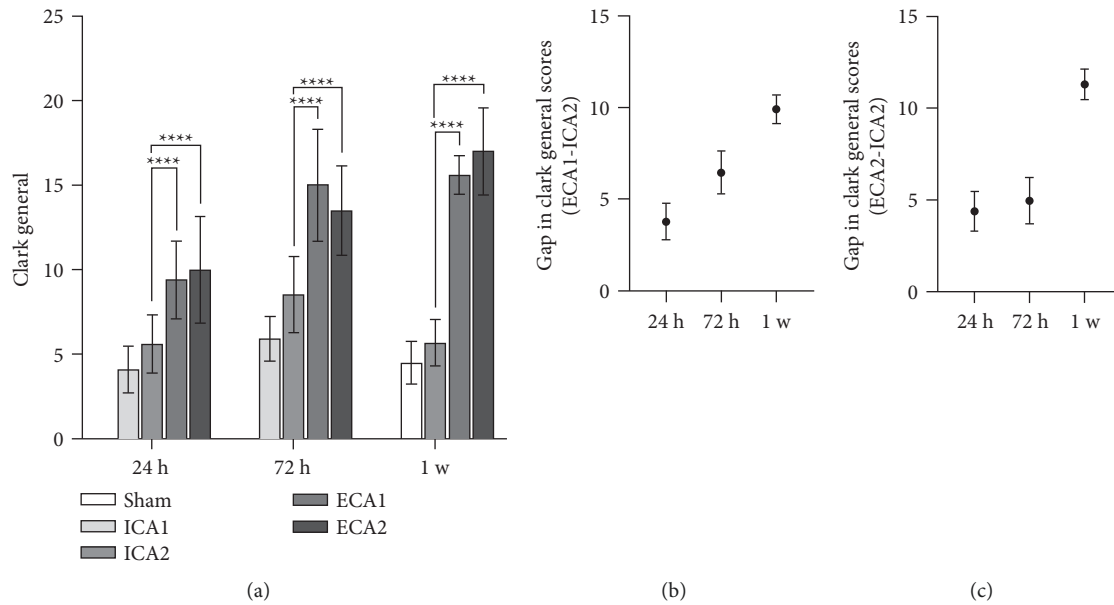


FIGURE 8: Analysis of Clark's general scores at different postoperative time points. (a) A significant difference in the ICA2 group compared to the ECA1 and ECA2 groups in Clark general scores at 3 postoperative time points 24 h, 72 h, and 1 w. **** $P < 0.0001$, $n = 15$, (b) difference in Clark general scores between ICA2 group and ECA1 group at different time points. (c) the difference in Clark general scores between ICA2 and ECA2 groups at different time points.

present study corroborate this conclusion), both of which increase mortality in mice and resulting discrepancies between behavioural assessments and the actual brain damage [35]. This method is therefore difficult to apply to systematic studies of cerebral ischemia-reperfusion injury. Subsequently, the use of bioadhesive for CCA repair was proposed as a feasible [18], but costly method with negligible damage to the endothelial injury can be followed by massive thrombosis, CCA occlusion, and failure to achieve reperfusion.

During the animal experiments, there are many other factors that affect the success of the mouse brain ischemia-reperfusion model, and the matters related to the surgery are summarized as follows. Select mice with appropriate body weight for surgery; too heavy models have a high failure rate and too light are prone to skull base haemorrhage. It is important to be proficient in the surgical approach. Careful separation of the PPA, ICA, and other vessels is essential for smooth insertion of the monofilament because of the potential for vascular variants at the carotid bifurcation. During the procedure we found abundant reverse blood flow in the PPA. In the classical surgical approach of ECA access, PPA can achieve compensation through the caudal part of the thin monofilament to the middle cerebral artery (MCA) and its surrounding branch arteries, ultimately leading to poor model consistency or even modelling failure [36]. It has been proposed to Permanent suture PPA on top of the classic surgical approach of ECA access, which has branches including the ophthalmic, pterygoid, pharyngeal, and other important branch arteries and is bound to have a serious impact on the well-being of the mice. The optimised surgical approach in this study therefore avoids both compensatory perfusions of the MCA by the PPA and damage to the PPA.

There are various ways to determine the success of a mouse brain ischemia-reperfusion model, noninvasive methods such as neurological deficit scoring, which is too subjective and less accurate, and invasive methods such as TTC staining, which is intuitive but the mice have been executed after the staining is completed, are now widely used for transcranial Doppler flow monitoring. The results of this experiment suggest that by monitoring the cerebral blood flow in the middle cerebral artery of mice, it can be judged that all groups can form effective embolization of the MCA trunk during the operation, but only the ICA2 and ECA2 groups formed a prolonged and effective interruption of blood flow in the middle cerebral artery before the end of the operation, and the ICA2 modelling success rate reached 93.3%. Middle cerebral artery flow is restored in the ICA1 and ECA1 groups, with a modelling success rate of only 26.7%–33.3%, this is still mainly due to the abundant intracranial arterial collateral circulation in mice [37], which cannot be reoperated again even if significant intraoperative MCA blood flow fluctuations are monitored, inevitably resulting in wasted samples. The silicone coating of fine monofilaments is therefore of sufficient length to embolize parts of the ACA and PCoA to reduce collateral compensation is key to increasing the success of moulding and improving the stability of the model.

To further improve the reproducibility and consistency of the mouse ischemia-reperfusion model, the diameter of the silicone monofilaments needs to be further investigated according to the mouse strain, body weight, and intracranial vessel diameter. The number of mice in this experiment is limited and a large sample size will be required to reach a conclusion worthy of recommendation.

Data Availability

The datasets used and analyzed during the current study are available from the corresponding author upon request.

Conflicts of Interest

The authors declare that they have no conflicts of interest.

References

- [1] F. Z. Caprio and F. A. Sorond, "Cerebrovascular disease," *Medical Clinics of North America*, vol. 103, no. 2, pp. 295–308, 2019.
- [2] A. S. Go, D. Mozaffarian, V. L. Roger et al., "Heart disease and stroke statistics--2014 update: a report from the American Heart Association," *Circulation*, vol. 129, no. 3, pp. e28–e292, 2014.
- [3] J. O. Ström, E. Ingberg, A. Theodorsson, and E. Theodorsson, "Method parameters' impact on mortality and variability in rat stroke experiments: a meta-analysis," *BMC Neuroscience*, vol. 14, p. 41, 2013.
- [4] S. Lee, Y. Hong, S. Park, S.-R. Lee, K.-T. Chang, and Y. Hong, "Comparison of surgical methods of transient middle cerebral artery occlusion between rats and mice," *Journal of Veterinary Medical Science*, vol. 76, no. 12, pp. 1555–1561, 2014.
- [5] R. Hata, K. Maeda, D. Hermann, G. Mies, and K.-A. Hossmann, "Evolution of brain infarction after transient focal cerebral ischemia in mice," *Journal of Cerebral Blood Flow and Metabolism*, vol. 20, no. 6, pp. 937–946, 2000.
- [6] H. Yao, S. Ibayashi, F. Anaga-Akiyoshi, K. Fukuda, and M. Fujishima, "[YAG laser-induced reperfusion of photo-thrombotic middle cerebral artery occlusion in rats]," *Nō to shinkei = Brain and nerve*, vol. 53, no. 3, p. 253, 2001.
- [7] S. Ansari, E. Chatzikonstantinou, A. Wistuba-Schier et al., "Characterization of a new model of thromboembolic stroke in C57 black/6J mice," *Translational Stroke Research*, vol. 5, no. 4, pp. 526–533, 2014.
- [8] K. J. Schunke, T. K. Toung, J. Zhang et al., "A novel atherothrombotic model of ischemic stroke induced by injection of collagen into the cerebral vasculature," *Journal of Neuroscience Methods*, vol. 239, pp. 65–74, 2015.
- [9] Y. Chen, W. Zhu, W. Zhang, and N. Libal, "A novel mouse model of thromboembolic stroke," *J Neurosci Methods*, vol. 256, pp. 203–211.
- [10] M. Ren, Z.-J. Lin, H. Qian et al., "Emboic middle cerebral artery occlusion model using thrombin and fibrinogen composed clots in rat," *Journal of Neuroscience Methods*, vol. 211, no. 2, pp. 296–304, 2012.
- [11] X. Fan, J. Qiu, Z. Yu et al., "A rat model of studying tissue-type plasminogen activator thrombolysis in ischemic stroke with diabetes," *Stroke*, vol. 43, no. 2, pp. 567–570, 2012.
- [12] E. B. Ringelstein, R. Biniek, C. Weiller, B. Ammeling, P. N. Nolte, and A. Thron, "Type and extent of hemispheric brain infarctions and clinical outcome in early and delayed middle cerebral artery recanalization," *Neurology*, vol. 42, no. 2, p. 289, 1992.
- [13] S. Ansari, H. Azari, D. J. McConnell, A. Afzal, and J. Mocco, "Intraluminal middle cerebral artery occlusion (MCAO) model for ischemic stroke with laser Doppler flowmetry guidance in mice," *Journal of Visualized Experiments*, vol. 8, no. 51, p. 2849, 2011.
- [14] N. Shimamura and H. Ohkuma, "Novel rat middle cerebral artery occlusion model: trans-femoral artery approach combined with preservation of the external carotid artery," *Journal of Neuroscience Methods*, vol. 184, no. 2, pp. 195–198, 2010.
- [15] Q. Cai, G. Xu, J. Liu et al., "A modification of intraluminal middle cerebral artery occlusion/reperfusion model for ischemic stroke with laser Doppler flowmetry guidance in mice," *Neuropsychiatric Disease and Treatment*, pp. 2851–2858, 2016.
- [16] G. P. Morris, A. L. Wright, R. P. Tan, A. Gladbach, L. M. Ittner, and B. Vissel, "A comparative study of variables influencing ischemic injury in the longa and koizumi methods of intraluminal filament middle cerebral artery occlusion in mice," *PLoS One*, vol. 11, no. 2, p. e0148503, 2016.
- [17] E. S. Connolly, C. J. Winfree, D. M. Stern, R. A. Solomon, and D. J. Pinsky, "Procedural and strain-related variables significantly affect outcome in a murine model of focal cerebral ischemia," *Neurosurgery*, vol. 38, no. 3, pp. 523–532, 1996, discussion 532.
- [18] M. Trotman-Lucas, M. E. Kelly, J. Janus, R. Fern, and C. L. Gibson, "An alternative surgical approach reduces variability following filament induction of experimental stroke in mice," *Disease Models and Mechanisms*, vol. 10, no. 7, pp. 931–938, 2017.
- [19] J.-i. Koizumi, Y. Yoshida, T. Nakazawa, and G. Ooneda, "Experimental studies of ischemic brain edema," *Nosotchu*, vol. 8, no. 1, pp. 1–8, 1986.
- [20] E. Z. Longa, P. R. Weinstein, S. Carlson, and R. Cummins, "Reversible middle cerebral artery occlusion without craniectomy in rats," *Stroke*, vol. 20, no. 1, pp. 84–91, 1989.
- [21] B. W. Mccoll, H. V. Carswell, J. Mcculloch, and K. Horsburgh, "Extension of cerebral hypoperfusion and ischaemic pathology beyond MCA territory after intraluminal filament occlusion in C57Bl/6J mice," *Brain Research*, vol. 997, no. 1, pp. 15–23, 2004.
- [22] H. K. Smith, J. M. Russell, D. N. Granger, and F. N. E. Gavins, "Critical differences between two classical surgical approaches for middle cerebral artery occlusion-induced stroke in mice," *Journal of Neuroscience Methods*, vol. 249, pp. 99–105, 2015.
- [23] M. Dittmar, T. Spruss, G. Schuierer, and M. Horn, "External carotid artery territory ischemia impairs outcome in the endovascular filament model of middle cerebral artery occlusion in rats," *Stroke*, vol. 34, no. 9, pp. 2252–2257, 2003.
- [24] M. S. Dittmar, B. Vatankhah, N. P. Fehm et al., "The role of ECA transection in the development of masticatory lesions in the MCAO filament model," *Experimental Neurology*, vol. 195, no. 2, pp. 372–378, 2005.
- [25] R. C. Trueman, D. J. Harrison, D. M. Dwyer, S. B. Dunnett, M. Hoehn, and T. D. Farr, "A critical Re-examination of the intraluminal filament MCAO model: impact of external carotid artery transection," *Translational Stroke Research*, vol. 2, no. 4, pp. 651–661, 2011.
- [26] A. Lourbopoulos, U. Mamrak, S. Roth et al., "Inadequate food and water intake determine mortality following stroke in mice," *Journal of Cerebral Blood Flow and Metabolism*, vol. 37, no. 6, pp. 2084–2097, 2017.
- [27] K. Kaawa, "Cerebral ischemia after bilateral carotid artery occlusion and intraluminal suture occlusion in mice: evaluation of the patency of the posterior communicating artery," *Journal of Cerebral Blood Flow and Metabolism*, vol. 18, no. 5, pp. 570–579, 1998.
- [28] Y. Akamatsu, H. Shimizu, A. Saito, M. Fujimura, and T. Tominaga, "Consistent focal cerebral ischemia without posterior cerebral artery occlusion and its real-time

- monitoring in an intraluminal suture model in mice,” *Journal of Neurosurgery*, vol. 116, no. 3, pp. 657–664, 2012.
- [29] S. Ansari, H. Azari, D. J. McConnell, A. Afzal, and J. Mocco, “Intraluminal middle cerebral artery occlusion (MCAO) model for ischemic stroke with laser Doppler flowmetry guidance in mice,” *Journal of Visualized Experiments*, vol. 8, no. 51, p. 2879, 2011.
 - [30] J. Chen, P. R. Sanberg, Y. Li et al., “Intravenous administration of human umbilical cord blood reduces behavioral deficits after stroke in rats,” *Stroke*, vol. 32, no. 11, pp. 2682–2688, 2001.
 - [31] R. A. Swanson and F. R. Sharp, “Infarct measurement methodology,” *Journal of Cerebral Blood Flow and Metabolism*, vol. 14, no. 4, p. 697, 1994.
 - [32] W. M. Clark, “Monofilament intraluminal middle cerebral artery occlusion in the mouse,” *Neurological Research*, vol. 19, no. 6, pp. 641–648, 1997.
 - [33] B. S. Aspey, F. L. Taylor, M. Terruli, and M. J. G. Harrison, “Temporary middle cerebral artery occlusion in the rat: consistent protocol for a model of stroke and reperfusion,” *Neuropathology and Applied Neurobiology*, vol. 26, no. 3, pp. 232–242, 2000.
 - [34] A. Rosell, V. Agin, M. Rahman et al., “Distal occlusion of the middle cerebral artery in mice: are we ready to assess long-term functional outcome,” *Transl Stroke Res*, vol. 4, no. 3, pp. 297–307, 2013.
 - [35] M. Bieber, J. Gronewold, A.-C. Scharf et al., “Validity and reliability of neurological scores in mice exposed to middle cerebral artery occlusion,” *Stroke*, vol. 50, no. 10, pp. 2875–2882, 2019.
 - [36] Y. Chen, A. Ito, K. Takai, and N. Saito, “Blocking pterygopalatine arterial blood flow decreases infarct volume variability in a mouse model of intraluminal suture middle cerebral artery occlusion,” *Journal of Neuroscience Methods*, vol. 174, no. 1, pp. 18–24, 2008.
 - [37] Z. Hua, P. Prabhakar, R. Sealock et al., “Faber JEWide genetic variation in the native pial collateral circulation is a major determinant of variation in severity of stroke. J Cereb Blood Flow Metab 30:923-934,” *Journal of the International Society of Cerebral Blood Flow & Metabolism*, vol. 30, no. 5, pp. 923–934, 2010.

Retraction

Retracted: Implementation of Evidence in Preventing Postoperative Sore Throat of Patients Undergoing General Anesthesia Intubation Using the i-PARIHS Framework

Computational Intelligence and Neuroscience

Received 25 July 2023; Accepted 25 July 2023; Published 26 July 2023

Copyright © 2023 Computational Intelligence and Neuroscience. This is an open access article distributed under the Creative Commons Attribution License, which permits unrestricted use, distribution, and reproduction in any medium, provided the original work is properly cited.

This article has been retracted by Hindawi following an investigation undertaken by the publisher [1]. This investigation has uncovered evidence of one or more of the following indicators of systematic manipulation of the publication process:

- (1) Discrepancies in scope
- (2) Discrepancies in the description of the research reported
- (3) Discrepancies between the availability of data and the research described
- (4) Inappropriate citations
- (5) Incoherent, meaningless and/or irrelevant content included in the article
- (6) Peer-review manipulation

The presence of these indicators undermines our confidence in the integrity of the article's content and we cannot, therefore, vouch for its reliability. Please note that this notice is intended solely to alert readers that the content of this article is unreliable. We have not investigated whether authors were aware of or involved in the systematic manipulation of the publication process.

In addition, our investigation has also shown that one or more of the following human-subject reporting requirements has not been met in this article: ethical approval by an Institutional Review Board (IRB) committee or equivalent, patient/participant consent to participate, and/or agreement to publish patient/participant details (where relevant).

Wiley and Hindawi regrets that the usual quality checks did not identify these issues before publication and have since put additional measures in place to safeguard research integrity.

We wish to credit our own Research Integrity and Research Publishing teams and anonymous and named external researchers and research integrity experts for contributing to this investigation.

The corresponding author, as the representative of all authors, has been given the opportunity to register their agreement or disagreement to this retraction. We have kept a record of any response received.

References

- [1] Q. Liu, Y. Wang, R. Zhuang, L. Bao, L. Zhu, and Y. Zhou, "Implementation of Evidence in Preventing Postoperative Sore Throat of Patients Undergoing General Anesthesia Intubation Using the i-PARIHS Framework," *Computational Intelligence and Neuroscience*, vol. 2022, Article ID 3151423, 9 pages, 2022.

Research Article

Implementation of Evidence in Preventing Postoperative Sore Throat of Patients Undergoing General Anesthesia Intubation Using the i-PARIHS Framework

Qian Liu,¹ Yiting Wang,¹ Ruo Zhuang^{ID},¹ Lei Bao,¹ Liqun Zhu,¹ and Yingfeng Zhou²

¹Anesthesia Operating Room, Affiliated Hospital of Jiangsu University, Zhenjiang City, China

²Evidence-Based Nursing Cooperation Center of Fudan University, School of Nursing, Fudan University, Shanghai, China

Correspondence should be addressed to Ruo Zhuang; 1923507921@139.com

Received 10 May 2022; Revised 1 June 2022; Accepted 2 June 2022; Published 5 July 2022

Academic Editor: Dong Chen

Copyright © 2022 Qian Liu et al. This is an open access article distributed under the Creative Commons Attribution License, which permits unrestricted use, distribution, and reproduction in any medium, provided the original work is properly cited.

Objective. The aim of the study was to assess the effectiveness of the implementation of the best evidence in preventing postoperative sore throat in patients undergoing general anesthesia intubation. **Methods.** The related topics of the postoperative sore throat of patients undergoing general anesthesia intubation were systematically searched in the database and evaluated using the Integrated Promoting Action on Research Implementation in Health Services (i-PARIHS) framework. Combined with clinical needs and evidence-based professional judgment, 20 pieces of evidence and 6 examination standards on the management process and evidence implementation plan for the prevention of postoperative sore throat in patients with general anesthesia intubation are summarized, implementing the best evidence into clinical practice in anesthesiology, general surgery, orthopedics, thoracic surgery, and gynecology. **Results.** Nurses' knowledge scores and evidence compliance significantly improved after the implementation of the best evidence ($P < 0.05$); the incidence of the postoperative sore throat in patients undergoing general anesthesia intubation decreased from 41.7% to 28.1%. **Conclusion.** The i-PARIHS framework effectively prevents postoperative sore throat in patients, providing an effective case for translating evidence into practice based on the i-PARIHS framework.

1. Introduction

Postoperative sore throat (POST) is the nociceptive pain caused by the throat and tracheal mucosa injury during tracheal intubation under general anesthesia. The main clinical manifestations are postoperative sore throat, local congestion, and redness, accompanied by hoarseness, low voice, and cough. It will affect eating or even cause fatal injury in severe cases [1]. It has been reported that the incidence of postoperative pharyngolaryngitis and hoarseness is as high as 6.9%~90.0% [2–4], which causes pain, aggravates patients' difficulty in swallowing and speaking, reduces postoperative comfort, and prolongs patients' hospital stay [5–7]. Therefore, the effective control of POST has great significance in improving the management quality of general anesthesia intubation and the safety of patients. However, there is a lack of clinical practice guidelines and systematic intervention for POST prevention in China, and

most measures taken by nurses in a clinic are based on experience and routine. Therefore, this study aims to explore the best evidence for postoperative sore throat prevention in patients with general anesthesia intubation and to conduct clinical translation and implementation to address postoperative sore throat and thus improve the quality of care.

2. Methods

2.1. Setting and Participants. This study uses the i-PARIHS framework and adopts a controlled before-and-after study. Clinical research was carried out in the anesthesia department, general surgery department, orthopedics department, thoracic surgery department, and gynecology department of a third-class hospital from June 2019 to June 2021, including baseline review before evidence implementation, practice reform, and effect evaluation after evidence implementation.

Five wards in the Affiliated Hospital of Jiangsu University were selected. 151 patients with general anesthesia intubation, patients, and 140 clinical medical staff were included as research objects before and after the implementation of evidence.

The inclusion criteria for patients are as follows: (1) adult (age ≥ 18 years old); (2) patients undergoing elective general anesthesia; (3) no other underlying medical conditions; (4) patients have no contraindications to anesthesia.

The exclusion criteria for patients are as follows: (1) patients who suspend surgery for some reason; (2) patients who subjectively refuse to participate in the study; (3) patients who objectively cannot cooperate due to mental and audio-visual disorders; (4) patients who lacked complete medical record data; (5) patients who withdraw halfway through the course of treatment. The inclusion criteria for nurses are working for more than 6 months and obtaining a nurse practice certificate; the exclusion criteria for nurses do not agree to participate in the study.

2.2. Baseline Survey

2.2.1. Team Formation. Evidence-based expert team and evidence review team include (1) establishment of a review team which consists of 10 members, including one head nurse of the anesthesiology department as the team leader, who plans the overall project and trains the team members to ensure the implementation of evidence transformation. One nursing department director ensures project resources; one teaching secretary is responsible for process decision-making and departmental consultation. Six head nurses and directors are responsible for project support and coordination; one graduate student is responsible for data collection and analysis. (2) There are two members in the evidence-based expert group, including one deputy head of the evidence-based committee who is responsible for the project quality control and guiding the practice plan. A tutor from the Evidence-based Center of Fudan University Nursing tracked, guided, and reviewed the whole project.

2.2.2. Determination of Review Indicators and Review Methods. In addition to the 12 members of the project team, two anesthesiologists from our hospital were invited to evaluate the best evidence of integration in four dimensions, namely, feasibility, suitability, clinical significance, and effectiveness according to the FAME principle.

Combined with the clinical environment of evidence transformation and the resources of our hospital, we turn the items related to the best evidence for clinical implementation into 16 quality inspection indicators (please refer to the Summary of the Best Evidence for Prevention of Throat Pain after General Anesthesia and Tracheal Intubation in the journal of nursing science in 2021 for specific evidence items) and determine the inspection objects and methods of the inspection indicators one by one, as shown in Table 1.

2.2.3. Evaluation Index. (1) Incidence of postoperative sore throat (%) and (2) severity of postoperative sore throat (using Prince-Henry sore throat score [8]) are divided into four grades: no pain feeling when coughing is 0 point; occasionally, there is a pain when coughing, but the absence of pain during deep breathing is 1 point; pain occurs during deep breathing, and it is relieved when quiet is 2 points; there is pain feeling in a quiet state, but within the tolerable range, it is 3 points; when in a quiet state, the pain is severe and unbearable is 4 points. (3) The time at which the patient eats after surgery, (4) the amount of food for patients after the operation, (5) the degree and level of dysphagia were recorded, and Wada test was put forward by Japanese scholar Toshio Wada in 1982 [9], which is the most classic method of swallowing function screening. Washi's drinking water experiment is as follows: patients sit flat and fill a cup of warm water (capacity 30 ml), so that the patient can drink it in a normal state. Carefully observe the patient's drinking process and make records to realize the swallowing function of the patient during this process.

(1) The Evaluation of the Grade. Scoring criteria are as follows: 1. Grade I: the patient drank it all at once, and there was no abnormality; 2. Grade II: the time is 0~5 s, and there was no bucking after drinking twice; 3. Grade III: there is bucking, and the time is 5~10 s after drinking once; 4. Grade IV: the cough is mild, and the time is 5~10 s after drinking many times; 5. Grade V: frequent bucking, difficulty in drinking water, time >10 s; (6) comfort (VAS score [10]) was evaluated when the patient was awake. Scoring criteria are as follows: the feeling of no pain at the wound is 0 points; slight pain in the wound is 1~2 points; the pain in the wound was slightly obvious, and the number of times of pain was 3~points. The pain in the wound is obvious, but within the tolerable range, it is 5~7 points; the acute pain in the wound cannot be tolerated for 8~10 points; and (7) investigation and analysis of the mastery of the knowledge (knowledge, attitude, practice KAP).

2.3. i-PARIHS. Evidence-based practice model was used to analyze the obstacle factors of clinical transformation of evidence for preventing postoperative sore throat in patients undergoing general anesthesia intubation. It was analyzed from three dimensions: change (change brought by evidence), receiver, and organizational environment (Table 2).

It can be seen from the analysis of the above obstacle factors that evidence needs to be further transformed into a form that is accessible and useable for nurses, such as nursing operation procedures or paths. However, the implementation of some evidence will change the existing procedures, such as preoperative assessment of a patient's throat. The willingness and ability of evidence recipients need to be strengthened and improved, for example, the lack of knowledge and skills related to intubation assessment. Therefore, there is a lack of resources in the organizational environment, especially human resources for anesthesia nurses.

TABLE 1: Review indicators and review methods based on the i-PARIHS framework.

Serial number	Review indicators	Review methods
1	Before an operation, doctors and nurses should evaluate the basic condition of patients and actively treat them	Check the nursing record sheet
2	During the operation, anesthesiologists should evaluate the high-risk factors affecting postoperative throat pain	Check the anesthesia record sheet and field survey
3	Anesthesiologists should make a comprehensive assessment of patients with difficult airways and follow-up	Check the preoperative evaluation sheet and postoperative visit records
4	Doctors and nurses should pay attention to the comfort and satisfaction of sore throat	Check the nursing record sheet and field survey
5	Select a video laryngoscope to assist with intubation first	Check the anesthesia record sheet and field survey
6	Anesthesiologists should master the measures to reduce postoperative throat pain and choose the most suitable endotracheal tube	Field survey
7	According to the contraindications of patients, magnesium, licorice, diphenhydramine, corticosteroids (dexamethasone, betamethasone), ketamine, lidocaine, etc., are used locally or intravenously	Check the anesthesia record sheet
8	During the operation, according to factors such as time and body position change, timely use of pressure measuring device to regularly monitor the pressure of the cuff to maintain 25–30cmH ₂ O, and it is not allowed to be measured by the finger sensing method	Field survey
9	When suctioning sputum, anesthesiologists should control the negative pressure of sputum suction at 80–120 mmHg and fully suck it in every time to avoid repeated operation	Field survey
10	Anesthesiology doctors and nurses should exhaust all the gas in the cuff when extubating the trachea, and gently extubate	Field survey
11	Anesthesiology department doctors and nurses should suck sputum according to the situation of sputum	Field survey
12	Pay attention to your movements when suctioning sputum, please be gentle	Field survey
13	For those with sticky sputum, which is inconvenient to attract, fiber-optic bronchoscopy can be used for sputum aspiration	Field survey

2.4. Transformation Strategy of Evidence Transformation.

In the process of promoting the clinical transformation of evidence, establishing effective strategies is the guarantee to promote the success of the reform. We should seek available resources and take effective and feasible action plans to promote the success of the change based on understanding the obstacles. A focus group discussion was held to further qualitatively understand the obstacles and promoting factors according to the baseline survey results. Each group consists of 5–9 team members led by a head nurse, and the discussion lasts for 60–120 minutes, which continues until the theoretical arguments are saturated. In the baseline survey, the coincidence rate of 5 review standards in 16 review standards was less than 60%, of which the compliance rate of 2 standards was 0.

As described above, the obstacle factors in the process of evidence transformation are analyzed from three dimensions: change, receiver, and organizational environment, and the change strategy will also aim at these three dimensions.

2.4.1. Strategy of Change Dimension

- (1) The evaluation list of sore throat prevention after intubation under general anesthesia was determined, printed out, and used through a literature search.

- (2) I-PARIHS framework helps promote the clinical implementation of research results and guides the analysis of obstacles and promoting factors in the implementation of evidence.
- (3) Converting the contents and items of measures to prevent sore throat into a flowchart, which is easy to understand and operate.
- (4) The nursing routine was revised. The content of evaluating intubated patients and the treatment of extubation for intubated patients were written into relevant systems and routines so that the content of the reform was clearly in place in the practice process.
- (5) Clarifying the links of major changes in the nursing process, such as detailing the medical history of respiratory diseases related to POST and including it in the hospitalization evaluation sheet. Multidisciplinary cooperation is needed to complete the change plan. Unifying evaluation methods and tools. Strengthening the work habits of accurate intubation pipe diameters and operation of each link.

2.4.2. Change Strategy of the Receiver Dimension

- (1) Enhancing the recipient's willingness to change: it was found that nurses expressed their desire to do

TABLE 2: Obstacles and promoters based on the i-PARIHS framework.

Review indicators	Obstacle factors	Promoting factors
Review indicator 1	I: evidence needs to change the process and system R: knowledge and skills are not fully mastered C: at present, hospitals lack relevant admission evaluation procedures and methods	Team members come from various specialties There are information systems that can be optimized
Review indicator 2	I: evidence needs to change the process and system R: there are many diseases, and medical care may not be able to cure them completely C: there are many patients in each ward, so it is impossible to do fine management	Hospital consultation can get specialist treatment guidance
Review indicator 6	I: evidence content is not included in the evaluation system R: the workload of nurses in the ward increased, and their compliance was insufficient C: there is no publicity material for the patients evaluated in this way	In each stage of the perioperative period, there are various forms of publicity tools, and in some links, human resources can be adjusted
Review indicator 8	I: the evidence failed to transform into an acceptable process and form R: anesthesiologists do not fully understand the content of the evidence C: teaching hospitals, with a large number of personnel for training and further education, are difficult to intubate all at once successfully	The Anesthesiology Department of our hospital is a training base with detailed operation procedures and training methods to facilitate training and assessment
Review indicator 9	I: the measures to reduce postoperative sore throat are not specific enough, and some techniques have certain learning curves R: there is no accurate tracheal diameter working habit, and some links are not finely operated C: there are no catheters of various types that can meet the demand, and there is no cuff management flow standard and process	Doctors and nurses have realized the importance of cuff management
Review indicator 10	I: evidence needs to change existing work habits and processes R: medical staff cannot fully grasp the timing of medication C: some medicines cannot be provided	The description of the medication process in the literature is relatively detailed
Review indicator 11	I: the evidence may conflict with the working environment of doctors and nurses R: the workload of medical evaluation is large, which is influenced by the cooperation of operation, and it also increases the possibility of forgetting C: there are not enough pressure measuring devices	The price of a pressure measuring device is acceptable
Review indicator 12	I:— R: it is difficult for staff to avoid repeated operations C: the negative pressure gauge value is unclear, and the pressure is not allowed	Fully attract relevant documents and materials
Review indicator 14	I:— R: the understanding of gentleness among the staff is not consistent enough C: there is no specific illustration of the operation	The medical staff realizes the importance of gently sucking sputum
Review indicator 16	I:— R: I am used to using a small syringe to deflate C: when the patient is restless, it is more difficult to gently pull the tube	There are consensus and guidelines for extubation

something for patients through the investigation, but they had no guidance and did not know how to do it. With these schemes, they could guide nursing work. In order to promote the health of patients, the nursing team retained nurses with relevant health

education majors to guide patients and their families; holding a mobilization meeting to allow core personnel such as the director of anesthesiology to support the relevant personnel involved in the practice; any good outcome and the importance

of bagging management in practice are important factors to enhance the willingness to change.

- (2) Enhancing the receiver's knowledge and skills: adopting various forms of training, such as lectures, medical record explanations, watching videos, reading educational manuals, and sputum suction maps; strengthening the training and assessment of nurses and interns in intubation, sputum suction, extubation, and POST safety awareness; strengthening the training of anesthesiologists on the timing, methods, and tools of cuff pressure measurement.
- (3) Empowerment: the visiting class will assess the POST risk of patients with general anesthesia one day before operation; strengthen the PACU responsibility system and meticulous nursing; and dynamically monitor patients to eliminate the causes of restlessness as soon as possible.
- (4) Establishing a multidisciplinary team cooperation mechanism: using the Internet such as WeChat to establish communication channels and timely communicate and treat the illness. In-hospital consultation, specialist guidance, and formulation of a POST treatment plan can guarantee the effective implementation of perioperative throat pain care.

2.4.3. Change Strategy of Organizational Environment Dimension

- (1) The Department of Anesthesiology of our hospital is a training base for regular training and specialized training in Zhenjiang City. It has detailed operating procedures and training methods, which are convenient for training and assessment.
- (2) Improving the allocation of human nursing resources: there are different forms of propaganda tools in each stage of the perioperative period, and human resources can be adjusted in different links.
- (3) Formulating the perioperative management path of POST: based on the "Management Pathway for Throat Pain in Patients with Tracheal Intubation under General Anesthesia during Perioperative Period," evidence was completed, which promoted the pathization of POST management.
- (4) Optimizing the hospital information system: POST is used as a routine monitoring indicator after general anesthesia and tracheal intubation, and normalized monitoring after extubation and postoperative follow-up is included in the doctor's order system; cuff management standards are formulated and included in surgical quality management information quality control.
- (5) Using of tools: using ultrasound or CT to measure the diameter of the trachea; applying for a patent for continuous measurement of cuff pressure; PACU is equipped with a system negative pressure gauge; contacting the instrument department to purchase a cuff pressure gauge. Through expert correspondence and

evidence-based group discussion, the assessment record sheet for prevention of sore throat in patients with general anesthesia and intubation was jointly revised, including the contents of the recommendations.

2.5. The Process of Evidence Implementation. It lasted for 5 months (from June 1, 2020, to October 30, 2020). In June, preparations such as writing health education, nursing manuals, and training nurses were completed before the evidence was implemented. The training content is designed as a small video and courseware, which is placed on the Jingyi teaching platform in the hospital, allowing nurses to participate in the learning, and setting questions for nurses to participate. Evidence-based implementation was implemented from June 1 to October 30, and 192 patients were included.

During the implementation of the evidence, nurses' knowledge of POST prevention was investigated using a questionnaire we designed and compared with the questionnaire in the baseline survey. The questionnaire content was designed based on the best evidence. After the questionnaire was completed, 3 anesthesiologists, 2 evidence-based specialists, and 1 otolaryngologist were consulted. The questionnaire was revised and improved according to expert opinion. The questionnaire consists of 3 parts (dimensions are divided into knowledge, attitude, and behavior). Including 37 questions, each question has a maximum score of 5 points and a minimum score of 1 point, with a total score of 185 points. Questionnaires are sent to nurses through online software. After nurses complete and submit the questionnaires, the system automatically scores the questionnaires. The study found that after the implementation of the evidence, the compliance rate of each item and the score of the questionnaire were improved compared with the baseline survey.

Two graduate students and interns performed data collection according to the review methodology. During the baseline survey and evidence implementation, 5 participants from students studying in the anesthesia operating room participated in data collection. The intern did not know the grouping of patients, and the nurse did not know which patient was performing evidence implementation to avoid the Hawthorne effect. Two graduate students collected the data on the occurrence of POST in patients, and the patient record sheet included general information stating whether POST occurred on admission, and provided admission, operation time, ward, intubation status (intubation size, single-lumen or dual-lumen line), difficult airway, successful extubation, medical information, and equipment involved in POST. To compare the incidence of postoperative POST in intubated patients with general anesthesia after the baseline survey and evidence implementation, patients participating in baseline surveys and evidence implementation should be different.

2.6. Statistical Methods. The data were statistically analyzed by SPSS22.0 software, and the counting data were expressed by $[n(\%)]$. By using χ^2 test, the VAS score of comfort and the

knowledge, belief, and behavior of medical staff were tested by independent sample *T*-test, and the test level $\alpha = 0.05$, with $P < 0.05$ as the difference with statistical significance.

3. Results

3.1. Structural Dimension System Level. The clinical pathway of intubation for patients under general anesthesia was established (see Figure 1). New technology of selecting suitable endotracheal tube by B-ultrasound to evaluate the tube diameter and setting and monitoring the cuff pressure of endotracheal tube by pressure tester was developed. The follow-up record and quality control book after anesthesia were updated, improving the perioperative throat pain management, endotracheal tube cuff management, post-anesthesia visit, and complication management process.

Step 1: preoperative evaluation to identify high-risk patients with respiratory diseases such as bronchitis and asthma, difficulty airway, and gastrointestinal surgery. In high-risk patients, preventive medication will be given.

Step 2: intubation management-item preparation: visual intubation equipment, airway nebulizer, ultrasound, tracheal tube, and preventive medication are on standby.

Step 3: cuff management-airbag pressure filling method: fixed volume injection method, minimum occlusion volume method, minimum lateral leakage test method, dynamic assessment of cuff pressure: 25–30 cm H₂O, evaluation timing: after tracheal intubation, after a body position change, after pneumoperitoneum, the operation time >6 hours, and after entering the recovery room.

Step 4: extubation management-sputum suction pressure: 80–100 mmHg; extubation method: a large syringe exhausts the cuff contents and gently removes them to reduce extubation injury.

Step 5: after extubation, the patient's throat pain and other conditions were promptly assessed, and shifts were handed over and recorded.

3.2. Process Dimension Practitioner Level

- (1) Compliance with evidence-based practices of medical staff: a method similar to the status review was used to review the compliance of the review indicators. A total of 16 indicators were reviewed before and after the implementation of evidence. The results are shown in Figure 2.
- (2) The score of knowledge-belief-action evaluation of medical staff on the management of intubation prevention for sore throat in patients with general anesthesia: the biggest impact of evidence in the process of clinical translation is the change of practitioners' knowledge, attitude, and behavior (see Table 3).

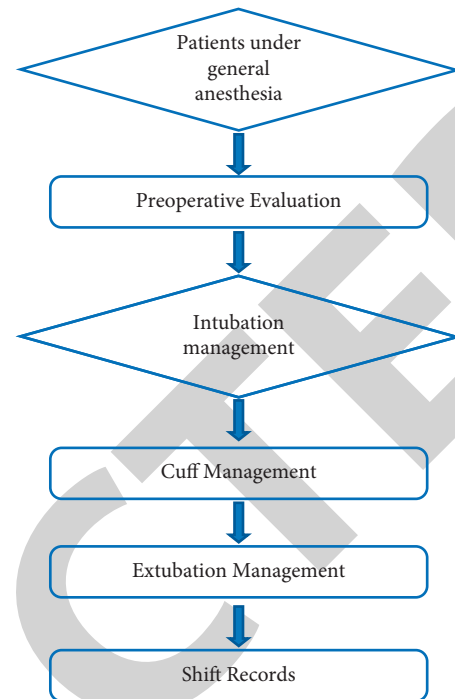


FIGURE 1: Clinical pathway of intubation for patients under general anesthesia.

3.3. Outcome Dimension Patient Level

3.3.1. Before and after the Implementation of Evidence. Before and after the implementation of evidence, 151 and 192 patients with general anesthesia who met the inclusion and exclusion criteria were obtained, respectively. There was no statistical difference between the two groups in age, gender, lung disease, department, and body position (see Table 4).

3.3.2. By Comparing the Clinical Outcome Indicators of the Two Groups of Patients. By comparing the clinical outcome indicators of the two groups of patients, the incidence of the sore throat under resting state in patients with general anesthesia and intubation before and after the implementation of evidence, the effect of pain on eating and rest, and the patient's comfort were significantly different ($P < 0.05$). However, there was no significant difference in the incidence of the sore throat under swallowing before and after the implementation of the evidence ($P > 0.05$), as shown in Table 5.

4. Discussion

Clinically, less attention is paid to the problem of postoperative sore throat in patients with general anesthesia and intubation. In contrast, we pay more attention to surgical patients' recurrence rate and wound pain after treatment. However, the rehabilitation of patients not only is about unilateral surgical treatment but also needs to pay attention to psychological treatment, prevention of postoperative complications, and comprehensive health guidance. Therefore,

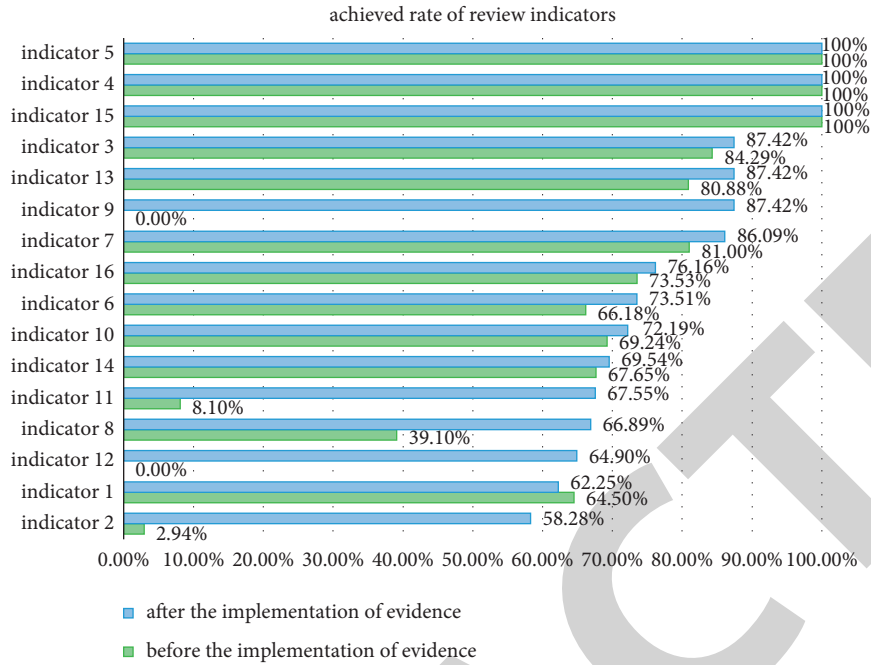


FIGURE 2: Achieved rate of review indicators before and after the implementation of evidence.

TABLE 3: KAP of surgical medical staff before and after implementation of evidence (score, $\bar{x} \pm S$).

	Knowledge	Attitude	Behavior
Before implementation of evidence	58.91 \pm 8.18	35.24 \pm 4.55	16.57 \pm 4.89
After implementation of the evidence	68.14 \pm 6.40	41.47 \pm 3.52	21.72 \pm 3.36
<i>t</i>	-10.516	-12.816	-10.267
<i>P</i>	<0.001	<0.001	<0.001

TABLE 4: General situation of research objects (*n*(%)).

Project		Before implementation of evidence <i>N</i> = 151	After implementation of evidence <i>N</i> = 192	χ^2	<i>P</i>
Age	<60 years old	107 (70.9)	149 (77.6)	2.03	0.154
	\geq 60 years old	44 (29.1)	43 (22.4)		
Gender	Man	56 (37.1)	78 (40.6)	0.445	0.505
	Woman	95 (62.9)	114 (59.4)		
Dept.	Gastrointestinal surgery	31 (20.5)	43 (22.4)	1.618	0.806
	Chest surgery	27 (17.9)	35 (18.2)		
	Gynecology	33 (21.9)	36 (18.8)		
	Urology	31 (20.5)	39 (20.3)		
	Spine 1	29 (19.2)	39 (20.3)		
Posture	Supine position	45 (29.8)	44 (22.9)	2.762	0.430
	Lateral position	37 (24.5)	52 (27.1)		
	Stone cutting position	34 (22.5)	48 (25.0)		
	Prone position	35 (23.2)	48 (25.0)		
Lung disease	Have	10 (6.6)	17 (8.9)	0.58	0.446
	Without	141 (93.4)	175 (91.1)		

scientific, standardized, and systematic nursing also plays a very important role [11]. Some studies have also pointed out that traditional surgical care has been unable to meet the development of modern nursing [12]. This study assessed the

implementation of evidence to prevent POST in general anesthesia intubated patients and described the evidence implementation process using the i-PARIHS framework. Evidence implementation is a complex and ongoing process.

TABLE 5: Comparison of incidence and comfort of the sore throat before and after implementation of evidence ($n(\%)$).

Time	Case number	Sore throat at rest	Sore throat in swallowing state	Effect of pain on eating	Effect of pain on rest	Comfort level
Before implementation of evidence	151	63 (41.7)	36 (23.8)	53 (35.1)	52 (34.4)	5.83 (1,10)
After implementation of evidence	192	54 (28.1)	37 (19.3)	20 (10.4)	13 (6.8)	6.65 (0,10)
χ^2/Z		6.953(1)	1.183(1)	30.738(1)	42.123(1)	19.955(2)
P		<0.05	>0.05	<0.05	<0.05	<0.05

Note: (1) is χ^2 value; (2) is the z value.

Evidence-based nursing can start from the actual condition of the patient through methods such as analyzing problems and finding evidence, to formulate a targeted evidence-based nursing plan for the patient, which can bring nursing intervention to the entire perioperative period and improve clinical efficacy. It has played an important role in relieving patients' negative emotions and improving clinical satisfaction [13, 14].

4.1. Clinical Practice Based on the Best Evidence Can Effectively Improve the Organizational Environment and Quality of Care.

In the past 10 years, both researchers and clinical nursing practitioners in the field of evidence-based nursing have been actively committed to promote the clinical translation of research evidence [15]. We mobilized all the resources throughout the evidence implementation process, with the support of the Nursing Department, Section Chief, and Head Nursing. Authorized by the "top-down" leadership, nurses can provide POST nursing training for patients as long as they have undergone systematic training and mastered relevant skill training. The evidence-based nursing practice for patients with general anesthesia and intubation has changed the previous method of selecting the type of tracheal tube based on estimation. Using B-ultrasound to measure the diameter of the tracheal tube, which is more accurate and less traumatic, changed the finger-feeling method to estimate the pressure and adopted a pressure test instrument to set and monitor endotracheal tube cuff pressure. Standardize endotracheal tube model selection, endotracheal tube cuff management, and endotracheal tube extraction, and incorporate them into quality management to ensure behavioral change. We need to pay attention to the patients themselves and then implement the personalized nursing practice in the process of promoting clinical translation. The problem of "evidence-based intervention can be replaced" also suggests that personalized nursing interventions need to be implemented in the process of evidence transformation. Some evidence needs to be based on the patient's situation and cannot be directly applied. Therefore, in the implementation of evidence, we must implement personalized nursing practice.

4.2. Clinical Practice Based on the Best Evidence Improves Nurses' Practice Compliance and Cultivates Nurses' Evidence-Based Concept. This study shows that the implementation rate of the 16 review indicators before and after the

implementation of evidence has increased significantly. After the implementation of evidence, in addition to the 62.25% in the first review indicator and the 58.28% in the second review indicator, the achieved rate of the 3 indicators has reached 100%, the rest of the achieved rates are above 60%, and nurses' POST-evidence-based compliance has improved. The evidence-based nursing practice of preventing sore throat in patients with general anesthesia intubation allows nursing staff to solve problems based on scientific evidence when they encounter problems and deal with problems at work, rather than solving problems by experience. For the sustainability of practice, we have repeatedly strengthened the concept of nursing staff from the observation records of baseline survey, training, implementation of the program, and re-examination, and trained and guided the content with low scores in the questionnaire, so that nurses can master nursing knowledge and practical skills, and adopted diversified training such as flowcharts, mission knowledge maps, videos, and case discussions. Propaganda and education are the keys to achieving knowledge, belief, and action that helps clinical staff establish risk awareness, understand the impact of postoperative sore throat, and enhance their execution ability later. The results showed that there was a statistically significant difference in the knowledge, belief, and behavior of clinical medical staff before and after the implementation of evidence ($P < 0.05$). The knowledge, attitude, and behavior were significantly improved, which is very beneficial for improving the compliance of nurses' clinical practice and cultivating nurses' evidence-based concept.

4.3. Clinical Practice Based on the Best Evidence Can Improve the Self-Management Ability of Patients with General Anesthesia Intubation to Prevent Sore Throat and Reduce the Incidence of Clinical Sore Throat. The results showed that the incidence of pharyngolaryngeal pain in patients undergoing general anesthesia intubation decreased from 41.7% to 28.1% after the evidence-based practice, and the effects of pain on eating and rest were all lower than before, with a statistically significant difference ($P < 0.05$). However, there was no significant difference in the incidence of sore throat in the swallowing state before and after the implementation of evidence ($P > 0.05$). It shows that the implementation of an evidence-based nursing practice scheme can effectively reduce the incidence of sore throat in patients with general anesthesia intubation at rest. In this study, 20 best pieces of

Retraction

Retracted: Analysis of Factors Related to Adolescents' Physical Activity Behavior Based on Multichannel LSTM Model

Computational Intelligence and Neuroscience

Received 25 July 2023; Accepted 25 July 2023; Published 26 July 2023

Copyright © 2023 Computational Intelligence and Neuroscience. This is an open access article distributed under the Creative Commons Attribution License, which permits unrestricted use, distribution, and reproduction in any medium, provided the original work is properly cited.

This article has been retracted by Hindawi following an investigation undertaken by the publisher [1]. This investigation has uncovered evidence of one or more of the following indicators of systematic manipulation of the publication process:

- (1) Discrepancies in scope
- (2) Discrepancies in the description of the research reported
- (3) Discrepancies between the availability of data and the research described
- (4) Inappropriate citations
- (5) Incoherent, meaningless and/or irrelevant content included in the article
- (6) Peer-review manipulation

The presence of these indicators undermines our confidence in the integrity of the article's content and we cannot, therefore, vouch for its reliability. Please note that this notice is intended solely to alert readers that the content of this article is unreliable. We have not investigated whether authors were aware of or involved in the systematic manipulation of the publication process.

Wiley and Hindawi regrets that the usual quality checks did not identify these issues before publication and have since put additional measures in place to safeguard research integrity.

We wish to credit our own Research Integrity and Research Publishing teams and anonymous and named external researchers and research integrity experts for contributing to this investigation.

The corresponding author, as the representative of all authors, has been given the opportunity to register their agreement or disagreement to this retraction. We have kept a record of any response received.

References

- [1] G. Chang and J. Liu, "Analysis of Factors Related to Adolescents' Physical Activity Behavior Based on Multichannel LSTM Model," *Computational Intelligence and Neuroscience*, vol. 2022, Article ID 1022421, 8 pages, 2022.

Research Article

Analysis of Factors Related to Adolescents' Physical Activity Behavior Based on Multichannel LSTM Model

Guiling Chang¹ and Jinfeng Liu² 

¹Xian University of Finance and Economics, Xian, Shaanxi 710100, China

²The Department of Physical Education, Huainan Normal University, Anhui, Huainan 232001, China

Correspondence should be addressed to Jinfeng Liu; cgl@xaufe.edu.cn

Received 7 May 2022; Revised 7 June 2022; Accepted 10 June 2022; Published 4 July 2022

Academic Editor: Dong Chen

Copyright © 2022 Guiling Chang and Jinfeng Liu. This is an open access article distributed under the Creative Commons Attribution License, which permits unrestricted use, distribution, and reproduction in any medium, provided the original work is properly cited.

The health problems of teenagers are closely related to their sports behavior. In order to understand the relevant factors of teenagers' sports behavior, we use a variety of research methods to make a brief theoretical analysis of the relevant factors of teenagers' sports behavior and analyze the impact of the model on teenagers' sports behavior from different levels. The model analyzes the factors affecting youth sports behavior, reveals the relationship between these factors, puts forward corresponding intervention strategies, and uses effective means to develop youth sports practice. Therefore, based on the analysis of the relevant factors of teenagers' sports behavior, this paper puts forward the LSTM model from many aspects, which shows that our model can be very effective in analyzing the factors affecting teenagers' sports behavior.

1. Introduction

The obesity rate in China has doubled in the last 30 years, according to The Times, UK. The rate of obesity and overweight among adults in developing countries increased from 250 million in 1980 to 904 million in 2008, and China now has a quarter of the obese and overweight population [1]. This study analyzes the factors influencing the physical activity behavior of adolescent students to provide a theoretical reference for physical education programs aimed at improving adolescent exercise behavior and promoting adolescent health [2].

At this stage, there are various factors that influence adolescent physical activity behavior. Individual factors are the primary factors of adolescent physical exercise behavior, which are necessary for exercise behavior. Individual physiological factors determine individual exercise behavior, and psychological factors promote the development of individual motor behavior [3]. Individual physiological factors are one of the important factors influencing adolescent physical exercise behavior, and factors such as height, weight, physical health status, and body size of adolescents

are common research variables in studies. For example, [4] in a study on the formation factors of exercise habits among college students, it was pointed out that the motivation to lose weight and build physical beauty could promote the change of exercise behavior among college students, and individual athletic ability influenced by congenital genetic factors could also affect the exercise behavior of individuals. [5] The amount of physical activity of adolescents was studied in terms of gender, age, height, and weight, and the influence of physiological, psychological, sociocultural, and environmental factors on the physical activity of adolescents was studied. As far as psychological factors are concerned, there is a relationship between individual achievement and individual personality. The study of [6] has pointed out that those adolescents who are adventurous and challenging may prefer competitive sports programs, where exercise provides satisfaction and pleasure, and the act of physical activity provides individuals with the opportunity to demonstrate their level of athletic ability, strengthening their self-esteem and pride. The motivation that is motivational and persistent and determines the intensity of behavior is an essential factor in motivating individuals to participate in sports.

Family factors are both physical environmental factors that satisfy the conditions and environment of adolescents' exercise, and internal psychological factors that promote individual adolescents' internal motivation and increase the level of individual exercise motivation [7]. Parents' exercise awareness and exercise behavior, cultural level, and socioeconomic status are important. School physical education is the main form of physical activity behavior of young students, and it is the main channel of physical activity of young people [8]. A reasonable physical education program can stimulate students' motivation to exercise, induce behavior change, satisfy students' self-actualization and sense of accomplishment, and also explain the causes of behavior change and its internal mechanism of action [9]. However, a common phenomenon in primary and secondary schools in China is that the number of physical education classes per week, the number of recesses, and the participation in school sports all decrease with grade level, and school sports become the main place to train students who have neither the awareness nor the ability to exercise [10].

Physical education teachers are the implementers of physical education and the organizers of extracurricular physical activities, and the amount of physical activity in schools for young students is closely related to the physical education teachers. Issues such as the number of games and competitions organized in school, the physical culture of the school, and exercise peers are the main factors that limit students' exercise behavior [11]. The phenomenon of physical education classes being squeezed is an important factor that currently restricts the development of physical education in schools, and "exam-oriented education" has seriously skewed educational values, with many schools pursuing the promotion rate unilaterally and squeezing and diverting students' physical education classes and extracurricular physical activities at will.

Social support, community exercise environment, and safety issues in the community were the main social level factors that governed youth physical activity behavior. Parental support, sibling support, school teacher support among school factors, and peer friend support were the main components of social support. Adolescents' perceived social support is closely related to their physical activity behavior and has a direct or indirect effect on self-efficacy. Researchers have compared parent-child communication, parental support, and adolescent psychological risk factors in obese and normal weight adolescents and found that parent-child communication and parental support had a significant impact on normal weight adolescents, while parental support had a more significant impact on obese adolescents. The lack of sports facilities is the main objective factor affecting individual exercise behavior. Studies on community exercise behavior found that the lack of public sports facilities in the community is the main factor affecting the physical exercise behavior of urban adolescents. The convenience of sports facilities and field equipment around the home, the good or bad exercise environment, and the development of sports activities all have an impact on the form of adolescent physical exercise behavior, the choice of

sports, exercise attitude, exercise awareness, exercise behavior, effort, and persistence.

2. Related Work

The factors influencing adolescent children's physical activity behaviors were studied in terms of subjective beliefs of both parents, objective material conditions, and work-life environment [12]. The study showed that parents' physical activity behaviors play a major role in promoting the formation of adolescents' sports perceptions, and that parents' actual exercise behaviors and exercise perceptions can contribute to adolescent children's internal motivation to exercise [13]. The stronger the family members' beliefs about exercise, the better the family exercise climate, and the stronger the family members' motivation to exercise and the greater the likelihood of physical activity behaviors.

In terms of family socioeconomic status, [14] a study of the family cultural level was conducted to explore the effects of different cultural level levels of youth physical activity behavior, and the results showed that the effect of family cultural level on youth exercise perceptions reached significant levels. The higher the literacy level of parents, the greater the possibility of active intake of family education knowledge and the more scientific the attitude of educating their children. For the study of economic status, [15] concluded that parents' exercise commitment was positively associated with adolescents' exercise behavior, but the level of parental exercise commitment perceived by adolescents was low, and that adolescent children's exercise behavior would be better developed if the intensity of commitment was increased. Parental encouragement and support are particularly important for the physical activity behaviors of 13- to 16-year-olds, and physical activity behaviors need to be sustained based on parental material support.

Safety issues and the safety of school sports equipment are key factors that limit physical activity and have a direct impact on youth physical activity behaviors. Studies by foreign scholars on safety have focused on whether relevant sports equipment meets national safety standards, whether schools regularly inspect sports equipment, the safe sports environment created by the joint efforts of schools and society, and the convenience of access to drinking water and sports rest areas during individual adolescent physical activity behaviors. The study of [16] found that low levels of community safety were strongly associated with physical activity levels and that residents of communities with lower levels of safety had higher rates of obesity and larger BMI indices.

Factor 1 mainly focused on reflecting motivation, interest in physical activity, sense of achievement in sports, enjoyable experience of sports, positive expectation of sports outcome, positive self-evaluation, and attitude toward sports knowledge. Among them, the sense of achievement in sports and interest in sports were the most highly correlated with F1, indicating that they are the more important factors in explaining the physical activity behavior of adolescents [17]. The sense of achievement in sports can lead to psychological

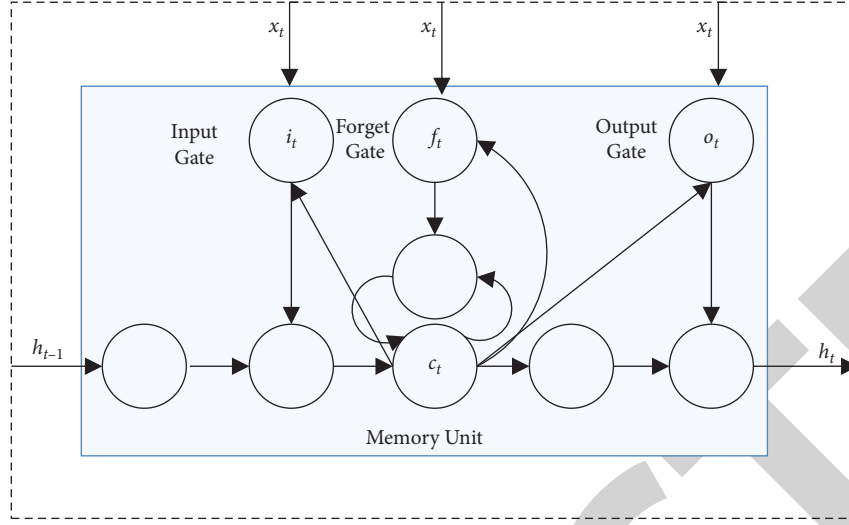


FIGURE 1: LSTM unit.

tendencies of pleasure and success from the heart, which all stem from the individual's active participation in sports. Sports behavior formed by sports interest can make individuals gain more knowledge about sports and health, improve motor skills, and promote healthy physical and mental development, as well as produce pleasant emotional experiences. In addition, the motivation of sports is also a factor that should not be neglected, as shown in a study by the authors of [18], motivation for physical activity is positively correlated with exercise adherence, and extrinsic motivation motivates people to participate in physical activity. Attitudes toward physical education knowledge had a slightly lower correlation with factor 1, suggesting less importance in comparison to other factors. The study of [1] showed that students' perceived value and role of physical activity showed a high correlation ($r = 0.87$) with adherence to physical activity in the long term, indicating that the perception of the value and role of physical education itself is an important factor influencing students' adherence to physical activity. This shows that there are some differences in the role played by the attitude factor of physical education knowledge in two different stages of physical activity behavior.

Factor 2 concentrates on the individual's physical quality, health status, and the degree of importance. Among them, an individual's health status and physical fitness have a high correlation, and it can be said that an individual's physical fitness and health status are necessary prerequisites for realizing a variety of psychological factors and are the physical basis of physical exercise behavior. Therefore, physical health factors and psychological factors complement each other, physical health factors are the basis of psychological factors, and psychological factors play a role in promoting physical health [19].

3. Methods

A single-channel LSTM-based method for analyzing factors related to youth physical activity behavior mainly includes

LSTMs use memory units to avoid gradient disappearance and gradient explosion during backpropagation, can learn long-term dependencies, and make full use of historical information. The LSTM was improved and extended, making it widely used in natural language processing, speech recognition, and other fields.

The LSTM unit is shown in Figure 1.

The updating process of the LSTM unit at time t is as follows:

$$\begin{aligned}
 i_t &= \sigma(W_i x_t + U_i h_{t-1} + V_i c_{t-1}), \\
 c_t &= \tanh(W_c x_t + U_c h_{t-1}), \\
 f_t &= \sigma(W_f x_t + U_f h_{t-1} + V_f c_{t-1}), \\
 c_t &= f_t \odot c_{t-1} + i_t \odot c_t, \\
 o_t &= \sigma(W_o x_t + U_o h_{t-1} + V_o c_t), \\
 h_t &= o_t \odot \tanh(c_t),
 \end{aligned} \tag{1}$$

where x_t is the input data of the memory unit, σ is the logistic sigmoid function, and the symbol \odot is the dot product operation between vectors. i_t, o_t, f_t, c_t are the values of the input gate, output gate, forgetting gate, and memory cell at time t , respectively, c_t are the values of the candidate memory states of the memory cell and h_t are the outputs of the LSTM cell at time t .

For the analysis of the factors associated with youth physical activity behavior, we obtain a balanced sample of the factors associated with each youth physical activity behavior and then used a single-channel LSTM as the classification method as shown in Figure 2. The input feature vectors are passed through the LSTM layer to obtain high-dimensional vectors, which can learn deeper features that can better describe the samples. The fully-connected layer is receiving all the outputs from the previous layer, weighting and summing these output vectors, and propagating the weighted outputs through the excitation function to the Dropout layer. In this experiment, the excitation function is shown in the following equation:

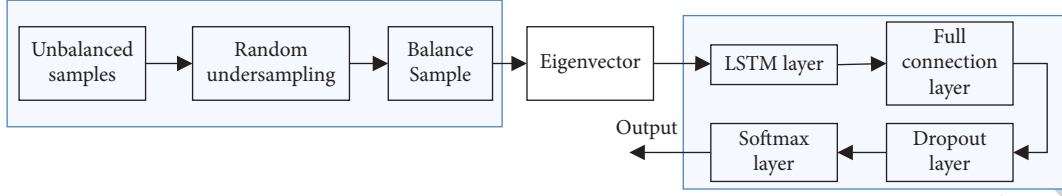


FIGURE 2: Single-channel LSTM classifier framework.

$$g(x) = \max(0, x), \quad (2)$$

where x is the output vector and the ReLU function sets all values less than 0 to 0, with the ability to bootstrap moderate sparsity. The Dropout layer is shown in following equation:

$$g = h^* \bullet D(p). \quad (3)$$

Finally, the output of the single-channel LSTM model is used to classify the samples by the Softmax output layer.

$$\text{label}_{\text{pred}} = \text{argmax}_i P(Y = i | \mathbf{x}, W, U, V), \quad (4)$$

where x is the upper layer output vector, i is the label prediction, W, U, V are the coefficient matrices in the LSTM update method, and $\text{label}_{\text{pred}}$ is the predicted label with the highest posterior probability.

The application of random undersampling and single-channel LSTM for the analysis of factors related to youth physical activity behavior has an obvious drawback: because undersampling only selects some samples from multiple classes and a large number of unselected samples. The method undersamples the imbalanced samples several times to obtain multiple sets of balanced samples, uses each set of balanced samples to learn an LSTM model, and uses the Merge layer to jointly learn multiple LSTMs.

The multichannel LSTM classifier framework is shown in Figure 3.

In the process of model training, we minimize,

$$J = - \sum_{i=1}^N \sum_{l=1}^m [\mathbf{1}\{t_i = l\} \log(y_l)] + \frac{\lambda}{2N} \sum_{k=1}^n \left(\sum_{\epsilon \in \omega} \|\mathbf{w}_{\epsilon}^k\|_F^2 + \sum_{\epsilon \in \mu} \|\mathbf{U}_{\epsilon}^k\|_F^2 + \sum_{\epsilon \in \gamma} \|\mathbf{V}_{\epsilon}^k\|_F^2 \right). \quad (5)$$

In the loss function, in addition to minimizing the negative log likelihood, the L2 regularization of W, U, V is added because the parameters of the Softmax function are redundant, i.e., the minima are not unique, and the addition of the regularization term can make the minima unique. The penalty factor λ regulates the weight of the regularization term, and the larger the value, the greater the penalty for large parameters.

4. Experiments

The analysis of the contents of the family's lifestyle, the way of interaction with the children, the interaction with the children, the parents' sports knowledge structure, sports habits and sports awareness and behavior, the level of

support from the relatives, and the family recreation side was carried out according to the different influencing factors. The reliability statistics under different influencing factors are in Table 1.

The factors with a high correlation with factor 1 include family sports atmosphere, family lifestyle, and tutoring style. It indicates that these factors exert an important influence in adolescent physical exercise behavior, and adolescent physical exercise behavior is often closely linked to the sports atmosphere of the family, and parents' sports ideology, attitude, awareness, and behavior habits towards sports all have a subtle influence on their children. The results in Table 2 show that exercisers and nonexercisers show significant differences in the dimensions of physical exercise attitudes.

Based on the above-given correlation analysis of each factor of exercise attitudes and the correlation analysis of exercise attitudes and physical behavior, the path relationships among the variables were further explored in conjunction with the theory relied on in this study. The path relationships among the variables were examined behavioral intentions on physical activity behaviors; and behavioral habits, behavioral attitudes, and sense of behavioral control on physical activity behaviors, while constructing path diagrams based on them.

Behavioral attitudes can have an impact on sport behavior only through the intermediate variable of behavioral perceptions, see Figure 4.

Specifically, the specific parameters we used are shown in Table 3.

Accuracy and geometric mean (G-mean) were used as a measure of classification effectiveness. The geometric mean is calculated as shown in the following equation:

$$G - \text{mean} = \sqrt[n]{\prod_{i=1}^n \text{Recall}_i}, \quad (6)$$

where Recall_i denotes the recall of category i , n is the number of categories, and n is taken as 7 in this experiment.

In the experiment, we implemented the following methods to deal with the analysis of factors related to youth physical activity behavior:

- (1) Full training + maximum entropy (FullT + Maxent), all the remaining samples of each class are used as training samples and the maximum entropy classifier is used.
- (2) Random oversampling + maximum entropy (Over-S + Maxent), let the maximum number of remaining

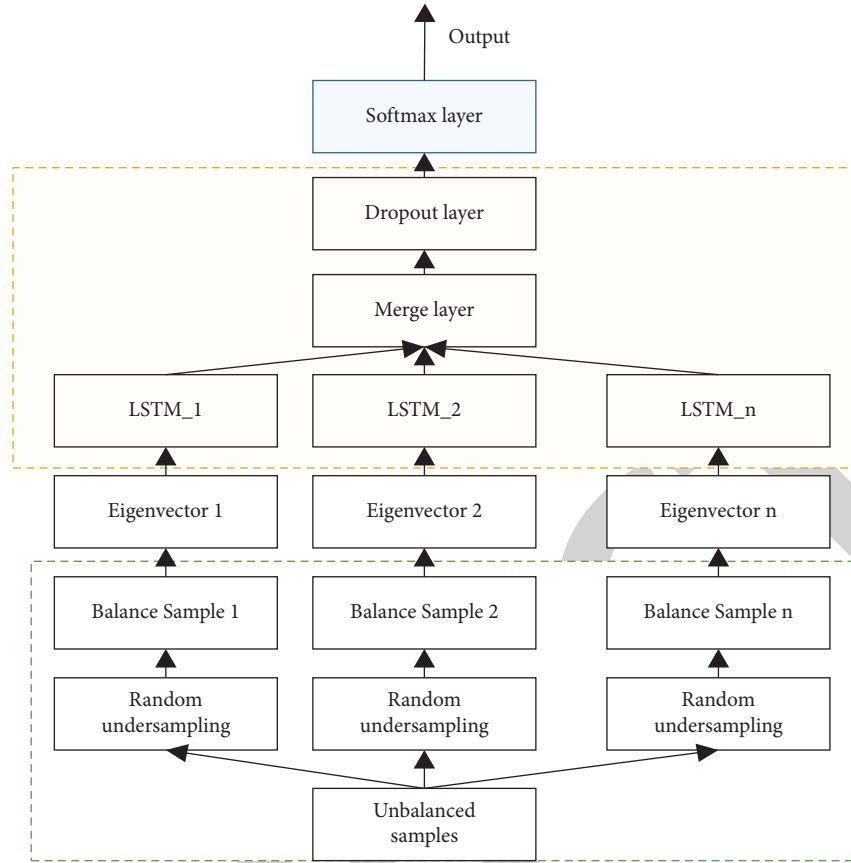


FIGURE 3: Multichannel LSTM classifier framework.

TABLE 1: Reliability statistics for each subscale of the influencing factors of youth physical activity behavior.

Scale level	Cronbach α coefficient	Standardized α coefficient	# Subscale question items
Individual level	0.878	0.879	12
Family level	0.915	0.916	11
School level	0.902	0.903	9
Community level	0.918	0.919	13
Policy level	0.939	0.939	10

TABLE 2: Summary of the scores of adolescents' attitudes toward physical exercise.

	Exercisers ($N = 100$)		Nonexercisers ($N = 251$)		T	P
	M	SD	M	SD		
Behavioral attitudes	31.0500	4.759	26.4548	4.915	7.968	0.0001
Target attitudes	48.6500	8.042	45.7812	6.051	3.678	0.0001
Behavioral cognition	29.0600	3.555	27.9525	3.309	0.878	0.004
Behavioral habits	37.1500	6.305	31.1995	6.405	7.885	0.0001
Behavioral intention	27.3200	3.502	24.1875	4.018	6.815	0.0001
Emotional experience	38.1800	5.855	34.2235	5.845	5.715	0.0001
Behavioral control	25.1500	4.935	20.9845	4.161	7.989	0.0001
Subjective standards	18.3800	4.295	20.7575	3.999	-4.865	0.0001

samples of each class (preference class) be n_{\max} and use the random oversampling technique to extract n_{\max} samples from the remaining samples of each class as training samples, using the maximum entropy classifier.

(3) Random undersampling + maximum entropy (UnderS + Maxent), let the number of remaining samples of the second smallest class (surprise class) be n_{\min} , and n_{\min} samples from the remaining

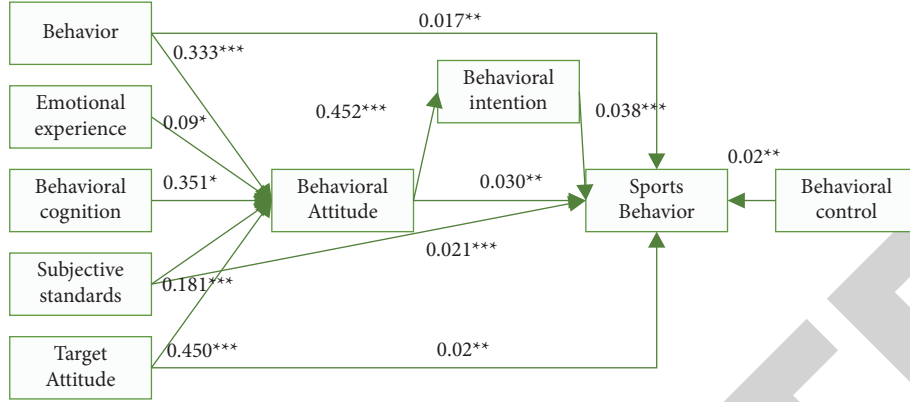


FIGURE 4: Path diagram of the influence of exercise attitude on physical behavior.

TABLE 3: Parameter settings in the LSTM.

Parameter expression	Parameter value
Input vector length	120
LSTM layer output dimension	128
Fully connected layer output dimension	64
Dropout parameter	0.5
#iterations	20

samples of each class are used as training samples using the random undersampling technique, and the maximum entropy classifier is used.

- (4) Random undersampling + single channel LSTM (UnderS + LSTM), using the sampling method in (3) to obtain the training samples, and the classifier uses a single channel LSTM.
- (5) Random undersampling + single-channel CNN (UnderS + CNN), using the sampling method in (3) to obtain the training samples, and the classifier uses a single-channel CNN.
- (6) Random undersampling + integrated learning (Ensemble-Maxent), multiple sets of training samples (5 sets for this experiment) are obtained using the sampling method in (3), and multiple base classifiers are built. Finally, integrated learning is performed by fusing the results of these base classifiers, where the base classifier is chosen as the maximum entropy classifier.
- (7) Random undersampling + multichannel LSTM (Multi-LSTM), using the sampling method in (5) to obtain multiple sets of training samples (5 sets in this experiment), and the classifier using a multichannel (5-channel) LSTM neural network [20–22].
- (8) Random undersampling + multichannel CNN (Multi-CNN), using the sampling method in (5) to obtain multiple sets of training samples (5 sets for this experiment), and a multichannel (5-channel) CNN for the classifier.

Figure 5 compares the classification effects of fully trained, randomly oversampled, and randomly under-sampled methods in the analysis of factors related to youth

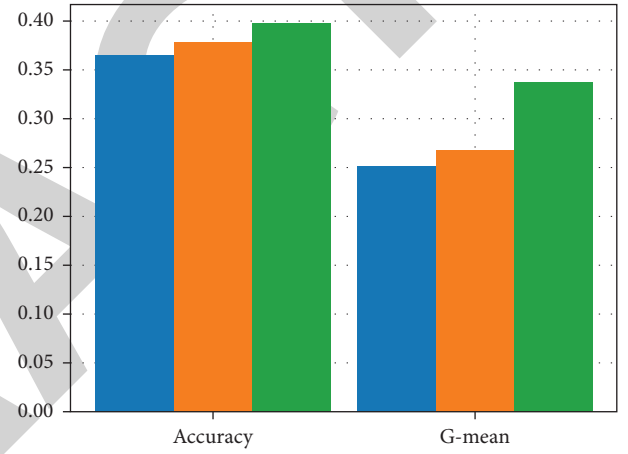


FIGURE 5: Comparison of classification performance of traditional methods for analyzing factors related to youth physical activity behavior.

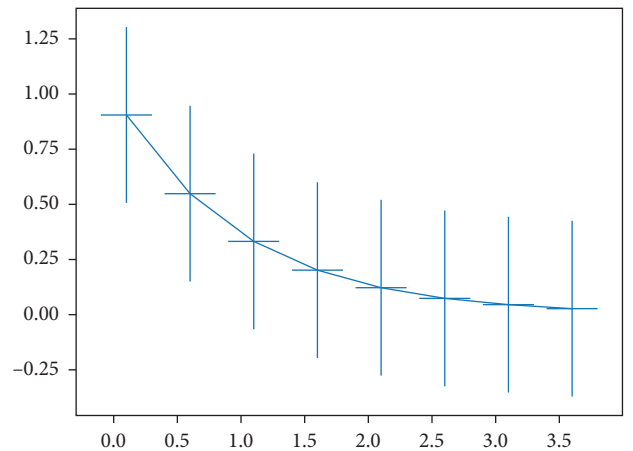


FIGURE 6: Error accumulation results.

physical activity behavior. We can see that the random nonpublic classification is obviously better than the first two methods, and its advantage is particularly obvious in the average value of g . The main reason for this phenomenon is that in the complete training and random sampling

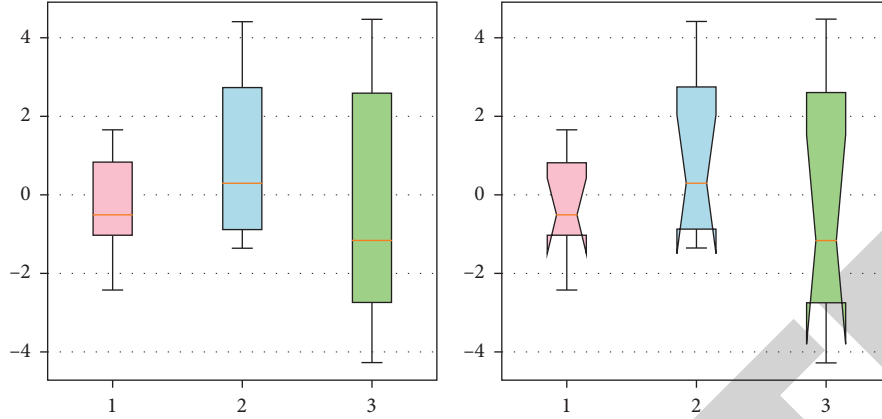


FIGURE 7: Comparison of classification performance of maximum entropy and neural networks.

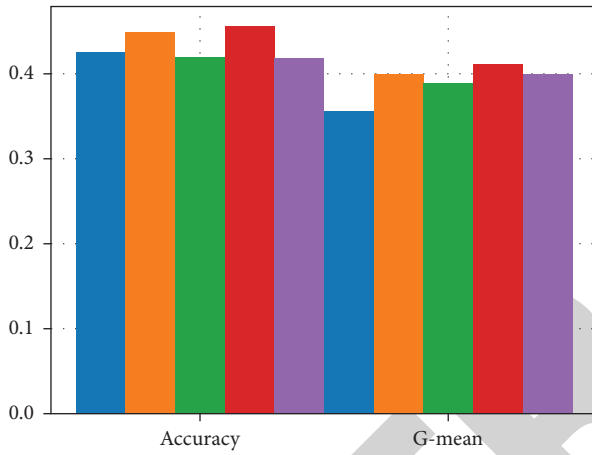


FIGURE 8: Comparison of classification performance between integrated learning and multichannel neural networks.

methods, the classification algorithm is very inclined to take more samples by category, resulting in the number of samples being less than the feedback category.

The error accumulation results of this method are shown in Figure 6.

Next, we compare the classification performance of the maximum entropy and LSTM under the random undersampling method. Figure 6 shows that the classification performance of single-channel LSTM is better than that of maximum entropy, with an improvement of 1.8% and 1.2% in accuracy and G-mean, respectively. We analyze that the main reason is that the LSTM can use the historical information and can learn the long-term dependence between samples. In addition, we also implemented a convolutional neural network (CNN)-based classification method. From Figure 7, we can see that the classification performance of LSTM and CNN are comparable, with LSTM having a slight advantage in accuracy and CNN having a slightly higher G-mean.

In the problem of analyzing factors related to youth physical activity behavior, the undersampling-based integrated learning approach performs better to use all labeled samples while maintaining a balance between training

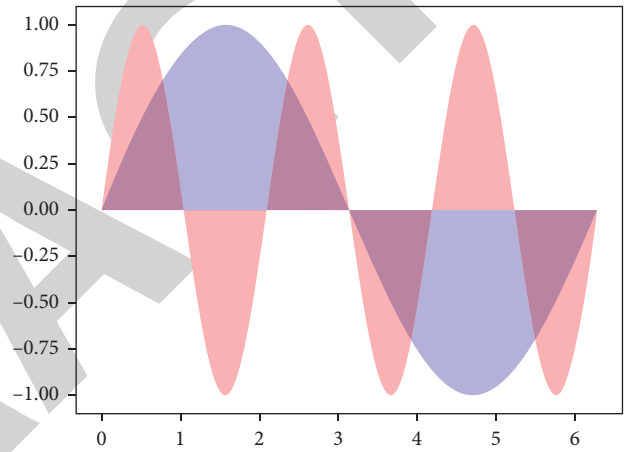


FIGURE 9: The importance of different factors.

samples. Next, we will compare the classification performance of the undersampling-based integrated learning approach with our proposed multichannel LSTM classification approach, as shown in Figure 8.

The results in Figure 8 show that the multichannel LSTM-based classification method improves 1.5% in accuracy and 2.8% in G-mean over the integrated learning method when the hidden layer features are fused using sum; the multichannel LSTM-based classification method improves 1.5% in accuracy and 2.8% in G-mean over the integrated learning method when the hidden layer features are fused using concatenate.

As in Figure 9, when the hidden features are fused using concatenate, the multichannel LSTM-based classification method improves by 1.0% in accuracy and 2.1% in G-mean over the integrated learning method. These results indicate that the multichannel LSTM-based classification method is very effective for analyzing factors related to youth physical activity behavior.

5. Conclusion

Factors affecting adolescents' physical activity behavior, namely, there are internal factors of individuals as well as family, school, and social factors closely related to

Research Article

The Application of Image Processing Technology in Camera Picture

Yun Hong 

Xi'an International University, Humanities and Arts College, Shaanxi, Xi'an 710077, China

Correspondence should be addressed to Yun Hong; 2016150291@jou.edu.cn

Received 25 April 2022; Revised 5 May 2022; Accepted 9 May 2022; Published 30 June 2022

Academic Editor: Dong Chen

Copyright © 2022 Yun Hong. This is an open access article distributed under the Creative Commons Attribution License, which permits unrestricted use, distribution, and reproduction in any medium, provided the original work is properly cited.

The application scene of camera pictures in our life is very huge, and the effect of information conveyed by images is more intense than words and language, so it is very important for us to make good use of pictures obtained by photography or even pictures obtained by other means. Aiming at the processing problem of camera pictures, we have adopted image scaling method, camera picture color change method, gray degree processing method, image color space change method, image brightness processing method, and other methods to solve the processing problems of camera pictures. After reasonable processing, the presentation effect of camera pictures will be greatly improved, and the utilization efficiency will be greatly improved.

1. Introduction

In this paper, based on the processing technology of camera pictures, all kinds of camera pictures or other image resources we get in our lives need us to process certain data. If we make good use of ways and means, the value of original film samples can become higher, which provides great convenience and help for our related research and life. We mainly digitize the attributes of photographic images and then use related algorithms to change the target values to achieve our goals and find the changing rules of other indicators of the images with changed attributes. One of the goals of this paper is an overview of the latest technologies for PDE-based image enhancement and smoothing methods. A unified description of the basic idea is that the generalization and application of relevant values and results can find historical remarks and the policy of opening up problems. Another goal is to propose an in-depth processing method and an interesting parabolic-like equation that can bridge the gap between the problem and the recovery method [1]. In this paper, one-dimensional interpolation function and two-bit separable extended application image data are derived. Cubic convolution interpolation has ideal characteristics and is very useful in image processing. This technique can be implemented stably and effectively in

digital computers and related problems in image processing [2]. The research based on morphology needs to design a computer-based image processing algorithm to reduce the background noise to enhance the image and propose a robust segmentation algorithm to extract geometric features, compactness, axial ratio, and so on. According to the results of image processing, classification and comparison can be carried out [3]. In this paper, a new low-level image processing technology is proposed, which mainly deals with edge and corner detection and keeps the noise reduction of the structure when processing the image. Nonlinear filtering is used to define the image part and pixel correlation. The new feature detector is based on the minimization of the local image area, and the measured area will be used as the smoothing field [4]. One of the aims of modern microscopes is to quantify two-dimensional, three-dimensional, and four-dimensional phenomena in biology, medicine, and medical materials. The design of the IMAGIC-5 software system explains the requirements of this data processing, and the image processing is special. The image will include a multivariate statistical analysis of collected data, and the resolution will be significantly improved by using a new angle reconstruction method to determine the three-dimensional structure of amorphous molecules [5]. Image processing must meet a series of formal requirements,

architectural requirements such as locality, progressiveness, and causality of space, stability requirements, and morphological requirements, which correspond to shape-preserving properties (rotation invariance and scale invariance). A complete classification of all images with various scale changes meeting these requirements is given [6]. This text provides depth and extensive coverage of all topics encountered in the field of image processing and machine vision and can be used as a readable reference for all groups of people. It is not just image processing and machine vision courses but also makes difficult concepts easy to understand and provides a large number of carefully selected problems and examples for learning and reference [7]. In a display system for the display of a graphical object generated by a machine screen, the graphs to be displayed require data of a standardized representation in a memory, a position between the graphs displayed in the machine, a horizontal width, an angle of rotation, a brightness of the graphs, and an inverse weight step value between the graphs [8]. Interconnectivity between digital cameras and other devices is one of the major problems for consumers and digital camera manufacturers. Interconnectivity allows for more user-friendly use, appropriate application layer software, and digital photos to be sent to target disk storage, printers, websites, e-mail messages, or prints [9]. In a display system for generating a graphic object on a camera screen, there is a need for data [10] that can convert a specification and perform a specification in a memory, an initial position at the start of each conversion between an identified camera picture and the object, a conversion width, a brightness in the image object, and a weight step value corresponding to the conversion width. With appropriate application layer software, digital photos can be sent directly from the camera to the desired target. The interconnection function of the digital camera allows consumers to use the function to take pictures more conveniently, using specially designed communication protocols and picture transfer protocols [9]. The digital camera inputs the captured image data from the key input unit to the e-mail address data, stores it in the flash memory so that the data are associated with each other, and then transmits the image data and the address data to the computer through the port and the infrared communication unit [11]. In a camera system of an image sensor apparatus for sensing and storing images, a professional processing apparatus processes uploaded sensed pictures. The supply device print head senses the image and prints on a print medium stored inside the camera system [12]. An electronic device can send viewpoint information to a server, and a search of an image database in the server can find pictures taken from relevant viewpoints and can provide a user with an option to save or pair multiple images instead of images captured by the electronic device [13]. A panoramic moving image camera for continuously exposing a film in a photographic picture includes a fixed housing portion and a rotating housing portion and comprises a lens device, a main film sprocket, a feed sprocket, a bow reel coaxially arranged in a spaced planar area, and a motor device for providing the main film sprocket in a fixed housing portion [14].

2. Image Processing-Related Operations

2.1. Image Size Processing. It is not very difficult to get pictures, and the pictures we get are processed in the planning so that we can better achieve the desired effect. If the size is inappropriate, we should change the size of the image. Particularly, the photos taken by high-position digital cameras are often too large to be reasonably inserted into media courseware. If we do not insert it according to the requirements, it will make the courseware resources occupy more space. At this time, we need to compress the pictures and process them in many ways. We can use algorithms to modify the attributes of the pictures and process the color attributes, brightness, and grayscale in the right positions. If you need to crop the image, you can also use Photoshop tools to crop the image size. Of course, if the size of the processing can be used in a variety of ways, using software facilities and hardware facilities, plus appropriate algorithms to deal with the size of the picture, can achieve higher requirements.

2.2. Image Watermarking. In many scenes, when we use certain pictures as materials or need to show them in public, most of the images with watermarks obtained in the network will bring us some troubles. With the continuous development of computer networks and the continuous enrichment of knowledge and information resources, the difficulty of obtaining resources is declining, and watermarking processing is also an urgent need. We can still use Photoshop technology for processing, and the repair brush tool can color the redundant marks on the image, so that the marks are close to the main colors of the picture, so that the marks can be integrated into the image. But sometimes when we need to add our own watermark to the picture, we can also operate the picture, select the text tool in Photoshop to fill in the watermark text we want, and set the attributes such as transparency to add the watermark to the picture perfectly.

2.3. Photographic Image Processing. We need to solve the problem of white spots in the postprocessing camera pictures. The grayscale table has a range, and the brightest point is the endpoint of the range that can be debugged. The maximum hue value is 255. The maximum grayscale is set to pure white without other details. The color temperature of the light source needs to be considered when defining white. Whether in shooting or postprocessing, it is to restore the true color of the image. The visual elements of photographic pictures include composition, color, and form. Visual language uses corresponding patterns to draw people's emotions, and concrete or abstract elements are used as media to show the author's inner feelings.

(1) The purpose of photographic pictures of life comes from recording life. Photographers have different purposes for different feelings, which can be to restore the truest shooting moment or to make the photographs more aesthetic in a specific direction and have different tastes. (2) Photographic pictures used in commercial nature need more professional technical processing, from the aspects of tone, sharpness, saturation, how to cut, secondary composition,

black-and-white processing, color temperature, exposure, and so on, so as to achieve the eye-catching effect with the best quality; thus, better publicity can be carried out.

3. Overview of Image Processing Algorithms

3.1. Image Color Space Transformation Method. In order to change the image, we can choose to change the basic hue of the image to achieve the effect of independent components of the color space of the picture. The effect of Lab color space is better than that of RGB, which cannot describe the visual effect of color quantitatively, so it is necessary to transform them into space. By analyzing the color of natural images, the statistical distribution results are transformed into uniform color space Lab in statistical sense. The orthogonal linear change is used to transform the red, green, and blue signals that can be felt by the human visual system into three irrelevant color variables. Matrix calculus is given here to realize the spatial transformation from RGB space to Lab, and the spatial transformation relationship of color is as follows:

$$\begin{bmatrix} x \\ y \\ z \end{bmatrix} = \begin{bmatrix} 0.412245 & 0.357580 & 0.180423 \\ 0.212671 & 0.715160 & 0.072169 \\ 0.019334 & 0.119193 & 0.950227 \end{bmatrix} \begin{bmatrix} R \\ G \\ B \end{bmatrix}. \quad (1)$$

The values of each component in the XYZ space are changed to the corresponding Lab component values according to the function $f(x)$ as follows:

$$\begin{cases} L^* = 116f\left(\frac{Y}{Y_n}\right) - 16, \\ a^* = 500\left[f\left(\frac{X}{X_n}\right) - f\left(\frac{Y}{Y_n}\right)\right], \\ b^* = 200\left[f\left(\frac{Y}{Y_n}\right) - f\left(\frac{Z}{Z_n}\right)\right]. \end{cases} \quad (2)$$

The above $F(x)$ specific function is described as follows:

$$f(t) = \begin{cases} t^{1/3} & \text{if } t > \left(\frac{6}{29}\right)^3 \\ \frac{1}{3}\left(\frac{29}{6}\right)^2 t + \frac{4}{29} & \text{otherwise} \end{cases}. \quad (3)$$

L^* , a^* , and b^* are the last color space values, XYZ is the conversion value of RGB after XYZ, and the conversion from Lab to RGB color space also needs XYZ as the basis and then changes the color space. The component of Lab needs to change according to the function and then become the component of XYZ as follows:

$$\begin{cases} X = X_n f^{-1}\left(\frac{1}{116}(L^* + 16) + \frac{1}{500}a^*\right), \\ Y = Y_n f^{-1}\left(\frac{1}{116}(L^* + 16)\right), \\ Z = Z_n f^{-1}\left(\frac{1}{116}\left((L^* + 16) - \frac{1}{200}b^*\right)\right). \end{cases} \quad (4)$$

After the above formula, the $f^{-1}(x)$ function is as follows:

$$f^{-1}(t) = \begin{cases} t^3, & \text{if } t > \frac{6}{29} \\ 3\left(\frac{6}{29}\right)^2\left(t - \frac{4}{29}\right), & \text{otherwise} \end{cases}. \quad (5)$$

Each component of XYZ is converted to an RGB component as shown in the following formula:

$$\begin{bmatrix} R \\ G \\ B \end{bmatrix} = \begin{bmatrix} 3.240479 & -1.537150 & -0.498353 \\ -0.969256 & 1.875992 & 0.041556 \\ 0.055648 & -0.204023 & 1.057311 \end{bmatrix} \begin{bmatrix} X \\ Y \\ Z \end{bmatrix}. \quad (6)$$

3.2. Image Relational Mapping Processing. After having the color table of the template and the color table of the target picture, we need to consider which colors and how to use the matching relationship to allocate the color table. For the purpose of reconstructing the image color selected in the template image guide, the matching color table must also consist of the color of the target image as much as possible. The relationship of color composition is divided into visual contrast between colors, proportion of color distribution, coordination of color matching, and so on. According to the relationship between the three-dimensional color of the object scene image, we can define the part which is suitable for the large range of color transformation according to the color correlation between the object scene image and the background image and adjust the attribute between the object color correlation image and the object color table from different angles. Visual difference relationship between $M = \{C_1, C_2, \dots, C_n\}$ colors in the target color table, relationship between color tables M and C , and relationship between different color points are described as follows:

$$\{\text{mean}(M) \rightarrow c_i; i, j \in n \& i \neq j. C_i \rightarrow C_j\}. \quad (7)$$

According to the purpose of color transition, by matching the visual difference relationship between the color table and the target color table, the visual difference relationship between the target colors is maintained. In the separation of foreground and background, the ratio of the total number of pixels of a certain color to the total number of pixels of the foreground is adopted to maximize the proportion of the color of the matching template image in the target image. A matching color table is generated according to the brightness rules in the target color table. When creating a new set of color tables, you need to adjust the proportion of the color tables matched with the selected color table according to the brightness distribution of the color table and adjust and calculate the proportion between the matched color table and the selected color table according to the brightness distribution of the color table. The figure is defined as follows for E_p :

$$E_p = \sum_i^n \{T_i | M_i\}. \quad (8)$$

T_i, M_i represents a certain element, where n represents the number of elements. Visual difference is the main factor affecting the generation of matching color table. If you need to maintain the visual differences of the color table, you need to maximize the similarity of the contrast matrix. Make sure that the visual difference between the two color tables is much larger than the previous data. The comparison matrices of the two color tables need to be standardized after interpolation and comparison:

$$C^* = \frac{c - u}{\delta}. \quad (9)$$

C^* is our standard value after processing, C is the value before processing, u is the mean of all samples, δ is the standard deviation in all data, and the root mean square error of normalized values of all data is used to measure the visual similarity between two color tables:

$$E_c = \sqrt{\frac{\sum_{i=1}^n |C^*|^2}{n}}. \quad (10)$$

If we consider the contrast of the color table from another aspect, we cannot grasp the overall effect of the color table as a whole. We need to pay attention to the visual difference between the color points in the table and the overall average value. The total contrast of the color table is

$$E_{ca} = E_{c1} + E_{c2}. \quad (11)$$

In this formula, E_{c1} is the contrast difference representing the average value M in the color table, E_{c2} is the contrast difference between the color points in the color table M , and quantizing the color table matching effect into the energy value E can be recorded as

$$E = E_p + E_{ca}. \quad (12)$$

3.3. Adaptive Processing of Picture Brightness. The background color attribute of the scene image is simplified, and the overall brightness is changed to adapt to the desired effect. In particular, a color template provided to a landscape image within a camera screen cannot easily find a color suitable for the background image of the scene. The color processing of the background part is divided into two types: one is to specify the corresponding color interactively, and the other is to adjust the color adaptively. Our brightness processing must keep the relationship between the parts of the object image and the brightness adjustment function:

$$\frac{It_l - c_{tl}}{pt_l - It_l} = \frac{Im_l - Cm_l}{Pm_l - Im_l}. \quad (13)$$

After scene image segmentation, the subimages are processed with heavy color. Image segmentation has certain particularity, which cannot achieve complete and accurate segmentation. In the combination process of each image, color jump is easy to occur. Partial overlap and partial information loss will occur in the part near the edge. In addition, there will be blank points of information loss in the edge points of the reconstructed map, and the migration of combined colors between segmented submaps is not smooth. To solve the manhole problem, the first problem to be solved is to distinguish the manhole types. The edge position of the reconstructed image is misaligned and missing to a certain extent, and the edge position of the subimage is determined by the edge pixels of the target image. The edge detection algorithm is used to realize the edge detection of the object image. The probability of judging a pixel as a boundary point is described as the edge intensity of the pixel, that is, the brightness value of the edge detection image. Longitudinal arrangement and transverse arrangement are cavity point arrangement. It can be determined that a cavity point may be an edge point by calculating an edge intensity between a plurality of pixels in the arrangement gradient direction of the cavity point as follows:

$$\text{Longitudinal} \begin{cases} \max(\phi(w1), \phi(h2), \phi(w2)) == \phi(h2), h2\text{Isanedgepoint}, \\ \max(\phi(l1), \phi(h2), \phi(w2)) \neq \phi(h2), h2\text{Non-edgepoint}. \end{cases} \quad (14)$$

When we may face the problem of color jump, we need to consider the problem of partial overlap and information loss near the edge SSO, which is the edge point, retrieve the blank points lost in the edge points of the reconstruction

image, and determine the edge position of the subimage and the edge pixel of the target image SSO, so that the migration between the combined colors of the segmented subimages can be smoother.

$$\text{Lateral} \begin{cases} \max(\phi(l1), \phi(h2), \phi(l2)) == \phi(h2), h2\text{Isanedgepoint}, \\ \max(\phi(l1), \phi(h2), \phi(l2)) \neq \phi(h2), h2\text{Non-edgepoint}. \end{cases} \quad (15)$$

3.4. Image Processing Experiment. Color conversion has important application value. The color region is selected according to the interaction between the input target image and the template image, and the color of the input target

image is added by using the color average value. Image color transfer effects corresponding to different regions of the target image are interactively selected for the input template image, details of which are as follows:

$$l = \left\{ \begin{array}{l} T1 \longrightarrow R1 \\ T2 \longrightarrow R2 \\ T3 \longrightarrow R3 \end{array} \right\}, (T1, T2, T3) \in T. \quad (16)$$

According to formula (16), we can find the selected color area for interaction between the target image T and the template image R and add the color of the input target image R to the image T by using the color average value. If formula (16) is missing, the interaction mode is unknown, and the transmission effect of the corresponding image cannot be observed.

3.5. Power Consumption for Pixel Processing. In order to optimize the actual power consumption of the shooting equipment on the screen, it is necessary to establish a power consumption evaluation model of the shooting screen and then evaluate the power consumption of the shooting image in the later stage. The OLED screen displays colors through three independent light sources, and the function of calculating the power consumption per pixel of the screen can be described as follows:

$$E_{\text{scrrtn}}(r, g, b) = (f(R_i) + f(G_i) + f(B_i)). \quad (17)$$

The left side of the equation is the power consumption of each pixel of the picture when emitting light, and the right side is the power consumption of red, green, and blue color components and the power consumption of the whole image processing:

$$E_{\text{scrrtn}} = C + \sum_{i=1}^n (f(R_i) + f(G_i) + f(B_i)). \quad (18)$$

Here, C is a constant; that is, according to the obtained data, the power consumption when displaying a black image on the screen is calculated, and a fitting curve is generated. The universal function fitting degree of color component of function fitting curve is as follows: red = 0.996, green = 0.969, and blue = 0.985. The starting point of image capture is the power consumption required when displaying black images on the screen, which is collectively referred to as the power consumption of image processing devices. The power consumption required by image processing equipment is constant, and the test value at this time is $C = 0.5856$ W. The overall trend of function adaptation image is that the power consumption curve increases with the increase of CL, basically at the same starting point, reflecting the power consumption value of camera equipment. The performance relationship is as follows:

$$\left\{ \begin{array}{l} E_{\text{blue}} \gg E_{\text{green}} \sim E_{\text{red}}, CL \leq 17, \\ E_{\text{blue}} \gg E_{\text{green}} > E_{\text{red}}, CL > 17. \end{array} \right. \quad (19)$$

The power consumption of blue is the largest among the three types. The power consumption curves of the front green and red treatments are relatively close, and the back part of green is obviously greater than red.

3.6. Color Reconstruction of Image. Through the corresponding reconstruction algorithm, the input image I is

repainted and then output, so that the processed image meets a better image visual effect. The color channel separates $I = \{I_r, I_g, I_b\}$ and converts $I = \{I_r, I_g, I_b\}$ into the HSL color space. According to each subgraph of the color table, each subgraph is converted into a component gallery C , and the RGB component corresponds to each gallery:

$$\left\{ \begin{array}{l} IrC \\ Ig \\ Ib \end{array} \right\} \longrightarrow \left\{ \begin{array}{l} Irc1, Irc2, \dots Ircn, \\ Igc1, Igc2, \dots Igcn, \\ Ibc1, Ibc2, \dots Ibcn. \end{array} \right. \quad (20)$$

The goal of color reconstruction is to select the corresponding RGB component mapping from C and to ensure that I , J , and K are not equal while minimizing the power consumption of the combined image.

3.7. Image Color Table Generation Method. The color table C is made by image clustering. This method is a common method because of the large amount of computation, the results obtained by the clustering method are simple and not inclusive, and the visual distance between colors cannot be guaranteed. Therefore, it is of great significance to find a variety of color table synthesis methods that can not only reduce the amount of calculation but also ensure the visual distance between colors. CIELab is abstracted as a three-dimensional sphere, and the radius of the sphere is set to $r = 100$ (corresponding to the color space). The possible ranges of a and b vary depending on the value of L , and the origin of the coordinate system coincides with the center of the sphere. Since the range of Z coordinates ($-50, 50$) and L ($0, 100$) of the sphere is different, the input value of L must be converted and input L to calculate the xL value:

$$\left\{ \begin{array}{l} \frac{xL}{100} = \frac{L-50}{50}, L > 50, \\ \frac{100-xL}{100} = \frac{L}{50}, L \leq 50. \end{array} \right. \quad (21)$$

It takes a lot of computation to get the set of color combinations by image clustering. The clustering method is not inclusive, and the visual distance between colors is not guaranteed. The significance of formula (21) lies in reducing the calculation amount and ensuring the visual distance between colors. CIELab is abstracted into a sphere, and the range of related attributes is set. After that, it is very convenient to operate according to the formula.

When the value of L is determined, the cross-sectional range of the corresponding color space is determined, and the radius of the cross-sectional circle is calculated:

$$r = \sqrt{R^2 - (xL)^2}. \quad (22)$$

Map the points on the coordinate system to CIELAB by selecting the difference between the points on the coordinate system and the CIELAB value range, as follows:

$$\left\{ \begin{array}{l} \left\{ \begin{array}{l} \frac{x}{100} = \frac{a}{127}, x \leq 0; \\ \frac{x}{100} = \frac{a}{128}, x > 0; \end{array} \right. \left\{ \begin{array}{l} \frac{y}{100} = \frac{b}{127}, y \leq 0; \\ \frac{y}{100} = \frac{b}{128}, y > 0; \end{array} \right. \end{array} \right. (x \longrightarrow a)(y \longrightarrow b). \quad (23)$$

It is judged that the newly generated color point P satisfies the relationship of the color point set D :

$$\left\{ \begin{array}{l} d(i)(L_i, a_i, b_i) \in D; \\ Ed_i = \sqrt{(L - L_i)^2 + (a - a_i)^2 + (b - b_i)^2}, \\ Ed_i \geq E0. \end{array} \right. \quad (24)$$

3.8. Color Table Combination Algorithm. The combination algorithm solves the problem of selecting the best combination of subimages from component library R and converts each component of the target image according to the color table hue to generate the corresponding color component library. Each color channel has a sublibrary of corresponding components, and the number of images in the sublibrary is the number of colors in the reference color table. The power consumption of each subgraph is calculated by using the power consumption evaluation model, and the power consumption matrix of each subgraph is established:

$$E_{\text{matrix}} = \begin{bmatrix} E_{r1} & E_{r2} & \dots & E_{rn} \\ E_{g1} & E_{g2} & \dots & E_{gn} \\ E_{b1} & E_{b2} & \dots & E_{bn} \end{bmatrix}. \quad (25)$$

E_{matrix} elements in the same column have the same hue, while elements in the same row correspond to the color table one by one, and the RGB component area of the target image is represented by different lines. Select three factors from E_{matrix} to keep the combined power consumption optimal. The selected element must satisfy the restriction, and the relationship is as follows:

$$\left\{ \begin{array}{l} E_{ri}, E_{gi}, E_{bk}, \\ \min(E_{ri} + E_{gi} + E_{bk}), \\ i \neq j \neq k. \end{array} \right. \quad (26)$$

4. Processing Methods of Photographic Pictures

4.1. Image Scaling Method. We have a certain operation and arrangement for picture processing. We can separate the processing of pictures independently and implement single operation after dividing them into several types of modules. Image data scaling and tone modification need the help of algorithms; in the case of interpolation points will not change, we need to change the interpolation according to different and relatively appropriate algorithms, using filters to achieve different image data processing under different algorithms. Compared with multiple data changes, the asynchronous FIFO of data buffer and LineBuffer of line buffer are of

appropriate size, which can realize data migration and change of scaling ratio. The timing control module is used instead of the traditional MCU module, which saves some resources. In the system, the image data is input and then detected (including high-precision capture of the image data, the configuration parameters are stored in the storage area), and the control block Ctrl, the multilevel scaling kernel (asynchronous FIFO, horizontal and vertical scaling, and line memory), the timing module, and the processing contents after data modification are shown in Figure 1.

According to different and relatively appropriate algorithms, the interpolation is changed, and the filter is used to realize the processing of picture data. Because the data needs to be changed many times, the data buffer asynchronous FIFO and the line buffer LineBuffer can realize the data migration and the change of scaling ratio, and the timing control module can replace the traditional MCU module, which can improve the efficiency.

Image scaling kernel processing: according to the above horizontal structure of the secondary image processing scaling kernel architecture, you can give the specific operation division of the core scaling module, as shown in Figure 2.

We input the detected image signal to identify its color coding format and the polarity of horizontal and vertical synchronization signals, send the calculated information to the receiving module, and control the scaling image processing according to different input information. At the same time, in order to save hardware resources while processing data in real time, the calculated data should be stored in ROM in advance, and the filter coefficients corresponding to configuration information should be found out in the table for interpolation processing. We input the detected image signal to identify its color coding format and the polarity of horizontal and vertical synchronization signals. The filter coefficients of the corresponding configuration information are found out in the table and provided for interpolation processing. The output images with different scaling ratios will be divided into many pixel blocks, which leads to the prominent mosaic phenomenon. The image quality is not very good; especially, the smaller the PSNR, the worse the imaging quality.

The output image with different scaling ratio will be divided into small pixel blocks, the mosaic phenomenon is prominent, the picture quality is not very good, and there will be pixel blocks when the scaling ratio is 0.5. Bicubic different scaling ratio display effect is good and according to the four-point two-segment interpolation effect will be better, using built-in functions to get objective scores of several algorithms, and in the case of magnification scaling ratio greater than 1, the larger the value of scaling ratio, the smaller the PSNR, the worse the imaging quality, and the smaller the scaling ratio less than 1 under reduced imaging. Scale ratio can be infinitely large in theory; most of the algorithms in the case of large scale ratio of the image imaging display effect is average.

The display effect of bicubic in different scaling ratios is OK. The nearest algorithm produces a block of pixels at a scale of 0.5, and therefore, compared with bicubic, the effect

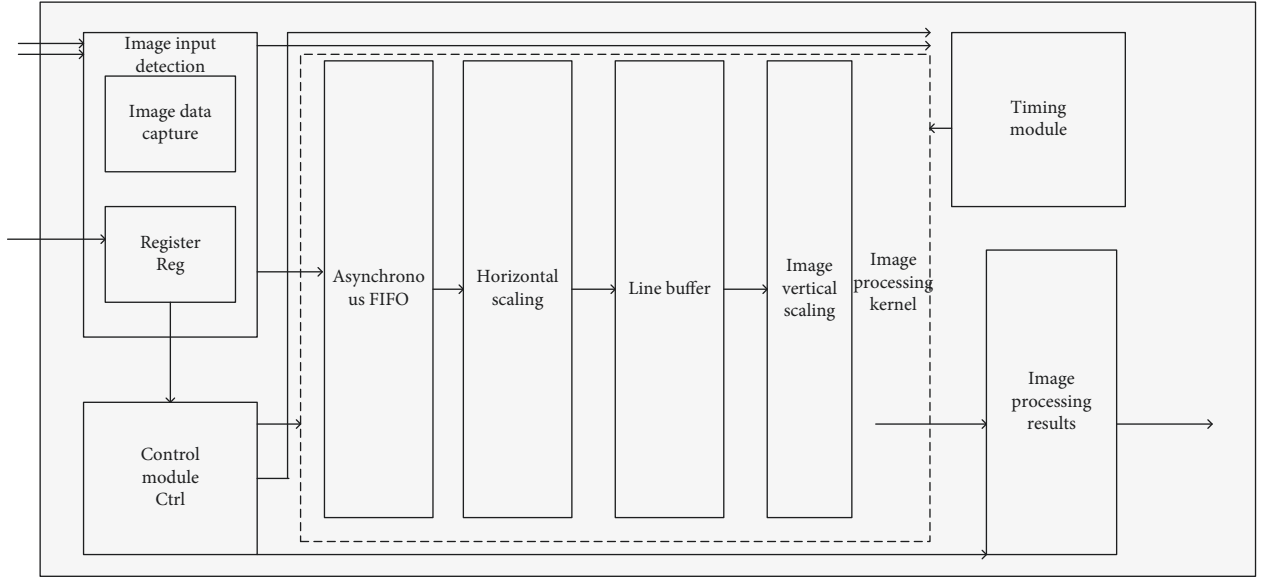


FIGURE 1: Image data and hue operation flow.

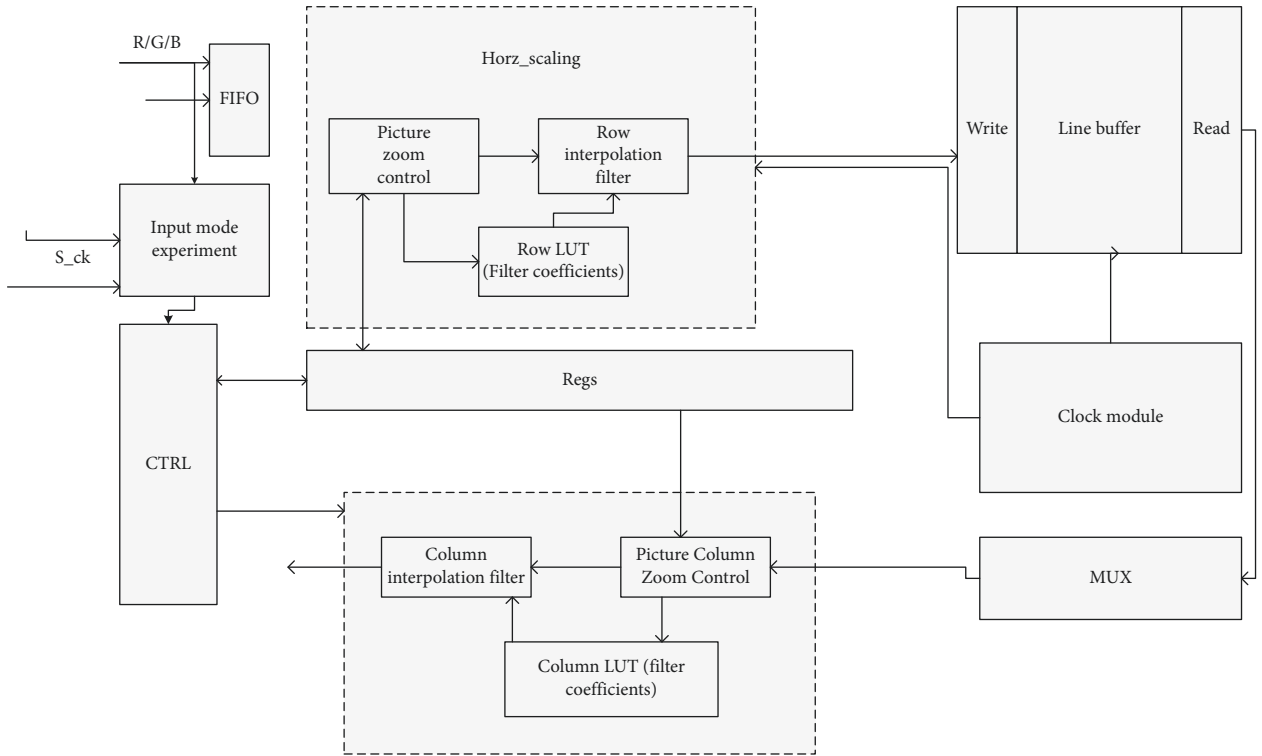


FIGURE 2: Scaling core processing flow.

will be a little worse. The larger the scaling ratio obtained by using the four algorithms with built-in functions, the smaller the PSNR and the worse the imaging quality. In theory, it can be infinitely enlarged. In fact, the imaging display effect of superlarge scaling ratio images is also general.

For example, Tables 1 and 2 are used to count the average scaling time required for image processing of different algorithms used in our experiments. According to the above data, we can see that the processing speed of bicubic

interpolation is slower than that of the nearest algorithm, and it is the slowest. The processing speed of the bilinear algorithm is close to that of piecewise quadratic processing, and the speed of both is far higher than that of bicubic interpolation. According to the above discussion, the scaling effect of the piecewise quadratic interpolation algorithm is worse than that of the bicubic interpolation algorithm, and its advantages are obvious. It has good low-pass characteristics and will not be easily distorted. All the above

TABLE 1: PSNR index of each algorithm of bikes in standard diagram.

Scale ratio	P SNR-bikes/unit: dB				
	2	4	8	0.3	0.5
Nearest	31.2873	27.9418	23.9202	22.3221	20.7878
Bilinear	35.7905	30.8422	30.8422	25.0325	23.2467
Bicubic	37.6688	31.7796	31.7886	26.1759	23.5067
Piecewise quadratic	36.4299	31.2586	31.2696	25.8461	23.4166

TABLE 2: PSNR index of each algorithm of caps in standard diagram.

Scale ratio	P SNR-bikes/unit: dB				
	2	4	8	0.3	0.5
Nearest	25.8943	22.6036	20.2453	20.0272	19.0793
Bilinear	28.6147	24.9835	23.0147	22.9415	22.0353
Bicubic	31.3147	26.6023	24.0458	24.0612	23.8647
Piecewise quadratic	29.9941	25.5041	23.9498	23.8701	23.6724

algorithms need to be implemented according to hardware, and the scaling speed of picture processing is better than the typical picture processing scaling algorithm, so we need to compare and select the core picture processing scaling algorithm suitable for the scene (Table 3).

Under various image processing scaling algorithm schemes, all four algorithms have their own degrees of freedom a. When calculating filter coefficients, only a and interpolation decimal offset are considered, and parameter a is adjusted to change the spectrum characteristics of the filter to suppress aliasing. After the algorithms are distinguished, the scaling processing effect of pictures will be different, and the processing speed and resource consumption will be different, as shown in Figure 3.

After selecting different parameter a, the rendering effect of the image will be different. We will pay attention to the consumption of hardware while operating, and we need to concentrate on the performance of hardware facilities to process the image centrally. In order to process the image better and get a better visual effect, we need to know the passband characteristics. The comparison of passband characteristics is shown in Figure 4.

4.2. Color Change Method of Photographic Image. Image color reconstruction algorithm is mainly used in image color conversion, and color reconstruction can make us change pictures more freely. Image reconstruction is quite different from ordinary attribute single change. Direct reconstruction is to change our key parts, and the degree is controlled by ourselves. A single image resource is not conducive to the efficiency evaluation of image color processing, and the algorithm will have shortcomings. We need to select multiple scene images and other template images to process the color and evaluate the efficiency of the algorithm. The input image is subjected to a color migration algorithm for about 10 times for an available template image, and finally, a large

TABLE 3: Statistics of average image processing time of each algorithm.

	Nearest	Bilinear	Bicubic	Piecewise quadratic
Processing reduction time/s	1.31	5.71	14.32	6.14
Processing amplification time/s	1.11	1.18	1.29	1.09

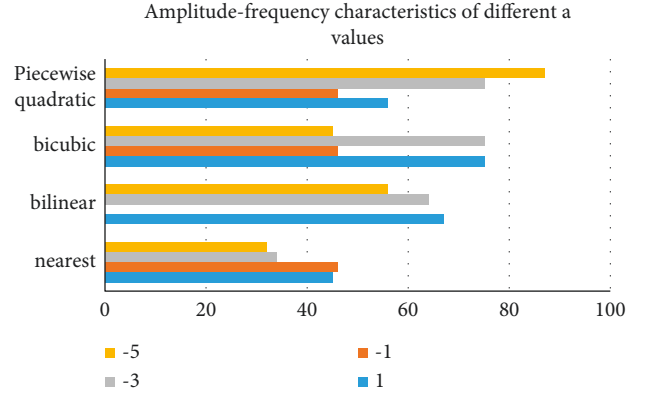


FIGURE 3: Amplitude-frequency characteristics of different parameter a under four algorithms in image processing.

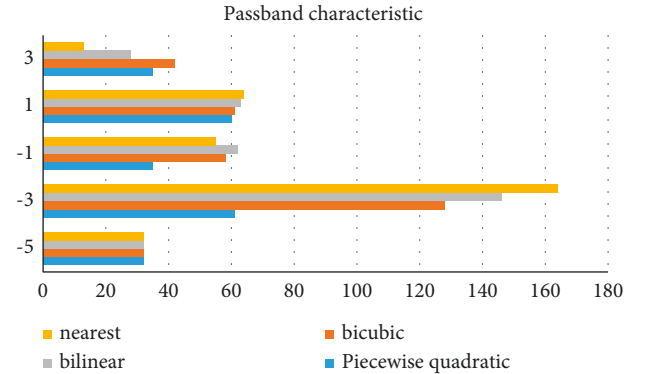


FIGURE 4: Passband characteristics under different parameter a.

amount of data is analyzed. The color reconstruction operation of the camera image is in Figure 5.

In the experiment, SSO is the image data we use as the template, SSO is our target image data, and using the algorithm can achieve the ideal migration probability of about 71%. Template image color transfer processing effect is not good, the same template image for different target image data has some differences, specifically, and the compatibility of image color has a great relationship, as shown in Figure 6.

The image is composed of pixels, and the color is expressed according to the actual situation of RGB components. Images of various RGB components can be used as the basis for testing. Because (0,255) is the value range of the color channel, it is actually difficult to compare the color difference by adding 1 color change. We cross eight color levels at a time, and the visual effect (roughly divided into



FIGURE 5: Color reconstruction picture.

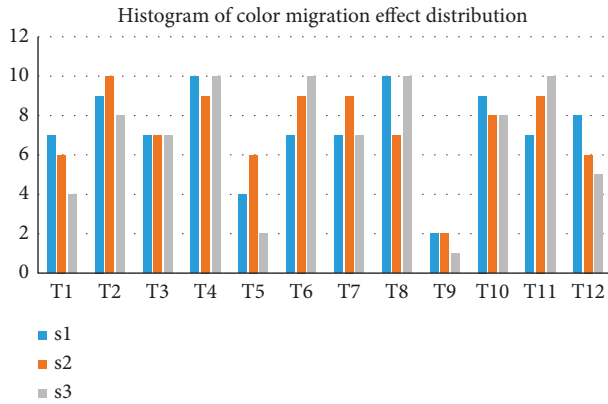


FIGURE 6: Color migration effect.

five effect degrees, 1–5) changes roughly in the process of change. The RGB color component has 32 color levels (0–255 difference is 8 to 1). The RGB values of different levels are displayed on the hardware screen, so we need to switch and record the change of the display effect of image color transformation regularly. Finally, we need to repeat the operation to take the average value (about 10 times), as shown in Figure 7.

In the three numerical changes of R , G , and B , the regular increase of 8 orders of magnitude can make the change effect more gentle and the visual effect more intuitive (Figure 7). Comparing the change display effect is more convenient for us to summarize the rules and methods.

4.3. Gray Degree Processing of Photographic Images. Image processing algorithm plays a very important role in image processing. We can use it to process photographic pictures, which also has a great influence on the posteffect and quality effect of the processed photographic pictures. Our preprocessing algorithm mainly calculates and processes the grayscale of the images, which can improve the image contrast and other parameters to a certain extent. By changing the brightness and shade of different brightness areas and increasing the numerical distribution of image gray space, the contrast of the image in different situations can be greatly improved, and the foreground target can be greatly highlighted. The gray processing of the picture is shown in Figure 8.

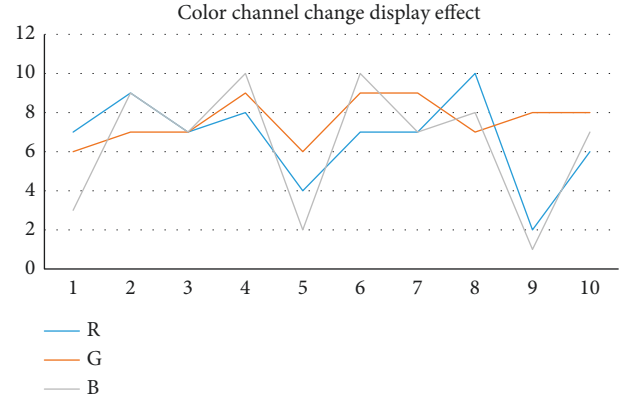


FIGURE 7: Color channel changes display effect.



FIGURE 8: Grayscale processing picture.

Linear transformation algorithm is one of the most basic algorithms in image transformation. The gray value of the initial image has a linear relationship with the gray value of the transformed image, as shown in Figure 9.

We need to consider that, in order to achieve the purpose of reconstructing the selected colors of the photographic picture template, the matched color table must be as similar to or even composed of the colors of the target image M as possible. The distribution of color table C also needs to grasp the relationship of color composition from multiple dimensions and also needs to adjust the attribute of M between the target color associated image C and the target color table from different angles so as to achieve the reasonable distribution of color table.

The gray space can change between 0 and 255. In order to prevent the grayscale from being displayed due to leap-frogging, we need to increase the contrast of different grayscale spaces in a certain application scene, compare with a single linear algorithm, and propose a method of different transformation functions in different grayscale intervals, so as to achieve the linear exchange of different grayscale intervals shown in Figure 10.

The gray level change of image has important significance and value. According to Figures 9 and 10, we can know that there are linear processing methods and nonlinear processing methods. The single linear algorithm is compared, and the linear exchange between different gray levels is realized. In the nonlinear change algorithm, the nonlinear function of power law change and exponential change is

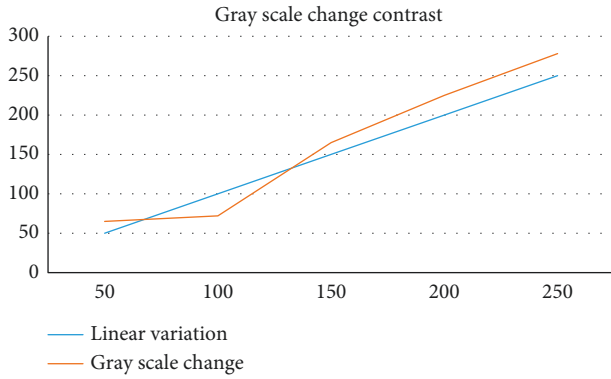


FIGURE 9: Comparison of image gray level change effect.

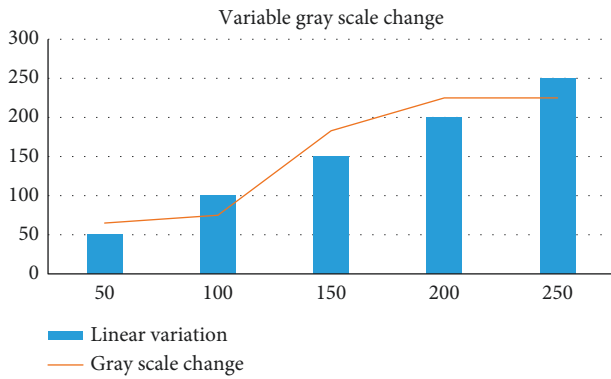


FIGURE 10: Image variability gray level change.

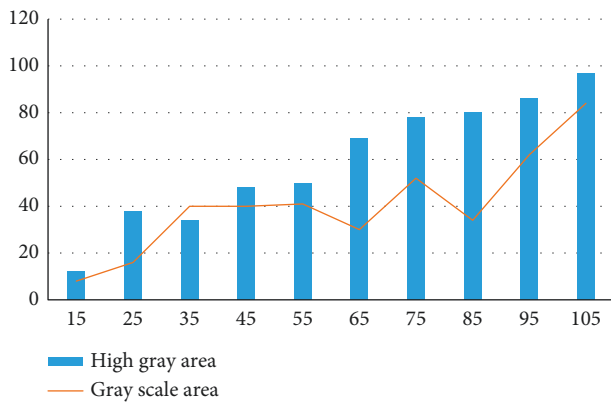


FIGURE 11: Image power change.

used to deal with the pixels of the image, which better avoids the distortion of the image. The single linear change is simple and convenient, and the nonlinear flexible change space is large. Both of them have their own advantages and have very important use significance.

In the algorithm of image nonlinear change, the basic principle of nonlinear change is to use the nonlinear function of power law change or exponential change to process every pixel of the image. The logarithmic change firstly takes the original image as input and calculates the gray value of each pixel by logarithmic calculation. Due to the distribution characteristics of the exponential function,

the exponential fluctuation amplitude in low-gray area is obvious, which can effectively improve the detail contrast in dark area of image. The operation of power law transformation takes the gray value of the image as the bottom of the power law function and other parameters as the coefficients and power values of power operation, which are similar to exponential changes to prevent image distortion. The change needs to be operated by power law transformation according to different parameters. When the parameter is less than 0, the power law transform can improve the contrast ability of dark area and ensure the color range of high-brightness area. When the input parameter is greater than 0, the switch can be changed to improve the intensity of the brightness area and the contrast of the high-brightness area so as to ensure that the image in the low brightness area is not distorted, as shown in Figure 11.

5. Concluding Remarks

The image processing technology written in this paper is applied to photographic images. We provide many aspects of image processing and how to make the image resources obtained by shooting use algorithms to change their attributes. For image processing is the focus of color and size processing, we can simply change not only the value of a single attribute but also the color reconstruction of large and free modification. Visually meticulous processing sometimes depends on contrast, and the difference is subtle, but the attribute of contrast is also very important. The contrast between the high-brightness area and the low-gray area will also have an impact on the final quality of the camera pictures in our hands, and the scaling of the image at the pixel block level should also be paid attention to. We know the rules clearly and master the methods so that we can better deal with the image processing problems.

Data Availability

The experimental data used to support the findings of this study are available from the corresponding author upon request.

Conflicts of Interest

The author declares that there are no conflicts of interest regarding this work.

References

- [1] J. Weickert, "Anisotropic diffusion in image processing," *B.g.teubner Stuttgart*, vol. 16, no. 1, p. 272, 1998.
- [2] R. G. Keys, "Cubic convolution interpolation for digital image processing," *IEEE Transactions on Acoustics, Speech, & Signal Processing*, vol. 29, no. 5, p. 567, 2003.
- [3] Y. Y. Bo, C. Elbuken, and C. L. Ren, "Image processing and classification algorithm for yeast cell morphology in a microfluidic chip," *Journal of Biomedical Optics*, vol. 16, no. 6, Article ID 066008, 2011.
- [4] S. M. Smith and J. M. Brady, "SUSAN—a new approach to low level image processing," *International Journal of Computer Vision*, vol. 23, no. 1, pp. 45–78, 1997.

- [5] M. van Heel, G. Harauz, E. V. Orlova, R. Schmidt, and M. Schatz, "A new generation of the IMAGIC image processing system," *Journal of Structural Biology*, vol. 116, no. 1, pp. 17–24, 1996.
- [6] L. Alvarez, F. Guichard, P. L. Lions, and J. M. Morel, "Axioms and fundamental equations of image processing," *Archive for Rational Mechanics and Analysis*, vol. 123, no. 3, pp. 199–257, 1993.
- [7] K. Saarinen, "Image processing, analysis and machine vision," *Signal Processing*, vol. 35, no. 1, pp. 102–104, 1994.
- [8] G. Sun, W. Qian, W. Huang et al., "Stochastic adaptive robust dispatch for virtual power plants using the binding scenario identification approach," *Energies*, vol. 12, no. 10, p. 1918, 2019.
- [9] P. Bigioi, G. Susanu, P. Corcoran, and I. Mocanu, "Digital camera connectivity solutions using the picture transfer protocol (PTP)," *IEEE Transactions on Consumer Electronics*, vol. 48, no. 3, pp. 417–427, 2002.
- [10] N. Jan and H. I. Myung, "Teacher-student relationship and peer disliking and liking across grades 1-4," *Photo Development*, vol. 87, no. 2, pp. 593–611, 2016.
- [11] Y. Yang, G. Hulot, P. Vigneron et al., "The CSES global geomagnetic field model (CGGM): an IGRF-type global geomagnetic field model based on data from the China Seismo-Electromagnetic Satellite," *Earth Planets and Space*, vol. 73, no. 1, pp. 1–21, 2021.
- [12] Y. Liu, T. S. Huang, and O. D. Faugeras, "Determination of Camera Location from 2D to 3D Line and point correspondences," in *Proceedings of the Conference on Computer Vision & Pattern Recognition*, June 1988.
- [13] E. Mendoza, P. R. Martineau, E. Brenner, and R. Dirzo, "A novel method to improve individual animal identification based on camera-trapping data," *Journal of Wildlife Management*, vol. 75, no. 4, pp. 973–979, 2011.
- [14] H. Griffin, "The wall motion picture camera," *Journal of the Society of Motion Picture Engineers*, vol. 25, no. 4, pp. 363–366, 1935.

Research Article

Management and Analysis of Sports Health Level of the Elderly Based on Deep Learning

Liping Xiao¹,¹ Limin Huang,² Hongxia Chang,¹ Li Ji,³ and Ji Li¹

¹College of Sports Science, Harbin Normal University, Harbin 150025, China

²College of Sports and Human Sciences, Harbin Sport University, Harbin 150008, China

³Administration of Sport for Persons with Disabilities, Beijing 101318, China

Correspondence should be addressed to Liping Xiao; xiaolp@hrbnu.edu.cn

Received 9 May 2022; Revised 6 June 2022; Accepted 10 June 2022; Published 30 June 2022

Academic Editor: Dong Chen

Copyright © 2022 Liping Xiao et al. This is an open access article distributed under the Creative Commons Attribution License, which permits unrestricted use, distribution, and reproduction in any medium, provided the original work is properly cited.

With the accelerating rate of population aging in China, the health of the elderly has received more and more attention and has become one of the most important issues in the elderly care industry. Because of insufficient research on the personal health of the elderly, the value of medical examination data cannot be fully exploited, many physical indicators have a certain impact on overall health or heart health, and there are few studies on heart health assessment. This paper proposes a deep learning-based elderly management analysis method of human exercise health level, using the exercise health management model to evaluate the heart health level of the elderly. Firstly, the indicators to measure heart health are proposed through traditional expert knowledge and personal health index to analyze heart health. Through dynamic assessment, predict the heart health status at the next time point, analyze possible heart diseases, and provide corresponding methods for the health of the elderly, which helps improve the physical health of the elderly. Quality of life provides assistance to meet the needs of improving the health of older adults.

1. Introduction

Studies have confirmed that long-term regular exercise in the mode of exercise health management can significantly improve the heart health of the elderly and improve the physical health and quality of life of the elderly [1–3]. In the late 1950s, the United States first proposed the concept of health management. Its core content is that medical insurance institutions carry out systematic health management for their medical insurance customers (including disease patients or high-risk groups), including disease prevention, All aspects of clinical diagnosis and treatment, rehabilitation, and health care are the whole process of comprehensive monitoring, analysis, evaluation, prediction, prevention, and maintenance of health risk factors of healthy people, subhealthy people, and diseased people and strive to effectively control the occurrence or development of diseases, significantly reducing the probability of an accident and actual medical expenses, thereby reducing the purpose

of medical insurance compensation losses [4–9]. This is generalized health management. In a relatively narrow sense, health management (Health Management) refers to the purpose of preventing and controlling the occurrence and development of diseases, reducing medical expenses, and improving the quality of life [10–15]. Chinese scholars have combined several representative definitions of health management at home and abroad to define health management as a process of comprehensively managing the health needs of individuals and groups [16–19]. Here, health needs can be a health risk factor, such as hypertension and obesity, or a disease state, such as coronary heart disease or diabetes. In short, it is the process of planning, organizing, directing, coordinating, and controlling health resources for health needs [2].

The United States is a pioneer in promoting health through exercise. Since 1980, exercise has been incorporated into the health management system. After years of development, the United States has established an exercise

promotion and health guidance service platform that is led by the government, supplemented by scientific research institutions and sports social organizations, and combines medical and health services with physical fitness services [20–24]. Based on inspecting the American sports promotion health guidance service platform, from the establishment of the “medicine and body integration” linkage management mechanism, to play the role of social organizations such as the Chinese Society of Sports Science, to refine the implementation goals of sports to promote health, and to strengthen compound sports to promote health. My country has built a national fitness service system in terms of guiding personnel training and other aspects. Physical exercise is an important embodiment of a healthy lifestyle, but exercise must also have a degree, that is, scientific exercise management methods are needed. Sports health management is to apply modern medical knowledge and scientific sports methods to systematically pay attention to and maintain the physical health of sportsmen from the perspectives of sociology, physiology, and psychology. Sports health management refers to understanding the needs and goals of sports from physical fitness assessment, sports consultation, and communication based on the health status, living status, and exercise habits provided by the individual, establishing a personal exercise prescription, and providing safe, effective, Reasonable exercise plan, guided by practical teaching methods, combined with comprehensive health services for exercise effect tracking, help improve personal physical fitness and fitness, and then achieve the goal of personal exercise and fitness and physical health.

Existing studies have shown that sports health management is based on the change in people’s health outlook. We review the research on sports health management, then expound on the basic elements of the public sports health management service model and the relationship between the elements, and demonstrate the operation mechanism of the service model and make corresponding recommendations. According to the health status, living status, and exercise habits provided by the individual, from physical fitness assessment, exercise consultation, and communication, to understand their exercise needs and goals, establish a personal exercise prescription, and provide a safe, effective, and reasonable exercise plan to Practical teaching methods are provided for guidance, combined with a full range of health services to track exercise results, to help improve personal physical fitness and fitness, and then achieve the goal of personal exercise and fitness and physical health. Some studies prove that exercise can enhance physical fitness, promote the overall development of the human body, enhance the human body’s resistance and prolong life, and improve the health level of patients with certain diseases; it is a kind of active rest, which makes people energetic and relieves life, work, and study tension and improves work efficiency. Exercise can effectively prevent psychological disorders, enhance the joy of life, and improve the quality of life. Exercise is an important part of the health management process. In the development of a healthy experiment plan, the three aspects of healthy exercise, healthy diet, and health coaching can be combined. Physical activity monitoring is

also a part of health monitoring, exercise health management is a part of exercise application in health management, and exercise prescription is a part of exercise health management. Health managers can guide and formulate healthy exercise for different groups of people according to the basic procedures of the survey.

As the elderly grow older, their physical condition also changes. The function of the heart will gradually deteriorate with aging, the systemic decline and functional degeneration of the elderly, and the immune system function of the elderly will decline significantly. The decline of the immune system function will directly affect the healthy life of the elderly, and the exercise of the elderly. The characteristics are also inseparable from their physiological characteristics; low-intensity, aerobic exercise for the elderly should not choose speed-type and strength-type sports, but whole-body sports that focus on aerobic metabolisms, such as Health Qigong, jogging, walking, and other projects.

To sum up, this paper proposes an analysis method for the management of the elderly’s exercise health level based on deep learning. Based on traditional expert knowledge and personal health index, it proposes indicators to measure heart health to analyze heart health. Sequence data set, perform a dynamic assessment of heart health, obtain the possible heart health status at the next time point, remind the risk of heart disease, and make appropriate adjustments to the body in time. Human physical health provides corresponding methods to help improve the physical health and quality of life of the elderly, so as to meet the needs of improving the health of the elderly.

2. Dynamic Assessment of Heart Health in the Elderly

2.1. Heart Health Indicators for the Elderly. Heart health problems in older adults are complex problem. As age continues to increase, the coordination ability between the various tissues of the human body will also decrease. Heart disease is a high-risk disease that threatens the health of the elderly. Pathogenesis is complex, and many indicators affect the health of the heart. Numerous studies have shown that senile heart disease mainly includes three types of hypertensive heart disease, coronary heart disease, and pulmonary heart disease. During the development of these three types of heart disease, the contraction force of the heart muscle will be weakened, which will cause a circulatory disturbance, become heart failure, and be life-threatening. In addition, these heart diseases may also cause heart rate disorder, which is manifested as a fast, slow, or irregular heartbeat. Therefore, in the process of studying the heart health of the elderly, it is necessary to analyze from multiple angles and multiple indicators. Heart disease is not diagnosed casually. It is not an arrhythmia or angina pectoris during exercise. It means that you have heart disease. Its diagnosis requires a professional doctor to use the diagnostic criteria of heart disease to judge. There are many manifestations of heart disease, such as cardiovascular problems and myocardial infarction problems, that is, individuals may suffer from coronary heart disease [25–27].

TABLE 1: Detailed information table of indicators to measure heart health.

Metrics	Reference range
Age	60+
Gender	{Male, female}
Blood pressure level	Systolic blood pressure: 90–14 mmHg Diastolic blood pressure: 60–90 mmHg
Types of chest pain	{ angina pectoris, non-angina pectoris, classic angina pain, and atypical angina }
Serum cholesterol	2.9~6.0 mmol/L
Blood sugar concentration	3.89~6.1 mmol/L
ECG results	{ normal, rising, falling }
Resting heart rate	60~100 times/min
Number of blood vessels	{0, 1, 2, 3}
PHI	[0, 1]

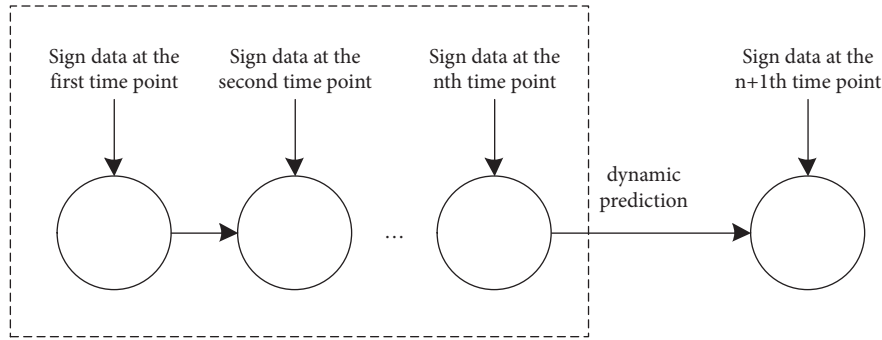


FIGURE 1: Detailed schematic diagram of dynamic assessment of heart health.

Heart health indicators are based on a combination of traditional expert knowledge, factors that cause senile heart disease, and personal health indexes. Most of the research in the field of heart disease is to predict the risk of heart disease or use a single attribute feature to analyze heart health changes, but few scholars start from multiple indicators and comprehensively consider changes in heart health. The detailed index description is shown in Table 1.

From the perspective of professional medicine, indicators such as blood pressure, cholesterol, and blood sugar play a very important role in the diagnosis of heart disease, and heart health is analyzed from a more comprehensive perspective, and relevant indicators need to be considered more comprehensively. And the rapid development of big data technology makes it possible to obtain knowledge from more physiological indicators.

2.2. Heart Health Dynamic Assessment Questions. For the elderly, as the age continues to increase, the functions of various tissues in the body continue to decline, and the body's self-regulation ability will also decrease. Once a certain index is abnormal, it is likely to occur in a short period changes in health status. For older adults without heart disease, changing data on signs of heart health may lead to an increased risk of heart health and, in turn, heart disease. For older adults with pre-existing heart disease, changing data on signs related to heart health may lead to worsening heart disease. In this section, heart health is dynamically assessed according to the continuous changes in the physical data. The detailed schematic diagram is shown

in Figure 1, which means that the physical data information of the previous n time points is used to predict the heart health status of the next time point. Dynamic evaluation, that is, to evaluate the possibility that the heart health state will evolve in a good or bad direction based on the sign data information at different time points.

Based on the above description of the problem of dynamic assessment of heart health, this section will analyze the dynamic assessment method and data preprocessing stage. Since it is a time-series dataset with multi-attribute features, the long short-term memory network (LSTM) in the field of deep learning has a good performance in processing long-term series data. But the input layer of the LSTM algorithm must be in canonical form, containing three dimensions, as follows.

Sample: all features at any time point are used as a single sample, and one or more samples constitute a batch.

Time step: each time point is a time step.

Features: the observed results for one-time step are called features.

Definition 1. $Series1: x_{11}, x_{12}, x_{13}, \dots, x_{1n}$, $Series2: x_{21}, x_{22}, x_{23}, \dots, x_{2n}$, $Seriesm: x_{m1}, x_{m2}, x_{m3}, \dots, x_{mn}$, are attribute sets of n features at m time points.

Before entering the LSTM, the dataset needs to be transformed into a 3D collection using the reshape method. There are a total of n time points, so the step size is n . Then the LSTM input layer input_shape (1, n , m). For the heart health data set, the vector similarity method is used to simulate a data set containing 5 time points, a total of 6166

individual data, so the input layer input_shape (5, 14, 5). The heart health state at the next time point is predicted from the personal sign data of the first n time points. The training set constructed is as follows:

$$\begin{aligned} \text{train_X} &= \begin{bmatrix} x_{11} & \cdots & x_{1(n-1)} \\ \cdots & \cdots & \cdots \\ x_{(m-1)1} & \cdots & x_{(m-1)(n-1)} \end{bmatrix}, \\ \text{train_Y} &= \begin{bmatrix} x_{1n} \\ \cdots \\ x_{mn} \end{bmatrix}. \end{aligned} \quad (1)$$

The test set is constructed in the same way as the training set.

3. Deep Learning Algorithms

3.1. RNN Neural Network. Often used in machine vision and natural language processing, recurrent neural networks (RNNs) have feature learning capabilities and are able to extract high-level features from input data. One-dimensional CNN (1D-RNN) can be used for time-series data processing, and two-dimensional CNN (2D-RNN) can be used for visual processing such as image recognition.

The structure of 1D-RNN is shown in Figure 2, which consists of an input layer, a convolutional layer, a pooling layer, a fully connected layer, and an output layer. The convolutional layer extracts features through convolution kernels of different sizes, and the pooling layer reduces the dimension of information by compressing the data. To efficiently extract and retain data features, convolutional layers, and pooling layers alternate. Fully connected layers will flatten the distribution features extracted from different spaces to achieve regression or classification. RNN focuses on local feature extraction and reduces weights through parameter sharing, which greatly reduces the computational parameters of the network.

3.2. LSTM Neural Network. Since there are many time points in the time-series data of the dynamic assessment of mental health of the elderly studied in this paper, it belongs to the long-term dependence problem. If RNN is used, there may be a problem that the gradient disappears during the backpropagation process. The gradient is the value used to update the weights during the neural network training process. If the gradient disappears, the training process will not continue. Therefore, this paper uses LSTM for research. The basic LSTM network structure is shown in Figure 3.

As can be seen from Figure 3, x_t represents the input of the data of the input layer, h_t represents the output of the data of the output layer, A represents the operation of each node in the hidden layer, and there is certain information transmission between the operations of different nodes. The structure is shown in Figure 4.

As shown in Figure 4, combined with Figure 3, a complete LSTM network structure diagram includes the input layer, forget gate, update gate and output gate. During

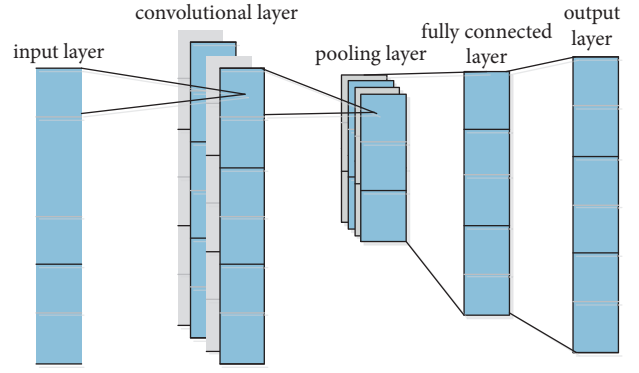


FIGURE 2: Structure of 1D-RNN.

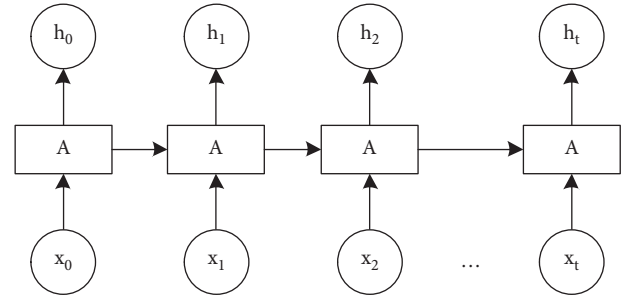


FIGURE 3: LSTM network structure diagram.

the learning process, the LSTM network structure will automatically store the historical information deemed useful to the $c(t)$, which represents the memory of the current LSTM unit, $c(t-1)$ represents the memory of the previous LSTM unit, $x(t)$ represents the input at time t , where “+” represents the added information, and “ \times ” represents the scaling information. The activation functions of the forget gate, update gate, and output gate are all sigmoid because the information processed by the sigmoid function will become 0 or 1, which can decide which information is forgotten or remembered after passing through the node. In addition, since the second derivative of tanh has a long distance when it keeps approaching zero, it can better overcome the problem of gradient disappearance during training. The formula for calculating the update gate at time t :

$$u(t) = \text{Sigmoid}(W_i[x(t); a(t-1) + b_i]), \quad (2)$$

where W_i is the weight of the update gate and b_i is the bias vector of the update gate.

The forgetting ratio in the forget gate is calculated as shown in

$$f(t) = \text{Sigmoid}(W_f[x(t); a(t-1)] + b_f), \quad (3)$$

where W_f is the weight of the forget gate and b_f is the bias vector of the forget gate. And the unit state at this moment is updated, as shown in

$$c(t) = f(t) * c(t-1) + u(t) * \tanh(W_s[x(t); a(t-1)] + b_s), \quad (4)$$

where W_s and b_s are the weight and bias vector of hidden units in the forget gate, respectively.

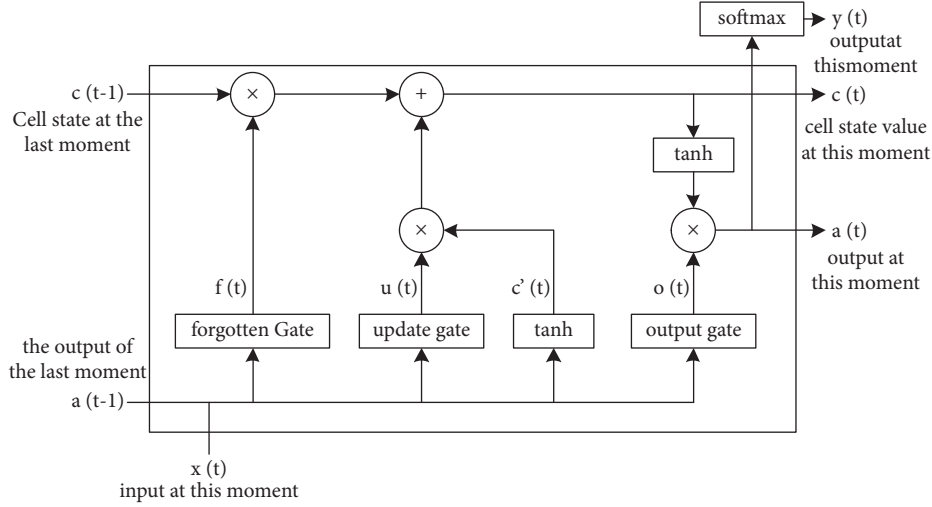


FIGURE 4: Detailed structure diagram of the LSTM computing unit.

Similarly, the update of the output gate information can be obtained, as shown in

$$o(t) = \text{Sigmoid}(W_o[x(t); a(t-1)]) + b_o, \quad (5)$$

$$y(t) = o(t) * \tanh(c(t)). \quad (6)$$

3.3. Deep Neural Network (DNN). In simple terms, DNN is an artificial neural network with multiple hidden layers, and the layers are fully connected. The model training process consists of two parts, one part is the forward propagation process, that is, starting from the input layer, calculating layer by layer until the calculation reaches the output layer. The other part is the backpropagation process. Before backpropagation, the loss between the predicted value and the output value needs to be calculated first, and then the loss function is optimized to find the minimum extreme value. The most common use of the gradient descent algorithm, and then reverse Update a series of W weight matrices and B bias vectors until the desired effect is achieved and stop training. The structure diagram of the 2-layer DNN network is shown in Figure 5.

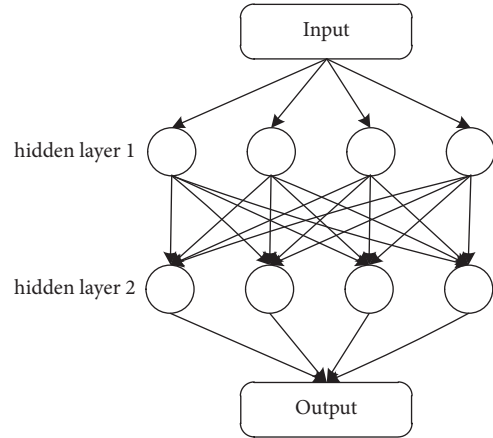


FIGURE 5: Schematic diagram of the 2-layer DNN network structure.

Step 1. Data preprocessing. Using the maximum and minimum normalization principle, the original data is normalized to the range of $[0, 1]$ according to the index, and the normalization formula is given by

$$x' = \frac{x - x_{\min}}{x_{\max} - x_{\min}}, \quad (7)$$

where x_{\max} is the maximum value of the indicator, x_{\min} is the minimum value of the indicator, and x is the value of the indicator for different sample data.

3.4. LSTM-DNN Model Construction. This paper will build the LSTM-DNN model and analyze it mainly from two aspects. First, the long-term sequence data set consider using the LSTM algorithm to learn the relationship between nodes at different times and make predictions; second, consider the particularity of the sign data because there may also be a certain relationship between different indicators, so use the DNN algorithm to learn the relationship between different indicators. The LSTM-DNN model structure is shown in Figure 6.

First perform data preprocessing, then input to the LSTM layer, then enter the DNN layer, and finally output a prediction result. The flow chart of the model operation is shown in Figure 7.

Step 2. Build a network training model. Assuming that the number of time points in the time dimension is n , the number of nodes in the LSTM layer is n . To solve the problem of gradient disappearance during the training process and improve the training speed of the model, the activation function uses ReLU. In the DNN layer, its essence is a fully connected layer, the number of hidden layers is set according to the size of the data, the activation function used is Sigmoid, and finally, the nodes of the output layer are set according to the category, if there are n categories, that is, set

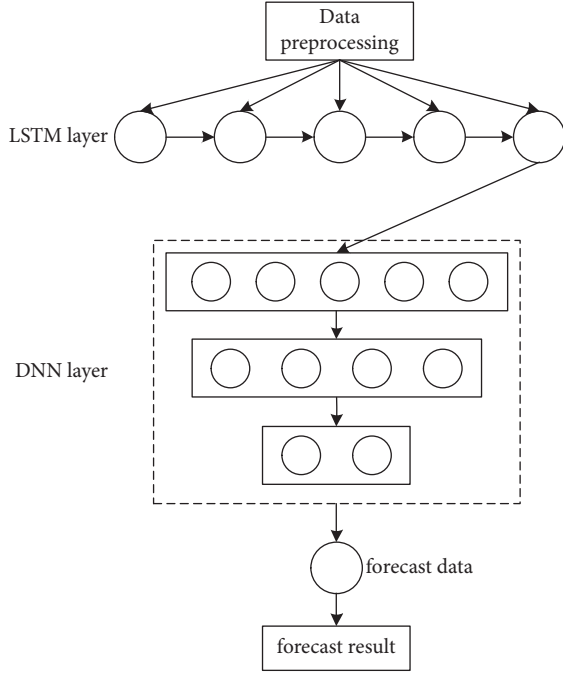


FIGURE 6: LSTM-DNN model structure diagram.

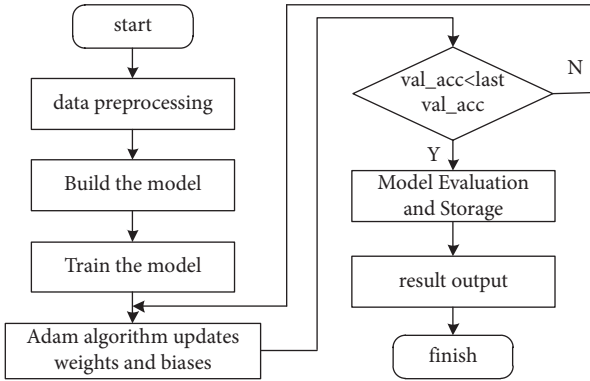


FIGURE 7: Model running flow chart.

n node. After configuring the network structure, a loss function needs to be defined to calculate the gradient and optimize it. The loss function uses the root mean square error method (RMSE), as shown in

$$f(x) = \max(0, x),$$

$$\text{RMSE} = \sqrt{\frac{1}{M} \sum_{i=1}^M (y^{(i)} - y'^{(i)})^2}. \quad (8)$$

Here, $y^{(i)}$ is the original value of the sample data, $y'^{(i)}$ is the predicted value of the model, M represents the size of the sample data, and i represents the i th sample.

Step 3. Train the network model. After completing the second step of network construction, start training, and configure parameters according to the size of the data set and

empirical knowledge, including the number of iterations epoch, and the batch size of the data sent into the network each time, which is used for verification after each epoch. In the evaluation function of the model, the parameter is set to “accuracy”, is simply by judging the ratio of the number of correct predictions to the total number in the test set. The optimizer in the training process uses the Adam algorithm. When the accuracy rate on the test set continues to increase and tends to be stable, it reaches the standard of the end of model training, that is, stops the training.

Step 4. Model evaluation and saving. After the set parameters are verified, when the accuracy rate of the test set reaches a stable level, the model training is regarded as the end, and the accuracy rate at this time is the optimal accuracy rate. The final values of the parameters and the model that are continuously adjusted during the training process are saved for application to other samples.

Step 5. Predict the resulting output. During the training process, the result accuracy rate and loss value of each iteration are printed, which is convenient for debugging parameters, and finally, the root mean square error of the test set and the result accuracy rate are output.

4. Experiment and Analysis

The medical examination data set used in this study comes from the public data of the National Health and Nutrition Examination Center in the United States, and only the elderly part is used, with a total of 6166 pieces of data. When analyzing heart health, indicators based on expert knowledge are the indicators used to measure heart disease. The reference data set is the standard data set of heart disease published by UCI. In the model training process, the heart health is measured by whether there is a heart disease, and the disease is mapped to 0, that is, the heart health is poor; otherwise, it is mapped to 1. The dynamic evaluation process uses all the index information of the first four time nodes to dynamically predict the heart health status at the fifth time point. The experimental environment is windows10, python3.6, and the model is built using the Keras framework in deep learning.

Since the number of time nodes in the dataset is 5, the LSTM part is configured with 5 nodes to learn the relationship between different time nodes. After many experiments, the number of DNN hidden layers is 2, the number of nodes is 4 and 2 respectively, the node of the output layer is set to 1, and finally, a prediction result is obtained. According to the size of the data set and related experience, after many attempts, the Epoch is set to 60, and the number of iterations and the corresponding accuracy result. When the number of iterations reaches 55, the accuracy of the result is the best, which is 79.6%, as shown in Figure 8.

Use the model in this chapter to compare and analyze the RNN algorithm and the BPNN algorithm. The precision rate, recall rate, and F1 value are used as evaluation indicators for analysis and comparison, and the experimental results are shown in Table 2.

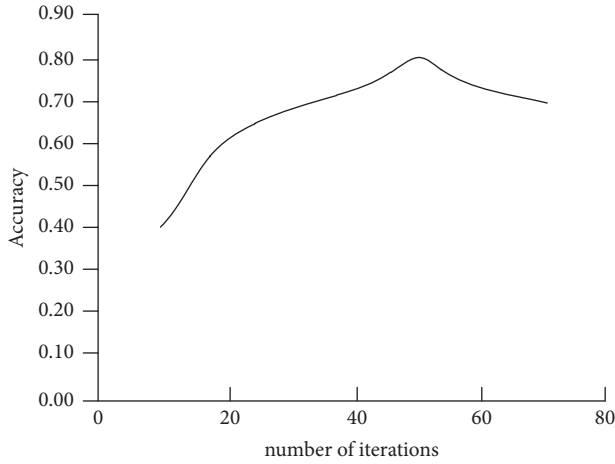


FIGURE 8: The number of iterations and their corresponding accuracy results.

TABLE 2: Comparison of experimental results.

Algorithm	Correct rate	Recall	F1 value
BPNN	0.725	0.668	0.702
RNN	0.764	0.725	0.742
LSTM-DNN	0.796	0.776	0.785

The experimental results show that the proposed LDNN model can better dynamically assess the state of heart health. The main reason is that the LSTM algorithm has better performance on long-term dependency problems and can better learn the correlation between different time points. And the result is processed by the DNN network structure with two hidden layers, and the relationship between the sample features is better learned, so the LDNN model constructed in this chapter has a better training effect and a higher prediction accuracy. Finally, in terms of the accuracy of the results, the LDNN model is 3% higher than the RNN algorithm on average and 7% higher than the BPNN algorithm.

5. Conclusion

Aiming at the heart health problems of the elderly in the elderly care industry, the related algorithms of deep learning are used to analyze and evaluate the heart health of the elderly. According to the time-series data set composed of indicators related to heart health, the problem of dynamic assessment of the heart health of the elderly is described and analyzed, and finally, the LSTM-DNN model is built for the dynamic assessment of the heart health of the elderly and combined with the RNN algorithm and BPNN. The algorithm compares the experimental results, and the accuracy of the evaluation results is increased by 3% and 7% respectively, which verifies the effectiveness of the model. Through the method in this paper, the possible heart health status at the next time point can be obtained, and the risk of heart disease can be reminded, so as to make appropriate adjustments to the body in time and improve the quality of life of the elderly. The evaluation method research in this

paper needs to be further improved: First, the data set comes from the data of Americans, which may be different from the physical data of Chinese people. Second, it is about the proposal of measuring heart health indicators. This paper only considers numerical data and does not involve text, type data, and image type data.

Data Availability

The dataset can be accessed upon request to the corresponding author.

Conflicts of Interest

The author declares that there are no conflicts of interest.

Acknowledgments

The authors thank the funding source supported by the Philosophy and Social Science Research Planning Project of Heilongjiang Province in 2018, Research on the Strategy of promoting the normalization of Youth Ice and Snow Sports in Heilongjiang during the Winter Olympic Games cycle, under Special Project 18TYD355.

References

- [1] W. Zhao, "Correlative analysis of occupational health management in construction companies to related factors based on fuzzy clustering and grey theory," *IOP Conference Series: Earth and Environmental Science*, vol. 267, no. 5, Article ID 052058, 2019.
- [2] M. M. Theilig, J. J. Korb, G. Mayer, C. Hoffmann, and R. Zarnekow, "SPECIAL SECTION ON DATA-ENABLED INTELLIGENCE FOR DIGITAL HEALTH—employing environmental data and machine learning to improve mobile health receptivity," *IEEE Access*, vol. 7, no. 1, pp. 179823–179841, 2019.
- [3] L. Zhang, J. Lin, B. Liu, Z. Zhang, X. Yan, and M. Wei, "A review on deep learning applications in prognostics and health management," *IEEE Access*, vol. 7, 2019.
- [4] M. R. Bleich, "The professional development educator role in leading population health management," *The Journal of Continuing Education in Nursing*, vol. 49, no. 11, pp. 496–497, 2018.
- [5] A. Pandey, M. LaMonte, L. Klein et al., "Relationship between physical activity, body mass index, and risk of heart failure," *Journal of the American College of Cardiology*, vol. 69, no. 9, pp. 1129–1142, 2017.
- [6] D. J. Moon, S. I. Lee, C. S. Lee, G. C. Kim, H. J. Kang, and Y. J. Yang, "A Suggestion on evaluating personal health state: health index," *Journal of Biomedical Engineering Research*, vol. 29, no. 5, pp. 400–407, 2008.
- [7] C. Ling, L. Xue, S. Wang et al., "Mining personal health index from annual geriatric medical examinations," in *Proceedings of the IEEE International Conference on Data Mining*, pp. 761–766, IEEE, Shenzhen, China, December 2014.
- [8] L. Chen, X. Li, Y. Yang, and H. Kurniawati, "Personal health indexing based on medical examinations: a data mining approach," *Decision Support Systems*, vol. 81, pp. 54–65, 2016.
- [9] H. Jung and K. Chung, "PHR based life health index mobile service using decision support model," *Wireless Personal Communications*, vol. 86, no. 1, pp. 315–332, 2016.

- [10] M. Esposito, A. Minutolo, R. Megna, and M. M. G. Forastiere, "A smart mobile, self-configuring, context-aware architecture for personal health monitoring," *Engineering Applications of Artificial Intelligence*, vol. 67, pp. 136–156, 2018.
- [11] G. Swapna, S. Kp, and R. Vinayakumar, "Automated detection of diabetes using CNN and CNN-LSTM network and heart rate signals," *Procedia Computer Science*, vol. 132, pp. 1253–1262, 2018.
- [12] G. Maragatham and S. Devi, "Retracted article: LSTM model for prediction of heart failure in big data," *Journal of Medical Systems*, vol. 43, no. 5, p. 111, 2019.
- [13] S. Saadatnejad, M. Oveisi, and M. Hashemi, "LSTM-based ECG classification for continuous monitoring on personal wearable devices," *IEEE Journal of Biomedical & Health Informatics*, vol. 24, no. 2, pp. 515–523, 2018.
- [14] F. Liu, X. Zhou, J. Cao, Z. Wang, H. Wang, and Y. Zhang, "A LSTM and CNN based assemble neural network framework for arrhythmias classification," in *Proceedings of the ICASSP 2019 - 2019 IEEE International Conference on Acoustics, Speech and Signal Processing (ICASSP)*, pp. 1303–1307, Brighton, UK, May 2019.
- [15] S. Mohammed, Y. Sha and M. D. Wang, "Early prediction of sepsis in EMR records using traditional ML techniques and deep learning LSTM networks," in *Proceedings of the 2018 40th Annual International Conference of the IEEE Engineering in Medicine and Biology Society (EMBC)*, pp. 4038–4041, Honolulu, HI, USA, May 2019.
- [16] L. Brunese, F. Martinelli, F. Mercaldo, and A. Santone, "Deep learning for heart disease detection through cardiac sounds," *Procedia Computer Science*, vol. 176, 2020.
- [17] F. López-Martínez, E. R. Núñez-Valdez, V. García-Díaz, and Z. Bursac, "A case study for a big data and machine learning platform to improve medical decision support in population health management," *Algorithms*, vol. 13, no. 4, p. 102, 2020.
- [18] D. J. Hunter and J. Brown, "A review of health management research," *European Journal of Public Health*, vol. 17, no. S1, pp. 33–37, 2007.
- [19] Y. Yang, C.-Huan Tian, J. Cao, and X.-J. Huang, "Research on the application of health management model based on the perspective of mobile health," *Medicine*, vol. 98, no. 33, Article ID e16847, 2019.
- [20] F. Ahmad, C. Guyeux, A. Makhoul, J. Ali, and R. Tawil, "On the coverage effects in wireless sensor networks based prognostic and health management," *International Journal of Sensor Networks*, vol. 28, no. 2, 2018.
- [21] P. Goe, H. Liu, D. Brown, and A. Datta, "On the use of spiking neural network for EEG classification," *International Journal of Knowledge-Based and Intelligent Engineering Systems*, vol. 12, no. 4, pp. 295–304, 2008.
- [22] D. J. Marino, "Building a value model for population health management," *Healthcare Financial Management: Journal of the Healthcare Financial Management Association*, vol. 71, no. 3, pp. 40–7, 2017.
- [23] K. Wei and Z. Zhou, "Adversarial attentive multi-modal embedding learning for image-text matching," *IEEE Access*, p. 1, 2020.
- [24] Z. Jia, Y. Lin, J. Wang, and X. Ning, "Multi-view spatial-temporal graph convolutional networks with domain generalization for sleep stage classification," *IEEE Transactions on Neural Systems and Rehabilitation Engineering*, vol. 29, pp. 1977–1986, 2021.
- [25] Y. J. Lee and Ha, "Consumer use of the internet for health management," *Journal of Consumer Health on the Internet*, vol. 20, no. 1-2, pp. 1–18, 2016.
- [26] T. Zhen, Yan, and P. Yuan, "Walking gait phase detection based on acceleration signals using LSTM-DNN algorithm," *Algorithms*, vol. 12, no. 12, p. 253, 2019.
- [27] J. Ospina, A. Newaz, and M. O. Faruque, "Forecasting of PV plant output using hybrid wavelet-based LSTM-DNN structure model," *IET Renewable Power Generation*, vol. 13, no. 7, pp. 1087–1095, 2019.

Research Article

Research on Land Use Planning Based on Multisource Remote Sensing Data

Wei Jia,¹ Tingting Pei,¹ and Kai Lei² 

¹*School of Food and Environment, Jinzhong College of Information, Jinzhong 030800, China*

²*School of Architecture and Urban Planning, Lanzhou Jiaotong University, Lanzhou 730070, China*

Correspondence should be addressed to Kai Lei; 11200657@stu.lzjtu.edu.cn

Received 10 May 2022; Revised 30 May 2022; Accepted 7 June 2022; Published 29 June 2022

Academic Editor: Dong Chen

Copyright © 2022 Wei Jia et al. This is an open access article distributed under the Creative Commons Attribution License, which permits unrestricted use, distribution, and reproduction in any medium, provided the original work is properly cited.

Land use changes are analyzed correctly, a series of improvements according to the changes are carried out appropriately, the relationship between land use development and economic and human survival is handled correctly, and the healthy and orderly development of the entire society is promoted. Aiming at the combination of multisource remote sensing data and monitoring changes in land planning, this study uses CBERS data and ASAR data as multisource remote sensing data sources to conduct in-depth research and discussion on the land use change in this area and uses the HPF pixel-level fusion method for data fusion to generate HPF. The data are integrated, and then, the CBERS data and HPF fusion data are used to extract the land use type information of Zhenning County, respectively, and a confusion matrix is built based on the field sample points to verify the accuracy, compare and analyze the relative error of the land use type information extraction before and after data fusion, and evaluate the CBERS data. Regarding the extraction effect of land use type information of fusion data with HPF, the results show that the two kinds of remote sensing data have good effects in extracting water body type information, and the accuracy has reached 100%. Using multisource remote sensing image processing can well summarize and analyze land use changes and make the changes in various indicators in the study area. Accurate statistics is obtained.

1. Introduction

To accelerate the pace of my country's economic construction, urbanization should be promoted. In the 2030s, my country should build a well-off society in an all-round way. The basic guarantee conditions for a moderately prosperous society are the construction of new towns, the rational use of limited land resources on the basis of existing rural land, and the completion of real estate construction and the construction of surrounding supporting facilities. The people-oriented concept to the stage of rural land planning is implemented, to achieve efficient use of existing land resources; in line with the basic concept of national construction at this stage, limited rural land resources must be planned and utilized in the early stage of construction, and to solve the problems that often occur in the land planning stage, people-oriented management concepts should be adopted to formulate and implement policies

[1, 2]. People-oriented management is in line with the future development of contemporary construction and management. It is people-oriented, implements basic concepts in the process of land planning, adopts strict management methods to reduce the occurrence of corruption incidents, and promotes the construction of new rural and urban systems in my country [3].

The virtuous circle of land use system is determined by the rationality of land use structure. Land use changes are analyzed correctly, a series of improvements are carried out appropriately according to the changes, the relationship between land use development and economic and human survival is handled correctly, and the healthy and orderly development of the entire society is promoted [4, 5]. This study analyzes the dynamic change characteristics of its land use and obtains the changes in cultivated land, vegetation, roads, residential land, and water areas, as well as the trend of human factors [3, 6, 7].

As a long-distance, noncontact target detection technology and method, remote sensing has the characteristics of multiplatform, multiband, and multilevel and has the advantages of abundant information, short information acquisition period, and strong real-time and dynamic characteristics. It can detect the target, obtain information, after processing, locate, and qualitatively and quantitatively describe the target [8–12]. Land use type information can be obtained by applying remote sensing technology and related geoscientific analysis, and thematic map production can be performed, which makes remote sensing technology have incomparable advantages in the field of land use type classification. Therefore, the use of remote sensing data to extract land use type information is an important means of classifying land use types. At present, the use of remote sensing data to quantitatively extract land use information in the study area is more and more important in the field of environmental science research such as large-scale regional soil erosion [13]. However, in the classification of land use types, there are limitations in data sources and extraction methods. The main problems are that the amount of data is small, the data source is single, mostly optical remote sensing, and radar data are rarely used, the spectrum is not rich, and the resolution needs to be improved. Multisource remote sensing data fusion can enrich the remote sensing information of various sensors, and use the redundancy and complementarity of multisource remote sensing information to describe the target or scene information to the greatest extent [14–16]. CBERS optical remote sensing spectral information is rich, but the spatial resolution is low, and it is easily affected by weather, while ASAR data have high spatial resolution and are less affected and restricted by weather. Therefore, the fusion of CBERS and ASAR remote sensing data can make CBERS optical remote sensing data and ASAR radar remote sensing data form complementary advantages, thereby improving the ability of target recognition, analysis, and interpretation [17–19].

This study uses CBERS and ASAR data as multisource remote sensing data sources, uses HPF pixel-level fusion method for data fusion, then uses the data before and after fusion to extract land use type information in Zhenning County, and compares and analyzes the relative error of land use type information before and after data fusion, and compares the extraction effect of land use types before and after fusion. The research results have important guiding significance for the extraction of land use type information in Zhenning County, a typical karst area with serious soil erosion and fragile ecological environment. In addition, land use type, as an important evaluation factor of soil erosion, is also the main parameter for constructing the soil erosion model in the study area. Therefore, the research on the extraction of land use type information based on multisource remote sensing data can provide a reference for the extraction of land use type information in large-scale soil erosion information and is of great significance for the analysis and evaluation of soil loss in large-scale research areas.

2. Research Progress of Remote Sensing Classification Based on Multisource Data

The accuracy of remote sensing classification is usually affected by the spatial and temporal resolution of the data. In the process of land use classification and crop planting information extraction, remote sensing images with a certain spatial resolution and time series are often required to ensure accuracy. Currently, remote sensing data have products with different temporal, spatial, and spectral resolutions. However, usually high spatial resolution data, due to the long return visit period, insufficient description of the key phenological period of crops, insufficient temporal characteristics, and small width, limit the application of the data in a large range; the ability to describe the space is not high, and there are many mixed pixels. The spatial and temporal resolutions often restrict each other, and it is difficult for the existing remote sensing data to take into account both and cannot satisfy the higher temporal and spatial resolutions at the same time. Therefore, many experts and scholars have carried out research on multisource data fusion technology to complement data from different sources, obtain as much spatial information and temporal features as possible, and obtain data with high spatial and temporal resolution. At present, fusion technology is mainly divided into two categories according to different goals: multisource data fusion technology that improves spatial resolution and temporal resolution. Through data fusion technology, the improvement of spatial resolution and the increase in spatial information can reduce the influence of mixed pixels on the accuracy, but there will still be certain errors, which will cause distortion of spectral information to a certain extent; for the improvement of temporal resolution, obtaining more specific time-series changes makes the temporal characteristic differences in ground objects more significant and reduces errors caused by the intersection of short-term phenological periods [20].

Due to the complex topography and changeable topography types in the study area, the distribution of ground objects is affected and the spatial heterogeneity is large. In addition, the agricultural planting structure in my country is complex and diverse, the fields are fragmented, the mixed pixel phenomenon is serious, and the fragmentation of the fields and other factors will also affect the classification accuracy of remote sensing. The accurate identification of ground objects and the correct classification of land use types require high spatial resolution of remote sensing data [21–23]. On the one hand, a reasonable model is used to decompose the mixed pixels, which can improve the classification accuracy to a certain extent. Jia et al. believed that the temporal features extracted from low-resolution images are of great significance for improving the classification accuracy of high spatial resolution remote sensing images; in particular, for vegetation types, the classification results have higher accuracy.

Multisource data fusion technology generally uses a certain method to process and operate remote sensing data from different sensor sources and different spatial

resolutions according to certain rules to obtain higher spatial resolution. This information includes spectral reflectance, backscattering coefficient, and time-series vegetation index. These methods are generally based on color correlation techniques, such as HIS transform method, or based on statistical methods, such as PCA, and Brovey and wavelet transform. The more extensive is in the data fusion of low spatial resolution and medium resolution with a certain time series.

Considering the texture features, spatial features, and other information of the study area is of great significance to further improve the accuracy of land use classification. The research shows that considering the spatial distribution characteristics and mutual correlation of ground objects can effectively make up for the shortcomings of pixel classification methods based on remote sensing images. Shao Wei et al. obtained the regional slope distribution law from the DEM statistical information of each category and used it as a classification rule in the classification postprocessing, which improved the problem of missing classification of some land categories. Jia et al. used the multitemporal HJ-1 satellite CCD data in 2010 as the main data source, supplemented by Landsat TM image, DEM, slope, and feature index data, and adopted the object-oriented classification method to extract the Guanzhong plain artificial surface information, higher classification accuracy. The object-based image analysis methods such as Jiang Fan comprehensively used the spectrum, texture, shape, slope, and other characteristics of image objects to realize the thematic mapping of land use/land cover in Qinqiangchuan area in various periods. It improves the classification efficiency and increases the reliability of the classification results. In addition, with the development of time-series analysis [24–28], some researchers combine time-series analysis methods to analyze.

3. Land and Building Research Model Based on Multisource Data Fusion

3.1. Research Area. Zhenning County is located in the southwest of the hilly plains in the central part of Guizhou, at $105^{\circ}35'10''$ – $106^{\circ}0'50''$ east longitude and $25^{\circ}25'19''$ – $26^{\circ}10'32''$ north latitude. The county has a land area of 1713.3 km^2 , and the terrain is high in the north and low in the south, with a large slope variation, with an altitude of 356–1678 m. Zhenning County is a typical karst area, with a mountainous area of 1098 km^2 and a hilly area of 157.8 km^2 , accounting for 64.08% and 9.21% of the county's total area, respectively. Karst landforms are widely distributed, accounting for more than 60% of the county's total area. The bedrock is mostly limestone, sand shale, dolomitic limestone, and siliceous limestone, and the soil is mostly yellow soil, red-yellow soil, and black lime soil.

3.2. Data Sources. CBERS data and ASAR data are taken as multisource remote sensing data sources. CBERS data come from the resource environment cloud platform, ASAR data come from ESA, and DEM data with 30 m resolution are

selected as auxiliary classification data. CBERS images have a large number of spectrums and have the advantages of better definition and higher geometric accuracy, but they also have some disadvantages such as a certain degree of fringe dislocation and poor resistance to atmospheric interference. ASAR images have high spatial resolution, all-weather, penetrability to the surface and clouds, and diversity of information carriers.

3.3. Image Preprocessing. CBERS data adopt the software ENVI 5.0 software, first synthesize the first 4 bands, select UTM for image projection, select ground control points (GCPs), perform geometric correction and fusion on the 5th band, and then use Zhenning County vector data to align the CBERS data. The CBERS image is cropped, and finally, the cropped data are processed by image transformation and enhancement to generate the CBERS image of the study area. After the ASAR data are processed by speckle noise removal, image calibration, filtering, and geometric correction are carried out, the ASAR image of the study area is cropped, and the CBERS and ASAR remote sensing images within the study area are fused by the high-pass filter (HPF) fusion method, to generate HPF fusion data.

3.4. Classification of Land Use Types. In this study, the random forest classification method is used to classify the study area, and the sample and feature space of each type of ground object are defined as the reference basis for classification, and the classification is performed according to the statistical characteristics of the image itself and the distribution of natural point groups. According to the research object and the standard of the national land use classification system, the land use types are divided into 8 categories: grassland, buildings or rocks, mountains, sloping farmland, forest land, other forest land, water body, and open land.

The random forest (RF) algorithm is a nonlinear and nonparametric classifier proposed by Breiman et al. in 2001, which allows the fusion of high-dimensional data from multiple sources, and has a high tolerance for missing values and outliers. It is suitable for high-dimensional complex datasets and can automatically judge the importance of variables. It takes the decision tree as the basic unit, integrates several decision trees through the idea of ensemble learning, uses multiple trees to train and predict the samples, and uses voting to determine the classification results of the samples. By constructing different sample training sets, random forest expands the difference between the classification models of decision tree, thereby improving the extrapolation prediction ability of the combined classification model. After obtaining a classification model sequence $\{h_1(X), h_2(X), \dots, h_K(X)\}$ through K rounds of training, a multiclassification model system is formed at this time, and the final classification result is obtained by adopting a simple majority voting decision. The classification decision is as follows:

$$H(x) = \operatorname{argmax} \sum_{i=1}^K I(h_i(x) = Y), \quad (1)$$

where $H(x)$ represents the combined classification model, h_i represents the single decision tree classification model, Y represents the output variable, and $I(\cdot)$ is the indicative function. In the process of constructing the random forest classification algorithm, it is necessary to set the number of decision trees and ensure the maximum number of features when the model is optimal. In this study, the grid search cross-validation method was used for parameter optimization. Through a large number of experiments, it is found that the error gradually converges and tends to be stable when it is set to 300. At this time, the maximum number of features is set to the square root of the total number of features n .

3.5. Classification Result Evaluation Method. In the accuracy evaluation, the sampling method is used to replace the whole image with some pixels or some categories to evaluate the accuracy of the image. Image accuracy refers to the degree of agreement between an image whose quality is unknown and a hypothetically accurate reference image or an image in the training area of a ground truth sample. An error matrix (or confusion matrix) is established to calculate various statistics and perform statistical tests and finally give the classification accuracy values for the overall and based on various ground types, error and misclassification error 4 indicators.

3.5.1. Drawing Accuracy. The likelihood is that the classifier can assign a pixel in a picture to class A, assuming the ground truth is class A. It is used to reflect how good or bad the method of producing this graph is.

$$P_{AJ} = \frac{P_A \text{ area}}{P_j \text{ area}}, \quad (2)$$

where P_{AJ} is the percentage, $P_A \text{ area}$ is the PA area, and $P_j \text{ area}$ is the PJ area.

3.5.2. User Precision. Assuming that the classifier assigns cells to class A, the corresponding ground truth class is the likelihood of A. It reflects the credibility of each category in the classification map, that is, the reliability of the map.

$$P_{Ui} = \frac{P_U \text{ area}}{P_i \text{ area}}, \quad (3)$$

where P_{Ui} is the percentage, $P_U \text{ area}$ is the PU area, and $P_i \text{ area}$ is the Pi area.

The mapping accuracy and user accuracy correspond to the missed classification error and misclassification error. The missed classification error shows how many of the actual objects of a certain type are wrongly classified into other

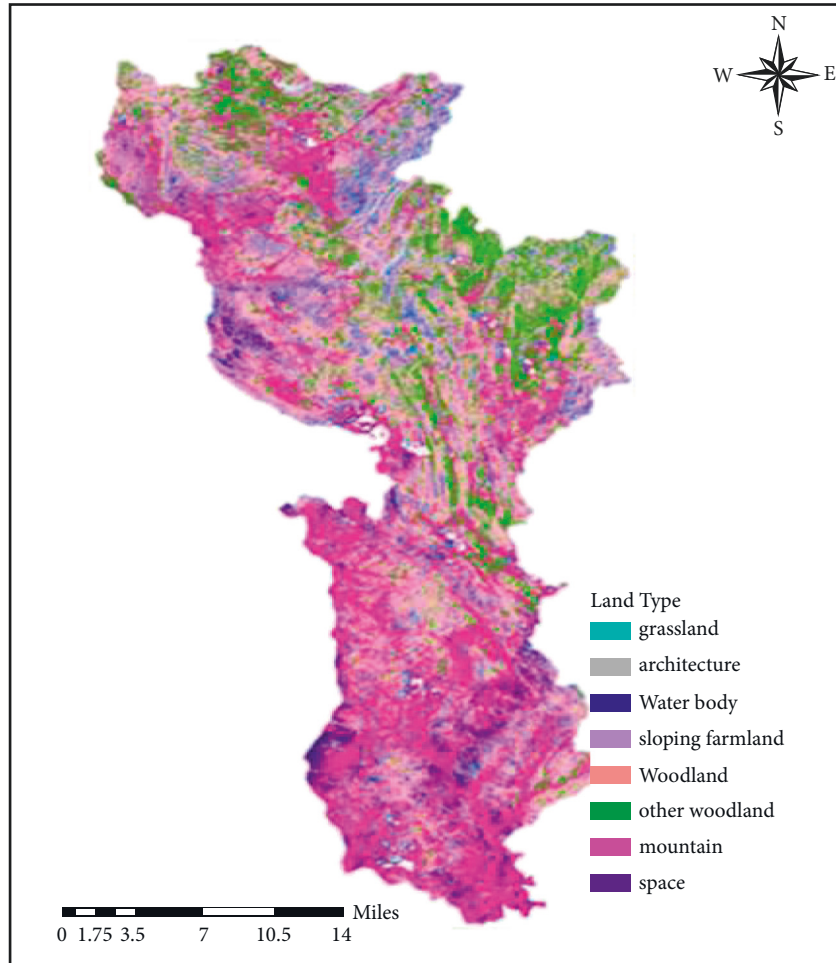


FIGURE 1: Classification of land use types in CBERS images.

categories, while the misclassification error shows how many of the objects classified as a certain type in the image should actually belong to other categories, the misclassification error is complementary to the mapping accuracy, and the misclassification error is complementary to the user's accuracy. 1 sampling point representing 8 land use types is selected on the CBERS image and HPF fusion image, respectively, a total of 16 sampling points, and each sampling point has an area of 667 m^2 ; a record table for the field survey and verification content of the land use types of the sampling points are formulated; field investigation and verification of sampling points are carried out, land use type information data are recorded in detail, the data of sampling points are summarized and counted to establish an error matrix formed by four indicators of mapping accuracy, user accuracy, missed classification error, and wrong classification error. The results of land use type information extracted from HPF fusion images were analyzed and evaluated.

4. Results and Analysis

4.1. Extract Results. The results of extracting land use type information based on CBERS images are shown in Figure 1, and the results of extracting land use type information based on HPF fusion images are shown in Figure 2.

4.2. Precision Analysis of Classification Results. The results and analysis of land use type information extraction are obtained based on CBERS images. Table 1 provides the results of land use type information extracted based on CBERS images: except for grassland types and other forest land types, which have relatively low accuracy, other types have relatively high accuracy and good classification effects. The architectural or rock mapping accuracy is 93.6%, and the user accuracy is 96.9%; the water system mapping accuracy and user accuracy are both 100%; the slope farmland

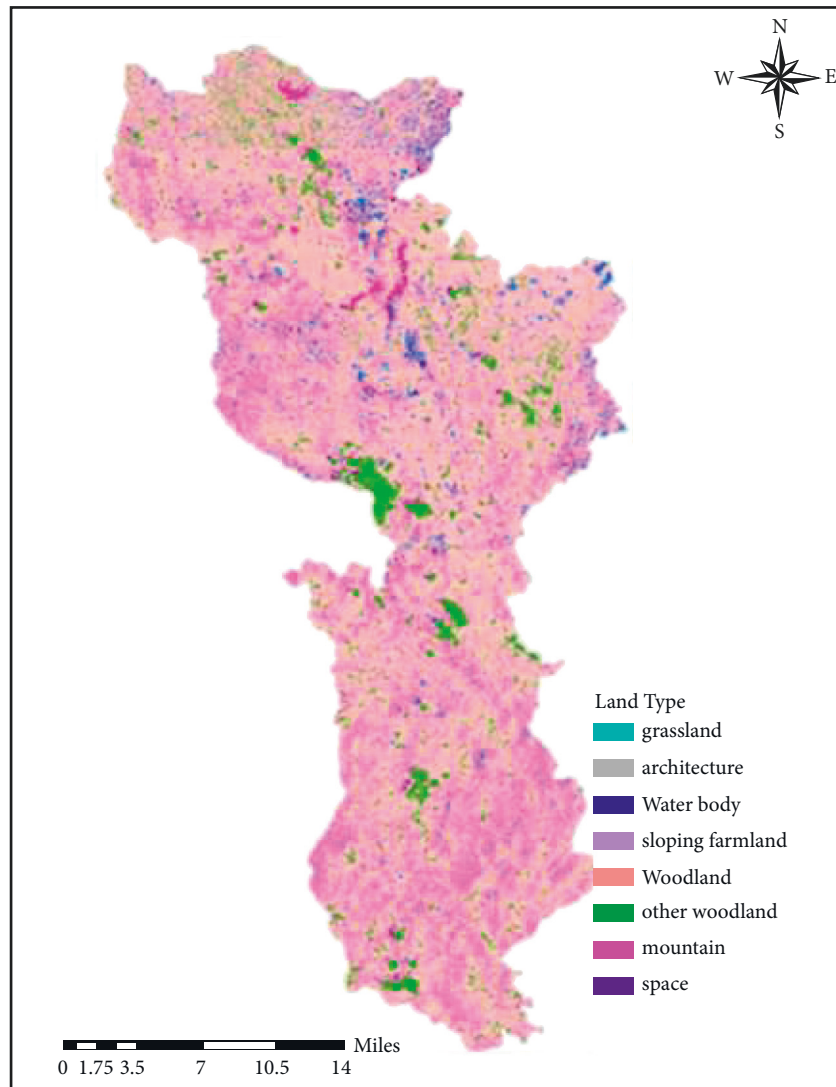


FIGURE 2: Classification of land use types of HPF fusion images.

TABLE 1: Error matrix of land use type information extraction results based on CBERS image and HPF fusion image.

Land use type		Field survey area (m ²)								Sum
		Grassland	Building or rock	Mountain	Sloping farmland	Woodland	Other woodland	Water body	Space	
CBERS image	Grassland	564	0	0	0	0	13	0	6	583
	Building or rock	7	638	0	0	0	0	16	12	659
	Mountain	10	0	651	7	0	0	0	0	670
	Sloping farmland	23	0	14	612	0	0	0	48	692
	Woodland	26	0	0	0	610	540	0	0	690
	Other woodland	36	0	0	15	58	113	0	0	714
	Water body	0	0	0	0	0	0	652	0	652
	Space	0	30	3	34	0	0	0	608	675
	Sum	668	668	668	668	668	668	668	668	5344
HPF fusion image	Grassland	642	0	0	1	15	0	1	0	659
	Building or rock	0	652	20	0	0	0	0	0	672
	Mountain	0	0	648	3	0	0	0	0	651
	Sloping farmland	0	16	0	663	0	0	0	0	679
	Woodland	0	0	0	0	638	0	0	0	638
	Other woodland	12	0	0	1	15	667	0	1	696
	Water body	14	0	0	0	0	0	667	0	681
	Space	0	0	0	0	0	1	0	667	668
	Sum	668	668	668	668	668	668	668	668	5344

mapping accuracy is 91.9%, and the user accuracy is 88.8%; the forest land mapping accuracy is 91.6%, and the user accuracy is 91.6%. The accuracy is 87.5%; the mountain mapping accuracy is 95.7%, and the user accuracy is 100.0%; the air-ground mapping accuracy is 91.2%, and the user accuracy is 89.9%. From Table 1, it can be seen that the mapping accuracy of grassland types is relatively low, and the phenomenon of missing classification is relatively serious. There are many pixels that belong to grassland types that are divided into other woodlands, but the user accuracy is high, and the misclassification error is small. The main reason is the spectral characteristics of CBERS. In the image, the texture and tone of each land use type are more obvious and easy to distinguish; the user accuracy of other forest land is low, and the misclassification error reaches 15.2%. The image boundary between shrubland and tree forest is not obvious, which leads to misclassification.

The results and analysis of land use type information extraction are obtained based on HPF fusion images. Table 2 provides the results of land use type information extracted based on HPF fusion images: each land use type has high mapping accuracy and user accuracy, and the missed classification error and misclassification error are small, and the classification effect is better. The water system mapping accuracy and user accuracy are both 100%; the grassland mapping accuracy is 96.5%, and the user accuracy is 98.8%; the building or rock mapping accuracy is 98.5%, and the user accuracy is 100%; the mountain system mapping accuracy is 97.1%, and the user accuracy is 97.1%; sloping farmland mapping accuracy is 96.3%, and user accuracy is 98.2%;

forest land mapping accuracy is 98.2%, and user accuracy is 97.9%; other forest land mapping accuracy is 96.1%, and user accuracy is 96.3%; open land mapping accuracy is 96.1%, and the user accuracy is 92.1%; the mapping accuracy and user accuracy of all land use types have reached more than 96%. From Table 2, it can be seen that only the other two types of forest land and open land are prone to misclassification, and there is a misclassification error, but the errors are small, all less than 10%, indicating that the HPF fusion image extracts land use type information with high accuracy, which is more accurate than fusion. The higher image resolution is related to the clearer texture, tone, and boundary of the image patch of land use type.

4.3. Classification Result Accuracy Evaluation. In general, HPF fusion images are better than CBERS images in extracting land use type information. In terms of user accuracy, the three land use types of water body, building or rock, and mountain body extracted from HPF fusion images can reach 100% accuracy, while CBERS images only reach 100% for mountain types, indicating that the range of land use types extracted from HPF fusion images is wider. The user accuracy of HPF fusion images is above 90%, and there are not many misclassifications, indicating that the extraction effect of HPF fusion images is significantly better than that of CBERS images. In terms of mapping accuracy, HPF fusion images extract water and open space types, and the accuracy reaches 100%, while CBERS images can only reach 100% for water types; in addition to water types, the

TABLE 2: Accuracy evaluation of land use type information extraction results based on CBERS images and HPF fusion images.

Land use type	CBERS image				HPF fusion image			
	Drawing accuracy (%)	Drawing accuracy (%)	User accuracy (%)	Misclassification error (%)	Drawing accuracy (%)	Drawing accuracy (%)	User accuracy (%)	Misclassification error (%)
Grassland	84.5	14.9	97.1	3.6	96.5	3.4	98.8	1.3
Building or rock	93.6	5.8	96.9	3.2	98.5	1.2	100.0	0.0
Mountain	95.7	3.5	100.0	0.0	97.1	2.3	100.0	0.0
Sloping farmland	91.9	8.1	88.8	11.5	96.3	3.1	98.2	1.2
Woodland	91.6	8.4	87.5	12.3	98.2	1.6	97.9	2.0
Other woodland	89.9	10.5	84.1	15.2	96.1	3.5	96.3	3.2
Water body	100.0	0.0	97.6	2.5	100.0	0.0	100.0	0.0
Space	91.2	9.8	89.9	10.8	100.0	0.0	92.1	7.3

mapping accuracy of other land use types and HPF fusion image accuracy all are higher than CBERS images, indicating that the HPF fusion images have less missed classification and better results in extracting land use type information.

5. Conclusion

Aiming at the combination of multisource remote sensing data and monitoring the change in land planning, this study conducts an in-depth study and discussion on the land use change in this area. Using CBERS image and HPF fusion image as data sources, HPF remote sensing image fusion is carried out, and the random forest classification method is used to extract it. The land use type information of Zhenning County and the results are as follows:

- (1) In general, the extraction of land use type information based on HPF fusion images has fewer missed points, and the effect of extracting land use type information is better. In terms of extracting water body types, the accuracy of both CBERS image and HPF fusion image has reached 100%, and both have the same effect; for the extraction of other land use type information, the accuracy of HPF fusion image is higher than that of CBERS image, and the effect of HPF fusion data is better than that of CBERS image.
- (2) Using CBERS and ASAR images for HPF fusion, generating HPF fusion images, and extracting land use type information from HPF fusion images are one of the effective ways to improve the accuracy of land use type classification

Data Availability

The data used to support this study are available from the corresponding author upon request.

Conflicts of Interest

The authors declare that there are no conflicts of interest.

References

- [1] R. Urrutia-Goyes and N. Ornelas-Soto, "The importance of land use definition in human health risk assessment related to lead in soils," *BioMed Research International*, vol. 2019, pp. 1–9, 2019.
- [2] S. N. Mahiga, P. Webala, M. J. Mware, and P. K. Ndong'ang'a, "Influence of land-use type on forest bird community composition in mount Kenya forest," *International Journal of Ecology*, vol. 2019, pp. 1–8, 2019.
- [3] Y. H. Ran, X. Li, L. Lu, and Z. Y. Li, "Large-scale land cover mapping with the integration of multi-source information based on the Dempster-Shafer theory," *International Journal of Geographical Information Science*, vol. 26, no. 1, pp. 169–191, 2012.
- [4] S. Liu, H. Su, R. Zhang et al., "Based on the Gaussian fitting method to derive daily evapotranspiration from remotely sensed instantaneous evapotranspiration," *Advances in Meteorology*, vol. 2019, pp. 1–13, 2019.
- [5] S. Park, K. C. Clarke, C. Choi, and J. Kim, "Simulating land use change in the seoul metropolitan area after greenbelt elimination using the SLEUTH model," *Journal of Sensors*, vol. 2017, pp. 1–18, 2017.
- [6] A. K. Hua, "Land use land cover changes in detection of water quality: a study based on remote sensing and multivariate statistics," *Journal of Environmental and Public Health*, vol. 2017, pp. 1–12, 2017.
- [7] W. Chen, R. He, and Q. Wu, "A Novel Efficiency Measure Model for Industrial Land Use Based on Subvector Data Envelope Analysis and Spatial Analysis Method," *Complexity*, vol. 2017, 2017.
- [8] D. Amarsaikhan, H. H. Blotevogel, J. L. van Genderen, M. Ganzorig, R. Gantuya, and B. Nergui, "Fusing high-resolution SAR and optical imagery for improved urban land cover study and classification," *International Journal of Image and Data Fusion*, vol. 1, no. 1, pp. 83–97, 2010.
- [9] S. F. Torres Mallma, "Mainstreaming land use planning into disaster risk management: trends in Lima, Peru," *International Journal of Disaster Risk Reduction*, vol. 62, p. 102404, 2021.
- [10] C. Wang, Z. Guo, S. Wang, L. Wang, C. Ma, and T. Jiao, "Improving hyperspectral image classification method for fine land use assessment application using semisupervised machine learning," *Journal of Spectroscopy*, vol. 2015, pp. 1–8, 2015.

- [11] S. Qadri, D. M. Khan, S. F. Qadri et al., "Multisource data fusion framework for land use/land cover classification using machine vision," *Journal of Sensors*, vol. 2017, pp. 1–8, 2017.
- [12] N. Farzana, W. Cherie, B. Noble, K. Belcher, and P. Lloyd-Smith, "Evaluation of alternative land-use scenarios using an ecosystem services-based strategic environmental assessment approach[J]," *Land Use Policy*, vol. 108, 2021.
- [13] S. Jerez, I. Dzib, and M. De la Sen, "A discrete method based on the CE-SE formulation for the fractional advection-dispersion equation," *Discrete Dynamics in Nature and Society*, vol. 2015, no. Pt.1, pp. 1–9, 2015.
- [14] H. Nathan, J. E. Gonzalez, and G. A. Isaac, "Impacts of aerosol particle size distribution and land cover land use on precipitation in a coastal urban environment using a cloud-resolving mesoscale model[J]," *Advances in Meteorology*, vol. 2014, no. Pt.1, 2014.
- [15] N. Caceres and F. G. Benitez, "Supervised land use inference from mobility patterns," *Journal of Advanced Transportation*, vol. 2018, pp. 1–12, 2018.
- [16] J. Yang, W. Liu, Y. Li, X. Li, Q. Ge, and M. Santos, "Simulating Intraurban Land Use Dynamics under Multiple Scenarios Based on Fuzzy Cellular Automata: A Case Study of Jinzhou District, Dalian," *Complexity*, vol. 2018, 2018.
- [17] S. N. Zudilin and Y. S. Iralieva, "Automation of land use planning based on geoinformation modeling," *IOP Conference Series: Earth and Environmental Science*, vol. 720, no. 1, p. 012039, 2021.
- [18] T. Lv, Li Wang, H. Xie, X. Zhang, and Y. Zhang, "Exploring the global research trends of land use planning based on a bibliometric analysis: current status and future prospects," *Land*, vol. 10, no. 3, p. 304, 2021.
- [19] R. Anna, P. Guido, L. Fabio, F. Francesco, and T. Laura, "GIS-based landslide susceptibility mapping for land use planning and risk assessment," *Land*, vol. 10, no. 2, 2021.
- [20] N. Xochitl, C.-G. Leticia, J. Rodríguez-Valadez Francisco, and S. Georgina, "Evaluation of yarrowia lipolytica oil for biodiesel production: land use oil yield, carbon, and energy balance.[J]," *Journal of lipids*, vol. 2018, 2018.
- [21] S. Schmidt and C. Barron, "Mapping impervious surfaces precisely—a GIS-based methodology combining vector data and high-resolution airborne imagery," *Journal of Geovisualization and Spatial Analysis*, vol. 4, no. 1, p. 14, 2020.
- [22] M. Masoudi, P. Jokar, and E. Ramezanipour, "A GIS-based quantitative model for land use planning in larestan county, Iran[J]," *EQA - International Journal of Environmental Quality*, vol. 40, no. 0, 2020.
- [23] T. Fasth, S. Bohman, A. Larsson, L. Ekenberg, and M. Danielson, "Portfolio decision analysis for evaluating stakeholder conflicts in land use planning," *Group Decision and Negotiation*, vol. 29, no. 2, pp. 321–343, 2020.
- [24] Z. Jia, X. Cai, Y. Hu, J. Ji, and Z. Jiao, "Delay propagation network in air transport systems based on refined nonlinear Granger causality[J]," *Transportation Business: Transport Dynamics*, pp. 1–13, 2022.
- [25] Z. Jia, X. Cai, and Z. Jiao, "Multi-modal physiological signals based squeeze-and-excitation network with domain adversarial learning for sleep staging[J]," *IEEE Sensors Journal*, 2022.
- [26] W. Ellen, "Land use planning, climate change, and changing natural hazards[J]," *Planning News*, vol. 46, no. 1, 2020.
- [27] Z. Jia, Y. Lin, J. Wang et al., "Multi-view spatial-temporal graph convolutional networks with domain generalization for sleep stage classification," *IEEE Transactions on Neural Systems and Rehabilitation Engineering*, vol. 29, pp. 1977–1986, 2021.
- [28] Z. Jia, Ji Junyu, X. Zhou, and Y. Zhou, "Hybrid Spiking Neural Network for Sleep EEG Encoding," *Science China Information Sciences*, 2022.

Retraction

Retracted: Meta-Analysis of Knee Joint Function Recovery after Anterior Cruciate Ligament Reconstruction by Accelerated Rehabilitation Surgery

Computational Intelligence and Neuroscience

Received 25 July 2023; Accepted 25 July 2023; Published 26 July 2023

Copyright © 2023 Computational Intelligence and Neuroscience. This is an open access article distributed under the Creative Commons Attribution License, which permits unrestricted use, distribution, and reproduction in any medium, provided the original work is properly cited.

This article has been retracted by Hindawi following an investigation undertaken by the publisher [1]. This investigation has uncovered evidence of one or more of the following indicators of systematic manipulation of the publication process:

- (1) Discrepancies in scope
- (2) Discrepancies in the description of the research reported
- (3) Discrepancies between the availability of data and the research described
- (4) Inappropriate citations
- (5) Incoherent, meaningless and/or irrelevant content included in the article
- (6) Peer-review manipulation

The presence of these indicators undermines our confidence in the integrity of the article's content and we cannot, therefore, vouch for its reliability. Please note that this notice is intended solely to alert readers that the content of this article is unreliable. We have not investigated whether authors were aware of or involved in the systematic manipulation of the publication process.

Wiley and Hindawi regrets that the usual quality checks did not identify these issues before publication and have since put additional measures in place to safeguard research integrity.

We wish to credit our own Research Integrity and Research Publishing teams and anonymous and named external researchers and research integrity experts for contributing to this investigation.

The corresponding author, as the representative of all authors, has been given the opportunity to register their agreement or disagreement to this retraction. We have kept a record of any response received.

References

- [1] J. Xu, M. Zheng, Z. Feng, L. Pan, and Z. Peng, "Meta-Analysis of Knee Joint Function Recovery after Anterior Cruciate Ligament Reconstruction by Accelerated Rehabilitation Surgery," *Computational Intelligence and Neuroscience*, vol. 2022, Article ID 5085143, 8 pages, 2022.

Research Article

Meta-Analysis of Knee Joint Function Recovery after Anterior Cruciate Ligament Reconstruction by Accelerated Rehabilitation Surgery

Junxiang Xu , Minzhe Zheng, Zongxian Feng, Lingxiao Pan, and Zhaoxiang Peng

Orthopedics department Ningbo Medical Center Lihuili Hospital, Ningbo 315000, China

Correspondence should be addressed to Junxiang Xu; 631607010126@mails.cqjtu.edu.cn

Received 9 May 2022; Revised 6 June 2022; Accepted 10 June 2022; Published 29 June 2022

Academic Editor: Dong Chen

Copyright © 2022 Junxiang Xu et al. This is an open access article distributed under the Creative Commons Attribution License, which permits unrestricted use, distribution, and reproduction in any medium, provided the original work is properly cited.

Objective. This investigation was undertaken to systematically assess the impact of increasingly rapid recovery treatment on the functional status of the knee following anterior cruciate ligament restructuring. **Methods.** Computer search from the establishment of the database to March 2022 in China Knowledge Network Database (CNKI), PubMed, EMBASE, ScienceDirect, CochraneLibrary, China VIP Database, Wanfang Database, and China Biomedical Literature Database (CBM). The control group was given only traditional rehabilitation training, and the observation group was treated with perioperative accelerated rehabilitation surgery intervention randomized controlled trial (RCT). Data for all included studies were extracted by two independent researchers, and the risk of bias for the quality of each included study was assessed by the Cochrane Handbook 5.1.0 criteria. Meta-analysis of the collected data by using RevMan5.4 statistical software. **Results.** A total of 593 articles were retrieved from the computer database and 8 RCT articles with a total of 636 samples were finally included for meta-analysis. According to the Jadad scale, the RCT score of 8 articles was ≥ 4 points. Meta-analysis was performed on the postoperative VAS scores of the ERAS group and the traditional rehabilitation group, and the heterogeneity test showed $\chi^2 = 288.60$, $df = 5$, $P < 0.00001$, and $I^2 = 99\%$. There was a statistically significant difference in the postoperative VAS scale between the intervention and the traditional rehabilitation model ($P < 0.05$). Eight articles reported the effect of accelerated rehabilitation surgery on the recovery of knee joint motion after ACL rehabilitation. After meta-analysis, the heterogeneity test showed $\chi^2 = 314.98$, $df = 7$, $P < 0.00001$, and $I^2 = 98\%$, and it can be concluded from the analysis that, compared with the traditional rehabilitation model, the enhanced rehabilitation surgery has an effect on the joint function after anterior cruciate ligament reconstruction. The improvement effect was more significant, and the difference was statistically significant ($P < 0.05$). Four articles reported the effect of enhanced recovery after surgery intervention on the range of motion of the knee joint of patients, the heterogeneity test showed $\chi^2 = 117.52$, $df = 2$, $P < 0.00001$, and $I^2 = 98\%$, through analysis, and compared with the traditional rehabilitation model and the enhanced recovery. The effect of surgery on the range of motion of the knee joint after ACL reconstruction was more significant, and the difference was statistically significant ($P < 0.05$). The effect of enhanced recovery after surgery and traditional rehabilitation mode on the incidence of postoperative adverse reactions in patients undergoing ACL reoperation was analyzed. The results of heterogeneity test showed that $\chi^2 = 1.59$, $df = 2$, $P = 0.66 > 0.05$, and $I^2 = 98\%$, and the analysis showed that, compared with the traditional rehabilitation mode, enhanced rehabilitation surgery can significantly reduce the risk of adverse reactions after anterior cruciate ligament reconstruction ($P < 0.05$). An inverted funnel plot was used to analyze publication bias in studies with quality of life as an outcome measure. The results showed that Egger's test $P = 0.0005 < 0.001$ suggesting that there may be a certain degree of publication bias. **Conclusion.** The existing research evidence shows that accelerating the reconstruction of anterior cruciate ligament can effectively promote the recovery of knee joint function, reduce the pain of patients, and reduce postoperative complications. However, more research is needed to further verify this.

1. Introduction

The knee joint anterior cruciate ligament (ACL) is one of the crucial structures to keep the knee joint stable. Rupture can lead to anterior instability and further cause knee joint subsidiary damage [1–3]. The anatomical basis, tissue structure, and biomechanical function of ACL, as well as regional economic and social factors, determine the epidemiological characteristics of ACL. ACL injury is different from other types of knee joint diseases. The particularity of ACL injury has different distribution of injured patients, and the injury mechanism of ACL also has its unique performance. According to the report, the overall incidence of former cross patients in the United States is 100/300,000, while the prevalence rate of people engaged in special sports, such as football or basketball, is as high as 60/100,000, and that of skiers is 70/100,000, which is significantly higher than that of the general population [4]. And, because the knee ligament relaxation of female is higher than that of male, the muscle strength of posterior group of thigh is worse, and the diameter of ACL is smaller, so the incidence of ACL injury in female is significantly higher than that in male. At the same time, sports injury is the main cause of ACL injury. Some steering movements require higher stability of the knee joint, while producing greater traction and torsion load; sports enthusiasts often ignore the practice of muscle strength when they focus on their favorite sports, and the low level of physical quality makes the knee joint lack of reliable muscle protection during exercise, which increases the risk of injury of knee joint ACL and other stable structures. At present, arthroscopy-assisted ACL reconstruction has been very mature, and the basic research and clinical research on ACL injury and treatment at home and abroad have been very extensive and in-depth, mainly focused on the anatomical reconstruction of ligament, biomechanical reconstruction, tendon healing, renewal of fixation methods and fixation materials, durability of graft, arthroscopic minimally invasive reconstruction, postoperative rehabilitation, research and development of advanced surgical equipment, etc.

The stiffness of knee joint after ACL damage is a hot topic studied at home and abroad for many years. The postoperative recovery of knee joint function is generally poor, and this problem needs to be seriously studied and solved. In addition, the anatomical and histological features of the ACL determine its poor blood supply [5]. Therefore, after the rupture of the anterior cruciate ligament, conservative treatment cannot restore the original state. The functional instability of the affected limb cannot be corrected by nonoperative treatment [6–8] and cannot meet the needs of patients. However, with further research, most experts believe that early surgical reconstruction is needed after ACL injury, which can regain the anterior knee joint stabilization and correct rotation and prevent the further aggravation of intra-articular secondary injury. This is of great significance to the management of complications, the protection of meniscus, the protection of articular cartilage, and the protection of other ligaments in the joint.

With the progress of arthroscopic surgery, arthroscopic ACL reconstruction has become a routine treatment for

ACL injury and multiple ligament injuries of the knee joint [9]. However, a series of symptoms represented by the limitation of limb movement after ACL reconstruction is a great obstacle to the recovery of limb function after the operation. Miao Shuai et al. [10] proposed that the incidence of joint stiffness and the limitation of limb movement after ACL reconstruction after ACL injury for 3 or more weeks were lower. However, a study by Guo et al. [11] and Lin et al. did not find any great differences in the incidence of joint adhesion between early and late reconstruction of ACL injury [11, 12].

The current literature [11, 13] has proved that accelerating rehabilitation surgery can promote the cases' knee joint functional recovery after ACL restructure, but the study has not been randomly assigned, and the sample size is small and lack of credibility. Therefore, through meta analysis, this study quantitatively synthesized the published randomized controlled trials (RCT), expanded the sample size, increased the statistical efficiency and the accuracy of estimated effect values, and enhanced the reliability and objectivity of the results [13]. In order to provide evidence-based evidence for postoperative rehabilitation of patients with knee anterior cruciate ligament injury.

2. Research Contents and Methods

2.1. The Sources and Retrieval Methods of Documents. Computer search was carried out from the establishment of the database to March 2022 in China Knowledge Network Database (CNKI), PubMed, EMBASE, ScienceDirect, CochraneLibrary, ChinaVIPDatabase, Wanfang Database, and China Biomedical Literature Database (CBM). The control group was given traditional rehabilitation training only, while the observation group was treated with accelerated rehabilitation surgery intervention (RCT). Literature retrieval was conducted in the way of free words and subject words, with the key words of accelerated rehabilitation surgery, nursing intervention, anterior cruciate ligament reconstruction, knee joint function, and so on.

2.2. Literature Inclusion Criteria and Exclusion Criteria

2.2.1. Literature Inclusion Criteria

- (1) Type of study: all domestic patients after ACL reoperation received a randomized control test of accelerated rehabilitation surgery and traditional rehabilitation intervention (RCT). The language was limited to Chinese.
- (2) Participants: CT, MRI, and other imaging methods were used to confirm the diagnosis of anterior cruciate ligament injury.
- (3) Intervention: control patients accepted rehabilitation training and experimental patients accepted accelerated rehabilitation surgery. The main results are as follows: (1) the mode of operation: anterior cruciate ligament reconstruction. (2) Intervention: the control group was given only traditional rehabilitation training, and the study group received

accelerated rehabilitation surgery during the peri-operative period. (3) Outcome indicators: peri-operative indicators (length of stay, postoperative complications, serum factor levels, etc.), quality of life score, VAS score, joint function score, and quality of life score.

2.2.2. Literature Exclusion Criteria. The literature exclusion criteria are as follows:

(1) It is not a randomized controlled study; (2) the data report is incomplete, and the data cannot be used; (3) repeat the research content and take the latest research; (4) the expression of the research index is not clear.

2.3. Quality Evaluation and Data Extraction

- (1) Quality evaluation: the qualities of the enrolled literature were assessed by the Jadad scale, which was evaluated according to random, blind method, and loss of follow-up/withdrawal. 0–5 points were used to count. When the literature quality is less than 2 points, it is lower, and when it is ≥ 3 points, it is higher. The specific evaluation is as follows: (1) random: (1) 2 points: “random distribution” is mentioned in the literature and described in detail and correctly. (2) 1 score: “random distribution” is only mentioned in the literature but not explained. (3) 0: the random allocation method/random allocation/pseudorandom allocation was not mentioned in the literature. (2) Blind method: (1) 2 points: the “double-blind” method is used in the literature, and the specific process is described correctly. (2) 1: the “double-blind” method is not specifically described in the literature. (3) 0: no “double-blind” method/method error. (3) withdrawal/loss of follow-up: (1) 1: the number and reasons of withdrawal and loss of follow-up are described in detail in the literature. (2) 0: it is not mentioned in the literature.
- (2) Data extraction: data for all included studies were extracted by two independent researchers, and the risk of bias for the quality of each included study was assessed by the Cochrane Handbook 5.1.0 criteria. When the two people had differences, they reached an agreement through consultation. It includes study author, publication time, sample size, treatment method, and curative effect evaluation method.

2.4. Statistical Processing. RevMan5 software originated from the Cochrane Collaboration Network for Meta Analysis. The mean and standard deviation of the net change difference of serum albumin, prealbumin, and hemoglobin in the experiment and the control cohorts were input into RevMan5 for analysis. Because the index is a continuous variable, the weighted mean difference (WMD) is used as the effect scale, and 95% confidence interval is selected. First, the X^2 test is used to determine whether there is heterogeneity between the studies. If $P > 0.05$ and $I^2 < 50\%$, it is considered

that the included study is homogeneous, and the modified impact model can be collected for meta-analysis; if $P < 0.05$ and $I^2 \geq 50\%$, when judging the homogeneity of the included study, the combined effect is needed and then choose the random effect model; if $P < 0.05$ and the source of heterogeneity could not be judged, meta analysis was not performed, and descriptive analysis was used.

3. Results and Analysis

3.1. Literature Search Results and Basic Information of Included Literature. 593 articles were retrieved through computer database retrieval, 281 articles were obtained after excluding duplicate studies, 136 articles were obtained through preliminary reading of the titles and abstracts of the articles, irrelevant studies, reviews, case reports, and uncontrolled articles were excluded, and 35 articles were initially included, and then the full text of the literature was carefully read, 27 literature with incomplete data and no primary outcome indicators were excluded, and 8 RCTs were finally included with overall 636 cases for meta analysis. The general aspects of the collected publications are displayed in Table 1.

3.2. Evaluation of the Quality of the Methodology Included in the Literature. Eight RCT articles included in this meta-analysis reported the baseline of patients, of which five RCT were randomized by random number table, and the other three articles did not mention the specific method of random grouping. Among them, 7 studies all gave detailed intervention measures, and 3 studies did not specify the follow-up time. The number and reasons of blind method and loss of follow-up or withdrawal were not described in detail in eight RCT articles. According to the Jadad scale, we can see that eight articles have RCT scores ≥ 4 . The results are shown in Table 2. The results of the literature quality evaluation showed that five articles [12, 15–18] were of low risk and three [19–21] were of medium risk. The studies that were rated as medium-risk mainly showed distribution hidden bias and report bias. Risk bias is shown in Figure 1.

3.3. Meta Analysis Result

3.3.1. VAS Scoring. Through the meta-analysis postoperative VAS scores of 636 samples from the 8 ERAS groups compared with the traditional rehabilitation group in the RCT study, the postoperative VSA scores were revealed in the overall enrolled six articles. The heterogeneity test showed that $\text{Chi}^2 = 288.60$, $\text{df} = 5$, $P < 0.00001$, and $I^2 = 99\%$, indicating that there was heterogeneity among the included research data. The postoperative VAS scores of patients after ACL reconstruction using enhanced recovery surgery intervention were significantly different from those of the traditional rehabilitation model ($P < 0.05$). The results are shown in Figure 2.

3.3.2. Lysholm Scoring. The effect of accelerated rehabilitation surgery on patients' knee joint functional after ACL

TABLE 1: Basic information of included studies.

Included literature	Year of publication	N (T/C)	Study group interventions	Control group interventions	Follow-up time	Observation indicator
Guo et al. [13]	2022	30/30	Accelerated rehabilitation surgery	Traditional rehabilitation	12 months	①②④
Lin et al. [12]	2020	61/57	Accelerated rehabilitation surgery	Traditional rehabilitation	Unknown	①②③
Qin et al. [14]	2020	43/42	Accelerated rehabilitation surgery	Traditional rehabilitation	6 months	①②④
Zhang et al. [15]	2020	44/44	Accelerated rehabilitation surgery	Traditional rehabilitation	Unknown	②④
Xu et al. [16]	2020	37/38	Accelerated rehabilitation surgery	Traditional rehabilitation	3 months	①②③④
Zhao et al. [17]	2021	37/38	Accelerated rehabilitation surgery	Traditional rehabilitation	Unknown	①②
Ge et al. [18]	2021	50/25	Accelerated rehabilitation surgery	Traditional rehabilitation	2 weeks after operation	①②
Yan et al. [19]	2020	30/30	Accelerated rehabilitation surgery	Traditional rehabilitation	On the day of discharge	1 ②

Note: ① VAS score; ② knee joint function score; ③ postoperative complication; ④ range of motion of joint.

TABLE 2: Results of methodological quality evaluation.

First author and year of publication	Random	Randomized hiding	Blind method	Withdrawal and dropouts	Total	Quality grade
Guo et al. [13]	2	1	1	1	5	High
Lin et al. [12]	1	1	1	1	4	High
Qin et al. [14]	2	1	1	1	5	High
Zhang et al. [15]	2	1	1	1	5	High
Xu et al. [16]	2	1	1	1	5	High
Zhao et al. [17]	1	1	1	1	4	High
Ge et al. [18]	1	1	1	1	4	High
Yan et al. [19]	2	1	1	1	5	High

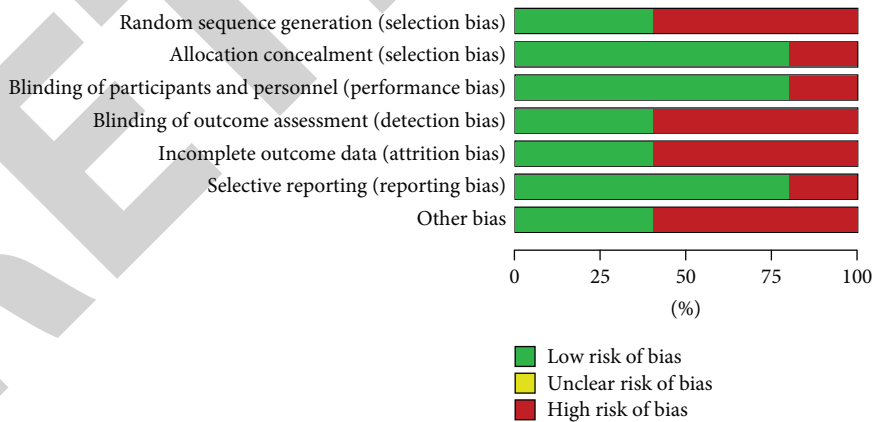


FIGURE 1: Risk of bias assessment of included studies.

reconstruction was reported in 8 literature studies. Meta analysis with random effect model showed that $\text{Chi}^2 = 314.98$, $df = 7$, $P < 0.00001$, and $I^2 = 98\%$, indicating that there was heterogeneity among the included research data. Compared with the traditional rehabilitation model, accelerated rehabilitation surgery has a more significant effect on the joint functional improvement after ACL reconstruction ($P < 0.05$). The results showed that the effect of

accelerated rehabilitation surgery on the joint function of patients after anterior cruciate ligament reconstruction was significantly better than that of traditional rehabilitation mode. The results are shown in Figure 3.

3.3.3. Range of Motion of Knee Joint. Among the eight articles included in the study, four reported the effect of

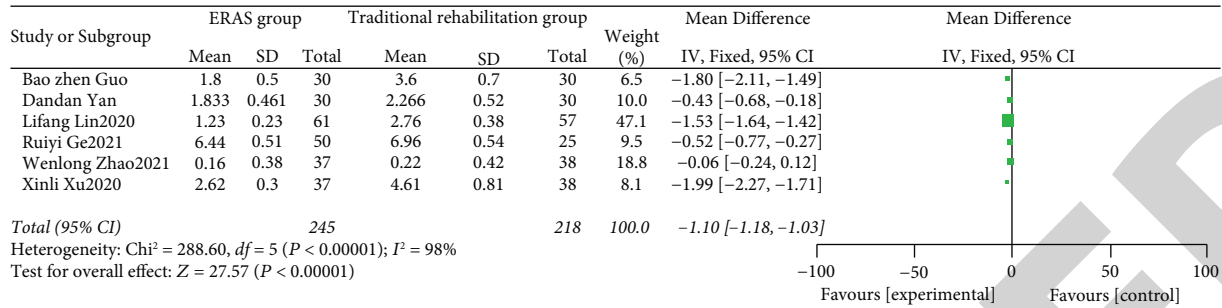


FIGURE 2: Forest plot of the impacts of accelerated rehabilitation surgery on the VAS scale.

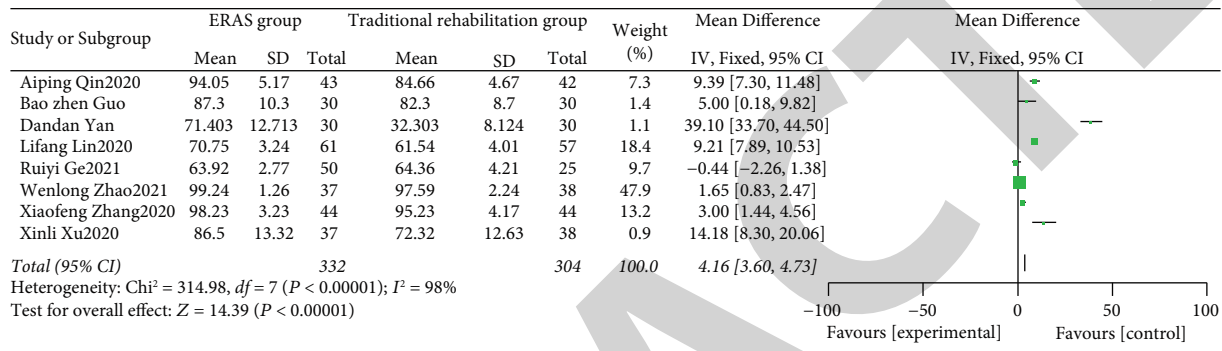


FIGURE 3: Forest plot of the joint function recovery.

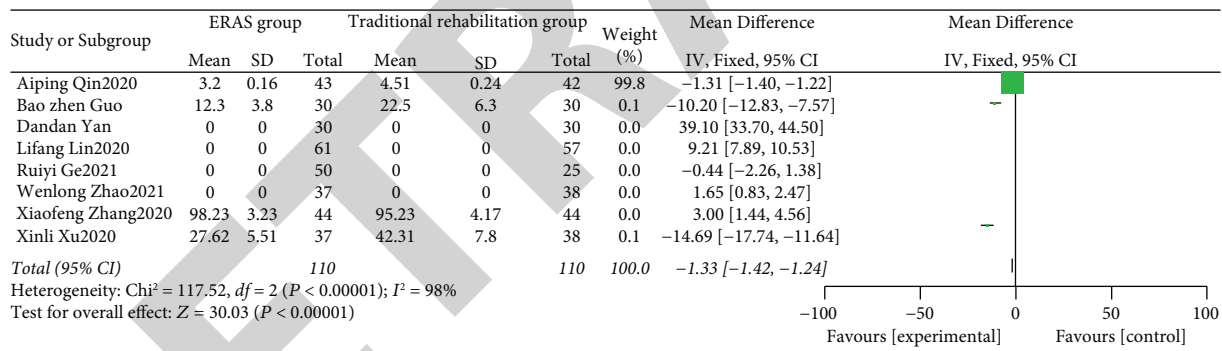


FIGURE 4: Forest plot of effect of accelerated rehabilitation surgery on the range of motion of knee joint.

accelerated rehabilitation surgical intervention on the range of motion of patients' knee joints. The heterogeneity test displayed $\chi^2 = 117.52$, $df = 2$, $P < 0.00001$, and $I^2 = 98\%$, indicating that there is heterogeneity among the included research data. Compared with the traditional rehabilitation model, accelerated rehabilitation surgery has a more significant effect on the scope of knee joint movements after ACL reconstruction ($P < 0.05$). The results are shown in Figure 4.

3.3.4. Complication. Four studies with extractable adverse reactions were analyzed by meta-analysis. The main adverse reactions included joint cavity effusion, joint cavity hemorrhage, infection, adhesive arthritis, and nerve injury, and no serious adverse reactions were reported. The effects of accelerated rehabilitation surgery and traditional rehabilitation model on the incidence of postoperative adverse reactions in patients with

anterior cruciate ligament reconstruction were compared with those in these four studies. The results of heterogeneity test showed that $\chi^2 = 1.59$, $df = 2$, $P = 0.66 > 0.05$, and $I^2 = 98\%$, indicating that there was no obvious heterogeneity among the included data, and the combined effect of WMD was analyzed by the fixed effect model. The combined effect size WMD test is $Z = 4.31$ ($P < 0.00001$). According to the analysis results, it can be considered that compared with the traditional rehabilitation mode, the use of enhanced recovery surgery can significantly reduce the number of patients after ACL rebuilding. The risk of adverse reactions was greatly distinct ($P < 0.05$). The results are shown in Figure 5.

3.3.5. Publication Bias Analysis. An inverted funnel plot was used to analyze the publication bias of studies with quality of life as the outcome indicator. The results are shown in Figure 6. The

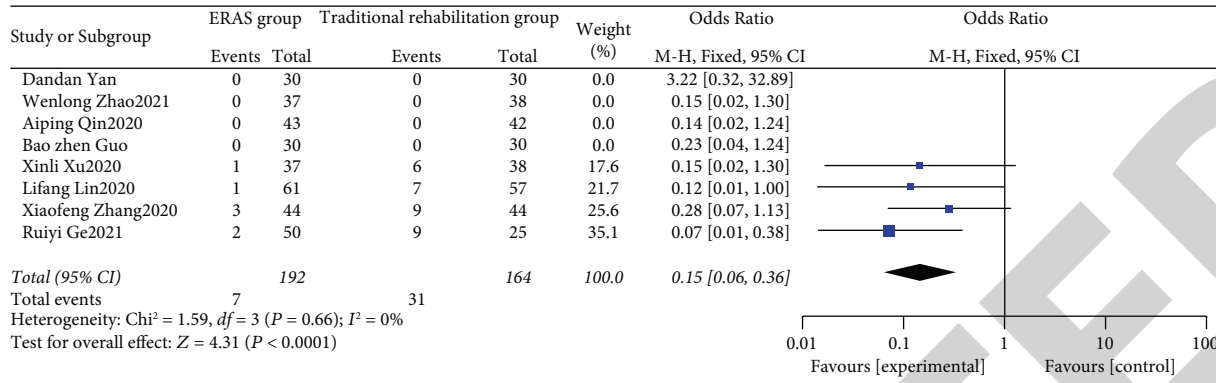


FIGURE 5: Forest plot of impacts of accelerated rehabilitation surgery on postoperative complications.

results showed that the graphs were not completely symmetrical, and the Egger's test showed $P = 0.0005 < 0.001$, suggesting that there may be a certain degree of publication bias.

4. Analysis and Discussion

Anterior cruciate ligament (ACL) is of remarkable meaningful for keeping the knee joint anterior stability and controlling the knee joint rotation. It is divided into the anterior medial bundle and the posterior lateral bundle. Its special anatomical characteristics determine that the tension of the two bundles of the knee joint is different during movement and changes accordingly with the extension and flexion of the knee joint. The anatomical position of the anteromedial ligament of the tibia determines its function, which mainly restricts the forward movement of the tibia and prevents the tibia from being damaged during movement. The anatomical position of the posterolateral bundle determines its function, which mainly restricts the backward movement of the knee joint. Therefore, the mechanism of its stability is to prevent the tibia from slipping forward in the joint during knee flexion, to prevent knee joint hyperextension during knee extension, and to actively control knee joint rotation and valgus under different knee flexion angles. According to Noyes's previous biomechanical tests, ACL assumed most of the antagonistic forces of the anterior drawer test when the knee was flexion 90° and the tibia was in a neutral position. ACL damage can cause knee joint instability to varying degrees and influence the knee joint functional activities, and the ACL rupture changes the stress form of meniscus and intra-articular cartilage itself. Therefore, to restore knee joint function to normal activity level as far as possible, most doctors advocate that ligament reconstruction should be actively carried out for patients with ACL [22]. Accelerating rehabilitation program is a more active rehabilitation strategy. It can reduce joint adhesion and increase joint range of motion in order to restore the intact structure and stabilization of the injured knee joint and eliminate the knee joint complications under conservative treatment [23].

With the renewal of the concept of knee rehabilitation, the recovery level of postoperative motor ability has been greatly

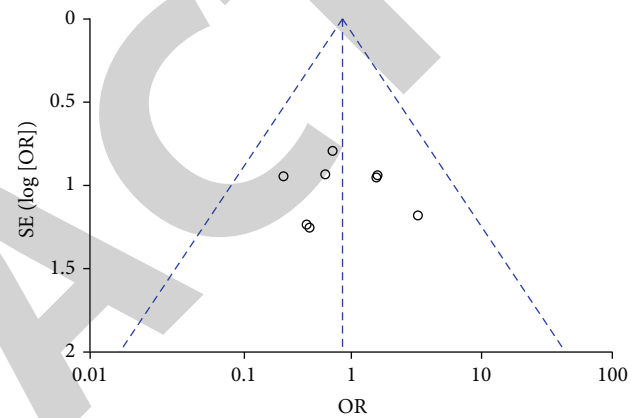


FIGURE 6: Inverted funnel plot of the impact of accelerated restore operation on the life quality of patients.

improved in the past 30 years. Accelerated rehabilitation surgery (ERAS) is a perioperative management method based on evidence-based medicine, which can reduce surgical trauma, reduce physical and psychological trauma stress, accelerate patient recovery, shorten hospital stay, and reduce hospitalization costs [24]. At the same time, it is a new type of perioperative medical cooperation project with surgery, anesthesiology, nursing, rehabilitation therapy, and so on. It includes reasonable perioperative management, such as fast-track anesthesia, minimally invasive surgery, best analgesic techniques, early postoperative feeding, and early getting out of bed. ERAS takes patient safety as the premise and rapid recovery as the goal, integrates various perioperative medical and nursing measures, and allows patients to pass through the perioperative period "safely and quickly." There was no significant difference between the accelerated rehabilitation program and the conventional rehabilitation program in joint range of motion, muscle strength, and stability, but the rehabilitation time was significantly longer than that of the conventional rehabilitation program [25, 26]. Early out-of-bed exercise and functional training can improve the symptoms of limited joint movement after ACL reconstruction, mostly in cases where knee joint movement is strictly restricted after the operation. Joint range of motion and weight-bearing activity aggravate lower limb muscle atrophy to some extent and promote the recovery of knee

joint function [27]. The concept of early active rehabilitation is to carry out functional exercise of rehabilitation nature as soon as possible, which can help shorten the time for functional recovery of the knee joint and help improve the effect of knee joint surgery [14, 28]. Although early studies have shown that accelerated rehabilitation programs do not adversely affect the prognosis of patients like conventional rehabilitation programs [29]. Most rehabilitation programs for ACL reconstruction take 6 months as a cycle.

At present, there is still a lack of high-level evidence-based evidence about the value of accelerated rehabilitation surgery [30]. Based on this, through meta-analysis, this paper systematically evaluates the effect of accelerated rehabilitation surgery on knee joint functional recovery after ACL reconstruction, so as to provide evidence-based reference for clinical treatment. Totally, eight RCT studies with overall 636 patients were enrolled in this investigation. Six of them scored postoperative VAS. A meta-analysis was performed on the postoperative VAS scores in these 6 studies. There was a large discrepancy in the following surgery VAS score between patients after enhanced rehabilitation surgery intervention for anterior cruciate ligament reconstruction and the traditional rehabilitation model ($P < 0.05$). Eight reported the effect of accelerated rehabilitation surgery on the knee joint functional restore after ACL operation. The effect of accelerated rehabilitation surgery on joint function of patients after anterior cruciate ligament reconstruction was more significant than that of traditional rehabilitation model ($P < 0.05$). Of the eight studies included in the study, four reported the effect of enhanced recovery after surgery intervention on the range of motion of the knee joint of patients. According to the different intervention measures, it was found that compared with the traditional rehabilitation model, upon the use of enhanced recovery after surgery, the improvement effect on the scope of knee joint motion in patients after ACL reoperation was more significant ($P < 0.05$). Four studies on the number of extractable ADR cases were analyzed by meta-analysis, and the occurrence of ADR was reported in all 4 studies. The main adverse reactions included articular effusion, articular hemorrhage, infection, adhesive arthritis, and nerve injury. No serious adverse reactions were reported. Among the eight articles included, four articles compared the effects of accelerated rehabilitation surgery and traditional rehabilitation model on the incidence of postoperative adverse reactions in patients with anterior cruciate ligament reconstruction. Accelerated rehabilitation surgery can significantly reduce the risk of adverse reactions in patients after ACL reoperation ($P < 0.05$). Among the studies included in this analysis, some studies have been observed for a short time, and the recovery of joint function is a long-term and chronic process. The effect of accelerated rehabilitation surgery on the knee joint functional improvement after ACL reoperation may be more significant after long-term follow-up, but the actual effect still needs a lot of studies to confirm.

Data Availability

No data were used to support this study.

Conflicts of Interest

The authors declare that they have no conflicts of interest.

Acknowledgments

This study was financially supported by the Effect of Macrophage Polarization on Proliferation and Differentiation of Tendon Stem Cells (2022KY1089).

References

- [1] H. Mistry, A. Metcalfe, J. Colquitt et al., "Autograft or allograft for reconstruction of anterior cruciate ligament: a health economics perspective," *Knee Surgery, Sports Traumatology, Arthroscopy*, vol. 27, no. 6, pp. 1782–1790, 2019.
- [2] P. A. Smith, D. M. Thomas, R. J. Pomajzl, J. A. Bley, F. M. Pfeiffer, and J. L. Cook, "A biomechanical study of the role of the anterolateral ligament and the deep iliotibial band for control of a simulated pivot shift with comparison of minimally invasive extra-articular anterolateral tendon graft reconstruction versus modified lemaire reconstruction after anterior cruciate ligament reconstruction," *Arthroscopy: The Journal of Arthroscopic & Related Surgery*, vol. 35, no. 5, pp. 1473–1483, 2019.
- [3] O. Riaz, A. Aqil, A. Mannan et al., "Quadriceps tendon-bone or patellar tendon-bone autografts when reconstructing the anterior cruciate ligament: a meta-analysis," *Clinical Journal of Sport Medicine*, vol. 28, no. 3, pp. 316–324, 2018.
- [4] C. Jin, E. K. Song, Q. H. Jin, N. H. Lee, and J. K. Seon, "Outcomes of simultaneous high tibial osteotomy and anterior cruciate ligament reconstruction in anterior cruciate ligament deficient knee with osteoarthritis," *BMC Musculoskeletal Disorders*, vol. 19, no. 1, pp. 1–6, 2018.
- [5] D. T. Trung, S. L. Manh, L. Nguyen Thanh, T. Chu Dinh, and T. Chu Dinh, "Preliminary result of arthroscopic anterior cruciate ligament reconstruction using anterior half of peroneus longus tendon autograft," *Open Access Macedonian Journal of Medical Sciences*, vol. 7, no. 24, pp. 4351–4356, 2019.
- [6] A. Rusanov, L. Kravchuk, O. Rusanova, Z. Vitaly, and S. Olga, "Physical Rehabilitation of patients who underwent the reconstruction of anterior cruciate ligament with arthroscopic surgical interventions," *Journal of Physical Education and Sport*, vol. 18, pp. 1896–1901, 2018.
- [7] X. Gu and X. Wei, "A meta analysis of early versus delayed reconstruction of anterior cruciate ligament injuries in adolescents is associated with the risks of meniscus and articular cartilage injury," *Osteoarthritis and Cartilage*, vol. 28, no. S1, p. 78, 2020.
- [8] L. Yang, C. Zou, Y. Mi, and Z. Wang, "All-inside reconstruction of anterior cruciate ligament with single-bundle autogenous peroneal longus tendon," *Orthopaedic Journal of Sports Medicine*, vol. 9, no. 62, pp. 11–12, 2021.
- [9] R. Gupta and A. Gupta, "A recent follow-up study on reconstruction of anterior cruciate ligament by arthroscopic free hamstring transplantation and retaining inserted hamstring transplantation," *Journal of Contemporary Medical Practice*, vol. 3, no. 2, Article ID 18019, 2021.
- [10] "Accelerated rehabilitation programme after arthroscopic reconstruction of anterior cruciate ligament," *Eur J Ther*, vol. 15, no. 1, p. 10, 2019.
- [11] B. Guo, J. du, and L. Wang, "Effect of accelerated rehabilitation surgery on function after anterior cruciate ligament

Research Article

Xingnao Kaiqiao Acupuncture Method Combined with Temporal Three-Needle in the Treatment of Acute Ischemic Stroke: A Randomized Controlled Trial

Zhongtao Song , Qingyuan Huang, Yuxia Guo, Xiaodong Song, Xuan Zhang, and Huajun Xiao

Meizhou People's Hospital, Meizhou 514031, Guangdong, China

Correspondence should be addressed to Zhongtao Song; 2016150190@jou.edu.cn

Received 11 May 2022; Revised 1 June 2022; Accepted 6 June 2022; Published 29 June 2022

Academic Editor: Dong Chen

Copyright © 2022 Zhongtao Song et al. This is an open access article distributed under the Creative Commons Attribution License, which permits unrestricted use, distribution, and reproduction in any medium, provided the original work is properly cited.

Objective. The objective of this study was to investigate the difference between the clinical effectiveness of two acupuncture methods in the treatment of acute ischemic stroke (AIS) and provide more evidence-based medical evidence of acupuncture's effectiveness in stroke rehabilitation. **Methods.** We conducted an outcome assessor-and data analyst-blinded, randomized, and controlled trial. Seventy-two participants were randomly allocated to the observation group and control group with a 1 : 1 allocation ratio by the generating of a random number table. The observation group received the "Xingnao kaiqiao" acupuncture method combined with "Temporal three needles," and the control group received conventional acupuncture "Scalp acupuncture" combined with the traditional "body acupuncture" method. The acupuncture treatment was performed once per day for one week by trained acupuncturists. Both groups underwent secondary prevention of cerebral infarction and received a 3-months' followup. After a 1-week acupuncture intervention, the changes of NIHSS (National Institutes of Health Stroke Scale) scores, Percent Change and Absolute Change of NIHSS scores, MBI (Modified Barthel Index), and the rate of MBI ≥ 80 in two groups were observed. After 3 months' followup, the mRS (Modified Ranking Scale) and the clinical efficacy of the two groups were compared. **Results.** The apparent efficiency rate of the observation group was 63.9%, higher than 19.4% of the control group, and the difference was significant ($P < 0.05$). After treatment, NIHSS scores, Percent Change, and Absolute Change of NIHSS scores in the observation group had a significant reduction than the control group (all $P < 0.05$). MBI in the observation group increased significantly more than in the control group ($P < 0.05$), but the rate of MBI ≥ 80 in the two groups was not significantly different ($P > 0.05$). After 3 months' of followup, the mRS score frequencies of the observation group were not statistically different from the control group ($P > 0.05$). The rate of mRS scores of 0–1 in the observation and control group were 55.6% and 38.9%, and there was no significant difference either ($P > 0.05$). **Conclusion.** Compared with "Scalp acupuncture" combined with "body acupuncture," "Xingnao kaiqiao" acupuncture method combined with "Temporal three-needle" had superiority in the improvement of neurological deficit, potential functional disability, and score of basic activities of daily living. As to the independent rate to basic activities of daily living and good prognosis of 3 months, there were no statistical differences.

1. Introduction

Ischemic stroke, with the common impairments that include motor and sensory loss or alteration [1], seriously affects the quality of life of patients and causes a tremendous burden to the whole society. Acute ischemic stroke is the most important stage to develop effective early interventions to

improve the prognosis for patients. Currently, administration of recombinant tissue plasminogen activator (rtPA) within 3 h of stroke onset improves clinical outcomes, large vessel occlusions that fail to open with intravenous (IV) rtPA alone are candidates for endovascular revascularization [2]. Endovascular therapy coupled with mechanical thrombectomy is the preferred choice to improve the reperfusion rate

TABLE 1: Comparison of general data between two groups.

Groups	<i>n</i>	Gender		Youngest	Age (years)		Time since stroke onset (days)		
		Male	Female		Eldest	Average ($\bar{x} \pm s$)	Shortest	Longest	<i>M</i> (P_{25}, P_{75})
Observation	36	19	17	33	87	67.28 ± 13.34	0.25	14	2(1–3.75)
Control	36	21	15	45	87	66.17 ± 10.69	0.25	14	2(1–4)
Statistical value		0.225 ^a				0.390 ^b			0.034 ^c
<i>P</i> -value		0.635				0.698			0.973

a. χ^2 -value; b. *t*-value; c. *Z*-value.

[3]. However, both therapies are severely restricted by the treatment time window [4] and the related risk of bleeding concerns patients and their families greatly.

Acupuncture, widely used for thousands of years in China [5], play an important role in the rehabilitation treatment for the patients with ischemic stroke. Up to now, there are two main representative methods involving scalp acupuncture combined with traditional body acupuncture and “Xingnao kaiqiao” (restoring consciousness and inducing resuscitation) acupuncture technique [6]. Intending to investigate the difference between the effectiveness of two acupuncture methods in the treatment of acute ischemic stroke, we conduct an outcome assessor-and data analyst-blinded, randomized, and controlled trial.

2. Clinical Data

2.1. General Data. All participants were collected from in-patients from the Department of Chinese Medicine and Neurology of Meizhou People’s Hospital, from May 1, 2019 to January 1, 2021. A total of 72 patients were included and they were randomly allocated to the observation group and control group with a 1 : 1 allocation ratio by the generating of a random number table. There were 36 cases in the observation group, aged from 33 to 87 years old, averagely (67.28 ± 13.34) years old, with the time since stroke onset 0.25 to 14 days, the Median (P_{25}, P_{75}) of which is 2(1–3.75) days. In the control group, 36 cases aged from 45 to 87, averagely (66.17 ± 10.69) years old, with the time since stroke onset 0.25 to 14 days, the Median (P_{25}, P_{75}) of which is 2(1–4) days. Regarding the age and disease duration of the subjects, there was no significant difference between groups, which made them comparable. The protocol was approved by the ethics committee of Meizhou People’s Hospital on April 9, 2019. Table 1 shows the comparison of general data between the two groups.

2.2. Diagnosis Criteria. The diagnosis criteria of traditional Chinese medicine were in reference with the standard for diagnosis and efficacy evaluation of stroke (Trial); the diagnosis criteria of western medicine were in reference with the diagnostic criteria of acute ischemic stroke according to the Chinese guidelines for diagnosis and treatment of acute ischemic stroke 2018 [1].

2.3. Inclusion Criteria. Patients are eligible for study inclusion if they: (1) were aged 18–80 years; (2) met the diagnostic criteria of acute ischemic stroke; (3) the onset was less than 2 weeks and the vital signs were stable; (4) there

were obvious physical activity, language dysfunction and other symptoms; (5) Glasgow coma scale (GCS) > 8; (6) First onset or previous stroke without neurological deficit; (7) were willing to accept and complete the course of treatment; (8) patients or family members informed consent to accept the clinical trial.

2.4. Exclusion Criteria. Patients will be excluded if they have any one of the following: (1) the patient was diagnosed with hemorrhagic stroke; (2) the patient had taken thrombectomy or intravenous thrombolysis; (3) the patient had serious cardiovascular, liver, kidney, or hematopoietic system disease; (4) the patient had an infection of the respiratory system, urinary system, digestive system, or other parts of the body; (5) the patient was a pregnant or lactating woman; (6) the patient had psychotic, dementia, or others problems that unable to cooperate with treatment; (7) the patient had neurological deficit or motor dysfunction caused by past or other reasons.

2.5. Withdrawal or Dropout Criteria. Participants will be terminated to continue this trial according to the following criteria: (1) the participants who have a deteriorated condition or have had a serious adverse event; (2) the participants who suffer from certain complications or specific physiological changes during the study may not be appropriate to continue; (3) the participants who fail to complete the course of treatment.

3. Treatment Methods

All patients were given second prevention of ischemic stroke in accordance with the Chinese guidelines for the diagnosis and treatment of acute ischemic stroke, to monitor and control the high blood pressure, high cholesterol, sugar metabolic disorder, and risk factors such as diabetes.

3.1. Observation Group. Received “Xingnao kaiqiao” acupuncture method combined with “Temporal three-needle,” the parameters of which were set as follows:

- (1) Acupoint: Neiguan (PC6, bilateral), Renzhong (DU26, unilateral), Sanyinjiao (SP6, unilateral), Temporal three-needle (unilateral, the affected side).

The point location has referred the nomenclature and location of acupuncture points (GB/T12346-2006) [7], temporal three-needle is one of Jin’s three-needle therapy systems created by Professor Jinrui,

the temporal I needle is located on the hairline 2 cun above the apex of the ear; the temporal II needle and the temporal III needle are located 1 cun from the temporal I needle on either side in the horizontal direction [8].

- (2) Acupuncture manipulation: participants were asked to adopt a supine position, then Neiguan (PC6) was punctured bilaterally to a depth of 0.5–1.0 cun and stimulated with the reducing method by lifting and thrusting with simultaneous twirling manipulation for 1 min. After this, Renzhong (DU26) was punctured obliquely toward the nasal septum to a depth of 0.3–0.5 cun with bird-pecking needling until the eyes became wet or developed tears. Subsequently, Sanyinjiao (SP6) was punctured on the affected side obliquely along with the medial border of the tibia and at a 45° angle to the skin to a depth of 0.5–1.0 cun, with lifting and thrusting reinforcing manipulation, thrusts with heavy strength and lifting with gentle strength until calf twitch for 3 times. At last, the temporal three-needle was punctured in sequence at an approximately 15-degree angle to a depth of 0.8–1.2 cun, with the needle rotated for at least 200 revolutions per minute for 1 minute.

3.2. Control Group. “Scalp acupuncture” combined with “body acupuncture” method was received once per day for 1 week. The parameters for “scalp acupuncture” combined with the “body acupuncture” acupuncture method are set as follows:

- (1) Acupoints: the motor area of Jiao’s scalp acupuncture (unilateral, the affected side), Jianyu (LI15, unilateral), Quchi (LI11, unilateral), Waiguan (SJ5, unilateral), Hegu (LI4, unilateral), Yanglingquan (GB34, unilateral), Zusanli (ST36, unilateral), Fenglong (ST40, unilateral), Kunlun (BL60, unilateral). Acupoint location has referred the Nomenclature and Location of acupuncture Points (GB/T12346-2006) [7]. The motor area of Jiao’s scalp acupuncture is a line starting from a point (known as the upper point of the motor area) 0.5 cm posterior to the midpoint of the anterior-posterior midline of the head and stretching diagonally to the juncture between the eyebrow-occipital line and the anterior border of the corner of the temporal hairline, which is indistinct. Draw a vertical line upwards from the middle point of the zygomatic arch to the eyebrow-occipital line; the intersection of the two lines is the projection of the motor area [9]. The motor area of the cerebral infarction lesion’s side is selected as the site for acupuncture treatment, and the paralytic side is selected for the other acupoints.
- (2) Acupuncture manipulation: Participants were asked to adopt the supine position, then needles were manually inserted at an approximately 15-degree angle to a depth of 0.8–1.0 cun respectively along the line of the motor area on the scalp. The needles were

rotated for at least 200 revolutions per minute for 1 minute. For other acupoints, needles were punctured to a depth of 0.8–1.0 cun, then the lifting, thrusting, and twirling manipulation was performed until the sensation of Deqi. All the needles were retained for 30 minutes.

For acupuncture therapy mentioned in both groups, disposable stainless steel needles (size 0.30 mm × 40 mm, Tony brand, manufactured by Suzhou Medical Appliance) were used after routinely disinfecting the local skin of acupoints with 75% alcohol cotton swabs. The acupuncture treatment was performed once per day for one week by a trained acupuncturist with more than 3 years of clinical experience.

After the 1-week treatment observation, all patients will start an additional 3-month followup period. Because of the specificity of stroke patients’ recovery, patients from both groups would need to attend rehabilitation treatment during the followup period.

4. Therapeutic Effect Observation

4.1. Observation Indicators

4.1.1. NIHSS (National Institutes of Health Stroke Scale). The National Institutes of Health Stroke Scale, a 15-item scale, allows consistent reporting of neurological deficits in acute-stroke studies, which contains quantified basic neurological examination. The NIHSS provides an ordinal, nonlinear measure of acute stroke-related impairments by assigning numerical values to various aspects of neurological function [10]. NIHSS scores range from 0 to 42, with higher scores indicating a more severe neurological deficit. The NIHSS has a high reliability to observe after only a few hours of training, is easy and quick to assess and is a valid measure of stroke severity. In this study, the NIHSS was assessed at admission, after the interventional period (at 1 week). Percent Change NIHSS was defined as $[\text{admission NIHSS score} - 1\text{-week NIHSS score}] \times 100 / \text{admission NIHSS score}$. Absolute Change NIHSS was defined as $[\text{admission NIHSS score} - 1\text{-week NIHSS score}]$.

4.1.2. Modified Ranking Scale (mRS). The ranking scale was a scale introduced by Dr. John Rankin in 1957 and modified to its current form by Charles Warlow in the 1980s, which has grown in popularity for almost all acute stroke trials [11, 12]. The mRS is now the most commonly used functional measure in stroke trials and has been the primary or coprimary outcome in most recent large-scale stroke trials [10]. The mRS has many potential strengths, and it is well accepted by both patients and assessors, with a nonstandardized interview taking around 5 minutes to complete. There are seven potential scores on the mRS (0–6), describing a full range of stroke outcomes from perfect health without symptoms to death. In this trial, the mRS was assessed when the followup period ended (at 3 months). An mRS score of 0–1 is considered as a good recovery.

4.1.3. Modified Barthel Index (MBI). The Barthel Index is a scale that measures ten basic aspects of daily life activities related to self-care and mobility [13]. For the Chinese MBI version, the ten items are continence of bowels and bladder, feeding, dressing, entering and leaving a toilet, grooming, bathing, moving from a wheelchair to a bed and returning to a wheelchair, walking on a level surface for 45 m, and ascending and descending stairs. Each item (activity) can be divided into five levels; each level represents a different degree of independence, the lowest level being 1 and the highest being, and the higher the level, the greater the independence. The total possible score is 100. Subjects with an independent living ability score 80 or more; lower scores represent assisted or totally dependent living [14]. The MBI was assessed at admission, and after the interventional period (at 1 week).

4.2. Effect Criteria. The therapeutic effect evaluation standard was set as follows:

Basically cured: NIHSS score reduction $\geq 90\%$, and mRS = 0

Markedly effective: NIHSS score reduction $\geq 46\%$, but $< 90\%$, and mRS = 1, 2, 3

Effective: NIHSS score reduction $\geq 18\%$, but $< 46\%$

Invalid: NIHSS score reduction $< 18\%$

The Sum of basically cured and markedly effective cases were calculated for apparent efficiency rate.

4.3. Statistical Methods. SPSS 22.0 software (SPSS Inc., Chicago, IL, USA) was employed for all statistical analyses. Normal distribution quantitative data were expressed as $\bar{x} \pm s$ and analyzed by independent *t*-test or paired *t*-test, non-normal distribution quantitative data were expressed as *M* (*P*₂₅, *P*₇₅) and analyzed by Mann-Whitney test. The enumeration data were expressed as counts (percentages). The rank-sum test was adopted to analyze categorical data, and $P < 0.05$ indicated that the difference was statistically significant.

5. Results

5.1. Comparison of the Clinical Effect. The apparent efficiency rate of the observation group was 63.9%, higher than 19.4% of the control group, and the difference was significant ($P > 0.05$). The overall curative effect of the observation group was better than that of the control group ($P > 0.05$), as shown in Table 2.

5.2. Comparison of NIHSS Score (before and after Treatment) and Percent Change NIHSS. Before treatment, there was no statistical significance in NIHSS scores between the two groups ($P > 0.05$). After treatment, NIHSS scores in both groups were reduced than before (both $P < 0.05$), and the reduction in the observation group was more obvious compared with the control group. There was a statistical significance difference between the two groups ($P < 0.05$).

In a comparison of Percent Change and Absolute Change of NIHSS in the observation and control group, a significant difference was observed ($P < 0.05$) as shown in Tables 3 and 4.

5.3. Comparison of MBI (before and after Treatment) and the Percent of MBI ≥ 80 after Treatment. Before treatment, there was no statistical significance in MBI between the two groups ($P > 0.05$). After treatment, MBI in both groups were increased more than before, but the improvement in the observation group was more obvious and there was statistical significance between groups ($P < 0.05$). Although the percent of MBI ≥ 80 in the observation group was higher than that in the control group, but the difference was not statistically significant ($P > 0.05$) as shown in Table 5.

5.4. Comparison of mRS Score Frequencies after 3-Month Followup. After 3-month followup, mRS score frequencies of the observation group were not statistically different from the control group ($P > 0.05$). The rate of mRS score of 0–1 in the observation and control groups were 55.6% and 38.9%, and there was no significant difference ($P > 0.05$), although the proportion in the observation group had possible higher trend than that in the control group as shown in Table 6.

6. Discussion

The NIHSS within 1 week satisfies the requirements for a surrogate end point and may be used as a primary outcome measure in trials of acute treatment for ischemic stroke [15]. It measures neurological deficit rather than the functional outcome. The early NIHSS is a very useful primary outcome measure in clinical trials testing the effect of new therapeutic interventions for ischemic stroke. The 7-day relative neurological improvement on NIHSS can predict 90-day functional outcomes after therapeutic interventions better than the 24-hour relative neurological improvement [16]. Percent Change NIHSS and Absolute Change NIHSS have powerful abilities to predict the functional outcome of the patients with stroke, and Percent Change NIHSS has the better predictive ability [17]. In this study, the NIHSS score, Percent Change NIHSS, and Absolute Change NIHSS of the observation group improved more obviously than the control group, which marked a good outcome. Barthel Index is the most commonly used functional measure in stroke-rehabilitation settings and the second most commonly used functional outcome measure across stroke trials. Most Chinese researchers usually use a slightly modified edition of the BI to adapt to China's condition without changing the validity of this tool and the accuracy of responses. It is usually believed that subjects with MBI > 80 are generally independent. As Results showed previously, after a 1-week acupuncture intervention independent (to basic activities of daily living) rate of participants in the observation group was not significantly higher than the control group. Although the original Rankin Scale was not originally intended as an assessment for clinical trials, a slightly modified version of Rankin's eponymous scale was used as an end point in the

TABLE 2: Comparison of the clinical effect.

Groups	<i>n</i>	Basically cured	Markedly effective	Effective	Invalid	Apparent efficiency rate
Observation	36	4(11.1%)	19(52.8%)	3(8.3%)	10(27.8%)	63.9%
Control	36	4(11.1%)	3(8.3%)	11(30.6%)	18(58.0%)	19.4%
Statistical value			2.701 ^a			14.629 ^b
<i>P</i> -value			0.007			0.000

a.Z-value; b. χ^2 -value.

TABLE 3: Comparison of NIHSS score (before and after treatment).

Groups	<i>n</i>	NIHSS(before treatment)		NIHSS(after treatment)	
		<i>M</i> (<i>P</i> ₂₅ , <i>P</i> ₇₅)	Range	<i>M</i> (<i>P</i> ₂₅ , <i>P</i> ₇₅)	Range
Observation	36	4(3–7)	1–15	2(1–3.75) ^b	0–13
Control	36	5(3–9)	1–16	4(2–7) ^a	0–16
Z-value		0.958		2.928	
<i>P</i> -value		0.338		0.003	

TABLE 4: Comparison of percent change and absolute change of NIHSS.

Groups	<i>n</i>	Percent change NIHSS				Absolute change NIHSS <i>M</i> (min, max)
		≤25%	>25%, and ≤50%	>50%, and ≤75%	>75%	
Observation	36	4(11.1%)	19(52.8%)	3(8.3%)	10(27.8%)	2(–4,11)
Control	36	4(11.1%)	3(8.3%)	11(30.6%)	18(58.0%)	1(–3,6)
Z-value				–3.312		–2.780
<i>P</i> -Value				0.001		0.005

TABLE 5: Comparison of MBI (before and after treatment) and the percent of MBI ≥ 80 after treatment.

Groups	<i>n</i>	MBI (before treatment)		MBI (after treatment)		Percent of MBI ≥ 80
		<i>M</i> (<i>P</i> ₂₅ , <i>P</i> ₇₅)	Range	<i>M</i> (<i>P</i> ₂₅ , <i>P</i> ₇₅)	Range	
Observation	36	60(35–75)	20–100	85(65–100)	20–100	58.3%
Control	36	60(36.25–80)	20–100	65(40–85)	15–100	38.9%
Statistical value		0.384 ^a		–2.273 ^a		2.724 ^b
<i>P</i> -value		0.701		0.023		0.099

a.Z-value; b. χ^2 -value.

TABLE 6: mRS score frequencies after 3-month followup.

Groups	<i>n</i>	0	1	2	3	4	5	6	The rate of 0–1
Observation	36	8 (22.2%)	12 (33.3%)	7 (19.4%)	4 (11.1%)	5 (13.9%)	0 (0%)	0 (0%)	55.6%
Control	36	7 (19.4%)	7 (19.4%)	7 (19.4%)	10 (27.8%)	4 (11.1%)	1 (2.8%)	0 (0%)	38.9%
Statistical value					1.181 ^a				2.006 ^b
<i>P</i> -value					0.238				0.157

a.Z-value; b. χ^2 -value.

first multicenter stroke trial (the UK TIA study) [18]. Recent studies have quantified the responsiveness of the mRS and proven excellent construct and convergent validity of the scale. Now, the mRS has grown to be the most prevalent functional outcome measure in contemporary stroke trials and has been used in several landmark studies [19, 20]. As the results shown, the observation group failed to make a better recovery (3 months after acupuncture intervention) than the control group.

There are many acupuncture techniques in the treatment of ischemic stroke. Scalp acupuncture has shown a remarkable treatment efficacy on motor dysfunction in patients with stroke in China, especially in the motor area of Jiao's scalp acupuncture, which is the most widely used treatment [21]. Many studies have shown that scalp

acupuncture has a remarkable treatment efficacy on motor dysfunction in stroke patients in China. In clinical practice, scalp acupuncture often combines with traditional body acupuncture. The traditional body acupuncture treatment of stroke patients mostly selects acupoints on Yang meridians, which has the theoretical basis "To treat paralysis, take "Yangming Meridian alone" recorded in *Huangdi Neijing* (Inner Canon of the Yellow Emperor). The "Xingnao kaiqiao" acupuncture technique was developed by Xue-min Shi in 1972 for the treatment of stroke [22], especially ischemic stroke, based on traditional Chinese medicine theory, modern medicine theory, and clinical treatment experience over 30 years and made a great contribution [23]. It is a special acupuncture therapy system, that contained its own theory about the cause and pathogenesis of stroke, the

principle of treatment, the formula of acupoint selection, and the quantitative standard of acupuncture manipulation. It was totally different from the traditional acupuncture therapy. According to the “Xingnao kaiqiao” acupuncture theory, the most important pathogenesis of stroke is the hidden of mind induced by the occlusion of cerebral orifices. The principle of acupuncture treatment is based on “restoring consciousness and inducing resuscitation, nourishing the liver and kidney,” and “unblocking the meridians” as the supplement. Acupoints selected were mainly on Yin Meridians, and corresponding manipulations were quantitatively prescribed for the optimal stimulus amount and the objective response of the patients. Evidence from previous studies [24–26] has shown that the Xingnao Kaiqiao acupuncture achieved satisfactory treatment effects on stroke. But the contrast study of the curative effect between the two major acupuncture methods is rare. In order to compare the advantages of the two acupuncture methods in neurological deficit, quality of life, and good prognosis, we conducted this study.

Results of this study confirmed that the “Xingnao kaiqiao” acupuncture method combined with the “Temporal three-needle” had a better clinical efficacy on AIS than the conventional acupuncture method, as previous studies [27, 28] had shown. And, according to the results, the NIHSS score of the observation group significantly improved than the control group after a 1-week acupuncture intervention. Both Absolute Change and Percent Change of NIHSS in observation group were better than that in the control group which indicated the potential functional disability of participants got improved more effectively in the observation group. The “Xingnao kaiqiao” acupuncture method combined with the “Temporal three-needle” had advantages in improving neurological deficits and potential functional disability of patients with AIS. The MBI score of the observation group was significantly higher than the control group after a 1-week acupuncture intervention, which indicated the basic ability of daily living of patients in the observation group got improved better than the control group, but the ratio of $MBI \geq 80$ in the observation group was not significantly higher than that in the control group ($P > 0.05$). The independent (to basic activities of daily living) rate of patients in the two groups was not significantly different. The “Xingnao kaiqiao” acupuncture method combined with the “Temporal three-needle” had advantages in improving activities of daily living of patients with AIS, but failed to increase their independent rate of them. Based on the results mentioned above, mRS score frequencies of the observation group were not statistically different from the control group, so as the proportion of mRS score of 0–1. In other words, there was no significant difference in the prognosis between the two groups when the 3-month followup ended.

Modern research studies have shown that the “Xingnao Kaiqiao” acupuncture method has an obvious brain protective effect, of which mechanism may be interfering inflammatory response in the brain after cerebral ischemia reperfusion [29], regulating the opening of brain KATP channel, reducing neuronal apoptosis [30], and starting the

endogenous protection mechanisms from the overall level. Furthermore, the “Xingnao Kaiqiao” acupuncture improved the cognitive function of patients, and its mechanism may be related to down regulating the levels of serum MMP-2 and MMP-9 and increasing the level of IGF-1 [31]. Based on the above advantages, the “Xingnao Kaiqiao” acupuncture method has possibility to achieve a better curative effect. This study verified the therapeutic effect of the “Xingnao Kaiqiao” acupuncture method on patients with AIS, such as the improvement of neurological impairment, potential functional disability, and the basic ability of daily living but not including good prognosis after 3 months of followup. The clinical efficiency of the conventional acupuncture method is mainly reflected in the long term prognosis, the possible reason of which estimated by us was that the method was summarised and refined based on evidence of long term clinical practice of so many acupuncturists. The mechanism of acupuncture in the treatment of ischemic stroke is not clear yet, more in-depth research is needed.

7. Conclusion

Compared with “Scalp acupuncture” combined with “body acupuncture,” the “Xingnao kaiqiao” acupuncture method combined with “Temporal three-needle” had superiority in the improvement of neurological deficit, potential functional disability, and score of basic activities of daily living. As to the independent rate to basic activities of daily living and good prognosis of 3 months, there were no statistical differences.

Data Availability

The data used to support the findings of this study are available from the corresponding author upon request.

Ethical Approval

This study was approved by the Ethics Committee of Meizhou People’s Hospital and was conducted in accordance with the principles of the Declaration of Helsinki.

Conflicts of Interest

The authors declare that they have no conflicts of interest.

Acknowledgments

The study was supported by Meizhou Medical and Health Research Project (Grant no. 2020B67), and the Special Funds for Inheritance and Development of TCM in Guangdong (research project of Guangdong Provincial Bureau of TCM) (Grant no. 20202206).



References

- [1] Chinese Society of Neurology and Chinese Stroke Society, “Chinese guidelines for diagnosis and treatment of acute ischemic stroke 2018,” *Chinese Journal of Neurology*, vol. 9, pp. 666–682, 2018.

- [2] Intercollegiate Stroke Working Party, *National Clinical Guideline for Stroke*, Royal College of Physicians, London, UK, 2012.
- [3] A. A. Rabinstein, "Update on treatment of acute ischemic stroke," *Continuum: Lifelong Learning in Neurology*, vol. 26, no. 2, pp. 268–286, 2020.
- [4] A. Moussaddy, A. M. Demchuk, and M. D. Hill, "Thrombolytic therapies for ischemic stroke: triumphs and future challenges," *Neuropharmacology*, vol. 134, no. Pt B, pp. 272–279, 2018.
- [5] P. Wu, E. Mills, D. Moher, and D. Seely, "Acupuncture in post stroke rehabilitation: a systematic review and meta-analysis of randomized trials," *Stroke*, vol. 41, no. 4, pp. e171–e179, 2010.
- [6] L. F. Chen, J. Q. Fang, L. N. Chen, and C. Wang, "[Achievements and enlightenment of modern acupuncture therapy for stroke based on the neuroanatomy]," *Zhen ci yan jiu*, vol. 39, no. 2, pp. 164–168, 2014.
- [7] Gb/T12346-2006, *The Nomenclature and Location of Acupuncture Points*, Beijing, China, 2006.
- [8] Shanghai Science and Technology Literature Press, *Chinese-English Explanation of Jin's 3-Needle Technique*, pp. 55–60, Shanghai Science and Technology Literature Press, Shanghai, China, 2004.
- [9] China Traditional Chinese Medicine Press, *Jiao Shunfa Scalp Acupuncture*, Vol. 27, China Traditional Chinese Medicine Press, , Hong Kong, 2009.
- [10] J. K. Harrison, K. S. McArthur, and T. J. Quinn, "Assessment scales in stroke: clinimetric and clinical considerations," *Clinical Interventions in Aging*, vol. 8, pp. 201–211, 2013.
- [11] T. J. Quinn, J. Dawson, and M. Walters, "Dr John Rankin; his life, legacy and the 50th anniversary of the Rankin stroke scale," *Scottish Medical Journal*, vol. 53, no. 1, pp. 44–47, 2008.
- [12] J. P. Broderick, O. Adeoye, and J. Elm, "Evolution of the modified Rankin scale and its use in future stroke trials," *Stroke*, vol. 48, no. 7, pp. 2007–2012, 2017.
- [13] F. I. Mahoney and D. W. Barthel, "Functional evaluation: the Barthel Index," *Md Maryland State Medical Journal*, vol. 14, no. 14, pp. 61–65, 1965.
- [14] T. Ohura, K. Hase, Y. Nakajima, and T. Nakayama, "Validity and reliability of a performance evaluation tool based on the modified Barthel Index for stroke patients," *BMC Medical Research Methodology*, vol. 17, no. 1, p. 131, 2017.
- [15] M. D. Vicky Chalos, A. M. Nadinda, M. D. van der Ende, F. Hester, and P. Lingsma, "National Institutes of health stroke scale An alternative primary outcome measure for trials of acute treatment for ischemic stroke," *Stroke*, vol. 51, no. 1, pp. 282–290, 2020.
- [16] J. Pu, H. Wang, M. Tu et al., "Combination of 24-hour and 7-day relative neurological improvement strongly predicts 90-day functional outcome of endovascular stroke therapy," *Journal of Stroke and Cerebrovascular Diseases*, vol. 27, no. 5, pp. 1217–1225, 2018.
- [17] P. P. Wang, Y. Gao, and L. Liu, "The comparison research of the absolute change of National Institutes of Health Stroke Scale(NIHSS) scores with the percent change of NIHSS scores to predict the functional outcome of the patients with stroke [J]," *Journal of Apoplexy and Nervous Diseases*, vol. 28, no. 2, pp. 156–158, 2011.
- [18] W. Hacke, "Intravenous thrombolysis with recombinant tissue plasminogen activator for acute hemispheric stroke," *JAMA*, vol. 274, no. 13, 1995.
- [19] A. Shuaib, K. R. Lees, P. Lyden et al., "NXY-059 for the treatment of acute ischemic stroke," *New England Journal of Medicine*, vol. 357, no. 6, pp. 562–571, 2007.
- [20] A. Ganesh, S. A. Gutnikov, and P. M. Rothwell, "Late functional improvement after lacunar stroke: a population-based study," *Journal of Neurology Neurosurgery and Psychiatry*, vol. 89, no. 12, pp. 1301–1307, 2018.
- [21] M. Xu, D. Li, and S. Zhang, "Acupuncture for acute stroke," *Cochrane Database of Systematic Reviews*, vol. 3, no. 7, 2018.
- [22] X. M. Shi, "Clinical research on the treatment of 9005 cases of apoplexy with the acupuncture method of sharpening mind and inducing consciousness," *Zhongyiyao Daobao*, vol. 11, pp. 3–5, 2005.
- [23] Y. P. Guo, "Contribution of Xingnao Kaiqiao acupuncture on acupuncture and moxibustion treatment of apoplexy," *Zhenjiu Linchuang*, vol. 11, pp. 1–3, 2007.
- [24] L. Guo and X. M. Shi, "The treatment of 750 cases of apoplexy with Xingnao Kaiqiao needling method," *Zhongguo Chuangtong Yixue Zazhi*, vol. 47, 2006.
- [25] Z. X. Yang and X. M. Shi, "[Systematic evaluation of the therapeutic effect and safety of Xingnao Kaiqiao needling method in treatment of stroke]," *Zhongguo Zhen Jiu*, vol. 27, no. 8, pp. 601–608, 2007.
- [26] L. J. Sun, Z. L. Zhang, and X. Q. Ji, "Clinical advancement of needling method of open the orifices on each stage of wind stroke," *Liaoning Zhongyi*, vol. 36, pp. 153–154, 2009.
- [27] Z. L. Chen and G. X. Ni, "New process of the clinical applications of Xingnao Kaiqiao needling method," *Tianjin Zhongyi*, vol. 30, pp. 765–768, 2013.
- [28] H. Liu, Y. Wang, H. Ren, W. M. Wang, and S. P. Ma, "An effect of acupuncture on ADL and cognitive function in patients with ischemic stroke," *Zhongguo Kangfu Yixue*, vol. 21, pp. 444–448, 2006.
- [29] G. X. Ni, X. M. Shi, and Z. K. Wang, "Resuscitating acupuncture effects on mRNA expression of IL-1RI and TNFR-I in brain tissues of rat with cerebral ischemia reperfusion," *Journal of Nanjing University of Traditional Chinese Medicine*, vol. 28, no. 6, pp. 538–540, 2012.
- [30] J. Chen, "Effect of Xingnao kaiqiao acupuncture on IGF-1, MMP-2 and MMP-9 expression in patients with vascular dementia," *Zhong Yi Xue Bao*, vol. 32, no. 10, pp. 2022–2025, 2017.
- [31] H. F. Wei, L. F. Zhang, and Y. Zheng, "Instant effect of Xingnao Kaiqiao acupuncture therapy on content of blood plasma ET, CGRP and ANGII in rats with cerebral ischemia-reperfusion," *China Journal of Traditional Chinese Medicine and Pharmacy*, vol. 25, no. 6, pp. 933–935, 2010.

Research Article

Integration of Genetic and Immune Infiltration Insights into Data Mining of Multiple Sclerosis Pathogenesis

Xiaoyun Zhang ¹, Ying Song,² Xiao Chen,² Xiaojia Zhuang,² Zhiqiang Wei,² and Li Yi ²

¹Department of Rehabilitation, Shenzhen Longhua District Central Hospital, Shenzhen 518000, China

²Department of Neurology, Peking University Shenzhen Hospital, Shenzhen 518000, China

Correspondence should be addressed to Xiaoyun Zhang; 13xyzhang3@stu.edu.cn and Li Yi; yilitj@hotmail.com

Received 7 May 2022; Revised 7 June 2022; Accepted 8 June 2022; Published 27 June 2022

Academic Editor: Dong Chen

Copyright © 2022 Xiaoyun Zhang et al. This is an open access article distributed under the Creative Commons Attribution License, which permits unrestricted use, distribution, and reproduction in any medium, provided the original work is properly cited.

Background. Multiple sclerosis (MS) is an immune-mediated demyelinating disease of the central nervous system. MS pathogenesis is closely related to the environment, genetic, and immune system, but the underlying interactions have not been clearly elucidated. This study aims to unveil the genetic basis and immune landscape of MS pathogenesis with bioinformatics. **Methods.** Gene matrix was retrieved from the gene expression database NCBI-GEO. Then, bioinformatics was used to standardize the samples and obtain differentially expressed genes (DEGs). The protein-protein interaction network was constructed with DEGs on the STRING website. Cytohubba plug-in and MCODE plug-in were used to mine hub genes. Meanwhile, the CIBERSORTX algorithm was used to explore the characteristics of immune cell infiltration in MS brain tissues. Spearman correlation analysis was performed between genes and immune cells, and the correlation between genes and different types of brain tissues was also analyzed using the WGCNA method. **Results.** A total of 90 samples from 2 datasets were included, and 882 DEGs and 10 hub genes closely related to MS were extracted. Functional enrichment analysis suggested the role of immune response in MS. Besides, CIBERSORTX algorithm results showed that MS brain tissues contained a variety of infiltrating immune cells. Correlation analysis suggested that the hub genes were highly relevant to chronic active white matter lesions. Certain hub genes played a role in the activation of immune cells such as macrophages and natural killer cells. **Conclusions.** Our study shall provide guidance for the further study of the genetic basis and immune infiltration mechanism of MS.

1. Background

Multiple sclerosis (MS) is an immune-mediated demyelinating disease of the central nervous system (CNS) [1], which predominantly occurs in Caucasians and can cause severe neurological dysfunctions in advanced stages [2, 3]. The current knowledge has indicated that environmental and genetic factors jointly mediate the occurrence of MS. Although genes play an important role in the pathogenesis of MS, the concordant rate among identical twins was 30%, and a meta-analysis estimated that genetic factors accounted for only 50% of the risk of MS [4, 5], suggesting that nongenetic factors also greatly influence the susceptibility to the disease. Environmental risk factors such as vitamin D deficiency, smoking, and Epstein-Barr virus (EB virus) infection [6] can

interact with genetic variations of MS and thus lead to immune dysregulation. However, the researches on the interaction between environment and gene are still in progress.

Peripheral immune cells, especially B cells and T cells, are implicated in the pathogenesis of MS. In the early stages of MS, the innate immune system dominated by macrophages promotes the proinflammatory response of T and B cells, leading to tissue damage. Early microglial activation may also be one of the initial events in the development of MS. Activated microglia contribute to disease progression by releasing proinflammatory cytokines, free radicals, and glutamate. In the progressive stages, pathological changes such as axonal degeneration, focal to diffuse white matter injury, microglial cell activation, lymphocyte diffusion,

monocyte infiltration, and cortical involvement occur [7, 8]. On the one hand, immune cells are involved in promoting inflammatory response, demyelination, axon damage, and disease plaque formation. On the other hand, some immune cells also exert anti-inflammatory effects and inhibit disease progression by promoting tissue repair. The alterations of the immune system are complex in MS patients, and the contributions of immune cells to the pathology of MS have not been fully clarified.

Emerging studies on the subtypes of infiltrating immune cells in the brain of MS patients or experimental autoimmune encephalomyelitis (EAE) have revealed that both Th1 and Th17 CD4⁺ T lymphocytes are involved in disease initiation after in situ reactivation. However, the details of the immune microenvironment of intracranial lesions in MS patients remain unclear. Accumulating studies focus on the role of certain types of immune cells and their plasticity in the interaction with cytokines, chemokines, and brain compartments [9].

As early as 20 years ago, sequencing technology emerged, and gene chips contained a large number of biological information [10]. Databases of gene expression, gene polymorphism, protein structure, and genetic map are expanding. Gene microarray is an emerging technology that bears the advantage of an efficient and large-scale collection of gene expression profile data of diseases, which has been widely used in bioinformatics research [11]. A large amount of gene data has aroused the demand for bioinformatics [12]. In this backdrop, we can extract, process, and analyze microarray data more effectively with bioinformatic tools. With the emerging technique CIBERSORT, we can analyze the compositions of immune cells based on gene chips.

In the current study, combined with microarray data extracted from the existing MS samples, we used *R* language, STRING, and Cytoscape to calculate hub genes, annotate, and perform gene enrichment analysis. We used the CIBERSORT algorithm to infer the proportion of peripheral immune cells in brain lesions. Moreover, we calculated the correlation between hub genes and immune cells and used the weighted gene coexpression network (WGCNA) to further compare the internal gene differences in the dataset and analyze the correlation between hub genes and lesion sites. This study aimed to explore susceptibility genes and immune cell infiltration in brain lesions of MS patients, hoping to confer novel insights into MS prevention and treatment.

2. Methods

2.1. Differentially Expressed Genes (DEGs) Screening. Gene Expression Omnibus [13] (GEO; <https://www.ncbi.nlm.nih.gov/geo/>) is an open genomics database. Human expression profile datasets of MS (GSE108000 and GSE135511) were downloaded from the GEO database. Then, the datasets were divided into the control group and the MS group. And we used the `normalizeBetweenArrays` function in the *R* language “limma” package to normalize the datasets and eliminate intragroup differences. GSE108000 and GSE135511 were combined with “SVA” *R* package [14] to

remove batches. DEGs with $p < 0.05$ and $|\log_2\text{FC}| > 0.5$ were considered statistically significant. Based on the obtained DEGs, we used *R* package “ggplot2” [15] to draw a volcano plot to view the differences between upregulated and downregulated genes and used a heatmap to view the differences of genes between the disease group and control group.

2.2. Construction of Protein-Protein Interaction (PPI) Networks. STRING (<https://string-db.org/>) is a database for the study of PPI networks. The data are derived from published experimental data, and genes come from computer mining, prediction, and fusion. In our study, we used STRING 11.0 to analyze the DEGs obtained. The confidence score was set as 0.9. Since the regions with more interconnections in the PPI network have a higher probability of participating in the biological regulation, and the dissociated gene nodes seldom play a key role in the entire network, we chose to eliminate the dissociated gene nodes in our study. After that, we downloaded the network file for subsequent analysis.

Cytoscape is software for network analysis, which contains plug-ins such as Cytohubba, Molecular Complex Detection (MCODE), and ClueGo. Cytohubba can rank network nodes via various topological analysis methods. Among all the topological methods, the MCC method has the most accurate prediction value. MCODE can detect closely related regions in the PPI network and then infer different molecular complexes. With the Cytohubba plug-in and MCC method, we ranked network nodes and selected the top ten genes for further analysis. With the MCODE plug-in, we divided the network into different subnetworks and analyzed the first five subnetworks.

2.3. Enrichment Analysis. The commonly used enrichment analysis methods mainly include Gene Ontology (GO) [cellular component (CC), biological process (BP), and molecular function (MF)] and Kyoto Encyclopedia of Genes and Genomes (KEGG), which can reveal the functional tendency of gene sets. The commonly used enrichment tools include the DAVID database, KOBAS database, and key *R* package (clusterProfiler) [16]. The plug-ins include Funrich, ClueGo, Cluepedia, Metascape, etc. In our study, we used Cytoscape ClueGo (version 2.5.7) and Cluepedia (version 1.5.7) plug-ins to perform gene annotation analysis on the gene sets obtained from step 2 using MCODE and Cytohubba methods and used “ClusterProfiler” *R* package to analyze the DEGs obtained from step 1. The pathways with $p < 0.05$ and $Q < 0.05$ were screened out. The top 30 GO and KEGG enrichment results were selected and shown as bubble plots. Upregulated and downregulated genes of the KEGG pathways of interest were visualized using “Pathview” *R* package [17].

2.4. Evaluation of Immune Infiltration of Brain Tissues. Currently, flow cytometry is accepted as the primary way to evaluate the infiltration of immune cells. However, it may take a lot of time to excavate the potential immune cells and determine the functional phenotypes of tissues in large

samples only using flow cytometry. CIBERSORT (cell-type identification by estimating relative subsets of RNA transcript) algorithm can simplify the process by deconvolution of peripheral immune cell subtypes based on linear support vector regression. CIBERSORT is one of the current methods to calculate immune cell subtypes based on gene expression profiles. In our study, we used CIBERSORT to analyze the characteristics of immune cell infiltration in brain tissues of MS. We input the merged dataset into the CIBERSORTX website (<https://CIBERSORTx.stanford.edu/>) and set simulation calculation times as 100 times to obtain the proportion of 22 immune cells. Then, we filtered out statistically significant data with the criterion of $p < 0.05$ for further analysis. The stacked bar chart was employed to visualize the composition of different immune cells. The correlation coefficient between different immune cells was determined and presented as a correlation heatmap. The differences between the MS group and the control group were compared using the Wilcoxon rank-sum test. The differences in immune cell infiltration between the disease group and control group were visualized by violin map using the “ggplot2” package in R. We also drew a two-dimensional PCA cluster plot to visualize the differences in immune cell infiltration between the MS group and control group using the “ggplot2” package in R.

2.5. Correlation Analysis between Hub Genes and Immune Cells. We obtained the proportion of 22 immune cells in the brain tissues of MS patients using the CIBERSORT deconvolution method in Step 4. Spearman correlation analysis was performed on the first 5 hub genes of Cytohubba and the infiltrating immune cells in the samples, which were presented as correlation maps using the “ggplot2” package in R.

2.6. Construction of Weighted Gene Coexpression Network. WGCNA [18] is an open-source R package that can be used to construct gene coexpression networks based on the following two points. One is that genes with similar expression patterns may be functionally related or have a coregulatory network; the other is that the connection between genes conforms to scale-free distribution [18]. In our study, we used the step-by-step method to analyze the combined gene set. Firstly, the best soft threshold β was calculated. Then, a hierarchical clustering tree was constructed based on the genetic correlation coefficient, and genes were assigned into different modules according to gene expression patterns. Afterward, we set the appropriate minimum quantity of gene modules and shear height threshold to further merge similar genes. The absolute value of Pearson correlation was used to measure the connectivity of genes in modules. Genes with high connectivity within the module were considered the hub genes of the module. The hub genes within a specific module often had a strong correlation with a specific trait. After obtaining the gene module of the specific trait we aimed to analyze, we used the “ggplot2” package to acquire the intersection of gene sets including MCODE Cluster 1 gene set, Cytohubba Top 10 gene set, and specific gene

module from the WGCNA to observe the relationships between genes clusters.

3. Result

3.1. DEG Screening. We included GSE108000 and GSE135511 for analysis. The description of the datasets is shown in Table 1. GSE108000 dataset collected gene expression profiles of pathological specimens of brain motor cortex from 20 MS patients (specimens with or without meningeal infiltration were collected) and motor cortex specimens from 10 patients without neurological diseases. GSE135511 dataset collected gene expression profiles of 30 white matter lesions from MS patients (7 patients with chronic active lesions and 8 patients with inactive lesions) and 10 white matter samples from controls. All specimens were nonliving specimens.

We downloaded the gene matrix from GSE108000 and GSE135511. GSE108000 contained gene expression profiles of white matter specimens from 30 MS patients and 10 controls. GSE135511 dataset contained gene expression data of gray matter specimens from 40 MS patients and 10 controls. We combined and normalized the two datasets, removed the batch effect between groups, and got the merged dataset. We set the threshold of significant difference of DEGs as $p < 0.05$ and $|\log_2FC| > 0.5$ to obtain more DEGs. Finally, we got 882 DEGs between the MS group and control group, including 399 upregulated genes and 483 downregulated genes (Figures 1(a), 1(b)).

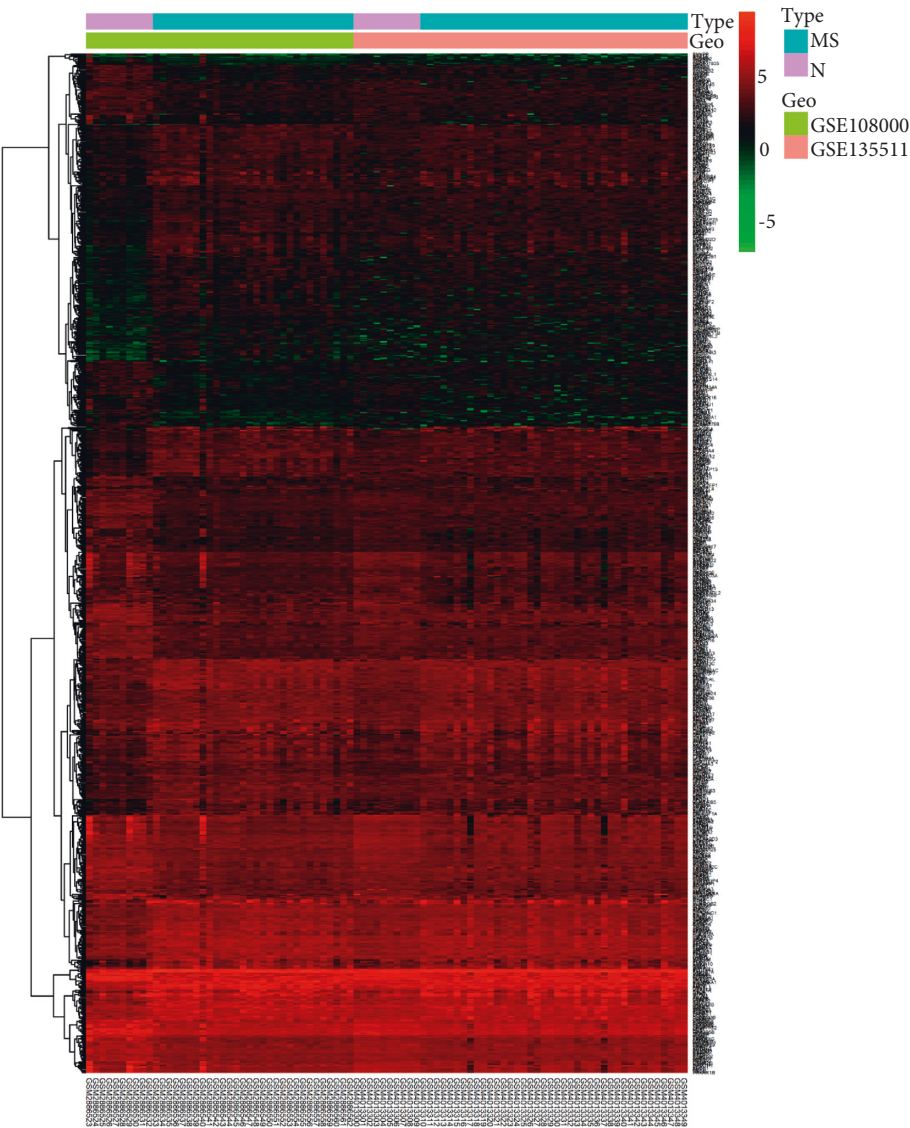
3.2. Construction of PPI Network. We input 882 DEGs into the STRING website, set the confidence score as 0.9, and removed the isolated genes. Then, we obtained a PPI network containing 872 nodes and 1265 edges. We downloaded network information and used Cytohubba plug-in MCC method to get the top 10 hub genes, as shown in Table 2. The genes were displayed in different color levels according to the critical degree of genes in the network, as shown in Figure 2(a). The PPI network of 872 nodes was analyzed using the MCODE plug-in, and 24 subnetworks were obtained. The first 5 subnetworks (as shown in Table 2 and Figures 2(b)–2(f)) were selected for further gene enrichment analysis.

3.3. Functional Enrichment Analysis of DEGs, Hub Genes, and Subnetwork Genes. GO and KEGG enrichment analysis of the first 10 hub genes was conducted using Cytoscape plug-ins ClueGo and Cluepedia. As shown in Figure 3(a), the highest GO enrichment intensity suggested that the molecular functions of the 10 hub genes were closely related to the activity of MHC class II receptors, polypeptide antigens, polysaccharides binding, ER-phagosome pathway, and cytokine signal transduction in the immune system. The top 5 hub genes with the highest KEGG enrichment intensity were closely related to allograft rejection, graft-versus-host disease, type 1 diabetes, asthma, and autoimmune thyroid disease, as shown in Figure 3(b). The enrichment results of Cluster 1 obtained from MCODE were similar to those of the

TABLE 1: Basic information of data from GSE108000 and GSE135511.

Dataset ID	Sample source	Data platform	Sample grouping	Disease subtypes	Sample number	Published date
GSE108000	Brain tissue	GPL13497 (agilent)	Multiple sclerosis and control	SPMS	40 (7M/18F)	Jan-18
GSE135511	Brain tissue	GPL6883 (illumina)	Multiple sclerosis and control	No specific	50 (14F/16M)	Dec-19

SPMS, secondary progressive multiple sclerosis; M, male; F, female.



(a)
FIGURE 1: Continued.

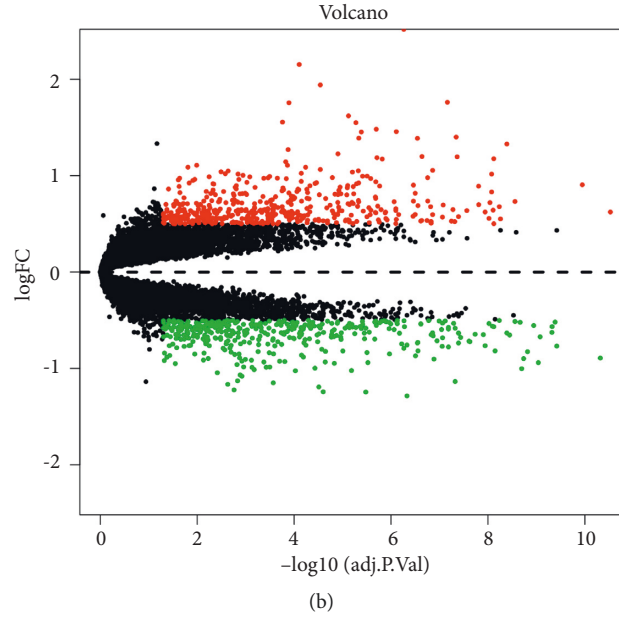


FIGURE 1: Volcano map and heat map of differentially expressed genes (DEGs). (a) The distributions of DEGs in a merged dataset of GSE108000 and GSE135511. MS refers to the multiple sclerosis group, and N refers to the control group. (b) The distribution of upregulated DEGs and downregulated DEGs in the multiple sclerosis group and control group. Color green represents downregulated DEGs and color red represents upregulated DEGs.

TABLE 2: The first 10 core genes obtained from Cytohubba plug-in and genes of 5 gene sets from the MCODE plug-in.

Gene sets	Gene lists
Top 10 hub genes	HLA-DRA, HLA-DRB1, HLA-DRB5, HLA-DQB2, HLA-DPA1, HLA-DQB1, HLA-E, HLA-C, GBP2, CD44
Cluster 1	ACTR1B, HLA-DRB5, HLA-DQB2, HLA-DPA1, HLA-DMB, B2M, HLA-DRA, HLA-DMA, HLA-DRB1, HLA-DQB1, IRF8, KLC2, DYNLL2, DYNLC11, GBP2, GBP1, DNAJC3, HLA-C, HLA-E, IFI30, CD44, IRF3, TMEM132A, LGALS1, PRKCSH, FSTL1, LTBP1, IGFBP7, CHGB, ADCY1, CALU, DRD4, HSP90B1, GNB4, HTR5A, CXCL16, CP, GNG3, CCR1, SPP1, C5AR1, ANXA1, GNG12, ADORA1, GNAI3, APOE, TIMP1
Cluster 2	WWP1, FBXO30, KLHL22, FBXO44, FBXL4, UBE2S, DTX3L, MGRN1, RNF126
Cluster 3	CD2BP2, PAPOLA, SYMPK, FUS, U2AF1L4, POLR2G, ELAVL2, PLRG1, PRPF31
Cluster 4	OLR1, CD300A, TMEM63A, ITGAV, COL8A1, ATP6V0C, P4HA1, PLOD2, COL1A2, COL9A3, COL8A2, P4HA2, COL4A2, CYBA, COL4A1, CD33, SERPINH1, CD53
Cluster 5	GPR65, GNRH1, P2RY2, CCKBR, TAC3, CCK, PIK3CA

first 10 genes obtained from Cytohubba. GO analysis suggested that the gene set was related to MHC-II, MHC-I, glycation, growth factor binding, and amyloidosis. Cluster 2 was associated with the ubiquitin-mediated proteolysis pathway. Cluster 3 was related to spliceosome and mRNA surveillance pathway, and Cluster 4 was related to ROS and RNS production and collagen degradation by phagocytes. Cluster 5 was associated with the regulation and signal transduction of TRP pathways by inflammatory mediators.

GO (BP, CC, and MF) enrichment analysis was performed on the DEGs obtained in step 1 using “Cluster-profiler” in the R package. The most significant pathways are displayed in Figure 4(a). The most significant BPs in GO showed negative immunoregulation, myeloid differentiation, antigen and positive regulation of cytokines production, control of protein catabolism, glial cell activity, and response to the IFN γ pathway, etc. The CCs were mainly related to collagen fibers, extracellular matrix,

adhesion plaques, endocytic vesicles, endocytic vesicle membrane, secretory granular membrane, MHC protein complex, etc. MFs were related to amide binding, protein serine/threonine kinase activity, polypeptide binding, carboxylic acid-binding, organic acid-binding, cytokine binding, immune receptor activity, cell adhesion mediator activity, and MHC class II receptor activity. The results of the KEGG enrichment analysis are shown in Figure 4(b). Enrichment pathways can be classified into virus infection (such as human papillomavirus, swine flu, cytomegalovirus, EB virus, etc.), bacterial infection (such as salmonella, *Staphylococcus aureus*, etc.), autoimmune diseases (including inflammatory bowel disease, type 1 diabetes, autoimmune thyroid disease, asthma, etc.), and others (including atherosclerosis, endogenous ligand, and other related pathways).

GO and KEGG enrichment results of the first 10 hub genes obtained by Cytoscape and Cytohubba plug-ins and

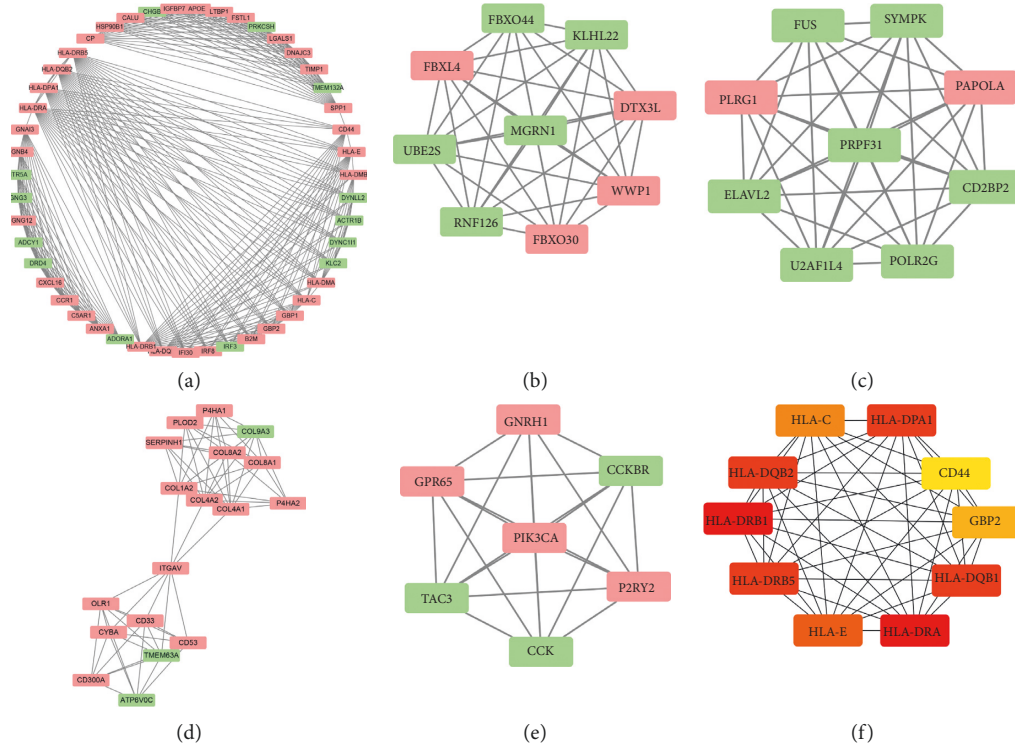


FIGURE 2: Protein-protein interaction networks of hub genes and subnetwork genes. (a)–(e) The top 5 protein-protein interaction networks obtained from the MCODE algorithm. In (a)–(e), color green represents downregulated genes and color red represents upregulated genes. The connection lines indicate the correlations between genes. (f) The interaction network of the first 10 genes obtained from the Cytohubba algorithm. The 10 genes are all upregulated genes and the color levels indicate the degree of genes in the network.

the first subgene set Cluster 1 obtained by MCODE plug-in were consistent with the enrichment results of DEGs, which mainly focused on immune regulatory pathways and immune-related disease pathways. However, the enrichment results of DEGs were more comprehensive, suggesting that in addition to immune response, the response of glial cells to antigens in brain tissues also played an essential role in the pathological mechanisms.

In our study, we also selected the Epstein-Barr virus pathway to explore the interaction between specific environmental factors and susceptibility genes of MS. The pathways were visualized using the “PathView” package in R. As shown in Figure 5, the Epstein-Barr virus mainly acted on B cells through B cell receptors such as MHC-II and TLR2. After entering B cells, Epstein-Barr virus further affected the immune activation pathway and upregulated genes related to antigen presentation of MHC-I, which further activated cytotoxic T cells. In addition, the Epstein-Barr virus might indirectly activate the PI3K pathway and affect cell proliferation and cell cycle.

3.4. Characteristics of Immune Infiltration in Brain Tissues of MS Patients. To explore the characteristics of immune infiltration in brain tissues of MS at the cellular level, we uploaded the merged dataset through the CIBERSORTX website, calculated 100 times using the CIBERSORT deconvolution method, and finally obtained the proportion

of 22 immune cells in different samples. A total of 70 samples with a relatively stable proportion of immune cells (including 12 control samples and 58 MS samples) were screened out by $p < 0.05$, as shown in Figure 6. The proportion of resting mast cells, macrophage M2, neutrophils, plasma cells, T cells CD8, and macrophage M0 was relatively high in MS brain tissues.

The correlation heatmap of immune cells between the MS group and control group is shown in Figure 7(a). The correlation between follicular helper T cells and eosinophils showed a correlation coefficient with the highest absolute value ($R = 0.5$), suggesting that there was a certain positive correlation between follicular helper T cells and eosinophils. The correlation coefficient of macrophage M0 and neutrophils ($R = -0.41$) was followed, suggesting the negative correlation between macrophage M0 and neutrophils. Overall, the correlation between immune cells in the specimens was weak to moderate. The differentiation of immune cells in MS and control samples was analyzed and shown in the violin diagram. As shown in Figure 7(b), the naive $CD4^+$ T cells were significantly reduced ($P = 0.013$), but the resting synaptic cells were significantly increased ($P = 0.003$) in the MS sample compared with those in the healthy control samples. The PCA cluster diagram showed that there were differences in the level of immune cell infiltration between MS and healthy control samples (Figure 7(c)).

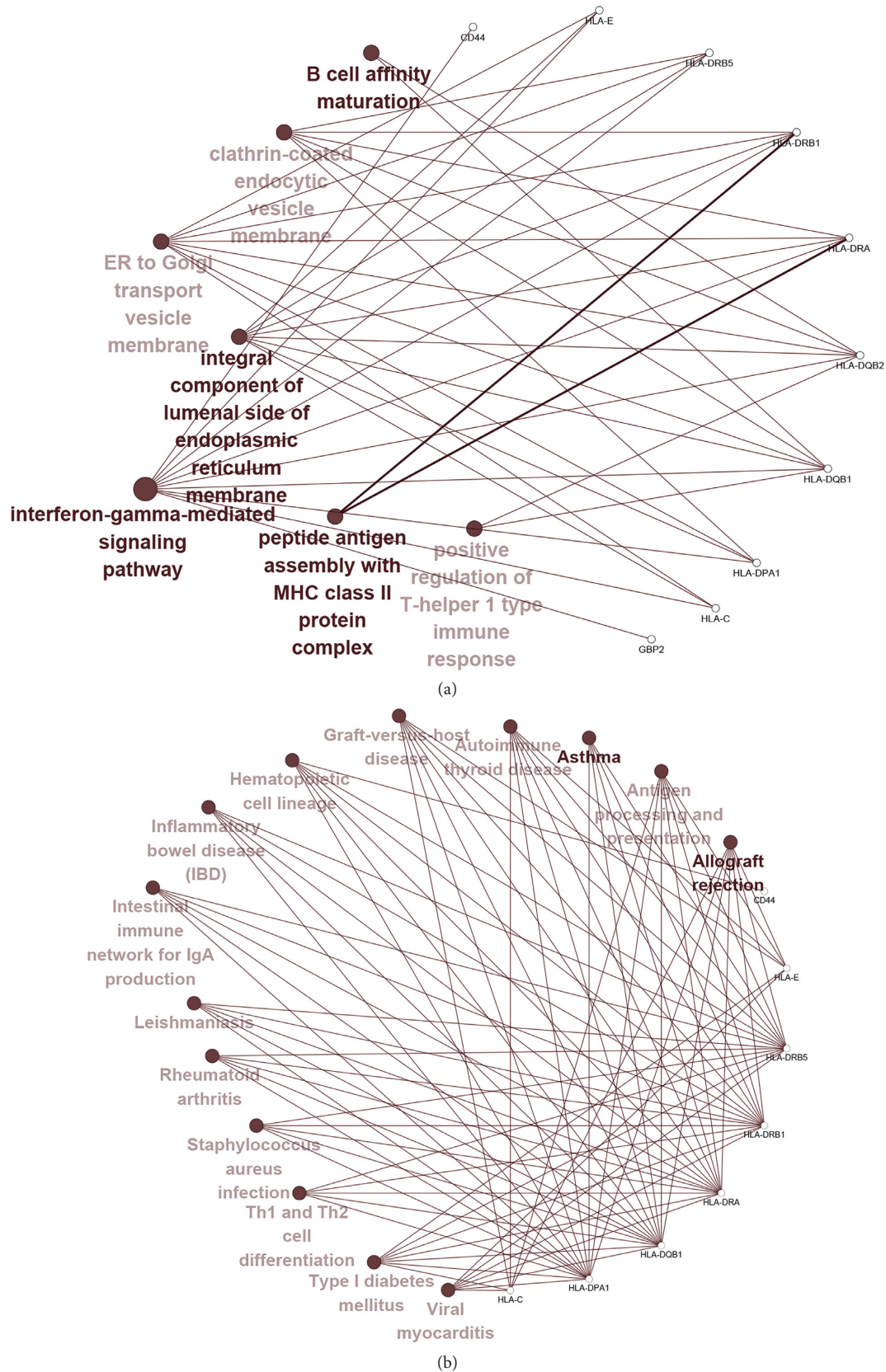


FIGURE 3: GO KEGG enrichment pathway network of the first 10 hub genes ($p < 0.05$). (a) The enrichment network of GO pathway (including BP, CC and MF) and (b) the enrichment network of KEGG pathway. The connection of the enrichment pathway suggests that there are connections between pathways and genes and between pathways. The darker the color and the larger the volume of the circle, the greater the significance of the pathway.

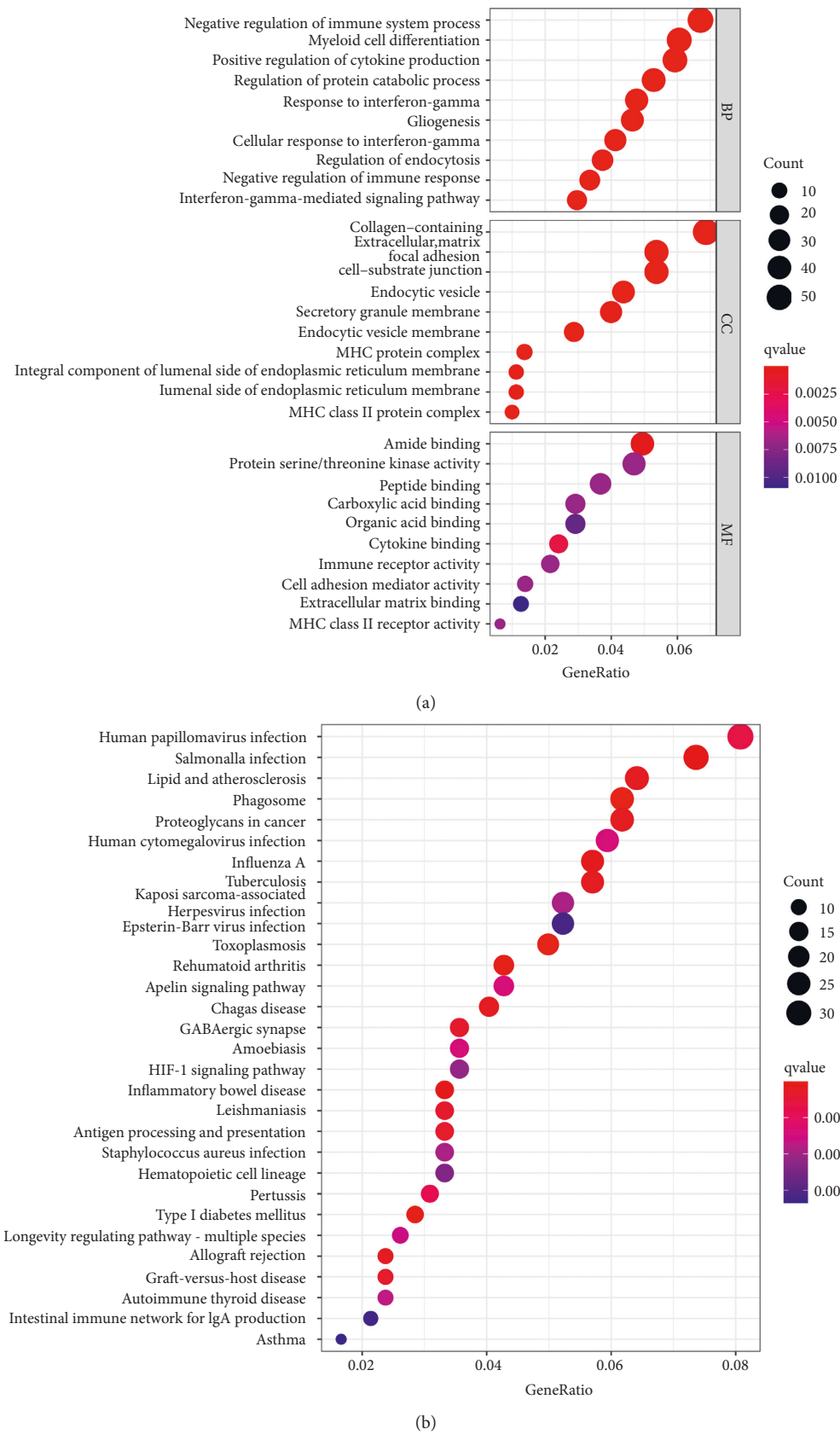


FIGURE 4: Gene Ontology (GO) and Kyoto Encyclopedia of Genes and Genomes (KEGG) analyses of DEGs. (a) GO enrichment analysis of DEGs, the top 10 enrichment pathways of biological process (BP), cellular component (CC) and molecular function (MF). Bubble size represents the number of genes related to the specific pathway. The larger the quantity of genes, the larger the bubble. And the color of the bubble represents the size of Q value. The smaller the q value, the redder the bubble. (b) The top 30 enrichment pathways in KEGG analysis. The bubble size represents the number of genes related to the pathway, and the more the number of genes, the larger the bubble. While the color of the bubble represents the size of the Q value. The smaller the q value, the redder the bubble.

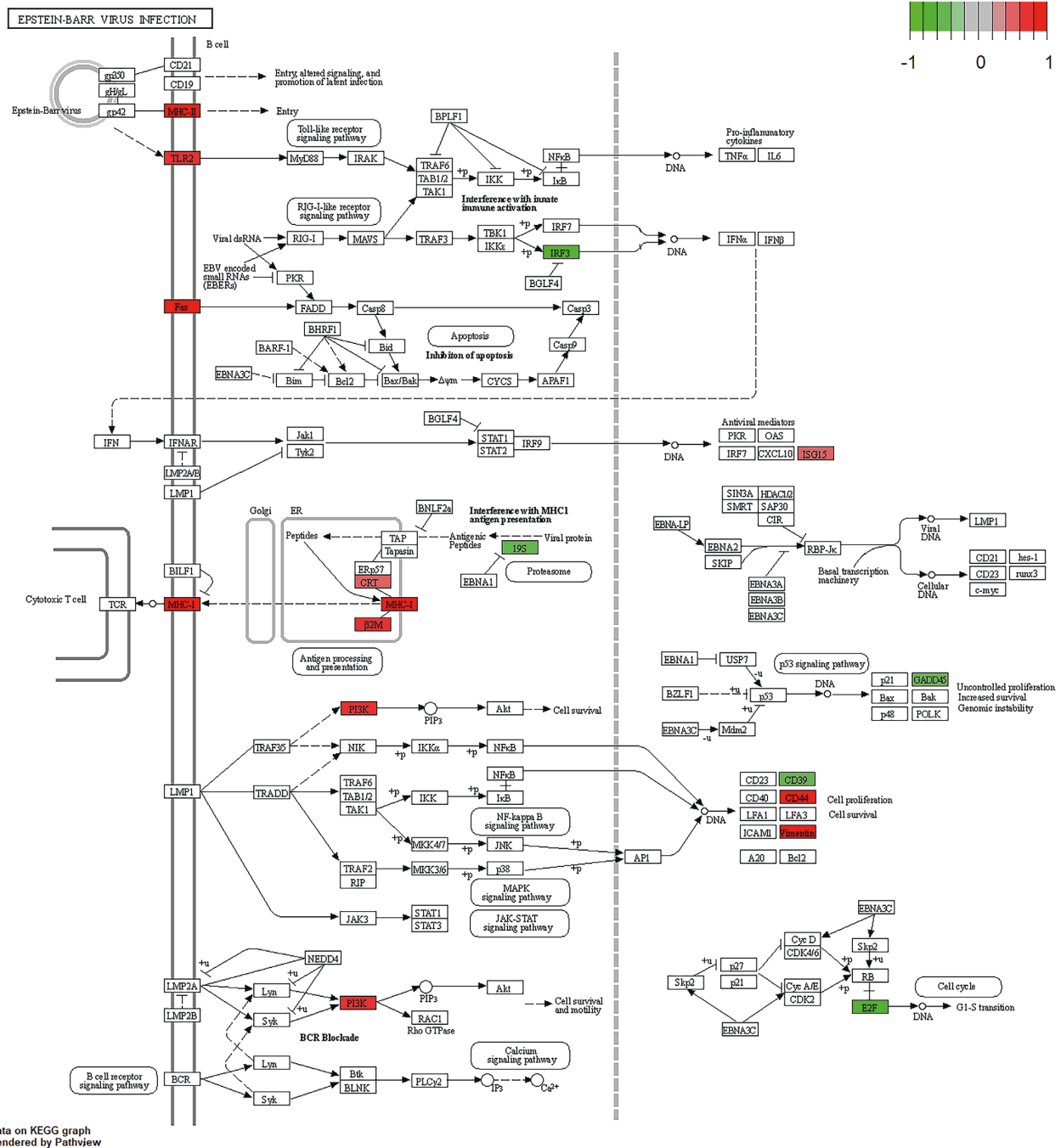


FIGURE 5: Signaling pathways associated with EB virus infection and differential gene expression in multiple sclerosis. In the figure, upregulated genes are indicated in red and downregulated genes are in green.

3.5. Construction of Weighted Gene Coexpression Network. To further observe the differences in gene expression in different brain regions, we also performed WGCNA on the merged dataset to observe the differences in gene expression in white matter lesions, normal white matter tissues, gray matter lesions, and normal gray matter tissues of MS patients. The variance of all genes was extracted and the top 25% of the variance was extracted to obtain the expression profiles of 3709 genes as the input dataset of WGCNA. Based on the parameters of R2, slope, and mean k , the optimal soft threshold β value was calculated to be 4. In this study,

$R^2 = 0.95$, which meant that the connectivity degree of the scaling-free network construction was optimal (Figure 8). The network was constructed using the step-by-step method, and the minimum number of genes in the module was set as 30. Then, the modules with a similarity above 0.75 were merged, and finally, 11 different modules were obtained (Figure 9). We further draw the correlation heatmap between gene modules and tissue characteristics (Figure 10). Among the modules obtained, the one with the most genes and the highest correlation with traits was the turquoise module (946 genes). The correlation analysis between gene

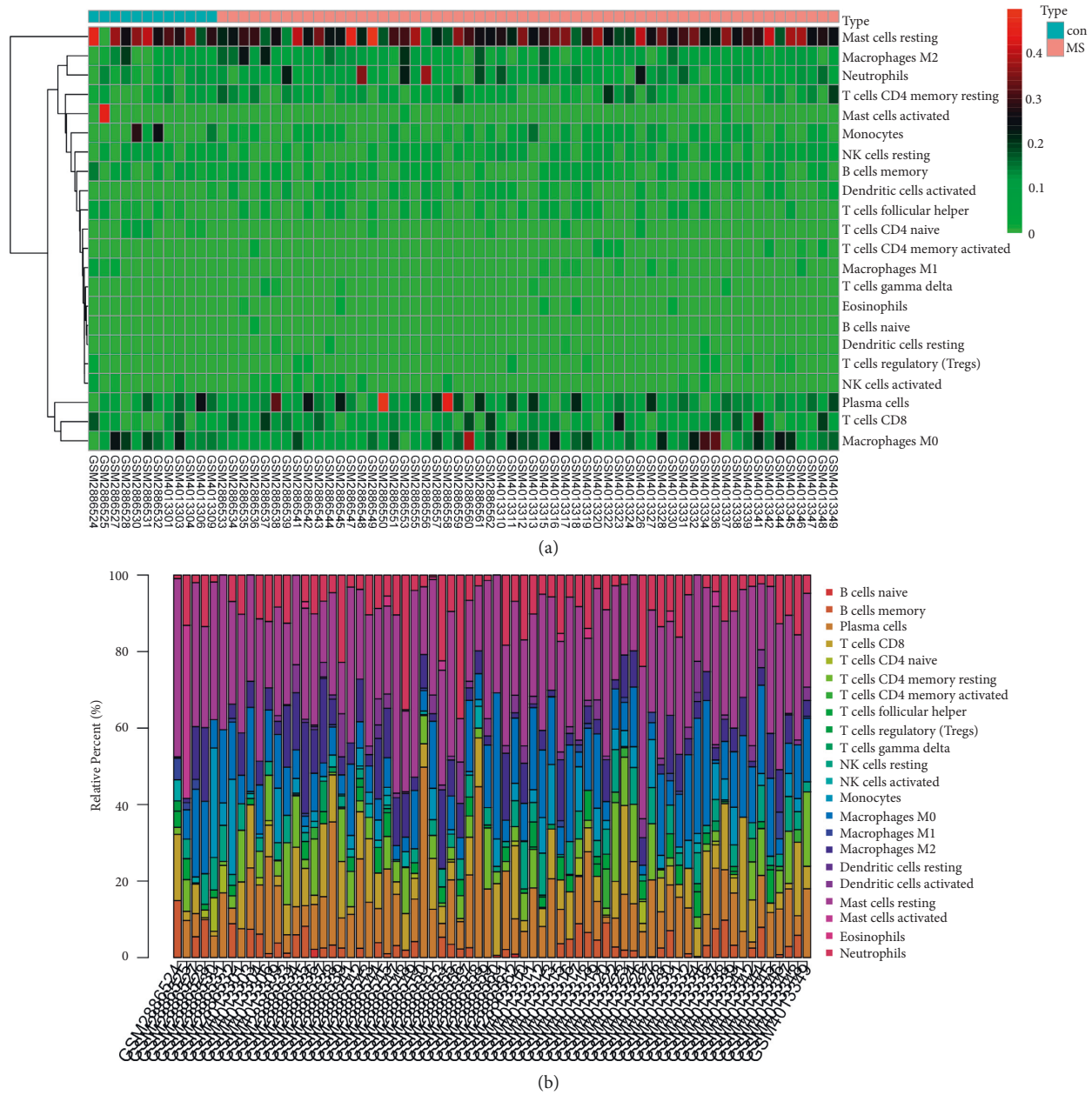


FIGURE 6: Heat map and stacking bar chart of proportions of infiltrating immune cells in the samples. (a) The expression level of immune cells in brain tissue. The darker the color, the larger the proportion. CON group represents the brain tissue samples of the control group, and the MS group represents the brain tissue samples of the multiple sclerosis group. (b) The proportion of immune cells in different tissues. The longer the bar chart, the higher the proportion of infiltrating immune cells in the tissues.

modules and tissue traits showed that there were significant differences in gene expression between the white matter of the MS group and the control group and between the gray matter of the MS group and the control group. The module with the greatest correlation with traits (turquoise module) may well distinguish the control group and disease group. There was also a certain degree of differentiation between the chronic active white matter lesions and the adjacent tissues of chronic active lesions in the disease group, but there was no effective gene module to clearly distinguish the gray matter lesions from the normal gray matter tissues. In our study, we further compared the turquoise gene module with

the hub genes obtained in Step 2 and found that all the hub genes were in the turquoise module (Figure 11), suggesting a strong correlation between the hub genes and chronic active white matter lesions. There was no significant difference between normal gray matter and pathological gray matter in MS samples, but significant differences could be observed between the two gray matters and the control samples. However, in the correlation diagram between gene modules and traits, the modules with the greatest difference correlation fell in the gray module, which belonged to the unclassified gene module. In brief, compared with the control population without neurological diseases, MS patients

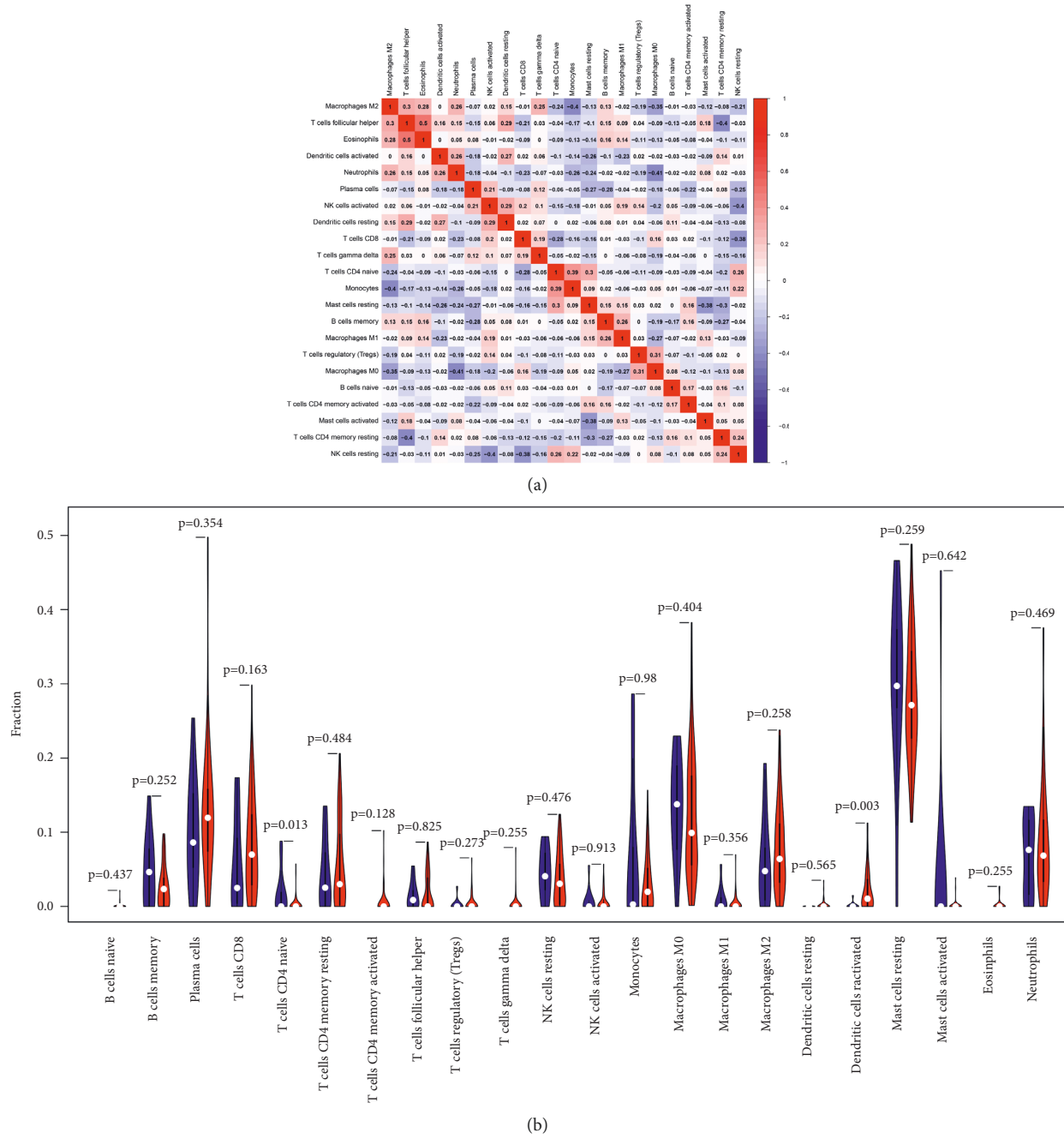


FIGURE 7: Continued.

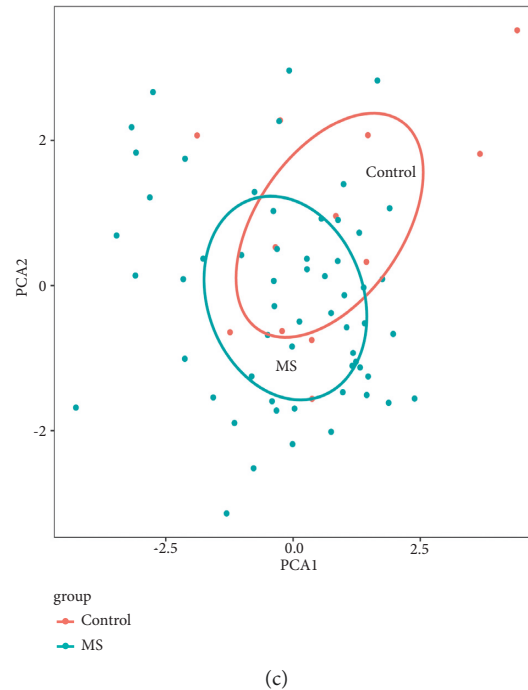


FIGURE 7: Evaluation and visualization of immune cell infiltration. (a) The correlation heat map of 22 types of immune cells. The darker the color, the stronger the correlation; color red indicates a positive correlation, while blue indicates a negative correlation. (b) The violin diagram of proportion of 22 types of immune cells between multiple sclerosis group and control group. Color red represents the multiple sclerosis group, while the color blue represents the control group. $p < 0.05$ indicates a significant difference. (c) The PCA cluster plot of infiltrating immune cells between the multiple sclerosis group and the control group.

generally had abnormal gene expression profiles in both gray matter and white matter of brain tissues. The turquoise module gene set could further distinguish chronic active lesions from the adjacent tissues of chronic active lesions in MS patients. Further information on genes belonging to eleven modules was listed in Supplementary Table S1.

3.6. Correlation Test between Hub Genes and Immune Cells. Spearman correlation analysis was performed between the first 5 hub genes of Cytohubba (HLA-DRA, HLA-DRB1, HLA-DRA5, HLA-DRA, and HLA-DPA1) and the 22 immune cells in the samples obtained from CIBERSORT. It was found that the expressions of the 5 hub genes were all negatively correlated with the number of M0, and positively correlated with the number of M1/M2 and the number of gamma delta in T cells. In neuroinflammatory diseases, macrophages play a dual role in the process of tissue damage according to their activation state (M1/M2). Macrophage M1 can damage neurons, while M2 macrophages are believed to facilitate the regeneration and repair of neurons, and M0 is at the resting state. The correlation diagrams of the analyzed gene correlations ($p < 0.05$) are shown as scatter plots in Figure 12.

4. Discussion

Multiple sclerosis is characterized by complex immune mechanisms. Specific genomic alterations drive the formation of heterogeneity in prognosis. Although there are

some single genes and risk models linked to multiple sclerosis patients' prognosis, few studies were reported for analysis on the relationships of genes and immune infiltration in multiple sclerosis. The initial objective of our study was to identify the relationships between hub genes in different brain lesions and the infiltrating immune cells in brain tissues of multiple sclerosis patients.

Most hub genes identified are located in HLA-DR loci in the MHC region and are associated with immunity. The screening of the functions of hub genes also confirms that the 10 genes are susceptibility genes to MS [19–29]. However, due to the lack of previous treatment information of included patients in the original literature, we failed to determine whether the mutation is germline or influenced by treatment. WGCNA algorithm in our study also demonstrated that the 10 genes were closely related to chronic active white matter lesions. We hypothesized that the hub genes obtained in this study were significantly expressed in chronic active white matter lesions, but we could not clarify whether these genes also affected the nonlesional regions. At present, there are relatively few studies on the relationship between genes and brain regions. Some studies have evaluated the pathogenicity of NF- κ B signaling pathway-related genes in different brain regions of MS patients and found that genes differentially expressed in specific brain regions regulate each other [30]. The comparison of miRNAs in different brain regions of MS patients [30] has revealed that active and chronic inactive white matter lesions share regulatory miRNAs, which are mainly involved in astrocyte

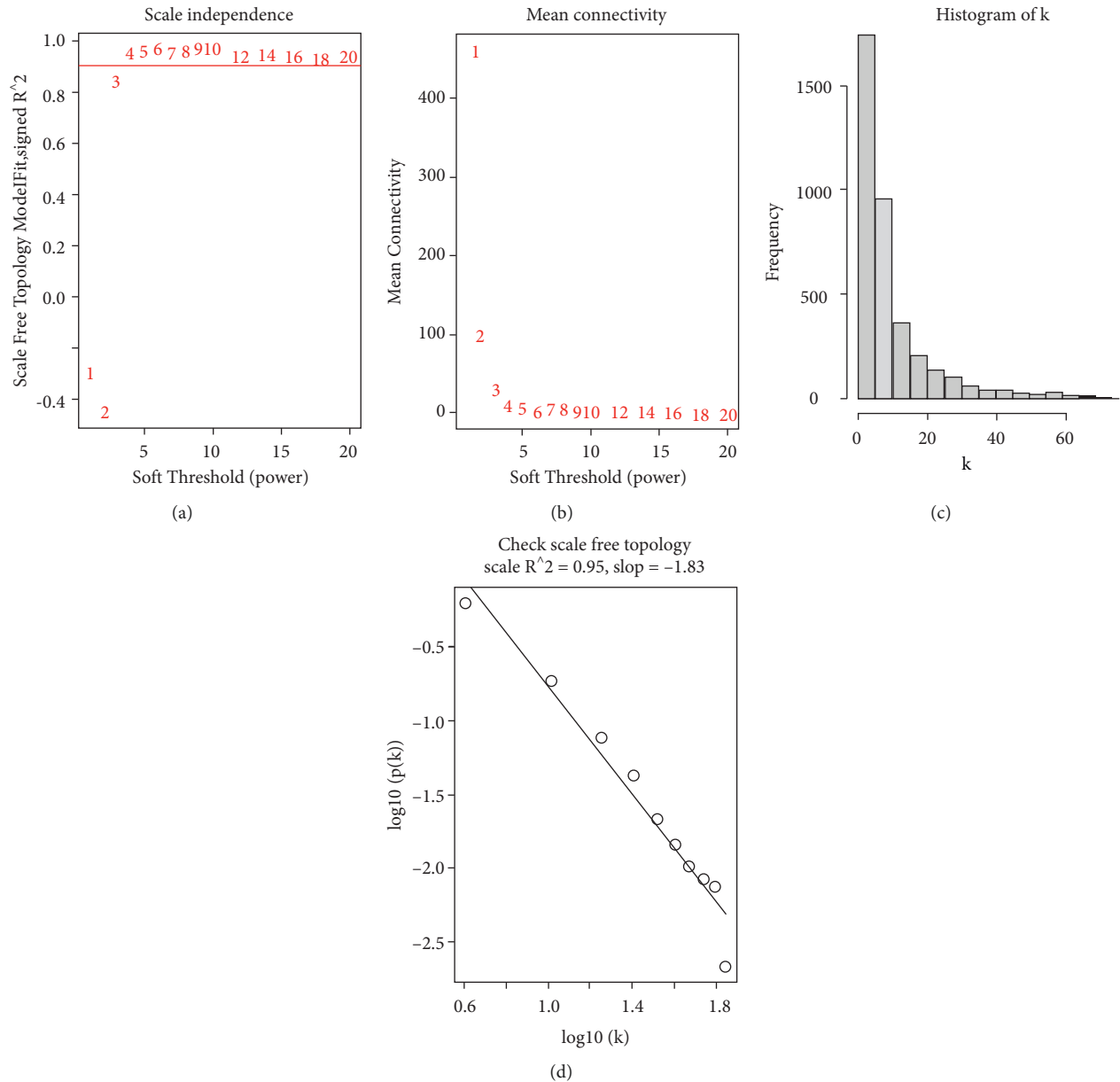


FIGURE 8: Soft threshold distribution and K value histogram. (a) shows the distribution of soft threshold. (b) The distribution of average connectivity and soft threshold. (c) The histogram of K value. (d) The graph of $\log_{10}(p(K))$ VS $\log_{10}(K)$, where R^2 is the correlation square between $\log(p(K))$ and $\log(K)$. The closer the R^2 value is next to 1, the stronger the linear relationship between $\log(p(k))$ and $\log(k)$, and the closer the constructed network to scaleless network distribution.

proliferation, microglial proliferation, and demyelination. However, microglia activation and inflammatory infiltration are not obvious in chronic inactive white matter lesions. miRNA overlap in chronic inactive white matter lesions and gray matter lesions is related to the response of astrocytes to inflammatory stimulation, maintenance of inflammatory cytokines, and apoptosis and regeneration of glial cells. Exploring gene expression in different brain tissues probably contributes to uncovering the pathological proinflammatory and anti-inflammatory mechanisms in brain tissues of MS patients.

GO analysis indicated that the hub genes were significantly enriched in immune pathways including antigen

presentation, antibody production, and T cell activation, proliferation, and differentiation. GO analysis of DEGs also suggested that glial cell proliferation contributed to the pathogenesis of MS. The overall pathogenesis of MS involves peripheral immune cells and a cascade of brain glial cell activation, which is consistent with the review of Bhise [31]. Previous studies have shown that glial cells have bidirectional interactions with components of the immune system, which not only mediate tissue damage and immunity repair but also directly participate in inflammatory processes, thereby further aggravating inflammation and axon injury [32–34]. Signal transduction between inflammatory cells and target tissues may also be bidirectional. The toxic

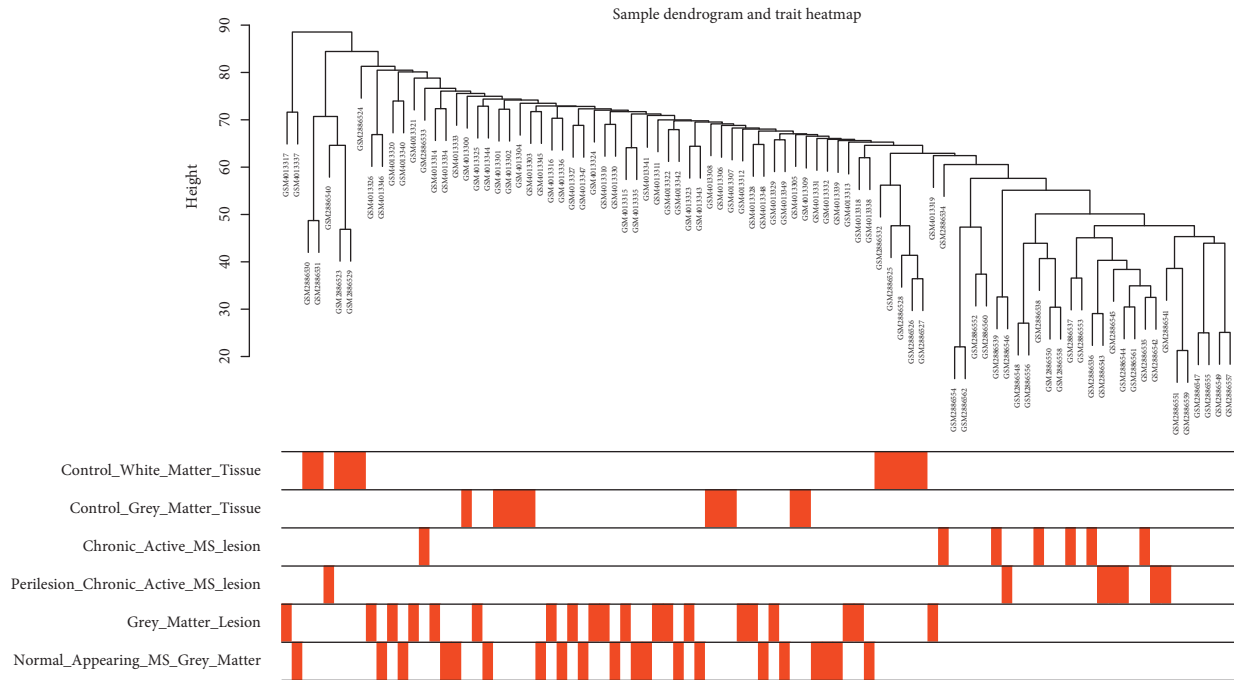


FIGURE 9: Clustering diagram of gene modules. Control_white_matter_tissue, white matter tissues of the control group; Control_gray_matter_tissue, gray matter tissues of the control group; chronic_active_MS_lesion, chronic active lesions of MS patients; perilesion_chronic_active_MS_lesion, perilesions of chronic active lesions of MS patients; gray_matter_lesion, gray matter lesions of MS patients; normal_appearing_MS_gray_matter, normal appearing gray matter of MS patients.

microenvironment mediated by immune cells (peripheral or central nerve cell compartmentalization) and resident cells of CNS (microglia and astrocytes) can produce inflammatory mediators, reactive oxygen species, and iron deposition, leading to chronic demyelination and axonal lesions. The structural damage of myelin oligodendrocytes and the loss of nutritional support lead to the increase of energy demand for nerve impulse transmission, while mitochondrial damage and disruption of ion homeostasis further impair normal electrical activity. The above processes jointly promote brain atrophy and explain the pathological mechanism of brain atrophy in patients with advanced MS [35, 36]. KEGG enrichment analysis in this study suggested that MS was closely related to environmental risk factors including viral infection, bacterial infection, and certain autoimmune diseases. The Epstein-Barr virus is regarded as the leading environmental risk factor [37]. The cross-reactivity of CD4⁺ T cells also partly explained the synergistic effect between EBV infection and genetic susceptibility to MS [38]. However, the pathway interaction between EB virus and DEGs of MS in our study remained to be verified. KEGG pathway analysis also suggested that MS was associated with other acquired autoimmune diseases such as inflammatory bowel disease, type 1 diabetes, autoimmune thyroid disease, and rheumatoid arthritis. MHC gene mutation is a significant contributor to the pathogenesis of most autoimmune diseases, affecting the immune cell response, T cell differentiation, cytokine secretion, and so on. Most of these autoimmune diseases are characterized by recurrent attacks and chronic progression [39].

To further explore the role of immune cells in the brain tissues of MS, we used the CIBERSORTX algorithm to analyze the brain tissue samples from MS patients. In general, the number of CD4⁺ T cells in MS samples is more than that in control samples. Our results showed a decrease in initial CD4⁺ T cells, suggesting that the proportion of CD4⁺ T cells in brain tissues of MS patients may vary with cell subtypes [40]. CD8⁺ T lymphocytes are resident cells of the brain and spinal cord tissues and transmit neuroinflammation locally when the cells encounter homologous antigens [41]. MS has long been viewed as a disease mediated by T cells, but in recent years, accumulating studies have focused on other important components including B cells, endothelial cells, complements, autoantibodies, cytokines, and chemokines [42]. B cells and myeloid cells are equally important in the inflammatory response of CNS. At present, anti-CD20 monoclonal antibodies (such as rituximab) are clinically used to deplete B cells, which can reduce the recurrence and retard the progression of the disease, further verifying the important roles of B cells and antibodies in MS progression [43]. Macrophages and microglia have similar inflammatory effects, and the infiltration of macrophages is strongly correlated with the model of advanced EAE [44], suggesting the role of macrophages in the advanced stage of the disease. EAE-related studies have found that the inactivation of macrophages can improve the severity of the disease [45]. Permanent myeloid cells can be found in all tissues and organs. In the case of infection or tissue injury, monocytes or granulocytes (especially neutrophils) can be recruited from the circulation to participate in the

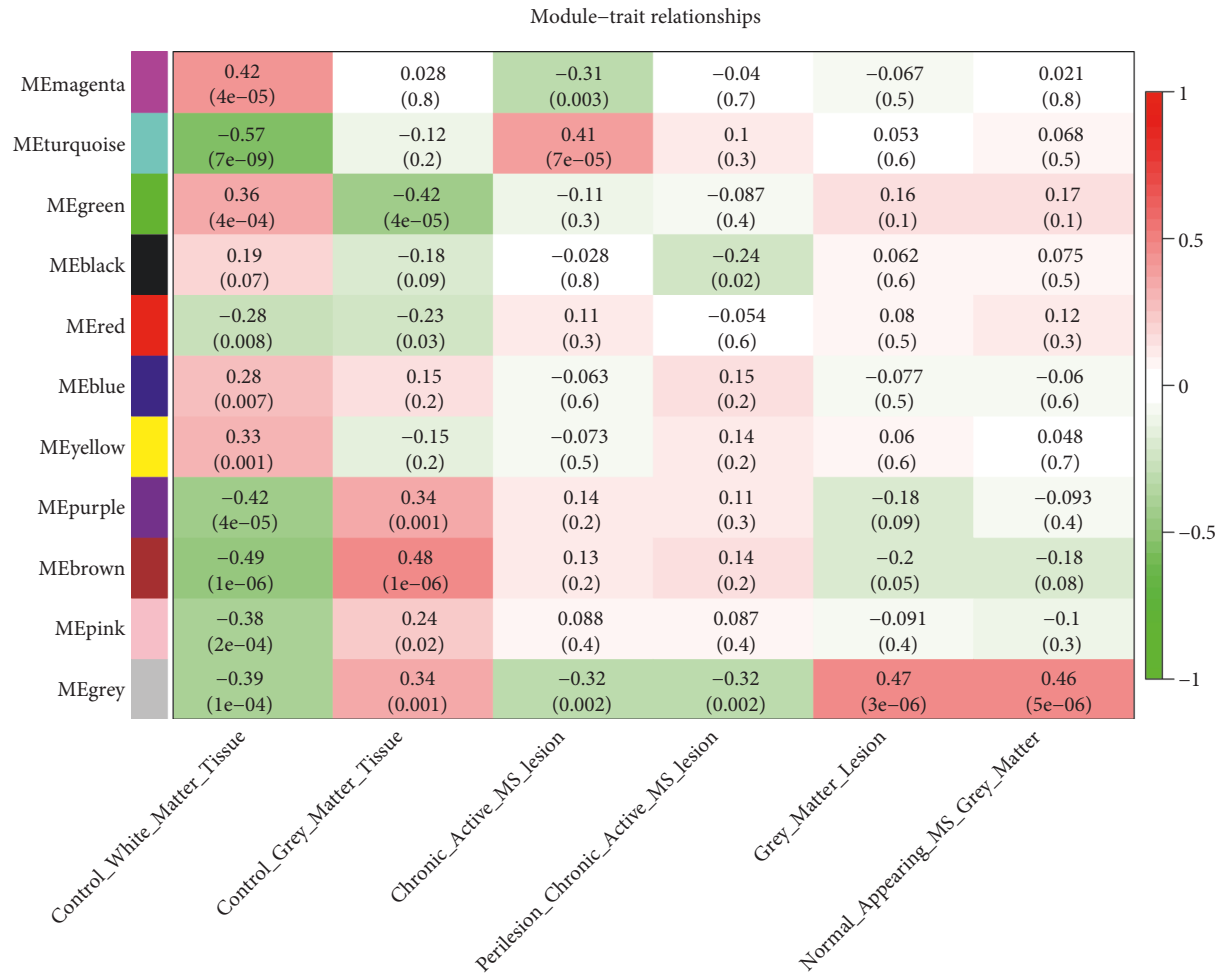


FIGURE 10: Scatterplot of correlation between genes modules and sample traits. The darker the color, the stronger the correlation between the genes module and sample trait. The color red indicates a positive correlation, while green indicates a negative correlation. Control_white_matter_tissue, white matter tissues of control group; Control_gray_matter_tissue, gray matter tissues of control group; chronic_active_MS_lesion, chronic active lesions of MS patients; perilesion_chronic_active_MS_lesion, perilesions of chronic active lesions of MS patients; gray_matter_lesion, gray matter lesions of MS patients; normal_appearing_MS_gray_matter, normal appearing gray matter of MS patients.

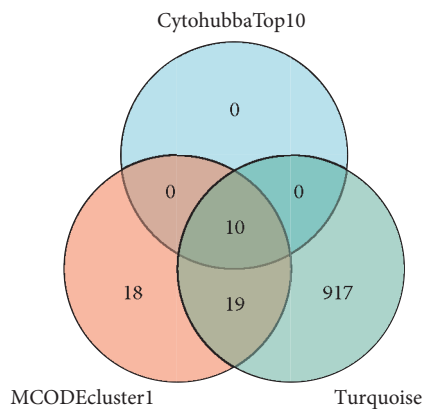


FIGURE 11: Venn diagram of intersection genes. 3 gene sets, including MCODE Cluster 1 gene set, Cytohubba Top 10 gene set, and WGCNA turquoise module genes were intersected. All top 10 genes from Cytohubba were located in the MCODE Cluster 1 gene set and the WGCNA turquoise module.

promotion of inflammatory response at the beginning and play the roles in tissue repair and regeneration at the later stage [46, 47]. The previous study on immune cell patterns of gene expression has suggested that the development of MS is caused by a wide subset of cells [42]. Patients may have a dysregulated proportion of immune cells, which results in differences in treatment responses. Susceptibility genes for major cell subsets are responsible for transcription factors, chemokines, receptors, intracellular enzymes, and signal transduction factors that control cell proportion, cell differentiation, and cell status [42]. Identifying the target antigens by tissue-hosting CD8⁺ T cells and B cells and recognizing the molecular properties and corresponding gene targets of soluble inflammatory mediators that may cause tissue damage are conducive to the treatment of MS [41]. Some hub genes were found negatively correlated with immune cells at the resting state and positively correlated with immune cells at the active state, suggesting that certain hub genes were related to the activation of peripheral

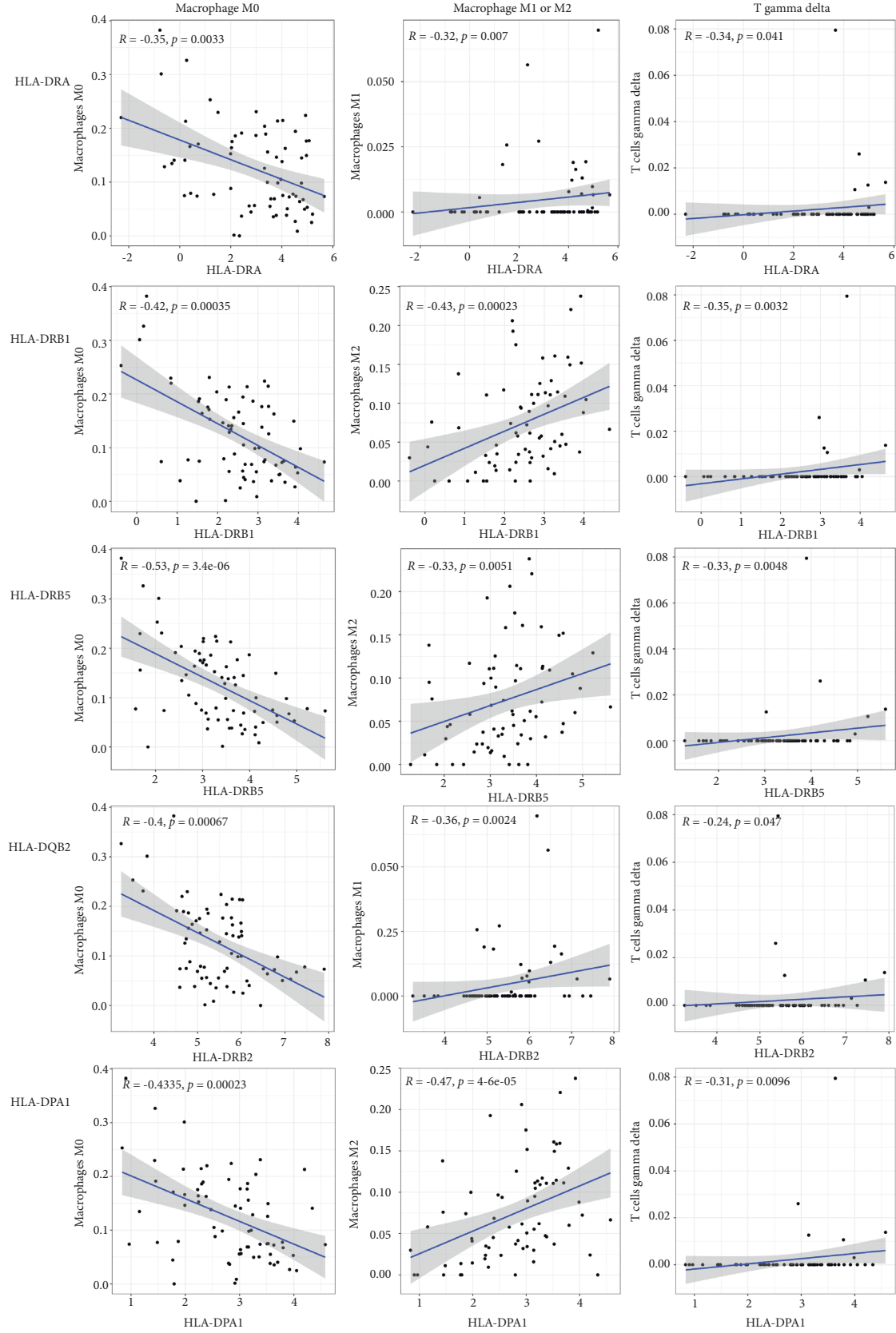


FIGURE 12: Scatterplot of correlation between top 5 hub genes (HLA-DRA, HLA-DRB1, HLA-DRB5, HLA-DQB2, and HLA-DPA1) and immune cells (including macrophage and T cells gamma delta) ($p < 0.05$).

immune cells such as macrophages. However, the role of genes in the regulation of immune cells in MS patients remained to be further investigated.

The 2019 International Multiple Sclerosis Genetics Consortium (IMSGC) explores the expression of MS genomewide immune cells and immune organs [8]. IMSGC annotates genomewide gene fragments of interest using gene expression profiles and epigenetic signature information and demonstrates that MS susceptibility loci are significantly enriched in many different immune cell types and tissues, including natural killer cells, dendritic cells, and thymus. Different from the IMSGC study, our study intuitively shows the changes of the pathological microenvironment of brain tissues.

However, our study has the following limitations, similar to most bioinformatics studies. Firstly, the sample size and patient information are limited, and we can not eliminate the bias of gender, comorbidity, disease stage, and medications. Secondly, although the merged data increase the sample size, the systematic error caused by different research methods and experimental conditions still cannot be eliminated. Thirdly, the samples in this study are from cadavers, and the gene expression profiles of these samples may be affected by the sample storage time and processing methods, which are somewhat different from living tissues. Although most of the results obtained in our study are consistent with previous studies, more studies are needed for further verification.

Given the fact that MS is not a simple genetic disease, and there are complex interactions among genetics, environment, and immunity, it is difficult to realize the application of genes in the clinical diagnosis and treatment of MS. Currently, more and more studies focus on the interaction between genes and the environment and the underlying immune mechanism. However, future studies should consider more information including clinical phenotypes, prognosis and treatment response, genetic (including epigenetic), and pathology characteristics. Moreover, it is necessary to expand the sample size to further explore the molecular mechanism of clinical phenotype and therapeutic prognosis heterogeneity, which will contribute to further clarifying the molecular classifications of the disease and guiding disease prevention and medication development of MS.

5. Conclusion

In this study, 10 key genes of MS including HLA-DRA, HLA-DRB1, HLA-DRB5, HLA-DQB2, HLA-DPA1, HLA-DQB1, HLA-E, HLA-C, GBP2, and CD44 are obtained using the algorithm. Enrichment pathways are associated with T cell activation, proliferation and differentiation, antigen presentation, autoantibody production, and glial cell proliferation, suggesting that the pathogenesis of MS was correlated with the involvement of the peripheral immune system and a cascade of brain glial cell activation. The infiltrating immune cells in brain tissues are diverse and are not only related to T cells but also B cells, macrophages, granulocytes, and other peripheral immune cells. The key genes are correlated with some immune cells, indicating the

role of susceptibility genes in promoting the activation of macrophages and natural killer cells. The gene expression profiles in MS brain tissues (including gray matter and white matter) are significantly different from those in the control samples, with the chronic active white matter lesions showing the most significant differences, followed by the tissues adjacent to chronic active white matter lesions. The 10 key genes are closely related to chronic active white matter lesions. The analysis of DEG pathway enrichment and peripheral immune cell infiltration can confer novel insights into the etiological and pathological mechanisms of MS. The gene expression profiles and underlying mechanisms of immune infiltration in MS and their correlations with environment and disease stage need further exploration.

Data Availability

The datasets analyzed during the current study are available in the National Center for Biotechnology Information-Gene Expression Omnibus (NCBI-GEO) database (<https://www.ncbi.nlm.nih.gov/geo/>). We downloaded two datasets: GSE108000 and GSE135511.

Conflicts of Interest

The authors declare no conflicts of interest.

Supplementary Materials

Supplement Table S1. Coexpressed genes of the eleven modules. (*Supplementary Materials*)

References

- [1] F. Rinaldi, M. Calabrese, P. Grossi, M. Puthenparampil, P. Perini, and P. Gallo, "Cortical lesions and cognitive impairment in multiple sclerosis," *Neurological Sciences: Official Journal of the Italian Neurological Society and of the Italian Society of Clinical Neurophysiology*, vol. 31, no. 2, pp. S235–S237, 2010.
- [2] H. M. B. Lunde, J. Assmus, K.-M. Myhr, L. Bø, and N. Grytten, "Survival and cause of death in multiple sclerosis: a 60-year longitudinal population study," *Journal of Neurology, Neurosurgery & Psychiatry*, vol. 88, no. 8, pp. 621–625, 2017.
- [3] T. Wallin, J. Culpepper, N. Nichols, and A. Bhutta, "Global, regional, and national burden of multiple sclerosis 1990–2016: a systematic analysis for the Global Burden of Disease Study 2016," *The Lancet Neurology*, vol. 18, no. 3, pp. 269–285, 2019.
- [4] H. Kuusisto, J. Kaprio, E. Kinnunen, T. Luukkaala, M. Koskenvuo, and I. Elovaara, "Concordance and heritability of multiple sclerosis in Finland: study on a nationwide series of twins," *European Journal of Neurology*, vol. 15, no. 10, pp. 1106–1110, 2008.
- [5] C. Fagnani, M. C. Neale, L. Nisticò et al., "Twin studies in multiple sclerosis: a meta-estimation of heritability and environmentality," *Multiple Sclerosis Journal*, vol. 21, no. 11, pp. 1404–1413, 2015.
- [6] L. Belbasis, V. Bellou, E. Evangelou, J. P. A. Ioannidis, and I. Tzoulaki, "Environmental risk factors and multiple sclerosis: an umbrella review of systematic reviews and meta-

- analyses," *The Lancet Neurology*, vol. 14, no. 3, pp. 263–273, 2015.
- [7] B. Hemmer, M. Kerschensteiner, and T. Korn, "Role of the innate and adaptive immune responses in the course of multiple sclerosis," *The Lancet Neurology*, vol. 14, no. 4, pp. 406–419, 2015.
 - [8] N. Patsopoulos, E. Baranzini, A. Santaniello, and P. Shoostari, "Multiple sclerosis genomic map implicates peripheral immune cells and microglia in susceptibility," *Science*, vol. 365, no. 6460, 2019.
 - [9] W. N. Brandão, M. G. De Oliveira, R. T. Andreoni, H. Nakaya, A. S. Farias, and J. P. S. Peron, "Neuroinflammation at single cell level: what is new?" *Journal of Leukocyte Biology*, vol. 108, no. 4, pp. 1129–1137, 2020.
 - [10] A. Butte, "The use and analysis of microarray data," *Nature Reviews Drug Discovery*, vol. 1, no. 12, pp. 951–960, 2002.
 - [11] H. R. Ali, L. Chlon, P. D. Pharoah, F. Markowitz, and C. Caldas, "Patterns of immune infiltration in breast cancer and their clinical implications: a gene-expression-based retrospective study," *PLoS Medicine*, vol. 13, no. 12, Article ID e1002194, 2016.
 - [12] I. S. Kohane, "Butte A.: Bioinformatics in Functional Genomics," *Encyclopedia of Biostatistics*, Wiley, Hoboken, NJ, USA, 2000.
 - [13] T. Barrett, S. E. Wilhite, P. Ledoux et al., "NCBI geo: archive for functional genomics data sets--update," *Nucleic Acids Research*, vol. 41, pp. D991–D995, 2013.
 - [14] H. S. Parker, J. T. Leek, A. V. Favorov et al., "Preserving biological heterogeneity with a permuted surrogate variable analysis for genomics batch correction," *Bioinformatics*, vol. 30, no. 19, pp. 2757–2763, 2014.
 - [15] L. Wilkinson, "Ggplot2: elegant graphics for data analysis by Wickham, H.," *Biometrics*, vol. 67, no. 2, pp. 678–679, 2011.
 - [16] G. Yu, L.-G. Wang, Y. Han, and Q.-Y. He, "ClusterProfiler: an R package for comparing biological themes among gene clusters," *OMICS: A Journal of Integrative Biology*, vol. 16, no. 5, pp. 284–287, 2012.
 - [17] W. Luo and C. Brouwer, "Pathview: an R/Bioconductor package for pathway-based data integration and visualization," *Bioinformatics*, vol. 29, no. 14, pp. 1830–1831, 2013.
 - [18] P. Langfelder and S. Horvath, "Fast R functions for robust correlations and hierarchical clustering," *Journal of Statistical Software*, vol. 46, no. 11, 2012.
 - [19] D. A. Hafler, D. A. Hafler, A. Compston et al., "Risk alleles for multiple sclerosis identified by a genomewide study," *New England Journal of Medicine*, vol. 357, no. 9, pp. 851–862, 2007.
 - [20] H. L. E. Lang, H. Jacobsen, S. Ikemizu et al., "A functional and structural basis for TCR cross-reactivity in multiple sclerosis," *Nature Immunology*, vol. 3, no. 10, pp. 940–943, 2002.
 - [21] S. Saidha and P. A. Calabresi, "Anti-interleukin-2 receptor alpha for multiple sclerosis?" *The Lancet*, vol. 381, no. 9884, pp. 2141–2143, 2013.
 - [22] L. Lorefice, G. Fenu, C. Sardù et al., "Multiple sclerosis and HLA genotypes: a possible influence on brain atrophy," *Multiple Sclerosis Journal*, vol. 25, no. 1, pp. 23–30, 2019.
 - [23] S. A. Joosten, L. C. Sullivan, and T. H. Ottenhoff, "Characteristics of HLA-E restricted T-cell responses and their role in infectious diseases," *Journal of immunology research*, vol. 2016, Article ID 2695396, 9 pages, 2016.
 - [24] P. F. Durrenberger, L. V. Webb, M. J. W. Sim, R. S. Nicholas, D. M. Altmann, and R. J. Boyton, "Increased HLA -E expression in white matter lesions in multiple sclerosis," *Immunology*, vol. 137, no. 4, pp. 317–325, 2012.
 - [25] F. Ye, J. Liang, J. Li, H. Li, and W. Sheng, "Development and validation of a five-gene signature to predict relapse-free survival in multiple sclerosis," *Frontiers in Neurology*, vol. 11, Article ID 579683, 2020.
 - [26] N. L. Fransen, C.-C. Hsiao, M. van der Poel et al., "Tissue-resident memory T cells invade the brain parenchyma in multiple sclerosis white matter lesions," *Brain*, vol. 143, no. 6, pp. 1714–1730, 2020.
 - [27] K. M. Flynn, M. Michaud, and J. A. Madri, "CD44 deficiency contributes to enhanced experimental autoimmune encephalomyelitis: a role in immune cells and vascular cells of the blood-brain barrier," *American Journal Of Pathology*, vol. 182, no. 4, pp. 1322–1336, 2013.
 - [28] K. N. Chitralla, H. Guan, N. P. Singh et al., "CD44 deletion leading to attenuation of experimental autoimmune encephalomyelitis results from alterations in gut microbiome in mice," *European Journal of Immunology*, vol. 47, no. 7, pp. 1188–1199, 2017.
 - [29] J. A. Hollenbach and J. R. Oksenberg, "The immunogenetics of multiple sclerosis: a comprehensive review," *Journal of Autoimmunity*, vol. 64, pp. 13–25, 2015.
 - [30] T. Fazio, A. Nova, D. Gentilini et al., "Investigating the causal effect of brain expression of CCL2, NFKB1, MAPK14, TNFRSF1A, CXCL10 genes on multiple sclerosis: a two-sample mendelian randomization approach," *Frontiers in Bioengineering and Biotechnology*, vol. 8, p. 397, 2020.
 - [31] V. Bhise and S. Dhib-Jalbut, "Further understanding of the immunopathology of multiple sclerosis: impact on future treatments," *Expert Review of Clinical Immunology*, vol. 12, no. 10, pp. 1069–1089, 2016.
 - [32] L. M. Healy, M. Yaqubi, S. Ludwin, and J. P. Antel, "Species differences in immune-mediated CNS tissue injury and repair: a (neuro)inflammatory topic," *Glia*, vol. 68, no. 4, pp. 811–829, 2020.
 - [33] J. Gruchot, V. Weyers, P. Göttele et al., "The molecular basis for remyelination failure in multiple sclerosis," *Cells*, vol. 8, no. 8, 2019.
 - [34] A. Geladaris, D. Hausler, and M. S. Weber, "Microglia: the missing link to decipher and therapeutically control MS progression?" *International Journal of Molecular Sciences*, vol. 22, no. 7, 2021.
 - [35] M. A. Friesse, B. Schattling, and L. Fugger, "Mechanisms of neurodegeneration and axonal dysfunction in multiple sclerosis," *Nature Reviews Neurology*, vol. 10, no. 4, pp. 225–238, 2014.
 - [36] D. H. Mahad, B. D. Trapp, and H. Lassmann, "Pathological mechanisms in progressive multiple sclerosis," *The Lancet Neurology*, vol. 14, no. 2, pp. 183–193, 2015.
 - [37] T. Olsson, "Epstein Barr virus infection and immune defense related to HLA-DR15: consequences for multiple sclerosis," *European Journal of Immunology*, vol. 51, no. 1, pp. 56–59, 2021.
 - [38] H. Zdimerova, A. Murer, C. Engelmann et al., "Attenuated immune control of Epstein-Barr virus in humanized mice is associated with the multiple sclerosis risk factor HLA-DR15," *European Journal of Immunology*, vol. 51, no. 1, pp. 64–75, 2021.
 - [39] R. Horton, L. Wilming, V. Rand et al., "Gene map of the extended human MHC," *Nature Reviews Genetics*, vol. 5, no. 12, pp. 889–899, 2004.
 - [40] B. Arneth, "Activated CD4+ and CD8+ T cell proportions in multiple sclerosis patients," *Inflammation*, vol. 39, no. 6, pp. 2040–2044, 2016.

- [41] H. Lassmann, "Pathogenic mechanisms associated with different clinical courses of multiple sclerosis," *Frontiers in Immunology*, vol. 9, p. 3116, 2018.
- [42] G. P. Parnell and D. R. Booth, "The multiple sclerosis (MS) genetic risk factors indicate both acquired and innate immune cell subsets contribute to MS pathogenesis and identify novel therapeutic opportunities," *Frontiers in Immunology*, vol. 8, p. 425, 2017.
- [43] G. Comi, A. Bar-Or, H. Lassmann et al., "Role of B Cells in multiple sclerosis and related disorders," *Annals of Neurology*, vol. 89, no. 1, pp. 13–23, 2021.
- [44] B. Ajami, J. L. Bennett, C. Krieger, K. M. McNagny, and F. M. V. Rossi, "Infiltrating monocytes trigger EAE progression, but do not contribute to the resident microglia pool," *Nature Neuroscience*, vol. 14, no. 9, pp. 1142–1149, 2011.
- [45] E. D. Ponomarev, T. Veremeyko, N. Barteneva, A. M. Krichevsky, and H. L. Weiner, "MicroRNA-124 promotes microglia quiescence and suppresses EAE by deactivating macrophages via the C/EBP- α -PU.1 pathway," *Nature Medicine*, vol. 17, no. 1, pp. 64–70, 2011.
- [46] T. Owens, A. Benmamar-Badel, A. Wlodarczyk et al., "Protective roles for myeloid cells in neuroinflammation," *Scandinavian Journal of Immunology*, vol. 92, no. 5, Article ID e12963, 2020.
- [47] X. Zhang, Y. Song, X. Chen, X. Zhuang, Z. Wei, and Li Yi, "Integration of genetic and immune infiltration insights into data mining of multiple sclerosis pathogenesis," 2021, <https://www.researchsquare.com/article/rs-642302/v2>.

Research Article

Design of Digital and Intelligent Financial Decision Support System Based on Artificial Intelligence

Tiejun Jia , Cheng Wang, Zhiqiang Tian, Bingyin Wang, and Feng Tian

Shenhua Group Zhungeer Energy CO. LTD., Ordos, Inner Mongolia 017000, China

Correspondence should be addressed to Tiejun Jia; 20203107663@hainanu.edu.cn

Received 23 April 2022; Revised 11 May 2022; Accepted 19 May 2022; Published 20 June 2022

Academic Editor: Dong Chen

Copyright © 2022 Tiejun Jia et al. This is an open access article distributed under the Creative Commons Attribution License, which permits unrestricted use, distribution, and reproduction in any medium, provided the original work is properly cited.

The quality of financial decision-making is very important to the future development of an enterprise, but it is often affected by the completeness of useful information for decision-making and the subjective factors of decision makers, and is often unstable. With the development of computer technology, the financial decision support system came into being, which improved the quality of financial decision to some extent. However, although the existing financial decision support system has achieved dataization to a certain extent, it still faces problems such as artificial leadership, insufficient intelligence, and poor decision-making efficiency, and cannot fully meet the needs of decision-makers. The explosion of artificial intelligence technology in recent years has provided potential improvements to financial decision support systems. In this article, we conduct a detailed analysis of the deficiencies in the current financial decision support system, build the mechanism and implementation path of the financial decision support system under artificial intelligence, and design a digital and intelligent financial decision support system. At the same time, we apply the proposed financial decision support system to the financial practice of X enterprise. Through the questionnaire survey, it is found that through the comprehensive application of artificial intelligence technology, the new system has a higher degree of intelligence than the existing system, and its construction can effectively improve the timeliness and accuracy of financial decision-making, while reducing the cost of financial decision-making. It is conducive to promoting the integration of management accounting and financial accounting.

1. Introduction

The quality of financial decision-making is the life source of an enterprise and is of great significance to the sustainable and stable development of the enterprise. For a long time, the construction of a financial decision support system has been the concern of scholars. The financial decision support system realizes scientific and effective financial decision-making by comprehensively managing the upstream and downstream financial information of the enterprise, integrating the actual financial situation of the enterprise in the whole process, and integrating internal and external information [1–3]. In recent years, with the vigorous development of computer technology, the concepts of digitization and intelligence have emerged in the management information system [4], [5]. Through the digitalization and intelligence of the financial decision-making system, a more

complete financial operation environment can be created for enterprises, the behavior of financial personnel can be standardized, and the transparency of financial information can be realized, which has become an important trend of enterprise financial management in the future.

The traditional financial decision support system cannot effectively mine the financial information of enterprises, resulting in the inability to distinguish the value of information, including information and usage information. Judging from the decision analysis system and big data technology implemented by some listed companies and Internet companies, the full mining of data value can greatly improve the efficiency and quality of decision-making [6]. However, most of the current financial decision support systems only implement digital information systems. However, the level of intelligence of financial decision support systems is not satisfactory. Zhao et al. pointed out

that the current large-scale financial decision support systems in enterprises are insufficient in intelligence. Specifically, most of the decisions are still judged by junior financial personnel, and the intelligent system cannot make judgments adaptively according to the actual situation. Therefore, the intelligent financial decision support system still has great potential [7].

In order to effectively improve the quality of corporate financial decision-making and promote the deep integration of artificial intelligence technology and the financial field, it is the general trend to build a financial decision support system under artificial intelligence. In order to lay a foundation for the construction of the financial decision support system under artificial intelligence in theory, so as to better guide its construction and application in practice, this article conducts in-depth research on its mechanism and implementation path. Based on artificial intelligence technology, this article investigates the application status of the existing financial decision support system and the necessity and feasibility of the elements contained in the mechanism and implementation path of the financial decision support system under artificial intelligence. On this basis, this article constructs the mechanism and implementation path of the financial decision support system under artificial intelligence. Finally, through the case analysis of the A group that applied the system, the results prove the effectiveness of our proposed system.

2. Related Work

The study of decision support systems (DSSs) began in the 1970s, when Scott et al. first proposed the term management decision systems and proposed the application of computers in the decision-making process [8]. The development of the decision support system has gone through five stages: the decision support system with the model base system as the core, the intelligent decision support system (IDSS) combining knowledge reasoning and model calculation, the decision support system based on the data warehouse (DW), the decision support system based on the data warehouse (DW), and client/server (C/S) decision support system and web service-based decision support system. Foreign financial decision support systems started in the 1980s. At the beginning of this century, EXCUCON Systems, Capex, and American Airlines developed and put into use a number of financial decision support systems. At the same time, scholars are constantly proposing new design schemes for financial decision support systems, which greatly strengthens its functions and expands its application fields. Eom et al. proposed a multicriteria decision support system based on an objective planning model to meet the needs of global financial planning of multinational companies [9]. Rigopoulos et al. proposed an intelligent module for strengthening group financial decision support systems, and the operation method of this module is based on multicriteria analysis and is dedicated to helping the financial department to make complex group financial decisions [10].

At the same time, with the development of computer and Internet technology, foreign scholars are also deepening the

research on new financial decision support systems, and they have put forward suggestions for improving financial decision support systems from the perspective of specific technical applications. Rupnik and Kukkar proposed the application of data mining technology in decision support systems [11]. Tang et al. proposed a financial decision support system based on information entropy and applied fuzzy logic theory, adaptive genetic algorithm, and other technologies. Marcin et al. believe that many factors can assist financial decision-making, including statistical methods, mathematical methods, behavioral methods, artificial intelligence, and sensitivity analysis of expert opinions. But it is very difficult to predict the market due to uncertainty and risk. In order to better solve this problem, they designed a group financial decision support system based on a consensus method. The design was tested by the data of the Warsaw Stock Exchange [12]. Tang and Leung pointed out that uncertainty has a great impact on the decision-making process, but the existing decision support tools are difficult to solve the instability impact of uncertainty on decision-making [13]. Xiao et al. pointed out the problems in the data collection of the existing system. The existing financial decision support system is established and developed on the basis of the traditional accounting information system. The financial and nonfinancial data obtained through the accounting information system are huge in scale, but contain very little information, which seriously affects the efficiency of financial decision-making [14]. In recent years, artificial intelligence technology has been gradually applied to financial decision support systems. However, Frantz et al. pointed out that the operation of expert systems often requires massive data, but for a long time, these data rely on manual input, and the dependence on manual input data has become a bottleneck in artificial intelligence applications [15].

3. The Proposed System

3.1. Analysis of Digital and Intelligent Financial Decision Support System. The existing system mainly assists financial decision-making by providing information, which makes it actually mainly play the function of a calculator, and cannot directly provide decision-making suggestions to managers [16–18], as shown in Figure 1. The formulas and decision models stored in the existing system are difficult to update, and the support for financial decision-making is limited to the provision of common financial analysis functions such as DuPont analysis, which makes the output results lack pertinence, especially in the face of unstructured finance. When making decisions, it often fails to provide the analysis results or decision-making solutions that decision makers really need. In addition, as the basis of financial decision-making, the quality of data is very important to the accuracy of financial decision-making, but it is difficult for the existing system to judge the authenticity and reliability of the data collected, which makes decision makers always keep vigilant and guard against data distortion has a limited impact on financial decisions and thus has limited reliance on existing systems.

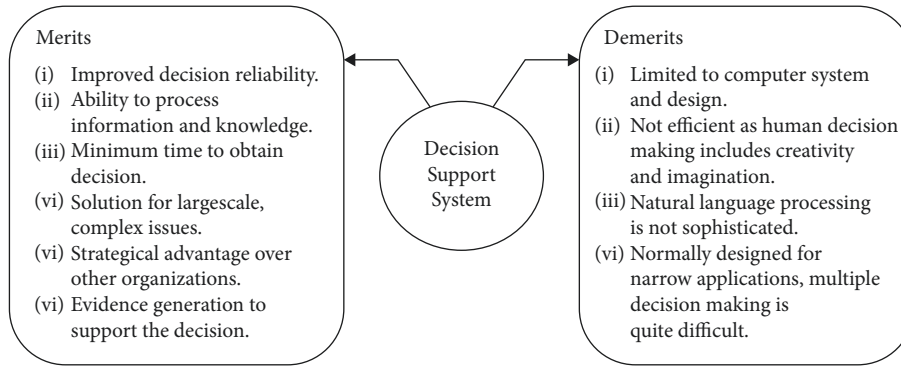


FIGURE 1: Merits and demerits of the current financial decision support system.

The financial decision support effect of the existing system is not good [19–21]. In terms of useful information for decision-making, the existing system focuses on the collection of internal business and financial information of the enterprise, while ignoring the collection of external information such as industry information, policy information, and macroeconomic information, and even some key decision-making useful information needs to be supplemented by decision makers, which leads to insufficient decision-making useful information integrity and reduces the quality of decision-making useful information [22–25]. The low quality of useful information for decision-making directly affects the quality of financial decision-making. In addition, for some large group companies, the subordinate companies have their own financial software, the data format is difficult to unify, and the real-time collection and aggregation cannot be realized, which makes these subordinate companies become information islands and increases the difficulty of financial decision-making at the group level. Because the support effect and versatility of the existing systems cannot be achieved at the same time, in order to ensure the quality of decision-making, most of the existing systems are designed for a certain kind of financial decision-making, and it is difficult to solve other financial decision-making problems. At the same time, the construction cost of the financial decision support system is usually high, and it is impossible to build a corresponding system for all problems, so the decision support cost is high and the scope of application is small.

3.2. Design of Our Proposed Structure. Overall structure of our proposed system is shown in Figure 2.

The data layer mainly performs data collection, cleaning, data mining, and storage. With the help of automatic data transmission programs and natural language processing technology, it is possible to quickly obtain useful information for internal decision-making such as business and financial information, audit information, and credit information stored in the local database, as well as government policy information, tax information, exchange rate information, and market information published on the Internet information, legal information, macroeconomic information, and other external information. These massive

heterogeneous data are cleaned and mined to form multi-dimensional useful information for decision-making, and are classified and stored in the data warehouse. The data warehouse lays a strong data foundation for the deep learning of the new system and financial decision-making. At the same time, the advance processing and classification of data also provides a guarantee for the timeliness of financial decision-making.

The analysis layer is responsible for carrying out financial analysis, financial forecasting, and financial decision-making activities. Financial analysis is the basis for carrying out financial forecasting and decision-making, and financial decision-making depends on the results of financial analysis and financial forecasting. The analysis layer includes knowledge base, method base, model base, and their respective management systems and artificial intelligence analysis system. The knowledge base stores various financial knowledge, common sense and reasoning rules, and other data, the method base stores financial analysis, forecasting, and decision-making methods, and the model base stores financial analysis models. On the one hand, the management systems of the three databases are responsible for receiving the instructions of the artificial intelligence analysis system and fetching the required knowledge, methods, and models from the corresponding libraries, and on the other hand, they embed deep learning algorithms to automatically carry out new knowledge, new methods, and models in the background. The establishment of new models and the improvement of existing knowledge, methods, and models, so as to update the knowledge base, method base, and model base in time. The artificial intelligence analysis system is responsible for receiving the financial decision-making goals conveyed by the human-computer interaction system and accordingly sends instructions to the database management systems and data warehouses, receives data for analysis, and finally feeds the results back to the human-computer interaction system. The artificial intelligence analysis system includes several inference engines embedded with deep learning algorithms. Some of these inference engines are responsible for determining the types of knowledge, methods, models, and portraits required according to financial decision-making goals, and the other is responsible for financial analysis to

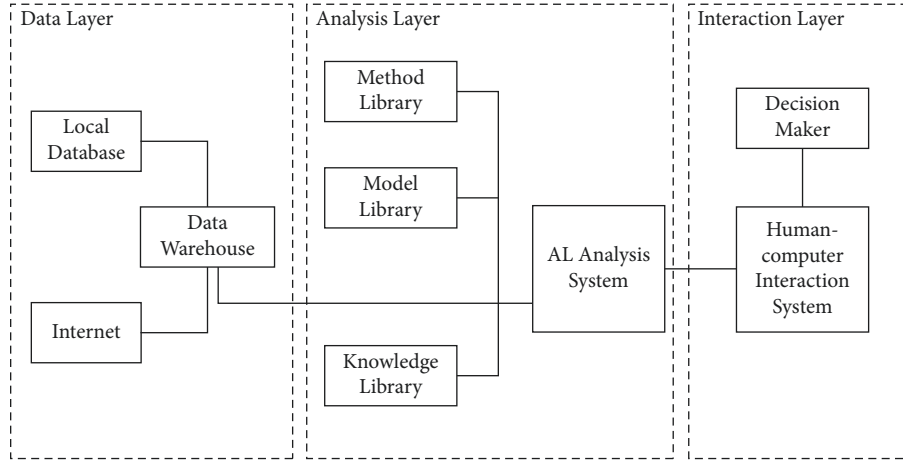


FIGURE 2: Overall structure of our proposed system.

generate various portraits. A part is responsible for the generation of financial forecasts and decisions.

The interaction layer is the link between the new system and decision-makers. Human-computer interaction systems use speech recognition and natural language processing technology, so decision-makers can use natural language to communicate with new systems. In the process of financial decision-making, the human-computer interaction system forms financial decision-making goals through the processing of natural language and at the same time communicates the financial decision-making goals to the artificial intelligence analysis system. After completing the financial decision, through the human-computer interaction system, output the financial analysis report, the financial forecast report and the financial decision report that integrates the above report information, or the customized report prepared according to the needs of the decision-maker.

3.3. The Digital and Intelligent Mechanism. With the help of the Internet, the new system can obtain massive amounts of structured, semi-structured, and unstructured data such as financial statement information, supply chain information, market information, industry information, securities market information, and online public opinion information in real time. These raw data describe the company's own financial situation and the external financial decision-making environment it faces from many aspects, but these data are chaotic in structure and uneven in quality, and cannot be directly used for financial analysis, so data cleaning and data mining are required. The raw data processed by big data technology have become multidimensional decision-making useful information and is classified and stored by subject. Taking a certain type of product as an example, through multidimensional decision-making useful information, we can extract relevant information from multiple dimensions such as product model, output, sales volume, and main market and quickly obtain the sales of the product at a certain time and place. Just as the liquidity of assets can be judged by indicators such as current ratio and quick ratio, and through these multidimensional decision-making useful

information, deep learning algorithms will determine the solvency, profitability, operating ability, growth ability, risk tolerance, risk appetite, and other factors should be evaluated and judged. Compared with the previous evaluation results obtained by solidified indicators, the results obtained by artificial intelligence technology based on exponential indicators are more accurate, thus ensuring the appropriateness of financial decisions. Further carry out financial analysis, financial forecasting, and financial decision-making based on useful information for decision-making. With the help of existing financial analysis methods and corresponding deep learning algorithms, it is possible to analyze and evaluate the solvency, development, profitability, and operational capabilities of enterprises. The financial analysis data together with the enterprise characteristic data constitute the enterprise portrait.

Similarly, through the analysis and processing of useful information for multidimensional decision-making on other topics, various types of financial decision-making information groups such as external environment portraits, asset portraits, and customer portraits can be obtained. When the financial decision target is generated, according to the model obtained by the deep learning algorithm during training, the new portrait is customized, and the various portraits are matched with each other and the future under different matching paths.

Predicting and analyzing the results of financial activities is to obtain financial forecast data. On this basis, the action path that can meet the financial decision-making objective to the greatest extent is selected as the financial decision. Decision-makers can revise the output financial decision through man-machine dialogue, and the revision process will affect the final decision model to improve the quality of the next decision. After obtaining a satisfactory financial decision, decision-makers can choose to output a general financial decision report or customize a personalized report. Useful information for decision-making is the starting point for financial decision-making. Therefore, the new system does not screen information when collecting information, so as to ensure the comprehensiveness of useful information for decision-making. Further processing of these data is

required to improve the relevance and availability of useful information for decision-making. For unstructured data, it uses natural language processing technology for structured processing, extracts key entity information, and mines the data relationships contained in this information.

Combining data mining with data-cleaned structured data, the new system can obtain high-quality decision-making useful information including the data itself and the complex relationship between the data. Financial decision-making methods and models are the link between useful information for decision-making and financial decision-making, reflecting the logical relationship and causal relationship between the two. Therefore, financial decision-making methods and models have a significant impact on the quality of financial decision-making. Here, we introduce two classical deep learning methods as decision models, namely, recurrent neural network (RNN) and long short-term memory. The equation for RNN is denoted as

$$\begin{aligned} o_t &= g(W_o s_t), \\ s_t &= f(W_x x_t + W_s s_{t-1}). \end{aligned} \quad (1)$$

For LSTM, the equation is denoted as

$$\begin{aligned} f_t &= \sigma(W_f x_t + U_f h_{t-1} + b_f), \\ i_t &= \sigma(W_i x_t + U_i h_{t-1} + b_i), \\ o_t &= \sigma(W_o x_t + U_o h_{t-1} + b_o), \\ c_t &= f_t \odot c_{t-1} + i_t \odot \sigma(W_c x_t + U_c h_{t-1} + b_c), \\ h_t &= o_t \odot \sigma(c_t), \end{aligned} \quad (2)$$

where x_t is the input features, which consist of price features and technical indicator. f_t , i_t , and o_t represent forget gate, input gate, and output gate, respectively. c_t and h_t represent cell state and hidden state, respectively.

Because our model is deployed on a financial system, computational complexity is a consideration, we improve the LSTM so that it can be deployed on high-traffic financial decision support systems. Specifically, the improved LSTM formula is as follows:

$$\begin{aligned} z_t &= \sigma(W_z[h_{t-1}, x_t]), \\ r_t &= \sigma(W_r[h_{t-1}, x_t]), \\ \hat{h}_t &= \tanh(W[r_t h_{t-1}, x_t]), \\ h_t &= (1 - z_t)h_{t-1} + z_t \hat{h}_t. \end{aligned} \quad (3)$$

Meanwhile, considering the black-box characteristics of the deep learning model, we added attention mechanism in the improved LSTM to improve the interpretability of the model. The attention mechanism enables models to adaptively discover potential patterns in input data, thereby improving model performance by identifying important features. Besides, the identification of important features also provides guidance for financial personnel to explain the

decision-making process of the model. The formula for the attention mechanism is as follows:

$$\begin{aligned} e_t &= h_t W c_T, \\ \alpha_t &= \frac{\exp(e_t)}{\sum_{t=1}^T \exp(e_t)}, \\ h &= \sum_{t=1}^T \alpha_t e_t \end{aligned} \quad (4)$$

Using deep learning algorithms, we feed the new system with decision-making information, and if it makes the right financial decision, we give the neural network that made the right decision more weight, and less weight if it does not. This process is the training process of the new system. After training enough times, the new system will sum up its own financial decision-making methods and models, making financial decisions without human involvement. These financial decision-making methods and models may be different from the current solidified models. Compared with solidified models, these methods and models are more complex functional systems and have a higher degree of fitting to the data. And as the number of training increases, these methods and models will become more complex, and the quality of financial decisions will continue to improve. When the new system receives the financial decision objective, the financial decision support process is initiated. The new system will select the financial decision-making methods and models that have been trained according to the financial decision-making objectives and select useful information for decision-making according to the methods and models. After calculation and analysis, a financial decision is finally generated.

4. Empirical Study

We execute real applications at X company and collect data for assessment in order to verify the efficacy of the suggested financial decision support system. Internal demands, rules, objectives, and external pressures are all factors that financial decision support systems consider. As a result, before the update, each category is assessed against the planned structure and compared to Enterprise X's decision support system: S1 for internal pressure, T1 external pressure, U1 goals and financial criteria, with subgoals, JA1 job satisfaction (common to financial employees), JA2 cognitive skills, JA3 employee contribution to the company, JA4 employee strength, JA5 individual effort, JA6 timely reaction, JA7 accessible resources, JA8 organizational characteristics, and JA9 maturity to company activities. The classification results are grouped into U1 and U2 groups, and the final classification result is generated as an output of the organizational development decision support system.

The priority function value is obtained based on the consistency of the clusters and thresholds. If the value is below 0.1, it is acceptable, and others are considered unacceptable. Based on the weights, the priority value of the proposed system is measured and compared with the previous system, as shown in Figure 3. By evaluating employees,

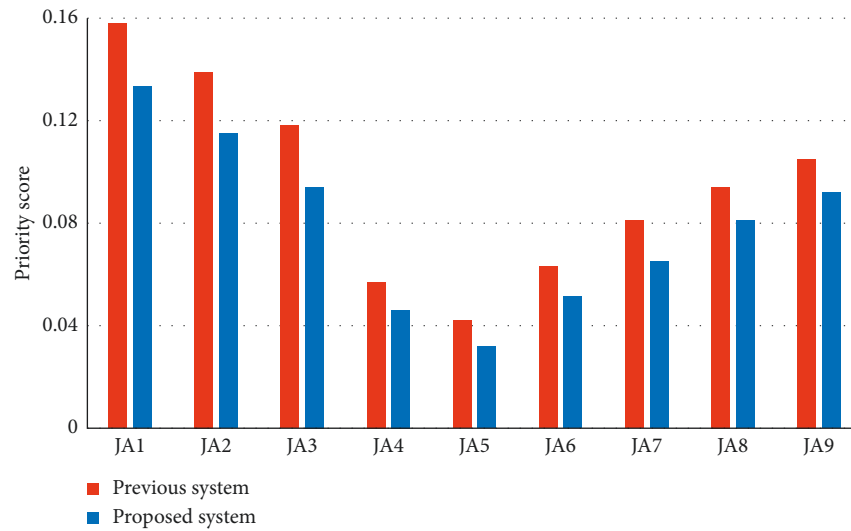


FIGURE 3: The results of the priority assessment comparison.

stack holders, and management, it was observed that the proposed model had better priority value opinions. While the previous system has a lower priority value due to its inefficient evaluation strategy.

The priority values of our proposed system are assessed and compared to the existing system using the weights, as illustrated in Figure 3. It was discovered that the suggested approach had superior priority value opinions after examining workers, stack holders, and management. Other models, on the other hand, have lower priority ratings owing to ineffective assessment techniques.

5. Conclusion

The application of the financial decision support system can have a positive impact on enterprise financial decision-making, including making financial analysis more comprehensive and accurate, improving the comprehensiveness of useful information for decision-making, and improving the timeliness of financial decision-making. However, the existing system is not widely used, and its functions are not comprehensive enough to meet all the decision-making needs of decision makers. The main reason for this situation is that the existing systems generally have the problems of low degree of intelligence, high cost of system construction and operation, insufficient timeliness of decision-making support, and poor decision-making effect. By realizing the extensive application of artificial intelligence technology in financial decision support systems, a financial decision support system under artificial intelligence can be constructed. The application of digital and intelligent systems can provide decision-makers with more comprehensive and accurate decision-making useful information, and under the condition of ensuring the principle of cost and benefit, expand the scope of financial decision support, improve the scientificity and objectivity of financial decision-making, and reduce the probability of irrational decision-making. It will improve the overall financial decision-making quality of the enterprise and ensure the long-term stable and healthy

development of the enterprise. This article proposes a financial decision support system composed of data layer, analysis layer, and interaction layer. Driven by digitalization and intelligence, it provides financial analysis, forecasting, and decision support services including financing decisions, investment decisions, cost decisions, dividend distribution decisions, and special financial decisions. AI technology is applied throughout the financial decision-making process. First of all, the new system mines and organizes the data collected in each basic database, draws various portraits, and stores them in the data warehouse. When the decision-making target is received, it supplements the decision-making useful information according to the decision-making target, and performs portrait matching, so as to obtain financial decision-making. Subsequently, the scheme can be modified and improved with the help of human-computer interaction to form the final scheme. The empirical research on the actual application of X enterprise shows that the system we propose not only inherits the digital characteristics of the existing system but also better utilizes intelligent technology to organize the flow of data, and realizes the improvement of decision-making efficiency.

Data Availability

The data used to support the findings of this study are available from the corresponding author upon request.

Conflicts of Interest

The authors declare that they have no conflicts of interest.

References

- [1] Z. Janková and P. Dostál, "Type-2 fuzzy expert system Approach for decision-making of financial assets and investing under different uncertainty," *Mathematical Problems in Engineering*, vol. 2021, pp. 1–16, Article ID 3839071, 2021.
- [2] M. Lai, "Smart Financial Management System Based on Data Mining and Man-Machine Management," *Wireless*

- Communications and Mobile Computing*, vol. 2022, pp. 1–10, Article ID 2717982, 2022.
- [3] L. Li, T. Qu, Y. Liu, and R. Y. Zhong, “Sustainability assessment of intelligent manufacturing supported by digital twin,” *IEEE Access*, vol. 8, pp. 174988–175008, 2020.
 - [4] H. Xiaolong, Z. Huiqi, Z. Lunchao, S. Nazir, D. Deng, and A. S. Khan, “Soft Computing and Decision Support System for Software Process Improvement: A Systematic Literature Review,” *Scientific Programming*, vol. 2021, pp. 1–14, Article ID 7295627, 2021.
 - [5] H. Ma, “Optimization of hotel financial management information system based on computational intelligence,” *Wireless Communications and Mobile Computing*, vol. 2021, pp. 1–11, Article ID 8680306, 2021.
 - [6] L. Li, B. Lei, and C. Mao, “Digital twin in smart manufacturing,” *Journal of Industrial Information Integration*, vol. 26, no. 9, Article ID 100289, 2022.
 - [7] Y. Zhao, “Decision Support System for Economic Management of Large Enterprises Based on Artificial Intelligence,” *Wireless Communications and Mobile Computing*, Article ID 9453580, 2022.
 - [8] M. C. Er, “Decision Support Systems: a summary, problems, and future trends,” *Decision Support Systems*, vol. 4, no. 3, pp. 355–363, 1988.
 - [9] H. B. Eom, S. M. Lee, C. A. Snyder, and F. N. Ford, “A multiple criteria decision support system for global financial planning,” *Journal of Management Information Systems*, vol. 4, no. 3, pp. 94–113, 1987.
 - [10] G. Rigopoulos, N. Karadimas, A. Orsoni, and J. Otamendi, “An interactive web based decision support system for financial decisions within a team,” in *Proceedings of the 2007 Innovations in Information Technologies (IIT)*, pp. 546–550, IEEE, Dubai, United Arab Emirates, 18–20 Nov. 2007.
 - [11] R. Rupnik and M. Kukar, “Decision support system to support decision processes with data mining[J],” *Journal of Information and Organizational Sciences*, vol. 31, no. 1, pp. 217–232, 2007.
 - [12] M. Hernes and J. Sobieska-Karpińska, “Application of the consensus method in a multiagent financial decision support system,” *Information Systems and E-Business Management*, vol. 14, no. 1, pp. 167–185, 2016.
 - [13] L. C. M. Tang and A. Y. T. Leung, “An entropy-based financial decision support system (e-FDSS) for project analysis in construction SMEs,” *Construction Management & Economics*, vol. 27, no. 5, pp. 499–513, 2009.
 - [14] M. Xiao, H. Xiaoli, and L. Gaojin, “Research on application of data mining technology in financial decision support system,” *IEEE in Proceedings of the 2010 3rd international conference on information management, innovation management and industrial engineering*, vol. 4, pp. 381–384, Kunming, China, 26–28 Nov. 2010.
 - [15] F. Vichot, F. Wolinski, H.-C. Ferri, and D. Urbani, “Feeding a financial decision support system with textual information [J],” *Journal of Intelligent and Robotic Systems*, vol. 26, no. 2, pp. 157–166, 1999.
 - [16] S. Gao, H. Wang, D. Xu, and Y. Wang, “An intelligent agent-assisted decision support system for family financial planning,” *Decision Support Systems*, vol. 44, no. 1, pp. 60–78, 2007.
 - [17] M. A. H. Dempster and A. M. Ireland, “A financial expert decision support system[J],” *Mathematical models for decision support*, vol. 48, pp. 415–440, 1988.
 - [18] C.-F. Tsai, “Financial decision support using neural networks and support vector machines,” *Expert Systems*, vol. 25, no. 4, pp. 380–393, 2008.
 - [19] L. Li and C. Mao, “Big data supported PSS evaluation decision in service-oriented manufacturing,” *IEEE Access*, vol. 8, no. 99, pp. 154663–154670, 2020.
 - [20] L. Li, C. Mao, H. Sun, and Y. B. Yuan, “Digital twin driven green performance evaluation methodology of intelligent manufacturing: hybrid model based on fuzzy rough-sets AHP, multistage weight synthesis, and PROMETHEE II,” *Complexity*, vol. 2020, no. 6, pp. 1–24, Article ID 3853925, 2020.
 - [21] S. Khademolqorani, A. Zeinal Hamadani, F. Mokhtab Rafiei, and Farimah, “A hybrid analysis approach to improve financial distress forecasting: empirical evidence from Iran,” *Mathematical Problems in Engineering*, vol. 2015, pp. 1–9, Article ID 178197, 2015.
 - [22] C. Gu, “Application of data mining technology in financial intervention based on data fusion information entropy,” *Journal of Sensors*, vol. 2022, pp. 1–10, Article ID 2192186, 2022.
 - [23] Q. Gao and H. Fan, “Effect of the dynamic macroeconomic fluctuation on the stability of a banking network system with scale-free structure,” *Mathematical Problems in Engineering*, vol. 2020, pp. 1–11, Article ID 7158506, 2020.
 - [24] A. Hasan, O. Kalipsız, and S. Akyokuş, “Modeling Traders’ Behavior with Deep Learning and Machine Learning Methods: Evidence from BIST 100 Index,” *Complexity*, vol. 2020, pp. 1–16, Article ID 8285149, 2020.
 - [25] S. Zhu, Y. Chen, and W. Wang, “Risk Assessment of Biological Asset Mortgage Loans of China’s New Agricultural Business Entities,” *Complexity*, vol. 2020, pp. 1–12, Article ID 8865840, 2020.

Research Article

A Study on the Hedging Function of Gold in the Light of Economic Policy Uncertainty

Borui Xiao 

Hainan University, Haikou, Hainan 570228, China

Correspondence should be addressed to Borui Xiao; 19120202210019@hainanu.edu.cn

Received 19 April 2022; Revised 12 May 2022; Accepted 16 May 2022; Published 16 June 2022

Academic Editor: Dong Chen

Copyright © 2022 Borui Xiao. This is an open access article distributed under the Creative Commons Attribution License, which permits unrestricted use, distribution, and reproduction in any medium, provided the original work is properly cited.

This paper focuses on the empirical analysis of the closing price of gold, the SSE Index, and the China Economic Policy Uncertainty Index by means of a GARCH model to study the main characteristics of their movements. The series of gold closing price returns are analysed for linkage using the current mainstream VAR model, so as to analyse and compare the hedging function of gold. The article selects the closing price of gold, the SSE Index, and the China News-Based EPU from June 2005 to June 2019 as the sample series for the study. The background of the study and the theoretical knowledge of VAR and GARCH models are first introduced, and then, the GARCH family model and statistical analysis methods are used to derive the respective movements of the log returns of gold closing price, SSE index log returns, and China News-Based EPU log volatilities. The results show that the movements of the closing price of gold, the SSE Index, and the China News-Based EPU have the characteristics of financial assets in general, such as spikes and thick tails, agglomeration, and leverage effects. For the empirical study of the linkage between the three, this paper first considers only three variables, namely gold closing price, SSE index, and EPU. In order to investigate whether there is a co-integration relationship between them, a vector autoregressive model is established, followed by the corresponding impulse response analysis and variance decomposition. The analysis of the linkage between the closing price of gold, the SSE index, and the EPU concluded that changes in the EPU had a greater impact on the changes in the closing price of gold, while changes in the SSE index had a smaller impact on the changes in the closing price of gold. Finally, the conclusion of this article is some advice to investors on gold investment.

1. Introduction

1.1. Background and Significance of the Study. Economic uncertainty is the inability of economic agents to predict if, when, and how the government will change existing economic policies. Gold is a special product with characteristics such as commodity, currency, and risk aversion. Risk aversion means that gold is a safe source of capital in times of major economic change and crisis. In the context of a worldwide economic recession, gold has become a “safe haven” for many investors. Due to the regular volatility of financial markets, investors worldwide are more than happy to add gold to their investment portfolios.

The risk-averse function of gold is usually applied in two situations.

Firstly, when global inflationary pressures increase, a rise in inflation means a reduction in the real value of paper

money. Then, holding paper money will be at risk of devaluation and investors will invest relatively more in gold for the purpose of preserving its value.

Secondly, in the context of a shrinking world economy, the global economic downturn has also exacerbated the market fears caused by the global recession. As a result, investors prefer to protect themselves from risk by holding gold.

When the price of gold falls temporarily, discounts can be obtained until it rises again. If the price rises, there is the option of continuing to observe or analyse the need to sell gold based on the factors affecting the price of gold, which, although a long-term investment, are a viable way of maintaining the value of the asset.

Therefore, this paper builds on previous research and takes into account the current volatility in the capital markets to investigate the hedging and hedging of gold, with

a view to compensating to some extent for the lack of research on risk-hedging assets in the capital markets.

1.2. Research Objectives. This paper will focus on the linkage between gold and Chinese economic policy uncertainty and examine the hedging function of gold. Empirical analysis will be conducted using VAR (vector of autoregression) and DARCH models. At the same time, the application of one model to the risk aversion capability of the gold market is an attempt and innovation of very practical importance to risk management in the gold market.

The following questions are addressed: (1) Is there a linkage between the gold price and the China Economic Policy Uncertainty Index? (2) Is there a correlation between the gold price and the SSE index? (3) Can gold be used as a hedging asset in extreme situations to bypass the sharp rise in economic policy uncertainty, and based on the above research, we analyse the hedging ability of gold and make more suitable investment recommendations to regulators and investors.

2. Review of the Literature

As an important component of commodities, gold's relationship with the economy and policy is at the heart of the debate. The relevant literature suggests that the disclosure of macroeconomic information has a significant impact on gold yields, with some studies, suggesting that the impact is more pronounced in times of economic contraction. Abken, for example, notes that the price of gold can change dramatically due to extreme political or economic uncertainty. [1] Ciner, Batten et al. suggest that gold became a refuge for the US stock market in the early 1990s and during the global financial crisis of 2008. [2]

Shafiee and Topal systematically collate and summarise the various factors that influence the price of gold and highlight that the short-term surge in gold prices is due to the fact that gold can act as a hedge against large fluctuations in traditional asset prices in times of financial market instability. [3] Batten et al. classify the real economy-related factors that may cause changes in commodity markets for precious metals such as gold, silver, platinum, and palladium into three types: variables that reflect the elasticity of the monetary environment, such as inflation rates and monetary aggregates; variables that reflect business prosperity, such as industrial GDP; and variables that reflect, for example, the exchange rate of the US dollar, returns on stock indices, and consumer confidence financial market variables such as the US dollar exchange rate, stock index returns, and consumer confidence indices. It was found that a certain degree of volatility in gold returns could be explained by the above economic variables. Chrtstie-David et al. investigated 23 macro indicators in the United States and found that the volatility of gold returns increased substantially over the reporting period, especially the volatility of gold returns in response to changes in capacity utilisation, CPI, and GDP. [4]

Cai et al. reported that the sale of the PBOC's gold reserves would lead to a fall in the price of gold. [5] Roache

and Rossi's study of 11 macroeconomic indicators and 6 commodities including gold shows that nonagricultural wage indicators, consumer confidence indicators, and interest rates have a significant impact on gold, and that gold's reaction to bearish information reflects a value-protective, safe-haven nature and is therefore different from the other 5 commodities. [6] When gold is used as both a hedging asset and a safe-haven asset, Baur and Lucey present the first statistical test, showing that gold can be used as both a hedging and a safe-haven asset against the US dollar. [7] Elder et al. examined the relationship between gold returns, trading volume and volatility, and the publication of macro information and shows that gold has a significant and rapid response to economic information, with nonagricultural pay and nonconsumer orders being particularly influential in economic information. [8] In addition to this, gold is also sensitive to macro supply and demand information. Reboredo examines the correlation between daily data on the exchange rates of major international currencies against the US dollar and the gold price between 2000 and 2012. He extends Baur and Lucey's definition of safe-haven and hedging assets by arguing that safe-haven and hedging assets among financial assets can be measured by general and dynamic correlation coefficients. The results show that the gold price is generally correlated with the US dollar exchange rate, with a positive dynamic correlation coefficient, confirming Reboredo (2010) findings. [9].

In recent years, with the rapid development and expansion of capital markets, more and more scholars are studying how gold hedges risk and the information about it is becoming more comprehensive and complete. Xu verified that gold prices have a good hedging effect on the consumer price index as well as the US dollar index, and can be used as an indicator of inflation through Granger causality tests of the VEC model. [10] Yuan and Yang examined the feasibility of gold futures to hedge real foreign exchange risk. [11] Yang studied Shandong gold as a representative, and the results showed that: firstly, the SSE Composite Index is not the Granger cause of Shandong gold, while the international gold price is the Granger cause of Shandong gold; secondly, the impact effect of the international gold price on Shandong gold is extremely obvious, about twice that of the SSE Composite Index; thirdly, both the SSE Composite Index and the international gold price have a long-term impact on Shandong gold. Finally, the international gold price explains the rate of change in Shandong gold prices much more strongly than the SSE Composite Index. [12] Nian examined the effect of gold hedging in different countries from different perspectives in a comprehensive manner. The study shows that in the long run, gold investment has an anti-inflationary effect, and therefore, gold is an effective long-term hedge, especially during periods of accelerating inflation, when gold investment returns are particularly significant. [13] Hu and Zhao conducted an empirical analysis by building a GARCH-like model, revealing that there are heteroscedasticity effects, asymmetric spillover effects, and significant asymmetry in both the stock market and the gold market. [14] Ni and Yu used a BEKK-GARCH model to study the risk aversion ability of the Chinese gold market,

and the results showed that gold only has certain hedging ability in the short term. [15]

In conclusion, gold is closely linked to the global real economy as well as to international financial markets. Gold is sensitive and responsive to timely macro information, suggesting that economic policy uncertainty has a significant impact on gold. We will judge whether gold can be used as a safe-haven asset to hedge against risks in the real economy or equity markets based on an examination of the linkage between gold and economic policy uncertainty.

3. Model Theory Research

This paper focuses on the hedging capacity of gold based on economic policy uncertainty. The relationship between the price of gold and future trading volume, and the policy uncertainty index is studied, and then, the covering capacity of gold is analysed based on the relationship between them. *Analysis of gold hedging capacity.* VAR models and GARCH-type models are used in this thesis, and this chapter provides a detailed introduction to VAR models and GARCH-type models.

3.1. VAR Model

3.1.1. Definitions. If the n -dimensional time series $\{Y_t\}$, $t \in T$, $T = \{1, 2, \dots\}$, the $Y_t = C + \theta_1 Y_{t-1} + \dots + \theta_p Y_{t-p} + \varepsilon_t$, satisfying, where $E(\varepsilon_t) = 0$, and $E(\varepsilon_t, \varepsilon_t) = \Omega t = \tau / 0t \neq \tau$

This is then a p -order vector autoregressive mode.

If ε_t mutually independent and identically distributed and follows a normal distribution, then the stochastic process of the model is the autocorrelation process of the P -order vector, which is a standard VAR model, and the model is called VAR(P).

3.1.2. Characteristics of the Standard VAR Model

- (1) Each component is an endogenous variable.
- (2) Each equation has the same explanatory variables.
- (3) Y_t the p -order lag of can then depict its dynamic structure that Y_t . there is no response to variables prior to the p moment.
- (4) The VAR model is a simplified form of joint cubic equation.

3.1.3. VAR Model Fixed Order. AIC (Akaike) and SC (Schwarz) guidelines are as follows:

$$\begin{aligned} \text{AIC}(p) &= \text{Indet}\left(\widehat{\sum p}\right) + \frac{2n^2 p}{T}, \\ \text{SIC}(p) &= \text{Indet}\left(\widehat{\sum p}\right) + \frac{n^2 p \ln T}{T}. \end{aligned} \quad (1)$$

N is the vector size, T is the sample size, p is the lag order, \det is the determinant of the solution matrix, and $\widehat{\sum p}$

is an estimate of the residual vector covariance matrix for a lag length of p .

If the same lag order is chosen as for the univariate model, the following problems will arise.

- (1) The choice of criterion is subjective and arbitrary. Depending on the choice of criterion, the lag order may also vary.
- (2) The actual series can sometimes be a nonfinite dimensional process of random probability events, and although there are large quantities of time series that are not smooth, modelling the smooth time series with a finite lag length VAR model can lead to an exciting conclusion.
- (3) Even if the series is smooth, if the actual lag order is greater than Q , the correct lag length cannot be obtained.

3.2. Introduction to GARCH-like Models. GARCH-type models usually consist of two equations consisting of a conditional mean equation and a conditional variance equation. Before building a GARCH-type model, it is often necessary to test for the smoothness of the series and the ARCH effect. And the ARCH effect means that future fluctuations can be predicted using historical fluctuations. Therefore, GARCH-type models are often used to study time series volatility and correlation with historical data and to predict future data. Therefore, the conditional variance equation is extremely important, while the conditional mean equation is relatively straightforward. [16]

The mean value model is

$$r_i = \mu + \varepsilon_i, \quad (2)$$

where μ is the unconditional mean, which is a constant, and ε_i is a random disturbance term. There are different criteria for classifying GARCH models: (1) according to the conditional mean equation, there are GARCH models and ARCH-mean models, that is, GARCH-M models; (2) whether they are symmetric, EGARCH, and RGARCH models

3.2.1. Univariate GARCH. Bollerslev (1986) extended the scope of Engle's original model, the Arch model, by introducing a method in the Arch model that allowed the conditional variance to be transformed into an ARMA process.

The generalised ARCH or GARCH (p, q) is as follows:

$$h_t^2 = \sum_{i=1}^p \beta_i \varepsilon_{t-i}^2 + \sum_{i=1}^q \alpha_i h_{t-i}^2. \quad (3)$$

The parameter p is also called the order of the ARCH term and the parameter q is the order of the GARCH term, $\alpha_0 \geq 0$, $\alpha_1 \geq 0$, $\beta_j \geq 0$.

3.2.2. GARCH-M Model. In addition to introducing the residual squared term of the conditional mean into the

conditional variance equation, the conditional characteristics of the residual term can also be used as an explanatory variable affecting the $\{Y_t\}$ mean, and this type of model is called an ARCH mean model or GARCH-M model.

The GARCH-M model (Engle) and other academics proposed in 1988 to describe the change in risk premiums over time.

The GARCH-M model is as follows:

$$\begin{aligned} y_t &= \beta + \delta h_t + \varepsilon_t, \\ h_t^2 &= r + \alpha \sum_{j=1}^i \varepsilon_{t-j}^2 + \sum_{j=1}^i h_{t-j}^2. \end{aligned} \quad (4)$$

3.2.3. Exponential GARCH: E-GARCH. The E-GARCH (exponential GARCH) model proposed by Nelson (1991) is as follows:

$$\ln h_t^2 = \alpha_0 + \sum_{i=1}^p \alpha_i \frac{|\varepsilon_t| - 1}{h_t} + \sum_{i=1}^q \beta_i \ln h_{t-i}^2 + \sum_{k=1}^r \lambda_k \frac{\varepsilon_{t-k}}{\sqrt{h_{t-i}}}. \quad (5)$$

$\lambda < 0$, then the existence of a leverage effect is indicated. $\lambda \neq 0$, impact of the shock is the asymmetric.

3.2.4. The TGAECH Model

Simple modified symmetry. The GAECH framework can describe the consequences of asymmetries of positive and negative disturbances. The TGAECH model proposed by Zakoian (1990) and Glosten, Jaganathan, and Runkle (1993) is as follows:

$$h_t^2 = \alpha_0 + \sum_{i=1}^p \rho_i h_{t-i} + \sum_{i=1}^q \alpha_i \varepsilon_{t-i}^2 + \gamma \varepsilon_{t-1}^2 d_{t-1}. \quad (6)$$

4. Data Selection, Description, and Changes

4.1. EPU and Data Selection. The Economic Policy Uncertainty Index, or EPU Index for short, is an index of economic policy uncertainty. It is compiled by Scott R. Baker, Nicholas Bloom, and Steven J. Davis and is generally used to reflect economic and policy uncertainty in the world's major economies. Their research has shown that the EPU Index has an apparently contradictory relationship with actual measures of macroeconomic indicators and can even explain to some extent the dramatic fluctuations in equity markets. In China, the EPU Index has a positive relationship with the bond market and a negative relationship with the stock market.

In this paper, gold (Au $T+d$) closing price, volume, turnover, weighted average price, position, SSE Index (SSEC), and Economic Policy Uncertainty Index (China News-Based EPU) are selected as the research samples. The frequency of the data selected is monthly, spanning 14 years from June 2005 to June 2019, with 169 sets of observations from the CSMAR database. Since the closing price, volume,

turnover, weighted average price, and position of gold (Au $T+d$) are identical to the modelling process of the SSE Index and the Economic Policy Uncertainty Index, this paper will only model the closing price return r_t with the SSE Index volatility r_s and the Economic Policy Uncertainty Index volatility r_e .

As shown in Figure 1, the overall trend in the volatility of the closing price of gold has been up and then down, rising from June 2005, peaking in November 2011, and then gradually declining.

The data were all logarithmically processed to obtain a series of log returns (log volatilities).

$$\text{Return} = \ln(p_t) - \ln(p_{t-1}). \quad (7)$$

4.2. An Empirical Study of the Volatility Characteristics of Gold Closing Prices. There are many modelling approaches to empirically analyse the characteristics of changes in financial assets, and here, we have chosen the GARCH family of models. In this chapter, the GARCH (1, 1), GARCH-M, EGARCH, and TGARCH models are used to analyse the patterns of change. The model coefficients are estimated using great likelihood, and correlations are tested using the ARCH-LM method. The selection of optimality for each model is judged using the AIC and SC criteria.

4.2.1. Basic Processing of Gold Closing Price Data

(1) Descriptive Statistics of Gold Closing Prices.

Table 1 shows that the skewness is -0.352225 , so the log return series of gold closing prices is left skewed (the skewness of the normal distribution is 0); the kurtosis is 4.010878 and $4.010878 > 3$, and 3 is the kurtosis of the normal distribution, so we can conclude that the log return series of gold closing prices has "sharp peaks and thick tails." Jarque-Bera is a χ^2 statistic that is often used to test whether a series follows a normal distribution. At the same time, the statistical properties of the log returns indicate that the original hypopaper is rejected and the distribution is not normal.

This paper therefore establishes a GARCH model, which is able to balance the time-varying characteristics that the sample data have. Based on the findings, it can be seen that the gold yield series does not exactly obey the standard normal distribution. In this case, based on the results of previous scholars, using a distribution can better fit the distribution characteristics of the sample data. So, as to arrive at optimal empirical results, this paper also examines the sample data using the GARCH equation under a T distribution. Ultimately, however, one must also take into account that the T distribution of the sample series is more consistent with the normal distribution, and this paper then proceeds to simulate a model based on the normal distribution. Based on the fact that after the normality test has been done above, the statistical characteristics of the time series that need to be examined if a GARCH model is to be built, this paper will therefore do a smoothness test, a data

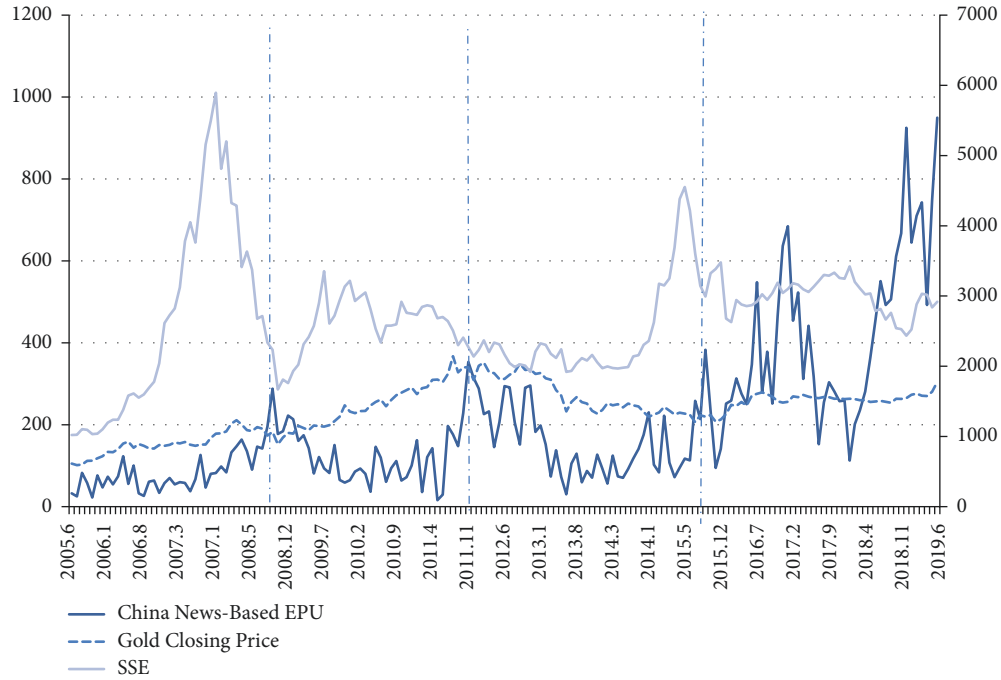


FIGURE 1: Gold closing price, SSE, and EPU chart, June 2005–June 2019.

TABLE 1: Descriptive statistics for log returns on the closing price of gold.

	Average value	Maximum value	Minimum value	Standard deviation	Skewness	Kurtosis	Jarque–Bera statistic
Rt	0.006159	0.122465	-0.172233	0.047912	-0.352225	4.010878	10.69012

autocorrelation test, and an effects test on the sample time series.

(2) *Statistical Characteristics of Gold Closing Prices and Correlation Tests.* The statistical analysis above shows that the log return series of the closing price of gold has the characteristics of a spike with a thick tail and its volatility series does not obey a normal distribution as known by the chemical statistics. To fully illustrate its disobedience to a normal distribution, a normal QQ plot is plotted, see Figure 2.

As shown in Figure 2, a large number of points are scattered outside the straight line of the normal distribution; thus, the actual distribution of the log return series of gold closing prices has a thick tail. The ADF unit root test for its smoothness, without the intercept term and without the time trend term, is shown in Figure 3, and the P -value of the ADF test for the log return time series of gold closing prices is 0, rejecting the null hypothesis of containing a unit root, which indicates that the series is stable.

(3) *Autocorrelation Test.* It is a test for serial autocorrelation. Many distributions of returns are not only kurtic and skewed and move over time, but the returns of successive adjacent periods are not necessarily independent of each other, a phenomenon known as autocorrelation of a return series. Sequences are autocorrelated because of the inertia and stickiness of their own series, which leads to correlation

between residuals. Therefore, in order to better create a VAR-GARCH model, this paper needs to examine the autocorrelation of the return series.

The yield series were tested with the autocorrelation function (ACF) and the partial correlation function (PACF), as shown in Figure 4, after which the results of the study were obtained for the lags to maturity: rt has 6th-order autocorrelation.

Based on the previous analysis, it is clear that the log return series of the closing price of gold is smooth, with clustering of its fluctuations and possible conditional heteroscedasticity, a distinctive feature of the GARCH model is that it allows the time series to have time-varying conditional variance.

(4) *Conditional Heteroscedasticity Test and ARCH Test.* Assuming that the residuals of the log return series of the closing price of gold obey a normal distribution (Bollerslev and Wooldridge have done a study where, as long as the mean coincident variance equation is set in the correct form, the maximum-likelihood estimates are still consistent even if the assumption of conditional normal distribution does not hold), a maximum-likelihood estimate of the log return series of the closing price of gold with a 6th-order lag is performed, and then, ARCH effect test was then performed on its residual term. The results are shown in Figure 5. The P -value of the LM statistic is 0.0048, which is smaller than the significance level of 0.05. This means that the log return

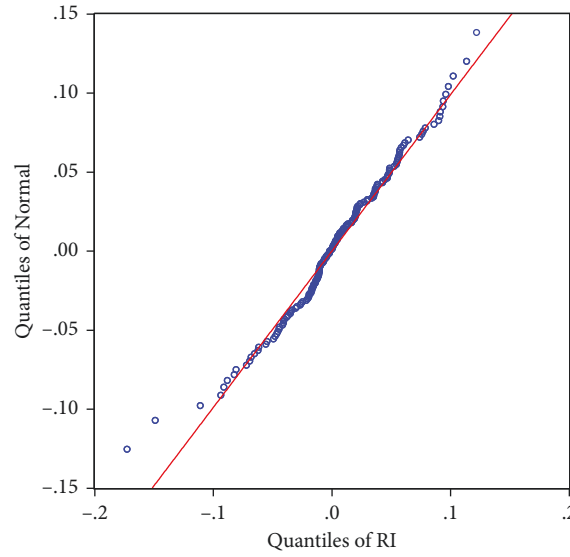


FIGURE 2: Normal QQ plot of the log return series for the closing price of gold.

Augmented Dickey-Fuller Unit Root Test on RT		
	t-Statistic	Prob.*
Augmented Dickey-Fuller test statistic	-13.93852	0.0000
Test critical values:		
1% level	-2.578799	
5% level	-1.942733	
10% level	-1.615446	

*MacKinnon (1996) one-sided p-values.

FIGURE 3: Smoothing test for the log return series of the closing price of gold.

series of the closing price of gold contains a higher order ARCH effect and can be modelled using a GARCH model.

4.2.2. GARCH-like Model Analysis

- (1) The GARCH (1, 1) model, the GARCH-M model, the EGARCH model, and the TGARCH model are modelled assuming a t-distribution of the error term of the log return on the closing price of gold.

GARCH (1, 1) model with mean equation is as follows:

$$\begin{aligned}
 RT_t &= 0.002354 \\
 &+ 0.192813RT_{t-6} \\
 &+ \hat{u}_t (0.779734) (2.492220), \\
 R^2 &= 0.33933, \\
 DW &= 2.176027.
 \end{aligned} \tag{8}$$

Corresponding GARCH (1,1) equation is as follows:

$$\begin{aligned}
 \sigma_t^2 &= 0.0000503 + 0.274179u_{t-1}^2 \\
 &+ 0.708382\sigma_{t-1}^2 (0.973159) (2.347141) (9.371286).
 \end{aligned} \tag{9}$$

GARCH-M model with mean equation is as follows:

$$\begin{aligned}
 RT_t &= -0.353251 + 0.157942RT_{t-6} + 7.543124\sqrt{\sigma_t^2} + \hat{u}_t \\
 &(-0.817324) (2.173317) (0.809165) \\
 R^2 &= 0.056204 \quad DW = 2.086611.
 \end{aligned} \tag{10}$$

GARCH-M equation is as follows:

$$\begin{aligned}
 \sigma_t^2 &= 0.001544 + 0.025769u_{t-1}^2 + 0.294520\sigma_{t-1}^2 \\
 &(1.72235) (0.751752) (0.856811).
 \end{aligned} \tag{11}$$

EGARCH model with mean equation is as follows:

$$\begin{aligned}
 RT_t &= 0.002639 + 0.200228RT_{t-6} + \hat{u}_t (0.812466) \\
 &(2.547833) \\
 R^2 &= 0.034358 \quad DW = 2.19355.
 \end{aligned} \tag{12}$$

EGARCH equation is as follows:

$$\begin{aligned}
 \ln(\sigma_t^2) &= -0.941444 + 0.497627|u_{t-1}/\sigma_{t-1}| \\
 &- 0.000486u_{t-1}/\sigma_{t-1} + 0.910791 \ln(\sigma_{t-1}^2) \\
 &(2.180059) (2.835271) (0.005617) (15.33532).
 \end{aligned} \tag{13}$$

TGARCH model with mean equation is as follows:

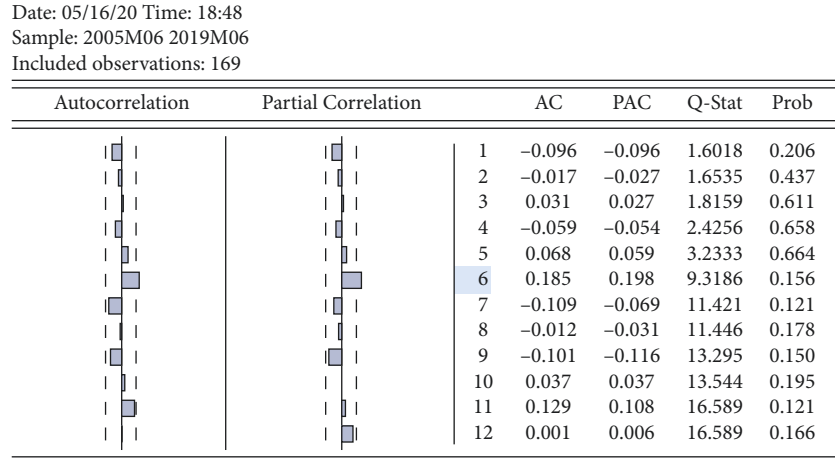


FIGURE 4: Autocorrelation test for log return series of gold closing prices.

F-statistic	8.162320	Prob. F (1,160)	0.0048
Obs*R-squared	7.863211	Prob. Chi-Square (1)	0.0050

FIGURE 5: ARCH-LM test table for the log return series of the closing price of gold.

$$RT_t = 0.002212 + 0.192738RT_{t-6} + \hat{u}_t (0.714730) (0.0077217),$$

$$R^2 = 0.033669 \quad DW = 2.171473.$$

(14)

TGARCH equation is as follows:

$$\sigma_t^2 = 0.0005 + 0.263328u_{t-1}^2 + 0.025729u_{t-1}^2d_{t-1} + 0.747799\sigma_{t-1}^2$$

$$(0.966826) (1.976846) (0.155165) (9.28640).$$

(15)

The specific GARCH estimation model was determined by selecting the GARCH model that corresponds to when the AIC and SC values are minimised according to the Akaike information criterion and the Schwarz criterion, that is, the AIC criterion and the SC criterion. Using the graphs above, Table 2 can be obtained.

In summary, by comparing the GARCH (1,1) model, GARCH-M model, EGARCH model, and TGARCH model for fitting parameters, according to the Akaike information criterion and Schwarz criterion, that is, AIC criterion and SC criterion, the GARCH (1,1) model, AIC value, and SC value reach the minimum, and GARCH (1,1) for the three sets of data GARCH (1,1) was chosen as the best fit for the residual series of log returns.

GARCH (1, 1) model with mean equation is as follows:

$$RT_t = 0.002354 + 0.192813RT_{t-6} + \hat{u}_t (0.779734) (2.492220),$$

$$R^2 = 0.33933,$$

$$DW = 2.176027.$$

(16)

Corresponding GARCH (1,1) equation is as follows.

$$\sigma_t^2 = 0.0000503 + 0.274179u_{t-1}^2 + 0.708382\sigma_{t-1}^2 (0.973159)$$

$$(2.347141) (9.371286).$$

(17)

The coefficients of both the ARCH and GARCH terms in the GARCH (1,1) equation are significant, and the sum of the coefficients of the ARCH and GARCH terms are $0.274179 + 0.708382 = 0.982561 < 1$, satisfying the constraints on the parameters. Since the sum of the coefficients is very close to 1, it means that this conditional variance is subject to continuous shocks; that is, it has great predictive power for the future.

4.3. An Empirical Study of the Volatility Characteristics of the SSE Index. Similar to the empirical study of the volatility characteristics of the closing price of gold in 4.2 above:

4.3.1. Descriptive Statistics and Trends of the SSE Index.

From Table 3, we can find that the skewness is -0.64021 , so the series is left-skewed (the skewness of the normal distribution is 0); the kurtosis is $4.801406 > 3$, thus determining that the SSE log return series is characterised by “sharp peaks and thick tails.” The Jarque–Bera statistic also shows the rejection of the normal distribution hypothesis. Figure 6 shows the trend of the log returns of the SSE index.

TABLE 2: GARCH model information criterion test results.

	GARCH(1,1) model	GARCH-M model	EGARCH model	TGARCH model
AIC	-3.253605	-3.332335	-3.342026	-3.320252
SC	-3.120745	-3.218454	-3.209165	-3.187391

TABLE 3: Descriptive statistics of log returns of SSE indices.

	Average value	Maximum value	Minimum value	Standard deviation	Skewness	Kurtosis	Jarque-Bera statistic
Rs	0.00611	0.242526	-0.28278	0.082856	-0.64021	4.801406	34.39535

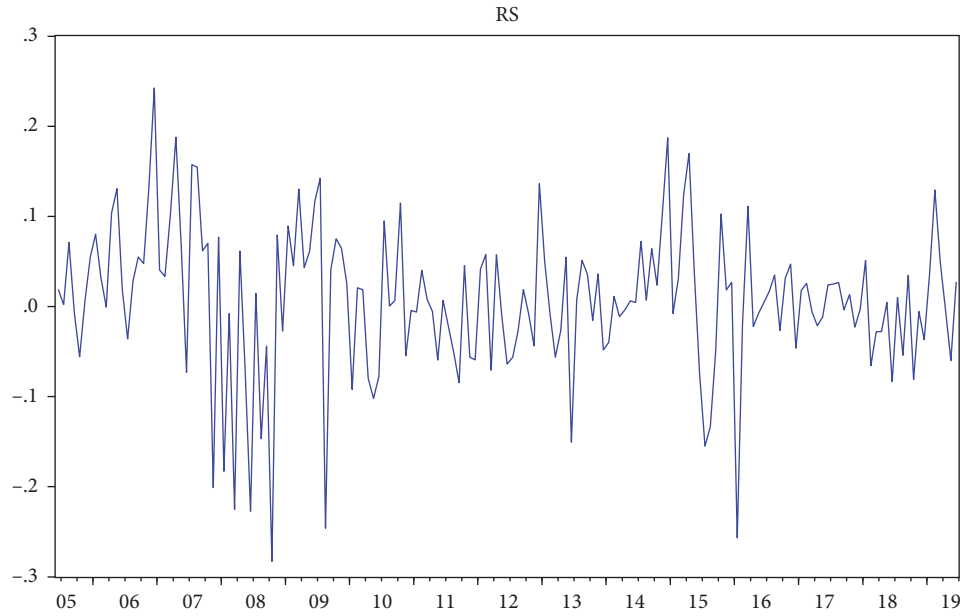


FIGURE 6: Trend in log returns of the SSE Index.

Augmented Dickey-Fuller Unit Root Test on RS		
Null Hypothesis: RS has a unit root		
Exogenous: None		
Lag Length: 0 (Automatic - based on SIC, maxlag = 13)		
	t-Statistic	Prob.*
Augmented Dickey-Fuller test statistic	-11.31340	0.0000
Test critical values:		
1% level	-2.578799	
5% level	-1.942733	
10% level	-1.615446	

*MacKinnon (1996) one-sided p-values.

FIGURE 7: ADF test for the log return series of the SSE Index.

4.3.2. Statistical Characteristics of the SSE Index and Correlation Tests. The ADF unit root test for its smoothness, without the intercept term and without the time trend term, can be seen in Figure 7, where the ADF test P -value for the log return time series of the SSE index is 0, rejecting the null hypothesis of containing a unit root, then indicating that the series is smooth.

4.3.3. Autocorrelation Test. The SSE log return series was tested for autocorrelation function (ACF) and partial correlation function (PACF), as shown in Figure 8, after which

the findings for the lags to maturity were obtained: rs has 4th-order autocorrelation.

4.3.4. Conditional Heteroscedasticity Test and ARCH Test. As can be seen from Figure 9, the LM statistic P -value of 0.9316 is significantly greater than the significance level of 0.05, which would indicate that there is no higher order ARCH effect in the effective exchange rate log return series and that the GARCH model cannot be used further to study its movement. This can be attributed to the data selection problem; the GARCH family of models is generally

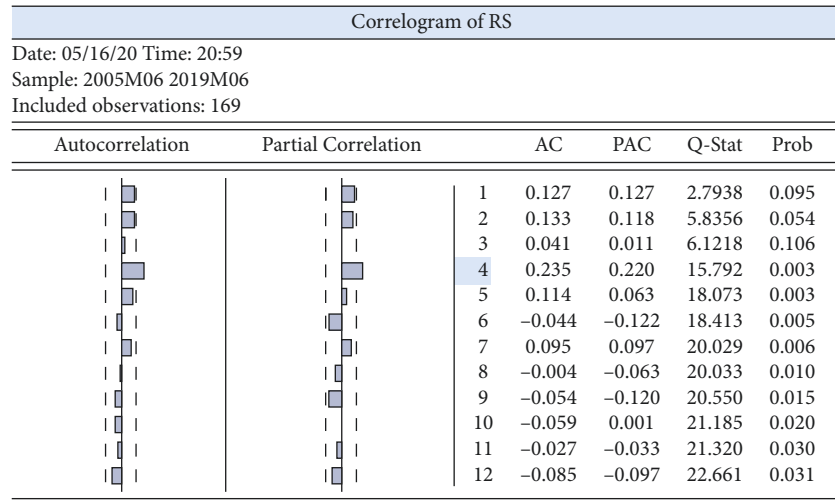


FIGURE 8: Log return series autocorrelation test for the SSE Index.

Heteroskedasticity Test: ARCH

F-statistic	0.007398	Prob. F (1,162)	0.9316
Obs*R-squared	0.007489	Prob. Chi-Square (1)	0.9310

FIGURE 9: ARCH-LM test table for the log return series of the SSE index.

TABLE 4: Descriptive statistics for the rate of change of EPU.

	Average value	Maximum value	Minimum value	Standard deviation	Skewness	Kurtosis	Jarque-Bera statistic
Re	0.13074	1.656059	-1.76689	0.480191	-0.15141	4.135166	9.719588

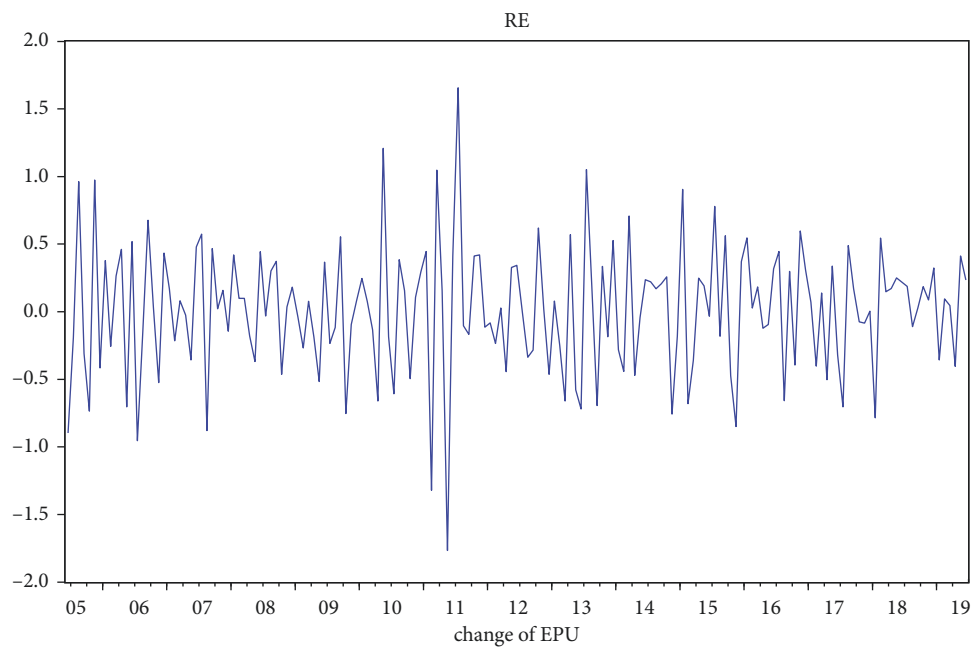


FIGURE 10: Trends in the rate of change of EPU.

applicable to high-frequency data, and only monthly data from June 2005 to June 2019 were chosen for this study, and the sample size is far less than high-frequency data, so the model simulation effect may not be ideal. But it does not negate the fact that SSE index movements are agglomerative and leveraged. From the statistical description of SSE index fluctuations in the previous section and the series trend graph, the trend of SSE index movements can still be derived.

4.4. Empirical Study of EPU Volatility Characteristics. Similar to the empirical study of the volatility characteristics of the closing price of gold in 4.2 above:

4.4.1. Descriptive Statistics and Trends in EPU. From Table 4, we can see that the skewness is -0.15141 , so the EPU rate of change return series is left-skewed (the skewness of the normal distribution is 0); the kurtosis is $4.135106 > 3$, respectively, which leads to the conclusion that the EPU rate of change series is characterized by “sharp peaks and thick tails.” The Jarque–Bera statistic also shows that the assumption of a normal distribution is rejected. Figure 10 shows the trend of the EPU rate of change.

4.4.2. Statistical Characteristics of EPU and Correlation Test. When the ADF unit root test for its smoothness is performed, without the intercept term and without the time trend term, it can be seen from Figure 11 that the P -value of the ADF test for the log return time series of the SSE index is 0, which rejects the null hypothesis of containing a unit root, and then indicates that the series is smooth.

4.4.3. Autocorrelation Test. Autocorrelation functions (ACF) and partial correlation functions (PACF) were performed on the EPU rate of change series, as shown in Figure 12, after which findings were obtained for the lags due to re with 1st- and 2nd-order autocorrelation.

4.4.4. Conditional Heteroscedasticity Test and ARCH Test. As can be seen from Figure 13, the LM statistic P -value of 0.3436 is significantly greater than the significance level of 0.05, which would indicate that there is no higher order ARCH effect in the effective exchange rate log return series and that the GARCH model cannot be used further to study its movement. This can be attributed to the data selection problem; the GARCH family of models is generally applicable to high-frequency data, and only monthly data from June 2005 to June 2019 were chosen for this study, and the sample size is far less than high-frequency data, so the model simulation effect may not be ideal. However, it does not negate the fact that the SSE index movements have a clustering and futile pole effect. From the statistical description of SSE index fluctuations in the previous section and the series trend graph, the trend of SSE index movements can still be derived.

5. Empirical Analysis of the Linkage between the Closing Price of Gold and the SSE Index and the China Policy Uncertainty Index

As China’s economic system continues to reform and the gold market process advances, many changes have occurred in China’s economic environment, which inevitably lays the foundation for further strengthening the linkage between the closing price of gold and the SSE and the China Policy Uncertainty Indices. Chapter 3 describes some common GARCH models, and in Chapter 4, we empirically analyse the movements of the log returns of the gold closing price, the log returns of the SSE, and the log volatility of the China Policy Uncertainty Index, thus providing a clearer picture of their patterns of movement. This chapter builds on the previous chapters on the linkages between the closing price of gold and the SSE and China Policy Uncertainty Index linkages. The first step is to test whether there is a long-run co-integration relationship between the gold closing price and the SSE and China Policy Uncertainty Indices, establish a vector autoregressive (VAR) model, and conduct impulse response analysis. The Johansen test is used to establish the co-integration equation and vector error correction model for the long-term equilibrium relationship between the closing price of gold and the China Policy Uncertainty Index; the impulse response and variance decomposition are used to analyse the direction and extent of their influence.

As can be seen from Chapter 4, both sets of data, the log return on the closing price of gold, the log return on the SSE, and the rate of change of the EPU are non-normally distributed series.

5.1. ADF Test. In order to avoid pseudoregression, we need to first perform a unit root test on the data to determine the stability of the data. The results of the ADF test are shown in Table 5, where c , t , and k represent the constant term, the time trend term, and the optimal lag order of the ADF test, respectively, and the P -value is obtained from the AIC minimum principle.

As can be seen from Table 5, rt , rs , and re are all smooth series at the 5% level of significance and no co-integration test is required.

5.2. Determination of the Lag Order. As the lag order affects the stability of the model, it is important that the lag order is set correctly before modelling. The longer the lag order, the better the fit of the model, but higher lag orders also entail a higher loss of degrees of freedom. Here, we will first determine the optimum number of lags. There are various criteria for judging the lag order, such as likelihood ratio (LR), AIC, and SC. The results of the tests are shown in Figure 14.

From Figure 14, it can be seen that the best lag order is 2; that is, the optimal lag order is set to 2.

Augmented Dickey-Fuller Unit Root Test on RE		
Null Hypothesis: RE has a unit root		
Exogenous: None		
Lag Length: 1 (Automatic -based on SIC, maxlag = 13)		
	t-Statistic	Prob.*
Augmented Dickey-Fuller test statistic	-17.40418	0.0000
Test critical values:		
1% level	-2.578883	
5% level	-1.942745	
10% level	-1.615438	

*MacKinnon (1996) one-sided p-values.

FIGURE 11: ADF test for EPU's log-volatility series.


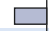






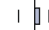












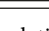

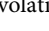
Correlogram of RE						
Date: 05/16/20 Time: 21:33						
Sample: 2005M06 2019M06						
Included observations: 169						
Autocorrelation	Partial Correlation		AC	PAC	Q-Stat	Prob
		1	-0.302	-0.302	15.675	0.000
		2	-0.326	-0.459	34.094	0.000
		3	0.280	-0.004	47.712	0.000
		4	-0.006	-0.047	47.718	0.000
		5	-0.144	-0.047	51.375	0.000
		6	0.061	-0.040	52.036	0.000
		7	0.016	-0.050	52.084	0.000
		8	-0.012	0.009	52.110	0.000
		9	-0.064	-0.095	52.860	0.000
		10	0.080	0.034	54.027	0.000
		11	0.057	0.068	54.628	0.000
		12	-0.106	0.002	56.692	0.000

FIGURE 12: Log volatility series autocorrelation test for EPU.

Heteroskedasticity Test: ARCH			
F-statistic	0.902286	Prob. F (1,164)	0.3436
Obs*R-squared	0.908292	Prob. Chi-Square (1)	0.3406

FIGURE 13: ARCH-LM test table for log volatility series of EPU.

TABLE 5: ADF test results.

Variables	ADF values	Test form (c,t,k)	P-value	Stability
rt	-13.9385	(0, 0, 0)	0.001	Stable
rs	-11.3134	(0, 0, 0)	0.001	Stable
re	-17.4042	(0, 0, 1)	0.001	Stable

5.3. Granger Causality Test. A further Granger causality test was done on the trivariate series of the gold closing price and the SSE and China Policy Uncertainty Indices. As shown in Figure 15, the probability that rs is not rt's Granger causality is 0.6671, which cannot reject the original hypopaper at the 5% significant level; that is, rs has no predictive power for rt; the probability that re is not rt's Granger causality is 0.0400,

which rejects the original hypopaper at the 5% significant level; that is, re has predictive power for rt.

5.4. VAR Model Development and Analysis of Results. A VAR (2) model is developed, and its estimation results (Table 6) are as follows:

VAR Lag Order Selection Criteria
 Endogenous variables: RT RS RE
 Exogenous variables: C
 Date: 05/17/20 Time: 14:15
 Sample: 2005M06 2019M06
 Included observations: 161

Lag	LogL	LR	FPE	AIC	SC	HQ
0	329.5178	NA	3.48e-06	-4.056122	-3.998705*	-4.032808
1	343.9246	28.09759	3.25e-06	-4.123287	-3.893617	-4.030031
2	369.7184	49.34481*	2.64e-06*	-4.331906*	-3.929984	-4.168709*
3	375.0730	10.04398	2.76e-06	-4.286621	-3.712447	-4.053483
4	382.2007	13.10431	2.83e-06	-4.263363	-3.516936	-3.960283
5	384.2382	3.669963	3.09e-06	-4.176872	-3.258192	-3.803850
6	392.8953	15.27095	3.10e-06	-4.172612	-3.081680	-3.729650
7	398.0587	8.915634	3.26e-06	-4.124952	-2.861768	-3.612048
8	401.2945	5.466683	3.51e-06	-4.053347	-2.617910	-3.470502

*indicates lag order selected by the criterion

LR: sequential modified LR test statistic (each test at 5% level)

FPE: Final prediction error

AIC: Akaike information criterion

SC: Schwarz information criterion

HQ: Hannan-Quinn information criterion

FIGURE 14: Optimal lag order test.

VAR Granger Causality/Block Exogeneity Wald Tests
 Date: 05/18/20 Time: 04:09
 Sample: 2005M06 2019M06
 Included observations: 167

Dependent variable: RT

Excluded	Chi-sq	df	Prob.
RS	0.809607	2	0.6671
RE	6.439416	2	0.0400
All	7.545919	4	0.1097

Dependent variable: RS

Excluded	Chi-sq	df	Prob.
RT	0.883294	2	0.6430
RE	0.367814	2	0.8320
All	1.080441	4	0.8974

Dependent variable: RE

Excluded	Chi-sq	df	Prob.
RT	2.144480	2	0.3422
RS	6.157160	2	0.0460
All	7.524766	4	0.1106

FIGURE 15: Granger causality test results.

TABLE 6: Coefficients and t-statistics of the VAR model.

	RT(-1)	RT(-2)	RS(-1)	RS(-2)	RE(-1)	RE(-2)	C
Coefficient	-0.070468	-0.01272	-0.03861	0.018914	0.008292	-0.01549	0.006776
	0.08046	0.07889	0.04595	0.04583	0.00836	0.00836	0.00375
T-statistic	[-0.87583]	[-0.16124]	[-0.84036]	[0.41265]	[0.99159]	[-1.85214]	[1.80610]

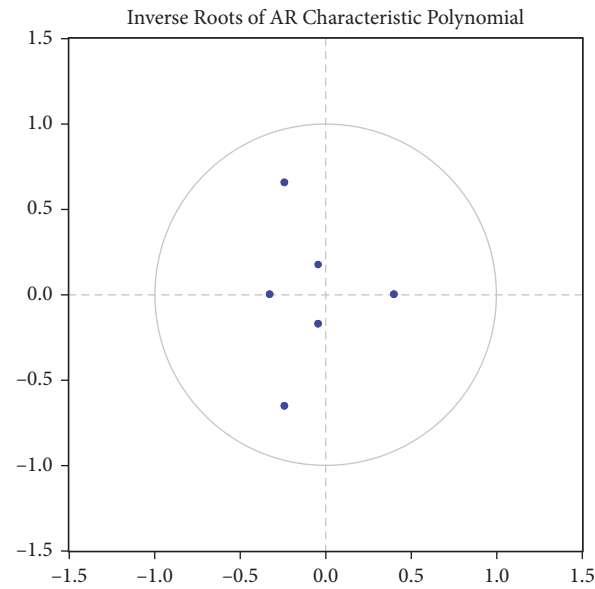


FIGURE 16: VAR (1) unit root test.

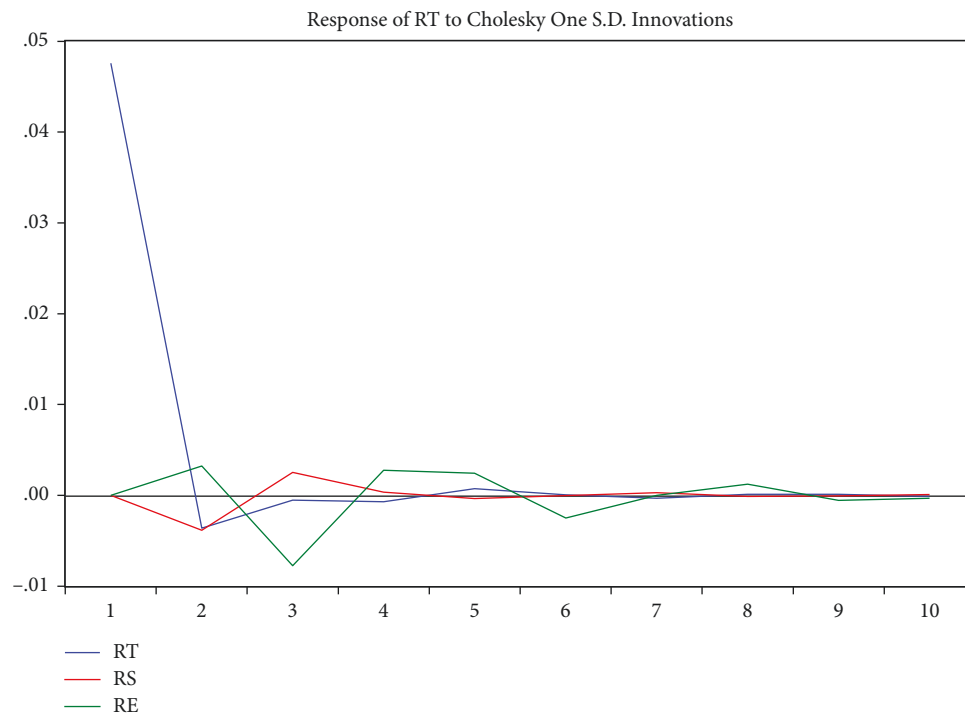


FIGURE 17: Impulse response diagram.

TABLE 7: Variance decomposition table.

Period	S.E.	RT	RS	RE
1	0.047576	100.0000	0.000000	0.000000
2	0.047978	98.90152	0.648567	0.449911
3	0.048668	96.13051	0.897432	2.972055
4	0.048752	95.81839	0.899005	3.282602
5	0.048820	95.57686	0.902164	3.520980
6	0.048883	95.32839	0.899865	3.771741
7	0.048885	95.32503	0.903522	3.771446
8	0.048901	95.26552	0.903542	3.830940
9	0.048904	95.25221	0.903639	3.844147
10	0.048906	95.24788	0.903966	3.848156
Cholesky ordering		: RT RS RE		

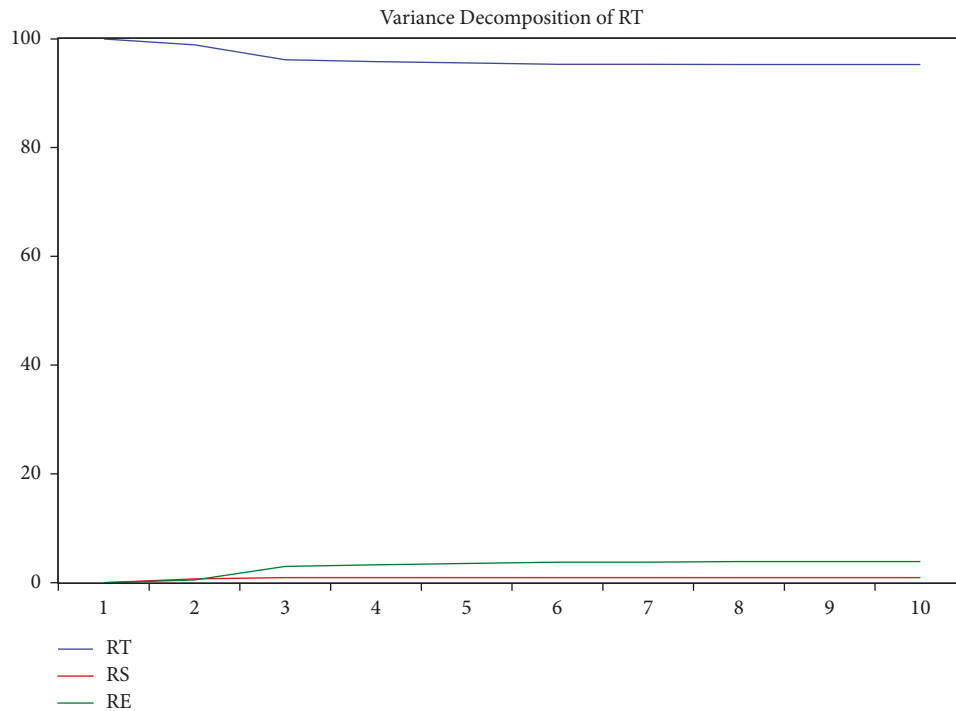


FIGURE 18: Variance decomposition plot for rt.

$$\begin{aligned}
 RT = & -0.0794677159514 * RT(-1) - 0.0127198550478 \\
 & * RT(-2) - 0.386137808512 * RS(-1) \\
 & + 0.0189136417895 * RS(-2) + 0.00829161885013 \\
 & * (-1) - 0.0154847640009 * \\
 & RE(-2) + 0.00677555375429.
 \end{aligned}
 \tag{18}$$

The F -test values from the VAR(2) equation are coincidentally 83.24589711, respectively, which shows that the equation is estimated to be significant. From the T -statistic of each coefficient of the equation, the absolute value of the coefficient of $re(-2)$ is larger and more significant than the T -statistic of 1.64 at the 10% level, while the coefficients of the remaining variables are not significant, indicating that the log return of the closing price of gold is mainly

influenced by the 2nd-order lag of EPU. However, when analysed by the magnitude of the coefficients, a 1% change in the 2nd-order lag of EPU results in a 1.549% change in the log return of the closing price of gold. This shows that there is a linkage between the log return on the closing price of gold and the rate of change of the EPU.

5.5. Impulse Response Analysis

5.5.1. Model Stability Tests. Before impulse response analysis, the stability of the established VAR (2) model needs to be tested. The impulse response analysis will only be more meaningful if the model is stable. This section uses the eigenroot test (AR) method, which means that the model is stable if the reciprocal of all the root modes of the VAR model is less than 1; that is, the eigenroots of the model all lie

within the unit circle. The results are shown in Figure 16, where all the characteristic roots of the model lie within the unit circle, which indicates that the model is stable and allows for impulse response analysis.

5.5.2. Response Analysis. The impulse response function analysis method is used to describe the response of an endogenous variable to a shock caused by an error term; that is, the effect on the current and future values after a shock of a standard deviation size is applied to the random error term. As can be seen from Figure 17, rt 's shock to itself slowly becomes smaller from period 1, reaches a minimum in period 2, is an assignment, then slowly becomes larger, crosses 0, reaches an extreme value in period 8, and converges to 0 thereafter; rs 's shock to rt starts at 0 in period 1, gradually becomes smaller, reaches a minimum in period 2, and gradually becomes larger across 0, reaches a maximum in period 3, and then fluctuates up and down of convergence with 0; re 's shock to rt , starts at 0 in the first period, gradually becomes larger, reaches a maximum in the second period, and gradually becomes smaller across 0, reaches a minimum in the third period, and then fluctuates up and down convergence with 0.

5.6. Variance Decomposition. The basic idea of variance decomposition is to decompose the fluctuations of all the variables in the system (k) into k components associated with each equation's new interest by their causes, thus obtaining the relative importance of the new interest to the model's endogenous variables.

As can be seen from Table 7 and Figure 18, in period 1, a perturbation of rt acts entirely on rt itself, but gradually decreases over time, but more slowly, and by period 10, the contribution is still 95.24788. In the process of rt being gradually weakened by its own perturbation, the contribution of rs and re to the effect of rt gradually increases, with re increasing more, and in period 10, it increases to 4.75212. However, relative to the 95.24788 contribution of rt to itself, the impact of rs and re on rt is small; that is, its transmission mechanism is hindered.

Therefore, the variance decomposition of the log return of the closing price of gold with the log return of the SSE Index and the rate of change of the EPU shows that although there is a linkage between them, the linkage is not strong. The impact of the change of the EPU on the change of the closing price of gold is stronger, and the impact of the change of the SSE Index on the change of the closing price of gold is weaker.

6. Conclusions and Recommendations

The article begins with a detailed description of the models used and then applies these models to an empirical analysis of gold closing price movements, focusing on the linkages between gold closing prices and the SSE Index and the China Economic Policy Uncertainty Index. The general idea of the empirical analysis section is as follows: (1) to carry out an empirical analysis of the closing price of gold, the SSE Index,

and the China Economic Policy Uncertainty Index, and to study the main characteristics of their movements; (2) to analyse the linkage between the closing price of gold and the SSE Index and the China Economic Policy Uncertainty Index. The above study leads to the empirical results. The autoregressive model shows that there is a linkage relationship between the China Economic Policy Uncertainty Index and the closing price of gold. Impulse response analysis was carried out, and the direction of change between them was derived from the impulse response results. Given a standard deviation shock to the SSE Index, the direction of change of the gold closing price was negative and then positive and finally stabilised, and given a standard deviation shock to the China Policy Uncertainty Index, the direction of change of the gold closing price was positive, first increasing then decreasing until it stabilised. The impact of the SSE on the closing price of gold is greater than the impact on the China Policy Uncertainty Index. From the variance decomposition, it is obvious that the closing price of gold explains itself to the greatest extent, the SSE index, and China economic policy uncertainty index explain the closing price of gold to a lesser extent, while the China economic policy uncertainty index explains the closing price of gold to a greater extent.

The hedging of gold should be adjusted accordingly to the economic policy environment in order to ultimately preserve and hedge risk. The increased demand for the protective properties of gold is also a result of the dynamics of the gold market, which developed after the dematerialisation of gold as it met the demand for protected investments, which was changed by investors' distrust of credit currencies. Gold is one of the most liquid of all asset classes around the world and is the only asset that does not need to be liquidated through domestic credit or corporate debt. People readily accept gold, which tends to move faster than other assets, for large transactions. Not only can gold be sold on the financial markets, but also it is increasingly becoming a recognised collateral, thus further increasing its liquidity and protection function.

Data Availability

The data are available from the corresponding author upon request.

Conflicts of Interest

The authors declared that they have no conflicts of interest.

References

- [1] P. A. Abken, "The Economics of Gold Price Movements," *Federal Reserve Bank of Richmond*, vol. 66, no. 2, pp. 3–13, 1980.
- [2] J. A. Batten, C. Ciner, B. M. Lucey, and P. G. Szilagyi, "The structure of gold and silver spread returns," *Quantitative Finance*, vol. 13, no. 4, pp. 561–570, 2013.
- [3] S. Shafiee and E. Topal, "An overview of global gold market and gold price forecasting," *Resources Policy*, vol. 35, no. 3, pp. 178–189, 2010.

- [4] R. Christie- David, M. Chaudhry, and T. W. Koch, "Do macroeconomics news releases affect gold and silver prices," *Journal of Economics and Business*, vol. 52, no. 5, pp. 405–421, 2000.
- [5] J. Cai, Y.-L. Cheung, and M. C. S. Wong, "What moves the gold market?" *Journal of Futures Markets*, vol. 21, no. 3, pp. 257–278, 2001.
- [6] S. K. Roache and M. Rossi, *The Effects of Economic News on Commodity Prices: Is Gold Just Another Commodity?* International Monetary Fund, Washington, D.C, USA, 2009.
- [7] D. G. Baur and B. M. Lucey, "Is gold a hedge or a safe haven? An analysis of stocks, bonds and gold," *Financial Review*, vol. 45, no. 2, pp. 217–229, 2010.
- [8] J. Elder, H. Miao, and S. Ramchander, "Impact of macroeconomic news on metal futures," *Journal of Banking & Finance*, vol. 36, no. 1, pp. 51–65, 2012.
- [9] J. C. Reboredo, "Is gold a hedge or safe haven against oil price movements?" *Resources Policy*, vol. 38, no. 2, pp. 130–137, 2013.
- [10] B. Xu, *An Empirical Analysis of the Relationship between Gold and Inflation*, Jiangsu University, Zhenjiang, China, 2010.
- [11] K. Yuan and Ye Yang, "Implied RMB forward exchange rate and hedging application of domestic and overseas gold futures," *Statistics & Decisions*, no. 12, pp. 143–145, 2010.
- [12] Y. Fan, "Analysis of the impact of international gold price and SSE Composite Index on gold mining stocks: the case of Shandong Gold," *Gold*, vol. 31, no. 12, pp. 4–8, 2010.
- [13] S. Nian, "Can gold investment fight inflation: implications for the development of commercial banks Gold Business," *Shanghai Finance*, no. 3, pp. 89–93, 2011.
- [14] Q. Hu and J. Zhao, "Study on the spillover effect of stock market and gold market yield volatility," *Statistics & Decisions*, no. 1, pp. 144–146, 2011.
- [15] He Ni and Yu Lu, "An analysis of gold's hedging power on Chinese stock market based on BEKK-GARCH model," *Collected Essays on Finance and Economics*, no. 5, pp. 48–56, 2012.
- [16] T. J. Watsham and P. Keith, *Translated by chen Gongmeng, Chen shoudong. Quantitative methods in finance*, Shanghai People's Publishing House, Shanghai, China, 2004.

Research Article

Analysis of the Relationship between Transformational Leadership and Educational Management in Higher Education Based on Deep Learning

Haiying Meng 

School of Business Sanda University, Shanghai 201209, China

Correspondence should be addressed to Haiying Meng; yhmeng@sandau.edu.cn

Received 29 April 2022; Revised 18 May 2022; Accepted 24 May 2022; Published 15 June 2022

Academic Editor: Dong Chen

Copyright © 2022 Haiying Meng. This is an open access article distributed under the Creative Commons Attribution License, which permits unrestricted use, distribution, and reproduction in any medium, provided the original work is properly cited.

Leadership behavior has been emphasized as one of the most important influencing factors in the innovation process. Leaders can encourage subordinates to innovate by creating the right environment, promoting knowledge integration, and setting specific goals. However, different leadership styles make different decisions and behaviors in the innovation process, and the final innovation effect is also different. Today, in the context of China, most business leaders still adopt “paternalistic” or “authoritarian” leadership behaviors, but more and more entrepreneurs and scholars are aware of the importance of this leadership style in enhancing employee creativity. Authoritarian leaders are more likely to exercise more control and supervision over team members, limit the autonomy of team members, and reduce work initiative and creativity. Although the positive effect of transformational leadership on employee creativity has been recognized by some scholars, in the real work environment, this leadership style rarely appears, especially in the context of China. This study first constructs a theoretical model of how transformational leaders in colleges and universities affect educational management innovation through the atmosphere of school organizational innovation, based on the deep learning theory and other related research results, and then puts forward research hypotheses on this basis. Secondly, a measurement scale was designed according to the existing research results, and the scale was revised through the pretest to form the formal questionnaire of this study. This research uses cluster sampling and random sampling to conduct a questionnaire survey on 1022 college teachers and uses the SPSS20.0 and AMOS21.0 to conduct an empirical analysis on the survey data. Each measurement scale was tested by exploratory factor analysis and confirmatory factor analysis. The experimental results show that the transformational leadership style of college principals has a positive impact on teachers’ teaching innovation. There is a positive correlation between the influence of charisma and teachers’ teaching management, and there is a positive correlation between intellectual stimulation and teachers’ teaching management.

1. Introduction

The rapid growth and increasing globalization of technology have brought complex challenges and significant changes to higher education institutions since the twenty-first century; Basham, for colleges and universities, effectively solves problems and makes full use available resources. Therefore, there is a huge demand for new definitions and approaches to the leadership and management of higher education institutions. Leaders are expected to work more effectively in rapidly changing environments and to respond appropriately

to these challenges. To facilitate change, leaders must respect each other’s knowledge and find new ways to identify and solve complex problems and challenges. Since James McGregor Burns first conceptualized leadership as transactional or transformational leadership in 1978, transformational leadership has quickly become the choice for a large number of studies and applications of leadership theory. A wealth of evidence has accumulated to demonstrate the effectiveness of transformational leaders in a variety of settings around the world. Much of the leadership literature asserts the positive effects of transformational leadership on

followers. In addition, numerous studies have shown that transformational leadership has a profoundly beneficial impact on the achievement of organizational goals. In higher education, academics have spent years studying the needs, multiple roles, and criticality of organizational leaders. Research shows that leadership styles at all levels of higher education institutions are complex and multidimensional. This research focuses on uncovering how transformational leadership is applied in higher education management settings. Specifically, two research questions are mainly discussed: (1) Is transformational leadership considered to be effective leadership in an academic setting? (2) How does transformational leadership affect performance? By exploring the hypothesis of the relationship between various related variables between transformational leadership and educational management, it is expected to provide corresponding inspiration based on the analysis results and the current situation of educational management development [1–9].

2. Related Work

After entering the 1970s, leadership theory was influenced by various academic thoughts, such as business leadership theories, new philosophies, and social thoughts, which led to the emergence of new leadership theories such as transactional, transformational, charismatic, and ethical leadership. Among them, the most influential and most respected leadership theory in management practice is the transformational leadership proposed by Burns. Over the past few decades, many researchers have studied transformational leadership and performance in a variety of settings. In higher education, several scholars have explored the effectiveness of transformational leadership in relation to the president. Others surveyed middle-level transformational leaders, including department chairs and deans. Basham focuses on the characteristics and traits of college presidents who are considered transformational leaders in America. His research supports the published and perceived characteristics of higher education leaders and their approaches to changing the learning climate in their organizations. The research highlights the group and individual qualities needed to create a transformative environment that fosters transformational leadership. Mattar aims to explore whether the characteristics and leadership styles of effective university leaders in Lebanon match those of transformational leaders. The results show that an effective leader largely accounts for most of the traits and attitudes that define transformational leaders. A transformational leader inspires and motivates all employees on campus, including faculty and staff, by fostering the spirit of co-workers, creating a friendly work environment, and respecting teamwork. On the other hand, the leadership styles of middle managers and their relationship with leader effectiveness were studied in different cultural contexts. Jones and Rudd found similar results that transformational leadership behaviors were used more often by the most effective and successful leaders, followed by transactional leadership and less laissez-faire leadership. Pixi et al. sought to find out whether the characteristics and leadership styles of effective heads of

academic departments in Malaysian universities are related to transformational leadership. In their study, inspirational motivation and idealized influence received the highest average scores, while intellectual stimulation and personalized consideration received the lowest average scores. The findings also suggest that, as a dimension of transactional leadership, contingent rewards have a significant impact on leadership effectiveness. These findings are consistent with many previous studies. Leaders' scores on the MLQ's Transformational Leadership Scale correlated significantly with measures of leader effectiveness. Furthermore, contingent rewards are often closely related to a leader's effectiveness. Existing studies have shown that transformational and transactional leadership theories have always been hotspots in management and school management research fields, and there have been relatively abundant studies on theoretical overview and dimensional structure. However, in the field of schools, transformational leadership mostly focuses on the influence of the principal's leadership style on teachers' psychological motivation and sense of efficacy and is limited to the single leadership style of transformational leadership. Based on the existing research, this research will focus on sorting out the role of transformational leadership in the atmosphere of school organization and teaching management, discussing their impact on teachers' teaching management, and exploring the mechanism of action between variables. Comparative analysis is beneficial to teachers' teaching [10–15].

3. Study Design

3.1. Conceptual Model. This study proposes a research framework for university leadership, school organizational innovation, and teacher teaching management. The principal's leadership is the independent variable, the teachers' teaching management is the dependent variable, and the school's organizational management climate is the mediating variable. Referring to Bass's classic literature, it can be seen that leadership effectiveness, organizational philosophy, team operation, learning growth, working conditions, environmental atmosphere, educational value, and policy are the main measures of college leadership management. Dimensions are more of a measure of transformational leadership, including leadership effectiveness, organizational philosophy, team operation, learning and growth, working conditions, environmental atmosphere, and the seven dimensions of educational value and policy. According to Chen Shuangcai, Wang Zhenhong, and You Xuqun's related research studies, teachers' teaching management is divided into five dimensions: conceptual thinking management, teaching content management, teaching method management, teaching resource management, and multievaluation management [16].

3.2. Research Hypothesis. There has been extensive and rich research in the corporate field on the impact of leadership styles on subordinates' innovative behavior. Among the many factors that affect the innovation performance of

organizational members, the behavior of leaders is considered to be the primary condition for introducing innovative ideas, promoting organizational change, setting innovation performance goals, and providing members with innovative resources, which can create a sustainable innovation environment for organizational members. Summarizing existing research, the principal's leadership style has an important impact on the school organization. Effective leadership not only pays attention to the realization of organizational goals but also pays attention to the overall cohesion of the school, the individual development of teachers, and their satisfaction with their work. Teachers demonstrate organizational goals and provide a rich teaching resource environment and a reasonable innovation mechanism. School leaders with transformational leadership have a positive role in guiding the innovation of the entire organization. Existing theories widely believe that transformational leadership has a more positive impact on organizational innovation than transactional leadership. Second, transformational leadership supports innovative learning processes in the organization and focuses on building mutual trust with teachers. The principal pursues organizational reform and innovation by taking himself as an example and fully encourages active and adventurous reform behaviors, thereby stimulating teachers' active exploration of teaching methods and teaching content and constantly seeking new and changing learning. The environment leads teachers to achieve the shared vision of the school. Based on the above analysis, we propose the following assumptions:

H1: the transformational leadership of college principals has a positive impact on teachers' teaching management

H1a: there is a positive correlation between charisma influence and teacher teaching management

H1b: there is a positive correlation between vision motivation and teacher teaching management

H1c: there is a positive correlation between individualized care and teacher teaching management

H1d: there is a positive correlation between intellectual stimulation and teacher teaching management

3.3. Research Tools. The part of measuring transformational leadership style in the Multifactor Leadership Questionnaire (Form5X) compiled by Bass was used, which was later revised by domestic scholar Li Chaoping. This article adopts the domestic revision, in which the transformational leadership style has four dimensions: charismatic influence, individualized care, intellectual stimulation, and vision stimulation. This study follows Bass's multifactor leadership style questionnaire to measure transactional leadership, including contingency rewards, active exception management, and passive exception management. The scale includes 35 items, measured on a 5-point scale (from 5 = completely agree to 1 = completely disagree) [17–19]. The details are shown in Table 1.

3.4. Data Collection Methods. The main research object of this research is college teachers. A total of 300 teachers from colleges and universities in the survey area were randomly selected to fill in the questionnaire as the survey sample for the test; a formal questionnaire survey was conducted. First, select 30 colleges and universities in the H region by the cluster sampling method, and then select 100 teachers from each school by the random sampling method. Teachers' personal information includes teachers' gender, teaching age, education background, job title, professional title, teaching period, and teaching subject. It mainly focuses on the school's leadership style perceived by teachers, the school's innovative atmosphere, and the level of teaching innovation they have [20].

4. Empirical Research

4.1. Reliability and Validity Test. To test the validity and reliability of the scale, the reliability test of the formal questionnaire still uses the Cronbach alpha coefficient. According to Bryman et al. (1997), if the internal reliability α coefficient is above 0.8, it means that the scale has high reliability; if the reliability of the prepared research tool is below 0.6, the measurement tool needs to be recompiled. Table 2 shows the reliability analysis of the formal questionnaire.

The above reliability test results show that the Cronbach α coefficients of transformational leadership, transactional leadership, school organizational innovation atmosphere, teacher teaching innovation scale, and subdimensions are all above 0.7, indicating that the reliability level of the scale is high. Each measurement item has a high internal consistency, which enables further analysis of the data.

4.2. Validity Test. According to the previous validity analysis results, the measurement tools used are mature scales that have been widely used and modified, indicating that the questionnaire has high content validity after factor analysis and principal component analysis (principal component analysis) to obtain the optimal factor structure of the scale, which ensures the construct validity of the scale. At this point, all factors and items of the scale have been determined. What needs to be explored is whether the factor structure model of the scale is consistent with the actual search data and whether the index variable can be effectively used as the measurement variable of the factor construct. The factor analysis procedure is confirmatory factor analysis (referred to as CFA). In this study, seven goodness-of-fit indicators (X^2/df , RMR, GFI, IFI, CFI, TLI, and RMSEA) were used to evaluate the model fit.

- (1) The chi-square degree of freedom ratio X^2/df can be used as an indicator of whether the model fits. The smaller the value is, the better the covariance matrix of the model fits the observed data. The chi-squared degrees of freedom ratios between 1 and 5 indicate an acceptable fit of the hypothesized model to the sample data.
- (2) The residual mean square and square root RMR refer to the difference between the variance-

TABLE 1: Transformational leadership style measurement items.

Transformational leadership style	Variable dimension	Measurement item
	Glamour influence	Sacrificing personal interests for the collective good
		Talk about important values and beliefs
		Emphasize the importance of a school's collective sense of mission
		Actively talk about what needs to be done
		Do not take the fruits of other people's labor as your own
	Vision incentive	Allow teachers to understand the development prospects of the school
		Show power and confidence
		Allow teachers to understand the school's development philosophy and development goals
		A promising future for everyone
		Explain the long-term significance of the work to the teacher
	Intellectual stimulation	Provide teachers with clear goals and directions
		Frequently work with teachers to analyze the impact of their work on the overall goals of the school
		Willingness to increase teacher effort
		Re-examine whether key assumptions are correct
		Always encourage teachers to use various methods to solve problems
	Personalized care	Often suggest new work, teaching methods to me
		Guide teachers to consider problems with new thinking and complete set tasks
		Old problems also require us to think differently
		In the process of dealing with teachers, the actual situation of teachers will be considered
		Frequent communication with teachers to understand teachers' work, life, and family situations
		Patiently teach teachers and answer questions for teachers
		See teachers as individuals, not just general members of the organization
		Focus on creating conditions for teachers to give full play to their strengths

TABLE 2: Reliability analysis of the questionnaire.

Variables and dimensions	Number of measurement items	Cronbach's alpha coefficient	Reliability level
Transformational leadership	17	0.975	Very high
Glamour influence	4	0.892	High
Vision incentive	4	0.929	Very high
Intellectual stimulation	5	0.932	Very high
Personalized care	4	0.942	Very high

covariance matrix of the measured data and the variance-covariance matrix implied by the theoretical model. According to Qiu Haozheng, when the RMR value is below 0.05, it is an acceptable fit model.

- (3) The fitness index GFI is used to represent the ratio of "the sum of the squares of the difference between the observation matrix of the sample data and the theoretically constructed replication matrix" and the "observed variance." When the GFI value is greater than 0.9, it represents the actual data and model path map has a good fit.
- (4) The value of the modified fitting index IFI and the modified fitting index CFI is between 0 and 1. The closer to 1, the better the fit of the model, which is generally used to judge whether the model path map is suitable for the actual data. The standard is above 0.9.
- (5) The nonregular fit index TLI is used to compare the degree of fit between two opposing models. The data of this index is between 0 and 1, and the standard or critical value of general fit is also above 0.9.

- (6) The asymptotic residual mean square and square root RMSEA is an absolute value indicator that does not require a baseline model. Steiger (1989) believes that when the RMSEA value is less than 0.05, it means that the model has a high degree of fitness. The details are shown in Table 3.

Confirmatory factor analysis on transformational leadership and its four dimensions found that among the evaluation indicators of the overall model goodness of fit, the chi-square degree of freedom χ^2/df ratio was less than 3, the fitness index GFI was greater than 0.9, and the progressive residual mean square and square root RMSEA were less than 0.08, and the other indicators all met the discriminant criteria. It can be seen that the overall model has good goodness of fit, and the model chart hypothesis of the scale's confirmatory factor analysis is statistically supported. The details are shown in Figure 1.

4.3. Descriptive Statistics of the Data. Before conducting formal data analysis, in order to ensure the accuracy of data analysis, the discrete level and concentration degree of the

TABLE 3: Evaluation indicators for the goodness of fit of the transformational leadership overall model.

Statistical test	χ^2/df	RMSEA	RMR	TLI	GFI	CFI	IFI
Fit criteria	1–5	<0.08	<0.05	>0.90	>0.90	>0.90	>0.90
Inspection data	4.711	0.060	0.012	0.973	0.941	0.978	0.978

variables of transformational leadership, transactional leadership, school organizational innovation, and teachers' teaching innovation variables were analyzed first, that is, the average of each variable (Mean) and standard deviation (Std. deviation), which improves the validity of data analysis results to a certain extent, but simply comparing the mean of each variable does not indicate that the difference has reached a statistically significant level, and a dependent sample variance analysis at each level is required.

The results of descriptive statistics and dependent sample variance analysis of the Transformational Leadership Scale show that the overall test of the mean difference of the four dimensions has reached a significant level, and the post hoc test shows that the average score of charisma is significantly higher than the average of the other three dimensions. The average score of individualized care is significantly lower than the average score of the other three dimensions. It can be considered that the teacher's perception of the principal's personal concern for himself is the least, and the feeling of the influence of charm is the strongest. At the same time, the standard deviation of each variable is less than 1, indicating that the level of the sample data set is relatively high. The details are shown in Table 4.

4.4. Regression Analysis considering the Influence of Control Variables. When two variables are significantly correlated, correlation analysis can only reflect the degree and direction of the correlation between the two variables. Regression analysis is based on the linear relationship between variables, further predicts the causal relationship between two variables, and uses an independent variable to predict the situation of the calibration variable. Under the premise of controlling for background variables such as gender and age of teachers, this study uses the principal's transformational leadership and transactional leadership as predictors to test the regression relationship between teachers' teaching innovation and the school standard variable and uses the stepwise multiple regression analysis method (Stepwise) to test the mediating effect of the school's organizational innovation climate. In the process of using multiple regression analysis, it is necessary to pay attention to whether there is a collinearity problem between the variables, that is, the correlation between the independent variables is too high, which will interfere with the fitting of the regression model. In order to test whether there is collinearity between independent variables, this study uses three indicators: tolerance (Tolerance), variance inflation factor (VIF), and serial correlation (Durbin–Watson).

4.4.1. Collinearity Diagnosis.

- (1) Tolerance: tolerance is equal to $(1-R^2)$, where R^2 represents the square of the multivariate correlation coefficient between independent variables. The value

range of tolerance is between 0 and 1. If the tolerance of an independent variable is too small, it means that there is a collinearity problem between the variable and other independent variables; if the value is close to 0, it means that this variable is almost a linear combination of other variables. The estimated value of the regression coefficient of the variable is not stable enough, and the calculated value of the regression coefficient will also have a large error.

- (2) Variance inflation factor: the variance inflation factor (VIF) is the reciprocal of tolerance, which reflects the possible common change trend between independent variables. If there is a high correlation, it means that the distortion of the regression model is more serious. Usually, the larger the value of VIF, the smaller the tolerance between independent variables and the more likely there is a collinearity problem. When the VIF value in the regression model is greater than 0 and less than 10, it can be considered that there is no multicollinearity between independent variables; if it is greater than 10, it means that the multicollinearity between independent variables is serious.
- (3) Sequence correlation: sequence correlation (Durbin–Watson) is a kind of correlation that exists in the regression model, that is, the significant correlation between different sample points. Serial correlation can be found by computing the Durbin–Watson value in the regression model, which can range from 0 to 4. When $DW = 0$, it means that there is a positive correlation between the residual values; when the value approaches 2, it means that there is no correlation between the residual items; when the DW value tends to 4, it means there is no serial correlation between them.

4.4.2. Regression Analysis between Variables. The details are shown in Table 5. Firstly, under the premise of controlling demographic variables such as teacher gender, teaching age, education background, and teaching subject, transformational leadership was introduced into the first-level regression model, and the Durbin–Watson value of the serial correlation was 1.881, ranging from 0 to 1.4, indicating that there is no autocorrelation in the model. The tolerance value is between 0.454 and 0.978, the maximum value of the variance inflation factor VIF is 2.203, and there is no serious collinearity in the model. Its multivariate correlation coefficient R value is 0.621, the coefficient of determination R^2 value is 0.386, the adjusted R square value is equal to 0.381, and the estimated standard error is 9.272, so transformational leadership can explain 38.6% of the total variance of teacher teaching innovation in the dependent variable. The standardized regression coefficient β value is 0.615, which shows that transformational

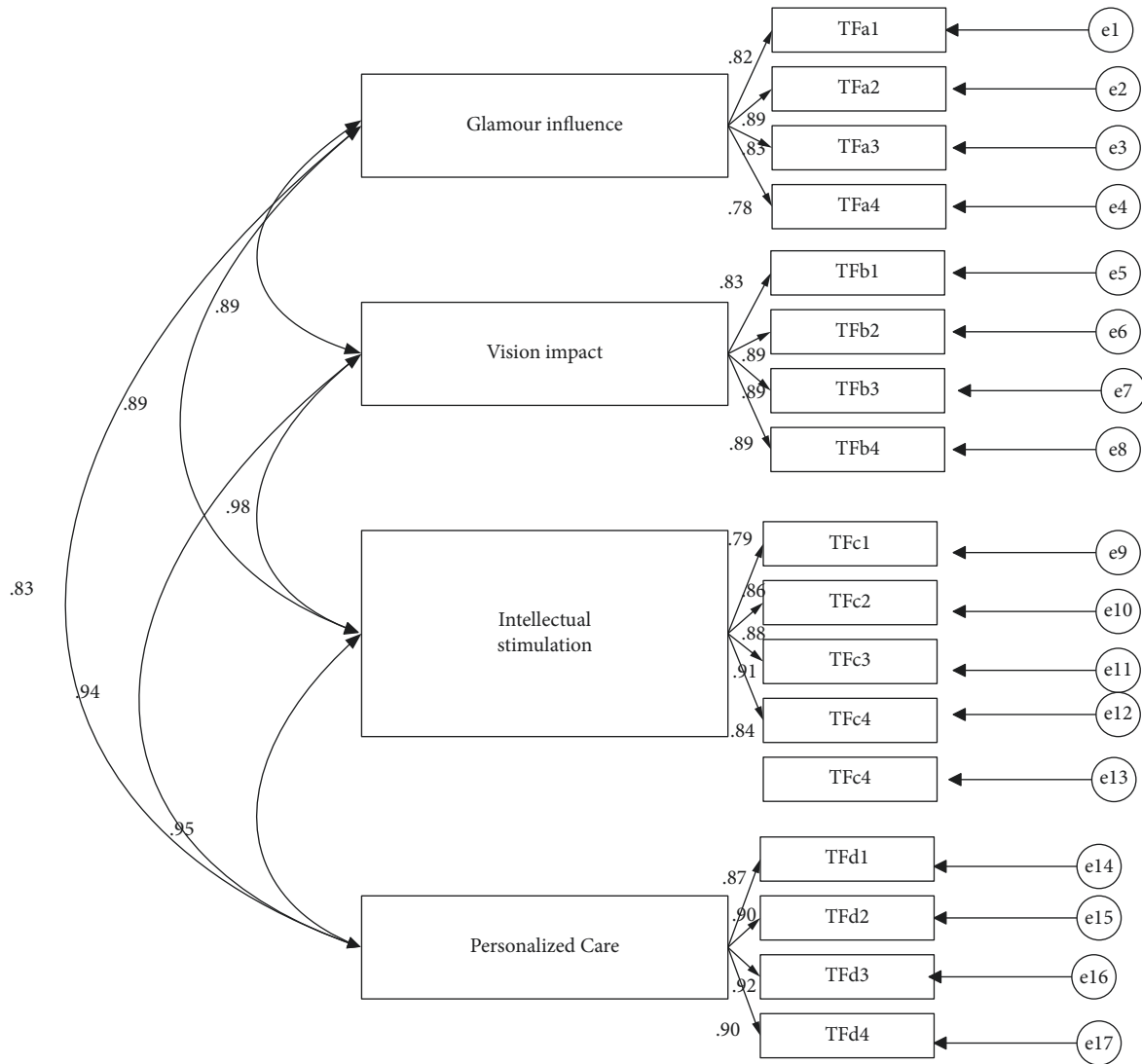


FIGURE 1: Confirmatory factor analysis model.

TABLE 4: Descriptive statistical analysis of transformational leadership.

Variables and dimensions	Average value	Standard deviation	Post hoc multiple comparisons ($P < 0.05$)
Transformational leadership	4.1686	0.63583	
Glamour influence	4.2554	0.58808	
Vision incentive	4.1580	0.69812	Charisma influence > vision inspiration > personalized care
Intellectual stimulation	4.1466	0.64921	
Personalized care	4.1201	0.76199	

leadership has a significant positive impact on teachers' teaching innovation and that transformational leadership has a positive predictive effect on teachers' teaching innovation as a whole. Next, the subdimension of transformational leadership is introduced into the second-layer model. The Durbin-Watson coefficient of multiple regression is 1.876, the tolerance is between 0 and 1, and the maximum value of the variance inflation factor VIF is 2.205. The regression model has no autocorrelation and common linearity. The dimensions entered into the regression model after stepwise analysis include intelligence stimulation and charisma influence. The

model explained a total of 39.7% of teachers' teaching innovation, of which intelligence stimulation explained 36.7% of teachers' teaching innovation and charisma influence explained 1.5%. The joint prediction variance of the second-level regression model relative to the control variable increased by 0.011, indicating that the introduction of transformational leadership dimensions into the regression model increased the model's interpretation by 1.1%. From the perspective of standardized regression coefficients, the β coefficients of intelligence stimulation and charisma are 0.438 and 0.213, respectively. These two dimensions have a positive impact on

TABLE 5: Transformational leadership and the impact of its dimensions on teacher teaching innovation.

Variable	Level one			Second floor			Multicollinearity test			
	Beta B	Sig Beta	B Sig	Beta B	Sig Beta	B Sig	Tol	VIF	Tol	VIF
Gender	-0.015	0.599	0.425	-0.014	-0.552	0.458	0.893	1.120	0.893	1.120
Teaching age	0.003	0.035	0.915	0.003	0.030	0.925	0.454	2.203	0.453	2.206
Education	0.020	0.809	0.359	0.024	0.941	0.282	0.674	1.483	0.674	1.484
School section	-0.010	-0.245	0.675	-0.004	-0.104	0.859	0.579	1.728	0.573	1.745
Job title	-0.054	-1.474	0.037	-0.050	-1.373	0.050	0.506	1.976	0.506	1.977
School	-0.024	-1.212	0.217	-0.024	-1.217	0.211	0.890	1.124	0.889	1.125
Subject	-0.003	-0.032	0.878	-0.004	-0.038	0.855	0.814	1.228	0.814	1.229
Change leadership	0.806	1.342	0.000				0.978	1.023		
Intellectual stimulation				0.388	2.154	0.000			0.130	7.680
Personal care				0.308	1.821	0.000			0.182	5.481
Vision incentive				0.143	0.920	0.003			0.144	6.937
R2		0.662			0.669		DW			1.748
$\Delta R2$		0.659			0.666					1.788
F		247.862			204.520					

TABLE 6: Analysis of regression results.

Assumption	Hypothetical content	Validation results
H1	The transformational leadership style of college principals has a positive impact on teachers' teaching innovation	Support
H1a	There is a positive correlation between the influence of charm and teachers' teaching management	Support
H1b	There is a positive correlation between vision incentive and teacher teaching management	Does not support
H1c	There is a positive correlation between individualized care and teachers' teaching management	Does not support
H1d	There is a positive correlation between intellectual stimulation and teachers' teaching management	Support

teachers' teaching innovation, while other control variables have no significant impact on teachers' teaching innovation. Therefore, it can be concluded that both intellectual stimulation and charismatic influence in transformational leadership can promote teachers' teaching innovation, while vision stimulation and individualized care have no significant correlation with teaching innovation. The standardized regression equation can be expressed as teacher teaching innovation = $0.438 \times$ intelligence stimulation + $0.213 \times$ charisma influence.

4.5. Analysis of Results. Under the premise of controlling for demographic variables such as teacher gender, age, and teaching subject, this research uses transformational leadership as the explanatory variable, teacher teaching management as the explained variable, and the school's organizational innovation atmosphere as the mediating variable for regression analysis. The inspection yielded the following results. The transformational leadership of principals perceived by teachers has a significant predictive effect on teachers' teaching management, indicating that the practice of transformational leadership by principals is a necessary path to improve the teaching management level of school teachers. Its sub-dimension intelligence stimulation and charismatic influence also have a positive effect on teaching innovation, while vision stimulation and individualized care have no significant impact on teaching innovation, and the positive effects of transformational leadership should be properly used. Research hypotheses H1, H1a, and H1d are verified, but H1b and H1c cannot be verified. The details are shown in Table 6.

5. Conclusion

In the descriptive statistical analysis of this study, the transformational leadership style of college principals has a positive impact on teachers' teaching innovation. There is a positive correlation between charisma and teachers' teaching management, and there is a positive correlation between intellectual stimulation and teachers' teaching management. From the data, it can be concluded that the average score of individualized care in the subdimension of transformational leadership is much lower than the scores of other dimensions. And it reaches a statistically significant level, indicating that teachers' perceived leadership care and the work support is far from the expected level. To a certain extent, the principal's excessive alienation and weakening of communication with teachers is a true portrayal of the bureaucratic tendency of the current primary and secondary school organizations, which is not conducive to the effective development of teaching innovation activities. The score is much higher than other dimensions, indicating that the principal is actively exerting personal influence, prompting teachers to resonate with the school's collective mission, and at the same time fully publicizing their own personality charm and noble character, and stimulating teachers' worship and awe of themselves through various methods. Transformational leadership and its sub-dimension intelligence stimulation and charismatic influence can effectively predict teachers' innovative teaching levels; that is, the higher the principal's transformational leadership level, the stronger teachers' teaching innovation ability and the predictive effect of intelligence stimulation on teachers'

teaching innovation. There are also some shortcomings in this study. For example, the influence of factors such as teachers' interpersonal relationships and organizational learning was not considered in the questionnaire design, and these factors were not controlled in the subsequent empirical analysis.

Data Availability

The dataset can be accessed upon request.

Conflicts of Interest

The authors declare that they have no conflicts of interest.

References

- [1] B. M. Bass and B. J. Avolio, *Improving Organizational Effectiveness through transformational leadership*, Sage Publications, Thousand Oaks, CA, USA, 1994.
- [2] B. M. Bass, *Leadership and Performance Beyond Expectations*, Free Press, New York, NY, USA, 1985.
- [3] W. Bennis and B. Nanus, *Leaders: The Strategies for Taking charge*, HarperCollins, New York, NY, USA, 1985.
- [4] P. M. Blau, *Exchange and Power in Social life*, John Wiley, New York, NY, USA, 1964.
- [5] F. E. Fiedler, *A Theory of Leadership effectiveness*, McGraw-Hill, New York, NY, USA, 1967.
- [6] A. W. Halpin and D. B. Croft, *The Organizational Climate of schools*, Midwest Administration Center, University of Chicago, Chicago, IL, USA, 1962.
- [7] A. Aydin, Y. Sarier, and S. Uysal, "The effect of school principals leadership styles on Teachers Organizational commitment and job satisfaction[J]," *Educational Sciences: Theory and Practice*, vol. 13, no. 2, pp. 806–811, 2013.
- [8] A. Bandura, "Self-efficacy: toward a unifying theory of behavioral change," *Psychological Review*, vol. 84, no. 2, pp. 191–215, 1977.
- [9] R. M. Baron and D. A. Kenny, "The moderator–mediator variable distinction in social psychological research: conceptual, strategic, and statistical considerations," *Journal of Personality and Social Psychology*, vol. 51, no. 6, pp. 1173–1182, 1987.
- [10] S. Bharadwaj and A. Menon, "Making innovation Happen in organizations: individual creativity mechanisms, organizational creativity mechanisms or both?" *Journal of Product Innovation Management*, vol. 17, no. 6, pp. 424–434, 2000.
- [11] C. Binnewies and M. Gromer, "Creativity and innovation at work: the role of work characteristics and personal initiative," *Psicothema*, vol. 24, no. 1, pp. 100–105, 2012.
- [12] R. Borasi and K. Finnigan, "Entrepreneurial attitudes and behaviors that can help Prepare successful change-Agents in education," *The New Educator*, vol. 6, no. 1, pp. 1–29, 2010.
- [13] A. Britz, *The Assessment of Climate for Innovation in organizations*, Unpublished master's thesis, technische hochschule Darmstadt, linstitut für betriebswirtschaftslehre, Darmstadt, Germany, 1995.
- [14] F. W. Brown and D. Moshavi, "Herding academic cats: faculty Reactions to transformational and contingent reward leadership by department chairs," *Journal of Leadership Studies*, vol. 8, no. 3, pp. 79–93, 2002.
- [15] A. Carmeli, R. Meitar, and J. Weisberg, "Self-leadership skills and innovative behavior at work," *International Journal of Manpower*, vol. 27, no. 1, pp. 75–90, 2006.
- [16] C.-P. Chang, H.-W. Chuang, and L. Bennington, "Organizational climate for innovation and creative teaching in urban and rural schools," *Quality and Quantity*, vol. 45, no. 4, pp. 935–951, 2011.
- [17] C. Day, A. Harris, and M. Hadfield, "Challenging the orthodoxy of effective school leadership," *International Journal of Leadership in Education*, vol. 4, no. 1, pp. 39–56, 2001.
- [18] S. Li and S. Liao, "Help others and Yourself Eventually: exploring the relationship between help-Giving and employee creativity under the model of perspective taking," *Frontiers in Psychology*, vol. 8, p. 1030, 2017.
- [19] J. Duan, C. Li, and Y. Xu, "Transformational leadership and employee voice behavior: a Pygmalion mechanism," *Journal of Organizational Behavior*, vol. 38, no. 5, pp. 650–670, 2017.
- [20] H. H. M. Tse and W. C. K. Chiu, "Transformational leadership and job performance: a social identity perspective," *Journal of Business Research*, vol. 67, no. 1, pp. 2827–2835, 2014.

Research Article

Metal Jewelry Craft Design Based on Computer Vision

Nan Li 

Design College, Shandong University of Arts, Jinan 250300, Shandong, China

Correspondence should be addressed to Nan Li; z00548@sdca.edu.cn

Received 24 April 2022; Revised 24 May 2022; Accepted 30 May 2022; Published 15 June 2022

Academic Editor: Dong Chen

Copyright © 2022 Nan Li. This is an open access article distributed under the Creative Commons Attribution License, which permits unrestricted use, distribution, and reproduction in any medium, provided the original work is properly cited.

Combining computer vision technology with process design, a new design and production method is obtained, which breaks through the limitations of traditional jewelry creation and provides new possibilities for the realization of complex jewelry structures. When technology no longer becomes the bottleneck of artistic expression, the space of art will be greatly expanded. Science and technology leading design method has become a new way to assist jewelry artists in subjective creation. According to various thoughts and ideas in design, establishing the corresponding algorithm rules and parameters can generate the scheme through calculation. The design result obtained in this way not only has a scientifically logical basis but also obtains the result beyond the normal imagination space due to the intelligent design process. This paper tries to apply computer vision technology to modern jewelry design, analyzes several aspects of computer vision application in process design, and combines the latest technical means to put forward algorithms for verification. The results prove that computer vision can improve the efficiency of crafts design significantly.

1. Introduction

With the rapid development of the global economy and culture, mankind has entered an era of information explosion and rapid development of science and technology. A variety of information sources can impact people's senses through various media such as graphics and sound. In the modern society where productivity has been greatly improved, art has gradually been integrated into people's lives. Modern people are no longer only satisfied with the practicality of products but also have new artistic and ideological requirements [1]. It can be seen from the gold and silver jewelry brands and stores everywhere that the metal art embodied in metal jewelry has catered to the emotional and spiritual needs of most people [2].

In the 21st century, human beings are in a pluralistic information society. Culture and art have been different from the single form of the previous society. After the development of religious function and social functions in ancient times, the decorative function of jewelry has been gradually strengthened. Jewelry design and research not only cater to religious etiquette and reflect class wealth but also have become a conscious and controllable behavior

gradually. Modern jewelry design and research pay more attention to the pursuit of decorative meaning, and this pure pursuit of decoration is also the development of humanities in different periods [3]. With a specific historical background, there are often costume cultural characteristics corresponding to it. After human society has developed to a certain extent, jewelry design reflects the most direct and pure decorative needs through certain research means. Modern jewelry design also needs effective research and development ways to excavate people's most urgent desire for jewelry decoration [4, 5].

Nowadays, the pace of life is getting faster and faster, and the rapid spread of Internet information makes the cultural industry face great challenges. Culture is also facing a crisis of convergence. In the field of jewelry design, jewelry products also lack cultural connotation and cannot realize cultural inheritance [6]. Many consumers with high quality and high artistic aesthetics are also eager to have jewelry works with far-reaching cultural connotations. Therefore, modern jewelry design and research need to pay attention to humanistic needs, use an effective research and development method to care about modern people's nostalgic mood, and explore people's inner intuition and desire for jewelry [7].

The most natural and pure decoration consciousness in people's hearts is the most direct display.

The rapid development of technology does not kill the art of metalworking but has encouraged the emergence of new industries. At present, the development of metal surface technology is led by the progress of science and technology [8], which has become the "processing type" metal surface technology. In the future, it is necessary to combine the "creative type" metal surface technology with brain and processing practice. Their mutual traction and influence can create works with more manual processing technology and modern machine production level. On the basis of studying the existing technologies, the metal surface technology will be carried forward and recreated, so that the metal surface technology can serve today's jewelry industry, humanities, and public aesthetics or provide materials and technology for the creation of artists [9].

Algorithm technology can tap the creative potential of designers and give designers more abundant imagination space. Computer technology plays an important role in the three-dimensional structure of the process and innovation, so this paper studies the application of jewelry design based on modern metal technology. We use a computer vision algorithm to analyze the different features of metal jewelry and further use network combination features to classify. After the primary classification of intelligent algorithms, new features are created in reverse through network algorithms, and these new features are applied to industrial models, so as to obtain the artistic products jointly created by machines and humans.

2. Related Work

Since humans started to smelt metal, they have begun to use metal to make all kinds of jewelry to decorate themselves. From the Stone Age to the use of simple and grinding tools to master the technology of smelting bronze and smelting silver to the blowing method [10] and then to the emergence of the smelting process, jewelry culture has experienced from grinding carved jade culture to bronze culture and the transition of precious metal gold and silver jewelry through attributes to various kinds of jewelry materials, design, and production. Historically, jewelry has an important status in clothing and ornaments. Ancient woman's crowns and jewelry are famous for their exquisite design at home and abroad. Men also pay attention to the role of jewelry seriously [11]. His jade pendants and hand-wearing-BanZhi are symbols of identity and grade. The delicacy of accessories not only reflects the superb craft level and technology but also represents the status of each class, so the ancient people attached great importance to the status of jewelry accessories.

The industrial revolution in Britain at the end of the 18th century brought about great social changes. Productivity rose dramatically, and handicraft workshops were replaced by large-scale mechanized production [12]. There was no doubt that the development of machinery aimed to serve human life. Labor force and time had been unusually saved and efficiency had also been improved. Cheap products were

shipped all over the world. At the same time, the destruction of handicrafts brought by mechanized large-scale production was immeasurable. In the field of jewelry design, mechanized mass production was still the main production and development mode of jewelry products [13]. However, with the development of society and the improvement of people's aesthetic awareness, more and more consumers pursue the uniqueness of design, so limited sales and customization models came into being. Limiting the number of products and advocating unique design and research mode solved this problem.

At present, the demand for ornaments is growing, and the types are becoming richer and richer. People's pursuit of jewelry has not only stayed at the beautiful level but also seeks a sense of science and technology. The development of new jewelry and sensor is pluralistic and refined. The demand for creativity makes everyone more practical, so the development of science and technology application jewelry has certain progress and innovation at home and abroad. With the rise of the "Art Nouveau" movement, the choice of jewelry materials has also undergone great changes. Cheap and renewable materials have been widely used in jewelry production. These abundant simple materials with decorative functions have gradually replaced precious gold, silver, and gem materials that occupy an important position in the history of jewelry culture. Jewelry designers have also become clearheaded and slowly put their eyes on the beauty and touch of the material itself [14]. For jewelry design, computer-aided technology has come into people's sight. But in the early design, as the computer is expensive and complicated, much design work cannot be completed on the computer. Computer-aided technology only represents a new possibility and a new direction. With the rapid development and popularity of computer technology, more and more jewelry design software came into being to let computers become a common tool for jewelry designers [15].

At the present stage, one of the most widely used technologies is MBD (Model-Based Definition). Before this, technicians used two-dimension drawings to describe products and transfer information, which had great shortcomings [16]. At present, digital design and manufacturing technology is adopted to directly utilize the digital information data of information transmission, process design, and manufacturing mode based on a 3D digital model in product manufacturing [17]. The process information, tooling design, product quality inspection, and other information in the product can be obtained by the MBD model, which can shorten the research and development design cycle and improve the design quality of the products. However, for the model itself, due to its complicated three-dimensional model, the file occupies a large memory space, usually more than 100 MB or even several GB. MBD model has a large amount of information, which is not conducive to the acquisition of data information and the disadvantages of model anytime viewing due to a large amount of data when it is transmitted between different departments, such as slow viewing or slow information acquisition due to a large amount of data, or the failure of computer hardware to meet

requirements [18]. In order to meet the demand for manufacturing, many scholars at home and abroad have done a lot of research studies on the lightweight of 3D digital MBD model data processing.

In the application of digital metal design and manufacturing, not only are 3D models used to replace the current 2D and 3D drawing conversion problems, but also design, process modeling, and simulation technology are used to improve the efficiency of product design and process production. For example, Wu et al. specially studied the application of complex shell MBD digital model in digital engineering in literature [19], compared four lightweight file formats, analyzed the advantages and disadvantages of the four formats, and verified their application in different application scenarios. Huang et al. introduced a method of extracting subcomponents from models in literature [20]. During the manufacturing process, effective parts of CAD models are retrieved to complete the reuse of 3D models. Balic et al. introduced a method to extract information from the model in literature [21] and studied the required functions of feature extraction of their CAD model based on the method of milling strategy prediction. The method adopted by Zhu et al. in literature [22] is to simplify the analysis by adding 3D model data information on the basis of a 2D model. Wang et al. studied the basis of the MBD model design in the literature [23], together with the present situation of the production process of soft and hardware environment; in the process of mechanical product manufacturing process model lightweight and visualization, 3D key technologies were analyzed, and the state of the extracted information into the feature information layer, three layers, and process chain used a recursive depth-first walk. The process information of constructing the lightweight model was extracted from the source point, the information file of the lightweight model was compressed, then the model was reconstructed to simplify the 3D model, and the visualization technology was used to realize the visualization of the 3D model.

With the deepening of research, more and more science and technology are introduced into metal design and manufacturing. People not only need to improve the process but also need to compute more flexibly and adopt light processing. In literature [24], Huang et al., in order to highlight the effect of display and reduce the amount of design data, adopted the method of artistic rendering to achieve this goal without the requirement of computer equipment. Although the sense of unreality of the artistic method can speed up the modeling, this method is operated on the original model. Although it achieves the effect of lightweight model data, the complete data information of the model is broken or even changed, which is not suitable for those applications requiring high model accuracy. The earliest Taubin and Ouma proposed a geometric lossless compression coding algorithm [25] based on grid processing, which is an efficient coding algorithm form that decomposes complex grid models into simple topological structure information compression coding, vertex prediction estimation, and compression. The grid model simplification algorithm is the most commonly used method to

deal with the browsing and display of 3D models. Under the requirement of model accuracy, the number of triangular meshes can be reduced to the maximum. The most commonly used algorithms include surface merging, vertex deletion, and other mesh simplification algorithms [26]. Most of the lightweight processing of 3D MBD model data is aimed at the lightweight processing of ontology solid model, for the purpose of fast 3D browsing and visualization. A small amount of research on the lightweight processing of 3D MBD model data is in transmission and storage. At present, in the era of big data, there is almost no research on the lightweight transfer of MBD model data to local terminals in the cloud. With the rapid development of intelligent devices and sensors, technology represented by computer vision will continue to replace traditional metal design.

3. Intelligent Metal Jewelry Design

With the change in people's ideology, the modern art design is also looking for various new forms of expression and development direction. With the advent of the information society, the design expression form accepted by people is no longer limited to a regional style. Considering the current cultural background and social background, on the one hand, the public's preference and aesthetic appreciation of modern design cannot be directly investigated by referring to the selection and evaluation criteria of traditional art. On the other hand, based on machine intelligence, people analyze metal jewelry data through computer vision, get a large number of metal jewelry features through training, and further classify them using the network. With the development of research, people reversely use the obtained features for recreation. Let network learning products and intelligent design meet human needs of modern products, and metal jewelry network flow based on computer vision is shown in Figure 1.

3.1. Traditional Metal Design. The traditional metal design method is the accumulation of human beings for thousands of years, which has an important position. The common forming process is mainly divided into forging, chiseling, welding, and casting [27].

- (1) Forging: the use of good ductility of metal, the metal plate after the high temperature is hammered plastic constantly, and finally made into relief, utensils, sculptures, etc.
- (2) Chisel: the use of the hammer, chisel, iron horse, and other tools on the metal surface carving pattern
- (3) Welding: it refers to the metal material pressure or heating, which can be used or not to fill the materials combined with the workpiece
- (4) Casting: the molten metal is injected into the mold and directly formed. Then, the surface process is treated

Traditional metal surface technology includes hammer forging, chisel, welding, gilding, silk inlay, hollowing,

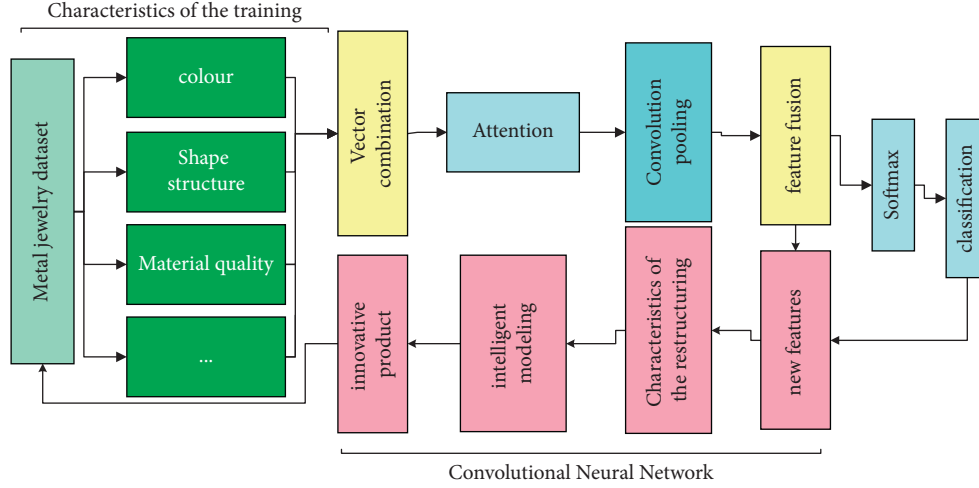


FIGURE 1: Network diagram of intelligent metal jewelry design.

misplaced inlay, and gold and silver off. Ancient craftsmen expressed the texture of the metal surface in different ways through various metal surface processes. In an excellent process, designers can often dig out the biggest characteristics and natural beauty of the material itself through various processes. The following is a brief introduction to some common traditional crafts.

Welding process: the forming method of the metal bead is to cut the metal sheet into small sections through high-temperature heating to make it fuse into granules naturally. The welding process is to heat and melt the metal beads and fuses them onto the surface of the metal product directly, forming a pattern composed of gold beads. Compared with the welding method using solder, the advantage of molten metal particles is that the welding area is small and the performance effect is clean.

Gilding process: gilding is a mixture of pure gold and mercury plated on bronze ware, which is called “gold amalgam.” Since gold is dissolved in mercury and can flow freely, these two things boil at different points. Heating vaporizes the mercury, leaving the gold to adhere to the surface to form gold patterns.

Silk inlaying process: silk process is to process gold or pure silver into the silk of different thicknesses for bending, pinching, filling, stacking, and other operations and the production of gold and silver jewelry fine gold process. Different decorative parts can be made into different patterns of silk, such as arch silk, bamboo silk, and wheat silk, and other shoulders can be welded to the shoulder of gold and silver utensils, becoming independent decorations.

Gold foil process: because of the good ductility and plasticity of gold, it is hammered into thin slices for pasting Buddha statues, utensils, etc. This craft is the traditional craft of the Chinese nation, which has a history of nearly 1700 years. The unique gold foil forging technique born in Nanjing was listed as the first batch of national intangible cultural heritage by The State Council.

Gold sticking process: gold sticking process is a traditional process with the emergence of gold foil. It has the same meaning as modern gold coating technology. That is,

the use of the adhesion of very thin gold foil, the mutual absorption of some smooth surface materials, and the gold foil package affixed to the surface of the utensils play protective and decorative roles.

Gold coating process: the gold foil is coated on the surface of copper, aluminum, zinc, iron, or other alloy materials and hammered solid so that the gold foil is attached to the surface of the body and the formation of concave and convex texture is consistent with the surface of the body to play the role of decoration and protection. The gold foil used for coating gold is usually gold with higher purity.

Gold and silver off process: it is developed by the Shang dynasty gold foil decal process, which is a famous ancient Chinese decoration process. Usually, the gold foil and silver foil are processed to the desired pattern and then coated in layers of paint and ground until the gold and silver reveal the corresponding pattern.

Misplaced gold and silver: chiseling and carving shallow grooves of patterns in the surface of the metals. Then, gold and silver wires, pieces, or beads are wedged into the groove, finally, beating and using grindstones to make them flat. This is a new development of the traditional bronze Mosaic technique. The gold and silver leveling and stripping technology used for lacquer surface decoration belong to a special form of gold and silver splicing technology.

Dotted jade craft: dotted jade craft is a traditional Chinese jewelry-making craft. It is one of China’s national treasures along with gilding and enamel. First, gold or gold-plating metal is used to make different patterns of the base. Then, the bright blue kingfisher back feathers are carefully inlaid on the table to make a variety of jewelry. After this, the color of the jewelry is bright and will never fade [28].

3.2. Modern Metal Working Based on Computer Vision

3.2.1. Metal Forming Technology. With the continuous improvement of the modern industrial level, the requirements of material production scale, production reliability, and production quality are also improved. In this context, it

is imperative to achieve the automatic production of materials. At the same time, the automatic production of materials can also effectively solve the problems of manual operation errors, low production efficiency, and low prominence and ultimately achieve the purpose of improving production efficiency and ensuring product quality.

Machine tool intelligent investment casting: it is the use of CNC machine tools according to computer vision 3D modeling or existing products directly to the metal cutting, grinding, and other processes. Due to the technical limitations of machine tools themselves, such as less axial direction, tool selection, and other reasons, machine tools are generally used to produce products whose shapes are combined on the basis of basic geometry.

3D printing technology: 3D printing is the crystallization of computer vision highly applied technology, that is, a kind of rapid prototyping technology by using powdery metal or plastic and other adhesive materials with layer printing and stacking model structure. Later, 3D printing technology has gradually matured and finished products can be directly printed by 3D printers.

Science and technology and traditional craftwork must be combined to achieve better development. With the progress of technology, many excellent and exquisite metalworking techniques have been lost due to various reasons, but the retained techniques are still worth learning and studying by modern metal artists. For example, forging, chisel, welding, gilding, filaments inlaid, hollowing, inlaid wrong, and gold and silver off in modern metal art design can still be referred to for reference and application. Its practical application is also in metalworking teaching practice in colleges and some personal metal studios.

3.2.2. Metal Surface Technology. Modern intelligent metal surface treatment technology is of great significance. The intelligent surface treatment technology greatly improves product quality and saves valuable materials, realizing material surface compounds. Solving problems cannot be solved by a single material to repair the overall advantage, saving energy and materials significantly.

Polishing process: it is the use of a polishing machine to complete the polishing process. When the polishing wheel rotates at high speed, high temperature is generated between the jewelry and the polishing wheel as well as the molten polishing wax, which improves the plasticity of the metal, the surface fine unbalances, and the brightness of the jewelry. If the surface of the material is rough, it is difficult to plate a solid and corrosion-resistant coating. Even if the coating is barely on, the jewelry coating will exuviate, bubble, pit, speckle, and has other undesirable phenomena in a short time. Therefore, the workpiece must be polished before electroplating. Metal polishing based on computer vision, using the algorithm to calculate the time and strength in advance, reduces the loss of materials. And it can accurately control the completion of the process.

Electroplating process: after the precious metal jewelry workpiece is processed and formed, the surface color is its inherent color. However, sometimes, it is necessary to

change the surface color of the metal jewelry to achieve a special effect. After the object is polished, processed, and electroplated before plating, the electroplating coating is formed, which makes the surface luster of the object strong. The main purpose of electroplating is to enhance the corrosion resistance of the metal, increasing the appearance and surface hardness. Electroplating is a chemical surface treatment process. It is prepared according to the requirements of jewelry electroplating special gold-plating solution in a certain PH value and temperature conditions through the electrochemical reaction between positive-negative electrode current and electroplating solution so that the gold ions of the gold-plating solution are gradually transferred to the metal surface of the jewelry.

Electrocasting is a new jewelry production process. Its principle is similar to electroplating, and casting in the solution is negative mold whose surface activation is treated after the generation of the conductive layer. Through the action of electrophoresis, metal will be gradually deposited on the negative mold surface, and the thickness can be removed after grinding and welding. This surface treatment is electrocasting the jewelry. This kind of jewelry has a beautiful appearance, large size, lightweight, fast electroforming speed, and high or low output, which is easy to master flexibly. At present, gold ornaments on the market such as mascots, Buddha, and zodiac are mostly hollowed into gold ornaments by electrocasting.

Sandblasting process: the metal surface is sandblasted according to the design requirements so that the metal surface shows the frosted texture. Compared with other surface textures, it enhances the artistic performance of the product and has increased its aesthetics.

Imprint process: it is also known as indentation, which is a decorative technique to produce texture properties on the metal surface. It is a process that makes the pattern needed to be designed into a mold and presses out the texture on the surface of the metal through stamping by using the characteristics of metal molding and ductility. Impression can only be made on one face of the metal plate. The texture of each imprint is mainly determined by the chisel.

Wood grain metal surface process: wood grain gold process is derived from the traditional Japanese sword-making technology, which is a metal-making process studied by sword casting division when forging swords. Swordsmith uses layers of metal in an attempt to mimic the ancient Chinese lacquer technique of stacking vermilion. Lacquers overlay layers of paint on vessels and, then, carve curving grooves on the surface of tang grass or swirls to reveal a continuous pattern of stripes of various colors. Grain gold is called "grain metal" because the visual effect of the metal layer is similar to the grain of wood.

Enamel process: enamel process is a unique combination of porcelain and metal processes. In the polished metal substrate surface, it is coated with a layer of glass gloss enamel. After drying and burning, it becomes a magnificent and colorful craft. It not only has the characteristics of precious and solid metal but also has the characteristics of crystal clear enamel glaze, which is smooth and suitable for decoration. Enamel works mainly include painting enamel,

wire drawing enamel, hammer forging enamel, and tire enamel.

3.3. Generative Adversarial Network

3.3.1. Metal Jewelry Image Processing

(1) *Image Denoising.* The purpose of image denoising is to remove the noise while preserving the important signal features as much as possible. In the process of image acquisition, there are many noises and interferences. Noise can be understood as the interference signal that hinders the process of image observation and information extraction. Noise may be introduced in every link of image generation and transmission, among which additive White Gaussian noise and salt and pepper noise are more common. The interference of the image noise irreversibly destroys the information of the image. The image noise model can be roughly approximated as

$$f(x) = u(x) + n(x), \quad (1)$$

where $u(x)$ represents the real signal value, and $n(x)$ represents the noise at position x .

The mean filter replaces the value of the window center with the average value of the pixel values covered by the window. The existence of noise causes a sharp gray difference in the image at the noise point, and it is this gray jump that leads to the observation obstacle. Eliminating the noise through the neighborhood method will also lead to the blurring of the edge part with the same sharp gray difference. Suppose the image is $f(x, y)$, and the image after mean filtering is defined as

$$\hat{f}(x, y) = \frac{1}{mn} \sum_{(s,t) \in S_{xy}} f(s, t), \quad (2)$$

where m and n are, respectively, the height and width of the filter window, S_{xy} represents the location set of all pixels in the window, and s and t are the locations of pixels in the window.

A median filter provides excellent noise reduction capability for some types of random noise, which can effectively smooth sharp noise and better retain an edge, and it is often used to filter salt and pepper noise. To a certain extent, isolated noise can be distinguished from image features that need to be preserved, such as image edges and lines.

(2) *Image Enhancement and Morphological Processing.* Image enhancement enhances the discrimination ability of some information according to specific needs while weakening or removing some unwanted information interference so that the processed image is more convenient for the subsequent processing links and more suitable for the current task needs.

Histogram equalization is a common technique to enhance image appearance. For an overall dark image, its histogram will be tilted toward the lower end of the grayscale. If we can “extend” the gray level of the dark end so that

the gray value is evenly distributed in $[0, 255]$, the gray-level difference between the background and the object in the image will be enlarged. Thus, it will increase the contrast of the image and make the image clearer. It can be found that there are scratches and macula defects on the surface of metal products. If the original image is directly used for defect detection, macula defects are not obvious and it is not easy to detect defects. Through image enhancement, the defect areas are highlighted. Morphology is mainly used in image preprocessing, enhancing object structure, and adjusting shape features, and it is widely used in image analysis. Corrosion and swelling are basic morphological changes based on which more morphological operations can be defined.

(3) *Image Segmentation.* Image segmentation is a prerequisite for image processing. Through image segmentation, the image is divided into regions with different features, and the region of interest is extracted. Usually, it can be segmented by grayscale, texture, color, and other features. There are many methods and types of image segmentation, among which the threshold-based image segmentation method is suitable for grayscale images with a large grayscale difference between target and background, which is simple and quick, so this paper mainly adopts threshold-based segmentation. The key to threshold segmentation lies in the determination of the threshold and a good segmentation method is conducive to the identification and analysis of subsequent targets.

The least mean square error method is one of the commonly used threshold segmentation methods, where z represents the gray value and $P(z)$ is the probability density estimation of the gray value. Two probability density functions P_1 and P_2 are defined, corresponding to the gray values of background and foreground, respectively. Then, the mixing density function of the whole image is

$$p(z) = p_1 p_1(z) + p_2 p_2(z), \quad (3)$$

$$p_1 + p_2 = 1.$$

So, the pixels in the image are divided into foreground and background. The aim of the least mean square error method is to minimize the probability of prediction error when selecting the threshold T . Based on computer vision, metal products are generally divided into three regions, namely, texture region, smooth region, and outer circle region, so it is defined as

$$F(x, y) = T(x, y) + S(x, y) + C(x, y), \quad (4)$$

where $F(x, y)$ is the original image, $T(x, y)$ represented the texture region image, $S(x, y)$ is the smooth region image, and $C(x, y)$ is the outer circle region image. The texture area is special. The surface is not smooth but has certain texture characteristics, which needs to be extracted separately for special treatment. The smooth area of normal metal products is relatively flat. For the smooth area of different products, the gray value trend of normal products is flat while defective products fluctuate. This area can be extracted separately to

make better use of this advantage. In this paper, two ring masks are used to separate the texture region, smooth region, and outer circle region.

Setting different threshold values for different regions can reduce the adverse effects of uneven illumination, which is easier to feature extraction of the metal products. For instance, if metal product surface polishing on the right side is bright, and the mean gray level is higher than the left, then setting the threshold can appropriately increase (such as using the grayscale average as discriminant conditions, A compared to B in the region, and gray-level threshold can be appropriately increased). Similarly, on the left side of the metal product, the gray mean value is low, so the set threshold can be appropriately reduced.

3.3.2. Computer Vision Metal Surface Classification.

Traditional image classification is often aimed at a specific recognition task, with small data scale and poor generalization ability. It is difficult to achieve an accurate recognition effect in practical applications for huge image data and serious image interference. In addition, traditional image processing methods often require complex threshold settings for defect recognition, which are sensitive to environmental factors such as illumination conditions and background. If environmental factors change, the settings of these thresholds need to be carefully adjusted; otherwise, the algorithm cannot adapt to the new environment and will lack adaptability and robustness. In feature extraction, it is easy to ignore or fail to understand some complex, hidden, or nonintuitive phenomena and ignore some feature variables depending on researchers' prior knowledge and cognition of classification tasks, while the extracted features directly affect the performance of the system.

In feature extraction, deep learning can automatically extract higher-dimensional and more abstract features from raw data instead of complicated manual feature description and extraction. In contrast, in the field of computer vision, a network model based on deep learning has a stronger ability for feature learning and feature expression. Neural networks can reveal more features that affect the quality of recognition in a positive way and build more general and accurate recognition methods. CNN performs convolution operation on the input 2D image through a series of convolutions with adjustable parameters and further convolves the obtained results to form a cascade, so as to realize the localization of network connection and reduce the number of parameters through weight sharing. A cascaded neural network can extract pattern features of different levels in the input image by gradually expanding the perception domain, which can be used to process different types of tasks.

(1) *Convolution Layer.* The convolutional layer extracts different hierarchical features of the input image. Each element of the convolution kernel is constantly adjusted by the error backpropagation method during training. The convolution operation realizes local connection and weight sharing through sliding Windows, which increases the translation invariance of images and is conducive to better

generalization performance, and can greatly reduce the number of parameters compared with multilayer perceptron.

Assuming that the input size is (H, W) , the filter size is (FH, FW) , the output size is (OH, OW) , the filling is P , and the step is S , we calculate the values of OH and OW as follows:

$$\begin{aligned} OH &= \frac{H + 2P - FH}{S} + 1, \\ OW &= \frac{W + 2P - FW}{S} + 1. \end{aligned} \quad (5)$$

The pooling layer can achieve three functions: feature invariance, feature dimension reduction, and overfitting prevention. Concerning the average (maximum) pooling during each operation, the average (maximum) of the area covered by the pooling core is used as the pooling result.

The function of activation is to introduce nonlinearity into the network and determine how to activate the sum of input signals. The sigmoid function used to play an important role in the development of neural networks, but it will produce a gradient "saturation effect." Relu is one of the most commonly used activation functions in deep convolutional neural networks. The Sigmoid function is defined as

$$\sigma(x) = \frac{1}{1 + \exp(-x)}. \quad (6)$$

Relus is considered to have more biological characterization, which can yield more favorable results for image recognition tasks because the function is less susceptible to the vanishing gradient problem and can produce a sparser and efficient representation. The Relu function is defined as

$$\max\{0, x\} = \begin{cases} x, & x \geq 0, \\ 0, & x < 0. \end{cases} \quad (7)$$

(2) *Full Connection.* For image classification problems, the full connection layer is connected at the end of the network, used to vectorize the feature map, and used this vector to calculate the classification results. In the last few layers of convolution and pooling of the network, high-level semantic information of the image has been extracted, which exists in the feature map. Vectorization of the feature map can be considered to obtain the feature vector of the source image. The fully connected layer has a large number of parameters, and a small number of computing layers involved in the final decision adopt the fully connected structure.

4. Application Simulation Experiment

4.1. *Data Preparation and Evaluation Indicators.* Since computer vision requires a large amount of data support, and metal jewelry design covers trade secrets and copyright, we choose Kolektor Surface Defect Dataset. Traditional machine learning can usually learn a model based on a given sufficient training data and then use that model to make predictions. In order to reduce the interference of invalid

regions on feature extraction, improve the training speed, and reduce memory consumption, the input object is processed to some extent, and only the measured object is retained in the final effect. The data set was randomly divided into training data set, test data set, and verification data set in the ratio of 8 : 1 : 1. Experimental data preparation is shown in Table 1.

The training set is used to fit the classifier parameters, and the verification set is used to adjust the classifier parameters. In the training stage, the test set is encapsulated, and in the final stage, the generalization ability of the trained model in practice is estimated by the test set. At the same time, the sample size is expanded by means of data augmentation. The system mainly adopts random horizontal flip, random vertical flip, and random rotation of 180 degrees.

In order to evaluate the performance of the metal surface classification system based on neural network architecture in practical application, the commonly used evaluation indexes for multiclassification tasks mainly include accuracy (Acc), precision (P), recall (R), $F1$ -score, and confusion matrix. In classification tasks, accuracy, also called precision, is the most commonly used index. Accuracy refers to the ratio of the number of samples correctly predicted to the total number of samples participating in the prediction. Corresponding to accuracy, the evaluation index is the error rate, which refers to the ratio of the number of samples that are wrong in prediction to the total number of samples that participate in prediction. Both measure the prediction of the global sample.

$$\begin{aligned}
 \text{Accuracy} &= \frac{TP + TN}{TP + TN + FP + FN}, \\
 \text{Precision} &= \frac{TP}{TP + FP}, \\
 \text{Recall} &= \frac{TP}{TP + FN}, \\
 F1 &= \frac{2 \times \text{Precision} \times \text{Recall}}{\text{Precision} + \text{Recall}}.
 \end{aligned} \tag{8}$$

4.2. Experimental Verification. Metal jewelry data is different from the conventional computer vision data set. In order to make the verification results more authentic, we choose transfer learning. It can migrate a large network trained on a large data set to a small data set so that good results can be achieved only with a little training. To some extent, transfer learning increases the utilization rate of the model and solves the problem of missing data, which is exactly what metal jewelry needs. In order to verify the network model based on CNN improved pretraining proposed in this paper, we simultaneously analyzed several mature models, VGG19, ResNet, and DenseNet, fine-tuned their structures, migrated to the local metal surface in the way of pretraining, and made the score as close as possible to the real metal jewelry.

4.2.1. Basic Experiment Preparation. Before the loss change experiment, the basic parameters of training need to be set. For the SGD optimizer, good performance can be

TABLE 1: Preparation of experimental data.

	Scratch	Normal	Crack
Train	400	200	240
Verify	50	25	30
Test	50	25	30
Total	500	250	300

achieved when the initial learning rate is 0.001. The best performance is achieved when the momentum decay factor is 0.9. For Adam optimizer, better performance can be achieved when the initial learning rate is 0.0001. When the momentum attenuation factor is 0.8, the performance can be significantly optimized. For the RMSProp optimizer, better performance can be achieved when the initial learning rate is 0.0001. However, the training process and verification process corresponding to the optimizer fluctuate greatly, so it is not recommended to be used in the current metal surface defect classification system. After several tests, the SGD optimizer was finally selected, with a learning rate of 0.001 and a momentum decay factor of 0.9.

The learning rate also directly affects the efficiency of the network model, and the performance of the system in the practical application can be measured by its performance in the validation set. In terms of accuracy and loss function, the system performs worst when the learning rate is 0.05. When the learning rate is 0.001, the system has the best performance, which is close to the performance when the learning rate is 0.0005 and can achieve the best accuracy and minimum loss function value on the verification set. Therefore, the final learning rate is determined to be 0.001.

In the training stage, the topological structure and hyperparameters of the transfer module can remain unchanged. According to whether the weight parameters are retrained according to the new data set, the transfer learning mode can be divided into pretraining mode and fixed-value mode. In the pretraining mode, the migrated weight is regarded as the initial weight of the new network, and the value will be changed by the gradient descent method during the training process. In this way, not only can the migrated knowledge be retained but also flexible adaptability can be ensured so that the migrated knowledge can be flexibly adjusted through the training of the new network on the new data. In contrast, in the fixed-value mode, the structure and weight of some migrated networks remain fixed, and the training process is only targeted at the fully connected network behind the migrated modules. Therefore, there are fewer parameters to be adjusted, and the learning convergence speed is faster. The performance of the two training methods using transfer learning is better than that of the training method without transferring in terms of accuracy and loss function value, and the epoch value is 50.

4.2.2. Loss Function. The improved CNN architecture in this paper is due to its lower computation and parameter quantity than other network models while ensuring accuracy. For different network architectures, we compared

VGG19, ResNet, and DenseNet. In the comparative experiment, the pretraining mode of transfer learning was uniformly adopted to fine-tune the network architectures. As can be seen from Figure 2, the improved model based on the pretrained CNN network has the best performance. On the one hand, the loss starting point is low and the overall curve is flat; on the other hand, the model in this paper is stable when the epoch is 50. Among them, the VGG model changes greatly and may have the problem of a huge model. The loss changes of ResNet and DenseNet models are very similar, but the overall results are still not as stable as the model in this paper.

4.2.3. Model Computation. In order to further verify the quality of the model, we verified the efficiency of the model mainly through model parameters and model computation, as shown in Table 2. By comparison, it is found that it is difficult for these models to achieve a high recognition rate with less model parameters and less model computation, and the recognition rate is always proportional to the complexity and computation.

From the perspective of the number of model parameters and the amount of model calculation, the number of model parameters and the amount of model calculation of the ResNet network model are 22M and 7000M, respectively, which are lower than the number of parameters and the amount of model calculation of the model in this paper, which are more conducive to the application of embedded terminals and other platforms. However, the traditional model has the worst performance in the accuracy of the verification and training phase, and it is difficult to meet the actual needs of the industry in the accuracy of basic metal surface recognition. VGG network architecture in the verification stage, the number of parameters, and the amount of computation corresponding to the network architecture are 140M and 35000M, respectively, which is obviously not suitable for the deployment of embedded terminals.

4.2.4. Accuracy. The accuracy rate directly reflects the quality of the model and determines whether the model can adapt to practical application, as shown in Figure 3.

As can be seen from the experimental results, the model in this paper has been ahead of other methods at the beginning of training, but unfortunately DenseNet model is significantly lower than other models. With the progress of training, ResNet and DenseNet were getting closer and closer and basically reached a flat state in 40epoch after the DenseNet surpassed them. For the variation curves of the model in this paper, VGG19 and DenseNet were very similar, reaching the peak around 50epoch and beginning to decline afterward. ResNet requires a longer training time and slower model response.

4.2.5. Other Indicators. Whether the computer algorithm can be applied to metal design needs to be considered in many ways, not only testing accuracy but also other indicators. The metal surface recognition and classification

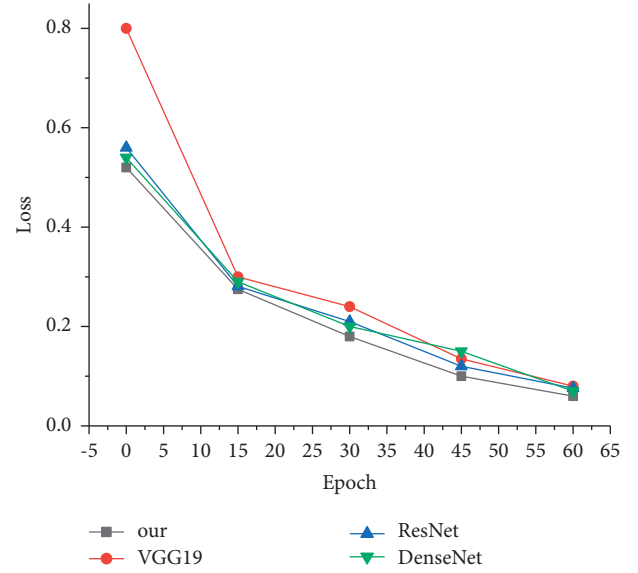


FIGURE 2: Comparative experiment of loss function change.

TABLE 2: Model parameters and calculation.

Model	Parameters	MAdd
Our	2M	600M
VGG19	140M	35000M
ResNet	22M	7000M
DenseNet	7M	5500M

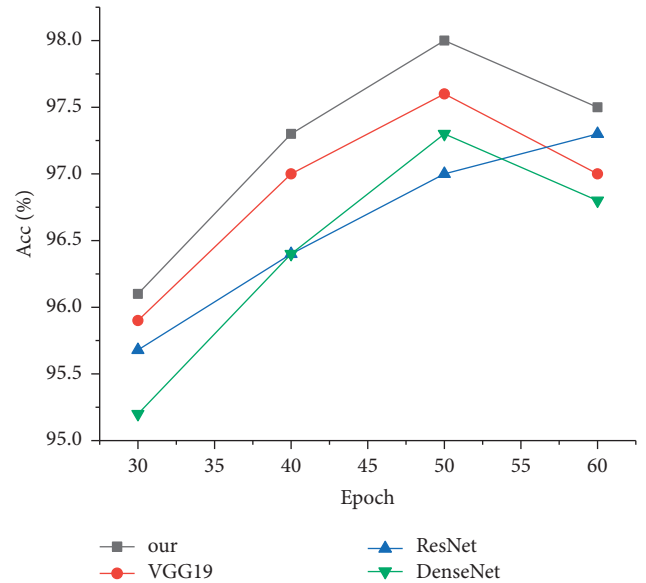


FIGURE 3: Accuracy comparison experiment.

system can correctly identify test data, or the phenomenon of the wrong classification can occur. Even if the metal surface is close to each other, its performance is still better than the metal surface detection system based on traditional methods. Due to various factors such as oxidation, scratches, and impurities in the actual production, distinguishing is also difficult to quantify, because with the passage of time,

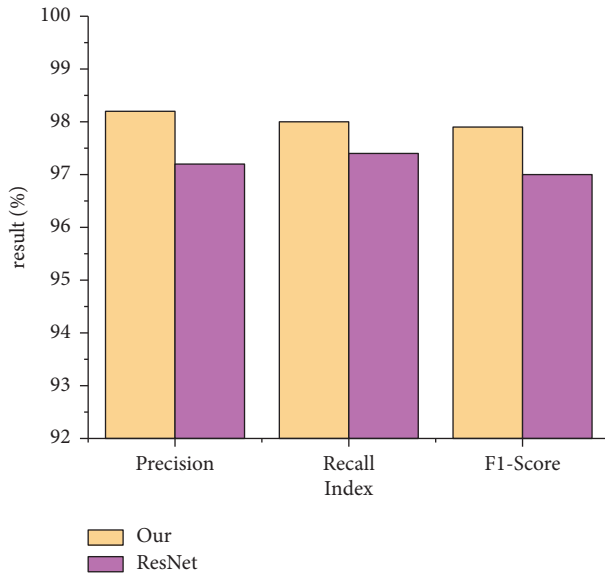


FIGURE 4: Comprehensive experimental index comparison.

the scratches are easily transformed into impurities, black points, or line even areas, leading to two defective characteristics of overlap, as shown in Figure 4 in this paper, the model of various other indexes.

5. Conclusion

Using computer vision to process design is a new means and thinking mode of computer-aided design, which provides a new possibility for modern jewelry design. Artificial intelligence technology provides a richer source of inspiration for jewelry, and jewelry also speaks for science and technology as a new medium. Jewelry designers only need to formulate and select algorithms according to the leading factors and then carry out the calculation through the computer; the results will be far beyond the designer's imagination. For modern jewelry, innovation based on traditional design methods is very important. As an auxiliary design tool, the participation of algorithm technology is positive for the design and production of modern jewelry. In this paper, it is proposed that computer vision technology can be applied to modern jewelry design, and a detailed theoretical analysis has been made to prove the necessity and feasibility and to provide new ideas and new methods for jewelry design. It extends the original thinking limitations by relying on the computer ability for data analysis and graphics generation and enriches the possibility of jewelry.

Data Availability

The experimental data used to support the findings of this study are available from the corresponding author upon request.

Conflicts of Interest

The author declares that there are no conflicts of interest to report regarding the present study.

References

- [1] B. Xia, "Construction and promotion of the added value of art design products," in *Proceedings of the International Innovation Design and Management Summit Forum and the Second World Chinese Design Academic Symposium*, Tianjin, China, December, 2011.
- [2] Li. Peng and Yi. Zhou, "The Artistic expression of metal jewelry," in *Proceedings of the 2009 China Jewelry Academic Exchange Conference*, National Jewelry and Jade Quality Supervision and Inspection Center, Beijing, China, November, 2012.
- [3] H. E. Meng, L. Hao, and S. O. Civil, "Outline of digital jewelry design and research direction," *Journal of Gems & Gemmology*, vol. 2, 2017.
- [4] S. Ramljak, "Unique by design: contemporary jewelry in the donna schneier collection," *Metropolitan Museum of Art Bulletin*, Yale University Press, London, England, 2014.
- [5] W. Zhao, "Application of Chinese traditional cloud pattern in modern jewelry design," *Journal of Gems & Gemmology*, vol. 4, 2016.
- [6] X. C. Yan and H. G. University, "The inheritance and manifestation of traditional silk craftwork in modern jewelry design," *Art and Design*, vol. 1, 2018.
- [7] J. Zhang, "Research on the application of comprehensive materials in contemporary art jewelry design," *Industrial Design*, vol. 2, no. 4, 2017.
- [8] L. Yizhong, "The development tendency and new progress of metal base composite material," *Journal of Institute of Disaster-Prevention Science and Technology*, vol. 7, 2006.
- [9] T. Wen, "Analysis on the application of folk metal craft in contemporary jewelry design teaching," *Art Education*, vol. 1, no. 11, p. 2, 2019.
- [10] H. Guo, "New exploration of metal materials in contemporary jewelry art," *Shanghai Arts and Crafts*, no. 1, p. 3, 2013.
- [11] J. Hu, "Discussion on the application of metal coloring in modern jewelry design," *Art and Design: Theory Edition*, vol. 9, no. A07, p. 3, 2012.
- [12] J. Hu, "Inspiration of modern European and American arts and crafts revolution from the arts and crafts movement to bauhaus practice in the United States," *Shanghai Arts and Crafts*, vol. 1, no. 1, p. 4, 2015.
- [13] C. Zhao, "Application of mass customization production mode in modern manufacturing industry," *Development and Innovation of Electromechanical Products*, vol. 019, no. 005, pp. 81–83, 2006.
- [14] M. Chen, *Research on the Application of Computer Technology in Jewelry Production and Processing*, China University of Geosciences, Beijing, China, 2020.
- [15] Yi. Yu, "On the application of computer technology in art design work," *Education*, vol. 000, no. 021, p. 6, 2015.
- [16] L. Qu, B. Ye, and Y. Sun, "Case study: The advantageous partnership between Black Controls and Rittal," *Manufacturing Automation*, vol. 37, no. 16, p. 3, 2015.
- [17] N. Wang, J. Zhao, and R. Mo, "Three dimensional procedure model creation methods," *Defense Manufacturing Technology*, vol. 17, no. 10, pp. 2112–2118, 2011.
- [18] Q. Virqilio, R. Louis, and P. Robert, "Will model-based definition replace engineering drawings throughout the product lifecycle. A global perspective from aerospace industry," *Computers in Industry*, vol. 61, pp. 497–508, 2010.
- [19] Z. Wu and H. Chen, "Application of MBD Digital Model for Lightweight Engineering of Complex Shell," *Science and technology innovation and application*, no. 16, p. 2, 2017.

- [20] R. Huang, S. S. Zhang, and X. L. Bai, "An effective subpart retrieval approach of 3D CAD models for manufacturing process reuse," *Computers in Industry*, vol. 67, pp. 38–53, 2014.
- [21] J. Balic, S. Klancnik, and S. Brezovnik, "Feature extraction from CAD model for milling strategy prediction," *Strojniski Vestnik-Journal of Mechanical Engineering*, vol. 54, no. 5, pp. 301–307, 2008.
- [22] L. Zhu and J. Hyyppä, "An approach of 3D model simplification of mobile phone based navigation application," *IEEE, in Proceedings of the Ubiquitous Positioning Indoor Navigation and Location Based Service (UPINLBS)*, pp. 1–4, Wuhan, China, March 2010.
- [23] Y. Wang, W. Ji, and D. Qian, "Research on 3D lightweight visualization of mechanical products in MBD mode," *Modular Machine Tool & Automatic Manufacturing Technique*, vol. 000, no. 005, pp. 107–110, 2015.
- [24] J. Huang, B. Bue, A. Pattath, D. S. Ebert, and K. M. Thomas, "Interactive illustrative rendering on mobile devices," *IEEE Computer Graphics and Applications*, vol. 27, no. 3, pp. 48–56, 2007.
- [25] G. Taubin and J. Rossignac, "Geometric compression through topological surgery," *ACM Transactions on Graphics*, vol. 17, no. 2, pp. 84–115, 1998.
- [26] A. D. Kalvin and R. H. Taylor, "Superfaces: polygonal mesh simplification with bounded error," *IEEE Computer Graphics and Applications*, vol. 16, no. 3, pp. 64–77, 1996.
- [27] H. Wan, Q. Yan, and M. Hu, "Forming process of hand-shaped metal art casting," in *Casting Technology*, p. 27, 2006.
- [28] N. Ding, "The importance of forging in metal craft specialty," *Art and Design: Theory Edition*, vol. 3, no. 4X, p. 2, 2011.

Research Article

Art Design Method of Industrial Products Based on Internet of Things Technology and Virtual VR

Yu Yu 

School of Design and Creativity, Fujian Jiangxia University, Fuzhou, Fujian 350108, China

Correspondence should be addressed to Yu Yu; hiphop1234@fjxxu.edu.cn

Received 23 April 2022; Revised 17 May 2022; Accepted 21 May 2022; Published 14 June 2022

Academic Editor: Dong Chen

Copyright © 2022 Yu Yu. This is an open access article distributed under the Creative Commons Attribution License, which permits unrestricted use, distribution, and reproduction in any medium, provided the original work is properly cited.

The Internet of Things technology transmits and shares physical information on the Internet, and describes the continuous world through scattered data. From the perspective of internal characteristics, the efficient interconnection of large-scale heterogeneous network elements is composed of the Internet of Things and imported from abroad, so there has been a high degree of accumulation in foreign countries so far. In 1980, the United States proposed a virtual reality concept called VR for short. Embedded virtual VR technology usually uses equipment to close the user's senses and temporarily isolate the user from the actual environment. This article also discusses the design of industrial products, the continuous development of big data, artificial intelligence, and additive material manufacturing technology to make the design methods and manufacturing processes of industrial products more scientific and systematic, and promote the diversity and precision of industrial product design. Social informatization plays an important role in all areas of digital technology design. Parametric design has changed the design thinking mode of designers and formed new design trends and styles. Taking the search for relationships and rules as the starting point of the design and the algorithm as the core content of the design are very different from traditional design ideas. The computer age has not only cultivated new styles but also cultivated new artistic design techniques for industrial products. Designers should strive to explore the potential functions of algorithm technology and focus on smarter and more logical design and production processes. In this paper, through the research of the Internet of Things technology and virtual VR, it is applied to the research of the artistic design method of industrial products, aiming to promote its better development.

1. Introduction

Beginning in 1999, the Massachusetts Institute of Technology in the United States began to study the Internet of Things in the laboratory. In 2005, the International Telecommunication Union officially defined the concept of the Internet of Things. The goal of information and communication technology has evolved from people-to-people exchanges to connections and mutual exchanges between people and things, and between things and things [1]. The Internet era of Internet of Things technology with all things interconnected is about to begin [2]. In addition, we also studied virtual reality technology. Virtual reality technology is a computer simulation system that can create and experience a virtual world [3]. By using a computer to generate

a simulation environment, users can have a sense of immersion in the environment [4]. Virtual VR technology combines virtual VR technology with various output devices through the use of data used in real life and electronic signals generated by computer technology to transform it into a phenomenon that people can feel [5, 6]. These phenomena are objects in reality, or matter that we cannot see, and they are displayed in front of us by three-dimensional models [7]. Because we cannot directly see these phenomena through the naked eye, but need to simulate the real world by computer technology, it is also called virtual reality [8]. This article also discusses the work on industrial products and their design. At the beginning of the industrial revolution, the esthetic issues of industrial products attracted the attention of many scholars and companies. Social practice has

proved that esthetic value is an indispensable part of successful products [9]. After the twenty-first century, esthetic culture has become more and more prevalent, especially the development of culture and creative industries, which comprehensively promotes the continuous development of the state of esthetic values [10]. Today, under the guidance of the national innovation strategy, various industries are innovating product design and supply-side reform through more digital, networked, and intelligent technologies [11]. Under the new circumstances, the esthetic value of the product has undergone major changes in both its connotation and extension [12]. The esthetic value of a product is not only an incidental value but also a spokesperson for product quality. With the continuous development of science and technology and social economy, social material production has become more and more abundant [13]. The concept of product design and production has shifted from centering on “manufacturing as the direction, product as the center” to “market as the direction and user as the center” trend. The consumer’s concept of consumption has shifted from focusing on basic performance to focusing on esthetic characteristics and experience [14]. Most consumers evaluate and choose most products from an esthetic point of view, and consumers’ esthetics and judgment have been double-improved [15]. In this context, the combination of the innovation of art design and the esthetic economy has become the most important productive force for social development [16].

2. Related Work

The literature introduces the origin and development of the Internet of Things, introduces the inevitability of the meaning of the Internet of Things, and then focuses on the hierarchical service model of the Internet of Things ontology, and introduces in detail the architecture of the intermediate links of the Internet of Things based on the ontology [17]. The literature puts forward the problems of IoT service discovery, analyzes the service discovery process based on its meaning, and discusses the semantic orientation, classification, and matching calculation methods of IoT service discovery [19]. The literature shows that taking the wiring shell as an example, the process structure of the part is analyzed. Based on the mold flow analysis, the best molding process parameters of the part are determined through experiments, combined with the structural characteristics and parameter analysis, and calculation and inspection are used for the molding of plastic parts [20]. The key components of the inlaid side core injection model have been designed and gradually calculated and corrected for its pouring system, molded part mechanism and cooling mechanism, side core mechanism, ejection system, and other related structures, completing the finite element correction of cavity load finally; the working principle of the mold and the simulation of the mold opening and closing movement process were completed; and the overall design of the wiring shell mold structure was realized [21, 22]. The literature introduces the architecture and mode of the intermediate links of the Internet of Things,

and discusses the reasoning based on the formalization of rules and ontology knowledge, and finally proposes a dynamic service mode based on the context of the ontology [23]. The literature shows that for molds with complex structures and high assembly accuracy requirements, the method of establishing physical prototypes is used in design assembly engineering. The design requires repeated assembly and changes, and the modification process needs to rely on the physical model. Through virtual assembly technology, a VR intelligent system for mold assembly that combines VR equipment and data gloves is developed. A virtual prototype of a complex structure and high-precision design mold is constructed in a virtual space, and it is applied to physical drag-and-drop assembly [24]. The designer himself can perform perceptual identification verification on the rationality and standardization of the product design, the possibility and difficulty of assembly, and other factors [25].

3. Internet of Things and Virtual VR Technology

3.1. Internet of Things. In this article, we have studied and analyzed the significance of the IoT architecture model, and proposed a semantic-based IoT service system model to realize the regional positioning of the IoT. Considering the diversity of IoT devices, this model integrates the IoT divided into physical space, information space, user needs, and service resources; IoT service resources are reflected in the actual physical space through the operation of the information space; and changes in the physical space are transmitted to the information space, affecting users and IoT services. The interaction model of user needs, service resources, physical space, and information space on the Internet of Things is shown in Figure 1.

3.2. Virtual VR Technology. Sphere form: the sphere is the most effective and flexible 3D model. It is defined as the smallest volume sphere that can wrap an object. On the surface of the center and radius of the sphere, we measure the distance between all the end points of the part to find the maximum value, that is, the radius of the sphere. The half point of this line is the center of the sphere.

$$R = \left\{ (x, y, z) | (x - O_x)^2 + (y - O_y)^2 + (z - O_z)^2 < r^2 \right\}. \quad (1)$$

The formula of ball center is as follows:

$$\begin{aligned} O_x &= \frac{1}{2} (x_{\max} + x_{\min}), \\ O_y &= \frac{1}{2} (y_{\max} + y_{\min}), \\ O_z &= \frac{1}{2} (z_{\max} + z_{\min}). \end{aligned} \quad (2)$$

The formula of ball radius is as follows:

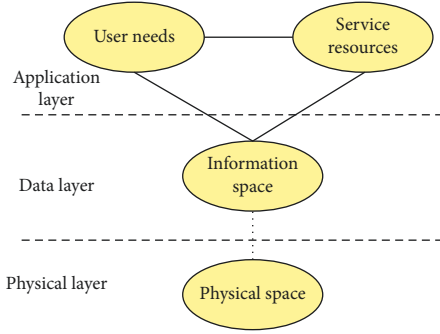


FIGURE 1: Information interaction model of the internet of things.

$$r = \frac{1}{2} \sqrt{(x_{\max} - x_{\min})^2 + (y_{\max} - y_{\min})^2 + (z_{\max} - z_{\min})^2}. \quad (3)$$

The detection of the intersection of the spheres is relatively simple, and only the relationship between the center distance and the radii of the two outer spheres needs to be determined. If the formula is valid, the overlap of the balls will cause collision detection.

$$|c_1 c_2| < (r_1 + r_2). \quad (4)$$

The AABB bounding box along the coordinate axis is the most commonly used detection method in the research of collision detection algorithms. Since the AABB bounding box is composed of the smallest hexahedron whose edges are parallel to the coordinate axis, only six scalars are needed to construct the AABB bounding box. The formula for the radius of the center position is as follows:

$$R = \left\{ (x, y, z) \mid |x_c - x| \leq r_x, |y_c - y| \leq r_y, |z_c - z| \leq r_z \right\}. \quad (5)$$

The formula of the ball center is as follows:

$$\begin{aligned} x_c &= \frac{1}{2} (x_{\max} + x_{\min}), \\ y_c &= \frac{1}{2} (y_{\max} + y_{\min}), \\ z_c &= \frac{1}{2} (z_{\max} + z_{\min}). \end{aligned} \quad (6)$$

The formula of ball radius is as follows:

$$r_x = x_c + \frac{1}{2} x_{\min}, r_y = y_c + \frac{1}{2} y_{\min}, r_z = z_c + \frac{1}{2} z_{\min}. \quad (7)$$

The OBB bounding box is also called the direction bounding box. However, collision detection calculations are relatively complicated, and OBB has good agility. It can make real entities better to create and help to better complete collision detection. The formula for the direction bounding box area is as follows:

$$R = \{O + ar_1 v_1 + ar_2 v_2 + ar_3 v_3 \mid a, b, c \in (-1, 1)\}. \quad (8)$$

Here, O represents the center of the OBB, and v_1, v_2 , and v_3 can determine the vector target whose direction bounding box positively intersects with the absolute coordinates.

$$a_{XY} = \frac{1}{3(n-1)} \sum_{i=1}^n (M_x^i - U_x)(M_Y^i - U_Y),$$

$$C_{3 \times 3} = (a_{mn})m, \quad n \in \{X, Y, Z\}, \quad (9)$$

$$U = \frac{1}{3n} \sum_{i=1}^n (M^i + N^i + K^i).$$

Through actual verification, by increasing the cross-sectional area of the gating system, the warping deformation of the plastic parts can be reduced from 0.373 to 0.370, the effect is not obvious, and there is no need to increase the cross-sectional area of the gating system. Therefore, the three performance parameters that have a great influence on warpage as shown in Table 1 are designed as variables for the MJ1504 wiring housing for process optimization.

In this experiment, the optimization method shown in Table 2 is used as the conditional boundary of the wiring housing, the melting temperature, and the cooling material index are used as variables, and the cooling time and warpage deformation are used as the quality benchmark. The purpose is to reduce the cooling time and improve the production efficiency of the product by adjusting the target variable while ensuring the slight warpage of the plastic part.

As shown in Figure 2, under certain cooling water temperature conditions, as the melting temperature increases, the cooling time of plastic parts increases significantly; at the same melting temperature, the cooling time can be greatly shortened by reducing the cooling water temperature. Therefore, in order to shorten the cooling time of plastic parts, it is mainly to reduce the molding temperature and the inlet temperature of the cooling material, and to strengthen the cooling.

By comparing the deformation of the plastic part in the x , y , and z directions, it is found that the deformation of the plastic part is mainly in the x direction. It is found from the response surface that the melting temperature has the greatest influence on the uneven shrinkage and deformation of plastic parts. On the premise that there is no change in other molding conditions, by increasing the melting temperature, uneven shrinkage and deformation can be reduced, and at the same time, by reducing the temperature of the cooling material, the deformation of the plastic part can be greatly reduced, as shown in Figure 3.

The warpage deformation response surface is shown in Figure 4.

The casting mold is subjected to various pressures during casting. If the strength of the cavity is not enough, the plastic parts will be deformed or cracked. When the rigidity is insufficient, under the action of elastic deformation, the joint surface of the mold is deformed, and cracks caused by flash burrs. After the forming pressure disappears, the mold elastically recovers, causing serious shrinkage, which affects the quality of the plastic parts and destroys the plastic parts. Therefore, the mold design must meet the requirements of strength and rigidity.

TABLE 1: Process plan comparison.

Performance parameter	Original plan	Scheme 1	Scheme 2	Scheme 3
Melting temperature (°C)	240	240	240	210
Mold temperature (°C)	90	90	90	90
Injection time (s)	4	4	4	4
Injection + holding pressure + cooling time (s)	48	48	48	42
Maximum holding pressure (MPa)	80	100	100	80
Holding time (s)	20	20	25	20
Warpage (mm)	0.373	0.209	0.199	0.405
Sink mark (mm)	0.186	0.077	0.078	0.176
Scheme variables	—	Increase the holding pressure	Pressurize, extend the holding time	Reduce melt and mold temperature

TABLE 2: DOE optimization process plan.

—	Scheme 1	DOE optimization 1	DOE optimization 2
Melt temperature (°C)	240	210	210
Mold temperature (°C)	90	60	60
Coolant inlet temperature (°C)	30	30	20
Maximum holding pressure (MPa)	100	80	100
Holding time (s)	25	20	20
Injection + holding pressure + cooling time (s)	48	39	31
Deformation (mm)	0.209	0.405	0.231
Sink mark (mm)	0.077	0.176	0.129
Scheme variables	—	Melt temperature	Melt, coolant and mold temperature

Cooling time [cooling][DOE]: response surface graph
X: Melt temperature
Y: Coolant inlet properties (default): Coolant inlet temperature

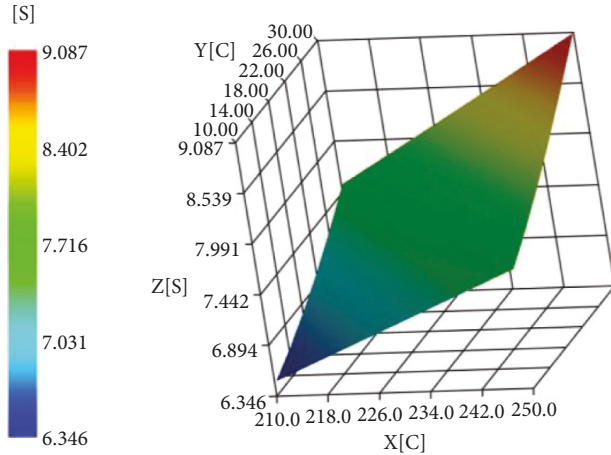


FIGURE 2: Cooling time response surface.

Deformation, all due to the case: X direction [DOE] : response surface
X: Melt temperature
Y: Coolant inlet properties (default): Coolant inlet temperature

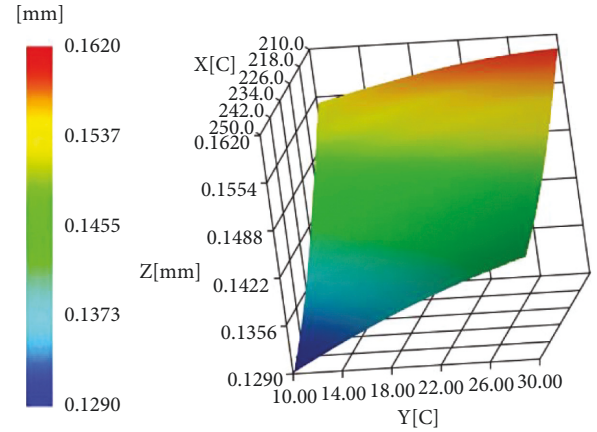


FIGURE 3: Warping deformation response surface in X direction.

We calculate the thickness of the mold cavity wall according to the formula:

$$S_c = \sqrt[3]{\frac{cpa^4}{E\delta}}. \quad (10)$$

We determine the thickness of the cavity bottom plate according to the formula:

$$S_h = \sqrt[3]{\frac{cpb^4}{E\delta}}. \quad (11)$$

The thickness of the dynamic mold support plate directly affects the strength and rigidity of the cavity bottom plate. It is necessary to calculate the force of the dynamic mold support plate and design its thickness. We calculate the thickness of the support plate according to the formula:

Deformation, all factors: Deformation [DOE]: Response surface plot
 X: Melt temperature
 Y: Coolant inlet properties (default): Coolant inlet temperature

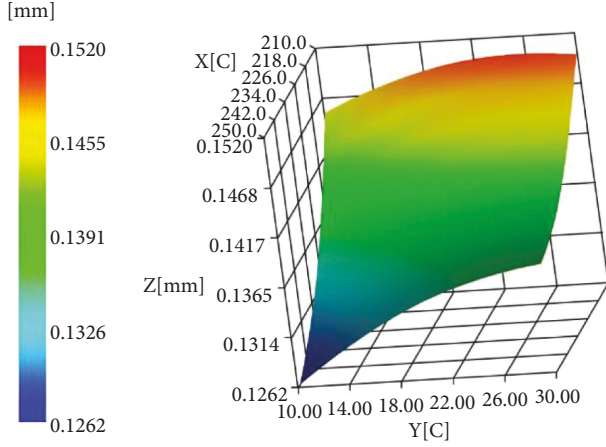


FIGURE 4: Warpage response surface of all factors.

$$h = K \sqrt{\frac{FL}{2B[\sigma]}} = K \sqrt{\frac{ApL}{2B[\sigma]}}$$

$$= 0.75 \times \sqrt{\frac{45 \times 18557 \times 294}{2 \times 450 \times 200}} = 38\text{mm}. \quad (12)$$

$$h = K \sqrt{\frac{FL}{2B[\sigma]}} = K \sqrt{\frac{ApL}{2B[\sigma]}}$$

We calculate the tensile force of the core-pulling mechanism according to the formula:

$$Q = \ln p_2 (f_2 \cos \theta - \sin \theta). \quad (13)$$

For safety reasons, the pulling-out distance of the side core is usually greater than the depth of the undercut structure, so that the core-pulling mechanism can completely pull out the undercut structure. We calculate the core-pulling distance according to the formula:

$$S = H + (2 \sim 3). \quad (14)$$

In the core-pulling process, the tensile force and the inclination angle of the inclined guide column directly affect the bending force. The bending force is calculated according to the formula as follows:

$$P = \frac{Q}{\cos \alpha}. \quad (15)$$

We calculate the diameter of the inclined guide column according to the formula:

$$d = \sqrt[3]{\frac{PH}{0.1 \cos \alpha [\sigma]}}. \quad (16)$$

We calculate the total length of the inclined guide column according to the formula:

TABLE 3: Marked dimensions and dimensional tolerances of plastic parts.

Plastic part dimensioning (mm)	Plastic part size tolerance (mm) (tolerance size is 3 precision)
Dimensions	
43.5	43.5 ⁰ _{-0.33}
33.4	33.4 ⁰ _{-0.29}
10.2	10.20 ⁰ _{-0.17}
7	7 ⁰ _{-0.15}
5.7	5.7 ⁰ _{-0.13}
30.1	30.1 ⁰ _{-0.29}
1.7	1.7 ⁰ _{-0.11}
Internal size	
10	10 ⁰ _{+0.17}
5	5 ⁰ _{+0.13}
3.3	3.3 ⁰ _{+0.13}
6.7	6.7 ⁰ _{+0.15}
1.5	1.5 ⁰ _{+0.11}
9.1	9.1 ⁰ _{+0.15}
11.7	11.7 ⁰ _{+0.17}
15.1	15.1 ⁰ _{+0.19}

$$L = \frac{h}{\cos \alpha^\circ} + \frac{S}{\sin \alpha^\circ} + \frac{1}{2} D \tan \alpha^\circ + (5 \sim 10). \quad (17)$$

The melting temperature of plastic casting is about 230°C, and the temperature of the plastic part that reaches the peak condition is about 88°C. A lot of heat is released during the molding process. In order to reduce the temperature of plastic parts and molds, the natural cooling effect is poor and the time is long, so in order to speed up the cooling rate, a cooling system needs to be set.

We calculate the volume flow of heat and cooling water according to the formula:

$$q_v = \frac{WQ_1}{\rho c_1 (\theta_1 - \theta_2)}, \quad (18)$$

$$Q_1 = c_2 (\theta_3 - \theta_4) + h.$$

The terminal housing is a thin-walled section with a rectangular cross section. We calculate the lock tension according to the formula:

$$F = \frac{8\delta_2 E S l \cos \varphi (f - \tan \varphi)}{(1 - \mu) k_2} + 0.1 A. \quad (19)$$

We calculate the diameter of the push rod according to the formula:

$$d = \psi \left(\frac{L^2 F}{n E} \right)^{1/4}. \quad (20)$$

We check the strength of the putter. The material of the push rod is T8a, and the allowable stress is 120 MPa. We use 20 push rods on a plastic part according to the formula:

$$\sigma_c = \frac{4F}{n\pi d^2} \leq [\sigma]. \quad (21)$$

The marked dimensions and dimensional tolerances of plastic parts are shown in Table 3.

The radial dimensions of the cavity and core are shown in Table 4.

The maximum and minimum displacement nodes of the cavity in the x , y , and z directions are represented by cloud diagrams. As shown in Table 5, the maximum displacement of the cavity node is 0.007 mm, and the deformation is very small.

4. Industrial Product Art Design Method and Application Research

4.1. Parametric Design of Industrial Products. Parametric is a term widely used in various fields from mathematics to design. Specifically, it refers to the calculation of a pre-determined value. Parametric design mainly refers to the way of design thinking, rather than using some software or some modeling techniques. It is based on mechanical design, and industrial designers draw on its thinking mode. The conventional design method is implemented in stages. If the plan is changed, it needs to be redesigned from scratch. Parametric design reveals many factors that affect the design form, describes the inherent logical relationship of computer language, and constructs a parametric model on a digital platform. In parametric design, parameters reflect the logical relationship between design elements. Changes to any one component will affect its related components. The relationship between components is dynamic and changes with the change of design conditions, as shown in Figure 5.

With the advancement of digital technology, it provides a source of power for design conversion, and the design software is always upgraded with the advancement of hardware technology. Software developers include many functional functions and logical rules. Designers can quickly create logical relationships between variables as needed and generate necessary design results by controlling predefined rules. The use of parametric design software leads to the uncertainty and complexity of the design, and simulates the complex natural phenomena in the evolution of logic. Based on the visual programming platform of industrial aided design, the complete model generation logic is constructed through a series of modular calculation units, which are usually used for the visual performance of animation. The main modeling method is polygon modeling, when it is used for parameter design at the same time, it must use the basic programming language. A certain mathematical calculation software is usually used for complex mathematics and engineering problems. The programming language used for parameter design has strong expansion capabilities, but it is difficult for general designers to master it.

4.2. Parametric Design Elements. Points and vectors are the basic elements of three-dimensional space and the basis of parameter design. In geometry, a point represents a position in space. A vector is an abstract element with a direction and length, and has no fixed position. Vectors and points are represented by (x, y, z) , but they are different. Vector calculations are often used in parameter design, as shown in Figure 6.

There are three ways to form the surface of the polygonal mesh through the parametric design method. In the first type, the mesh surface is generated by topology, and the vertices determine the topology of the mesh surface. A mesh surface can be generated from multiple points by components, but manual point distribution is very troublesome. Usually, the vertices and components of the existing model are combined and extracted to generate a new mesh surface. The second is to generate a mesh surface through the triangular surface algorithm. This algorithm can maximize the internal angle of the generated triangles, thereby uniformly generating a reasonable triangle mesh surface to prevent the surface of the triangle from becoming smaller.

Most of the research on curves and surfaces is about how to generate curves and surfaces. In the parameter control generation method, it is very important to study the analysis method of curve and surface. Parameter design can repeatedly adjust the shape of the curve according to the operating curve data and continuously optimize the function parameters and shape parameters to meet the design requirements. This is a new curve design method. The Nurbs curve is the basis for the construction of the shape and is a derivative of the previous Bezier curve. The algorithm of the Nurbs curve is more complicated than the Bezier curve, but the control is also easier. Only one parameter T of the curve is one-dimensional, and the two-dimensional surface has two parameters U and V , respectively. The curve is divided into positive and negative directions, and its surface is equivalent to the vertical direction W . Compared with the curvature of the curve, the curvature of the curved surface is not intuitive. The curvature of the point P on the curved surface refers to the deviation from the tangent plane of the point P . We use the point P to make several sections and calculate the point P at the intersection of the section and the surface. Because countless sections passing through point P can be made, there are countless curvatures K , the highest curvature is $K1$, and the lowest curvature is $K2$. Gaussian curvature and minimum curvature are two important surface theories. The Gaussian curvature formula is $g = k1 * k2$. When the Gaussian curvature is greater than 0, the surface is convex, and when the Gaussian curvature is less than 0, the surface is concave.

4.3. Data Structure and Processing. Data collection is the preliminary work of parameter design. Through investigation, all design requirements are digitized to form parametric variables. The starting point of the design is to meet the design requirements of human actions. The data of this information can change the design requirements into parameters that can be recognized by the computer, which is the basis for parameter generation. Data structure is the core of parameter design and the form of parameter storage. The deeper the design logic, the more complex the data structure. Different platforms have different data structure processing methods. In parametric modeling software, tree data is the core concept of platform data operation. This data structure includes multiple parallel data list groups, which can separately process any data in the group. Linear data is the

TABLE 4: Radial and axial dimensions of cavity and core.

Plastic part size (mm)	Calculation formula	Core or cavity working size (mm)
Radial size of cavity	$A_M + {}^{\xi z} = \{(1 + S)A_S - X\Delta\} + {}^{\xi z}$	$43.5_0^{+0.34}$
		$33.4_0^{+0.30}$
		$10.2_0^{+0.18}$
		$5.7_0^{+0.14}$
		$30.1_0^{+0.30}$
		$1.7_0^{+0.12}$
Radial size of core	$B_M - {}^{\xi z} = \{(1 + s)AS + X\Delta\} - {}^{\xi z}$	$11.7_0^{+0.18}$
		$5_0^{+0.14}$
		$6.7_0^{+0.16}$
		$1.5_0^{+0.12}$
		$9.10_0^{+0.16}$
Radial size of cavity	$H_M + {}^{\xi z} = \{(1 + s)H_S - 2/3\Delta\} + {}^{\xi z}$	$7_0^{+0.12}$
		$2.4_0^{+0.14}$
Axial dimension of cavity	$h_M - {}^{\xi z} = \{(1 + s)h_S + 2/3\Delta\} - {}^{\xi z}$	$11.7_0^{+0.18}$
		$15.1_0^{+0.20}$
		$15.31_0^{+0.07}$

TABLE 5: Maximum and minimum node displacement table.

Direction	Max displacement (mm)	Minimum displacement (mm)
x	0.003	-0.002
y	0.007	-0.005
z	0.007	-0.002

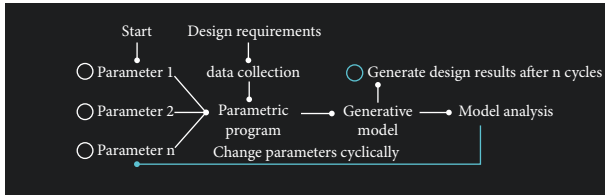


FIGURE 5: Flowchart of parametric design.

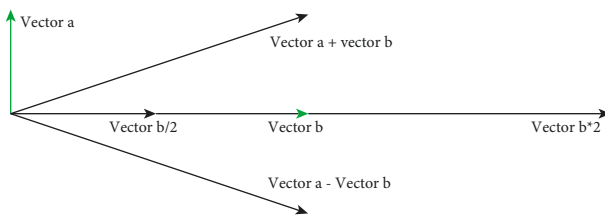


FIGURE 6: Illustration of basic vector operations.

simplest data structure; that is, sequence groups are sorted and placed in lists and then divided into long lists, short lists, and crossover operations. The long list is the default algorithm of Grasshopper. Tree data is similar to nested lists and consists of multiple parallel data lists. The arithmetic processing of tree data is actually to process linear data list operations of multiple lists in order. The two core algorithms of the overall data structure are the long list algorithm and the sequence correspondence operation. Two ordinary data must be correspondingly operated one by one. If the tree data corresponds to the normal data, all the normal data is used to calculate each group of the tree data, and the tree data is calculated correspondingly within the group.

4.4. Art Design Path of Industrial Products. Positioning refers to the company's unique value positioning in the minds of target customers by designing its own product image. Positioning is not to focus on the target of the product object but what the target consumer wants to do. By speculating on the consumer's psychological needs, how to emphasize the consumer's product differentiation in a limited psychological space is the criterion for judgment. The esthetic value of the product is an important overall plan and strategy formulated by the company to pursue and maintain a lasting competitive advantage as the basic point of the company's future. The overall strategy is divided into three levels: overall, business units, and functions. According to the different levels of corporate strategy and the state of corporate design innovation, the design strategy can be divided into three levels: overall design, competitive design, and functional design. What kind of design innovation strategy an enterprise adopts and how to execute the strategy must be determined by analyzing the opportunities and threats of the external environment, and the advantages and disadvantages of internal capabilities according to the company's development goals.

The development of an enterprise is inseparable from strategic guidance. Different environments and their own conditions determine that companies need to adopt different strategies to maintain long-term development. As a design strategy, the design innovation of product esthetic value requires different choices under different circumstances.

A stable strategy means that the company maintains the same development model and development goals as in the past, and the commercial scope of products and services is basically unchanged. When industrial technological innovation is at a mature stage, when consumer preference goals and intra-industry competition tend to stabilize, companies generally adopt this strategy. Under the stable strategy, the focus of design innovation is to maintain the combination and design direction of the original product design, and change the design style and form. The esthetic value of a product is to maintain the original brand image of the product, and to meet the basic esthetic needs of consumers is to change the design form.

Expansion strategy means that companies continue to increase their business and scope and increase their market share. Development is the instinct for survival, and most companies will go through this strategic period. Under the guidance of this strategy, companies generally achieve expansion goals through horizontal integration, vertical integration, and various developments. Under the expansion strategy, the design innovation of the company is very active, the product design is diversified, and the design organization is flexible and diverse. Designing a good product is favored by more markets and consumers. Understanding the corporate brand image is the core of corporate design innovation in this period. Therefore, the esthetic value of products plays an important role in design innovation. At this point, product esthetic value design innovation activities should be very active. It requires breakthrough innovations in different consumer target markets from multiple levels, and esthetic value design innovation from multiple levels.

The shrinking strategy means that the company retreats or shrinks from the existing business area, concentrates resources to respond to environmental changes, and maintains the company's survival. The shrinkage strategy is a negative strategy, generally a short-term strategy adopted during the period when the external environment is strongly impacted or when the enterprise is facing a downturn. The contraction strategy can be divided into active contraction and passive contraction. Under the active contraction strategy, product esthetic value design innovation must find the right position, emphasize the characteristics of the product, and increase the value of the product to consumers. Under the passive strategy, product esthetic value design innovation needs to reduce the enterprise's resource investment and maintain product image by integrating micro- and external resources. Due to the functionality of the main product, in some cases, companies can abandon the design innovation of the esthetic value of the product.

The competitive analysis framework crosses the boundaries of industries, specific technologies, or management methods. The emergence of the Internet has changed the barriers to industrial participation, redefined the power of buyers, and promoted the emergence of new alternative models. On the other hand, the basic driving force of industrial competition remains unchanged.

The cost leadership strategy means that the company reduces operating costs and product costs as much as possible, and takes low prices, small profits, and high profits as its overall goals. In order to achieve the total cost, it is necessary to comprehensively manage the human, material, and financial resources of the enterprise, and formulate a series of control and optimization plans in the process of product research, trial production, production, and sales. Reduce experience costs and indirect costs, and achieve efficient production. Total cost leadership is a cost management strategy, and the ultimate goal is to achieve the largest sales of products on the market. In order to curb costs, if product quality is reduced, the importance of cost leadership will be lost. The design innovation of product esthetic value can not only directly reduce the cost of products but also indirectly reduce the relative cost of products. In the context of the declining natural resources of

the era, it provides us with a powerful set of tools to survive and develop. Minimalist style is the world's mainstream esthetic style. It is not only an economic method to achieve low prices and high value, but also a method to promote environmental protection by reducing materials and unnecessary functions. The minimalist style reduces manufacturing costs such as the complexity of manufacturing raw materials, production procedures, and production processes by modeling simplified design, modulus design, and standardized design of constituent elements. Although the total product cost will rise with the design innovation, the esthetic value of the product increases the overall value of the product, so the design innovation of the product esthetic value is valuable. Through the strategy of leading total cost, a domestic mobile phone brand continues to innovate product designs, quickly occupy the market, and quickly grow into one of China's top mobile Internet technology companies to achieve high cost performance.

Differentiation strategy refers to the difference between an enterprise and a competing company in terms of brand positioning, product style, and operation mode. Due to the development of the times, the differentiation strategy of enterprises has experienced three development stages: product differentiation, image differentiation, and operation mode differentiation. Samsung Electronics is the largest electronics industry in South Korea. In terms of differentiation strategy, it mainly conducts product differentiation management through independent research and development, including breaking three-dimensional thinking, vertical integration, and strong cooperation. Not the same, improving the supply chain and circulation. Generally speaking, companies can use four methods to reflect product differentiation. First, high quality means that the product is more durable, safer, and more stable than other companies. A well-known mobile phone brand has excellent quality, stable signal, and good quality characteristics; the second is beautiful design, which is more reasonable and more beautiful than other companies' products. A well-known brand attaches great importance to product design, emphasizing the grade, and quality of the product; third, higher cost performance, that is, the ratio of the product function perceived by consumers to the quality of the purchase price is very high. The low price strategy is a common method to achieve high cost performance, but the high performance of the product does not necessarily depend on low prices. Fourth, new concepts, that is, products bring new cultural experiences and new lifestyles. This approach often brings breakthrough innovation, which is the combined effect of technology, design, and culture. The differentiation of the design innovation of the esthetic value of the product means that the difference between the products of the enterprise and the competing companies needs to be realized through one or more methods such as difference in perception, difference in function experience, or difference in image. Through the differentiated design of products, companies can not only avoid direct competition with competitors but also enrich product categories and provide consumers with more choices.

5. Conclusion

At present, molds with complex structures and assembly precision need to adopt the method of establishing physical prototypes to design the assembly process. Therefore, it is necessary to repeatedly assemble and change the design, and rely on the physical model in the change process. Through virtual assembly technology, a mold assembly virtual VR system that combines VR equipment and data gloves is developed. A virtual prototype of a complex structure and high-precision design mold is constructed in a virtual space, and it is applied to physical drag-and-drop assembly to allow design. The author can conduct verifiable research on the rationality and standardization of product design, the possibility and difficulty of assembly, and other factors. The esthetic value of a product is based on a specific historical and cultural background, taking material as a carrier, through design innovation or cultural accumulation, so that the artistic design of the product can meet people's esthetic needs, and bring people the intangible value of esthetic pleasure and spiritual enjoyment. The esthetic value of the product has the basic characteristics of esthetic entertainment, value dependence, rapid observation, diverse forms, and dynamic changes. Material factors, technical factors, and spiritual factors are the three major bearing factors of product esthetic value, from the macro social environment to the research and development of related enterprises, production, and sales, and microconsumption behavior will affect the esthetic value of the product.

Data Availability

The data set can be accessed upon request.

Conflicts of Interest

The author declared that there are no conflicts of interest.

References

- [1] M. Abu-Lebdeh, F. Belqasmi, and R. Glitho, "An architecture for QoS-enabled mobile video surveillance applications in a 4G EPC and M2M environment," *IEEE Access*, vol. 4, pp. 4082–4093, 2016.
- [2] I. F. Akyildiz, T. Melodia, and K. R. Chowdhury, "A survey on wireless multimedia sensor networks," *Computer Networks*, vol. 51, no. 4, pp. 921–960, 2007.
- [3] M. M. Alam and E. Ben Hamida, "Strategies for optimal mac parameters tuning in IEEE 802.15.6 wearable wireless sensor networks," *Journal of Medical Systems*, vol. 39, no. 9, p. 106, 2015.
- [4] A. B. Ammar, O. Bouattay, A. Dziri, M. Terre, and H. Youssef, "Performance Analysis of AODV and AOMDV over SMAC and IEEE 802.15.4 in wireless multimedia sensor network," in *Proceedings of the Wireless Communications and Mobile Computing Conference (IWCMC)—IEEE*, Dubrovnik, Croatia, August, 2015, <https://doi.org/10.1109/IWCMC.2015.7289298>.
- [5] L. Li, B. Lei, and C. Mao, "Digital twin in smart manufacturing," *Journal of Industrial Information Integration*, vol. 26, no. 9, Article ID 100289, 2022.
- [6] L. Li, T. Qu, Y. Liu et al., "Sustainability assessment of intelligent manufacturing supported by digital twin," *IEEE Access*, vol. 8, Article ID 174988, 2020.
- [7] N. N. Y. Chu and W. Luptow, "CE standards of interest: wearables and wireless TV [standards]," *IEEE Consumer Electronics Magazine*, vol. 6, no. 2, pp. 114–117, 2017.
- [8] S. Deshpande, "Adaptive low-bitrate streaming over IEEE 802.15.4 low rate wireless personal area networks (LR-WPAN) based on link quality indication," in *Proceedings of the 2006 international conference on Communications and mobile computing - IWCMC '06*, July, 2006.
- [9] A. Farhad, Y. Zia, and F. Bashir Hussain, "Survey of dynamic super-frame adjustment schemes in beacon-enabled IEEE 802.15.4 networks: AN application's perspective," *Wireless Personal Communications*, vol. 91, no. 1, 2016, <https://link.springer.com/article/10.1007/s11277-016-3448-9>.
- [10] A.-J. Garcia-Sanchez, F. Losilla, D. Rodenas-Herraz, F. Cruz-Martinez, and F. Garcia-Sanchez, "On the feasibility of wireless multimedia sensor networks over IEEE 802.15.5 mesh topologies," *Sensors*, vol. 16, no. 5, pp. 643–669, 2016.
- [11] L. Li and C. Mao, "Big data supported PSS evaluation decision in service-oriented manufacturing," *IEEE Access*, vol. 8, no. 99, Article ID 154663, 2020.
- [12] L. Li, C. Mao, H. Sun, Y. Yuan, and B. Lei, "Digital twin driven green performance evaluation methodology of intelligent manufacturing: hybrid model based on fuzzy rough-sets AHP, multistage weight synthesis, and PROMETHEE II," *Complexity*, vol. 2020, no. 6, 24 pages, Article ID 3853925, 2020.
- [13] N. M. Khoi, S. Saguna, K. Mitra, and C. A'hlund, "IREHMO: an efficient IOT-based remote health monitoring system for smart regions," in *Proceedings of the International Conference on E-Health Networking, Application & Services (Health-Com)—IEEE*, Boston, MA, USA, October, 2015.
- [14] P. Krawiec, M. Sosnowski, J. Mongay Batalla, C. X. Mavromoustakis, and G. Mastorakis, "DASCo: dynamic adaptive streaming over CoAP," *Multimedia Tools and Applications*, vol. 77, no. 4, pp. 4641–4660, 2018.
- [15] A. Liekens, "Universal LoRa (WAN) gateway limitations, because physics?," 2016, <https://www.thethingsnetwork.org/forum/t/universal-lora-wan-gateway-limitations-because-physics/1749>.
- [16] R. Minerva, A. Biru, D. Rotondi, and D. W. Engels, "Towards a definition of the internet of things (IoT)," *IEEE, iot.ieee.org*, vol. 2015, 2015.
- [17] J. Pedro Martinez, E. Torroglosa Garcia, J. Ortiz Murillo, and A. F. Skarmeta, "Evaluating video streaming in network architectures for the internet of things," in *Proceedings of the Innovative mobile and Internet Services in Ubiquitous Computing*, IEEE, Taichung, Taiwan, July, 2013.
- [18] R. Pereira and E. Pereira, "Video streaming: H.264 and the internet of things," in *Proceedings of the IEEE International Conference on Advanced Information Networking and Applications Workshops*, Gwangju, Korea (South), March, 2015.
- [19] J. E. Pezora, "Optimizing mission allocation in wireless sensor networks under geographically correlated failures," in *Proceedings of the ACM SenSys*, pp. 57–63, November, 2013, <https://doi.org/10.1145/2517351.2517435>.
- [20] S. A. Alvi, B. Afzal, G. A. Shah, L. Atzori, and W. Mahmood, "Internet of multimedia things: vision and challenges," *Ad Hoc Networks*, vol. 33, pp. 87–111, 2015.
- [21] M. Taneja, "A framework to support real-time applications over IEEE802.15.4 DSME," in *Proceedings of the IEEE Tenth International Conference on Intelligent Sensors, Sensor*

- Networks and Information Processing (ISSNIP)*, Singapore, April, 2015.
- [22] G. Tanganelli, C. Vallati, and E. Mingozzi, "Ensuring quality of service in the internet of things," in *New Advances in the Internet of Things*, R. R. Yager and J. P. Espada, Eds., Springer, New York, USA, pp. 139–163, 2018.
 - [23] E. P. Thubert, H. Brandt, L. Kelsey, S. Pister, and V. Alexander, *IPv6 Routing Protocol for Low-Power and Lossy Networks. Internet Engineering Task Force (IETF)*, 2012.
 - [24] J. Xu, Y. Andreopoulos, Y. Xiao, and M. van der Schaar, "Non-stationary resource allocation policies for delay-constrained video streaming: application to video over internet-of-things-enabled networks," *IEEE Journal on Selected Areas in Communications*, vol. 32, no. 4, pp. 782–794, 2014.
 - [25] X. P. Yang and C. H. Yin, "Research of reliability indexes of complex network," *Journal of Beijing Information Science and Technology University*, vol. 25, no. 3, pp. 92–96, 2010.

Research Article

Effects of Aerobic Exercise on the Serum Leptin Level and Heart Rate Variability in the Obese Girl Children

Cuihan Li , Shaojun Lyu, and Jianwei Zhang 

College of P.E. and Sports, Beijing Normal University, Beijing 100875, China

Correspondence should be addressed to Cuihan Li; 11132020301@bnu.edu.cn

Received 20 April 2022; Revised 20 May 2022; Accepted 26 May 2022; Published 10 June 2022

Academic Editor: Dong Chen

Copyright © 2022 Cuihan Li et al. This is an open access article distributed under the Creative Commons Attribution License, which permits unrestricted use, distribution, and reproduction in any medium, provided the original work is properly cited.

Objective. The present study examined the effects of a 16-week aerobic exercise (AE) on the serum leptin level and heart rate variability (time domain and frequency domain) in the obese girl children and correlation coefficients of changes between the serum leptin level and heart rate variability after a 16-week AE intervention. **Methods.** 36 participants were randomly assigned to either aerobic exercise (AE, $n = 18$) or obese group ($n = 18$). The obese girl children in the AE group conducted a 16-week (4 times per week and 60 min per time) exercise protocols, and the obese group did not perform regular physical training during 16 weeks of study. Then, the serum leptin level and HRV (time domain and frequency domain) were measured in all subjects before and after AE intervention. **Results.** (1) After 16-week AE intervention, compared with pre-exercise, LF/HF decreased ($P < 0.05$), HF, SDNN, and RMSSD significantly increased ($P < 0.05$ and $P < 0.01$), and there was no significant difference in LF ($P > 0.05$) in the AE group. Nevertheless, there was no significant change before and after the test in the serum leptin level and HRV of the obese group ($P > 0.05$, respectively). (2) After 16-week AE intervention, compared with the obese group, SDNN and HF significantly increased ($P < 0.05$, respectively), LF/HF significantly decreased ($P < 0.05$) in the AE group, but there was no significant difference in RMSSD and LF between the obese group and AE group. (3) The reduction variables of the serum leptin level before and after the AE intervention are positively correlated with the reduction in the LF/HF ($r = 0.478$, $P < 0.05$) and negatively correlated with the increasing in the RMSSD ($r = -0.482$, $P < 0.05$). But there is no significant association between the reduction in the serum leptin level and the change of LF, HF, and SDNN ($P > 0.05$, respectively). **Conclusion.** 16-week AE significantly reduced the serum leptin level and improved cardiac autonomic function in the obese girl children. Moreover, the reduction in the serum leptin level was associated with the increase in parasympathetic activation and improved sympathetic-vagus balance after AE intervention. More research is needed to see whether the effect of exercise on leptin levels in obese girl children can reduce the risk of cardiovascular disease in adulthood.

1. Introduction

With economic development and improvement of living standards, the number of children with obesity is rapidly increasing around the world, which seriously affects the children's growth, development, and physical and mental health. Studies suggest that obesity increases the risk of cardiovascular disease; moreover, dysregulation of autonomic nerve function (ANS) is one of the potential mechanisms and causes the changes in cardiometabolism of obese patients [1]. In addition, ANS is an important system of regulating energy balance and plays an important role in the pathophysiology of obesity [2]. Therefore, ANS has

important clinical significance in the study of obesity patients. Heart rate variability (HRV) has been recognized as a quantitative measure for noninvasive assessment of cardiac autonomic regulation (cardiac, parasympathetic, and sympathetic). Knutson et al. [3] found that obese children showed the sympathovagal dysregulation and lower heart rate variability than normal-weight children. Another study found that overweight and/or obese children showed the sympathetic hyperactivity and decreased the parasympathetic function when compared with normal-weight children, especially at night [4]. Therefore, it is crucial to balance the activity of the sympathovagal nervous system in obese patients. Most studies have shown that regular exercise can

enhance vagus nerve activity in obese patients which contribute to reduce the risk of cardiovascular disease and sudden cardiac death [5], but the mechanism is unclear.

Leptin is a 16 kDa peptide hormone and mainly derives from adipose tissue which suppresses appetite, increases energy expenditure, and reduces body weight by acting its receptors in the hypothalamus [6]. Studies have shown that overweight and obese patients have higher leptin concentrations, and most obese individuals exist “leptin resistance” [7]. In addition, elevated leptin levels have been shown to be directly associated with systemic inflammation, immune-mediated disease, cerebrovascular and cardiovascular disease, and it can lead to the autonomic dysregulation. Charles et al. [8] found that leptin levels were significantly negatively correlated with HRV, especially among officers with higher body weight ($\text{BMI} \geq 25 \text{ kg/m}^2$) through a study of 388 public security personnel, which suggested that elevated leptin levels may be associated with cardiovascular disease. And, animal studies have shown that the increasing leptin level on sympathetic nerve activity was dose-dependent, and it could lead to autonomic dysfunction and was associated with cardiovascular morbidity and mortality [9]. Therefore, it may be considered that leptin may play an important role in sympathovagal imbalance of obese children. Meta-analysis showed that regular exercise, especially aerobic exercise, can significantly reduce serum leptin levels in obese children [10]. And, scholars have found that aerobic exercise intervention has been shown to improve cardiac automatic rhythm function in adults and children [11]. However, there are few studies on whether the improvement of cardiac autonomic regulation in obese children by aerobic exercise is related to the decrease of serum leptin. Therefore, the present study examined the effects of a 16-week aerobic exercise (AE) on the serum leptin level and heart rate variability (time domain and frequency domain) in the obese girl children and determined whether these effects were related to changes in serum leptin levels in order to provide a theoretical basis for aerobic exercise to improve cardiovascular health in obese children.

2. Research Objects and Methods

2.1. Subjects. According to the standard height and weight value of Chinese students aged 7–22, those whose actual weight is more than 20% of the standard weight are regarded as obese, mildly obese (20–29% overweight), moderately obese (30–49% overweight), and more than 50% were severely obese [12]. According to the above criteria, 36 obese female children from Affiliated Primary School of Beijing Normal University were recruited. The subjects were all simple obesity and were randomly divided into obesity group ($n = 18$) and aerobic exercise group ($n = 18$). As shown in Table 1, there was no significant difference in age, height, weight, and BMI between the two groups by independent samples *T*-test (all $P > 0.05$).

2.1.1. Inclusion Criteria. The subjects who had been diagnosed without hypertension, diabetes, dyslipidemia, and cardiovascular

disease or who were not consuming weight-reducing medicine or no regular exercise program or physical activity in the past 3 months were included. All participants and their parents or guardians were informed of the purpose of the experiment and voluntarily participated in the exercise training and signed informed consent before training.

2.2. Research Methods

2.2.1. Aerobic Exercise Program [10]. From March to July in 2020, obese female children in the aerobic exercise group were given 16 weeks of aerobic exercise (badminton, aerobics, jogging, power cycling, and sports games), 4 times a week, each exercise for 60 minutes (warm up for 5 minutes, formal training for 50 minutes, and relaxation training for 5 minutes), and exercise intensity of $220\text{-age} \times 65\% \text{--} 70\%$; the whole training process is guided by professional physical education teachers, and the exercise intensity is supervised by polar table.

2.2.2. HRV Indicator Evaluation. Before and after the exercise intervention, the subjects wore the heart rate of Polar Team 2 (made in Finland) and measured the HRV of subjects. After the height, weight, date of birth, and other information were put into the computer of the subjects and rest 5 min with eyes closed in a quiet environment. Subsequently, the heart rate for 10 min (10 subjects for each test) was recorded, and then the Kubios HRV software is used to calculate the HRV time domain and frequency domain indicators.

Time domain indexes include SDNN (standard deviation of all R-R intervals, ms) and RMSSD (square root of the sum of the mean of the difference between adjacent RR intervals, ms). Frequency domain indicators include low frequency power (LF, 0.04–0.15 Hz; sympathetic activity index) and high frequency power (HF, 0.15–0.40 Hz; vagus nerve activity level index) and LF/HF ratio (sympathetic-vagus nerve balance index).

2.2.3. Measurement of the Blood Leptin Level. Before and after the exercise intervention, blood samples from all subjects were collected at our laboratory at 08:00 following a 12-hour overnight fast. After a 10-minute rest in a comfortable chair, fasting blood was collected from the median cubital vein into a plain tube. Each blood sample was centrifuged at 3,000g for 10 minutes at 4°C, and serum leptin levels were determined by radioimmunoassay (according to the instructions).

2.3. Data Analysis. All experimental data were expressed as mean \pm standard deviation, and the data were analyzed using SPSS 19.0. All experimental data belonged to the normal distribution by K-S test. Paired *t*-test was used to compare the differences in the levels of leptin and HRV parameters before and after the experiment, and independent samples *t*-test was used to compare the differences in the above data between obese group and aerobic exercise group. The

TABLE 1: Basic information of the objects ($\bar{x} \pm s$).

Group	Age	Height (m)	Weight (kg)	BMI (kg/m ²)
Obese group	11.58 \pm 0.27	1.53 \pm 3.02	58.12 \pm 2.64	24.12 \pm 3.08
Aerobic exercise group	12.04 \pm 0.96	1.54 \pm 4.12	58.86 \pm 2.82	24.59 \pm 3.36
<i>P</i>	0.098	0.078	0.063	0.096

correlation of the changes in serum leptin levels and HRV parameters after aerobic exercise intervention was analyzed by Pearson correlation, and a *P* value of 0.05 indicated that the difference was considered statistically significant.

3. Research Results

3.1. The Effect of Aerobic Exercise on Serum Leptin Level in Obese Female Children. As shown in Table 2, after 16 weeks of aerobic exercise intervention, compared with pre-exercise, the serum leptin level of the obese exercise group significantly decreased ($P < 0.01$) by 13.06%. Independent sample *T*-test showed that there was no significant difference in serum leptin level between the obese group and the obese exercise group before aerobic exercise intervention ($t = -0.155$, $P = 0.878$). After 16 weeks of aerobic exercise, compared with the obese group, the serum leptin level in the obese exercise group significantly decreased by 15.21% ($t = 2.645$, $P = 0.012$).

3.2. Effects of Aerobic Exercise on HRV in Obese Female Children. As shown in Table 3, after 12 weeks of aerobic exercise intervention, SDNN and RMSSD in the obese exercise group significantly increased compared with those pre-exercise (all $P < 0.01$); The frequency domain index LF/HF significantly decreased, and HF significantly increased ($P < 0.05$). There was no significant change in LF before and after exercise intervention ($P > 0.05$). There was no significant difference in the above indicators in the obese group before and after the experiment (all $P > 0.05$).

Independent sample *T* test showed that there was no significant difference in HRV parameters between the two groups before aerobic exercise intervention (all $P > 0.05$). After 16-week aerobic exercise, compared with the obese group, SDNN of HRV time domain index significantly increased ($t = -2.641$, $P = 0.012$) in the obese exercise group. There was no significant difference in RMSSD and frequency domain LF ($t = -0.783$, $P = 0.439$; $t = -0.103$, $P = 0.918$) between the two groups. While LF/HF in the obese exercise group was significantly lower than that of the obese group ($t = 2.334$, $P = 0.026$), and HF was significantly higher than that of the obese group ($t = -2.111$, $P = 0.045$).

3.3. Correlation Analysis between Changes in Serum Leptin Levels and HRV Parameters after Aerobic Exercise Intervention. As shown in Table 4, Pearson correlation analysis showed that, after 16 weeks of aerobic exercise intervention, the change of serum leptin was significantly negatively correlated with the change of HRV time domain index RMSSD ($r = -0.482$, $P < 0.05$) and significantly positively correlated with the change of HRV frequency domain

index LF/HF ($r = 0.512$, $r = 0.478$, $P < 0.05$). There was no significant correlation with the changes of LF, HF, and SDNN (all $P > 0.05$).

4. Discussion

4.1. The Effect of Aerobic Exercise on HRV in Obese Female Children. Studies suggest that cardiovascular risk factors such as hyperglycemia, hypertension, and abnormal plasma lipoprotein levels in obese children which increase the likelihood of developing atherosclerotic cardiovascular disease in adulthood, and changes of ANS play an important role in the pathogenesis of these diseases [13]. HRV has emerged as a reliable noninvasive method to assess ANS activity, especially SDNN can reflect the overall activity of ANS. Low frequency (LF) is mainly mediated by sympathetic activity, and RMSSD and HF are associated with vagal activity [14]. Prior study found that compared with normal weight children (BMI: 17.7 ± 2.8 kg/m²) and obese children (11.6 ± 3.8 years old; BMI: 29.8 ± 4.6 kg/m²), the heart rate variability indicators SDNN, RMSSD, and pNN50 significantly decreased in the obese group which suggested that obesity may lead to sympathovagal imbalance or disorder and increase the risk of cardiovascular disease in obese children [15]. Paschoal et al. [16] found that compared with normal-weight children (10.2 ± 0.7 years), HRV frequency domain indicators LFn and LF/HF ratio significantly decreased and HFn significantly increased in the standing position of the obese children, indicating that cardiac sympathetic nerve activity was enhanced and parasympathetic nerve activity was weakened. Therefore, improvement of ANS activity is critical in obese children. The prior study found that the level of physical exercise can affect the cardiac autonomic function, and the study showed that regular exercise increased the HF of obese children, while the decreasing of RMSSD stopped after exercise, indicating that regular physical exercise had a good effect on the parasympathetic (vagus) activity of obese children [17]. However, the conclusion that physical exercise improving ANS in obese children is inconsistent. Gutin et al. [18] conducted a 12-month moderate-intensity exercise intervention (5 days/week, 20 min each time, heart rate 130–140 bpm) in obese children (6–11 years old) and found that exercise significantly increased HF and decreased LF in obese children, which suggested that moderate-intensity physical activity improves sympathetic and vagal activity in obese children. And, LI [19] found that Taijiquan exercise can improve the integration and regulation function of cardiac autonomic nerve, especially vagus nerve activity. In addition, Biljon et al. [20] found that moderate-intensity aerobic exercise (exercise intensity: 65–70% HRmax) might increase vagal activity (increasing in HF) in normal-weight children (11.07 ± 0.81 years) and cause sympathovagal balance (ratio of

TABLE 2: Results of the serum leptin level in each group of obese female children ($\bar{x} \pm s$).

Group	<i>n</i>	Before serum leptin level, $\mu\text{g/L}$	After serum leptin level, $\mu\text{g/L}$	<i>t</i> value	<i>P</i> value
Obese group	18	21.83 ± 3.73	22.61 ± 3.18	-1.740	0.100
Aerobic exercise group	18	22.05 ± 4.80	$19.17 \pm 4.51^{\Delta\Delta\#}$	10.363	0.000

Note. $\Delta P < 0.05$ and $\Delta\Delta P < 0.01$, comparison before and after the experiment; $\#P < 0.05$, comparison between obese group and obese exercise group.

TABLE 3: Results of the HRV in each group of obese female children ($\bar{x} \pm s$).

HRV	Group	Before	After	<i>T</i> value	<i>P</i> value
SDNN (ms)	Obese group	126.67 ± 13.05	128.89 ± 10.72	-0.885	0.388
	Obese exercise group	128.88 ± 10.72	$139.67 \pm 13.59^{\Delta\Delta\#}$	-10.361	0.000
RMSSD (ms)	Obese group	46.06 ± 8.33	46.89 ± 8.33	-0.995	0.334
	Obese exercise group	45.17 ± 8.83	$49.28 \pm 8.86^{\Delta\Delta}$	-10.719	0.000
LF (ms^2)	Obese group	1026.67 ± 424.51	1008.44 ± 396.05	0.663	0.516
	Obese exercise group	1078.39 ± 474.39	1023.94 ± 497.93	1.831	0.085
HF (ms^2)	Obese group	677.71 ± 304.81	645.03 ± 303.79	0.386	0.705
	Obese exercise group	697.09 ± 306.98	$986.03 \pm 614.45^{\Delta\#}$	-2.728	0.014
LF/HF	Obese group	1.73 ± 0.86	1.74 ± 0.75	-0.065	0.949
	Obese exercise group	1.79 ± 1.09	$1.20 \pm 0.63^{\Delta\#}$	2.706	0.015

Note. $\Delta P < 0.05$ and $\Delta\Delta P < 0.01$, comparison before and after the experiment; $\#P < 0.05$, comparison between obese group and obese exercise group.

TABLE 4: Correlation coefficients (*r*) of changes between serum leptin level and heart rate variability after a 16-week aerobic exercise intervention ($\bar{x} \pm s$).

		ΔHF (ms^2)	ΔLF (ms^2)	$\Delta\text{LF}/\text{HF}$	ΔSDNN (ms)	ΔRMSSD (ms)
Δ serum leptin level ($\mu\text{g/L}$)	<i>r</i>	-0.070	0.159	0.478*	0.258	-0.482*
	<i>P</i>	0.782	0.530	0.046	0.301	0.043

LF/HF decreasing) which seemed to induce superior alterations in cardiac ANS activity in normal-weight children. Mandigout et al. [21] conducted a 13-week endurance training program (exercise intensity $>80\%$ HRmax) in 19 obese children (10–11 years old) and found that LF and HF of obese children after endurance training were significantly higher than those before training, but the LF/HF ratio did not significantly change. The results showed that endurance training had a positive effect on HRV in healthy children, but did not induce sympathetic and parasympathetic modifications. The results of current study are consistent with previous studies that the moderate-intensity exercise program improves the HRV in obese children. The results of current study shows that time domain indicators SDNN and RMSSD significantly increased, the frequency domain HF increased, the ratio of LF/HF decreased, but LF did not significantly change in the obese exercise group when compared with the obese children group which indicated that physical exercise can increase heart rate variability and stimulate vagal tone, but has no effect on sympathetic nerve activity. Different results are obtained for different studies, which may be related to different exercise time, intensity, and research objects.

4.2. The Effect of Aerobic Exercise on the Serum Leptin Level in Obese Female Children. Leptin reduces food intake and increases the activity of the sympathetic nervous system by acting relevant receptors in the hypothalamus. It can reduce fatty acid (FFA) and lipid synthesis and also directly act on

adipocytes in the body to inhibit fat synthesis. It plays an important role in body weight regulation and leptin resistance in overweight and obese individuals, and it plays an important factor in weight control [22]. And, studies suggest that there is a positive correlation between circulating leptin levels and greater future BMI or body adiposity, which can predict the risk of future obesity in children [23], so lowering leptin levels is crucial for obese children. Most scholars believe that the reduction of body fat is the main reason that exercise affects leptin levels, and Willis et al. [24] found that compared with resistance training and resistance training combined with aerobic exercise, aerobic exercise is considered to be the best way to reduce body fat, but the effect on serum leptin levels is more controversial. Meta-analysis showed that physical exercise can increase adiponectin, reduce the plasma levels of leptin and IL-6, and significantly improve the inflammatory status of obese children without changing dietary habits or other lifestyles [10]. And, Zhang et al. [25] thought that long-term Taijiquan practice reduced the concentration of blood-insulin and leptin, promote the fat catabolism, and was helpful for health, fitness, and losing weight. However, Zguira et al. [26] conducted 8 weeks (90 min, 3 days/week) training on obese patients with metabolic syndrome (14 ± 2 years) and found that serum leptin level did not significantly change before and after exercise. The results of this study are the same as those of the former study. After 16 weeks of aerobic exercise intervention, compared with the obese children, the serum leptin level of the obese exercise group significantly decreased.

Zhiping et al. [27] believed that the decrease in leptin concentration after aerobic exercise intervention may be related to the reduction of body fat and the negative energy balance caused by exercise training; and García-Hermoso et al. [28] believed that the longer the exercise time (≥ 60 min), the higher the energy expenditure (≥ 800 kcal) and the lower the leptin concentration which indicated that the duration of exercise training and the time of every exercise training were significantly negatively correlated with the leptin level. Therefore, it can be considered that the decreasing of serum leptin level in obese children after 16-week aerobic exercise intervention in this study may be related to the reduction of body fat in obese children, and the different changes in the leptin level after exercise intervention may be related to exercise training time and exercise training intensity.

4.3. Correlation Analysis of the Serum Leptin Level and Heart Rate Variability. Studies suggested that leptin is independently correlated with different markers of autonomic nervous activity [29]. In addition, Paolisso et al. [30] found that leptin is positively correlated with heart rate variability index LF and LF/HF ratio in 120 normal males (42.5 ± 1.9 years old), which reflected that leptin level is closely correlated with the increasing sympathetic nervous activity. The same results were obtained in adult women (20.9 ± 0.33 years old) by Flanagan et al. [31]. There was a positive correlation between the leptin level and LF or LF/HF in adult women, and the leptin level had a greater impact on the sympathetic nervous system of women with high body fat. However, there was no significant correlation between LF or LF/HF in males (20.9 ± 0.22 years). Wille [32] found that the serum leptin level was significantly positively correlated with LF or LF/HF in male and female children and negatively correlated with parasympathetic activity (HF and pNN50) in male children, but without significantly associated with parasympathetic activity in female children through follow-up (6.7–12.2 y) study of children (4.4 to 11.0 years old). In the current study, correlation analysis showed that the decreased level of serum leptin was significantly positively correlated with the decrease in HRV frequency domain index LF/HF, but not with the change of LF and HF before and after aerobic exercise intervention in obese female children. This study also found a significant negative correlation between decreased serum leptin level and increased RMSSD, suggesting a significant negative correlation between serum leptin level and parasympathetic neural activity in female children, which is different from the above results. Umetani et al. [33] believe that HRV is related to gender and age. Therefore, it can be considered that the difference between our study, and the above research results may be related to the selection of research objects.

Data Availability

The experimental data used to support the findings of this study are available from the corresponding author upon request.

Additional Points

16-week aerobic exercise significantly reduced serum leptin level and improved cardiac autonomic function in obese female children, and the decreasing of serum leptin concentration after aerobic exercise intervention was associated with the increasing of sympathetic vagus nerve balance to parasympathetic nerve activity. But more research is needed to confirm whether the effect of exercise on leptin levels in obese female children can reduce the risk of cardiovascular disease in adulthood.

Conflicts of Interest

The authors declare that they have no conflicts of interest to report regarding the present study.

Acknowledgments

The study was supported by the National Social Science Fund of China, China (Grant no. 2020CTY002) and Fundamental Research Funds for the Central Universities, China (Grant no. 2020NTSS08).

References

- [1] U. Sheema and B. Malipatil, "A cross-sectional study on effect of body mass index on the spectral analysis of heart rate variability," *National Journal of Physiology, Pharmacy and Pharmacology*, vol. 5, no. 3, pp. 250–252, 2015.
- [2] D. C. Jarrin, J. J. McGrath, P. Poirier, and Quality Cohort Collaborative Group, "Autonomic dysfunction: a possible pathophysiological pathway underlying the association between sleep and obesity in children at-risk for obesity," *Journal of Youth and Adolescence*, vol. 44, no. 2, pp. 285–297, 2015.
- [3] K. L. Knutson, "Does inadequate sleep play a role in vulnerability to obesity?" *American Journal of Human Biology*, vol. 24, no. 3, pp. 361–371, 2012.
- [4] P. Baum, D. Petroff, J. Classen, W. Kiess, and S. Blüher, "Dysfunction of autonomic nervous system in childhood obesity: a cross-sectional study," *PLoS One*, vol. 8, no. 1, Article ID e54546, 2013.
- [5] S. Abolahrari-Shirazi, J. Kojuri, Z. Bagheri, and Z. Rojhani-Shirazi, "Effect of exercise training on heart rate variability in patients with heart failure after percutaneous coronary intervention," *J Biomed Phys Eng*, vol. 9, no. 1, pp. 97–104, 2019.
- [6] J. M. Friedman and J. L. Halaas, "Leptin and the regulation of body weight in mammals," *Nature*, vol. 395, no. 6704, pp. 763–770, 1998.
- [7] M. Vadacca, D. P. Margiotta, L. Navarini, and A. Afeltra, "Leptin in immuno-rheumatological diseases," *Cellular and Molecular Immunology*, vol. 8, no. 3, pp. 203–212, 2011.
- [8] L. E. Charles, C. M. Burchfiel, K. Sarkisian et al., "Leptin, adiponectin, and heart rate variability among police officers," *American Journal of Human Biology*, vol. 27, no. 2, pp. 184–191, 2015.
- [9] W. G. Haynes, D. A. Morgan, S. A. Walsh, A. L. Mark, and W. I. Sivitz, "Receptor-mediated regional sympathetic nerve activation by leptin," *Journal of Clinical Investigation*, vol. 100, no. 2, pp. 270–278, 1997.
- [10] F. Sirico, A. Bianco, G. D'Alicandro et al., "Effects of physical exercise on adiponectin, leptin, and inflammatory markers in

- childhood obesity: systematic review and meta-analysis," *Childhood Obesity*, vol. 14, no. 4, pp. 207–217, 2018.
- [11] G. R. H. Sandercock, P. D. Bromley, and D. A. Brodie, "Effects of exercise on heart rate variability: inferences from meta-analysis," *Medicine & Science in Sports & Exercise*, vol. 37, no. 3, pp. 433–439, 2005.
 - [12] Chinese Students physical and health Research Group, *Study on Chinese Students' Physical and health*, People's Education Press, Beijing, China, 1988.
 - [13] Y. Zhou, G. Xie, J. Wang, and S. Yang, "Cardiovascular risk factors significantly correlate with autonomic nervous system Activity in children," *Canadian Journal of Cardiology*, vol. 28, no. 4, pp. 477–482, 2012.
 - [14] Li Guangxin, Z. Wang, W. Lv, and L. Zhao, "Effect of aerobic exercise on Heart rate Variability in obese adolescents," *Journal of Jilin University (Earth Science Edition)*, vol. 40, no. 5, pp. 1093–1097, 2014.
 - [15] C. Baumann, U. Rakowski, and R. Buchhorn, "Omega-3 fatty acid supplementation improves heart rate variability in obese children," *International Journal of Pediatrics*, vol. 2018, pp. 1–5, 2018.
 - [16] M. A. Paschoal, P. F. Trevizan, and N. F. Scodeler, "Variabilidade da frequência cardíaca, lípides e capacidade física de crianças obesas e não-obesas," *Arquivos Brasileiros de Cardiologia*, vol. 93, no. 3, pp. 239–246, 2009.
 - [17] G. Martini, P. Riva, F. Rabbia et al., "Heart rate variability in childhood obesity," *Clinical Autonomic Research: Official Journal of the Clinical Autonomic Research Society*, vol. 11, no. 2, pp. 87–91, 2001.
 - [18] B. Gutin, P. Barbeau, M. S. Litaker, M. Ferguson, and S. Owens, "Heart rate variability in obese children: relations to total body and visceral adiposity, and changes with physical training and detraining," *Obesity Research*, vol. 8, no. 1, pp. 12–19, 2000.
 - [19] L. I. Wenjuan, *The Influence of Eight Weeks of TaiChi Training on Heart Rate Variability and Other Biochemical Indexes of Healthy university Female students*, Beijing Sport University, Beijing, China, 2010.
 - [20] A. van Biljon, A. J. McKune, K. D. DuBose, U. Kolanisi, and S. J. Semple, "Short-term high-intensity interval training is superior to moderate-intensity continuous training in improving cardiac autonomic function in children," *Cardiology*, vol. 141, no. 1, pp. 1–8, 2018.
 - [21] S. Mandigout, A. Melin, L. Fauchier, L. D. N'Guyen, D. Courteix, and P. Obert, "Physical training increases heart rate variability in healthy prepubertal children," *European Journal of Clinical Investigation*, vol. 32, no. 7, pp. 479–487, 2002.
 - [22] J. Shang, X. Zhao, S. He, J. Li, and S. Wang, "Meta analysis on the association between adipocytokines and obesity in Chinese children and adolescents," *Chinese Journal School Health*, vol. 35, no. 7, pp. 1049–1052, 2014.
 - [23] M. Zhang, H. Cheng, X. Zhao et al., "Leptin and leptin-to-adiponectin ratio predict adiposity gain in nonobese children over a six-year period," *Childhood Obesity*, vol. 13, no. 3, pp. 213–221, 2017.
 - [24] L. H. Willis, C. A. Slentz, L. A. Bateman et al., "Effects of aerobic and/or resistance training on body mass and fat mass in overweight or obese adults," *Journal of Applied Physiology*, vol. 113, no. 12, pp. 1831–1837, 2012.
 - [25] H. Zhang and H. Zhang, "Effects of long-term taijiquan practice on lipid metabolism and related hormone levels of obese university students," *Journal of Shenyang Sport University*, vol. 30, no. 6, pp. 95–98, 2011.
 - [26] M. S. Zguira, M. Slimani, N. L. Bragazzi et al., "Effect of an 8-week individualized training program on blood biomarkers, adipokines and endothelial function in obese young adolescents with and without metabolic syndrome," *International Journal of Environmental Research and Public Health*, vol. 16, no. 5, p. 751, 2019.
 - [27] Z. Xu, W. Liu, P. Wang, Y. Hu, and Y. Jin, "Effects of aerobic exercise prescription to leptin levels and leptin receptor mRNA expressions in peripheral blood of female obese college students," *Journal of Beijing Sport University*, vol. 34, no. 11, pp. 58–61, 2011.
 - [28] A. García-Hermoso, R. J. M. Ceballos-Ceballos, C. E. Poblete-Aro, A. C. Hackney, J. Mota, and R. Ramírez-Vélez, "Exercise, adipokines and pediatric obesity: a meta-analysis of randomized controlled trials," *International Journal of Obesity*, vol. 41, no. 4, pp. 475–482, 2017.
 - [29] C. Pieterse, R. Schutte, and A. E. Schutte, "Autonomic activity and leptin in Africans and whites," *Journal of Hypertension*, vol. 32, no. 4, pp. 826–833, 2014.
 - [30] G. Paolisso, D. Manzella, N. Montano, A. Gambardella, and M. Varricchio, "Plasma leptin concentrations and cardiac autonomic nervous system in healthy subjects with different body weights," *Journal of Clinical Endocrinology & Metabolism*, vol. 85, no. 5, pp. 1810–1814, 2000.
 - [31] D. E. Flanagan, J. C. Vaile, G. W. Petley et al., "Gender differences in the relationship between leptin, insulin resistance and the autonomic nervous system," *Regulatory Peptides*, vol. 140, no. 1–2, pp. 37–42, 2007.
 - [32] R. Van De Wille and N. Michels, "Longitudinal associations of leptin and adiponectin with heart rate variability in children," *Frontiers in Physiology*, vol. 8, pp. 498–505, 2017.
 - [33] K. Umetani, D. H. Singer, R. McCraty, and M. Atkinson, "Twenty-four hour time domain heart rate variability and heart rate: relations to age and gender over nine decades," *Journal of the American College of Cardiology*, vol. 31, no. 3, pp. 593–601, 1998.

Research Article

Research on Mechanical and Carbonization Properties of Hybrid Fiber Iron Tailings Concrete Based on Deep Learning

Wenbo Zheng¹, Sheliang Wang,² Yang Qu,¹ Kangning Liu,² and Liangwei Jia²

¹School of Civil Engineering, Xijing University, Xi'an 710123, China

²School of Civil Engineering, Xi'an University of Architecture and Technology, Xi'an 710055, China

Correspondence should be addressed to Wenbo Zheng; 2008590003043@stu.xijing.edu.cn

Received 26 April 2022; Revised 15 May 2022; Accepted 23 May 2022; Published 9 June 2022

Academic Editor: Dong Chen

Copyright © 2022 Wenbo Zheng et al. This is an open access article distributed under the Creative Commons Attribution License, which permits unrestricted use, distribution, and reproduction in any medium, provided the original work is properly cited.

Iron tailings sand is a kind of mineral waste, and open-air storage is a common treatment method for iron tailings, which not only has a huge impact on the ecological environment but also occupies a lot of land resources. Therefore, the preparation of high-ductility fiber reinforced iron tailings concrete and its application in practical engineering structures have good application prospects. This paper is based on the deep learning research on the mechanical and carbonization properties of hybrid fiber iron tailings concrete. Therefore, tailings sands with different substitution rates, single-mixed steel fiber, and mixed steel-PVA fiber concrete were prepared in this paper. Its compressive strength, split tensile strength, axial compressive strength, elastic modulus, strain, and carbonization depth were tested. Through the existing concrete compressive stress-strain curve equations, the nonlinear calculation of each group of concrete compressive stress-strain curve equations in this paper is carried out, some parameters are determined, and the carbonation depth equation is established. The results show that, with the increase of tailings content, the properties of concrete increase first and then decrease and the addition of fibers can effectively improve the strength, elastic modulus, peak strain, and carbonization depth of concrete. However, with the increase of PVA fiber content, its performance enhancement effect decreased.

1. Related Introduction

In China, the comprehensive utilization of iron tailings sand began in the 1990s. After years of experimental research, a relatively mature conclusion has been achieved in the use of iron tailings sand for the preparation of iron tailings concrete. The preparation, mechanical properties, and durability of tailings concrete were further researched and developed. In the process of iron ore mining, a large amount of solid waste will be produced. Processing tailings waste into building materials is the most effective way to absorb mineral waste and has high ecological benefits and engineering value. Due to the high compressive strength, rough texture, and angular shape of iron tailings particles, iron tailings-made concrete has better ITZ properties and durability than ordinary concrete. By using mechanical activation to improve the pozzolanic activity and hydration performance of iron tailings, secondary hydration reaction

occurs with cement to improve concrete strength. A large number of experimental studies have shown that, with the increase of iron tailings replacement rate, the workability of concrete decreases, which may be due to the high water absorption and specific surface area of iron tailings material, which leads to a decrease in workability. Although iron tailings as fine aggregates can improve the compressive strength of concrete, considering that it will reduce the workability of concrete, it is generally recommended to use iron tailings not exceeding 30% as fine aggregates. Lv conducted a comparative study by completely replacing ordinary aggregates with iron tailings in dam concrete with different grades.

It can be seen from the above literature that scholars have little research on the carbonization properties of iron tailings and hybrid fibers. Therefore, this paper studies its mechanical properties such as compressive strength, axial compressive strength, elastic modulus, stress-strain, and

TABLE 1: Chemical composition of cement and fly ash.

Quality score	SiO ₂	Al ₂ O ₃	CaO	MgO	Fe ₂ O ₃	TiO ₂	SO ₃	Other
Cement	55.7	42.5	0.4	—	0.3	0.9	—	0.2
Fly ash	52.97	29.96	3.66	1.52	7.98	—	0.65	3.26

TABLE 2: Physical properties of fly ash.

Physical properties of fly ash (%)				
Moisture	Loss on ignition	Water demand ratio	Fineness (45 μ m square hole sieve allowance)	Density (g/cm ³)
0.29	3.52	93	12	2.11

TABLE 3: Physical properties of fine aggregates.

Aggregate type	Apparent area (kg/m ³)	Loose packing (kg/m ³)	Void ratio (%)	Water absorption (%)	Mud content (%)	Crush indicator (%)
Thin bone material	River sand	2689	1655	—	0.5	3.1
	Iron tailings sand	2745	1824	8.7	2.9	19.53

TABLE 4: Physical properties of fibers.

Fiber type	Length (mm)	Diameter (μ m)	Aspect ratio	Density (g/cm ³)	Tensile strength (MPa)	Elastic modulus (GPa)
Steel fiber (SF)	16	220	72.73	7.8	2500	210
Polyethylene fiber (PVA)	12	24	500	0.97–0.98	3000	160

carbonization depth and provides a basis for the carbonization performance of iron tailings hybrid fibers in a wider range of applications [1–10].

2. Related Tests

2.1. Materials

2.1.1. Cementitious Material. The cementitious material used in this test consists of two parts, Qinling brand ordinary Portland cement and fly ash with a strength grade of P-O 42.5R. The minerals and physical properties of the two materials are shown in Tables 1 and 2, respectively.

2.1.2. Aggregate. The aggregate is composed of natural crushed stone and fine aggregate, and the fine aggregate is river sand and natural sand. The physical properties of the tested aggregate are shown in Table 3.

2.1.3. Fiber. The fibers used in the test are steel fibers and PVA fibers, and the performance indicators of the two fibers are shown in Table 4.

2.2. Mixing Ratio. This test is divided into ordinary concrete (NC), iron tailings concrete (TAC), steel fiber concrete (TAC-S), and steel-polyvinyl alcohol fiber concrete (TAC-S-P) according to the iron tailings replacement rate

and fiber content. . The replacement rate of iron tailings is 30%, 50%, and 100%. In most studies, the optimal dosage of steel fiber is roughly 1.5%. The effects of polyvinyl alcohol fiber content of 0, 0.3%, 0.6%, and 0.9% on the mechanical properties and carbonation durability of concrete were discussed [11].

This article refers to the requirements of the “Ordinary Concrete Mix Proportion Design Regulations” (JGJ55-2011) and other specifications. After the previous trial and adjustment, the concrete mix design is shown in Table 5. Among them, the water-cement ratio of each group of mixing ratios is 0.4, and the sand ratio is 0.37.

*1 is for number naming; take “T30-S1.5-P0.3 as an example;” T stands for iron tailings, S stands for steel fiber, P stands for PVA fiber, the number “30” means 30% iron tailings replacement rate, and the number “0.3” means that the PVA fiber content is 0.3%.

2.3. Preparation of Test Pieces. According to the mixing ratio of 5 in Table 5, 12 samples were prepared in each group, including 9 cube samples of 100 mm \times 100 mm \times 100 mm; the compressive strength of the cubes at carbonization ages of 0 d, 7 d, 14 d, 28 d, and 56 d was tested, respectively, and three prisms with a sample size of 100 mm \times 100 mm \times 300 mm were tested for axial compressive strength, stress-strain curve, elastic modulus, and stress-strain [12].

TABLE 5: Design of concrete mix ratio.

Serial number	Block coding	Water-cement ratio	Cementitious material		Coarse aggregate		Fine aggregate	Fiber type	Water	
			Cement	Fly ash	Stone	River sand			PV	Water reducer
1	NC	0.4	440	110	1103	656	0	0	0	220
2	T30	0.4	440	110	1103	459.2	196.8	0	0	220
3	T50	0.4	440	110	1103	328	328	0	0	220
4	T100	0.4	440	110	1103	0	656	0	0	220
5	T100-S1.5	0.4	440	110	1103	0	656	117	0	220
6	T100-S1.5-P0.3	0.4	440	110	1103	0	656	117	2.94	220
7	T100-S1.5-P0.6	0.4	440	110	1103	0	656	117	5.88	220
8	T100-S1.5-P0.9	0.4	440	110	1103	0	656	117	8.82	220

2.4. Test Instruments and Programs. The carbonization experiment was carried out in a carbonization test chamber, the CO₂ concentration was kept at $(20 \pm 3)\%$, the humidity was controlled at $(70 \pm 5)\%$, the temperature in the chamber was controlled at $(20 \pm 2)^\circ\text{C}$, and the carbonization ages were 7, 14, 28, and 56 days.

3. Analysis of Test Results Based on Deep Learning

3.1. Cube Compressive Strength

3.1.1. Compressive Strength of Iron Tailings Concrete before and after Carbonization. Figure 1 shows the effects of iron tailings replacement rate and carbonation age on compressive strength under different compressive strength. It can be seen from the test results that when the replacement rate of iron tailings is increased, the concrete strength increases first and then decreases. When the replacement rate of iron tailings is 30%, the compressive strength of concrete reaches the highest, the strength increases by 7.6%, the replacement rate is 50% and 100%, and the strength decreases by 5.8% and 18.9%, respectively.

With the increasing carbonation age, the compressive strength of concrete always maintains a stable growth trend. When the carbonation age reaches 7d, the increase of compressive strength is the largest, and the compressive strength increases by 5.5%, 3.5%, 8.2%, and 10.2%, respectively. With the increase of age, the growth of carbonation compressive strength gradually stabilized.

When the concrete carbonizes, the chemical composition and pore structure inside the matrix change. CO₂ reacts with Ca (OH)₂ to form water-insoluble calcium carbonate. Calcium carbonate fills the cemented pores and microcracks inside the concrete, weakens the subsequent diffusion of CO₂, and increases the density and strength of the concrete [13, 14].

3.1.2. Compressive Strength of Fiber Iron Tailings Concrete before and after Carbonization. Figure 2 studies the effect of fiber content and carbonization age on compressive strength, and fiber addition has a positive effect on concrete strength. With the increase of PVA fiber content, the strength of concrete increases at first and then decreases, and

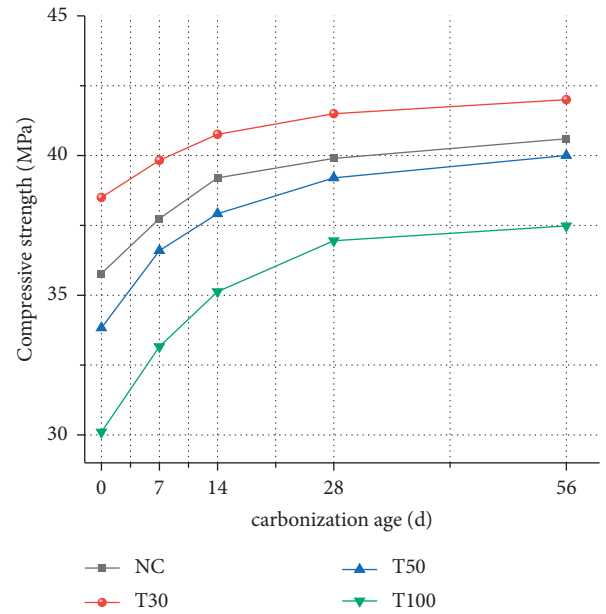


FIGURE 1: Compressive strength of iron tailings concrete.

the strength of concrete mixed with fiber is greater than that of steel fiber alone. Fiber reinforced concrete strength increased by 14%, 19%, 22.8%, and 16.4%, respectively.

Carbonation has little effect on the strength of fiber reinforced concrete, because the addition of fibers improves the internal structure of the concrete, making it difficult for CO₂ to penetrate into the concrete. After carbonization for 7d, the compressive strength of concrete increased by 5.5%, 1.9%, 4.7%, and 5.4%, respectively.

The improvement of fiber reinforced concrete strength is mainly due to two aspects of crack resistance and toughening. The anticracking effect of fibers depends on the distribution of fibers in concrete. When only steel fibers are mixed into concrete, since the density of steel fibers is greater than that of the matrix, it will sink under the action of self-weight and vibration, resulting in steel fibers in the concrete. The uneven distribution in the concrete can easily cause local stress concentration during compression, resulting in premature failure of the specimen. The increase in toughness is due to the fiber bridging-debonding-slip failure mode,

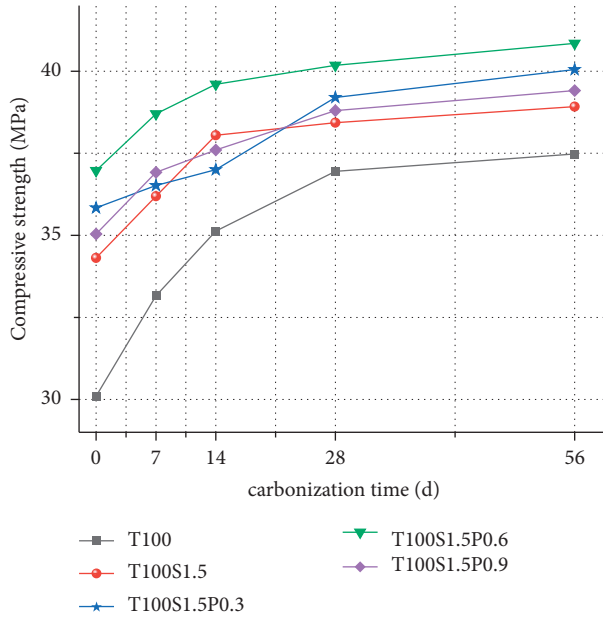


FIGURE 2: Compressive strength of fiber reinforced concrete.

which generates more dissipated energy. There are hydroxyl groups in the molecular chain of PVA fiber, which can form a strong bond between the fiber and the concrete matrix. A large number of fine PVA fibers will increase the surface area in contact with the concrete matrix, which can better transmit stress through cracks. After adding PVA fiber, a complex three-dimensional fiber network is formed with the random distribution of steel fiber. The steel fiber can inhibit the large cracks in the concrete, and the PVA fiber inhibits the early plastic shrinkage and drying shrinkage microcracks. And as a steel fiber hybrid carrier, the steel fiber is evenly dispersed in the matrix, which produces a good synergy with the steel fiber, produces a positive hybrid effect, and improves the strength of the concrete.

With the increase of PVA fiber content, it is relatively difficult to disperse too much PVA fiber, and there will be obvious agglomeration phenomenon, resulting in the formation of new weak areas where there are no fibers or less fibers in the concrete. The intervention of fibers causes the redistribution and transfer of concrete stress. If the distribution of this stress cannot achieve a true equilibrium, new stress concentrations may be formed, resulting in cracking in the area where fibers are lacking [15].

3.2. Cube Splitting Tensile Strength

3.2.1. Splitting Tensile Strength of Iron Tailings Concrete before and after Carbonization. Figure 3 investigates the effect of different iron tailings substitution rate and carbonization age on splitting tensile strength. It can be seen from the figure that, with the increase of iron tailings substitution rate, the splitting tensile strength of concrete increases first and then decreases. The tensile strength is the highest when the substitution rate is 30%, and the splitting

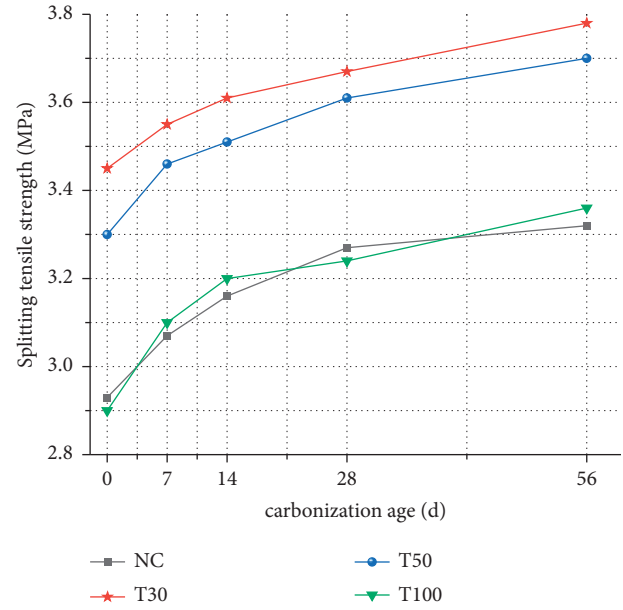


FIGURE 3: Splitting tensile strength of iron tailings concrete.

tensile strength of T30, T50, and T100 is the highest. The strength increased by 17.7%, 12.6%, and -1%, respectively. With the increase of carbonization age, the overall splitting tensile strength is in a steady growth trend, and the tensile strength of carbonized 28d increases by 11.6%, 6.4%, 9.4%, and 11.7%, respectively.

Tensile strength is an important index to determine the crack resistance in concrete design, and it is also a key parameter to indirectly determine the bond strength of each component of concrete. In this experiment, 30% of iron tailings was the optimal replacement level, the concrete had the densest filling structure, and the bonding performance between the aggregate and the cement mortar was improved. As the content of iron tailings increases, the bonding properties between aggregates deteriorate, resulting in a decrease in tensile strength.

Carbonization makes the splitting tensile strength value of concrete more complicated. With the increase of carbonization age, the carbonization strength value fluctuates greatly. The addition of iron tailings has a great influence on the strength value of the low carbonization period. When the carbonization cycle is long, the effect is relatively small. For example, when the dosage is 100%, the strength value increases by 6.9%, 3.2%, 1.25%, and 3.7%, respectively, at the carbonization age of 7d, 14d, 28d, and 56d. The reason is that as the carbonization time increases, the hydration products gradually fill the pores in the concrete after carbonization, so that there are fewer channels for CO₂ to enter and leave the concrete, which reduces the impact of carbonization [16–20].

3.2.2. Splitting Tensile Strength of Fiber Reinforced Concrete before and after Carbonization. It can be seen from Figure 4 that the addition of fibers has a significant effect on improving the splitting tensile strength value of concrete and

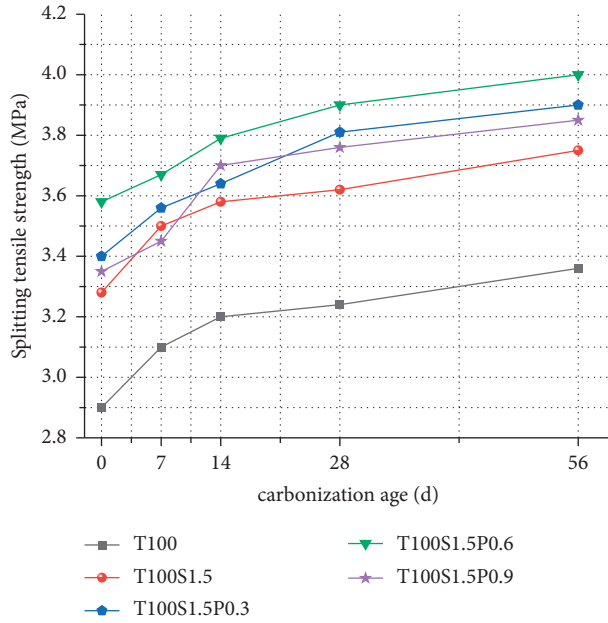


FIGURE 4: Splitting tensile strength of fiber reinforced concrete.

the concrete strength is increased by 13.1%, 17.2%, 23.4%, and 15.5%, respectively.

The effect of single-doped steel fiber on the splitting tensile properties of iron tailings concrete can be explained as follows: due to the rough surface of iron tailings, the bonding performance between steel fibers and aggregates is enhanced, and when the concrete is loaded, the steel fibers are difficult to be pulled out or break, thereby increasing the tensile strength value. Second, steel fibers can inhibit the development of cracks. Third, the tensile force is transmitted to the steel fibers through the concrete matrix, and the bridging effect between the steel fibers and the concrete makes up for the defects of the concrete matrix. During the splitting and tensile failure of concrete, steel fibers absorb a lot of energy.

Mixing fibers can significantly improve the tensile strength value of concrete, and the mixing effect is better than that of steel fibers alone. When steel fibers are mixed with PVA fibers, PVA fibers form a fiber grid, evenly dispersed in concrete. It has a good synergistic effect with steel fiber, and a positive hybrid effect occurs, which greatly improves the tensile strength value of concrete. With the increase of PVA fiber volume ratio, the tensile strength value of hybrid fiber reinforced concrete showed an increasing trend. This is because, with the increase of PVA fiber content, the fiber spacing is relatively low in concrete, which can effectively limit the development of primary cracks caused by factors such as segregation and shrinkage, thereby improving the tensile strength value. When the fiber content is more than 0.6%, the tensile strength value of concrete will be reduced. According to the analysis of the compressive test above, if too much PVA fiber is added, there will be obvious agglomeration, so that the fibers are not uniformly distributed in the concrete, and the fiber distribution is too sparse or too dense at the splitting interface, resulting in a

larger concentrated stress reducing the tensile strength value.

With the increase of carbonization age, the value of splitting tensile strength has been increasing. It may be because in the early stage of carbonization CO_2 in the air penetrates into the internal pores of the concrete and dissolves the water in the pores. The carbonization reaction of the hydration product generates calcium carbonate, which fills part of the pores, and the bridging effect of the PVA fiber and the matrix makes the expansion stress distribution of the concrete pores more uniform. In the later stage of carbonization, the generated calcium carbonate fills the internal pores of the concrete, and the addition of fibers also reduces the cracks of the concrete, and it is difficult for CO_2 to enter the concrete again, so the effect of increasing the tensile strength value in the later stage of carbonization is not obvious.

When the steel fiber is used alone, due to the high density and thick diameter of the steel fiber, the volume ratio of the steel fiber contained in the same volume of concrete is larger, the fiber spacing of the steel fiber is significantly higher than that of other fibers, and CO_2 easily enters the concrete. After adding PVA fiber, steel fiber and PVA fiber have a good synergistic effect, reducing the fiber spacing between fibers, and its effect on capillary thinning and blocking is more obvious, thereby reducing the pore channel of CO_2 in the concrete, so the mixing effect is due to the single mixing of steel fibers [21, 22].

3.3. The Mechanism of Fiber Crack Inhibition. The strength, deformation, and failure of concrete are related to the propagation of cracks. The essence of concrete failure is the expansion and penetration of original microcracks until macroscopic cracks are produced, which eventually lead to concrete instability and failure. Fiber can effectively prevent the generation and development of cracks and improve the crack resistance of concrete. The main reason is that when fibers are added to the concrete, they are evenly distributed in the concrete. As a result of fiber and concrete, there is a very strong grasp force; when the crack is further expanded, it can be timely blocked by adjacent fiber, in order to prevent crack expansion and improve the resistance of concrete cracking. The fiber forms a uniform three-dimensional chaotic support system in concrete, which can weaken the plastic shrinkage of mortar and disperse the shrinkage energy to the fiber filaments, thus effectively enhancing the toughness of concrete and reducing the cracks caused by the shrinkage of mortar. At the same time, the formation of uniform chaotic support system can effectively prevent aggregate segregation and ensure the uniform seepage of mortar in the early stage, so as to prevent the formation of settlement cracks. When the concrete bears the larger compression load and crack, the crack tip will produce stress concentration, and the crack will continue to expand under the continuous action of load. When the crack tip intersects with the fiber, the fiber can offset part of the stress and effectively prevent the crack from developing into a penetrating crack. With the decrease of fiber spacing, the stress

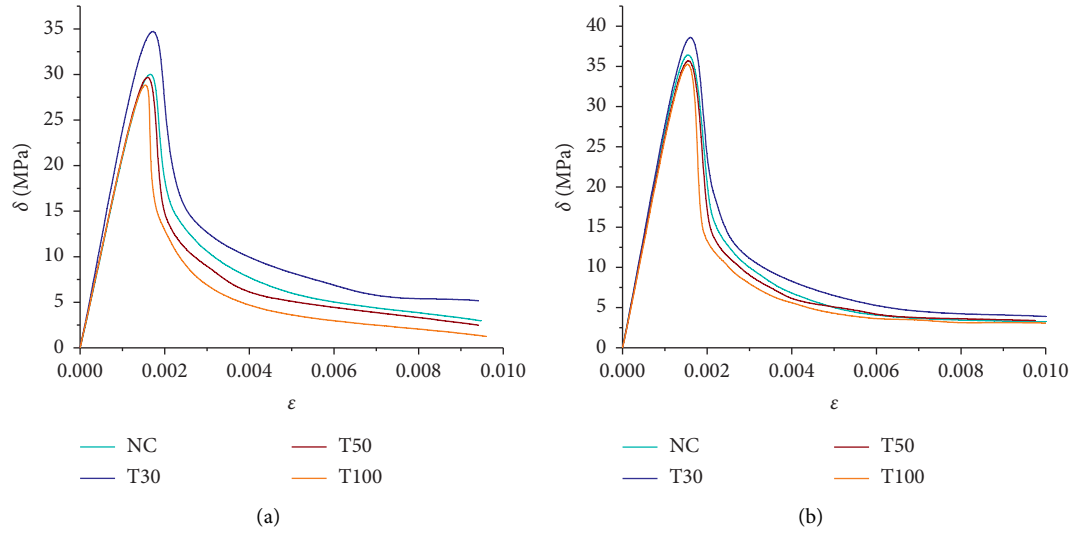


FIGURE 5: Effect of carbonization on the stress-strain curve of iron-added tailings concrete. (a) Carbide 0d. (b) Carbide 56d.

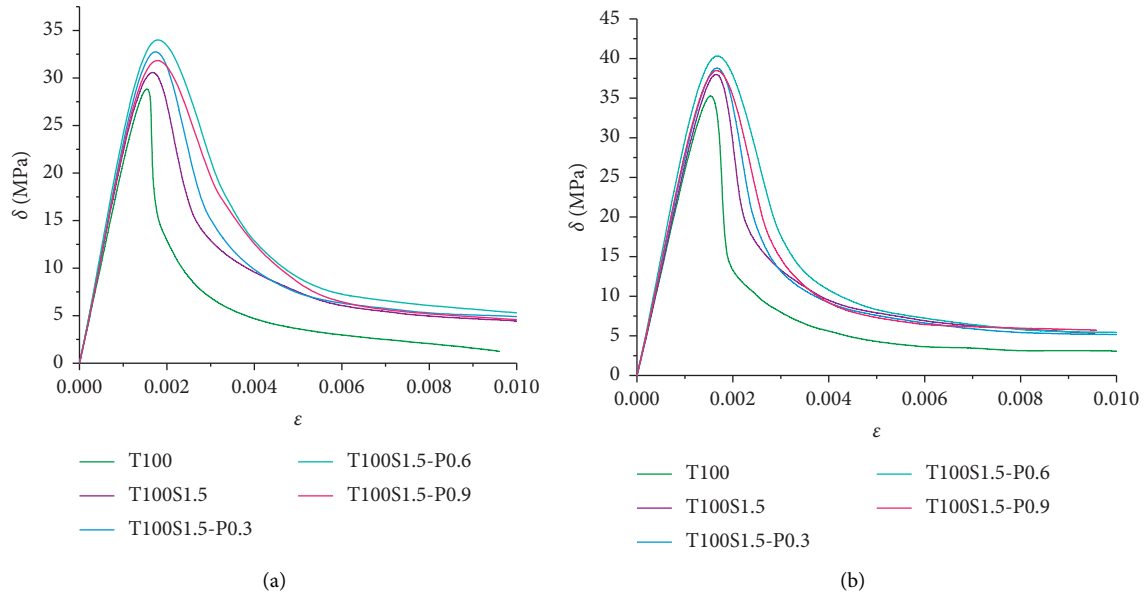


FIGURE 6: Effect of carbonization on the stress-strain curve of fiber reinforced concrete. (a) Carbide 0d. (b) Carbide 56d.

concentration at the crack tip is gradually relieved or even disappears.

3.4. Uniaxial Compression

3.4.1. Stress-Strain Curve. The stress-strain relationship is a key parameter to measure the mechanical properties of concrete, and it is the main basis for analyzing the bearing capacity and deformation of concrete structures. The stress-strain curve of concrete includes an ascending segment and a descending segment, which is a comprehensive macroscopic response of the basic characteristics such as the appearance and development of plastic strain, the generation of microcracks, internal defects and damage, ultimate strength,

residual strength, and deformation. In this paper, the stress-strain curves of concrete in carbonation 0d (28d natural curing) and 56d are studied by adding different performance reinforcing materials, as shown in Figures 5 and 6, respectively.

From Figure 5, the stress-strain curves of the tailings concrete before and after carbonization are essentially the same, with a small change in the ascending section and a large change in the descending section, indicating that the amount of tailings and carbonation has a greater impact on the descending section of the concrete. The descending section of concrete mixed with a small amount of iron tailings is almost the same as that of ordinary concrete. The larger the amount of tailings added, the steeper the descending section. With the increase of the amount of

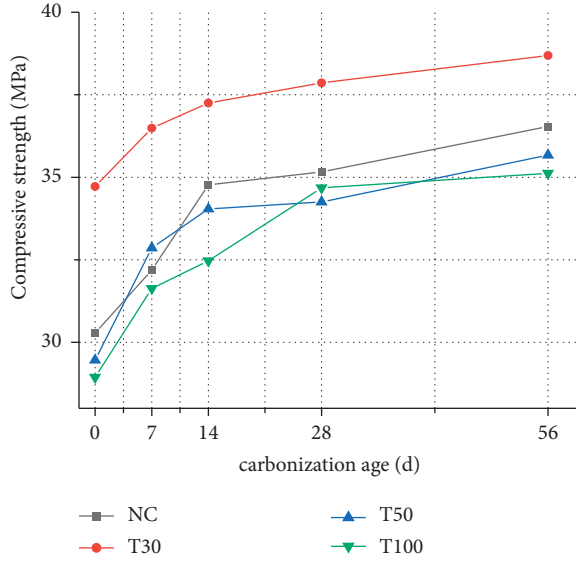


FIGURE 7: Axial compressive strength of iron tailings concrete.

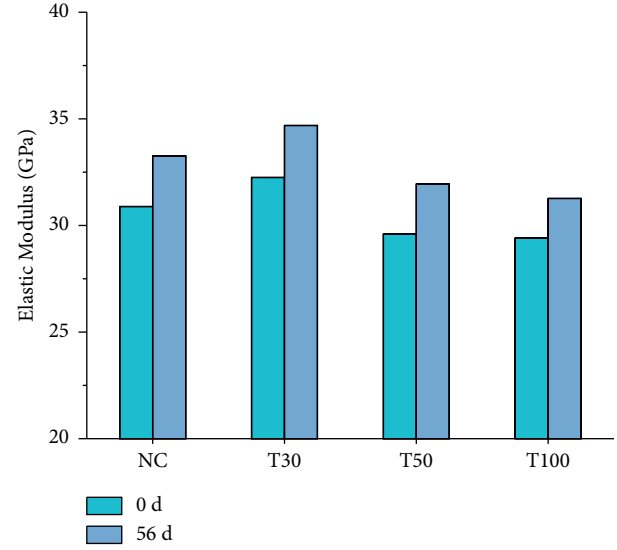


FIGURE 9: Elastic modulus of iron tailings concrete.

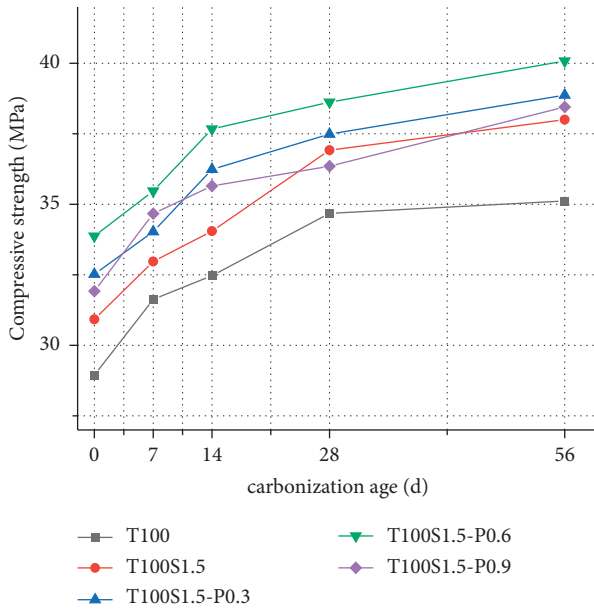


FIGURE 8: Axial compressive strength of fiber reinforced concrete.

tailings, the stiffness of concrete decreases, the ability of resisting elastic deformation weakens, and the brittleness increases. The longer the carbonization period, the steeper the descending section of the curve, indicating that the plastic deformation capacity is reduced and the failure process is more rapid.

It can be seen from Figure 6 that the addition of fibers increases the peak stress, peak strain, and residual stress of the stress-strain curve. Compared with ordinary concrete, the behavior after cracking changes, and the curve after cracking is relatively flat, indicating that the brittleness of the material is reduced and the area of the lower region increases, indicating that more energy can be absorbed. Compared with the single-doped steel fiber, the stress drop

rate of the hybrid fiber after the peak is slower, the residual stress is higher, and the toughness and deformation properties of the specimen are significantly improved, which proves that the PVA fiber has a positive effect on improving the ductility of concrete. With the increase of PVA fiber content, the peak stress decreased slightly, and the slope of the downward branch of the stress-strain curve decreased slightly with the increase of PVA fiber content. Similar to the effect of adding iron tailings, the longer the carbonization period, the steeper the descending section, and the more increased the concrete brittleness.

3.4.2. Axial Compressive Strength. The axial compressive strength of each mix ratio is shown in Figures 7 and 8. Similar to the cube compressive strength discussed previously, the addition of iron tailings and fibers effectively increases the axial compressive strength of concrete, and, with carbonization and the increase of age, the axial compressive strength increases steadily. The strength of tailings concrete increased by 14.7%, -3.3%, and -4.4%, and the strength of fiber concrete increased by 6.8%, 12.4%, 17%, and 10.3%, respectively. It can be seen from the above that the compressive strength of concrete decreases with the increase of PVA fiber content, which is the same as the compressive strength of cubes.

3.4.3. Modulus of Elasticity

(1) Elastic Modulus of Iron Tailings Concrete before and after Carbonization. Figure 9 shows the elastic modulus of iron tailings concrete at different ages before and after carbonization. It can be seen that the elastic modulus of iron tailings increases first and then decreases. The compressive strength of concrete is achieved by homogenizing the constituent materials and their strength. Therefore, the elastic modulus of concrete increases with the increase of concrete strength. The elastic modulus represents the deformation resistance of

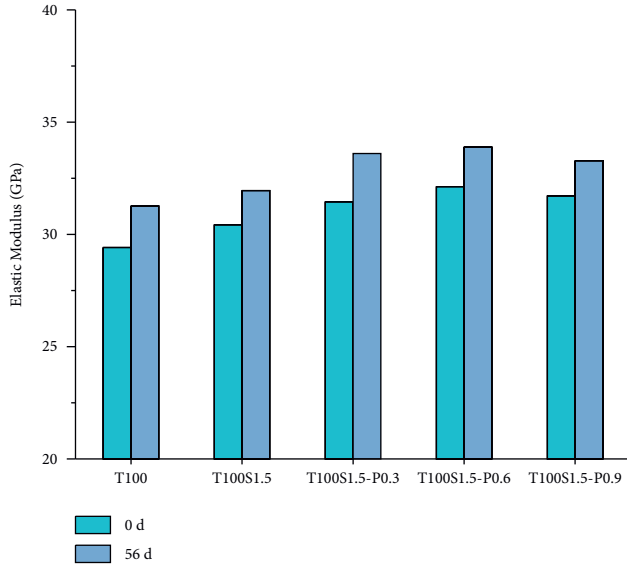


FIGURE 10: Modulus of elasticity of fiber reinforced concrete.

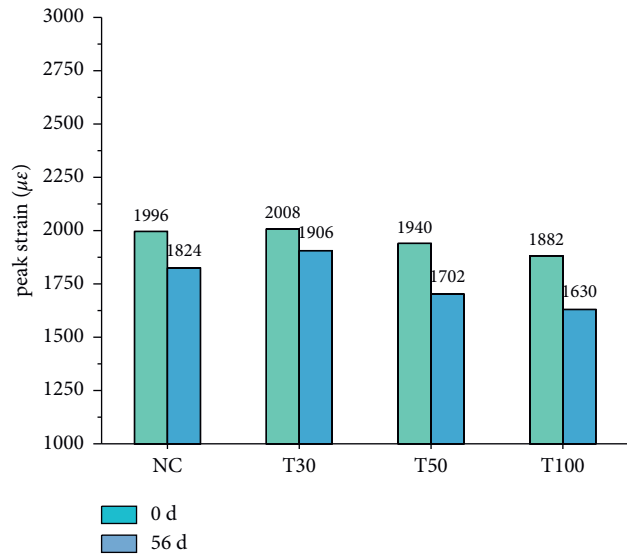


FIGURE 11: Peak strain of tailings concrete.

the material under stress, that is, the stiffness of the material. The addition of tailings reduces the stiffness of the concrete, and the ability of resisting elastic deformation is weakened, resulting in varying degrees of reduction in elastic modulus. With the extension of carbonation age, the elastic modulus of concrete with each mix ratio increases, possibly due to the formation of water-insoluble CaCO_3 in the carbonization process to fill the pores of the concrete and improve the compactness of the concrete, thereby increasing the elastic modulus of the concrete.

(2) *Elastic Modulus of Fiber Reinforced Concrete before and after Carbonization.* Figure 10 shows the elastic modulus of fiber concrete at different ages before and after carbonization. It can be seen that the addition of fibers increases the

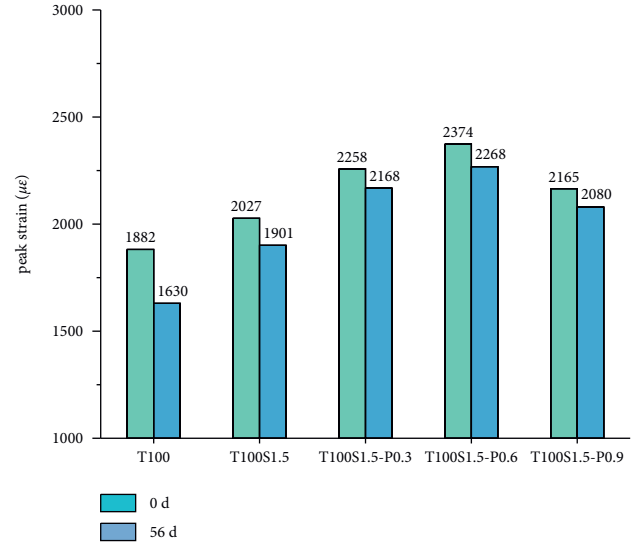


FIGURE 12: Peak strain of fiber concrete.

elastic modulus of concrete. This is because the addition of fibers delays the formation of microcracks, while the elastic modulus decreases with the increase of PVA fiber content, which may be caused by the uneven distribution of excessive fibers in the concrete. When the PVA fiber content was 0.6%, the elastic modulus increased the most, which increased by 11.8%, 10%, and 9.2%, respectively. When the content was 0.9%, the elastic modulus increased by 8.2%, 9.3%, and 7.8%, respectively. Like tailings concrete, with the increase of carbonization age, the elastic modulus of fiber reinforced concrete increases, among which tailings concrete increases the most, followed by single-mixed steel fiber and hybrid fiber. Fiber reinforced concrete has less effect.

3.4.4. Peak Strain

(1) *Peak Strain of Iron Tailings Concrete before and after Carbonization.* Figure 11 shows the peak strain of tailings concrete. It can be seen that the peak strain of ordinary concrete is small, because the mechanical behavior of ordinary concrete is brittle in nature, and the postpeak performance decreases during the compression process due to the limited lateral strain capacity of the material. With the increase of tailings content, the peak strain first increased and then decreased. The addition of low-volume tailings optimizes the internal pore structure of the concrete and slightly increases the peak strain of the concrete. The increase of the tailings content is not conducive to the compact formation of the concrete, which increases the brittleness of the concrete and causes the concrete to break more rapidly, resulting in a decrease in the peak strain. Although the compressive strength of concrete increases after carbonization, the brittleness of concrete increases and the peak strain decreases.

(2) *Peak Strain before and after Carbonization of Fiber Reinforced Concrete.* It can be seen from Figure 12 that the addition of fibers greatly increases the peak strain of concrete

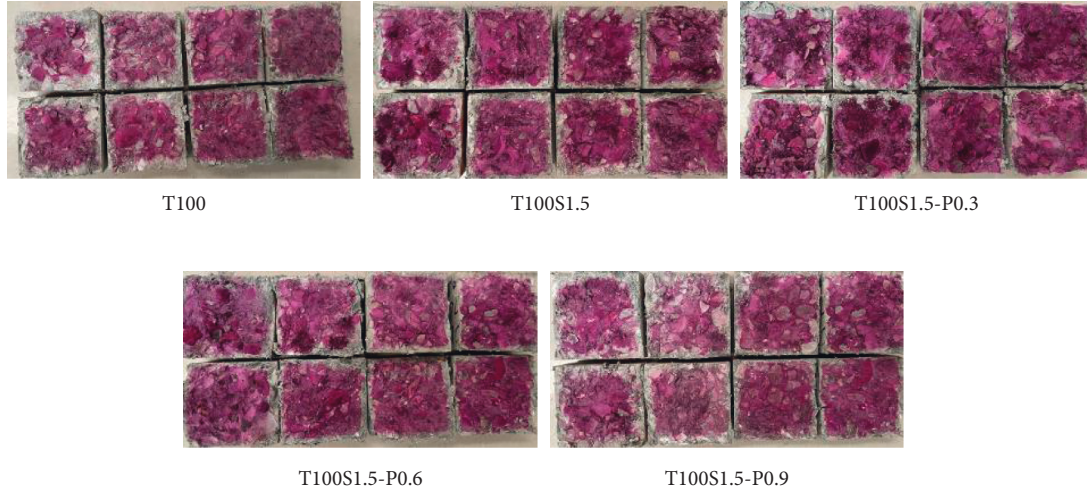


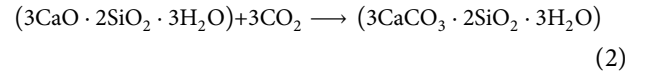
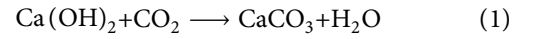
FIGURE 13: Concrete carbonation depth.

and the peak strain reflects the deformation ability of the specimen under the ultimate strength. The main function of fibers is to improve the postcompression performance of concrete, and fibers will continue to prevent the expansion of cracks after the concrete is compressed, so that the concrete can continue to withstand higher strains. In addition, the fibers constrain the formation of axial cracks in concrete and also increase the strain of peak stress significantly. Compared with ordinary concrete, the descending section of the stress-strain curve can act as a bridge and continue to bear the load due to the existence of fibers, so the descending section is more gentle. The peak strains increased by 7.7%, 20%, 26%, and 15%, respectively, because the addition of high-ductility PVA fibers increased the deformation of concrete before the ultimate compressive load and had a positive confounding effect with steel fibers. When the PVA fiber content is 0.9, the peak strain decreases, which may be due to the poor dispersion of more PVA fibers in the matrix.

4. Related Discussion

Based on the test results of deep learning, relevant discussions are mainly made from the carbonation depth of iron tailings concrete and the carbonation depth of fiber reinforced concrete. The main point of view is that, with the increase of carbonization age, the carbonation depth of concrete increases. Moreover, the carbonation depth of concrete also showed a state of first increase and then decrease, but with the increase of PVA fiber content the carbonation depth of concrete increased, showing a decreasing and then increasing trend.

4.1. Carbonation Depth of Iron Tailings Concrete. As shown in Figure 13, with the increase of carbonization age, the carbonation depth of concrete increases. With the increase of iron tailings replacement rate, the concrete carbonation depth first decreases and then increases. When the iron tailings content is 30%, the carbonation depth is the smallest.



Iron tailings are low-activity mineral admixtures with small particle size, which can exert the microaggregate effect, fill the pores between the matrix particles, make the concrete more compact, and be beneficial to the carbonization resistance of the concrete. And iron tailings have potential hydraulic and pozzolanic activity. With the increase of carbonization age, the activity of iron tailings will undergo secondary hydration reaction with $\text{Ca}(\text{OH})_2$, the main hydration product of cement, to generate hydrated silicic acid. Calcium and calcium aluminate hydrate improve the internal pore structure of concrete, thereby improving the compactness of concrete. Another reason may be that iron tailings have higher water absorption than river sand and adding an appropriate proportion of iron tailings reduces the relative humidity inside the concrete, which is not conducive to the entry of CO_2 . With the increase of the replacement rate of iron tailings, the secondary hydration reaction of iron tailings leads to a large consumption of $\text{Ca}(\text{OH})_2$, the hydration product of cement, which reduces the alkalinity of the hydration solution and causes the carbonization and neutralization of the concrete to be shortened, thus making the concrete carbonization and neutralization shorter. The anticarbonation performance decreased.

4.2. Carbonation Depth of Fiber Reinforced Concrete. As shown in Table 6, the addition of fiber significantly improves the carbonization resistance of concrete. The same as the previous law, the carbonization resistance of hybrid fiber is better than that of single-doped steel fiber. With the increase of PVA fiber content, the carbonization depth of concrete shows an increasing trend after decreasing.

The anticarbonation performance of fiber reinforced concrete is mainly reflected in two aspects: filling internal

TABLE 6: Carbonation depth of fiber reinforced concrete.

Test number carbonization age	0	7	14	28	56
T100-S1.5	0	5.3	7.34	8.5	9.7
T100-S1.5-P0.3	0	4.32	6.27	7.58	8.1
T100-S1.5-P0.6	0	3.98	5.52	6.95	7.24
T100-S1.5-P0.9	0	4.77	6.8	8.11	8.36

pores and reducing cracks. After a certain amount of steel fibers are mixed into the concrete, a complex three-dimensional chaotic support system is formed inside the matrix, which inhibits the subsidence of the aggregate and makes the mortar distribution more uniform, thereby improving the compactness of the concrete; at the same time, the steel is distributed in the concrete. The fibers make the capillary pores in the mortar smaller, and the capillaries are thinned or even blocked. In addition, when the concrete shrinks, the steel fiber can bear more shrinkage stress, which enhances the bonding force between the aggregate and the mortar and inhibits the formation of microcracks and the expansion of macrocracks. However, as CO₂ continues to diffuse, it may lead to corrosion of steel fibers, and the formation of rust will destroy the bond between fibers and mortar, thus providing conditions for the penetration and diffusion of CO₂.

Mixing steel-PVA fibers in concrete will further improve the carbonization resistance of concrete. Due to the high density and thick diameter of steel fibers, the spacing of steel fibers in concrete is too large, and the grid effect formed by steel fibers in concrete is weakened. After adding PVA fibers, the fiber spacing becomes smaller, and the fiber network formed by fiber bridging can better hinder the expansion of pores and cracks in the concrete. On the other hand, PVA fiber is a relatively hydrophilic fiber, and a large amount of water will accumulate on the surface of the fiber, which creates conditions for cement hydration, inhibits early plastic shrinkage and drying shrinkage cracks, reduces its cracking temperature, and improves concrete crack resistance.

With the increase of PVA fiber content, a large number of disordered distribution of PVA fibers in concrete will hinder the cement mortar from filling the pores of coarse aggregate, resulting in the increase of pores in the concrete. When the amount of PVA fiber increases, the mortar required to wrap the fiber is relatively reduced, which will cause concrete agglomeration during the mixing process and reduce the density of the concrete. Microscopically, there are weak interfaces intertwined between fibers and concrete. With the increase of fiber content, the number of weak interfaces in concrete increases, which provides conditions for the penetration of CO₂.

5. Conclusion

Based on in-depth learning, this paper studies the mechanical and carbonation properties of concrete with different iron tailings replacement rates, single steel fiber, and mixed steel-PVA fiber concrete. Through the analysis of the test structure, the following conclusions are drawn:

- (1) After adding iron tailings, its compressive strength, splitting tensile strength, axial compressive strength, elastic modulus, and peak strain are enhanced in varying degrees, and the carbonation depth is reduced. With the increase of substitution rate, the performance enhancement effect shows a downward trend, but after the addition of fiber the failure form of concrete presents ductile failure, and its performance has been improved in all aspects.
- (2) Through the existing concrete compressive stress-strain curve equation, the nonlinear calculation of each group of concrete compressive stress-strain curve in this paper is carried out, and some parameters are determined. The calculated results are in good agreement with the experimental results.
- (3) With the increase of carbonation age, its compressive strength, splitting tensile strength, axial compressive strength, elastic modulus, and carbonation depth increase, the peak strain decreases, and the brittleness of concrete increases.

Data Availability

The dataset can be accessed upon request.

Conflicts of Interest

The authors declare that they have no conflicts of interest.

References

- [1] V. C. Li, "From micromechanics to structural engineering-the design of cementitious composites for civil engineering application," *JSCE Journal of Mechanics and Earthquake Engineering*, vol. 10, no. 2, pp. 37–48, 1993.
- [2] T. Kanda and S. Watanabe, *Application of Pseudo Strain Hardening Cement Itious Composites to Shear Resistant Structural Elements in Fracture Mechanics of Conc-Rete Structures Proc.*, D-79104Freiburg Germany: FRAMCOS-3 AEDIFICATIO Publishers, Freiburg, Germany, 1998.
- [3] C. Ren, "Experimental research on high performance concrete admixture of tailing: information engineering research institute, USA," in *Proceedings of the 2016 5th International Conference on Materials Engineering for Advanced Technologies*, ICMEAT, Qingdao, China, March 2016.
- [4] C. Ding, L. Guo, and B. Chen, "An optimum polyvinyl alcohol fiber length for reinforced high ductility cementitious composites based on theoretical and experimental analyses," *Construction and Building Materials*, vol. 259, pp. 119–824, 2020.
- [5] Z. Wang, J. Zuo, X. Zhang, G. Jiang, and L. Feng, "Stress-strain behaviour of hybrid-fibre engineered cementitious composite in compression," *Advances in Cement Research*, vol. 32, no. 2, pp. 53–65, 2020.
- [6] L.-I. Kan, R.-x. Shi, and J. Zhu, "Effect of fineness and calcium content of fly ash on the mechanical properties of Engineered Cementitious Composites (ECC)," *Construction and Building Materials*, vol. 209, pp. 476–484, 2019.
- [7] H. Xiaoyan, R. Ravi, and C. L. Victor, "Feasibility study of developing green ECC using iron ore tailings powder as

- cement replacement,” *Journal of Materials in Civil Engineering*, vol. 25, no. 7, 2013.
- [8] Jci, *JSCE-SF4 Method of Test for Flexural Strength and Ilex-Ural Toughness of Fiber Reinforced concrete* Tokyo: Japan Concrete Institute, Tokyo, Japan, 1984.
 - [9] G. Shan, Z. Guohao, G. Lanhui, L. Zhou, and K. Yuan, “Utilization of coal gangue as coarse aggregates in structural concrete,” *Construction and Building Materials*, vol. 268, 2020.
 - [10] M. Kassem, A. Soliman, and H. E. Nagggar, “Sustainable approach for recycling treated oil sand waste in concrete: Engineering properties and potential applications,” *Journal of Cleaner Production*, vol. 204, 2018.
 - [11] Aci Committee 318, *Building Code Requirements for Structural concrete (ACI 318-95) and Commentary (ACI 318-95)*, Detroit: American Concrete Institute, Farmington Hills, Michigan, 1995.
 - [12] J.-Z. Xiao, J.-B. Li, and C. Zhang, “On relationships between the mechanical properties of recycled aggregate concrete: an overview,” *Materials and Structures*, vol. 39, no. 6, pp. 655–664, 2006.
 - [13] K. E. Loland, “Continuous damage model for load response estimation of concrete,” *Cem, Concre.res*, vol. 10, p. 392, 1980.
 - [14] N. Duy-Lien, T. Duc-Kien, and N. Tri-Thuong, “Weibull modulus from size effect of high-performance fiber-reinforced concrete under compression and flexure,” *Construction and Building Materials*, vol. 226, pp. 226–743, 2019.
 - [15] L. M. Kachanov, *Introduction to Continuum Damage mechanics*, Nijhoff, Netherlands Dordrecht, 1986.
 - [16] S. Z. Kumar and Li Lin, *Material Characterization Techniques*, CRC Press: Boca Raton, Boca Raton, FL, USA, 2008.
 - [17] C. Leech, D. Lockington, and P. Dux, “Unsaturated diffusivity functions for concrete derived from NMR images,” *Materials and Structures*, vol. 36, no. 6, pp. 413–418, 2003.
 - [18] R. Sun, X. Hu, Y. Ling, Z. Zho, P. Zhuang, and F. Wang, “Chloride diffusion behavior of engineered cementitious composite under dry-wet cycles,” *Construction and Building Materials*, vol. 260, no. 11, pp. 43–99, 2020.
 - [19] C. E. T. Matheus, F. F. Jefferson, S. V. Queilla, P. V. Alan, and F. M. Rafael, “Study on the feasibility of using iron ore tailing (iot) on technological properties of concrete roof tiles,” *Construction and Building Materials*, vol. 279, 2021.
 - [20] J. S. Zhao, K. Ni, Y. P. Su, and Y. Shi, “An evaluation of iron ore tailings characteristics and iron ore tailings concrete properties,” *Construction and Building Materials*, vol. 286, 2021.
 - [21] B. Karthikeyan, R. Kathyayini, V. Aravind Kumar, V. Utra, and S. K. Selvarj, “Effect of dumped iron ore tailing waste as fine aggregate with steel and basalt fibre in improving the performance of concrete,” *Materials Today Proceedings*, vol. 46, no. 17, 2021.
 - [22] F. Xu, S. L. Wang, T. Li, B. Li, T. Liu, and Y. Zhou, “Mechanical properties and pore structure of recycled aggregate concrete made with iron ore tailings and polypropylene fibers,” *Journal of Building Engineering*, vol. 33, 2021.

Research Article

Novel High-Efficiency Nanocomposite Gate Design of Quantum-Dot Cellular Automata Based on Deep Learning

Yourun Zhu , **Senlin Ren**, and **Xiaolong Li**

College of Electronic Information, Jiangsu University of Science and Technology, Zhenjiang, Jiangsu 212100, China

Correspondence should be addressed to Yourun Zhu; 192030055@stu.just.edu.cn

Received 21 April 2022; Revised 10 May 2022; Accepted 16 May 2022; Published 8 June 2022

Academic Editor: Dong Chen

Copyright © 2022 Yourun Zhu et al. This is an open access article distributed under the Creative Commons Attribution License, which permits unrestricted use, distribution, and reproduction in any medium, provided the original work is properly cited.

With the development of science and technology, the feature size of CMOS devices will always shrink to the limit. Therefore, some new nanodevices will eventually become substitutes for microelectronic devices. A new electronic revolution will break out. Nanoscience and technology is the high-tech frontier technology of the century and one of the main contents of scientific development in the new era. Its development will have a profound impact on other disciplines, industries, and society. Nanoelectronics is an important part of the discipline of nanoscience and technology, which represents the development trend of microelectronics and will become the foundation of the next generation of electronic science and technology. With the development of ultra-large-scale integrated circuits, the feature size of electronic devices is getting smaller and smaller and has entered the nanoscale from the microscale. When the size of the system is small enough to be compared with the wavelength of electrons, the quantum effect becomes the dominant current-carrying main factor in child behavior. While these new phenomena and new effects bring challenges to the original semiconductor devices, they also provide opportunities for the development of new devices. Evolutionary circuit design is based on cellular neural network and quantum-dot cells, designs combinational logic circuits through the evolutionary algorithm, uses the logic gate based on cellular neural network design as the population gene of evolutionary circuit design, enriches the diversity of the population, and improves the evolutionary algorithm at the same time, the success rate of the improved genetic algorithm for evolutionary circuits has been greatly improved, and the failure rate has been reduced from 14% to 2%, obtaining a faster evolution speed and improving the performance of the evolution circuit.

1. Introduction

In the nineteenth century, scientists discovered silicon experimentally and then began a wide range of research and applications, including the preparation of crystalline silicon and the exploration of its applications. Silicon is a special material with both metallic and nonmetallic properties, that is, a semiconductor material in the usual sense. Its discovery and research play a crucial role in the emergence and continuous development of integrated circuits. Nanotechnology is the science and technology of using atoms or molecules with a scale of 0.1 to 100 nm to manufacture substances, and nanoelectronics is the science of studying nanodevices. At present, due to the characteristics of new physical theories and unique working methods, nanoelectronics technology has caused extensive research in academia. The main purposes of studying nanoelectronics

are to explore more advanced manufacturing technology to break through the physical size and technical limits of devices under traditional processes and then to prepare new nanomaterials and nanodevices with brand-new functions and, similar to traditional circuits, to explore nanodevices applications in the construction of electronic systems, thereby greatly improving the level of information storage and processing in electronic systems. The different-plane crossing in the current QCA circuit solves the problem of signal crosstalk caused by coplanar crossing, but it is quite difficult to physically realize the different-plane crossing. At present, there is no actual experimental result to realize the different-plane crossing special physical structure. The advantages and disadvantages of the evaluation circuit in the classic circuit can be evaluated by the number of devices, power consumption, and other evaluation criteria, but the QCA circuit is still an immature research content, and its

evaluation criteria have not been unified. At present, there are only complexity, delay, area, power consumption, and other factors that determine the merits of this QCA circuit. Although these evaluation criteria are still very simple, a comprehensive evaluation of the overall performance of the circuit has not been made, and large-scale mass production is still difficult. Among all nanodevice research, QCA is considered to be the most promising new generation of new nanoelectronic components [1–8].

2. Related Work

Quantum-dot cellular automata (QCA) were first proposed in 1993 by Lent et al. Since QCA was proposed, it has received extensive attention and research from domestic and foreign researchers. In the QCA circuit, the core idea of studying the QCA circuit is to use the special properties and unique rules of the QCA itself to realize various unit devices and large-scale circuits in the classical circuit. Different from the basic logic gates in the classical circuit, QCA mainly realizes the circuit by the multiple gate, the NOT gate, and the derivative gate of the multiple gate. Since the two most typical circuit structures of the NOT gate are fixed, while the majority gate and the crossover are not fixed, the two structures are converted into corresponding structures according to the needs of the circuit structure. At present, the research on three-input and five-input majority gates is more extensive, and most of the majority gates used in circuits are these two structures. For example, Dharmendra Kumar et al. published in *Microelectronics Journal* 2016 a fault-tolerant majority gate that not only occupies a small area but also has incredible reliability; Sen et al. in the *Journal of 2016 Computational Electronics* has published a majority gate implemented by rotating cells, and the fault tolerance rate is close to 100% even in the case of a missing cell. In addition, when reducing circuit complexity, a five-input majority gate is a better choice. For example, Shadi Sheikhfaal et al. published a five-input multiple gate with low energy consumption and low complexity in *Microelectronics Journal* in 2015, and the use of the five-input multiple gate to realize the XOR gate can simplify the overall. Therefore, when a large-scale circuit is realized based on the exclusive OR gate, the complexity of the circuit is reduced. Sankit Kassa et al. proposed a five-input majority gate with the lowest complexity so far in the *Journal of Computational Electronics* in 2016 and published the verification of the physical calculation process. The above is a demonstration of the research results of the majority gate of the basic device, and then the majority of scientific researchers have launched the research and design of combinational logic circuits; for example, adders, comparators, subtractors, dividers, and other circuits have been designed and implemented. In 2006–2008, Huang et al. successively published the design concept based on orthogonal modules in the *Journal of Electronic Testing-theory and Applications and Proceedings of the 18th ACM Great Lakes Symposium on VLSI* and realized 2–4 lines decoder, and the fault tolerance performance is also theoretically analyzed on this decoder. High-bit current-carrying adders and multipliers were published

by Cho et al. in 2009, and the advantages compared with the previous adders and multipliers were analyzed in detail. Until today, many QCA circuits designed using quantum cellular automata have been theoretically confirmed and experimentally tested. QCA circuit design has also become a key research branch of nanoelectronics, and many classic circuits such as adders, multipliers, and flip-flops have been transplanted into QCA circuits. Throughout the development of nanoelectronics technology, its technological development is based on novel physical theories and guided by the most advanced process technology. The development of electronic technology needs to break through the bottleneck of traditional physical size and technical limits, develop the structural potential of substances, and develop nanodevices with brand-new concepts. According to the current development of nanoelectronic technology, there are two main research approaches for nanoelectronic devices: one is new nanoelectronic devices such as resonant tunnel diodes, single-electron transistors, carbon nanotubes, and quantum cellular automata. The second is the assembly of molecules to form devices with certain functions, such as organic thin films and transparent oxide thin-film transistors. Although there has been a lot of progress in the design and research of QCA circuits in recent years, there are still many problems, such as the degradation of the stability of the QCA circuit caused by the coplanar cross-linking of the lines and the division of clock regions in the QCA circuit. Although there are still many problems, quantum cellular automata are still considered to be one of the next-generation electronic components with the most potential to replace CMOS technology [9–15].

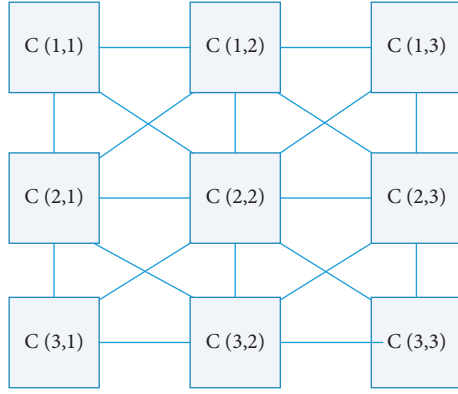
3. Related Theoretical Methods

3.1. Cellular Neural Network. The structure of the cellular neural network is similar to cellular automata, each neuron is only connected to its surrounding neurons, and information can be directly transmitted between adjacent cells. They are not directly connected but can influence each other indirectly. The figure shows a two-dimensional cellular neural network. In theory, we can define cellular neural networks of any dimension but usually focus on the two-dimensional case and its application in image processing, as shown in Figure 1 [16].

For example, an $M \times N$ cellular neural network has $M \times N$ neurons, arranged in M rows and N columns; we can express the neurons in the i -th row and the j -th column as $\text{cell}(i, j)$, abbreviated as $C(i, j)$; the cell neuron in its neighborhood is defined as

$$N_r(i, j) = \{C(k, l) | \max\{|k - i|, |l - j|\} \leq r, 1 \leq k \leq M; 1 \leq l \leq N\}. \quad (1)$$

A cellular neural network is a spatial array of locally coupled cells, each of which is a dynamical system. It consists of input variables, output variables, and state variables that change according to some prescribed dynamic laws. To be precise, it consists of two mathematical elements. (1) It consists of a spatially discrete collection of continuous

FIGURE 1: A 3×3 CNN structure diagram.

nonlinear dynamical systems called cells, where each cell is loaded with information through input variables, initial states, and thresholds. (2) Each cell is centered on its own and is connected with all other cells within the radius of the sphere of influence through a coupling law.

3.2. QCA Cells. The basic device unit of the QCA circuit is the cell, and the cell is the basic device of the circuit, so the basic research on the circuit is the research on the cell. In the research field of QCA, first of all, from the perspective of the composition mechanism of the cell, among the currently known cells, a single cell is usually composed of two or four or five or six or even eight quantum dots and free electrons, which is the basic composition of the cell [17]. Furthermore, from the perspective of circuit operation mechanism, free electrons tunnel between quantum dots to realize information transmission, such as a five-quantum-dot cell, removing the central quantum dot, and the remaining four quantum dots are composed of four-quantum-dot cells., the operation mechanism of the two is the same, but the four-quantum-dot cell is more suitable as the basic cell of the QCA circuit, and the five-quantum-dot cell is suitable for calculating the kink energy between quantum dots. Although the above five cell structures look similar in shape, they have the same structural form, and the common point is that they all have bistable characteristics, which ensures that the cell can transmit signals correctly and effectively and effectively avoid it to solve the problem of signal weakening and crosstalk.

3.2.1. Four-Quantum-Dot Cell. A standard QCA cell of four quantum dots is mainly composed of quantum dots, electrons that can move freely in the quantum dots, and a tunnel structure. But their actual structure depends on the specific implementation. The earliest experimental verification was the cell composed of silicon-based metal semiconductors. In a standard four-quantum-dot cell, two electrons that move freely in the quantum dot can be accommodated. However, due to the high potential barrier height between cells, it is impossible for electrons to tunnel between cells, and the range of electron activity is regulated within a cell. Two free electrons tend to occupy two quantum dots on the diagonal

under the Coulomb interaction. There are only two states on the diagonal in the cell. These two states are stable and unique. The two states of the cell are the characterization of the cell in the polarized state; that is, the polarizability $P = 1$ or $P = -1$, respectively, represents the “1” and logical “0” of binary information, as shown in Figure 2. This can be obtained using the polarization calculation formula, such as equation (1). In the formula, p_1 to p_4 represent the potential energy occupied by each quantum dot, respectively [18].

$$P = \frac{(P_1 + P_3) - (P_2 + P_4)}{P_1 + P_2 + P_3 + P_4}. \quad (2)$$

3.2.2. Five-Quantum-Dot Cell. In Figure 3, the five-quantum-dot cell has one more quantum dot in the center than the four-quantum-dot cell, and we number it as 0. In order to calculate the kink energy between the quantum dots, the polarity of the cell can be calculated. Since the five-quantum-dot cell and the four-quantum-dot cell are the same, they also contain two free electrons. Since there is a quantum dot in the center of the five-quantum-dot cell, the free electrons can be transmitted diagonally, thus realizing diagonal quantum dot tunneling, which is lacking in four-quantum-dot cells. When there is no external magnetic field or electric field in the cell, the free electrons are distributed probabilistically in the five quantum dots of the cell. When there is an external magnetic field or electric field, the two free electrons show a diagonal distribution state in the cell due to the action of the external force, that is, the two cell polarization states of the above four quantum dots, which is the polarization of the cell. Its polarity calculation formula is shown in [19]

$$P = \frac{(P_1 + P_3) - (P_2 + P_4)}{P_0 + P_1 + P_2 + P_3 + P_4}. \quad (3)$$

3.3. QCA Basic Device Unit

3.3.1. Transmission Line. Transmission lines are indispensable in QCA circuits and play an extremely important role. The same or opposite information transmission is required between devices. Therefore, almost every circuit must have the participation of transmission lines. Therefore, the study of transmission lines is also particularly important, but transmission lines are also relatively simple; it has two transmission forms, namely, straight transmission line and angled transmission line, specifically as shown in Figure 4 [20].

When simplifying the circuit and reducing the area occupied by the circuit, the right-angle transmission line is a transmission line that must be considered. The right-angle transmission line plays a role in the information transmission of the devices in the horizontal and vertical directions. Figure 5 is a schematic diagram of a right-angle transmission line.

Angled transmission lines are often used in QCA circuits to connect two devices that are not on the same line.

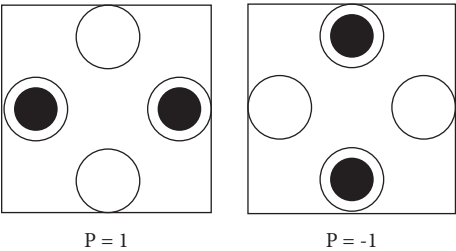


FIGURE 2: Cells in two polarization states.

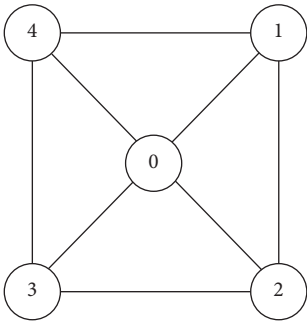


FIGURE 3: Five-quantum dot cell.

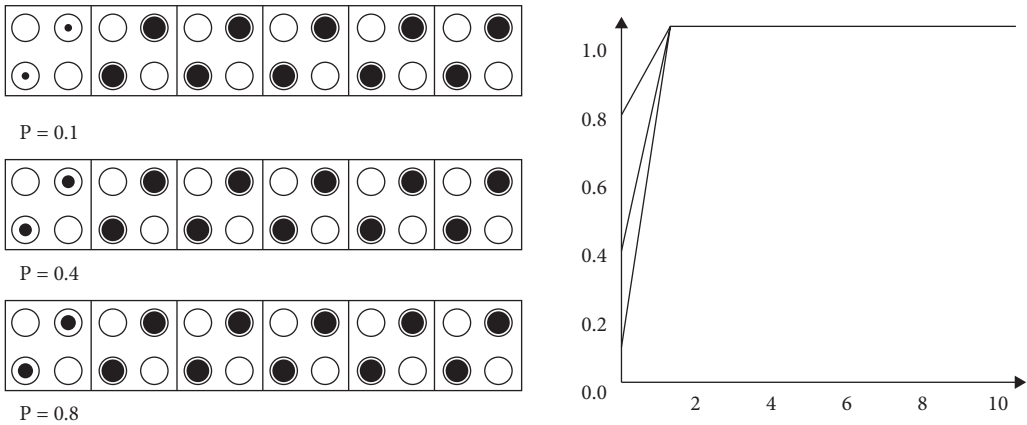


FIGURE 4: Transmission line polarization diagrams with different polarity inputs.

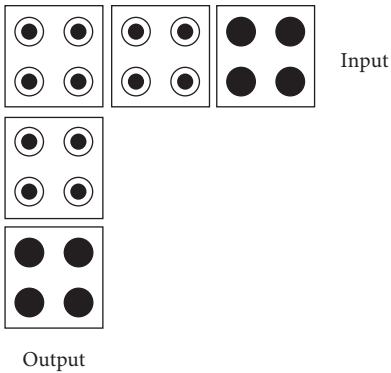


FIGURE 5: Schematic diagram of the right-angle transmission line.

Sometimes, the use of angled transmission lines in circuit design will reduce the circuit area. The polarity of the cells does not change during transmission. In addition, fan-out transmission lines are used when multiplexed signals are required. Sometimes, an input signal can be used by several devices, which has to consider the fan-out transmission line, which serves as an input signal that can transmit the same signal in different directions at the same time, and the fan-out transmission line has such a function. In the QCA circuit, the fan-out transmission line has the following two structures. Figure 6(a) shows a three-fan-out transmission line; Figure 6(b) shows a two-fan-out transmission line.

3.3.2. Inverter. The inverter plays a vital role in the QCA circuit. Although there are only three structures of the inverter, the choice is very flexible when choosing its construction circuit, because it greatly simplifies the complexity of the QCA circuit degree and area, and the structure of the circuit tends to be simple. Its structure is shown in Figure 7. The following three structures are briefly analyzed.

3.3.3. Three-Input Multiple Gate. The QCA circuit is superior to the classical CMOS circuit. Another reason for the device is that the QCA circuit can realize the multigate structure with the least number of cells, which cannot be achieved in the CMOS circuit. Then, the multigate plays a very important role in the QCA circuit. It is a very important logic device in the QCA circuit. Figure 8 is the cell diagram of the three-input majority gate and the logic diagram of its classical circuit.

4. Evolutionary Circuit Design Based on Cellular Neural Network

The circuit structure of the basic logic function of the cellular neural network is similar, and the logic function corresponding to different parameters is also different, which determines the reconfigurability of the cellular circuit. Using this property combined with the intelligent algorithm can constitute the two elements of the evolutionary circuit design. This paper mainly studies the evolutionary circuit design based on a cellular neural network and evolves the combinational logic circuit by improving the genetic algorithm.

4.1. Evolutionary Circuit Design Algorithm. Traditional circuit design depends on the knowledge reserve, ability, and experience of developers and the progressiveness of the design platform. When a circuit is successfully designed, its hardware circuit structure is fixed and cannot be modified. If we want to design other circuits, we need to rebuild their circuit structure, which is cumbersome and expensive. Therefore, Friedman first proposed the idea of studying evolutionary combinational logic circuits in his paper in the 1950s. He mainly proposed an idea to evolve a series of control circuit units through a “selective feedback” similar to the neural network. In the 1990s, the idea of applying this evolutionary design to circuits was called evolvable hardware (EHW).

The application of evolvable hardware enables researchers to deal with the design of more complex circuits without relying on prior knowledge and evolves design schemes that researchers cannot think of. Evolvable hardware refers to a system that uses intelligent algorithms, such as genetic algorithm (GA), evolutionary strategy (ES), particle swarm optimization algorithms (PSO), and genetic programming (GP) [30], to automatically design circuits, including reconfigurable hardware and intelligent algorithms. Evolutionary hardware has a wide range of research fields, including digital filter design, function level image filter design, robot controller design, equalizer design, combinational circuit design, sequential circuit design, embryonic electronic system design, fault-tolerant system design, analog circuit design, and polymorphic circuit design.

Evolvable hardware has two evolution situations. The first is to design circuits based on existing electronic components, such as basic components (triode, FET, resistance, inductance, and capacitance) and basic logic gates (and gate, or gate and not gate). Among them, using logic gate circuit as population design, the combinatorial logic circuit is called evolutionary circuit design. This paper studies evolutionary circuit design based on the logic gate.

The second is to find the optimal parameters of the circuit; for example, the design of a digital filter and equalizer is to find the optimal parameters fundamentally. For example, in the evolutionary design of analog circuits, when the framework of the circuit has been determined, and the important goal of its evolution is the parameters corresponding to the components, this goal is also called the design of evolutionary hardware.

At present, the main problem faced by evolutionary circuit design is scalability. Scalability is an important reason why evolvable hardware is difficult to be applied to practical engineering. It is mainly reflected in that when the input increases, the evolutionary scale increases and the time spent increases rapidly. At the same time, evolutionary algebra also increases rapidly because of the expansion of the scale of the problem. Therefore, the evolutionary ability decreases accordingly, so satisfactory results can not be obtained. At present, there are four main methods to solve the above problems: optimization of evolutionary algorithm, decomposition of input problem, improvement of “genotype-phenotype” mapping relationship, and taking function level module as the basic construction unit. The first method and the third method can partially solve this problem, and the fourth method has a certain improvement. At present, the second decomposition method is relatively good, but it requires too many resources. In general, scalability is a long-standing problem, which needs further research.

The evolution of combinational logic circuits using genetic algorithms first came from Louis’ research. He combined the knowledge content of circuits with a genetic algorithm and used a masked Crossover Genetic operator to replace the classical crossover operator to optimize the evolution process. Although it can not completely solve the design problem of combinational circuits, the results also opened up a new development direction for researchers.

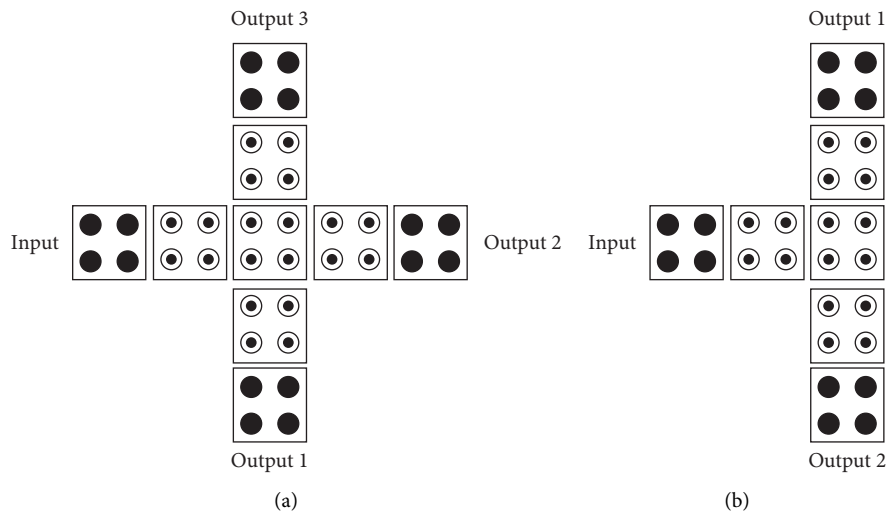


FIGURE 6: Three- and two-fan-out cables.

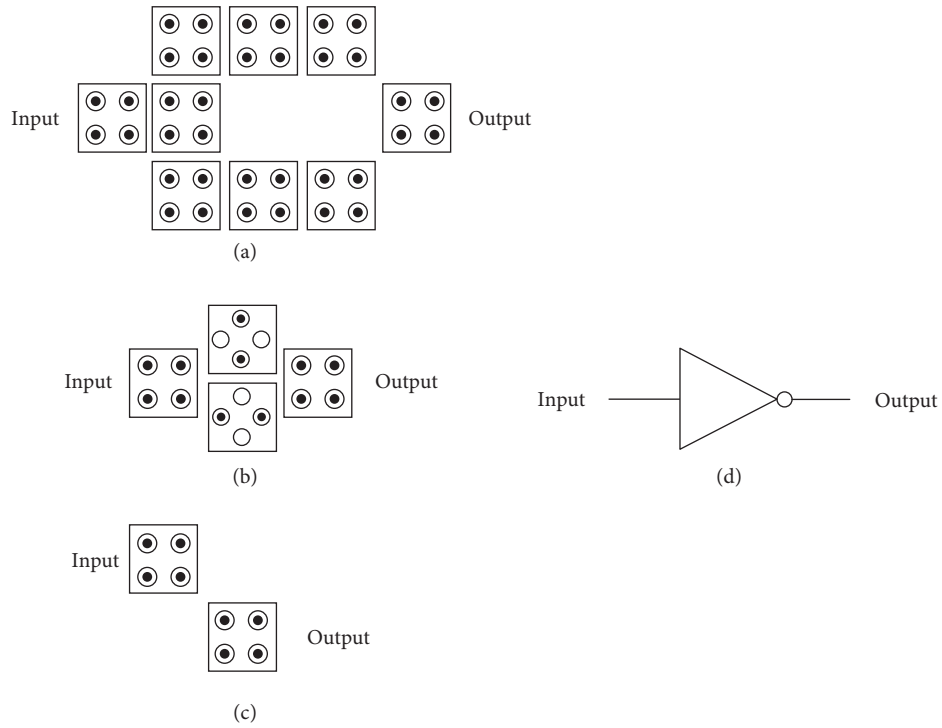


FIGURE 7: Inverter.

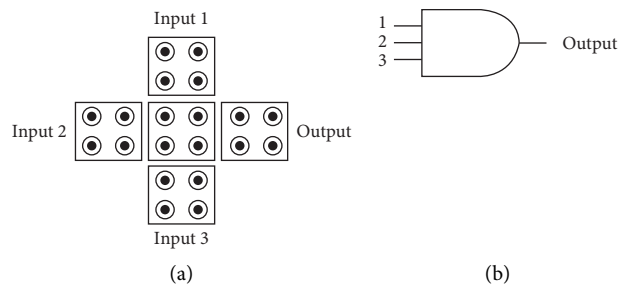


FIGURE 8: Three-input multiple-choice gate. (a) Cell diagram. (b) Logical diagram.

The genetic algorithm is a very important intelligent algorithm for computer simulation of biological behavior. It can be used for the optimization of complex systems. It has the following characteristics:

- (1) Genetic algorithm realizes pure mathematical operation by coding the problem. In particular, for problems that cannot be expressed by numerical values, the way of coding processing shows its advantages.
- (2) Genetic algorithm only converts the objective function into a fitness function and then carries out genetic and mutation operations on the fitness function without the help of other information and derivation. On the one hand, it reduces the complexity of the operation; on the other hand, it improves search efficiency.
- (3) Genetic algorithm has the characteristics of parallelism. The traditional optimization algorithm starts from a certain point for the iterative search. The single-point search contains less information; the search efficiency is low and even easy to fall into local optimization. The genetic algorithm starts from the whole population, which is composed of multiple individuals rather than a single individual. When the genetic operator operates on each generation of the population, it will produce a new generation of population, and there is an interactive relationship between individuals in the population. This information can be used by the genetic algorithm. Therefore, it is equivalent to searching multiple points at the same time, which speeds up the search speed.
- (4) The probability genetic algorithm is used. The operations of genetic operators are carried out under a certain probability, and the mutual transfer between search points is uncertain, which increases the diversity of individuals in the process of algorithm and avoids being limited to local optimization.

Using the characteristics of the circuit and genetic algorithm, the process of evolutionary circuit design is to encode the structure and parameters of the circuit, calculate its fitness function value, and observe whether the fitness value meets the requirements. If it meets the requirements, the process can be ended. Otherwise, according to the fitness value, carry out a series of operations such as cross mutation on individuals, and then repeat the above process. If the set maximum evolutionary algebra is reached in this process, the algorithm will be terminated. The coding methods include direct coding and indirect coding. This paper adopts indirect coding, which corresponds to the external evolution method. When the evolved circuit individual meets the requirements, the circuit structure corresponding to the coding is restored.

4.2. Improved Genetic Algorithm for Evolutionary Circuit Design

4.2.1. Improvement of Selection Operator. A selection operator commonly used in basic genetic algorithms is the

roulette selection operator. Due to the large selection error of the roulette wheel, degeneration sometimes occurs; that is, individuals with high fitness lose the opportunity to choose, making it difficult for the algorithm to converge to the optimal solution. Based on this, some scholars proposed a multi-round roulette selection operator, let M be the population size, the fitness of each individual i is F_i , and the selection probability calculated according to the fitness of these M individuals is $[0, 1]$ divided into M intervals, $\xi_1, \xi_2, \dots, \xi_M$ which are M integers, which, respectively, represent the number of random numbers in these M intervals. The algorithm performs multiple rounds of roulette selection. During the multi-round roulette selection process, the generated M random numbers are used for one round of selection, and the ξ values of each interval are counted to obtain $\xi_1, \xi_2, \dots, \xi_M$, and take the maximum ξ value. The individual corresponding to the interval is the individual selected in this round, and the above operation is repeated M times to obtain M individuals.

In the above algorithm, the selection of each individual needs to perform M roulettes, and each generation of individuals needs to perform M^2 roulettes. Although this method reduces the randomness of the selection, it reduces the evolution speed. Through the analysis, it can be seen that when the differences between individuals are relatively large, the use of multiple rounds of roulette selection can reduce the randomness. When the difference between individuals is relatively small, the advantage of multi-round roulette selection is not significant, and since the number of roulette selections M is unchanged, it will greatly reduce the population evolution speed. Therefore, the number of multi-round roulette selections can be appropriately reduced to increase the speed of evolution. Based on the above analysis, this paper proposes an improved multi-round roulette selection operator; that is, the number of roulette rounds in each round changes with the variability of individuals. The specific number of roulettes is determined by the following formula:

$$m = \left\lceil M \left(1 - \frac{F_{\text{avg}}}{F_{\text{MAX}}} \right) \right\rceil + 1, \quad (4)$$

where m is the number of roulettes in each generation, M is the population number, F_{avg} is the average fitness value of the current generation population, F_{max} is the highest fitness value of the current generation individual, and $\lceil \cdot \rceil$ means rounding. Through this method, the number of roulette selections can be dynamically adjusted, which increases the evolution speed while reducing randomness.

4.2.2. Improvement of Crossover Operator. In the basic crossover operation, individuals in the population use a fixed crossover probability for the crossover operation. However, this method of fixing the crossover probability has certain defects. As the crossover probability increases, the frequency of gene exchange between individuals also increases. However, when the crossover probability is too large, the genes of individuals with high fitness inherited will be more likely to be destroyed; if the crossover probability is too

small, the frequency of gene exchange between individuals will be reduced, and the diversity of the population will be reduced, which is not conducive to jumping out local optimum. In the process of genetic evolution, the population is always changing, and the fixed crossover probability cannot adapt to the changing population. Therefore, this paper proposes a crossover operator that dynamically adjusts the crossover probability. The specific adjustment formula (5) of the crossover probability is

$$P_c = P_{c1} - (P_{c1} - P_{c2}) \times \left(\frac{F_{\text{avg}} - F_{\text{min}}}{F_{\text{max}} - F_{\text{min}}} \right). \quad (5)$$

In the formula, P_c represents the actual crossover probability, $P_{c1}=0.9$, $P_{c2}=0.4$, F_{avg} represents the average fitness value of all individuals in the current generation population, F_{max} is the highest fitness value of the current generation individual, and F_{min} is the current generation individual minimum fitness value. From the analysis of the formula, it can be seen that when the gap between the average fitness of the population and the minimum fitness value is larger, it means that the population as a whole is concentrated near the maximum fitness value, and there are many excellent individuals. In crossover probability, when the gap between the average fitness of the population and the minimum fitness value is smaller, it means that the population as a whole is concentrated near the lowest fitness value. At this time, there are few excellent individuals, and the crossover probability should be increased to generate more excellent individuals. By adopting a crossover operator that dynamically adjusts the crossover probability, it can tend to generate more excellent individuals in order to achieve the global optimum.

4.2.3. Improvement of Mutation Operator. In the basic mutation operation, individuals in the population use a fixed mutation probability for mutation operation. However, this method of fixing the probability of mutation has certain drawbacks. When the mutation probability is too large, the excellent individuals in the population are easily destroyed; when the mutation probability is too small, it is not conducive to jumping out of the local optimum. Therefore, this paper proposes a mutation operator that dynamically changes the mutation probability, which is determined by the following formula:

$$P_m = P_{m1} - (P_{m1} - P_{m2}) \times \left(\frac{F - F_{\text{min}}}{F_{\text{max}} - F_{\text{min}}} \right). \quad (6)$$

In the formula, P_m represents the actual mutation probability, $P_{m1}=0.1$, $P_{m2}=0.001$, F represents the fitness of the current individual, F_{max} is the highest fitness value of the current generation individual, and F_{min} is the lowest fitness value of the current generation individual. It can be seen from the formula that the larger the individual fitness is, the smaller the mutation probability is, and the easier it is for the excellent individual to be retained; the smaller the individual fitness is, the

larger the mutation probability is, and the easier the population is to jump out of the local optimum. By using a mutation operator that dynamically adjusts the mutation probability, the population can be kept from falling into the local optimum while retaining excellent individuals, and finally, the global optimum can be achieved.

4.3. Analysis of Experimental Results. The Ackley function is used as the objective function, and the function has a minimum value, but the genetic algorithm used in this paper operates on the principle that the larger the fitness value, the better, so it is necessary to convert the minimum value of the objective function to the maximum value of the fitness function and, at the same time, consider the selection. The operator requires that the fitness values are all positive numbers, so the fitness function is selected as

$$F = 20 - \text{ACKley}(x_1, x_2). \quad (7)$$

When $(x_1, x_2) = (0, 0)$, the Ackley function obtains the minimum value of 0, and the fitness function obtains the maximum value of 20 at this time. The value range of x_1 and x_2 is $[-10, 10]$. At this time, the maximum value of the Ackley function does not exceed 20. Therefore, the fitness function takes 20 and the inverse of the function to ensure that all fitness values are positive numbers. In the genetic algorithm, the population size is 50, and the terminating evolutionary generation is 100. In the basic genetic algorithm, the roulette selection method is used as the selection operator, the single-point crossover is used as the crossover operator, and the nonuniform mutation is used as the mutation operator. Select a fixed value of 0.7 for crossover probability and 0.01 for mutation probability. From this, the change curve of the fitness function can be obtained as shown below. In the 100th iteration, $x_1=0.0147$, $x_2=-0.1026$, and the corresponding optimal fitness value is 19.4440.

It can be seen from the fitness value curve in Figure 9 that the basic genetic algorithm is not easy to retain the optimal individual, the fitness value oscillates obviously, it is easy to fall into the local optimum, and the convergence accuracy is poor. The values of the variables x_1 and x_2 corresponding to the fitness function are shown in the following figure. It can be seen from Figure 10 that there are many value points near the value $(0, 0)$ range, but they have not converged to one point. The center of the circle in the figure is the location of the optimal value $(0, 0)$. The nearby values are not completely concentrated in the circle and are scattered around the circle so that the optimal value cannot be obtained. Therefore, it proves the poor convergence of the basic genetic algorithm.

Apply the improved genetic algorithm to the Ackley function by setting the operator parameters of the genetic algorithm. Also take the population size as 50 and the number of termination iterations as 100. The fitness curve of the improved genetic algorithm can be obtained as shown below, in which, at the 100th iteration, $x_1=0.0049$,

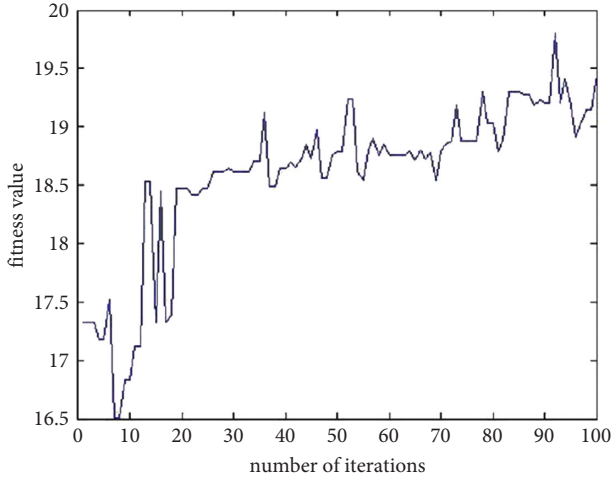


FIGURE 9: Basic genetic algorithm fitness curve.

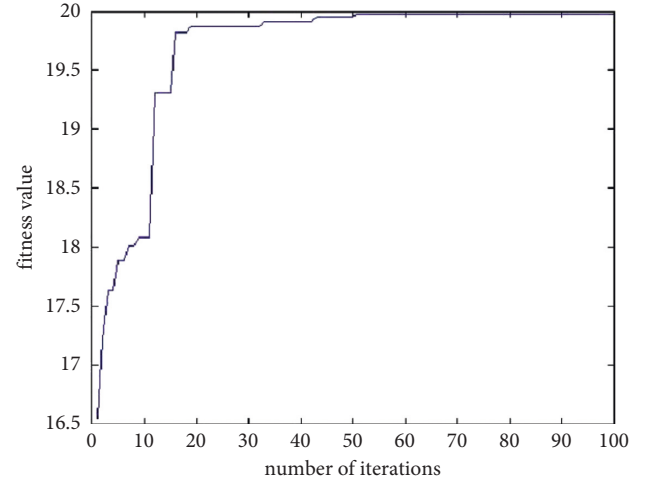
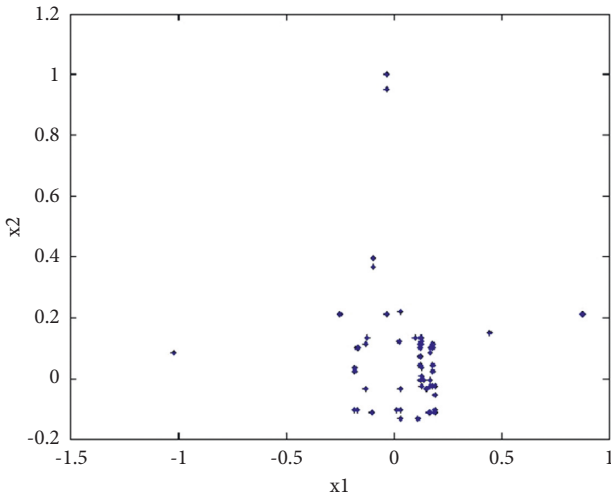
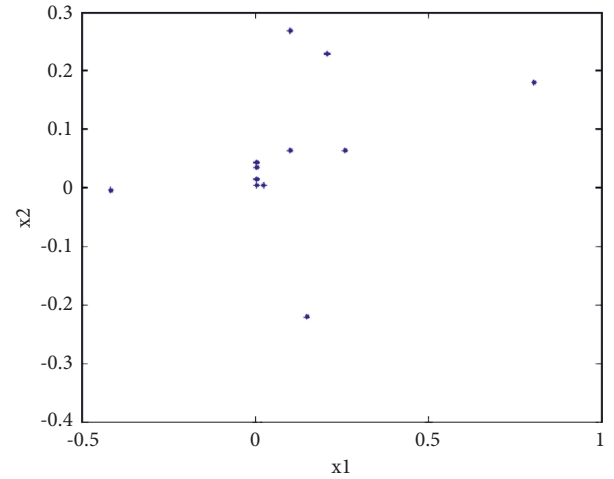


FIGURE 11: Improved genetic algorithm fitness curve.

FIGURE 10: Distribution of input variables x_1 and x_2 of basic genetic algorithm.FIGURE 12: Distribution of input variables x_1 and x_2 of the improved genetic algorithm.

$x_2 = -0.0049$, and the corresponding optimal fitness value is 19.9792.

It can be seen from Figure 11 that in the 20th iteration, the optimal fitness is already around 19.8. From the overall change trend of the curve, it can be seen that the fitness is rapidly approaching the global maximum value and continues to approach the global maximum value. The maximum error is very small. It can be seen that the improved genetic algorithm has no obvious oscillation, the global convergence is good, and the speed is fast. It can jump out of the local optimum and achieve the global optimum. The values of the variables x_1 and x_2 corresponding to the fitness function are shown in Figure 12. Compared with the basic genetic algorithm, the number of points shown in the figure is very small. It can be seen that the convergence speed is fast, near (0, 0), and they are all in the circles in the figure. Therefore, it can be verified that the improved genetic algorithm has good convergence and high precision.

4.3.1. Evolving a One-Bit Full Adder. The most basic components of a computer are basic logic gates, bit-by-bit arithmetic addition operations, and computational storage units. Among them, addition is the most basic form of computer operation, and the adder is the most basic combinational logic circuit, which can be used for binary subtraction, multiplication, and other operations, and arithmetic operations in the digital system are all performed by addition. Therefore, a full adder is analyzed and evolved to verify the superiority of the improved genetic algorithm. The experiment uses a 4×4 matrix to implement a one-bit full adder. The number of populations is 50, and the maximum number of generations is set to 1000. The basic genetic algorithm parameter setting is as follows: crossover probability is 0.7; mutation probability is 0.01; improved genetic algorithm parameter setting is dynamic change.

Through two genetic algorithms, run 50 times, respectively, the performance of the algorithm is shown in Table 1.

TABLE 1: List of algorithm performance parameters.

Algorithm choice	Number of runs	Average fitness	Best convergent algebra	Failure rate (%)
Basic genetic algorithm	50	13.238	854	14
Improved genetic algorithm	50	14.562	530	2

From Table 1, it can be concluded that the success rate of the improved genetic algorithm for the evolution circuit is greatly improved, and the failure rate is reduced from 14% to 2%. It is determined by experiments that the rate ratio of the basic genetic algorithm and the improved genetic algorithm is 1:1.24 under the same number of iterations. Compared with the basic genetic algorithm, the optimal convergence algebra of the improved genetic algorithm is reduced by 37.94%, so the overall speed is increased by 23%. The fitness value curve for one of the evolutionary processes is shown in the figure. The analysis shows that after the basic genetic algorithm reaches the maximum fitness value of 875, the improved genetic algorithm achieves the maximum fitness value of about 535. It can be seen that the convergence speed of the improved genetic algorithm is accelerated.

5. Conclusion

This paper is based on the evolutionary circuit design of the cellular neural network. Firstly, the principle of evolutionary circuit design and its algorithm are expounded, the performance of the genetic algorithm is analyzed, and the genetic algorithm is determined as the algorithm for evolutionary circuit design; then, the three-input linear distributable function is added as the population gene to improve the diversity of genes and enrich circuits. The diversity of evolution improves the effectiveness of the circuit; then, an improved genetic algorithm is proposed, which improves the selection operator, the crossover operator, and the mutation operator, and compared with the basic genetic algorithm, the failure rate of the improved genetic algorithm for the evolutionary circuit is reduced from 14% to 2%, the optimal convergence algebra is reduced by 37.94%, and the overall speed is increased by 23%, so as to improve the evolution rate and the overall performance of the circuit. Finally, the improved genetic algorithm is used to evolve a one-bit full adder and two-bit multiplier, and a more simplified circuit design is obtained.

Data Availability

The dataset can be accessed upon request.

Conflicts of Interest

The authors declare that they have no conflicts of interest.

Acknowledgments

This paper was supported by the general project of the National Natural Science Foundation of China, 61671221.

References

- [1] S. Sinha and W. Ditto, "Dynamics based computation," *Physical Review Letters*, vol. 81, no. 10, pp. 2156–2159, 1998.
- [2] K. Murali, A. Miliotis, W. L. Ditto, and S. Sinha, "Logic from nonlinear dynamical evolution," *Physics Letters A*, vol. 373, no. 15, pp. 1346–1351, 2009.
- [3] K. R. Crounse, E. L. Fung, and L. O. Chua, "Efficient implementation of neighborhood logic for cellular automata via the cellular neural network universal machine," *IEEE Transactions on Circuits and Systems I: Fundamental Theory and Applications*, vol. 44, no. 4, pp. 355–361, 1997.
- [4] L. O. Chua and P. Gea, "Nonlinear dynamics perspective OF WOLFRAM'S new kind OF science. Part XIV: MORE Bernoulli sigma(tau)-SHIFT RULES," *International Journal of Bifurcation and Chaos*, vol. 20, no. 8, pp. 2253–2425, 2010.
- [5] K. Dharmendra and M. Debasis, "Design of a practical fault-tolerant adder in QCA," *Microelectronics Journal*, vol. 53, no. 1, pp. 90–104, 2016.
- [6] B. Sen, M. Dutta, and R. Mukherjee, "Towards the design of hybrid QCA tiles targeting high fault tolerance," *Journal of Computational Electronics*, vol. 15, no. 1, pp. 4722–4736, 2016.
- [7] S. Shadi, A. Shaahin, S. Soheil, and M. Hossein, "Designing efficient QCA logic circuits with power dissipation analysis," *Microelectronics Journal*, vol. 46, no. 1, pp. 462–471, 2015.
- [8] R. K. Sankit and R. K. Nagaria, "A novel design of quantum dot cellular automata 5-input majority gate with some physics proofs," *Journal of Computational Electronics*, vol. 15, no. 1, pp. 324–334, 2016.
- [9] H. Cho and E. E. Swartzlander, "Adder and multiplier design in quantum-dot cellular automata," *IEEE Transactions on Computers*, vol. 58, no. 6, pp. 721–727, 2009.
- [10] C. Labrado and H. Thapliyal, "Design of adder and subtractor circuits in majority logic-based field-coupled QCA nanocomputing," *Electronics Letters*, vol. 52, no. 6, pp. 464–466, 2016.
- [11] S. Sayedsalehi, M. Rahimi Azghadi, S. Angizi, and K. Navi, "Restoring and non-restoring array divider designs in quantum-dot cellular automata," *Information Sciences*, vol. 311, no. 1, pp. 86–101, 2015.
- [12] H. Lv and G. Xie, "Design of the quantum-dot encoder and decoder using QCA," *Acta Optica Sinica*, vol. 32, no. 1, pp. 1–7, 2012.
- [13] T. Oh, "Organic thin-film transistors using pentacene and SiOC film," *IEEE Transactions on Nanotechnology*, vol. 5, no. 1, pp. 23–29, 2006.
- [14] H. U. Li and T. N. Jackson, "Oxide semiconductor thin film transistors on thin solution-cast flexible substrates," *IEEE Electron Device Letters*, vol. 36, no. 1, pp. 35–37, 2015.
- [15] P. Jian, G. I. H. Sun, M. Pinaki, and M. Senior, "Resonant tunneling diodes: models and properties," *Proceedings of the IEEE*, vol. 86, no. 4, 1998.
- [16] W. Wei, J. Han, and F. Lombardi, "Robust HSPICE modeling of a single electron turnstile," *Microelectronics Journal*, vol. 45, no. 4, pp. 394–407, 2014.
- [17] J. Appenzeller, "Carbon nanotubes for high-performance electronics-progress and prospect," *Proceedings of the IEEE*, vol. 96, no. 2, pp. 201–211, 2008.

- [18] K. Walus and G. A. Jullien, "Design tools for an emerging SoC technology: quantum-dot cellular automata," *Proceedings of the IEEE*, vol. 94, no. 6, pp. 1225–1244, 2006.
- [19] S. Craig, P. D. T. Lent, and P. Wolfgang, "Bistable saturation in coupled quantum dots for quantum cellular automata," *Applied Physics Letters*, vol. 62, no. 7, pp. 714–716, 1993.
- [20] K. Walus, T. J. Dysart, G. A. Jullien, and R. A. Budiman, "QCADesigner: a rapid design and simulation tool for quantum-dot cellular automata," *IEEE Transactions on Nanotechnology*, vol. 3, no. 1, pp. 26–31, 2004.

Research Article

Monitoring and Analysis of Venture Capital and Corporate Fraud Based on Deep Learning

Ruijun Zhang and Lina Zheng 

School of Business, Renmin University of China, Beijing 100872, China

Correspondence should be addressed to Lina Zheng; zhenglina@ruc.edu.cn

Received 11 April 2022; Revised 21 April 2022; Accepted 5 May 2022; Published 31 May 2022

Academic Editor: Dong Chen

Copyright © 2022 Ruijun Zhang and Lina Zheng. This is an open access article distributed under the Creative Commons Attribution License, which permits unrestricted use, distribution, and reproduction in any medium, provided the original work is properly cited.

With the continuous expansion of global investment institutions, the development of the investment industry is gradually accelerating, but the risks behind the investment are also constantly increasing. Using the data of A-share companies in China's capital market from 2010 to 2019, this paper studies the impact of venture capital on corporate fraud. Empirical results show that venture capital holdings reduce the probability and frequency of corporate fraud. These findings remain robust after mitigating endogeneity using PSM, Heckman's two-step, one-step approach, suggesting a causal relationship between venture capital holdings and fraud reduction. Further research shows that the way venture capital holdings reduce corporate fraud is to suppress corporate fraud by improving the company's internal and external information environment. Furthermore, venture capital holdings play an important role in the governance of corporate disclosure fraud and operational fraud, but not in the governance of TMT fraud. In addition, the venture capital has better inhibitory effects on the supervision and governance of the fraud frequency of nonstate-owned enterprises compared with state-owned enterprises. The results of this research imply that venture capital shareholding plays an important role in preventing corporate fraud. This study contributes to the researches about the value-added role of venture capital and reveals the governance effect of venture capital on corporate fraud. Besides, it provides the theoretical evidence for capitals to better serve the real economy.

1. Introduction

In recent years, with the rapid development of the global venture capital industry, relevant research has sprung up. The value-added role of venture capital as an “active investor” is widely recognized in the study of start-ups. Related scholars Chemmanur and others found through research that the enterprises backed by corporate venture capital (CVC) are higher in risk than those backed by independent venture capital (IVC), but the returns are lower; however, measured by patents, an in-depth study of the innovation capabilities of companies found that companies backed by corporate venture capital (CVC) were more capable of innovation, for two possible reasons—failure tolerance and industry knowledge. Alvarez and Dushnitsky used the inherent dichotomy of independent venture capital and corporate investors to study the innovation results of venture capital and found that, in terms of innovation output rate,

corporate venture capital is higher than the enterprises backed by independent venture capital. Starting from the medical and health industry, Lehoux et al., when exploring the impact of venture capital on medical technology innovation, found that although there are differences in values and investment objectives of investors, after venture capital enters the medical field, it can promote technology developers and carry out exploration and research on new technologies and develop new medical technologies, thereby enhancing the innovation capability in this field. However, there is currently little research on the subsequent impact of venture capital on firms. The reason for this is the inherent cognitive assumption that VCs will quickly withdraw their investments after the IPO of the invested company and no longer play the role of the investor. However, due to the equity lock-up period, agreement and other reasons, the shares held by venture capital will be restricted from circulation within a certain period of time after the invested

company is listed. In addition, when a listed company has good development prospects, venture capital will gradually withdraw its investment from the invested company at an appropriate time in order to maximize the return on investment and obtain sustainable equity income. As mentioned earlier, from the listing of Winner Technology in 2017 to the latest shareholding reduction cycle in January 2022, Sequoia Juye has always been the major shareholder of Winner Technology with a shareholding ratio of more than 5%. Therefore, it is of significance to study the responsibilities of Sequoia Juye as a major shareholder. Based on the above discussion, the research on the supervision and inhibition of VC on corporate fraud is conducted from the perspective of corporate fraud, helping to fully understand the value-added role of VC and expanding the research scope of VC governance [1–10].

Therefore, the data of China's A-share companies from 2010 to 2019 is selected to study the impact of VC shareholding on corporate fraud, to verify the governance role of VC shareholding on companies. According to the research results, the VC-backed companies have a lower probability and frequency of fraud. The result is still valid after endogenous tests such as one period lag, propensity score matching (PSM) and Heckman two-step methods. Through the mechanism test, it is found that VC shareholding has a more significant impact on the fraud probability and fraud frequency of companies with poor internal corporate governance and poor external information environment. Further research found that VC shareholding mainly plays a governance role in the company operation fraud and has no obvious impact on information disclosure and TMT fraud. In the study of nonstate-owned enterprises, VC has a more significant inhibitory effect on the probability and frequency of fraud.

The possible marginal contributions of this paper are as follows. Firstly, this paper enriches the relevant literature on the factors affecting corporate fraud. Most existing studies focused on the effect of motivations and internal and external influence mechanisms on fraud. However, few studies exist on the effect of VC inhibiting corporate fraud. Secondly, this paper enriches the relevant research on the supervision and governance roles of VC. Existing studies on the supervision role of VC often focused on supervising the earnings management of senior executives and phased investment to supervise the development of the company. This study applies the supervision role of VC in the research on various frauds of companies for the first time, enriching the research results on the supervision role of VC.

2. Related Technical Methods

Machine learning is all about exploring and developing a set of algorithms that enable computers to learn and model all kinds of data on their own and make predictions using established models and new inputs without explicit instructions from the outside. It has been widely used in various branches of artificial intelligence, such as intelligent customer service in the financial field, robo-advising, behavior recognition, natural language understanding, and risk prediction. Common machine learning algorithms

include classification algorithms, regression algorithms, and aggregation algorithms. The working principle of machine learning is simply to substitute specific data samples into the machine learning algorithm for verification and testing. The model is repeatedly tuned, and then the process of application promotion is carried out. How machine learning works is shown in Figure 1 [11–15].

The current mainstream machine learning models are as follows:

- (1) Classification. Common classification algorithms include support vector machine (SVM) and logistic regression. SVM can quickly classify sample data by discovering the boundaries of separating classes with the widest possible edges. Logistic regression is a process of computing binomial and polynomial classification functions for linearly separable data sources.
- (2) Regression. A simple definition of regression analysis is the technique of predicting a dependent variable (y) based on one or more independent variables (x). Regression analysis is usually used for some business decisions, and the common application scenarios are as follows: One is to explain some incomprehensible things. The second is to forecast important business trends. The third is to choose a different option. Linear regression is the most commonly used regression technique. The purpose of linear regression is to find the line of best fit, known as the regression line through the points.
- (3) Clustering. The basic principle of clustering analysis can be summarized as follows: the aggregation of similar (homogeneous) individuals; that is, "things cluster together, and people are divided into groups." If you find this class, you can find the similarity of these objects (clusters). Calculations are performed through certain rules, and objects with similarities are aggregated. Common clustering algorithms include clustering of samples, that is, K-Means clustering. The main clustering type is to find the proximity of distance, clustering of variables, that is, unified clustering; the key is to find correlations. Proximity. K-Means clustering is currently widely used.

Based on machine learning, this paper monitors and experiments venture capital and corporate fraud.

3. Hypotheses Development

For companies, VC shareholding affects the motivation of committing fraud by the companies from two aspects. First, suppose that the cost of committing the fraud by the listed company is $c = p \times F$, where p is the probability of the inspection of the corporate fraud, and F is the loss of the company caused by the disclosure of the fraud, including the fine imposed by the regulator and the decline in stock price arising therefrom. The decline in stock price will deal a huge blow to both companies and investors, so it is paid more attention to by the company. In terms of the inspection probability (p), as a kind of financial intermediary or

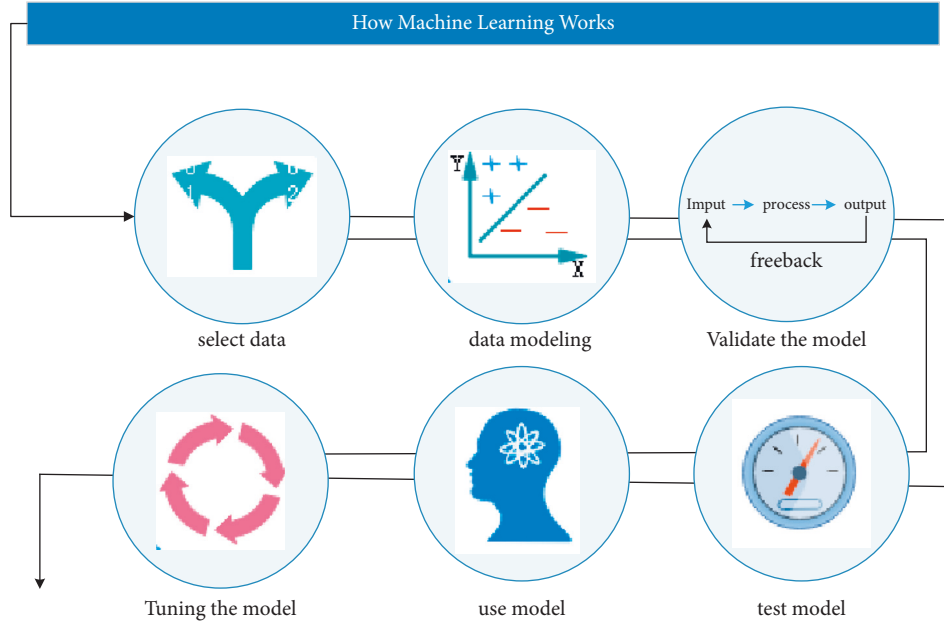


FIGURE 1: How machine learning works.

institutional investor, VC invests in the companies, often causing more analysts to track and analyze, and thus promoting the company to disclose more information to reduce the degree of information asymmetry [14], so as to improve the information transparency of the company. As “active investors,” VC has rich industry experience and professional analysts and advanced tools, so that it has inherent advantages in obtaining and analyzing information [14]. Therefore, it can be seen that the investment of VC will improve the information transparency of companies and thus improve the probability (p) of disclosing the fraud committed by the companies [16–20].

For the company’s losses caused by current disclosure fraud (f), VC shareholding may produce information spillover effect in some way, which will affect other investors and accelerate the dissemination of negative information of the company. In addition, venture capital holdings have attracted more analysts’ attention, which will also accelerate the dissemination of negative information and trigger stock price fluctuations. Therefore, considering the above formula, the possibility that VC holding shares of the company increases the fraud cost of the company does exist ($C = P \times F$). In conclusion, based on the above analysis, this chapter puts forward the following assumptions to be verified based on the above research results:

H1a: venture backed companies are less likely to commit fraud than nonventure backed companies.

H1b: compared with nonventure capital backed companies, venture capital backed companies have a lower frequency of fraud.

4. Data, Sample Selection, and Variables

4.1. Data and Sample. This paper takes the data of all shared companies from 2010 to 2019 as the initial sample, and the

relevant data of a company are public data with high authenticity. Through the screening and selection of samples, the details are as follows: (1) eliminate the sample of companies in the finance industry; (2) eliminate ST and *ST samples in abnormal business operation; (3) eliminate the variables and samples with missing values; (4) Winsorize all continuous variables to eliminate the extreme values. This paper mainly studies the variable, and the data on fraud comes from the fraud subdatabase of the China Stock Market and Accounting Research Database (CSMAR). The company’s financial data comes from other subdatabases of CSMAR. The relevant characteristic data such as the name of the VC and the number of investment events are all from the CVSource database. As an open database, CVSource database has certain authority and representativeness.

4.2. Variable Definition

4.2.1. Dependent Variable. The probability of fraud ($\text{Fraud}_{i,t+1}$): $\text{Fraud}_{i,t+1}$ measures whether the listed company commits fraud, and the data on fraud is cross-sectional data arranged by the fraud events in the subdatabase of the China Stock Market and Accounting Research Database (CSMAR). The data is reorganized into company-year panel data according to the information under the index of “fraud year” because the date of corporate fraud may not be in the same year as the date of fraud audit. If the listed company i commits fraud in the year $t + 1$, the $\text{Fraud}_{i,t+1}$ value is 1; otherwise, it is 0. The variable is lagged one period here to alleviate the reverse causality problem to a certain extent. The Probit model is constructed to demonstrate hypothesis H1a, that is, whether VC shareholding effectively reduces the probability of corporate fraud [21].

The frequency of fraud ($\text{Freq}_{i,t+1}$): $\text{Freq}_{i,t+1}$ is used to measure the frequency of fraud committed by the listed

TABLE 1: Variable definitions.

Variable name	Symbol	Description
<i>Main variable</i>		
Corporate fraud	$\text{Fraud}_{i,t+1}$	The dummy variable, is set to 1 if there is corporate fraud, otherwise it is 0
Fraud frequency	$\text{Freq}_{i,t+1}$	Count variable, corporate fraud frequency
Venture capital	$\text{VC}_{i,t}$	The dummy variable, is set to 1 if the VC holds the shares of companies in the current year, otherwise it is 0
<i>Control variable</i>		
Audit quality	Audit	The dummy variable, is set to 1 if audit institutions are big 4 accounting firms, otherwise it is 0
Company size	Size	Natural logarithm of total assets
Performance variable	Roa	Return on assets (ROA)
Board size	Bdsize	The logarithm of the number of directors by the end of the year
CEO duality	Dual	The value is set to 1 if the roles of the CEO and the chair of the board are combined, otherwise it is 0
Years of being companies	Age	The logarithm of years of being companies
Industry confidence	Tqmed	Median of TobinQ of all companies in the same industry by the end of the year
Industry dummy variable	Industry	Classified according to the industry classification standard of the China securities regulatory commission (CSRC) in 2012
Year dummy variable	Year	Year dummy variable

company i in the year $t + 1$. The variable is lagged one period here to alleviate the reverse causality problem to a certain extent. Poisson model is constructed to Hypothesis H1b, that is, whether VC shareholding reduces the frequency of corporate fraud.

4.2.2. Independent Variable. $\text{VC}_{i,t}$ is the main research object in this paper. Whether there is a VC among the top ten shareholders of companies is considered the main independent variable. $\text{VC}_{i,t}$ is a dummy variable and is set to 1 when there is a VC among the top ten shareholders of companies; otherwise, it is 0. The identification process of VC financing is as follows: firstly, confirm VC institutions according to the classification of shareholders of companies in the China Securities Regulatory Commission (CSMAR). Secondly, match the name of VC institutions with their characteristics obtained from the CVSource database by Stata. Finally, the matching result between the name of company shareholders and the full name of VCs is manually confirmed by referring to previous practices [10, 22]. The sample is finally determined through the above steps.

4.2.3. Control Variables. In the selection of control variables, based on the current research edge at home and abroad, this paper selects the following control variables to control other factors: audit quality (AUDIT), company size (scale), property right nature (state), independent director ratio (ind), board size (board size), debt asset ratio (Lev), company years (age), Revenue growth rate (growth), and industry confidence (tqmed). The variables involved in this model and their definitions are shown in Table 1.

5. Empirical Tests and Results

5.1. Empirical Model. To test hypothesis H1, that is, the impact of VC shareholding on corporate fraud, the model is constructed as follows:

$$Y_{i,t+1} = \beta_0 + \beta_1 \times \text{VC}_{i,t} + \beta_2 \times \text{Controls}_{i,t} + \text{Year}_{i,t} + \text{Industry}_{i,t} + \varepsilon_{i,t}. \quad (1)$$

where the dependent variable is the fraud status of the companies next year, and the reason to use one period lag is to alleviate the endogeneity problem such as reverse causality. $Y_{i,t+1}$ is expressed by $\text{Fraud}_{i,t+1}$ and $\text{Freq}_{i,t+1}$ respectively in this paper. In the regression process, the Probit model is used for the dummy variable Fraud; the Poisson model is used for the counting variable Freq. The main independent variable is whether there is VC ($\text{VC}_{i,t}$) among the top ten shareholders of companies; $\text{Control}_{i,t}$ is a series of control variables; in addition, the model also controls the annual and industry fixed effects. The regression coefficient β reflects the impact of the core independent variable “VC holdings” on corporate fraud, and it is the empirical result this paper focuses on. If VCs have a governance effect on companies, the fraud probability and fraud frequency of VC-backed companies are significantly lower than those of non-VC-backed companies; that is, β should be significantly negative [23].

5.2. Summary Statistics. In this paper, the summary statistics of all variables are shown in Table 2. The mean value of corporate fraud ($\text{Fraud}_{i,t+1}$) is 0.203, indicating that about 20.3% of companies commit fraud in all sample observations. The mean value of corporate fraud frequency ($\text{Freq}_{i,t+1}$) is 0.314, the standard deviation is 0.735, the minimum value is 0, and the maximum value is 4, indicating that the average frequency of corporate fraud is about 0.3 in the annual observations, and the fluctuation range around the mean value is large. In terms of independent variables, the mean value of VC ($\text{VC}_{i,t}$) is 0.266, indicating that the average proportion of companies with a VC shareholder among the top ten shareholders during the sample period is about 26.6% [24].

In addition, the summary statistics of the control variables show that the mean value of whether any of the big 4

TABLE 2: Descriptive statistics.

Variable	Sample size	Mean value	Standard deviation	Minimum value	Maximum value
Fraud	16347	0.203	0.402	0.000	1.000
Freq	16347	0.314	0.735	0.000	4.000
VC	16347	0.266	0.442	0.000	1.000
Audit	16347	0.040	0.195	0.000	1.000
Age	16347	1.886	0.926	0.000	3.178
Cash	16347	0.438	0.848	-2.355	3.748
Size	16347	22.265	1.199	20.085	25.884
ROA	16347	0.047	0.051	-0.155	0.197
Dual	16347	0.729	0.444	0.000	1.000
Top1	16347	0.353	0.150	0.090	0.750
BdSize	16347	2.143	0.195	1.609	2.708
Tqmed	16347	1.756	0.528	0.996	3.648

TABLE 3: VC shareholding and corporate fraud.

	(1)	(2)	(3)	(4)
	Probit		Poisson	
	Fraud _{t+1}	Fraud _{t+1}	Freq _{t+1}	Freq _{t+1}
VC	-0.0560* (-1.80)	-0.0642** (-2.03)	-0.134*** (-3.44)	-0.149*** (-3.80)
Age		-0.0333* (-1.87)		-0.0484** (-2.18)
Size		0.00923 (0.59)		0.0534*** (2.82)
ROA		-3.615*** (-11.13)		-6.101*** (-16.68)
Dual		-0.0912*** (-2.93)		-0.178*** (-4.77)
Audit		-0.243*** (-3.10)		-0.397*** (-3.72)
BdSize		0.156** (2.06)		0.171* (1.87)
Tqmed		-0.0552 (-0.89)		-0.146* (-1.90)
Cash		-0.0795*** (-4.42)		-0.133*** (-5.98)
Constant	-0.275 (-1.55)	-0.301 (-0.73)	-0.303* (-1.86)	-0.869* (-1.82)
Observations	12003	12003	12047	12047
Year&Industry	Yes	Yes	Yes	Yes
Pseudo R ²	0.018	0.036	0.024	0.047
AIC	12024.7	11819.1	18581.6	18156.5
Log likelihood	-5931.3	-5820.6	-9201.8	-8981.2

* $p < 0.10$, ** $p < 0.05$, and *** $p < 0.01$.

accounting firms are hired is 0.040, indicating that about 4% of the companies hire the big 4 accounting firms in annual observations of all companies. For corporate governance factors, the mean value of the CEO duality is 0.729; that is, the probability of the Chair of the Board concurrently serving as the CEO is up to 72.3% in the sample range of this study, indicating that the Chair of the Board concurrently serving as the CEO is a quite common phenomenon in the current situation of listed corporate governance in China. The mean value of the shareholding ratio of the largest shareholder (Top1) is 0.353, the minimum value is 0.09, and the maximum value is 0.75, indicating that there is a relatively large gap in the shareholding ratio of the largest

shareholder between China's companies, and the shareholding ratio is generally high. The mean value of the shareholding ratio is consistent with the existing research conclusions.

5.3. Basic Results. Table 3 shows the empirical results of the impact of VC shareholding ($VC_{i,t}$) on violations of companies. In the regression, the variables that may affect corporate fraud are controlled, as well as the fixed effects of year and industry. Columns (1) and (2) show the results of the impact of VC shareholding ($VC_{i,t}$) on corporate fraud ($Fraud_{i,t+1}$). Columns (3) and (4) show the results of the

impact of VC shareholding ($VC_{i,t}$) on the probability ($Freq_{i,t+1}$) of corporate fraud. According to column (2) of Table 3, the estimated coefficient of the impact of VC shareholding ($VC_{i,t}$) on corporate fraud ($Fraud_{i,t+1}$) is significantly negative at the significance level of 5% after the possible factors influencing the corporate fraud are controlled except for VC shareholding, indicating that the fraud probability of the VC-backed companies will significantly decrease in the next year. According to column (4) of Table 3, the estimated coefficient of the impact of VC shareholding ($VC_{i,t}$) on the fraud probability ($Freq_{i,t+1}$) of companies is significantly negative at the significance level of 1% after the possible factors influencing the corporate fraud are controlled except for VC shareholding, indicating that VC shareholding effectively will reduce the fraud frequency of the companies in the next year. To sum up, the hypothesis in this paper is confirmed; that is, VC significantly inhibits the occurrence of corporate fraud [25].

According to the results of control variables, the coefficient of audit quality (Audit) is significantly negative but not significant, indicating that independent high-quality external audit and supervision can effectively reduce the probability and frequency of corporate fraud and supervise and restrain the occurrence of corporate fraud. The coefficient of return on assets (ROA) is significantly negative possibly because there is less incentive to obtain illegitimate incomes by fraud when the return on assets is more. The coefficient of the board size (Bdsize) is significantly positive, indicating that larger board size is not equivalent to a higher board efficiency. The larger the size of the board of directors, the more likely there are differences in interests and failure of supervision. The coefficient of CEO duality (Dual) is negative, indicating that the higher the CEO duality, the less the frequency of fraud. The possible reason is that the person bears more responsibilities and receives more severe punishment when holding the positions of the Chair of Board and CEO concurrently, inhibiting the persons' motivation to commit fraud more effectively.

5.4. Mechanism Test. In this section, the internal and external governance environment mechanism of companies is tested to clarify whether VC affects corporate fraud by participating in the governance and supervision of the companies.

5.4.1. Internal Governance Environment. The internal governance environment affects the efficiency of supervisors. VC shareholding plays a positive role in the supervision of companies by means of participating in the general meeting of shareholders [12] and assigning directors to the investee company. The role of supervision of VC varies with internal governance environments. When the internal governance environment of the company is poor, the management and large shareholders have more motivations and opportunities to act in their own self-interest, so the fraud frequency of the companies is higher. In such a case, the impact of VC shareholding on the governance of corporate fraud is more significant. On the

contrary, if a company has a good original internal governance environment and a good supervision mechanism to restrict the self-interest motivation of insiders, then VC institutions, providing supplementary supervision for the internal governance of the company, only have small marginal benefits [22].

Furthermore, the benefit brought by active participation in supervision is far greater than the cost, so venture capitalists are motivated to implement active supervision. Active supervision helps improve the intrinsic value of companies and finally improves the exit return of VC, while negative supervision increases the cost: (1) it directly affects the stock price of companies and reduces the exit return of VC; (2) it indirectly affects the reputation accumulation of VC industry and then affects the subsequent financing and investment of venture capitalists. Therefore, venture capitalists are willing and motivated to supervise companies (Tam, 2010). Based on the above reasoning, the following inference is proposed:

Inference 1. The worse the internal governance environment, the more significant the impact of VC on corporate fraud.

The fund occupation is used as the proxy variable of the internal governance environment in this paper. Fund occupation is an important means for corporate insiders to seek private interests [11], so fund occupation is selected as the proxy variable of the internal governance environment. It is calculated by the following formula: $Occupancy = (\text{other receivables} - \text{other payables}) / \text{total assets}$. The greater the occupancy value, the more the occupied funds of the listed company, and the worse the internal governance environment of the company. In this section, the average value of the capital occupation level in the industry in the previous year is used as the grouped variable, and the sample is divided into two groups, namely, the group with good internal governance (Occupancy -L) and the group with poor internal governance (Occupancy -H). Table 4 shows the results of grouped regression.

According to the results in columns (1) and (2) of Table 4, the coefficient of the impact of VC shareholding ($VC_{i,t}$) on the fraud probability ($Fraud_{i,t+1}$) of companies is negative in the subsamples whether the internal environment is good or bad, but it is significantly negative in the subsamples with the poor internal environment (Occupancy-L). The results in columns (3) and (4) of Table 4 show that the coefficient of the impact of VC shareholding ($VC_{i,t}$) on the fraud frequency of companies ($Freq_{i,t+1}$) is also significantly negative in the group with the poor internal environment (Occupancy-L). The above results confirm the abovementioned Inference 1; that is, the worse the internal governance environment of the company, the more significant the impact of VC on fraud.

5.4.2. External Governance Environment. According to the modern information-based financial intermediary theory, information production is the root cause for the existence of financial intermediary [21]. The role of certification of VC

TABLE 4: Internal governance environment.

	(1)	(2)	(3)	(4)
	Fraud _{t+1}		Freq _{t+1}	
	Occupy-H	Occupy-L	Occupy-H	Occupy-L
VC	-0.043 (-1.10)	-0.089* (-1.66)	-0.058 (-1.21)	-0.277*** (-4.02)
Age	-0.040* (-1.76)	-0.022 (-0.72)	-0.070** (-2.48)	0.001 (0.02)
Size	0.018 (0.87)	0.003 (0.14)	0.074*** (2.99)	0.039 (1.27)
ROA	-4.405*** (-10.30)	-2.633*** (-5.15)	-6.711*** (-13.85)	-5.177*** (-9.11)
Dual	-0.037 (-0.93)	-0.186*** (-3.56)	-0.070 (-1.47)	-0.338*** (-5.55)
Audit	-0.311*** (-2.68)	-0.177 (-1.61)	-0.435*** (-2.80)	-0.346** (-2.29)
BdSize	0.062 (0.64)	0.286** (2.31)	-0.040 (-0.34)	0.433*** (2.88)
Tqmed	-0.080 (-0.99)	-0.031 (-0.30)	-0.207** (-2.06)	-0.065 (-0.54)
Cash	-0.072*** (-3.07)	-0.098*** (-3.37)	-0.148*** (-5.12)	-0.116*** (-3.24)
Constant	-0.096 (-0.18)	-0.619 (-0.93)	-0.498 (-0.82)	-1.578** (-1.99)
Observations	7478	4471	7508	4539
Year&Industry	Yes	Yes	Yes	Yes
Pseudo R ²	0.040	0.049	0.049	0.067
AIC	7423.775	4443.219	11370.060	6796.922
Log likelihood	-3622.888	-2139.610	-5588.030	-3307.461

* $p < 0.10$, ** $p < 0.05$, and *** $p < 0.01$.

shareholders on enterprises is reflected in its shareholding, conveying a “good profit” signal to the market. VC shareholding will release certification signals to the market, which will drive the stock trading volume of companies to rise. Existing studies have shown that stock liquidity is also an indirect governance mechanism [8, 20]. VCs are special financial investment institutions, so their investment projects are more likely to attract more attention from analysts, and more internal information of the investee company is transmitted to the market in the form of analyst reports, thus improving the information transparency of the enterprise. In addition, as a professional investment institution, VC can effectively identify the impact of various information on the company’s stock price and development prospects. Therefore, the shareholding status of VC implies the trend of the company’s future development [14].

The impact of the external information environment on the relationship between VC and corporate fraud is as follows: the original information transparency of companies will affect the relationship between the VC shareholding and corporate fraud. When the transparency of the company’s external information environment is low, investors lack approaches to acquiring the internal information of companies, resulting in a huge information gap. Under such circumstances, it is less likely to be found by the outside world even if the company commits fraud, or the adverse impact arising from corporate fraud is relatively small even if corporate fraud is found in an

audit. Therefore, there may be more serious fraud in such companies, the venture capitals are provided with good opportunities to play the role of governance, and the supervision role of VC shareholding in corporate governance will be more significant. On the contrary, if the external information transparency of the company is high, and the self-interest motivation of insiders can be effectively restrained, the governance space for VC is relatively small, so as an alternative to the external governance mechanism, the supervision role of VC will be inhibited to a certain extent. As an “active investor,” the VC-backed companies will attract more attention. For example, more analysts will disclose more enterprise information to the market, thus reducing the asymmetry between internal and external information [14]. The higher the information transparency, the greater the probability of fraud being found. The following inference is proposed based on the above analysis:

Inference 2. The worse the external information environment the company is in, the more significant the impact of VC on corporate fraud is.

According to the existing studies, the number of analysts tracking the companies is selected as the proxy variable of the external information environment. Firstly, the samples are grouped into better information environment (Analyst-H) and worse information environment (Analyst-L) according to the industry median of the number of analysts

TABLE 5: External governance environment.

	(1)	(2)	(3)	(4)
	Fraud _{t+1}		Freq _{t+1}	
	Analyst-H	Analyst-L	Analyst-H	Analyst-L
VC	-0.047 (-0.96)	-0.077* (-1.83)	-0.122 (-1.57)	-0.158*** (-3.09)
Age	-0.073** (-2.47)	-0.030 (-1.27)	-0.099*** (-2.60)	-0.038 (-1.36)
Size	-0.009 (-0.33)	0.063*** (2.85)	0.015 (0.45)	0.129*** (5.06)
ROA	-2.606*** (-4.98)	-3.853*** (-8.33)	-5.811*** (-9.20)	-5.759*** (-11.64)
Dual	-0.077 (-1.56)	-0.095** (-2.30)	-0.235*** (-3.94)	-0.135*** (-2.79)
Audit	-0.237** (-2.18)	-0.249** (-2.11)	-0.434*** (-2.80)	-0.365** (-2.42)
BdSize	0.208* (1.74)	0.129 (1.29)	0.146 (0.99)	0.184 (1.56)
Tqmed	0.009 (0.10)	-0.104 (-1.24)	-0.038 (-0.32)	-0.193* (-1.89)
Cash	-0.099*** (-3.59)	-0.064*** (-2.61)	-0.170*** (-4.74)	-0.105*** (-3.57)
Constant	-0.380 (-0.57)	-1.156** (-2.05)	-0.372 (-0.45)	-2.368*** (-3.78)
AME			-0.0334** (-1.96)	-0.0555*** (-3.08)
Observations	5374	6555	5459	6588
Year&Industry	Yes	Yes	Yes	Yes
Pseudo R ²	0.054	0.033	0.075	0.044
AIC	4922.074	6913.573	7433.147	10667.752
Log likelihood	-2377.037	-3370.786	-3619.573	-5242.876

* $p < 0.10$, ** $p < 0.05$, and *** $p < 0.01$.

in the previous year. Then, grouped regression is performed, and the regression results are shown in Table 5. The results in columns (1) and (2) show that the coefficient of the impact of VC shareholding on the probability of corporate fraud (Fraud_{t+1}) is significantly negative at the 10% level in the subsamples with poor external information environment (Analyst-L). The results in columns (3) and (4) show that the coefficient of the impact of VC shareholding on the frequency of corporate fraud (Freq_{t+1}) is significantly negative at the level of 1% in the subsamples with poor external information environment (Analyst-L). The above-mentioned Inference 2 is confirmed through the above results; that is, the worse the external information environment of the company, the more significant the impact of VC on corporate fraud.

6. Endogeneity and Robustness Test

6.1. Endogeneity Test. The variable such as the industry and year is controlled, and the corresponding control variables are selected according to different types, but there are still inevitable endogeneity problems. There may be the following endogenous problems in this paper: the first is reverse causality. VC shareholding can improve the governance and efficiency of companies and reduce the probability of corporate fraud through supervision and governance. Furthermore, venture investors do not

randomly choose companies for investment but tend to choose enterprises with good future development prospects, good company operation, good corporate governance, and fewer frauds. The second is selection bias, namely, self-selection bias and sample selection bias. In terms of self-selection bias, due to the “selection effect,” VC may choose enterprises with better corporate governance effect, thus resulting in the wrong identification of governance effects of VC. Furthermore, whether enterprises choose VC is self-selection and will be affected by various factors. In terms of sample selection bias, there may be some differences between VC-backed companies and non-VC-backed companies, leading to the differences in fraud between an experimental group and a control group. Endogeneity is tested as follows:

6.1.1. Reverse Causality. By referring to the research methods of the VC and other control variables are treated with a lag period, and then the fraud data of the company (i) in the current period (t) and the independent variables lagged one period are regressed. See Table 6 for the results.

The results in column (1) of Table 6 show that the coefficient of the impact of VC shareholding on the probability of corporate fraud (Fraud_t) is significantly negative at the significance level of 10%. The results in column (2) show that the coefficient of the impact of VC shareholding on the

TABLE 6: Variable lagged one period.

	(1) Fraud _t	(2) Freq _t
L.VC	-0.062* (-1.95)	-0.140*** (-3.60)
L.Age	-0.035** (-1.99)	-0.054** (-2.45)
L.Size	0.011 (0.68)	0.058*** (3.04)
L.ROA	-3.608*** (-11.11)	-6.081*** (-16.60)
L.Dual	-0.089*** (-2.86)	-0.174*** (-4.67)
L.Audit	-0.244*** (-3.11)	-0.404*** (-3.78)
L.BdSize	0.161** (2.12)	0.169* (1.84)
L.Tqmed	-0.029 (-0.50)	-0.088 (-1.22)
L.Cash	-0.079*** (-4.36)	-0.134*** (-6.02)
Constant	-0.400 (-0.98)	-1.093** (-2.32)
Observations	11998	12047
Year and industry	Yes	Yes
Pseudo R ²	0.035	0.046
AIC	11826.115	18162.879
Log likelihood	-5826.057	-8986.439

* $p < 0.10$, ** $p < 0.05$, and *** $p < 0.01$.

frequency of corporate fraud (Freq_{*i,t*}) is significantly negative at the significance level of 1%. To sum up, after considering the possible endogeneity problems such as reverse causality, the main test conclusion is still stable; that is, VC shareholding can effectively reduce the probability and the frequency of corporate fraud.

6.1.2. Self-Selection Problem. In this section, Heckman two-step method is used to handle the possible sample self-selection problems. The specific steps are as follows: the first step is that Probit regression is used to model the relationship between the dummy variable VC as the dependent variable and two relative exogenous variables (exclusion constraints) affecting the selection of investee companies by VC, and the inverse Mills ratio (IMR) is calculated. Exclusion constraints are strongly correlated with independent variables and will not directly affect the dependent variables. Based on the existing practices, whether the selected company is in the area with active VC investments and the period of rapid development of VC is used as exclusion constraints. For the identification of the areas with active VC investments, according to the Venture Capital Development in China, companies headquartered in Beijing, Jiangsu, and Guangdong are identified as the companies in areas with active VC investments and are set as a dummy variable Z1; for the identification of the development period of VC industry, China's venture capital industry began to develop rapidly after the "No. 1 Proposal" of the Chinese People's Political Consultative Conference (CPPCC) in 1998, so the

TABLE 7: Heckman two-step estimation result.

	(1) Step 1 VC	(2) Step 2 Fraud _{t+1}	(3) Freq _{t+1}
Z1	0.040* (1.67)		
Z2	0.093*** (4.00)		
VC		-0.065** (-2.04)	-0.149*** (-3.81)
IMR		-0.062 (-0.16)	-0.125 (-0.27)
Age		-0.031 (-1.60)	-0.045* (-1.88)
Size		0.008 (0.53)	0.053*** (2.77)
ROA		-3.603*** (-11.09)	-6.090*** (-16.64)
Dual		-0.092** (-2.93)	-0.178*** (-4.77)
Audit		-0.242*** (-3.09)	-0.397*** (-3.71)
BdSize		0.155** (2.05)	0.171* (1.86)
Tqmed		-0.064 (-1.02)	-0.153** (-1.98)
Cash		-0.080*** (-4.42)	-0.133*** (-5.97)
Constant	-1.228*** (-7.24)	-0.165 (-0.22)	-0.636 (-0.69)
Observations	16297	11966	12007
Year and industry	Yes	Yes	Yes
Pseudo R ²	0.074	0.035	0.046
AIC	17665.601	11803.346	18132.111
Log likelihood	-8746.800	-5813.673	-8973.055

* $p < 0.10$, ** $p < 0.05$, and *** $p < 0.01$.

value of the companies after 1998 is set to 1 in this paper, and such companies are easier to get the VC support. In the second step, the inverse Mills ratio (IMR) is used in the regression and regressed with VC and control variables. If the IMR coefficient is not significant, and the coefficient of VC is still significantly negative, it indicates that the model is still considered to be robust after the sample self-selection bias is taken into consideration. See Table 7 for specific estimation results. The results show that the impact of VC on the probability and frequency of corporate fraud is still significantly negative in the second step, indicating that the basic test in this paper is still robust after the self-selection problem is considered.

6.1.3. Sample Selection Bias. The above results may be affected by the sample selection bias, so there is a "selection effect" of VC on the investee company. The difference in fraud tendency between the treatment group and the control group of VC may be caused by inherent differences between the two groups of samples. To alleviate this problem, the propensity score matching method (PSM) is used to select the appropriate control group for VC enterprises to reduce the

TABLE 8: PSM.

Variable	Unmatched matched	Mean		%bias	% reduct bias	t -test t	$p > t $
		Treated	Control				
Z1	U	0.3731	0.3473	5.40		3.05	0.002
	M	0.3702	0.3822	-2.50	53.30	-1.16	0.248
Z2	U	0.5774	0.5285	9.80		5.55	0.000
	M	0.5749	0.5742	0.10	98.60	0.07	0.948
Age	U	1.9434	1.8646	8.50		4.82	0.000
	M	1.9415	1.9183	2.50	70.60	1.19	0.234
Size	U	22.5030	22.1790	26.40		15.37	0.000
	M	22.4870	22.4910	-0.30	99.00	-0.12	0.903
ROA	U	0.0469	0.0465	0.70		0.41	0.683
	M	0.0468	0.0471	-0.60	17.90	-0.28	0.779
Dual	U	0.7320	0.7279	0.90		0.52	0.604
	M	0.7325	0.7348	-0.50	43.30	-0.24	0.808
Audit	U	0.0552	0.0342	10.20		6.09	0.000
	M	0.0526	0.0556	-1.50	85.70	-0.62	0.536
BdSize	U	2.1602	2.1368	12.00		6.76	0.000
	M	2.1593	2.1583	0.50	95.50	0.25	0.805
Tqmed	U	1.8183	1.7334	15.80		9.11	0.000
	M	1.8137	1.8092	0.80	94.80	0.36	0.717
Cash	U	0.4736	0.4249	5.70		3.25	0.001
	M	0.4652	0.4662	-0.10	97.90	-0.05	0.956

systematic difference between enterprises with and without VC investments. The specific matching methods are as follows: firstly, the years from 2010 to 2019 are the sample period, the control group as the enterprises not selected by VC during the sample period, and the control variables in the benchmark model and the exclusion constraints in the Heckman selection model are used as covariates to perform Logit regression and the propensity matching score is obtained. Then, the nearest neighbor 1:1 and radius matching method is used to find an appropriate control group for the experimental group, and the caliper radius is selected to be 0.01.

The balance test results in Table 8 can reflect the matching effect of PSM. It can be seen from the test results of Table 8 that other covariates showed significant differences before matching except ROA and Dual, but the difference between covariates disappeared after PSM, indicating that PSM reduced the systematic difference between the experimental group and the control group and the matching effect of PSM was better. Additionally, from the perspective of deviation percentage, the standardization difference of covariates is less than 10%, and the standardization deviation of most variables is significantly reduced compared with that before matching. In conclusion, the matching method satisfies the equilibrium hypothesis well.

The main test for matched samples by PSM is regressed. The regression results for the matched samples by PSM are shown in Table 9. Columns (1) and (2) are the regression results by using nearest neighbor 1:1 matching. Columns (3) and (4) are the regression results by using nearest neighbor 1:2 matching. The results in Table 9 show that the coefficient of the impact of VC shareholding on the probability of corporate fraud ($Fraud_{i,t+1}$) and the frequency of corporate fraud ($Freq_{i,t+1}$) is significantly negative whether nearest neighbor 1:1 matching or nearest neighbor 1:2 matching is used; that

is, the conclusion of the basic test is still robust after the possible endogeneity problems are solved by PSM.

6.2. Robustness Test

6.2.1. Replace Method. To investigate whether the impact of VC shareholding on corporate fraud depends on the estimation method of the model, the Tobit model is first used to retest the impact of VC shareholding on the probability of corporate fraud. Subsequently, negative binomial regression is used to test the relationship between VC shareholding and the frequency of corporate fraud. The fraud frequency for only the company that commits fraud is non-zero, the independent variable changes from zero to non-zero, and then excessive dispersion may appear, so negative binomial regression is used instead of the abovementioned Poisson model to test robustness to avoid the impact of excessive dispersion on the research. The results of the robustness test are shown in Table 10. The results in column (1) show that the coefficient of the impact of VC shareholding on the probability of corporate fraud is still significantly negative after the replacement of the Tobit model; the results in column (2) show that the coefficient of the impact of VC shareholding on the frequency of corporate fraud is still significantly negative after the use of negative binomial regression. To sum up, the basic test results are still robust.

6.2.2. Sample Transformation and Winsorization Change. By referring to previous studies (Zou et al., 2019), the missing values are not eliminated, and winsorization is not used for samples. The basic test was regressed again with new samples, and the results are shown in Table 11. Without eliminating the missing value and without winsorization, the coefficient of the impact of VC shareholding ($VC_{i,t}$) on the

TABLE 9: Regression result based on PSM.

	(1) Radius-nearest neighbor (1 : 1) matching Fraud _{t+1}	(2) Freq _{t+1}	(3) Radius-nearest neighbor (1 : 2) matching Fraud _{t+1}	(4) Freq _{t+1}
VC	-0.084* (-1.92)	-0.152*** (-2.82)	-0.076** (-2.06)	-0.159*** (-3.52)
Age	-0.058** (-2.00)	-0.099*** (-2.76)	-0.057** (-2.42)	-0.085*** (-2.88)
Size	0.025 (1.01)	0.107*** (3.55)	0.015 (0.77)	0.084*** (3.43)
ROA	-3.562*** (-6.95)	-5.654*** (-9.24)	-3.566*** (-8.35)	-6.267*** (-12.51)
Dual	-0.048 (-0.97)	-0.128** (-2.17)	-0.043 (-1.06)	-0.110** (-2.25)
Audit	-0.305** (-2.55)	-0.335** (-2.19)	-0.214** (-2.22)	-0.234* (-1.90)
BdSize	0.222* (1.84)	0.196 (1.34)	0.230** (2.35)	0.198* (1.67)
Tqmed	-0.007 (-0.07)	-0.023 (-0.18)	-0.040 (-0.50)	-0.075 (-0.75)
Cash	-0.081*** (-2.91)	-0.139*** (-4.01)	-0.067*** (-2.88)	-0.120*** (-4.19)
Constant	-1.055 (-1.56)	-2.501*** (-3.15)	-0.758 (-1.41)	-1.748*** (-2.79)
Observations	4962	5002	7191	7226
Year&Industry	Yes	Yes	Yes	Yes
Pseudo R ²	0.046	0.054	0.039	0.050
AIC	4919.764	7447.950	7103.497	10869.554
Log likelihood	-2373.882	-3629.975	-3463.748	-5339.777

* $p < 0.10$, ** $p < 0.05$, and *** $p < 0.01$.

TABLE 10: Replace model.

	(1) Tobit Fraud _{t+1}	(2) Negative binomial regression Freq _{t+1}
VC	-0.018** (-2.09)	-0.132** (-2.55)
Age	-0.009* (-1.87)	-0.041 (-1.39)
Size	0.004 (0.84)	0.033 (1.25)
ROA	-0.999*** (-11.46)	-6.259*** (-11.75)
Dual	-0.026*** (-2.98)	-0.173*** (-3.42)
Audit	-0.056*** (-2.96)	-0.378*** (-2.85)
BdSize	0.037* (1.84)	0.239* (1.92)
Tqmed	-0.016 (-0.95)	-0.123 (-1.17)
Cash	-0.020*** (-4.25)	-0.134*** (-4.51)
Constant	0.375*** (3.32)	-0.662 (-0.98)
Observations	12047	12047
Year and industry	Yes	Yes
Pseudo R ²	0.037	0.028
AIC	11914.801	16851.091
Log likelihood	-5859.400	-8327.546

* $p < 0.10$, ** $p < 0.05$, and *** $p < 0.01$.

TABLE 11: Winsorization change without eliminating missing value.

	(1) Probit Fraud _{t+1}	(2) Poisson Freq _{t+1}
VC	-0.0483** (-2.01)	-0.133*** (-4.83)
Age	0.0133 (1.07)	0.0762*** (5.36)
Size	-0.0251** (-2.54)	-0.0252** (-2.25)
ROA	-2.653*** (-17.23)	-2.152*** (-27.42)
Dual	-0.118*** (-5.05)	-0.199*** (-7.73)
Audit	-0.276*** (-5.42)	-0.446*** (-6.76)
BdSize	0.0188 (0.35)	0.0289 (0.48)
Tqmed	-0.0397 (-1.07)	-0.0992** (-2.30)
Cash	-0.00302 (-0.85)	-0.0364*** (-4.27)
Constant	0.351 (1.33)	0.334 (1.16)
Observations	20749	20800
Year and industry	Yes	Yes
Pseudo R ²	0.035	0.044
AIC	21517.6	36832.0
Log likelihood	-10666.8	-18316.0

* $p < 0.10$, ** $p < 0.05$, and *** $p < 0.01$.

probability of corporate fraud ($\text{Fraud}_{i,t+1}$) is significantly negative at the significance level of 5%. The coefficient of the impact of the frequency of corporate fraud ($\text{Freq}_{i,t+1}$) is significantly negative at the significance level of 1%. The above results show that the conclusion of the basic test is still robust in this paper and will not be changed by changing the time range and winsorization of samples.

7. Conclusions

This paper selects all A-share companies from 2010 to 2019 as samples to study the impact of VC Shareholding on corporate fraud. According to the research results, firstly, the basic test confirms that, compared with non-VC supported companies, the possibility and frequency of fraud of VC supported companies are lower, and the influence coefficient of VC shareholding ($\text{VC}_{i,t}$) on the probability of corporate fraud ($\text{fraud}_{i,t+1}$) is significantly negative when the significance level is 5%. When the significance level is 1%, the influence coefficient of corporate fraud frequency ($\text{freq}_{i,t+1}$) is significantly negative. The above conclusions show that VC shareholding strengthens the supervision for companies and lowers the probability of the market punishment due to fraud by playing the role of supervision and governance, so the agency cost is reduced, and the governance mechanism of investee companies is improved. Secondly, through the mechanism test, it is found that the method of VC shareholding to reduce corporate fraud is to curb its fraud by improving the company's information environment. In terms of the internal governance environment, the coefficient of the impact of VC on the companies with a worse internal information environment is more significant; in terms of the external information environment, when the external information environment is poor, VC has a more significant inhibitory effect on the corporate fraud. Thirdly, the endogeneity and robustness are tested. To alleviate the possible endogeneity problems such as reverse causality, sample selection bias, and self-selection bias, this paper has confirmed that the conclusion is still robust after controlling the endogeneity problem through the methods of one period lag, Heckman two-step test, and propensity score matching (PSM). In addition, the robustness is tested by changing the estimation model and using the samples without eliminating missing values and without winsorization, and the results are still valid. Finally, further research found that VC shareholding plays an effective role in the governance of the company's information disclosure fraud and operation fraud but not a significant role in the governance of TMT fraud. Compared with state-owned enterprises, VC has a better inhibitory effect on the frequency of corporate fraud in nonstate-owned enterprises through its supervision and governance role.

Data Availability

The dataset can be accessed upon request.

Conflicts of Interest

The authors declare that they have no conflicts of interest.

References

- [1] E. Alvarez-Garrido and G. Dushnitsky, "Are entrepreneurial venture's innovation rates sensitive to investor complementary assets? Comparing biotech ventures backed by corporate and independent VCs, Atlanta, GA, US; Dushnitsky, Gary. London Business School, London, United Kingdom, gdushnitsky@london.edu. Are entrepreneurial venture's innovation rates sensitive to investor complementary assets? Comparing biotech ventures backed by corporate and independent VCs," *Strategic Management Journal*, vol. 37, no. 5, pp. 819–834, 2016.
- [2] P. Lehoux, F. A. Miller, and G. Daudelin, "How does venture capital operate in medical innovation?" *BMJ innovations*, vol. 2, no. 3, pp. 111–117, 2016.
- [3] E. Boxenbaum and L. Rouleau, "New knowledge products as b: metaphors and scripts in organizational theory," *Academy of Management Review*, vol. 36, no. 2, pp. 272–296, 2011.
- [4] A. Tiwana, *Platform Ecosystems: Aligning Architecture, Governance, and Strategy*, Elsevier, Waltham, MA, 2013.
- [5] S. Li Sun, V. Z. 2 Chen, S. A. 3 Sunny, and J. 1.4 Chen, "Venture capital as an innovation ecosystem engineer in an emerging market(Article)," *International Business Review*, vol. 28, no. 5, 2019.
- [6] X. Gu, Y. Xin, and F. Teng, "Does external enforcement actions have governance effect? Discussion on the duality of stock price synchronicity indicators," *Nankai Business Review*, vol. 19, no. 5, pp. 41–54, 2016.
- [7] F. Guo, T. R. Kubick, and A. Masli, "The effects of restatements for misreporting on auditor scrutiny of peer firms," *Accounting Horizons*, vol. 32, no. 1, pp. 65–85, 2017.
- [8] J. Helwege, V. J. Intintoli, and A. Zhang, "Voting with their feet or activism? Institutional investors' impact on CEO turnover," *Journal of Corporate Finance*, vol. 18, no. 1, pp. 22–37, 2012.
- [9] N. Jeppson and D. Salerno, "Innovation focused strategy and earnings management," *Economic and Business Review*, vol. 19, no. 1, pp. 19–49, 2017.
- [10] F. Jiang, B. Zhu, and Y. Wang, "Do managers' incentive contracts of state-owned enterprises pay less attention to performance," *Management World*, vol. 33, no. 9, pp. 143–159, 2014.
- [11] G. Jiang and H. Yue, "A study of the relationship between big shareholders' diverting listed companies' capital and the stock returns of these companies," *Management World*, vol. 24, no. 9, pp. 119–172, 2005.
- [12] J. M. Karpoff, "The impact of shareholder activism on target companies: a survey of empirical findings," *Social Science Electronic Publishing*, vol. 11–12, no. 2, pp. 22–23, 2006.
- [13] V. Khanna, E. H. Kim, and Y. Lu, "CEO connectedness and corporate fraud," *The Journal of Finance*, vol. 70, no. 3, pp. 1203–1252, 2015.
- [14] J. B. Kim and C. H. Yi, "Foreign versus domestic institutional investors in emerging markets: who contributes more to firm-specific information flow?" *China Journal of Accounting Research*, vol. 8, no. 1, pp. 1–23, 2015.
- [15] P. Li and Y. Shen, "The corporate governance role of media: empirical evidence from China," *Economic Research Journal*, vol. 45, no. 4, pp. 14–27, 2010.
- [16] P.-L. Li, Y. Zhang, and J. M. J. K. F. Abais, "Cyclic ADP-r in vascular regulation and diseases," *Messenger*, vol. 2, no. 2, pp. 63–85, 2013.

- [17] D. Lu, X. Xie, and D. Yang, "Independent directors' official background and corporate fraud," *Accounting Research*, no. 08, pp. 55–61+95, 2017.
- [18] Y. Lu, Y. Zhu, and X. Hu, "Institutional shareholding and corporate fraud: evidence from China," *Nankai Business Review*, vol. 15, no. 1, pp. 13–23, 2012.
- [19] W. L. Megginson and K. A. Weiss, "Venture capitalist certification in initial public offerings," *The Journal of Finance*, vol. 46, no. 3, pp. 879–903, 1991.
- [20] M. Qian, "Is "voting with your feet" an effective mutual fund governance mechanism?" *Journal of Corporate Finance*, vol. 17, no. 1, pp. 45–61, 2011.
- [21] R. T. S. Ramakrishnan and A. V. Thakor, "Information reliability and a theory of financial intermediation," *The Review of Economic Studies*, vol. 51, no. 3, pp. 415–432, 1984.
- [22] C. Wu, S. Wu, L. Cheng, and L. Wang, "The role of venture capital in the investment and financing behavior of listed companies: evidence from China," *Economic Research Journal*, vol. 47, no. 1, pp. 105–119+160, 2012.
- [23] W. A. Sahlman, "The structure and governance of venture-capital organizations," *Journal of Financial Economics*, vol. 27, no. 2, pp. 473–521, 1990.
- [24] J. Su, B. Wang, F. Cao, and X. Liu, "Does corporate strategy affect earnings management," *Management World*, no. 3, pp. 160–169, 2016.
- [25] X. Tian, G. Udell, and X. Yu, "Disciplining delegated monitors: the consequences of failing to prevent fraud," *Unpublished working paper*, 2011.

Research Article

Design and Implementation of 3D Animation Data Processing Development Platform Based on Artificial Intelligence

Quansheng Gao 

College for Creative Studies, Changzhou Vocational Institute of Textile and Garment, Changzhou, Jiangsu 213164, China

Correspondence should be addressed to Quansheng Gao; qsgao@cztgi.edu.cn

Received 20 April 2022; Revised 10 May 2022; Accepted 16 May 2022; Published 30 May 2022

Academic Editor: Dong Chen

Copyright © 2022 Quansheng Gao. This is an open access article distributed under the Creative Commons Attribution License, which permits unrestricted use, distribution, and reproduction in any medium, provided the original work is properly cited.

Based on the whole process of computer-aided technology, a 3D animation data processing development platform based on artificial intelligence is designed and implemented. A random forest model for animation data processing and development is designed to mine the experience that can guide animation generation from the accumulated animation data. Based on the design goal and implementation principle of animation data processing and development platform, the attributes and categories of random forest model are abstracted. After standardizing a large number of historical data, the training sample set is obtained, and the random forest model is obtained after training. The parameters of the random forest model are continuously optimized by experiments, so that the learning model can better guide the dynamic animation data processing and development platform to generate animation to the satisfaction of users. The designed three-dimensional animation data processing and development platform interacts with the animation generation module, users, and system administrators. It can continuously receive the sample data of the animation generation module, automatically expand the number of training samples, analyze the status of the sample database, and put forward suggestions to the system administrator to update the learning model, so as to realize the initiative of learning. The experimental results show that the designed 3D animation data processing and development platform is effective and feasible.

1. Introduction

Three-dimensional animation technology [1–3] mainly relies on computer image technology, using three-dimensional model, light, material, and shooting of its change process to simulate the real picture of birth, and can display the shocking picture beyond reality through special effects [4–10]. The research of three-dimensional animation technology began in North America. After in-depth research on three-dimensional animation theory and computer animation system, three-dimensional computer animation system appeared in the 1970s and realized commercialization in the following 10 years. By the 1990s, 3D animation technology had made new breakthroughs in the field of film stunts, and 3D animated films became fashionable for a time [2].

Machine learning is the most popular artificial intelligence science at present [11–13]. It establishes a prediction

model (training model) by learning the characteristics and results of known data sets (training samples). Using the model, the characteristics and results of unknown data can be predicted and measured. Classical machine learning algorithms include decision tree, neural network, support vector machine, etc.

At present, the traditional knowledge-based method faces two problems: (1) lack of learning ability, and a large amount of historical data is wasted; (2) the quality of finished animation can only depend on the level of the system designer and the user of the system—the user cannot participate in the generation of animation.

In view of this, this study builds a 3D animation data processing development platform based on machine learning algorithm to realize the learning ability of “continuous learning” of the platform. On the one hand, this platform solves the two inherent problems of the generation

system. On the other hand, by building a circular learning system, the generation system has the ability of “continuous learning.”

2. Framework of Platform

2.1. Overall Architecture of the Platform. In order to solve the above two problems, the 3D animation data processing and development platform proposed in this article takes the user’s evaluation of animation products and the historical data of the generation system as training samples and uses machine learning algorithm to generate a model with user evaluation as classification result to guide the generation system to generate animation that makes users more satisfied. However, users’ evaluation of animation is a subjective judgment. Users’ understanding of the text and users’ psychological state and the color, music, action, and other factors of the animation itself will affect the evaluation results. In order to make the learning purpose more clear and the guidance more targeted, we need to choose a more specific evaluation object.

Scene is the background of animation. For users, scene is the most intuitive content of animation; For the generation system, the spatial attributes and layout attributes of the scene directly affect the subsequent model addition, color, lighting, and a series of planning. This study selects the animation scene as the evaluation object of users. In addition, the selection of machine learning algorithm is a key problem in the implementation of 3D animation data processing and development platform. Among the machine learning methods, the method based on decision tree is widely used [14–19]. First, because the decision tree model is easy to understand, the problem-solving process can be intuitively understood through the working process of decision tree, and second because the decision tree can give accurate solutions to a wide range of problems. Random forest is an integrated learning device based on decision tree. It is known as “a method representing the level of integrated learning technology” because of its simplicity, easy implementation, low computational overhead, and strong performance in many real tasks.

2.2. Detailed Design of the Platform. The proposed 3D animation data processing and development platform is divided into two modules: generation system and learning system. Their design and implementation will be described below.

2.2.1. Generation Module. We build a sample database in generation module. The increase of sample data will stimulate the continuous updating of learning model, improve the guidance ability of learning system, and finally realize the ability of “continuous learning” of the system. The generation module (as shown in Figure 1) is divided into four core sub-modules: information extraction sub-module, scenario qualitative planning sub-module, animation quantitative calculation sub-module, and network rendering sub-module. Other auxiliary sub-modules are short message receiving and preprocessing sub-module, LAN transmission sub-

module of animation related files, and 3D animation website generation and sending sub-module.

The flow chart is shown in Figure 2.

The finished animation of the generation module depends on the animation material library. Animation material library mainly includes scene library, model library, background music library, etc. Both scene library and model library are Maya file libraries. The scene is the background scene where the animation takes place. A model is a physical model, such as a person, a flower, etc. First, the information extraction module extracts several topics and templates from the SMS text. Theme refers to the animation theme series extracted from SMS, such as birthday, playing basketball, new year, etc. Template is a concrete object, such as character template, location template, etc. For example, from the text message “I want to stay at home and don’t want to play football,” the theme “play football” and the template “action” and “character” are extracted. These lines of information are stored in the IE file and become the basis for the qualitative planning of the plot. In the generation module, we use the software Protégé to build ontology library (animation scene library class, theme library class, template library class, background picture library class, scene space class, animation three-dimensional model class, etc.) and use SWRL language to write rules (including theme class rules, animation scene class rules, adding class rules used to produce variability effects on animation, deleting class rules, changing class rules, etc.), so as to realize the specific expression of different knowledge and the complex reasoning relationship between different data. The plot qualitative planning sub-module calls the corresponding ontology library and rule library according to the information framework; infers and completes the planning of scene selection, model increase, and decrease, action, color, deformation, and illumination; and writes the planning results into the plot planning document. The results of qualitative planning will be used as the basis of quantitative planning module. The quantitative module carries out quantitative calculation, operates the animation file, and then generates the animation scene file that can be rendered. Finally, we enter the network rendering module for rendering, generate playable animation files, and return them to the user.

The material selection of the generation module adheres to the principles of rationality, randomness, and diversity, that is the material conforms to the transmission content of short message text. The selection of material selection within a reasonable range is not interfered by people. Different animations will be obtained if the same short message text is input multiple times. The specific strategy of scene selection is as follows: first, several candidate scenes are obtained according to the theme, template atom, model, or special effect corresponding to template atom of information extraction. Then each candidate scene is scored according to the set scoring items (time, character, action, etc.), and the final total score is calculated. Finally, a candidate scene is randomly selected as the final scene. The higher the total score, the more likely the candidate scene is to be selected.

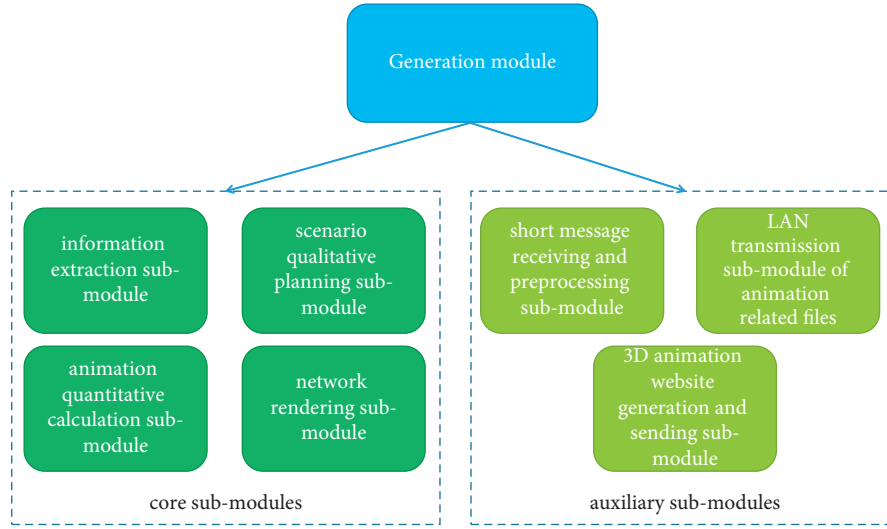


FIGURE 1: The generation module.

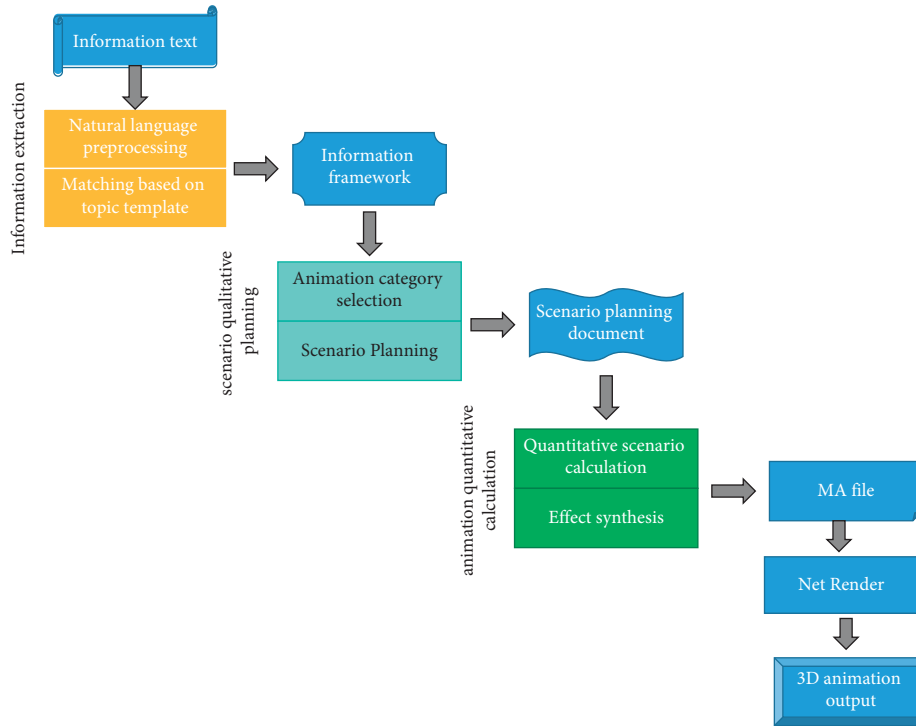


FIGURE 2: The flow chart of generation module.

2.3. Learning Module. The learning goal of the learning module is to help the generation system select more satisfactory scenes for users on the premise of adhering to the three principles of rationality, randomness, and diversity and finally improve users' satisfaction with animation. The learning module has three sub-modules: interaction sub-module, data management and analysis sub-module, and training sub-module. The flow chart is shown in Figure 3.

The interaction sub-module is responsible for interacting with the generation system and users. The historical data

obtained through interaction with the generation module, including IE files with information framework, ADL documents with qualitative data (with selected scenes), finished animation products, and the user's evaluation of scene selection obtained through interaction with the user, are jointly used as training sample data. At the same time, the interaction sub-module should continuously transmit the learning results (model data) to the generation module to help the generation module make better choices. Interaction sub-module is an important guarantee to achieve learning objectives.

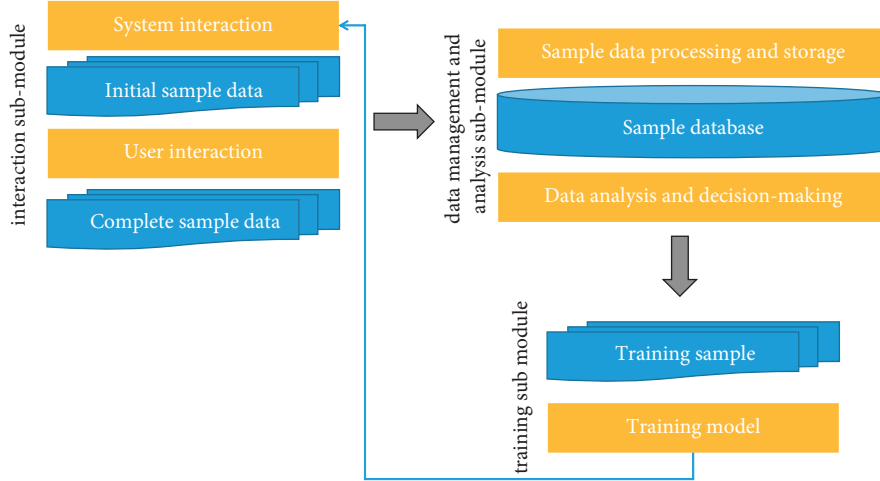


FIGURE 3: The flow chart of learning module.

The data management and analysis sub-module realizes the unified storage, management, analysis, and decision of sample data. First, it receives the complete sample data transmitted by the interactive sub-module, extracts and processes the information, obtains the standard sample data, and stores it in the database, and then the sub-module analyzes and makes decisions on the data in the sample database.

The attribute list of the database is shown in Table 1.

As shown in Table 1, the difference attribute is used to select the SMS animation that needs interaction. Difference and IsUsed jointly decide whether to retrain. The strategies are as follows: (1) When the number of unused samples in the database exceeds the limit value, it is suggested that the system manager retrain the data; (2) when the number of samples whose difference value exceeds the limit value in the database, it is suggested that the system manager retrain the data; and (3) when the above two situations occur at the same time, the system manager is required to retrain the data. The training module uses training samples for training, and the obtained learning model is returned to the interaction module. The module accepts the judgment of the data management and analysis module to decide whether to train or not, so as to ensure that the learning model can be updated continuously with the operation of the generation system.

2.4. Random Forest Model for 3D Animation Data Processing.

Random forest model [20–25] for 3D animation data processing is the key to realize the learning ability of animation data processing development platform. It can mine the experience that can guide animation generation from the accumulated animation data.

Decision tree [18, 19] is a kind of inductive learning, and its structure is shown in Figure 4. The generation of decision tree is a recursive process. The key of decision tree learning is how to select the optimal partition attribute.

ID3 algorithm divides attributes based on information gain [23–25]. Assuming that the proportion of the k th

TABLE 1: The attribute list of the database.

Number	Name	Meaning
1	ID	ID number
2	SMSN	SMS number
3	SSD	Standard sample data
4	IsUsed	Is this sample used as a trained sample
5	Difference	The distance value of the cluster closest to the sample
6	IsJudge	Is it rated by the user

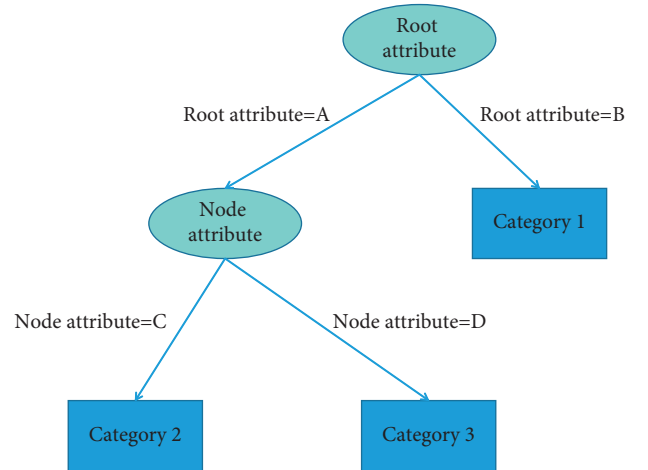


FIGURE 4: Decision tree.

sample in the current sample set D is p_k , $k = 1, 2, \dots, |y|$, the definition of information entropy of D is shown as

$$\text{Ent}(D) = - \sum_{k=1}^{|y|} p_k \log_2 p_k. \quad (1)$$

Assuming that there are V possible values $\{a^1, a^2, \dots, a^V\}$ for discrete attribute a , and the sample with value a^V on attribute a is recorded as D^V , the information gain obtained by dividing sample D by attribute a is as follows:

TABLE 2: Comparative experiment of specific information text on the selection probability of user's favorite/dislike scene.

	User favorite scene selection probability experiment			User aversion scene selection probability experiment		
	0 to 10%	10% to 25%	25 to 40%	-10% to 0	-25% to -10%	-40% to -25%
Growth rate of probability of learning module participating in favorite/disgust scene selection						
Number	3	9	5	5	4	8

TABLE 3: The background information of experimental users.

Age	Occupation	Number of men	Number of women	Total number
15-25	Student	3	4	7
25-35	Graduate student	5	6	11
25-45	Workers	4	7	11
45-55	Workers	8	2	10
55-65	Unemployed and retirees	2	4	6
Above 65	Unemployed and retirees	3	2	5

$$\text{Gain}(D, a) = \text{Ent}(D) - \sum_{v=1}^V \frac{|D^v|}{|D|} \text{Ent}(D^v). \quad (2)$$

Bootstrap sampling is a sampling with return, that is we randomly take a sample from the initial data set (assuming that it contains m samples) and put it into the sampling set, then put the sample back into the data set, and continue to do this until the new sampling set has m samples. Random forest is a model composed of multiple decision tree classification models, which is sampled by bootstrap sampling. The basic idea of the algorithm is to use the bootstrap method to extract t sampling sets containing m samples, and then use the decision tree algorithm to train t decision tree models.

Different from the traditional decision tree algorithm, the random forest introduces the random attribute selection in the training process of the decision tree. The traditional decision tree directly selects the optimal attribute when selecting the partition attribute, while the base decision tree of the random forest first randomly selects an attribute subset and selects the optimal attribute from the subset. The classification results of random forest are determined by all set decision trees through voting. The commonly used voting methods are absolute majority voting method and relative majority voting method. Among them, the relative majority voting method refers to the random selection of one of the markers with the most votes.

Random forest can increase the difference between classification models by constructing different training sets, so as to improve the extrapolation prediction ability of combined classification models. Compared with decision tree, random forest has good advantages in solving over fitting problem. It should be noted that generalization error may occur within a certain limit.

3. Experiment

3.1. Experiment 1. Experiment 1 verifies whether the random forest model of the learning module in the 3D animation data processing and development platform can

effectively learn users' preferences. Under specific text content, the animation scene with a user score of 1 is recorded as disgusting scene, and the animation scene with a user score of 5 is recorded as favorite scene. From the user's feedback on the animation, 18 text information animations with a score of 1 and 16 text information animations with a score of 5 are found; the corresponding text information, text content, and selected scene are extracted; and a comparative test on these 34 text information is conducted.

The specific operations are as follows: (1) Input the short message text into the generation module without learning module to get the scene selected by the system, and test the short message with the same content for 100 times; (2) input the text into the generation module guided by the learning module to get the scene selected by the system, and test the text with the same content for 100 times; and (3) compare the probability of disgusting scene/favorite scene between the two groups.

The comparison results are shown in Table 2.

3.2. Experiment 2. In the proposed 3D animation data processing and development platform, the main function of the learning module is to improve users' satisfaction with animation by helping the generation module select the scenes that users prefer. In Experiment 2, there were 50 experimental users—25 men and 25 women. The background information of experimental users is shown in Table 3.

We selected 500 animations from the original generation module. After the experimental user clearly understood the definition of the scene of the generation module, we scored the scene selection of these 500 animations, with an average score of 3.12. After the learning module was put into use, 100 animations were randomly selected to interact with experimental users to get score feedback. The average score was 3.71, an increase of 16.93%. The results show that the learning module can help the generation module to improve user satisfaction, and the growth rate has not increased significantly. The main reason is that users are not satisfied

with the scene production in the material library of the generation system, resulting in no breakthrough in the highest score of user evaluation.

We use two experiments to verify the effectiveness of the learning module in the three-dimensional animation data processing and development platform, that is the learning module can learn users' preferences for the scene and help the generation module improve users' satisfaction with the finished animation. However, due to the objective limitations of other factors in the generation module, and in order to ensure the randomness and diversity of the animation, this improvement is within a certain range.

4. Conclusions

In this research, we mainly build a three-dimensional animation data processing and development platform, in which the design and implementation of generation module and learning module is the focus of this research. The learning module helps the generation module to continuously learn experience from historical data and generate animations that are more satisfactory to users. At the same time, the implementation of the learning module enables the generation module to have the ability of "continuous learning." At present, the learning module mainly helps the generation module to select the scene. This learning mode can also be applied to the selection of model, character action, and background music, so that the user's opinions can act on all aspects of the finished animation. The learning module is still in the improvement stage, and a large number of experiments are needed to find better system parameters, such as the number of base learners, so as to better serve the generation module.

Future research will be carried out from the following aspects. (1) Expansion of learning mode. A complete animation synthesis mainly includes three aspects: background scene, model, and music. The animation data processing and development platform designed in this article starts from the perspective of background animation scene selection. Whether this learning mode around background scene can be extended to the design and selection of model and music is a problem needs further research. (2) Optimization of parameters of animation data processing development platform. Animation data processing and development platform is a system involving many system parameters, such as the number of basic decision trees of random forest model and the setting of boundary values in data management and analysis. These parameters need further experiments and time test to demonstrate their effectiveness. (3) How to reduce the workload of users and system administrators. The proposed 3D animation data processing and development platform is currently in a semiautomatic state, and the system administrator needs to participate in the update of the learning model. Manual participation can ensure the stability and controllability of the system in the initial stage of system operation. With the maturity of platform functions, manual participation needs to be gradually reduced. The 3D animation data processing and development platform adopts the active learning method to

obtain the user's evaluation marks for some text animation. At present, the interactive mode between the mobile platform and users is to show the text number to the user. The user accesses the platform and finds the text to be evaluated according to the number. The user evaluation is written into the sample database of the platform by the system administrator. In the next version of this platform, a more intuitive and convenient interactive interface for users can be built.

Data Availability

The data set can be accessed upon request.

Conflicts of Interest

The authors declare that there are no conflicts of interest.

References

- [1] J. Liu, "Research on the design and production of 3D animation," in *Proceedings of the 2nd International Conference on Computer Vision, Image, and Deep Learning*, Liuzhou, China, October 2021.
- [2] Lu Yi, "Computer digital art design based on 3D animation special effects," in *Proceedings of the 2021 International Conference on Computer Technology and Media Convergence Design, CTMCD*, pp. 30–33, Sanya, China, April 2021.
- [3] J. Zhao and X. Zhao, "Computer-aided graphic design for virtual reality-oriented 3D animation scenes," *Computer-Aided Design and Applications*, vol. 19, pp. 65–76, 2022.
- [4] H. Zhu, "The optimization function of computer image technology in processing oil painting creation," *Wireless Communications and Mobile Computing*, vol. 2022, Article ID 3188527, 2022.
- [5] L. Li, C. Mao, H. Sun, Y. Yuan, and B. Lei, "Digital twin driven green performance evaluation methodology of intelligent manufacturing: hybrid model based on fuzzy rough-sets AHP, multistage weight synthesis, and PROMETHEE II," *Complexity*, vol. 2020, no. 6, pp. 1–24, Article ID 3853925, 2020.
- [6] Y. Cheng, "Application of VR computer image technology in 3D virtualization of sports human science," *Concurrency and Computation: Practice and Experience*, vol. 30, 2018.
- [7] L. Li, T. Qu, Y. Liu et al., "Sustainability assessment of intelligent manufacturing supported by digital twin," *IEEE Access*, vol. 8, pp. 174988–175008, 2020.
- [8] L. Li, B. Lei, and C. Mao, "Digital twin in smart manufacturing," *Journal of Industrial Information Integration*, vol. 26, no. 9, Article ID 100289, 2022.
- [9] L. Fu, "Research on the role of computer image technology in visual communication design," *Journal of Physics: Conference Series*, vol. 3, Article ID 032093, 1992.
- [10] L. Li and C. Mao, "Big data supported PSS evaluation decision in service-oriented manufacturing," *IEEE Access*, vol. 8, pp. 154663–154670, 2020.
- [11] Y. Li and He Mao, "Study on machine learning applications in ideological and political education under the background of big data," *Scientific Programming*, vol. 2022, Article ID 3317876, 2022.
- [12] F. Shah, Y. Liu, A. Anwar et al., "Machine learning: the backbone of intelligent trade credit-based systems," *Security and Communication Networks*, vol. 2022, Article ID 7149902, 2022.

- [13] M. B. Butt, M. Alfayad, S. Saqib et al., "Diagnosing the stage of hepatitis C using machine learning," *Journal of Healthcare Engineering*, vol. 2021, Article ID 8062410, 2021.
- [14] S. Liao and Z. Liu, "Enterprise financial influencing factors and early warning based on decision tree model," *Scientific Programming*, vol. 2022, Article ID 6260809, 2022.
- [15] F. Wu, X. Liu, Y. Wang, X. Li, and M. Zhou, "Research on evaluation model of hospital informatization level based on decision tree algorithm," *Security and Communication Networks*, vol. 2022, Article ID 3777474, 2022.
- [16] B. Mahbooba, M. Timilsina, R. Sahal, and M. Serrano, "Explainable artificial intelligence (XAI) to enhance trust management in intrusion detection systems using decision tree model," *Complexity*, vol. 2021, Article ID 6634811, 2021.
- [17] P. Lu, Y. Zhang, B. Zhou et al., "Identification of arrhythmia by using a decision tree and gated network fusion model," *Computational and Mathematical Methods in Medicine*, vol. 2021, Article ID 6665357, 2021.
- [18] C. Jin, F. Li, S. Ma, and Y. Wang, "Sampling scheme-based classification rule mining method using decision tree in big data environment," *Knowledge-Based Systems*, vol. 244, no. 23, 2022.
- [19] W. He, Y. Wang, M. Zhou, and B. Wang, "A novel parameters correction and multivariable decision tree method for edge computing enabled HGR system," *Neurocomputing*, vol. 487, pp. 203–213, 2022.
- [20] J. Galasso, D. M. Cao, and R. Hochberg, "A random forest model for forecasting regional COVID-19 cases utilizing reproduction number estimates and demographic data," *Chaos, Solitons & Fractals*, vol. 156, Article ID 111779, 2022.
- [21] X. Wang, Z. Wen, G. Liu, H. Tao, and K. Song, "Remote estimates of total suspended matter in China's main estuaries using Landsat images and a weight random forest model," *ISPRS Journal of Photogrammetry and Remote Sensing*, vol. 183, pp. 94–110, 2022.
- [22] X. Li, J. Liu, D. Liu et al., "Measurement and analysis of regional agricultural water and soil resource composite system harmony with an improved random forest model based on a dragonfly algorithm," *Journal of Cleaner Production*, vol. 305, 2021.
- [23] Z. Liu, N. Su, Y. Qin, J. Lu, and X. Li, "A deep random forest model on spark for network intrusion detection," *Mobile Information Systems*, vol. 2020, Article ID 6633252, 2020.
- [24] H. Fu and K. Qi, "Evaluation model of teachers' teaching ability based on improved random forest with grey relation projection," *Scientific Programming*, vol. 2022, Article ID 5793459, 2022.
- [25] H. Xie, J. Dong, Y. Deng, and D. Yiwen, "Prediction model of the slope angle of rocky slope stability based on random forest algorithm," *Mathematical Problems in Engineering*, vol. 2022, Article ID 9441411, 2022.

Research Article

Fetal Meconium Peritonitis: A Clinical Study of Nine Cases

Fengping Fu , Xia Song , Fudan Huang , Hang Yuan , and Li Xiao 

Shandong Provincial Maternal and Child Health Care Hospital, Jinan City, Shandong Province, China

Correspondence should be addressed to Li Xiao; lixiao@sdmch.com.cn

Received 11 April 2022; Revised 5 May 2022; Accepted 12 May 2022; Published 27 May 2022

Academic Editor: Dong Chen

Copyright © 2022 Fengping Fu et al. This is an open access article distributed under the Creative Commons Attribution License, which permits unrestricted use, distribution, and reproduction in any medium, provided the original work is properly cited.

Objective. To explore the prenatal ultrasonographic characteristics and pregnancy outcomes of fetal meconium peritonitis (FMP). **Methods.** Nine patients diagnosed with FMP by routine prenatal examination between January 2015 and December 2020 were identified. Both prenatal ultrasonographic characteristics and pregnancy outcomes associated with these patients were retrospectively analyzed. **Results.** The mean gestational age at the time of FMP diagnosis was 31.3 ± 4.8 weeks, and the mean gestational age of delivery was 35.1 ± 5.1 weeks. Prenatal ultrasonographic findings at the time of diagnosis in these patients included intestinal dilatation (9/9, 100%), intraperitoneal calcification (8/9, 88.9%), fetal ascites (5/9, 55.6%), intraperitoneal pseudocyst (5/9, 55.6%), and polyhydramnios (6/9, 66.7%). Analyses of the etiological basis for meconium peritonitis in 5 of the 8 live births that underwent surgical treatment revealed 4 cases of congenital volvulus and 1 case of jejunal atresia. **Conclusion.** The prenatal ultrasound manifestations of fetal meconium peritonitis are diverse, and the different grades of prenatal ultrasound manifestations can provide important information for the treatment of perinatal infants.

1. Introduction

FMP (fetal meconium peritonitis) is a rare form of sterile chemical peritonitis that can occur in utero, primarily as a consequence of the flow of meconium into the abdominal cavity due to the perforation of the fetal intestine [1]. The incidence of FMP is low, about 1 in 30,000 [2]. Owing to its rarity and the limited amount of research conducted on this condition to date, FMP was associated with a case fatality rate of up to 43.7%–59.6% in 2003 [3]. The neonatal mortality associated with this condition has, however, declined in recent years owing to new advances in prenatal diagnostics, with the live birth rate of affected neonates now ranging from 80%–92.3% [4–6]. Herein, we conducted a retrospective analysis of the ultrasonographic findings and perinatal outcomes associated with 9 cases of prenatally diagnosed FMP in an effort to provide a better basis for prenatal diagnosis and management of this potentially dangerous condition.

2. Materials and Methods

2.1. Subjects. In total, data from 9 patients diagnosed with FMP during routine ultrasonographic prenatal

examinations from January 2015 to December 2020 were retrospectively analyzed. All pregnant women provided written informed consent to undergo these prenatal ultrasound examinations, and the ethics committee of our hospital approved the present retrospective study.

2.2. Research Methods. Clinical data pertaining to the 9 patients diagnosed with FMP were analyzed retrospectively, including prenatal ultrasound examination characteristics, the diagnosis made following postnatal imaging or surgical exploration, and associated neonatal outcomes. Correlations between prenatal ultrasonography and neonatal prognosis were additionally evaluated.

2.3. Diagnostic Criteria. Prenatal ultrasonographic findings of FMP are primarily associated with one or more of the following, with or without hyperhydramnios: (1) calcification in the abdominal cavity of the fetus; (2) fetal peritoneal effusion; (3) fetal intestinal dilatation; (4) pseudocyst in the fetal abdominal cavity [6]. The FMP ultrasonic classification standards are shown in Table 1 [7].

TABLE 1: Zangheri's FMP grading system [7].

Classification	Sonographic findings
0	Simple intraperitoneal calcification
1	1A Intraperitoneal calcification with ascites
	1B Intraperitoneal calcification with pseudocyst
	1C Intraperitoneal calcification with intestinal loop dilatation
2	Intraperitoneal calcification with the above two kinds of ultrasound abnormalities
3	Intraperitoneal calcification with ≥ 3 of the above related ultrasonographic abnormalities

TABLE 2: Ultrasonic characteristics and classifications.

Serial number	Sonographic findings	Classification
1	Fetal intestinal dilatation, fetal intraperitoneal calcification, fetal ascites, fetal intraperitoneal pseudocyst, hydramnios	3
2	Fetal intestinal dilatation, fetal peritoneal calcification, fetal ascites	2
3	Fetal intestinal dilatation, fetal peritoneal calcification, fetal ascites	2
4	Fetal intestinal dilatation, fetal intraperitoneal pseudocyst, hydramnios	Unrated
5	Fetal intestinal dilatation, fetal peritoneal calcification, fetal ascites, excessive amniotic fluid	2
6	Fetal intestinal dilatation, fetal peritoneal calcification, hydramnios	1C
7	Fetal intestinal dilatation, fetal peritoneal calcification, fetal peritoneal pseudocyst	2
8	Fetal intestinal dilatation, fetal intraperitoneal calcification, fetal ascites, fetal intraperitoneal pseudocyst, fetal hyperhydramnios, fetal edema, fetal right heart dilatation with pericardial effusion	3
9	Fetal intestinal dilatation, fetal peritoneal calcification, fetal intraperitoneal pseudocyst, hydramnios	2

3. Results

3.1. General Data and Clinical Outcomes. The mean gestational age of the 9 patients in this study was 29.6 ± 5.3 years old, the mean gestational age at diagnosis was 31.3 ± 4.8 weeks, and the mean gestational age at delivery was 35.1 ± 5.1 weeks. Among the 9 patients, there were 8 live births and 1 case of induced labor. The mean birth weight of the resultant newborns (6 males, 3 females) was 2795.6 ± 908.5 g, and of these 9 patients, 7 underwent delivery via cesarean section (77.8%), fetal movement decreased in 3 cases (33.3%), and 2 exhibited amniotic fluid meconium contamination degree II or III (22.2%). Of these 9 patients, 2 had undergone prenatal screening for serum toxoplasma, rubella virus, cytomegalovirus, and herpes simplex virus, with no abnormal findings. Three cases underwent ultrasound-guided amniocentesis for prenatal diagnosis, with no findings consistent with pathogenicity, and one case underwent ultrasound-guided fetal abdominal puncture before birth.

For these 9 cases, prenatal ultrasound suggested potential meconium peritonitis with fetal intestinal obstruction or intestinal atresia. In total, 5 out of 8 live births underwent surgical treatment, leading to the confirmation of congenital volvulus in 4 cases and jejunal atresia in 1 case. The remaining 3 cases improved upon conservative treatment.

3.2. Prenatal Ultrasound Findings. Upon prenatal ultrasonographic assessment of these 9 cases, 8 (88.9%) exhibited visible fetal intraabdominal calcifications, 5 (55.6%) exhibited visible fetal ascites, 5 (5/9, 55.6%) exhibited fetal intraabdominal pseudocyst, 6 (66.7%) exhibited hydramnios, and 1 exhibited fetal edema, fetal right heart enlargement, and pericardial effusion. The ultrasonographic

characteristics and grades associated with these 9 cases are shown in Table 2.

4. Discussion

The pathogenesis of FMP is poorly understood but may be associated with congenital ileus [8], congenital intestinal wall dysplasia [9], intrauterine infection, or other factors, with some cases additionally being associated with cystic fibrosis [10], chromosomal malformations, or spontaneous intestinal perforation of unknown cause. Congenital intestinal obstruction is the most common cause of FMP [8] and may arise as a consequence of intestinal atresia, intussusception, or intestinal volvulus [8]. The clinical presentation of patients with FMP varies depending on the timing of fetal intestinal perforation and whether the perforation is closed. In this study, 4 cases of FMP were confirmed by surgery as being associated with congenital intestinal obstruction and intestinal perforation resulting from intestinal torsion, while 1 case was associated with congenital jejunal atresia. There are some reports suggesting that there may be cases of familial FMP [11], but further research on this topic is warranted.

The prenatal diagnosis of FMP is primarily dependent upon ultrasound-based screening and detection at present. Prenatal ultrasound scans can detect FMP at a median gestational age of approximately 32 weeks, with a median gestational age at delivery of about 36 weeks [4]. In the present report, we similarly observed an average gestational age at diagnosis of 31.3 ± 4.8 weeks and an average gestational age at delivery of 35.1 ± 5.1 weeks, in line with these prior reports. FMP can be associated with diverse ultrasonographic manifestations, with the most common such

findings being fetal ascites, polyhydramnios, calcification in the fetal abdominal cavity, dilatation of the fetal intestinal loops, fetal edema, and pseudocyst formation [5]. The primary prenatal ultrasonography results used to guide the diagnosis of FMP include ascites, abdominal calcification, and intestinal perforation and/or dilatation. In the present study, the most common ultrasonographic findings were fetal intestinal dilatation, followed by fetal intraperitoneal calcification, fetal ascites with intestinal perforation and dilation of the oop intestine, and 1 case presenting with hyperhyniotic amniotic fluid. Some researchers classify FMP into three types depending on the presence of specific features, with type I FMP presenting with ascites, type II FMP being associated with cysts as a consequence of local ascites accumulation and adhesion in the bowel and greater omentum having resulted in pseudocyst formation, and type III FMP being associated with fibrous adhesions as a consequence of calcium salt closed perforation caused by the sedimentation of the bowel perforation position [4, 5, 12]. With intraperitoneal calcification as the common phenomenon, Zangheri et al. divided FMP into four levels according to the presence of other abnormal ultrasonographic situations: level 0 refers to the cases where only intraperitoneal calcification is observed, level 1 refers to the cases where intraperitoneal calcification and one abnormal ultrasonographic situation are observed, level 2 refers to the cases where intraperitoneal calcification and two abnormal ultrasonographic situations are observed, and level 3 refers to the cases where intraperitoneal calcification and three abnormal ultrasonographic situations are observed [7]. The majority of cases in the present study were of grade 2 or 3. In some prior studies, magnetic resonance imaging (MRI) has been used to guide the prenatal diagnosis of FMP, but at present prenatal ultrasound remains the primary diagnostic approach for this condition.

Prenatal diagnostic tests such as fetal chromosomal karyotyping, gene microarrays, and TORCH screening are recommended in cases of suspected prenatal FMP. If a gene fragment suspected to be pathogenic is identified, patients should undergo antenatal consultation to determine whether to continue the pregnancy. In this study, two patients underwent prenatal diagnosis, and no suspected pathogenic gene fragments were identified.

In this study, 7 of the 9 patients delivered via cesarean section, but there is no evidence that cesarean delivery can improve neonatal outcomes associated with FMP. The postnatal treatment and prognosis of FMP are closely linked to whether or not there is evidence of intestinal perforation and intestinal obstruction. According to the grading system proposed by Zangheri et al., grade 0 fetuses require no surgical intervention after birth, whereas approximately 50% of grade 1 fetuses will require surgical treatment, and almost all grade 2 and 3 fetuses will require postnatal surgery [7]. In this study, 5 of the 8 live neonates underwent postnatal surgery, all of whom were Zangheri grade 2 or grade 3 cases. Some studies have shown that pseudocyst, intestinal loop dilatation, and ascites are predictors of the need for neonatal surgical treatment [13]. Early diagnosis and early treatment are of particular importance in neonates with FMP

complicated by intestinal perforation and obstruction. The prognosis of all children in the present study was good.

In summary, while FMP remains a rare condition, its timely diagnosis and postnatal management are important as a means of improving neonatal prognosis. Prenatal ultrasonography is a key means of diagnosing FMP, which can allow for the dynamic monitoring of disease progression during pregnancy while offering guidance regarding neonatal clinical outcomes.

Data Availability

The datasets used to support the findings of this study are available from the corresponding author on reasonable request.

Ethical Approval

The study got the approval of the ethics committee of Shandong Provincial Maternal and Child Health Care Hospital.

Consent

Patients' family members fully knew the study process and they signed informed consent forms.

Disclosure

This study has been presented in International Conference on Advances in Biological Science and Technology ICABST2022 as a poster presentation.

Conflicts of Interest

The authors declare that they do not have any commercial or associative interest that represents a conflict of interest in connection with the work submitted.

References

- [1] F. Eckoldt, K. S. Heling, R. Woderich, S. Kraft, R. Bollmann, and H. Mau, "Meconium peritonitis and pseudo-cyst formation: prenatal diagnosis and post-natal course," *Prenatal Diagnosis*, vol. 23, no. 11, pp. 904–908, 2003.
- [2] N. Saleh, A. Geipel, U. Gembruch et al., "Prenatal diagnosis and postnatal management of meconium peritonitis," *Journal of Perinatal Medicine*, vol. 37, no. 5, pp. 535–538, 2009.
- [3] M. K. Shyu, J. C. Shih, C. N. Lee, H. L. Hwa, S. N. Chow, and F. J. Hsieh, "Correlation of prenatal ultrasound and postnatal outcome in meconium peritonitis," *Fetal Diagnosis and Therapy*, vol. 18, no. 4, pp. 255–261, 2003.
- [4] S. H. Nam, S. C. Kim, D. Y. Kim et al., "Experience with meconium peritonitis," *Journal of Pediatric Surgery*, vol. 42, no. 11, pp. 1822–1825, 2007.
- [5] M. H. Tsai, S. M. Chu, R. Lien, H. R. Huan, and C. C. Luo, "Clinical Manifestations in Infants with Symptomatic Meconium Peritonitis," *Pediatr Neonatol*.
- [6] C.-W. Chen, C.-C. Peng, C.-H. Hsu et al., "The prognosis of meconium peritonitis," *Comparison of outcomes of prenatal and postnatal diagnosis*, vol. 98, no. 39, 2019.

- [7] G. Zangheri, M. Andreani, E. Ciriello, G. Urban, M. Incerti, and P. Vergani, "Fetal intra-abdominal calcifications from meconium peritonitis: sonographic predictors of postnatal surgery," *Prenatal Diagnosis*, vol. 27, no. 10, pp. 960–963, 2007.
- [8] L. M. Ping, V. S. Rajadurai, S. E. Saffari, and S. Chandran, "Meconium peritonitis: correlation of antenatal diagnosis and postnatal outcome - an institutional experience over 10 years," *Fetal Diagnosis and Therapy*, vol. 42, no. 1, pp. 57–62, 2017.
- [9] S. Emil, T. Nguyen, J. Sills, and G. Padilla, "Meconium obstruction in extremely low-birth-weight neonates: guidelines for diagnosis and management," *Journal of Pediatric Surgery*, vol. 39, no. 5, pp. 731–737, 2004.
- [10] G. Casaccia, A. Trucchi, A. Nahom et al., "The impact of cystic fibrosis on neonatal intestinal obstruction: the need for prenatal/neonatal screening," *Pediatric Surgery International*, vol. 19, no. 1, pp. 75–78, 2003.
- [11] K. H. Park, M. H. Bae, N. R. Lee, Y. M. Han, S. Y. Byun, and H. Y. Kim, "Meconium peritonitis resulting from different etiologies in siblings: a case report," *BMC Pediatrics*, vol. 20, no. 1, p. 106, 2020.
- [12] G. L. Omansky, "Meconium peritonitis a case study," *Neonatal Netw*, vol. 37, no. 4, pp. 233–237, 2018.
- [13] S. Shinar, S. Agrawal, M. Ryu, A. Zani, P. Chiu, and D. Chitayat, "Fetal meconium peritonitis - prenatal findings and postnatal outcome: a case series, systematic review, and meta-analysis," *Ultraschall Med*, vol. 43, no. 2, pp. 194–203, 2020.